CONTENTS

PREFACE

1 MAXWELL'S INTEGRAL LAWS IN FREE SPACE

1.0 Introduction

Overview of Subject,

1.1 The Lorentz Law in Free Space

1.2 Charge and Current Densities

1.3 Gauss' Integral Law of Electric Field Density

Singular Charge Distributions,
Gauss' Continuity Condition,

1.4 Ampere's Integral Law

Singular Current Distributions,
Ampere's Continuity Condition,

1.5 Charge Conservation in Integral Form

Charge Conservation Continuity Condition,

1.6 Faraday's Integral Law

Electric Field Intensity Having No Circulation,
Electric Field Intensity With Circulation,
Faraday's Continuity Condition,

1.7 Gauss' Integral Law of Magnetic Flux

Magnetic Flux Continuity Condition,

1.8 Summary

2 MAXWELL'S DIFFERENTIAL LAWS IN FREE SPACE

2.0 Introduction

2.1 The Divergence Operator

2.2 Gauss' Integral Theorem

2.3 Gauss' Law, Magnetic Flux Continuity and Charge Conservation

2.4 The Curl Operator

2.5 Stokes' Integral Theorem

2.6 Differential Laws of Ampere and Faraday

2.7 Visualization of Fields and the Divergence and Curl

2.8 Summary of Maxwell's Differential Laws and Integral Theorems

3 INTRODUCTION TO ELECTROQUASISTATICS AND MAGNETOQUASISTATICS

3.0 Introduction

3.1 Temporal Evolution of World Governed by Laws of Maxwell, Lorentz, and Newton

3.2 Quasistatic Laws

3.3 Conditions for Fields to be Quasistatic

3.4 Quasistatic Systems

3.5 Overview of Applications

3.6 Summary

4 ELECTROQUASISTATIC FIELDS: THE SUPERPOSITION INTEGRAL POINT OF VIEW

4.0 Introduction

4.1 Irrotational Field Represented by Scalar Potential: The Gradient Operator and Gradient Integral Theorem

Visualization of Two-Dimensional Irrotational Fields.

4.2 Poisson's Equation

4.3 Superposition Principle

4.4 Fields Associated with Charge Singularities

Dipole at the Origin.
Pair of Charges at Infinity Having Equal Magnitude and Opposite Sign.
Other Charge Singularities.

4.5 Solution of Poisson's Equation for Specified Charge Distributions

Superposition Integral for Surface Charge Density.
Superposition Integral for Line Charge Density.
Two-Dimensional Charge and Field Distributions.
Potential of Uniform Dipole Layer.

4.6 Electroquasistatic Fields in the Presence of Perfect Conductors

Capacitance. .

4.7 Method of Images

4.8 Charge Simulation Approach to Boundary Value Problems

4.9 Summary

5 ELECTROQUASISTATIC FIELDS FROM THE BOUNDARY VALUE POINT OF VIEW

5.0 Introduction

5.1 Particular and Homogeneous Solutions to Poisson's and Laplace's Equations

Superposition to Satisfy Boundary Conditions.
Capacitance Matrix.

5.2 Uniqueness of Solutions of Poisson's Equation

5.3 Continuity Conditions

5.4 Solutions to Laplace's Equation in Cartesian Coordinates

5.5 Modal Expansions to Satisfy Boundary Conditions

5.6 Solutions to Poisson's Equation With Boundary Conditions

5.7 Solutions to Laplace's Equation in Polar Coordinates

5.8 Examples in Polar Coordinates

Simple Solutions.
Azimuthal Modes.
Radial Modes.

5.9 Three Solutions to Laplace's Equation in Spherical Coordinates

5.10 Three-Dimensional Solutions to Laplace's Equation

Cartesian Coordinate Product Solutions,
Modal Expansion in Cartesian Coordinates,
Modal Expansion in Other Coordinates,

5.11 Summary

6 POLARIZATION

6.0 Introduction

6.1 Polarization Density

6.2 Laws and Continuity Conditions with Polarization

Polarization Current Density and Ampere's Law,
Displacement Flux Density,

6.3 Permanent Polarization

6.4 Polarization Constitutive Laws

6.5 Fields in the Presence of Electrically Linear Dielectrics

Capacitance,
Induced Polarization Charge,

6.6 Piece-wise Uniform Electrically Linear Dielectrics

Uniform Dielectrics,
Piece-wise Uniform Dielectrics,

6.7 Smoothly Inhomogeneous Electrically Linear Dielectrics

6.8 Summary

7 CONDUCTION AND ELECTROQUASISTATIC CHARGE RELAXATION

7.0 Introduction

7.1 Conduction Constitutive Laws

Ohmic Conduction,
Unipolar Conduction,

7.2 Steady Ohmic Conduction

Continuity Conditions,
Conductance,
Qualitative View of Fields in Conductors,

7.3 Distributed Current Sources and Associated Fields

Distributed Current Source Singularities,
Fields Associated with Current Source Singularities,
Method of Images,

7.4 Superposition and Uniqueness of Steady Conduction Solutions

Superposition to Satisfy Boundary Conditions,
The Conductance Matrix,
Uniqueness,

7.5 Steady Currents in Piece-wise Uniform Conductors

Analogy to Fields in Linear Dielectrics,
Inside-Outside Approximations,

7.6 Conduction Analogs

Mapping Fields That Satisfy Laplace's Equation,

7.7 Charge Relaxation in Uniform Conductors

Net Charge on Bodies Immersed in Uniform Materials,

7.8 Electroquasistatic Conduction Laws for Inhomogeneous Material

Evolution of Unpaired Charge Density,
Electroquasistatic Potential Distribution,
Uniqueness,

7.9 Charge Relaxation in Uniform and Piece-Wise Uniform Systems

Fields in Regions Having Uniform Properties,
Continuity Conditions in Piece-Wise Uniform Systems,
Nonuniform Fields in Piece-Wise Uniform Systems,

7.10 Summary

8 MAGNETOQUASISTATIC FIELDS: SUPERPOSITION INTEGRAL AND BOUNDARY VALUE POINTS OF VIEW

8.0 Introduction

Vector Field Uniquely Specified,

8.1 The Vector Potential And the Vector Poisson Equation

Two-Dimensional Current and Vector Potential Distributions,

8.2 The Biot-Savart Superposition Integral

Stick Model for Computing Fields of Electromagnet,

8.3 The Scalar Magnetic Potential

The Scalar Potential of a Current Loop,

8.4 Magnetoquasistatic Fields in the Presence of Perfect Conductors

Boundary Conditions and Evaluation of Induced Surface Current Density.
Voltage at the Terminals of a Perfectly Conducting Coil.
Inductance.

8.5 Piece-Wise Magnetic Fields

8.6 Vector Potential and the Boundary Value Point of View

Vector Potential for Two-Dimensional Fields.
Vector Potential for Axisymmetric Fields in Spherical Coordinates.
Boundary Value Solution by "Inspection".
Method of Images.
Two-Dimensional Boundary Value Problems.

8.7 Summary

9 MAGNETIZATION

9.0 Introduction

9.1 Magnetization Density

9.2 Laws and Continuity Conditions with Magnetization

Faraday's Law Including Magnetization.
Magnetic Flux Density.
Terminal Voltage with Magnetization.

9.3 Permanent Magnetization

9.4 Magnetization Constitutive Laws

9.5 Fields in the Presence of Magnetically Linear Insulating Materials

Inductance in the Presence of Linearly Magnetizable Materials.
Induced Magnetic Charge: Demagnetization.

9.6 Fields in Piece-Wise Uniform Magnetically Linear Materials

Excitation in Region of High Permeability.
Excitation in Region of Low Permeability.

9.7 Magnetic Circuits

Electrical Terminal Relations and Characteristics.

9.8 Summary

10 MAGNETOQUASISTATIC RELAXATION AND DIFFUSION

10.0 Introduction

10.1 Magnetoquasistatic Electric Fields in Systems of Perfect Conductors

10.2 Nature of Fields Induced in Finite Conductors

10.3 Diffusion of Axial Magnetic Fields Through Thin Conductors

10.4 Diffusion of Transverse Magnetic Fields Through Thin Conductors

Response to a Step in Applied Field,

10.5 Magnetic Diffusion Laws

Physical Interpretation,

10.6 Magnetic Diffusion Transient Response

Product Solutions to the One-Dimensional Diffusion Equation,

10.7 Skin Effect

10.8 Summary

11 ENERGY, POWER FLOW AND FORCES

11.0 Introduction

Power Flow in a Circuit,
Overview,

11.1 Integral and Differential Conservation Statements

11.2 Poynting's Theorem

Systems Composed of Perfect Conductors and Free Space,

11.3 Ohmic Conductors with Linear Polarization and Magnetization

An Alternative Conservation Theorem for Electroquasistatic Systems,
Poynting Power Density Related to Circuit Power Input,
Poynting Flux and Electromagnetic Radiation,

11.4 Energy Storage

Energy Densities,
Energy Storage in Terms of Terminal Variables,

11.5 Electromagnetic Dissipation

Energy Conservation for Temporarily Periodic Systems,
Induction Heating,
Dielectric Heating,

Hysteresis Losses.

11.6 Electrical Forces on Macroscopic Media

11.7 Macroscopic Magnetic Forces

Reciprocity Conditions.
Finding the Coenergy.
Evaluation of the Force.
The Torque of Electrical Origin..

11.8 Forces on Macroscopic Electric and Magnetic Dipoles

Force on an Electric Dipole.
Force on Electric Charge Derived from Energy Principle.
Force on a Magnetic Charge and Magnetic Dipole.
Comparison of Coulomb's Force to the Force on a Magnetic Dipole..

11.9 Macroscopic Force Densities

The Lorentz Force Density.
The Kelvin Polarization Force Density.
The Kelvin Magnetization Force Density.
Alternative Force Densities.

11.10 Summary

12 ELECTRODYNAMIC FIELDS; THE SUPERPOSITION INTEGRAL POINT OF VIEW

12.0 Introduction

12.1 Electrodynamic Fields and Potentials

Superposition Principle.
Continuity Conditions.

12.2 Electrodynamic Fields of Source Singularities

Potential of a Point Charge.
Electric Dipole Field..
Electric Dipole in the Sinusoidal Steady State.
The Far-Field and Uniformly Polarized Plane Waves.
Magnetic Dipole Field.

12.3 Superposition Integral for Electrodynamic Fields

Transient Response..
Sinusoidal Steady State Response.

12.4 Antennae Radiation Fields in the Sinusoidal Steady State

Distributed Current Distribution.
Arrays.

Dipoles in Broadside Array,
Dipoles in End-Fire Array,
Finite Dipoles in End-Fire Array,
Gain,

12.5 Complex Poynting's Theorem and Radiation Resistance

Complex Poynting's Theorem,
Radiation Resistance,

12.6 Periodic Sheet-Source Fields: Uniform and Nonuniform Plane Waves

Transverse Magnetic (TM) Fields,
Product Solutions to the Helmhotz Equation,
Transverse Electric (TE) Fields,

12.7 Electrodynamic Fields in the Presence of Perfect Conductors

Method of Images,
Quarter-wave Antenna Above a Ground-plane,
Two-element Array over Ground Plane,
Ground-plane With Reflector,
Boundaries at the Nodes of Standing Waves,

12.8 Summary

13 ELECTRODYNAMIC FIELDS: THE BOUNDARY VALUE POINT OF VIEW

13.0 Introduction

13.1 Introduction to TEM Waves

The MQS Limit,
The MQS Approximation,
The EQS Limit,
The EQS Approximation,

13.2 Two-Dimensional Modes Between Parallel-Plates

13.3 TE and TM Standing Waves Between Parallel Plates

13.4 Rectangular Waveguide Modes

13.5 Dielectric Waveguides: Optical Fibers

13.6 Summary

14 ONE-DIMENSIONAL WAVE DYNAMICS

14.0 Introduction

14.1 Distributed Parameter Equivalents and Models

Plane Waves,

Ideal Transmission Line,
Quasi-One-Dimensional Models.

14.2 Transverse Electromagnetic Waves

No TEM Fields in Hollow Pipes,
Power-flow and Energy Storage,

14.3 Transients on Infinite Transmission Lines

Response to Initial Conditions,

14.4 Transients on Bounded Transmission Lines

Matching,

14.5 Transmission Lines in the Sinusoidal Steady State

Transmission Line Impedance,

14.6 Reflection Coefficient Representation of Transmission Lines

Smith Chart,
Standing Wave Ratio,
Admittance in the Reflection-Coefficient Plane,

14.7 Distributed Parameter Equivalents and Models With Dissipation

14.8 Uniform and TEM Waves in Ohmic Conductors

Displacement Current Much Greater Than Displacement Current,
Conduction Current Much Greater Than Conduction Current,

14.9 Quasi-One-Dimensional Models

Charge Diffusion Transmission-Line,
Skin-Depth small Compared to All Dimensions of Interest,

14.10 Summary

15 OVERVIEW OF ELECTROMAGNETIC FIELDS

15.0 Introduction

15.1 Source and Material Configurations

Incremental Dipoles,
Planar Periodic Configurations,
Cylindrical and Spherical,
Fields Between Plane Parallel Plates,
Axisymmetric (Coaxial) Fields,
TM and TE Fields with Longitudinal Boundary Conditions,
Cylindrical Conductor Pair and Conductor Plane,

15.2 Macroscopic Media

Source Representation of Macroscopic Media,
Material Idealizations,
The Relativity of Perfection,

15.3 Characteristic Times, Physical Processes, and Approximations

Self-Consistency of Approximate Laws,
Similitude and Maxwell's Equations,
Characteristic Times and Lengths,

15.4 Energy, Power, and Force

Energy and Quasistatics,.

APPENDICES

Appendix 1. Vector Operations

Vectors,
Vector Addition,
Definition of Scalar Product,
Definition of Vector Product,
The Scalar Triple Product,
The Double Cross-Product,

Appendix 2. Line and Surface Integrals and Proof that Curl is a Vector

Line Integrals,.
Surface Integrals,
Proof that the Curl Operation Results in a Vector,

0.1 PREFACE

The text is aimed at an audience that has seen Maxwell's equations in integral or differential form (second-term Freshman Physics) and had some exposure to integral theorems and differential operators (second term Freshman Calculus). The first two chapters and supporting problems and appendices are a review of this material.

In Chap. 3, a simple and physically appealing argument is presented to show that Maxwell's equations predict the time evolution of a field, produced by free charges, given the initial charge densities and velocities, and electric and magnetic fields. This is a form of the uniqueness theorem that is established more rigorously later. As part of this development, it is shown that a field is completely specified by its divergence and its curl throughout all of space, a proof that explains the general form of Maxwell's equations.

With this background, Maxwell's equations are simplified into their electroquasistatic (EQS) and magnetoquasistatic (MQS) forms. The stage is set for taking a structured approach that gives a physical overview while developing the mathematical skills needed for the solution of engineering problems.

The text builds on and reinforces an understanding of analog circuits. The fields are never static. Their dynamics are often illustrated with step and sinusoidal steady state responses in systems where the spatial dependence has been encapsulated in time-dependent coefficients (of solutions to partial differential equations) satisfying ordinary differential equations. However, the connection with analog circuits goes well beyond the same approach to solving differential equations as used in circuit theory. The approximations inherent in the development of circuit theory from Maxwell's equations are brought out very explicitly, so that the student appreciates under what conditions the assumptions implicit in circuit theory cease to be applicable.

To appreciate the organization of material in this text, it may be helpful to make a more subtle connection with electrical analog circuits. We think of circuit theory as being analogous to field theory. In this analogy, our development begins with capacitors– charges and their associated fields, equipotentials used to represent perfect conductors. It continues with resistors– steady conduction to represent losses. Then these elements are combined to represent charge relaxation, i.e. "RC" systems dynamics (Chaps. 4-7). Because EQS fields are not necessarily static, the student can appreciate R-C type dynamics, where the distribution of free charge is determined by the continuum analog of R-C systems.

Using the same approach, we then take up the continuum generalization of L-R systems (Chaps. 8–10). As before, we first are given the source (the current density) and find the magnetic field. Then we consider perfectly conducting systems and once again take the boundary value point of view. With the addition of finite conductivity to this continuum analog of systems of inductors, we arrive at the dynamics of systems that are L-R-like in the circuit analogy.

Based on an appreciation of the connection between sources and fields afforded by these quasistatic developments, it is natural to use the study of electric and magnetic energy storage and dissipation as an entree into electrodynamics (Chap. 11).

Central to electrodynamics are electromagnetic waves in loss-free media (Chaps. 12–14). In this limit, the circuit analog is a system of distributed differential induc-

tors and capacitors, an L-C system. Following the same pattern used for EQS and MQS systems, fields are first found for given sources– antennae and arrays. The boundary value point of view then brings in microwave and optical waveguides and transmission lines.

We conclude with the electrodynamics of lossy material, the generalization of L-R-C systems (Chaps. 14–15). Drawing on what has been learned for EQS, MQS, and electrodynamic systems, for example, on the physical significance of the dominant characteristic times, we form a perspective as to how electromagnetic fields are exploited in practical systems. In the circuit analogy, these characteristic times are RC, L/R, and $1/\sqrt{LC}$. One benefit of the field theory point of view is that it shows the influence of physical scale and configuration on the dynamics represented by these times. The circuit analogy gives a hint as to why it is so often possible to view the world as either EQS or MQS. The time $1/\sqrt{LC}$ is the geometric mean of RC and L/R. Either RC or L/R is smaller than $1/\sqrt{LC}$, but not both. For large R, RC dynamics comes first as the frequency is raised (EQS), followed by electrodynamics. For small R, L/R dynamics comes first (MQS), again followed by electrodynamics. Implicit is the enormous difference between what is meant by a "perfect conductor" in systems appropriately modeled as EQS and MQS.

This organization of the material is intended to bring the student to the realization that electric, magnetic, and electromagnetic devices and systems can be broken into parts, often described by one or another limiting form of Maxwell's equations. Recognition of these limits is part of the art and science of modeling, of making the simplifications necessary to make the device or system amenable to analytic treatment or computer analysis and of effectively using appropriate simplifications of the laws to guide in the process of invention.

With the EQS approximation comes the opportunity to treat such devices as transistors, electrostatic precipitators, and electrostatic sensors and actuators, while relays, motors, and magnetic recording media are examples of MQS systems. Transmission lines, antenna arrays, and dielectric waveguides (i.e., optical fibers) are examples where the full, dynamic Maxwell's equations must be used.

In connection with examples, about 40 demonstrations are described in this text. These are designed to make the mathematical results take on physical meaning. Based upon relatively simple configurations and arrangements of equipment, they incorporate no more complexity then required to make a direct connection between what has been derived and what is observed. Their purpose is to help the student observe physically what has been described symbolically. Often coming with a plot of the theoretical predictions that can be compared to data taken in the classroom, they give the opportunity to test the range of validity of the theory and to promulgate a quantitative approach to dealing with the physical world. More detailed consideration of the demonstrations can be the basis for special projects, often bringing in computer modeling. For the student having only the text as a resource, the descriptions of the experiments stand on their own as a connection between the abstractions and the physical reality. For those fortunate enough to have some of the demonstrations used in the classroom, they serve as documentation of what was done. All too often, students fail to profit from demonstrations because conventional note taking fails to do justice to the presentation.

The demonstrations included in the text are of physical phenomena more than of practical applications. To fill out the classroom experience, to provide the

engineering motivation, applications should also be exemplified. In the subject as we teach it, and as a practical matter, these are more of the nature of "show and tell" than of working demonstrations, often reflecting the current experience and interests of the instructor and usually involving more complexity than appropriate for more than a qualitative treatment.

The text provides a natural frame of reference for developing numerical approaches to the details of geometry and nonlinearity, beginning with the method of moments as the superposition integral approach to boundary value problems and culminating in energy methods as a basis for the finite element approach. Professor J. L. Kirtley and Dr. S. D. Umans are currently spearheading our efforts to expose the student to the "muscle" provided by the computer for making practical use of field theory while helping the student gain physical insight. Work stations, finite element packages, and the like make it possible to take detailed account of geometric effects in routine engineering design. However, no matter how advanced the computer packages available to the student may become in the future, it will remain essential that a student comprehend the physical phenomena at work with the aid of special cases. This is the reason for the emphasis of the text on simple geometries to provide physical insight into the processes at work when fields interact with media.

The mathematics of Maxwell's equations leads the student to a good understanding of the gradient, divergence, and curl operators. This mathematical conversance will help the student enter other areas– such as fluid and solid mechanics, heat and mass transfer, and quantum mechanics– that also use the language of classical fields. So that the material serves this larger purpose, there is an emphasis on source-field relations, on scalar and vector potentials to represent the irrotational and solenoidal parts of fields, and on that understanding of boundary conditions that accounts for finite system size and finite time rates of change.

Maxwell's equations form an intellectual edifice that is unsurpassed by any other discipline of physics. Very few equations encompass such a gamut of physical phenomena. Conceived before the introduction of relativity Maxwell's equations not only survived the formulation of relativity, but were instrumental in shaping it. Because they are linear in the fields, the replacement of the field vectors by operators is all that is required to make them quantum theoretically correct; thus, they also survived the introduction of quantum theory.

The introduction of magnetizable materials deviates from the usual treatment in that we use paired magnetic charges, magnetic dipoles, as the source of magnetization. The often-used alternative is circulating Ampèrian currents. The magnetic charge approach is based on the Chu formulation of electrodynamics. Chu exploited the symmetry of the equations obtained in this way to facilitate the study of magnetism by analogy with polarization. As the years went by, it was unavoidable that this approach would be criticized, because the dipole moment of the electron, the main source of ferromagnetism, is associated with the spin of the electron, i.e., seems to be more appropriately pictured by circulating currents.

Tellegen in particular, of Tellegen-theorem fame, took issue with this approach. Whereas he conceded that a choice between two approaches that give identical answers is a matter of taste, he gave a derivation of the force on a current loop (the Ampèrian model of a magnetic dipole) and showed that it gave a different answer from that on a magnetic dipole. The difference was small, the correction term was relativistic in nature; thus, it would have been difficult to detect the

effect in macroscopic measurements. It occurred only in the presence of a time-varying electric field. Yet this criticism, if valid, would have made the treatment of magnetization in terms of magnetic dipoles highly suspect.

The resolution of this issue followed a careful investigation of the force exerted on a current loop on one hand, and a magnetic dipole on the other. It turned out that Tellegen's analysis, in postulating a constant circulating current around the loop, was in error. A time-varying electric field causes changes in the circulating current that, when taken into account, causes an additional force that cancels the critical term. Both models of a magnetic dipole yield the same force expression. The difficulty in the analysis arose because the current loop contains "moving parts," i.e., a circulating current, and therefore requires the use of relativistic corrections in the rest-frame of the loop. Hence, the current loop model is inherently much harder to analyze than the magnetic charge–dipole model.

The resolution of the force paradox also helped clear up the question of the symmetry of the energy momentum tensor. At about the same time as this work was in progress, Shockley and James at Stanford independently raised related questions that led to a lively exchange between them and Coleman and Van Vleck at Harvard. Shockley used the term "hidden momentum" for contributions to the momentum of the electromagnetic field in the presence of magnetizable materials. Coleman and Van Vleck showed that a proper formulation based on the Dirac equation (i.e., a relativistic description) automatically includes such terms. With all this theoretical work behind us, we are comfortable with the use of the magnetic charge–dipole model for the source of magnetization. The student is not introduced to the intricacies of the issue, although brief mention is made of them in the text.

As part of curriculum development over a period about equal in time to the age of a typical student studying this material (the authors began their collaboration in 1968) this text fits into an evolution of field theory with its origins in the "Radiation Lab" days during and following World War II. Quasistatics, promulgated in texts by Professors Richard B. Adler, L.J. Chu, and Robert M. Fano, is a major theme in this text as well. However, the notion has been broadened and made more rigorous and useful by recognizing that electromagnetic phenomena that are "quasistatic," in the sense that electromagnetic wave phenomena can be ignored, can nevertheless be rate dependent. As used in this text, a quasistatic regime includes dynamical phenomena with characteristic times longer than those associated with electromagnetic waves. (A model in which no time-rate processes are included is termed "quasistationary" for distinction.)

In recognition of the lineage of our text, it is dedicated to Professors R. B. Adler, L. J. Chu and R. M. Fano. Professor Adler, as well as Professors J. Moses, G. L. Wilson, and L. D. Smullin, who headed the department during the period of development, have been a source of intellectual, moral, and financial support. Our inspiration has also come from colleagues in teaching– faculty and teaching assistants, and those students who provided insight concerning the many evolutions of the "notes." The teaching of Professor Alan J. Grodzinsky, whose latterday lectures have been a mainstay for the course, is reflected in the text itself. A partial list of others who contributed to the curriculum development includes Professors J. A. Kong, J. H. Lang, T. P. Orlando, R. E. Parker, D. H. Staelin, and M. Zahn (who helped with a final reading of the text). With "macros" written by Ms. Amy Hendrickson, the text was "Tex't" by Ms. Cindy Kopf, who managed to make the final publication process a pleasure for the authors.

1

MAXWELL'S INTEGRAL LAWS IN FREE SPACE

1.0 INTRODUCTION

Practical, intellectual, and cultural reasons motivate the study of electricity and magnetism. The operation of electrical systems designed to perform certain engineering tasks depends, at least in part, on electrical, electromechanical, or electrochemical phenomena. The electrical aspects of these applications are described by Maxwell's equations. As a description of the temporal evolution of electromagnetic fields in three-dimensional space, these same equations form a concise summary of a wider range of phenomena than can be found in any other discipline. Maxwell's equations are an intellectual achievement that should be familiar to every student of physical phenomena. As part of the theory of fields that includes continuum mechanics, quantum mechanics, heat and mass transfer, and many other disciplines, our subject develops the mathematical language and methods that are the basis for these other areas.

For those who have an interest in electromechanical energy conversion, transmission systems at power or radio frequencies, waveguides at microwave or optical frequencies, antennas, or plasmas, there is little need to argue the necessity for becoming expert in dealing with electromagnetic fields. There are others who may require encouragement. For example, circuit designers may be satisfied with circuit theory, the laws of which are stated in terms of voltages and currents and in terms of the relations imposed upon the voltages and currents by the circuit elements. However, these laws break down at high frequencies, and this cannot be understood without electromagnetic field theory. The limitations of circuit models come into play as the frequency is raised so high that the propagation time of electromagnetic fields becomes comparable to a period, with the result that "inductors" behave as "capacitors" and vice versa. Other limitations are associated with loss phenomena. As the frequency is raised, resistors and transistors are limited by "capacitive" effects, and transducers and transformers by "eddy" currents.

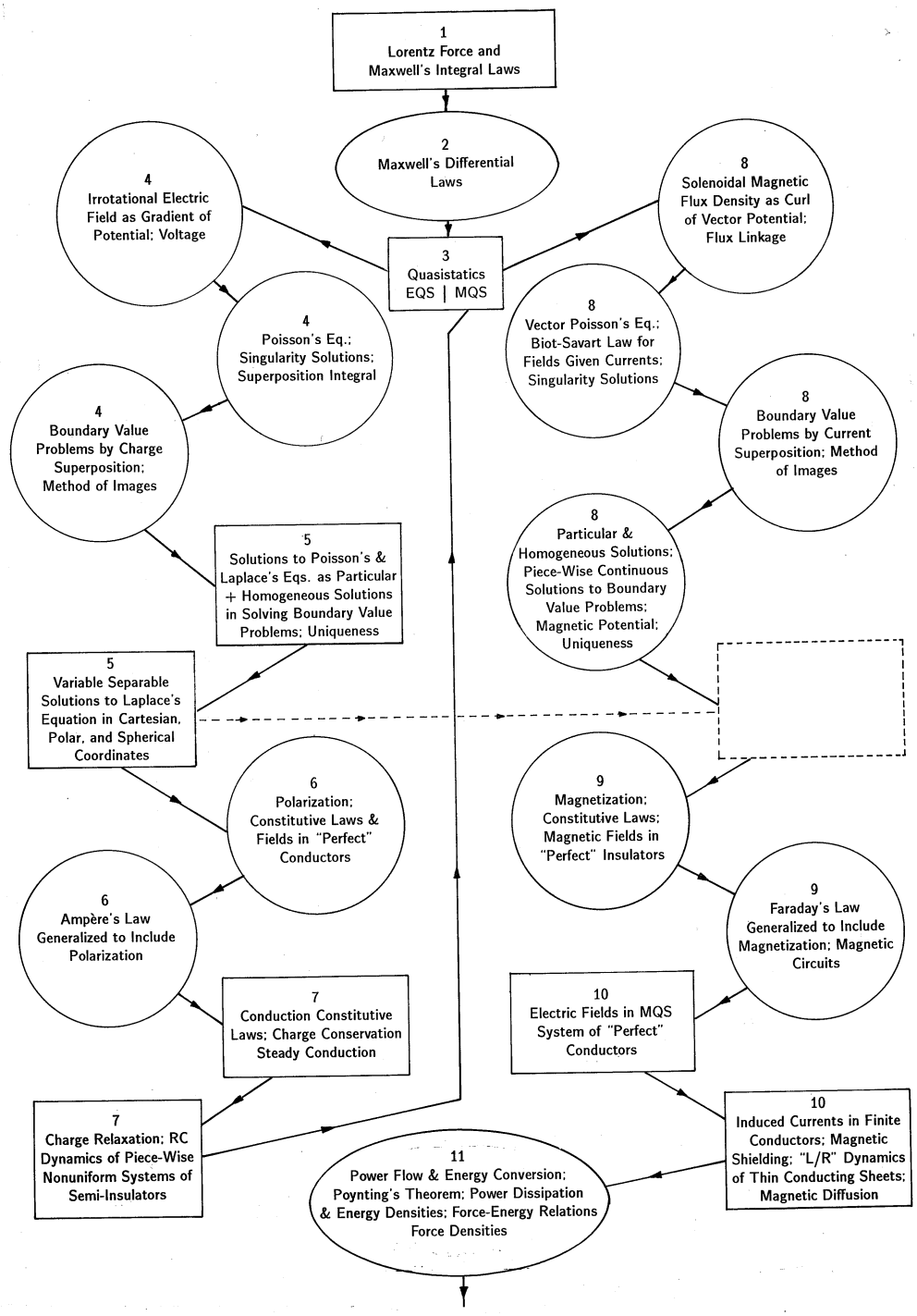
Anyone concerned with developing circuit models for physical systems requires a field theory background to justify approximations and to derive the values of the circuit parameters. Thus, the bioengineer concerned with electrocardiography or neurophysiology must resort to field theory in establishing a meaningful connection between the physical reality and models, when these are stated in terms of circuit elements. Similarly, even if a control theorist makes use of a lumped parameter model, its justification hinges on a continuum theory, whether electromagnetic, mechanical, or thermal in nature.

Computer hardware may seem to be another application not dependent on electromagnetic field theory. The software interface through which the computer is often seen makes it seem unrelated to our subject. Although the hardware is generally represented in terms of circuits, the practical realization of a computer designed to carry out logic operations is limited by electromagnetic laws. For example, the signal originating at one point in a computer cannot reach another point within a time less than that required for a signal, propagating at the speed of light, to traverse the interconnecting wires. That circuit models have remained useful as computation speeds have increased is a tribute to the solid state technology that has made it possible to decrease the size of the fundamental circuit elements. Sooner or later, the fundamental limitations imposed by the electromagnetic fields define the computation speed frontier of computer technology, whether it be caused by electromagnetic wave delays or electrical power dissipation.

Overview of Subject. As illustrated diagrammatically in Fig. 1.0.1, we start with Maxwell's equations written in integral form. This chapter begins with a definition of the fields in terms of forces and sources followed by a review of each of the integral laws. Interwoven with the development are examples intended to develop the methods for surface and volume integrals used in stating the laws. The examples are also intended to attach at least one physical situation to each of the laws. Our objective in the chapters that follow is to make these laws useful, not only in modeling engineering systems but in dealing with practical systems in a qualitative fashion (as an inventor often does). The integral laws are directly useful for (a) dealing with fields in this qualitative way, (b) finding fields in simple configurations having a great deal of symmetry, and (c) relating fields to their sources.

Chapter 2 develops a differential description from the integral laws. By following the examples and some of the homework associated with each of the sections, a minimum background in the mathematical theorems and operators is developed. The differential operators and associated integral theorems are brought in as needed. Thus, the divergence and curl operators, along with the theorems of Gauss and Stokes, are developed in Chap. 2, while the gradient operator and integral theorem are naturally derived in Chap. 4.

Static fields are often the first topic in developing an understanding of phenomena predicted by Maxwell's equations. Fields are not measurable, let alone of practical interest, unless they are dynamic. As developed here, fields are never truly static. The subject of quasistatics, begun in Chap. 3, is central to the approach we will use to understand the implications of Maxwell's equations. A mature understanding of these equations is achieved when one has learned how to neglect complications that are inconsequential. The electroquasistatic (EQS) and magne-


1
Lorentz Force and Maxwell's Integral Laws
2
Maxwell's Differential Laws
3
Quasistatics EQS | MQS
4
Irrotational Electric Field as Gradient of Potential; Voltage
4
Poisson's Eq.: Singularity Solutions; Superposition Integral
4
Boundary Value Problems by Charge Superposition; Method of Images
5
Solutions to Poisson's & Laplace's Eqs. as Particular + Homogeneous Solutions in Solving Boundary Value Problems; Uniqueness
5
Variable Separable Solutions to Laplace's Equation in Cartesian, Polar, and Spherical Coordinates
6
Polarization; Constitutive Laws & Fields in "Perfect" Conductors
6
Ampère's Law Generalized to Include Polarization
7
Conduction Constitutive Laws; Charge Conservation Steady Conduction
7
Charge Relaxation; RC Dynamics of Piece-Wise Nonuniform Systems of Semi-Insulators
8
Solenoidal Magnetic Flux Density as Curl of Vector Potential; Flux Linkage
8
Vector Poisson's Eq.: Biot-Savart Law for Fields Given Currents; Singularity Solutions
8
Boundary Value Problems by Current Superposition; Method of Images
8
Particular & Homogeneous Solutions; Piece-Wise Continuous Solutions to Boundary Value Problems; Magnetic Potential; Uniqueness
9
Magnetization; Constitutive Laws; Magnetic Fields in "Perfect" Insulators
9
Faraday's Law Generalized to Include Magnetization; Magnetic Circuits
10
Electric Fields in MQS System of "Perfect" Conductors
10
Induced Currents in Finite Conductors; Magnetic Shielding; "L/R" Dynamics of Thin Conducting Sheets; Magnetic Diffusion
11
Power Flow & Energy Conversion; Poynting's Theorem; Power Dissipation & Energy Densities; Force-Energy Relations Force Densities

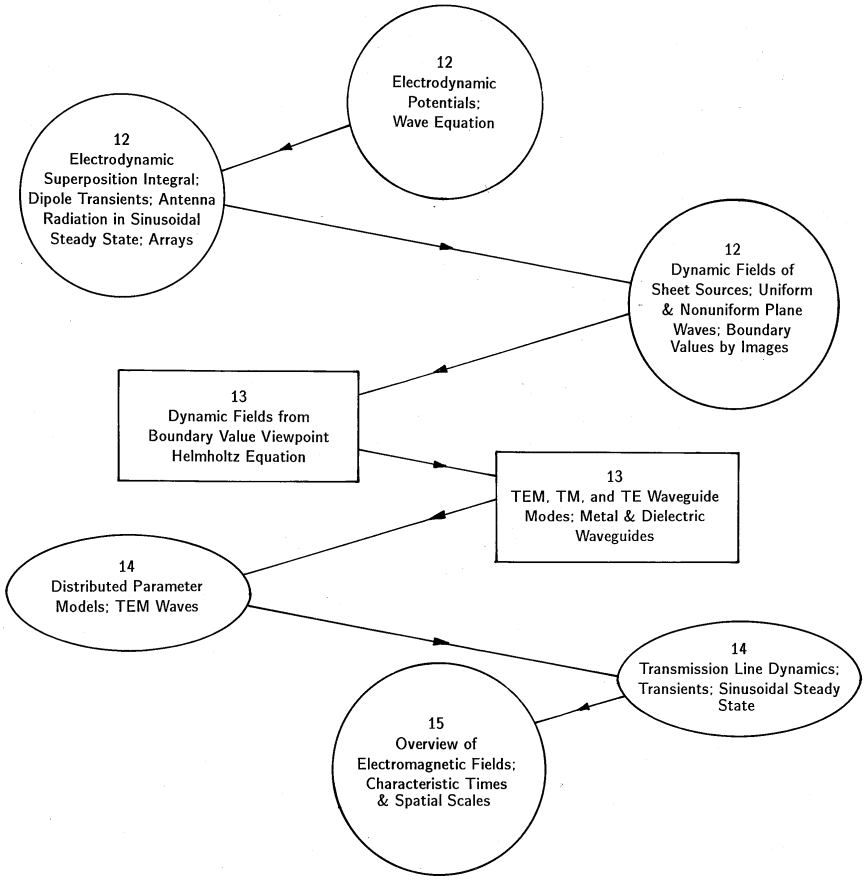


Fig. 1.0.1 Outline of Subject. The three columns, respectively for electroquasistatics, magnetoquasistatics and electrodynamics, show parallels in development.

toquasistatic (MQS) approximations are justified if time rates of change are slow enough (frequencies are low enough) so that time delays due to the propagation of electromagnetic waves are unimportant. The examples considered in Chap. 3 give some notion as to which of the two approximations is appropriate in a given situation. A full appreciation for the quasistatic approximations will come into view as the EQS and MQS developments are drawn together in Chaps. 11 through 15.

Although capacitors and inductors are examples in the electroquasistatic and magnetoquasistatic categories, respectively, it is not true that quasistatic systems can be generally modeled by frequency-independent circuit elements. High-frequency models for transistors are correctly based on the EQS approximation. Electromagnetic wave delays in the transistors are not consequential. Nevertheless, dynamic effects are important and the EQS approximation can contain the finite time for charge migration. Models for eddy current shields or heaters are correctly based on the MQS approximation. Again, the delay time of an electromagnetic wave is unimportant while the all-important diffusion time of the magnetic field

is represented by the MQS laws. Space charge waves on an electron beam or spin waves in a saturated magnetizable material are often described by EQS and MQS laws, respectively, even though frequencies of interest are in the GHz range.

The parallel developments of EQS (Chaps. 4–7) and MQS systems (Chaps. 8–10) is emphasized by the first page of Fig. 1.0.1. For each topic in the EQS column to the left there is an analogous one at the same level in the MQS column. Although the field concepts and mathematical techniques used in dealing with EQS and MQS systems are often similar, a comparative study reveals as many contrasts as direct analogies. There is a two-way interplay between the electric and magnetic studies. Not only are results from the EQS developments applied in the description of MQS systems, but the examination of MQS situations leads to a greater appreciation for the EQS laws.

At the tops of the EQS and the MQS columns, the first page of Fig. 1.0.1, general (contrasting) attributes of the electric and magnetic fields are identified. The developments then lead from situations where the field sources are prescribed to where they are to be determined. Thus, EQS electric fields are first found from prescribed distributions of charge, while MQS magnetic fields are determined given the currents. The development of the EQS field solution is a direct investment in the subsequent MQS derivation. It is then recognized that in many practical situations, these sources are induced in materials and must therefore be found as part of the field solution. In the first of these situations, induced sources are on the boundaries of conductors having a sufficiently high electrical conductivity to be modeled as "perfectly" conducting. For the EQS systems, these sources are surface charges, while for the MQS, they are surface currents. In either case, fields must satisfy boundary conditions, and the EQS study provides not only mathematical techniques but even partial differential equations directly applicable to MQS problems.

Polarization and magnetization account for field sources that can be prescribed (electrets and permanent magnets) or induced by the fields themselves. In the Chu formulation used here, there is a complete analogy between the way in which polarization and magnetization are represented. Thus, there is a direct transfer of ideas from Chap. 6 to Chap. 9.

The parallel quasistatic studies culminate in Chaps. 7 and 10 in an examination of loss phenomena. Here we learn that very different answers must be given to the question "When is a conductor perfect?" for EQS on one hand, and MQS on the other.

In Chap. 11, many of the concepts developed previously are put to work through the consideration of the flow of power, storage of energy, and production of electromagnetic forces. From this chapter on, Maxwell's equations are used without approximation. Thus, the EQS and MQS approximations are seen to represent systems in which either the electric or the magnetic energy storage dominates respectively.

In Chaps. 12 through 14, the focus is on electromagnetic waves. The development is a natural extension of the approach taken in the EQS and MQS columns. This is emphasized by the outline represented on the right page of Fig. 1.0.1. The topics of Chaps. 12 and 13 parallel those of the EQS and MQS columns on the previous page. Potentials used to represent electrodynamic fields are a natural generalization of those used for the EQS and MQS systems. As for the quasistatic fields, the fields of given sources are considered first. An immediate practical application is therefore the description of radiation fields of antennas.

The boundary value point of view, introduced for EQS systems in Chap. 5 and for MQS systems in Chap. 8, is the basic theme of Chap. 13. Practical examples include simple transmission lines and waveguides. An understanding of transmission line dynamics, the subject of Chap. 14, is necessary in dealing with the "conventional" ideal lines that model most high-frequency systems. They are also shown to provide useful models for representing quasistatic dynamical processes.

To make practical use of Maxwell's equations, it is necessary to master the art of making approximations. Based on the electromagnetic properties and dimensions of a system and on the time scales (frequencies) of importance, how can a physical system be broken into electromagnetic subsystems, each described by its dominant physical processes? It is with this goal in mind that the EQS and MQS approximations are introduced in Chap. 3, and to this end that Chap. 15 gives an overview of electromagnetic fields.

1.1 THE LORENTZ LAW IN FREE SPACE

There are two points of view for formulating a theory of electrodynamics. The older one views the forces of attraction or repulsion between two charges or currents as the result of action at a distance. Coulomb's law of electrostatics and the corresponding law of magnetostatics were first stated in this fashion. Faraday[1] introduced a new approach in which he envisioned the space between interacting charges to be filled with fields, by which the space is activated in a certain sense; forces between two interacting charges are then transferred, in Faraday's view, from volume element to volume element in the space between the interacting bodies until finally they are transferred from one charge to the other. The advantage of Faraday's approach was that it brought to bear on the electromagnetic problem the then well-developed theory of continuum mechanics. The culmination of this point of view was Maxwell's formulation[2] of the equations named after him.

From Faraday's point of view, electric and magnetic fields are defined at a point $\mathbf{r}$ even when there is no charge present there. The fields are defined in terms of the force that would be exerted on a test charge q if it were introduced at $\mathbf{r}$ moving at a velocity $\mathbf{v}$ at the time of interest. It is found experimentally that such a force would be composed of two parts, one that is independent of $\mathbf{v}$, and the other proportional to $\mathbf{v}$ and orthogonal to it. The force is summarized in terms of the *electric field intensity* $\mathbf{E}$ and *magnetic flux density* $\mu_o\mathbf{H}$ by the *Lorentz force law.* (For a review of vector operations, see Appendix 1.)

$$\boxed{\mathbf{f} = q(\mathbf{E} + \mathbf{v} \times \mu_o\mathbf{H})} \tag{1}$$

The superposition of electric and magnetic force contributions to (1) is illustrated in Fig. 1.1.1. Included in the figure is a reminder of the right-hand rule used to determine the direction of the cross-product of $\mathbf{v}$ and $\mu_o\mathbf{H}$. In general, $\mathbf{E}$ and $\mathbf{H}$ are not uniform, but rather are functions of position $\mathbf{r}$ and time t: $\mathbf{E} = \mathbf{E}(\mathbf{r}, t)$ and $\mu_o\mathbf{H} = \mu_o\mathbf{H}(\mathbf{r}, t)$.

In addition to the units of length, mass, and time associated with mechanics, a unit of charge is required by the theory of electrodynamics. This unit is the

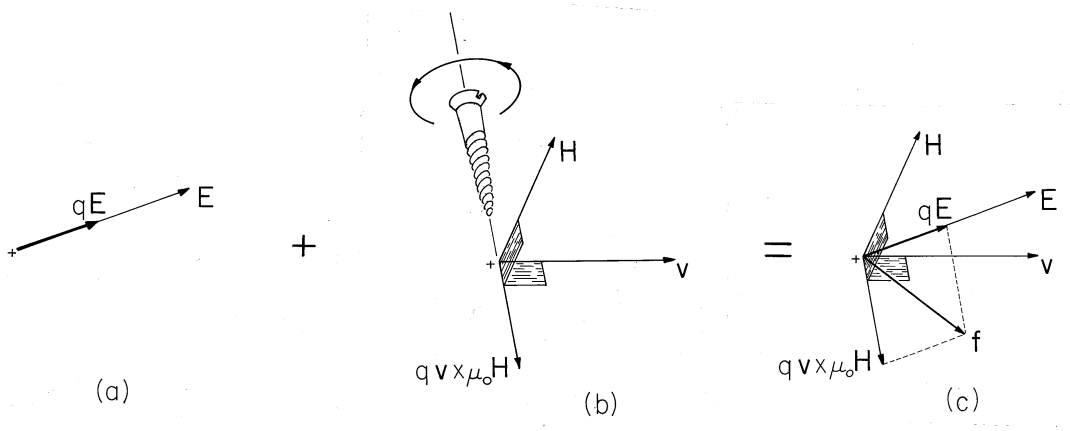


Fig. 1.1.1 Lorentz force **f** in geometric relation to the electric and magnetic field intensities, **E** and **H**, and the charge velocity **v**: (a) electric force, (b) magnetic force, and (c) total force.

coulomb. The Lorentz force law, (1), then serves to define the units of **E** and of $\mu_o\mathbf{H}$.

$$\text{units of } \mathbf{E} = \frac{\text{newton}}{\text{coulomb}} = \frac{\text{kilogram meter}/(\text{second})^2}{\text{coulomb}} \tag{2}$$

$$\text{units of } \mu_o\mathbf{H} = \frac{\text{newton}}{\text{coulomb meter/second}} = \frac{\text{kilogram}}{\text{coulomb second}} \tag{3}$$

We can only establish the units of the magnetic flux density $\mu_o\mathbf{H}$ from the force law and cannot argue until Sec. 1.4 that the derived units of **H** are ampere/meter and hence of μ_o are henry/meter.

In much of electrodynamics, the predominant concern is not with mechanics but with electric and magnetic fields in their own right. Therefore, it is inconvenient to use the unit of mass when checking the units of quantities. It proves useful to introduce a new name for the unit of electric field intensity– the unit of volt/meter.

In the summary of variables given in Table 1.8.2 at the end of the chapter, the fundamental units are SI, while the derived units exploit the fact that the unit of mass, kilogram = volt-coulomb-second^2/meter^2 and also that a coulomb/second = ampere. Dimensional checking of equations is guaranteed if the basic units are used, but may often be accomplished using the derived units. The latter communicate the physical nature of the variable and the natural symmetry of the electric and magnetic variables.

Example 1.1.1. Electron Motion in Vacuum in a Uniform Static Electric Field

In vacuum, the motion of a charged particle is limited only by its own inertia. In the uniform electric field illustrated in Fig. 1.1.2, there is no magnetic field, and an electron starts out from the plane $x = 0$ with an initial velocity v_i.
The "imposed" electric field is $\mathbf{E} = \mathbf{i_x}E_x$, where $\mathbf{i_x}$ is the unit vector in the x direction and E_x is a given constant. The trajectory is to be determined here and used to exemplify the charge and current density in Example 1.2.1.

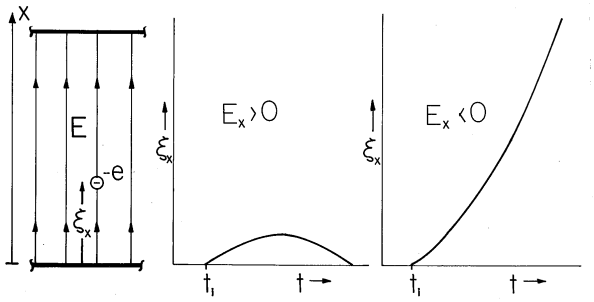


Fig. 1.1.2 An electron, subject to the uniform electric field intensity $\mathbf{E}_x$, has the position ξ_x, shown as a function of time for positive and negative fields.

With m defined as the electron mass, Newton's law combines with the Lorentz law to describe the motion.

$$m\frac{d^2\xi_x}{dt^2} = f = -eE_x \tag{4}$$

The electron position ξ_x is shown in Fig. 1.1.2. The charge of the electron is customarily denoted by e ($e = 1.6 \times 10^{-19}$ coulomb) where e is positive, thus necessitating an explicit minus sign in (4).

By integrating twice, we get

$$\xi_x = -\frac{1}{2}\frac{e}{m}E_x t^2 + c_1 t + c_2 \tag{5}$$

where c_1 and c_2 are integration constants. If we assume that the electron is at $\xi_x = 0$ and has velocity v_i when $t = t_i$, it follows that these constants are

$$c_1 = v_i + \frac{e}{m}E_x t_i; \qquad c_2 = -v_i t_i - \frac{1}{2}\frac{e}{m}E_x t_i^2 \tag{6}$$

Thus, the electron position and velocity are given as a function of time by

$$\xi_x = -\frac{1}{2}\frac{e}{m}E_x(t - t_i)^2 + v_i(t - t_i) \tag{7}$$

$$\frac{d\xi_x}{dt} = -\frac{e}{m}E_x(t - t_i) + v_i \tag{8}$$

With x defined as upward and $E_x > 0$, the motion of an electron in an electric field is analogous to the free fall of a mass in a gravitational field, as illustrated by Fig. 1.1.2. With $E_x < 0$, and the initial velocity also positive, the velocity is a monotonically increasing function of time, as also illustrated by Fig. 1.1.2.

Example 1.1.2. Electron Motion in Vacuum in a Uniform Static Magnetic Field

The magnetic contribution to the Lorentz force is perpendicular to both the particle velocity and the imposed field. We illustrate this fact by considering the trajectory

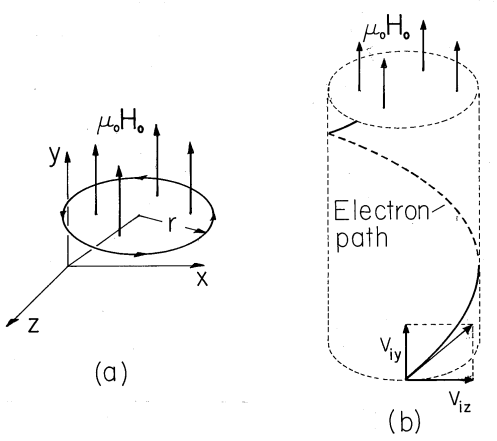


Fig. 1.1.3 (a) In a uniform magnetic flux density $\mu_o \mathbf{H}_o$ and with no initial velocity in the y direction, an electron has a circular orbit. (b) With an initial velocity in the y direction, the orbit is helical.

resulting from an initial velocity v_{iz} along the z axis. With a uniform constant magnetic flux density $\mu_o \mathbf{H}$ existing along the y axis, the force is

$$\mathbf{f} = -e(\mathbf{v} \times \mu_o \mathbf{H}) \tag{9}$$

The cross-product of two vectors is perpendicular to the two vector factors, so the acceleration of the electron, caused by the magnetic field, is always perpendicular to its velocity. Therefore, a magnetic field alone cannot change the magnitude of the electron velocity (and hence the kinetic energy of the electron) but can change only the direction of the velocity. Because the magnetic field is uniform, because the velocity and the rate of change of the velocity lie in a plane perpendicular to the magnetic field, and, finally, because the magnitude of $\mathbf{v}$ does not change, we find that the acceleration has a constant magnitude and is orthogonal to both the velocity and the magnetic field. The electron moves in a circle so that the centrifugal force counterbalances the magnetic force. Figure 1.1.3a illustrates the motion. The radius of the circle is determined by equating the centrifugal force and radial Lorentz force

$$e\mu_o |v| H_o = \frac{mv^2}{r} \tag{10}$$

which leads to

$$r = \frac{m}{e} \frac{|v|}{\mu_o H_o} \tag{11}$$

The foregoing problem can be modified to account for any arbitrary initial angle between the velocity and the magnetic field. The vector equation of motion (really three equations in the three unknowns ξ_x, ξ_y, ξ_z)

$$m \frac{d^2 \bar{\xi}}{dt^2} = -e\Big(\frac{d\bar{\xi}}{dt} \times \mu_o \mathbf{H}\Big) \tag{12}$$

is linear in $\bar{\xi}$, and so solutions can be superimposed to satisfy initial conditions that include not only a velocity v_{iz} but one in the y direction as well, v_{iy}. Motion in the same direction as the magnetic field does not give rise to an additional force. Thus,

the y component of (12) is zero on the right. An integration then shows that the y directed velocity remains constant at its initial value, v_{iy}. This uniform motion can be added to that already obtained to see that the electron follows a helical path, as shown in Fig. 1.1.3b.

It is interesting to note that the angular frequency of rotation of the electron around the field is independent of the speed of the electron and depends only upon the magnetic flux density, $\mu_o H_o$. Indeed, from (11) we find

$$\frac{v}{r} \equiv \omega_c = \frac{e}{m}\mu_o H_o \tag{13}$$

For a flux density of 1 volt-second/meter (or 1 tesla), the *cyclotron frequency* is $f_c = \omega_c/2\pi = 28\,\text{GHz}$. (For an electron, $e = 1.602\times10^{-19}$ coulomb and $m = 9.106\times10^{-31}$ kg.) With an initial velocity in the z direction of 3×10^7 m/s, the radius of gyration in the flux density $\mu_o H = 1$ tesla is $r = v_{iz}/\omega_c = 1.7\times10^{-4}$ m.

1.2 CHARGE AND CURRENT DENSITIES

In Maxwell's day, it was not known that charges are not infinitely divisible but occur in elementary units of 1.6×10^{-19} coulomb, the charge of an electron. Hence, Maxwell's macroscopic theory deals with continuous charge distributions. This is an adequate description for fields of engineering interest that are produced by aggregates of large numbers of elementary charges. These aggregates produce charge distributions that are described conveniently in terms of a charge per unit volume, a charge density ρ.

Pick an incremental volume and determine the net charge within. Then

$$\rho(\mathbf{r},t) \equiv \frac{\text{net charge in } \Delta\text{V}}{\Delta V} \tag{1}$$

is the *charge density* at the position $\mathbf{r}$ when the time is t. The units of ρ are coulomb/meter^3. The volume ΔV is chosen small as compared to the dimensions of the system of interest, but large enough so as to contain many elementary charges. The charge density ρ is treated as a continuous function of position. The "graininess" of the charge distribution is ignored in such a "macroscopic" treatment.

Fundamentally, current is charge transport and connotes the time rate of change of charge. Current density is a directed current per unit area and hence measured in (coulomb/second)/meter^2. A charge density ρ moving at a velocity $\mathbf{v}$ implies a rate of charge transport per unit area, a *current density* $\mathbf{J}$, given by

$$\mathbf{J} = \rho\mathbf{v} \tag{2}$$

One way to envision this relation is shown in Fig. 1.2.1, where a charge density ρ having velocity $\mathbf{v}$ traverses a differential area δa. The area element has a unit normal $\mathbf{n}$, so that a differential area vector can be defined as $\delta\mathbf{a} = \mathbf{n}\delta a$. The charge that passes during a differential time δt is equal to the total charge contained in the volume $\mathbf{v}\cdot\delta a dt$. Therefore,

$$d(\delta q) = \rho\mathbf{v}\cdot\delta\mathbf{a}dt \tag{3}$$

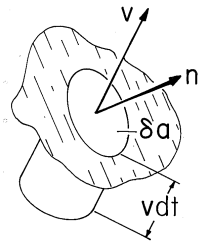


Fig. 1.2.1 Current density **J** passing through surface having a normal **n**.

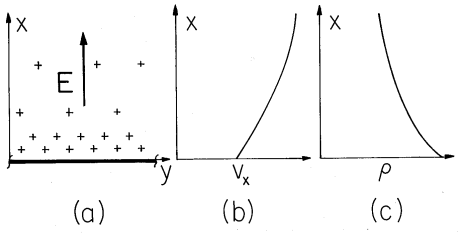


Fig. 1.2.2 Charge injected at the lower boundary is accelerated upward by an electric field. Vertical distributions of (a) field intensity, (b) velocity and (c) charge density.

Divided by dt, we expect (3) to take the form $\mathbf{J} \cdot \delta\mathbf{a}$, so it follows that the current density is related to the charge density by (2).

The velocity $\mathbf{v}$ is the velocity of the charge. Just how the charge is set into motion depends on the physical situation. The charge might be suspended in or on an insulating material which is itself in motion. In that case, the velocity would also be that of the material. More likely, it is the result of applying an electric field to a conductor, as considered in Chap. 7. For charged particles moving in vacuum, it might result from motions represented by the laws of Newton and Lorentz, as illustrated in the examples in Sec.1.1. This is the case in the following example.

Example 1.2.1. Charge and Current Densities in a Vacuum Diode

Consider the charge and current densities for electrons being emitted with initial velocity $\mathbf{v}$ from a "cathode" in the plane $x = 0$, as shown in Fig. 1.2.2a.[1]

Electrons are continuously injected. As in Example 1.1.1, where the motions of the individual electrons are considered, the electric field is assumed to be uniform. In the next section, it is recognized that charge is the source of the electric field. Here it is assumed that the charge used to impose the uniform field is much greater than the "space charge" associated with the electrons. This is justified in the limit of a low electron current. Any one of the electrons has a position and velocity given by (1.1.7) and (1.1.8). If each is injected with the same initial velocity, the charge and current densities in any given plane $x =$ constant would be expected to be independent of time. Moreover, the current passing any x-plane should be the same as that passing any other such plane. That is, in the steady state, the current density is independent

[1] Here we picture the field variables E_x, v_x, and ρ as though they were positive. For electrons, $\rho < 0$, and to make $v_x > 0$, we must have $E_x < 0$.

of not only time but x as well. Thus, it is possible to write

$$\rho(x)v_x(x) = J_o \tag{4}$$

where J_o is a given current density.

The following steps illustrate how this condition of current continuity makes it possible to shift from a description of the particle motions described with time as the independent variable to one in which coordinates (x, y, z) (or for short $\mathbf{r}$) are the independent coordinates. The relation between time and position for the electron described by (1.1.7) takes the form of a quadratic in $(t - t_i)$

$$\frac{1}{2}\frac{e}{m}E_x(t - t_i)^2 - v_i(t - t_i) + \xi_x = 0 \tag{5}$$

This can be solved to give the elapsed time for a particle to reach the position ξ_x. Note that of the two possible solutions to (5), the one selected satisfies the condition that when $t = t_i$, $\xi_x = 0$.

$$t - t_i = \frac{v_i - \sqrt{v_i^2 - 2\frac{e}{m}E_x\xi_x}}{\frac{e}{m}E_x} \tag{6}$$

With the benefit of this expression, the velocity given by (1.1.8) is written as

$$\frac{d\xi_x}{dt} = \sqrt{v_i^2 - \frac{2e}{m}E_x\xi_x} \tag{7}$$

Now we make a shift in viewpoint. On the left in (7) is the velocity v_x of the particle that is at the location $\xi_x = x$. Substitution of variables then gives

$$v_x = \sqrt{v_i^2 - 2\frac{e}{m}E_x x} \tag{8}$$

so that x becomes the independent variable used to express the dependent variable v_x. It follows from this expression and (4) that the charge density

$$\rho = \frac{J_o}{v_x} = \frac{J_o}{\sqrt{v_i^2 - \frac{2e}{m}E_x x}} \tag{9}$$

is also expressed as a function of x. In the plots shown in Fig. 1.2.2, it is assumed that $E_x < 0$, so that the electrons have velocities that increase monotonically with x. As should be expected, the charge density decreases with x because as they speed up, the electrons thin out to keep the current density constant.

1.3 GAUSS' INTEGRAL LAW OF ELECTRIC FIELD INTENSITY

The Lorentz force law of Sec. 1.1 expresses the effect of electromagnetic fields on a moving charge. The remaining sections in this chapter are concerned with the reaction of the moving charges upon the electromagnetic fields. The first of

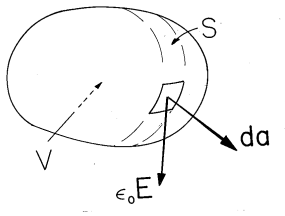


Fig. 1.3.1 General surface S enclosing volume V.

Maxwell's equations to be considered, *Gauss' law*, describes how the electric field intensity is related to its source. The net charge within an arbitrary volume V that is enclosed by a surface S is related to the net electric flux through that surface by

$$\boxed{\oint_S \epsilon_o \mathbf{E} \cdot d\mathbf{a} = \int_V \rho dv} \tag{1}$$

With the surface normal defined as directed outward, the volume is shown in Fig. 1.3.1. Here the *permittivity of free space*, $\epsilon_o = 8.854 \times 10^{-12}$ farad/meter, is an empirical constant needed to express Maxwell's equations in SI units. On the right in (1) is the net charge enclosed by the surface S. On the left is the summation over this same closed surface of the differential contributions of flux $\epsilon_o \mathbf{E} \cdot d\mathbf{a}$. The quantity $\epsilon_o \mathbf{E}$ is called the *electric displacement flux density* and, [from (1)], has the units of coulomb/meter^2. Out of any region containing net charge, there must be a net displacement flux.

The following example illustrates the mechanics of carrying out the volume and surface integrations.

Example 1.3.1. Electric Field Due to Spherically Symmetric Charge Distribution

Given the charge and current distributions, the integral laws fully determine the electric and magnetic fields. However, they are not directly useful unless there is a great deal of symmetry. An example is the distribution of charge density

$$\rho(r) = \begin{cases} \rho_o \frac{r}{R}; & r < R \\ 0; & r > R \end{cases} \tag{2}$$

in the spherical coordinate system of Fig. 1.3.2. Here ρ_o and R are given constants. An argument based on the spherical symmetry shows that the only possible component of $\mathbf{E}$ is radial.

$$\mathbf{E} = \mathbf{i_r} E_r(r) \tag{3}$$

Indeed, suppose that in addition to this r component the field possesses a ϕ component. At a given point, the components of $\mathbf{E}$ then appear as shown in Fig. 1.3.2b. Rotation of the system about the axis shown results in a component of $\mathbf{E}$ in some new direction perpendicular to r. However, the rotation leaves the source of that field, the charge distribution, unaltered. It follows that E_ϕ must be zero. A similar argument shows that E_θ also is zero.

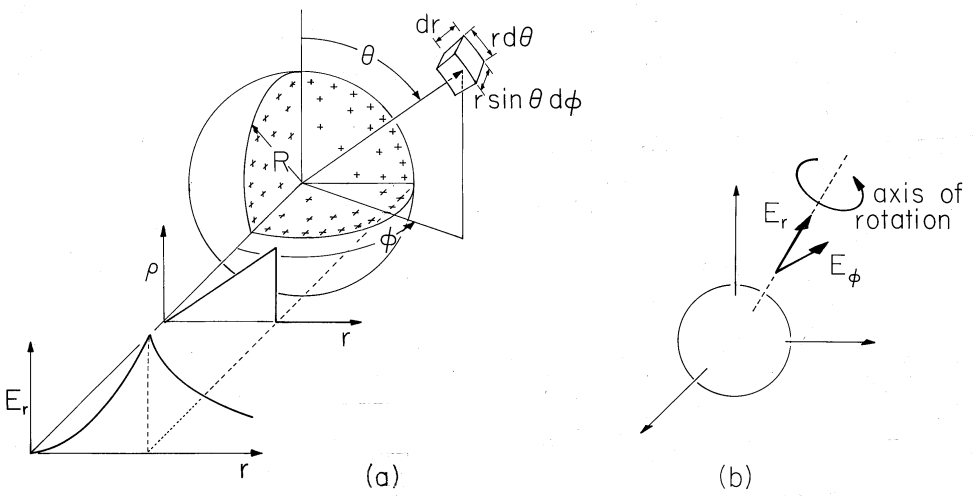


Fig. 1.3.2 (a) Spherically symmetric charge distribution, showing radial dependence of charge density and associated radial electric field intensity. (b) Axis of rotation for demonstration that the components of **E** transverse to the radial coordinate are zero.

The incremental volume element is

$$dv = (dr)(rd\theta)(r\sin\theta d\phi) \tag{4}$$

and it follows that for a spherical volume having arbitrary radius r,

$$\int_V \rho dv = \begin{cases} \int_0^r \int_0^\pi \int_0^{2\pi} \left[\rho_o \frac{r'}{R}\right](r'\sin\theta d\phi)(r' d\theta)dr' = \frac{\pi\rho_o}{R} r^4; & r < R \\ \int_0^R \int_0^\pi \int_0^{2\pi} \left[\rho_o \frac{r'}{R}\right](r'\sin\theta d\phi)(r' d\theta)dr' = \pi\rho_o R^3; & R < r \end{cases} \tag{5}$$

To evaluate the left-hand side of (1), note that

$$\mathbf{n} = \mathbf{i_r}; \qquad d\mathbf{a} = \mathbf{i_r}(rd\theta)(r\sin\theta d\phi) \tag{6}$$

Thus, for the spherical surface at the arbitrary radius r,

$$\oint_S \epsilon_o \mathbf{E}\cdot d\mathbf{a} = \int_0^\pi \int_0^{2\pi} \epsilon_o E_r (r\sin\theta d\phi)(rd\theta) = \epsilon_o E_r 4\pi r^2 \tag{7}$$

With the volume and surface integrals evaluated in (5) and (7), Gauss' law, (l), shows that

$$\epsilon_o E_r 4\pi r^2 = \frac{\pi\rho_o}{R} r^4 \Rightarrow E_r = \frac{\rho_o r^2}{4\epsilon_o R}; \qquad r < R \tag{8a}$$

$$\epsilon_o E_r 4\pi r^2 = \pi\rho_o R^3 \Rightarrow E_r = \frac{\rho_o R^3}{4\epsilon_o r^2}; \qquad R < r \tag{8b}$$

Inside the spherical charged region, the radial electric field increases with the square of the radius because even though the associated surface increases like the square

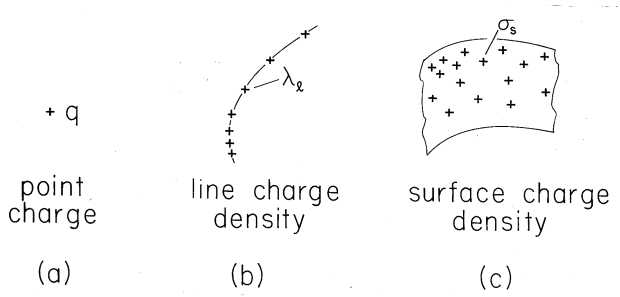


Fig. 1.3.3 Singular charge distributions: (a) point charge, (b) line charge, (c) surface charge.

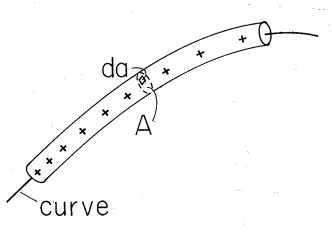


Fig. 1.3.4 Filamentary volume element having cross-section *da* used to define line charge density.

of the radius, the enclosed charge increases even more rapidly. Figure 1.3.2 illustrates this dependence, as well as the exterior field decay. Outside, the surface area continues to increase in proportion to r^2, but the enclosed charge remains constant.

Singular Charge Distributions. Examples of singular functions from circuit theory are impulse and step functions. Because there is only the one independent variable, namely time, circuit theory is concerned with only one "dimension." In three-dimensional field theory, there are three spatial analogues of the temporal impulse function. These are point, line, and surface distributions of ρ, as illustrated in Fig. 1.3.3. Like the temporal impulse function of circuit theory, these singular distributions are defined in terms of integrals.

A *point charge* is the limit of an infinite charge density occupying zero volume. With q defined as the net charge,

$$q = \lim_{\substack{\rho \to \infty \\ V \to 0}} \int_V \rho dv \tag{9}$$

the point charge can be pictured as a small charge-filled region, the outside of which is charge free. An example is given in Fig. 1.3.2 in the limit where the volume $4\pi R^3/3$ goes to zero, while $q = \pi \rho_o R^3$ remains finite.

A *line charge density* represents a two-dimensional singularity in charge density. It is the mathematical abstraction representing a thin charge filament. In terms of the filamentary volume shown in Fig. 1.3.4, the line charge per unit length λ_l (the line charge density) is defined as the limit where the cross-sectional area of the volume goes to zero, ρ goes to infinity, but the integral

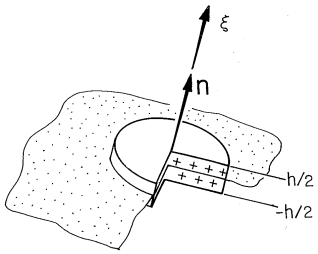


Fig. 1.3.5 Volume element having thickness h used to define surface charge density.

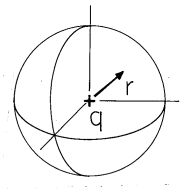


Fig. 1.3.6 Point charge q at origin of spherical coordinate system.

$$\lambda_l = \lim_{\substack{\rho\to\infty \\ A\to 0}} \int_A \rho da \tag{10}$$

remains finite. In general, λ_l is a function of position along the curve.

The one-dimensional singularity in charge density is represented by the *surface charge density.* The charge density is very large in the vicinity of a surface. Thus, as a function of a coordinate perpendicular to that surface, the charge density is a one-dimensional impulse function. To define the surface charge density, mount a pillbox as shown in Fig. 1.3.5 so that its top and bottom surfaces are on the two sides of the surface. The surface charge density is then defined as the limit

$$\sigma_s = \lim_{\substack{\rho\to\infty \\ h\to 0}} \int_{\xi-\frac{h}{2}}^{\xi+\frac{h}{2}} \rho d\xi \tag{11}$$

where the ξ coordinate is picked parallel to the direction of the normal to the surface, $\mathbf{n}$. In general, the surface charge density σ_s is a function of position in the surface.

Illustration. Field of a Point Charge

A point charge q is located at the origin in Fig. 1.3.6. There are no other charges. By the same arguments as used in Example 1.3.1, the spherical symmetry of the charge distribution requires that the electric field be radial and be independent of θ and ϕ. Evaluation of the surface integral in Gauss' integral law, (1), amounts to multiplying $\epsilon_o E_r$ by the surface area. Because all of the charge is concentrated at the origin, the volume integral gives q, regardless of radial position of the surface S. Thus,

$$4\pi r^2 \epsilon_o E_r = q \Rightarrow \mathbf{E} = \frac{q}{4\pi\epsilon_o r^2}\mathbf{i_r} \tag{12}$$

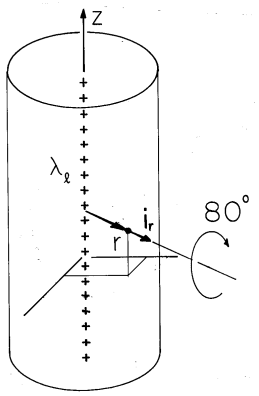


Fig. 1.3.7 Uniform line charge distributed from − infinity to + infinity along z axis. Rotation by 180 degrees about axis shown leads to conclusion that electric field is radial.

is the electric field associated with a point charge q.

Illustration. The Field Associated with Straight Uniform Line Charge

A uniform line charge is distributed along the z axis from $z = -\infty$ to $z = +\infty$, as shown in Fig. 1.3.7. For an observer at the radius r, translation of the line source in the z direction and rotation of the source about the z axis (in the ϕ direction) results in the same charge distribution, so the electric field must only depend on r. Moreover, $\mathbf{E}$ can only have a radial component. To see this, suppose that there were a z component of $\mathbf{E}$. Then a 180 degree rotation of the system about an axis perpendicular to and passing through the z axis must reverse this field. However, the rotation leaves the charge distribution unchanged. The contradiction is resolved only if $E_z = 0$. The same rotation makes it clear that E_ϕ must be zero.

This time, Gauss' integral law is applied using for S the surface of a right circular cylinder coaxial with the z axis and of arbitrary radius r. Contributions from the ends are zero because there the surface normal is perpendicular to $\mathbf{E}$. With the cylinder taken as having length l, the surface integration amounts to a multiplication of $\epsilon_o E_r$ by the surface area $2\pi rl$ while, the volume integral gives $l\lambda_l$ regardless of the radius r. Thus, (1) becomes

$$2\pi rl\epsilon_o E_r = \lambda_l l \Rightarrow \mathbf{E} = \frac{\lambda_l}{2\pi\epsilon_o r}\mathbf{i_r} \tag{13}$$

for the field of an infinitely long uniform line charge having density λ_l.

Example 1.3.2. The Field of a Pair of Equal and Opposite Infinite Planar Charge Densities

Consider the field produced by a surface charge density $+\sigma_o$ occupying all the $x-y$ plane at $z = s/2$ and an opposite surface charge density $-\sigma_o$ at $z = -s/2$.

First, the field must be z directed. Indeed there cannot be a component of $\mathbf{E}$ transverse to the z axis, because rotation of the system around the z axis leaves the same source distribution while rotating that component of $\mathbf{E}$. Hence, no such component exists.

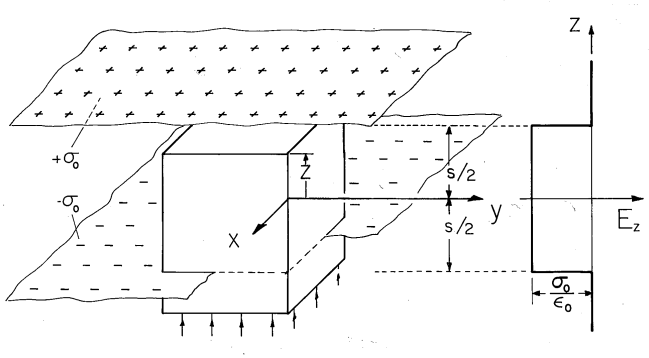


Fig. 1.3.8 Sheets of surface charge and volume of integration with upper surface at arbitrary position x. With field E_o due to external charges equal to zero, the distribution of electric field is the discontinuous function shown at right.

Because the source distribution is independent of x and y, E_z is independent of these coordinates. The z dependence is now established by means of Gauss' integral law, (1). The volume of integration, shown in Fig. 1.3.8, has cross-sectional area A in the $x-y$ plane. Its lower surface is located at an arbitrary fixed location below the lower surface charge distribution, while its upper surface is in the plane denoted by z. For now, we take E_z as being E_o on the lower surface. There is no contribution to the surface integral from the side walls because these have normals perpendicular to **E**. It follows that Gauss' law, (1), becomes

$$\begin{aligned} A(\epsilon_o E_z - \epsilon_o E_o) = 0; \qquad & -\infty < z < -\frac{s}{2} \Rightarrow E_z = E_o \\ A(\epsilon_o E_z - \epsilon_o E_o) = -A\sigma_o; \qquad & -\frac{s}{2} < z < \frac{s}{2} \Rightarrow E_z = -\frac{\sigma_o}{\epsilon_o} + E_o \\ A(\epsilon_o E_z - \epsilon_o E_o) = 0; \qquad & \frac{s}{2} < z < \infty \Rightarrow E_z = E_o \end{aligned} \tag{14}$$

That is, with the upper surface below the lower charge sheet, no charge is enclosed by the surface of integration, and E_z is the constant E_o. With the upper surface of integration between the charge sheets, E_z is E_o minus σ_o/ϵ_o. Finally, with the upper integration surface above the upper charge sheet, E_z returns to its value of E_o. The external electric field E_o must be created by charges at $z = +\infty$, much as the field between the charge sheets is created by the given surface charges. Thus, if these charges at "infinity" are absent, $E_o = 0$, and the distribution of E_z is as shown to the right in Fig. 1.3.8.

Illustration. Coulomb's Force Law for Point Charges

It is worthwhile to see that for charges at rest, Gauss' integral law and the Lorentz force law give the familiar action at a distance force law. The force on a charge q is given by the Lorentz law, (1.1.1), and if the electric field is caused by a second charge at the origin in Fig. 1.3.9, then

$$\mathbf{f} = q\mathbf{E} = \frac{q_1 q_2}{4\pi\epsilon_o r^2}\mathbf{i_r} \tag{15}$$

Coulomb's famous statement that the force exerted by one charge on another is proportional to the product of their charges, acts along a line passing through each

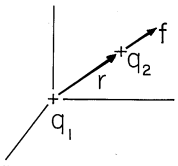


Fig. 1.3.9 Coulomb force induced on charge q_2 due to field from q_1.

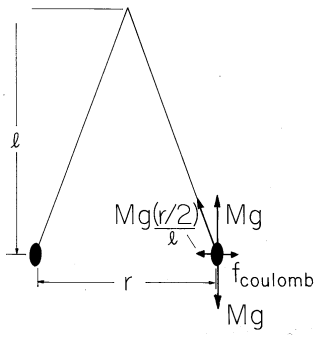


Fig. 1.3.10 Like-charged particles on ends of thread are pushed apart by the Coulomb force.

charge, and is inversely proportional to the square of the distance between them, is now demonstrated.

Demonstration 1.3.1. Coulomb's Force Law

The charge resulting on the surface of adhesive tape as it is pulled from a dispenser is a common nuisance. As the tape is brought toward a piece of paper, the force of attraction that makes the paper jump is an aggravating reminder that there are charges on the tape. Just how much charge there is on the tape can be approximately determined by means of the simple experiment shown in Fig. 1.3.10.

Two pieces of freshly pulled tape about 7 cm long are folded up into balls and stuck on the ends of a thread having a total length of about 20 cm. The middle of the thread is then tied up so that the charged balls of tape are suspended free to swing. (By electrostatic standards, our fingers are conductors, so the tape should be manipulated chopstick fashion by means of plastic rods or the like.) It is then easy to measure approximately l and r, as defined in the figure. The force of repulsion that separates the "balls" of tape is presumably predicted by (15). In Fig. 1.3.10, the vertical component of the tension in the thread must balance the gravitational force Mg (where g is the gravitational acceleration and M is the mass). It follows that the horizontal component of the thread tension balances the Coulomb force of repulsion.

$$\frac{q^2}{4\pi\epsilon_o r^2} = Mg\frac{(r/2)}{l} \Rightarrow q = \sqrt{\frac{Mgr^3 2\pi\epsilon_o}{l}} \tag{16}$$

As an example, tape balls having an area of $A = 14$ cm^2, (7 cm length of 2 cm wide tape) weighing 0.1 mg and dangling at a length $l = 20$ cm result in a distance of separation $r = 3$ cm. It follows from (16) (with all quantities expressed in SI units) that $q = 2.7 \times 10^{-9}$ coulomb. Thus, the average surface charge density is $q/A = 1.9 \times 10^{-6}$ coulomb/meter or 1.2×10^{13} electronic charges per square meter. If

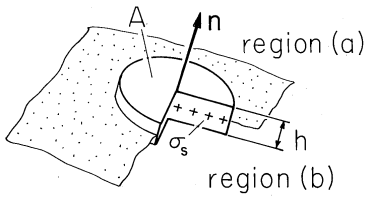


Fig. 1.3.11 Pillbox-shaped incremental volume used to deduce the jump condition implied by Gauss' integral law.

these charges were in a square array with spacing s between charges, then $\sigma_s = e/s^2$, and it follows that the approximate distance between the individual charge in the tape surface is $0.3\mu m$. This length is at the limit of an optical microscope and may seem small. However, it is about 1000 times larger than a typical atomic dimension.[2]

Gauss' Continuity Condition. Each of the integral laws summarized in this chapter implies a relationship between field variables evaluated on either side of a surface. These conditions are necessary for dealing with surface singularities in the field sources. Example 1.3.2 illustrates the jump in the normal component of $\mathbf{E}$ that accompanies a surface charge.

A surface that supports surface charge is pictured in Fig. 1.3.11, as having a unit normal vector directed from region (b) to region (a). The volume to which Gauss' integral law is applied has the pillbox shape shown, with endfaces of area A on opposite sides of the surface. These are assumed to be small enough so that over the area of interest the surface can be treated as plane. The height h of the pillbox is very small so that the cylindrical sideface of the pillbox has an area much smaller than A.

Now, let h approach zero in such a way that the two sides of the pillbox remain on opposite sides of the surface. The volume integral of the charge density, on the right in (1), gives $A\sigma_s$. This follows from the definition of the surface charge density, (11). The electric field is assumed to be finite throughout the region of the surface. Hence, as the area of the sideface shrinks to zero, so also does the contribution of the sideface to the surface integral. Thus, the displacement flux through the closed surface consists only of the contributions from the top and bottom surfaces. Applied to the pillbox, Gauss' integral law requires that

$$\boxed{\mathbf{n} \cdot (\epsilon_o \mathbf{E}^a - \epsilon_o \mathbf{E}^b) = \sigma_s} \tag{17}$$

where the area A has been canceled from both sides of the equation.

The contribution from the endface on side (b) comes with a minus sign because on that surface, $\mathbf{n}$ is opposite in direction to the surface element $d\mathbf{a}$.

Note that the field found in Example 1.3.2 satisfies this continuity condition at $z = s/2$ and $z = -s/2$.

[2] An alternative way to charge a particle, perhaps of low density plastic, is to place it in the corona discharge around the tip of a pin placed at high voltage. The charging mechanism at work in this case is discussed in Chapter 7 (Example 7.7.2).

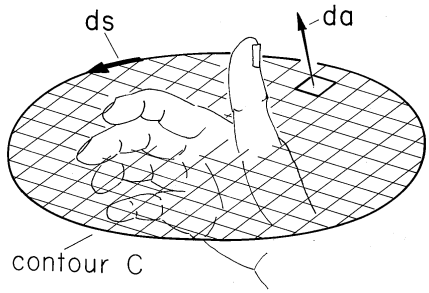


Fig. 1.4.1 Surface S is enclosed by contour C having positive direction determined by the right-hand rule. With the fingers in the direction of $d\mathbf{s}$, the thumb passes through the surface in the direction of positive $d\mathbf{a}$.

1.4 AMPÈRE'S INTEGRAL LAW

The law relating the *magnetic field intensity* $\mathbf{H}$ to its source, the current density $\mathbf{J}$, is

$$\boxed{\oint_C \mathbf{H} \cdot d\mathbf{s} = \int_S \mathbf{J} \cdot d\mathbf{a} + \frac{d}{dt} \int_S \epsilon_o \mathbf{E} \cdot d\mathbf{a}} \tag{1}$$

Note that by contrast with the integral statement of Gauss' law, (1.3.1), the surface integral symbols on the right do not have circles. This means that the integrations are over open surfaces, having edges denoted by the contour C. Such a surface S enclosed by a contour C is shown in Fig. 1.4.1. In words, Ampère's integral law as given by (1) requires that the line integral (circulation) of the magnetic field intensity $\mathbf{H}$ around a closed contour is equal to the net current passing through the surface spanning the contour plus the time rate of change of the net displacement flux density $\epsilon_o \mathbf{E}$ through the surface (the *displacement current*).

The direction of positive $d\mathbf{a}$ is determined by the right-hand rule, as also illustrated in Fig. 1.4.1. With the fingers of the right-hand in the direction of $d\mathbf{s}$, the thumb has the direction of $d\mathbf{a}$. Alternatively, with the right hand thumb in the direction of $d\mathbf{s}$, the fingers will be in the positive direction of $d\mathbf{a}$.

In Ampère's law, $\mathbf{H}$ appears without μ_o. This law therefore establishes the basic units of $\mathbf{H}$ as coulomb/(meter-second). In Sec. 1.1, the units of the flux density $\mu_o \mathbf{H}$ are defined by the Lorentz force, so the second empirical constant, the *permeability of free space*, is $\mu_o = 4\pi \times 10^{-7}$ henry/m (henry = volt sec/amp).

Example 1.4.1. Magnetic Field Due to Axisymmetric Current

A constant current in the z direction within the circular cylindrical region of radius R, shown in Fig. 1.4.2, extends from − infinity to + infinity along the z axis and is represented by the density

$$\mathbf{J} = \begin{cases} J_o\left(\frac{r}{R}\right); & r < R \\ 0; & r > R \end{cases} \tag{2}$$

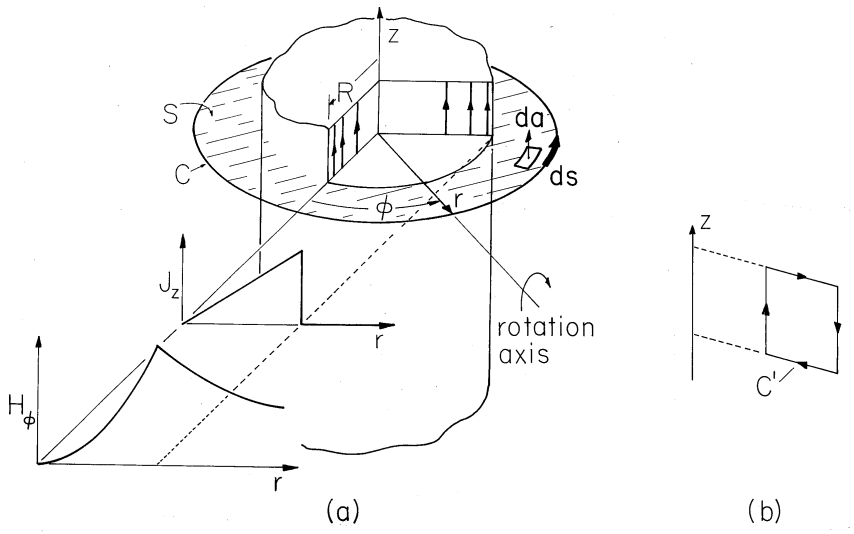


Fig. 1.4.2 Axially symmetric current distribution and associated radial distribution of azimuthal magnetic field intensity. Contour C is used to determine azimuthal $\mathbf{H}$, while C' is used to show that the z-directed field must be uniform.

where J_o and R are given constants. The associated magnetic field intensity has only an azimuthal component.

$$\mathbf{H} = H_\phi \mathbf{i}_\phi \tag{3}$$

To see that there can be no r component of this field, observe that rotation of the source around the radial axis, as shown in Fig. 1.4.2, reverses the source (the current is then in the $-z$ direction) and hence must reverse the field. But an r component of the field does not reverse under such a rotation and hence must be zero. The H_ϕ and H_z components are not ruled out by this argument. However, if they exist, they must not depend upon the ϕ and z coordinates, because rotation of the source around the z axis and translation of the source along the z axis does not change the source and hence does not change the field.

The current is independent of time and so we assume that the fields are as well. Hence, the last term in (1), the displacement current, is zero. The law is then used with S, a surface having its enclosing contour C at the arbitrary radius r, as shown in Fig. 1.4.2. Then the area and line elements are

$$d\mathbf{a} = rd\phi dr\mathbf{i}_z; \qquad d\mathbf{s} = \mathbf{i}_\phi r d\phi \tag{4}$$

and the right-hand side of (1) becomes

$$\int_S \mathbf{J} \cdot d\mathbf{a} = \begin{cases} \int_0^{2\pi} \int_0^r J_o \frac{r}{R} r d\phi dr = \frac{J_o r^3 2\pi}{3R}; & r < R \\ \int_0^{2\pi} \int_0^R J_o \frac{r}{R} r d\phi dr = \frac{J_o R^2 2\pi}{3}; & R < r \end{cases} \tag{5}$$

Integration on the left-hand side amounts to a multiplication of the ϕ independent H_ϕ by the length of C.

$$\oint_C \mathbf{H} \cdot d\mathbf{s} = \int_0^{2\pi} H_\phi r d\phi = H_\phi 2\pi r \tag{6}$$

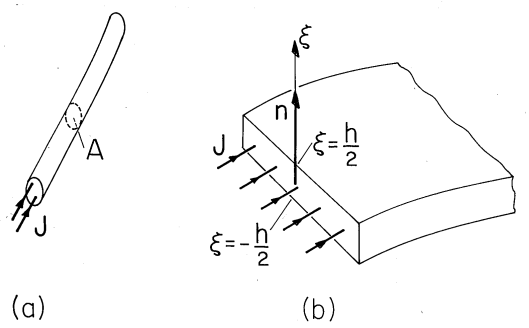


Fig. 1.4.3 (a) Line current enclosed by volume having cross-sectional area A. (b) Surface current density enclosed by contour having thickness h.

These last two expressions are used to evaluate (1) and obtain

$$2\pi r H_\phi = \frac{J_o r^3 2\pi}{3R} \Rightarrow H_\phi = \frac{J_o r^2}{3R}; \qquad r < R$$

$$2\pi r H_\phi = \frac{J_o R^2 2\pi}{3} \Rightarrow H_\phi = \frac{J_o R^2}{3r}; \qquad r < R \tag{7}$$

Thus, the azimuthal magnetic field intensity has the radial distribution shown in Fig. 1.4.2.

The z component of $\mathbf{H}$ is, at most, uniform. This can be seen by applying the integral law to the contour C', also shown in Fig. 1.4.2. Integration on the top and bottom legs gives zero because $H_r = 0$. Thus, to make the contributions due to H_z on the vertical legs cancel, it is necessary that H_z be independent of radius. Such a uniform field must be caused by sources at infinity and is therefore set equal to zero if such sources are not postulated in the statement of the problem.

Singular Current Distributions. The first of two singular forms of the current density shown in Fig. 1.4.3a is the *line current*. Formally, it is the limit of an infinite current density distributed over an infinitesimal area.

$$i = \lim_{\substack{|\mathbf{J}|\to\infty \\ A\to 0}} \int_A \mathbf{J} \cdot d\mathbf{a} \tag{8}$$

With i a constant over the length of the line, a thin wire carrying a current i conjures up the correct notion of the line current. However, in general, the current i may depend on the position along the line if it varies with time as in an antenna.

The second singularity, the *surface current density*, is the limit of a very large current density $\mathbf{J}$ distributed over a very thin layer adjacent to a surface. In Fig. 1.4.3b, the current is in a direction parallel to the surface. If the layer extends between $\xi = -h/2$ and $\xi = +h/2$, the *surface current density* $\mathbf{K}$ is defined as

$$\mathbf{K} = \lim_{\substack{|\mathbf{J}|\to\infty \\ h\to 0}} \int_{-\frac{h}{2}}^{\frac{h}{2}} \mathbf{J} d\xi \tag{9}$$

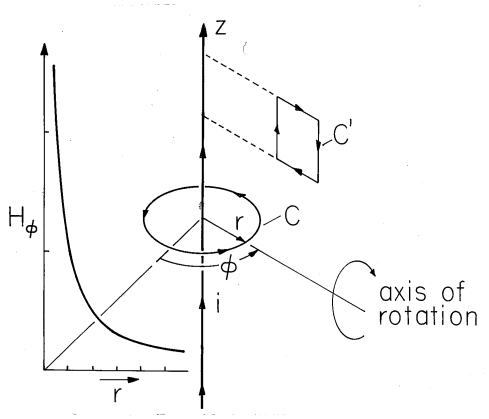


Fig. 1.4.4 Uniform line current with contours for determining **H**. Axis of rotation is used to deduce that radial component of field must be zero.

By definition, **K** is a vector tangential to the surface that has units of ampere/meter.

Illustration. *H* field Produced by a Uniform Line Current

A uniform line current of magnitude i extends from − infinity to + infinity along the z axis, as shown in Fig. 1.4.4. The symmetry arguments of Example 1.4.1 show that the only component of **H** is azimuthal. Application of Ampère's integral law, (1), to the contour of Fig. 1.4.4 having arbitrary radius r gives a line integral that is simply the product of H_ϕ and the circumference $2\pi r$ and a surface integral that is simply i, regardless of the radius.

$$2\pi r H_\phi = i \Rightarrow H_\phi = \frac{i}{2\pi r} \tag{10}$$

This expression makes it especially clear that the units of **H** are ampere/meter.

Demonstration 1.4.1. Magnetic Field of a Line Current

At 60 Hz, the displacement current contribution to the magnetic field of the experiment shown in Fig. 1.4.5 is negligible. So long as the field probe is within a distance r from the wire that is small compared to the distance to the ends of the wire or to the return wires below, the magnetic field intensity is predicted quantitatively by (10). The curve shown is typical of demonstration measurements illustrating the radial dependence. Because the Hall-effect probe fundamentally exploits the Lorentz force law, it measures the flux density $\mu_o\mathbf{H}$. A common unit for flux density is the Gauss. For conversion of units, 10,000 gauss = 1 tesla, where the tesla is the SI unit.

Illustration. Uniform Axial Surface Current

At the radius R from the z axis, there is a uniform z directed surface current density K_o that extends from - infinity to + infinity in the z direction. The symmetry arguments of Example 1.4.1 show that the resulting magnetic field intensity

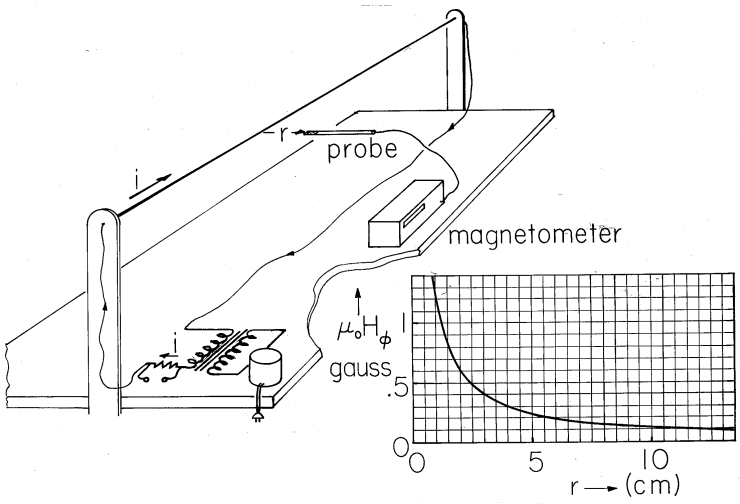


Fig. 1.4.5 Demonstration of peak magnetic flux density induced by line current of 6 ampere (peak).

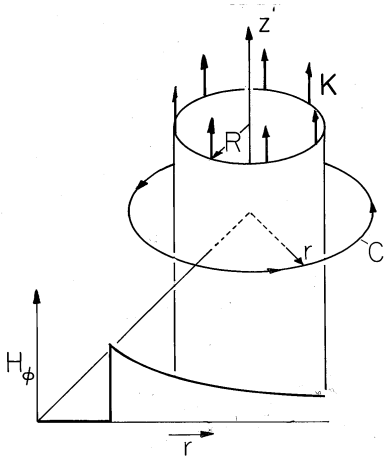


Fig. 1.4.6 Uniform current density K_o is z directed in circular cylindrical shell at $r = R$. Radially discontinuous azimuthal field shown is determined using the contour at arbitrary radius r.

is azimuthal. To determine that field, Ampère's integral law is applied to a contour having the arbitrary radius r, shown in Fig. 1.4.6. As in the previous illustration, the line integral is the product of the circumference and H_ϕ. The surface integral gives nothing if $r < R$, but gives $2\pi R$ times the surface current density if $r > R$. Thus,

$$2\pi r H_\phi = \begin{cases} 0; & r < R \\ 2\pi R K_o; & r > R \end{cases} \Rightarrow H_\phi = \begin{cases} 0; & r < R \\ K_o \frac{R}{r}; & r > R \end{cases} \tag{11}$$

Thus, the distribution of $\mathbf{H}_\phi$ is the discontinuous function shown in Fig. 1.4.6. The field tangential to the surface current undergoes a jump that is equal in magnitude

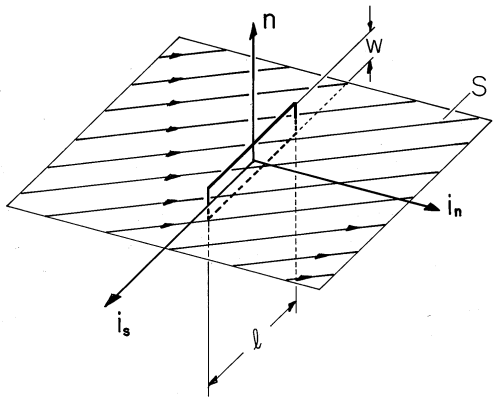


Fig. 1.4.7 Ampère's integral law is applied to surface S' enclosed by a rectangular contour that intersects a surface S carrying the current density $\mathbf{K}$. In terms of the unit normal to S, $\mathbf{n}$, the resulting continuity condition is given by (16).

to the surface current density.

Ampère's Continuity Condition. A surface current density in a surface S causes a discontinuity of the magnetic field intensity. This is illustrated in Fig. 1.4.6. To obtain a general relation between fields evaluated to either side of S, a rectangular surface of integration is mounted so that it intersects S as shown in Fig. 1.4.7. The normal to S is in the plane of the surface of integration. The length l of the rectangle is assumed small enough so that the surface of integration can be considered plane over this length. The width w of the rectangle is assumed to be much smaller than l . It is further convenient to introduce, in addition to the normal $\mathbf{n}$ to S, the mutually orthogonal unit vectors $\mathbf{i_s}$ and $\mathbf{i_n}$ as shown.

Now apply the integral form of Ampère's law, (1), to the rectangular surface of area lw. For the right-hand side we obtain

$$\int_{S'} \mathbf{J} \cdot d\mathbf{a} + \int_{S'} \frac{\partial}{\partial t} \epsilon_o \mathbf{E} \cdot d\mathbf{a} \simeq \mathbf{K} \cdot \mathbf{i}_n l \tag{12}$$

Only $\mathbf{J}$ gives a contribution, and then only if there is an infinite current density over the zero thickness of S, as required by the definition of the surface current density, (9). The time rate of change of a finite displacement flux density integrated over zero area gives zero, and hence there is no contribution from the second term.

The left-hand side of Ampère's law, (1), is a contour integral following the rectangle. Because w has been assumed to be very small compared with l, and $\mathbf{H}$ is assumed finite, no contribution is made by the two short sides of the rectangle. Hence,

$$l\ \mathbf{i}_s \cdot (\mathbf{H}^a - \mathbf{H}^b) = \mathbf{K} \cdot \mathbf{i}_n l \tag{13}$$

From Fig. 1.4.7, note that

$$\mathbf{i}_s = \mathbf{i}_n \times \mathbf{n} \tag{14}$$

The cross and dot can be interchanged in this scalar triple product without affecting the result (Appendix 1), so introduction of (14) into (13) gives

$$\mathbf{i}_n \cdot \mathbf{n} \times (\mathbf{H}^a - \mathbf{H}^b) = \mathbf{i}_n \cdot \mathbf{K} \tag{15}$$

Finally, note that the vector $\mathbf{i}_n$ is arbitrary so long as it lies in the surface S. Since it multiplies vectors tangential to the surface, it can be omitted.

$$\boxed{\mathbf{n} \times (\mathbf{H}^a - \mathbf{H}^b) = \mathbf{K}} \tag{16}$$

There is a jump in the tangential magnetic field intensity as one passes through a surface current. Note that (16) gives a prediction consistent with what was found for the illustration in Fig. 1.4.6.

1.5 CHARGE CONSERVATION IN INTEGRAL FORM

Embedded in the laws of Gauss and Ampère is a relationship that must exist between the charge and current densities. To see this, first apply Ampère's law to a closed surface, such as sketched in Fig. 1.5.1. If the contour $\mathbf{C}$ is regarded as the"drawstring" and S as the "bag," then this limit is one in which the "string" is drawn tight so that the contour shrinks to zero. Thus, the open surface integrals of (1.4.1) become closed, while the contour integral vanishes.

$$\oint_S \mathbf{J} \cdot d\mathbf{a} + \frac{d}{dt} \oint_S \epsilon_o \mathbf{E} \cdot d\mathbf{a} = 0 \tag{1}$$

But now, in view of Gauss' law, the surface integral of the electric displacement can be replaced by the total charge enclosed. That is, (1.3.1) is used to write (1) as

$$\boxed{\oint_S \mathbf{J} \cdot d\mathbf{a} + \frac{d}{dt} \int_V \rho dv = 0} \tag{2}$$

This is the law of conservation of charge. If there is a net current out of the volume shown in Fig. 1.5.2, (2) requires that the net charge enclosed be decreasing with time.

Charge conservation, as expressed by (2), was a compelling reason for Maxwell to add the electric displacement term to Ampère's law. Without the displacement current density, Ampère's law would be inconsistent with charge conservation. That is, if the second term in (1) would be absent, then so would the second term in (2). If the displacement current term is dropped in Ampère's law, then net current cannot enter, or leave, a volume.

The conservation of charge is consistent with the intuitive picture of the relationship between charge and current developed in Example 1.2.1.

Example 1.5.1. Continuity of Convection Current

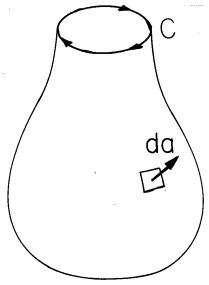


Fig. 1.5.1 Contour C enclosing an open surface can be thought of as the drawstring of a bag that can be closed to create a closed surface.

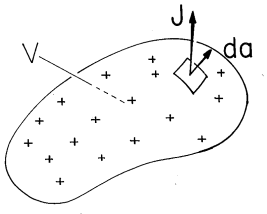


Fig. 1.5.2 Current density leaves a volume V and hence the net charge must decrease.

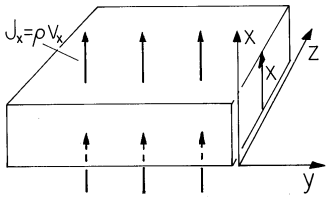


Fig. 1.5.3 In steady state, charge conservation requires that the current density entering through the $x = 0$ plane be the same as that leaving through the plane at $x = x$.

The steady state current of electrons accelerated through vacuum by a uniform electric field is described in Example 1.2.1 by assuming that in any plane $x =$ constant the current density is the same. That this must be true is now seen formally by applying the charge conservation integral theorem to the volume shown in Fig. 1.5.3. Here the lower surface is in the injection plane $x = 0$, where the current density is known to be J_o. The upper surface is at the arbitrary level denoted by x. Because the steady state prevails, the time derivative in (2) is zero. The remaining surface integral has contributions only from the top and bottom surfaces. Evaluation of these, with the recognition that the area element on the top surface is $(\mathbf{i_x}dydz)$ while it is $(-\mathbf{i_x}dydz)$ on the bottom surface, makes it clear that

$$AJ_x - AJ_o = 0 \Rightarrow \rho v_x = J_o \tag{3}$$

This same relation was used in Example 1.2.1, (1.2.4), as the basis for converting from a particle point of view to the one used here, where (x, y, z) are independent of t.

Example 1.5.2. Current Density and Time-Varying Charge

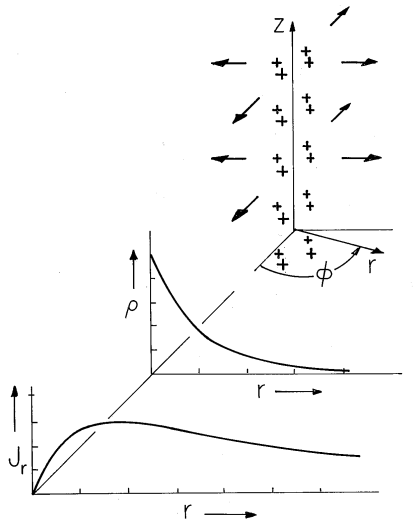


Fig. 1.5.4 With the given axially symmetric charge distribution positive and decreasing with time ($\partial\rho/\partial t < 0$), the radial current density is positive, as shown.

With the charge density a given function of time with an axially symmetric spatial distribution, (2) can be used to deduce the current density. In this example, the charge density is

$$\rho = \rho_o(t)e^{-r/a} \tag{4}$$

and can be pictured as shown in Fig. 1.5.4. The function of time ρ_o is given, as is the dimension a.

As the first step in finding $\mathbf{J}$, we evaluate the volume integral in (2) for a circular cylinder of radius r having z as its axis and length l in the z direction.

$$\begin{aligned}\int_V \rho dv &= \int_0^l \int_0^{2\pi} \int_0^r \rho_o e^{-\frac{r}{a}} dr(rd\phi)dz \\ &= 2\pi l a^2 \left[1 - e^{-\frac{r}{a}}\left(1 + \frac{r}{a}\right)\right]\rho_o\end{aligned} \tag{5}$$

The axial symmetry demands that $\mathbf{J}$ is in the radial direction and independent of ϕ and z. Thus, the evaluation of the surface integral in (2) amounts to a multiplication of J_r by the area $2\pi rl$, and that equation becomes

$$2\pi r l J_r + 2\pi l a^2 \left[1 - e^{-\frac{r}{a}}\left(1 + \frac{r}{a}\right)\right]\frac{d\rho_o}{dt} = 0 \tag{6}$$

Finally, this expression can be solved for J_r.

$$J_r = \frac{a^2}{r}\left[e^{-\frac{r}{a}}\left(1 + \frac{r}{a}\right) - 1\right]\frac{d\rho_o}{dt} \tag{7}$$

Under the assumption that the charge density is positive and decreasing, so that $d\rho_o/dt < 0$, the radial distribution of J_r is shown at an instant in time in

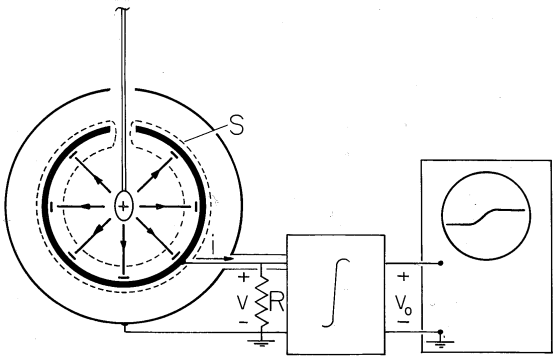


Fig. 1.5.5 When a charge q is introduced into an essentially grounded metal sphere, a charge $-q$ is induced on its inner surface. The integral form of charge conservation, applied to the surface S, shows that $i = dq/dt$. The net excursion of the integrated signal is then a direct measurement of q.

Fig. 1.5.4. In this case, the radial current density is positive at any radius r because the net charge within that radius, given by (5), is decreasing with time.

The integral form of charge conservation provides the link between the current carried by a wire and the charge. Thus, if we can measure a current, this law provides the basis for measuring the net charge. The following demonstration illustrates its use.

Demonstration 1.5.1. Measurement of Charge

In Demonstration 1.3.1, the net charge is deduced from mechanical measurements and Coulomb's force law. Here that same charge is deduced electrically. The "ball" carrying the charge is stuck to the end of a thin plastic rod, as in Fig. 1.5.5. The objective is to measure this charge, q, without removing it from the ball.

We know from the discussion of Gauss' law in Sec. 1.3 that this charge is the source of an electric field. In general, this field terminates on charges of opposite sign. Thus, the net charge that terminates the field originating from q is equal in magnitude and opposite in sign to q. Measurement of this "image" charge is tantamount to measuring q.

How can we design a metal electrode so that we are guaranteed that all of the lines of $\mathbf{E}$ originating from q will be terminated on its surface? It would seem that the electrode should essentially surround q. Thus, in the experiment shown in Fig. 1.5.5, the charge is transported to the interior of a metal sphere through a hole in its top. This sphere is grounded through a resistance R and also surrounded by a grounded shield. This resistance is made low enough so that there is essentially no electric field in the region between the spherical electrode, and the surrounding shield. As a result, there is negligible charge on the outside of the electrode and the net charge on the spherical electrode is just that inside, namely $-q$.

Now consider the application of (2) to the surface S shown in Fig. 1.5.5. The surface completely encloses the spherical electrode while excluding the charge q at its center. On the outside, it cuts through the wire connecting the electrode to the resistance R. Thus, the volume integral in (2) gives the net charge $-q$, while

contributions to the surface integral only come from where S cuts through the wire. By definition, the integral of $\mathbf{J}\cdot d\mathbf{a}$ over the cross-section of the wire gives the current i (amps). Thus, (2) becomes simply

$$i + \frac{d(-q)}{dt} = 0 \Rightarrow i = \frac{dq}{dt} \tag{8}$$

This current is the result of having pushed the charge through the hole to a position where all the field lines terminated on the spherical electrode.[3]

Although small, the current through the resistor results in a voltage.

$$v \simeq iR = R\frac{dq}{dt} \tag{9}$$

The integrating circuit is introduced into the experiment in Fig. 1.5.5 so that the oscilloscope directly displays the charge. With this circuit goes a gain A such that

$$v_o = A\int vdt = ARq \tag{10}$$

Then, the voltage v_o to which the trace on the scope rises as the charge is inserted through the hole reflects the charge q. This measurement of q corroborates that of Demonstration 1.3.1.

In retrospect, because S and V are arbitrary in the integral laws, the experiment need not be carried out using an electrode and shield that are spherical. These could just as well have the shape of boxes.

Charge Conservation Continuity Condition. The continuity condition associated with charge conservation can be derived by applying the integral law to the same pillbox-shaped volume used to derive Gauss' continuity condition, (1.3.17). It can also be found by simply recognizing the similarity between the integral laws of Gauss and charge conservation. To make this similarity clear, rewrite (2) putting the time derivative under the integral. In doing so, d/dt must again be replaced by $\partial/\partial t$, because the time derivative now operates on ρ, a function of t and $\mathbf{r}$.

$$\oint_S \mathbf{J}\cdot d\mathbf{a} + \int_V \frac{\partial\rho}{\partial t}dV = 0 \tag{11}$$

Comparison of (11) with Gauss' integral law, (1.3.1), shows the similarity. The role of $\epsilon_o\mathbf{E}$ in Gauss' law is played by $\mathbf{J}$, while that of ρ is taken by $-\partial\rho/\partial t$. Hence, by analogy with the continuity condition for Gauss' law, (1.3.17), the continuity condition for charge conservation is

[3] Note that if we were to introduce the charged ball without having the spherical electrode essentially grounded through the resistance R, charge conservation (again applied to the surface S) would require that the electrode retain charge neutrality. This would mean that there would be a charge q on the outside of the electrode and hence a field between the electrode and the surrounding shield. With the charge at the center and the shield concentric with the electrode, this outside field would be the same as in the absence of the electrode, namely the field of a point charge, (1.3.12).

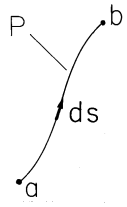


Fig. 1.6.1 Integration line for definition of electromotive force.

$$\boxed{\mathbf{n}\cdot(\mathbf{J}^a-\mathbf{J}^b)+\frac{\partial\sigma_s}{\partial t}=0} \tag{12}$$

Implicit in this condition is the assumption that $\mathbf{J}$ is finite. Thus, the condition does not include the possibility of a surface current.

1.6 FARADAY'S INTEGRAL LAW

The laws of Gauss and Ampère relate fields to sources. The statement of charge conservation implied by these two laws relates these sources. Thus, the previous three sections either relate fields to their sources or interrelate the sources. In this and the next section, integral laws are introduced that do not involve the charge and current densities.

Faraday's integral law states that the circulation of $\mathbf{E}$ around a contour C is determined by the time rate of change of the magnetic flux linking the surface enclosed by that contour (the magnetic induction).

$$\boxed{\oint_C \mathbf{E}\cdot d\mathbf{s}=-\frac{d}{dt}\int_S \mu_o\mathbf{H}\cdot d\mathbf{a}} \tag{1}$$

As in Ampère's integral law and Fig. 1.4.1, the right-hand rule relates $d\mathbf{s}$ and $d\mathbf{a}$.

The *electromotive force*, or EMF, between points (a) and (b) along the path P shown in Fig. 1.6.1 is defined as

$$\mathcal{E}_{ab}=\int_{(a)}^{(b)}\mathbf{E}\cdot\mathbf{ds} \tag{2}$$

We will accept this definition for now and look forward to a careful development of the circumstances under which the EMF is measured as a voltage in Chaps. 4 and 10.

Electric Field Intensity with No Circulation. First, suppose that the time rate of change of the magnetic flux is negligible, so that the electric field is essentially

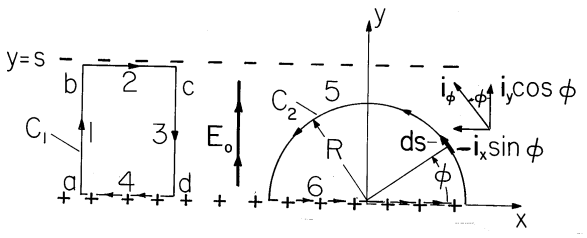


Fig. 1.6.2 Uniform electric field intensity E_o, between plane parallel uniform distributions of surface charge density, has no circulation about contours C_1 and C_2.

free of circulation. This means that no matter what closed contour C is chosen, the line integral of $\mathbf{E}$ must vanish.

$$\oint_C \mathbf{E} \cdot d\mathbf{s} = 0 \tag{3}$$

We will find that this condition prevails in electroquasistatic systems and that all of the fields in Sec. 1.3 satisfy this requirement.

Illustration. A Field Having No Circulation

A static field between plane parallel sheets of uniform charge density has no circulation. Such a field, $\mathbf{E} = E_o\mathbf{i_x}$, exists in the region $0 < y < s$ between the sheets of surface charge density shown in Fig. 1.6.2. The most convenient contour for testing this claim is denoted C_1 in Fig. 1.6.2.

Along path 1, $\mathbf{E} \cdot d\mathbf{s} = E_o dy$, and integration from $y = 0$ to $y = s$ gives sE_o for the EMF of point (a) relative to point (b). Note that the EMF between the plane parallel surfaces in Fig. 1.6.2 is the same regardless of where the points (a) and (b) are located in the respective surfaces.

On segments 2 and 4, $\mathbf{E}$ is orthogonal to $d\mathbf{s}$, so there is no contribution to the line integral on these two sections. Because $d\mathbf{s}$ has a direction opposite to $\mathbf{E}$ on segment 3, the line integral is the integral from $y = 0$ to $y = s$ of $\mathbf{E} \cdot d\mathbf{s} = -E_o dy$. The result of this integration is $-sE_o$, so the contributions from segments 1 and 3 cancel, and the circulation around the closed contour is indeed zero.[4]

In this planar geometry, a field that has only a y component cannot be a function of x without incurring a circulation. This is evident from carrying out this integration for such a field on the rectangular contour C_1. Contributions to paths 1 and 3 cancel only if $\mathbf{E}$ is independent of x.

Example 1.6.1. Contour Integration

To gain some appreciation for what it means to require of $\mathbf{E}$ that it have no circulation, no matter what contour is chosen, consider the somewhat more complicated contour C_2 in the uniform field region of Fig. 1.6.2. Here, C_2 is composed of the

[4] In setting up the line integral on a contour such as 3, which has a direction opposite to that in which the coordinate increases, it is tempting to double-account for the direction of $d\mathbf{s}$ not only be recognizing that $d\mathbf{s} = -\mathbf{i_y}dy$, but by integrating from $y = s$ to $y = 0$ as well.

semicircle (5) and the straight segment (6). On the latter, $\mathbf{E}$ is perpendicular to $d\mathbf{s}$ and so there is no contribution there to the circulation.

$$\oint_C \mathbf{E}\cdot d\mathbf{s} = \int_5 \mathbf{E}\cdot d\mathbf{s} + \int_6 \mathbf{E}\cdot d\mathbf{s} = \oint_5 \mathbf{E}\cdot d\mathbf{s} \tag{4}$$

On segment 5, the vector differential $d\mathbf{s}$ is first written in terms of the unit vector $\mathbf{i}_\phi$, and that vector is in turn written (with the help of the vector decomposition shown in the figure) in terms of the Cartesian unit vectors.

$$d\mathbf{s} = \mathbf{i}_\phi R d\phi; \qquad \mathbf{i}_\phi = \mathbf{i}_y \cos\phi - \mathbf{i}_x \sin\phi \tag{5}$$

It follows that on the segment 5 of contour C_2

$$\mathbf{E}\cdot d\mathbf{s} = E_o \cos\phi R d\phi \tag{6}$$

and integration gives

$$\oint_C \mathbf{E}\cdot d\mathbf{s} = \int_0^\pi E_o \cos\phi R d\phi = [E_o R \sin\phi]_0^\pi = 0 \tag{7}$$

So for contour C_2, the circulation of $\mathbf{E}$ is also zero.

When the electromotive force between two points is path independent, we call it the voltage between the two points. For a field having no circulation, the EMF must be independent of path. This we will recognize formally in Chap. 4.

Electric Field Intensity with Circulation. The second limiting situation, typical of the magnetoquasistatic systems to be considered, is primarily concerned with the circulation of $\mathbf{E}$, and hence with the part of the electric field generated by the time-varying magnetic flux density. The remarkable fact is that Faraday's law holds for any contour, whether in free space or in a material. Often, however, the contour of interest coincides with a conducting wire, which comprises a coil that links a magnetic flux density.

Illustration. Terminal EMF of a Coil

A coil with one turn is shown in Fig. 1.6.3. Contour (1) is inside the wire, while (2) joins the terminals along a defined path. With these contours constituting C, Faraday's integral law as given by (1) determines the terminal electromotive force. If the electrical resistance of the wire can be regarded as zero, in the sense that the electric field intensity inside the wire is negligible, the contour integral reduces to an integration from (b) to (a).[5] In view of the definition of the EMF, (2), this integration gives the negative of the EMF. Thus, Faraday's law gives the terminal EMF as

$$\mathcal{E}_{ab} = \frac{d}{dt}\lambda_f; \qquad \lambda_f \equiv \int_S \mu_o \mathbf{H}\cdot d\mathbf{a} \tag{8}$$

[5] With the objectives here limited to attaching an intuitive meaning to Faraday's law, we will give careful attention to the conditions required for this terminal relation to hold in Chaps. 8, 9, and 10.

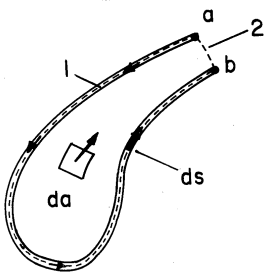


Fig. 1.6.3 Line segment (1) through a perfectly conducting wire and (2) joining the terminals (a) and (b) form closed contour.

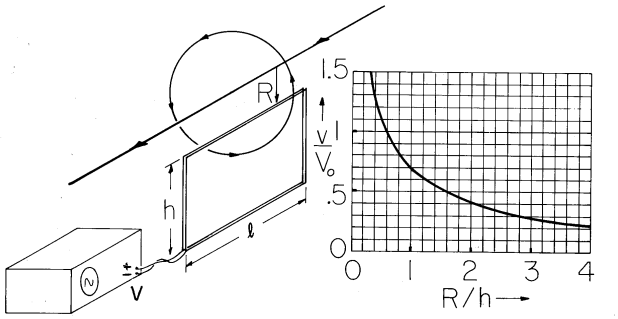


Fig. 1.6.4 Demonstration of voltmeter reading induced at terminals of a coil in accordance with Faraday's law. To plot data on graph, normalize voltage to V_o as defined with (11). Because I is the peak current, v is the peak voltage.

where λ_f, the total flux of magnetic field linking the coil, is defined as the flux linkage. Note that Faraday's law makes it possible to measure $\mu_o\mathbf{H}$ electrically (as now demonstrated).

Demonstration 1.6.1. Voltmeter Reading Induced by Magnetic Induction

The rectangular coil shown in Fig. 1.6.4 is used to measure the magnetic field intensity associated with current in a wire. Thus, the arrangement and field are the same as in Demonstration 1.4.1. The height and length of the coil are h and l as shown, and because the coil has N turns, it links the flux enclosed by one turn N times. With the upper conductors of the coil at a distance R from the wire, and the magnetic field intensity taken as that of a line current, given by (1.4.10), evaluation of (8) gives

$$\lambda_f = \mu_o N \int_z^{z+l} \int_R^{R+h} \frac{i}{2\pi r} dr dz = \left[\frac{\mu_o N l}{2\pi} ln\left(1 + \frac{h}{R}\right) \right] i \tag{9}$$

In the experiment, the current takes the form

$$i = I \sin \omega t \tag{10}$$

where $\omega = 2\pi(60)$. The EMF between the terminals then follows from (8) and (9) as

$$v = V_o ln\Big(1 + \frac{h}{R}\Big)\cos\omega t; \qquad V_o \equiv \frac{\mu_o N l \omega I}{2\pi} \tag{11}$$

A voltmeter reads the electromotive force between the two points to which it is connected, provided certain conditions are satisfied. We will discuss these in Chap. 8.

In a typical experiment using a 20-turn coil with dimensions of $h = 8$ cm, $l = 20$ cm, $I = 6$ amp peak, the peak voltage measured at the terminals with a spacing $R = 8$ cm is $v = 1.35$ mV. To put this data point on the normalized plot of Fig. 1.6.4, note that $R/h = 1$ and the measured $v/V_o = 0.7$.

Faraday's Continuity Condition. It follows from Faraday's integral law that the tangential electric field is continuous across a surface of discontinuity, provided that the magnetic field intensity is finite in the neighborhood of the surface of discontinuity. This can be shown by applying the integral law to the incremental surface shown in Fig. 1.4.7, much as was done in Sec. 1.4 for Ampère's law. With $\mathbf{J}$ set equal to zero, there is a formal analogy between Ampère's integral law, (1.4.1), and Faraday's integral law, (1). The former becomes the latter if $\mathbf{H} \to \mathbf{E}$, $\mathbf{J} \to \mathbf{0}$, and $\epsilon_o \mathbf{E} \to -\mu_o \mathbf{H}$. Thus, Ampère's continuity condition (1.4.16) becomes the continuity condition associated with Faraday's law.

$$\boxed{\mathbf{n} \times (\mathbf{E}^a - \mathbf{E}^b) = 0} \tag{12}$$

At a surface having the unit normal $\mathbf{n}$, the tangential electric field intensity is continuous.

1.7 GAUSS' INTEGRAL LAW OF MAGNETIC FLUX

The net magnetic flux out of any region enclosed by a surface S must be zero.

$$\boxed{\oint_S \mu_o \mathbf{H} \cdot d\mathbf{a} = 0} \tag{1}$$

This property of flux density is almost implicit in Faraday's law. To see this, consider that law, (1.6.1), applied to a closed surface S. Such a surface is obtained from an open one by letting the contour shrink to zero, as in Fig. 1.5.1. Then Faraday's integral law reduces to

$$\frac{d}{dt} \oint_S \mu_o \mathbf{H} \cdot \mathbf{da} = \mathbf{0} \tag{2}$$

Gauss' law (1) adds to Faraday's law the empirical fact that in the beginning, there was no closed surface sustaining a net outward magnetic flux.

Illustration. Uniqueness of Flux Linking Coil

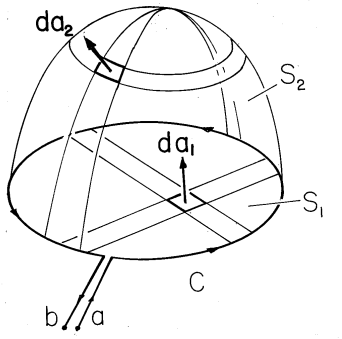


Fig. 1.7.1 Contour C follows loop of wire having terminals $a - b$. Because each has the same enclosing contour, the net magnetic flux through surfaces S_1 and S_2 must be the same.

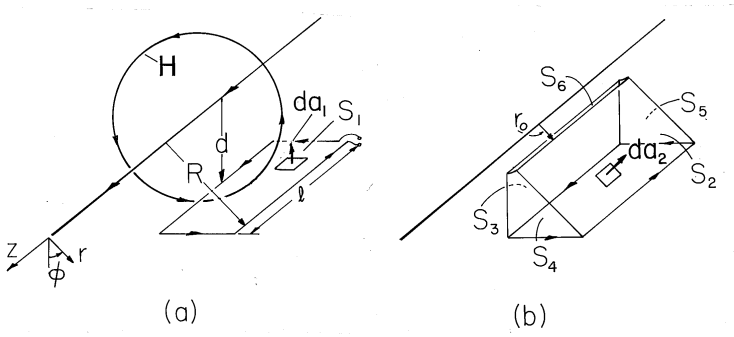


Fig. 1.7.2 (a) The field of a line current induces a flux in a horizontal rectangular coil. (b) The open surface has the coil as an enclosing contour. Rather than being in the plane of the contour, this surface is composed of the five segments shown.

An example is shown in Fig. 1.7.1. Here a wire with terminals $a - b$ follows the contour C. According to (1.6.8), the terminal EMF is found by integrating the normal magnetic flux density over a surface having C as its edge. But which surface? Figure 1.7.1 shows two of an infinite number of possibilities.

The terminal EMF can be unique only if the integrals over S_1 and S_2 result in the same answer. Taken together, S_1 and S_2 form a closed surface. The magnetic flux continuity integral law, (1), requires that the net flux out of this closed surface be zero. This is equivalent to the statement that the flux passing through S_1 in the direction of $d\mathbf{a}_1$ must be equal to that passing through S_2 in the direction of $d\mathbf{a}_2$. We will formalize this statement in Chap. 8.

Example 1.7.1. Magnetic Flux Linked by Coil and Flux Continuity

In the configuration of Fig. 1.7.2, a line current produces a magnetic field intensity that links a one-turn coil. The left conductor in this coil is directly below the wire at a distance d. The plane of the coil is horizontal. Nevertheless, it is convenient to specify the position of the right conductor in terms of a distance R from the line current. What is the net flux linked by the coil?

The most obvious surface to use is one in the same plane as the coil. However,

in doing so, account must be taken of the way in which the unit normal to the surface varies in direction relative to the magnetic field intensity. Selection of another surface, to which the magnetic field intensity is either normal or tangential, simplifies the calculation. On surfaces S_2 and S_3, the normal direction is the direction of the magnetic field. Note also that because the field is tangential to the end surfaces, S_4 and S_5, these make no contribution. For the same reason, there is no contribution from S_6, which is at the radius r_o from the wire. Thus,

$$\lambda_f \equiv \int_S \mu_o \mathbf{H} \cdot d\mathbf{a} = \int_{S_2} \mu_o \mathbf{H} \cdot d\mathbf{a} + \int_{S_3} \mu_o \mathbf{H} \cdot d\mathbf{a} \tag{3}$$

On S_2 the unit normal is $\mathbf{i}_\phi$, while on S_3 it is $-\mathbf{i}_\phi$. Therefore, (3) becomes

$$\lambda_f = \int_0^l \int_{r_o}^R \mu_o H_\phi dr dz - \int_0^l \int_{r_o}^d \mu_o H_\phi dr dz \tag{4}$$

With the field intensity for a line current given by (1.4.10), it follows that

$$\lambda_f = \frac{\mu_o li}{2\pi}\left(ln\frac{R}{r_o} - ln\frac{d}{r_o}\right) = \mu_o \frac{li}{2\pi} ln\left(\frac{R}{d}\right) \tag{5}$$

That r_o does not appear in the answer is no surprise, because if the surface S_1 had been used, r_o would not have been brought into the calculation.

Magnetic Flux Continuity Condition. With the charge density set equal to zero, the magnetic continuity integral law (1) takes the same form as Gauss' integral law (1.3.1). Thus, Gauss' continuity condition (1.3.17) becomes one representing the magnetic flux continuity law by making the substitution $\epsilon_o \mathbf{E} \rightarrow \mu_o \mathbf{H}$.

$$\boxed{\mathbf{n} \cdot (\mu_o \mathbf{H}^a - \mu_o \mathbf{H}^b) = 0} \tag{6}$$

The magnetic flux density normal to a surface is continuous.

1.8 SUMMARY

Electromagnetic fields, whether they be inside a transistor, on the surfaces of an antenna or in the human nervous system, are defined in terms of the forces they produce. In every example involving electromagnetic fields, charges are moving somewhere in response to electromagnetic fields. Hence, our starting point in this introductory chapter is the Lorentz force on an elementary charge, (1.1.1). Represented by this law is the effect of the field on the charge and current (charge in motion).

The subsequent sections are concerned with the laws that predict how the field sources, the charge, and current densities introduced in Sec. 1.2, in turn give rise to the electric and magnetic fields. Our presentation is aimed at putting these

laws to work. Hence, the empirical origins of these laws that would be evident from a historical presentation might not be fully appreciated. Elegant as they appear, Maxwell's equations are no more than a summary of experimental results. Each of our case studies is a potential test of the basic laws.

In the interest of being able to communicate our subject, each of the basic laws is given a name. In the interest of learning our subject, each of these laws should now be memorized. A summary is given in Table 1.8.1. By means of the examples and demonstrations, each of these laws should be associated with one or more physical consequences.

From the Lorentz force law and Maxwell's integral laws, the units of variables and constants are established. For the SI units used here, these are summarized in Table 1.8.2. Almost every practical result involves the free space permittivity ϵ_o and/or the free space permeability μ_o. Although these are summarized in Table 1.8.2, confidence also comes from having these natural constants memorized.

A common unit for measuring the magnetic flux density is the Gauss, so the conversion to the SI unit of Tesla is also given with the abbreviations.

A goal in this chapter has also been the use of examples to establish the mathematical significance of volume, surface, and contour integrations. At the same time, important singular source distributions have been defined and their associated fields derived. We will make extensive use of point, line, and surface sources and the associated fields.

In dealing with surface sources, a continuity condition should be associated with each of the integral laws. These are summarized in Table 1.8.3.

The continuity conditions should always be associated with the integral laws from which they originate. As terms are added to the integral laws to account for macroscopic media, there will be corresponding changes in the continuity conditions.

REFERENCES

[1] M. Faraday, **Experimental Researches in Electricity**, R. Taylor Publisher (1st-9th series), 1832-1835, 1 volume, various pagings; "From the Philosophical Transactions 1832-1835," London, England.

[2] J.C. Maxwell, **A Treatise on Electricity and Magnetism**, 3rd ed., 1891, reissued by Dover, N.Y. (1954).

TABLE 1.8.1

SUMMARY OF MAXWELL'S INTEGRAL LAWS IN FREE SPACE

NAME	INTEGRAL LAW	EQ. NUMBER
Gauss' Law	$\oint_S \epsilon_o \mathbf{E} \cdot d\mathbf{a} = \int_V \rho dv$	1.3.1
Ampere's Law	$\oint_C \mathbf{H} \cdot d\mathbf{s} = \int_S \mathbf{J} \cdot d\mathbf{a} + \frac{d}{dt} \int_S \epsilon_o \mathbf{E} \cdot d\mathbf{a}$	1.4.1
Faraday's Law	$\oint_C \mathbf{E} \cdot d\mathbf{s} = -\frac{d}{dt} \int_S \mu_o \mathbf{H} \cdot d\mathbf{a}$	1.6.1
Magnetic Flux Continuity	$\oint_S \mu_o \mathbf{H} \cdot d\mathbf{a} = 0$	1.7.1
Charge Conservation	$\oint_S \mathbf{J} \cdot d\mathbf{a} + \frac{d}{dt} \int_V \rho dv = 0$	1.5.2

TABLE 1.8.2

DEFINITIONS AND UNITS OF FIELD VARIABLES AND CONSTANTS

(basic unit of mass, kg, is replaced by V-C-s^2/m^2)

VARIABLE OR PARAMETER	NOMENCLATURE	BASIC UNITS	DERIVED UNITS
Electric Field Intensity	$\mathbf{E}$	V/m	V/m
Electric Displacement Flux Density	$\epsilon_o\mathbf{E}$	C/m^2	C/m^2
Charge Density	ρ	C/m^3	C/m^3
Surface Charge Density	σ_s	C/m^2	C/m^2
Magnetic Field Intensity	$\mathbf{H}$	C/(ms)	A/m
Magnetic Flux Density	$\mu_o\mathbf{H}$	Vs/m^2	T
Current Density	$\mathbf{J}$	C/(m^{2}s)	A/m^2
Surface Current Density	$\mathbf{K}$	C/(ms)	A/m
Free Space Permittivity	$\epsilon_o = 8.854 \times 10^{-12}$	C/(Vm)	F/m
Free Space Permeability	$\mu_o = 4\pi \times 10^{-7}$	Vs^2/(Cm)	H/m

UNIT ABBREVIATIONS

Ampère	A	Kilogram	kg	Volt	V
Coulomb	C	Meter	m		
Farad	F	Second	s		
Henry	H	Tesla	T (10^4 Gauss)		

TABLE 1.8.3
SUMMARY OF CONTINUITY CONDITIONS IN FREE SPACE

NAME	CONTINUITY CONDITION	EQ. NUMBER
Gauss' Law	$\mathbf{n}\cdot(\epsilon_o\mathbf{E}^a-\epsilon_o\mathbf{E}^b)=\sigma_s$	1.3.17
Ampère's Law	$\mathbf{n}\times(\mathbf{H}^a-\mathbf{H}^b)=\mathbf{K}$	1.4.16
Faraday's Law	$\mathbf{n}\times(\mathbf{E}^a-\mathbf{E}^b)=0$	1.6.14
Magnetic Flux Continuity	$\mathbf{n}\cdot(\mu_o\mathbf{H}^a-\mu_o\mathbf{H}^b)=0$	1.7.6
Charge Conservation	$\mathbf{n}\cdot(\mathbf{J}^a-\mathbf{J}^b)+\frac{\partial\sigma_s}{\partial t}=0$	1.5.12

PROBLEMS

1.1 The Lorentz Law in Free Space*

1.1.1* Assuming in Example 1.1.1 that $v_i = 0$ and that $E_x < 0$, show that by the time the electron has reached the position $x = h$, its velocity is $\sqrt{-2eE_xh/m}$. In an electric field of only $E_x = 1\text{v/cm} = 10^{-2}$ v/m, show that by the time it reaches $h = 10^{-2}$ m, the electron has reached a velocity of 5.9×10^3 m/s.

1.1.2 An electron moves in vacuum under the same conditions as in Example 1.1.1 except that the electric field takes the form $\mathbf{E} = E_x\mathbf{i_x} + E_y\mathbf{i_y}$ where E_x and E_y are given constants. When $t = 0$, the electron is at $\xi_x = 0$ and $\xi_y = 0$ and the velocity $d\xi_x/dt = v_i$ and $d\xi_y/dt = 0$.

(a) Determine $\xi_x(t)$ and $\xi_y(t)$.
(b) For $E_x > 0$, when and where does the electron return to the plane $x = 0$?

1.1.3* An electron, having velocity $\mathbf{v} = v_i\mathbf{i_z}$, experiences the field $\mathbf{H} = H_o\mathbf{i_y}$ and $\mathbf{E} = E_o\mathbf{i_x}$, where H_o and E_o are constants. Show that the electron retains this velocity if $E_o = v_i\mu_oH_o$.

1.1.4 An electron has the initial position $x = 0$, $y = 0$, $z = z_o$. It has an initial velocity $\mathbf{v} = v_o\mathbf{i_x}$ and moves in the uniform and constant fields $\mathbf{E} = E_o\mathbf{i_y}$, $\mathbf{H} = H_o\mathbf{i_y}$.

(a) Determine the position of the electron in the y direction, $\xi_y(t)$.
(b) Describe the trajectory of the electron.

1.2 Charge and Current Densities

1.2.1* The charge density is $\rho_o r/R$ coulomb/m^3 throughout the volume of a spherical region having radius R, with ρ_o a constant and r the distance from the center of the region (the radial coordinate in spherical coordinates). Show that the total charge associated with this charge density is $q = \pi\rho_oR^3$ coulomb.

1.2.2 In terms of given constants ρ_o and a, the net charge density is $\rho = (\rho_o/a^2)(x^2 + y^2 + z^2)$ coulomb/m^3. What is the total charge q (coulomb) in the cubical region $-a < x < a$, $-a < y < a$, $-a < z < a$?

* An asterisk on a problem number designates a "show that" problem. These problems are especially designed for self study.

1.2.3* With J_o and a given constants, the current density is $\mathbf{J} = (J_o/a^2)(y^2 + z^2)[\mathbf{i_x} + \mathbf{i_y} + \mathbf{i_z}]$. Show that the total current i passing through the surface $x = 0,\ -a < y < a,\ -a < z < a$ is $i = 8J_o a^2/3$ amp.

1.2.4 In cylindrical coordinates (r, ϕ, z) the current density is given in terms of constants J_o and a by $\mathbf{J} = J_o(r/a)^2\mathbf{i_z}$ (amp/m^2). What is the net current i (amp) through the surface $z = 0,\ r < a$?

1.2.5* In cylindrical coordinates, the electric field in the annular region $b < r < a$ is $\mathbf{E} = \mathbf{i_r}E_o(b/r)$, where E_o is a given negative constant. When $t = 0$, an electron having mass m and charge $q = -e$ has no velocity and is positioned at $r = \xi_r = b$.

(a) Show that, in vacuum, the radial motion of the electron is governed by the differential equation $m dv_r/dt = -eE_o b/\xi_r$, where $v_r = d\xi_r/dt$. Note that these expressions combine to provide one second-order differential equation governing ξ_r.

(b) By way of providing one integration of this equation, multiply the first of the first-order expressions by v_r and (with the help of the second first-order expression) show that the resulting equation can be written as $d[\frac{1}{2}mv_r^2 + eE_o b\ ln\xi_r]/dt = 0$. That is, the sum of the kinetic and potential energies (the quantity in brackets) remains constant.

(c) Use the result of (b) to find the electron velocity $v_r(r)$.

(d) Assume that this is one of many electrons that flow radially outward from the cathode at $r = b$ to $r = a$ and that the number of electrons passing radially outward at any location r is independent of time. The system is in the steady state so that the net current flowing outward through a surface of radius r and length l, $i = 2\pi r l J_r$, is the same at one radius r as at another. Use this fact to determine the charge density $\rho(r)$.

1.3 Gauss' Integral Law

1.3.1* Consider how Gauss' integral law, (1), is evaluated for a surface that is not naturally symmetric. The charge distribution is the uniform line charge of Fig. 1.3.7 and hence $\mathbf{E}$ is given by (13). However, the surface integral on the left in (1) is to be evaluated using a surface that has unit length in the z direction and a square cross-section centered on the z axis. That is, the surface is composed of the planes $z = 0,\ z = 1,\ x = \pm a$, and $y = \pm a$. Thus, we know from evaluation of the right-hand side of (1) that evaluation of the surface integral on the left should give the line charge density λ_l.

(a) Show that the area elements $d\mathbf{a}$ on these respective surfaces are $\pm\mathbf{i_z}dxdy$, $\pm\mathbf{i_x}dydz$, and $\pm\mathbf{i_y}dxdz$.

(b) Starting with (13), show that in Cartesian coordinates, $\mathbf{E}$ is

$$\mathbf{E} = \frac{\lambda_l}{2\pi\epsilon_o}\left(\frac{x}{x^2+y^2}\mathbf{i_x} + \frac{y}{x^2+y^2}\mathbf{i_y}\right) \tag{a}$$

(Standard Cartesian and cylindrical coordinates are defined in Table I at the end of the text.)

(c) Show that integration of $\epsilon_o\mathbf{E}\cdot d\mathbf{a}$ over the part of the surface at $x = a$ leads to the integral

$$\int \epsilon_o\mathbf{E}\cdot d\mathbf{a} = \frac{\lambda_l}{2\pi}\int_0^1\int_{-a}^{a}\frac{a}{a^2+y^2}dydz \tag{b}$$

(d) Finally, show that integration over the entire closed surface indeed gives λ_l.

1.3.2 Using the spherical symmetry and a spherical surface, the electric field associated with the point charge q of Fig. 1.3.6 is found to be given by (12). Evaluation of the left-hand side of (1) over any other surface that encloses the point charge must also give q. Suppose that the closed surface S is composed of a hemisphere of radius a in the upper half-plane, a hemisphere of radius b in the lower half-plane, and a washer-shaped flat surface that joins the two. In spherical coordinates (defined in Table I), these three parts of the closed surface S are defined by $(r = a,\ 0 < \theta < \frac{1}{2}\pi,\ 0 \le \phi < 2\pi)$, $(r = b, \frac{1}{2}\pi < \theta < \pi,\ 0 \le \phi < 2\pi)$, and $(\theta = \frac{1}{2}\pi,\ b \le r \le a,\ 0 \le \phi < 2\pi)$. For this surface, use (12) to evaluate the left-hand side of (1) and show that it results in q.

1.3.3* A cylindrically symmetric charge configuration extends to infinity in the $\pm z$ directions and has the same cross-section in any constant z plane. Inside the radius b, the charge density has a parabolic dependence on radius while over the range $b < r < a$ outside that radius, the charge density is zero.

$$\rho = \begin{cases} \rho_o(r/b)^2; & r < b \\ 0; & b < r < a \end{cases} \tag{a}$$

There is no surface charge density at $r = b$.

(a) Use the axial symmetry and Gauss' integral law to show that $\mathbf{E}$ in the two regions is

$$\mathbf{E} = \begin{cases} (\rho_o r^3/4\epsilon_o b^2)\mathbf{i_r}; & r < b \\ (\rho_o b^2/4\epsilon_o r)\mathbf{i_r}; & b < r < a \end{cases} \tag{b}$$

(b) Outside a shell at $r = a$, $\mathbf{E} = 0$. Use (17) to show that the surface charge density at $r = a$ is

$$\sigma_s = -\rho_o b^2/4a \tag{c}$$

(c) Integrate this charge per unit area over the surface of the shell and show that the resulting charge per unit length on the shell is the negative of the charge per unit length inside.
(d) Show that, in Cartesian coordinates, $\mathbf{E}$ is

$$\mathbf{E} = \frac{\rho_o}{4\epsilon_o} \begin{cases} [x(x^2+y^2)/b^2]\mathbf{i_x} + [y(x^2+y^2)/b^2]\mathbf{i_y}; & r < b \\ b^2 x(x^2+y^2)^{-1}\mathbf{i_x} + b^2 y(x^2+y^2)^{-1}\mathbf{i_y}; & b < r < a \end{cases} \tag{d}$$

Note that ($r = \sqrt{x^2+y^2},\ \cos\phi = x/r,\ \sin\phi = y/r,\ \mathbf{i_r} = \mathbf{i_x}\cos\phi + \mathbf{i_y}\sin\phi$) and the result takes the form $\mathbf{E} = E_x(x,y)\mathbf{i_x} + E_y(x,y)\mathbf{i_y}$.
(e) Now, imagine that the circular cylinder of charge in the region $r < b$ is enclosed by a cylindrical surface of square cross-section with the z coordinate as its axis and unit length in the z direction. The walls of this surface are at $x = \pm c,\ y = \pm c$ and $z = 0$ and $z = 1$. (To be sure that the cylinder of the charge distribution is entirely within the surface, $b < r < a,\ b < c < a/\sqrt{2}$.) Show that the surface integral on the left in (1) is

$$\oint_S \epsilon_o \mathbf{E}\cdot d\mathbf{a} = \frac{\rho_o b^2}{4}\left\{ \int_{-c}^{c} \left[\frac{c}{c^2+y^2} - \frac{(-c)}{c^2+y^2}\right] dy + \int_{-c}^{c} \left[\frac{c}{x^2+c^2} - \frac{(-c)}{x^2+c^2}\right] dx \right\} \tag{e}$$

Without carrying out these integrations, what is the answer?

1.3.4 In a spherically symmetric configuration, the region $r < b$ has the uniform charge density ρ_b and is surrounded by a region $b < r < a$ having the uniform charge density ρ_a. At $r = b$ there is no surface charge density, while at $r = a$ there is that surface charge density that assures $\mathbf{E} = 0$ for $a < r$.

(a) Determine $\mathbf{E}$ in the two regions.
(b) What is the surface charge density at $r = a$?
(c) Now suppose that there is a surface charge density given at $r = b$ of $\sigma_s = \sigma_o$. Determine $\mathbf{E}$ in the two regions and σ_s at $r = a$.

1.3.5* The region between the plane parallel sheets of surface charge density shown in Fig. 1.3.8 is filled with a charge density $\rho = 2\rho_o z/s$, where ρ_o is a given constant. Again, assume that the electric field below the lower sheet is $E_o\mathbf{i_z}$ and show that between the sheets

$$E_z = E_o - \frac{\sigma_o}{\epsilon_o} + \frac{\rho_o}{\epsilon_o s}\left[z^2 - (s/2)^2\right] \tag{a}$$

1.3.6 In a configuration much like that of Fig. 1.3.8, there are three rather than two sheets of charge. One, in the plane $z = 0$, has the given surface charge density σ_o. The second and third, respectively located at $z = s/2$ and

$z = -s/2$, have unknown charge densities σ_a and σ_b. The electric field outside the region $-\frac{1}{2}s < z < \frac{1}{2}s$ is zero, and $\sigma_a = 2\sigma_b$. Determine σ_a and σ_b.

1.3.7 Particles having charges of the same sign are constrained in their positions by a plastic tube which is tilted with respect to the horizontal by the angle α, as shown in Fig. P1.3.7. Given that the lower particle has charge Q_o and is fixed, while the upper one (which has charge Q and mass M) is free to move without friction, at what relative position, ξ, can the upper particle be in a state of static equilibrium?

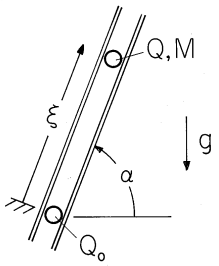


Fig. P1.3.7

1.4 Ampère's Integral Law

1.4.1* A static H field is produced by the cylindrically symmetric current density distribution $\mathbf{J} = J_o \exp(-r/a)\mathbf{i_z}$, where J_o and a are constants and r is the radial cylindrical coordinate. Use the integral form of Ampère's law to show that

$$H_\phi = \frac{J_o a^2}{r}\left[1 - e^{-r/a}\left(1 + \frac{r}{a}\right)\right] \qquad (a)$$

1.4.2* In polar coordinates, a uniform current density $J_o\mathbf{i_z}$ exists over the cross-section of a wire having radius b. This current is returned in the $-z$ direction as a uniform surface current at the radius $r = a > b$.

(a) Show that the surface current density at $r = a$ is

$$\mathbf{K} = -(J_o b^2/2a)\mathbf{i_z} \qquad (a)$$

(b) Use the integral form of Ampère's law to show that $\mathbf{H}$ in the regions $0 < r < b$ and $b < r < a$ is

$$\mathbf{H} = \begin{cases} (J_o r/2)\mathbf{i}_\phi; & r < b \\ (J_o b^2/2r)\mathbf{i}_\phi; & b < r < a \end{cases} \qquad (b)$$

(c) Use Ampère's continuity condition, (16), to show that $\mathbf{H} = 0$ for $r > a$.

(d) Show that in Cartesian coordinates, $\mathbf{H}$ is

$$\mathbf{H} = \frac{J_o}{2}\begin{cases} -y\mathbf{i_x} + x\mathbf{i_y}; & r < b \\ -b^2 y(x^2+y^2)^{-1}\mathbf{i_x} + b^2 x(x^2+y^2)^{-1}\mathbf{i_y}; & b < r < a \end{cases} \qquad (c)$$

(e) Suppose that the inner cylinder is now enclosed by a contour C that encloses a square surface in a constant z plane with edges at $x = \pm c$ and $y = \pm c$ (so that C is in the region $b < r < a,\ b < c < a/\sqrt{2}$). Show that the contour integral on the left in (1) is

$$\oint_C \mathbf{H}\cdot d\mathbf{s} = \int_{-c}^{c} \frac{J_o b^2}{2}\left(\frac{c}{c^2+y^2} - \frac{(-c)}{c^2+y^2}\right)dy + \int_{-c}^{c} \frac{J_o b^2}{2}\left(\frac{c}{x^2+c^2} - \frac{(-c)}{x^2+c^2}\right)dx \qquad (d)$$

Without carrying out the integrations, use Ampère's integral law to deduce the result of evaluating (d).

1.4.3 In a configuration having axial symmetry about the z axis and extending to infinity in the $\pm z$ directions, a line current I flows in the $-z$ direction along the z axis. This current is returned uniformly in the $+z$ direction in the region $b < r < a$. There is no current density in the region $0 < r < b$ and there are no surface current densities.

(a) In terms of I, what is the current density in the region $b < r < a$?
(b) Use the symmetry of the configuration and the integral form of Ampère's law to deduce $\mathbf{H}$ in the regions $0 < r < b$ and $b < r < a$.
(c) Express $\mathbf{H}$ in each region in Cartesian coordinates.
(d) Now, consider the evaluation of the left-hand side of (1) for a contour C that encloses a square surface S having sides of length $2c$ and the z axis as a perpendicular. That is, C lies in a constant z plane and has sides $x = \pm c$ and $y = \pm c$ with $c < a/\sqrt{2}$). In Cartesian coordinates, set up the line integral on the left in (1). Without carrying out the integrations, what must the answer be?

1.4.4* In a configuration having axial symmetry about the z axis, a line current I flows in the $-z$ direction along the z axis. This current is returned at the radii a and b, where there are uniform surface current densities K_{za} and K_{zb}, respectively. The current density is zero in the regions $0 < r < b,\ b < r < a$ and $a < r$.

(a) Given that $K_{za} = 2K_{zb}$, show that $K_{za} = I/\pi(2a+b)$.
(b) Show that $\mathbf{H}$ is

$$\mathbf{H} = -\frac{I}{2\pi}\mathbf{i}_\phi\begin{cases} 1/r; & 0 < r < b \\ 2a/r(2a+b); & b < r < a \end{cases} \qquad (a)$$

1.4.5 Uniform surface current densities $\mathbf{K} = \pm K_o \mathbf{i_y}$ are in the planes $z = \pm\frac{1}{2}s$, respectively. In the region $-\frac{1}{2}s < z < \frac{1}{2}s$, the current density is $\mathbf{J} = 2J_o z/s\mathbf{i_y}$. In the region $z < -\frac{1}{2}s$, $\mathbf{H} = 0$. Determine $\mathbf{H}$ for $-\frac{1}{2}s < z$.

1.5 Charge Conservation in Integral Form

1.5.1* In the region of space of interest, the charge density is uniform and a given function of time, $\rho = \rho_o(t)$. Given that the system has spherical symmetry, with r the distance from the center of symmetry, use the integral form of the law of charge conservation to show that the current density is

$$\mathbf{J} = -\frac{r}{3}\frac{d\rho_o}{dt}\mathbf{i_r} \qquad (a)$$

1.5.2 In the region $x > 0$, the charge density is known to be uniform and the given function of time $\rho = \rho_o(t)$. In the plane $x = 0$, the current density is zero. Given that it is x directed and only dependent on x and t, what is $\mathbf{J}$?

1.5.3* In the region $z > 0$, the current density $\mathbf{J} = 0$. In the region $z < 0$, $\mathbf{J} = J_o(x, y)\cos\omega t\mathbf{i_z}$, where J_o is a given function of (x, y). Given that when $t = 0$, the surface charge density $\sigma_s = 0$ over the plane $z = 0$, show that for $t > 0$, the surface charge density in the plane $z = 0$ is $\sigma_s(x, y, t) = [J_o(x, y)/\omega]\sin\omega t$.

1.5.4 In cylindrical coordinates, the current density $\mathbf{J} = 0$ for $r < R$, and $\mathbf{J} = J_o(\phi, z)\sin\omega t\mathbf{i_r}$ for $r > R$. The surface charge density on the surface at $r = R$ is $\sigma_s(\phi, z, t) = 0$ when $t = 0$. What is $\sigma_s(\phi, z, t)$ for $t > 0$?

1.6 Faraday's Integral Law

1.6.1* Consider the calculation of the circulation of $\mathbf{E}$, the left-hand side of (1), around a contour consisting of three segments enclosing a surface lying in the $x - y$ plane: from $(x, y) = (0, 0) \to (g, s)$ along the line $y = sx/g$; from $(x, y) = (g, s) \to (0, s)$ along $y = s$ and from $(x, y) = (0, s)$ to $(0, 0)$ along $x = 0$.

(a) Show that along the first leg, $d\mathbf{s} = [\mathbf{i_x} + (s/g)\mathbf{i_y}]dx$.
(b) Given that $\mathbf{E} = E_o\mathbf{i_y}$ where E_o is a given constant, show that the line integral along the first leg is sE_o and that the circulation around the closed contour is zero.

1.6.2 The situation is the same as in Prob. 1.6.1 except that the first segment of the closed contour is along the curve $y = s(x/g)^2$.

(a) Once again, show that for a uniform field $\mathbf{E} = E_o\mathbf{i_y}$, the circulation of $\mathbf{E}$ is zero.
(b) For $\mathbf{E} = E_o(x/g)\mathbf{i_y}$, what is the circulation around this contour?

1.6.3* The $\mathbf{E}$ field of a line charge density uniformly distributed along the z axis is given in cylindrical coordinates by (1.3.13).

(a) Show that in Cartesian coordinates, with $x = r\cos\phi$ and $y = r\sin\phi$,

$$\mathbf{E} = \frac{\lambda_l}{2\pi\epsilon_o}\left[\frac{x}{x^2+y^2}\mathbf{i_x} + \frac{y}{x^2+y^2}\mathbf{i_y}\right] \tag{a}$$

(b) For the contour shown in Fig. P1.6.3, show that

$$\oint_C \mathbf{E}\cdot d\mathbf{s} = \frac{\lambda_l}{2\pi\epsilon_o}\left[\int_k^g (1/x)dx + \int_0^h \frac{y}{g^2+y^2}dy - \int_k^g \frac{x}{x^2+h^2}dx - \int_0^h \frac{y}{k^2+y^2}dy\right] \tag{b}$$

and complete the integrations to prove that the circulation is zero.

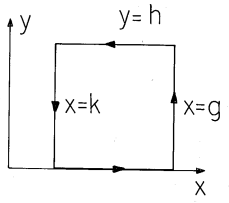


Fig. P1.6.3

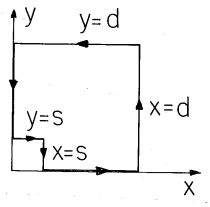


Fig. P1.6.4

1.6.4 A closed contour consisting of six segments is shown in Fig. P1.6.4. For the electric field intensity of Prob. 1.6.3, calculate the line integral of $\mathbf{E}\cdot d\mathbf{s}$ on each of these segments and show that the integral around the closed contour is zero.

1.6.5* The experiment in Fig. 1.6.4 is carried out with the coil positioned horizontally, as shown in Fig. 1.7.2. The left edge of the coil is directly below the wire, at a distance d, while the right edge is at the radial distance R from the wire, as shown. The area element $d\mathbf{a}$ is y directed (the vertical direction).

(a) Show that, in Cartesian coordinates, the magnetic field intensity due to the current i is

$$\mathbf{H} = \frac{i}{2\pi}\left(\frac{-\mathbf{i_x}y}{x^2+y^2} + \frac{\mathbf{i_y}x}{x^2+y^2}\right) \qquad (a)$$

(b) Use this field to show that the magnetic flux linking the coil is as given by (1.7.5).
(c) What is the circulation of $\mathbf{E}$ around the contour representing the coil?
(d) Given that the coil has N turns, what is the EMF measured at its terminals?

1.6.6 The magnetic field intensity is given to be $\mathbf{H} = H_o(t)(\mathbf{i_x} + \mathbf{i_y})$, where $H_o(t)$ is a given function of time. What is the circulation of $\mathbf{E}$ around the contour shown in Fig. P1.6.6?

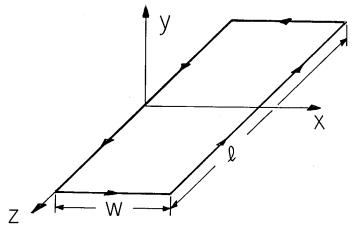


Fig. P1.6.6

1.6.7* In the plane $y = 0$, there is a uniform surface charge density $\sigma_s = \sigma_o$. In the region $y < 0$, $\mathbf{E} = E_1\mathbf{i_x} + E_2\mathbf{i_y}$ where E_1 and E_2 are given constants. Use the continuity conditions of Gauss and Faraday, (1.3.17) and (12), to show that just above the plane $y = 0$, where $y = 0^+$, the electric field intensity is $\mathbf{E} = E_1\mathbf{i_x} + [E_2 + (\sigma_o/\epsilon_o)]\mathbf{i_y}$.

1.6.8 Inside a circular cylindrical region having radius $r = R$, the electric field intensity is $\mathbf{E} = E_o\mathbf{i_y}$, where E_o is a given constant. There is a surface charge density $\sigma_o \cos\phi$ on the surface at $r = R$ (the polar coordinate ϕ is measured relative to the x axis). What is $\mathbf{E}$ just outside the surface, where $r = R^+$?

1.7 Integral Magnetic Flux Continuity Law

1.7.1* A region is filled by a uniform magnetic field intensity $H_o(t)\mathbf{i_z}$.

(a) Show that in spherical coordinates (defined in Fig. A.1.3 of Appendix 1), $\mathbf{H} = H_o(t)(\mathbf{i_r}\cos\theta - \mathbf{i}_\theta \sin\theta)$.
(b) A circular contour lies in the $z = 0$ plane and is at $r = R$. Using the enclosed surface in the plane $z = 0$ as the surface S, show that the circulation of $\mathbf{E}$ in the ϕ direction around C is $-\pi R^2 \mu_o dH_o/dt$.

(c) Now compute the same circulation using as a surface S enclosed by C the hemispherical surface at $r = R$, $0 \leq \theta < \frac{1}{2}\pi$.

1.7.2 With $H_o(t)$ a given function of time and d a given constant, three distributions of $\mathbf{H}$ are proposed.

$$\mathbf{H} = H_o(t)\mathbf{i_y} \tag{a}$$

$$\mathbf{H} = H_o(t)(x/d)\mathbf{i_x} \tag{b}$$

$$\mathbf{H} = H_o(t)(y/d)\mathbf{i_x} \tag{c}$$

Which one of these will not satisfy (1) for a surface S as shown in Fig. 1.5.3?

1.7.3* In the plane $y = 0$, there is a given surface current density $\mathbf{K} = K_o\mathbf{i_x}$. In the region $y < 0$, $\mathbf{H} = H_1\mathbf{i_y} + H_2\mathbf{i_z}$. Use the continuity conditions of (1.4.16) and (6) to show that just above the current sheet, where $y = 0^+$, $\mathbf{H} = (H_1 - K_o)\mathbf{i_y} + H_z\mathbf{i_z}$.

1.7.4 In the circular cylindrical surface $r = R$, there is a surface current density $\mathbf{K} = K_o\mathbf{i_z}$. Just inside this surface, where $r = R$, $\mathbf{H} = H_1\mathbf{i_r}$. What is $\mathbf{H}$ just outside the surface, where $r = R^+$?

2

MAXWELL'S DIFFERENTIAL LAWS IN FREE SPACE

2.0 INTRODUCTION

Maxwell's integral laws encompass the laws of electrical circuits. The transition from fields to circuits is made by associating the relevant volumes, surfaces, and contours with electrodes, wires, and terminal pairs. Begun in an informal way in Chap. 1, this use of the integral laws will be formalized and examined as the following chapters unfold. Indeed, many of the empirical origins of the integral laws are in experiments involving electrodes, wires and the like.

The remarkable fact is that the integral laws apply to any combination of volume and enclosing surface or surface and enclosing contour, whether associated with a circuit or not. This was implicit in our use of the integral laws for deducing field distributions in Chap. l.

Even though the integral laws can be used to determine the fields in highly symmetric configurations, they are not generally applicable to the analysis of realistic problems. Reasons for this lie beyond the geometric complexity of practical systems. Source distributions are not generally known, even when materials are idealized as insulators and "perfect" conductors. In actual materials, for example, those having finite conductivity, the self-consistent interplay of fields and sources, must be described.

Because they apply to *arbitrary* volumes, surfaces, and contours, the integral laws also contain the differential laws that apply at each point in space. The differential laws derived in this chapter provide a more broadly applicable basis for predicting fields. As might be expected, the point relations must involve information about the shape of the fields in the neighborhood of the point. Thus it is that the integral laws are converted to point relations by introducing partial derivatives of the fields with respect to the spatial coordinates.

The plan in this chapter is first to write each of the integral laws in terms of one type of integral. For example, in the case of Gauss' law, the surface integral is

converted to one over the volume V enclosed by the surface.

$$\int_V div(\epsilon_o \mathbf{E}) dv = \oint_S \epsilon_o \mathbf{E} \cdot d\mathbf{a} \tag{1}$$

Here *div* is some combination of spatial derivatives of $\epsilon_o \mathbf{E}$ to be determined in the next section. With this mathematical theorem accepted for now, Gauss' integral law, (1.3.1), can be written in terms of volume integrals.

$$\int_V div(\epsilon_o \mathbf{E}) dv = \int_V \rho dv \tag{2}$$

The desired differential form of Gauss' law is obtained by equating the integrands in this expression.

$$div(\epsilon_o \mathbf{E}) = \rho \tag{3}$$

Is it true that if two integrals are equal, their integrands are as well? In general, the answer is no! For example, if x^2 is integrated from 0 to 1, the result is the same as for an integration of $2x/3$ over the same interval. However, x^2 is hardly equal to $2x/3$ for every value of x.

It is because the volume V is arbitrary that we can equate the integrands in (1). For a one-dimensional integral, this is equivalent to having endpoints that are arbitrary. With the volume arbitrary (the endpoints arbitrary), the integrals can only be equal if the integrands are as well.

The equality of the three-dimensional volume integration on the left in (1) and the two-dimensional surface integration on the right is analogous to the case of a one-dimensional integral being equal to the function evaluated at the integration endpoints. That is, suppose that the operator *der* operates on $f(x)$ in such a way that

$$\int_{x_1}^{x_2} der(f) dx = f(x_2) - f(x_1) \tag{4}$$

The integration on the left over the "volume" interval between x_1 and x_2 is reduced by this "theorem" to an evaluation on the "surface," where $x = x_1$ and $x = x_2$.

The procedure for determining the operator *der* in (4) is analogous to that used to deduce the divergence and curl operators in Secs. 2.1 and 2.4, respectively. The point x at which *der* is to be evaluated is taken midway in the integration interval, as in Fig. 2.0.1. Then the interval is taken as incremental ($\Delta x = x_2 - x_1$) and for small Δx, (4) becomes

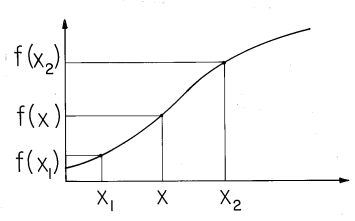


Fig. 2.0.1 General function of x defined between endpoints x_1 and x_2.

$$[der(f)]\Delta x = f(x_2) - f(x_1) \tag{5}$$

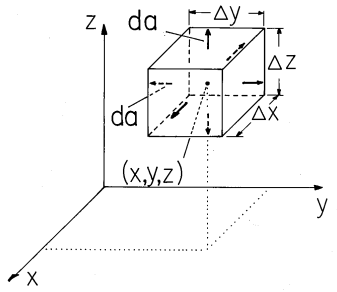


Fig. 2.1.1 Incremental volume element for determination of divergence operator.

It follows that

$$der = \lim_{\Delta x \to 0} \left[\frac{f\left(x + \frac{\Delta x}{2}\right) - f\left(x - \frac{\Delta x}{2}\right)}{\Delta x} \right] \tag{6}$$

Thus, as we knew to begin with, *der* is the derivative of f with respect to x.

Byproducts of the derivation of the divergence and curl operators in Secs. 2.1 and 2.4 are the integral theorems of Gauss and Stokes, derived in Secs. 2.2 and 2.5, respectively. A *theorem* is a mathematical relation and must be distinguished from a physical *law*, which establishes a physical relation among physical variables. The differential laws, together with the operators and theorems that are the point of this chapter, are summarized in Sec. 2.8.

2.1 THE DIVERGENCE OPERATOR

If Gauss' integral theorem, (1.3.1), is to be written with the surface integral replaced by a volume integral, then it is necessary that an operator be found such that

$$\int_V div\mathbf{A} dv = \oint_S \mathbf{A} \cdot d\mathbf{a} \tag{1}$$

With the objective of finding this *divergence operator*, *div*, (1) is applied to an incremental volume ΔV. Because the volume is small, the volume integral on the left can be taken as the product of the integrand and the volume. Thus, the divergence of a vector $\mathbf{A}$ is defined in terms of the limit of a surface integral.

$$div\mathbf{A} \equiv \lim_{\Delta V \to 0} \frac{1}{\Delta V} \oint_S \mathbf{A} \cdot d\mathbf{a} \tag{2}$$

Once evaluated, it is a function of $\mathbf{r}$. That is, in the limit, the volume shrinks to zero in such a way that all points on the surface approach the point $\mathbf{r}$. With this condition satisfied, the actual shape of the volume element is arbitrary.

In Cartesian coordinates, a convenient incremental volume is a rectangular parallelepiped $\Delta x \Delta y \Delta z$ centered at (x, y, z), as shown in Fig. 2.1.1. With the limit where $\Delta x \Delta y \Delta z \to 0$ in view, the right-hand side of (2) is approximated by

$$\begin{aligned}\oint_S \mathbf{A}\cdot d\mathbf{a} \simeq\ & \Delta y\Delta z\big[A_x\big(x+\frac{\Delta x}{2},y,z\big)-A_x\big(x-\frac{\Delta x}{2},y,z\big)\big]\\ &+\Delta z\Delta x\big[A_y\big(x,y+\frac{\Delta y}{2},z\big)-A_y\big(x,y-\frac{\Delta y}{2},z\big)\big]\\ &+\Delta x\Delta y\big[A_z\big(x,y,z+\frac{\Delta z}{2}\big)-A_z\big(x,y,z-\frac{\Delta z}{2}\big)\big]\end{aligned} \tag{3}$$

With the above expression used to evaluate (2), along with $\Delta V=\Delta x\Delta y\Delta z$,

$$\begin{aligned}div\mathbf{A}=\ & \lim_{\Delta x\to 0}\left[\frac{A_x\big(x+\frac{\Delta x}{2},y,z\big)-A_x\big(x-\frac{\Delta x}{2},y,z\big)}{\Delta x}\right]\\ &+\lim_{\Delta y\to 0}\left[\frac{A_y\big(x,y+\frac{\Delta y}{2},z\big)-A_y\big(x,y-\frac{\Delta y}{2},z\big)}{\Delta y}\right]\\ &+\lim_{\Delta z\to 0}\left[\frac{A_z\big(x,y,z+\frac{\Delta z}{2}\big)-A_z\big(x,y,z-\frac{\Delta z}{2}\big)}{\Delta z}\right]\end{aligned} \tag{4}$$

It follows that in Cartesian coordinates, the divergence operator is

$$\boxed{div\mathbf{A}=\frac{\partial A_x}{\partial x}+\frac{\partial A_y}{\partial y}+\frac{\partial A_z}{\partial z}} \tag{5}$$

This result suggests an alternative notation. The *del* operator is defined as

$$\boxed{\nabla\equiv\mathbf{i_x}\frac{\partial}{\partial x}+\mathbf{i_y}\frac{\partial}{\partial y}+\mathbf{i_z}\frac{\partial}{\partial z}} \tag{6}$$

so that (5) can be written as

$$div\mathbf{A}=\nabla\cdot\mathbf{A} \tag{7}$$

The *div* notation suggests that this combination of derivatives describes the outflow of $\mathbf{A}$ from the neighborhood of the point of evaluation. The definition (2) is independent of the choice of a coordinate system. On the other hand, the *del* notation suggests the mechanics of the operation in Cartesian coordinates. We will have it both ways by using the *del* notation in writing equations in Cartesian coordinates, but using the name divergence in the text.

Problems 2.1.4 and 2.1.6 lead to the divergence operator in cylindrical and spherical coordinates, respectively (summarized in Table I at the end of the text), and provide the opportunity to develop the connection between the general definition, (2), and specific representations.

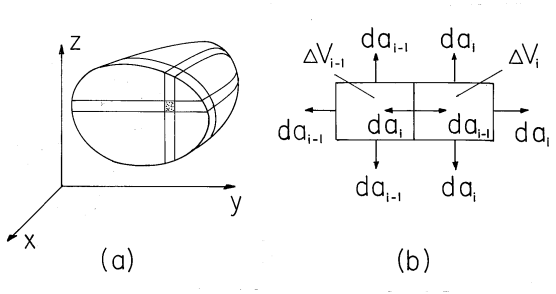


Fig. 2.2.1 (a) Three mutually perpendicular slices define an incremental volume in the volume V shown in cross-section. (b) Adjacent volume elements with common surface.

2.2 GAUSS' INTEGRAL THEOREM

The operator that is required for (2.1.1) to hold has been identified by considering an incremental volume element. But does the relation hold for volumes of finite size?

The volume enclosed by the surface S can be subdivided into differential elements, as shown in Fig. 2.2.1. Each of the elements has a surface of its own with the i-th being enclosed by the surface S_i. We now prove that the surface integral of the vector $\mathbf{A}$ over the surface S is equal to the sum of the surface integrals over each surface S

$$\oint_S \mathbf{A} \cdot d\mathbf{a} = \sum_i \Big[\int_{S_i} \mathbf{A} \cdot d\mathbf{a} \Big] \tag{1}$$

Note first that the surface normals of two surfaces between adjacent volume elements are oppositely directed, while the vector $\mathbf{A}$ has the same value for both surfaces. Thus, as illustrated in Fig. 2.2.1, the fluxes through surfaces separating two volume elements in the interior of S cancel.

The only contributions to the summation in (1) which do not cancel are the fluxes through the surfaces which do not separate one volume element from another, i.e., those surfaces that lie on S. But because these surfaces together form S, (1) follows. Finally, with the right-hand side rewritten, (1) is

$$\oint_S \mathbf{A} \cdot d\mathbf{a} = \sum_i \Big[\frac{\int_{S_i} \mathbf{A} \cdot d\mathbf{a}}{\Delta V_i} \Big] \Delta V_i \tag{2}$$

where ΔV_i is the volume of the i-th element. Because these volume elements are differential, what is in brackets on the right in (2) can be represented using the definition of the divergence operator, (2.1.2).

$$\oint_S \mathbf{A} \cdot d\mathbf{a} = \sum_i (\nabla \cdot \mathbf{A})_i \Delta V_i \tag{3}$$

Gauss' integral theorem follows by replacing the summation over the differential volume elements by an integration over the volume.

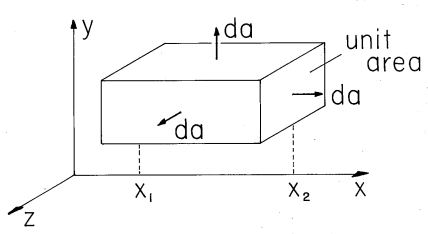


Fig. 2.2.2 Volume between planes $x = x_1$ and $x = x_2$ having unit area in $y - z$ planes.

$$\boxed{\oint_S \mathbf{A} \cdot d\mathbf{a} = \int_V \nabla \cdot \mathbf{A} dv} \tag{4}$$

Example 2.2.1. One-Dimensional Theorem

If the vector $\mathbf{A}$ is one-dimensional so that

$$\mathbf{A} = f(x)\mathbf{i}_x \tag{5}$$

what does Gauss' integral theorem say about an integration over a volume V between the planes $x = x_1$ and $x = x_2$ and of unit cross-section in any $y - z$ plane between these planes? The volume V and surface S are as shown in Fig. 2.2.2. Because $\mathbf{A}$ is x directed, the only contributions are from the right and left surfaces. These respectively have $d\mathbf{a} = \mathbf{i}_x dydz$ and $d\mathbf{a} = -\mathbf{i}_x dydz$. Hence, substitution into (4) gives the familiar form,

$$f(x_2) - f(x_1) = \int_{x_1}^{x_2} \frac{\partial f}{\partial x} dx \tag{6}$$

which is a reminder of the one-dimensional analogy discussed in the introduction. Gauss' theorem extends into three dimensions the relationship that exists between the derivative and integral of a function.

2.3 GAUSS' LAW, MAGNETIC FLUX CONTINUITY, AND CHARGE CONSERVATION

Of the five integral laws summarized in Table 1.8.1, three involve integrations over closed surfaces. By Gauss' theorem, (2.2.4), each of the surface integrals is now expressed as a volume integral. Because the volume is arbitrary, the integrands must vanish, and so the differential laws are obtained.

The *differential form of Gauss' law* follows from (1.3.1) in that table.

$$\boxed{\nabla \cdot \epsilon_o \mathbf{E} = \rho} \tag{1}$$

Magnetic flux continuity in differential form follows from (1.7.1).

$$\boxed{\nabla \cdot \mu_o \mathbf{H} = 0} \tag{2}$$

In the integral charge conservation law, (1.5.2), there is a time derivative. Because the geometry of the integral we are considering is fixed, the time derivative can be taken inside the integral. That is, the spatial integration can be carried out after the time derivative has been taken. But because ρ is not only a function of t but of (x, y, z) as well, the time derivative is taken holding (x, y, z) constant. Thus, the *differential charge conservation law* is stated using a partial time derivative.

$$\boxed{\nabla \cdot \mathbf{J} + \frac{\partial \rho}{\partial t} = 0} \tag{3}$$

These three differential laws are summarized in Table 2.8.1.

2.4 THE CURL OPERATOR

If the integral laws of Ampère and Faraday, (1.4.1) and (1.6.1), are to be written in terms of one type of integral, it is necessary to have an operator such that the contour integrals are converted to surface integrals. This operator is called the *curl*.

$$\int_S curl\ \mathbf{A} \cdot d\mathbf{a} = \oint_C \mathbf{A} \cdot d\mathbf{s} \tag{1}$$

The operator is identified by making the surface an incremental one, Δa. At the particular point $\mathbf{r}$ where the operator is to be evaluated, pick a direction $\mathbf{n}$ and construct a plane normal to $\mathbf{n}$ through the point $\mathbf{r}$. In this plane, choose a contour C around $\mathbf{r}$ that encloses the incremental area Δa. It follows from (1) that

$$(curl\ \mathbf{A})_n = \lim_{\Delta a \to 0} \frac{1}{\Delta a} \oint_C \mathbf{A} \cdot d\mathbf{s} \tag{2}$$

The shape of the contour C is arbitrary except that all its points are assumed to approach the point $\mathbf{r}$ under study in the limit $\Delta a \to 0$. Such an arbitrary elemental surface with its unit normal $\mathbf{n}$ is illustrated in Fig. 2.4.1a. The definition of the curl operator given by (2) is independent of the coordinate system.

To express (2) in Cartesian coordinates, consider the incremental surface shown in Fig. 2.4.1b. The center of Δa is at the location (x, y, z), where the operator is to be evaluated. The contour is composed of straight segments at $y \pm \Delta y/2$ and $z \pm \Delta z/2$. To first order in Δy and Δz, it follows that the $\mathbf{n} = \mathbf{i_x}$ component of (2) is

$$\begin{aligned}(curl\ \mathbf{A})_x = \lim_{\Delta y \Delta z \to 0} \frac{1}{\Delta y \Delta z} \Bigg\{ &\left[A_z\big(x, y + \frac{\Delta y}{2}, z\big) - A_z\big(x, y - \frac{\Delta y}{2}, z\big) \right] \Delta z \\ &- \left[A_y\big(x, y, z + \frac{\Delta z}{2}\big) - A_y\big(x, y, z - \frac{\Delta z}{2}\big) \right] \Delta y \Bigg\}\end{aligned} \tag{3}$$

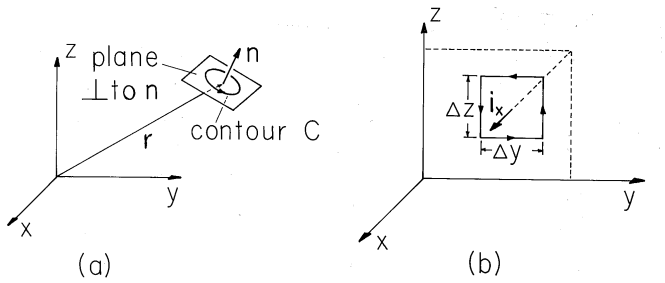


Fig. 2.4.1 (a) Incremental contour for evaluation of the component of the curl in the direction of **n**. (b) Incremental contour for evaluation of x component of curl in Cartesian coordinates.

Here the first two terms represent integrations along the vertical segments, first in the $+z$ direction and then in the $-z$ direction. Note that integration on this second leg results in a minus sign, because there, **A** is oppositely directed to $d\mathbf{s}$.

In the limit, (3) becomes

$$(curl\ \mathbf{A})_x = \frac{\partial A_z}{\partial y} - \frac{\partial A_y}{\partial z} \tag{4}$$

The same procedure, applied to elemental areas having normals in the y and z directions, result in three "components" for the *curl* operator.

$$\begin{aligned} curl\ \mathbf{A} = &\left(\frac{\partial A_z}{\partial y} - \frac{\partial A_y}{\partial z}\right)\mathbf{i_x} + \left(\frac{\partial A_x}{\partial z} - \frac{\partial A_z}{\partial x}\right)\mathbf{i_y} \\ &+ \left(\frac{\partial A_y}{\partial x} - \frac{\partial A_x}{\partial y}\right)\mathbf{i_z} \end{aligned} \tag{5}$$

In fact, we should be able to select the surface for evaluating (2) as having a unit normal **n** in any arbitrary direction. For (5) to be a vector, its dot product with **n** must give the same result as obtained for the direct evaluation of (2). This is shown to be true in Appendix 2.

The result of cross-multiplying **A** by the *del* operator, defined by (2.1.6), is the curl operator. This is the reason for the alternate notation for the curl operator.

$$curl\ \mathbf{A} = \nabla \times \mathbf{A} \tag{6}$$

Thus, in Cartesian coordinates

$$\boxed{\nabla \times \mathbf{A} = \begin{vmatrix} \mathbf{i_x} & \mathbf{i_y} & \mathbf{i_z} \\ \partial/\partial x & \partial/\partial y & \partial/\partial z \\ A_x & A_y & A_z \end{vmatrix}} \tag{7}$$

The problems give the opportunity to derive expressions having similar forms in cylindrical and spherical coordinates. The results are summarized in Table I at the end of the text.

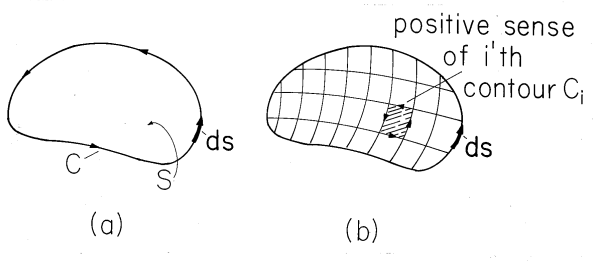


Fig. 2.5.1 Arbitrary surface enclosed by contour C is subdivided into incremental elements, each enclosed by a contour having the same sense as C.

2.5 STOKES' INTEGRAL THEOREM

In Sec. 2.4, *curl***A** was identified as that vector function which had an integral over a surface S that could be reduced to an integral on $\mathbf{A}$ over the enclosing contour C. This was done by applying (2.4.1) to an incremental surface. But does this relation hold for S and C of finite size and arbitrary shape?

The generalization to an arbitrary surface begins by subdividing S into differential area elements, each enclosed by a contour C . As shown in Fig. 2.5.1, each differential contour coincides in direction with the positive sense of the original contour. We shall now prove that

$$\oint_C \mathbf{A} \cdot d\mathbf{s} = \sum_i \oint_{C_i} \mathbf{A} \cdot d\mathbf{s} \tag{1}$$

where the sum is over all contours bounding the surface elements into which the surface S has been subdivided.

Because the segments are followed in opposite senses when evaluated for the adjacent area elements, line integrals along those segments of the contours which separate two adjacent surface elements add to zero in the sum of (1). Only those line integrals remain which pertain to the segments coinciding with the original contour. Hence, (1) is demonstrated.

Next, (1) is written in the slightly different form.

$$\oint_C \mathbf{A} \cdot d\mathbf{s} = \sum_i \left[\frac{1}{\Delta a_i} \oint_{C_i} \mathbf{A} \cdot d\mathbf{s} \right] \Delta a_i \tag{2}$$

We can now appeal to the definition of the component of the curl in the direction of the normal to the surface element, (2.4.2), and replace the summation by an integration.

$$\oint_C \mathbf{A} \cdot d\mathbf{s} = \int_S (curl\ \mathbf{A})_n da \tag{3}$$

Another way of writing this expression is to take advantage of the vector character of the *curl* and the definition of a vector area element, $d\mathbf{a} = \mathbf{n}da$:

$$\boxed{\oint_C \mathbf{A} \cdot d\mathbf{s} = \int_S \nabla \times \mathbf{A} \cdot d\mathbf{a}} \tag{4}$$

This is *Stokes' integral theorem*. If a vector function can be written as the *curl* of a vector $\mathbf{A}$, then the integral of that function over a surface S can be reduced to an integral of $\mathbf{A}$ on the enclosing contour C.

2.6 DIFFERENTIAL LAWS OF AMPÈRE AND FARADAY

With the help of Stokes' theorem, Ampère's integral law (1.4.1) can now be stated as

$$\int_S \nabla \times \mathbf{H} \cdot d\mathbf{a} = \int_S \mathbf{J} \cdot d\mathbf{a} + \frac{d}{dt} \int_S \epsilon_o \mathbf{E} \cdot d\mathbf{a} \tag{1}$$

That is, by virtue of (2.5.4), the contour integral in (1.4.1) is replaced by a surface integral. The surface S is fixed in time, so the time derivative in (1) can be taken inside the integral. Because S is also arbitrary, the integrands in (1) must balance.

$$\boxed{\nabla \times \mathbf{H} = \mathbf{J} + \frac{\partial \epsilon_o \mathbf{E}}{\partial t}} \tag{2}$$

This is the *differential form of Ampère's law*. In the last term, which is called the displacement current density, a partial time derivative is used to make it clear that the location (x, y, z) at which the expression is evaluated is held fixed as the time derivative is taken.

In Sec. 1.5, it was seen that the integral forms of Ampère's and Gauss' laws combined to give the integral form of the charge conservation law. Thus, we should expect that the differential forms of these laws would also combine to give the differential charge conservation law. To see this, we need the identity $\nabla \cdot (\nabla \times \mathbf{A}) = 0$ (Problem 2.4.5). Thus, the divergence of (2) gives

$$0 = \nabla \cdot \mathbf{J} + \frac{\partial}{\partial t}(\nabla \cdot \epsilon_o \mathbf{E}) \tag{3}$$

Here the time and space derivatives have been interchanged in the last term. By Gauss' differential law, (2.3.1), the time derivative is of the charge density, and so (3) becomes the differential form of charge conservation, (2.3.3). Note that we are taking a differential view of the interrelation between laws that parallels the integral developments of Sec. 1.5.

Finally, Stokes' theorem converts Faraday's integral law (1.6.1) to integrations over S only. It follows that the *differential form of Faraday's law* is

$$\boxed{\nabla \times \mathbf{E} = -\frac{\partial \mu_o \mathbf{H}}{\partial t}} \tag{4}$$

The differential forms of Maxwell's equations in free space are summarized in Table 2.8.1.

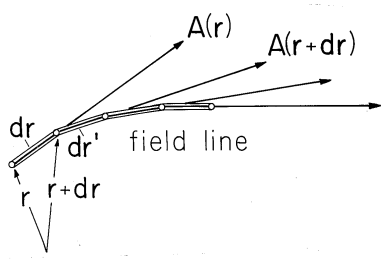


Fig. 2.7.1 Construction of field line.

2.7 VISUALIZATION OF FIELDS AND THE DIVERGENCE AND CURL

A three-dimensional vector field $\mathbf{A}(\mathbf{r})$ is specified by three components that are, individually, functions of position. It is difficult enough to plot a single scalar function in three dimensions; a plot of three is even more difficult and hence less useful for visualization purposes. Field lines are one way of picturing a field distribution.

A field line through a particular point $\mathbf{r}$ is constructed in the following way: At the point $\mathbf{r}$, the vector field has a particular direction. Proceed from the point $\mathbf{r}$ in the direction of the vector $\mathbf{A}(\mathbf{r})$ a differential distance $d\mathbf{r}$. At the new point $\mathbf{r} + d\mathbf{r}$, the vector has a new direction $\mathbf{A}(\mathbf{r} + d\mathbf{r})$. Proceed a differential distance $d\mathbf{r}'$ along this new (differentially different) direction to a new point, and so forth as shown in Fig. 2.7.1. By this process, a field line is traced out. The tangent to the field line at any one of its points gives the direction of the vector field $\mathbf{A}(\mathbf{r})$ at that point.

The magnitude of $\mathbf{A}(\mathbf{r})$ can also be indicated in a somewhat rough way by means of the field lines. The convention is used that the number of field lines drawn through an area element perpendicular to the field line at a point $\mathbf{r}$ is proportional to the magnitude of $\mathbf{A}(\mathbf{r})$ at that point. The field might be represented in three dimensions by wires.

If it has no divergence, a field is said to be *solenoidal*. If it has no curl, it is *irrotational*. It is especially important to conceptualize solenoidal and irrotational fields. We will discuss the nature of irrotational fields in the following examples, but become especially in tune with their distributions in Chap. 4. Consider now the "wire-model" picture of the solenoidal field.

Single out a surface with sides formed of a continuum of adjacent field lines, a "hose" of lines as shown in Fig. 2.7.2, with endfaces spanning across the ends of the hose. Then, because a solenoidal field can have no net flux out of this tube, the number of field lines entering the hose through one endface must be equal to the number of lines leaving the hose through the other end. Because the hose is picked arbitrarily, we conclude that a solenoidal field is represented by lines that are continuous; they do not appear or disappear within the region where they are solenoidal.

The following examples begin to develop an appreciation for the attributes of the field lines associated with the divergence and curl.

Example 2.7.1. Fields with Divergence but No Curl (Irrotational but Not Solenoidal)

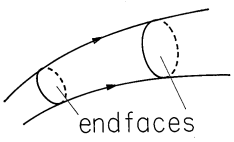


Fig. 2.7.2 Solenoidal field lines form hoses within which the lines neither begin nor end.

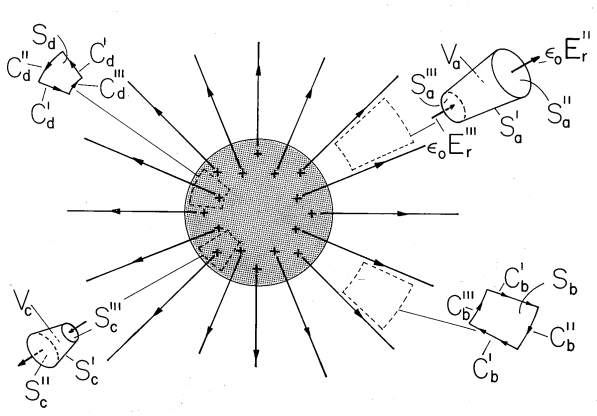


Fig. 2.7.3 Spherically symmetric field that is irrotational. Volume elements V_a and V_c are used with Gauss' theorem to show why field is solenoidal outside the sphere but has a divergence inside. Surface elements C_b and C_d are used with Stokes' theorem to show why fields are irrotational everywhere.

The spherical region $r < R$ supports a charge density $\rho = \rho_o r/R$. The exterior region is free of charge. In Example 1.3.1, the radially symmetric electric field intensity is found from the integral laws to be

$$\mathbf{E} = \mathbf{i_r} \frac{\rho_o}{4\epsilon_o} \begin{cases} \frac{r^2}{R}; & r < R \\ \frac{R^3}{r^2}; & r > R \end{cases} \tag{1}$$

In spherical coordinates, the divergence operator is (from Table I)

$$\nabla \cdot \mathbf{E} = \frac{1}{r^2}\frac{\partial}{\partial r}(r^2 E_r) + \frac{1}{r\sin\theta}\frac{\partial}{\partial \theta}(\sin\theta E_\theta) + \frac{1}{r\sin\theta}\frac{\partial E_\phi}{\partial \phi} \tag{2}$$

Thus, evaluation of Gauss' differential law, (2.3.1), gives

$$\epsilon_o \nabla \cdot \mathbf{E} = \begin{cases} \frac{\rho_o r}{R}; & r < R \\ 0; & r > R \end{cases} \tag{3}$$

which of course agrees with the charge distribution used in the original derivation. This exercise serves to emphasize that the differential laws apply point by point throughout the region.

The field lines can be sketched as in Fig. 2.7.3. The magnitude of the charge density is represented by the density of + (or −) symbols.

Where in this plot does the field have a divergence? Because the charge density has already been pictured, we already know the answer to this question. The field has divergence only where there is a charge density. Thus, even though the field lines are thinning out with increasing radius in the exterior region, at any given point in this region the field has no divergence. The situation in this region is typified by the flux of $\mathbf{E}$ through the "hose" defined by the volume V_a. The field does indeed decrease with radius, but the cross-sectional area of the hose increases so as to exactly compensate and maintain the net flux constant.

In the interior region, a volume element having the shape of a tube with sides parallel to the radial field can also be considered, volume V_c. That the field is not solenoidal is evident from the fact that its intensity is least over the cross-section of the tube having the least area. That there must be a net outward flux is evidence of the net charge enclosed. Field lines originate inside the volume on the enclosed charges.

Are the field lines in Fig. 2.7.3 irrotational? In spherical coordinates, the *curl* is

$$\begin{aligned}\nabla \times \mathbf{E} =& \mathbf{i_r} \frac{1}{r \sin\theta}\left[\frac{\partial}{\partial\theta}(E_\phi \sin\theta) - \frac{\partial E_\theta}{\partial\phi}\right] \\ &+ \mathbf{i}_\theta\left[\frac{1}{r\sin\theta}\frac{\partial E_r}{\partial\phi} - \frac{1}{r}\frac{\partial}{\partial r}(rE_\phi)\right] \\ &+ \mathbf{i}_\phi\left[\frac{1}{r}\frac{\partial}{\partial r}(rE_\theta) - \frac{1}{r}\frac{\partial E_r}{\partial\theta}\right]\end{aligned} \tag{4}$$

and it follows from a substitution of (1) that there is no curl, either inside or outside. This result is corroborated by evaluating the circulation of $\mathbf{E}$ for contours enclosing areas Δa having normals in any one of the coordinate directions. [Remember the definition of the *curl*, (2.4.2).] Examples are the contours enclosing the surfaces S_b and S_d in Fig. 2.7.3. Contributions to the C'' and C''' segments vanish because these are perpendicular to $\mathbf{E}$, while (because $\mathbf{E}$ is independent of ϕ and θ) the contribution from one C' segment cancels that from the other.

Example 2.7.2. Fields with Curl but No Divergence (Solenoidal but Not Irrotational)

A wire having radius R carries an axial current density that increases linearly with radius. Ampère's integral law was used in Example 1.4.1 to show that the associated magnetic field intensity is

$$\mathbf{H} = \mathbf{i}_\phi \frac{J_o}{3}\begin{cases} r^2/R; & r < R \\ R^2/r; & r > R \end{cases} \tag{5}$$

Where does this field have curl? The answer follows from Ampère's law, (2.6.2), with the displacement current neglected. The curl is the current density, and hence restricted to the region $r < R$, where it tends to be concentrated at the periphery. Evaluation of the *curl* in cylindrical coordinates gives a result consistent with this expectation.

$$\begin{aligned}\nabla \times \mathbf{H} &= \mathbf{i_r}\left(\frac{1}{r}\frac{\partial H_z}{\partial\phi} - \frac{\partial H_\phi}{\partial z}\right) + \mathbf{i}_\phi\left(\frac{\partial H_r}{\partial z} - \frac{\partial H_z}{\partial r}\right) \\ &\quad + \mathbf{i_z}\left(\frac{1}{r}\frac{\partial}{\partial r}(rH_\phi) - \frac{1}{r}\frac{\partial H_r}{\partial\phi}\right) \\ &= \begin{cases} J_o r/R\mathbf{i_z}; & r < R \\ 0; & r > R \end{cases}\end{aligned} \tag{6}$$

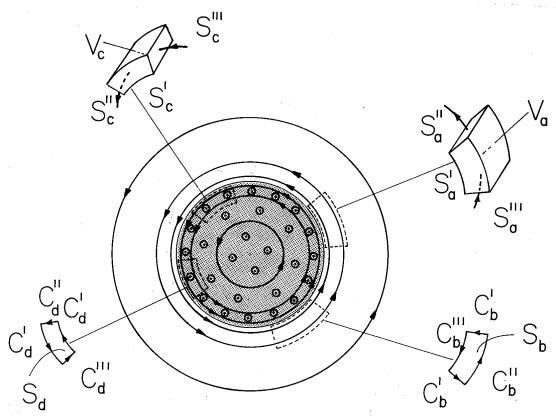


Fig. 2.7.4 Cylindrically symmetric field that is solenoidal. Volume elements V_a and V_c are used with Gauss' theorem to show why the field has no divergence anywhere. Surface elements S_b and S_d are used with Stokes' theorem to show that the field is irrotational outside the cylinder but does have a curl inside.

The current density and magnetic field intensity are sketched in Fig. 2.7.4. In accordance with the "wire" representation, the spacing of the field lines indicates their intensity. A similar convention applies to the current density. When seen "end-on," a current density headed out of the paper is indicated by $\odot$, while $\otimes$ indicates the vector is headed into the paper. The suggestion is of the vector pictured as an arrow, with the symbols representing its tip and feathers, respectively.

Can the azimuthally directed field vary with r (a direction perpendicular to ϕ) and still have no curl in the outer region? The integration of $\mathbf{H}$ around the contour C_b in Fig. 2.7.4 shows why it can. The contours C_b' are arranged to make $d\mathbf{s}$ perpendicular to $\mathbf{H}$, so that $\mathbf{H} \cdot d\mathbf{s} = 0$ there. Integrations on the segments C_b''' and C_b'' cancel because the difference in the length of the segments just compensates the decrease in the field with radius.

In the interior region, a similar integration surely gives a finite result. On the contour C_d, the field is larger on the outside leg where the contour length is larger, so it is clear that the curl must be finite. Of course, this field shape simply reflects the presence of the current density.

The field is solenoidal everywhere. This can be checked by taking the divergence of (5) in each of the regions. In cylindrical coordinates, Table I gives

$$\nabla \cdot \mathbf{H} = \frac{1}{r}\frac{\partial}{\partial r}(rH_r) + \frac{1}{r}\frac{\partial H_\phi}{\partial \phi} + \frac{\partial H_z}{\partial z} \tag{7}$$

The flux tubes defined as incremental volumes V_a and V_c in Fig. 2.7.4, in the exterior and interior regions, respectively, clearly sustain no net flux through their surfaces. That the field lines circulate in tubes without originating or disappearing in certain regions is the hallmark of the solenoidal field.

It is important to distinguish between fields "in the large" (in terms of the integral laws written for volumes, surfaces, and contours of finite size) and "in the small" (in terms of differential laws). To this end, consider some questions that might be raised.

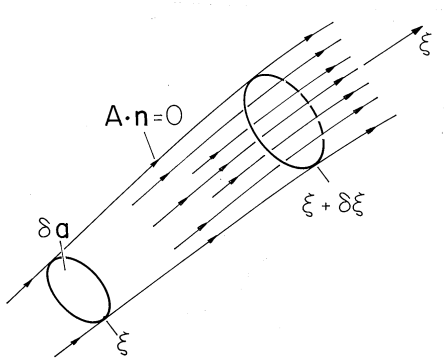


Fig. 2.7.5 Volume element with sides tangential to field lines is used to interpret divergence from field coordinate system.

Is it possible for a field that has no divergence at each point on a closed surface S to have a net flux through that surface? Example 2.7.1 illustrates that the answer is yes. At each point on a surface S that encloses the charged interior region, the divergence of $\epsilon_o\mathbf{E}$ is zero. Yet integration of $\epsilon_o\mathbf{E}\cdot d\mathbf{a}$ over such a surface gives a finite value, indeed, the net charge enclosed.

The divergence can be viewed as a weighted derivative along the direction of the field, or along the field "hose." With $\delta\mathbf{a}$ defined as the cross-sectional area of such a tube having sides parallel to the field $\epsilon_o\mathbf{E}$, as shown in Fig. 2.7.5, it follows from (2.1.2) that the divergence is

$$\nabla\cdot\mathbf{A}=\lim_{\substack{\delta a\to 0\\ \delta\xi\to 0}}\frac{1}{\delta a}\left(\frac{\mathbf{A}\cdot\delta\mathbf{a}|_{\xi+\Delta\xi}-\mathbf{A}\cdot\delta\mathbf{a}|_{\xi}}{\delta\xi}\right) \tag{8}$$

The minus sign in the second term results because $d\mathbf{a}$ and $\delta\mathbf{a}$ are negatives on the left surface. Written in this form, the divergence is the derivative of $e_o\mathbf{E}\cdot\delta\mathbf{a}$ with respect to a coordinate in the direction of $\mathbf{E}$. Examples of such tubes are volumes V_a and V_c in Fig. 2.7.3. That the divergence is zero in the exterior region of that example is equivalent to having a radial derivative of the displacement flux $\epsilon_o\mathbf{E}\cdot\delta\mathbf{a}$ that is zero.

A further observation returns to the distinction between fields as they are described "in the large" by means of the integral laws and as they are represented "in the small" by the differential laws. Is it possible for a field to have a circulation on some contour C and yet be irrotational at each point on C? Example 2.7.2 shows that the answer is again yes. The exterior magnetic field encircles the center current-carrying region. Therefore, it has a circulation on any contour that encloses the center region. Yet at all exterior points, the *curl* of $\mathbf{H}$ is zero.

The cross-product of two vectors is perpendicular to both vectors. Is the *curl* of a vector necessarily perpendicular to that vector? Example 2.7.2 would seem to say yes. There the current density is the curl of $\mathbf{H}$ and is in the z direction, while $\mathbf{H}$ is in the azimuthal direction. However, this time the answer is no. By definition we can add to $\mathbf{H}$ any irrotational field without altering the curl. If that irrotational field has a component in the direction of the curl, then the curl of the combined fields is not perpendicular to the combined fields.

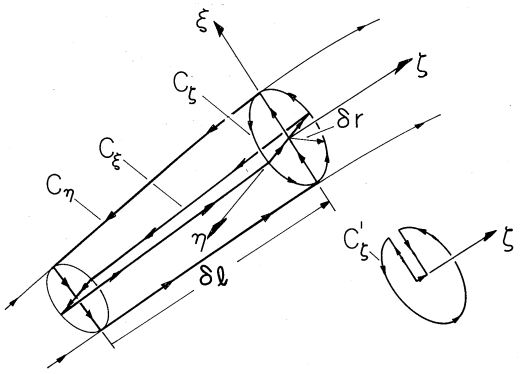


Fig. 2.7.6 Three surfaces, having orthogonal normal vectors, have geometry determined by the field hose. Thus, the curl of the field is interpreted in terms of a field coordinate system.

Illustration. A Vector Field Not Perpendicular to Its Curl

In the interior of the conductor shown in Fig. 2.7.4, the magnetic field intensity and its curl are

$$\mathbf{H} = \frac{J_o}{3}\frac{r^2}{R}\mathbf{i}_\phi; \qquad \nabla \times \mathbf{H} = \mathbf{J} = \frac{J_o r}{R}\mathbf{i_z} \tag{9}$$

Suppose that we add to this $\mathbf{H}$ a field that is uniform and z directed.

$$\mathbf{H} = \frac{J_o r^2}{3R}\mathbf{i}_\phi + H_o\mathbf{i_z} \tag{10}$$

Then the new field has a component in the z direction and yet has the same z-directed curl as given by (9). Note that the new field lines are helixes having increasingly tighter pitches as the radius is increased.

The curl can also be viewed in terms of a field hose. The definition, (2.4.2), is applied to any one of the three contours and associated surfaces shown in Fig. 2.7.6. Contours C_ξ and C_η are perpendicular and across the hose while (C_ζ) is around the hose. The former are illustrated by contours C_b and C_d in Fig. 2.7.4.

The component of the *curl* in the ξ direction is the limit in which the area $2\delta r\delta l$ goes to zero of the circulation around the contour C_ξ divided by that area. The contributions to this line integration from the segments that are perpendicular to the ζ axis are by definition zero. Thus, for this component of the *curl*, transverse to the field, (2.4.2) becomes

$$(\nabla \times \mathbf{H})_\xi = \lim_{\substack{\delta l \to 0 \\ \delta\xi \to 0}} \frac{1}{\delta l}\left(\frac{\delta\mathbf{l}\cdot\mathbf{H}|_{\eta+\frac{\delta\eta}{2}} - \delta\mathbf{l}\cdot\mathbf{H}|_{\eta-\frac{\delta\eta}{2}}}{\delta\eta}\right) \tag{11}$$

The transverse components of the *curl* can be regarded as derivatives with respect to transverse directions of the vector field weighted by incremental line elements δl.

At its center, the surface enclosed by the contour C_ζ has its normal in the direction of the field. It would seem that the curl in the ζ direction would therefore have to be zero. However, the previous discussion and illustration give a warning that the contour integral around C_ζ is not necessarily zero.

Even though, to zero order in the diameter of the hose, the field is perpendicular to the contour, to higher order it can have components parallel to the contour. This means that if the contour C_ζ were actually perpendicular to the field at each point, it would not close on itself. An equivalent contour, shown by the inset to Fig. 2.7.6, begins and terminates on the central field line. With the exception of the segment in the ζ direction used to close this contour, each segment is now by definition perpendicular to ζ. The contribution to the circulation around the contour now comes from the ζ-directed segment. Remember that the length of this segment is determined by the shape of the field lines. Thus, it is proportional to $(\delta r)^2$, and therefore so also is the circulation. The limit defined by (2.1.2) can result in a finite value in the ζ direction. The "cross-product" of an operator with a vector has properties that are not identical with the cross-product of two vectors.

2.8 SUMMARY OF MAXWELL'S DIFFERENTIAL LAWS AND INTEGRAL THEOREMS

In this chapter, the divergence and curl operators have been introduced. A third, the gradient, is naturally defined where it is put to use, in Chap. 4. A summary of these operators in the three standard coordinate systems is given in Table I at the end of the text. The problems for Secs. 2.1 and 2.4 outline the derivations of the gradient and curl operators in cylindrical and spherical coordinates.

The integral theorems of Gauss and Stokes are two of three theorems summarized in Table II at the end of the text. Gauss' theorem states how the volume integral of any scalar that can be represented as the divergence of a vector can be reduced to an integration of the normal component of that vector over the surface enclosing that volume. A volume integration is reduced to a surface integration. Similarly, Stokes' theorem reduces the surface integration of any vector that can be represented as the *curl* of another vector to a contour integration of that second vector. A surface integral is reduced to a contour integral.

These generally useful theorems are the basis for moving from the integral law point of view of Chap. 1 to a differential point of view. This transition from a global to a point-wise view of fields is summarized by the shift from the integral laws of Table 1.8.1 to the differential laws of Table 2.8.1.

The aspects of a vector field encapsulated in the divergence and curl can always be recalled by returning to the fundamental definitions, (2.1.2) and (2.4.2), respectively. The divergence is indeed defined to represent the net outward flux through a closed surface. But keep in mind that the surface is incremental, and that the divergence describes only the neighborhood of a given point. Similarly, the curl represents the circulation around an incremental contour, not around one that is of finite size.

What should be committed to memory from this chapter? The theorems of Gauss and Stokes are the key to relating the integral and differential forms of Maxwell's equations. Thus, with these theorems and the integral laws in mind,

TABLE 2.8.1

MAXWELL'S DIFFERENTIAL LAWS IN FREE SPACE

NAME	DIFFERENTIAL LAW	EQ. NUMBER
Gauss' Law	$\nabla \cdot \epsilon_o \mathbf{E} = \rho$	2.3.1
Ampère's Law	$\nabla \times \mathbf{H} = \mathbf{J} + (\partial \epsilon_o \mathbf{E})/(\partial t)$	2.6.2
Faraday's Law	$\nabla \times \mathbf{E} = -(\partial \mu_o \mathbf{H})/(\partial t)$	2.6.4
Magnetic Flux Continuity	$\nabla \cdot \mu_o \mathbf{H} = 0$	2.3.2
Charge Conservation	$\nabla \cdot \mathbf{J} + \frac{\partial \rho}{\partial t} = 0$	2.3.3

it is easy to remember the differential laws. Applied to differential volumes and surfaces, the theorems also provide the definitions (and hence the significances) of the divergence and curl operators independent of the coordinate system. Also, the evaluation in Cartesian coordinates of these operators should be remembered.

PROBLEMS

2.1 The Divergence Operator

2.1.1* In Cartesian coordinates, $\mathbf{A} = (A_o/d^2)(x^2\mathbf{i_x} + y^2\mathbf{i_y} + z^2\mathbf{i_z})$, where A_o and d are constants. Show that $div\mathbf{A} = 2A_o(x + y + z)/d^2$.

2.1.2* In Cartesian coordinates, three vector functions are

$$\mathbf{A} = (A_o/d)(y\mathbf{i_x} + x\mathbf{i_y}) \quad (a)$$

$$\mathbf{A} = (A_o/d)(x\mathbf{i_x} - y\mathbf{i_y}) \quad (b)$$

$$\mathbf{A} = A_o e^{-ky}(\cos kx\mathbf{i_x} - \sin kx\mathbf{i_y}) \quad (c)$$

where A_o, k, and d are constants.

(a) Show that the divergence of each is zero.
(b) Devise three vector functions that have a finite divergence and evaluate their divergences.

2.1.3 In cylindrical coordinates, the divergence operator is given in Table I at the end of the text. Evaluate the divergence of the following vector functions.

$$\mathbf{A} = (A_o/d)(r\cos 2\phi\mathbf{i_r} - r\sin 2\phi\mathbf{i}_\phi) \quad (a)$$

$$\mathbf{A} = A_o(\cos\phi\mathbf{i_r} - \sin\phi\mathbf{i}_\phi) \quad (b)$$

$$\mathbf{A} = (A_o r^2/d^2)\mathbf{i_r} \quad (c)$$

2.1.4* In cylindrical coordinates, unit vectors are as defined in Fig. P2.1.4a. An incremental volume element having sides $(\Delta r, r\Delta\phi, \Delta z)$ is as shown in Fig. P2.1.4b. Determine the divergence operator by evaluating (2), using steps analogous to those leading from (3) to (5). Show that the result is as given in Table I at the end of the text. (Hint: In carrying out the integrations over the surface elements in Fig. P2.1.4b having normals $\pm\mathbf{i_r}$, note that not only is A_r evaluated at $r = r \pm \frac{1}{2}\Delta r$, but so also is r. For this reason, it is most convenient to group A_r and r together in manipulating the contributions from this surface.)

2.1.5 The divergence operator is given in spherical coordinates in Table I at the end of the text. Use that operator to evaluate the divergence of the following vector functions.

$$\mathbf{A} = (A_o/d^3)r^3\mathbf{i_r} \quad (a)$$

$$\mathbf{A} = (A_o/d^2)r^2\mathbf{i}_\phi \quad (b)$$

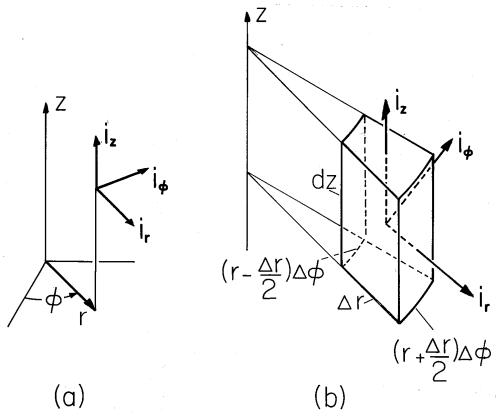


Fig. P2.1.4

$$\mathbf{A} = A_o(\cos\theta\mathbf{i_r} - \sin\theta\mathbf{i}_\theta) \qquad (c)$$

2.1.6* In spherical coordinates, an incremental volume element has sides Δr, $r\Delta\theta$, $r\ \sin\theta\Delta\phi$. Using steps analogous to those leading from (3) to (5), determine the divergence operator by evaluating (2.1.2). Show that the result is as given in Table I at the end of the text.

2.2 Gauss' Integral Theorem

2.2.1* Given a well-behaved vector function $\mathbf{A}$, Gauss' theorem shows that the same result will be obtained by integrating its divergence over a volume V or by integrating its normal component over the surface S that encloses that volume. The following steps exemplify this fact. Consider the particular vector function $\mathbf{A} = (A_o/d)(x\mathbf{i_x}+y\mathbf{i_y})$ and a cubical volume having surfaces in the planes $x = \pm d$, $y = \pm d$, and $z = \pm d$.

(a) Show that the area elements on these surfaces are respectively $d\mathbf{a} = \pm\mathbf{i_x}dydz$, $\pm\mathbf{i_y}dxdz$, and $\pm\mathbf{i_z}dydx$.

(b) Show that evaluation of the left-hand side of (4) gives

$$\oint_S \mathbf{A}\cdot d\mathbf{a} = \frac{A_o}{d}\left[\int_{-d}^{d}\int_{-d}^{d}(d)dydz - \int_{-d}^{d}\int_{-d}^{d}(-d)dydz + \int_{-d}^{d}\int_{-d}^{d}(d)dxdz - \int_{-d}^{d}\int_{-d}^{d}(-d)dxdz\right]$$
$$= 16\ A_o d^2$$

(c) Evaluate the divergence of $\mathbf{A}$ and the right-hand side of (4) and show that it gives the same result.

2.2.2 With $\mathbf{A} = (A_o/d^3)(xy^2\mathbf{i_x} + x^2y\mathbf{i_y})$, carry out the steps in Prob. 2.2.1.

2.3 Differential Forms of Gauss' Law, Magnetic Flux Continuity, and Charge Conservation

2.3.1* For a line charge along the z axis of Prob. 1.3.1, $\mathbf{E}$ was written in Cartesian coordinates as (a).

(a) Use Gauss' differential law in Cartesian coordinates to show that the charge density is indeed zero everywhere except along the z axis.
(b) Obtain the same result by evaluating Gauss' law using $\mathbf{E}$ as given by (1.3.13) and the divergence operator from Table I in cylindrical coordinates.

2.3.2* Show that at each point $r < a$, $\mathbf{E}$ and ρ as given respectively by (b) and (a) of Prob. 1.3.3 are consistent with Gauss' differential law.

2.3.3* For the flux linkage λ_f to be independent of S, (2) must hold. Return to Prob. 1.6.6 and check to see that this condition was indeed satisfied by the magnetic flux density.

2.3.4* Using $\mathbf{H}$ expressed in cylindrical coordinates by (1.4.10), show that the magnetic flux density of a line current is indeed solenoidal (has no divergence) everywhere except at $r = 0$.

2.3.5 Use the differential law of magnetic flux continuity, (2), to answer Prob. 1.7.2.

2.3.6* In Prob. 1.3.5, $\mathbf{E}$ and ρ are found for a one-dimensional configuration using the integral charge conservation law. Show that the differential form of this law is satisfied at each position $-\frac{1}{2}s < z < \frac{1}{2}s$.

2.3.7 For $\mathbf{J}$ and ρ as found in Prob. 1.5.1, show that the differential form of charge conservation, (3), is satisfied.

2.4 The Curl Operator

2.4.1* Show that the curls of the three vector functions given in Prob. 2.1.2 are zero. Devise three such functions that have finite curls (are rotational) and give their curls.

2.4.2 Vector functions are given in cylindrical coordinates in Prob. 2.1.3. Using the curl operator as given in cylindrical coordinates by Table I at the end of the text, show that all of these functions are irrotational. Devise three functions that are rotational and give their curls.

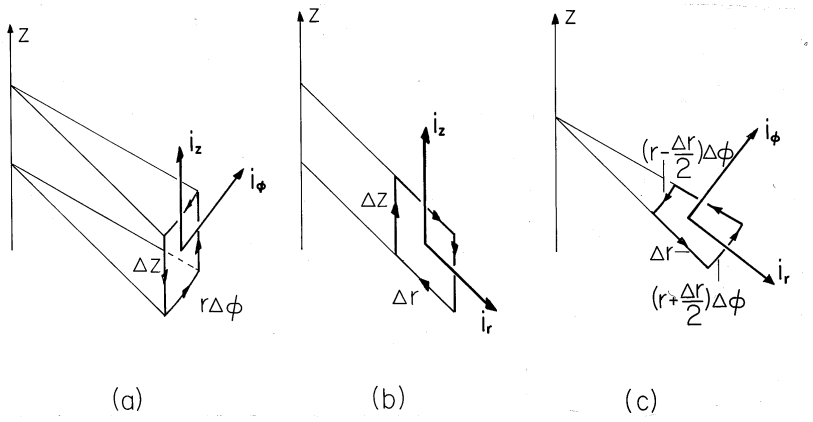


Fig. P2.4.3

2.4.3* In cylindrical coordinates, define incremental surface elements having normals in the r, ϕ and z directions, respectively, as shown in Fig. P2.4.3. Determine the r, ϕ, and z components of the curl operator. Show that the result is as given in Table I at the end of the text. (Hint: In integrating in the $\pm\phi$ directions on the outer and inner incremental contours of Fig. P2.4.3c, note that not only is A_ϕ evaluated at $r = r \pm \frac{1}{2}\Delta r$, respectively, but so also is r. It is therefore convenient to treat $A_\phi r$ as a single function.)

2.4.4 In spherical coordinates, incremental surface elements have normals in the r, θ, and ϕ directions, respectively, as described in Appendix 1. Determine the r, θ, and ϕ components of the curl operator and compare to the result given in Table I at the end of the text.

2.4.5 The following is an identity.

$$\nabla \cdot (\nabla \times \mathbf{A}) = 0 \qquad (a)$$

This can be shown in two ways.

(a) Apply Stokes' theorem to an arbitrary but closed surface S (one having no edge, so $C = 0$) and then Gauss' theorem to argue the identity.
(b) Write out the the divergence of the curl in Cartesian coordinates and show that it is indeed identically zero.

2.5 Stokes' Integral Theorem

2.5.1* To exemplify Stokes' integral theorem, consider the evaluation of (4) for the vector function $\mathbf{A} = (A_o/d^2)x^2\mathbf{i_y}$ and a rectangular contour consisting of the segments at $x = g + \Delta$, $y = h$, $x = g$, and $y = 0$. The direction of the contour is such that $d\mathbf{a} = \mathbf{i_z}dxdy$.

(a) Show that the left-hand side of (4) is $hA_o[(g+\Delta)^2 - g^2]d^2$.
(b) Verify (4) by obtaining the same result integrating $curl\mathbf{A}$ over the area enclosed by C.

2.5.2 For the vector function $\mathbf{A} = (A_o/d)(-\mathbf{i_x}y + \mathbf{i_y}x)$, evaluate the contour and surface integrals of (4) on C and S as prescribed in Prob. 2.5.1 and show that they are equal.

2.6 Differential Laws of Ampère and Faraday

2.6.1* In Prob. 1.4.2, $\mathbf{H}$ is given in Cartesian coordinates by (c). With $\partial\epsilon_o\mathbf{E}/\partial t = 0$, show that Ampère's differential law is satisfied at each point $r < a$.

2.6.2* For the $\mathbf{H}$ and $\mathbf{J}$ given in Prob. 1.4.1, show that Ampère's differential law, (2), is satisfied with $\partial\epsilon_o\mathbf{E}/\partial t = 0$.

2.7 Visualization of Fields and the Divergence and Curl

2.7.1 Using the conventions exemplified in Fig. 2.7.3,

(a) Sketch the distributions of charge density ρ and electric field intensity $\mathbf{E}$ for Prob. 1.3.5 and with $E_o = 0$ and $\sigma_o = 0$.
(b) Verify that $\mathbf{E}$ is irrotational.
(c) From observation of the field sketch, why would you suspect that $\mathbf{E}$ is indeed irrotational?

2.7.2 Using Fig. 2.7.4 as a model, sketch $\mathbf{J}$ and $\mathbf{H}$

(a) For Prob. 1.4.1.
(b) For Prob. 1.4.4.
(c) Verify that in each case, $\mathbf{H}$ is solenoidal.
(d) From observation of these field sketches, why would you suspect that $\mathbf{H}$ is indeed solenoidal?

2.7.3 Three two-dimensional vector fields are shown in Fig. P2.7.3.

(a) Which of these is irrotational?
(b) Which are solenoidal?

2.7.4 For the fields of Prob. 1.6.7, sketch $\mathbf{E}$ just above and just below the plane $y = 0$ and σ_s in the surface $y = 0$. Assume that $E_1 = E_2 = \sigma_o/\epsilon_o > 0$ and adhere to the convention that the field intensity is represented by the spacing of the field lines.

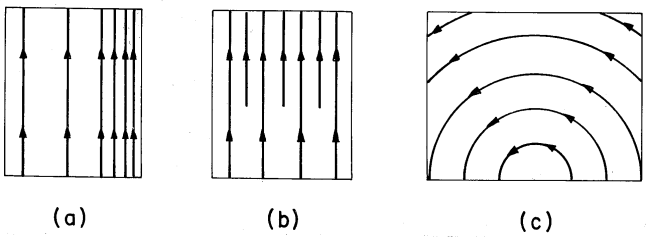


Fig. P2.7.3

2.7.5 For the fields of Prob. 1.7.3, sketch **H** just above and just below the plane $y = 0$ and **K** in the surface $y = 0$. Assume that $H_1 = H_2 = K_o > 0$ and represent the intensity of **H** by the spacing of the field lines.

2.7.6 Field lines in the vicinity of the surface $y = 0$ are shown in Fig. P2.7.6.

(a) If the field lines represent **E**, there is a surface charge density σ_s on the surface. Is σ_s positive or negative?
(b) If the field lines represent **H**, there is a surface current density $\mathbf{K} = K_z\mathbf{i_z}$ on the surface. Is K_z positive or negative?

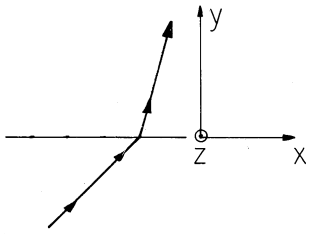


Fig. P2.7.6

3

INTRODUCTION TO ELECTROQUASISTATICS AND MAGNETOQUASISTATICS

3.0 INTRODUCTION

The laws represented by Maxwell's equations are remarkably general. Nevertheless, they are deceptively simple. In differential form they are

$$\nabla \times \mathbf{E} = -\frac{\partial \mu_o \mathbf{H}}{\partial t} \tag{1}$$

$$\nabla \times \mathbf{H} = \mathbf{J} + \frac{\partial \epsilon_o \mathbf{E}}{\partial t} \tag{2}$$

$$\nabla \cdot \epsilon_o \mathbf{E} = \rho \tag{3}$$

$$\nabla \cdot \mu_o \mathbf{H} = 0 \tag{4}$$

The sources of the electric and magnetic field intensities, $\mathbf{E}$ and $\mathbf{H}$, are the charge and current densities, ρ and $\mathbf{J}$.

If, at an initial instant, electric and magnetic fields are specified throughout all of a source-free space, then Maxwell's equations in their differential form predict these fields as they subsequently evolve in space and time. Proof of this assertion is our starting point in Sec. 3.1. This makes it natural to attribute a physical significance to the fields in their own right. Fields can exist in regions far removed from their sources because they can propagate as electromagnetic waves. An introduction to such waves is given in Sec. 3.2. It is shown that the coupling between $\mathbf{E}$ and $\mathbf{H}$ produced by the *magnetic induction* in Faraday's law, the term on the right in (1) and the *displacement current density* in Ampère's law, the time derivative term on the right in (2), gives rise to electromagnetic waves.

Even though fields can propagate without sources, where they are initiated or detected they must be related to their sources or sinks. To do this, the Lorentz force law must be brought into play. In Sec. 3.1, this law is used to complete Newton's law

and describe the evolution of a charge distribution. Generally, the Lorentz force law does not act so directly as it does in this example; nevertheless, it usually underlies a constitutive law for conduction that is added to Maxwell's equations to relate the fields to the sources. The most commonly used constitutive law is Ohm's law, which is not introduced until Chap. 7. However, in the intervening chapters we will often model electrodes and wires as being *perfectly conducting* in the sense that Lorentz's law is responsible for making the charges move in just such a way that there is effectively no electric field intensity in the material.

Maxwell's equations describe the most intricate electromagnetic wave phenomena. Of course, the analysis of such fields is difficult and not always necessary. Wave phenomena occur on short time scales or at high frequencies that are often of no practical concern. If this is the case, the fields may be described by truncated versions of Maxwell's equations applied to relatively long time scales and low frequencies (quasistatics). The objective in Sec. 3.3 is to identify the two quasistatic approximations and rank the laws in order of importance in these approximations.

In Sec. 3.4, we find what turns out to be one typical condition that must be satisfied if either of these quasistatic approximations is to be justified. Thus, we will find that a system composed of perfect conductors and free space is either electroquasistatic (EQS) or magnetoquasistatic (MQS) if an electromagnetic wave can propagate through a typical dimension of the system in a time that is shorter than times of interest.

If fulfillment of the same condition justifies either the EQS or MQS approximation, how do we know which to use? We begin to form insights in this regard in Sec. 3.4.

A formal justification of the quasistatic approximations would be based on what might be termed a time-rate expansion. As time rates of change are increased, more terms are required in a series having its first term predicted by the appropriate quasistatic laws. In Sec. 3.4, a specific example is used to illustrate this expansion and the error committed by omission of the higher-order terms.

Whether they be electromagnetic, or perhaps thermal or mechanical, dynamical systems that proceed from one state to another as though they are static are commonly said to be quasistatic in their behavior. In this text, the quasistatic fields are indeed related to their sources as if they were truly static. That is, given the charge or current distribution, $\mathbf{E}$ or $\mathbf{H}$ are determined without regard for the dynamics of electromagnetism. However, other dynamical processes can play a role in determining the source distributions.

In the systems we are prepared to consider in this chapter, composed of free space and perfect conductors, the quasistatic source distributions within a given quasistatic subregion do not depend on time rates of change. Thus, for now, we will find that geometry and spatial and temporal scales alone determine whether a subregion is magnetoquasistatic or electroquasistatic. Illustrated in Sec. 3.5 is the interconnection of such subsystems. In a way that is familiar from circuit theory, the resulting model for the total system has apportionments of sources in the subregions (charges in the EQS regions and currents in the MQS regions) that do depend on the time rates of change. After we have considered effects of finite conductivity in Chaps. 7 and 10, it will be clear that there are many other situations where quasistatic models represent dynamical processes.

Again, Sec. 3.6 provides an overview, this time not of the laws but rather of the parts of the physical world to which they pertain. The discussion is qualitative

and the section is for "feet on the table" reading. Finally, Sec. 3.7 summarizes the electroquasistatic and magnetoquasistatic field laws that, respectively, are the themes of Chaps. 4–7 and 8–10.

We return to the subject of quasistatic approximations in Chap. 12, where electromagnetic waves are again considered. In Chap. 15 we will come to recognize that the concept of quasistatics promulgated in Chaps. 7 and 10 (where loss phenomena are considered) has made the classification into electroquasistatic and magnetoquasistatic regions depend not only on geometry and spatial and temporal scales, but on material properties as well.

3.1 TEMPORAL EVOLUTION OF WORLD GOVERNED BY LAWS OF MAXWELL, LORENTZ, AND NEWTON

If certain initial conditions are given, Maxwell's equations, along with the Lorentz law and Newton's law, describe the time evolution of $\mathbf{E}$ and $\mathbf{H}$. This can be argued by expressing Maxwell's equations, (1)–(4), with the time derivatives and charge density on the left.

$$\frac{\partial \mathbf{H}}{\partial t} = -\frac{1}{\mu_o}(\nabla \times \mathbf{E}) \tag{1}$$

$$\frac{\partial \mathbf{E}}{\partial t} = \frac{1}{\epsilon_o}(\nabla \times \mathbf{H} - \mathbf{J}) \tag{2}$$

$$\rho = \nabla \cdot \epsilon_o \mathbf{E} \tag{3}$$

$$0 = \nabla \cdot \mu_o \mathbf{H} \tag{4}$$

The region of interest is vacuum, where particles having a mass m and charge q are subject only to the Lorentz force. Thus, Newton's law (here used in its nonrelativistic form), also written with the time derivative (of the particle velocity) on the left, links the charge distribution to the fields.

$$m\frac{d\mathbf{v}}{dt} = q(\mathbf{E} + \mathbf{v} \times \mu_o \mathbf{H}) \tag{5}$$

The Lorentz force on the right is given by (1.1.1).

Suppose that at a particular instant, $t = t_o$, we are given the fields throughout the entire space of interest, $\mathbf{E}(\mathbf{r}, t_o)$ and $\mathbf{H}(\mathbf{r}, t_o)$. Suppose we are also given the velocity $\mathbf{v}(\mathbf{r}, t_o)$ of all the charges when $t = t_o$. It follows from Gauss' law, (3), that at this same instant, the distribution of charge density is known.

$$\rho(\mathbf{r}, t_o) = \nabla \cdot \epsilon_o \mathbf{E}(\mathbf{r}, t_o) \tag{6}$$

Then the current density at the time $t = t_o$ follows as

$$\mathbf{J}(\mathbf{r}, t_o) = \rho(\mathbf{r}, t_o)\mathbf{v}(\mathbf{r}, t_o) \tag{7}$$

So that (4) is satisfied when $t = t_o$, we must require that the given distribution of $\mathbf{H}$ be solenoidal.

The curl operation involves only spatial derivatives, so the right-hand sides of the remaining laws, (1), (2), and (5), can now be evaluated. Thus, the time rates of change of the quantities, $\mathbf{E}$, $\mathbf{H}$, and $\mathbf{v}$, given when $t = t_o$, are now known. This allows evaluation of these quantities an instant later, when $t = t_o + \Delta t$. For example, at this later time,

$$\mathbf{E} = \mathbf{E}(\mathbf{r}, t_o) + \Delta t \frac{\partial \mathbf{E}}{\partial t}\Big|_{(\mathbf{r},t_o)} \tag{8}$$

Thus, when $t = t_o + \Delta t$ we have the same three vector functions throughout all space we started with. This process can be repeated iteratively to determine the distributions at an arbitrary later time. Note that if the initial distribution of $\mathbf{H}$ is solenoidal, as required by (4), all subsequent distributions will be solenoidal as well. This follows by taking the divergence of Faraday's law, (1), and noting that the divergence of the curl is zero.

The left-hand side of (5) is written as a total derivative because it is required to represent the time derivative as measured by an observer moving with a given particle.

The preceding argument shows that in free space, for given initial $\mathbf{E}$, $\mathbf{H}$, and $\mathbf{v}$, the Lorentz law (here used with Newton's law) and Maxwell's equations determine the charge distributions and the associated fields for all later time. In this sense, Maxwell's equations and the Lorentz law may be said to provide a complete description of electrodynamic interactions in free space. Commonly, more than one species of charge is involved and the charged particles respond to the field in a manner more complex than simply represented by the laws of Newton and Lorentz. In that case, the role played by (5) is taken by a conduction constitutive law which nevertheless reflects the Lorentz force law.

Another interesting property of Maxwell's equations emerges from the preceding discussion. The electric and magnetic fields are coupled. The temporal evolution of $\mathbf{E}$ is determined in part by the *curl* of $\mathbf{H}$, (2), and, similarly, it is the *curl* of $\mathbf{E}$ that determines how fast $\mathbf{H}$ is changing in time, (1).

Example 3.1.1. Evolution of an Electromagnetic Wave

The interplay of the magnetic induction and the electric displacement current is illustrated by considering fields that evolve in Cartesian coordinates from the initial distributions

$$\mathbf{E} = E_o \mathbf{i}_\mathbf{x} e^{-z^2/2a^2} \tag{9}$$

$$\mathbf{H} = \sqrt{\epsilon_o/\mu_o} E_o \mathbf{i}_\mathbf{y} e^{-z^2/2a^2} \tag{10}$$

In this example, we let $t_o = 0$, so these are the fields when $t = 0$. Shown in Fig. 3.1.1, these fields are transverse, in that they have a direction perpendicular to the coordinate upon which they depend. Thus, they are both solenoidal, and Gauss' law makes it clear that the physical situation we consider does not involve a charge density. It follows from (7) that the current density is also zero.

With the initial fields given and $\mathbf{J} = 0$, the right-hand sides of (1) and (2) can be evaluated to give the rates of change of $\mathbf{H}$ and $\mathbf{E}$.

$$\mu_o \frac{\partial \mathbf{H}}{\partial t} = -\nabla \times \mathbf{E} = -\mathbf{i}_\mathbf{y} \frac{\partial E_x}{\partial z} = -\mathbf{i}_\mathbf{y} E_o \frac{d}{dz} e^{-z^2/2a^2} \tag{11}$$

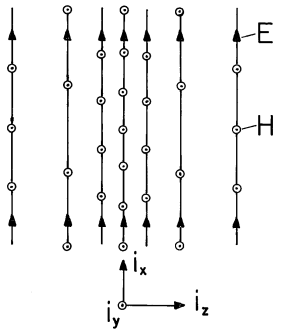


Fig. 3.1.1 A schematic representation of the **E** and **H** fields of Example 3.2.1. The distributions move to the right with the speed of light, c.

$$\epsilon_o \frac{\partial \mathbf{E}}{\partial t} = \nabla \times \mathbf{H} = -\mathbf{i_x}\sqrt{\epsilon_o/\mu_o}E_o \frac{d}{dz}e^{-z^2/2a^2} \tag{12}$$

It follows from (11), Faraday's law, that when $t = \Delta t$,

$$\mathbf{H} = \mathbf{i_y}\sqrt{\epsilon_o/\mu_o}E_o\left(e^{-z^2/2a^2} - c\Delta t\frac{d}{dz}e^{-z^2/2a^2}\right) \tag{13}$$

where $c = 1/\sqrt{\epsilon_o\mu_o}$, and from (12), Ampère's law, that the electric field is

$$\mathbf{E} = E_o\mathbf{i_x}\left(e^{-z^2/2a^2} - c\Delta t\frac{d}{dz}e^{-z^2/2a^2}\right) \tag{14}$$

When $t = \Delta t$, the **E** and **H** fields are equal to the original Gaussian distribution minus $c\Delta t$ times the spatial derivatives of these Gaussians. But these represent the original Gaussians shifted by $c\Delta t$ in the $+z$ direction. Indeed, witness the relation applicable to any function $f(z)$.

$$f(z - \Delta z) = f(z) - \Delta z\frac{df}{dz}. \tag{15}$$

On the left, $f(z - \Delta z)$ is the function $f(z)$ shifted by Δz. The Taylor expansion on the right takes the same form as the fields when $t = \Delta t$, (13) and (14). Thus, within Δt, the **E** and **H** field distributions have shifted by $c\Delta t$ in the $+z$ direction. Iteration of this process shows that the field distributions shown in Fig. 3.1.1 travel in the $+z$ direction without change of shape at the speed c, the speed of light.

$$\boxed{c = \frac{1}{\sqrt{\epsilon_o\mu_o}} \cong 3 \times 10^8 \text{m/sec}} \tag{16}$$

Note that the derivation would not have changed if we had substituted for the initial Gaussian functions any other continuous functions $f(z)$.

In retrospect, it should be recognized that the initial conditions were premeditated so that they would result in a single wave propagating in the $+z$ direction. Also, the method of solution was really not numerical. If we were interested in pursuing the numerical approach, care would have to be taken to avoid the accumulation of errors.

The above example illustrated that the electromagnetic wave is caused by the interplay of the magnetic induction and the displacement current, the terms on the left in (1) and (2). Through Faraday's law, (1), the curl of an initial **E** implies that an instant later, the initial **H** is altered. Similarly, Ampère's law requires that the curl of an initial **H** leads to a change in **E**. In turn, the curls of the altered **E** and **H** imply further changes in **H** and **E**, respectively.

There are two main points in this section. First, Maxwell's equations, augmented by laws describing the interaction of the fields with the sources, are sufficient to describe the evolution of electromagnetic fields.

Second, in regions well removed from materials, electromagnetic fields evolve as electromagnetic waves. Typically, the time required for fields to propagate from one region to another, say over a distance L, is

$$\tau_{em} = \frac{L}{c} \tag{17}$$

where c is the velocity of light. The origin of these waves is the coupling between the laws of Faraday and Ampère afforded by the magnetic induction and the displacement current. If either one or the other of these terms is neglected, so too is any electromagnetic wave effect.

3.2 QUASISTATIC LAWS

The quasistatic laws are obtained from Maxwell's equations by neglecting either the magnetic induction or the electric displacement current.

ELECTROQUASTATIC		**MAGNETOQUASISTATIC**	
$\nabla \times \mathbf{E} = -\dfrac{\partial \mu_o \mathbf{H}}{\partial t} \simeq 0$	$(1a)$	$\nabla \times \mathbf{E} = -\dfrac{\partial \mu_o \mathbf{H}}{\partial t}$	$(1b)$
$\nabla \times \mathbf{H} = \dfrac{\partial \epsilon_o \mathbf{E}}{\partial t} + \mathbf{J}$	$(2a)$	$\nabla \times \mathbf{H} = \dfrac{\partial \epsilon_o \mathbf{E}}{\partial t} + \mathbf{J} \simeq \mathbf{J}$	$(2b)$
$\nabla \cdot \epsilon_o \mathbf{E} = \rho$	$(3a)$	$\nabla \cdot \epsilon_o \mathbf{E} = \rho$	$(3b)$
$\nabla \cdot \mu_o \mathbf{H} = 0$	$(4a)$	$\nabla \cdot \mu_o \mathbf{H} = 0$	$(4b)$

The electromagnetic waves that result from the coupling of the magnetic induction and the displacement current are therefore neglected in either set of quasistatic laws. Before considering order of magnitude arguments in support of these approximate laws, we recognize their differing orders of importance.

In Chaps. 4 and 8 it will be shown that if the curl and divergence of a vector are specified, then that vector is determined.

In the EQS approximation, (1a) requires that $\mathbf{E}$ is essentially irrotational. It then follows from (3a) that if the charge density is given, both the curl and divergence of $\mathbf{E}$ are specified. Thus, Gauss' law and the EQS form of Faraday's law come first.

$$\nabla \cdot \epsilon_o \mathbf{E} = \rho \qquad (5a)$$

$$\nabla \times \mathbf{E} = 0 \qquad (6a)$$

In the MQS approximation, the displacement current is negligible in (2b), while (4b) requires that $\mathbf{H}$ is solenoidal. Thus, if the current density is given, both the curl and divergence of $\mathbf{H}$ are known. Thus, the MQS form of Ampère's law and the flux continuity condition come first.

$$\nabla \times \mathbf{H} = \mathbf{J}; \quad \nabla \cdot \mathbf{J} = 0 \qquad (5b-c)$$

$$\nabla \cdot \mu_o \mathbf{H} = 0 \qquad (6b)$$

Implied by the approximate form of Ampère's law is the continuity condition of $\mathbf{J}$, given also by (5b).

In these relations, there are no time derivatives. This does not mean that the sources, and hence the fields, are not functions of time. But given the sources at a certain instant, the fields at that same instant are determined without regard for what the sources of fields were an instant earlier. Figuratively, a snapshot of the source distribution determines the field distribution at the same instant in time.

Generally, the sources of the fields are not known. Rather, because of the Lorentz force law, which acts to set charges into motion, they are determined by the fields themselves. It is for this reason that time rates of change come into play. We now bring in the equation retaining a time derivative.

Because $\mathbf{H}$ is often not crucial to the EQS motion of charges, it is eliminated from the picture by taking the divergence of (2a).

$$\nabla \cdot \mathbf{J} + \frac{\partial \rho}{\partial t} = 0 \qquad (7a)$$

Faraday's law makes it clear that a time varying $\mathbf{H}$ implies an induced electric field.

$$\nabla \times \mathbf{E} = \frac{-\partial \mu_o \mathbf{H}}{\partial t} \qquad (7b)$$

In the EQS approximation, **H** is usually a "leftover" quantity. In any case, once **E** and **J** are determined, **H** can be found by solving (2a) and (4a).

$$\nabla \times \mathbf{H} = \frac{\partial \epsilon_o \mathbf{E}}{\partial t} + \mathbf{J} \qquad (8a)$$

$$\nabla \cdot \mu_o \mathbf{H} = 0 \qquad (9a)$$

In the MQS approximation, the charge density is a "leftover" quantity, which can be found by applying Gauss' law, (3b), to the previously determined electric field intensity.

$$\nabla \cdot \epsilon_o \mathbf{E} = \rho \qquad (8b)$$

In the EQS approximation, it is clear that with **E** and **J** determined from the "zero order" laws (5a)–(7a), the curl and divergence of **H** are known [(8a) and (9a)]. Thus, **H** can be found in an "after the fact" way. Perhaps not so obvious is the fact that in the MQS approximation, the divergence and curl of **E** are also determined without regard for ρ. The curl of **E** follows from Faraday's law, (7b), while the divergence is often specified by combining a conduction constitutive law with the continuity condition on **J**, (5b).

The differential quasistatic laws are summarized in Table 3.6.1 at the end of the chapter. Because there is a direct correspondence between terms in the differential and integral laws, the quasistatic integral laws are as summarized in Table 3.6.2. The conditions under which these quasistatic approximations are valid are examined in the next section.

3.3 CONDITIONS FOR FIELDS TO BE QUASISTATIC

An appreciation for the quasistatic approximations will come with a consideration of many case studies. Justification of one or the other of the approximations hinges on using the quasistatic fields to estimate the "error" fields, which are then hopefully found to be small compared to the original quasistatic fields.

In developing any mathematical "theory" for the description of some part of the physical world, approximations are made. Conclusions based on this "theory" should indeed be made with a concern for implicit approximations made out of ignorance or through oversight. But in making quasistatic approximations, we are fortunate in having available the "exact" laws. These can always be used to test the validity of a tentative approximation.

Provided that the system of interest has dimensions that are all within a factor of two or so of each other, order of magnitude arguments easily illustrate how the error fields are related to the quasistatic fields. The examples shown in Fig. 3.3.1 are not to be considered in detail, but rather should be regarded as prototypes. The candidate for the EQS approximation in part (a) consists of metal spheres that are insulated from each other and driven by a source of EMF. In the case of part (b), which is proposed for the MQS approximation, a current source drives a current around a one-turn loop. The dimensions are "on the same order" if the diameter of one of the spheres, is within a factor of two or so of the spacing between spheres

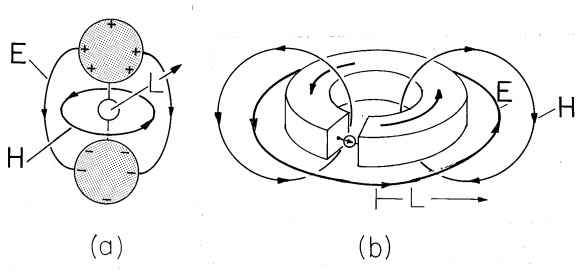


Fig. 3.3.1 Prototype systems involving one typical length. (a) EQS system in which source of EMF drives a pair of perfectly conducting spheres having radius and spacing on the order of L. (b) MQS system consisting of perfectly conducting loop driven by current source. The radius of the loop and diameter of its cross-section are on the order of L.

and if the diameter of the conductor forming the loop is within a similar factor of the diameter of the loop.

If the system is pictured as made up of "perfect conductors" and "perfect insulators," the decision as to whether a quasistatic field ought to be classified as EQS or MQS can be made by a simple rule of thumb: Lower the time rate of change (frequency) of the driving source so that the fields become static. If the magnetic field vanishes in this limit, then the field is EQS; if the electric field vanishes the field is MQS. In reality, materials are not "perfect," neither perfect conductors nor perfect insulators. Therefore, the usefulness of this rule depends on understanding under what circumstances materials tend to behave as "perfect" conductors, and insulators. Fortunately, nature provides us with metals that are extremely good conductors– and with gases, liquids, and solids that are very good insulators– so that this rule is a good intuitive starting point. Chapters 7, 10, and 15 will provide a more mature view of how to classify quasistatic systems.

The quasistatic laws are now used in the order summarized by (3.2.5)-(3.2.9) to estimate the field magnitudes. With only one typical length scale L, we can approximate spatial derivatives that make up the curl and divergence operators by $1/L$.

ELECTROQUASISTATIC

Thus, it follows from Gauss' law, (3.2.5a), that typical values of $\mathbf{E}$ and ρ are related by

$$\frac{\epsilon_o E}{L} = \rho \Rightarrow E = \frac{\rho L}{\epsilon_o} \qquad (1a)$$

MAGNETOQUASISTATIC

Thus, it follows from Ampère's law, (3.2.5b), that typical values of $\mathbf{H}$ and $\mathbf{J}$ are related by

$$\frac{H}{L} = J \Rightarrow H = JL \qquad (1b)$$

As suggested by the integral forms of the laws so far used, these fields and their sources are sketched in Fig. 3.3.1. The EQS laws will predict $\mathbf{E}$ lines that originate on the positive charges on one electrode and terminate on the negative charges on the other. The MQS laws will predict lines of $\mathbf{H}$ that close around the circulating current.

If the excitation were sinusoidal in time, the characteristic time τ for the

sinusoidal steady state response would be the reciprocal of the angular frequency ω. In any case, if the excitations are time varying, with a characteristic time τ, then

the time varying charge implies a current, and this in turn induces an **H**. We could compute the current in the conductors from charge conservation, (3.2.7a), but because we are interested in the induced **H**, we use Ampère's law, (3.2.8a), evaluated in the free space region. The electric field is replaced in favor of the charge density in this expression using (1a).

$$\frac{H}{L} = \frac{\epsilon_o E}{\tau} \Rightarrow \quad H = \frac{\epsilon_o E L}{\tau} = \frac{L^2 \rho}{\tau} \tag{2a}$$

the time-varying current implies an **H** that is time-varying. In accordance with Faraday's law, (3.2.7b), the result is an induced **E**. The magnetic field intensity is replaced by **J** in this expression by making use of (1b).

$$\frac{E}{L} = \frac{\mu_o H}{\tau} \Rightarrow \quad E = \frac{\mu_o H L}{\tau} = \frac{\mu_o J L^2}{\tau} \tag{2b}$$

What errors are committed by ignoring the magnetic induction and displacement current terms in the respective EQS and MQS laws?

The electric field induced by the quasistatic magnetic field is estimated by using the **H** field from (2a) to estimate the contribution of the induction term in Faraday's law. That is, the term originally neglected in (3.2.1a) is now estimated, and from this a *curl* of an error field evaluated.

$$\frac{E_{\text{error}}}{L} = \frac{\mu_o \rho L^2}{\tau^2} \Rightarrow \quad E_{\text{error}} = \frac{\mu_o \rho L^3}{\tau^2} \tag{3a}$$

The magnetic field induced by the displacement current represents an error field. It can be estimated from Ampère's law, by using (2b) to evaluate the displacement current that was originally neglected in (3.2.2b).

$$\frac{H_{\text{error}}}{L} = \frac{\epsilon_o \mu_o J L^2}{\tau^2} \Rightarrow \quad H_{\text{error}} = \frac{\epsilon_o \mu_o J L^3}{\tau^2} \tag{3b}$$

It follows from this expression and (1a) that the ratio of the error field to the quasistatic field is

$$\frac{E_{\text{error}}}{E} = \frac{\mu_o \epsilon_o L^2}{\tau^2} \qquad (4a)$$

It then follows from this and (1b) that the ratio of the error field to the quasistatic field is

$$\frac{H_{\text{error}}}{H} = \frac{\epsilon_o \mu_o L^2}{\tau^2} \qquad (4b)$$

For the approximations to be justified, these error fields must be small compared to the quasistatic fields. Note that whether (4a) is used to represent the EQS system or (4b) is used for the MQS system, the conditions on the spatial scale L and time τ (perhaps the reciprocal frequency) are the same.

Both the EQS and MQS approximations are predicated on having sufficiently slow time variations (low frequencies) and sufficiently small dimensions so that

$$\frac{\mu_o \epsilon_o L^2}{\tau^2} \ll 1 \Rightarrow \frac{L}{c} \ll \tau \qquad (5)$$

where $c = 1/\sqrt{\epsilon_o \mu_o}$. The ratio L/c is the time required for an electromagnetic wave to propagate at the velocity c over a length L characterizing the system. Thus, either of the quasistatic approximations is valid if an electromagnetic wave can propagate a characteristic length of the system in a time that is short compared to times τ of interest.

If the conditions that must be fulfilled in order to justify the quasistatic approximations are the same, how do we know which approximation to use? For systems modeled by free space and perfect conductors, such as we have considered here, the answer comes from considering the fields that are retained in the static limit (infinite τ or zero frequency ω).

Recapitulating the rule expressed earlier, consider the pair of spheres shown in Fig. 3.3.1a. Excited by a constant source of EMF, they are charged, and the charges give rise to an electric field. But in this static limit, there is no current and hence no magnetic field. Thus, the static system is dominated by the electric field, and it is natural to represent it as being EQS even if the excitation is time-varying.

Excited by a dc source, the circulating current in Fig. 3.3.1b gives rise to a magnetic field, but there are no charges with attendant electric fields. This time it is natural to use the MQS approximation when the excitation is time varying.

Example 3.3.1. Estimate of Error Introduced by Electroquasistatic Approximation

Consider a simple structure fed by a set of idealized sources of EMF as shown in Fig. 3.3.2. Two circular metal disks, of radius b, are spaced a distance d apart. A distribution of EMF generators is connected between the rims of the plates so that the complete system, plates and sources, is cylindrically symmetric. With the understanding that in subsequent chapters we will be examining the underlying physical processes, for now we assume that, because the plates are highly conducting, $\mathbf{E}$ must be perpendicular to their surfaces.

The electroquasistatic field laws are represented by (3.2.5a) and (3.2.6a). A simple solution for the electric field between the plates is

$$\mathbf{E} = \frac{\mathcal{E}}{d}\mathbf{i_z} \equiv E_o \mathbf{i_z} \qquad (6)$$

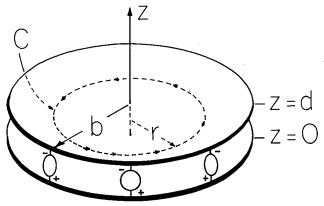


Fig. 3.3.2 Plane parallel electrodes having no resistance, driven at their outer edges by a distribution of sources of EMF.

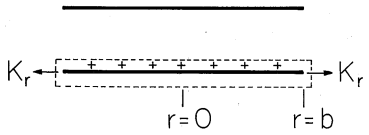


Fig. 3.3.3 Parallel plates of Fig. 3.3.2, showing volume containing lower plate and radial surface current density at its periphery.

where the sign definition of the EMF, $\mathcal{E}$, is as indicated in Fig. 3.3.2. The field of (6) satisfies (3.2.5a) and (3.2.6a) in the region between the plates because it is both irrotational and solenoidal (no charge is assumed to exist in the region between the plates). Further, the field has no component tangential to the plates which is consistent with the assumption of plates with no resistance. Finally, Gauss' jump condition, (1.3.17), can be used to find the surface charges on the top and bottom plates. Because the fields above the upper plate and below the lower plate are assumed to be zero, the surface charge densities on the bottom of the top plate and on the top of the bottom plate are

$$\sigma_s = \begin{cases} -\epsilon_o E_z(z=d) = -\epsilon_o E_o; & z = d \\ \epsilon_o E_z(z=0) = \epsilon_o E_o; & z = 0 \end{cases} \tag{7}$$

There remains the question of how the electric field in the neighborhood of the distributed source of EMF is constrained. We assume here that these sources are connected in such a way that they make the field uniform right out to the outer edges of the plates. Thus, it is consistent to have a field that is uniform throughout the entire region between the plates. Note that the surface charge density on the plates is also uniform out to $r = b$. At this point, (3.2.5a) and (3.2.6a) are satisfied between and on the plates.

In the EQS order of laws, conservation of charge comes next. Rather than using the differential form, (3.2.7a), we use the integral form, (1.5.2). The volume V is a cylinder of circular cross-section enclosing the lower plate, as shown in Fig. 3.3.3. Because the radial surface current density in the plate is independent of ϕ, integration of $\mathbf{J} \cdot d\mathbf{a}$ on the enclosing surface amounts to multiplying K_r by the circumference, while the integration over the volume is carried out by multiplying σ_s by the surface area, because the surface charge density is uniform. Thus,

$$K_r 2\pi b + \pi b^2 \epsilon_o \frac{dE_o}{dt} = 0 \Rightarrow K_r\big|_{r=b} = -\frac{b\epsilon_o}{2}\frac{dE_o}{dt} \tag{8}$$

In order to find the magnetic field, we make use of the "secondary" EQS laws, (3.2.8a) and (3.2.9a). Ampère's law in integral form, (1.4.1), is convenient for the present case of high symmetry. The displacement current is z directed, so the

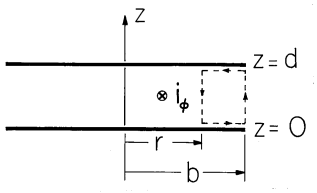


Fig. 3.3.4 Cross-section of system shown in Fig. 3.3.2 showing surface and contour used in evaluating correction **E** field.

surface S is taken as being in the free space region between the plates and having a z-directed normal.

$$\oint_C \mathbf{H} \cdot d\mathbf{s} = \int_S \frac{\partial \epsilon_o \mathbf{E}}{\partial t} \cdot \mathbf{i_z} da \tag{9}$$

The symmetry of structure and source suggests that **H** must be ϕ independent. A centered circular contour of radius r, as in Fig. 3.3.2, with z in the range $0 < z < d$, gives

$$H_\phi 2\pi r = \epsilon_o \frac{dE_o}{dt} \pi r^2 \Rightarrow H_\phi = \frac{r}{2} \epsilon_o \frac{dE_o}{dt} \tag{10}$$

Thus, for this specific configuration, we are at a point in the analysis represented by (2a) in the order of magnitude arguments.

Consider now "higher order" fields and specifically the error committed by neglecting the magnetic induction in the EQS approximation. The correct statement of Faraday's law is (3.2.1a), with the magnetic induction retained. Now that the quasistatic **H** has been determined, we are in a position to compute the curl of **E** that it generates.

Again, for this highly symmetric configuration, it is best to use the integral law. Because **H** is ϕ directed, the surface is chosen to have its normal in the ϕ direction, as shown in Fig. 3.3.4. Thus, Faraday's integral law (1.6.1) becomes

$$\oint_C \mathbf{E} \cdot d\mathbf{s} = -\int_S \frac{\partial \mu_o H_\phi}{\partial t} \mathbf{i}_\phi \cdot d\mathbf{a} \tag{11}$$

We use the contour shown in Fig. 3.3.4 and assume that the **E** induced by the magnetic induction is independent of z. Because the tangential **E** field is zero on the plates, the only contributions to the line integral on the left in (11) come from the vertical legs of the contour. The surface integral on the right is evaluated using (10).

$$\begin{aligned} [E_z(b) - E_z(r)]d &= \frac{\mu_o \epsilon_o d}{2} \int_r^b r' dr' \frac{d^2 E_o}{dt^2} \\ &= \frac{\mu_o \epsilon_o d}{4} (b^2 - r^2) \frac{d^2 E_o}{dt^2} \end{aligned} \tag{12}$$

The field at the outer edge is constrained by the EMF sources to be E_o, and so it follows from (12) that to this order of approximation the electric field is

$$E_z = E_o + \frac{\epsilon_o \mu_o}{4} \frac{d^2 E_o}{dt^2} (r^2 - b^2) \tag{13}$$

We have found that the electric field at $r \neq b$ differs from the field at the edge. How big is the difference? This depends on the time rate of variation of the electric field.

For purposes of illustration, assume that the electric field is sinusoidally varying with time.

$$E_o(t) = A \cos \omega t \tag{14}$$

Thus, the time characterizing the dynamics is $1/\omega$.

Introducing this expression into (13), and calling the second term the "error field," the ratio of the error field and the field at the rim, where $r = b$, is

$$\frac{|E_{\text{error}}|}{E_o} = \frac{1}{4}\omega^2 \epsilon_o \mu_o (b^2 - r^2) \tag{15}$$

The error field will be negligible compared to the quasistatic field if

$$\frac{\omega^2 \epsilon_o \mu_o b^2}{4} \ll 1 \tag{16}$$

for all r between the plates. In terms of the free space wavelength λ, defined as the distance an electromagnetic wave propagates at the velocity $c = 1/\sqrt{\epsilon_o \mu_o}$ in one cycle $2\pi/\omega$

$$\frac{\lambda}{c} = \frac{2\pi}{\omega} : \qquad c \equiv 1/\sqrt{\mu_o \epsilon_o} \tag{17}$$

(16) becomes

$$b^2 \ll (\lambda/\pi)^2 \tag{18}$$

In free space and at a frequency of 1 MHz, the wavelength is 300 meters. Hence, if we build a circular disk capacitor and excite it at a frequency of 1 MHz, then the quasistatic laws will give a good approximation to the actual field as long as the radius of the disk is much less than 300 meters.

The correction field for a MQS system is found by following steps that are analogous to those used in the previous example. Once the magnetic and electric fields have been determined using the MQS laws, the error magnetic field induced by the displacement current can be found.

3.4 QUASISTATIC SYSTEMS[1]

Whether we ignore the magnetic induction and use the EQS approximation, or neglect the displacement current and make a MQS approximation, times of interest τ must be long compared to the time τ_{em} required for an electromagnetic wave to propagate at the velocity c over the largest length L of the system.

$$\tau_{em} = \frac{L}{c} \ll \tau \tag{1}$$

[1] This section makes use of the integral laws at a level somewhat more advanced than necessary in preparation for the next chapter. It can be skipped without loss of continuity.

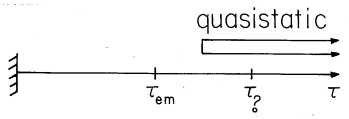


Fig. 3.4.1 Range of characteristic times over which quasistatic approximation is valid. The transit time of an electromagnetic wave is τ_{em} while $\tau_?$ is a time characterizing the dynamics of the quasistatic system.

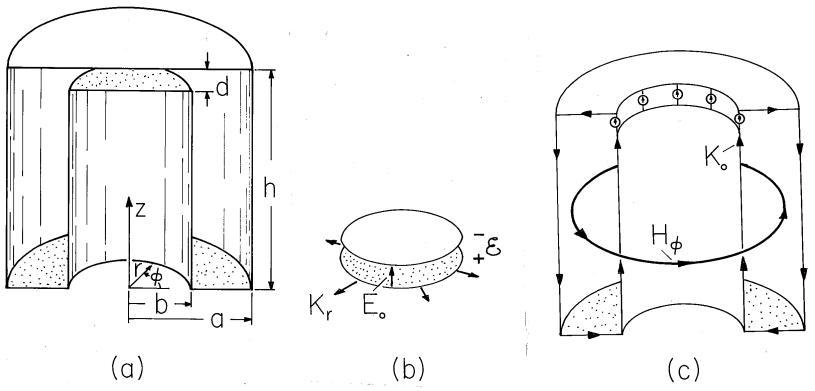


Fig. 3.4.2 (a) Quasistatic system showing (b) its EQS subsystem and (c) its MQS subsystem.

This requirement is given a graphic representation in Fig. 3.4.1.

For a given characteristic time (for example, a given reciprocal frequency), it is clear from (1) that the region described by the quasistatic laws is limited in size. Systems can often be divided into subregions that are small enough to be quasistatic but, by virtue of being interconnected through their boundaries, are dynamic in their behavior. With the elements regarded as the subregions, electric circuits are an example. In the physical world of perfect conductors and free space (to which we are presently limited), it is the topology of the conductors that determines whether these subregions are EQS or MQS.

A system that is described by quasistatic laws but retains a dynamical behavior exhibits one or more characteristic times. On the characteristic time axis in Fig. 3.4.1, $\tau_?$ is one such time. The quasistatic system model provides a meaningful description provided that the one or more characteristic times $\tau_?$ are long compared to τ_{em}. The following example illustrates this concept.

Example 3.4.1. A Quasistatic System Exhibiting Resonance

Shown in cross-section in Fig. 3.4.2 is a resonator used in connection with electron beam devices at microwave frequencies. The volume enclosed by its perfectly conducting boundaries can be broken into the two regions shown. The first of these is bounded by a pair of circular plane parallel conductors having spacing d and radius b. This region is EQS and described in Example 3.3.1.

The second region is bounded by coaxial, perfectly conducting cylinders which form an annular region having outside radius a and an inside radius b that matches up to the outer edge of the lower plate of the EQS system. The coaxial cylinders are

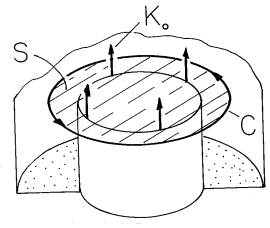


Fig. 3.4.3 Surface S and contour C for evaluating **H**-field using Ampère's law.

shorted by a perfectly conducting plate at the bottom, where $z = 0$. A similar plate at the top, where $z = h$, connects the outer cylinder to the outer edge of the upper plate in the EQS subregion.

For the moment, the subsystems are isolated from each other by driving the MQS system with a current source K_o (amps/meter) distributed around the periphery of the gap between conductors. This gives rise to axial surface current densities of K_o and $-K_o(b/a)$ on the inner and outer cylindrical conductors and radial surface current densities contributing to $\mathbf{J} \cdot d\mathbf{a}$ in the upper and lower plates, respectively. (Note that these satisfy the MQS current continuity requirement.)

Because of the symmetry, the magnetic field can be determined by using the integral MQS form of Ampère's law. So that there is a contribution to the integration of $\mathbf{J} \cdot d\mathbf{a}$, a surface is selected with a normal in the axial direction. This surface is enclosed by a circular contour having the radius r, as shown in Fig. 3.4.3. Because of the axial symmetry, H_ϕ is independent of ϕ, and the integrations on S and C amount to multiplications.

$$\oint_C \mathbf{H} \cdot d\mathbf{s} = \int_S \mathbf{J} \cdot \mathbf{i_z} da \Rightarrow 2\pi r H_\phi = 2\pi b K_o \tag{2}$$

Thus, in the annulus,

$$H_\phi = \frac{b}{r} K_o \tag{3}$$

In the regions outside the annulus, **H** is zero. Note that this is consistent with Ampère's jump condition, (1.4.16), evaluated on any of the boundaries using the already determined surface current densities. Also, we will find in Chap. 10 that there can be no time-varying magnetic flux density normal to a perfectly conducting boundary. The magnetic field given in (3) satisfies this condition as well.

In the hierarchy of MQS laws, we have now satisfied (3.2.5b) and (3.2.6b) and come next to Faraday's law, (3.2.7b). For the present purposes, we are not interested in the details of the distribution of electric field. Rather, we use the integral form of Faraday's law, (1.6.1), integrated on the surface S shown in Fig. 3.4.4. The integral of $\mathbf{E} \cdot d\mathbf{s}$ along the perfect conductor vanishes and we are left with

$$\mathcal{E}_{ab} = \int_a^b \mathbf{E} \cdot d\mathbf{s} = \frac{d\lambda_f}{dt} \tag{4}$$

where the EMF across the gap is as defined by (1.6.2), and the flux linked by C is consistent with (1.6.8).

$$\lambda_f = h \int_b^a \mu_o H_\phi dr = \mu_o b h K_o \int_b^a \frac{dr}{r} = \mu_o h b \, ln\big(\frac{a}{b}\big) K_o \tag{5}$$

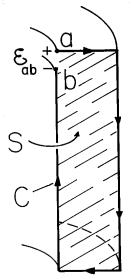


Fig. 3.4.4 Surface S and contour C used to determine EMF using Faraday's law.

These last two expressions combine to give

$$\mathcal{E}_{ab} = \mu_o hb\, ln\Big(\frac{a}{b}\Big)\frac{dK_o}{dt} \tag{6}$$

Just as this expression serves to relate the EMF and surface current density at the gap of the MQS system, (3.3.8) relates the gap variables defined in Fig. 3.4.2b for the EQS subsystem. The subsystems are now interconnected by replacing the distributed current source driving the MQS system with the peripheral surface current density of the EQS system.

$$K_r + K_o = 0 \tag{7}$$

In addition, the EMF's of the two subsystems are made to match where they join.

$$-\mathcal{E} = \mathcal{E}_{ab} \tag{8}$$

With (3.3.8) and (3.3.6), respectively, substituted for K_r and $\mathcal{E}_{ab}$, these expressions become two differential equations in the two variables E_o and K_o describing the complete system.

$$-\frac{b\epsilon_o}{2}\frac{dE_o}{dt} + K_o = 0 \tag{9}$$

$$-dE_o = \mu_o bh\, ln\Big(\frac{a}{b}\Big)\frac{dK_o}{dt} \tag{10}$$

Elimination of K_o between these expressions gives

$$\frac{d^2E_o}{dt^2} + \omega_o^2 E_o = 0 \tag{11}$$

where ω_o is defined as

$$\omega_o^2 = \frac{2d}{\epsilon_o\mu_o hb^2\, ln\big(\frac{a}{b}\big)} \tag{12}$$

and it follows that solutions are a linear combination of $\sin\omega_o t$ and $\cos\omega_o t$.

As might have been suspected from the outset, what we have found is a response to initial conditions that is oscillatory, with a natural frequency ω_o. That is, the parallel plate capacitor that comprises the EQS subsystem, connected in parallel with the one-turn inductor that is the MQS subsystem, responds to initial values of E_o and K_o with an oscillation that at one instant has E_o at its peak magnitude and $K_o = 0$, and a quarter cycle later has $E_o = 0$ and K_o at its peak magnitude.

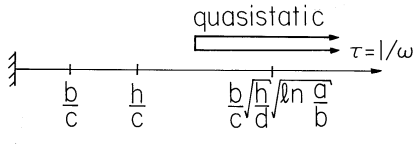


Fig. 3.4.5 In terms of characteristic time τ, the dynamic regime in which the system of Fig. 3.4.2 is quasistatic but capable of being in a state of resonance.

Remember that $\epsilon_o E_o$ is the surface charge density on the lower plate in the EQS section. Thus, the oscillation is between the charges in the EQS subsystem and the currents in the MQS subsystem. The distribution of field sources in the system as a whole is determined by a dynamical interaction between the two subsystems.

If the system were driven by a current source having the frequency ω, it would display a resonance at the natural frequency ω_o. Under what conditions can the system be in resonance and still be quasistatic? In this case, the characteristic time for the system dynamics is the reciprocal of the resonance frequency. The EQS subsystem is indeed EQS if $b/c \ll \tau$, while the annular subsystem is MQS if $h/c \ll \tau$. Thus, the resonance is correctly described by the quasistatic model if the times have the ordering shown in Fig. 3.4.5. Essentially, this is achieved by making the spacing d in the EQS section very small.

With the region of interest containing media, the appropriate quasistatic limit is often as much determined by the material properties as by the topology. In Chaps. 7 and 10, we will consider lossy materials where the distributions of field sources depend on the time rates of change and a given region can be EQS or MQS depending on the electrical conductivity. We return to the subject of quasistatics in Chaps. 12 and 14.

3.5 OVERVIEW OF APPLICATIONS

Electroquasistatics is the subject of Chaps. 4–7 and magnetoquasistatics the topic of Chaps. 8–10. Before embarking on these subjects, consider in this section some practical examples that fall in each category, and some that involve the electrodynamics of Chaps. 12–14.

Our starting point is at location A at the upper right in Fig. 3.5.1. With frequencies that range from 60-400 MHz, television signals propagate from remote locations to our homes as electromagnetic waves. If the frequency is f, the field passes through one period in the time $1/f$. Setting this equal to the transit time, (3.1.l7) gives an expression for the wavelength, the distance the wave travels during one cycle.

$$L \equiv \lambda = \frac{c}{f}$$

Thus, for channel 2 (60 MHz) the wavelength is about 5 m, while for channel 54 it is about 20 cm. The distance between antenna and receiver is many wavelengths, and hence the fields undergo many oscillations while traversing the space between the two. The dynamics is not quasistatic but rather intimately involves the electromagnetic wave represented by inset B and described in Sec. 3.1.

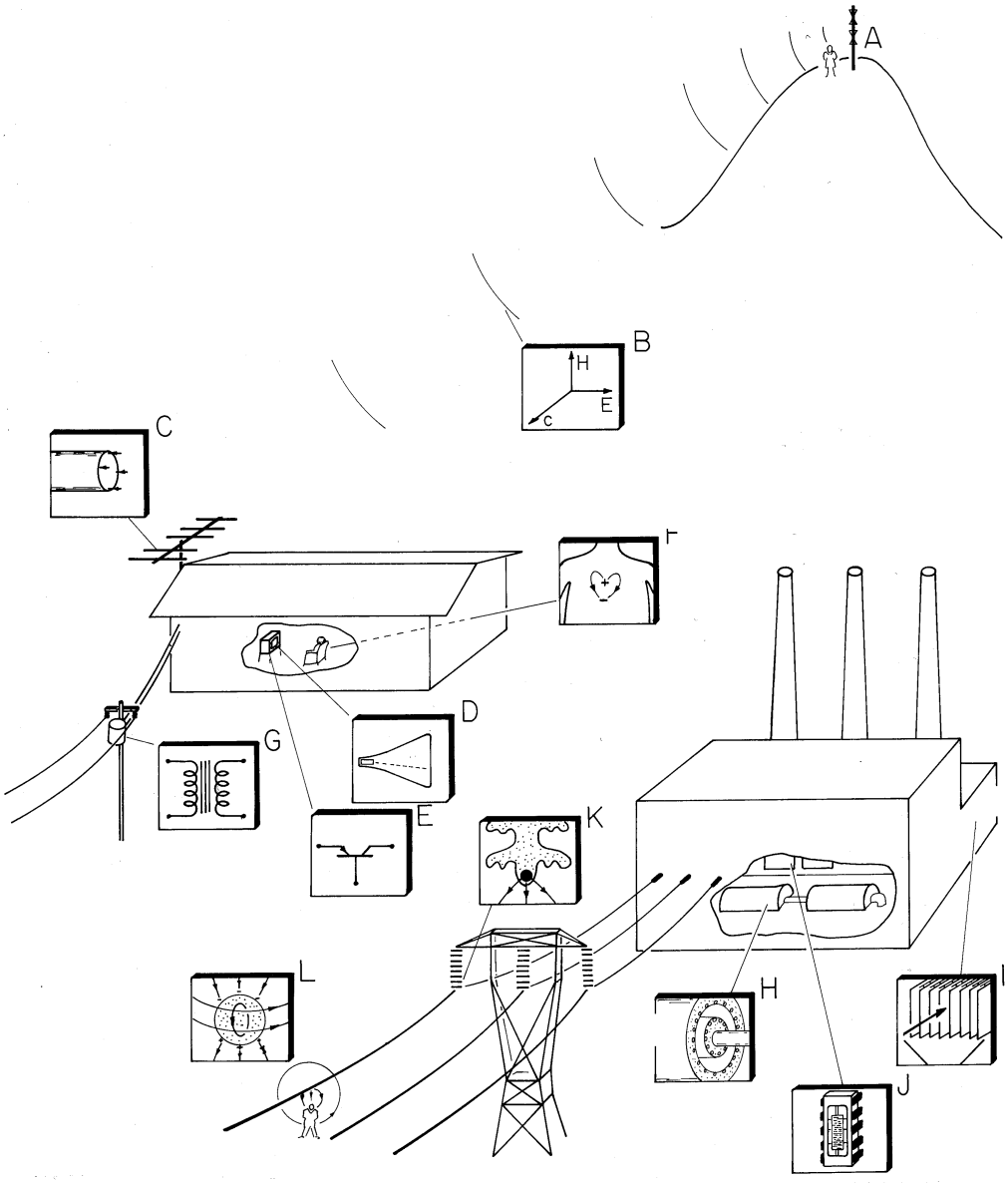


Fig. 3.5.1 Quasistatic and electrodynamic fields in the physical world.

The field induces charges and currents in the antenna, and the resulting signals are conveyed to the TV set by a transmission line. At TV frequencies, the line is likely to be many wavelengths long. Hence, the fields surrounding the line are also not quasistatic. But the radial distributions of current in the elements of the antennas and in the wires of the transmission line are governed by magnetoquasistatic (MQS) laws. As suggested by inset C, the current density tends to concentrate

adjacent to the conductor surfaces and this skin effect is MQS.

Inside the television set, in the transistors and picture tube that convert the signal to an image and sound, electroquasistatic (EQS) processes abound. Included are dynamic effects in the transistors (E) that result from the time required for an electron or hole to migrate a finite distance through a semiconductor. Also included are the effects of inertia as the electrons are accelerated by the electric field in the picture tube (D). On the other hand, the speaker that transduces the electrical signals into sound is most likely MQS.

Electromagnetic fields are far closer to the viewer than the television set. As is obvious to those who have had an electrocardiogram, the heart (F) is the source of a pulsating current. Are the distributions of these currents and the associated fields described by the EQS or MQS approximation? On the largest scales of the body, we will find that it is MQS.

Of course, there are many other sources of electrical currents in the body. Nerve conduction and other electrical activity in the brain occur on much smaller length scales and can involve regions of much less conductivity. These cases can be EQS.

Electrical power systems provide diverse examples as well. The step-down transformer on a pole outside the home (G) is MQS, with dynamical processes including eddy currents and hysteresis.

The energy in all these examples originates in the fuel burned in a power plant. Typically, a steam turbine drives a synchronous alternator (H). The fields within this generator of electrical power are MQS. However, most of the electronics in the control room (J) are described by the EQS approximation. In fact, much of the payoff in making computer components smaller is gained by having them remain EQS even as the bit rate is increased. The electrostatic precipitator (I), used to remove flyash from the combustion gases before they are vented from the stacks, seems to be an obvious candidate for the EQS approximation. Indeed, even though some modern precipitators use pulsed high voltage and all involve dynamic electrical discharges, they are governed by EQS laws.

The power transmission system is at high voltage and therefore might naturally be regarded as EQS. Certainly, specification of insulation performance (K) begins with EQS approximations. However, once electrical breakdown has occurred, enough current can be faulted to bring MQS considerations into play. Certainly, they are present in the operation of high-power switch gear. To be even a fraction of a wavelength at 60 Hz, a line must stretch the length of California. Thus, in so far as the power frequency fields are concerned, the system is quasistatic. But certain aspects of the power line itself are MQS, and others EQS, although when lightning strikes it is likely that neither approximation is appropriate.

Not all fields in our bodies are of physiological origin. The man standing under the power line (L) finds himself in both electric and magnetic fields. How is it that our bodies can shield themselves from the electric field while being essentially transparent to the magnetic field without having obvious effects on our hearts or nervous systems? We will find that currents are indeed induced in the body by both the electric and magnetic fields, and that this coupling is best understood in terms of the quasistatic fields. By contrast, because the wavelength of an electromagnetic wave at TV frequencies is on the order of the dimensions of the body, the currents induced in the person standing in front of the TV antenna at A are not quasistatic.

As we make our way through the topics outlined in Fig. 3.5.1, these and other physical situations will be taken up by the examples.

3.6 SUMMARY

From a mathematical point of view, the summary of quasistatic laws given in Table 3.6.1 is an outline of the next seven chapters.

An excursion down the left column and then down the right column of the outline represented by Fig. 1.0.1 carries us down the corresponding columns of the table. Gauss' law and the requirement that **E** be irrotational, (3.2.5a) and (3.2.6a), are the subjects of Chaps. 4–5. In Chaps. 6 and 7, two types of charge density are distinguished and used to represent the effects of macroscopic media on the electric field. In Chap. 6, where polarization charge is used to represent insulating media, charge is automatically conserved. But in Chap. 7, where unpaired charges are created through conduction processes, the charge conservation law, (3.2.7a), comes into play on the same footing as (3.2.5a) and (3.2.6a). In stages, starting in Chap. 4, the ability to predict self-consistent distributions of **E** and ρ is achieved in this last EQS chapter.

Ampére's law and magnetic flux continuity, (3.2.5b) and (3.2.6b), are featured in Chap. 8. First, the magnetic field is determined for a given distribution of current density. Because current distributions are often controlled by means of wires, it is easy to think of practical situations where the MQS source, the current density, is known at the outset. But even more, the first half of Chap. 7 was already devoted to determining distributions of "stationary" current densities. The MQS current density is always solenoidal, (3.2.5c), and the magnetic induction on the right in Faraday's law, (3.2.7b), is sometimes negligible so that the electric field can be essentially irrotational. Thus, the first half of Chap. 7 actually starts the sequence of MQS topics. In the second half of Chap. 8, the magnetic field is determined for systems of perfect conductors, where the source distribution is not known until the fields meet certain boundary conditions. The situation is analogous to that for EQS systems in Chap. 5. Chapters 9 and 10 distinguish between effects of magnetization and conduction currents caused by macroscopic media. It is in Chap. 10 that Faraday's law, (3.2.7b), comes into play in a field theoretical sense. Again, in stages, in Chaps. 8–10, we attain the ability to describe a self-consistent field and source evolution, this time of **H** and its sources, **J**.

The quasistatic approximations and ordering of laws can just as well be stated in terms of the integral laws. Thus, the differential laws summarized in Table 3.6.1 have the integral law counterparts listed in Table 3.6.2.

TABLE 3.6.1
SUMMARY OF QUASISTATIC DIFFERENTIAL LAWS IN FREE SPACE

ELECTROQUASISTATIC	MAGNETOQUASISTATIC	Reference Eq.
$\nabla \cdot \epsilon_o \mathbf{E} = \rho$	$\nabla \times \mathbf{H} = \mathbf{J}; \quad \nabla \cdot \mathbf{J} = 0$	(3.2.5)
$\nabla \times \mathbf{E} = 0$	$\nabla \cdot \mu_o \mathbf{H} = 0$	(3.2.6)
$\nabla \cdot \mathbf{J} + \dfrac{\partial \rho}{\partial t} = 0$	$\nabla \times \mathbf{E} = \dfrac{-\partial \mu_o \mathbf{H}}{\partial t}$	(3.2.7)
Secondary		
$\nabla \times \mathbf{H} = \mathbf{J} + \dfrac{\partial \epsilon_o \mathbf{E}}{\partial t}$	$\nabla \cdot \epsilon_o \mathbf{E} = \rho$	(3.2.8)
$\nabla \cdot \mu_o \mathbf{H} = 0$		(3.2.9)

TABLE 3.6.2
SUMMARY OF QUASISTATIC INTEGRAL LAWS IN FREE SPACE

(a) ELECTROQUASISTATIC	(b) MAGNETOQUASISTATIC	Eq.
$\oint_S \epsilon_o \mathbf{E} \cdot d\mathbf{a} = \int_V \rho dv$	$\oint_C \mathbf{H} \cdot d\mathbf{s} = \int_S \mathbf{J} \cdot d\mathbf{a}; \quad \oint_S \mathbf{J} \cdot d\mathbf{a} = 0$	(1)
$\oint_C \mathbf{E} \cdot d\mathbf{s} = 0$	$\oint_S \mu_o \mathbf{H} \cdot d\mathbf{a} = 0$	(2)
$\oint_S \mathbf{J} \cdot d\mathbf{a} + \frac{d}{dt} \int_V \rho dV = 0$	$\int_C \mathbf{E} \cdot d\mathbf{s} = -\frac{d}{dt} \int_S \mu_0 \mathbf{H} \cdot d\mathbf{a}$	(3)
Secondary		
$\oint_C \mathbf{H} \cdot d\mathbf{s} = \int_S \mathbf{J} \cdot d\mathbf{a} + \frac{d}{dt} \int_S \epsilon_o \mathbf{E} \cdot d\mathbf{a}$	$\oint_S \epsilon_o \mathbf{E} \cdot d\mathbf{a} = \int_V \rho dv$	(4)
$\oint_S \mu_o \mathbf{H} \cdot d\mathbf{a} = 0$		(5)

PROBLEMS

3.1 Temporal Evolution of World Governed by Laws of Maxwell, Lorentz, and Newton

3.1.1 In Example 3.1.1, it was shown that solutions to Maxwell's equations can take the form $\mathbf{E} = E_x(z - ct)\mathbf{i_x}$ and $\mathbf{H} = H_y(z - ct)\mathbf{i_y}$ in a region where $\mathbf{J} = 0$ and $\rho = 0$.

(a) Given $\mathbf{E}$ and $\mathbf{H}$ by (9) and (10) when $t = 0$, what are these fields for $t > 0$?
(b) By substituting these expressions into (1)–(4), show that they are exact solutions to Maxwell's equations.
(c) Show that for an observer at $z = ct+$ constant, these fields are constant.

3.1.2* Show that in a region where $\mathbf{J} = 0$ and $\rho = 0$ and a solution to Maxwell's equations $\mathbf{E}(\mathbf{r}, t)$ and $\mathbf{H}(\mathbf{r}, t)$ has been obtained, a second solution is obtained by replacing $\mathbf{H}$ by $-\mathbf{E}$, $\mathbf{E}$ by $\mathbf{H}$, ϵ by μ and μ by ϵ.

3.1.3 In Prob. 3.1.1, the initial conditions given by (9) and (10) were arranged so that for $t > 0$, the fields took the form of a wave traveling in the $+z$ direction.

(a) How would you alter the magnetic field intensity, (10), so that the ensuing field took the form of a wave traveling in the $-z$ direction?
(b) What would you make $\mathbf{H}$, so that the result was a pair of electric field intensity waves having the same shape, one traveling in the $+z$ direction and the other traveling in the $-z$ direction?

3.1.4 When $t = 0$, $\mathbf{E} = E_o\mathbf{i_z}\cos\beta x$, where E_o and β are given constants. When $t = 0$, what must $\mathbf{H}$ be to result in $\mathbf{E} = E_o\mathbf{i_z}\cos\beta(x - ct)$ for $t > 0$.

3.2 Quasistatic Laws

3.2.1 In Sec. 13.1, we will find that fields of the type considered in Example 3.1.1 can exist between the plane parallel plates of Fig. P3.2.1. In the particular case where the plates are "open" at the right, where $z = 0$, it will be found that between the plates these fields are

$$\mathbf{E} = E_o\frac{\cos\beta z}{\cos\beta l}\cos\omega t\mathbf{i_x} \qquad (a)$$

$$\mathbf{H} = E_o\sqrt{\frac{\epsilon_o}{\mu_o}}\frac{\sin\beta z}{\cos\beta l}\sin\omega t\mathbf{i_y} \qquad (b)$$

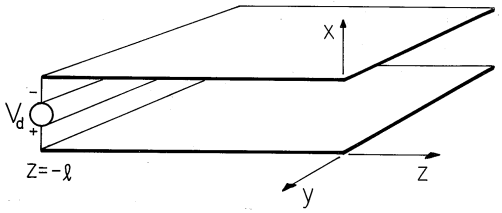


Fig. P3.2.1

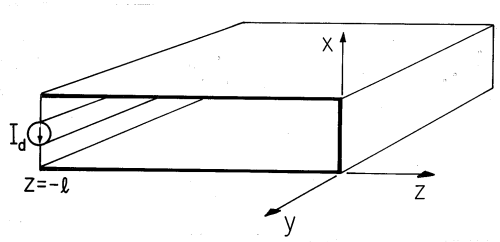


Fig. P3.2.2

where $\beta = \omega\sqrt{\mu_o\epsilon_o}$ and E_o is a constant established by the voltage source at the left.

(a) By substitution, show that in the free space region between the plates (where $\mathbf{J} = 0$ and $\rho = 0$), (a) and (b) are exact solutions to Maxwell's equations.
(b) Use trigonometric identities to show that these fields can be decomposed into sums of waves traveling in the $\pm z$ directions. For example, $E_x = E_+(z - ct) + E_-(z + ct)$, where c is defined by (3.1.16) and $E_\pm$ are functions of $z \mp ct$, respectively.
(c) Show that if $\beta l \ll 1$, the time l/c required for an electromagnetic wave to traverse the length of the electrodes is short compared to the time $\tau \equiv 1/\omega$ within which the driving voltage is changing.
(d) Show that in the limit where this is true, (a) and (b) become

$$\mathbf{E} \rightarrow E_o \cos\omega t \mathbf{i}_\mathbf{x} \tag{c}$$

$$\mathbf{H} \rightarrow E_o\epsilon_o\omega z \sin\omega t \mathbf{i}_\mathbf{y} \tag{d}$$

so that the electric field between the plates is uniform.
(e) With the frequency low enough so that (c) and (d) are good approximations to the fields, do these solutions satisfy the EQS or MQS laws?

3.2.2 In Sec. 13.1, it will be shown that the electric and magnetic fields between the plane parallel plates of Fig. P3.2.2 are

$$\mathbf{E} = \sqrt{\frac{\mu_o}{\epsilon_o}} H_o \frac{\sin\beta z}{\cos\beta l} \sin\omega t \mathbf{i}_\mathbf{x} \tag{a}$$

$$\mathbf{H} = H_o \frac{\cos \beta z}{\cos \beta l} \cos \omega t \mathbf{i_y} \qquad (b)$$

where $\beta = \omega\sqrt{\mu_o \epsilon_o}$ and H_o is a constant determined by the current source at the left. Note that because the plates are "shorted" at $z = 0$, the electric field intensity given by (a) is zero there.

(a) Show that (a) and (b) are exact solutions to Maxwell's equations in the region between the plates where $\mathbf{J} = 0$ and $\rho = 0$.
(b) Use trigonometric identities to show that these fields take the form of waves traveling in the $\pm z$ directions with the velocity c defined by (3.1.16).
(c) Show that the condition $\beta l \ll 1$ is equivalent to the condition that the wave transit time l/c is short compared to $\tau \equiv 1/\omega$.
(d) For the frequency ω low enough so that the conditions of part (c) are satisfied, give approximate expressions for $\mathbf{E}$ and $\mathbf{H}$. Describe the distribution of $\mathbf{H}$ between the plates.
(e) Are these approximate fields governed by the EQS or the MQS laws?

3.3 Conditions for Fields to be Quasistatic

3.3.1 Rather than being in the circular geometry of Example 3.3.1, the configuration considered here and shown in Fig. P3.3.1 consists of plane parallel rectangular electrodes of (infinite) width w in the y direction, spacing d in the x direction and length $2l$ in the z direction. The region between these electrodes is free space. Voltage sources constrain the integral of $\mathbf{E}$ between the electrode edges to be the same functions of time.

$$v = \int_0^d E_x(z = \pm l) dx \qquad (a)$$

(a) Assume that the voltage sources are varying so slowly that the electric field is essentially static (irrotational). Determine the electric field between the electrodes in terms of v and the dimensions. What is the surface charge density on the inside surfaces of the electrodes? (These steps are very similar to those in Example 3.3.1.)
(b) Use conservation of charge to determine the surface current density K_z on the electrodes.
(c) Now use Ampère's integral law and symmetry arguments to find $\mathbf{H}$. With this field between the plates, use Ampère's continuity condition, (1.4.16), to find $\mathbf{K}$ in the plates and show that it is consistent with the result of part (b).
(d) Because of the $\mathbf{H}$ found in part (c), $\mathbf{E}$ is not irrotational. Return to the integral form of Faraday's law to find a corrected electric field intensity, using the magnetic field of part (c). [Note that the electric field found in part (a) already satisfies the conditions imposed by the voltage sources.]

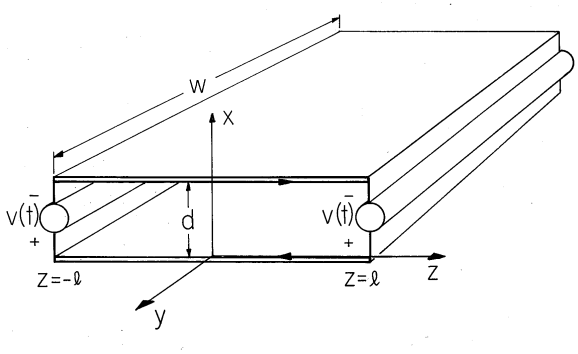


Fig. P3.3.1

(e) If the driving voltage takes the form $v = v_o \cos \omega t$, determine the ratio of the correction (error) field to the quasistatic field of part (a).

3.3.2 The configuration shown in Fig. P3.3.2 is similar to that for Prob. 3.3.1 except that the sources distributed along the left and right edges are current rather than voltage sources and are of opposite rather than the same polarity. Thus, with the current sources varying slowly, a (z-independent) surface current density $K(t)$ circulates around a loop consisting of the sources and the electrodes. The roles of **E** and **H** are the reverse of what they were in Example 3.3.1 or Prob. 3.3.1. Because the electrodes are pictured as having no resistance, the low-frequency electric field is zero while, even if the excitations are constant in time, there is an **H**. The following steps answer the question, Under what circumstances is the electric displacement current negligible compared to the magnetic induction?

(a) Determine **H** in the region between the electrodes in a manner consistent with there being no **H** outside. (Ampère's continuity condition relates **H** to **K** at the electrodes. Like the **E** field in Example 3.3.1 or Prob. 3.3.1, the **H** is extremely simple.)

(b) Use the integral form of Faraday's law to determine **E** between the electrodes. Note that symmetry requires that this field be zero where $z = 0$.

(c) Because of this time-varying **E**, there is a displacement current density between the electrodes in the x direction. Use Ampère's integral law to find the correction (error) **H**. Note that the quasistatic field already meets the conditions imposed by the current sources where $z = \pm l$.

(d) Given that the driving currents are sinusoidal with angular frequency ω, determine the ratio of the "error" of **H** to the MQS field of part (a).

3.4 Quasistatic Systems

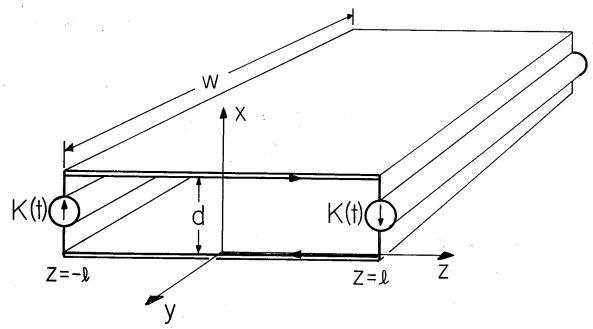


Fig. P3.3.2

3.4.1 The configuration shown in cutaway view in Fig. P3.4.1 is essentially the outer region of the system shown in Fig. 3.4.2. The object here is to determine the error associated with neglecting the displacement current density in this outer region. In this problem, the region of interest is pictured as bounded on three sides by material having no resistance, and on the fourth side by a distributed current source. The latter imposes a surface current density K_o in the z direction at the radius $r = b$. This current passes radially outward through a plate in the $z = h$ plane, axially downward in another conductor at the radius $r = a$, and radially inward in the plate at $z = 0$.

(a) Use the MQS form of Ampère's integral law to determine **H** inside the "donut"-shaped region. This field should be expressed in terms of K_o. (Hint: This step is essentially the same as for Example 3.4.1.)

(b) There is no **H** outside the structure. The interior field is terminated on the boundaries by a surface current density in accordance with Ampère's continuity condition. What is **K** on each of the boundaries?

(c) In general, the driving current is time varying, so Faraday's law requires that there be an electric field. Use the integral form of this law and the contour C and surface S shown in Fig. P3.4.2 to determine **E**. Assume that **E** tangential to the zero-resistance boundaries is zero. Also, assume that **E** is z directed and independent of z.

(d) Now determine the error in the MQS **H** by using Ampère's integral law. This time the displacement current density is not approximated as zero but rather as implied by the **E** found in part (c). Note that the MQS **H** field already satisfies the condition imposed by the current source at $r = b$.

(e) With $K_o = K_p \cos \omega t$, write the condition for the error field to be small compared to the MQS field in terms of ω, c, and l.

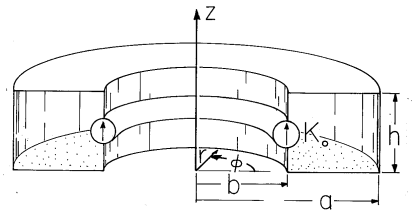


Fig. P3.4.1

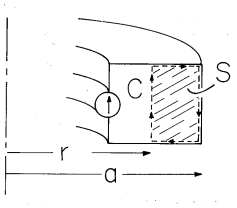


Fig. P3.4.2

4

ELECTROQUASISTATIC FIELDS: THE SUPERPOSITION INTEGRAL POINT OF VIEW

4.0 INTRODUCTION

The reason for taking up electroquasistatic fields first is the relative ease with which such a vector field can be represented. The EQS form of Faraday's law requires that the electric field intensity $\mathbf{E}$ be irrotational.

$$\nabla \times \mathbf{E} = 0 \tag{1}$$

The electric field intensity is related to the charge density ρ by Gauss' law.

$$\nabla \cdot \epsilon_o \mathbf{E} = \rho \tag{2}$$

Thus, the source of an electroquasistatic field is a scalar, the charge density ρ. In free space, the source of a magnetoquasistatic field is a vector, the current density. Scalar sources, are simpler than vector sources and this is why electroquasistatic fields are taken up first.

Most of this chapter is concerned with finding the distribution of $\mathbf{E}$ predicted by these laws, given the distribution of ρ. But before the chapter ends, we will be finding fields in limited regions bounded by conductors. In these more practical situations, the distribution of charge on the boundary surfaces is not known until after the fields have been determined. Thus, this chapter sets the stage for the solving of boundary value problems in Chap. 5.

We start by establishing the electric potential as a scalar function that uniquely represents an irrotational electric field intensity. Byproducts of the derivation are the gradient operator and gradient theorem.

The scalar form of Poisson's equation then results from combining (1) and (2). This equation will be shown to be linear. It follows that the field due to a superposition of charges is the superposition of the fields associated with the individual charge components. The resulting superposition integral specifies how the

potential, and hence the electric field intensity, can be determined from the given charge distribution. Thus, by the end of Sec. 4.5, a general approach to finding solutions to (1) and (2) is achieved.

The art of arranging the charge so that, in a restricted region, the resulting fields satisfy boundary conditions, is illustrated in Secs. 4.6 and 4.7. Finally, more general techniques for using the superposition integral to solve boundary value problems are illustrated in Sec. 4.8.

For those having a background in circuit theory, it is helpful to recognize that the approaches used in this and the next chapter are familiar. The solution of (1) and (2) in three dimensions is like the solution of circuit equations, except that for the latter, there is only the one dimension of time. In the field problem, the driving function is the charge density.

One approach to finding a circuit response is based on first finding the response to an impulse. Then the response to an arbitrary drive is determined by superimposing responses to impulses, the superposition of which represents the drive. This response takes the form of a superposition integral, the convolution integral. The impulse response of Poisson's equation that is our starting point is the field of a point charge. Thus, the theme of this chapter is a convolution approach to solving (1) and (2).

In the boundary value approach of the next chapter, concepts familiar from circuit theory are again exploited. There, solutions will be divided into a particular part, caused by the drive, and a homogeneous part, required to satisfy boundary conditions. It will be found that the superposition integral is one way of finding the particular solution.

4.1 IRROTATIONAL FIELD REPRESENTED BY SCALAR POTENTIAL: THE GRADIENT OPERATOR AND GRADIENT INTEGRAL THEOREM

The integral of an irrotational electric field from some reference point $\mathbf{r}_{\text{ref}}$ to the position $\mathbf{r}$ is independent of the integration path. This follows from an integration of (1) over the surface S spanning the contour defined by alternative paths I and II, shown in Fig. 4.1.1. Stokes' theorem, (2.5.4), gives

$$\int_S \nabla \times \mathbf{E} \cdot d\mathbf{a} = \oint_C \mathbf{E} \cdot d\mathbf{s} = 0 \tag{1}$$

Stokes' theorem employs a contour running around the surface in a single direction, whereas the line integrals of the electric field from $\mathbf{r}$ to $\mathbf{r}_{\text{ref}}$, from point a to point b, run along the contour in opposite directions. Taking the directions of the path increments into account, (1) is equivalent to

$$\oint_C \mathbf{E} \cdot d\mathbf{s} = \int_{a_{\text{path I}}}^{b} \mathbf{E} \cdot d\mathbf{s} - \int_{a_{\text{path II}}}^{b} \mathbf{E} \cdot d\mathbf{s}' = 0 \tag{2}$$

and thus, for an irrotational field, the EMF between two points is independent of path.

$$\int_{a_{\text{path I}}}^{b} \mathbf{E} \cdot d\mathbf{s} = \int_{a_{\text{path II}}}^{b} \mathbf{E} \cdot d\mathbf{s}' \tag{3}$$

$$\int_S \nabla \times \mathbf{E} \cdot d\mathbf{a} = \oint_C \mathbf{E} \cdot d\mathbf{s} = 0$$

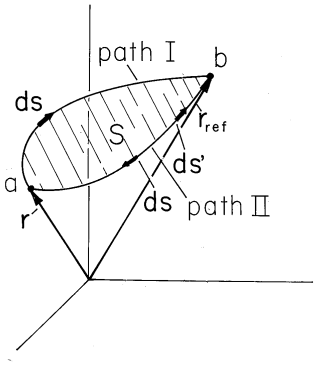


Figure 4.1
positions r
S.

Stokes' theorem employs a contour running around th
whereas the line integrals of the electric field from $\mathbf{r}$ to $\mathbf{r}_{\text{ref}}$

Sec. 4.1 Irrotational Field

Fig. 4.1.1 Paths I and II between positions $\mathbf{r}$ and $\mathbf{r}_{\text{ref}}$ are spanned by surface S.

A field that assigns a unique value of the line integral between two points independent of path of integration is said to be *conservative.*

With the understanding that the reference point is kept fixed, the integral is a scalar function of the integration endpoint $\mathbf{r}$. We use the symbol $\Phi(\mathbf{r})$ to define this scalar function

$$\Phi(\mathbf{r}) - \Phi(\mathbf{r}_{\text{ref}}) = \int_{\mathbf{r}}^{\mathbf{r}_{\text{ref}}} \mathbf{E} \cdot d\mathbf{s} \tag{4}$$

and call $\Phi(\mathbf{r})$ the *electric potential* of the point $\mathbf{r}$ with respect to the reference point. With the endpoints consisting of "nodes" where wires could be attached, the potential difference of (1) would be the *voltage* at $\mathbf{r}$ relative to that at the reference. Typically, the latter would be the "ground" potential. Thus, for an irrotational field, the EMF defined in Sec. 1.6 becomes the voltage at the point a relative to point b.

We shall show that specification of the scalar function $\Phi(\mathbf{r})$ contains the same information as specification of the field $\mathbf{E}(\mathbf{r})$. This is a remarkable fact because a vector function of $\mathbf{r}$ requires, in general, the specification of three scalar functions of $\mathbf{r}$, say the three Cartesian components of the vector function. On the other hand, specification of $\Phi(\mathbf{r})$ requires one scalar function of $\mathbf{r}$.

Note that the expression $\Phi(\mathbf{r}) =$ constant represents a surface in three dimensions. A familiar example of such an expression describes a spherical surface having radius R.

$$x^2 + y^2 + z^2 = R^2 \tag{5}$$

Surfaces of constant potential are called *equipotentials.*

Shown in Fig. 4.1.2 are the cross-sections of two equipotential surfaces, one passing through the point $\mathbf{r}$, the other through the point $\mathbf{r} + \Delta\mathbf{r}$. With $\Delta\mathbf{r}$ taken as a differential vector, the potential at the point $\mathbf{r} + \Delta\mathbf{r}$ differs by the differential

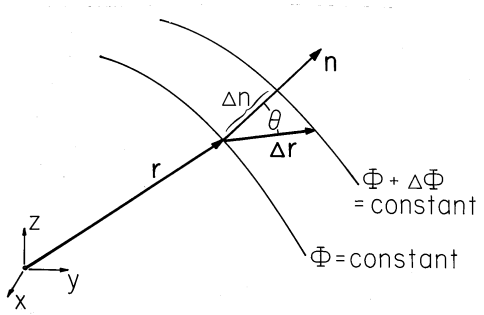


Fig. 4.1.2 Two equipotential surfaces shown cut by a plane containing their normal, **n**.

amount $\Delta\Phi$ from that at $\mathbf{r}$. The two equipotential surfaces cannot intersect. Indeed, if they intersected, both points $\mathbf{r}$ and $\mathbf{r}+\Delta\mathbf{r}$ would have the same potential, which is contrary to our assumption.

Illustrated in Fig. 4.1.2 is the shortest distance Δn from the point $\mathbf{r}$ to the equipotential at $\mathbf{r}+\Delta\mathbf{r}$. Because of the differential geometry assumed, the length element Δn is perpendicular to both equipotential surfaces. From Fig. 4.1.2, $\Delta n = \cos\theta\Delta r$, and we have

$$\Delta\Phi = \frac{\Delta\Phi}{\Delta n}\cos\theta\Delta r = \frac{\Delta\Phi}{\Delta n}\mathbf{n}\cdot\Delta\mathbf{r} \tag{6}$$

The vector $\Delta\mathbf{r}$ in (6) is of arbitrary direction. It is also of arbitrary differential length. Indeed, if we double the distance Δn, we double $\Delta\Phi$ and Δr; $\Delta\Phi/\Delta n$ remains unchanged and thus (6) holds for any Δr (of differential length). We conclude that (6) assigns to every differential vector length element $\Delta\mathbf{r}$, originating from $\mathbf{r}$, a scalar of magnitude proportional to the magnitude of $\Delta\mathbf{r}$ and to the cosine of the angle between $\Delta\mathbf{r}$ and the unit vector $\mathbf{n}$. This assignment of a scalar to a vector is representable as the scalar product of the vector length element $\Delta\mathbf{r}$ with a vector of magnitude $\Delta\Phi/\Delta n$ and direction $\mathbf{n}$. That is, (6) is equivalent to

$$\Delta\Phi = grad\ \Phi\cdot\Delta\mathbf{r} \tag{7}$$

where the gradient of the potential is defined as

$$grad\ \Phi \equiv \frac{\Delta\Phi}{\Delta n}\mathbf{n} \tag{8}$$

Because it is independent of any particular coordinate system, (8) provides the best way to conceptualize the gradient operator. The same equation provides the algorithm for expressing $grad\ \Phi$ in any particular coordinate system. Consider, as an example, Cartesian coordinates. Thus,

$$\mathbf{r} = x\mathbf{i_x} + y\mathbf{i_y} + z\mathbf{i_z}; \qquad \Delta\mathbf{r} = \Delta x\mathbf{i_x} + \Delta y\mathbf{i_y} + \Delta z\mathbf{i_z} \tag{9}$$

and an alternative to (6) for expressing the differential change in Φ is

$$\begin{aligned}\Delta\Phi &= \Phi(x+\Delta x, y+\Delta y, z+\Delta z) - \Phi(x,y,z)\\ &= \frac{\partial\Phi}{\partial x}\Delta x + \frac{\partial\Phi}{\partial y}\Delta y + \frac{\partial\Phi}{\partial z}\Delta z.\end{aligned} \tag{10}$$

In view of (9), this expression is

$$\Delta\Phi = \left(\mathbf{i_x}\frac{\partial\Phi}{\partial x} + \mathbf{i_y}\frac{\partial\Phi}{\partial y} + \mathbf{i_z}\frac{\partial\Phi}{\partial z}\right)\cdot\Delta\mathbf{r} = \nabla\Phi\cdot\Delta\mathbf{r} \tag{11}$$

and it follows that in Cartesian coordinates the gradient operation, as defined by (7), is

$$grad\ \Phi \equiv \nabla\Phi = \frac{\partial\Phi}{\partial x}\mathbf{i_x} + \frac{\partial\Phi}{\partial y}\mathbf{i_y} + \frac{\partial\Phi}{\partial z}\mathbf{i_z} \tag{12}$$

Here, the del operator defined by (2.1.6) is introduced as an alternative way of writing the gradient operator.

Problems at the end of this chapter serve to illustrate how the gradient is similarly determined in other coordinates, with results summarized in Table I at the end of the text.

We are now ready to show that the potential function $\Phi(\mathbf{r})$ defines $\mathbf{E}(\mathbf{r})$ uniquely. According to (4), the potential changes from the point $\mathbf{r}$ to the point $\mathbf{r}+\Delta\mathbf{r}$ by

$$\begin{aligned}\Delta\Phi &= \Phi(\mathbf{r}+\Delta\mathbf{r}) - \Phi(\mathbf{r})\\ &= -\int_{\mathbf{r}_{\rm ref}}^{\mathbf{r}+\Delta\mathbf{r}} \mathbf{E}\cdot d\mathbf{s} + \int_{\mathbf{r}_{\rm ref}}^{\mathbf{r}} \mathbf{E}\cdot d\mathbf{s}\\ &= -\int_{\mathbf{r}}^{\mathbf{r}+\Delta\mathbf{r}} \mathbf{E}\cdot d\mathbf{s}\end{aligned} \tag{13}$$

The first two integrals in (13) follow from the definition of Φ, (4). By recognizing that $d\mathbf{s}$ is $\Delta\mathbf{r}$ and that $\Delta\mathbf{r}$ is of differential length, so that $\mathbf{E}(\mathbf{r})$ can be considered constant over the length of the vector $\Delta\mathbf{r}$, it can be seen that the last integral in (13) becomes

$$\Delta\Phi = -\mathbf{E}\cdot\Delta\mathbf{r} \tag{14}$$

The vector element $\Delta\mathbf{r}$ is arbitrary. Therefore, comparison of (14) to (7) shows that

$$\boxed{\mathbf{E} = -\nabla\Phi} \tag{15}$$

Given the potential function $\Phi(\mathbf{r})$, the associated electric field intensity is the negative gradient of Φ.

Note that we also obtained a useful integral theorem, for if (15) is substituted into (4), it follows that

$$\boxed{\int_{\mathbf{r}_{\rm ref}}^{\mathbf{r}} \nabla\Phi\cdot d\mathbf{s} = \Phi(\mathbf{r}) - \Phi(\mathbf{r}_{\rm ref})} \tag{16}$$

That is, the line integration of the gradient of Φ is simply the difference in potential between the endpoints. Of course, Φ can be any scalar function.

In retrospect, we can observe that the representation of $\mathbf{E}$ by (15) guarantees that it is irrotational, for the vector identity holds

$$\nabla\times(\nabla\Phi) = 0 \tag{17}$$

The curl of the gradient of a scalar potential Φ vanishes. Therefore, given an electric field represented by a potential in accordance with (15), (4.0.1) is automatically satisfied.

Because the preceding discussion shows that the potential Φ contains full information about the field $\mathbf{E}$, the replacement of $\mathbf{E}$ by *grad* (Φ) constitutes a general solution, or integral, of (4.0.1). Integration of a first-order ordinary differential equation leads to one arbitrary integration constant. Integration of the first-order vector differential equation *curl* $\mathbf{E} = 0$ yields a scalar function of integration, $\Phi(\mathbf{r})$.

Thus far, we have not made any specific assignment for the reference point $\mathbf{r}_{\text{ref}}$. Provided that the potential behaves properly at infinity, it is often convenient to let the reference point be at infinity. There are some exceptional cases for which such a choice is not possible. All such cases involve problems with infinite amounts of charge. One such example is the field set up by a charge distribution that extends to infinity in the $\pm z$ directions, as in the second Illustration in Sec. 1.3. The field decays like $1/r$ with radial distance r from the charged region. Thus, the line integral of $\mathbf{E}$, (4), from a finite distance out to infinity involves the difference of $ln\ r$ evaluated at the two endpoints and becomes infinite if one endpoint moves to infinity. In problems that extend to infinity but are not of this singular nature, we shall assume that the reference is at infinity.

Example 4.1.1. Equipotential Surfaces

Consider the potential function $\Phi(x, y)$, which is independent of z:

$$\Phi(x, y) = V_o \frac{xy}{a^2} \tag{18}$$

Surfaces of constant potential can be represented by a cross-sectional view in any $x - y$ plane in which they appear as lines, as shown in Fig. 4.1.3. For the potential given by (18), the equipotentials appear in the $x - y$ plane as hyperbolae. The contours passing through the points (a, a) and $(-a, -a)$ have the potential V_o, while those at $(a, -a)$ and $(-a, a)$ have potential $-V_o$.

The magnitude of $\mathbf{E}$ is proportional to the spatial rate of change of Φ in a direction perpendicular to the constant potential surface. Thus, if the surfaces of constant potential are sketched at equal increments in potential, as is done in Fig. 4.1.3, where the increments are $V_o/4$, the magnitude of $\mathbf{E}$ is inversely proportional to the spacing between surfaces. The closer the spacing of potential lines, the higher the field intensity. Field lines, sketched in Fig. 4.1.3, have arrows that point from high to low potentials. Note that because they are always perpendicular to the equipotentials, they naturally are most closely spaced where the field intensity is largest.

Example 4.1.2. Evaluation of Gradient and Line Integral

Our objective is to exemplify by direct evaluation the fact that the line integration of an irrotational field between two given points is independent of the integration path. In particular, consider the potential given by (18), which, in view of (12), implies the electric field intensity

$$\mathbf{E} = -\nabla\Phi = -\frac{V_o}{a^2}(y\mathbf{i}_\mathbf{x} + x\mathbf{i}_\mathbf{y}) \tag{19}$$

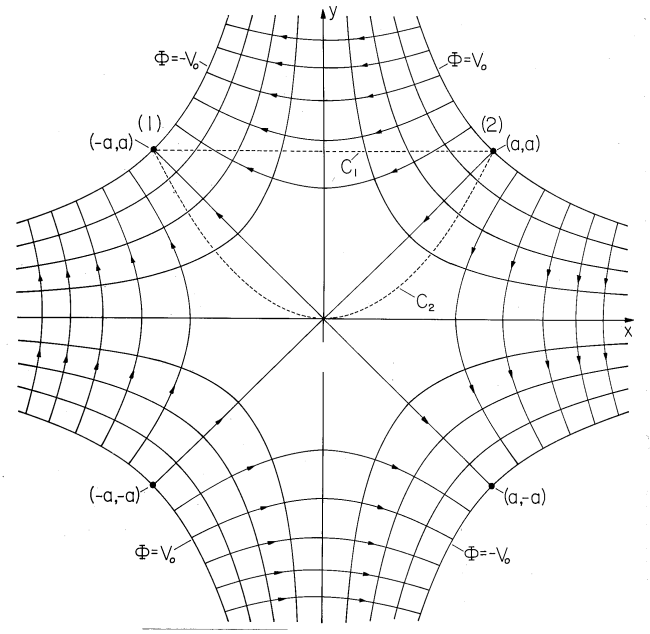


Fig. 4.1.3 Cross-sectional view of surfaces of constant potential for two-dimensional potential given by (18).

We integrate this vector function along two paths, shown in Fig. 4.1.3, which join points (1) and (2). For the first path, C_1, y is held fixed at $y = a$ and hence $d\mathbf{s} = dx\mathbf{i_x}$. Thus, the integral becomes

$$\int_{C_1} \mathbf{E} \cdot d\mathbf{s} = \int_{-a}^{a} E_x(x, a)dx = -\int_{-a}^{a} \frac{V_o}{a^2} a dx = -2V_o \tag{20}$$

For path C_2, $y - x^2/a = 0$ and in general, $d\mathbf{s} = dx\mathbf{i_x} + dy\mathbf{i_y}$, so the required integral is

$$\int_{C_2} \mathbf{E} \cdot d\mathbf{s} = \int_{C_2} (E_x dx + E_y dy) \tag{21}$$

However, for the path C_2 we have $dy - (2x)dx/a = 0$, and hence (21) becomes

$$\begin{aligned} \int_{C_2} \mathbf{E} \cdot d\mathbf{s} &= \int_{-a}^{a} \Big(E_x + \frac{2x}{a} E_y\Big) dx \\ &= \int_{-a}^{a} -\frac{V_o}{a^2} \left(\frac{x^2}{a} + \frac{2x^2}{a} \right) dx = -2V_o \end{aligned} \tag{22}$$

Because $\mathbf{E}$ is found by taking the negative gradient of Φ, and is therefore irrotational, it is no surprise that (20) and (22) give the same result.

Example 4.1.3. Potential of Spherical Cloud of Charge

A uniform static charge distribution ρ_o occupies a spherical region of radius R. The remaining space is charge free (except, of course, for the balancing charge at infinity). The following illustrates the determination of a piece-wise continuous potential function.

The spherical symmetry of the charge distribution imposes a spherical symmetry on the electric field that makes possible its determination from Gauss' integral law. Following the approach used in Example 1.3.1, the field is found to be

$$E_r = \begin{cases} \frac{r\rho_o}{3\epsilon_o}; & r < R \\ \frac{R^3\rho_o}{3\epsilon_o r^2}; & r > R \end{cases} \tag{23}$$

The potential is obtained by evaluating the line integral of (4) with the reference point taken at infinity, $r = \infty$. The contour follows part of a straight line through the origin. In the exterior region, integration gives

$$\Phi(r) = \int_r^\infty E_r dr = \frac{4\pi R^3}{3}\rho_o\Big(\frac{1}{4\pi\epsilon_o r}\Big); \qquad r > R \tag{24}$$

To find Φ in the interior region, the integration is carried through the outer region, (which gives (24) evaluated at $r = R$) and then into the radius r in the interior region.

$$\Phi(r) = \frac{4\pi R^3}{3}\rho_o\Big(\frac{1}{4\pi\epsilon_o R}\Big) + \frac{\rho_o}{6\epsilon_o}(R^2 - r^2) \tag{25}$$

Outside the charge distribution, where $r \geq R$, the potential acquires the form of the coulomb potential of a point charge.

$$\Phi = \frac{q}{4\pi\epsilon_o r}; \qquad q \equiv \frac{4\pi R^3}{3}\rho_o \tag{26}$$

Note that q is the net charge of the distribution.

Visualization of Two-Dimensional Irrotational Fields. In general, equipotentials are three-dimensional surfaces. Thus, any two-dimensional plot of the contours of constant potential is the intersection of these surfaces with some given plane. If the potential is two-dimensional in its dependence, then the equipotential surfaces have a cylindrical shape. For example, the two-dimensional potential of (18) has equipotential surfaces that are cylinders having the hyperbolic cross-sections shown in Fig. 4.1.3.

We review these geometric concepts because we now introduce a different point of view that is useful in picturing *two-dimensional* fields. A three-dimensional picture is now made in which the third dimension represents the amplitude of the potential Φ. Such a picture is shown in Fig. 4.1.4, where the potential of (18) is used as an example. The floor of the three-dimensional plot is the $x - y$ plane, while the vertical dimension is the potential. Thus, contours of constant potential are represented by lines of constant altitude.

The surface of Fig. 4.1.4 can be regarded as a membrane stretched between supports on the periphery of the region of interest that are elevated or depressed in proportion to the boundary potential. By the definition of the gradient, (8), the lines of electric field intensity follow contours of steepest descent on this surface.

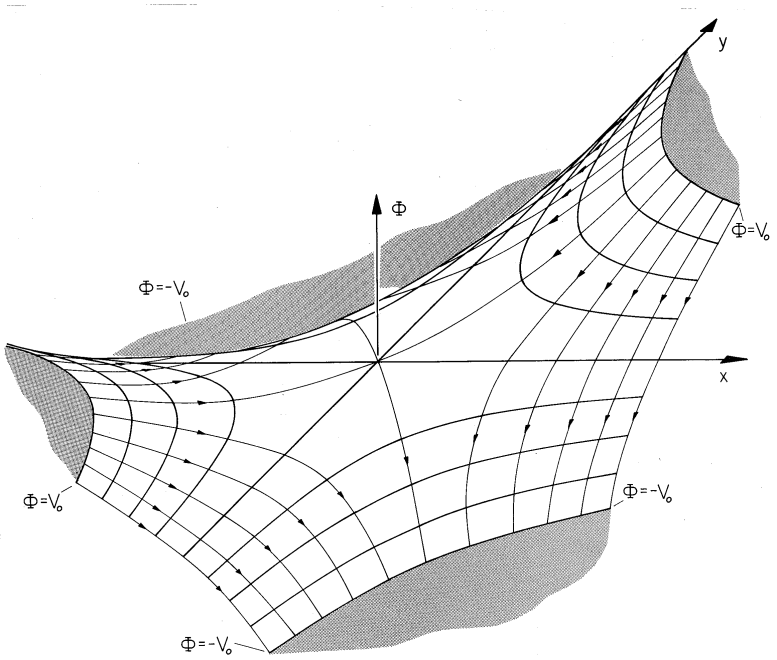


Fig. 4.1.4 Two-dimensional potential of (18) and Fig. 4.1.3 represented in three dimensions. The vertical coordinate, the potential, is analogous to the vertical deflection of a taut membrane. The equipotentials are then contours of constant altitude on the membrane surface.

Potential surfaces have their greatest value in the mind's eye, which pictures a two-dimensional potential as a contour map and the lines of electric field intensity as the flow lines of water streaming down the hill.

4.2 POISSON'S EQUATION

Given that **E** is irrotational, (4.0.1), and given the charge density in Gauss' law, (4.0.2), what is the distribution of electric field intensity? It was shown in Sec. 4.1 that we can satisfy the first of these equations identically by representing the vector **E** by the scalar electric potential Φ.

$$\mathbf{E} = -\nabla\Phi \tag{1}$$

That is, with the introduction of this relation, (4.0.1) has been integrated.

Having integrated (4.0.1), we now discard it and concentrate on the second equation of electroquasistatics, Gauss' law. Introduction of (1) into Gauss' law, (1.0.2), gives

$$\nabla \cdot \nabla\Phi = -\frac{\rho}{\epsilon_o}$$

which is identically

$$\boxed{\nabla^2\Phi = -\frac{\rho}{\epsilon_o}} \tag{2}$$

Integration of this *scalar Poisson's equation*, given the charge density on the right, is the objective in the remainder of this chapter.

By analogy to the ordinary differential equations of circuit theory, the charge density on the right is a "driving function." What is on the left is the operator ∇^2, denoted by the second form of (2) and called the *Laplacian* of Φ. In Cartesian coordinates, it follows from the expressions for the divergence and gradient operators, (2.1.5) and (4.1.12), that

$$\frac{\partial^2\Phi}{\partial x^2} + \frac{\partial^2\Phi}{\partial y^2} + \frac{\partial^2\Phi}{\partial z^2} = \frac{-\rho}{\epsilon_o} \tag{3}$$

The Laplacian operator in cylindrical and spherical coordinates is determined in the problems and summarized in Table I at the end of the text. In Cartesian coordinates, the derivatives in this operator have constant coefficients. In these other two coordinate systems, some of the coefficients are space varying.

Note that in (3), time does not appear explicitly as an independent variable. Hence, the mathematical problem of finding a quasistatic electric field at the time t_o for a time-varying charge distribution $\rho(\mathbf{r}, t)$ is the same as finding the static field for the time-independent charge distribution $\rho(\mathbf{r})$ equal to $\rho(\mathbf{r}, t = t_o)$, the charge distribution of the time-varying problem at the particular instant t_o.

In problems where the charge distribution is given, the evaluation of a quasistatic field is therefore equivalent to the evaluation of a succession of static fields, each with a different charge distribution, at the time of interest. We emphasize this here to make it understood that the solution of a static electric field has wider applicability than one would at first suppose: Every static field solution can represent a "snapshot" at a particular instant of time. Having said that much, we shall not indicate the time dependence of the charge density and field explicitly, but shall do so only when this is required for clarity.

4.3 SUPERPOSITION PRINCIPLE

As illustrated in Cartesian coordinates by (4.2.3), Poisson's equation is a linear second-order differential equation relating the potential $\Phi(\mathbf{r})$ to the charge distribution $\rho(\mathbf{r})$. By "linear" we mean that the coefficients of the derivatives in the differential equation are not functions of the dependent variable Φ. An important consequence of the linearity of Poisson's equation is that $\Phi(\mathbf{r})$ obeys the superposition principle. It is perhaps helpful to recognize the analogy to the superposition principle obeyed by solutions of the linear ordinary differential equations of circuit theory. Here the principle can be shown as follows.

Consider two different spatial distributions of charge density, $\rho_a(\mathbf{r})$ and $\rho_b(\mathbf{r})$. These might be relegated to different regions, or occupy the same region. Suppose we have found the potentials Φ_a and Φ_b which satisfy Poisson's equation, (4.2.3),

with the respective charge distributions ρ_a and ρ_b. By definition,

$$\nabla^2\Phi_a(\mathbf{r}) = -\frac{\rho_a(\mathbf{r})}{\epsilon_o} \tag{1}$$

$$\nabla^2\Phi_b(\mathbf{r}) = -\frac{\rho_b(\mathbf{r})}{\epsilon_o} \tag{2}$$

Adding these expressions, we obtain

$$\nabla^2\Phi_a(\mathbf{r}) + \nabla^2\Phi_b(\mathbf{r}) = -\frac{1}{\epsilon_o}[\rho_a(\mathbf{r}) + \rho_b(\mathbf{r})] \tag{3}$$

Because the derivatives called for in the Laplacian operation– for example, the second derivatives of (4.2.3)– give the same result whether they operate on the potentials and then are summed or operate on the sum of the potentials, (3) can also be written as

$$\nabla^2[\Phi_a(\mathbf{r}) + \Phi_b(\mathbf{r})] = -\frac{1}{\epsilon_o}[\rho_a(\mathbf{r}) + \rho_b(\mathbf{r})] \tag{4}$$

The mathematical statement of the superposition principle follows from (1) and (2) and (4). That is, if

$$\begin{aligned} \rho_a &\Rightarrow \Phi_a \\ \rho_b &\Rightarrow \Phi_b \end{aligned} \tag{5}$$

then

$$\rho_a + \rho_b \Rightarrow \Phi_a + \Phi_b \tag{6}$$

The potential distribution produced by the superposition of the charge distributions is the sum of the potentials associated with the individual distributions.

4.4 FIELDS ASSOCIATED WITH CHARGE SINGULARITIES

At least three objectives are set in this section. First, the superposition concept from Sec. 4.3 is exemplified. Second, we begin to deal with fields that are not highly symmetric. The potential proves invaluable in picturing such fields, and so we continue to develop ways of picturing the potential and field distribution. Finally, the potential functions developed will reappear many times in the chapters that follow. Solutions to Poisson's equation as pictured here filling all of space will turn out to be solutions to Laplace's equation in subregions that are devoid of charge. Thus, they will be seen from a second point of view in Chap. 5, where Laplace's equation is featured.

First, consider the potential associated with a point charge at the origin of a spherical coordinate system. The electric field was obtained using the integral form of Gauss' law in Sec. 1.3, (1.3.12). It follows from the definition of the potential, (4.1.4), that the potential of a point charge q is

$$\Phi = \frac{q}{4\pi\epsilon_o r} \tag{1}$$

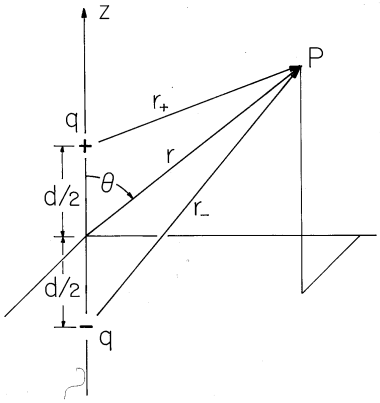


Fig. 4.4.1 Point charges of equal magnitude and opposite sign on the z axis.

This "impulse response" for the three-dimensional Poisson's equation is the starting point in derivations and problem solutions and is worth remembering.

Consider next the field associated with a positive and a negative charge, located on the z axis at $d/2$ and $-d/2$, respectively. The configuration is shown in Fig. 4.4.1. In (1), r is the scalar distance between the point of observation and the charge. With P the observation position, these distances are denoted in Fig. 4.4.1 by r_+ and r_-. It follows from (1) and the superposition principle that the potential distribution for the two charges is

$$\Phi = \frac{q}{4\pi\epsilon_o}\left(\frac{1}{r_+} - \frac{1}{r_-}\right) \tag{2}$$

To find the electric field intensity by taking the negative gradient of this function, it is necessary to express r_+ and r_- in Cartesian coordinates.

$$r_+ = \sqrt{x^2 + y^2 + \left(z - \frac{d}{2}\right)^2}; \qquad r_- = \sqrt{x^2 + y^2 + \left(z + \frac{d}{2}\right)^2} \tag{3}$$

Thus, in these coordinates, the potential for the two charges given by (2) is

$$\Phi = \frac{q}{4\pi\epsilon_o}\left(\frac{1}{\sqrt{x^2 + y^2 + \left(z - \frac{d}{2}\right)^2}} - \frac{1}{\sqrt{x^2 + y^2 + \left(z + \frac{d}{2}\right)^2}}\right) \tag{4}$$

Equation (2) shows that in the immediate vicinity of one or the other of the charges, the respective charge dominates the potential. Thus, close to the point charges the equipotentials are spheres enclosing the charge. Also, this expression makes it clear that the plane $z = 0$ is one of zero potential.

One straightforward way to plot the equipotentials in detail is to program a calculator to evaluate (4) at a specified coordinate position. To this end, it is convenient to normalize the potential and the coordinates such that (4) is

$$\underline{\Phi} = \frac{1}{\sqrt{\underline{x}^2 + \underline{y}^2 + \left(\underline{z} - \frac{1}{2}\right)^2}} - \frac{1}{\sqrt{\underline{x}^2 + \underline{y}^2 + \left(\underline{z} + \frac{1}{2}\right)^2}} \tag{5}$$

where

$$\underline{x} = \frac{x}{d}, \quad \underline{y} = \frac{y}{d}, \quad \underline{z} = \frac{z}{d}, \quad \underline{\Phi} = \frac{\Phi}{(q/4\pi d\epsilon_o)}$$

By evaluating Φ for various coordinate positions, it is possible to zero in on the coordinates of a given equipotential in an iterative fashion. The equipotentials shown in Fig. 4.4.2a were plotted in this way with $\underline{x} = 0$. Of course, the equipotentials are actually three-dimensional surfaces obtained by rotating the curves shown about the z axis.

Because $\mathbf{E}$ is the negative gradient of Φ, lines of electric field intensity are perpendicular to the equipotentials. These can therefore be easily sketched and are shown as lines with arrows in Fig. 4.4.2a.

Dipole at the Origin. An important limit of (2) corresponds to a view of the field for an observer far from either of the charges. This is a very important limit because charge pairs of opposite sign are the model for polarized atoms or molecules. The dipole is therefore at center stage in Chap. 6, where we deal with polarizable matter. Formally, the dipole limit is taken by recognizing that rays joining the point of observation with the respective charges are essentially parallel to the r coordinate when $r \gg d$. The approximate geometry shown in Fig. 4.4.3 motivates the approximations.

$$r_+ \simeq r - \frac{d}{2}\cos\theta; \qquad r_- \simeq r + \frac{d}{2}\cos\theta \tag{6}$$

Because the first terms in these expressions are very large compared to the second, powers of r_+ and r_- can be expanded in a binomial expansion.

$$(a+b)^n = a^n + na^{n-1}b + \dots \tag{7}$$

With $n = -1$, (2) becomes approximately

$$\begin{aligned}\Phi &= \frac{q}{4\pi\epsilon_o}\left[\left(\frac{1}{r} + \frac{d}{2r^2}\cos\theta + \dots\right)\right. \\ &\quad \left. - \left(\frac{1}{r} - \frac{d}{2r^2}\cos\theta + \dots\right)\right] \\ &= \frac{qd}{4\pi\epsilon_o}\frac{\cos\theta}{r^2}\end{aligned} \tag{8}$$

Remember, the potential is pictured in spherical coordinates.

Suppose the equipotential is to be sketched that passes through the z axis at some specified location. What is the shape of the potential as we move in the positive θ direction? On the left in (8) is a constant. With an increase in θ, the cosine function on the right decreases. Thus, to stay on the surface, the distance r from the origin must decrease. As the angle approaches $\pi/2$, the cosine decreases to zero, making it clear that the equipotential must approach the origin. The equipotentials and associated lines of $\mathbf{E}$ are shown in Fig. 4.4.2b.

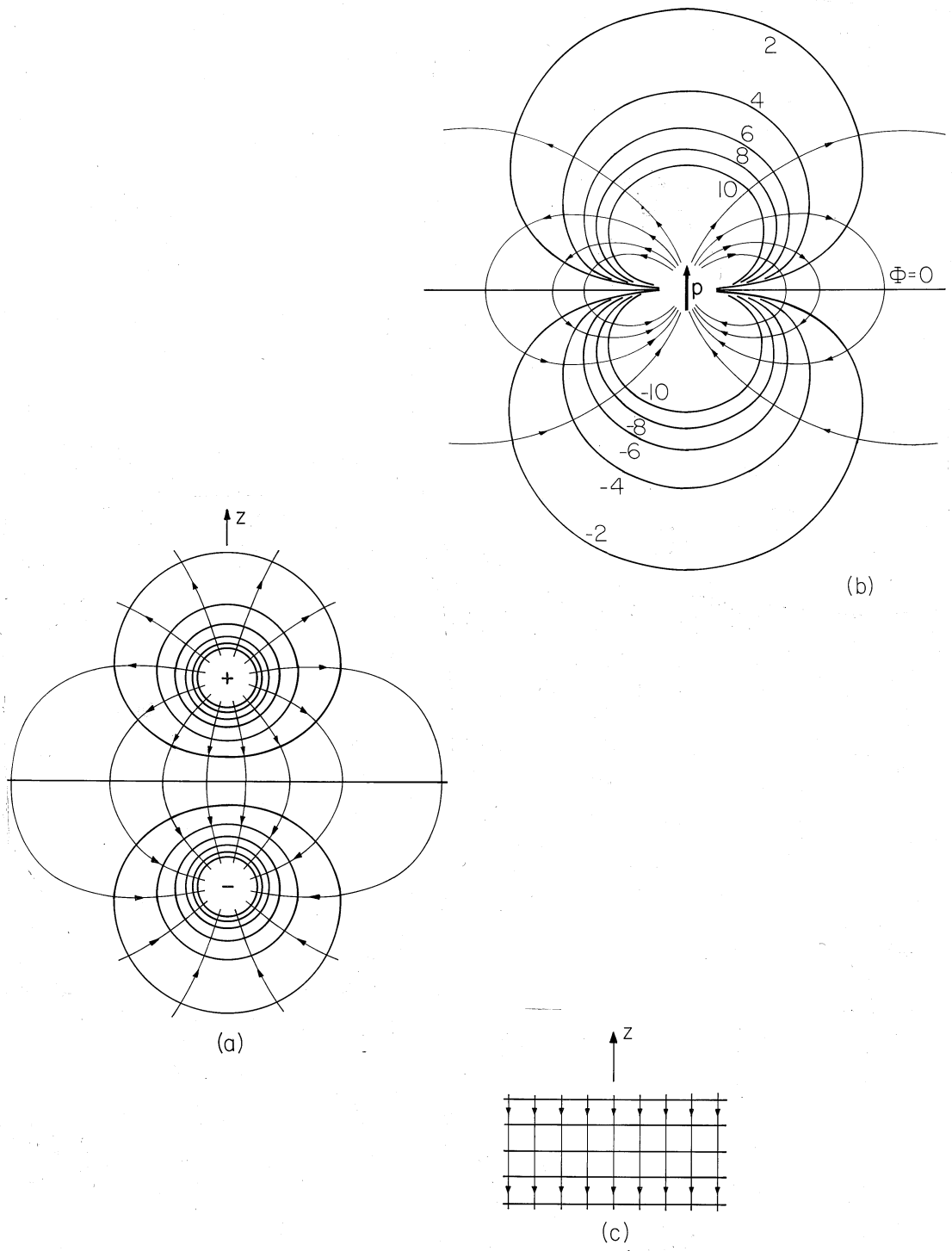


Fig. 4.4.2 (a) Cross-section of equipotentials and lines of electric field intensity for the two charges of Fig. 4.4.1. (b) Limit in which pair of charges form a dipole at the origin. (c) Limit of charges at infinity.

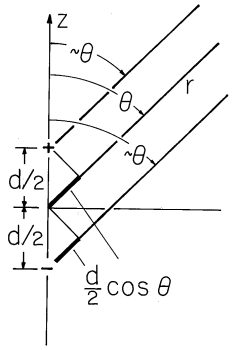


Fig. 4.4.3 Far from the dipole, rays from the charges to the point of observation are essentially parallel to r coordinate.

The dipole model is made mathematically exact by defining it as the limit in which two charges of equal magnitude and opposite sign approach to within an infinitesimal distance of each other while increasing in magnitude. Thus, with the dipole moment p defined as

$$p = \lim_{\substack{d\to 0 \\ q\to\infty}} qd \tag{9}$$

the potential for the dipole, (8), becomes

$$\Phi = \frac{p}{4\pi\epsilon_o}\frac{\cos\theta}{r^2} \tag{10}$$

Another more general way of writing (10) with the dipole positioned at an arbitrary point $\mathbf{r}'$ and lying along a general axis is to introduce the dipole moment vector. This vector is defined to be of magnitude p and directed along the axis of the two charges pointing from the $-$ charge to the $+$ charge. With the unit vector $\mathbf{i}_{\mathbf{r}'\mathbf{r}}$ defined as being directed from the point $\mathbf{r}'$ (where the dipole is located) to the point of observation at $\mathbf{r}$, it follows from (10) that the generalized potential is

$$\Phi = \frac{\mathbf{p}\cdot\mathbf{i}_{\mathbf{r}'\mathbf{r}}}{4\pi\epsilon_o|\mathbf{r}-\mathbf{r}'|^2} \tag{11}$$

Pair of Charges at Infinity Having Equal Magnitude and Opposite Sign. Consider next the appearance of the field for an observer located between the charges of Fig. 4.4.2a, in the neighborhood of the origin. We now confine interest to distances from the origin that are small compared to the charge spacing d. Effectively, the charges are at infinity in the $+z$ and $-z$ directions, respectively.

With the help of Fig. 4.4.4 and the three-dimensional Pythagorean theorem, the distances from the charges to the observer point are expressed in spherical coordinates as

$$r_+ = \sqrt{\left(\frac{d}{2} - r\cos\theta\right)^2 + (r\sin\theta)^2}; \qquad r_- = \sqrt{\left(\frac{d}{2} + r\cos\theta\right)^2 + (r\sin\theta)^2} \tag{12}$$

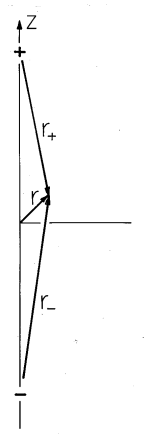


Fig. 4.4.4 Relative displacements with charges going to infinity.

In these expressions, d is large compared to r, so they can be expanded by again using (7) and keeping only linear terms in r.

$$r_+^{-1} \simeq \frac{2}{d} + \frac{4r}{d^2}\cos\theta; \qquad r_-^{-1} \simeq \frac{2}{d} - \frac{4r}{d^2}\cos\theta \tag{13}$$

Introduction of these approximations into (2) results in the desired expression for the potential associated with charges that are at infinity on the z axis.

$$\Phi \rightarrow \frac{2(q/d^2)}{\pi\epsilon_o} r\cos\theta \tag{14}$$

Note that $z = r\cos\theta$, so what appears to be a complicated field in spherical coordinates is simply

$$\Phi \rightarrow \frac{2q/d^2}{\pi\epsilon_o} z \tag{15}$$

The z coordinate can just as well be regarded as Cartesian, and the electric field evaluated using the gradient operator in Cartesian coordinates. Thus, the surfaces of constant potential, shown in Fig. 4.4.2c, are horizontal planes. It follows that the electric field intensity is uniform and downward directed. Note that the electric field that follows from (15) is what is obtained by direct evaluation of (1.3.12) as the field of point charges q at a distance $d/2$ above and below the point of interest.

Other Charge Singularities. A two-dimensional dipole consists of a pair of oppositely charged parallel lines, rather than a pair of point charges. Pictured in a plane perpendicular to the lines, and in polar coordinates, the equipotentials appear similar to those of Fig. 4.4.2b. However, in three dimensions the surfaces are cylinders of circular cross-section and not at all like the closed surfaces of revolution that are the equipotentials for the three-dimensional dipole. Two-dimensional dipole fields are derived in Probs. 4.4.1 and 4.4.2, where the potentials are given for reference.

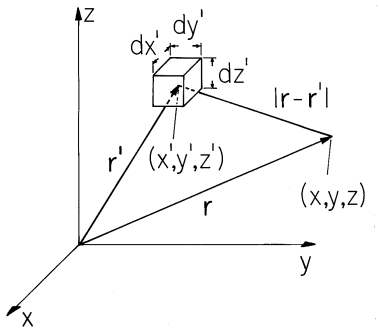


Fig. 4.5.1 An elementary volume of charge at $\mathbf{r}'$ gives rise to a potential at the observer position $\mathbf{r}$.

There is an infinite number of charge singularities. One of the "higher order" singularities is illustrated by the quadrupole fields developed in Probs. 4.4.3 and 4.4.4. We shall see these same potentials again in Chap. 5.

4.5 SOLUTION OF POISSON'S EQUATION FOR SPECIFIED CHARGE DISTRIBUTIONS

The superposition principle is now used to find the solution of Poisson's equation for any given charge distribution $\rho(\mathbf{r})$. The argument presented in the previous section for singular charge distributions suggests the approach.

For the purpose of representing the arbitrary charge density distribution as a sum of "elementary" charge distributions, we subdivide the space occupied by the charge density into elementary volumes of size $dx'dy'dz'$. Each of these elements is denoted by the Cartesian coordinates (x', y', z'), as shown in Fig. 4.5.1. The charge contained in one of these elementary volumes, the one with the coordinates (x', y', z'), is

$$dq = \rho(\mathbf{r}')dx'dy'dz' = \rho(\mathbf{r}')dv' \tag{1}$$

We now express the total potential due to the charge density ρ as the superposition of the potentials $d\Phi$ due to the differential elements of charge, (1), positioned at the points $\mathbf{r}'$. Note that each of these elementary charge distributions has zero charge density at all points outside of the volume element dv' situated at $\mathbf{r}'$. Thus, they represent point charges of magnitudes dq given by (1). Provided that $|\mathbf{r} - \mathbf{r}'|$ is taken as the distance between the point of observation $\mathbf{r}$ and the position of one incremental charge $\mathbf{r}'$, the potential associated with this incremental charge is given by (4.4.1).

$$d\Phi(\mathbf{r}, \mathbf{r}') = \frac{\rho(\mathbf{r}')dv'}{4\pi\epsilon_o|\mathbf{r} - \mathbf{r}'|} \tag{2}$$

where in Cartesian coordinates

$$|\mathbf{r} - \mathbf{r}'| = \sqrt{(x - x')^2 + (y - y')^2 + (z - z')^2}$$

Note that (2) is a function of two sets of Cartesian coordinates: the (observer) coordinates (x, y, z) of the point $\mathbf{r}$ at which the potential is evaluated and the

(source) coordinates (x', y', z') of the point $\mathbf{r}'$ at which the incremental charge is positioned.

According to the superposition principle, we obtain the total potential produced by the sum of the differential charges by adding over all differential potentials, keeping the observation point (x, y, z) fixed. The sum over the differential volume elements becomes a volume integral over the coordinates (x', y', z').

$$\boxed{\Phi(\mathbf{r}) = \int_{V'} \frac{\rho(\mathbf{r}')dv'}{4\pi\epsilon_o|\mathbf{r} - \mathbf{r}'|}} \tag{3}$$

This is the *superposition integral* for the electroquasistatic potential.

The evaluation of the potential requires that a triple integration be carried out. With the help of a computer, or even a programmable calculator, this is a straightforward process. There are few examples where the three successive integrations are carried out analytically without considerable difficulty.

There are special representations of (3), appropriate in cases where the charge distribution is confined to surfaces, lines, or where the distribution is two dimensional. For these, the number of integrations is reduced to two or even one, and the difficulties in obtaining analytical expressions are greatly reduced.

Three-dimensional charge distributions can be represented as the superposition of lines and sheets of charge and, by exploiting the potentials found analytically for these distributions, the numerical integration that might be required to determine the potential for a three-dimensional charge distribution can be reduced to two or even one numerical integration.

Superposition Integral for Surface Charge Density. If the charge density is confined to regions that can be described by surfaces having a very small thickness Δ, then one of the three integrations of (3) can be carried out in general. The situation is as pictured in Fig. 4.5.2, where the distance to the observation point is large compared to the thickness over which the charge is distributed. As the integration of (3) is carried out over this thickness Δ, the distance between source and observer, $|\mathbf{r} - \mathbf{r}'|$, varies little. Thus, with ξ used to denote a coordinate that is locally perpendicular to the surface, the general superposition integral, (3), reduces to

$$\Phi(\mathbf{r}) = \int_{A'} \frac{da'}{4\pi\epsilon_o|\mathbf{r} - \mathbf{r}'|} \int_0^{\Delta} \rho(\mathbf{r}')d\xi \tag{4}$$

The integral on ξ is by definition the surface charge density. Thus, (4) becomes a form of the superposition integral applicable where the charge distribution can be modeled as being on a surface.

$$\boxed{\Phi(\mathbf{r}) = \int_{A'} \frac{\sigma_s(\mathbf{r}')da'}{4\pi\epsilon_o|\mathbf{r} - \mathbf{r}'|}} \tag{5}$$

The following example illustrates the application of this integral.

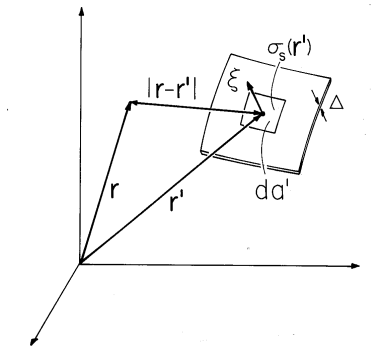


Fig. 4.5.2 An element of surface charge at the location $\mathbf{r}'$ gives rise to a potential at the observer point $\mathbf{r}$.

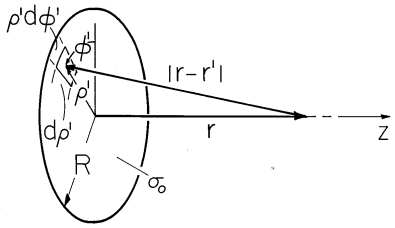


Fig. 4.5.3 A uniformly charged disk with coordinates for finding the potential along the z axis.

Example 4.5.1. Potential of a Uniformly Charged Disk

The disk shown in Fig. 4.5.3 has a radius R and carries a uniform surface charge density σ_o. The following steps lead to the potential and field on the axis of the disk.

The distance $|\mathbf{r}-\mathbf{r}'|$ between the point $\mathbf{r}'$ at radius ρ and angle ϕ (in cylindrical coordinates) and the point $\mathbf{r}$ on the axis of the disk (the z axis) is given by

$$|\mathbf{r}-\mathbf{r}'| = \sqrt{\rho'^2 + z^2} \tag{6}$$

It follows that (5) is expressible in terms of the following double integral

$$\begin{aligned} \Phi &= \frac{\sigma_o}{4\pi\epsilon_o}\int_0^{2\pi}\int_0^R \frac{\rho' d\rho' d\phi'}{\sqrt{\rho'^2+z^2}} \\ &= \frac{\sigma_o}{4\pi\epsilon_o} 2\pi \int_0^R \frac{\rho' d\rho'}{\sqrt{\rho'^2+z^2}} \\ &= \frac{\sigma_o}{2\epsilon_o}\left(\sqrt{R^2+z^2}-|z|\right) \end{aligned} \tag{7}$$

where we have allowed for both positive z, the case illustrated in the figure, and negative z. Note that these are points on opposite sides of the disk.

The axial field intensity E_z can be found by taking the gradient of (7) in the z direction.

$$\begin{aligned} E_z = -\frac{\partial \Phi}{\partial z} &= -\frac{\sigma_o}{2\epsilon_o}\frac{d}{dz}\left(\sqrt{R^2+z^2}-|z|\right) \\ &= -\frac{\sigma_o}{2\epsilon_o}\left(\frac{z}{\sqrt{R^2+z^2}}\mp 1\right) \end{aligned} \tag{8}$$

The upper sign applies to positive z, the lower sign to negative z.

The potential distribution of (8) can be checked in two limiting cases for which answers are easily obtained by inspection: the potential at a distance $|z| \gg R$, and the field at $|z| \ll R$.

(a) At a very large distance $|z|$ of the point of observation from the disk, the radius of the disk R is small compared to $|z|$, and the potential of the disk must approach the potential of a point charge of magnitude equal to the total charge of the disk, $\sigma_o \pi R^2$. The potential given by (7) can be expanded in powers of R/z

$$\sqrt{R^2+z^2}-|z| = |z|\left(1+\frac{1}{2}\frac{R^2}{z^2}\right) \tag{9}$$

to find that Φ indeed approaches the potential function

$$\Phi \simeq \frac{\sigma_o}{4\pi\epsilon_o}\pi R^2 \frac{1}{|z|} \tag{10}$$

of a point charge at distance $|z|$ from the observation point.

(b) At $|z| \ll R$, on either side of the disk, the field of the disk must approach that of a charge sheet of very large (infinite) extent. But that field is $\pm\sigma_o/2\epsilon_o$. We find, indeed, that in the limit $|z| \to 0$, (8) yields this limiting result.

Superposition Integral for Line Charge Density. Another special case of the general superposition integral, (3), pertains to fields from charge distributions that are confined to the neighborhoods of lines. In practice, dimensions of interest are large compared to the cross-sectional dimensions of the area A' of the charge distribution. In that case, the situation is as depicted in Fig. 4.5.4, and in the integration over the cross-section the distance from source to observer is essentially constant. Thus, the superposition integral, (3), becomes

$$\Phi(\mathbf{r}) = \int_{L'} \frac{dl'}{4\pi\epsilon_o|r-r'|}\int_{A'}\rho(\mathbf{r}')da' \tag{11}$$

In view of the definition of the line charge density, (1.3.10), this expression becomes

$$\boxed{\Phi(\mathbf{r}) = \int_{L'}\frac{\lambda_l(\mathbf{r}')dl'}{4\pi\epsilon_o|r-r'|}} \tag{12}$$

Example 4.5.2. Field of Collinear Line Charges of Opposite Polarity

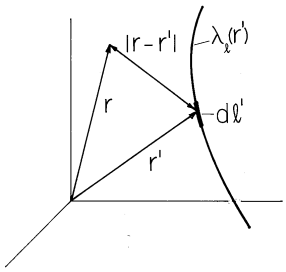


Fig. 4.5.4 An element of line charge at the position $\mathbf{r}'$ gives rise to a potential at the observer location $\mathbf{r}$.

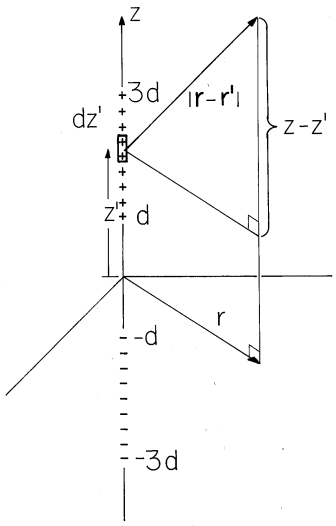


Fig. 4.5.5 Collinear positive and negative line elements of charge symmetrically located on the z axis.

A positive line charge density of magnitude λ_o is uniformly distributed along the z axis between the points $z = d$ and $z = 3d$. Negative charge of the same magnitude is distributed between $z = -d$ and $z = -3d$. The axial symmetry suggests the use of the cylindrical coordinates defined in Fig. 4.5.5.

The distance from an element of charge $\lambda_o dz'$ to an arbitrary observer point (r, z) is

$$|\mathbf{r} - \mathbf{r}'| = \sqrt{r^2 + (z - z')^2} \tag{13}$$

Thus, the line charge form of the superposition integral, (12), becomes

$$\Phi = \frac{\lambda_o}{4\pi\epsilon_o}\left(\int_d^{3d} \frac{dz'}{\sqrt{(z-z')^2 + r^2}} - \int_{-3d}^{-d} \frac{dz'}{\sqrt{(z-z')^2 + r^2}}\right) \tag{14}$$

These integrations are carried out to obtain the desired potential distribution

$$\underline{\Phi} = ln\, \frac{\left(3 - \underline{z} + \sqrt{(3-\underline{z})^2 + \underline{r}^2}\right)\left(\underline{z} + 1 + \sqrt{(\underline{z}+1)^2 + \underline{r}^2}\right)}{\left(1 - \underline{z} + \sqrt{(1-\underline{z})^2 + \underline{r}^2}\right)\left(\underline{z} + 3 + \sqrt{(\underline{z}+3)^2 + \underline{r}^2}\right)} \tag{15}$$

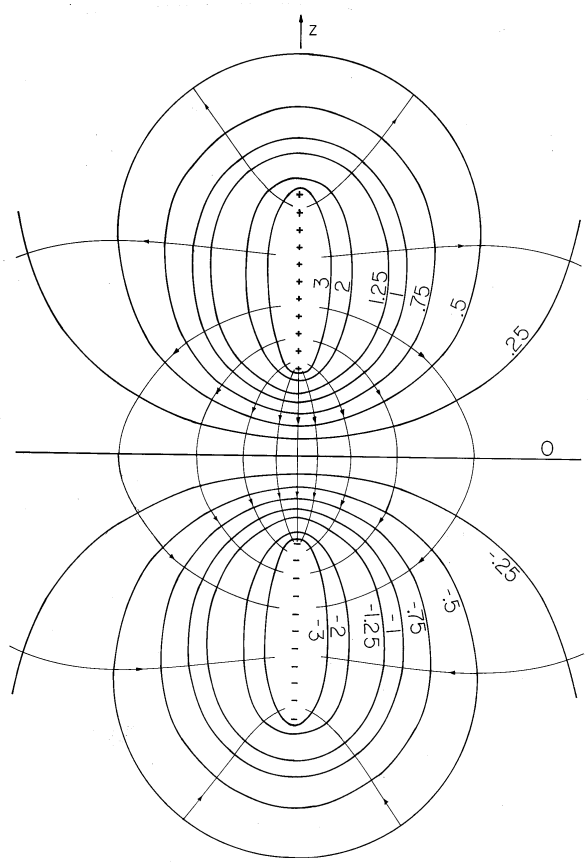


Fig. 4.5.6 Cross-section of equipotential surfaces and lines of electric field intensity for the configuration of Fig. 4.5.5.

Here, lengths have been normalized to d, so that $\underline{z} = z/d$ and $\underline{r} = r/d$. Also, the potential has been normalized such that

$$\underline{\Phi} \equiv \frac{\Phi}{(\lambda_o/4\pi\epsilon_o)} \tag{16}$$

A programmable calculator can be used to evaluate (15), given values of $(\underline{r}, \underline{z})$. The equipotentials in Fig. 4.5.6 were, in fact, obtained in this way, making it possible to sketch the lines of field intensity shown. Remember, the configuration is axisymmetric, so the equipotentials are surfaces generated by rotating the cross-section shown about the z axis.

Two-Dimensional Charge and Field Distributions. In two-dimensional configurations, where the charge distribution uniformly extends from $z = -\infty$ to $z = +\infty$, one of the three integrations of the general superposition integral is carried out by representing the charge by a superposition of line charges, each extending from $z = -\infty$ to $z = +\infty$. The fundamental element of charge, shown in

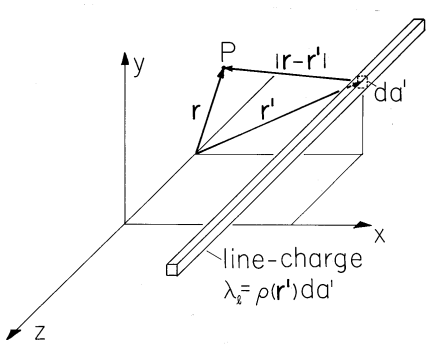


Fig. 4.5.7 For two-dimensional charge distributions, the elementary charge takes the form of a line charge of infinite length. The observer and source position vectors, $\mathbf{r}$ and $\mathbf{r}'$, are two-dimensional vectors.

Fig. 4.5.7, is not the point charge of (1) but rather an infinitely long line charge. The associated potential is not that of a point charge but rather of a line charge.

With the line charge distributed along the z axis, the electric field is given by (1.3.13) as

$$E_r = -\frac{\partial \Phi}{\partial r} = \frac{\lambda_l}{2\pi\epsilon_o r} \tag{17}$$

and integration of this expression gives the potential

$$\Phi = \frac{-\lambda_l}{2\pi\epsilon_o} ln\left(\frac{r}{r_o}\right) \tag{18}$$

where r_o is a reference radius brought in as a constant of integration. Thus, with da denoting an area element in the plane upon which the source and field depend and $\mathbf{r}$ and $\mathbf{r}'$ the vector positions of the observer and source respectively in that plane, the potential for the incremental line charge of Fig. 4.5.7 is written by making the identifications

$$\lambda_l \rightarrow \rho(\mathbf{r}')da'; \qquad r \rightarrow |\mathbf{r} - \mathbf{r}'| \tag{19}$$

Integration over the given two-dimensional source distribution then gives as the two-dimensional superposition integral

$$\boxed{\Phi = -\int_{S'} \frac{\rho(\mathbf{r}')da'\, ln|\mathbf{r} - \mathbf{r}'|}{2\pi\epsilon_o}} \tag{20}$$

In dealing with charge distributions that extend to infinity in the z direction, the potential at infinity can not be taken as a reference. The potential at an arbitrary finite position can be defined as zero by adding an integration constant to (20).

The following example leads to a result that will be found useful in solving boundary value problems in Sec. 4.8.

Example 4.5.3. Two-Dimensional Potential of Uniformly Charged Sheet

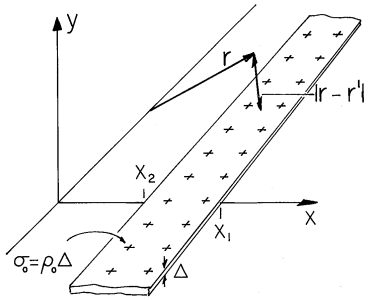


Fig. 4.5.8 Strip of uniformly charged material stretches to infinity in the $\pm z$ directions, giving rise to two-dimensional potential distribution.

A uniformly charged strip lying in the $y = 0$ plane between $x = x_2$ and $x = x_1$ extends from $z = +\infty$ to $z = -\infty$, as shown in Fig. 4.5.8. Because the thickness of the sheet in the y direction is very small compared to other dimensions of interest, the integrand of (20) is essentially constant as the integration is carried out in the y direction. Thus, the y integration amounts to a multiplication by the thickness Δ of the sheet

$$\rho(\mathbf{r}')da' = \rho(\mathbf{r}')\Delta dx = \sigma_s dx \tag{21}$$

and (20) is written in terms of the surface charge density σ_s as

$$\Phi = -\int \frac{\sigma_s(x')dx'\ ln|\mathbf{r} - \mathbf{r}'|}{2\pi\epsilon_o} \tag{22}$$

If the distance between source and observer is written in terms of the Cartesian coordinates of Fig. 4.5.8, and it is recognized that the surface charge density is uniform so that $\sigma_s = \sigma_o$ is a constant, (22) becomes

$$\Phi = -\frac{\sigma_o}{2\pi\epsilon_o}\int_{x_2}^{x_1} ln\sqrt{(x - x')^2 + y^2}dx' \tag{23}$$

Introduction of the integration variable $u = x - x'$ converts this integral to an expression that is readily integrated.

$$\begin{aligned}\Phi &= \frac{\sigma_o}{2\pi\epsilon_o}\int_{x-x_2}^{x-x_1} ln\sqrt{u^2 + y^2}du \\ &= \frac{\sigma_o}{2\pi\epsilon_o}\Bigg[(x - x_1)ln\sqrt{(x - x_1)^2 + y^2} \\ &\quad - (x - x_2)ln\sqrt{(x - x_2)^2 + y^2} + y\tan^{-1}\Big(\frac{x - x_1}{y}\Big) \\ &\quad - y\tan^{-1}\Big(\frac{x - x_2}{y}\Big) + (x_1 - x_2)\Bigg]\end{aligned} \tag{24}$$

Two-dimensional distributions of surface charge can be piece-wise approximated by uniformly charged planar segments. The associated potentials are then represented by superpositions of the potential given by (24).

Potential of Uniform Dipole Layer. The potential produced by a dipole of charges $\pm q$ spaced a vector distance $\mathbf{d}$ apart has been found to be given by (4.4.11)

$$\Phi = \frac{\mathbf{p} \cdot \mathbf{i}_{\mathbf{r}'\mathbf{r}}}{4\pi\epsilon_o} \frac{1}{|\mathbf{r} - \mathbf{r}'|^2} \tag{25}$$

where

$$\mathbf{p} \equiv q\mathbf{d}$$

A *dipole layer*, shown in Fig. 4.5.9, consists of a pair of surface charge distributions $\pm\sigma_s$ spaced a distance $\mathbf{d}$ apart. An area element $d\mathbf{a}$ of such a layer, with the direction of $d\mathbf{a}$ (pointing from the negative charge density to the positive one), can be regarded as a differential dipole producing a (differential) potential $d\Phi$

$$d\Phi = \frac{(\sigma_s d)d\mathbf{a} \cdot \mathbf{i}_{\mathbf{r}'\mathbf{r}}}{4\pi\epsilon_o} \frac{1}{|\mathbf{r} - \mathbf{r}'|^2} \tag{26}$$

Denote the surface dipole density by π_s where

$$\pi_s \equiv \sigma_s d \tag{27}$$

and the potential produced by a surface dipole distribution over the surface S is given by

$$\boxed{\Phi = \frac{1}{4\pi\epsilon_o} \int_S \frac{\pi_s \mathbf{i}_{\mathbf{r}'\mathbf{r}}}{|\mathbf{r} - \mathbf{r}'|^2} \cdot d\mathbf{a}} \tag{28}$$

This potential can be interpreted particularly simply if the dipole density is constant. Then π_s can be pulled out from under the integral, and there Φ is equal to $\pi_s/(4\pi\epsilon_o)$ times the integral

$$\Omega \equiv \int_S \frac{\mathbf{i}_{\mathbf{r}'\mathbf{r}} \cdot d\mathbf{a}'}{|\mathbf{r} - \mathbf{r}'|^2} \tag{29}$$

This integral is dimensionless and has a simple geometric interpretation. As shown in Fig. 4.5.9, $\mathbf{i}_{\mathbf{r}'\mathbf{r}} \cdot d\mathbf{a}$ is the area element projected into the direction connecting the source point to the point of observation. Division by $|\mathbf{r} - \mathbf{r}'|^2$ reduces this projected area element onto the unit sphere. Thus, the integrand is the differential solid angle subtended by $d\mathbf{a}$ as seen by an observer at $\mathbf{r}$. The integral, (29), is equal to the solid angle subtended by the surface S when viewed from the point of observation $\mathbf{r}$. In terms of this solid angle,

$$\boxed{\Phi = \frac{\pi_s}{4\pi\epsilon_o}\Omega} \tag{30}$$

Next consider the discontinuity of potential in passing through the surface S containing the dipole layer. Suppose that the surface S is approached from the + side; then, from Fig. 4.5.10, the surface is viewed under the solid angle Ω_o.

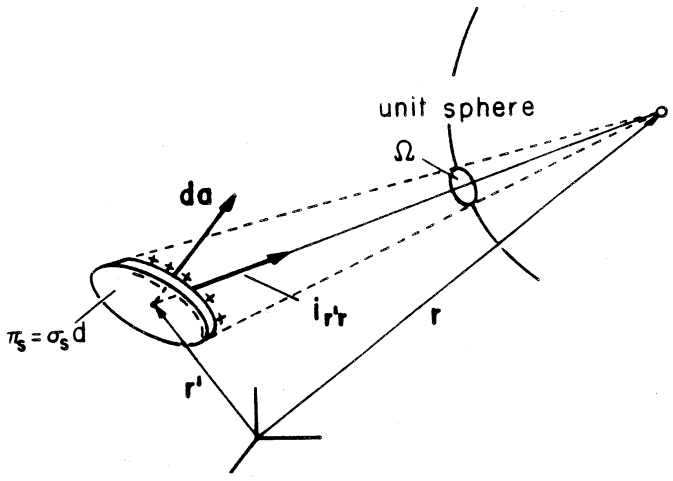


Fig. 4.5.9 The differential solid angle subtended by dipole layer of area *da*.

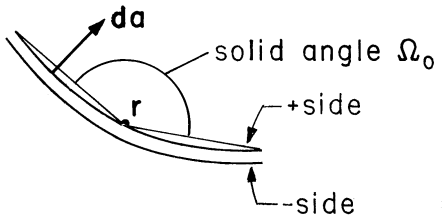


Fig. 4.5.10 The solid angle from opposite sides of dipole layer.

Approached from the other side, the surface subtends the solid angle $-(4\pi - \Omega_o)$. Thus, there is a discontinuity of potential across the surface of

$$\Delta\Phi = \frac{\pi_s}{4\pi\epsilon_o}\Omega_o - \frac{\pi_s}{4\pi\epsilon_o}(\Omega_s - 4\pi) = \frac{\pi_s}{\epsilon_o} \tag{31}$$

Because the dipole layer contains an infinite surface charge density σ_s, the field within the layer is infinite. The "fringing" field, i.e., the external field of the dipole layer, is finite and hence negligible in the evaluation of the internal field of the dipole layer. Thus, the internal field follows directly from Gauss' law under the assumption that the field exists solely between the two layers of opposite charge density (see Prob. 4.5.12). Because contributions to (28) are dominated by π_s in the immediate vicinity of a point $\mathbf{r}$ as it approaches the surface, the discontinuity of potential is given by (31) even if π_s is a function of position. In this case, the tangential $\mathbf{E}$ is not continuous across the interface (Prob. 4.5.12).

4.6 ELECTROQUASISTATIC FIELDS IN THE PRESENCE OF PERFECT CONDUCTORS

In most electroquasistatic situations, the surfaces of metals are equipotentials. In fact, if surrounded by insulators, the surfaces of many other conducting materials

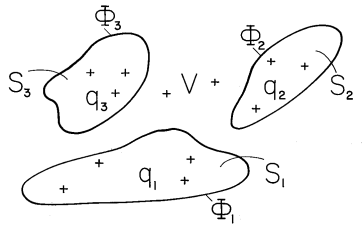


Fig. 4.6.1 Once the superposition principle has been used to determine the potential, the field in a volume V confined by equipotentials is just as well induced by perfectly conducting electrodes having the shapes and potentials of the equipotentials they replace.

also tend to form equipotential surfaces. The electrical properties and dynamical conditions required for representing a boundary surface of a material by an equipotential will be identified in Chap. 7.

Consider the situation shown in Fig. 4.6.l, where three surfaces S_i, $i = 1, 2, 3$ are held at the potentials Φ_1, Φ_2, and Φ_3, respectively. These are presumably the surfaces of conducting electrodes. The field in the volume V surrounding the surfaces S_i and extending to infinity is not only due to the charge in that volume but due to charges outside that region as well. Fields normal to the boundaries terminate on surface charges. Thus, as far as the fields in the region of interest are concerned, the sources are the charge density in the volume V (if any) and the surface charges on the surrounding electrodes.

The superposition integral, which is a solution to Poisson's equation, gives the potential when the volume and surface charges are known. In the present statement of the problem, the volume charge densities are known in V, but the surface charge densities are not. The only fact known about the latter is that they must be so distributed as to make the S_i's into equipotential surfaces at the potentials Φ_i.

The determination of the charge distribution for the set of specified equipotential surfaces is not a simple matter and will occupy us in Chap. 5. But many interesting physical situations are uncovered by a different approach. Suppose we are given a potential function $\Phi(\mathbf{r})$. Then any equipotential surface of that potential can be replaced by an electrode at the corresponding potential. Some of the electrode configurations and associated fields obtained in this manner are of great practical interest.

Suppose such a procedure has been followed. To determine the charge on the i-th electrode, it is necessary to integrate the surface charge density over the surface of the electrode.

$$q_i = \int_{S_i} \sigma_s da = \int_{S_i} \epsilon_o \mathbf{E} \cdot d\mathbf{a} \tag{1}$$

In the volume V, the contributions of the surface charges on the equipotential surfaces are exactly equivalent to those of the charge distribution inside the regions enclosed by the surface S_i causing the original potential function. Thus, an alternative to the use of (1) for finding the total charge on the electrode is

$$q_i = \int_{V_i} \rho dv \tag{2}$$

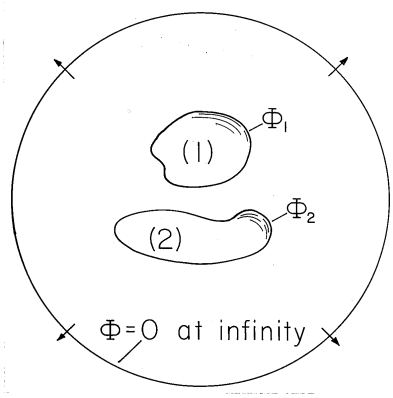


Fig. 4.6.2 Pair of electrodes used to define capacitance.

where V_i is the volume *enclosed* by the surface S_i and ρ is the charge density *inside* S_i associated with the *original* potential.

Capacitance. Suppose the system consists of only two electrodes, as shown in Fig. 4.6.2. The charges on the surfaces of conductors (1) and (2) can be evaluated from the assumedly known solution by using (1).

$$q_1 = \oint_{S_1} \epsilon_o \mathbf{E} \cdot d\mathbf{a}; \qquad q_2 = \oint_{S_2} \epsilon_o \mathbf{E} \cdot d\mathbf{a} \tag{3}$$

Further, there is a charge at infinity of

$$q_\infty = \oint_{S_\infty} \epsilon_o \mathbf{E} \cdot d\mathbf{a} = -q_1 - q_2 \tag{4}$$

The charge at infinity is the negative of the sum of the charges on the two electrodes. This follows from the fact that the field is divergence free, and all field lines originating from q_1 and q_2 must terminate at infinity. Instead of the charges, one could specify the potentials of the two electrodes with respect to infinity. If the charge on electrode 1 is brought to it by a voltage source (battery) that takes charge away from electrode 2 and deposits it on electrode 1, the normal process of charging up two electrodes, then $q_1 = -q_2$. A capacitance C between the two electrodes can be defined as the ratio of charge on electrode 1 divided by the voltage between the two electrodes. In terms of the fields, this definition becomes

$$C = \frac{\oint_{S_1} \epsilon_o \mathbf{E} \cdot d\mathbf{a}}{\int_{(1)}^{(2)} \mathbf{E} \cdot d\mathbf{s}} \tag{5}$$

In order to relate this definition to the capacitance concept used in circuit theory, one further observation must be made. The capacitance relates the charge of one electrode to the voltage between the two electrodes. In general, there may also exist a voltage between electrode 1 and infinity. In this case, capacitances must

also be assigned to relate the voltage with regard to infinity to the charges on the electrodes. If the electrodes are to behave as the single terminal-pair element of circuit theory, these capacitances must be negligible. Returning to (5), note that C is independent of the magnitude of the field variables. That is, if the magnitude of the charge distribution is doubled everywhere, it follows from the superposition integral that the potential doubles as well. Thus, the electric field in the numerator and denominator of (3) is doubled everywhere. Each of the integrals therefore also doubles, their ratio remaining constant.

Example 4.6.1. Capacitance of Isolated Spherical Electrodes

A spherical electrode having radius a has a well-defined capacitance C relative to an electrode at infinity. To determine C, note that the equipotentials of a point charge q at the origin

$$\Phi = \frac{q}{4\pi\epsilon_o r} \tag{6}$$

are spherical. In fact, the equipotential having radius $r = a$ has a voltage with respect to infinity of

$$\Phi = v = \frac{q}{4\pi\epsilon_o a} \tag{7}$$

The capacitance is defined as the the net charge on the surface of the electrode per unit voltage, (5). But the net charge found by integrating the surface charge density over the surface of the sphere is simply q, and so the capacitance follows from (7) as

$$C = \frac{q}{v} = 4\pi\epsilon_o a \tag{8}$$

By way of illustrating the conditions necessary for the capacitance to be well defined, consider a pair of spherical electrodes. Electrode (1) has radius a while electrode (2) has radius R. If these are separated by many times the larger of these radii, the potentials in their vicinities will again take the form of (6). Thus, with the voltages v_1 and v_2 defined relative to infinity, the charges on the respective spheres are

$$q_1 = 4\pi\epsilon_o a v_1; \qquad q_2 = 4\pi\epsilon_o R v_2 \tag{9}$$

With all of the charge on sphere (1) taken from sphere (2),

$$q_1 = -q_2 \Rightarrow a v_1 = -R v_2 \tag{10}$$

Under this condition, all of the field lines from sphere (1) terminate on sphere (2). To determine the capacitance of the electrode pair, it is necessary to relate the charge q_1 to the voltage difference between the spheres. To this end, (9) is used to write

$$\frac{q_1}{4\pi\epsilon_o a} - \frac{q_2}{4\pi\epsilon_o R} = v_1 - v_2 \equiv v \tag{11}$$

and because $q_1 = -q_2$, it follows that

$$q_1 = vC; \qquad C \equiv \frac{4\pi\epsilon_o}{\left(\frac{1}{a} + \frac{1}{R}\right)} \tag{12}$$

where C is now the capacitance of one sphere relative to the other.

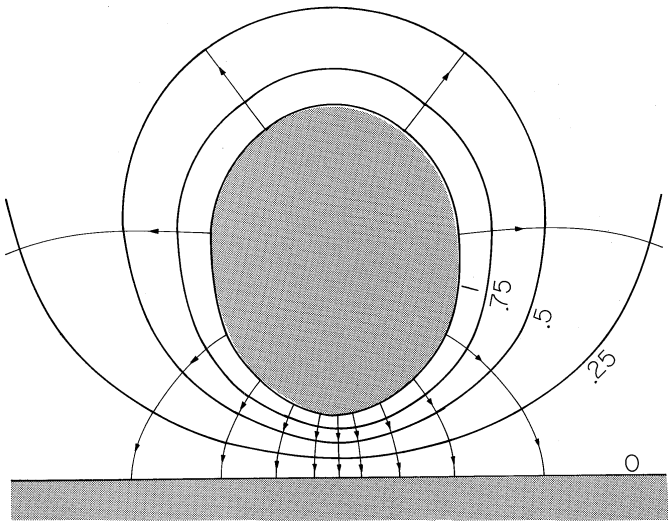


Fig. 4.6.3 The $\underline{\Phi} = 1$ and $\underline{\Phi} = 0$ equipotentials of Fig. 4.5.6 are turned into perfectly conducting electrodes having the capacitance of (4.6.16).

Note that in order to maintain no net charge on the two spheres, it follows from (9), (10), and (12) that the average of the voltages relative to infinity must be retained at

$$\frac{1}{2}(v_1 + v_2) = \frac{1}{2}\left(\frac{q_1}{4\pi\epsilon_o a} + \frac{q_2}{4\pi\epsilon_o R}\right) = \frac{1}{2}v\frac{\left(\frac{1}{a} - \frac{1}{R}\right)}{\left(\frac{1}{a} + \frac{1}{R}\right)} \tag{13}$$

Thus, the average potential must be raised in proportion to the potential difference v.

Example 4.6.2. Field and Capacitance of Shaped Electrodes

The field due to oppositely charged collinear line charges was found to be (4.5.15) in Example 4.5.2. The equipotential surfaces, shown in cross-section in Fig. 4.5.6, are melon shaped and tend to enclose one or the other of the line charge elements.

Suppose that the surfaces on which the normalized potentials are equal to 1 and to 0, respectively, are turned into electrodes, as shown in Fig. 4.6.3. Now the field lines originate on positive surface charges on the upper electrode and terminate on negative charges on the ground plane. By contrast with the original field from the line charges, the field in the region now inside the electrodes is zero.

One way to determine the net charge on one of the electrodes requires that the electric field be found by taking the gradient of the potential, that the unit normal vector to the surface of the electrode be determined, and hence that the surface charge be determined by evaluating $\epsilon_o \mathbf{E} \cdot d\mathbf{a}$ on the electrode surface. Integration of this quantity over the electrode surface then gives the net charge. A far easier way to determine this net charge is to recognize that it is the same as the net charge enclosed by this surface for the original line charge configuration. Thus, the net charge is simply $2d\lambda_l$, and if the potentials of the respective electrodes are taken as $\pm V$, the capacitance is

$$C \equiv \frac{q}{v} = \frac{2d\lambda_l}{V} \tag{14}$$

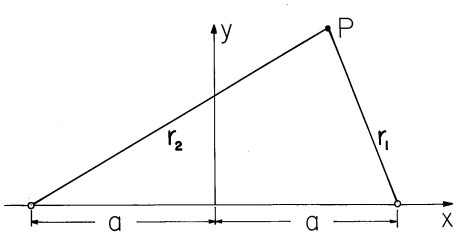


Fig. 4.6.4 Definition of coordinates for finding field from line charges of opposite sign at $x = \pm a$. The displacement vectors are two dimensional and hence in the $x - y$ plane.

For the surface of the electrode in Fig. 4.6.3,

$$\frac{V}{\lambda_l/4\pi\epsilon_o} = 1 \Rightarrow \frac{\lambda_l}{V} = 4\pi\epsilon_o \tag{15}$$

It follows from these relations that the desired capacitance is simply

$$C = 8\pi\epsilon_o d \tag{16}$$

In these two examples, the charge density is zero everywhere between the electrodes. Thus, throughout the region of interest, Poisson's equation reduces to Laplace's equation.

$$\nabla^2\Phi = 0 \tag{17}$$

The solution to Poisson's equation throughout all space is tantamount to solving Laplace's equation in a limited region, subject to certain boundary conditions. A more direct approach to finding such solutions is taken in the next chapter. Even then, it is well to keep in mind that solutions to Laplace's equation in a limited region are solutions to Poisson's equation throughout the entire space, including those regions that contain the charges.

The next example leads to an often-used result, the capacitance per unit length of a two-wire transmission line.

Example 4.6.3. Potential of Two Oppositely Charged Conducting Cylinders

The potential distribution between two equal and opposite parallel line charges has circular cylinders for its equipotential surfaces. Any pair of these cylinders can be replaced by perfectly conducting surfaces so as to obtain the solution to the potential set up between two perfectly conducting parallel cylinders of circular cross-section.

We proceed in the following ways: (a) The potentials produced by two oppositely charged parallel lines positioned at $x = +a$ and $x = -a$, respectively, as shown in Fig. 4.6.4, are superimposed. (b) The intersections of the equipotential surfaces with the $x - y$ plane are circles. The above results are used to find the potential distribution produced by two parallel circular cylinders of radius R with their centers spaced by a distance $2l$. (c) The cylinders carry a charge per unit length λ_l and have a potential difference V, and so their capacitance per unit length is determined.

(a) The potential associated with a single line charge on the z axis is most easily obtained by integrating the electric field, (1.3.13), found from Gauss' integral

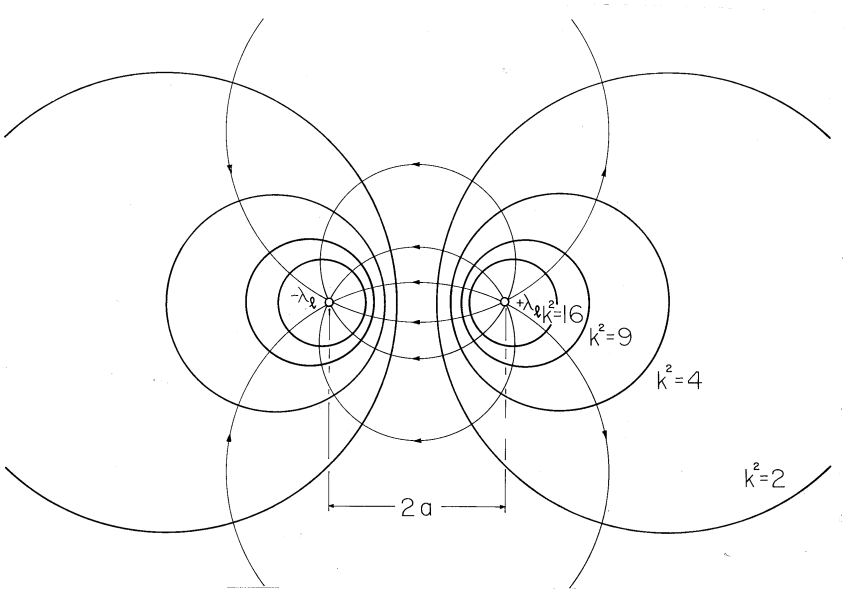


Fig. 4.6.5 Cross-section of equipotentials and electric field lines for line charges.

law. It follows by superposition that the potential for two parallel line charges of charge per unit length $+\lambda_l$ and $-\lambda_l$, positioned at $x = +a$ and $x = -a$, respectively, is

$$\Phi = \frac{-\lambda_l}{2\pi\epsilon_o} ln\ r_1 + \frac{\lambda_l}{2\pi\epsilon_o} ln\ r_2 = \frac{-\lambda_l}{2\pi\epsilon_o} ln\ \frac{r_1}{r_2} \tag{18}$$

Here r_1 and r_2 are the distances of the field point P from the + and − line charges, respectively, as shown in Fig. 4.6.4.

(b) On an equipotential surface, $\Phi = U$ is a constant and the equation for that surface, (18), is

$$\frac{r_2}{r_1} = \exp\left(\frac{2\pi\epsilon_o U}{\lambda_l}\right) = \text{const} \tag{19}$$

where in Cartesian coordinates

$$r_2^2 = (a+x)^2 + y^2; \qquad r_1^2 = (a-x)^2 + y^2$$

With the help of Fig. 4.6.4, (19) is seen to represent cylinders of circular cross-section with centers on the x axis. This becomes apparent when the equation is expressed in Cartesian coordinates. The equipotential circles are shown in Fig. 4.6.5 for different values of

$$k \equiv \exp\left(\frac{2\pi\epsilon_o U}{\lambda_l}\right) \tag{20}$$

(c) Given two conducting cylinders whose centers are a distance $2l$ apart, as shown in Fig. 4.6.6, what is the location of the two line charges such that their field

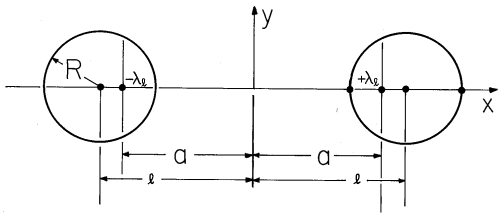


Fig. 4.6.6 Cross-section of parallel circular cylinders with centers at $x = \pm l$ and line charges at $x = \pm a$, having equivalent field.

has equipotentials coincident with these two cylinders? In terms of k as defined by (20), (19) becomes

$$k^2 = \frac{(x+a)^2 + y^2}{(x-a)^2 + y^2} \tag{21}$$

This expression can be written as a quadratic function of x and y.

$$x^2 - 2xa\frac{(k^2+1)}{(k^2-1)} + a^2 + y^2 = 0 \tag{22}$$

Equation (22) confirms that the loci of constant potential in the $x - y$ plane are indeed circles. In order to relate the radius and location of these circles to the parameters a and k, note that the expression for a circle having radius R and center on the x axis at $x = l$ is

$$(x-l)^2 + y^2 - R^2 = 0 \Rightarrow x^2 - 2xl + (l^2 - R^2) + y^2 = 0 \tag{23}$$

We can make (22) identical to this expression by setting

$$-2l = -2a\frac{(k^2+1)}{(k^2-1)} \tag{24}$$

and

$$a^2 = l^2 - R^2 \tag{25}$$

Given the spacing $2l$ and radius R of parallel conductors, this last expression can be used to locate the positions of the line charges. It also can be used to see that $(l-a) = R^2/(l+a)$, which can be used with (24) solved for k^2 to deduce that

$$k = \frac{l+a}{R} \tag{26}$$

Introduction of this expression into (20) then relates the potential of the cylinder on the right to the line charge density. The net charge per unit length that is actually on the surface of the right conductor is equal to the line charge density λ_l. With the voltage difference between the cylinders defined as $V = 2U$, we can therefore solve for the capacitance per unit length.

$$C = \frac{\lambda_l}{V} = \frac{\pi\epsilon_o}{ln\left[\frac{l}{R} + \sqrt{(l/R)^2 - 1}\right]} \tag{27}$$

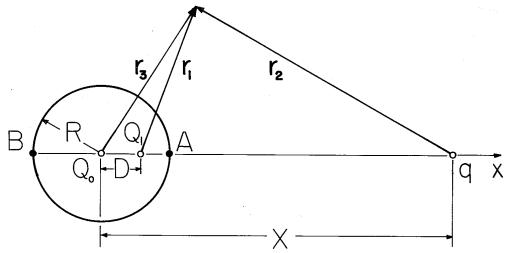


Fig. 4.6.7 Cross-section of spherical electrode having radius R and center at the origin of x axis, showing charge q at $x = X$. Charge Q_1 at $x = D$ makes spherical surface an equipotential, while Q_o at origin makes the net charge on the sphere zero without disturbing the equipotential condition.

Often, the cylinders are wires and it is appropriate to approximate this result for large ratios of l/R.

$$\frac{l}{R} + \sqrt{(l/R)^2 - 1} = \frac{l}{R}\left[1 + \sqrt{1 - (R/l)^2}\right] \simeq \frac{2l}{R} \tag{28}$$

Thus, the capacitance per unit length is approximately

$$\frac{\lambda_l}{V} \equiv C = \frac{\pi\epsilon_o}{ln\,\frac{2l}{R}} \tag{29}$$

This same result can be obtained directly from (18) by recognizing that when $a \gg l$, the line charges are essentially at the center of the cylinders. Thus, evaluated on the surface of the right cylinder where the potential is $V/2$, $r_1 \simeq R$ and $r_2 \simeq 2l$, (18) gives (29).

Example 4.6.4. Attraction of a Charged Particle to a Neutral Sphere

A charged particle facing a conducting sphere induces a surface charge distribution on the sphere. This distribution adjusts itself so as to make the spherical surface an equipotential. In this problem, we take advantage of the fact that two charges of opposite sign produce a potential distribution, one equipotential surface of which is a sphere.

First we find the potential distribution set up by a perfectly conducting sphere of radius R, carrying a net charge Q, and a point charge q at a distance X ($X \geq R$) from the center of the sphere. Then the result is used to determine the force on the charge q exerted by a *neutral* sphere ($Q = 0$)! The configuration is shown in Fig. 4.6.7.

Consider first the potential distribution set up by a point charge Q_1 and another point charge q. The construction of the potential is familiar from Sec. 4.4.

$$\Phi(\mathbf{r}) = \frac{q}{4\pi\epsilon_o r_2} + \frac{Q_1}{4\pi\epsilon_o r_1} \tag{30}$$

In general, the equipotentials are not spherical. However, the surface of zero potential

$$\Phi(\mathbf{r}) = 0 = \frac{q}{4\pi\epsilon_o r_2} + \frac{Q_1}{4\pi\epsilon_o r_1} \tag{31}$$

is described by

$$\frac{r_2}{r_1} = -\frac{q}{Q_1} \tag{32}$$

and if $q/Q_1 \leq 0$, this represents a sphere. This can be proven by expressing (32) in Cartesian coordinates and noting that in the plane of the two charges, the result is the equation of a circle with its center on the axis intersecting the two charges [compare (19)].

Using this fact, we can apply (32) to the points A and B in Fig. 4.6.7 and eliminate q/Q_1. Taking R as the radius of the sphere and D as the distance of the point charge Q_1 from the center of the sphere, it follows that

$$\frac{R-D}{X-R} = \frac{R+D}{X+R} \Rightarrow D = \frac{R^2}{X} \tag{33}$$

This specifies the distance D of the point charge Q_1 from the center of the equipotential sphere. Introduction of this result into (32) applied to point A gives the (fictitious) charge Q_1.

$$-Q_1 = q\frac{R}{X} \tag{34}$$

With this value for Q_1 located in accordance with (33), the surface of the sphere has zero potential. Without altering its equipotential character, the potential of the sphere can be shifted by positioning another fictitious charge at its center. If the net charge of the spherical conductor is to be Q, then a charge $Q_o = Q - Q_1$ is to be positioned at the center of the sphere. The net field retains the sphere as an equipotential surface, now of nonzero potential. The field outside the sphere is the sought-for solution. With r_3 defined as the distance from the center of the sphere to the point of observation, the field outside the sphere is

$$\Phi = \frac{q}{4\pi\epsilon_o r_2} + \frac{Q_1}{4\pi\epsilon_o r_1} + \frac{Q-Q_1}{4\pi\epsilon_o r_3} \tag{35}$$

With $Q = 0$, the force on the charge follows from an evaluation of the electric field intensity directed along an axis passing through the center of the sphere and the charge q. The self-field of the charge is omitted from this calculation. Thus, along the x axis the potential due to the fictitious charges within the sphere is

$$\Phi = \frac{Q_1}{4\pi\epsilon_o(x-D)} - \frac{Q_1}{4\pi\epsilon_o x} \tag{36}$$

The x directed electric field intensity, and hence the required force, follows as

$$f_x = qE_x = -q\frac{\partial\Phi}{\partial x} = \frac{qQ_1}{4\pi\epsilon_o}\left[\frac{1}{(x-D)^2} - \frac{1}{x^2}\right]_{x=X} \tag{37}$$

In view of (33) and (34), this can be written in terms of the actual physical quantities as

$$f_x = -\frac{q^2 R}{4\pi\epsilon_o X^3}\left[\frac{1}{\left[1-(R/X)^2\right]^2} - 1\right] \tag{38}$$

The field implied by (34) with $Q = 0$ is shown in Fig. 4.6.8. As the charge approaches the spherical conductor, images are induced on the nearest parts of the surface. To

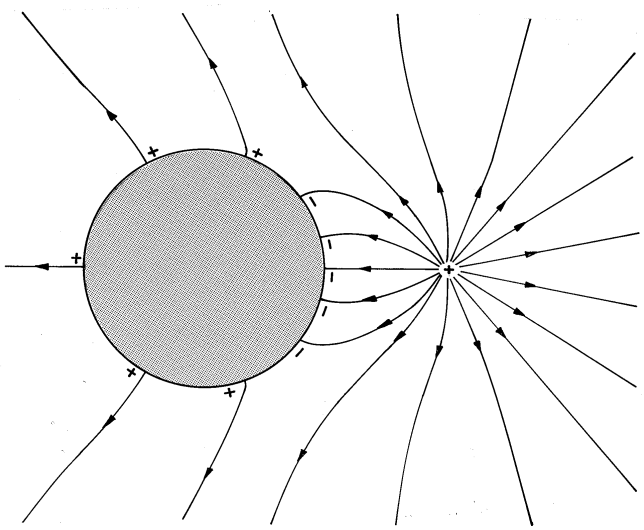


Fig. 4.6.8 Field of point charge in vicinity of neutral perfectly conducting spherical electrode.

keep the net charge zero, charges of opposite sign must be induced on parts of the surface that are more remote from the point charge. The force of attraction results because the charges of opposite sign are closer to the point charge than those of the same sign.

4.7 METHOD OF IMAGES

Given a charge distribution throughout all of space, the superposition integral can be used to determine the potential that satisfies Poisson's equation. However, it is often the case that interest is confined to a limited region, and the potential must satisfy a boundary condition on surfaces bounding this region. In the previous section, we recognized that any equipotential surface could be replaced by a physical electrode, and found solutions to boundary value problems in this way. The art of solving problems in this "backwards" fashion can be remarkably practical but hinges on having a good grasp of the relationship between fields and sources.

Symmetry is often the basis for superimposing fields to satisfy boundary conditions. Consider for example the field of a point charge a distance $d/2$ above a plane conductor, represented by an equipotential. As illustrated in Fig. 4.7.1a, the field $\mathbf{E}_+$ of the charge by itself has a component tangential to the boundary, and hence violates the boundary condition on the surface of the conductor.

To satisfy this condition, forget the conductor and consider the field of two charges of equal magnitude and opposite signs, spaced a distance $2d$ apart. In the symmetry plane, the normal components add while the tangential components cancel. Thus, the composite field is normal to the symmetry plane, as illustrated in the figure. In fact, the configuration is the same as discussed in Sec. 4.4. The

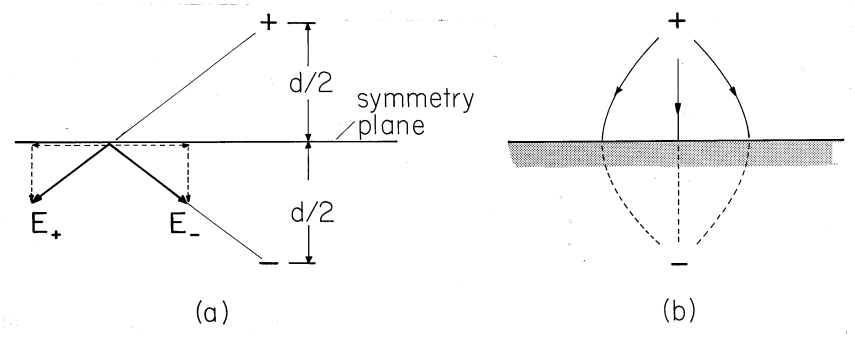


Fig. 4.7.1 (a) Field of positive charge tangential to horizontal plane is canceled by that of symmetrically located image charge of opposite sign. (b) Net field of charge and its image.

fields are as in Fig. 4.4.2a, where now the planar $\Phi = 0$ surface is replaced by a conducting sheet.

This method of satisfying the boundary conditions imposed on the field of a point charge by a plane conductor by using an opposite charge at the mirror image position of the original charge, is called the *method of images*. The charge of opposite sign at the mirror-image position is the "image-charge."

Any superposition of charge pairs of opposite sign placed symmetrically on two sides of a plane results in a field that is normal to the plane. An example is the field of the pair of line charge elements shown in Fig. 4.5.6. With an electrode having the shape of the equipotential enclosing the upper line charge and a ground plane in the plane of symmetry, the field is as shown in Fig. 4.6.3. This identification of a physical situation to go with a known field was used in the previous section. The method of images is only a special case involving planar equipotentials.

To compare the replacement of the symmetry plane by a planar conductor, consider the following demonstration.

Demonstration 4.7.1. Charge Induced in Ground Plane by Overhead Conductor

The circular cylindrical conductor of Fig. 4.7.2, separated by a distance l from an equipotential (grounded) metal surface, has a voltage $U = U_o \cos \omega t$. The field between the conductor and the ground plane is that of a line charge inside the conductor and its image below the ground plane. Thus, the potential is that determined in Example 4.6.3. In the Cartesian coordinates shown, (4.6.18), the definitions of r_1 and r_2 with (4.6.19) and (4.6.25) (where $U = V/2$) provide the potential distribution

$$\Phi = -\frac{\lambda_l}{2\pi\epsilon_o} ln \frac{\sqrt{(a-x)^2 + y^2}}{\sqrt{(a+x)^2 + y^2}} \tag{1}$$

The charge per unit length on the cylinder is [compare (4.6.27)]

$$\lambda_l = CU; \qquad C = \frac{2\pi\epsilon_o}{ln\left[\frac{l}{R} + \sqrt{\left(\frac{l}{R}\right)^2 - 1}\right]} \tag{2}$$

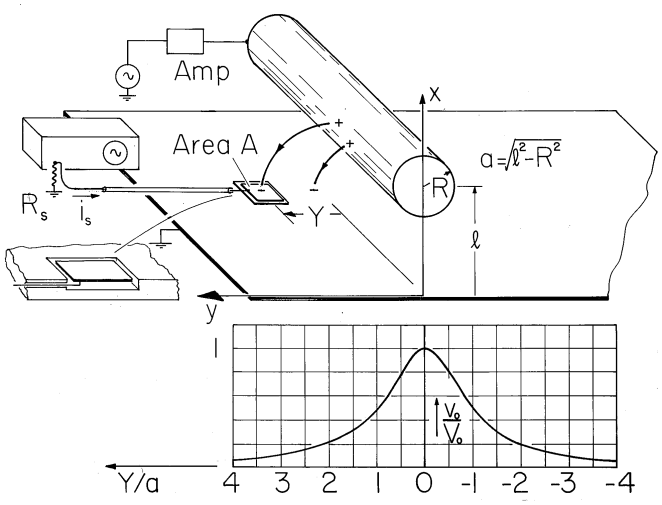


Fig. 4.7.2 Charge induced on ground plane by overhead conductor is measured by probe. Distribution shown is predicted by (4.7.7).

In the actual physical situation, images of this charge are induced on the surface of the ground plane. These can be measured by using a flat probe that is connected through the cable to ground and insulated from the ground plane just below. The input resistance of the oscilloscope is low enough so that the probe surface is at essentially the same (zero) potential as the ground plane. What is the measured current, and hence voltage v_o, as a function of the position Y of the probe?

Given the potential, the surface charge is (1.3.17)

$$\sigma_s = \epsilon_o E_x(x=0) = -\epsilon_o \left.\frac{\partial \Phi}{\partial x}\right|_{x=0} \tag{3}$$

Evaluation of this expression using (1) gives

$$\begin{aligned}\sigma_s &= \frac{CU}{2\pi}\left[-\frac{(a-x)}{(a-x)^2+y^2}-\frac{(a+x)}{(a+x)^2+y^2}\right]_{x=0} \\ &= -\frac{CU}{\pi}\frac{a}{a^2+y^2}\end{aligned} \tag{4}$$

Conservation of charge requires that the probe current be the time rate of change of the charge q on the probe surface.

$$i_s = \frac{dq}{dt} \tag{5}$$

Because the probe area is small, the integration of the surface charge over its surface is approximated by the product of the area and the surface charge evaluated at the position Y of its center.

$$q = \int_A \sigma_s dy dz \simeq A\sigma_s \tag{6}$$

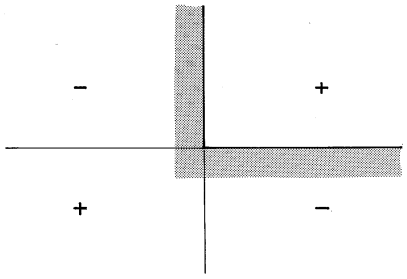


Fig. 4.7.3 Image charges arranged to satisfy equipotential conditions in two planes.

Thus, it follows from (4)–(6) that the induced voltage, $v_o = -R_s i_s$, is

$$v_o = -V_o \sin \omega t \frac{1}{1 + (Y/a)^2}; \qquad V_o \equiv \frac{R_s ACU_o \omega}{a\pi} \tag{7}$$

This distribution of the induced signal with probe position is shown in Fig. 4.7.2.

In the analysis, it is assumed that the plane $x = 0$, including the section of surface occupied by the probe, is constrained to zero potential. In first computing the current to the probe using this assumption and then finding the probe voltage, we are clearly making an approximation that is valid only if the voltage is "small." This can be insured by making the resistance R_s small.

The usual scope resistance is $1M\Omega$. It may come as a surprise that such a resistance is treated here as a short. However, the voltage given by (7) is proportional to the frequency, so the value of acceptable resistance depends on the frequency. As the frequency is raised to the point where the voltage of the probe does begin to influence the field distribution, some of the field lines that originally terminated on the electrode are diverted to the grounded part of the plane. Also, charges of opposite polarity are induced on the other side of the probe. The result is an output signal that no longer increases with frequency. A frequency response of the probe voltage that does not increase linearly with frequency is therefore telltale evidence that the resistance is too large or the frequency too high. In the demonstration, where "desk-top" dimensions are typical, the frequency response is linear to about 100 Hz with a scope resistance of $1M\Omega$.

As the frequency is raised, the system becomes one with two excitations contributing to the potential distribution. The multiple terminal-pair systems treated in Sec. 5.1 start to model the full frequency response of the probe.

Symmetry also motivates the use of image charges to satisfy boundary conditions on more than one planar surface. In Fig. 4.7.3, the objective is to find the field of the point charge in the first quadrant with the planes $x = 0$ and $y = 0$ at zero potential. One image charge gives rise to a field that satisfies one of the boundary conditions. The second is satisfied by introducing an image for the *pair* of charges.

Once an image or a system of images has been found for a point charge, the same principle of images can be used for a continuous charge distribution. The charge density distributions have density distributions of image charges, and the total field is again found using the superposition integral.

Even where symmetry is not involved, charges located outside the region of interest to produce fields that satisfy boundary conditions are often referred to

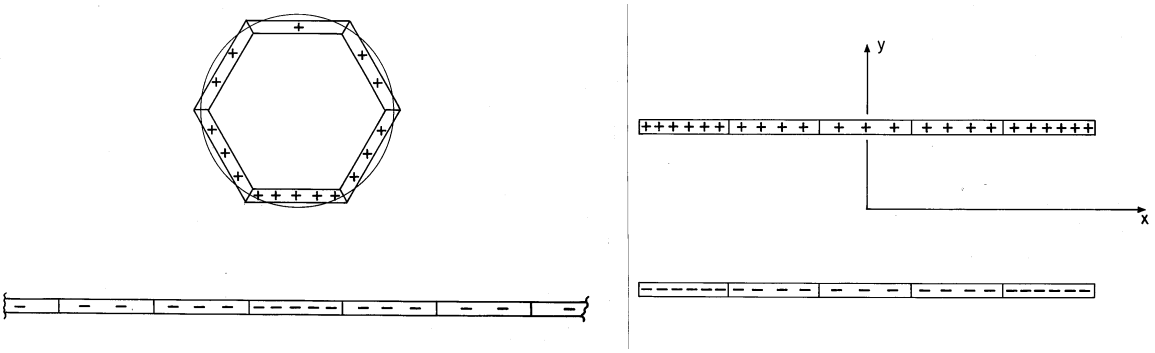


Fig. 4.8.1 (a) Surface of circular cylinder over a ground plane broken into planar segments, each having a uniform surface charge density. (b) Special case where boundaries are in planes $y =$ constant.

as image charges. Thus, the charge Q_1 located within the spherical electrode of Example 4.6.4 can be regarded as the image of q.

4.8 CHARGE SIMULATION APPROACH TO BOUNDARY VALUE PROBLEMS

In solving a boundary value problem, we are in essence finding that distribution of charges external to the region of interest that makes the total field meet the boundary conditions. Commonly, these external charges are actually on the surfaces of conductors bounding or embedded in the region of interest. By way of preparation for the boundary value point of view taken in the next chapter, we consider in this section a direct approach to adjusting surface charges so that the fields meet prescribed boundary conditions on the potential. Analytically, the technique is cumbersome. However, with a computer, it becomes one of a class of powerful numerical techniques[1] for solving boundary value problems.

Suppose that the fields are two dimensional, so that the region of interest can be "enclosed" by a surface that can be approximated by strip segments, as illustrated in Fig. 4.8.1a. This example becomes an approximation to the circular conductor over a ground plane (Example 4.7.1) if the magnitudes of the charges on the strips are adjusted to make the surfaces approximate appropriate equipotentials.

With the surface charge density on each of these strips taken as *uniform*, a "stair-step" approximation to the actual distribution of charge is obtained. By increasing the number of segments, the approximation is refined. For purposes of illustration, we confine ourselves here to boundaries lying in planes of constant y, as shown in Fig. 4.8.1b. Then the potential associated with a single uniformly charged strip is as found in Example 4.5.3.

Consider first the potential due to a strip of width (a) lying in the plane $y = 0$ with its center at $x = 0$, as shown in Fig. 4.8.2a. This is a special case of the configuration considered in Example 4.5.3. It follows from (4.5.24) with $x_1 = a/2$ and $x_2 = -a/2$ that the potential at the observer location (x, y) is

$$\Phi(x, y) = \sigma_o S(x, y) \tag{1}$$

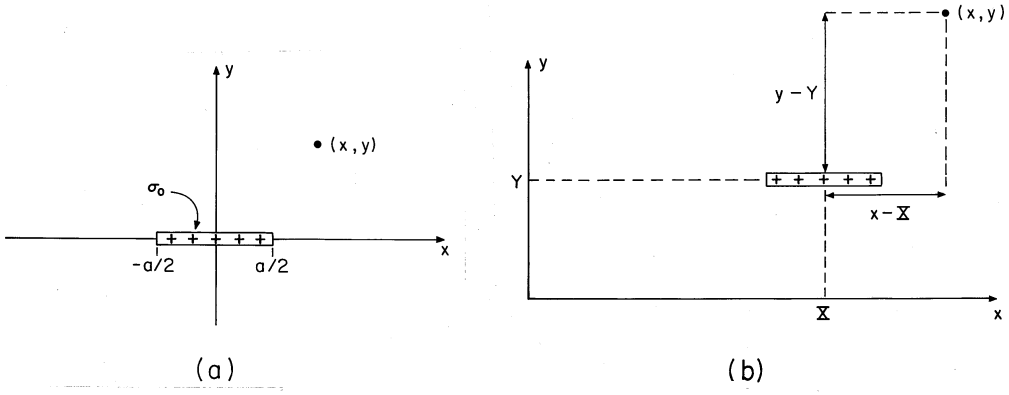


Fig. 4.8.2 (a) Charge strip of Fig. 4.5.8 centered at origin. (b) Charge strip translated so that its center is at (X, Y).

where

$$S(x,y) \equiv \Bigg[\left(x - \frac{a}{2}\right) ln \sqrt{\left(x - \frac{a}{2}\right)^2 + y^2} - \left(x + \frac{a}{2}\right) ln \sqrt{\left(x + \frac{a}{2}\right)^2 + y^2} + y \tan^{-1}\left(\frac{x - a/2}{y}\right) - y \tan^{-1}\left(\frac{x + a/2}{y}\right) + a \Bigg] / 2\pi\epsilon_o \tag{2}$$

With the strip located at $(x, y) = (X, Y)$, as shown in Fig. 4.8.2b, this potential becomes

$$\Phi(x,y) = \sigma_o S(x - X, y - Y) \tag{3}$$

In turn, by superposition we can write the potential due to N such strips, the one having the uniform surface charge density σ_i being located at $(x, y) = (X_i, Y_i)$.

$$\Phi(x,y) = \sum_{i=1}^{N} \sigma_i S_i; \qquad S_i \equiv S(x - X_i, y - Y_i) \tag{4}$$

Given the surface charge densities, σ_i, the potential at any given location (x, y) can be evaluated using this expression. We assume that the net charge on the strips is zero, so that their collective potential goes to zero at infinity.

With the strips representing surfaces that are constrained in potential (for example, perfectly conducting boundaries), the charge densities are adjusted to meet boundary conditions. Each strip represents part of an electrode surface. The potential V_j at the center of the j-th strip is set equal to the known voltage of the electrode to which it belongs. Evaluating (4) for the center of the j-th strip one obtains

$$\sum_{i=1}^{N} \sigma_i S_{ij} = V_j; \qquad S_{ij} \equiv S(x_j - X_i, y_j - Y_i), \qquad j = 1, \ldots N \tag{5}$$

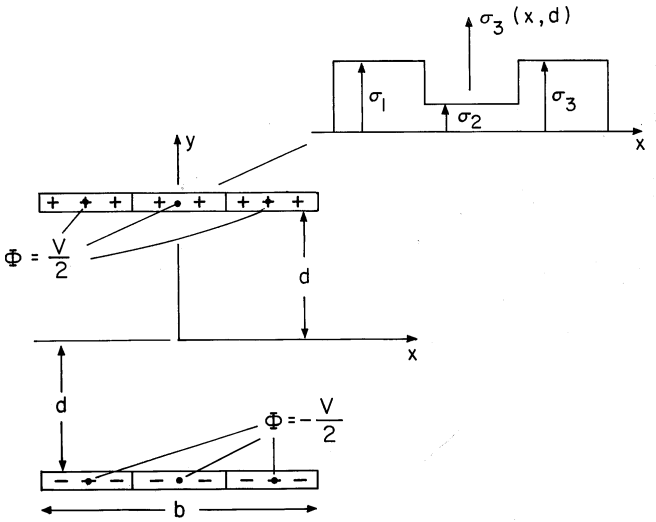


Fig. 4.8.3 Charge distribution on plane parallel electrodes approximated by six uniformly charged strips.

This statement can be made for each of the strips, so that it holds with $j = 1, \ldots N$. These relations comprise N equations that are linear in the N unknowns $\sigma_1 \ldots \sigma_N$.

$$\begin{pmatrix} C_{11} & C_{12} & \cdots \\ C_{21} & & \\ \cdots & & C_{NN} \end{pmatrix} \begin{pmatrix} \sigma_1 \\ \vdots \\ \sigma_N \end{pmatrix} = \begin{pmatrix} V_1 \\ \vdots \\ V_N \end{pmatrix} \tag{6}$$

The potentials $V_1 \ldots V_N$ on the right are known, so these expressions can be solved for the surface charge densities. Thus, the potential that meets the approximate boundary conditions, (4), has been determined. We have found an approximation to the surface charge density needed to meet the potential boundary condition.

Example 4.8.1. Fields of Finite Width Parallel Plate Capacitor

In Fig. 4.8.3, the parallel plates of a capacitor are divided into six segments. The potentials at the centers of those in the top row are required to be $V/2$, while those in the lower row are $-V/2$. In this simple case of six segments, symmetry gives

$$\sigma_1 = \sigma_3 = -\sigma_4 = -\sigma_6, \qquad \sigma_2 = -\sigma_5 \tag{7}$$

and the six equations in six unknowns, (6) with $N = 6$, reduces to two equations in two unknowns. Thus, it is straightforward to write analytical expressions for the surface charge densities (See Prob. 4.8.1).

The equipotentials and associated surface charge distributions are shown in Fig. 4.8.4 for increasing numbers of charge sheets. The first is a reminder of the distribution of potential for uniformly charged sheets. Shown next are the equipotentials that result from using the six-segment approximation just evaluated. In the last case, 20 segments have been used and the inversion of (6) carried out by means of a computer.

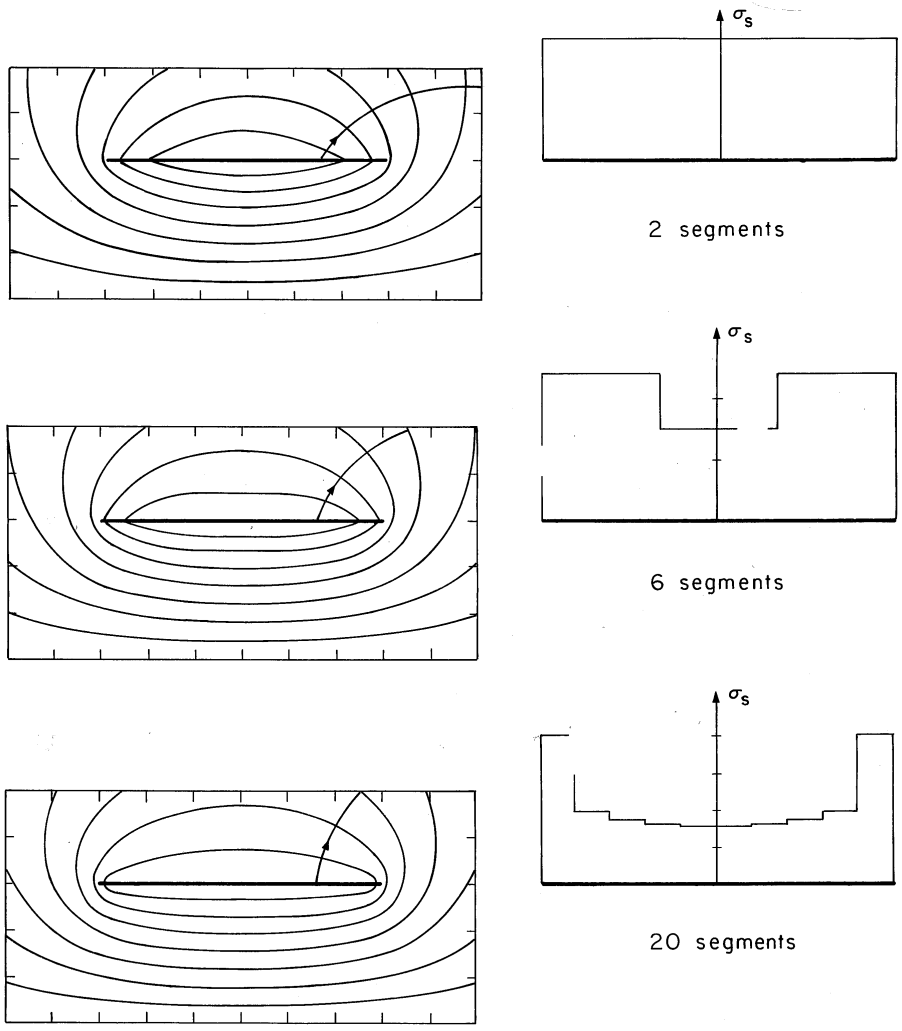


Fig. 4.8.4 Potential distributions using 2, 6, and 20 sheets to approximate the fields of a plane parallel capacitor. Only the fields in the upper half-plane are shown. The distributions of surface charge density on the upper plate are shown to the right.

Note that the approximate capacitance per unit length is

$$C = \frac{1}{V}\sum_{i=1}^{N/2}\frac{b}{(N/2)}\sigma_i \tag{8}$$

This section shows how the superposition integral point of view can be the basis for a numerical approach to solving boundary value problems. But as we

proceed to a more direct approach to boundary value problems, it is especially important to profit from the physical insight inherent in the method used in this section.

We have found a mathematical procedure for adjusting the distributions of surface charge so that boundaries are equipotentials. Conducting surfaces surrounded by insulating material tend to become equipotentials by similarly redistributing their surface charge. For example, consider how the surface charge redistributes itself on the parallel plates of Fig. 4.8.4. With the surface charge uniformly distributed, there is a strong electric field tangential to the surface of the plate. In the upper plate, the charges move radially outward in response to this tangential field. Thus, the charge redistributes itself as shown in the subsequent cases. The correct distribution of surface charge density is the one that makes this tangential electric field approach zero, which it is when the surfaces become equipotentials. Thus, the surface charge density is higher near the edges of the plates than it is in the middle. The additional surface charges near the edges result in just that inward-directed electric field which is needed to make the net field perpendicular to the surfaces of the electrodes.

We will find in Sec. 8.6 that the solution to a class of two-dimensional MQS boundary value problems is completely analogous to that for EQS systems of perfect conductors.

4.9 SUMMARY

The theme in this chapter is set by the two equations that determine $\mathbf{E}$, given the charge density ρ. The first of these, (4.0.1), requires that $\mathbf{E}$ be irrotational. Through the representation of $\mathbf{E}$ as the negative gradient of the electric potential, Φ, it is effectively integrated.

$$\mathbf{E} = -\nabla\Phi \tag{1}$$

This gradient operator, determined in Cartesian coordinates in Sec. 4.1 and found in cylindrical and spherical coordinates in the problems of that section, is summarized in Table I. The associated gradient integral theorem, (4.1.16), is added for reference to the integral theorems of Gauss and Stokes in Table II.

The substitution of (1) into Gauss' law, the second of the two laws forming the theme of this chapter, gives Poisson's equation.

$$\nabla^2\Phi = -\frac{\rho}{\epsilon_o} \tag{2}$$

The Laplacian operator on the left, defined as the divergence of the gradient of Φ, is summarized in the three standard coordinate systems in Table I.

It follows from the linearity of (2) that the potential for the superposition of charge distributions is the superposition of potentials for the individual charge distributions. The potentials for dipoles and other singular charge distributions are therefore found by superimposing the potentials of point or line charges. The superposition integral formalizes the determination of the potential, given the distribution of charge. With the surface and line charges recognized as special (singular) volume charge densities, the second and third forms of the superposition integral

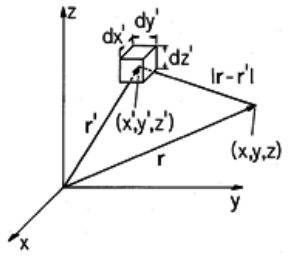
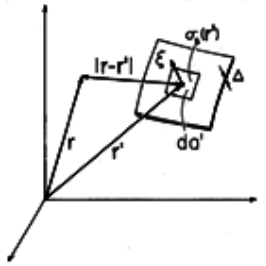
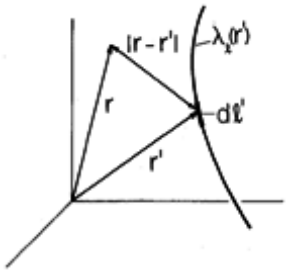
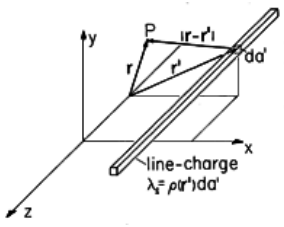
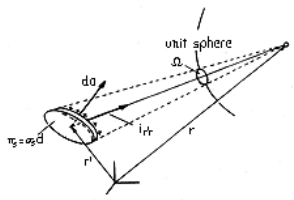
summarized in Table 4.9.1 follow directly from the first. The fourth is convenient if the source and field are two dimensional.

Through Sec. 4.5, the charge density is regarded as given throughout all space. From Sec. 4.6 onward, a shift is made toward finding the field in confined regions of space bounded by surfaces of constant potential. At first, the approach is opportunistic. Given a solution, what problems have been solved? However, the numerical convolution method of Sec. 4.8 is a direct and practical approach to solving boundary value problems with arbitrary geometry.

REFERENCES

[1] R. F. Harrington, **Field Computation by Moment Methods**, MacMillan, NY (1968).

TABLE 4.9.1
SUPERPOSITION INTEGRALS FOR ELECTRIC POTENTIAL

Volume Charge (4.5.3)	$\Phi = \int_{V'} \frac{\rho(\mathbf{r}')dv'}{4\pi\epsilon_o\|\mathbf{r}-\mathbf{r}'\|}$	
Surface Charge (4.5.5)	$\Phi = \oint_{A'} \frac{\sigma_s(\mathbf{r}')da'}{4\pi\epsilon_o\|\mathbf{r}-\mathbf{r}'\|}$	
Line Charge (4.5.12)	$\Phi = \int_{L'} \frac{\lambda_l(\mathbf{r}')dl'}{4\pi\epsilon_o\|\mathbf{r}-\mathbf{r}'\|}$	
Two-dimensional (4.5.20)	$\Phi = -\int_{S'} \frac{\rho(\mathbf{r}')ln\|\mathbf{r}-\mathbf{r}'\|da'}{2\pi\epsilon_o}$	
Double-layer (4.5.28)	$\Phi = \frac{\pi_s}{4\pi\epsilon_o}\Omega$ $\Omega \equiv \int_S \frac{\mathbf{i}_{r'r}\cdot d\mathbf{a}}{\|\mathbf{r}-\mathbf{r}'\|^2}$	

PROBLEMS

4.1 Irrotational Field Represented by Scalar Potential: The Gradient Operator and Gradient Integral Theorem

4.1.1 Surfaces of constant Φ that are spherical are given by

$$\Phi = \frac{V_o}{a^2}(x^2 + y^2 + z^2) \tag{a}$$

For example, the surface at radius a has the potential V_o.

(a) In Cartesian coordinates, what is grad(Φ)?
(b) By the definition of the gradient operator, the unit normal $\mathbf{n}$ to an equipotential surface is

$$\mathbf{n} = \frac{\nabla\Phi}{|\nabla\Phi|} \tag{b}$$

Evaluate $\mathbf{n}$ in Cartesian coordinates for the spherical equipotentials given by (a) and show that it is equal to $\mathbf{i_r}$, the unit vector in the radial direction in spherical coordinates.

4.1.2 For Example 4.1.1, carry out the integral of $\mathbf{E}\cdot d\mathbf{s}$ from the origin to $(x, y) = (a, a)$ along the line $y = x$ and show that it is indeed equal to $\Phi(0, 0) - \Phi(a, a)$.

4.1.3 In Cartesian coordinates, three two-dimensional potential functions are

$$\Phi = \frac{V_o x}{a} \tag{a}$$

$$\Phi = \frac{V_o y}{a} \tag{b}$$

$$\Phi = \frac{V_o}{a^2}(x^2 - y^2) \tag{c}$$

(a) Determine $\mathbf{E}$ for each potential.
(b) For each function, make a sketch of Φ and $\mathbf{E}$ using the conventions of Fig. 4.1.3.
(c) For each function, make a sketch using conventions of Fig. 4.1.4.

4.1.4* A cylinder of rectangular cross-section is shown in Fig. P4.1.4. The electric potential inside this cylinder is

$$\Phi = \frac{\rho_o(t)}{\epsilon_o\left[\left(\frac{\pi}{a}\right)^2 + \left(\frac{\pi}{b}\right)^2\right]} \sin\frac{\pi}{a}x \sin\frac{\pi}{b}y \tag{a}$$

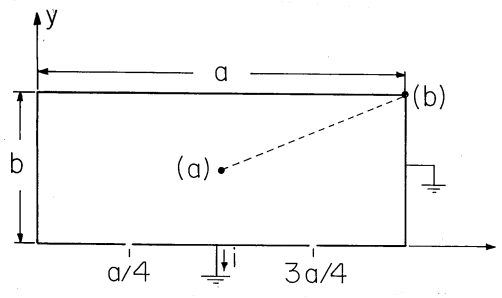


Fig. P4.1.4

where $\rho_o(t)$ is a given function of time.

(a) Show that the electric field intensity is

$$\mathbf{E} = \frac{-\rho_o(t)}{\epsilon_o\left[\left(\frac{\pi}{a}\right)^2 + \left(\frac{\pi}{b}\right)^2\right]}\left[\frac{\pi}{a}\cos\frac{\pi}{a}x\sin\frac{\pi}{b}y\mathbf{i_x} + \frac{\pi}{b}\sin\frac{\pi}{a}x\cos\frac{\pi}{b}y\mathbf{i_y}\right] \tag{b}$$

(b) By direct evaluation, show that $\mathbf{E}$ is irrotational.

(c) Show that the charge density ρ is

$$\rho = \rho_o(t)\sin\frac{\pi}{a}x\sin\frac{\pi}{b}y \tag{c}$$

(d) Show that the tangential $\mathbf{E}$ is zero on the boundaries.

(e) Sketch the distributions of Φ, ρ, and $\mathbf{E}$ using conventions of Figs. 2.7.3 and 4.1.3.

(f) Compute the line integral of $\mathbf{E}\cdot d\mathbf{s}$ between the center and corner of the rectangular cross-section (points shown in Fig. P4.1.4) and show that it is equal to $\Phi(a/2, b/2, t)$. Why would you expect the integration to give the same result for any path joining the point (a) to any point on the wall?

(g) Show that the net charge inside a length d of the cylinder in the z direction is

$$Q = d\rho_o 4\frac{ab}{\pi^2} \tag{d}$$

first by integrating the charge density over the volume and then by using Gauss' integral law and integrating $\epsilon_o\mathbf{E}\cdot d\mathbf{a}$ over the surface enclosing the volume.

(h) Find the surface charge density on the electrode at $y = 0$ and use your result to show that the net charge on the electrode segment between $x = a/4$ and $x = 3a/4$ having depth d into the paper is

$$q = -\frac{\sqrt{2}\frac{a}{b}d\rho_o}{\left[\left(\frac{\pi}{a}\right)^2 + \left(\frac{\pi}{b}\right)^2\right]} \tag{e}$$

(i) Show that the current, $i(t)$, to this electrode segment is

$$i = \frac{\sqrt{2}\frac{ad}{b}\frac{d\rho_o}{dt}}{\left[\left(\frac{\pi}{a}\right)^2 + \left(\frac{\pi}{b}\right)^2\right]} \tag{f}$$

4.1.5 Inside the cylinder of rectangular cross-section shown in Fig. P4.1.4, the potential is given as

$$\Phi = \frac{\rho_o(t)}{\epsilon_o\left[\left(\frac{\pi}{a}\right)^2 + \left(\frac{\pi}{b}\right)^2\right]} \cos\frac{\pi}{a}x \cos\frac{\pi}{b}y \tag{a}$$

where $\rho_o(t)$ is a given function of time.

(a) Find $\mathbf{E}$.
(b) By evaluating the *curl*, show that $\mathbf{E}$ is indeed irrotational.
(c) Find ρ.
(d) Show that $\mathbf{E}$ is tangential to all of the boundaries.
(e) Using the conventions of Figs. 2.7.3 and 4.1.3, sketch Φ, ρ, and $\mathbf{E}$.
(f) Use $\mathbf{E}$ as found in part (a) to compute the integral of $\mathbf{E} \cdot d\mathbf{s}$ from (a) to (b) in Fig. P4.1.4. Check your answer by evaluating the potential difference between these points.
(g) Evaluate the net charge in the volume by first using Gauss' integral law and integrating $\epsilon_o \mathbf{E} \cdot d\mathbf{a}$ over the surface enclosing the volume and then by integrating ρ over the volume.

4.1.6 Given the potential

$$\Phi = A \sinh mx \sin k_y y \sin k_z z \sin \omega t \tag{a}$$

where A, m, and ω are given constants.

(a) Find $\mathbf{E}$.
(b) By direct evaluation, show that $\mathbf{E}$ is indeed irrotational.
(c) Determine the charge density ρ.
(d) Can you adjust m so that $\rho = 0$ throughout the volume?

4.1.7 The system, shown in cross-section in Fig. P4.1.7, extends to $\pm\infty$ in the z direction. It consists of a cylinder having a square cross-section with sides which are resistive sheets (essentially many resistors in series). Thus, the voltage sources $\pm V$ at the corners of the cylinder produce linear distributions of potential along the sides. For example, the potential between the corners at $(a, 0)$ and $(0, a)$ drops linearly from V to $-V$.

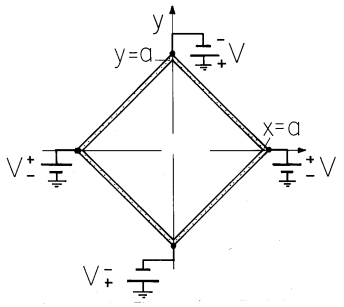


Fig. P4.1.7

(a) Show that the potential inside the cylinder can match that on the walls of the cylinder if it takes the form $A(x^2 - y^2)$. What is A?
(b) Determine $\mathbf{E}$ and show that there is no volume charge density ρ within the cylinder.
(c) Sketch the equipotential surfaces and lines of electric field intensity.

4.1.8 Figure P4.1.8 shows a cross-sectional view of a model for a "capacitance" probe designed to measure the depth h of penetration of a tool into a metallic groove. Both the "tool" and the groove can be considered constant potential surfaces having the potential difference $v(t)$ as shown. An insulating segment at the tip of the tool is used as a probe to measure h. This is done by measuring the charge on the surface of the segment. In the following, we start with a field distribution that can be made to fit the problem, determine the charge and complete some instructive manipulations along the way.

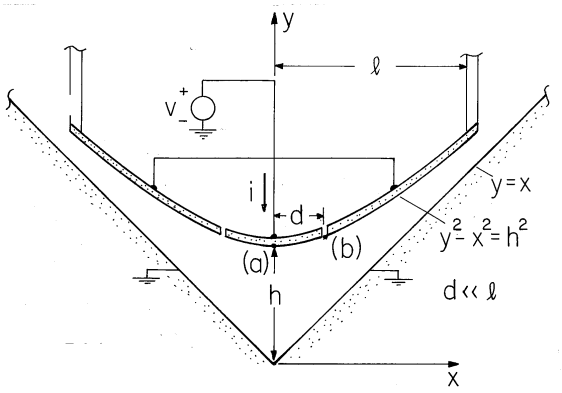


Fig. P4.1.8

(a) Given that the electric field intensity between the groove and tool takes the form

$$\mathbf{E} = C[x\mathbf{i}_\mathbf{x} - y\mathbf{i}_\mathbf{y}] \qquad (a)$$

show that $\mathbf{E}$ is irrotational and evaluate the coefficient C by computing the integral of $\mathbf{E} \cdot d\mathbf{s}$ between point (a) and the origin.

(b) Find the potential function consistent with (a) and evaluate C by inspection. Check with part (a).
(c) Using the conventions of Figs. 2.7.3 and 4.1.3, sketch lines of constant potential and electric field $\mathbf{E}$ for the region between the groove and the tool surfaces.
(d) Determine the total charge on the insulated segment, given $v(t)$. (Hint: Use the integral form of Gauss' law with a convenient surface S enclosing the electrode.)

4.1.9* In cylindrical coordinates, the incremental displacement vector, given in Cartesian coordinates by (9), is

$$\Delta\mathbf{r} = \Delta r\mathbf{i}_\mathbf{r} + r\Delta\phi\mathbf{i}_\phi + \Delta z\mathbf{i}_\mathbf{z} \qquad (a)$$

Using arguments analogous to (7)–(12), show that the gradient operator in cylindrical coordinates is as given in Table I at the end of the text.

4.1.10* Using arguments analogous to those of (7)–(12), show that the gradient operator in spherical coordinates is as given in Table I at the end of the text.

4.2 Poisson's Equation

4.2.1* In Prob. 4.1.4, the potential Φ is given by (a). Use Poisson's equation to show that the associated charge density is as given by (c) of that problem.

4.2.2 In Prob. 4.1.5, Φ is given by (a). Use Poisson's equation to find the charge density.

4.2.3 Use the expressions for the divergence and gradient in cylindrical coordinates from Table I at the end of the text to show that the Laplacian operator is as summarized in that table.

4.2.4 Use the expressions from Table I at the end of the text for the divergence and gradient in spherical coordinates to show that the Laplacian operator is as summarized in that table.

4.3 Superposition Principle

4.3.1 A current source $I(t)$ is connected in parallel with a capacitor C and a resistor R. Write the ordinary differential equation that can be solved for the voltage $v(t)$ across the three parallel elements. Follow steps analogous to those used in this section to show that if $I_a(t) \Rightarrow v_a(t)$ and $I_b(t) \Rightarrow v_b(t)$, then $I_a(t) + I_b(t) \Rightarrow v_a(t) + v_b(t)$.

4.4 Fields Associated with Charge Singularities

4.4.1* A two-dimensional field results from parallel uniform distributions of line charge, $+\lambda_l$ at $x = d/2,\ y = 0$ and $-\lambda_l$ at $x = -d/2,\ y = 0$, as shown in Fig. P4.4.1. Thus, the potential distribution is independent of z.

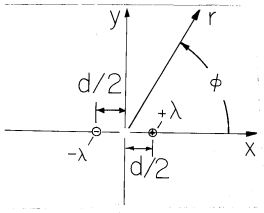


Fig. P4.4.1

(a) Start with the electric field of a line charge, (1.3.13), and determine Φ.
(b) Define the two-dimensional dipole moment as $p_\lambda = d\lambda_l$ and show that in the limit where $d \to 0$ (while this moment remains constant), the electric potential is

$$\Phi = \frac{p_\lambda}{2\pi\epsilon_o}\frac{\cos\phi}{r} \qquad (a)$$

4.4.2* For the configuration of Prob. 4.4.1, consider the limit in which the line charge spacing d goes to infinity. Show that, in polar coordinates, the potential distribution is of the form

$$\Phi \to Ar\cos\phi \qquad (a)$$

Express this in Cartesian coordinates and show that the associated $\mathbf{E}$ is uniform.

4.4.3 A two-dimensional charge distribution is formed by pairs of positive and negative line charges running parallel to the z axis. Shown in cross-section in Fig. P4.4.3, each line is at a distance $d/2$ from the origin. Show that in the limit where $d \ll r$, this potential takes the form $A\cos 2\phi/r^n$. What are the constants A and n?

4.4.4 The charge distribution described in Prob. 4.4.3 is now at infinity ($d \gg r$).

(a) Show that the potential in the neighborhood of the origin takes the form $A(x^2 - y^2)$.
(b) How would you position the line charges so that in the limit where they moved to infinity, the potential would take the form of (4.1.18)?

4.5 Solution of Poisson's Equation for Specified Charge Distributions

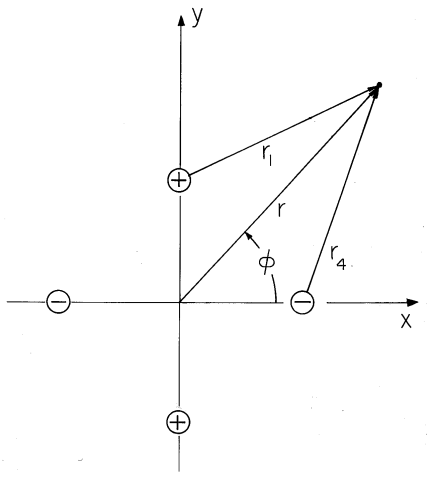


Fig. P4.4.3

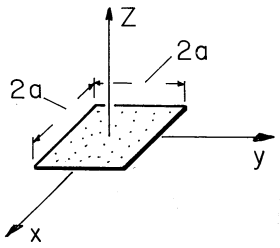


Fig. P4.5.1

4.5.1 The only charge is restricted to a square patch centered at the origin and lying in the $x - y$ plane, as shown in Fig. P4.5.1.

(a) Assume that the patch is very thin in the z direction compared to other dimensions of interest. Over its surface there is a given surface charge density $\sigma_s(x, y)$. Express the potential Φ along the z axis for $z > 0$ in terms of a two-dimensional integral.

(b) For the particular surface charge distribution $\sigma_s = \sigma_o|xy|/a^2$ where σ_o and a are constants, determine Φ along the positive z axis.

(c) What is Φ at the origin?

(d) Show that Φ has a z dependence for $z \gg a$ that is the same as for a point charge at the origin. In this limit, what is the equivalent point charge for the patch?

(e) What is $\mathbf{E}$ along the positive z axis?

4.5.2* The highly insulating spherical shell of Fig. P4.5.2 has radius R and is "coated" with a surface charge density $\sigma_s = \sigma_o \cos\theta$, where σ_o is a given constant.

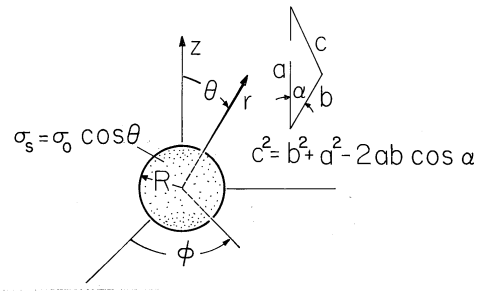


Fig. P4.5.2

(a) Show that the distribution of potential along the z axis in the range $z > R$ is

$$\Phi = \frac{\sigma_o R^3}{3\epsilon_o z^2} \tag{a}$$

[Hint: Remember that for the triangle shown in the figure, the law of cosines gives $c = (b^2 + a^2 - 2ab\cos\alpha)^{1/2}$.]

(b) Show that the potential distribution for the range $z < R$ along the z axis inside the shell is

$$\Phi = \frac{\sigma_o z}{3\epsilon_o} \tag{b}$$

(c) Show that along the z axis, $\mathbf{E}$ is

$$\mathbf{E} = \mathbf{i_z} \begin{cases} \frac{2\sigma_o R^3}{3\epsilon_o z^3} & R < z \\ -\frac{\sigma_o}{3\epsilon_o} & R > z \end{cases} \tag{c}$$

(d) By comparing the z dependence of the potential to that of a dipole polarized in the z direction, show that the equivalent dipole moment is $qd = (4\pi/3)\sigma_o R^3$.

4.5.3 All of the charge is on the surface of a cylindrical shell having radius R and length $2l$, as shown in Fig. P4.5.3. Over the top half of this cylinder at $r = R$ the surface charge density is σ_o (coulomb/m^2), where σ_o is a positive constant, while over the lower half it is $-\sigma_o$.

(a) Find the potential distribution along the z axis.
(b) Determine $\mathbf{E}$ along the z axis.
(c) In the limit where $z \gg l$, show that Φ becomes that of a dipole at the origin. What is the equivalent dipole moment?

4.5.4* A uniform line charge of density λ_l and length d is distributed parallel to the y axis and centered at the point $(x, y, z) = (a, 0, 0)$, as shown in Fig. P4.5.4. Use the superposition integral to show that the potential $\Phi(x, y, z)$ is

$$\Phi = \frac{\lambda_l}{4\pi\epsilon_o} ln\left[\frac{\frac{d}{2} - y + \sqrt{(x-a)^2 + \left(\frac{d}{2} - y\right)^2 + z^2}}{-\frac{d}{2} - y + \sqrt{(x-a)^2 + \left(\frac{d}{2} + y\right)^2 + z^2}}\right] \tag{a}$$

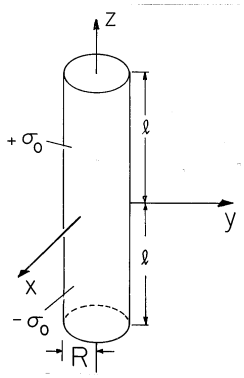


Fig. P4.5.3

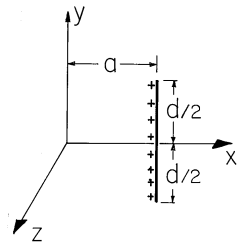


Fig. P4.5.4

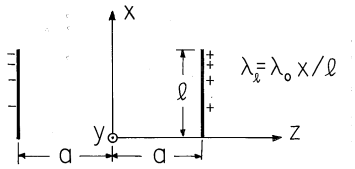


Fig. P4.5.5

4.5.5 Charge is distributed with density $\lambda_l = \pm\lambda_o x/l$ coulomb/m along the lines $z = \pm a,\ y = 0$, respectively, between the points $x = 0$ and $x = l$, as shown in Fig. P4.5.5. Take λ_o as a given charge per unit length and note that λ_l varies from zero to λ_o over the lengths of the line charge distributions. Determine the distribution of Φ along the z axis in the range $0 < z < a$.

4.5.6 Charge is distributed along the z axis such that the charge per unit length $\lambda_l(z)$ is given by

$$\lambda_l = \begin{cases} \frac{\lambda_o z}{a} & -a < z < a \\ 0 & z < -a;\ a < z \end{cases} \qquad (a)$$

Determine Φ and $\mathbf{E}$ at a position $z > a$ on the z axis.

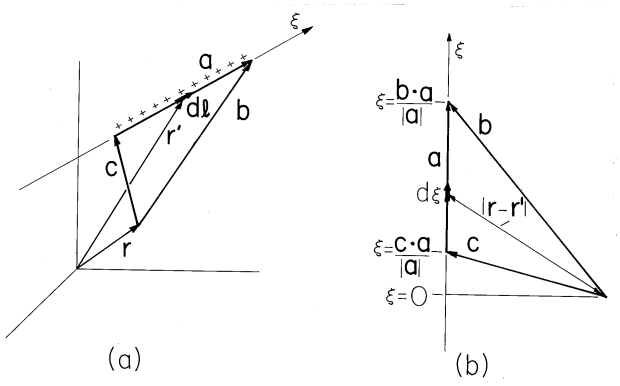


Fig. P4.5.9

4.5.7* A strip of charge lying in the $x-z$ plane between $x=-b$ and $x=b$ extends to $\pm\infty$ in the z direction. On this strip the surface charge density is

$$\sigma_s = \sigma_o \frac{(d-b)}{(d-x)} \tag{a}$$

where $d > b$. Show that at the location $(x,y)=(d,0)$, the potential is

$$\Phi(d,0) = \frac{\sigma_o}{4\pi\epsilon_o}(d-b)\{[ln(d-b)]^2 - [ln(d+b)]^2\} \tag{b}$$

4.5.8 A pair of charge strips lying in the $x-z$ plane and running from $z=+\infty$ to $z=-\infty$ are each of width $2d$ with their left and right edges, respectively, located on the z axis. The one between the z axis and $(x,y)=(2d,0)$ has a uniform surface charge density σ_o, while the one between $(x,y)=(-2d,0)$ and the z axis has $\sigma_s=-\sigma_o$. (Note that the symmetry makes the plane $x=0$ one of zero potential.) What must be the value of σ_o if the potential at the center of the right strip, where $(x,y)=(d,0)$, is to be V?

4.5.9* Distributions of line charge can be approximated by piecing together uniformly charged segments. Especially if a computer is to be used to carry out the integration by summing over the fields due to the linear elements of line charge, this provides a convenient basis for calculating the electric potential for a given line distribution of charge. In the following, you determine the potential at an arbitrary observer coordinate $\mathbf{r}$ due to a line charge that is uniformly distributed between the points $\mathbf{r}+\mathbf{b}$ and $\mathbf{r}+\mathbf{c}$, as shown in Fig. P4.5.9a. The segment over which this charge (of line charge density λ_l) is distributed is denoted by the vector $\mathbf{a}$, as shown in the figure.

Viewed in the plane in which the position vectors $\mathbf{a}, \mathbf{b}$, and $\mathbf{c}$ lie, a coordinate ξ denoting the position along the line charge is as shown in Fig. P4.5.9b. The origin of this coordinate is at the position on the line segment collinear with $\mathbf{a}$ that is nearest to the observer position $\mathbf{r}$.

(a) Argue that in terms of ξ, the base and tip of the $\mathbf{a}$ vector are as designated in Fig. P4.5.9b along the ξ axis.
(b) Show that the superposition integral for the potential due to the segment of line charge at $\mathbf{r}'$ is

$$\Phi = \int_{\mathbf{c}\cdot\mathbf{a}/|\mathbf{a}|}^{\mathbf{b}\cdot\mathbf{a}/|\mathbf{a}|} \frac{\lambda_l d\xi}{4\pi\epsilon_o|\mathbf{r}-\mathbf{r}'|} \tag{a}$$

where

$$|\mathbf{r}-\mathbf{r}'| = \sqrt{\xi^2 + \frac{|\mathbf{b}\times\mathbf{a}|^2}{|\mathbf{a}|^2}} \tag{b}$$

(c) Finally, show that the potential is

$$\Phi = \frac{\lambda}{4\pi\epsilon_o} ln \frac{\left| \frac{\mathbf{b}\cdot\mathbf{a}}{|\mathbf{a}|} + \sqrt{\left(\frac{\mathbf{b}\cdot\mathbf{a}}{|\mathbf{a}|}\right)^2 + \frac{|\mathbf{b}\times\mathbf{a}|^2}{|\mathbf{a}|^2}} \right|}{\left| \frac{\mathbf{c}\cdot\mathbf{a}}{|\mathbf{a}|} + \sqrt{\left(\frac{\mathbf{c}\cdot\mathbf{a}}{|\mathbf{a}|}\right)^2 + \frac{|\mathbf{b}\times\mathbf{a}|^2}{|\mathbf{a}|^2}} \right|} \tag{c}$$

(d) A straight segment of line charge has the uniform density λ_o between the points $(x, y, z) = (0, 0, d)$ and $(x, y, z) = (d, d, d)$. Using (c), show that the potential $\phi(x, y, z)$ is

$$\Phi = \frac{\lambda_o}{4\pi\epsilon_o} ln \left| \frac{2d - x - y + \sqrt{2[(d-x)^2 + (d-y)^2 + (d-z)^2]}}{-x - y + \sqrt{2[x^2 + y^2 + (d-z)^2]}} \right| \tag{d}$$

4.5.10* Given the charge distribution, $\rho(\mathbf{r})$, the potential Φ follows from (3). This expression has the disadvantage that to find $\mathbf{E}$, derivatives of Φ must be taken. Thus, it is not enough to know Φ at one location if $\mathbf{E}$ is to be determined. Start with (3) and show that a superposition integral for the electric field intensity is

$$\mathbf{E} = \frac{1}{4\pi\epsilon_o} \int_{V'} \frac{\rho(\mathbf{r}')\mathbf{i}_{r'r} dv'}{|\mathbf{r}-\mathbf{r}'|^2} \tag{a}$$

where $\mathbf{i}_{r'r}$ is a unit vector directed from the source coordinate $\mathbf{r}'$ to the observer coordinate $\mathbf{r}$. (Hint: Remember that when the gradient of Φ is taken to obtain $\mathbf{E}$, the derivatives are with respect to the observer coordinates with the source coordinates held fixed.) A similar derivation is given in Sec. 8.2, where an expression for the magnetic field intensity $\mathbf{H}$ is obtained from a superposition integral for the vector potential $\mathbf{A}$.

4.5.11 For a better understanding of the concepts underlying the derivation of the superposition integral for Poisson's equation, consider a hypothetical situation where a somewhat different equation is to be solved. The charge

density is assumed in part to be a predetermined density $s(x,y,z)$, and in part to be induced at a given point (x,y,z) in proportion to the potential itself at that same point. That is,

$$\rho = s - \epsilon_o \kappa^2 \Phi \tag{a}$$

(a) Show that the expression to be satisfied by Φ is then not Poisson's equation but rather

$$\nabla^2 \Phi - \kappa^2 \Phi = -\frac{s}{\epsilon_o} \tag{b}$$

where $s(x,y,z)$ now plays the role of ρ.

(b) The first step in the derivation of the superposition integral is to find the response to a point source at the origin, defined such that

$$\lim_{R \to 0} \int_0^R s 4\pi r^2 dr = Q \tag{c}$$

Because the situation is then spherically symmetric, the desired response to this point source must be a function of r only. Thus, for this response, (b) becomes

$$\frac{1}{r^2}\frac{\partial}{\partial r}\left(r^2 \frac{\partial \Phi}{\partial r}\right) - \kappa^2 \Phi = -\frac{s}{\epsilon_o} \tag{d}$$

Show that for $r \neq 0$, a solution is

$$\Phi = A\frac{e^{-\kappa r}}{r} \tag{e}$$

and use (c) to show that $A = Q/4\pi\epsilon_o$.

(c) What is the superposition integral for Φ?

4.5.12* Because there is a jump in potential across a dipole layer, given by (31), there is an infinite electric field within the layer.

(a) With $\mathbf{n}$ defined as the unit normal to the interface, argue that this internal electric field is

$$\mathbf{E}_{int} = -\epsilon_o \sigma_s \mathbf{n} \tag{a}$$

(b) In deriving the continuity condition on $\mathbf{E}$, (1.6.12), using (4.1.1), it was assumed that $\mathbf{E}$ was finite everywhere, even within the interface. With a dipole layer, this assumption cannot be made. For example, suppose that a nonuniform dipole layer $\pi_s(x)$ is in the plane $y = 0$. Show that there is a jump in tangential electric field, E_x, given by

$$E_x^a - E_x^b = -\epsilon_o \frac{\partial \pi_s}{\partial x} \tag{b}$$

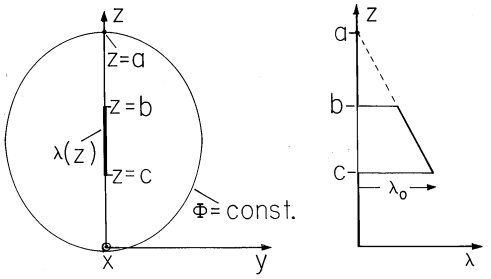


Fig. P4.6.1

4.6 Electroquasistatic Fields in the Presence of Perfect Conductors

4.6.1* A charge distribution is represented by a line charge between $z = c$ and $z = b$ along the z axis, as shown in Fig. P4.6.1a. Between these points, the line charge density is given by

$$\lambda_l = \lambda_o \frac{(a-z)}{(a-c)} \tag{a}$$

and so it has the distribution shown in Fig. P4.6.1b. It varies linearly from the value λ_o where $z = c$ to $\lambda_o(a-b)/(a-c)$ where $z = b$. The only other charges in the system are at infinity, where the potential is defined as being zero.

An equipotential surface for this charge distribution passes through the point $z = a$ on the z axis. [This is the same "a" as appears in (a).] If this equipotential surface is replaced by a perfectly conducting electrode, show that the capacitance of the electrode relative to infinity is

$$C = 2\pi\epsilon_o(2a - c - b) \tag{b}$$

4.6.2 Charges at "infinity" are used to impose a uniform field $\mathbf{E} = E_o\mathbf{i_z}$ on a region of free space. In addition to the charges that produce this field, there are positive and negative charges, of magnitude q, at $z = +d/2$ and $z = -d/2$, respectively, as shown in Fig. P4.6.2. Spherical coordinates (r, θ, ϕ) are defined in the figure.

(a) The potential, radial coordinate and charge are normalized such that

$$\underline{\Phi} = \frac{\Phi}{E_o d}; \qquad \underline{r} = \frac{r}{d}; \qquad \underline{q} = \frac{q}{4\pi\epsilon_o E_o d^2} \tag{a}$$

Show that the normalized electric potential $\underline{\Phi}$ can be written as

$$\underline{\Phi} = -\underline{r}\cos\theta + \underline{q}\left\{\left[\underline{r}^2 + \frac{1}{4} - \underline{r}\cos\theta\right]^{-1/2} - \left[\underline{r}^2 + \frac{1}{4} + \underline{r}\cos\theta\right]^{-1/2}\right\} \tag{b}$$

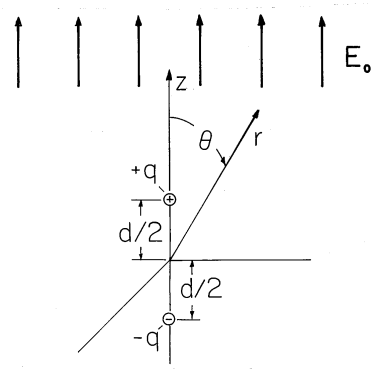


Fig. P4.6.2

(b) There is an equipotential surface $\Phi = 0$ that encloses these two charges. Thus, if a "perfectly conducting" object having a surface taking the shape of this $\Phi = 0$ surface is placed in the initially uniform electric field, the result of part (a) is a solution to the boundary value problem representing the potential, and hence electric field, around the object. The following establishes the shape of the object. Use (b) to find an implicit expression for the radius r at which the surface intersects the z axis. Use a graphical solution to show that there will always be such an intersection with $r > d/2$. For $\underline{q} = 2$, find this radius to two-place accuracy.

(c) Make a plot of the surface $\underline{\Phi} = 0$ in a $\phi =$ constant plane. One way to do this is to use a programmable calculator to evaluate $\underline{\Phi}$ given $\underline{r}$ and θ. It is then straightforward to pick a θ and iterate on $\underline{r}$ to find the location of the surface of zero potential. Make $\underline{q} = 2$.

(d) We expect **E** to be largest at the poles of the object. Thus, it is in these regions that we expect electrical breakdown to first occur. In terms of $\underline{E}_o$ and with $\underline{q} = 2$, what is the electric field at the north pole of the object?

(e) In terms of E_o and d, what is the total charge on the northern half of the object. [Hint: A numerical calculation is *not* required.]

4.6.3* For the disk of charge shown in Fig. 4.5.3, there is an equipotential surface that passes through the point $z = d$ on the z axis and encloses the disk. Show that if this surface is replaced by a perfectly conducting electrode, the capacitance of this electrode relative to infinity is

$$C = \frac{2\pi R^2 \epsilon_o}{(\sqrt{R^2 + d^2} - d)} \qquad (a)$$

4.6.4 The purpose of this problem is to get an estimate of the capacitance of, and the fields surrounding, the two conducting spheres of radius R shown in Fig. P4.6.4, with the centers separated by a distance h. We construct

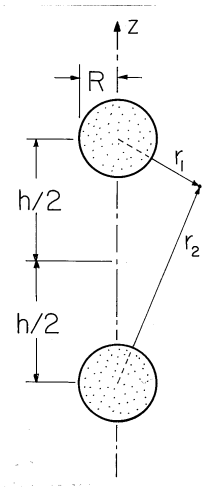


Fig. P4.6.4

an approximate field solution for the field produced by charges $\pm Q$ on the two spheres, as follows:

(a) First we place the charges at the centers of the spheres. If $R \ll h$, the two equipotentials surrounding the charges at $r_1 \approx R$ and $r_2 \approx R$ are almost spherical. If we assume that they *are* spherical, what is the potential difference between the two spherical conductors? Where does the maximum field occur and how big is it?

(b) We can obtain a better solution by noting that a spherical equipotential coincident with the top sphere is produced by a set of three charges. These are the charge $-Q$ at $z = -h/2$ and the two charges inside the top sphere properly positioned according to (33) of appropriate magnitude and total charge $+Q$. Next, we replace the charge $-Q$ by two charges, just like we did for the charge $+Q$. The net field is now due to four charges. Find the potential difference and capacitance for the new field configuration and compare with the previous result. Do you notice that you have obtained higher-order terms in R/h? You are in the process of obtaining a rapidly convergent series in powers of R/h.

4.6.5 This is a continuation of Prob. 4.5.4. The line distribution of charge given there is the only charge in the region $0 \leq x$. However, the $y - z$ plane is now a perfectly conducting surface, so that the electric field is normal to the plane $x = 0$.

(a) Determine the potential in the half-space $0 \leq x$.

(b) For the potential found in part (a), what is the equation for the equipotential surface passing through the point $(x, y, z) = (a/2, 0, 0)$?

(c) For the remainder of this problem, assume that $d = 4a$. Make a sketch of this equipotential surface as it intersects the plane $z = 0$. In doing this, it is convenient to normalize x and y to a by defining $\xi = x/a$ and

$\eta = y/a$. A good way to make the plot is then to compute the potential using a programmable calculator. By iteration, you can quickly zero in on points of the desired potential. It is sufficient to show that in addition to the point of part (a), your curve passes through three well-defined points that suggest its being a closed surface.

(d) Suppose that this closed surface having potential V is actually a metallic (perfect) conductor. Sketch the lines of electric field intensity in the region between the electrode and the ground plane.

(e) The capacitance of the electrode relative to the ground plane is defined as $C = q/V$, where q is the total charge on the surface of the electrode having potential V. For the electrode of part (c), what is C?

4.7 Method of Images

4.7.1* A point charge Q is located on the z axis a distance d above a perfect conductor in the plane $z = 0$.

(a) Show that Φ above the plane is

$$\Phi = \frac{Q}{4\pi\epsilon_o}\left\{\frac{1}{[x^2+y^2+(z-d)^2]^{1/2}} - \frac{1}{[x^2+y^2+(z+d)^2]^{1/2}}\right\} \tag{a}$$

(b) Show that the equation for the equipotential surface $\Phi = V$ passing through the point $z = a < d$ is

$$[x^2+y^2+(z-d)^2]^{-1/2} - [x^2+y^2+(z+d)^2]^{-1/2} = \frac{2a}{d^2-a^2} \tag{b}$$

(c) Use intuitive arguments to show that this surface encloses the point charge. In terms of a, d, and ϵ_o, show that the capacitance relative to the ground plane of an electrode having the shape of this surface is

$$C = \frac{2\pi\epsilon_o(d^2-a^2)}{a} \tag{c}$$

4.7.2 A positive uniform line charge is along the z axis at the center of a perfectly conducting cylinder of square cross-section in the $x-y$ plane.

(a) Give the location and sign of the image line charges.

(b) Sketch the equipotentials and $\mathbf{E}$ lines in the $x-y$ plane.

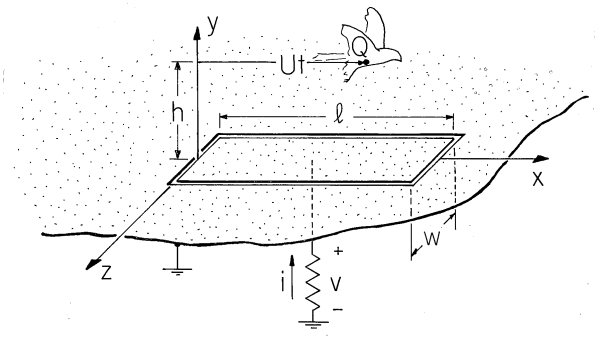


Fig. P4.7.3

4.7.3 When a bird perches on a dc high-voltage power line and then flies away, it does so carrying a net charge.

(a) Why?
(b) For the purpose of measuring this net charge Q carried by the bird, we have the apparatus pictured in Fig. P4.7.3. Flush with the ground, a strip electrode having width w and length l is mounted so that it is insulated from ground. The resistance, R, connecting the electrode to ground is small enough so that the potential of the electrode (like that of the surrounding ground) can be approximated as zero. The bird flies in the x direction at a height h above the ground with a velocity U. Thus, its position is taken as $y = h$ and $x = Ut$.
(c) Given that the bird has flown at an altitude sufficient to make it appear as a point charge, what is the potential distribution?
(d) Determine the surface charge density on the ground plane at $y = 0$.
(e) At a given instant, what is the net charge, q, on the electrode? (Assume that the width w is small compared to h so that in an integration over the electrode surface, the integration in the z direction is simply a multiplication by w.)
(f) Sketch the time dependence of the electrode charge.
(g) The current through the resistor is dq/dt. Find an expression for the voltage, v, that would be measured across the resistance, R, and sketch its time dependence.

4.7.4* Uniform line charge densities $+\lambda_l$ and $-\lambda_l$ run parallel to the z axis at $x = a, y = 0$ and $x = b, y = 0$, respectively. There are no other charges in the half-space $0 < x$. The $y - z$ plane where $x = 0$ is composed of finely segmented electrodes. By connecting a voltage source to each segment, the potential in the $x = 0$ plane can be made whatever we want. Show that the potential distribution you would impose on these electrodes to insure that there is no normal component of $\mathbf{E}$ in the $x = 0$ plane, $E_x(0, y, z)$, is

$$\Phi(0, y, z) = -\frac{\lambda_l}{2\pi\epsilon_o} ln \frac{(a^2 + y^2)}{(b^2 + y^2)} \qquad (a)$$

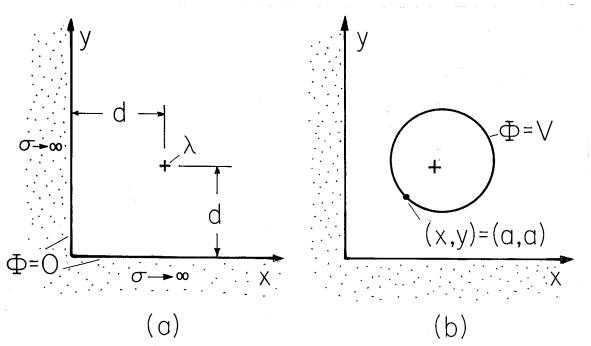


Fig. P4.7.5

4.7.5 The two-dimensional system shown in cross-section in Fig. P4.7.5 consists of a uniform line charge at $x = d, y = d$ that extends to infinity in the $\pm z$ directions. The charge per unit length in the z direction is the constant λ. Metal electrodes extend to infinity in the $x = 0$ and $y = 0$ planes. These electrodes are grounded so that the potential in these planes is zero.

(a) Determine the electric potential in the region $x > 0, y > 0$.

(b) An equipotential surface passes through the line $x = a, y = a (a < d)$. This surface is replaced by a metal electrode having the same shape. In terms of the given constants a, d, and ϵ_o, what is the capacitance per unit length in the z direction of this electrode relative to the ground planes?

4.7.6* The disk of charge shown in Fig. 4.5.3 is located at $z = s$ rather than $z = 0$. The plane $z = 0$ consists of a perfectly conducting ground plane.

(a) Show that for $0 < z$, the electric potential along the z axis is given by

$$\Phi = \frac{\sigma_o}{2\epsilon_o}\left[\left(\sqrt{R^2 + (z-s)^2} - |z-s|\right) - \left(\sqrt{R^2 + (z+s)^2} - |z+s|\right)\right] \qquad (a)$$

(b) Show that the capacitance relative to the ground plane of an electrode having the shape of the equipotential surface passing through the point $z = d < s$ on the z axis and enclosing the disk of charge is

$$C = \frac{2\pi R^2 \epsilon_o}{\left[\sqrt{R^2 + (d-s)^2} - \sqrt{R^2 + (d+s)^2} + 2d\right]} \qquad (b)$$

4.7.7 The disk of charge shown in Fig. P4.7.7 has radius R and height h above a perfectly conducting plane. It has a surface charge density $\sigma_s = \sigma_o r/R$. A perfectly conducting electrode has the shape of an equipotential surface

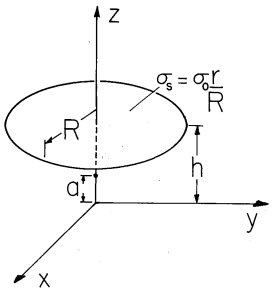


Fig. P4.7.7

that passes through the point $z = a < h$ on the z axis and encloses the disk. What is the capacitance of this electrode relative to the plane $z = 0$?

4.7.8 A straight segment of line charge has the uniform density λ_o between the points $(x, y, z) = (0, 0, d)$ and $(x, y, z) = (d, d, d)$. There is a perfectly conducting material in the plane $z = 0$. Determine the potential for $z \geq 0$. [See part (d) of Prob. 4.5.9.]

4.8 Charge Simulation Approach to Boundary Value Problems

4.8.1 For the six-segment approximation to the fields of the parallel plate capacitor in Example 4.8.1, determine the respective strip charge densities in terms of the voltage V and dimensions of the system. What is the approximate capacitance?

5

ELECTROQUASISTATIC FIELDS FROM THE BOUNDARY VALUE POINT OF VIEW

5.0 INTRODUCTION

The electroquasistatic laws were discussed in Chap. 4. The electric field intensity $\mathbf{E}$ is irrotational and represented by the negative gradient of the electric potential.

$$\mathbf{E} = -\nabla\Phi \tag{1}$$

Gauss' law is then satisfied if the electric potential Φ is related to the charge density ρ by Poisson's equation

$$\nabla^2\Phi = -\frac{\rho}{\epsilon_o} \tag{2}$$

In charge-free regions of space, Φ obeys Laplace's equation, (2), with $\rho = 0$.

The last part of Chap. 4 was devoted to an "opportunistic" approach to finding boundary value solutions. An exception was the numerical scheme described in Sec. 4.8 that led to the solution of a boundary value problem using the source-superposition approach. In this chapter, a more direct attack is made on solving boundary value problems without necessarily resorting to numerical methods. It is one that will be used extensively not only as effects of polarization and conduction are added to the EQS laws, but in dealing with MQS systems as well.

Once again, there is an analogy useful for those familiar with the description of linear circuit dynamics in terms of ordinary differential equations. With time as the independent variable, the response to a drive that is turned on when $t = 0$ can be determined in two ways. The first represents the response as a superposition of impulse responses. The resulting convolution integral represents the response for all time, before and after $t = 0$ and even when $t = 0$. This is the analogue of the point of view taken in the first part of Chap. 4.

The second approach represents the history of the dynamics prior to when $t = 0$ in terms of initial conditions. With the understanding that interest is confined to times subsequent to $t = 0$, the response is then divided into "particular"

and "homogeneous" parts. The particular solution to the differential equation representing the circuit is not unique, but insures that at each instant in the temporal range of interest, the differential equation is satisfied. This particular solution need not satisfy the initial conditions. In this chapter, the "drive" is the charge density, and the particular potential response guarantees that Poisson's equation, (2), is satisfied everywhere in the spatial region of interest.

In the circuit analogue, the homogeneous solution is used to satisfy the initial conditions. In the field problem, the homogeneous solution is used to satisfy boundary conditions. In a circuit, the homogeneous solution can be thought of as the response to drives that occurred prior to when $t = 0$ (outside the temporal range of interest). In the determination of the potential distribution, the homogeneous response is one predicted by Laplace's equation, (2), with $\rho = 0$, and can be regarded either as caused by fictitious charges residing outside the region of interest or as caused by the surface charges induced on the boundaries.

The development of these ideas in Secs. 5.1–5.3 is self-contained and does not depend on a familiarity with circuit theory. However, for those familiar with the solution of ordinary differential equations, it is satisfying to see that the approaches used here for dealing with partial differential equations are a natural extension of those used for ordinary differential equations.

Although it can often be found more simply by other methods, a particular solution always follows from the superposition integral. The main thrust of this chapter is therefore toward a determination of homogeneous solutions, of finding solutions to Laplace's equation. Many practical configurations have boundaries that are described by setting one of the coordinate variables in a three-dimensional coordinate system equal to a constant. For example, a box having rectangular cross-sections has walls described by setting one Cartesian coordinate equal to a constant to describe the boundary. Similarly, the boundaries of a circular cylinder are naturally described in cylindrical coordinates. So it is that there is great interest in having solutions to Laplace's equation that naturally "fit" these configurations. With many examples interwoven into the discussion, much of this chapter is devoted to cataloging these solutions. The results are used in this chapter for describing EQS fields in free space. However, as effects of polarization and conduction are added to the EQS purview, and as MQS systems with magnetization and conduction are considered, the homogeneous solutions to Laplace's equation established in this chapter will be a continual resource.

A review of Chap. 4 will identify many solutions to Laplace's equation. As long as the field source is outside the region of interest, the resulting potential obeys Laplace's equation. What is different about the solutions established in this chapter? A hint comes from the numerical procedure used in Sec. 4.8 to satisfy arbitrary boundary conditions. There, a superposition of N solutions to Laplace's equation was used to satisfy conditions at N points on the boundaries. Unfortunately, to determine the amplitudes of these N solutions, N equations had to be solved for N unknowns.

The solutions to Laplace's equation found in this chapter can also be used as the terms in an infinite series that is made to satisfy arbitrary boundary conditions. But what is different about the terms in this series is their orthogonality. This property of the solutions makes it possible to explicitly determine the individual amplitudes in the series. The notion of the orthogonality of functions may already

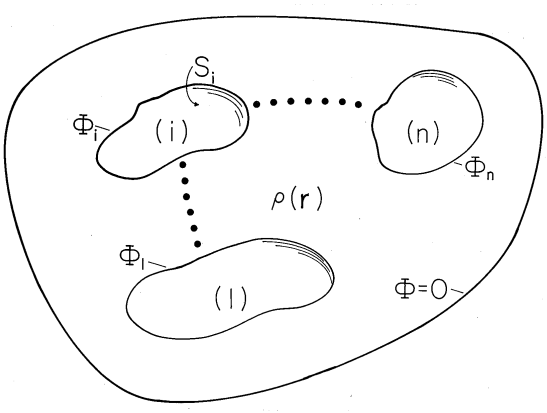


Fig. 5.1.1 Volume of interest in which there can be a distribution of charge density. To illustrate bounding surfaces on which potential is constrained, n isolated surfaces and one enclosing surface are shown.

be familiar through an exposure to Fourier analysis. In any case, the fundamental ideas involved are introduced in Sec. 5.5.

5.1 PARTICULAR AND HOMOGENEOUS SOLUTIONS TO POISSON'S AND LAPLACE'S EQUATIONS

Suppose we want to analyze an electroquasistatic situation as shown in Fig. 5.1.1. A charge distribution $\rho(\mathbf{r})$ is specified in the part of space of interest, designated by the volume V. This region is bounded by perfect conductors of specified shape and location. Known potentials are applied to these conductors and the enclosing surface, which may be at infinity.

In the space between the conductors, the potential function obeys Poisson's equation, (5.0.2). A particular solution of this equation within the prescribed volume V is given by the superposition integral, (4.5.3).

$$\Phi_p(\mathbf{r}) = \int_{V'} \frac{\rho(\mathbf{r}')dv'}{4\pi\epsilon_o|\mathbf{r}-\mathbf{r}'|} \tag{1}$$

This potential obeys Poisson's equation at each point within the volume V. Since we do not evaluate this equation outside the volume V, the integration over the sources called for in (1) need include no sources other than those within the volume V. This makes it clear that the particular solution is not unique, because the addition to the potential made by integrating over arbitrary charges outside the volume V will only give rise to a potential, the Laplacian derivative of which is zero within the volume V.

Is (1) the complete solution? Because it is not unique, the answer must be, surely not. Further, it is clear that no information as to the position and shape of the conductors is built into this solution. Hence, the electric field obtained as the negative gradient of the potential Φ_p of (1) will, in general, possess a finite tangential component on the surfaces of the electrodes. On the other hand, the conductors

have surface charge distributions which adjust themselves so as to cause the net electric field on the surfaces of the conductors to have vanishing tangential electric field components. The distribution of these surface charges is not known at the outset and hence cannot be included in the integral (1).

A way out of this dilemma is as follows: The potential distribution we seek within the space not occupied by the conductors is the result of two charge distributions. First is the prescribed volume charge distribution leading to the potential function Φ_p, and second is the charge distributed on the conductor surfaces. The potential function produced by the surface charges must obey the source-free Poisson's equation in the space V of interest. Let us denote this solution to the homogeneous form of Poisson's equation by the potential function Φ_h. Then, in the volume V, Φ_h must satisfy Laplace's equation.

$$\nabla^2 \Phi_h = 0 \tag{2}$$

The superposition principle then makes it possible to write the total potential as

$$\Phi = \Phi_p + \Phi_h \tag{3}$$

The problem of finding the complete field distribution now reduces to that of finding a solution such that the net potential Φ of (3) has the prescribed potentials v_i on the surfaces S_i. Now Φ_p is known and can be evaluated on the surface S_i. Evaluation of (3) on S_i gives

$$v_i = \Phi_p(S_i) + \Phi_h(S_i) \tag{4}$$

so that the homogeneous solution is prescribed on the boundaries S_i.

$$\Phi_h(S_i) = v_i - \Phi_p(S_i) \tag{5}$$

Hence, the determination of an electroquasistatic field with prescribed potentials on the boundaries is reduced to finding the solution to Laplace's equation, (2), that satisfies the boundary condition given by (5).

The approach which has been formalized in this section is another point of view applicable to the boundary value problems in the last part of Chap. 4. Certainly, the abstract view of the boundary value situation provided by Fig. 5.1.1 is not different from that of Fig. 4.6.1. In Example 4.6.4, the field shown in Fig. 4.6.8 is determined for a point charge adjacent to an equipotential charge-neutral spherical electrode. In the volume V of interest outside the electrode, the volume charge distribution is singular, the point charge q. The potential given by (4.6.35), in fact, takes the form of (3). The particular solution can be taken as the first term, the potential of a point charge. The second and third terms, which are equivalent to the potentials caused by the fictitious charges within the sphere, can be taken as the homogeneous solution.

Superposition to Satisfy Boundary Conditions. In the following sections, superposition will often be used in another way to satisfy boundary conditions.

Suppose that there is no charge density in the volume V, and again the potentials on each of the n surfaces S_j are v_j. Then

$$\nabla^2\Phi = 0 \tag{6}$$

$$\Phi = v_j \quad \text{on} \quad S_j,\ j = 1, \dots n \tag{7}$$

The solution is broken into a superposition of solutions Φ_j that meet the required condition on the j-th surface but are zero on all of the others.

$$\Phi = \sum_{j=1}^{n} \Phi_j \tag{8}$$

$$\Phi_j \equiv \begin{cases} v_j & \text{on } S_j \\ 0 & \text{on } S_1 \dots S_{j-1},\ S_{j+1} \dots S_n \end{cases} \tag{9}$$

Each term is a solution to Laplace's equation, (6), so the sum is as well.

$$\nabla^2\Phi_j = 0 \tag{10}$$

In Sec. 5.5, a method is developed for satisfying arbitrary boundary conditions on one of four surfaces enclosing a volume of interest.

Capacitance Matrix. Suppose that in the n electrode system the net charge on the i-th electrode is to be found. In view of (8), the integral of $\mathbf{E} \cdot d\mathbf{a}$ over the surface S_i enclosing this electrode then gives

$$q_i = -\oint_{S_i} \epsilon_o \nabla\Phi \cdot d\mathbf{a} = -\oint_{S_i} \epsilon_o \sum_{j=1}^{n} \nabla\Phi_j \cdot d\mathbf{a} \tag{11}$$

Because of the linearity of Laplace's equation, the potential Φ_j is proportional to the voltage exciting that potential, v_j. It follows that (11) can be written in terms of capacitance parameters that are independent of the excitations. That is, (11) becomes

$$q_i = \sum_{j=1}^{n} C_{ij} v_j \tag{12}$$

where the *capacitance coefficients* are

$$C_{ij} = \frac{-\oint_{S_i} \epsilon_o \nabla\Phi_j \cdot d\mathbf{a}}{v_j} \tag{13}$$

The charge on the i-th electrode is a linear superposition of the contributions of all n voltages. The coefficient multiplying its own voltage, C_{ii}, is called the *self-capacitance*, while the others, $C_{ij},\ i \neq j$, are the *mutual capacitances*.

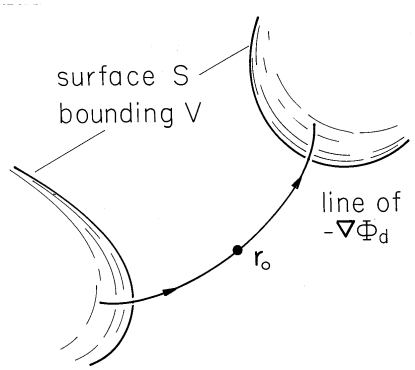


Fig. 5.2.1 Field line originating on one part of bounding surface and terminating on another after passing through the point $\mathbf{r}_o$.

5.2 UNIQUENESS OF SOLUTIONS TO POISSON'S EQUATION

We shall show in this section that a potential distribution obeying Poisson's equation is completely specified within a volume V if the potential is specified over the surfaces bounding that volume. Such a uniqueness theorem is useful for two reasons: (a) It tells us that if we have found such a solution to Poisson's equation, whether by mathematical analysis or physical insight, then we have found the only solution; and (b) it tells us what boundary conditions are appropriate to uniquely specify a solution. If there is no charge present in the volume of interest, then the theorem states the uniqueness of solutions to Laplace's equation.

Following the method "reductio ad absurdum", we assume that the solution is not unique– that two solutions, Φ_a and Φ_b, exist, satisfying the same boundary conditions– and then show that this is impossible. The presumably different solutions Φ_a and Φ_b must satisfy Poisson's equation with the same charge distribution and must satisfy the same boundary conditions.

$$\nabla^2\Phi_a = -\frac{\rho}{\epsilon_o}; \qquad \Phi_a = \Phi_i \quad \text{on} \quad S_i \tag{1}$$

$$\nabla^2\Phi_b = -\frac{\rho}{\epsilon_o}; \qquad \Phi_b = \Phi_i \quad \text{on} \quad S_i \tag{2}$$

It follows that with Φ_d defined as the difference in the two potentials, $\Phi_d = \Phi_a - \Phi_b$,

$$\nabla^2\Phi_d \equiv \nabla\cdot(\nabla\Phi_d) = 0; \qquad \Phi_d = 0 \quad \text{on} \quad S_i \tag{3}$$

A simple argument now shows that the only way Φ_d can both satisfy Laplace's equation and be zero on all of the bounding surfaces is for it to be zero. First, it is argued that Φ_d cannot possess a maximum or minimum at any point within V. With the help of Fig. 5.2.1, visualize the negative of the gradient of Φ_d, a field line, as it passes through some point $\mathbf{r}_o$. Because the field is solenoidal (divergence free), such a field line cannot start or stop within V (Sec. 2.7). Further, the field defines a potential (4.1.4). Hence, as one proceeds along the field line in the direction of the negative gradient, the potential has to decrease until the field line reaches one of the surfaces S_i bounding V. Similarly, in the opposite direction, the potential has to increase until another one of the surfaces is reached. Accordingly, all maximum and minimum values of $\Phi_d(\mathbf{r})$ have to be located on the surfaces.

The difference potential at any interior point cannot assume a value larger than or smaller than the largest or smallest value of the potential on the surfaces. But the surfaces are themselves at zero potential. It follows that the difference potential is zero everywhere in V and that $\Phi_a = \Phi_b$. Therefore, only one solution exists to the boundary value problem stated with (1).

5.3 CONTINUITY CONDITIONS

At the surfaces of metal conductors, charge densities accumulate that are only a few atomic distances thick. In describing their fields, the details of the distribution within this thin layer are often not of interest. Thus, the charge is represented by a surface charge density (1.3.11) and the surface supporting the charge treated as a surface of discontinuity.

In such cases, it is often convenient to divide a volume in which the field is to be determined into regions separated by the surfaces of discontinuity, and to use piece-wise continuous functions to represent the fields. Continuity conditions are then needed to connect field solutions in two regions separated by the discontinuity. These conditions are implied by the differential equations that apply throughout the region. They assure that the fields are consistent with the basic laws, even in passing through the discontinuity.

Each of the four Maxwell's equations implies a continuity condition. Because of the singular nature of the source distribution, these laws are used in integral form to relate the fields to either side of the surface of discontinuity. With the vector $\mathbf{n}$ defined as the unit normal to the surface of discontinuity and pointing from region (b) to region (a), the continuity conditions were summarized in Table 1.8.3.

In the EQS approximation, the laws of primary interest are Faraday's law without the magnetic induction and Gauss' law, the first two equations of Chap. 4. Thus, the corresponding EQS continuity conditions are

$$\mathbf{n} \times [\mathbf{E}^a - \mathbf{E}^b] = 0 \tag{1}$$

$$\mathbf{n} \cdot (\epsilon_o \mathbf{E}^a - \epsilon_o \mathbf{E}^b) = \sigma_s \tag{2}$$

Because the magnetic induction makes no contribution to Faraday's continuity condition in any case, these conditions are the same as for the general electrodynamic laws. As a reminder, the contour enclosing the integration surface over which Faraday's law was integrated (Sec. 1.6) to obtain (1) is shown in Fig. 5.3.1a. The integration volume used to obtain (2) from Gauss' law (Sec. 1.3) is similarly shown in Fig. 5.3.1b.

What are the continuity conditions on the electric potential? The potential Φ is continuous across a surface of discontinuity even if that surface carries a surface charge density. This will be the case when the $\mathbf{E}$ field is finite (a dipole layer containing an infinite field causes a jump of potential), because then the line integral of the electric field from one side of the surface to the other side is zero, the path-length being infinitely small.

$$\Phi^a - \Phi^b = 0 \tag{3}$$

To determine the jump condition representing Gauss' law through the surface of discontinuity, it was integrated (Sec. 1.3) over the volume shown intersecting the

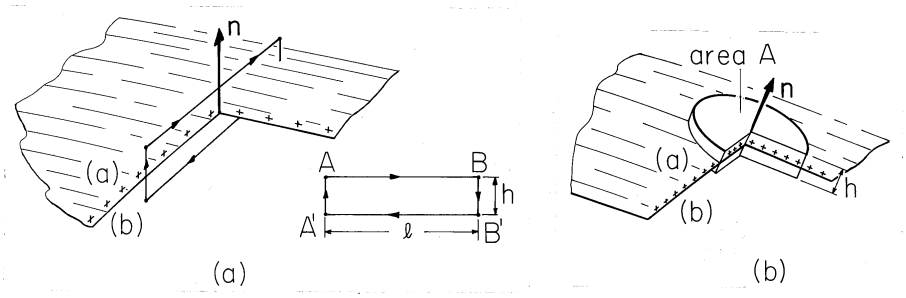


Fig. 5.3.1 (a) Differential contour intersecting surface supporting surface charge density. (b) Differential volume enclosing surface charge on surface having normal **n**.

surface in Fig. 5.3.1b. The resulting continuity condition, (2), is written in terms of the potential by recognizing that in the EQS approximation, $\mathbf{E} = -\nabla\Phi$.

$$\mathbf{n} \cdot [(\nabla\Phi)^a - (\nabla\Phi)^b] = -\frac{\sigma_s}{\epsilon_o} \tag{4}$$

At a surface of discontinuity that carries a surface charge density, the normal derivative of the potential is discontinuous.

The continuity conditions become boundary conditions if they are made to represent physical constraints that go beyond those already implied by the laws that prevail in the volume. A familiar example is one where the surface is that of an electrode constrained in its potential. Then the continuity condition (3) requires that the potential in the volume adjacent to the electrode be the given potential of the electrode. This statement cannot be justified without invoking information about the physical nature of the electrode (that it is "infinitely conducting," for example) that is not represented in the volume laws and hence is not intrinsic to the continuity conditions.

5.4 SOLUTIONS TO LAPLACE'S EQUATION IN CARTESIAN COORDINATES

Having investigated some general properties of solutions to Poisson's equation, it is now appropriate to study specific methods of solution to Laplace's equation subject to boundary conditions. Exemplified by this and the next section are three standard steps often used in representing EQS fields. First, Laplace's equation is set up in the coordinate system in which the boundary surfaces are coordinate surfaces. Then, the partial differential equation is reduced to a set of ordinary differential equations by separation of variables. In this way, an infinite set of solutions is generated. Finally, the boundary conditions are satisfied by superimposing the solutions found by separation of variables.

In this section, solutions are derived that are natural if boundary conditions are stated along coordinate surfaces of a Cartesian coordinate system. It is assumed that the fields depend on only two coordinates, x and y, so that Laplace's equation

is (Table I)

$$\frac{\partial^2 \Phi}{\partial x^2} + \frac{\partial^2 \Phi}{\partial y^2} = 0 \tag{1}$$

This is a partial differential equation in two independent variables. One time-honored method of mathematics is to reduce a new problem to a problem previously solved. Here the process of finding solutions to the partial differential equation is reduced to one of finding solutions to ordinary differential equations. This is accomplished by the *method of separation of variables*. It consists of assuming solutions with the special space dependence

$$\Phi(x, y) = X(x)Y(y) \tag{2}$$

In (2), X is assumed to be a function of x alone and Y is a function of y alone. If need be, a general space dependence is then recovered by superposition of these special solutions. Substitution of (2) into (1) and division by Φ then gives

$$\frac{1}{X(x)} \frac{d^2 X(x)}{dx^2} = -\frac{1}{Y(y)} \frac{d^2 Y(y)}{dy^2} \tag{3}$$

Total derivative symbols are used because the respective functions X and Y are by definition only functions of x and y.

In (3) we now have on the left-hand side a function of x alone, on the right-hand side a function of y alone. The equation can be satisfied independent of x and y only if each of these expressions is constant. We denote this "separation" constant by k^2, and it follows that

$$\frac{d^2 X}{dx^2} = -k^2 X \tag{4}$$

and

$$\frac{d^2 Y}{dy^2} = k^2 Y \tag{5}$$

These equations have the solutions

$$X \sim \cos kx \qquad \text{or} \qquad \sin kx \tag{6}$$

$$Y \sim \cosh ky \qquad \text{or} \qquad \sinh ky \tag{7}$$

If $k = 0$, the solutions degenerate into

$$X \sim \text{ constant} \qquad \text{or} \qquad x \tag{8}$$

$$Y \sim \text{ constant} \qquad \text{or} \qquad y \tag{9}$$

The product solutions, (2), are summarized in the first four rows of Table 5.4.1. Those in the right-hand column are simply those of the middle column with the roles of x and y interchanged. Generally, we will leave the prime off the k' in writing these solutions. Exponentials are also solutions to (7). These, sometimes more convenient, solutions are summarized in the last four rows of the table.

The solutions summarized in this table can be used to gain insight into the nature of EQS fields. A good investment is therefore made if they are now visualized.

The fields represented by the potentials in the left-hand column of Table 5.4.1 are all familiar. Those that are linear in x and y represent uniform fields, in the x and y directions, respectively. The potential xy is familiar from Fig. 4.1.3. We will use similar conventions to represent the potentials of the second column, but it is helpful to have in mind the three-dimensional portrayal exemplified for the potential xy in Fig. 4.1.4. In the more complicated field maps to follow, the sketch is visualized as a contour map of the potential Φ with peaks of positive potential and valleys of negative potential.

On the top and left peripheries of Fig. 5.4.1 are sketched the functions $\cos kx$ and $\cosh ky$, respectively, the product of which is the first of the potentials in the middle column of Table 5.4.1. If we start out from the origin in either the $+y$ or $-y$ directions (north or south), we climb a potential hill. If we instead proceed in the $+x$ or $-x$ directions (east or west), we move downhill. An easterly path begun on the potential hill to the north of the origin corresponds to a decrease in the $\cos kx$ factor. To follow a path of equal elevation, the $\cosh ky$ factor must increase, and this implies that the path must turn northward.

A good starting point in making these field sketches is the identification of the contours of zero potential. In the plot of the second potential in the middle column of Table 5.4.1, shown in Fig. 5.4.2, these are the y axis and the lines $kx = +\pi/2,\ +3\pi/2$, etc. The dependence on y is now odd rather than even, as it was for the plot of Fig. 5.4.1. Thus, the origin is now on the side of a potential hill that slopes downward from north to south.

The solutions in the third and fourth rows of the second column possess the same field patterns as those just discussed provided those patterns are respectively shifted in the x direction. In the last four rows of Table 5.4.1 are four additional possible solutions which are linear combinations of the previous four in that column. Because these decay exponentially in either the $+y$ or $-y$ directions, they are useful for representing solutions in problems where an infinite half-space is considered.

The solutions in Table 5.4.1 are nonsingular throughout the entire $x-y$ plane. This means that Laplace's equation is obeyed everywhere within the finite $x-y$ plane, and hence the field lines are continuous; they do not appear or disappear. The sketches show that the fields become stronger and stronger as one proceeds in the positive and negative y directions. The lines of electric field originate on positive charges and terminate on negative charges at $y \to \pm\infty$. Thus, for the plots shown in Figs. 5.4.1 and 5.4.2, the charge distributions at infinity must consist of alternating distributions of positive and negative charges of infinite amplitude.

Two final observations serve to further develop an appreciation for the nature of solutions to Laplace's equation. First, the third dimension can be used to represent the potential in the manner of Fig. 4.1.4, so that the potential surface has the shape of a membrane stretched from boundaries that are elevated in proportion to their potentials.

Laplace's equation, (1), requires that the sum of quantities that reflect the curvatures in the x and y directions vanish. If the second derivative of a function is positive, it is curved upward; and if it is negative, it is curved downward. If the curvature is positive in the x direction, it must be negative in the y direction. Thus, at the origin in Fig. 5.4.1, the potential is cupped downward for excursions in the

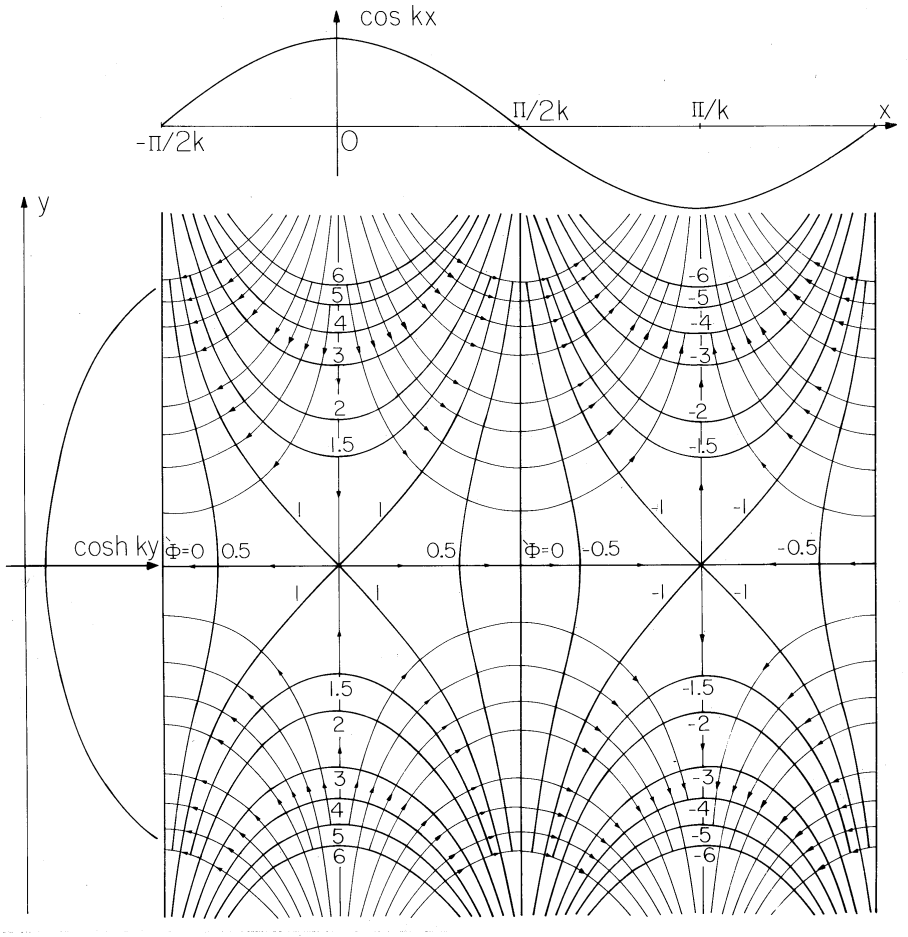


Fig. 5.4.1 Equipotentials for $\Phi = \cos(kx)\cosh(ky)$ and field lines. As an aid to visualizing the potential, the separate factors $\cos(kx)$ and $\cosh(ky)$ are, respectively, displayed at the top and to the left.

x direction, and so it must be cupped upward for variations in the y direction. A similar deduction must apply at every point in the $x - y$ plane.

Second, because the k that appears in the periodic functions of the second column in Table 5.4.1 is the same as that in the exponential and hyperbolic functions, it is clear that the more rapid the periodic variation, the more rapid is the decay or apparent growth.

5.5 MODAL EXPANSION TO SATISFY BOUNDARY CONDITIONS

Each of the solutions obtained in the preceding section by separation of variables could be produced by an appropriate potential applied to pairs of parallel surfaces

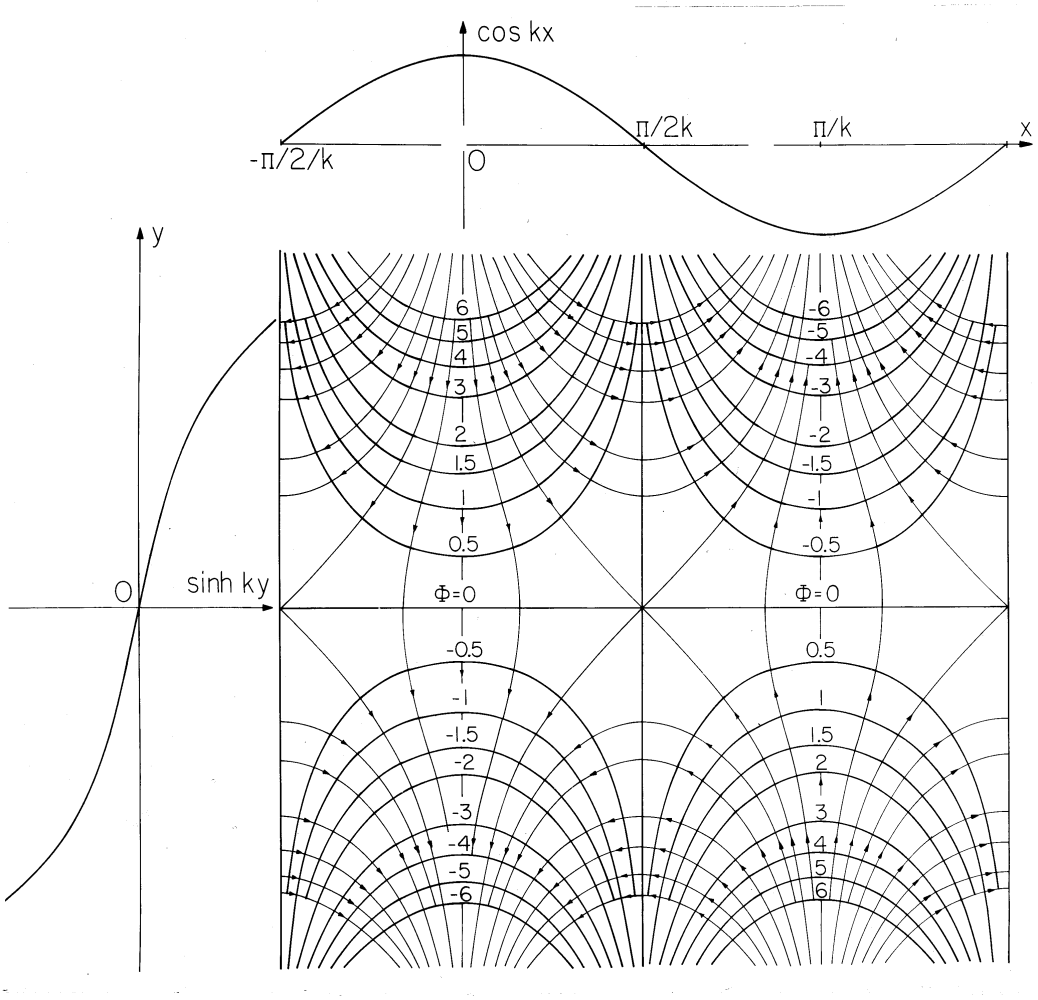


Fig. 5.4.2 Equipotentials for $\Phi = \cos(kx)\sinh(ky)$ and field lines. As an aid to visualizing the potential, the separate factors $\cos(kx)$ and $\sinh(ky)$ are, respectively, displayed at the top and to the left.

in the planes $x =$ constant and $y =$ constant. Consider, for example, the fourth solution in the column $k^2 \geq 0$ of Table 5.4.1, which with a constant multiplier is

$$\Phi = A \sin kx \sinh ky \tag{1}$$

This solution has $\Phi = 0$ in the plane $y = 0$ and in the planes $x = n\pi/k$, where n is an integer. Suppose that we set $k = n\pi/a$ so that $\Phi = 0$ in the plane $y = a$ as well. Then at $y = b$, the potential of (1)

$$\Phi(x, b) = A \sinh \frac{n\pi}{a} b \sin \frac{n\pi}{a} x \tag{2}$$

TABLE 5.4.1
TWO-DIMENSIONAL CARTESIAN SOLUTIONS
OF LAPLACE'S EQUATION

$k = 0$	$k^2 \geq 0$	$k^2 \leq 0$ $(k \rightarrow jk')$
Constant	$\cos kx \cosh ky$	$\cosh k'x \cos k'y$
y	$\cos kx \sinh ky$	$\cosh k'x \sin k'y$
x	$\sin kx \cosh ky$	$\sinh k'x \cos k'y$
xy	$\sin kx \sinh ky$	$\sinh k'x \sin k'y$
	$\cos kx\, e^{ky}$	$e^{k'x} \cos k'y$
	$\cos kx\, e^{-ky}$	$e^{-k'x} \cos k'y$
	$\sin kx\, e^{ky}$	$e^{k'x} \sin k'y$
	$\sin kx\, e^{-ky}$	$e^{-k'x} \sin k'y$

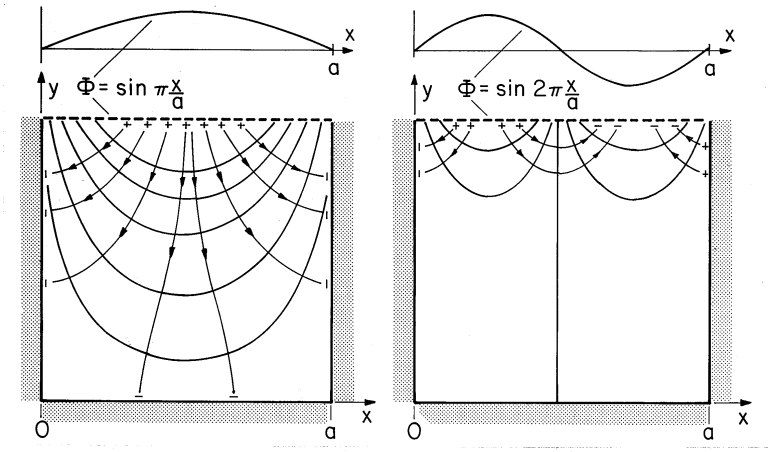


Fig. 5.5.1 Two of the infinite number of potential functions having the form of (1) that will fit the boundary conditions $\Phi = 0$ at $y = 0$ and at $x = 0$ and $x = a$.

has a sinusoidal dependence on x. If a potential of the form of (2) were applied along the surface at $y = b$, and the surfaces at $x = 0$, $x = a$, and $y = 0$ were held at zero potential (by, say, planar conductors held at zero potential), then the potential, (1), would exist within the space $0 < x < a$, $0 < y < b$. Segmented electrodes having each segment constrained to the appropriate potential could be used to approximate the distribution at $y = b$. The potential and field plots for $n = 1$ and $n = 2$ are given in Fig. 5.5.1. Note that the theorem of Sec. 5.2 insures

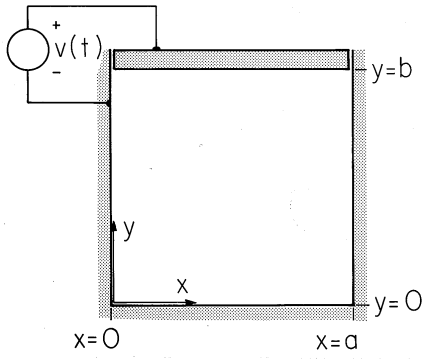


Fig. 5.5.2 Cross-section of zero-potential rectangular slot with an electrode having the potential v inserted at the top.

that the specified potential is unique.

But what can be done to describe the field if the wall potentials are not constrained to fit neatly the solution obtained by separation of variables? For example, suppose that the fields are desired in the same region of rectangular cross-section, but with an electrode at $y = b$ constrained to have a potential v that is independent of x. The configuration is now as shown in Fig. 5.5.2.

A line of attack is suggested by the infinite number of solutions, having the form of (1), that meet the boundary condition on three of the four walls. The superposition principle makes it clear that any linear combination of these is also a solution, so if we let A_n be arbitrary coefficients, a more general solution is

$$\Phi = \sum_{n=1}^{\infty} A_n \sinh \frac{n\pi}{a} y \sin \frac{n\pi}{a} x \tag{3}$$

Note that k has been assigned values such that the sine function is zero in the planes $x = 0$ and $x = a$. Now how can we adjust the coefficients so that the boundary condition at the driven electrode, at $y = b$, is met? One approach that we will not have to use is suggested by the numerical method described in Sec. 4.8. The electrode could be divided into N segments and (3) evaluated at the center point of each of the segments. If the infinite series were truncated at N terms, the result would be N equations that were linear in the N unknowns A_n. This system of equations could be inverted to determine the A_n's. Substitution of these into (3) would then comprise a solution to the boundary value problem. Unfortunately, to achieve reasonable accuracy, large values of N would be required and a computer would be needed.

The power of the approach of variable separation is that it results in solutions that are orthogonal in a sense that makes it possible to determine explicitly the coefficients A_n. The evaluation of the coefficients is remarkably simple. First, (3) is evaluated on the surface of the electrode where the potential is known.

$$\Phi(x, b) = \sum_{n=1}^{\infty} A_n \sinh \frac{n\pi b}{a} \sin \frac{n\pi}{a} x \tag{4}$$

On the right is the infinite series of sinusoidal functions with coefficients that are to be determined. On the left is a given function of x. We multiply both sides of the expression by $\sin(m\pi x/a)$, where m is one integer, and then both sides of the expression are integrated over the width of the system.

$$\int_0^a \Phi(x,b)\sin\frac{m\pi}{a}xdx = \sum_{n=1}^{\infty} A_n \sinh\frac{n\pi b}{a}\int_0^a \sin\frac{m\pi}{a}x\sin\frac{n\pi}{a}xdx \tag{5}$$

The functions $\sin(n\pi x/a)$ and $\sin(m\pi x/a)$ are orthogonal in the sense that the integral of their product over the specified interval is zero, unless $m = n$.

$$\int_0^a \sin\frac{m\pi}{a}x\sin\frac{n\pi}{a}xdx = \begin{cases} 0, & n \neq m \\ \frac{a}{2}, & n = m \end{cases} \tag{6}$$

Thus, all the terms on the right in (5) vanish, except the one having $n = m$. Of course, m can be any integer, so we can solve (5) for the m-th amplitude and then replace m by n.

$$A_n = \frac{2}{a\sinh\frac{n\pi b}{a}}\int_0^a \Phi(x,b)\sin\frac{n\pi}{a}xdx \tag{7}$$

Given any distribution of potential on the surface $y = b$, this integral can be carried out and hence the coefficients determined. In this specific problem, the potential is v at each point on the electrode surface. Thus, (7) is evaluated to give

$$A_n = \frac{2v(t)}{n\pi}\frac{(1-\cos\pi n)}{\sinh\left(\frac{n\pi b}{a}\right)} = \begin{cases} 0; & n \text{ even} \\ \frac{4v}{n\pi}\frac{1}{\sinh\left(\frac{n\pi b}{a}\right)}; & n \text{ odd} \end{cases} \tag{8}$$

Finally, substitution of these coefficients into (3) gives the desired potential.

$$\Phi = \sum_{\substack{n=1 \\ \text{odd}}}^{\infty} \frac{4v(t)}{\pi}\frac{1}{n}\frac{\sinh\left(\frac{n\pi}{a}y\right)}{\sinh\left(\frac{n\pi b}{a}\right)}\sin\frac{n\pi}{a}x \tag{9}$$

Each product term in this infinite series satisfies Laplace's equation and the zero potential condition on three of the surfaces enclosing the region of interest. The *sum* satisfies the potential condition on the "last" boundary. Note that the sum is not itself in the form of the product of a function of x alone and a function of y alone.

The modal expansion is applicable with an arbitrary distribution of potential on the "last" boundary. But what if we have an arbitrary distribution of potential on all four of the planes enclosing the region of interest? The superposition principle justifies using the sum of four solutions of the type illustrated here. Added to the series solution already found are three more, each analogous to the previous one, but rotated by 90 degrees. Because each of the four series has a finite potential only on the part of the boundary to which its series applies, the sum of the four satisfy all boundary conditions.

The potential given by (9) is illustrated in Fig. 5.5.3. In the three-dimensional portrayal, it is especially clear that the field is infinitely large in the corners where

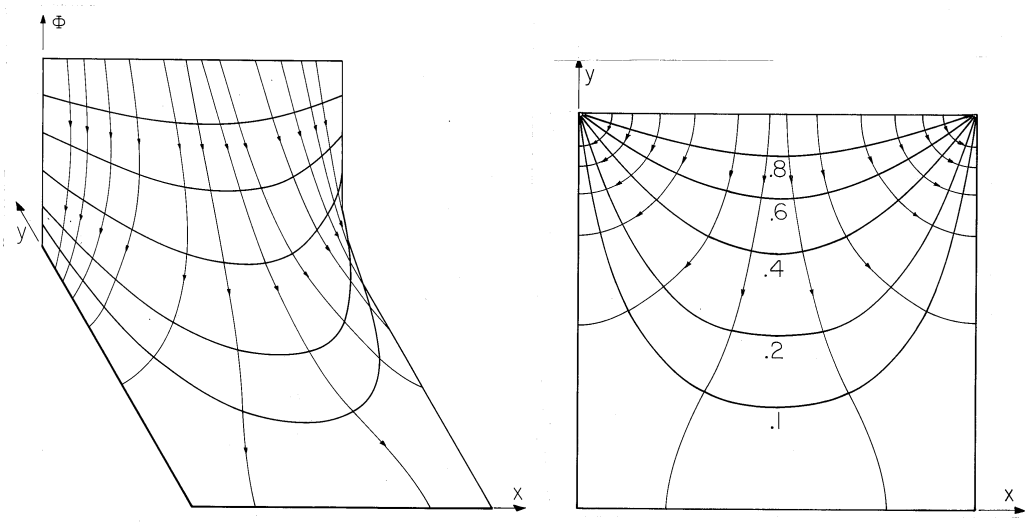


Fig. 5.5.3 Potential and field lines for the configuration of Fig. 5.5.2, (9), shown using vertical coordinate to display the potential and shown in $x-y$ plane.

the driven electrode meets the grounded walls. Where the electric field emanates from the driven electrode, there is surface charge, so at the corners there is an infinite surface charge density. In practice, of course, the spacing is not infinitesimal and the fields are not infinite.

Demonstration 5.5.1. Capacitance Attenuator

Because neither of the field laws in this chapter involve time derivatives, the field that has been determined is correct for $v = v(t)$, an arbitrary function of time. As a consequence, the coefficients A_n are also functions of time. Thus, the charges induced on the walls of the box are time varying, as can be seen if the wall at $y = 0$ is isolated from the grounded side walls and connected to ground through a resistor. The configuration is shown in cross-section by Fig. 5.5.4. The resistance R is small enough so that the potential v_o is small compared with v.

The charge induced on this output electrode is found by applying Gauss' integral law with an integration surface enclosing the electrode. The width of the electrode in the z direction is w, so

$$q = \oint_S \epsilon_o \mathbf{E} \cdot d\mathbf{a} = \epsilon_o w \int_0^a E_y(x,0)dx = -\epsilon_o w \int_0^a \frac{\partial \Phi}{\partial y}(x,0)dx \tag{10}$$

This expression is evaluated using (9).

$$q = -C_m v; \qquad C_m \equiv \frac{8\epsilon_o w}{\pi} \sum_{\substack{n=1 \\ \text{odd}}}^{\infty} \frac{1}{n \sinh\left(\frac{n\pi b}{a}\right)} \tag{11}$$

Conservation of charge requires that the current through the resistance be the rate of change of this charge with respect to time. Thus, the output voltage is

$$v_o = -R\frac{dq}{dt} = RC_m \frac{dv}{dt} \tag{12}$$

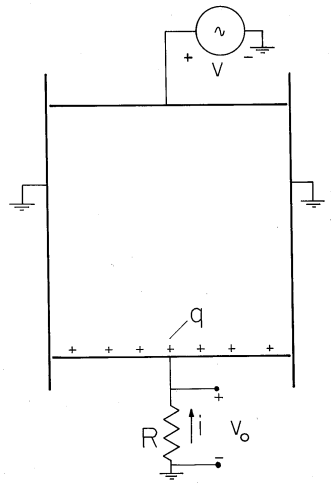


Fig. 5.5.4 The bottom of the slot is replaced by an insulating electrode connected to ground through a low resistance so that the induced current can be measured.

and if $v = V \sin \omega t$, then

$$v_o = RC_m \omega V \cos \omega t \equiv V_o \cos \omega t \tag{13}$$

The experiment shown in Fig. 5.5.5 is designed to demonstrate the dependence of the output voltage on the spacing b between the input and output electrodes. It follows from (13) and (11) that this voltage can be written in normalized form as

$$\frac{V_o}{U} = \sum_{\substack{n=1 \\ \text{odd}}}^{\infty} \frac{1}{2n \sinh\left(\frac{n\pi b}{a}\right)}; \qquad U \equiv \frac{16\epsilon_o w \omega R}{\pi} V \tag{14}$$

Thus, the natural log of the normalized voltage has the dependence on the electrode spacing shown in Fig. 5.5.5. Note that with increasing b/a the function quickly becomes a straight line. In the limit of large b/a, the hyperbolic sine can be approximated by $\exp(n\pi b/a)/2$ and the series can be approximated by one term. Thus, the dependence of the output voltage on the electrode spacing becomes simply

$$ln\left(\frac{V_o}{U}\right) = ln\, e^{-(\pi b/a)} = -\pi \frac{b}{a} \tag{15}$$

and so the asymptotic slope of the curve is $-\pi$.

Charges induced on the input electrode have their images either on the side walls of the box or on the output electrode. If b/a is small, almost all of these images are on the output electrode, but as it is withdrawn, more and more of the images are on the side walls and fewer are on the output electrode.

In retrospect, there are several matters that deserve further discussion. First, the potential used as a starting point in this section, (1), is one from a list of four in Table 5.4.1. What type of procedure can be used to select the appropriate form? In general, the solution used to satisfy the zero potential boundary condition on the

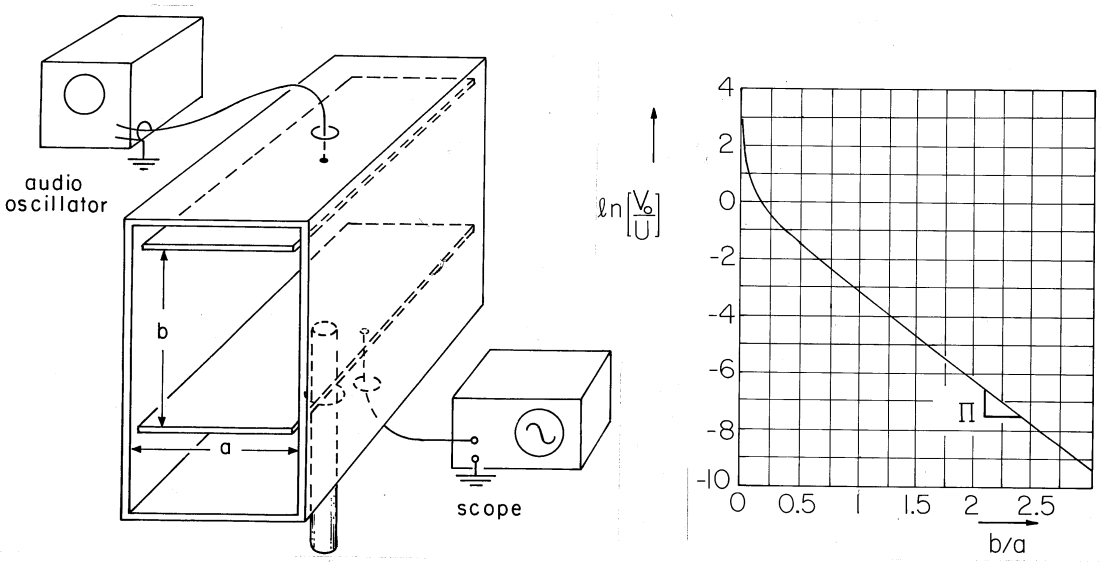


Fig. 5.5.5 Demonstration of electroquasistatic attenuator in which normalized output voltage is measured as a function of the distance between input and output electrodes normalized to the smaller dimension of the box. The normalizing voltage U is defined by (14). The output electrode is positioned by means of the attached insulating rod. In operation, a metal lid covers the side of the box.

"first" three surfaces is a linear combination of the four possible solutions. Thus, with the A's denoting undetermined coefficients, the general form of the solution is

$$\begin{aligned}\Phi = {} & A_1 \cos kx \cosh ky + A_2 \cos kx \sinh ky \\ & + A_3 \sin kx \cosh ky + A_4 \sin kx \sinh ky\end{aligned} \tag{16}$$

Formally, (1) was selected by eliminating three of these four coefficients. The first two must vanish because the function must be zero at $x = 0$. The third is excluded because the potential must be zero at $y = 0$. Thus, we are led to the last term, which, if $A_4 = A$, is (1).

The methodical elimination of solutions is necessary. Because the origin of the coordinates is arbitrary, setting up a simple expression for the potential is a matter of choosing the origin of coordinates properly so that as many of the solutions (16) are eliminated as possible. We purposely choose the origin so that a single term from the four in (16) meets the boundary condition at $x = 0$ and $y = 0$. The selection of product solutions from the list should interplay with the choice of coordinates. Some combinations are much more convenient than others. This will be exemplified in this and the following chapters.

The remainder of this section is devoted to a more detailed discussion of the expansion in sinusoids represented by (9). In the plane $y = b$, the potential distribution is of the form

$$\Phi(x, b) = \sum_{n=1}^{\infty} V_n \sin \frac{n\pi}{a} x \tag{17}$$

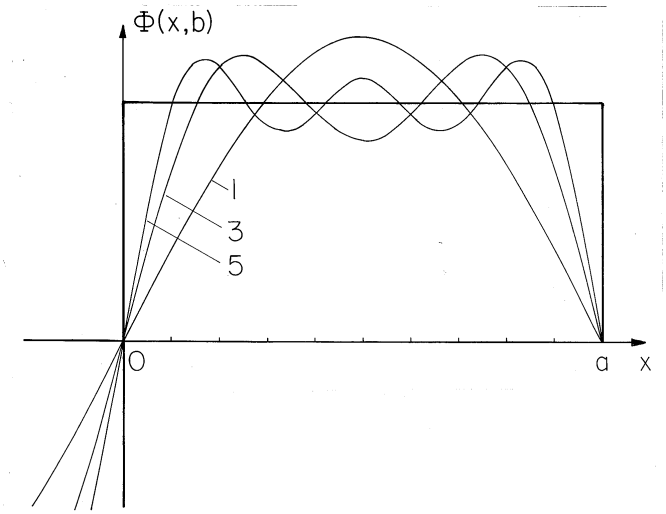


Fig. 5.5.6 Fourier series approximation to square wave given by (17) and (18), successively showing one, two, and three terms. Higher-order terms tend to fill in the sharp discontinuity at $x = 0$ and $x = a$. Outside the range of interest, the series represents an odd function of x having a periodicity length $2a$.

where the procedure for determining the coefficients has led to (8), written here in terms of the coefficients V_n of (17) as

$$V_n = \begin{cases} 0, & n \text{ even} \\ \frac{4v}{n\pi}, & n \text{ odd} \end{cases} \tag{18}$$

The approximation to the potential v that is uniform over the span of the driving electrode is shown in Fig. 5.5.6. Equation (17) represents a square wave of period $2a$ extending over all x, $-\infty < x < +\infty$. One half of a period appears as shown in the figure. It is possible to represent this distribution in terms of sinusoids alone because it is odd in x. In general, a periodic function is represented by a Fourier series of both sines and cosines. In the present problem, cosines were missing because the potential had to be zero at $x = 0$ and $x = a$. Study of a Fourier series shows that the series converges to the actual function in the sense that in the limit of an infinite number of terms,

$$\int_0^a [\Phi^2(x) - F^2(x)]dx = 0 \tag{19}$$

where $\Phi(x)$ is the actual potential distribution and $F(x)$ is the Fourier series approximation.

To see the generality of the approach exemplified here, we show that the orthogonality property of the functions $X(x)$ results from the differential equation and boundary conditions. Thus, it should not be surprising that the solutions in other coordinate systems also have an orthogonality property.

In all cases, the orthogonality property is associated with any one of the factors in a product solution. For the Cartesian problem considered here, it is $X(x)$ that satisfies boundary conditions at two points in space. This is assured by adjusting

the eigenvalue $k_n = n\pi/a$ so that the eigenfunction or mode, $\sin(n\pi x/a)$, is zero at $x = 0$ and $x = a$. This function satisfies (5.4.4) and the boundary conditions.

$$\frac{d^2X_m}{dx^2} + k_m^2 X_m = 0; \qquad X_m = 0 \quad \text{at} \quad x = 0, a \tag{20}$$

The subscript m is used to recognize that there is an infinite number of solutions to this problem. Another solution, say the n-th, must also satisfy this equation and the boundary conditions.

$$\frac{d^2X_n}{dx^2} + k_n^2 X_n = 0; \qquad X_n = 0 \quad \text{at} \quad x = 0, a \tag{21}$$

The orthogonality property for these modes, exploited in evaluating the coefficients of the series expansion, is

$$\int_0^a X_m X_n dx = 0, \qquad n \neq m \tag{22}$$

To prove this condition in general, we multiply (20) by X_n and integrate between the points where the boundary conditions apply.

$$\int_0^a X_n \frac{d}{dx}\left(\frac{dX_m}{dx}\right)dx + \int_0^a k_m^2 X_m X_n dx = 0 \tag{23}$$

By identifying $u = X_n$ and $v = dX_m/dx$, the first term is integrated by parts to obtain

$$\int_0^a X_n \frac{d}{dx}\left(\frac{dX_m}{dx}\right)dx = X_n \frac{dX_m}{dx}\bigg|_0^a - \int_0^a \frac{dX_n}{dx}\frac{dX_m}{dx}dx \tag{24}$$

The first term on the right vanishes because of the boundary conditions. Thus, (23) becomes

$$-\int_0^a \frac{dX_m}{dx}\frac{dX_n}{dx}dx + k_m^2 \int_0^a X_m X_n dx = 0 \tag{25}$$

If these same steps are completed with n and m interchanged, the result is (25) with n and m interchanged. Because the first term in (25) is the same as its counterpart in this second equation, subtraction of the two expressions yields

$$(k_m^2 - k_n^2)\int_0^a X_m X_n dx = 0 \tag{26}$$

Thus, the functions are orthogonal provided that $k_n \neq k_m$. For this specific problem, the eigenfunctions are $X_n = \sin(n\pi/a)$ and the eigenvalues are $k_n = n\pi/a$. But in general we can expect that our product solutions to Laplace's equation in other coordinate systems will result in a set of functions having similar orthogonality properties.

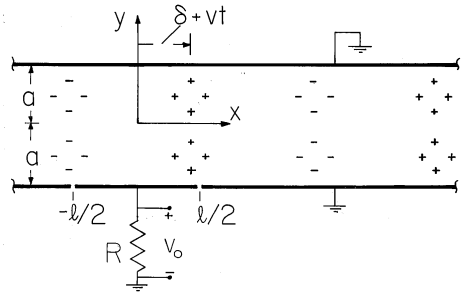


Fig. 5.6.1 Cross-section of layer of charge that is periodic in the x direction and bounded from above and below by zero potential plates. With this charge translating to the right, an insulated electrode inserted in the lower equipotential is used to detect the motion.

5.6 SOLUTIONS TO POISSON'S EQUATION WITH BOUNDARY CONDITIONS

An approach to solving Poisson's equation in a region bounded by surfaces of known potential was outlined in Sec. 5.1. The potential was divided into a particular part, the Laplacian of which balances $-\rho/\epsilon_o$ throughout the region of interest, and a homogeneous part that makes the sum of the two potentials satisfy the boundary conditions. In short,

$$\Phi = \Phi_p + \Phi_h \tag{1}$$

$$\nabla^2\Phi_p = -\frac{\rho}{\epsilon_o} \tag{2}$$

$$\nabla^2\Phi_h = 0 \tag{3}$$

and on the enclosing surfaces,

$$\Phi_h = \Phi - \Phi_p \qquad \text{on} \quad S \tag{4}$$

The following examples illustrate this approach. At the same time they demonstrate the use of the Cartesian coordinate solutions to Laplace's equation and the idea that the fields described can be time varying.

Example 5.6.1. Field of Traveling Wave of Space Charge between Equipotential Surfaces

The cross-section of a two-dimensional system that stretches to infinity in the x and z directions is shown in Fig. 5.6.1. Conductors in the planes $y = a$ and $y = -a$ bound the region of interest. Between these planes the charge density is periodic in the x direction and uniformly distributed in the y direction.

$$\rho = \rho_o \cos \beta x \tag{5}$$

The parameters ρ_o and β are given constants. For now, the segment connected to ground through the resistor in the lower electrode can be regarded as being at the same zero potential as the remainder of the electrode in the plane $x = -a$ and the electrode in the plane $y = a$. First we ask for the field distribution.

Remember that any particular solution to (2) will do. Because the charge density is independent of y, it is natural to look for a particular solution with the same property. Then, on the left in (2) is a second derivative with respect to x, and the equation can be integrated twice to obtain

$$\Phi_p = \frac{\rho_o}{\epsilon_o \beta^2} \cos \beta x \tag{6}$$

This particular solution is independent of y. Note that it is not the potential that would be obtained by evaluating the superposition integral over the charge between the grounded planes. Viewed over all space, that charge distribution is not independent of y. In fact, the potential of (6) is associated with a charge distribution as given by (5) that extends to infinity in the $+y$ and $-y$ directions.

The homogeneous solution must make up for the fact that (6) does not satisfy the boundary conditions. That is, at the boundaries, $\Phi = 0$ in (1), so the homogeneous and particular solutions must balance there.

$$\Phi_h \Big|_{y=\pm a} = -\Phi_p \Big|_{y=\pm a} = -\frac{\rho_o}{\epsilon_o \beta^2} \cos \beta x \tag{7}$$

Thus, we are looking for a solution to Laplace's equation, (3), that satisfies these boundary conditions. Because the potential has the same value on the boundaries, and the origin of the y axis has been chosen to be midway between, it is clear that the potential must be an even function of y. Further, it must have a periodicity in the x direction that matches that of (7). Thus, from the list of solutions to Laplace's equation in Cartesian coordinates in the middle column of Table 5.4.1, $k = \beta$, the $\sin kx$ terms are eliminated in favor of the $\cos kx$ solutions, and the $\cosh ky$ solution is selected because it is even in y.

$$\Phi_h = A \cosh \beta y \cos \beta x \tag{8}$$

The coefficient A is now adjusted so that the boundary conditions are satisfied by substituting (8) into (7).

$$A \cosh \beta a \cos \beta x = -\frac{\rho_o}{\epsilon_o \beta^2} \cos \beta x \rightarrow A = -\frac{\rho_o}{\epsilon_o \beta^2 \cosh \beta a} \tag{9}$$

Superposition of the particular solution, (7), and the homogeneous solution given by substituting the coefficient of (9) into (8), results in the desired potential distribution.

$$\Phi = \frac{\rho_o}{\epsilon_o \beta^2} \left(1 - \frac{\cosh \beta y}{\cosh \beta a} \right) \cos \beta x \tag{10}$$

The mathematical solutions used in deriving (10) are illustrated in Fig. 5.6.2. The particular solution describes an electric field that originates in regions of positive charge density and terminates in regions of negative charge density. It is purely x directed and is therefore tangential to the equipotential boundary. The homogeneous solution that is added to this field is entirely due to surface charges. These give rise to a field that bucks out the tangential field at the walls, rendering them surfaces of constant potential. Thus, the sum of the solutions (also shown in the figure), satisfies Gauss' law and the boundary conditions.

With this static view of the fields firmly in mind, suppose that the charge distribution is moving in the x direction with the velocity v.

$$\rho = \rho_o \cos \beta (x - vt) \tag{11}$$

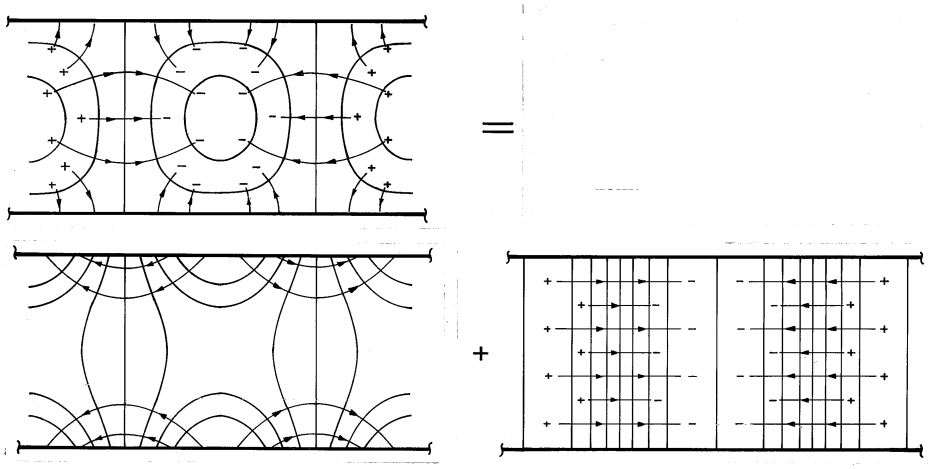


Fig. 5.6.2 Equipotentials and field lines for configuration of Fig. 5.6.1 showing graphically the superposition of particular and homogeneous parts that gives the required potential.

The variable x in (5) has been replaced by $x - vt$. With this moving charge distribution, the field also moves. Thus, (10) becomes

$$\Phi = \frac{\rho_o}{\epsilon_o \beta^2}\left(1 - \frac{\cosh \beta y}{\cosh \beta a}\right)\cos \beta(x - vt) \tag{12}$$

Note that the homogeneous solution is now a linear combination of the first and third solutions in the middle column of Table 5.4.1.

As the space charge wave moves by, the charges induced on the perfectly conducting walls follow along in synchronism. The current that accompanies the redistribution of surface charges is detected if a section of the wall is insulated from the rest and connected to ground through a resistor, as shown in Fig. 5.6.1. Under the assumption that the resistance is small enough so that the segment remains at essentially zero potential, what is the output voltage v_o?

The current through the resistor is found by invoking charge conservation for the segment to find the current that is the time rate of change of the net charge on the segment. The latter follows from Gauss' integral law and (12) as

$$\begin{aligned} q &= w \int_{-l/2}^{l/2} \epsilon_o E_y \Big|_{y=-a} dx \\ &= -\frac{w\rho_o}{\beta^2} \tanh \beta a \big[\sin \beta\big(\frac{l}{2} - vt\big) \\ &\quad + \sin \beta\big(\frac{l}{2} + vt\big)\big] \end{aligned} \tag{13}$$

It follows that the dynamics of the traveling wave of space charge is reflected in a measured voltage of

$$v_o = -R\frac{dq}{dt} = -\frac{2Rw\rho_o v}{\beta} \tanh \beta a \sin \frac{\beta l}{2} \sin \beta vt \tag{14}$$

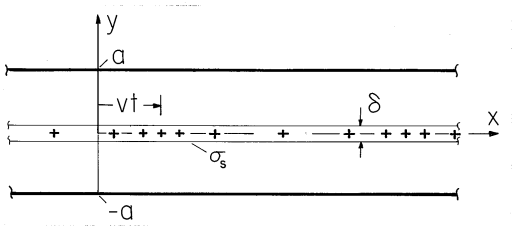


Fig. 5.6.3 Cross-section of sheet beam of charge between plane parallel equipotential plates. Beam is modeled by surface charge density having dc and ac parts.

In writing this expression, the double-angle formulas have been invoked.

Several predictions should be consistent with intuition. The output voltage varies sinusoidally with time at a frequency that is proportional to the velocity and inversely proportional to the wavelength, $2\pi/\beta$. The higher the velocity, the greater the voltage. Finally, if the detection electrode is a multiple of the wavelength $2\pi/\beta$, the voltage is zero.

If the charge density is concentrated in surface-like regions that are thin compared to other dimensions of interest, it is possible to solve Poisson's equation with boundary conditions using a procedure that has the appearance of solving Laplace's equation rather than Poisson's equation. The potential is typically broken into piece-wise continuous functions, and the effect of the charge density is brought in by Gauss' continuity condition, which is used to splice the functions at the surface occupied by the charge density. The following example illustrates this procedure. What is accomplished is a solution to Poisson's equation in the entire region, including the charge-carrying surface.

Example 5.6.2. Thin Bunched Charged-Particle Beam between Conducting Plates

In microwave amplifiers and oscillators of the electron beam type, a basic problem is the evaluation of the electric field produced by a bunched electron beam. The cross-section of the beam is usually small compared with a free space wavelength of an electromagnetic wave, in which case the electroquasistatic approximation applies.

We consider a strip electron beam having a charge density that is uniform over its cross-section δ. The beam moves with the velocity v in the x direction between two planar perfect conductors situated at $y = \pm a$ and held at zero potential. The configuration is shown in cross-section in Fig. 5.6.3. In addition to the uniform charge density, there is a "ripple" of charge density, so that the net charge density is

$$\rho = \begin{cases} 0 & a > y > \frac{\delta}{2} \\ \rho_o + \rho_1 \cos\left[\frac{2\pi}{\Lambda}(x - vt)\right] & \frac{\delta}{2} > y > -\frac{\delta}{2} \\ 0 & -\frac{\delta}{2} > y > -a \end{cases} \tag{15}$$

where ρ_o, ρ_1, and Λ are constants. The system can be idealized to be of infinite extent in the x and y directions.

The thickness δ of the beam is much smaller than the wavelength of the periodic charge density ripple, and much smaller than the spacing $2a$ of the planar conductors. Thus, the beam is treated as a sheet of surface charge with a density

$$\sigma_s = \sigma_o + \sigma_1 \cos\left[\frac{2\pi}{\Lambda}(x - vt)\right] \tag{16}$$

where $\sigma_o = \rho_o\delta$ and $\sigma_1 = \rho_1\delta$.

In regions (a) and (b), respectively, above and below the beam, the potential obeys Laplace's equation. Superscripts (a) and (b) are now used to designate variables evaluated in these regions. To guarantee that the fundamental laws are satisfied within the sheet, these potentials must satisfy the jump conditions implied by the laws of Faraday and Gauss, (5.3.4) and (5.3.5). That is, at $y = 0$

$$\Phi^a = \Phi^b \tag{17}$$

$$-\epsilon_o\left(\frac{\partial\Phi^a}{\partial y} - \frac{\partial\Phi^b}{\partial y}\right) = \sigma_o + \sigma_1\cos\left[\frac{2\pi}{\Lambda}(x - vt)\right] \tag{18}$$

To complete the specification of the field in the region between the plates, boundary conditions are, at $y = a$,

$$\Phi^a = 0 \tag{19}$$

and at $y = -a$,

$$\Phi^b = 0 \tag{20}$$

In the respective regions, the potential is split into dc and ac parts, respectively, produced by the uniform and ripple parts of the charge density.

$$\Phi = \Phi_o + \Phi_1 \tag{21}$$

By definition, Φ_o and Φ_1 satisfy Laplace's equation and (17), (19), and (20). The dc part, Φ_o, satisfies (18) with only the first term on the right, while the ac part, Φ_1, satisfies (18) with only the second term.

The dc surface charge density is independent of x, so it is natural to look for potentials that are also independent of x. From the first column in Table 5.4.1, such solutions are

$$\Phi^a = A_1 y + A_2 \tag{22}$$

$$\Phi^b = B_1 y + B_2 \tag{23}$$

The four coefficients in these expressions are determined from (17)–(20), if need be, by substitution of these expressions and formal solution for the coefficients. More attractive is the solution by inspection that recognizes that the system is symmetric with respect to y, that the uniform surface charge gives rise to uniform electric fields that are directed upward and downward in the two regions, and that the associated linear potential must be zero at the two boundaries.

$$\Phi_o^a = \frac{\sigma_o}{2\epsilon_o}(a - y) \tag{24}$$

$$\Phi_o^b = \frac{\sigma_o}{2\epsilon_o}(a + y) \tag{25}$$

Now consider the ac part of the potential. The x dependence is suggested by (18), which makes it clear that for product solutions, the x dependence of the potential must be the cosine function moving with time. Neither the sinh nor the cosh functions vanish at the boundaries, so we will have to take a linear combination of these to satisfy the boundary conditions at $y = +a$. This is effectively done by inspection if it is recognized that the origin of the y axis used in writing the

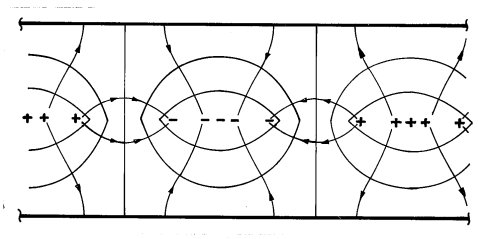


Fig. 5.6.4 Equipotentials and field lines caused by ac part of sheet charge in the configuration of Fig. 5.6.3.

solutions is arbitrary. The solutions to Laplace's equation that satisfy the boundary conditions, (19) and (20), are

$$\Phi_1^a = A_3 \sinh \frac{2\pi}{\Lambda}(y-a)\, \cos\left[\frac{2\pi}{\Lambda}(x-vt)\right] \tag{26}$$

$$\Phi_1^b = B_3 \sinh \frac{2\pi}{\Lambda}(y+a) \cos\left[\frac{2\pi}{\Lambda}(x-vt)\right] \tag{27}$$

These potentials must match at $y = 0$, as required by (17), so we might just as well have written them with the coefficients adjusted accordingly.

$$\Phi_1^a = -C \sinh \frac{2\pi}{\Lambda}(y-a) \cos\left[\frac{2\pi}{\Lambda}(x-vt)\right] \tag{28}$$

$$\Phi_1^b = C \sinh \frac{2\pi}{\Lambda}(y+a) \cos\left[\frac{2\pi}{\Lambda}(x-vt)\right] \tag{29}$$

The one remaining coefficient is determined by substituting these expressions into (18) (with σ_o omitted).

$$C = \frac{\sigma_1}{2\epsilon_o}\frac{\Lambda}{2\pi} \Big/ \cosh\left(\frac{2\pi a}{\Lambda}\right) \tag{30}$$

We have found the potential as a piece-wise continuous function. In region (a), it is the superposition of (24) and (28), while in region (b), it is (25) and (29). In both expressions, C is provided by (30).

$$\Phi^a = \frac{\sigma_o}{2\epsilon_o}(a-y) - \frac{\sigma_1}{2\epsilon_o}\frac{\Lambda}{2\pi}\frac{\sinh\left[\frac{2\pi}{\Lambda}(y-a)\right]}{\cosh\left(\frac{2\pi}{\Lambda}a\right)} \cos\left[\frac{2\pi}{\Lambda}(x-vt)\right] \tag{31}$$

$$\Phi^b = \frac{\sigma_o}{2\epsilon_o}(a+y) + \frac{\sigma_1}{2\epsilon_o}\frac{\Lambda}{2\pi}\frac{\sinh\left[\frac{2\pi}{\Lambda}(y+a)\right]}{\cosh\left(\frac{2\pi}{\Lambda}a\right)} \cos\left[\frac{2\pi}{\Lambda}(x-vt)\right] \tag{32}$$

When $t = 0$, the ac part of this potential distribution is as shown by Fig. 5.6.4. With increasing time, the field distribution translates to the right with the velocity v. Note that some lines of electric field intensity that originate on the beam terminate elsewhere on the beam, while others terminate on the equipotential walls. If the walls are even a wavelength away from the beam ($a = \Lambda$), almost all the field lines terminate elsewhere on the beam. That is, coupling to the wall is significant only if the wavelength is on the order of or larger than a. The nature of solutions to Laplace's equation is in evidence. Two-dimensional potentials that vary rapidly in one direction must decay equally rapidly in a perpendicular direction.

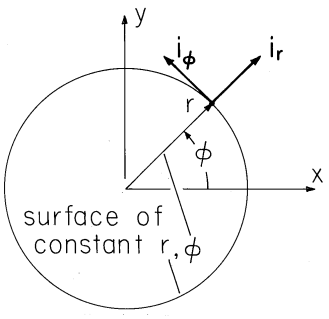


Fig. 5.7.1 Polar coordinate system.

A comparison of the fields from the sheet beam shown in Fig. 5.6.4 and the periodic distribution of volume charge density shown in Fig. 5.6.2 is a reminder of the similarity of the two physical situations. Even though Laplace's equation applies in the subregions of the configuration considered in this section, it is really Poisson's equation that is solved "in the large," as in the previous example.

5.7 SOLUTIONS TO LAPLACE'S EQUATION IN POLAR COORDINATES

In electroquasistatic field problems in which the boundary conditions are specified on circular cylinders or on planes of constant ϕ, it is convenient to match these conditions with solutions to Laplace's equation in polar coordinates (cylindrical coordinates with no z dependence). The approach adopted is entirely analogous to the one used in Sec. 5.4 in the case of Cartesian coordinates.

As a reminder, the polar coordinates are defined in Fig. 5.7.1. In these coordinates and with the understanding that there is no z dependence, Laplace's equation, Table I, (8), is

$$\frac{1}{r}\frac{\partial}{\partial r}\left(r\frac{\partial \Phi}{\partial r}\right)+\frac{1}{r^2}\frac{\partial^2 \Phi}{\partial \phi^2}=0 \tag{1}$$

One difference between this equation and Laplace's equation written in Cartesian coordinates is immediately apparent: In polar coordinates, the equation contains coefficients which not only depend on the independent variable r but become singular at the origin. This singular behavior of the differential equation will affect the type of solutions we now obtain.

In order to reduce the solution of the partial differential equation to the simpler problem of solving total differential equations, we look for solutions which can be written as products of functions of r alone and of ϕ alone.

$$\Phi = R(r)F(\phi) \tag{2}$$

When this assumed form of ϕ is introduced into (1), and the result divided by ϕ and multiplied by r, we obtain

$$\frac{r}{R}\frac{d}{dr}\left(r\frac{dR}{dr}\right)=-\frac{1}{F}\frac{d^2F}{d\phi^2} \tag{3}$$

We find on the left-hand side of (3) a function of r alone and on the right-hand side a function of ϕ alone. The two sides of the equation can balance if and only if the function of ϕ and the function of r are both equal to the same constant. For this "separation constant" we introduce the symbol $-m^2$.

$$\frac{d^2F}{d\phi^2} = -m^2F \tag{4}$$

$$r\frac{d}{dr}\left(r\frac{dR}{dr}\right) = m^2R \tag{5}$$

For $m^2 > 0$, the solutions to the differential equation for F are conveniently written as

$$F \sim \cos m\phi \qquad \text{or} \qquad \sin m\phi \tag{6}$$

Because of the space-varying coefficients, the solutions to (5) are not exponentials or linear combinations of exponentials as has so far been the case. Fortunately, the solutions are nevertheless simple. Substitution of a solution having the form r^n into (5) shows that the equation is satisfied provided that $n = \pm m$. Thus,

$$R \sim r^m \qquad \text{or} \qquad r^{-m} \tag{7}$$

In the special case of a zero separation constant, the limiting solutions are

$$F \sim \text{ constant or } \phi \tag{8}$$

and

$$R \sim \text{ constant or } ln\, r \tag{9}$$

The product solutions shown in the first two columns of Table 5.7.1, constructed by taking all possible combinations of these solutions, are those most often used in polar coordinates. But what are the solutions if $m^2 < 0$?

In Cartesian coordinates, changing the sign of the separation constant k^2 amounts to interchanging the roles of the x and y coordinates. Solutions that are periodic in the x direction become exponential in character, while the exponential decay and growth in the y direction becomes periodic. Here the geometry is such that the r and ϕ coordinates are not interchangeable, but the new solutions resulting from replacing m^2 by $-p^2$, where p is a real number, essentially make the oscillating dependence radial instead of azimuthal, and the exponential dependence azimuthal rather than radial. To see this, let $m^2 = -p^2$, or $m = jp$, and the solutions given by (7) become

$$R \sim r^{jp} \qquad \text{or} \qquad r^{-jp} \tag{10}$$

These take a more familiar appearance if it is recognized that r can be written identically as

$$r \equiv e^{lnr} \tag{11}$$

Introduction of this identity into (10) then gives the more familiar complex exponential, which can be split into its real and imaginary parts using Euler's formula.

$$R \sim r^{\pm jp} = e^{\pm jp\, ln\, r} = \cos(p\, ln\, r) \pm j \sin(p\, ln\, r) \tag{12}$$

Thus, two independent solutions for $R(r)$ are the cosine and sine functions of $p\,ln\,r$. The ϕ dependence is now either represented by $\exp \pm p\phi$ or the hyperbolic functions that are linear combinations of these exponentials. These solutions are summarized in the right-hand column of Table 5.7.1.

In principle, the solution to a given problem can be approached by the methodical elimination of solutions from the catalogue given in Table 5.7.1. In fact, most problems are best approached by attributing to each solution some physical meaning. This makes it possible to define coordinates so that the field representation is kept as simple as possible. With that objective, consider first the solutions appearing in the first column of Table 5.7.1.

The constant potential is an obvious solution and need not be considered further. We have a solution in row two for which the potential is proportional to the angle. The equipotential lines and the field lines are illustrated in Fig. 5.7.2a. Evaluation of the field by taking the gradient of the potential in polar coordinates (the gradient operator given in Table I) shows that it becomes infinitely large as the origin is reached. The potential increases from zero to 2π as the angle ϕ is increased from zero to 2π. If the potential is to be single valued, then we cannot allow that ϕ increase further without leaving the region of validity of the solution. This observation identifies the solution with a physical field observed when two semi-infinite conducting plates are held at different potentials and the distance between the conducting plates at their junction is assumed to be negligible. In this case, shown in Fig. 5.7.2, the outside field between the plates is properly represented by a potential proportional to ϕ.

With the plates separated by an angle of 90 degrees rather than 360 degrees, the potential that is proportional to ϕ is seen in the corners of the configuration shown in Fig. 5.5.3. The $m^2 = 0$ solution in the third row is familiar from Sec. 1.3, for it is the potential of a line charge. The fourth $m^2 = 0$ solution is sketched in Fig. 5.7.3.

In order to sketch the potentials corresponding to the solutions in the second column of Table 5.7.1, the separation constant must be specified. For the time being, let us assume that m is an integer. For $m = 1$, the solutions $r\cos\phi$ and $r\sin\phi$ represent familiar potentials. Observe that the polar coordinates are related to the Cartesian ones defined in Fig. 5.7.1 by

$$\begin{aligned} r\cos\phi &= x \\ r\sin\phi &= y \end{aligned} \tag{13}$$

The fields that go with these potentials are best found by taking the gradient in Cartesian coordinates. This makes it clear that they can be used to represent uniform fields having the x and y directions, respectively. To emphasize the simplicity of these solutions, which are made complicated by the polar representation, the second function of (13) is shown in Fig. 5.7.4a.

Figure 5.7.4b shows the potential $r^{-1}\sin\phi$. To stay on a contour of constant potential in the first quadrant of this figure as ϕ is increased toward $\pi/2$, it is necessary to first increase r, and then as the sine function decreases in the second quadrant, to decrease r. The potential is singular at the origin of r; as the origin is approached from above, it is large and positive; while from below it is large and negative. Thus, the field lines emerge from the origin within $0 < \phi < \pi$ and converge toward the origin in the lower half-plane. There must be a source at

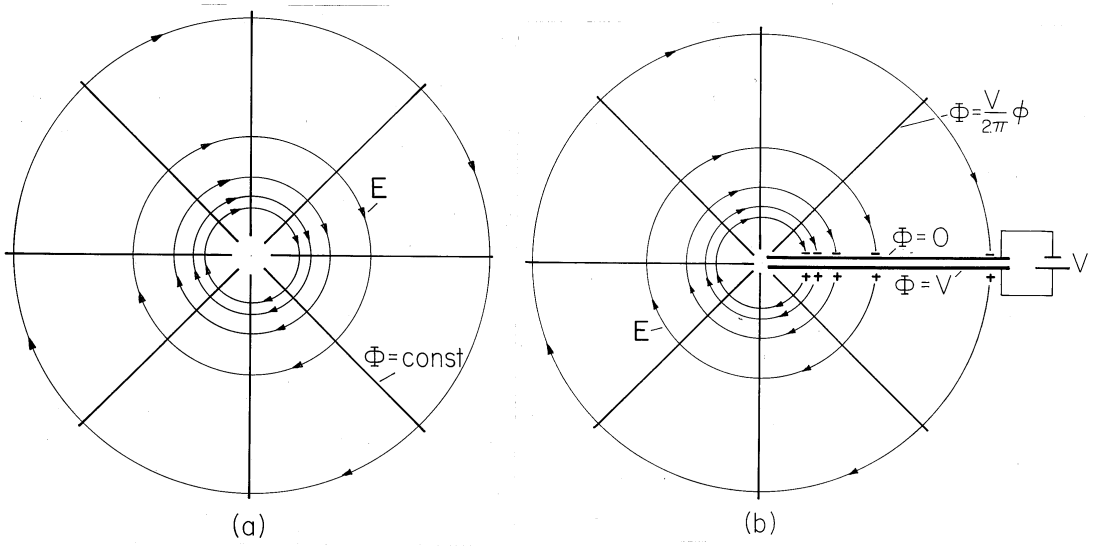


Fig. 5.7.2 Equipotentials and field lines for (a) $\Phi = \phi$, (b) region exterior to planar electrodes having potential difference V.

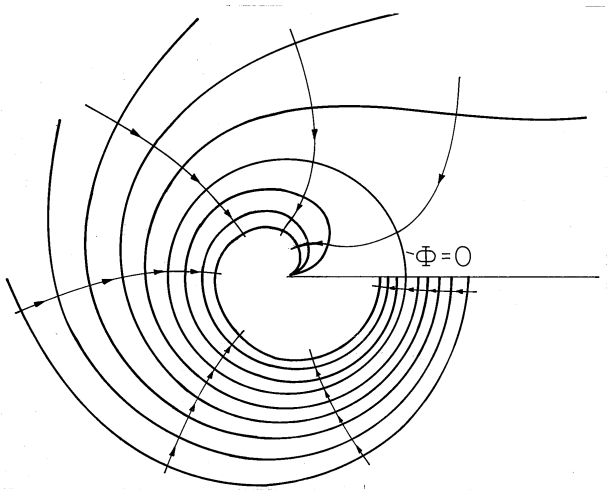


Fig. 5.7.3 Equipotentials and field lines for $\Phi = \phi\, ln(\mathbf{r})$.

the origin composed of equal and opposite charges on the two sides of the plane $r \sin \phi = 0$. The source, which is uniform and of infinite extent in the z direction, is a line dipole.

This conclusion is confirmed by direct evaluation of the potential produced by two line charges, the charge $-\lambda_l$ situated at the origin, the charge $+\lambda_l$ at a very small distance away from the origin at $r = d$, $\phi = \pi/2$. The potential follows from

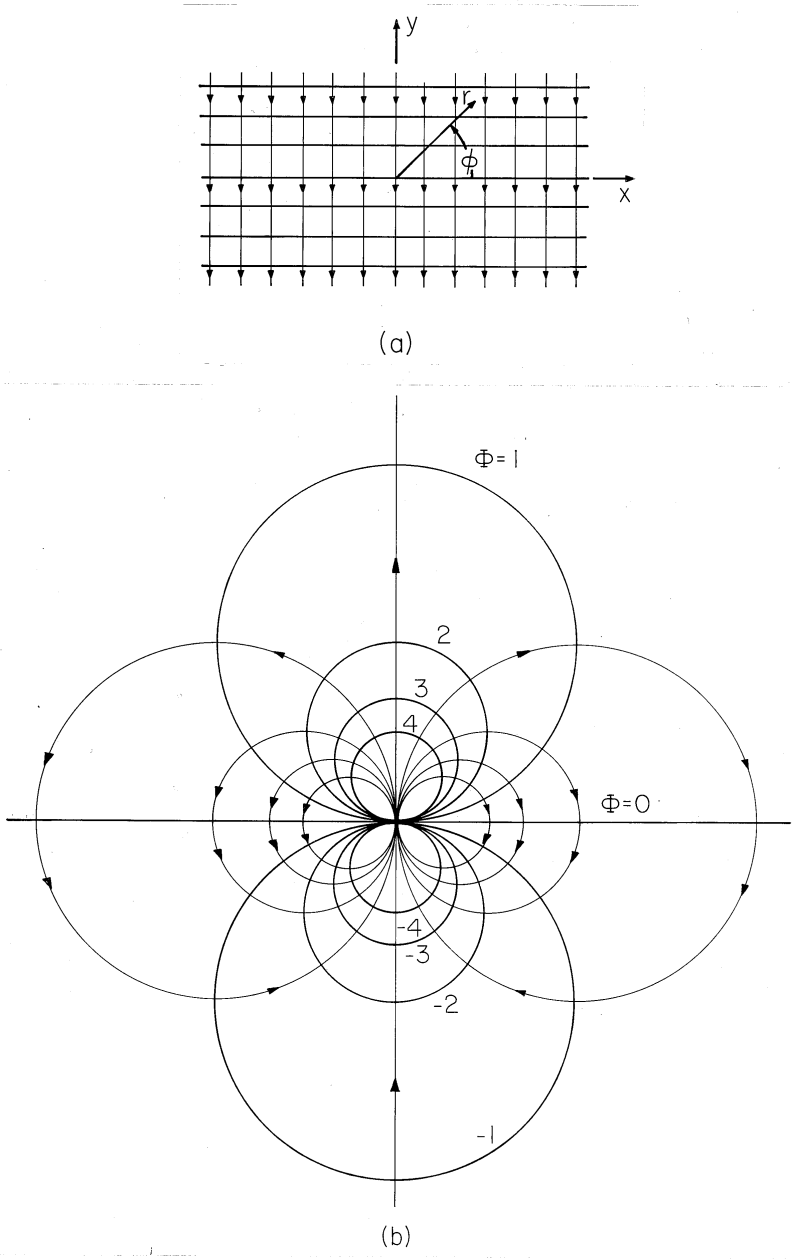


Fig. 5.7.4 Equipotentials and field lines for (a) $\Phi = r\sin(\phi)$, (b) $\Phi = \mathbf{r}^{-1}\sin(\phi)$.

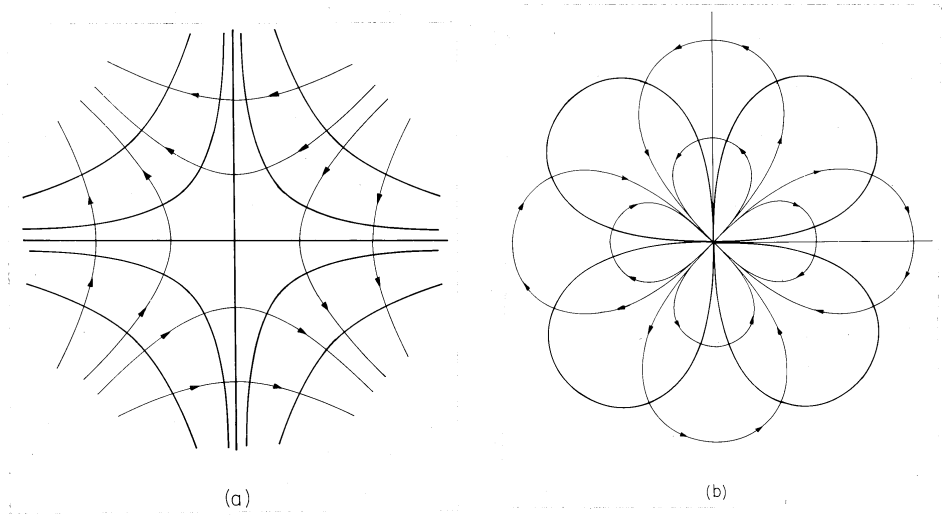


Fig. 5.7.5 Equipotentials and field lines for (a) $\Phi = r^2 \sin(2\phi)$, (b) $\Phi = r^{-2} \sin(2\phi)$.

steps paralleling those used for the three-dimensional dipole in Sec. 4.4.

$$\Phi = \lim_{\substack{d \to 0 \\ \lambda_l \to \infty}} \left[-\frac{\lambda_l}{2\pi\epsilon_o} ln(r - d\sin\phi) + \frac{\lambda_l}{2\pi\epsilon_o} ln\, r \right] = \frac{p_\lambda}{2\pi\epsilon_o} \frac{\sin\phi}{r} \tag{14}$$

The spatial dependence of the potential is indeed $\sin\phi/r$. In an analogy with the three-dimensional dipole of Sec. 4.4, $p_\lambda \equiv \lambda_l d$ is defined as the line dipole moment. In Example 4.6.3, it is shown that the equipotentials for parallel line charges are circular cylinders. Because this result is independent of spacing between the line charges, it is no surprise that the equipotentials of Fig. 5.7.4b are circular.

In summary, the $m = 1$ solutions can be thought of as the fields of dipoles at infinity and at the origin. For the sine dependencies, the dipoles are y directed, while for the cosine dependencies they are x directed.

The solution of Fig. 5.7.5a, $\phi \propto r^2 \sin 2\phi$, has been met before in Cartesian coordinates. Either from a comparison of the equipotential plots or by direct transformation of the Cartesian coordinates into polar coordinates, the potential is recognized as xy.

The $m = 2$ solution that is singular at the origin is shown in Fig. 5.7.5b. Field lines emerge from the origin and return to it twice as ϕ ranges from 0 to 2π. This observation identifies four line charges of equal magnitude, alternating in sign as the source of the field. Thus, the $m = 2$ solutions can be regarded as those of quadrupoles at infinity and at the origin.

It is perhaps a bit surprising that we have obtained from Laplace's equation solutions that are singular at the origin and hence associated with sources at the origin. The singularity of one of the two independent solutions to (5) can be traced to the singularity in the coefficients of this differential equation.

From the foregoing, it is seen that increasing m introduces a more rapid variation of the field with respect to the angular coordinate. In problems where

TABLE 5.7.1

SOLUTIONS TO LAPLACE'S EQUATION

IN POLAR COORDINATES

$m = 0$	$m^2 \geq 0$	$m^2 \leq 0$ $(m \rightarrow jp)$
Constant		$\cos[p\,ln(r)]\ \cosh\ p\phi$
ϕ		$\cos[p\,ln(r)]\ \sinh\ p\phi$
$ln\,r$		$\sin\,[p\,ln(r)]\ \cosh\ p\phi$
$\phi\,ln\,r$		$\sin\,[p\,ln(r)]\ \sinh\ p\phi$
	$r^m \cos\ m\phi$	$\cos\,[p\,ln(r)]\,e^{p\phi}$
	$r^m \sin\ m\phi$	$\cos\,[p\,ln(r)]\,e^{-p\phi}$
	$r^{-m}\ \cos\ m\phi$	$\sin\,[p\,ln(r)]\,e^{p\phi}$
	$r^{-m} \sin\ m\phi$	$\sin\,[p\,ln(r)]\,e^{-p\phi}$

the region of interest includes all values of ϕ, m must be an integer to make the field return to the same value after one revolution. But, m does not have to be an integer. If the region of interest is pie shaped, m can be selected so that the potential passes through one cycle over an arbitrary interval of ϕ. For example, the periodicity angle can be made ϕ_o by making $m\phi_o = n\pi$ or $m = n\pi/\phi_o$, where n can have any integer value.

The solutions for $m^2 < 0$, the right-hand column of Table 5.7.1, are illustrated in Fig. 5.7.6 using as an example essentially the fourth solution. Note that the radial phase has been shifted by subtracting $p\,ln(b)$ from the argument of the sine. Thus, the potential shown is

$$\Phi = \sin\left[p\,ln(r/b)\right]\sinh p\phi \tag{15}$$

and it automatically passes through zero at the radius $r = b$. The distances between radii of zero potential are not equal. Nevertheless, the potential distribution is qualitatively similar to that in Cartesian coordinates shown in Fig. 5.4.2. The exponential dependence is azimuthal; that direction is thus analogous to y in Fig. 5.4.2. In essence, the potentials for $m^2 < 0$ are similar to those in Cartesian coordinates but wrapped around the z axis.

5.8 EXAMPLES IN POLAR COORDINATES

With the objective of attaching physical insight to the polar coordinate solutions to Laplace's equation, two types of examples are of interest. First are certain classic

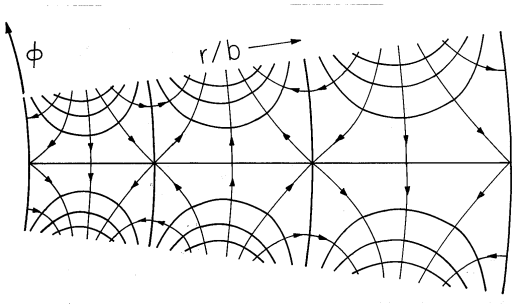


Fig. 5.7.6 Equipotentials and field lines representative of solutions in right-hand column of Table 5.7.1. Potential shown is given by (15).

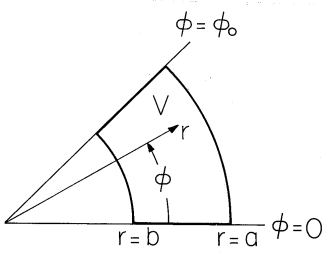


Fig. 5.8.1 Natural boundaries in polar coordinates enclose region V.

problems that have simple solutions. Second are examples that require the generally applicable modal approach that makes it possible to satisfy arbitrary boundary conditions.

The equipotential cylinder in a uniform applied electric field considered in the first example is in the first category. While an important addition to our resource of case studies, the example is also of practical value because it allows estimates to be made in complex engineering systems, perhaps of the degree to which an applied field will tend to concentrate on a cylindrical object.

In the most general problem in the second category, arbitrary potentials are imposed on the polar coordinate boundaries enclosing a region V, as shown in Fig. 5.8.1. The potential is the superposition of four solutions, each meeting the potential constraint on one of the boundaries while being zero on the other three. In Cartesian coordinates, the approach used to find one of these four solutions, the modal approach of Sec. 5.5, applies directly to the other three. That is, in writing the solutions, the roles of x and y can be interchanged. On the other hand, in polar coordinates the set of solutions needed to represent a potential imposed on the boundaries at $r = a$ or $r = b$ is different from that appropriate for potential constraints on the boundaries at $\phi = 0$ or $\phi = \phi_o$. Examples 5.8.2 and 5.8.3 illustrate the two types of solutions needed to determine the fields in the most general case. In the second of these, the potential is expanded in a set of orthogonal functions that are not sines or cosines. This gives the opportunity to form an appreciation for an orthogonality property of the product solutions to Laplace's equation that prevails in many other coordinate systems.

Simple Solutions. The example considered now is the first in a series of "cylinder" case studies built on the same $m = 1$ solutions. In the next chapter, the cylinder will become a polarizable dielectric. In Chap. 7, it will have finite conductivity and provide the basis for establishing just how "perfect" a conductor must be to justify the equipotential model used here. In Chaps. 8–10, the field will be magnetic and the cylinder first perfectly conducting, then magnetizable, and finally a shell of finite conductivity. Because of the simplicity of the dipole solutions used in this series of examples, in each case it is possible to focus on the physics without becoming distracted by mathematical details.

Example 5.8.1. Equipotential Cylinder in a Uniform Electric Field

A uniform electric field E_a is applied in a direction perpendicular to the axis of a (perfectly) conducting cylinder. Thus, the surface of the conductor, which is at $r = R$, is an equipotential. The objective is to determine the field distribution as modified by the presence of the cylinder.

Because the boundary condition is stated on a circular cylindrical surface, it is natural to use polar coordinates. The field excitation comes from "infinity," where the field is known to be uniform, of magnitude E_a, and x directed. Because our solution must approach this uniform field far from the cylinder, it is important to recognize at the outset that its potential, which in Cartesian coordinates is $-E_a x$, is

$$\Phi(r \to \infty) \to -E_a r \cos\phi \tag{1}$$

To this must be added the potential produced by the charges induced on the surface of the conductor so that the surface is maintained an equipotential. Because the solutions have to hold over the entire range $0 < \phi < 2\pi$, only integer values of the separation constant m are allowed, i.e., only solutions that are periodic in ϕ. If we are to add a function to (1) that makes the potential zero at $r = R$, it must cancel the value given by (1) at each point on the surface of the cylinder. There are two solutions in Table 5.7.1 that have the same $\cos\phi$ dependence as (1). We pick the $1/r$ dependence because it decays to zero as $r \to \infty$ and hence does not disturb the potential at infinity already given by (1). With A an arbitrary coefficient, the solution is therefore

$$\Phi = -E_a r \cos\phi + \frac{A}{r}\cos\phi \tag{2}$$

Because $\Phi = 0$ at $r = R$, evaluation of this expression shows that the boundary condition is satisfied at every angle ϕ if

$$A = E_a R^2 \tag{3}$$

and the potential is therefore

$$\Phi = -E_a R\left[\frac{r}{R} - \frac{R}{r}\right]\cos\phi \tag{4}$$

The equipotentials given by this expression are shown in Fig. 5.8.2. Note that the $x = 0$ plane has been taken as having zero potential by omitting an additive constant in (1). The field lines shown in this figure follow from taking the gradient of (4).

$$\mathbf{E} = \mathbf{i}_r E_a\left[1 + \left(\frac{R}{r}\right)^2\right]\cos\phi - \mathbf{i}_\phi E_a\left[1 - \left(\frac{R}{r}\right)^2\right]\sin\phi \tag{5}$$

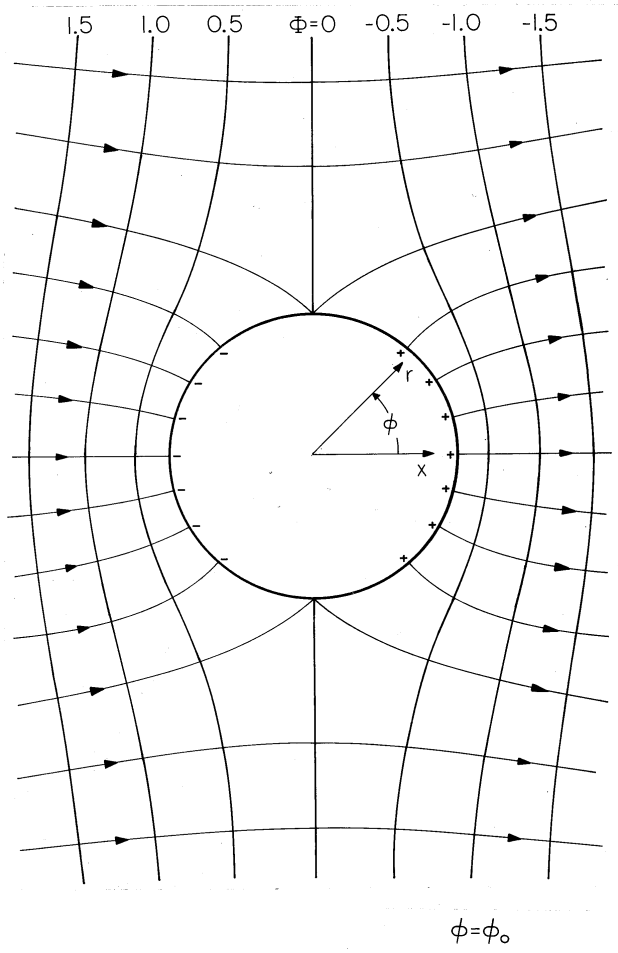


Fig. 5.8.2 Equipotentials and field lines for perfectly conducting cylinder in initially uniform electric field.

Field lines tend to concentrate on the surface where $\phi = 0$ and $\phi = \pi$. At these locations, the field is maximum and twice the applied field. Now that the boundary value problem has been solved, the surface charge on the cylindrical conductor follows from Gauss' jump condition, (5.3.2), and the fact that there is no field inside the cylinder.

$$\sigma_s = \mathbf{n} \cdot \epsilon_o \mathbf{E} = \epsilon_o E_r \Big|_{r=R} = 2\epsilon_o E_a \cos\phi \tag{6}$$

In retrospect, the boundary condition on the circular cylindrical surface has been satisfied by adding to the uniform potential that of an x directed line dipole. Its moment is that necessary to create a field that cancels the tangential field on the surface caused by the imposed field.

Azimuthal Modes. The preceding example considered a situation in which Laplace's equation is obeyed in the entire range $0 < \phi < 2\pi$. The next two examples

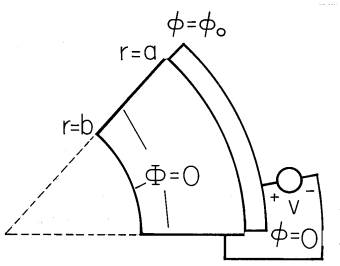


Fig. 5.8.3 Region of interest with zero potential boundaries at $\phi = 0$, $\Phi = \phi_o$, and $r = b$ and electrode at $r = a$ having potential v.

illustrate how the polar coordinate solutions are adapted to meeting conditions on polar coordinate boundaries that have arbitrary locations as pictured in Fig. 5.8.1.

Example 5.8.2. Modal Analysis in ϕ: Fields in and around Corners

The configuration shown in Fig. 5.8.3, where the potential is zero on the walls of the region V at $r = b$ and at $\phi = 0$ and $\phi = \phi_o$, but is v on a curved electrode at $r = a$, is the polar coordinate analogue of that considered in Sec. 5.5. What solutions from Table 5.7.1 are pertinent? The region within which Laplace's equation is to be obeyed does not occupy a full circle, and hence there is no requirement that the potential be a single-valued function of ϕ. The separation constant m can assume noninteger values.

We shall attempt to satisfy the boundary conditions on the three zero-potential boundaries using individual solutions from Table 5.7.1. Because the potential is zero at $\phi = 0$, the cosine and $ln(r)$ terms are eliminated. The requirement that the potential also be zero at $\phi = \phi_o$ eliminates the functions ϕ and $\phi ln(r)$. Moreover, the fact that the remaining sine functions must be zero at $\phi = \phi_o$ tells us that $m\phi_o = n\pi$. Solutions in the last column are not appropriate because they do not pass through zero more than once as a function of ϕ. Thus, we are led to the two solutions in the second column that are proportional to $\sin(n\pi\phi/\phi_o)$.

$$\Phi = \sum_{n=1}^{\infty} \left[A_n \left(\frac{r}{b}\right)^{n\pi/\phi_o} + B_n \left(\frac{r}{b}\right)^{-n\pi/\phi_o} \right] \sin\left(\frac{n\pi\phi}{\phi_o}\right) \tag{7}$$

In writing these solutions, the r's have been normalized to b, because it is then clear by inspection how the coefficients A_n and B_n are related to make the potential zero at $r = b$, $A_n = -B_n$.

$$\Phi = \sum_{n=1}^{\infty} A_n \left[\left(\frac{r}{b}\right)^{n\pi/\phi_o} - \left(\frac{r}{b}\right)^{-n\pi/\phi_o} \right] \sin\left(\frac{n\pi\phi}{\phi_o}\right) \tag{8}$$

Each term in this infinite series satisfies the conditions on the three boundaries that are constrained to zero potential. All of the terms are now used to meet the condition at the "last" boundary, where $r = a$. There we must represent a potential which jumps abruptly from zero to v at $\phi = 0$, stays at the same v up to $\phi = \phi_o$, and then jumps abruptly from v back to zero. The determination of the coefficients in (8) that make the series of sine functions meet this boundary condition is the same as for (5.5.4) in the Cartesian analogue considered in Sec. 5.5. The parameter $n\pi(x/a)$

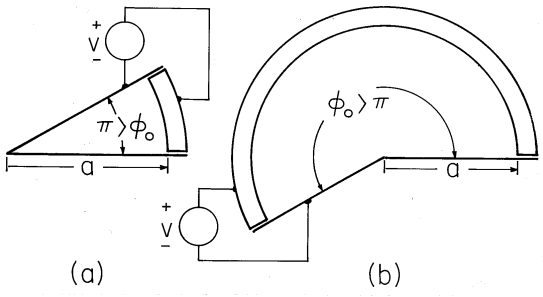


Fig. 5.8.4 Pie-shaped region with zero potential boundaries at $\phi = 0$ and $\phi = \phi_o$ and electrode having potential v at $r = a$. (a) With included angle less than 180 degrees, fields are shielded from region near origin. (b) With angle greater than 180 degrees, fields tend to concentrate at origin.

of Sec. 5.5 is now to be identified with $n\pi(\phi/\phi_o)$. With the potential given by (8) evaluated at $r = a$, the coefficients must be as in (5.5.17) and (5.5.18). Thus, to meet the "last" boundary condition, (8) becomes the desired potential distribution.

$$\Phi = \sum_{\substack{n=1 \\ \text{odd}}}^{\infty} \frac{4v}{n\pi} \frac{\left[\left(\frac{r}{b}\right)^{n\pi/\phi_o} - \left(\frac{r}{b}\right)^{-n\pi/\phi_o}\right]}{\left[\left(\frac{a}{b}\right)^{n\pi/\phi_o} - \left(\frac{a}{b}\right)^{-n\pi/\phi_o}\right]} \sin\left(\frac{n\pi}{\phi_o}\phi\right) \tag{9}$$

The distribution of potential and field intensity implied by this result is much like that for the region of rectangular cross-section depicted in Fig. 5.5.3. See Fig. 5.8.3.

In the limit where $b \to 0$, the potential given by (9) becomes

$$\Phi = \sum_{\substack{n=1 \\ \text{odd}}}^{\infty} \frac{4v}{n\pi} \left(\frac{r}{a}\right)^{n\pi/\phi_o} \sin\frac{n\pi}{\phi_o}\phi \tag{10}$$

and describes the configurations shown in Fig. 5.8.4. Although the wedge-shaped region is a reasonable "distortion" of its Cartesian analogue, the field in a region with an outside corner ($\pi/\phi_o < 1$) is also represented by (10). As long as the leading term has the exponent $\pi/\phi_o > 1$, the leading term in the gradient [with the exponent $(\pi/\phi_o) - 1$] approaches zero at the origin. This means that the field in a wedge with $\phi_o < \pi$ approaches zero at its apex. However, if $\pi/\phi_o < 1$, which is true for $\pi < \phi_o < 2\pi$ as illustrated in Fig. 5.8.4b, the leading term in the gradient of Φ has the exponent $(\pi/\Phi_o) - 1 < 0$, and hence the field approaches infinity as $r \to 0$. We conclude that the field in the neighborhood of a sharp edge is infinite. This observation teaches a lesson for the design of conductor shapes so as to avoid electrical breakdown. Avoid sharp edges!

Radial Modes. The modes illustrated so far possessed sinusoidal ϕ dependencies, and hence their superposition has taken the form of a Fourier series. To satisfy boundary conditions imposed on constant ϕ planes, it is again necessary to have an infinite set of solutions to Laplace's equation. These illustrate how the

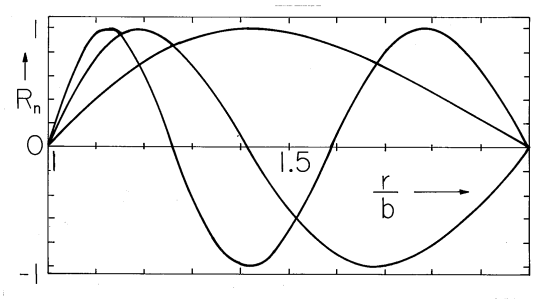


Fig. 5.8.5 Radial distribution of first three modes given by (13) for $a/b = 2$. The $n = 3$ mode is the radial dependence for the potential shown in Fig. 5.7.6.

product solutions to Laplace's equation can be used to provide orthogonal modes that are not Fourier series.

To satisfy zero potential boundary conditions at $r = b$ and $r = a$, it is necessary that the function pass through zero at least twice. This makes it clear that the solutions must be chosen from the last column in Table 5.7.1. The functions that are proportional to the sine and cosine functions can just as well be proportional to the sine function shifted in phase (a linear combination of the sine and cosine). This phase shift is adjusted to make the function zero where $r = b$, so that the radial dependence is expressed as

$$R(r) = \sin[p\,ln(r) - p\,ln(b)] = \sin[p\,ln(r/b)] \tag{11}$$

and the function made to be zero at $r = a$ by setting

$$p\,ln(a/b) = n\pi \Rightarrow p = \frac{n\pi}{ln(a/b)} \tag{12}$$

where n is an integer.

The solutions that have now been defined can be superimposed to form a series analogous to the Fourier series.

$$S(r) = \sum_{n=1}^{\infty} S_n R_n(r); \qquad R_n \equiv \sin\left[n\pi \frac{ln(r/b)}{ln(a/b)}\right] \tag{13}$$

For $a/b = 2$, the first three terms in the series are illustrated in Fig. 5.8.5. They have similarity to sinusoids but reflect the polar geometry by having peaks and zero crossings skewed toward low values of r.

With a weighting function $g(r) = r^{-1}$, these modes are orthogonal in the sense that

$$\int_b^a \frac{1}{r} \sin\left[n\pi \frac{ln(r/b)}{ln(a/b)}\right] \sin\left[m\pi \frac{ln(r/b)}{ln(a/b)}\right] dr = \begin{cases} \frac{1}{2} ln(a/b), & m = n \\ 0, & m \neq n \end{cases} \tag{14}$$

It can be shown from the differential equation defining $R(r)$, (5.7.5), and the boundary conditions, that the integration gives zero if the integration is over

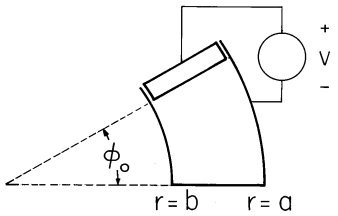


Fig. 5.8.6 Region with zero potential boundaries at $r = a,\ r = b$, and $\phi = 0$. Electrode at $\phi = \phi_o$ has potential v.

the product of different modes. The proof is analogous to that given in Cartesian coordinates in Sec. 5.5.

Consider now an example in which these modes are used to satisfy a specific boundary condition.

Example 5.8.3. Modal Analysis in r

The region of interest is of the same shape as in the previous example. However, as shown in Fig. 5.8.6, the zero potential boundary conditions are at $r = a$ and $r = b$ and at $\phi = 0$. The "last" boundary is now at $\phi = \phi_o$, where an electrode connected to a voltage source imposes a uniform potential v.

The radial boundary conditions are satisfied by using the functions described by (13) for the radial dependence. Because the potential is zero where $\phi = 0$, it is then convenient to use the hyperbolic sine to represent the ϕ dependence. Thus, from the solutions in the last column of Table 5.7.1, we take a linear combination of the second and fourth.

$$\Phi = \sum_{n=1}^{\infty} A_n \sin\left[n\pi \frac{ln(r/b)}{ln(a/b)}\right] \sinh\left[\frac{n\pi}{ln(a/b)}\phi\right] \tag{15}$$

Using an approach that is analogous to that for evaluating the Fourier coefficients in Sec. 5.5, we now use (15) on the "last" boundary, where $\phi = \phi_o$ and $\Phi = v$, multiply both sides by the mode R_m defined with (13) and by the weighting factor $1/r$, and integrate over the radial span of the region.

$$\begin{aligned}\int_b^a \frac{1}{r}\Phi(r,\phi_o)\sin\left[m\pi\frac{ln(r/b)}{ln(a/b)}\right]dr = \sum_{n=1}^{\infty}\int_b^a \frac{A_n}{r}\sinh\left[\frac{n\pi}{ln(a/b)}\phi_o\right] \\ \cdot \sin\left[n\pi\frac{ln(r/b)}{ln(a/b)}\right]\sin\left[m\pi\frac{ln(r/b)}{ln(a/b)}\right]dr\end{aligned} \tag{16}$$

Out of the infinite series on the right, the orthogonality condition, (14), picks only the m-th term. Thus, the equation can be solved for A_m and $m \to n$. With the substitution $u = m\pi ln(r/b)/ln(a/b)$, the integrals can be carried out in closed form.

$$A_n = \begin{cases} \frac{4v}{n\pi \sinh\left[\frac{n\pi}{ln(a/b)}\phi_o\right]}, & n \text{ odd} \\ 0, & n \text{ even} \end{cases} \tag{17}$$

A picture of the potential and field intensity distributions represented by (15) and its negative gradient is visualized by "bending" the rectangular region shown by Fig. 5.5.3 into the curved region of Fig. 5.8.6. The role of y is now played by ϕ.

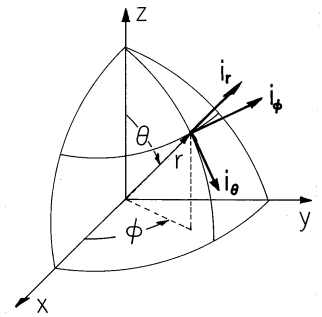


Fig. 5.9.1 Spherical coordinate system.

5.9 THREE SOLUTIONS TO LAPLACE'S EQUATION IN SPHERICAL COORDINATES

The method employed to solve Laplace's equation in Cartesian coordinates can be repeated to solve the same equation in the spherical coordinates of Fig. 5.9.1. We have so far considered solutions that depend on only two independent variables. In spherical coordinates, these are commonly r and θ. These two-dimensional solutions therefore satisfy boundary conditions on spheres and cones.

Rather than embark on an exploration of product solutions in spherical coordinates, attention is directed in this section to three such solutions to Laplace's equation that are already familiar and that are remarkably useful. These will be used to explore physical processes ranging from polarization and charge relaxation dynamics to the induction of magnetization and eddy currents.

Under the assumption that there is no ϕ dependence, Laplace's equation in spherical coordinates is (Table I)

$$\frac{1}{r^2}\frac{\partial}{\partial r}\left(r^2\frac{\partial \Phi}{\partial r}\right)+\frac{1}{r^2\sin\theta}\frac{\partial}{\partial \theta}\left(\sin\theta\frac{\partial \Phi}{\partial \theta}\right)=0 \tag{1}$$

The first of the three solutions to this equation is independent of θ and is the potential of a point charge.

$$\Phi \sim \frac{1}{r} \tag{2}$$

If there is any doubt, substitution shows that Laplace's equation is indeed satisfied. Of course, it is not satisfied at the origin where the point charge is located.

Another of the solutions found before is the three-dimensional dipole, (4.4.10).

$$\Phi \sim \frac{\cos\theta}{r^2} \tag{3}$$

This solution factors into a function of r alone and of θ alone, and hence would have to turn up in developing the product solutions to Laplace's equation in spherical coordinates. Substitution shows that it too is a solution of (1).

The third solution represents a uniform z-directed electric field in spherical coordinates. Such a field has a potential that is linear in z, and in spherical coordinates, $z = r\cos\theta$. Thus, the potential is

$$\Phi \sim r\cos\theta \tag{4}$$

These last two solutions, for the three-dimensional dipole at the origin and a field due to ± charges at $z \to \pm\infty$, are similar to those for dipoles in two dimensions, the $m = 1$ solutions that are proportional to cos ϕ from the second column of Table 5.7.1. However, note that the two-dimensional dipole potential varies as r^{-1}, while the three dimensional dipole potential has an r^{-2} dependence. Also note that whereas the polar coordinate dipole can have an arbitrary orientation (can be a sine as well as a cosine function of ϕ, or any linear combination of these), the three-dimensional dipole is z directed. That is, do not replace the cosine function in (3) by a sine function and expect that the potential will satisfy Laplace's equation in spherical coordinates.

Example 5.9.1. Equipotential Sphere in a Uniform Electrical Field

Consider a raindrop in an electric field. If in the absence of the drop, that field is uniform over many drop radii R, the field in the vicinity of the drop can be computed by taking the field as being uniform "far from the sphere." The field is z directed and has a magnitude E_a. Thus, on the scale of the drop, the potential must approach that of the uniform field (4) as $r \to \infty$.

$$\Phi(r \to \infty) \to -E_a r \cos\theta \tag{5}$$

We will see in Chap. 7 that it takes only microseconds for a water drop in air to become an equipotential. The condition that the potential be zero at $r = R$ and yet approach the potential of (5) as $r \to \infty$ is met by adding to (5) the potential of a dipole at the origin, an adjustable coefficient times (3). By writing the r dependencies normalized to the drop radius R, it is possible to see directly what this coefficient must be. That is, the proposed solution is

$$\Phi = -E_a R \cos\theta \Big[\frac{r}{R} + A\Big(\frac{R}{r}\Big)^2\Big] \tag{6}$$

and it is clear that to make this function zero at $r = R$, $A = -1$.

$$\Phi = -E_a R \cos\theta \Big[\frac{r}{R} - \Big(\frac{R}{r}\Big)^2\Big] \tag{7}$$

Note that even though the configuration of a perfectly conducting rod in a uniform transverse electric field (as considered in Example 5.8.1) is very different from the perfectly conducting sphere in a uniform electric field, the potentials are deduced from very similar arguments, and indeed the potentials appear similar. In cross-section, the distribution of potential and field intensity is similar to that for the cylinder shown in Fig. 5.8.2. Of course, their appearance in three-dimensional space is very different. For the polar coordinate configuration, the equipotentials shown are the cross-sections of cylinders, while for the spherical drop they are cross-sections of surfaces of revolution. In both cases, the potential acquired (by the sphere or the rod) is that of the symmetry plane normal to the applied field.

The surface charge on the spherical surface follows from (7).

$$\sigma_s = -\epsilon_o \mathbf{n} \cdot \nabla\Phi\Big|_{r=R} = \epsilon_o E_r\Big|_{r=R} = 3\epsilon_o E_a \cos\theta \tag{8}$$

Thus, for $E_a > 0$, the north pole is capped by positive surface charge while the south pole has negative charge. Although we think of the second solution in (7) as being

due to a fictitious dipole located at the sphere's center, it actually represents the field of these surface charges. By contrast with the rod, where the maximum field is twice the uniform field, it follows from (8) that the field intensifies by a factor of three at the poles of the sphere.

In making practical use of the solution found here, the "uniform field at infinity E_a" is that of a field that is slowly varying over dimensions on the order of the drop radius R. To demonstrate this idea in specific terms, suppose that the imposed field is due to a distant point charge. This is the situation considered in Example 4.6.4, where the field produced by a point charge and a conducting sphere is considered. If the point charge is very far away from the sphere, its field at the position of the sphere is essentially uniform over the region occupied by the sphere. (To relate the directions of the fields in Example 4.6.4 to the present case, mount the $\theta = 0$ axis from the center of the sphere pointing towards the point charge. Also, to make the field in the vicinity of the sphere positive, make the point charge negative, $q \to -q$.)

At the sphere center, the magnitude of the field intensity due to the point charge is

$$E_a = \frac{q}{4\pi\epsilon_o X^2} \tag{9}$$

The magnitude of the image charge, given by (4.6.34), is

$$Q_1 = \frac{|q|R}{X} \tag{10}$$

and it is positioned at the distance $D = R^2/X$ from the center of the sphere. If the sphere is to be charge free, a charge of strength $-Q_1$ has to be mounted at its center. If X is very large compared to R, the distance D becomes small enough so that this charge and the charge given by (10) form a dipole of strength

$$p = \frac{Q_1 R^2}{X} = \frac{|q|R^3}{X^2} \tag{11}$$

The potential resulting from this dipole moment is given by (4.4.10), with p evaluated using this moment. With the aid of (9), the dipole field induced by the point charge is recognized as

$$\Phi = \frac{p}{4\pi\epsilon_o r^2}\cos\theta = E_a \frac{R^3}{r^2}\cos\theta \tag{12}$$

As witnessed by (7), this potential is identical to the one we have found necessary to add to the potential of the uniform field in order to match the boundary conditions on the sphere.

Of the three spherical coordinate solutions to Laplace's equation given in this section, only two were required in the previous example. The next makes use of all three.

Example 5.9.2. Charged Equipotential Sphere in a Uniform Electric Field

Suppose that the highly conducting sphere from Example 5.9.1 carries a net charge q while immersed in a uniform applied electric field E_a. Thunderstorm electrification is evidence that raindrops are often charged, and E_a could be the field they generate collectively.

In the absence of this net charge, the potential is given by (7). On the boundary at $r = R$, this potential remains uniform if we add the potential of a point charge at the origin of magnitude q.

$$\Phi = -E_a R\cos\theta\Big[\frac{r}{R} - \Big(\frac{R}{r}\Big)^2\Big] + \frac{q}{4\pi\epsilon_o r} \tag{13}$$

The surface potential has been raised from zero to $q/4\pi\epsilon_o R$, but this potential is independent of ϕ and so the tangential electric field remains zero.

The point charge is, of course, fictitious. The actual charge is distributed over the surface and is found from (13) to be

$$\sigma_s = -\epsilon_o \frac{\partial\Phi}{\partial r}\Big|_{r=R} = 3\epsilon_o E_a\Big(\cos\theta + \frac{q}{q_c}\Big); \qquad q_c \equiv 12\pi\epsilon_o E_a R^2 \tag{14}$$

The surface charge density switches sign when the term in parentheses vanishes, when $q/q_c < 1$ and

$$-\cos\theta_c = \frac{q}{q_c} \tag{15}$$

Figure 5.9.2a is a graphical solution of this equation. For E_a and q positive, the positive surface charge capping the sphere extends into the southern hemisphere. The potential and electric field distributions implied by (13) are illustrated in Fig. 5.9.2b. If q exceeds $q_c \equiv 12\pi\epsilon_o E_a R^2$, the entire surface of the sphere is covered with positive surface charge density and $\mathbf{E}$ is directed outward over the entire surface.

5.10 THREE-DIMENSIONAL SOLUTIONS TO LAPLACE'S EQUATION

Natural boundaries enclosing volumes in which Poisson's equation is to be satisfied are shown in Fig. 5.10.1 for the three standard coordinate systems. In general, the distribution of potential is desired within the volume with an arbitrary potential distribution on the bounding surfaces.

Considered first in this section is the extension of the Cartesian coordinate two-dimensional product solutions and modal expansions introduced in Secs. 5.4 and 5.5 to three dimensions. Given an arbitrary potential distribution over one of the six surfaces of the box shown in Fig. 5.10.1, and given that the other five surfaces are at zero potential, what is the solution to Laplace's equation within? If need be, a superposition of six such solutions can be used to satisfy arbitrary conditions on all six boundaries.

To use the same modal approach in configurations where the boundaries are natural to other than Cartesian coordinate systems, for example the cylindrical and spherical ones shown in Fig. 5.10.1, essentially the same extension of the basic ideas already illustrated is used. However, the product solutions involve less familiar functions. For those who understand the two-dimensional solutions, how they are used to meet arbitrary boundary conditions and how they are extended to three-dimensional Cartesian coordinate configurations, the literature cited in this section should provide ready access to what is needed to exploit solutions in new coordinate systems. In addition to the three standard coordinate systems, there are many

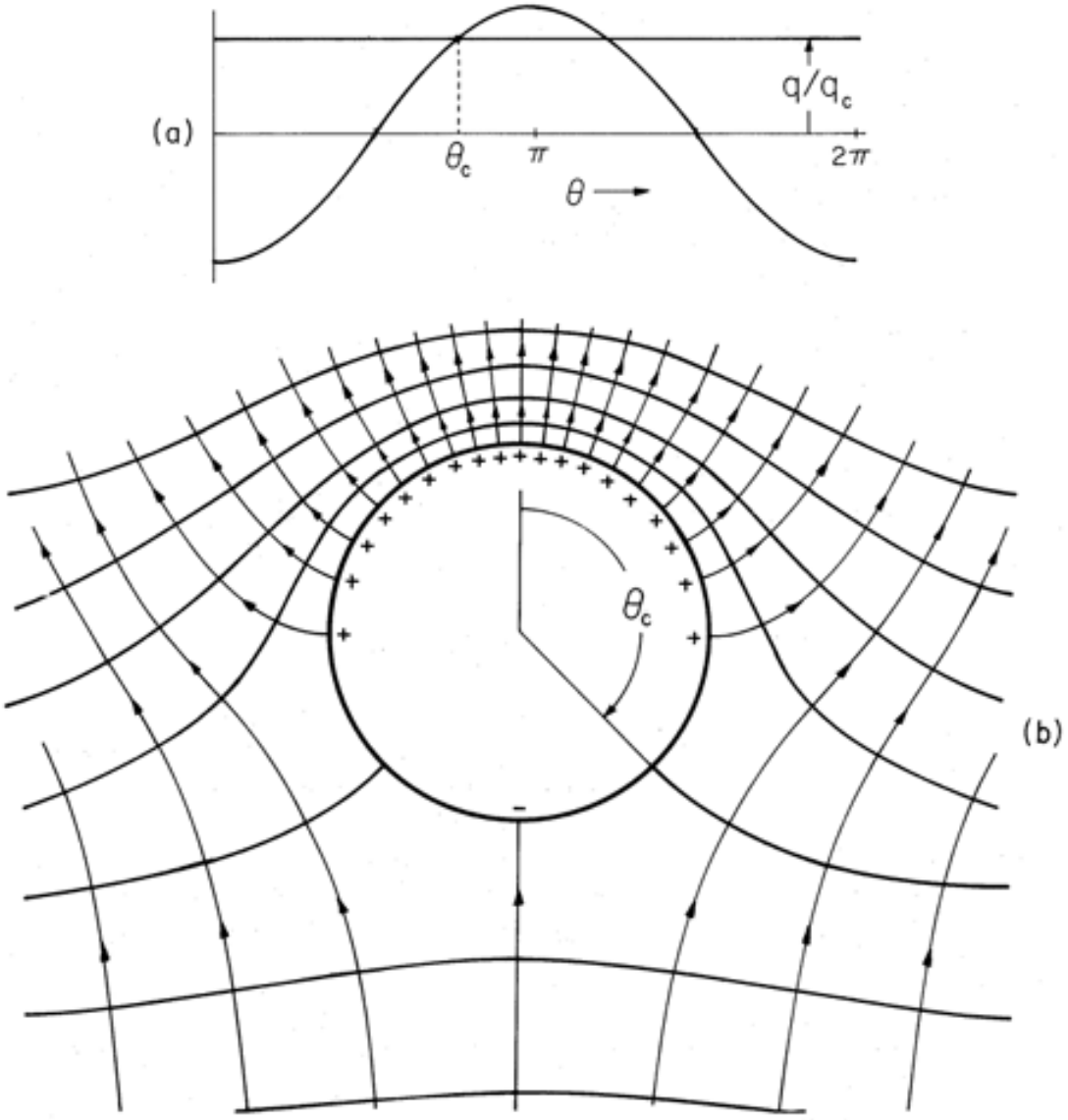


Fig. 5.9.2 (a) Graphical solution of (15) for angle θ_c at which electric field switches from being outward to being inward directed on surface of sphere. (b) Equipotentials and field lines for perfectly conducting sphere having net charge q in an initially uniform electric field.

others in which Laplace's equation admits product solutions. The latter part of this section is intended as an introduction to these coordinate systems and associated product solutions.

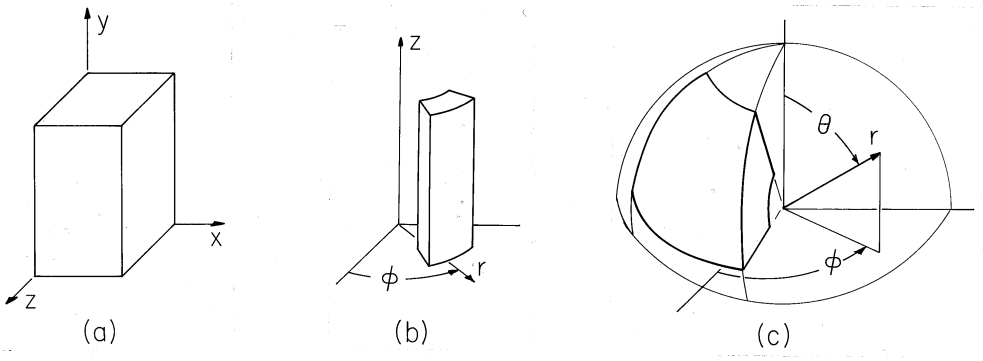


Fig. 5.10.1 Volumes defined by natural boundaries in (a) Cartesian, (b) cylindrical, and (c) spherical coordinates.

Cartesian Coordinate Product Solutions. In three-dimensions, Laplace's equation is

$$\frac{\partial^2\Phi}{\partial x^2}+\frac{\partial^2\Phi}{\partial y^2}+\frac{\partial^2\Phi}{\partial z^2}=0 \tag{1}$$

We look for solutions that are expressible as products of a function of x alone, $X(x)$, a function of y alone, $Y(y)$, and a function of z alone, $Z(z)$.

$$\Phi=X(x)Y(y)Z(z) \tag{2}$$

Introducing (2) into (1) and dividing by Φ, we obtain

$$\frac{1}{X}\frac{d^2X}{dx^2}+\frac{1}{Y}\frac{d^2Y}{dy^2}+\frac{1}{Z}\frac{d^2Z}{dz^2}=0 \tag{3}$$

A function of x alone, added to one of y alone and one of of z alone, gives zero. Because x, y, and z are independent variables, the zero sum is possible only if each of these three "functions" is in fact equal to a constant. The sum of these constants must then be zero.

$$\frac{1}{X}\frac{d^2X}{dx^2}=-k_x^2; \qquad \frac{1}{Y}\frac{d^2Y}{dy^2}=k_y^2; \qquad \frac{1}{Z}\frac{d^2Z}{dz^2}=-k_z^2 \tag{4}$$

$$-k_x^2+k_y^2-k_z^2=0 \tag{5}$$

Note that if two of these three separation constants are positive, it is then necessary that the third be negative. We anticipated this by writing (4) accordingly. The solutions of (4) are

$$\begin{aligned} X &\sim \cos k_x x \quad \text{or} \quad \sin k_x x \\ Y &\sim \cosh k_y y \quad \text{or} \quad \sinh k_y y \\ Z &\sim \cos k_z z \quad \text{or} \quad \sin k_z z \end{aligned} \tag{6}$$

where

$$k_y^2=k_x^2+k_z^2.$$

Of course, the roles of the coordinates can be interchanged, so either the x or z directions could be taken as having the exponential dependence. From these solutions it is evident that the potential cannot be periodic or be exponential in its dependencies on all three coordinates and still be a solution to Laplace's equation. In writing (6) we have anticipated satisfying potential constraints on planes of constant y by taking X and Z as periodic.

Modal Expansion in Cartesian Coordinates. It is possible to choose the constants and the solutions from (6) so that zero potential boundary conditions are met on five of the six boundaries. With coordinates as shown in Fig. 5.10.1a, the sine functions are used for X and Z to insure a zero potential in the planes $x = 0$ and $z = 0$. To make the potential zero in planes $x = a$ and $z = w$, it is necessary that

$$\sin k_x a = 0; \qquad \sin k_z w = 0 \tag{7}$$

Solution of these eigenvalue equations gives $k_x = m\pi/a,\ k_z = n\pi/w$, and hence

$$XZ \sim \sin \frac{m\pi}{a} x \sin \frac{n\pi}{w} z \tag{8}$$

where m and n are integers.

To make the potential zero on the fifth boundary, say where $y = 0$, the hyperbolic sine function is used to represent the y dependence. Thus, a set of solutions, each meeting a zero potential condition on five boundaries, is

$$\Phi \sim \sin \frac{m\pi}{a} x \sin \frac{n\pi}{w} z \sinh k_{mn} y \tag{9}$$

where in view of (5)

$$k_{mn} \equiv \sqrt{(m\pi/a)^2 + (n\pi/w)^2}$$

These can be used to satisfy an arbitrary potential constraint on the "last" boundary, where $y = b$. The following example, which extends Sec. 5.5, illustrates this concept.

Example 5.10.1. Capacitive Attenuator in Three Dimensions

In the attenuator of Example 5.5.1, the two-dimensional field distribution is a good approximation because one cross-sectional dimension is small compared to the other. In Fig. 5.5.5, $a \ll w$. If the cross-sectional dimensions a and w are comparable, as shown in Fig. 5.10.2, the field can be represented by the modal superposition given by (9).

$$\Phi = \sum_{m=1}^{\infty} \sum_{n=1}^{\infty} A_{mn} \sin \frac{m\pi}{a} x \sin \frac{n\pi}{w} z \sinh k_{mn} y \tag{10}$$

In the five planes $x = 0,\ x = a,\ y = 0,\ z = 0$, and $z = w$ the potential is zero. In the plane $y = b$, it is constrained to be v by an electrode connected to a voltage source.

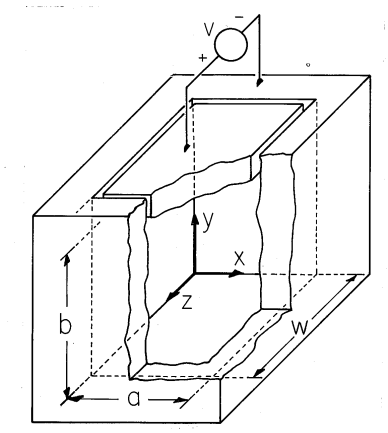


Fig. 5.10.2 Region bounded by zero potentials at $x = 0,\ x = a,\ z = 0,\ z = w$, and $y = 0$. Electrode constrains plane $y = b$ to have potential v.

Evaluation of (10) at the electrode surface must give v.

$$v = \sum_{m=1}^{\infty}\sum_{n=1}^{\infty} A_{mn} \sinh k_{mn} b \sin \frac{m\pi}{a} x \sin \frac{n\pi}{w} z \tag{11}$$

The coefficients A_{mn} are determined by exploiting the orthogonality of the eigenfunctions. That is,

$$\int_0^a X_m X_i dx = \begin{cases} 0, & m \neq i \\ \frac{a}{2}, & m = i \end{cases}; \qquad \int_0^w Z_n Z_j dz = \begin{cases} 0, & n \neq j \\ \frac{w}{2}, & n = j \end{cases} \tag{12}$$

where

$$X_m \equiv \sin \frac{m\pi}{a} x; \qquad Z_n \equiv \sin \frac{n\pi}{w} z.$$

The steps that now lead to an expression for any given coefficient A_{mn} are a natural extension of those used in Sec. 5.5. Both sides of (11) are multiplied by the eigenfunction $X_i Z_j$ and then both sides are integrated over the surface at $y = b$.

$$\begin{aligned} \int_0^a \int_0^w v X_i Z_j dx dz = \sum_{m=1}^{\infty}\sum_{n=1}^{\infty} A_{mn} \sinh(k_{mn} b) \\ \int_0^a \int_0^w X_m X_i Z_n Z_j dx dz \end{aligned} \tag{13}$$

Because of the product form of each term, the integrations can be carried out on x and z separately. In view of the orthogonality conditions, (12), the only none-zero term on the right comes in the summation with $m = i$ and $n = j$. This makes it possible to solve the equation for the coefficient A_{ij}. Then, by replacing $i \to m$ and $j \to n$, we obtain

$$A_{mn} = \frac{\int_0^a \int_0^w v \sin \frac{m\pi}{a} x \sin \frac{n\pi}{w} z dx dz}{\frac{aw}{4} \sinh(k_{mn} b)} \tag{14}$$

The integral can be carried out for any given distribution of potential. In this particular situation, the potential of the surface at $y = b$ is uniform. Thus, integration gives

$$A_{mn} = \begin{cases} \frac{16v}{mn\pi^2} \frac{1}{\sinh(k_{mn}b)} & \text{for } m \text{ and } n \text{ both odd} \\ 0 & \text{for either } m \text{ or } n \text{ even} \end{cases} \tag{15}$$

The desired potential, satisfying the boundary conditions on all six surfaces, is given by (10) and (15). Note that the first term in the solution we have found is not the same as the first term in the two-dimensional field representation, (5.5.9). No matter what the ratio of a to w, the first term in the three-dimensional solution has a sinusoidal dependence on z, while the two-dimensional one has no dependence on z.

For the capacitive attenuator of Fig. 5.5.5, what output signal is predicted by this three dimensional representation? From (10) and (15), the charge on the output electrode is

$$q = \int_0^a \int_0^w \Big[-\epsilon_o \frac{\partial \Phi}{\partial y} \Big]_{y=0} dxdz \equiv -C_M v \tag{16}$$

where

$$C_M = \frac{64}{\pi^4} \epsilon_o a w \sum_{\substack{m=1 \\ \text{odd}}}^{\infty} \sum_{\substack{n=1 \\ \text{odd}}}^{\infty} \frac{k_{mn}}{m^2 n^2 \sinh(k_{mn}b)}$$

With $v = V \sin \omega t$, we find that $v_o = V_o \cos \omega t$ where

$$V_o = RC_n \omega V \tag{17}$$

Using (16), it follows that the amplitude of the output voltage is

$$\frac{V_o}{U'} = \sum_{\substack{m=1 \\ \text{odd}}}^{\infty} \sum_{\substack{n=1 \\ \text{odd}}}^{\infty} \frac{a k_{mn}}{2\pi m^2 n^2 \sinh\left[(k_{mn}a)\frac{b}{a}\right]} \tag{18}$$

where the voltage is normalized to

$$U' = \frac{128 \epsilon_o w R \omega V}{\pi^3}$$

and

$$k_{mn}a = \sqrt{(n\pi)^2 + (m\pi)^2 (a/w)^2}$$

This expression can be used to replace the plot of Fig. 5.5.5. Here we compare the two-dimensional and three-dimensional predictions of output voltage by considering (18) in the limit where $b \gg a$. In this limit, the hyperbolic sine is dominated by one of its exponentials, and the first term in the series gives

$$ln\Big(\frac{V_o}{U'}\Big) \to ln\sqrt{1 + (a/w)^2} - \pi \sqrt{1 + (a/w)^2}\ \frac{b}{a} \tag{19}$$

In the limit $a/w \ll 1$, the dependence on spacing between input and output electrodes expressed by the right hand side becomes identical to that for the two-dimensional model, (5.5.15). However, $U' = (8/\pi^2)U$ regardless of a/w.

This three-dimensional Cartesian coordinate example illustrates how the orthogonality property of the product solution is exploited to provide a potential

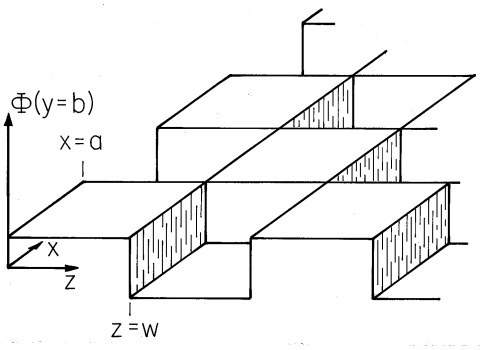


Fig. 5.10.3 Two-dimensional square wave function used to represent electrode potential for system of Fig. 5.10.2 in plane $y = b$.

that is zero on five of the boundaries while assuming any desired distribution on the sixth boundary. On this sixth surface, the potential takes the form

$$\Phi = \sum_{\substack{m=1 \\ \text{odd}}}^{\infty} \sum_{\substack{n=1 \\ \text{odd}}}^{\infty} V_{mn} F_{mn} \tag{20}$$

where

$$F_{mn} \equiv X_m Z_n \equiv \sin \frac{m\pi}{a} x \sin \frac{n\pi}{w} z$$

The two-dimensional functions F_{mn} have been used to represent the "last" boundary condition. This two-dimensional Fourier series replaces the one-dimensional Fourier series of Sec. 5.5 (5.5.17). In the example, it represents the two-dimensional square wave function shown in Fig. 5.10.3. Note that this function goes to zero along $x = 0$, $x = a$ and $z = 0$, $z = w$, as it should. It changes sign as it passes through any one of these "nodal" lines, but the range outside the original rectangle is of no physical interest, and hence the behavior outside that range does not affect the validity of the solution applied to the example. Because the function represented is odd in both x and y, it can be represented by sine functions only.

Our foray into three-dimensional modal expansions extends the notion of orthogonality of functions with respect to a one-dimensional interval to orthogonality of functions with respect to a two-dimensional section of a plane. We are able to determine the coefficients V_{mn} in (20) as it is made to fit the potential prescribed on the "sixth" surface because the terms in the series are orthogonal in the sense that

$$\int_0^a \int_0^w F_{mn} F_{ij} dx dz = \begin{cases} 0 & m \neq i \text{ or } n \neq j \\ \frac{aw}{4} & m = i \text{ and } n = j \end{cases} \tag{21}$$

In other coordinate systems, a similar orthogonality relation will hold for the product solutions evaluated on one of the surfaces defined by a constant natural coordinate. In general, a weighting function multiplies the eigenfunctions in the integrand of the surface integral that is analogous to (21).

Except for some special cases, this is as far as we will go in considering three-dimensional product solutions to Laplace's equation. In the remainder of this section, references to the literature are given for solutions in cylindrical, spherical, and other coordinate systems.

Modal Expansion in Other Coordinates. A general volume having natural boundaries in cylindrical coordinates is shown in Fig. 5.10.1b. Product solutions to Laplace's equation take the form

$$\Phi = R(r)F(\phi)Z(z) \tag{22}$$

The polar coordinates of Sec. 5.7 are a special case where $Z(z)$ is a constant.

The ordinary differential equations, analogous to (4) and (5), that determine $F(\phi)$ and $Z(z)$, have constant coefficients, and hence the solutions are sines and cosines of $m\phi$ and kz, respectively. The radial dependence is predicted by an ordinary differential equation that, like (5.7.5), has space-varying coefficients. Unfortunately, with the z dependence, solutions are not simply polynomials. Rather, they are Bessel's functions of order m and argument kr. As applied to product solutions to Laplace's equation, these functions are described in standard fields texts[1−4]. Bessel's and associated functions are developed in mathematics texts and treatises[5−8].

As has been illustrated in two- and now three-dimensions, the solution to an arbitrary potential distribution on the boundaries can be written as the superposition of solutions each having the desired potential on one boundary and zero potential on the others. Summarized in Table 5.10.1 are the forms taken by the product solution, (22), in representing the potential for an arbitrary distribution on the specified surface. For example, if the potential is imposed on a surface of constant r, the radial dependence is given by Bessel's functions of real order and imaginary argument. What is needed to represent Φ in the constant r surface are functions that are periodic in ϕ and z, so we expect that these Bessel's functions have an exponential-like dependence on r.

In spherical coordinates, product solutions take the form

$$\Phi = R(r) \ominus (\theta)F(\phi) \tag{23}$$

From the cylindrical coordinate solutions, it might be guessed that new functions are required to describe $R(r)$. In fact, these turn out to be simple polynomials. The ϕ dependence is predicted by a constant coefficient equation, and hence represented by familiar trigonometric functions. But the θ dependence is described by Legendre functions. By contrast with the Bessel's functions, which are described by infinite polynomial series, the Legendre functions are finite polynomials in $\cos(\theta)$. In connection with Laplace's equation, the solutions are summarized in fields texts[1−4]. As solutions to ordinary differential equations, the Legendre polynomials are presented in mathematics texts[5,7].

The names of other coordinate systems suggest the surfaces generated by setting one of the variables equal to a constant: Elliptic-cylinder coordinates and prolate spheroidal coordinates are examples in which Laplace's equation is separable[2]. The first step in exploiting these new systems is to write the Laplacian and other differential operators in terms of those coordinates. This is also described in the given references.

5.11 SUMMARY

There are two themes in this chapter. First is the division of a solution to a partial differential equation into a particular part, designed to balance the "drive" in the

TABLE 5.10.1

FORM OF SOLUTIONS TO LAPLACE'S EQUATION IN CYLINDRICAL COORDINATES WHEN POTENTIAL IS CONSTRAINED ON GIVEN SURFACE AND OTHERS ARE AT ZERO POTENTIAL

Surface of Constant	$R(r)$	$F(\phi)$	$Z(z)$
r	Bessel's functions of real order and imaginary argument (modified Bessel's functions)	trigonometric functions of real argument	trigonometric functions of real argument
ϕ	Bessel's functions of imaginary order and imaginary argument	trigonometric functions of imaginary argument	trigonometric functions of real argument
z	Bessel's functions of real order and real argument	trigonometric functions of real argument	trigonometric functions of imaginary argument

differential equation, and a homogeneous part, used to make the total solution satisfy the boundary conditions. This chapter solves Poisson's equation; the "drive" is due to the volumetric charge density and the boundary conditions are stated in terms of prescribed potentials. In the following chapters, the approach used here will be applied to boundary value problems representing many different physical situations. Differential equations and boundary conditions will be different, but because they will be linear, the same approach can be used.

Second is the theme of product solutions to Laplace's equation which by virtue of their orthogonality can be superimposed to satisfy arbitrary boundary conditions. The thrust of this statement can be appreciated by the end of Sec. 5.5. In the configuration considered in that section, the potential is zero on all but one of the natural Cartesian boundaries of an enclosed region. It is shown that the product solutions can be superimposed to satisfy an arbitrary potential condition on the "last" boundary. By making the "last" boundary any one of the boundaries and, if need be, superimposing as many series solutions as there are boundaries, it is then possible to meet arbitrary conditions on all of the boundaries. The section on polar coordinates gives the opportunity to extend these ideas to systems where the coordinates are not interchangeable, while the section on three-dimensional Cartesian solutions indicates a typical generalization to three dimensions.

In the chapters that follow, there will be a frequent need for solving Laplace's equation. To this end, three classes of solutions will often be exploited: the Cartesian solutions of Table 5.4.1, the polar coordinate ones of Table 5.7.1, and the three

spherical coordinate solutions of Sec. 5.9. In Chap. 10, where magnetic diffusion phenomena are introduced and in Chap. 13, where electromagnetic waves are described, the application of these ideas to the diffusion and the Helmholtz equations is illustrated.

REFERENCES

[1] M. Zahn, **Electromagnetic Field Theory: A Problem Solving Approach**, John Wiley and Sons, N.Y. (1979).

[2] P. Moon and D. E. Spencer, **Field Theory for Engineers**, Van Nostrand, Princeton, N.J. (1961).

[3] S. Ramo, J. R. Whinnery, and T. Van Duzer, **Fields and Waves in Communication Electronics**, John Wiley and Sons, N.Y. (1967).

[4] J. R. Melcher, **Continuum Electromechanics**, M.I.T. Press, Cambridge, Mass. (1981).

[5] F. B. Hildebrand, **Advanced Calculus for Applications**, Prentice-Hall, Inc, Englewood Cliffs, N.J. (1962).

[6] G. N. Watson, **A Treatise on the Theory of Bessel Functions**, Cambridge University Press, London E.C.4. (1944).

[7] P. M. Morse and H. Feshbach, **Methods of Theoretical Physics**, McGraw-Hill Book Co., N.Y. (1953).

[8] N. W. McLachlan, **Bessel Functions for Engineers**, Oxford University Press, London E.C.4 (1941).

PROBLEMS

5.1 Particular and Homogeneous Solutions to Poisson's and Laplace's Equations

5.1.1 In Problem 4.7.1, the potential of a point charge over a perfectly conducting plane (where $z > 0$) was found to be Eq. (a) of that problem. Identify particular and homogeneous parts of this solution.

5.1.2 A solution for the potential in the region $-a < y < a$, where there is a charge density ρ, satisfies the boundary conditions $\Phi = 0$ in the planes $y = +a$ and $y = -a$.

$$\Phi = \frac{\rho_o}{\epsilon_o \beta^2}\left(1 - \frac{\cosh \beta y}{\cosh \beta a}\right)\cos \beta x \qquad (a)$$

(a) What is ρ in this region?
(b) Identify Φ_p and Φ_h. What boundary conditions are satisfied by Φ_h at $y = +a$ and $y = -a$?
(c) Illustrate another combination of Φ_p and Φ_h that could just as well be used and give the boundary conditions that apply for Φ_h in that case.

5.1.3* The charge density between the planes $x = 0$ and $x = d$ depends only on x.

$$\rho = \frac{4\rho_o(x-d)^2}{d^2} \qquad (a)$$

Boundary conditions are that $\Phi(x = 0) = 0$ and $\Phi(x = d) = V$, so $\Phi = \Phi(x)$ is independent of y and z.

(a) Show that Poisson's equation therefore reduces to

$$\frac{\partial^2 \Phi}{\partial x^2} = -\frac{4\rho_o}{d^2 \epsilon_o}(x-d)^2 \qquad (b)$$

(b) Integrate this expression twice and use the boundary conditions to show that the potential distribution is

$$\Phi = -\frac{\rho_o}{3d^2\epsilon_o}(x-d)^4 + (\frac{V}{d} - \frac{\rho_o d}{3\epsilon_o})x + \frac{\rho_o d^2}{3\epsilon_o} \qquad (c)$$

(c) Argue that the first term in (c) can be Φ_p, with the remaining terms then Φ_h.
(d) Show that in that case, the boundary conditions satisfied by Φ_h are

$$\Phi_h(0) = \frac{\rho_o d^2}{3\epsilon_o}; \qquad \Phi_h(d) = V \qquad (d)$$

5.1.4 With the charge density given as

$$\rho = \rho_o \sin \frac{\pi x}{d} \tag{a}$$

carry out the steps in Prob. 5.1.3.

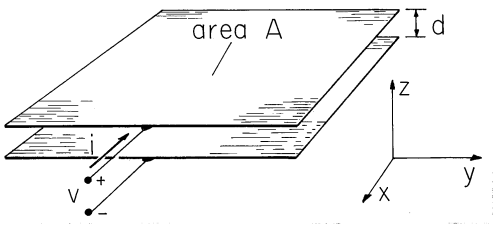


Fig. P5.1.5

5.1.5* A frequently used model for a capacitor is shown in Fig. P5.1.5, where two plane parallel electrodes have a spacing that is small compared to either of their planar dimensions. The potential difference between the electrodes is v, and so over most of the region between the electrodes, the electric field is uniform.

(a) Show that in the region well removed from the edges of the electrodes, the field $\mathbf{E} = -(v/d)\mathbf{i_z}$ satisfies Laplace's equation and the boundary conditions on the electrode surfaces.
(b) Show that the surface charge density on the lower surface of the upper electrode is $\sigma_s = \epsilon_o v/d$.
(c) For a single pair of electrodes, the capacitance C is defined such that $q = Cv$ (13). Show that for the plane parallel capacitor of Fig. P5.1.5, $C = A\epsilon_o/d$, where A is the area of one of the electrodes.
(d) Use the integral form of charge conservation, (1.5.2), to show that $i = dq/dt = Cdv/dt$.

5.1.6* In the three-electrode system of Fig. P5.1.6, the bottom electrode is taken as having the reference potential. The upper and middle electrodes then have potentials v_1 and v_2, respectively. The spacings between electrodes, $2d$ and d, are small enough relative to the planar dimensions of the electrodes so that the fields between can be approximated as being uniform.

(a) Show that the fields denoted in the figure are then approximately $E_1 = v_1/2d$, $E_2 = v_2/d$ and $E_m = (v_1 - v_2)/d$.
(b) Show that the net charges q_1 and q_2 on the top and middle electrodes, respectively, are related to the voltages by the capacitance matrix [in the form of (12)]

$$\begin{bmatrix} q_1 \\ q_2 \end{bmatrix} = \begin{bmatrix} \epsilon_o w(L+l)/2d & -\epsilon_o wl/d \\ -\epsilon_o wl/d & 2\epsilon_o wl/d \end{bmatrix} \begin{bmatrix} v_1 \\ v_2 \end{bmatrix} \tag{a}$$

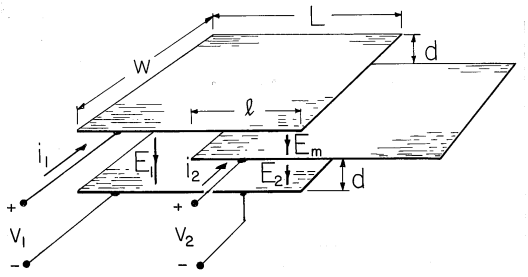


Fig. P5.1.6

5.3 Continuity Conditions

5.3.1* The electric potentials Φ^a and Φ^b above and below the plane $y = 0$ are

$$\begin{aligned} \Phi^a &= V\cos\beta x\exp(-\beta y); \qquad y > 0 \\ \Phi^b &= V\cos\beta x\exp(\beta y); \qquad y < 0 \end{aligned} \tag{a}$$

(a) Show that (4) holds. (The potential is continuous at $y = 0$.)
(b) Evaluate $\mathbf{E}$ tangential to the surface $y = 0$ and show that it too is continuous. [Equation (1) is then automatically satisfied at $y = 0$.]
(c) Use (5) to show that in the plane $y = 0$, the surface charge density, $\sigma_s = 2\epsilon_o\beta V\cos\beta x$, accounts for the discontinuity in the derivative of Φ normal to the plane $y = 0$.

5.3.2 By way of appreciating how the continuity of Φ guarantees the continuity of tangential $\mathbf{E}$ [(4) implies that (1) is satisfied], suppose that the potential is given in the plane $y = 0$: $\Phi = \Phi(x, 0, z)$.

(a) Which components of $\mathbf{E}$ can be determined from this information alone?
(b) For example, if $\Phi(x, 0, z) = V\sin(\beta x)\sin(\beta z)$, what are those components of $\mathbf{E}$?

5.4 Solutions to Laplace's Equation in Cartesian Coordinates

5.4.1* A region that extends to $\pm\infty$ in the z direction has the square cross-section of dimensions as shown in Fig. P5.4.1. The walls at $x = 0$ and $y = 0$ are at zero potential, while those at $x = a$ and $y = a$ have the linear distributions shown. The interior region is free of charge density.

(a) Show that the potential inside is

$$\Phi = \frac{V_o xy}{a^2} \tag{a}$$

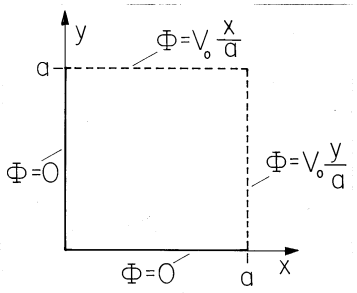


Fig. P5.4.1

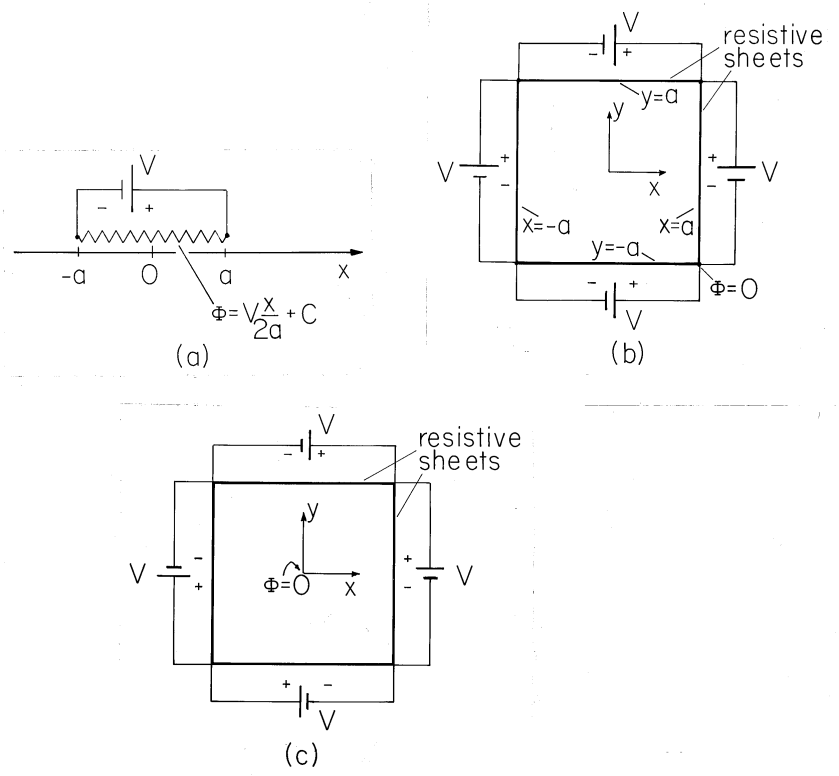


Fig. P5.4.2

(b) Show that plots of Φ and $\mathbf{E}$ are as shown in the first quadrant of Fig. 4.1.3.

5.4.2 One way to constrain a boundary so that it has a potential distribution that is a linear function of position is shown in Fig. P5.4.2a. A uniformly resistive sheet having a length $2a$ is driven by a voltage source V. For the coordinate x shown, the resulting potential distribution is the linear function of x shown. The constant C is determined by the definition of where the potential is zero. In the case shown in Fig. 5.4.2a, if Φ is zero at

$x = 0$, then $C = 0$.

(a) Suppose a cylindrical region having a square cross-section of length $2a$ on a side, as shown in Fig. 5.4.2b, is constrained in potential by resistive sheets and voltage sources, as shown. Note that the potential is defined to be zero at the lower right-hand corner, where $(x, y) = (a, -a)$. Inside the cylinder, what must the potential be in the planes $x = \pm a$ and $y = \pm a$?

(b) Find the linear combination of the potentials from the first column of Table 5.4.1 that satisfies the conditions on the potentials required by the resistive sheets. That is, if Φ takes the form

$$\Phi = Ax + By + C + Dxy \tag{a}$$

so that it satisfies Laplace's equation inside the cylinder, what are the coefficients A, B, C, and D?

(c) Determine $\mathbf{E}$ for this potential.

(d) Sketch Φ and $\mathbf{E}$.

(e) Now the potential on the walls of the square cylinder is constrained as shown in Fig. 5.4.2c. This time the potential is zero at the location $(x, y) = (0, 0)$. Adjust the coefficients in (a) so that the potential satisfies these conditions. Determine $\mathbf{E}$ and sketch the equipotentials and field lines.

5.4.3* Shown in cross-section in Fig. P5.4.3 is a cylindrical system that extends to infinity in the $\pm z$ directions. There is no charge density inside the cylinder, and the potentials on the boundaries are

$$\Phi = V_o \cos \frac{\pi}{a} x \quad \text{at} \quad y = \pm b \tag{a}$$

$$\Phi = 0 \qquad \text{at} \qquad x = \pm \frac{a}{2} \tag{b}$$

(a) Show that the potential inside the cylinder is

$$\Phi = V_o \cos \frac{\pi x}{a} \cosh \frac{\pi y}{a} / \cosh \frac{\pi b}{a} \tag{c}$$

(b) Show that a plot of Φ and $\mathbf{E}$ is as given by the part of Fig. 5.4.1 where $-\pi/2 < kx < \pi/2$.

5.4.4 The square cross-section of a cylindrical region that extends to infinity in the $\pm z$ directions is shown in Fig. P5.4.4. The potentials on the boundaries are as shown.

(a) Inside the cylindrical space, there is no charge density. Find Φ.

(b) What is $\mathbf{E}$ in this region?

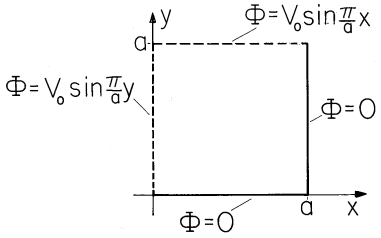


Fig. P5.4.4

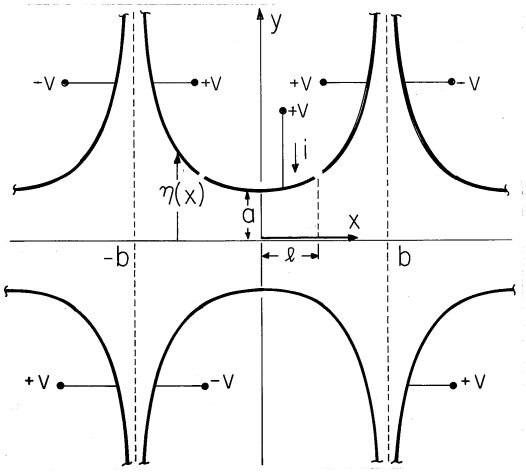


Fig. P5.4.5

(c) Sketch Φ and $\mathbf{E}$.

5.4.5* The cross-section of an electrode structure which is symmetric about the $x = 0$ plane is shown in Fig. P5.4.5. Above this plane are electrodes that alternately either have the potential $v(t)$ or the potential $-v(t)$. The system has depth d (into the paper) which is very long compared to such dimensions as a or l. So that the current $i(t)$ can be measured, one of the upper electrodes has a segment which is insulated from the rest of the electrode, but driven by the same potential. The geometry of the upper electrodes is specified by giving their altitudes above the $x = 0$ plane. For example, the upper electrode between $y = -b$ and $y = b$ has the shape

$$\eta = \frac{1}{k}\sinh^{-1}\left(\frac{\sinh ka}{\cos kx}\right); \qquad k = \frac{\pi}{2b} \tag{a}$$

where η is as shown in Fig. P5.4.5.

(a) Show that the potential in the region between the electrodes is

$$\Phi = v(t)\cos kx \sinh ky/\sinh ka \tag{b}$$

(b) Show that **E** in this region is

$$\mathbf{E} = \frac{v(t)}{\sinh\left(\frac{\pi a}{2b}\right)}\left(\frac{\pi}{2b}\right)\left[\sin\left(\frac{\pi x}{2b}\right)\sinh\left(\frac{\pi y}{2b}\right)\mathbf{i_x} - \cos\left(\frac{\pi x}{2b}\right)\cosh\left(\frac{\pi y}{2b}\right)\mathbf{i_y}\right] \tag{c}$$

(c) Show that plots of Φ and **E** are as shown in Fig. 5.4.2.
(d) Show that the net charge on the upper electrode segment between $y = -l$ and $y = l$ is

$$q = \frac{2\epsilon_o d}{\sinh ka}\sin kl\left[1 + \left(\frac{\sinh ka}{\cos kl}\right)^2\right]^{1/2} v(t) = Cv \tag{d}$$

(Because the surface S in Gauss' integral law is arbitrary, it can be chosen so that it both encloses this electrode and is convenient for integration.)
(e) Given that $v(t) = V_o \sin \omega t$, where V_o and ω are constants, show that the current to the electrode segment $i(t)$, as defined in Fig. P5.4.5, is

$$i = \frac{dq}{dt} = C\frac{dv}{dt} = C\omega V_o \cos \omega t \tag{e}$$

5.4.6 In Prob. 5.4.5, the polarities of all of the voltage sources driving the lower electrodes are reversed.

(a) Find Φ in the region between the electrodes.
(b) Determine **E**.
(c) Sketch Φ and **E**.
(d) Find the charge q on the electrode segment in the upper middle electrode.
(e) Given that $v(t) = V_o \cos \omega t$, what is $i(t)$?

5.5 Modal Expansion to Satisfy Boundary Conditions

5.5.1* The system shown in Fig. P5.5.1a is composed of a pair of perfectly conducting parallel plates in the planes $x = 0$ and $x = a$ that are shorted in the plane $y = b$. Along the left edge, the potential is imposed and so has a given distribution $\Phi_d(x)$. The plates and short have zero potential.

(a) Show that, in terms of $\Phi_d(x)$, the potential distribution for $0 < y < b$, $0 < x < a$ is

$$\Phi = \sum_{n=1}^{\infty} A_n \sin\left(\frac{n\pi x}{a}\right)\sinh\left[\frac{n\pi}{a}(y - b)\right] \tag{a}$$

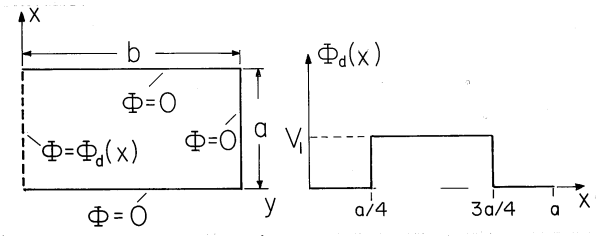


Fig. P5.5.1

where

$$A_n = \frac{2}{a \sinh\left(-\frac{n\pi b}{a}\right)} \int_0^a \Phi_d(x) \sin\left(\frac{n\pi x}{a}\right) dx \tag{b}$$

(At this stage, the coefficients in a modal expansion for the field are left expressed as integrals over the yet to be specified potential distribution.)

(b) In particular, if the imposed potential is as shown in Fig. P5.5.1b, show that A_n is

$$A_n = -\frac{4V_1}{n\pi} \frac{\cos\left(\frac{n\pi}{4}\right)}{\sinh\left(\frac{n\pi b}{a}\right)} \tag{c}$$

5.5.2* The walls of a rectangular cylinder are constrained in potential as shown in Fig. P5.5.2. The walls at $x = a$ and $y = b$ have zero potential, while those at $y = 0$ and $x = 0$ have the potential distributions $V_1(x)$ and $V_2(y)$, respectively.

In particular, suppose that these distributions of potential are uniform, so that $V_1(x) = V_a$ and $V_2(y) = V_b$, with V_a and V_b defined to be independent of x and y.

(a) The region inside the cylinder is free space. Show that the potential distribution there is

$$\Phi = \sum_{\substack{n=1 \\ \text{odd}}}^{\infty} \left[-\frac{4V_b}{n\pi} \frac{\sinh\frac{n\pi}{b}(x-a)}{\sinh\frac{n\pi a}{b}} \sin\frac{n\pi y}{b} - \frac{4V_a}{n\pi} \frac{\sinh\frac{n\pi}{a}(y-b)}{\sinh\frac{n\pi b}{a}} \sin\frac{n\pi x}{a} \right] \tag{a}$$

(b) Show that the distribution of surface charge density along the wall at $x = a$ is

$$\sigma_s = \sum_{\substack{n=1 \\ \text{odd}}}^{\infty} \left[-\frac{4\epsilon_o V_b}{b} \frac{\sin\frac{n\pi}{b}y}{\sinh\frac{n\pi a}{b}} + \frac{4\epsilon_o V_a}{a} \frac{\sinh\frac{n\pi}{a}(y-b)}{\sinh\frac{n\pi b}{a}} \right] \tag{b}$$

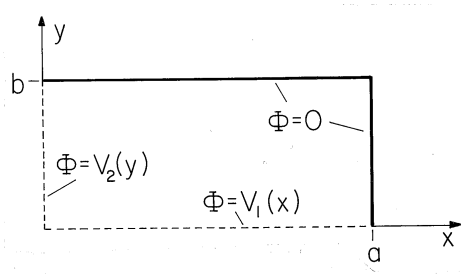


Fig. P5.5.2

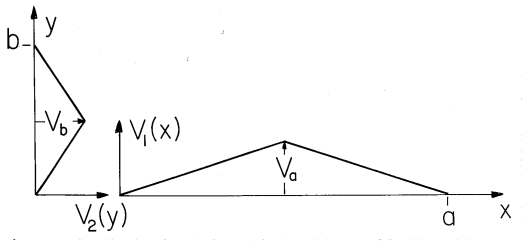


Fig. P5.5.3

5.5.3 In the configuration described in Prob. 5.5.2, the distributions of potentials on the walls at $x = 0$ and $y = 0$ are as shown in Fig. P5.5.3, where the peak voltages V_a and V_b are given functions of time.

(a) Determine the potential in the free space region inside the cylinder.
(b) Find the surface charge distribution on the wall at $y = b$.

5.5.4* The cross-section of a system that extends to "infinity" out of the paper is shown in Fig. P5.5.4. An electrode in the plane $y = d$ has the potential V. A second electrode has the shape of an "L." One of its sides is in the plane $y = 0$, while the other is in the plane $x = 0$, extending from $y = 0$ almost to $y = d$. This electrode is at zero potential.

(a) The electrodes extend to infinity in the $-x$ direction. Show that, far to the left, the potential between the electrodes tends to

$$\Phi = \frac{Vy}{d} \tag{a}$$

(b) Using this result as a part of the solution, Φ_a, the potential between the plates is written as $\Phi = \Phi_a + \Phi_b$. Show that the boundary conditions that must be satisfied by Φ_b are

$$\Phi_b = 0 \qquad \text{at} \quad y = 0 \quad \text{and} \quad y = d \tag{b}$$

$$\Phi_b \to 0 \qquad \text{as} \quad x \to -\infty \tag{c}$$

$$\Phi_b = -\frac{Vy}{d} \qquad \text{at} \quad x = 0 \tag{d}$$

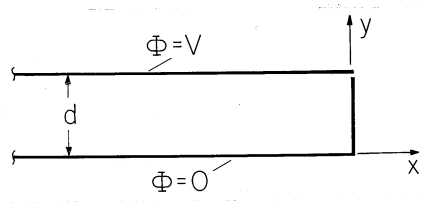


Fig. P5.5.4

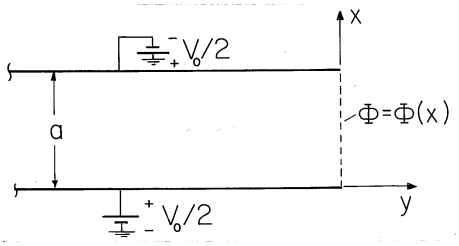


Fig. P5.5.5

(c) Show that the potential between the electrodes is

$$\Phi = \frac{Vy}{d} + \sum_{n=1}^{\infty} \frac{2V}{n\pi}(-1)^n \sin\frac{n\pi y}{d} \exp\left(\frac{n\pi x}{d}\right) \qquad (e)$$

(d) Show that a plot of Φ and $\mathbf{E}$ appears as shown in Fig. 6.6.9c, turned upside down.

5.5.5 In the two-dimensional system shown in cross-section in Fig. P5.5.5, plane parallel plates extend to infinity in the $-y$ direction. The potentials of the upper and lower plates are, respectively, $-V_o/2$ and $V_o/2$. The potential over the plane $y = 0$ terminating the plates at the right is specified to be $\Phi_d(x)$.

(a) What is the potential distribution between the plates far to the left?
(b) If Φ is taken as the potential Φ_a that assumes the correct distribution as $y \to -\infty$, plus a potential Φ_b, what boundary conditions must be satisfied by Φ_b?
(c) What is the potential distribution between the plates?

5.5.6 As an alternative (and in this case much more complicated) way of expressing the potential in Prob. 5.4.1, use a modal approach to express the potential in the interior region of Fig. P5.4.1.

5.5.7* Take an approach to finding the potential in the configuration of Fig. 5.5.2 that is an alternative to that used in the text. Let $\Phi = (Vy/b) + \Phi_1$.

(a) Show that the boundary conditions that must be satisfied by Φ_1 are that $\Phi_1 = -Vy/b$ at $x = 0$ and at $x = a$, and $\Phi_1 = 0$ at $y = 0$ and $y = b$.

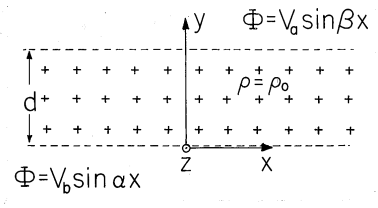


Fig. P5.6.1

(b) Show that the potential is

$$\Phi = \frac{Vy}{b} + \sum_{n=1}^{\infty} A_n \cosh \frac{n\pi}{b}\left(x - \frac{a}{2}\right) \sin \frac{n\pi y}{b} \qquad (a)$$

where

$$A_n = \frac{2V(-1)^n}{\cosh\left(\frac{n\pi a}{2b}\right)} \qquad (b)$$

(It is convenient to exploit the symmetry of the configuration about the plane $x = a/2$.)

5.6 Solutions to Poisson's Equation with Boundary Conditions

5.6.1* The potential distribution is to be determined in a region bounded by the planes $y = 0$ and $y = d$ and extending to infinity in the x and z directions, as shown in Fig. P5.6.1. In this region, there is a uniform charge density ρ_o. On the upper boundary, the potential is $\Phi(x, d, z) = V_a \sin(\beta x)$. On the lower boundary, $\Phi(x, 0, z) = V_b \sin(\alpha x)$. Show that $\Phi(x, y, z)$ throughout the region $0 < y < d$ is

$$\begin{aligned}\Phi =& V_a \sin\beta x \frac{\sinh \beta y}{\sinh \beta d} - V_b \sin \alpha x \frac{\sinh \alpha(y-d)}{\sinh \alpha d} \\ &- \frac{\rho_o}{\epsilon_o}\left(\frac{y^2}{2} - \frac{yd}{2}\right)\end{aligned} \qquad (a)$$

5.6.2 For the configuration of Fig. P5.6.1, the charge is again uniform in the region between the boundaries, with density ρ_o, but the potential at $y = d$ is $\Phi = \Phi_o \sin(kx)$, while that at $y = 0$ is zero (Φ_o and k are given constants). Find Φ in the region where $0 < y < d$, between the boundaries.

5.6.3* In the region between the boundaries at $y = \pm d/2$ in Fig. P5.6.3, the charge density is

$$\rho = \rho_o \cos k(x - \delta); \qquad -\frac{d}{2} < y < \frac{d}{2} \qquad (a)$$

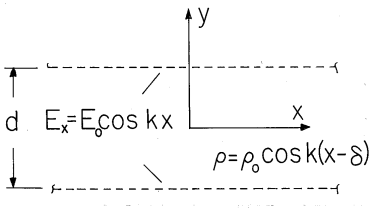


Fig. P5.6.3

where ρ_o and δ are given constants. Electrodes at $y = \pm d/2$ constrain the tangential electric field there to be

$$E_x = E_o \cos kx \tag{b}$$

The charge density might represent a traveling wave of space charge on a modulated particle beam, and the walls represent the traveling-wave structure which interacts with the beam. Thus, in a practical device, such as a traveling-wave amplifier designed to convert the kinetic energy of the moving charge to ac electrical energy available at the electrodes, the charge and potential distributions move to the right with the same velocity. This does not concern us, because we consider the interaction at one instant in time.

(a) Show that a particular solution is

$$\Phi_p = \frac{\rho_o}{\epsilon_o k^2} \cos k(x - \delta) \tag{c}$$

(b) Show that the total potential is the sum of this solution and that solution to Laplace's equation that makes the total solution satisfy the boundary conditions.

$$\Phi = \Phi_p - \frac{\cosh ky}{\cosh\left(\frac{kd}{2}\right)} \left[\frac{E_o}{k} \sin kx + \frac{\rho_o}{\epsilon_o k^2} \cos k(x - \delta) \right] \tag{d}$$

(c) The force density (force per unit volume) acting on the charge is $\rho\mathbf{E}$. Show that the force f_x acting on a section of the charge of length in the x direction $\lambda = 2\pi/k$ spanning the region $-d/2 < y < d/2$ and unit length in the z direction is

$$f_x = \frac{2\pi\rho_o E_o}{k^2} \tanh\left(\frac{kd}{2}\right) \cos k\delta \tag{e}$$

5.6.4 In the region $0 < y < d$ shown in cross-section in Fig. P5.6.4, the charge density is

$$\rho = \rho_o \cos k(x - \delta); \qquad 0 < y < d \tag{a}$$

where ρ_o and δ are constants. Electrodes at $y = d$ constrain the potential there to be $\Phi(x, d) = V_o \cos(kx)$ (V_o and k given constants), while an electrode at $y = 0$ makes $\Phi(x, 0) = 0$.

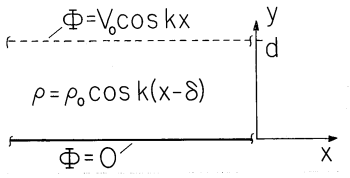


Fig. P5.6.4

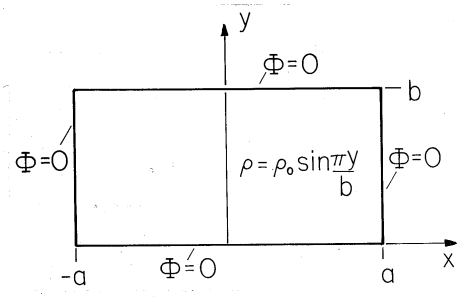


Fig. P5.6.5

(a) Find a particular solution that satisfies Poisson's equation everywhere between the electrodes.
(b) What boundary conditions must the homogeneous solution satisfy at $y = d$ and $y = 0$?
(c) Find Φ in the region $0 < y < d$.
(d) The force density (force per unit volume) acting on the charge is $\rho\mathbf{E}$. Find the total force f_x acting on a section of the charge spanning the system from $y = 0$ to $y = d$, of unit length in the z direction and of length $\lambda = 2\pi/k$ in the x direction.

5.6.5* A region that extends to infinity in the $\pm z$ directions has a rectangular cross-section of dimensions $2a$ and b, as shown in Fig. P5.6.5. The boundaries are at zero potential while the region inside has the distribution of charge density

$$\rho = \rho_o \sin\left(\frac{\pi y}{b}\right) \tag{a}$$

where ρ_o is a given constant. Show that the potential in this region is

$$\Phi = \frac{\rho_o}{\epsilon_o}(b/\pi)^2 \sin\left(\frac{\pi y}{b}\right)\left[1 - \cosh\ \frac{\pi x}{b}/\cosh\ \frac{\pi a}{b}\right] \tag{b}$$

5.6.6 The cross-section of a two-dimensional configuration is shown in Fig. P5.6.6. The potential distribution is to be determined inside the boundaries, which are all at zero potential.

(a) Given that a particular solution inside the boundaries is

$$\Phi_p = V \sin\left(\frac{\pi y}{b}\right) \sin \beta x \tag{a}$$

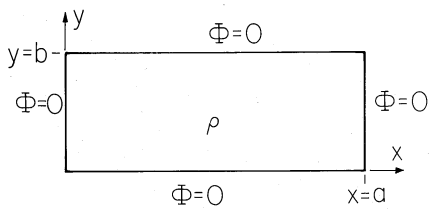


Fig. P5.6.6

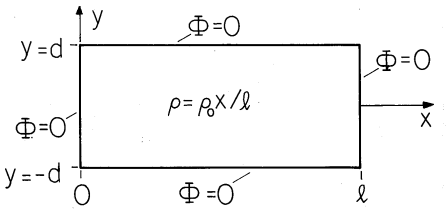


Fig. P5.6.7

where V and β are given constants, what is the charge density in that region?

(b) What is Φ?

5.6.7 The cross-section of a metal box that is very long in the z direction is shown in Fig. P5.6.7. It is filled by the charge density $\rho_o x/l$. Determine Φ inside the box, given that $\Phi = 0$ on the walls.

5.6.8* In region (b), where $y < 0$, the charge density is $\rho = \rho_o \cos(\beta x) e^{\alpha y}$, where ρ_o, β, and α are positive constants. In region (a), where $0 < y$, $\rho = 0$.

(a) Show that a particular solution in the region $y < 0$ is

$$\Phi_p = \frac{\rho_o}{\epsilon_o(\beta^2 - \alpha^2)} \cos(\beta x) \exp(\alpha y) \qquad (a)$$

(b) There is no surface charge density in the plane $y = 0$. Show that the potential is

$$\Phi = \frac{-\rho_o \cos \beta x}{\epsilon_o(\beta^2 - \alpha^2)2} \begin{cases} \left(\frac{\alpha}{\beta} - 1\right) \exp(-\beta y); & 0 < y \\ -2 \exp(\alpha y) + \left(\frac{\alpha}{\beta} + 1\right) \exp(\beta y); & y < 0 \end{cases} \qquad (b)$$

5.6.9 A sheet of charge having the surface charge density $\sigma_s = \sigma_o \sin \beta(x - x_o)$ is in the plane $y = 0$, as shown in Fig. 5.6.3. At a distance a above and below the sheet, electrode structures are used to constrain the potential to be $\Phi = V \cos \beta x$. The system extends to infinity in the x and z directions. The regions above and below the sheet are designated (a) and (b), respectively.

(a) Find Φ_a and Φ_b in terms of the constants V, β, σ_o, and x_o.

(b) Given that the force per unit area acting on the charge sheet is $\sigma_s E_x(x,0)$, what is the force acting on a section of the sheet having length d in the z direction and one wavelength $2\pi/\beta$ in the x direction?

(c) Now, the potential on the wall is made a traveling wave having a given angular frequency ω, $\Phi(x,\pm a,t) = V\cos(\beta x - \omega t)$, and the charge moves to the right with a velocity U, so that $\sigma_s = \sigma_o \sin\beta(x - Ut - x_o)$, where $U = \omega/\beta$. Thus, the wall potentials and surface charge density move in synchronism. Building on the results from parts (a)–(b), what is the potential distribution and hence total force on the section of charged sheet?

(d) What you have developed is a primitive model for an electron beam device used to convert the kinetic energy of the electrons (accelerated to the velocity v by a dc voltage) to high-frequency electrical power output. Because the system is free of dissipation, the electrical power output (through the electrode structure) is equal to the mechanical power input. Based on the force found in part (c), what is the electrical power output produced by one period $2\pi/\beta$ of the charge sheet of width w?

(e) For what values of x_o would the device act as a generator of electrical power?

5.7 Solutions to Laplace's Equation in Polar Coordinates

5.7.1* A circular cylindrical surface $r = a$ has the potential $\Phi = V\sin 5\phi$. The regions $r < a$ and $a < r$ are free of charge density. Show that the potential is

$$\Phi = V\begin{cases}(r/a)^5\sin 5\phi & r < a\\ (a/r)^5\sin 5\phi & a < r\end{cases} \qquad (a)$$

5.7.2 The $x - z$ plane is one of zero potential. Thus, the y axis is perpendicular to a zero potential plane. With ϕ measured relative to the x axis and z the third coordinate axis, the potential on the surface at $r = R$ is constrained by segmented electrodes there to be $\Phi = V\sin\phi$.

(a) If $\rho = 0$ in the region $r < R$, what is Φ in that region?

(b) Over the range $r < R$, what is the surface charge density on the surface at $y = 0$?

5.7.3* An annular region $b < r < a$ where $\rho = 0$ is bounded from outside at $r = a$ by a surface having the potential $\Phi = V_a\cos 3\phi$ and from the inside at $r = b$ by a surface having the potential $\Phi = V_b\sin\phi$. Show that Φ in the annulus can be written as the sum of two terms, each a combination of solutions to Laplace's equation designed to have the correct value at one radius while

being zero at the other.

$$\Phi = V_a \cos 3\phi \frac{[(r/b)^3 - (b/r)^3]}{[(a/b)^3 - (b/a)^3]} + V_b \sin\phi \frac{[(r/a) - (a/r)]}{[(b/a) - (a/b)]} \qquad (a)$$

5.7.4 In the region $b < r < a,\ 0 < \phi < \alpha,\ \rho = 0$. On the boundaries of this region at $r = a$, at $\phi = 0$ and $\phi = \alpha,\ \Phi = 0$. At $r = b,\ \Phi = V_b \sin(\pi\phi/\alpha)$. Determine Φ in this region.

5.7.5* In the region $b < r < a,\ 0 < \phi < \alpha,\ \rho = 0$. On the boundaries of this region at $r = a,\ r = b$ and at $\phi = 0,\ \Phi = 0$. At $\phi = \alpha$, the potential is $\Phi = V \sin[3\pi ln(r/a)/ln(b/a)]$. Show that within the region,

$$\Phi = V \sinh\left[\frac{3\pi\phi}{ln(b/a)}\right] \sin\left[3\pi \frac{ln(r/a)}{ln(b/a)}\right] \Big/ \sinh\left[\frac{3\pi\alpha}{ln(b/a)}\right] \qquad (a)$$

5.7.6 The plane $\phi = 0$ is at potential $\Phi = V$, while that at $\phi = 3\pi/2$ is at zero potential. The system extends to infinity in the $\pm z$ and r directions. Determine and sketch Φ and $\mathbf{E}$ in the range $0 < \phi < 3\pi/2$.

5.8 Examples in Polar Coordinates

5.8.1* Show that Φ and $\mathbf{E}$ as given by (4) and (5), respectively, describe the potential and electric field intensity around a perfectly conducting half-cylinder at $r = R$ on a perfectly conducting plane at $x = 0$ with a uniform field $E_a\mathbf{i_x}$ applied at $x \to \infty$. Show that the maximum field intensity is twice that of the applied field, regardless of the radius of the half-cylinder.

5.8.2 Coaxial circular cylindrical surfaces bound an annular region of free space where $b < r < a$. On the inner surface, where $r = b$, $\Phi = V_b > 0$. On the outer surface, where $r = a,\ \Phi = V_a > 0$.

(a) What is Φ in the annular region?
(b) How large must V_b be to insure that all lines of $\mathbf{E}$ are outward directed from the inner cylinder?
(c) What is the net charge per unit length on the inner cylinder under the conditions of (b)?

5.8.3* A device proposed for using the voltage v_o to measure the angular velocity Ω of a shaft is shown in Fig. P5.8.3a. A cylindrical grounded electrode has radius R. (The resistance R_o is "small.") Outside and concentric at $r = a$ is a rotating shell supporting the surface charge density distribution shown in Fig. P5.8.3b.

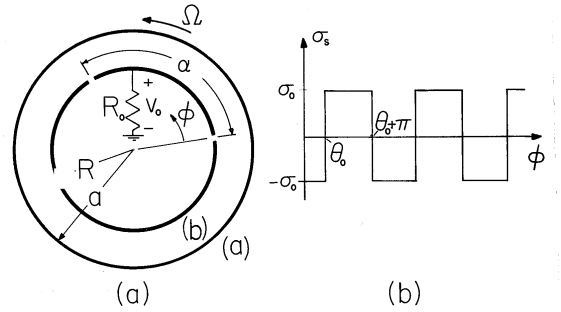


Fig. P5.8.3

(a) Given θ_o and σ_o, show that in regions (a) and (b), respectively, outside and inside the rotating shell,

$$\Phi = \frac{2\sigma_o a}{\pi\epsilon_o}\sum_{\substack{m=1\\ \text{odd}}}^{\infty}\frac{1}{m^2}\cdot \begin{cases} [(a/R)^m - (R/a)^m](R/r)^m \sin m(\phi-\theta_o); & a<r \\ (R/a)^m[(r/R)^m - (R/r)^m]\sin m(\phi-\theta_o); & R<r<a \end{cases} \qquad (a)$$

(b) Show that the charge on the segment of the inner electrode attached to the resistor is

$$q = \sum_{\substack{m=1\\ \text{odd}}}^{\infty} Q_m[\cos m\theta_o - \cos m(\alpha-\theta_o)]; \qquad Q_m \equiv \frac{4w\sigma_o a}{m^2\pi}(R/a)^m \qquad (b)$$

where w is the length in the z direction.

(c) Given that $\theta_o = \Omega t$, show that the output voltage is related to Ω by

$$v_o(t) = \sum_{\substack{m=1\\ \text{odd}}}^{\infty} Q_m m\Omega R_o[\sin m(\alpha-\Omega t) + \sin m\Omega t] \qquad (c)$$

so that its amplitude can be used to measure Ω.

5.8.4 Complete the steps of Prob. 5.8.3 with the configuration of Fig. P5.8.3 altered so that the rotating shell is inside rather than outside the grounded electrode. Thus, the radius a of the rotating shell is less than the radius R, and region (a) is $a < r < R$, while region (b) is $r < a$.

5.8.5* A pair of perfectly conducting zero potential electrodes form a wedge, one in the plane $\phi = 0$ and the other in the plane $\phi = \alpha$. They essentially extend to infinity in the $\pm z$ directions. Closing the region between the electrodes at $r = R$ is an electrode having potential V. Show that the potential inside the region bounded by these three surfaces is

$$\Phi = \sum_{\substack{m=1\\ \text{odd}}}^{\infty}\frac{4V}{m\pi}(r/R)^{m\pi/\alpha}\sin\left(\frac{m\pi\phi}{\alpha}\right) \qquad (a)$$

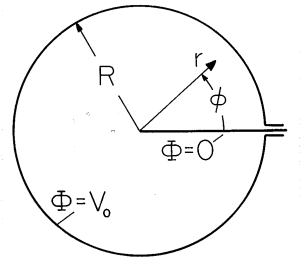


Fig. P5.8.7

5.8.6 In a two-dimensional system, the region of interest is bounded in the $\phi = 0$ plane by a grounded electrode and in the $\phi = \alpha$ plane by one that has $\Phi = V$. The region extends to infinity in the r direction. At $r = R$, $\Phi = V$. Determine Φ.

5.8.7 Figure P5.8.7 shows a circular cylindrical wall having potential V_o relative to a grounded fin in the plane $\phi = 0$ that reaches from the wall to the center. The gaps between the cylinder and the fin are very small.

(a) Find all solutions in polar coordinates that satisfy the boundary conditions at $\phi = 0$ and $\phi = 2\pi$. Note that you cannot accept solutions for Φ of negative powers in r.
(b) Match the boundary condition at $r = R$.
(c) One of the terms in this solution has an electric field intensity that is infinite at the tip of the fin, where $r = 0$. Sketch Φ and $\mathbf{E}$ in the neighborhood of the tip. What is the σ_s on the fin associated with this term as a function of r? What is the net charge associated with this term?
(d) Sketch the potential and field intensity throughout the region.

5.8.8 A two-dimensional system has the same cross-sectional geometry as that shown in Fig. 5.8.6 except that the wall at $\phi = 0$ has the potential v. The wall at $\phi = \phi_o$ is grounded. Determine the interior potential.

5.8.9 Use arguments analogous to those used in going from (5.5.22) to (5.5.26) to show the orthogonality (14) of the radial modes R_n defined by (13). [Note the comment following (14).]

5.9 Three Solutions to Laplace's Equation in Spherical Coordinates

5.9.1 On the surface of a spherical shell having radius $r = a$, the potential is $\Phi = V \cos\theta$.

(a) With no charge density either outside or inside this shell, what is Φ for $r < a$ and for $r > a$?
(b) Sketch Φ and $\mathbf{E}$.

5.9.2* A spherical shell having radius a supports the surface charge density $\sigma_o \cos\theta$.

(a) Show that if this is the only charge in the volume of interest, the potential is

$$\Phi = \frac{\sigma_o a}{3\epsilon_o} \begin{cases} (a/r)^2 \cos\theta & r \geq a \\ (r/a)\cos\theta & r \leq a \end{cases} \qquad (a)$$

(b) Show that a plot of Φ and $\mathbf{E}$ appears as shown in Fig. 6.3.1.

5.9.3* A spherical shell having zero potential has radius a. Inside, the charge density is $\rho = \rho_o \cos\theta$. Show that the potential there is

$$\Phi = \frac{a^2 \rho_o}{4\epsilon_o}[(r/a) - (r/a)^2]\cos\theta \qquad (a)$$

5.9.4 The volume of a spherical region is filled with the charge density $\rho = \rho_o (r/a)^m \cos\theta$, where ρ_o and m are given constants. If the potential $\Phi = 0$ at $r = a$, what is Φ for $r < a$?

5.10 Three-Dimensional Solutions to Laplace's Equation

5.10.1* In the configuration of Fig. 5.10.2, all surfaces have zero potential except those at $x = 0$ and $x = a$, which have $\Phi = v$. Show that

$$\Phi = \sum_{\substack{m=1 \\ \text{odd}}}^{\infty} \sum_{\substack{n=1 \\ \text{odd}}}^{\infty} A_{mn} \sin\left(\frac{m\pi y}{b}\right) \sin\left(\frac{n\pi z}{w}\right) \cosh k_{mn}\left(x - \frac{a}{2}\right) \qquad (a)$$

and

$$A_{mn} = \frac{16v}{mn\pi^2} \Big/ \cosh\frac{k_{mn} a}{2} \qquad (b)$$

5.10.2 In the configuration of Fig. 5.10.2, all surfaces have zero potential. In the plane $y = a/2$, there is the surface charge density $\sigma_s = \sigma_o \sin(\pi x/a)\sin(\pi z/w)$. Find the potentials Φ^a and Φ^b above and below this surface, respectively.

5.10.3 The configuration is the same as shown in Fig. 5.10.2 except that all of the walls are at zero potential and the volume is filled by the uniform charge density $\rho = \rho_o$. Write four essentially different expressions for the potential distribution.

6

POLARIZATION

6.0 INTRODUCTION

The previous chapters postulated surface charge densities that appear and disappear as required by the boundary conditions obeyed by surfaces of conductors. Thus, the idea that the distribution of the charge density may be linked to the field it induces is not new. Thus far, however, no consideration has been given in any detail to the physical laws which determine the occurrence and behavior of charge densities in matter.

To set the stage for this and the next chapter, consider two possible pictures that could be used to explain why an object distorts an initially uniform electric field. In Fig. 6.0.1a, the sphere is composed of a metallic conductor, and therefore composed of atoms having electrons that are free to move from one atomic site to another. Suppose, to begin with, that there are equal numbers of positive sites and negative electrons. In the absence of an applied field and on a scale that is large compared to the distance between atoms (that is, on a *macroscopic* scale), there is therefore no charge density at any point within the material.

When this object is placed in an initially uniform electric field, the electrons are subject to forces that tend to make them concentrate on the south pole of the sphere. This requires only that the electrons migrate downward slightly (on the average, less than an interatomic distance). Because the interior of the sphere must be field free in the final equilibrium (steady) state, the charge density remains zero at each point within the volume of the material. However, to preserve a zero net charge, the positive atomic sites on the north pole of the sphere are uncovered. After a time, the net result is the distribution of surface charge density shown in Fig. 6.0.1b. [In fact, provided the electrodes are well-removed from the sphere, this is the distribution found in Example 5.9.1.]

Now consider an alternative picture of the physics that can lead to a very similar result. As shown in Fig. 6.0.1c, the material is composed of atoms, molecules,

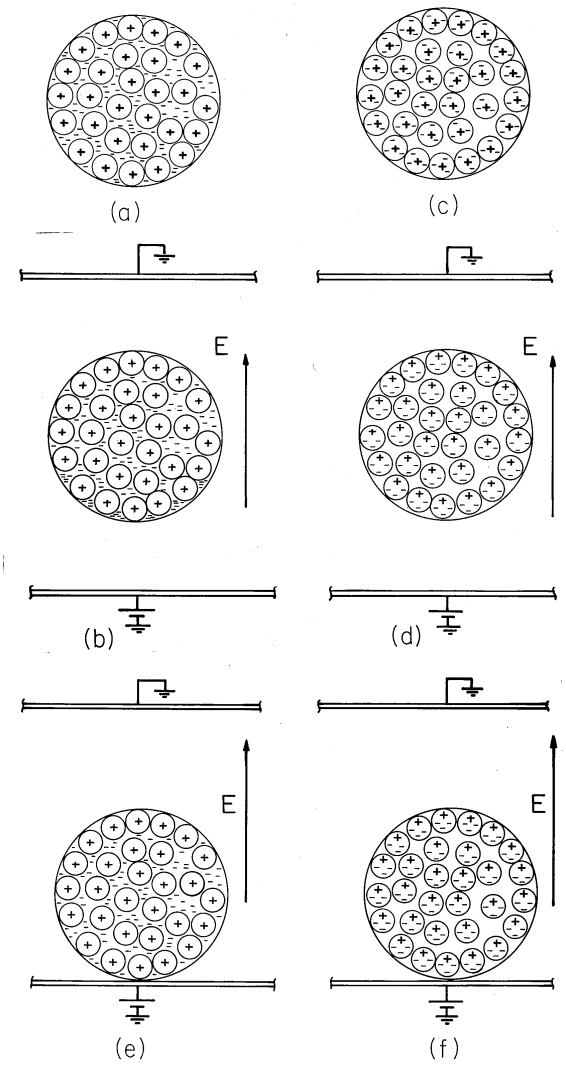


Fig. 6.0.1 In the left-hand sequence, the sphere is conducting, while on the right, it is polarizable and not conducting.

or groups of molecules (domains) in which the electric field induces dipole moments. For example, suppose that the dipole moments are of an atomic scale and, in the absence of an electric field, do not exist; the moments are induced because atoms contain positively charged nuclei and electrons orbiting around the nuclei. According to quantum theory, electrons orbiting the nuclei are not to be viewed as localized at any particular instant of time. It is more appropriate to think of the electrons as "clouds" of charge surrounding the nuclei. Because the charge of the orbiting electrons is equal and opposite to the charge of the nuclei, a neutral atom has no net charge. An atom with no permanent dipole moment has the further

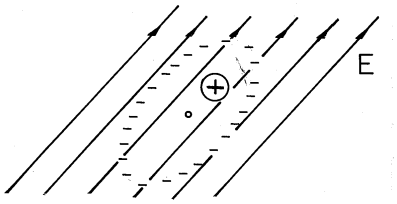


Fig. 6.0.2 Nucleus with surrounding electronic charge cloud displaced by applied electric field.

property that the center of the negative charge of the electron "clouds" coincides with the center of the positive charge of the nuclei. In the presence of an electric field, the center of positive charge is pulled in the direction of the field while the center of negative charge is pushed in the opposite direction. At the atomic level, this relative displacement of charge centers is as sketched in Fig. 6.0.2. Because the two centers of charge no longer coincide, the particle acquires a dipole moment. We can represent each atom by a pair of charges of equal magnitude and opposite sign separated by a distance d.

On the macroscopic scale of the sphere and in an applied field, the dipoles then appear somewhat as shown in Fig. 6.0.1d. In the interior of the sphere, the polarization leaves each positive charge in the vicinity of a negative one, and hence there is no net charge density. However, at the north pole there are no negative charges to neutralize the positive ones, and at the south pole no positive ones to pair up with the negative ones. The result is a distribution of surface charge density that does not differ qualitatively from that for the metal sphere.

How can we distinguish between these two very different situations? Suppose that the two spheres make contact with the lower electrode, as shown in parts (e) and (f) of the figure. By this we mean that in the case of the metal sphere, electrons are now free to pass between the sphere and the electrode. Once again, electrons move slightly downward, leaving positive sites exposed at the top of the sphere. However, some of those at the bottom flow into the lower electrode, thus reducing the amount of negative surface charge on the lower side of the metal sphere.

At the top, the polarized sphere shown by Fig. 6.0.1f has a similar distribution of positive surface charge density. But one very important difference between the two situations is apparent. On an atomic scale in the ideal dielectric, the orbiting electrons are paired with the parent atom, and hence the sphere must remain neutral. Thus, the metallic sphere now has a net charge, while the one made up of dipoles does not.

Experimental evidence that a metallic sphere had indeed acquired a net charge could be gained in a number of different ways. Two are clear from demonstrations in Chap. 1. A pair of spheres, each charged by "induction" in this fashion, would repel each other, and this could be demonstrated by the experiment in Fig. 1.3.10. The charge could also be measured by charge conservation, as in Demonstration 1.5.1. Presumably, the same experiments carried out using insulating spheres would demonstrate the existence of no net charge.

Because charge accumulations occur via displacements of paired charges (polarization) as well as of charges that can move far away from their partners of opposite sign, it is often appropriate to distinguish between these by separating the total charge density ρ into parts ρ_u and ρ_p, respectively, produced by unpaired and

paired charges.

$$\rho = \rho_u + \rho_p \tag{1}$$

In this chapter, we consider insulating materials and therefore focus on the effects of the paired or polarization charge density. Additional effects of unpaired charges are taken up in the next chapter.

Our first step, in Sec. 6.1, is to relate the polarization charge density to the density of dipoles– to the polarization density. We do this because it is the polarization density that can be most easily specified. Sections 6.2 and 6.3 then focus on the first of two general classes of polarization. In these sections, the polarization density is permanent and therefore specified without regard for the electric field. In Sec. 6.4, we discuss simple constitutive laws expressing the action of the field upon the polarization. This field-induced atomic polarization just described is typical of physical situations. The field action on the atom, molecule, or domain is accompanied by a reaction of the dipoles on the field that must be considered simultaneously. That is, within such a polarizable body placed into an electric field, a polarization charge density is produced which, in turn, modifies the electric field. In Secs. 6.5–6.7, we shall study methods by which self-consistent solutions to such problems are obtained.

6.1 POLARIZATION DENSITY

The following development is applicable to polarization phenomena having diverse microscopic origins. Whether representative of atoms, molecules, groups of ordered atoms or molecules (domains), or even macroscopic particles, the dipoles are pictured as opposite charges $\pm q$ separated by a vector distance $\mathbf{d}$ directed from the negative to the positive charge. Thus, the individual dipoles, represented as in Sec. 4.4, have moments $\mathbf{p}$ defined as

$$\mathbf{p} = q\mathbf{d} \tag{1}$$

Because $\mathbf{d}$ is generally smaller in magnitude than the size of the atom, molecule, or other particle, it is small compared with any macroscopic dimension of interest.

Now consider a medium consisting of N such polarized particles per unit volume. What is the net charge q contained within an arbitrary volume V enclosed by a surface S? Clearly, if the particles of the medium within V were unpolarized, the net charge in V would be zero. However, now that they are polarized, some charge centers that were contained in V in their unpolarized state have moved out of the surface S and left behind unneutralized centers of charge. To determine the net unneutralized charge left behind in V, we will assume (without loss of generality) that the negative centers of charge are stationary and that only the positive centers of charge are mobile during the polarization process.

Consider the particles in the neighborhood of an element of area $d\mathbf{a}$ on the surface S, as shown in Fig. 6.1.1. All positive centers of charge now outside S within the volume $dV = \mathbf{d} \cdot d\mathbf{a}$ have left behind negative charge centers. These contribute a net negative charge to V. Because there are $N\mathbf{d} \cdot d\mathbf{a}$ such negative centers of charge in dV, the net charge left behind in V is

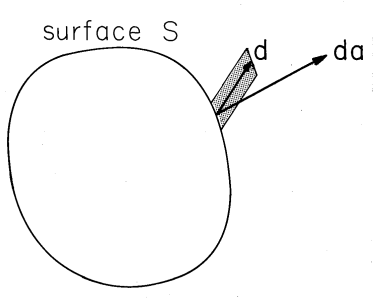


Fig. 6.1.1 Volume element containing positive charges which have left negative charges on the other side of surface S.

$$Q = -\oint_S (qN\mathbf{d}) \cdot d\mathbf{a} \tag{2}$$

Note that the integrand can be either positive or negative depending on whether positive centers of charge are leaving or entering V through the surface element $d\mathbf{a}$. Which of these possibilities occurs is reflected by the relative orientation of $\mathbf{d}$ and $d\mathbf{a}$. If $\mathbf{d}$ has a component parallel (anti-parallel) to $d\mathbf{a}$, then positive centers of charge are leaving (entering) V through $d\mathbf{a}$.

The integrand of (1) has the dimensions of dipole moment per unit volume and will therefore be defined as the *polarization density*.

$$\mathbf{P} \equiv Nq\mathbf{d} \tag{3}$$

Also by definition, the net charge in V can be determined by integrating the polarization charge density over its volume.

$$Q = \int_V \rho_p dV \tag{4}$$

Thus, we have two ways of calculating the net charge, the first by using the polarization density from (3) in the surface integral of (2).

$$Q = -\oint_S \mathbf{P} \cdot d\mathbf{a} = -\int_V \nabla \cdot \mathbf{P} dV \tag{5}$$

Here Gauss' theorem has been used to convert the surface integral to one over the enclosed volume. The charge found from this volume integral must be the same as given by the second way of calculating the net charge, by (4). Because the volume under consideration is arbitrary, the integrands of the volume integrals in (4) and (5) must be identical.

$$\boxed{\rho_p = -\nabla \cdot \mathbf{P}} \tag{6}$$

In this way, the polarization charge density ρ_p has been related to the polarization density $\mathbf{P}$.

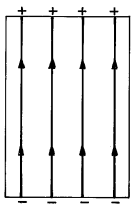


Fig. 6.1.2 Polarization surface charge due to uniform polarization of right cylinder.

It may seem that little has been accomplished in this development because, instead of the unknown ρ_p, the new unknown $\mathbf{P}$ appeared. In some instances, $\mathbf{P}$ is known. But even in the more common cases where the polarization density and hence the polarization charge density is not known a priori but is induced by the field, it is easier to directly link $\mathbf{P}$ with $\mathbf{E}$ than ρ_p with $\mathbf{E}$.

In Fig. 6.0.1, the polarized sphere could acquire no net charge. Our representation of the polarization charge density in terms of the polarization density guarantees that this is true. To see this, suppose V is interpreted as the volume containing the entire polarized body so that the surface S enclosing the volume V falls outside the body. Because $\mathbf{P}$ vanishes on S, the surface integral in (5) must vanish. Any distribution of charge density related to the polarization density by (6) cannot contribute a net charge to an isolated body.

We will often find it necessary to represent the polarization density by a discontinuous function. For example, in a material surrounded by free space, such as the sphere in Fig. 6.0.1, the polarization density can fall from a finite value to zero at the interface. In such regions, there can be a surface polarization charge density. With the objective of determining this density from $\mathbf{P}$, (6) can be integrated over a pillbox enclosing an incremental area of an interface. With the substitution $-\mathbf{P} \rightarrow \epsilon_o\mathbf{E}$ and $\rho_p \rightarrow \rho$, (6) takes the same form as Gauss' law, so the proof is identical to that leading from (1.3.1) to (1.3.17). We conclude that where there is a jump in the normal component of $\mathbf{P}$, there is a *surface polarization charge density*

$$\boxed{\sigma_{sp} = -\mathbf{n} \cdot (\mathbf{P}^a - \mathbf{P}^b)} \tag{7}$$

Just as (6) tells us how to determine the polarization charge density for a given distribution of $\mathbf{P}$ in the volume of a material, this expression serves to evaluate the singularity in polarization charge density (the surface polarization charge density) at an interface.

Note that according to (6), $\mathbf{P}$ originates on negative polarization charge and terminates on positive charge. This contrasts with the relationship between $\mathbf{E}$ and the charge density. For example, according to (6) and (7), the uniformly polarized cylinder of material shown in Fig. 6.1.2 with $\mathbf{P}$ pointing upward has positive σ_{sp} on the top and negative on the bottom.

6.2 LAWS AND CONTINUITY CONDITIONS WITH POLARIZATION

With the unpaired and polarization charge densities distinguished, Gauss' law becomes

$$\nabla \cdot \epsilon_o \mathbf{E} = \rho_u + \rho_p \tag{1}$$

where (6.1.6) relates ρ_p to $\mathbf{P}$.

$$\rho_p = -\nabla \cdot \mathbf{P} \tag{2}$$

Because $\mathbf{P}$ is an "averaged" polarization per unit volume, it is a "smooth" vector function of position on an atomic scale. In this sense, it is a macroscopic variable. The negative of its divergence, the polarization charge density, is also a macroscopic quantity that does not reflect the "graininess" of the microscopic charge distribution. Thus, as it appears in (1), the electric field intensity is also a macroscopic variable.

Integration of (1) over an incremental volume enclosing a section of the interface, as carried out in obtaining (1.3.7), results in

$$\mathbf{n} \cdot \epsilon_o (\mathbf{E}^a - \mathbf{E}^b) = \sigma_{su} + \sigma_{sp} \tag{3}$$

where (6.1.7) relates σ_{sp} to $\mathbf{P}$.

$$\sigma_{sp} = -\mathbf{n} \cdot (\mathbf{P}^a - \mathbf{P}^b) \tag{4}$$

These last two equations, respectively, give expression to the continuity condition of Gauss' law, (1), at a surface of discontinuity.

Polarization Current Density and Ampère's Law. Gauss' law is not the only one affected by polarization. If the polarization density varies with time, then the flow of charge across the surface S described in Sec. 6.1 comprises an electrical current. Thus, we need to investigate charge conservation, and more generally the effect of a time-varying polarization density on Ampére's law. To this end, the following steps lead to the polarization current density implied by a time-varying polarization density.

According to the definition of $\mathbf{P}$ evolved in Sec. 6.1, the process of polarization transfers an amount of charge dQ

$$dQ = \mathbf{P} \cdot d\mathbf{a} \tag{5}$$

through a surface area element $d\mathbf{a}$. This is perhaps envisioned in terms of the volume $\mathbf{d} \cdot d\mathbf{a}$ shown in Fig. 6.2.1. If the polarization density $\mathbf{P}$ varies with time, then according to this equation, charge is passed through the area element at a finite rate. For a change in $qN\mathbf{d}$, or $\mathbf{P}$, of $\Delta\mathbf{P}$, the amount of charge that has passed through the incremental area element $d\mathbf{a}$ is

$$\Delta(dQ) = \Delta\mathbf{P} \cdot d\mathbf{a} \tag{6}$$

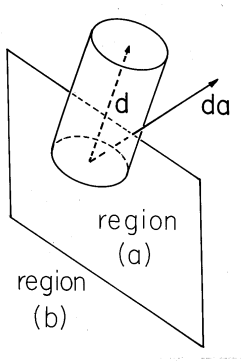


Fig. 6.2.1 Charges passing through area element $d\mathbf{a}$ result in polarization current density.

Note that we have two indicators of differentials in this expression. The d refers to the fact that Q is differential because $d\mathbf{a}$ is a differential. The rate of change with time of dQ, $\Delta(dQ)/\Delta t$, can be identified with a current di_p through $d\mathbf{a}$, from side (b) to side (a).

$$di_p = \frac{\Delta(dQ)}{\Delta t} = \frac{\partial \mathbf{P}}{\partial t} \cdot d\mathbf{a} \tag{7}$$

The partial differentiation symbol is used to distinguish the differentiation with respect to t from the space dependence of $\mathbf{P}$.

A current di_p through an area element $d\mathbf{a}$ is usually written as a current density dot-multiplied by $d\mathbf{a}$

$$di_p = \mathbf{J}_p \cdot d\mathbf{a} \tag{8}$$

Hence, we compare these last two equations and deduce that the polarization current density is

$$\mathbf{J}_p = \frac{\partial \mathbf{P}}{\partial t} \tag{9}$$

Note that $\mathbf{J}_p$ and ρ_p, via (2) and (9), automatically obey a continuity law having the same form as the charge conservation equation, (2.3.3).

$$\nabla \cdot \mathbf{J}_p + \frac{\partial \rho_p}{\partial t} = 0 \tag{10}$$

Hence, we can think of a rate of charge transport in a material medium as consisting of a current density of unpaired charges $\mathbf{J}_u$ and a polarization current density $\mathbf{J}_p$, each obeying its own conservation law. This is also implied by Ampère's law, as now generalized to include the effects of polarization.

In the EQS approximation, the magnetic field intensity is not usually of interest, and so Ampère's law is of secondary importance. But if $\mathbf{H}$ were to be determined, $\mathbf{J}_p$ would make a contribution. That is, Ampère's law as given by (2.6.2) is now written with the current density divided into paired and unpaired parts. With the latter given by (9), Ampère's differential law, generalized to include polarization, is

$$\nabla \times \mathbf{H} = \mathbf{J}_u + \frac{\partial}{\partial t}(\epsilon_o \mathbf{E} + \mathbf{P}) \tag{11}$$

This law is valid whether quasistatic approximations are to be made or not. However, it is its implication for charge conservation that is usually of interest in the EQS approximation. Thus, the divergence of (11) gives zero on the left and, in view of (1), (2), and (9), the expression becomes

$$\nabla \cdot \mathbf{J}_u + \frac{\partial \rho_u}{\partial t} + \nabla \cdot \mathbf{J}_p + \frac{\partial \rho_p}{\partial t} = 0 \tag{12}$$

Thus, with the addition of the polarization current density to (11), the divergence of Ampère's law gives the sum of the conservation equations for polarization charges, (10), and unpaired charges

$$\nabla \cdot \mathbf{J}_u + \frac{\partial \rho_u}{\partial t} = 0 \tag{13}$$

In the remainder of this chapter, it will be assumed that in the polarized material, ρ_u is usually zero. Thus, (13) will not come into play until Chap. 7.

Displacement Flux Density. Primarily in dealing with field-dependent polarization phenomena, it is customary to define a combination of quantities appearing in Gauss' law and Ampère's law as the *displacement flux density* $\mathbf{D}$.

$$\boxed{\mathbf{D} \equiv \epsilon_o \mathbf{E} + \mathbf{P}} \tag{14}$$

We regard $\mathbf{P}$ as representing the material and $\mathbf{E}$ as a field quantity induced by the external sources and the sources within the material. This suggests that $\mathbf{D}$ be considered a "hybrid" quantity. Not all texts on electromagnetism take this point of view. Our separation of all quantities appearing in Maxwell's equations into field and material quantities aids in the construction of models for the interaction of fields with matter.

With ρ_p replaced by (2), Gauss' law (1) can be written in terms of $\mathbf{D}$ defined by (14),

$$\boxed{\nabla \cdot \mathbf{D} = \rho_u} \tag{15}$$

while the associated continuity condition, (3) with σ_{sp} replaced by (4), becomes

$$\boxed{n \cdot (\mathbf{D}^a - \mathbf{D}^b) = \sigma_{su}} \tag{16}$$

The divergence of $\mathbf{D}$ and the jump in normal $\mathbf{D}$ determine the unpaired charge densities. Equations (15) and (16) hold, unchanged in form, both in free space and matter. To adapt the laws to free space, simply set $\mathbf{D} = \epsilon_o \mathbf{E}$.

Ampère's law is also conveniently written in terms of $\mathbf{D}$. Substitution of (14) into (11) gives

$$\boxed{\nabla \times \mathbf{H} = \mathbf{J}_u + \frac{\partial \mathbf{D}}{\partial t}} \tag{17}$$

Now the *displacement current density* $\partial\mathbf{D}/\partial t$ includes the polarization current density.

6.3 PERMANENT POLARIZATION

Usually, the polarization depends on the electric field intensity. However, in some materials a permanent polarization is "frozen" into the material. Ideally, this means that $\mathbf{P}(\mathbf{r},t)$ is prescribed, independent of $\mathbf{E}$. Electrets, used to make microphones and telephone speakers, are often modeled in this way.

With $\mathbf{P}$ a given function of space, and perhaps of time, the polarization charge density and surface charge density follow from (6.2.2) and (6.2.4) respectively. If the unpaired charge density is also given throughout the material, the total charge density in Gauss' law and surface charge density in the continuity condition for Gauss' law are known. [The right-hand sides of (6.2.1) and (6.2.3) are known.] Thus, a description of permanent polarization problems follows the same format as used in Chaps. 4 and 5.

Examples in this section are intended to develop an appreciation for the relationship between the polarization density $\mathbf{P}$, the polarization charge density ρ_p, and the electric field intensity $\mathbf{E}$. It should be recognized that once ρ_p is determined from the given $\mathbf{P}$, the methods of Chaps. 4 and 5 are directly applicable.

The distinction between paired and unpaired charges is sometimes academic. By subjecting an insulating material to an extremely large field, especially at an elevated temperature, it is possible to coerce molecules or domains of molecules into a polarization state that is retained for some period of time at lower fields and temperatures. It is natural to take this as a state of permanent polarization. But, if ions are made to impact the surface of the material, they can form sites of permanent charge. Certainly, the origin of these ions suggests that they be regarded as unpaired. Yet if the material attracts other charges to become neutral, as it tends to do, these permanent charges could also be regarded as due to polarization and represented by a permanent polarization charge density.

In this section, the EQS laws prevail. Thus, with the understanding that throughout the region of interest (exclusive of enclosing boundaries) the charge densities are given,

$$\mathbf{E} = -\nabla\Phi \tag{1}$$

$$\nabla^2\Phi = -\frac{1}{\epsilon_o}(\rho_u + \rho_p) \tag{2}$$

The example now considered is akin to that pictured qualitatively in Fig. 6.1.2. By making the uniformly polarized material spherical, it is possible to obtain a simple solution for the field distribution.

Example 6.3.1. A Permanently Polarized Sphere

A sphere of material having radius R is uniformly polarized along the z axis,

$$\mathbf{P} = P_o\mathbf{i_z} \tag{3}$$

Given that the surrounding region is free space with no additional field sources, what is the electric field intensity **E** produced by this permanent polarization?

The first step is to establish the distribution of ρ_p, in the material volume and on its surfaces. In the volume, the negative divergence of **P** is zero, so there is no volumetric polarization charge density (6.2.2). This is obvious with **P** written in Cartesian coordinates. It is less obvious when **P** is expressed in its spherical coordinate components.

$$\mathbf{P} = P_o \cos\theta \mathbf{i}_\mathbf{r} - P_o \sin\theta \mathbf{i}_\theta \tag{4}$$

Abrupt changes of the normal component of **P** entail polarization surface charge densities. These follow from using (4) to evaluate the continuity condition of (6.2.4) applied at $r = R$, where the normal component is $\mathbf{i}_\mathbf{r}$ and region (a) is outside the sphere.

$$\sigma_{sp} = P_o \cos\theta \tag{5}$$

This surface charge density gives rise to **E**.

Now that the field sources have been identified, the situation reverts to one much like that illustrated by Problem 5.9.2. Both within the sphere and in the surrounding free space, the potential must satisfy Laplace's equation, (2), with $\rho_u + \rho_p = 0$. In terms of Φ the continuity conditions at $r = R$ implied by (1) and (2) [(5.3.3) and (6.2.3)] with the latter evaluated using (5) are

$$\Phi^o - \Phi^i = 0 \tag{6}$$

$$-\epsilon_o \frac{\partial \Phi^o}{\partial r} + \epsilon_o \frac{\partial \Phi^i}{\partial r} = P_o \cos\theta \tag{7}$$

where (o) and (i) denote the regions outside and inside the sphere.

The source of the **E** field represented by this potential is a surface polarization charge density that varies cosinusoidally with θ. It is possible to fulfill the boundary conditions, (6) and (7), with the two spherical coordinate solutions to Laplace's equation (from Sec. 5.9) having the θ dependence $\cos\theta$. Because there are no sources in the region outside the sphere, the potential must go to zero as $r \to \infty$. Of the two possible solutions having the $\cos\theta$ dependence, the dipole field is used outside the sphere.

$$\Phi^o = A \frac{\cos\theta}{r^2} \tag{8}$$

Inside the sphere, the potential must be finite, so this solution is excluded. The solution is

$$\Phi^i = Br\cos\theta \tag{9}$$

which is that of a uniform electric field intensity. Substitution of these expressions into the continuity conditions, (6) and (7), gives expressions from which $\cos\theta$ can be factored. Thus, the boundary conditions are satisfied at every point on the surface if

$$\frac{A}{R^2} - BR = 0 \tag{10}$$

$$2\epsilon_o \frac{A}{R^3} + \epsilon_o B = P_o \tag{11}$$

These expressions can be solved for A and B, which are introduced into (8) and (9) to give the potential distribution

$$\Phi^o = \frac{P_o R^3}{3\epsilon_o} \frac{\cos\theta}{r^2} \tag{12}$$

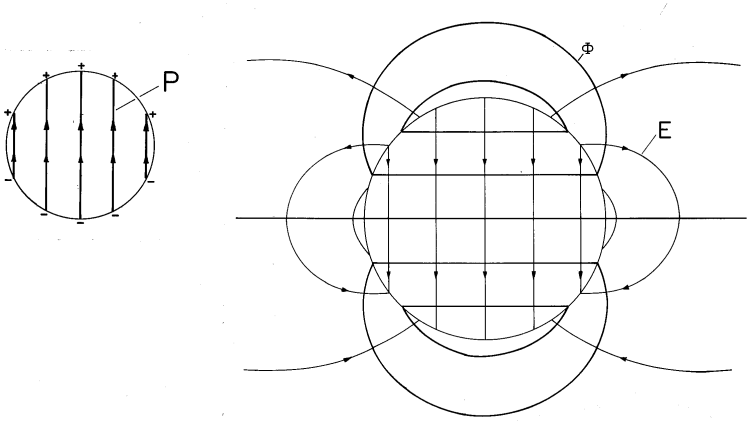


Fig. 6.3.1 Equipotentials and lines of electric field intensity of permanently polarized sphere having uniform polarization density. Inset shows polarization density and associated surface polarization charge density.

$$\Phi^i = \frac{P_o}{3\epsilon_o} r\cos\theta \tag{13}$$

Finally, the desired distribution of electric field is obtained by taking the negative gradient of this potential.

$$\mathbf{E}^o = \frac{P_o R^3}{3\epsilon_o r^3}(2\cos\theta\mathbf{i}_\mathbf{r} + \sin\theta\mathbf{i}_\theta) \tag{14}$$

$$\mathbf{E}^i = \frac{P_o}{3\epsilon_o}(-\cos\theta\mathbf{i}_\mathbf{r} + \sin\theta\mathbf{i}_\theta) \tag{15}$$

With the distribution of polarization density shown in the inset, Fig. 6.3.1 shows this electric field intensity. It comes as no surprise that the **E** lines originate on the positive charge and terminate on the negative. The polarization density originates on negative polarization charge and terminates on positive polarization charge. The resulting electric field is classic because outside it is exactly that of a dipole at the origin, while inside it is uniform.

What would be the moment of the dipole at the origin giving rise to the same external field as the uniformly polarized sphere? This can be seen from a comparison of (12) and (4.4.10).

$$|P| = \frac{4}{3}\pi R^3 P_o \tag{16}$$

The moment is simply the volume multiplied by the uniform polarization density.

There are two new ingredients in the next example. First, the region of interest has boundaries upon which the potential is constrained. Second, the given polarization density represents a volumetric distribution of polarization charge density rather than a surface distribution.

Example 6.3.2. Fields Due to Volume Polarization Charge with Boundary Conditions

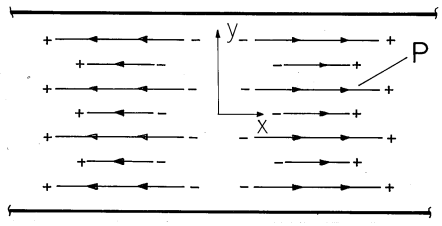


Fig. 6.3.2 Periodic distribution of polarization density and associated polarization charge density ($\rho_o < 0$) gives rise to potential and field shown in Fig. 5.6.2.

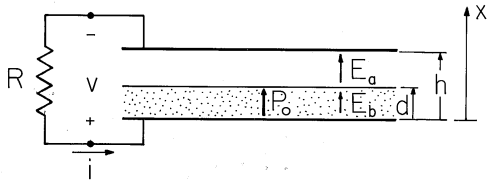


Fig. 6.3.3 Cross-section of electret microphone.

Plane parallel electrodes, in the planes $y = \pm a$, are constrained to zero potential. In the planar region between, the polarization density is the spatially periodic function

$$\mathbf{P} = -\mathbf{i_x}\frac{\rho_o}{\beta}\sin\beta x \tag{17}$$

We wish to determine the field distribution.

First, the distribution of polarization charge density is determined by taking the negative divergence of (17) [(17) is substituted into (6.1.6)].

$$\rho_p = \rho_o \cos\beta x \tag{18}$$

The distribution of polarization density and polarization charge density which has been found is shown in Fig. 6.3.2 ($\rho_o < 0$).

Now the situation reverts to solving Poisson's equation, given this source distribution and subject to the zero potential conditions on the boundaries at $y = \pm a$. The problem is identical to that considered in Example 5.6.1. The potential and field are the superposition of particular and homogeneous parts depicted in Fig. 5.6.2.

The next example illustrates how a permanent polarization can conspire with a mechanical deformation to produce a useful electrical signal.

Example 6.3.3. An Electret Microphone

Shown in cross-section in Fig. 6.3.3 is a thin sheet of permanently polarized material having thickness d. It is bounded from below by a fixed electrode having the potential v and from above by an air gap. On the other side of this gap is a conducting grounded diaphragm which serves as the movable element of a microphone. It is mounted so that it can undergo displacements. Thus, the spacing $h = h(t)$. Given $h(t)$, what is the voltage developed across a load resistance R?

In the sheet, the polarization density is uniform, with magnitude P_o, and directed from the lower electrode toward the upper one. This vector has no divergence,

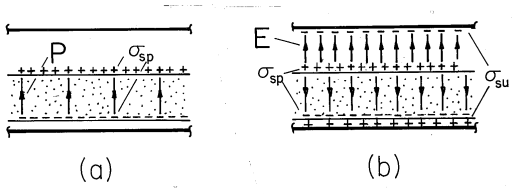


Fig. 6.3.4 (a) Distribution of polarization density and surface charge density in electret microphone. (b) Electric field intensity and surface polarization and unpaired charges.

and so evaluation of (6.1.6) shows that the polarization charge density is zero in the volume of the sheet. The polarization surface charge density on the electret air gap interface follows from (6.1.7) as

$$\sigma_{sp} = -\mathbf{n} \cdot (\mathbf{P}^a - \mathbf{P}^b) = P_o \tag{19}$$

Because σ_{sp} is uniform and the equipotential boundaries are plane and parallel, the electric field in the air gap [region (a)] and in the electret [region (b)] are taken as uniform.

$$\mathbf{E} = \mathbf{i_x} \begin{cases} E_a; & d < x < h \\ E_b; & 0 < x < d \end{cases} \tag{20}$$

Formally, we have just solved Laplace's equation in each of the bulk regions. The fields E_a and E_b must satisfy two conditions. First, the potential difference between the electrodes is v, so

$$v = \int_0^h E_x dx = dE_b + (h-d)E_a \tag{21}$$

Second, Gauss' jump condition at the electret air gap interface, (6.2.3), requires that

$$\epsilon_o E_a - \epsilon_o E_b = P_o \tag{22}$$

Simultaneous solution of these last two expressions evaluates the electric fields in terms of v and h.

$$E_a = \frac{v}{h} + \frac{d}{h}\frac{P_o}{\epsilon_o} \tag{24a}$$

$$E_b = \frac{v}{h} - \frac{(h-d)}{h}\frac{P_o}{\epsilon_o} \tag{24b}$$

What has been found is illustrated in Fig. 6.3.4. The uniform $\mathbf{P}$ and associated σ_{sp} shown in part (a) combine with the unpaired charges on the lower electrode and upper diaphragm to produce the fields shown in part (b). In this picture, it is assumed that v is positive and $(h-d)P_o/\epsilon_o > v$. In the air gap, the field due to the unpaired charges on the electrodes reinforces that due to σ_{sp}, while in the electret, it opposes the downward-directed field due to σ_{sp}.

To compute the current i, defined in Fig. 6.3.3, the lower electrode and the electret are enclosed by a surface S, and Gauss' law is used to evaluate the enclosed *unpaired* charge.

$$\nabla \cdot (\epsilon_o \mathbf{E} + \mathbf{P}) = \rho_u \Rightarrow q = \oint_S (\epsilon_o \mathbf{E} + \mathbf{P}) \cdot \mathbf{n} da \tag{25}$$

Just how the surface S cuts through the system does not matter. Here we take the surface as enclosing the lower electrode by passing through the air gap. It follows from (24) that the unpaired charge is

$$q = A\epsilon_o E_a = \frac{A\epsilon_o}{h}\left(v + \frac{dP_o}{\epsilon_o}\right) \tag{26}$$

where A is the area of the electrode.

Conservation of unpaired charge requires that the current be the rate of change of the total unpaired charge on the lower electrode.

$$i = \frac{dq}{dt} \tag{27}$$

With the resistor attached to the terminals (the input resistance of an amplifier driven by the microphone), the voltage and current must also satisfy Ohm's law.

$$v = -iR \tag{28}$$

These last three relations combine to give an expression for $v(t)$, given $h(t)$.

$$-\frac{v}{R} = -\frac{A\epsilon_o}{h^2}\left(v + \frac{dP_o}{\epsilon_o}\right)\frac{dh}{dt} + \frac{A\epsilon_o}{h}\frac{dv}{dt} \tag{29}$$

This differential equation has time-varying coefficients. Not only is this equation difficult to solve, but also the predicted voltage response cannot be a good replica of $h(t)$, as required for a good microphone, if all terms are of equal importance. That situation can be remedied if the deflections h_1 are kept small compared with the equilibrium position, $h_o \gg h_1$. In the absence of a time variation of h_1, it is clear from (29) that v is zero. By making h_1 small, we can make v small.

Expanding the right-hand side of (29) to first order in h_1, dh_1/dt, v, and dv/dt, we obtain

$$C_o\frac{dv}{dt} + \frac{v}{R} = \frac{C_o}{h_o}\left(\frac{dP_o}{\epsilon_o}\right)\frac{dh_1}{dt} \tag{30}$$

where $C_o = A\epsilon_o/h_o$.

We could solve this equation for its response to a sinusoidal drive. Alternatively, the resulting frequency response can be determined, with more physical insight, by considering two limits. First, suppose that time rate of change is so slow (frequencies so low) that the first term on the left is negligible compared to the second. Then the output voltage is

$$v = \frac{C_o R}{h_o}\left(\frac{dP_o}{\epsilon_o}\right)\frac{dh_1}{dt}; \qquad \omega RC_o \ll 1 \tag{31}$$

In this limit, the resistor acts as a short. The charge can be determined by the diaphragm displacement with the contribution of v ignored (i.e., the charge required to produce v by charging the capacitance C_o is ignored). The small but finite voltage is then obtained as the time rate of change of the charge multiplied by $-R$.

Second, suppose that time rates of change are so rapid that the second term is negligible compared to the first. Within an integration constant,

$$v = \frac{dP_o}{\epsilon_o}\frac{h_1}{h_o}; \qquad \omega RC_o \gg 1 \tag{32}$$

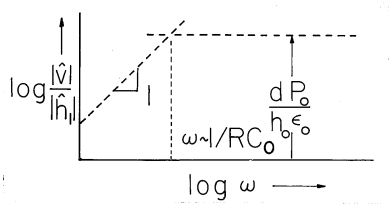


Fig. 6.3.5 Frequency response of electret microphone for imposed diaphragm displacement.

In this limit, the electrode charge is essentially constant. The voltage is obtained from (26) with q set equal to its equilibrium value, $(A\epsilon_o/h_o)(dP_o/\epsilon_o)$.

The frequency response gleaned from these asymptotic responses is in Fig. 6.3.5.

Because its displacement was taken as known, we have been able to ignore the dynamical equations of the diaphragm. If the mass and damping of the diaphragm are ignored, the displacement indeed reflects the pressure of a sound wave. In this limit, a linear distortion-free response of the microphone to pressure is assured at frequencies $\omega > 1/RC$. However, in predicting the response to a sound wave, it is usually necessary to include the detailed dynamics of the diaphragm.

In a practical microphone, subjecting the electret sheet to an electric field would induce some polarization over and beyond the permanent component P_o. Thus, a more realistic model would incorporate features of the linear dielectrics introduced in Sec. 6.4.

6.4 CONSTITUTIVE LAWS OF POLARIZATION

Dipole formation, or orientation of dipolar particles, usually depends on the local field in which the particles are situated. This local microscopic field is not necessarily equal to the macroscopic E field. Yet certain relationships between the macroscopic quantities $\mathbf{E}$ and $\mathbf{P}$ can be established without a knowledge of the relations between the local microscopic fields and the macroscopic E fields. Usually, these relations, called constitutive laws, originate in experimental observations characteristic of the material being investigated.

First, the permanent polarization model developed in the previous section is one constitutive law. In such a medium, $\mathbf{P}(\mathbf{r})$ is prescribed independent of $\mathbf{E}$.

There are media, and these are much more common, in which the polarization depends on $\mathbf{E}$. Consider an isotropic medium, which, in the absence of an electric field has no preferred orientation. Amorphous media such as glass are isotropic. Crystalline media, made up of randomly oriented microscopic crystals, also behave as isotropic media on a macroscopic scale. If we assume that the polarization $\mathbf{P}$ in an isotropic medium depends on the instantaneous field and not on its past history, then $\mathbf{P}$ is a function of $\mathbf{E}$

$$\mathbf{P} = \mathbf{P}(\mathbf{E}) \tag{1}$$

where $\mathbf{P}$ and $\mathbf{E}$ are parallel to each other. Indeed, if $\mathbf{P}$ were not parallel to $\mathbf{E}$, then a preferred direction different from the direction of $\mathbf{E}$ would need to exist in the medium, which contradicts the assumption of isotropy. A possible relation between

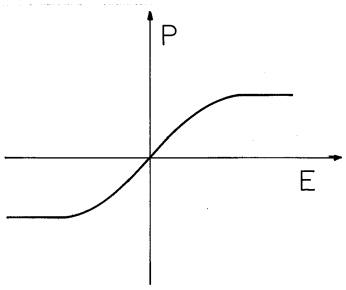


Fig. 6.4.1 Polarization characteristic for nonlinear isotropic material.

the magnitudes of **E** and **P** is shown in Fig. 6.4.1 and represents an "electrically nonlinear" medium for which **P** "saturates" for large values of **E**.

If the medium is electrically linear, in addition to being isotropic, then a linear relationship exists between **E** and **P**

$$\mathbf{P} = \epsilon_o \chi_e \mathbf{E} \tag{2}$$

where χ_e is the *dielectric susceptibility*. Typical values are given in Table 6.4.1. All isotropic media behave as linear media and obey (2) if the applied **E** field is sufficiently small. As long as **E** is small enough, any continuous function $\mathbf{P}(\mathbf{E})$ can be expanded in a Taylor series of **E** and broken off with the first term in **E**. (An isotropic medium cannot have a term in the Taylor expansion independent of **E**.)

For a linear isotropic material, where (2) is obeyed, it follows that **D** and **E** are related by

$$\mathbf{D} = \epsilon \mathbf{E} \tag{3}$$

where

$$\epsilon \equiv \epsilon_o (1 + \chi_e) \tag{4}$$

is the *permittivity* or *dielectric constant*. The permittivity normalized to ϵ_o, $(1+\chi_e)$, is the *relative dielectric constant*.

In our discussion, it has been assumed that the state of polarization depends only on the instantaneous electric field intensity. There are materials in which the polarization depends not only on the current electric field intensity but on the sequence of preceding states as well (hysteresis). Because we will find magnetization phenomena analogous in many ways to polarization phenomena, we will defer consideration of hysteretic phenomena to Chap. 9.

Many types of transducers exploit the dependence of polarization on variables other than the electric field. In pyroelectric materials, polarization is a function of temperature. Pyroelectrics are used for optical detectors of high-power infrared radiation. Piezoelectric materials have a polarization which is a function of strain (deformation). Such media are suited to low-power electromechanical energy conversion.

TABLE 6.4.1
MATERIAL DIELECTRIC SUSCEPTIBILITIES

Gases	χ_e
Air,	
0°C	0.00059
40 atmospheres	0.0218
80 atmospheres	0.0439
Carbon dioxide, 0°C	0.000985
Hydrogen, 0°C	0.000264
Water vapor, 145°C	0.00705

Liquids	χ_e
Acetone, 0°C	25.6
Air, -191°C	0.43
Alcohol	
amyl	16.0
ethyl	24.8
methyl	30.2
Benzene	1.29
Glycerine, 15°C	55.2
Oils,	
castor	3.67
linseed	2.35
corn	2.1
Water, distilled	79.1

Solids	χ_e
Diamond	15.5
Glass,	
flint, density 4.5	8.90
flint, density 2.87	5.61
lead, density 3.0-3.5	4.4-7.0
Mica	4.6-5.0
Paper (cable insulation)	1.0-1.5
Paraffin	1.1
Porcelain	4.7
Quartz,	
1 to axis	3.69
11 to axis	4.06
Rubber	1.3-3.0
Shellac	2.1

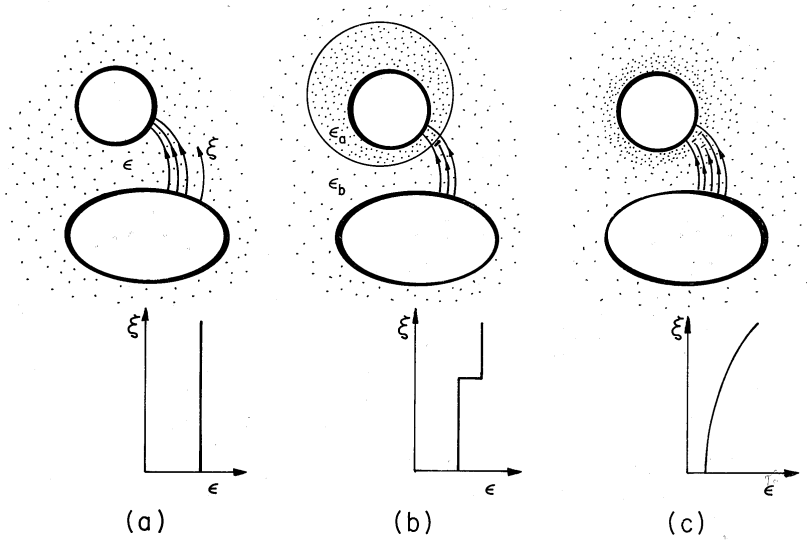


Fig. 6.5.1 Field region filled by (a) uniform dielectric, (b) piece-wise uniform dielectric and (c) smoothly varying dielectric.

6.5 FIELDS IN THE PRESENCE OF ELECTRICALLY LINEAR DIELECTRICS

In Secs. 6.2 and 6.3, the polarization density was given independently of the electric field intensity. In this and the next two sections, the polarization is induced by the electric field. Not only does the electric field give rise to the polarization, but in return, the polarization modifies the field. The polarization feeds back on the electric field intensity.

This "feedback" is described by the constitutive law for a linear dielectric. Thus, (6.4.3) and Gauss' law, (6.2.15), combine to give

$$\nabla \cdot \epsilon \mathbf{E} = \rho_u \tag{1}$$

and the electroquasistatic form of Faraday's law requires that

$$\nabla \times \mathbf{E} = 0 \Rightarrow \mathbf{E} = -\nabla \Phi \tag{2}$$

The continuity conditions implied by these two laws across an interface separating media having different permittivities are (6.2.16) expressed in terms of the constitutive law and either (5.3.1) or (5.3.4). These are

$$\mathbf{n} \cdot (\epsilon_a \mathbf{E}^a - \epsilon_b \mathbf{E}^b) = \sigma_{su} \tag{3}$$

$$\mathbf{n} \times (\mathbf{E}^a - \mathbf{E}^b) = 0 \Rightarrow \Phi^a - \Phi^b = 0 \tag{4}$$

Figure 6.5.1 illustrates three classes of situations involving linear dielectrics. In the first, the entire region of interest is filled with a *uniform* dielectric. In the second, the region of interest can be broken into uniform subregions within which

the permittivity is constant. The continuity conditions are needed to insure that the basic laws are satisfied through the interfaces between these regions. Systems of this type are said to be composed of *piece-wise uniform* dielectrics. Finally, the dielectric material may vary in its permittivity over dimensions that are on the same order as those of interest. Such a *smoothly inhomogeneous* dielectric is illustrated in Fig. 6.5.1c.

The remainder of this section makes some observations that are generally applicable provided that $\rho_u = 0$ throughout the volume of the region of interest. Section 6.6 is devoted to systems having uniform and piece-wise uniform dielectrics, while Sec. 6.7 illustrates fields in smoothly inhomogeneous dielectrics.

Capacitance. How does the presence of a dielectric alter the capacitance? To answer this question, recognize that conservation of unpaired charge, as expressed by (6.2.13), still requires that the current i measured at terminals connected to a pair of electrodes is the time rate of change of the *unpaired* charge on the electrode. In view of Gauss' law, with the effects of polarization included, (6.2.15), the net unpaired charge on an electrode enclosed by a surface S is

$$q = \int_V \rho_u dV = \int_V \nabla \cdot \mathbf{D} dV = \oint_S \mathbf{D} \cdot \mathbf{n} da \tag{5}$$

Here, Gauss' theorem has been used to convert the volume integral to a surface integral.

We conclude that the capacitance of an electrode (a) relative to a reference electrode (b) is

$$C = \frac{\oint_S \mathbf{D} \cdot \mathbf{n} da}{\int_{a\,C'}^{b} \mathbf{E} \cdot d\mathbf{s}} = \frac{\oint_S \mathbf{D} \cdot \mathbf{n} da}{v} \tag{6}$$

Note that this is the same as for electrodes in free space except that $\epsilon_o \mathbf{E} \rightarrow \mathbf{D}$. Because there is no unpaired charge density in the region between the electrodes, S is any surface that encloses the electrode (a). As before, with no polarization, $\mathbf{E}$ is irrotational, and therefore C' is any contour connecting the electrode (a) to the reference (b).

In an electrically linear dielectric, where $\mathbf{D} = \epsilon \mathbf{E}$, both the numerator and denominator of (6) are proportional to the voltage, and as a result, the capacitance C is independent of the voltage. However, with the introduction of an electrically nonlinear material, perhaps having the polarization constitutive law of Fig. 6.4.1, the numerator of (6) is not a linear function of the voltage. As defined by (6), the capacitance is then a function of the applied voltage.

Induced Polarization Charge. Stated as (1)–(4), the laws and continuity conditions for fields in a linear dielectric put the polarization charge out of view. Yet it is this charge that contains the effect of the dielectric on the field. Where does the polarization charge accumulate?

Again, assuming that ρ_u is zero, a vector identity casts Gauss' law as given by (1) into the form

$$\epsilon \nabla \cdot \mathbf{E} + \mathbf{E} \cdot \nabla \epsilon = 0 \tag{7}$$

Multiplied by ϵ_o and divided by ϵ, this expression can be written as

$$\nabla \cdot \epsilon_o \mathbf{E} = \frac{-\epsilon_o}{\epsilon} \mathbf{E} \cdot \nabla \epsilon \tag{8}$$

Comparison of this expression to Gauss' law written in terms of ρ_p, (6.2.1), shows that the polarization charge density is

$$\rho_p = -\frac{\epsilon_o}{\epsilon} \mathbf{E} \cdot \nabla \epsilon \tag{9}$$

This equation makes it clear that polarization charge will be induced only where there are gradients in ϵ. A special case is where there is an abrupt discontinuity in ϵ. Then the gradient in (9) is singular and represents a polarization surface charge density (the gradient represents the spatial derivative of a step function, which is an impulse). This surface charge density can best be determined by making use of the polarization charge density continuity condition, (6.1.7). Substitution of the constitutive law $\mathbf{P} = (\epsilon - \epsilon_o)\mathbf{E}$ then gives

$$\sigma_{sp} = -\mathbf{n} \cdot [(\epsilon_a - \epsilon_o)\mathbf{E}^a - (\epsilon_b - \epsilon_o)\mathbf{E}^b] \tag{10}$$

Because $\sigma_{su} = 0$, it follows from the jump condition for $\mathbf{n} \cdot \mathbf{D}$, (3), that

$$\sigma_{sp} = \mathbf{n} \cdot \epsilon_o \mathbf{E}^a \big(1 - \frac{\epsilon_a}{\epsilon_b}\big) \tag{11}$$

Remember that $\mathbf{n}$ is directed from region (b) to region (a).

Because $\mathbf{D}$ is solenoidal, we can construct tubes of $\mathbf{D}$ containing constant flux. Lines of $\mathbf{D}$ must therefore begin and terminate on the boundaries. The constitutive law, $\mathbf{D} = \epsilon\mathbf{E}$, requires that $\mathbf{D}$ is proportional to $\mathbf{E}$. Thus, although $\mathbf{E}$ can intensify or rarify as it passes through a flux tube, it can not reverse direction. Therefore, if we follow a bundle of electric field lines from the boundary point of high potential to the one of low potential, the polarization charge encountered [in accordance with (9) and (11)] is positive at points where ϵ is decreasing, negative where it is increasing.

Consider the examples in Fig. 6.5.1. In the case of the uniform dielectric, Fig. 6.5.1a, the typical flux tube shown passes through no variations in ϵ, and it follows from (8) that there is no volume polarization charge density. Thus, it will come as no surprise that the field distribution in this case is predicted by Laplace's equation.

In the piece-wise uniform dielectrics, there is no polarization charge density in a flux tube except where it passes through an interface. For the flux tube shown, (11) shows that if the upper region has the greater permittivity ($\epsilon_a > \epsilon_b$), then there is an accumulation of negative surface charge density at the interface. Thus, the field originating on positive charges at the lower electrode is in part terminated by negative polarization surface charge at the interface, and the field in the upper region tends to be weakened relative to that below.

In the smoothly inhomogeneous dielectric of Fig. 6.5.1c, the typical flux tube shown passes through a region where ϵ increases with ξ. It follows from (8) that negative polarization charge density is induced in the volume of the material. Here

again, the electric field associated with positive charge on the lower electrode is in part terminated on the polarization charge density induced in the volume. As a result, the dielectric tends to make the electric field weaken with increasing ξ.

The next two sections give the opportunity to solve for the fields in simple configurations and then see that the results are consistent with the physical picture that has been found here.

6.6 PIECE-WISE UNIFORM ELECTRICALLY LINEAR DIELECTRICS

In a region where the permittivity is uniform and where there is no unpaired charge, the electric potential obeys Laplace's equation.

$$\nabla^2\Phi = 0 \tag{1}$$

This follows from (6.5.1) and (6.5.2).

Uniform Dielectrics. If all of the region of interest is filled by a uniform dielectric, it is clear from the foregoing that all equations developed for fields in free space are now valid in the presence of the uniform dielectric. The only alteration is the replacement of the permittivity of free space ϵ_o by that of the uniform dielectric. In every problem from Chaps. 4 and 5 where Φ and $\mathbf{E}$ were determined in a region of free space bounded by equipotentials, that region could just as well be filled with a uniform dielectric, and for the same potentials the electric field intensity would be unaltered. However, the surface charge density σ_{su} on the boundaries would then be increased by the ratio ϵ/ϵ_o.

Illustration. Capacitance of a Sphere

A sphere having radius R has a potential v relative to infinity. Formally, the potential, and hence the electric field, follow from (1).

$$\Phi = v\frac{R}{r} \Rightarrow \mathbf{E} = v\frac{R}{r^2} \tag{2}$$

Evaluation of the capacitance, (6.5.6), then gives

$$C \equiv \frac{q}{v} = \frac{4\pi R^2}{v}\epsilon E_r|_{r=R} = 4\pi R\epsilon \tag{3}$$

The dielectric has increased the capacitance in the ratio of the dielectric constant of the material to the dielectric constant of free space.

The susceptibilities listed in Table 6.4.1 illustrate the increase in capacitance that would be observed if vacuum were replaced by one of the materials. In gases, atoms or molecules are so dilute that the increase in capacitance is usually negligible. With solids and liquids, the increase is of practical importance. Some, having

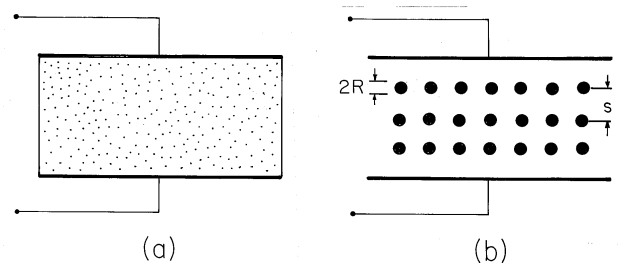


Fig. 6.6.1 (a) Plane parallel capacitor with region between electrodes occupied by a dielectric. (b) Artificial dielectric composed of cubic array of perfectly conducting spheres having radius R and spacing s.

molecules of large permanent dipole moments that are aligned by the field, increase the capacitance dramatically.

The following example is intended to provide an appreciation for why the polarized dielectric increases the capacitance.

Example 6.6.1. An Artificial Dielectric

In the plane parallel capacitor of Fig. 6.6.1, the electric field intensity is $(v/d)\mathbf{i_z}$. Thus, the unpaired charge density on the lower electrode is $D_z = \epsilon v/d$, and if the electrode area is A, the capacitance is

$$C \equiv \frac{q}{v} = \frac{A}{v} D_z|_{z=0} = \frac{A\epsilon}{d} \tag{4}$$

Here we assume that d is much less than either of the electrode dimensions, so the fringing fields can be ignored.

Now consider the plane parallel capacitor of Fig. 6.6.1b. The dielectric is composed of "molecules" that are actually perfectly conducting spheres. These have radius R and are in a cubic array with spacing $s >> R$. With the application of a voltage, the spheres acquire the positive and negative surface charges on their northern and southern poles required to make their surfaces equipotentials. In so far as the field outside the spheres is concerned, the system is modeled as an array of dipoles, each induced by the applied field.

If there are many of the spheres, the change in capacitance caused by inserting the array between the plates can be determined by treating it as a continuum. This we will do under the assumption that $s >> R$. In that case, the field in regions removed several radii from the sphere centers is essentially uniform, and taken as $E_z = v/d$. The resulting field in the vicinity of a sphere is then as determined in Example 5.9.1. The dipole moment of each sphere follows from a comparison of the potential for the perfectly conducting sphere in a uniform electric field, (5.9.7), with that of a dipole, (4.4.10).

$$p = 4\pi\epsilon_o R^3 E_a \tag{5}$$

The polarization density is the moment/dipole multiplied by the number of dipoles per unit volume, the number density N.

$$P_z = \epsilon_o(4\pi R^3 N)E_a \tag{6}$$

For the cubic array, a unit volume contains $1/s^3$ spheres, and so

$$N = \frac{1}{s^3} \tag{7}$$

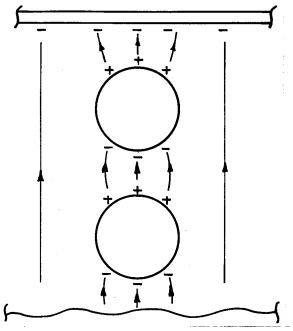


Fig. 6.6.2 From the microscopic point of view, the increase in capacitance results because the dipoles adjacent to the electrode induce image charges on the electrode in addition to those from the unpaired charges on the opposite electrode.

From (6) and (7) it follows that

$$\mathbf{P} = \epsilon_o\left[4\pi\left(\frac{R}{s}\right)^3\right]\mathbf{E} \tag{8}$$

Thus, the polarization density is a linear function of $\mathbf{E}$. The susceptibility follows from a comparison of (8) with (6.4.2) and, in turn, the permittivity is given by (6.4.4).

$$\chi_e = 4\pi\left(\frac{R}{s}\right)^3 \Rightarrow \epsilon = \left[1 + 4\pi\left(\frac{R}{s}\right)^3\right]\epsilon_o \tag{9}$$

Of course, this expression is accurate only if the interaction between spheres is negligible.

As the array of spheres is inserted between the electrodes, surface charges are induced, as shown in Fig. 6.6.2. Within the array, each cap of positive surface charge on the north pole of a sphere is compensated by an opposite charge on the south pole of a neighboring sphere. Thus, on a scale large compared to the spacing s, there is no charge density in the volume of the array. Nevertheless, the average field at the electrode is larger than the applied field $\mathbf{E}_a$. This is caused by surface charges on the last layers of spheres which have their images in unpaired charges on the electrodes. For a given applied voltage, the field between the top and bottom layers of spheres and the adjacent electrodes is increased, with an attendant increase in observed capacitance.

Demonstration 6.6.1. Artificial Dielectric

In Fig. 6.6.3, the artificial dielectric is composed of an array of ping-pong balls with conducting coatings. The parallel plate capacitor is in one leg of a bridge, as shown in the circuit pictured in Fig. 6.6.4. The resistors shunt the input terminals of balanced amplifiers so that the oscilloscope displays v_o. With the array removed, capacitor C_2 is adjusted to null the output voltage v_o. The output voltage resulting from the the insertion of the array is a measure of the change in capacitance. To simplify the interpretation of this voltage, the resistances R_s are made small compared to the impedance of the parallel plate capacitor. Thus, almost all of the applied voltage V appears across the lower legs of the bridge. With the introduction of the array, the change in current through the parallel plate capacitor is

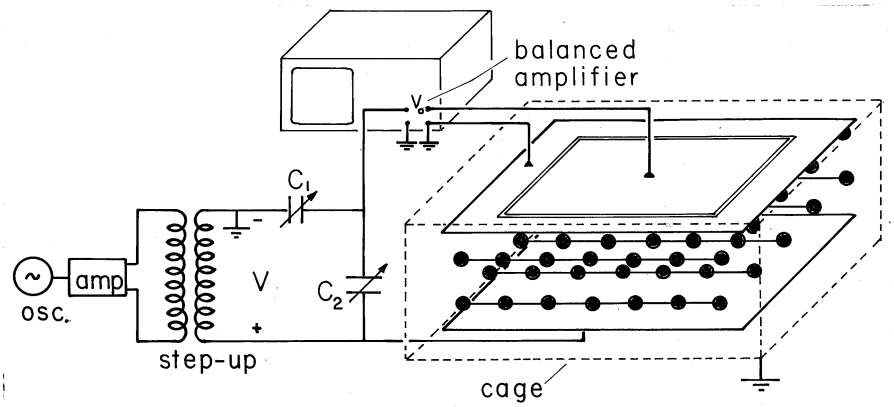


Fig. 6.6.3 Demonstration in which change in capacitance is used to measure the equivalent dielectric constant of an artificial dielectric.

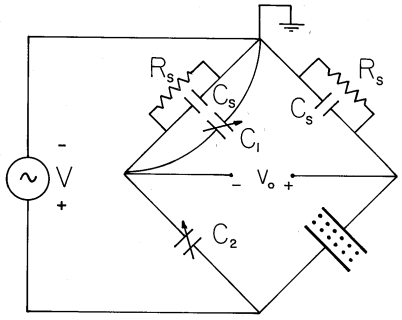


Fig. 6.6.4 Balanced amplifiers of oscilloscope, balancing capacitors, and demonstration capacitor shown in Fig. 6.6.4 comprise the elements in the bridge circuit. The driving voltage comes from the transformer, while v_o is the oscilloscope voltage.

$$|\Delta i| = \omega(\Delta C)|V| \tag{10}$$

Thus, there is a change of current through the resistance in the right leg and hence a change of voltage across that resistance given by

$$v_o = R_s\omega(\Delta C)V \tag{11}$$

Because the current through the left leg has remained the same, this change in voltage is the measured output voltage.

Typical experimental values are $R = 1.87$ cm, $s = 8$ cm, $A = (0.40)^2$ m^2, $d = 0.15$ m, $\omega = 2\pi$ (250 Hz), $R_s = 100$ kΩ and $V = 566$ v peak with a measured voltage of $v_o = 0.15$ V peak. From (4), (9), and (11), the output voltage is predicted to be 0.135 V peak.

Piece-Wise Uniform Dielectrics. So far we have only considered systems filled with uniform dielectrics, as in Fig. 6.5.1a. We turn now to the description of fields in piece-wise uniform dielectrics, as exemplified by Fig. 6.5.1b.

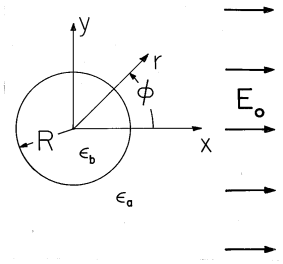


Fig. 6.6.5 Insulating rod having uniform permittivity ϵ_b surrounded by material of uniform permittivity ϵ_a. Uniform electric field is imposed by electrodes that are at "infinity."

In each of the regions of constant permittivity, the field distribution is described by Laplace's equation, (1). The field problem is attacked by solving this equation in each of the regions and then using the jump conditions to match these solutions at the surfaces of discontinuity between the dielectrics. The following example has a relatively simple solution that helps form further insights.

Example 6.6.2. Dielectric Rod in Uniform Transverse Field

A uniform electric field $E_o\mathbf{i_x}$, perhaps produced by means of a parallel plate capacitor, exists in a dielectric having permittivity ϵ_a. With its axis perpendicular to this field, a circular cylindrical dielectric rod having permittivity ϵ_b and radius R is introduced, as shown in Fig. 6.6.5. With the understanding that the electrodes are sufficiently far from the rod so that the field at "infinity" is essentially uniform, our objective is to determine and then interpret the electric field inside and outside the rod.

The shape of the circular cylindrical boundary suggests that we use polar coordinates. In these coordinates, $x = r\cos\phi$, and so the potential far from the cylinder is

$$\Phi(r \to \infty) \to -E_o r\cos\phi \tag{12}$$

Because this potential varies like the cosine of the angle, it is reasonable to attempt satisfying the jump conditions with solutions of Laplace's equation having the same ϕ dependence. Thus, outside the cylinder, the potential is assumed to take the form

$$\Phi^a = -E_o r\cos\phi + A\frac{R}{r}\cos\phi \tag{13}$$

Here the dipole field is multiplied by an adjustable coefficient A, but the uniform field has a magnitude set to match the potential at large r, (12).

Inside the cylinder, the solution with a $1/r$ dependence cannot be accepted because it becomes singular at the origin. Thus, the only solution having the cosine dependence on ϕ is a uniform field, with the potential

$$\Phi_b = B\frac{r}{R}\cos\phi \tag{14}$$

Can the coefficients A and B be adjusted to satisfy the two jump conditions implied by the laws of Gauss and Faraday, (6.5.3) and (6.5.4), at $r = R$?

$$\epsilon_a E_r^a - \epsilon_b E_r^b = 0 \tag{15}$$

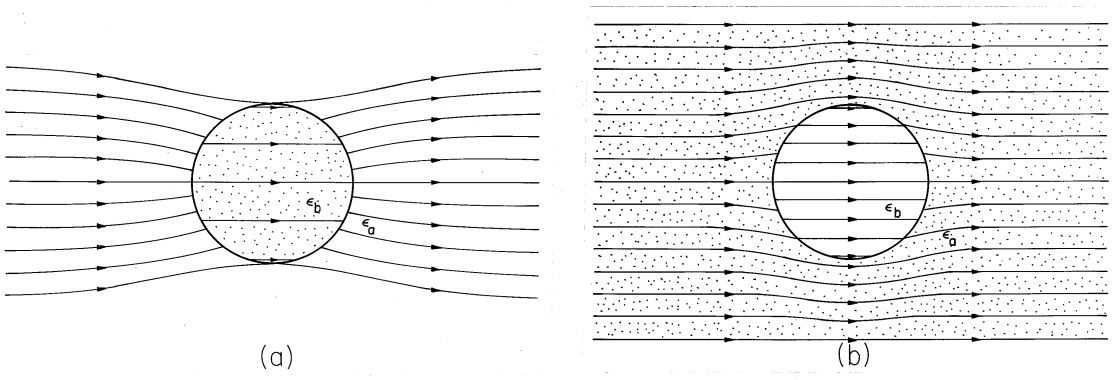


Fig. 6.6.6 Electric field intensity in and around dielectric rod of Fig. 6.6.5 for (a) $\epsilon_b > \epsilon_a$ and (b) $\epsilon_b \leq \epsilon_a$.

$$\Phi^a - \Phi^b = 0 \tag{16}$$

Substitution of (13) and (14) into these conditions shows that the answer is yes. Continuity of potential, (16), requires that

$$(-E_o R + A)\cos\phi = B\cos\phi \tag{17}$$

while continuity of normal $\mathbf{D}$, (15), is satisfied if

$$\Big(-\epsilon_a E_o - \epsilon_a \frac{A}{R}\Big)\cos\phi = \frac{\epsilon_b B}{R}\cos\phi \tag{18}$$

Note that these conditions contain the $\cos\phi$ dependence on both sides, and so can be satisfied at each angle ϕ. This confirms the correctness of the originally assumed ϕ dependence of our solutions. Simultaneous solution of (17) and (18) for A and B gives

$$A = \frac{\epsilon_b - \epsilon_a}{\epsilon_b + \epsilon_a} E_o R \tag{19}$$

$$B = \frac{-2\epsilon_a}{\epsilon_b + \epsilon_a} E_o R \tag{20}$$

Introducing these values of the coefficients into the potentials, (13) and (14), gives

$$\Phi_a = -RE_o\cos\phi\left[\Big(\frac{r}{R}\Big) - \Big(\frac{R}{r}\Big)\frac{(\epsilon_b - \epsilon_a)}{(\epsilon_b + \epsilon_a)}\right] \tag{21}$$

$$\Phi_b = \frac{-2\epsilon_a}{\epsilon_b + \epsilon_a} E_o r\cos\phi \tag{22}$$

The electric field is obtained as the gradient of this potential.

$$\mathbf{E}^a = E_o\left\{\mathbf{i}_\mathbf{r}\cos\phi\left[1 + \Big(\frac{R}{r}\Big)^2\frac{(\epsilon_b - \epsilon_a)}{(\epsilon_b + \epsilon_a)}\right] - \mathbf{i}_\phi\sin\phi\left[1 - \Big(\frac{R}{r}\Big)^2\frac{(\epsilon_b - \epsilon_a)}{\epsilon_b + \epsilon_a}\right]\right\} \tag{23}$$

$$\mathbf{E}^b = \frac{2\epsilon_a}{\epsilon_b + \epsilon_a} E_o(\mathbf{i}_\mathbf{r}\cos\phi - \mathbf{i}_\phi\sin\phi) \tag{24}$$

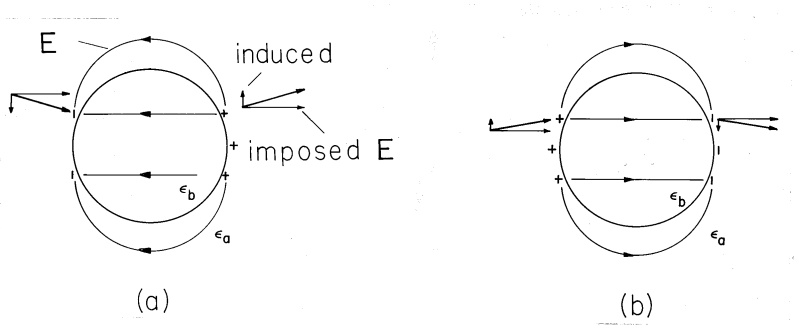


Fig. 6.6.7 Surface polarization charge density responsible for distortion of fields as shown in Fig. 6.6.6. (a) $\epsilon_b > \epsilon_a$, (b) $\epsilon_a > \epsilon_b$.

The electric field intensity given by these expressions is shown in Fig. 6.6.6. If the cylinder has the higher dielectric constant, as would be the case for a dielectric rod in air, the lines of electric field intensity tend to concentrate in the rod. In the opposite case– for example, representing a cylindrical void in a dielectric– the field lines tend to skirt the cylinder.

With an understanding of the relationship between the electric field intensity and the induced polarization charge comes the ability to see in advance how dielectrics distort the electric field. The circular cylindrical dielectric rod introduced into a uniform tranverse electric field in Example 6.6.2 serves as an illustration. Without carrying out the detailed analysis which led to (23) and (24), could we see in advance that the electric field has the distribution illustrated in Fig. 6.6.6?

The induced polarization charge provides the sources for the field induced by polarized material. For piece-wise uniform dielectrics, this is a polarization surface charge, given by (6.5.11).

$$\sigma_{sp} = \mathbf{n} \cdot \epsilon_o \mathbf{E}^a \big(1 - \frac{\epsilon_a}{\epsilon_b}\big) \tag{25}$$

The electric field intensity in the cylindrical rod example is generally directed to the right. It follows from (25) that the distribution of surface polarization charge at the cylindrical interface is as illustrated in Fig. 6.6.7. With the rod having the higher permittivity, Fig. 6.6.7a, the induced positive polarization surface charge density is at the right and the negative surface charge is at the left. These charges give rise to fields that generally originate at the positive charge and terminate at the negative. Thus, it is clear without any analysis that if $\epsilon_b > \epsilon_a$, the induced field inside tends to cancel the imposed field. In this case, the interior field is decreased or "depolarized." In the exterior region, vector addition of the induced field to the right-directed imposed field shows that incoming field lines at the left must be deflected inward, while outgoing ones at the right are deflected outward.

These same ideas, applied to the case where $\epsilon_a > \epsilon_b$, show that the interior field is increased while the exterior one tends to be ducted around the cylinder.

The circular cylinder is one of a series of examples having exact solutions. These give the opportunity to highlight the physical phenomena without encumbering mathematics. If it is actually necessary to account for detailed geometry,

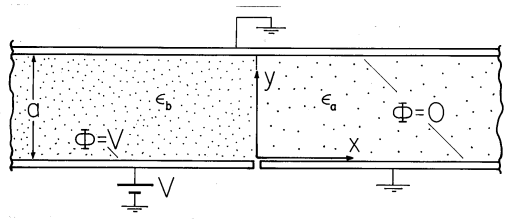


Fig. 6.6.8 Grounded upper electrode and lower electrode extending from $x = 0$ to $x \to \infty$ form plane parallel capacitor with fringing field that extends into the region $0 < x$ between grounded electrodes.

then some of the approaches introduced in Chaps. 4 and 5 can be used. The following example illustrates the use of the orthogonal modes approach introduced in Sec. 5.5.

Example 6.6.3. Fringing Field of Dielectric Filled Parallel Plate Capacitor

Fields are to be determined in the planar region between a grounded conductor in the plane $y = a$ and a pair of conductors in the plane $y = 0$, shown in Fig. 6.6.8. To the right of $x = 0$ in the $y = 0$ plane is a second grounded conductor. To the left of $x = 0$ in this same plane is an electrode at the potential V. The regions to the right and left of the plane $x = 0$ are, respectively, filled with uniform dielectrics having permittivities ϵ_a and ϵ_b. Under the assumption that the system extends to infinity in the $\pm x$ and $\pm z$ directions, we now determine the fringing fields in the vicinity of the interface between dielectrics.

Our approach is to write solutions to Laplace's equation in the respective regions that satisfy the boundary conditions in the planes $y = 0$ and $y = a$ and as $x \to \pm\infty$. These are then matched up by the jump conditions at the interface between dielectrics.

Consider first the region to the right, where $\Phi = 0$ in the planes $y = 0$ and $y = a$ and goes to zero as $x \to \infty$. From Table 5.4.1, we select the infinite set of solutions

$$\Phi^a = \sum_{n=1}^{\infty} A_n e^{-\frac{n\pi}{a}x} \sin\frac{n\pi}{a}y \tag{26}$$

Here we have set $k = n\pi/a$ so that the sine functions are zero at each of the boundaries.

In the region to the left, the field is uniform in the limit $x \to -\infty$. This suggests writing the solution as the sum of a "particular" part meeting the "inhomogeneous part" of the boundary condition and a homogeneous part that is zero on each of the boundaries.

$$\Phi^b = -V\Big(\frac{y}{a} - 1\Big) + \sum_{n=1}^{\infty} B_n e^{\frac{n\pi}{a}x} \sin\frac{n\pi}{a}y \tag{27}$$

The coefficients A_n and B_n must now be adjusted so that the jump conditions are met at the interface between the dielectrics, where $x = 0$. First, consider the jump condition on the potential, (6.5.4). Evaluated at $x = 0$, (26) and (27) must give the same potential regardless of y.

$$\Phi^a\Big|_{x=0} = \Phi^b\Big|_{x=0} \Rightarrow \sum_{n=1}^{\infty} A_n \sin\frac{n\pi}{a}y = -V\Big(\frac{y}{a} - 1\Big) + \sum_{n=1}^{\infty} B_n \sin\frac{n\pi}{a}y \tag{28}$$

To satisfy this relation at each value of y, expand the linear potential distribution on the right in a series of the same form as the other two terms.

$$-V\left(\frac{y}{a}-1\right)=\sum_{n=1}^{\infty}V_n\sin\frac{n\pi}{a}y \tag{29}$$

Multiplication of both sides by $\sin(m\pi y/a)$ and integration from $y=0$ to $y=a$ gives only one term on the right and an integral that can be carried out on the left. Hence, we can solve for the coefficients V_n in (29).

$$\int_0^a -V\left(\frac{y}{a}-1\right)\sin\frac{m\pi}{a}ydy=\frac{aV_m}{2}\Rightarrow V_n=\frac{2V}{n\pi} \tag{30}$$

Thus, the series provided by (29) and (30) can be substituted into (28) to obtain an expression with each term a sum over the same type of series.

$$\sum_{n=1}^{\infty}A_n\sin\frac{n\pi}{a}y=\sum_{n=1}^{\infty}\frac{2V}{n\pi}\sin\frac{n\pi}{a}y+\sum_{n=1}^{\infty}B_n\sin\frac{n\pi}{a}y \tag{31}$$

This expression is satisfied if the coefficients of the like terms are equal. Thus, we have

$$A_n=\frac{2V}{n\pi}+B_n \tag{32}$$

To make the normal component of $\mathbf{D}$ continuous at the interface,

$$\begin{aligned}-\epsilon_a\frac{\partial\Phi^a}{\partial x}\Big|_{x=0}=-\epsilon_b\frac{\partial\Phi^b}{\partial x}\Big|_{x=0}\Rightarrow\sum_{n=1}^{\infty}\epsilon_a\frac{n\pi}{a}A_n\sin\frac{n\pi}{a}y\\ =-\sum_{n=1}^{\infty}\epsilon_b\frac{n\pi}{a}B_n\sin\frac{n\pi}{a}y\end{aligned} \tag{33}$$

and a second relation between the coefficients results.

$$\epsilon_aA_n=-\epsilon_bB_n \tag{34}$$

The coefficients A_n and B_n are now determined by simultaneously solving (32) and (34). These are substituted into the original expressions for the potential, (26) and (27), to give the desired potential distribution.

$$\Phi^a=\sum_{n=1}^{\infty}\frac{2V}{n\pi\left(1+\frac{\epsilon_a}{\epsilon_b}\right)}e^{-\frac{n\pi}{a}x}\sin\frac{n\pi}{a}y \tag{35}$$

$$\Phi^b=-V\left(\frac{y}{a}-1\right)-\sum_{n=1}^{\infty}\frac{2}{n\pi}\frac{\epsilon_a}{\epsilon_b}\frac{V}{\left(1+\frac{\epsilon_a}{\epsilon_b}\right)}e^{\frac{n\pi}{a}x}\sin\frac{n\pi}{a}y \tag{36}$$

These potential distributions, and sketches of the associated fields, are illustrated in Fig. 6.6.9. Shown first is the uniform dielectric. Laplace's equation prevails throughout, even at the "interface." Far to the left, we know that the potential is

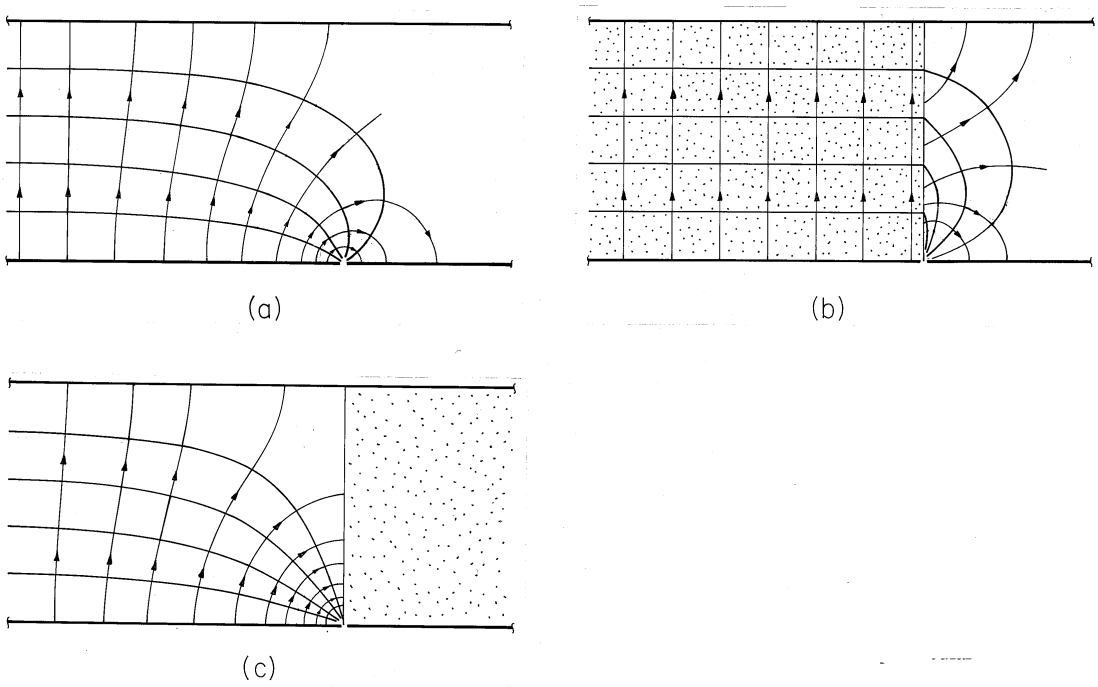


Fig. 6.6.9 Equipotentials and field lines for configuration of Fig. 6.6.8. (a) Fringing for uniform dielectric. (b) With high permittivity material between capacitor plates, field inside tends to become tangential to the interface and uniform throughout the region to the left. (c) With high permittivity material outside the region between the capacitor plates, the field inside tends to be perpendicular to the interface.

linear in y, and hence represented by the equally spaced parallel straight lines. These lines must end at other points on the bounding surface having the same potential. The only place where this is possible is in the singular region at the origin where the potential makes an abrupt change from V to 0. These observations provide a starting point in sketching the field lines.

Shown next is the field distribution in the limit where the permittivity between the capacitor plates (to the left) is very large compared to that outside. As is clear by taking the limit $\epsilon_a/\epsilon_b \to 0$ in (36), the field inside the capacitor tends to be uniform right up to the edge of the capacitor. The dielectric effectively ducts the electric field. As far as the field inside the capacitor is concerned, there tends to be no normal component of $\mathbf{E}$.

In the opposite extreme, where the region to the right has a high permittivity compared to that between the capacitor plates, the electric field inside the capacitor tends to approach the interface normally. As far as the potential to the left is concerned, the interface is an equipotential.

In Chap. 9, we find that magnetization and polarization phenomena are analogous. There we delve further into approximations on magnetic field distributions in the presence of magnetizable materials that can just as well be used to understand systems of piece-wise uniform dielectrics.

6.7 SMOOTHLY INHOMOGENEOUS ELECTRICALLY LINEAR DIELECTRICS

The potential distribution in a dielectric that is free of unpaired charge and which has a space-varying permittivity is governed by

$$\nabla \cdot \epsilon \nabla \Phi = 0 \tag{1}$$

This is (6.5.1) combined with (6.5.2) and with $\rho_u = 0$. The contribution of the spatially varying permittivity is emphasized by using the vector identity for the divergence of a scalar (ϵ) times a vector ($\nabla\Phi$).

$$\nabla^2 \Phi + \nabla \Phi \cdot \frac{\nabla \epsilon}{\epsilon} = 0 \tag{2}$$

With a spatially varying permittivity, polarization charge is induced in proportion to the component of $\mathbf{E}$ that is in the direction of the gradient in ϵ. Thus, in general, the potential is not a solution to Laplace's equation.

Equation (2) gives a different perspective to the approach taken in dealing with piece-wise uniform systems. In Sec. 6.6, the polarization charge density represented by the $\nabla\epsilon$ term in (2) is confined to interfaces and accounted for by jump conditions. Thus, the section was a variation on the theme of Laplace's equation. The theme of this section broadens the developments of Sec. 6.6.

It is the objective in this section to demonstrate how familiar methods are adapted to dealing with unfamiliar laws. In general, (2) has spatially varying coefficients. Thus, even though it is linear, we are not guaranteed simple closed-form solutions. However, if the spatial dependence of ϵ is exponential, the equation does have constant coefficients and simple solutions. Our example exploits this fact.

Example 6.7.1. Fields in an Exponentially Varying Dielectric

A dielectric has a permittivity that varies exponentially in the y direction, as illustrated in Fig. 6.7.1a.

$$\epsilon = \epsilon(y) = \epsilon_p e^{-\beta y} \tag{3}$$

Here ϵ_p and β are given constants.

In this example, the dielectric fills the rectangular region shown in Fig. 6.7.1b. This configuration is familiar from Sec. 5.5. The fields are two dimensional, $\Phi = 0$ at $x = 0$ and $x = a$ and $y = 0$. The potential on the "last" surface, where $y = b$, is $v(t)$.

It follows from (3) that

$$\nabla \Phi \cdot \frac{\nabla \epsilon}{\epsilon} = -\beta \frac{\partial \Phi}{\partial y} \tag{4}$$

and (2) becomes

$$\frac{\partial^2 \Phi}{\partial x^2} + \frac{\partial^2 \Phi}{\partial y^2} - \beta \frac{\partial \Phi}{\partial y} = 0 \tag{5}$$

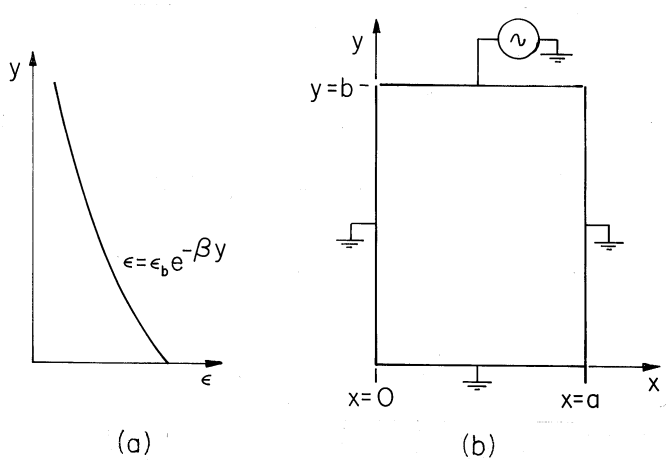


Fig. 6.7.1 (a) Smooth permittivity distribution of material enclosed by (b) zero potential boundaries at $x = 0$, $x = a$, and $y = 0$, and electrode at potential v at $y = b$.

The dielectric fills a region having boundaries that are natural in Cartesian coordinates. Thus, we look for product solutions having the form $\Phi = X(x)Y(y)$. Substitution into (5) gives

$$\frac{1}{Y}\left(\frac{d^2Y}{dy^2} - \frac{1}{\beta}\frac{dY}{dy}\right) + \frac{1}{X}\frac{d^2X}{dx^2} = 0 \tag{6}$$

The first term, a function of y alone, must sum with the function of x alone to give zero. Thus, the first is set equal to the separation coefficient k^2 and the second equal to $-k^2$.

$$\frac{d^2X}{dx^2} + k^2X = 0 \tag{7}$$

$$\frac{d^2Y}{dy^2} - \beta\frac{dY}{dy} - k^2Y = 0 \tag{8}$$

This assignment of sign for the separation coefficient is motivated by the requirement that $\Phi = 0$ at two locations. This results in periodic solutions for (7).

$$X = \begin{cases} \sin kx \\ \cos kx \end{cases} \tag{9}$$

Because it also has constant coefficients, the solutions to (8) are exponentials. Substitution of $\exp(py)$ shows that

$$p = \frac{\beta}{2} \pm \sqrt{\left(\frac{\beta}{2}\right)^2 + k^2} \tag{10}$$

and it follows that solutions are linear combinations of two exponentials.

$$Y = e^{\frac{\beta}{2}y}\begin{bmatrix} \cosh\sqrt{\left(\frac{\beta}{2}\right)^2 + k^2}\, y \\ \sinh\sqrt{\left(\frac{\beta}{2}\right)^2 + k^2}\, y \end{bmatrix} \tag{11}$$

For the specific problem at hand, we look for the products of these sets of solutions that satisfy the homogeneous boundary conditions. Those at $x = 0$ and $x = a$ are met by making $k = n\pi/a$, with n an integer. The origin of the y axis was made to coincide with the third zero potential boundary so that the hyperbolic sine function could be used. Thus, we arrive at an infinite series of solutions, each satisfying the homogeneous boundary conditions.

$$\Phi = \sum_{n=1}^{\infty} A_n e^{\frac{\beta}{2}y} \sinh \sqrt{\left(\frac{\beta}{2}\right)^2 + \left(\frac{n\pi}{a}\right)^2}\, y \sin\left(\frac{n\pi}{a}x\right) \tag{12}$$

The assignment of the coefficients so that the potential constraint at $y = b$ is met follows the procedure familiar from Sec. 5.5.

$$\Phi = \sum_{\substack{n=1 \\ \text{odd}}}^{\infty} \frac{4v}{n\pi} e^{\frac{\beta}{2}(y-b)} \frac{\sinh \sqrt{\left(\frac{\beta}{2}\right)^2 + \left(\frac{n\pi}{a}\right)^2}\, y}{\sinh \sqrt{\left(\frac{\beta}{2}\right)^2 + \left(\frac{n\pi}{a}\right)^2}\, b} \sin\left(\frac{n\pi}{a}x\right) \tag{13}$$

For interpretation of (13), suppose that β is positive so that ϵ decreases with y, as illustrated in Fig. 6.7.1a. Without the analysis, we know that the lines of $\mathbf{D}$ originate on the electrode at $y = b$ and terminate on the zero potential walls. This means that E lines either terminate on the grounded walls or on polarization charges induced in the volume. If $v > 0$, we can see from (6.5.9) that because $\mathbf{E} \cdot \nabla\epsilon$ is positive, the induced polarization charge density must be negative. Thus, some of the E lines terminate on this negative charge density and it comes as no surprise that we have found a potential that decays away from the excitation electrode at $y = b$ at a rate that is faster than if the potential were governed by Laplace's equation. The electric field is effectively shielded out of the lower region of higher permittivity by the induced polarization charge.

One approach to determining fields in spatially varying dielectrics is suggested in Fig. 6.7.2. The smooth distribution has been approximated by "stair steps." Physically, the equivalent system consists of uniform layers. Thus, the fields revert to the solutions of Laplace's equation matched to each other at the interfaces by the jump conditions. According to (6.5.11), E lines originating at $y = b$ and passing downward through these interfaces will induce positive surface polarization charge. Thus, replacing the smoothly varying dielectric with the layers of uniform dielectric is equivalent to representing the volume polarization charge density by a distribution of surface polarization charges.

6.8 SUMMARY

Table 6.8.1 is useful both as an outline of this chapter and as a reference. Gauss' theorem is the basis for deriving the surface relations in the right-hand column from the respective volume relations in the left-hand column. By remembering the volume relations, one is able to recall the surface relations.

Our first task, in Sec. 6.1, was to introduce the polarization density as a way of representing the polarization charge density. The first volume and surface

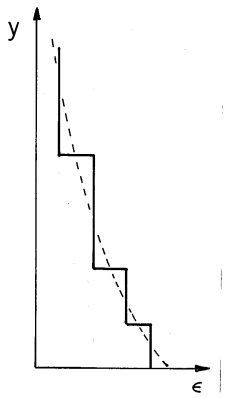


Fig. 6.7.2 Stair-step distribution of permittivity approximating smooth distribution.

relations resulted. These are deceptively similar in appearance to Gauss' law and the associated jump condition. However, they are not electric field laws. Rather, they simply relate the volume and surface sources representing the material to the polarization density.

Next we considered the fields due to permanently polarized materials. The polarization density was given. For this purpose, Gauss' law and the associated jump condition were conveniently written as (6.2.2) and (6.2.3), respectively.

With the polarization induced by the field itself, it was convenient to introduce the displacement flux density $\mathbf{D}$ and write Gauss' law and the jump condition as (6.2.15) and (6.2.16). In particular, for linear polarization, the equivalent constitutive laws of (6.4.2) and (6.4.3) were introduced.

The theme of this chapter has been the determination of EQS fields when the polarization charge density makes a contribution. In cases where the polarization density is given, this is easy to keep in mind, because the first step in formulating a problem is to evaluate ρ_p from the given $\mathbf{P}$. However, when ρ_p is induced, variables such as $\mathbf{D}$ are used and we must be reminded that when all is said and done, ρ_p (or its surface counterpart, σ_{sp}) is still responsible for the effect of the material on the field. The expressions for ρ_p and σ_{sp} given by the last two relations in the table are useful not only for interpreting the distributions of fields after they have been found but for forming an impression of the fields in complex systems where it would not be worthwhile to find an analytic solution. Remember that these relations hold only in regions where there is no unpaired charge density.

In Chap. 9, we will find that most of this chapter is directly applicable to the description of magnetization. There we will continue to develop insights that will be equally applicable to the polarization phenomena of this chapter.

TABLE 6.8.1

SUMMARY OF POLARIZATION RELATIONS AND LAWS

Polarization Charge Density and Polarization Density			
$\rho_p = -\nabla \cdot \mathbf{P}$	(6.1.6)	$\sigma_{sp} = -\mathbf{n} \cdot (\mathbf{P}^a - \mathbf{P}^b)$	6.1.7)
Gauss' Law with Polarization			
$\nabla \cdot \epsilon_o \mathbf{E} = \rho_p + \rho_u$	(6.2.1)	$n \cdot \epsilon_o(\mathbf{E}^a - \mathbf{E}^b) = \sigma_{sp} + \sigma_{su}$	(6.2.3)
$\nabla \cdot \mathbf{D} = \rho_u$	(6.2.15)	$n \cdot (\mathbf{D}^a - \mathbf{D}^b) = \sigma_{su}$	(6.2.16)
where			
$\mathbf{D} \equiv \epsilon_o \mathbf{E} + \mathbf{P}$	(6.2.14)		
Electrically Linear Polarization			
Constitutive Law			
$\mathbf{P} = \epsilon_o \chi_e \mathbf{E} = (\epsilon - \epsilon_o)\mathbf{E}$	(6.4.2)		
$\mathbf{D} = \epsilon \mathbf{E}$	(6.4.3)		
Source Distribution, $\rho_u = 0$			
$\rho_p = -\frac{\epsilon_o}{\epsilon} \mathbf{E} \cdot \nabla \epsilon$	(6.5.9)	$\sigma_{sp} = \mathbf{n} \cdot \epsilon_o \mathbf{E}^a \left(1 - \frac{\epsilon_a}{\epsilon_b}\right)$	(6.5.11)

PROBLEMS

6.1 Polarization Density

6.1.1 The layer of polarized material shown in cross-section in Fig. P6.1.1, having thickness d and surfaces in the planes $y = d$ and $y = 0$, has the polarization density $\mathbf{P} = P_o \cos \beta x (\mathbf{i_x} + \mathbf{i_y})$.

(a) Determine the polarization charge density throughout the slab.

(b) What is the surface polarization charge density on the layer surfaces?

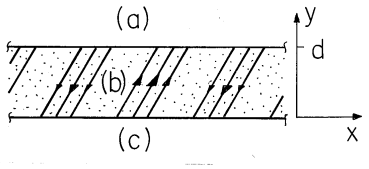


Fig. P6.1.1

6.2 Laws and Continuity Conditions with Polarization

6.2.1 For the polarization density given in Prob. 6.1.1, with $P_o(t) = P_o \cos\omega t$:

(a) Determine the polarization current density and polarization charge density.
(b) Using $\mathbf{J}_p$ and ρ_p, show that the differential charge conservation law, (10), is indeed satisfied.

6.3 Permanent Polarization

6.3.1* A layer of permanently polarized material is sandwiched between plane parallel perfectly conducting electrodes in the planes $x = 0$ and $x = a$, respectively, having potentials $\Phi = 0$ and $\Phi = -V$. The system extends to infinity in the $\pm y$ and $\pm z$ directions.

(a) Given that $\mathbf{P} = P_o \cos\beta x \mathbf{i}_\mathbf{x}$, show that the potential between the electrodes is

$$\Phi = \frac{P_o}{\beta\epsilon_o}(\sin\beta x - \frac{x}{a}\sin\beta a) - \frac{Vx}{a} \qquad (a)$$

(b) Given that $\mathbf{P} = P_o \cos\beta y \mathbf{i}_\mathbf{y}$, show that the potential between the electrodes is

$$\Phi = \frac{P_o}{\beta\epsilon_o}\sin\beta y\left[1 - \frac{\cosh\beta(x - a/2)}{\cosh(\beta a/2)}\right] - \frac{Vx}{a} \qquad (b)$$

6.3.2 The cross-section of a configuration that extends to infinity in the $\pm z$ directions is shown in Fig. P6.3.2. What is the potential distribution inside the cylinder of rectangular cross-section?

6.3.3* A polarization density is given in the semi-infinite half-space $y < 0$ to be $\mathbf{P} = P_o \cos[(2\pi/\Lambda)x]\mathbf{i}_\mathbf{y}$. There are no other field sources in the system and P_o and Λ are given constants.

(a) Show that $\rho_p = 0$ and $\sigma_{sp} = P_o \cos(2\pi x/\Lambda)$.

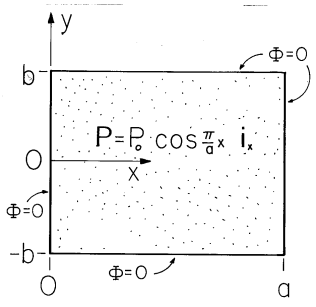


Fig. P6.3.2

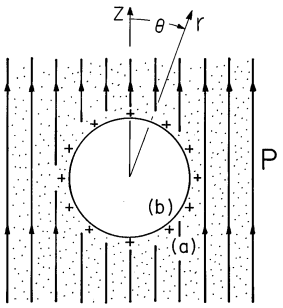


Fig. P6.3.5

(b) Show that

$$\Phi = \frac{P_o \Lambda}{4\epsilon_o \pi} \cos(2\pi x/\Lambda) \exp(\mp 2\pi y/\Lambda); \qquad y \gtrless 0 \qquad (a)$$

6.3.4 A layer in the region $-a < y < 0$ has the polarization density $\mathbf{P} = P_o \mathbf{i_y} \sin \beta(x - x_o)$. In the planes $y = \pm a$, the potential is constrained to be $\Phi = V \cos \beta x$, where P_o, β and V are given constants. The region $0 < y < a$ is free space and the system extends to infinity in the $\pm x$ and $\pm z$ directions. Find the potential in regions (a) and (b) in the free space and polarized regions, respectively. (If you have already solved Prob. 5.6.12, you can solve this problem by inspection.)

6.3.5* Figure P6.3.5 shows a material having the uniform polarization density $\mathbf{P} = P_o \mathbf{i_z}$, with a spherical cavity having radius R. On the surface of the cavity is a uniform distribution of unpaired charge having density $\sigma_{su} = \sigma_o$. The interior of the cavity is free space, and P_o and σ_o are given constants. The potential far from the cavity is zero. Show that the electric potential is

$$\Phi = \begin{cases} -\frac{P_o}{3\epsilon_o} r \cos\theta + \frac{\sigma_o R}{\epsilon_o}; & r \leq R \\ -\frac{P_o R^3}{3\epsilon_o r^2} \cos\theta + \frac{\sigma_o R^2}{\epsilon_o r}; & r \geq R \end{cases} \qquad (a)$$

6.3.6 The cross-section of a groove (shaped like a half-cylinder having radius R) cut from a uniformly polarized material is shown in Fig. P6.3.6. The

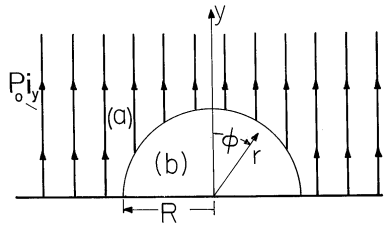


Fig. P6.3.6

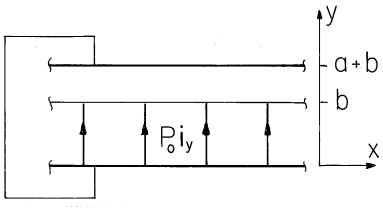


Fig. P6.3.7

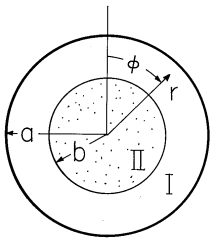


Fig. P6.3.8

material rests on a grounded perfectly conducting electrode at $y = 0$, and P_o is a given constant. Assume that the configuration extends to infinity in the y direction and find Φ in regions (a) and (b), respectively, outside and inside the groove.

6.3.7 The system shown in cross-section in Fig. P6.3.7 extends to infinity in the $\pm x$ and $\pm z$ directions. The electrodes at $y = 0$ and $y = a + b$ are shorted. Given P_o and the dimensions, what is $\mathbf{E}$ in regions (a) and (b)?

6.3.8* In the two-dimensional configuration shown in Fig. P6.3.8, a perfectly conducting circular cylindrical electrode at $r = a$ is grounded. It is coaxial with a rotor of radius b which supports the polarization density $\mathbf{P} = \nabla[P_o r \cos(\phi - \alpha)]$.

(a) Show that the polarization charge density is zero inside the rotor.
(b) Show that the potential functions Φ^I and Φ^{II} respectively in the regions outside and inside the rotor are

$$\Phi^I = \frac{P_o b^2}{2\epsilon_o}\left(\frac{1}{r} - \frac{r}{a^2}\right)\cos(\phi - \alpha) \qquad (a)$$

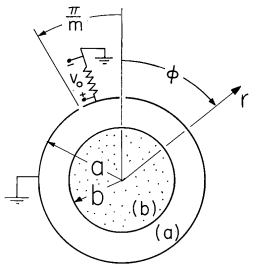


Fig. P6.3.9

$$\Phi^{II} = \frac{P_o(a^2 - b^2)}{2\epsilon_o a^2} r\cos(\phi - \alpha) \qquad (b)$$

(c) Show that if $\alpha = \Omega t$, where Ω is an angular velocity, the field rotates in the ϕ direction with this angular velocity.

6.3.9 A circular cylindrical material having radius b has the polarization density $\mathbf{P} = \nabla[P_o(r^{m+1}/b^m)\cos m\phi]$, where m is a given positive integer. The region $b < r < a$, shown in Fig. P6.3.9, is free space.

(a) Determine the volume and surface polarization charge densities for the circular cylinder.

(b) Find the potential in regions (a) and (b).

(c) Now the cylinder rotates with the constant angular velocity Ω. Argue that the resulting potential is obtained by replacing $\phi \rightarrow (\phi - \Omega t)$.

(d) A section of the outer cylinder is electrically isolated and connected to ground through a resistance R. This resistance is low enough so that, as far as the potential in the gap is concerned, the potential of the segment can still be taken as zero. However, as the rotor rotates, the charge induced on the segment is time varying. As a result, there is a current through the resistor and hence an output signal v_o. Assume that the segment subtends an angle π/m and has length l in the z direction, and find v_o.

6.3.10* Plane parallel electrodes having zero potential extend to infinity in the $x-z$ planes at $y = 0$ and $y = d$.

(a) In a first configuration, the region between the electrodes is free space, except for a segmented electrode in the plane $x = 0$ which constrains the potential there to be $V(y)$. Given $V(y)$, what is the potential distribution in the regions $0 < x$ and $x < 0$, regions (a) and (b), respectively?

(b) Now the segmented electrode is removed and the region $x < 0$ is filled with a permanently polarized material having $\mathbf{P} = P_o\mathbf{i_x}$, where P_o is a given constant. What continuity conditions must the potential satisfy in the $x = 0$ plane?

(c) Show that the potential is given by

$$\Phi = \frac{dP_o}{\epsilon_o} \sum_{n=1}^{\infty} \frac{[1-(-1)^n]}{(n\pi)^2} \sin \frac{n\pi}{d} y \exp\left(\mp \frac{n\pi}{d} x\right); \qquad x \gtrless 0 \qquad (a)$$

(The method used here to represent Φ is used in Example 6.6.3.)

6.3.11 In Prob. 6.1.1, there is a perfect conductor in the plane $y = 0$ and the region $d < y$ is free space. What are the potentials in regions (a) and (b), the regions where $d < y$ and $0 < y < d$, respectively?

6.4 Polarization Constitutive Laws

6.4.1 Suppose that a solid or liquid has a mass density of $\rho = 10^3 kg/m^3$ and a molecular weight of $M_o = 18$ (typical of water). [The number of molecules per unit mass is Avogadro's number ($A_o = 6.023 \times 10^{26}$ molecules/kg-mole) divided by M_o.] This material has a permittivity $\epsilon = 2\epsilon_o$ and is subject to an electric field intensity $E = 10^7 v/m$ (approaching the highest field strength that can be sustained without breakdown on scales of a centimeters in liquids and solids). Assume that each molecule has a polarization $q\mathbf{d}$ where $q = e = 1.6 \times 10^{-19}$ C, the charge of an electron). What is $|d|$?

6.5 Fields in the Presence of Electrically Linear Dielectrics

6.5.1* The plane parallel electrode configurations of Fig. P6.5.1 have in common the fact that the linear dielectrics have dielectric "constants" that are functions of x, $\epsilon = \epsilon(x)$. The systems have depth c in the z direction.

(a) Show that regardless of the specific functional dependence on x, $\mathbf{E}$ is uniform and simply $\mathbf{i_y} v/d$.

(b) For the system of Fig. P6.5.1a, where the dielectric is composed of uniform regions having permittivities ϵ_a and ϵ_b, show that the capacitance is

$$C = \frac{c}{d}(\epsilon_b b + \epsilon_a a) \qquad (a)$$

(c) For the smoothly inhomogeneous capacitor of Fig. P6.5.1b, $\epsilon = \epsilon_o(1 + x/l)$. Show that

$$C = \frac{3\epsilon_o c l}{2d} \qquad (b)$$

6.5.2 In the configuration shown in Fig. P6.5.1b, what is the capacitance C if $\epsilon = \epsilon_a(1 + \alpha \cos \beta x)$, where $0 < \alpha < 1$ and β are given constants?

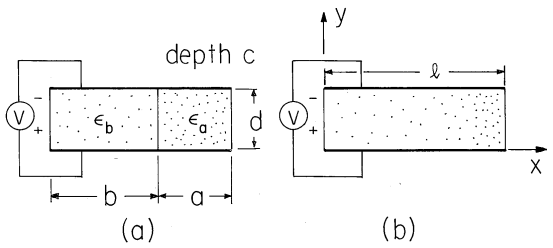


Fig. P6.5.1

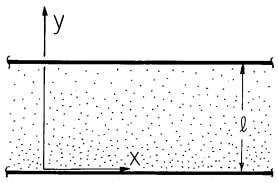


Fig. P6.5.3

6.5.3* The region of Fig. P6.5.3 between plane parallel perfectly conducting electrodes in the planes $y = 0$ and $y = l$ is filled by a uniformly inhomogeneous dielectric having permittivity $\epsilon = \epsilon_o[1+\chi_a(1+y/l)]$. The electrode at $y = 0$ has potential v relative to that at $y = l$. The electrode separation l is much smaller than the dimensions of the system in the x and z directions, so the fields can be regarded as not depending on x or z.

(a) Show that D_y is independent of y.
(b) With the electrodes having area A, show that the capacitance is

$$C = \frac{\epsilon_o A}{l}\chi_a / ln\Big[\frac{1+2\chi_a}{1+\chi_a}\Big] \qquad (a)$$

6.5.4 The dielectric in the system of Prob. 6.5.3 is replaced by one having permittivity $\epsilon = \epsilon_p \exp(-y/d)$, where ϵ_p is constant. What is the capacitance C?

6.5.5 In the two configurations shown in cross-section in Fig. P6.5.5, circular cylindrical conductors are used to make coaxial capacitors. In Fig. P6.5.5a, the linear dielectric has a wedge shape with interfaces with the free space region that are surfaces of constant ϕ. In Fig. P6.5.5b, the interface is at $r = R$.

(a) Determine $\mathbf{E}(\mathbf{r})$ in regions (1) and (2) in each configuration, showing that simple fields satisfy all boundary conditions on the electrode surfaces and at the interfaces between dielectric and free space.
(b) For lengths l in the z direction, what are the capacitances?

6.5.6* For the configuration of Fig. P6.5.5a, the wedge-shaped dielectric is replaced by one that fills the gap (over all ϕ as well as over the radius

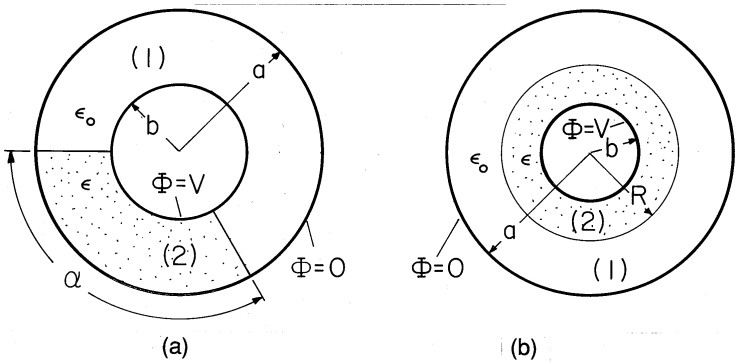


Fig. P6.5.5

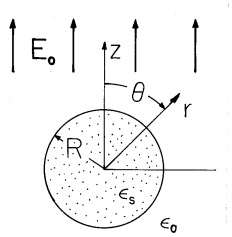


Fig. P6.6.1

$b < r < a$) with material having the permittivity $\epsilon = \epsilon_a + \epsilon_b \cos^2 \phi$, where ϵ_a and ϵ_b are constants. Show that the capacitance is

$$C = (2\epsilon_a + \epsilon_b)\pi l / ln(a/b) \tag{a}$$

6.6 Piece-Wise Uniform Electrically Linear Dielectrics

6.6.1* An insulating sphere having radius R and uniform permittivity ϵ_s is surrounded by free space, as shown in Fig. P6.6.1. It is immersed in an electric field $E_o(t)\mathbf{i_z}$ that, in the absence of the sphere, is uniform.

(a) Show that the potential is

$$\Phi = E_o(t) \begin{cases} -r\cos\theta + R^3 A \frac{\cos\theta}{r^2}; & R < r \\ Br\cos\theta; & r < R \end{cases} \tag{a}$$

where $A = (\epsilon_s - \epsilon_o)/(\epsilon_s + 2\epsilon_o)$ and $B = -3\epsilon_o/(\epsilon_s + 2\epsilon_o)$.

(b) Show that, in the limit where $\epsilon_s \to \infty$, the electric field intensity tangential to the surface of the sphere goes to zero. Thus, the surface becomes an equipotential.

(c) Show that the same solution is obtained for the potential outside the sphere as in the limit $\epsilon_s \to \infty$ if this boundary condition is used at the outset.

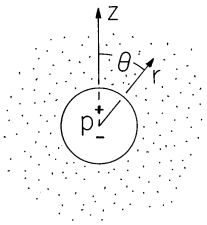


Fig. P6.6.2

6.6.2 An electric dipole having a z-directed moment p is situated at the origin, as shown in Fig. P6.6.2. Surrounding it is a spherical cavity of free space having radius a. Outside of the radius a is a linearly polarizable dielectric having permittivity ϵ.

(a) Determine Φ and $\mathbf{E}$ in regions (a) and (b) outside and inside the cavity.

(b) Show that in the limit where $\epsilon \to \infty$, the electric field intensity tangential to the interface of the dielectric goes to zero. That is, in this limit, the effect of the dielectric on the interior fields is the same as if the dielectric were a perfect conductor.

(c) Show that the same interior potential is obtained as in the limit $\epsilon \to \infty$ if this boundary condition is used at the outset.

6.6.3* In Example 6.6.1, an artificial dielectric is made from an array of perfectly conducting spheres. Here, an artificial dielectric is constructed using an array of rods, each having a circular cross-section with radius R. The rods run parallel to the capacitor plates and hence perpendicular to the imposed electric field intensity. The spacing between rod centers is s, and they are in a square array. Show that, for s large enough so that the fields induced by the rods do not interact, the equivalent electric susceptibility is $\chi_c = 2\pi(R/s)^2$.

6.6.4 Each of the conducting spheres in the artificial dielectric of Example 6.6.1 is replaced by the dielectric sphere of Prob. 6.6.1. Again, with the understanding that the spacing between spheres is large enough to justify ignoring their interaction, what is the equivalent susceptibility of the array?

6.6.5* A point charge finds itself at a height h above an infinite half-space of dielectric material. The charge has magnitude q, the dielectric has a uniform permittivity ϵ, and there are no unpaired charges in the volume of the dielectric or on its surface. The Cartesian coordinates x and z are in the plane of the dielectric interface, while y is directed perpendicular to the interface and into the free space region. Thus, the charge is at $y = h$. The field in the free space region can be taken as the superposition of a particular solution due to the point charge and a homogeneous solution due to a charge q_b at $y = -h$ below the interface. The field in the dielectric can be taken as that of a charge q_a at $y = h$.

(a) Show that the potential is given by

$$\Phi = \frac{1}{4\pi\epsilon_o}\begin{cases}(q/r_+) - (q_b/r_-); & 0 < y\\ q_a/r_+; & y < 0\end{cases}$$

where $r_\pm = \sqrt{x^2 + (y \mp h)^2 + z^2}$ and the magnitudes of the charges turn out to be

$$q_a = \frac{2q}{\left(\frac{\epsilon}{\epsilon_o} + 1\right)}; \qquad q_b = \frac{q\left(\frac{\epsilon}{\epsilon_o} - 1\right)}{\left(\frac{\epsilon}{\epsilon_o} + 1\right)} \tag{b}$$

(b) Show that the charge is attracted to the dielectric with the force

$$f = q\frac{q_b}{16\pi\epsilon_o h^2} \tag{c}$$

6.6.6 The half-space $y > 0$ is filled by a dielectric having uniform permittivity ϵ_a, while the remaining region $0 > y$ is filled by a dielectric having the uniform permittivity ϵ_b. Running parallel to the interface between these dielectrics along the line where $x = 0$ and $y = h$ is a uniform line charge of density λ. Determine the potentials in regions (a) and (b), respectively.

6.6.7* If the permittivities are nearly the same, so that $(1 - \epsilon_a/\epsilon_b) \equiv \kappa$ is small, the qualitative approach to determining the field distribution given in connection with Fig. 6.6.7 can be made quantitative. That is, if κ is small, the polarization charge induced by the imposed field can be determined to a good approximation and that charge, in turn, used to find the change in the applied field. Consider the following approximate approach to finding the fields in and around the dielectric cylinder of Example 6.6.2.

(a) In the limit where κ is zero, the field is equal to the applied field, both inside and outside the cylinder. Write this field in polar coordinates.
(b) Show that this field gives rise to $\sigma_{sp} = \epsilon_b E_o \kappa \cos\phi$ at the surface of the cylinder.
(c) Find the field due to this induced polarization surface charge and add it to the imposed field to show that, with the first-order contribution of the induced polarization surface charge, the field is

$$\Phi = -RE_o\begin{cases}\left(\frac{r}{R} - \frac{\kappa R}{2r}\right)\cos\phi; & r > R\\ \frac{r}{R}\left(1 - \frac{\kappa}{2}\right)\cos\phi; & r < R\end{cases} \tag{a}$$

(d) Expand the exact fields given by (21) and (22) to first order in κ and show that they are in agreement with this result.

6.6.8 As an illustration of how identification of the induced polarization charge can be used in a qualitative determination of the fields, consider the fields

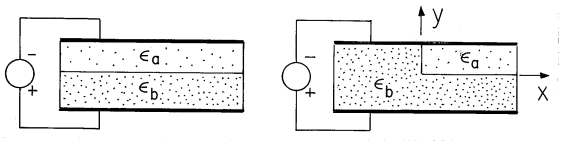


Fig. P6.6.8

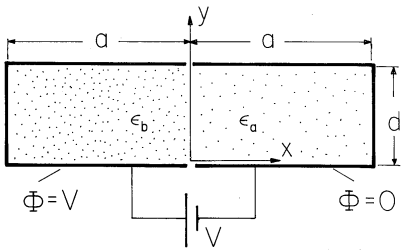


Fig. P6.6.9

between the plane parallel electrodes of Fig. P6.6.8. In Fig. P6.6.8a, there are two layers of dielectric.

(a) In the limit where $\kappa = (1 - \epsilon_a/\epsilon_b)$ is zero, what is the imposed $\mathbf{E}$?
(b) What is the σ_{sp} induced by this field at the interface between the dielectrics.
(c) For $\epsilon_a > \epsilon_b$, sketch the field lines in the two regions. (You should be able to see, from the superposition of the fields induced by this σ_{sp} and that imposed, which of the fields is the greater.)
(d) Now consider the more complicated geometry of Fig. 6.6.8b and carry out the same steps. Based on your deductions, draw a sketch of σ_{sp} and $\mathbf{E}$ for the case where $\epsilon_b > \epsilon_a$.

6.6.9 The configuration of perfectly conducting electrodes and perfectly insulating dielectrics shown in Fig. P6.6.9 is similar to that shown in Fig. 6.6.8 except that at the left and right, the electrodes are "shorted" together and the top electrode is also divided at the middle. Thus, the $\supset$ shaped electrode is grounded while the $\subset$ shaped one is at potential V.

(a) Determine Φ in regions (a) and (b).
(b) With the permittivities equal, sketch Φ and $\mathbf{E}$. (Use physical reasoning rather than the mathematical result.)
(c) Assuming that the permittivities are nearly equal, use the result of (b) to deduce σ_{sp} on the interface between dielectrics in the case where ϵ_a/ϵ_b is somewhat greater than and then somewhat less than 1. Sketch $\mathbf{E}$ deduced as the sum of the fields induced by these surface charges and the imposed field.
(d) With ϵ_a much greater that ϵ_b, draw a sketch of Φ and $\mathbf{E}$ in region (b).
(e) With ϵ_a much less than ϵ_b, sketch Φ and $\mathbf{E}$ in both regions.

6.7 Smoothly Inhomogeneous Electrically Linear Dielectrics

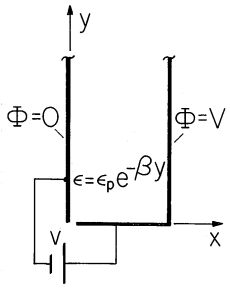


Fig. P6.7.1

6.7.1* For the two-dimensional system shown in Fig. P6.7.1, show that the potential in the smoothly inhomogeneous dielectric is

$$\Phi = \frac{Vx}{a} + \sum_{n=1}^{\infty} \left(\frac{2V}{n\pi}\right) e^{\beta y/2} \exp\left[-\sqrt{(\beta/2)^2 + (n\pi/a)^2}\, y\right] \sin\left(\frac{n\pi}{a}x\right) \qquad (a)$$

6.7.2 In Example 6.6.3, the dielectrics to right and left, respectively, have the permittivities $\epsilon_a = \epsilon_p \exp(-\beta x)$ and $\epsilon_b = \epsilon_p \exp(\beta x)$. Determine the potential throughout the dielectric regions.

6.7.3 A linear dielectric has the permittivity

$$\epsilon = \epsilon_a\{1 + \chi_p \exp[-(x^2 + y^2 + z^2)/a^2]\} \qquad (a)$$

An electric field that is uniform far from the origin (where it is equal to $E_o\mathbf{i_y}$) is imposed.

(a) Assume that ϵ/ϵ_o is not much different from unity and find ρ_p.
(b) With this induced polarization charge as a guide, sketch **E**.

7

CONDUCTION AND ELECTROQUASISTATIC CHARGE RELAXATION

7.0 INTRODUCTION

This is the last in the sequence of chapters concerned largely with electrostatic and electroquasistatic fields. The electric field $\mathbf{E}$ is still irrotational and can therefore be represented in terms of the electric potential Φ.

$$\boxed{\nabla \times \mathbf{E} = 0 \Leftrightarrow \mathbf{E} = -\nabla\Phi} \tag{1}$$

The source of $\mathbf{E}$ is the charge density. In Chap. 4, we began our exploration of EQS fields by treating the distribution of this source as prescribed. By the end of Chap. 4, we identified solutions to boundary value problems, where equipotential surfaces were replaced by perfectly conducting metallic electrodes. There, and throughout Chap. 5, the sources residing on the surfaces of electrodes as surface charge densities were made self-consistent with the field. However, in the volume, the charge density was still prescribed.

In Chap. 6, the first of two steps were taken toward a self-consistent description of the charge density in the volume. In relating $\mathbf{E}$ to its sources through Gauss' law, we recognized the existence of two types of charge densities, ρ_u and ρ_p, which, respectively, represented unpaired and paired charges. The paired charges were related to the polarization density $\mathbf{P}$ with the result that Gauss' law could be written as (6.2.15)

$$\boxed{\nabla \cdot \mathbf{D} = \rho_u} \tag{2}$$

where $\mathbf{D} \equiv \epsilon_o\mathbf{E} + \mathbf{P}$. Throughout Chap. 6, the volume was assumed to be perfectly insulating. Thus, ρ_p was either zero or a given distribution.

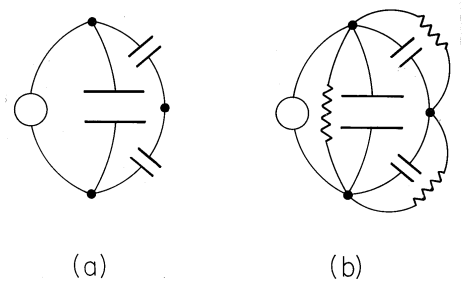


Fig. 7.0.1 EQS distributions of potential and current density are analogous to those of voltage and current in a network of resistors and capacitors. (a) Systems of perfect dielectrics and perfect conductors are analogous to capacitive networks. (b) Conduction effects considered in this chapter are analogous to those introduced by adding resistors to the network.

The second step toward a self-consistent description of the volume charge density is taken by adding to (1) and (2) an equation expressing conservation of the unpaired charges, (2.3.3).

$$\boxed{\nabla \cdot \mathbf{J}_u + \frac{\partial \rho_u}{\partial t} = 0} \tag{3}$$

That the charge appearing in this equation is indeed the unpaired charge density follows by taking the divergence of Ampère's law expressed with polarization, (6.2.17), and using Gauss' law as given by (2) to eliminate $\mathbf{D}$.

To make use of these three differential laws, it is necessary to specify $\mathbf{P}$ and $\mathbf{J}$. In Chap. 6, we learned that the former was usually accomplished by either specifying the polarization density $\mathbf{P}$ or by introducing a polarization constitutive law relating $\mathbf{P}$ to $\mathbf{E}$. In this chapter, we will almost always be concerned with linear dielectrics, where $\mathbf{D} = \epsilon\mathbf{E}$.

A new constitutive law is required to relate $\mathbf{J}_u$ to the electric field intensity. The first of the following sections is therefore devoted to the constitutive law of conduction. With the completion of Sec. 7.1, we have before us the differential laws that are the theme of this chapter.

To anticipate the developments that follow, it is helpful to make an analogy to circuit theory. If the previous two chapters are regarded as describing circuits consisting of interconnected capacitors, as shown in Fig. 7.0.1a, then this chapter adds resistors to the circuit, as in Fig. 7.0.1b. Suppose that the voltage source is a step function. As the circuit is composed of resistors and capacitors, the distribution of currents and voltages in the circuit is finally determined by the resistors alone. That is, as $t \to \infty$, the capacitors cease charging and are equivalent to open circuits. The distribution of voltages is then determined by the steady flow of current through the resistors. In this long-time limit, the charge on the capacitors is determined from the voltages already specified by the resistive network.

The steady current flow is analogous to the field situation where $\partial\rho_u/\partial t \to 0$ in the conservation of charge expression, (3). We will find that (1) and (3), the latter written with $\mathbf{J}_u$ represented by the conduction constitutive law, then fully determine the distribution of potential, of $\mathbf{E}$, and hence of $\mathbf{J}_u$. Just as the charges

on the capacitors in the circuit of Fig. 7.0.1b are then specified by the already determined voltage distribution, the charge distribution can be found in an after-the-fact fashion from the already determined field distribution by using Gauss' law, (2). After considering the physical basis for common conduction constitutive laws in Sec. 7.1, Secs. 7.2–7.6 are devoted to steady conduction phenomena.

In the circuit of Fig. 7.0.1b, the distribution of voltages an instant after the voltage step is applied is determined by the capacitors without regard for the resistors. From a field theory point of view, this is the physical situation described in Chaps. 4 and 5. It is the objective of Secs. 7.7–7.9 to form an appreciation for how this initial distribution of the fields and sources relaxes to the steady condition, already studied in Secs. 7.2–7.6, that prevails when $t \to \infty$.

In Chaps. 3–5 we invoked the "perfect conductivity" model for a conductor. For electroquasistatic systems, we will conclude this chapter with an answer to the question, "Under what circumstances can a conductor be regarded as perfect?"

Finally, if the fields and currents are essentially static, there is no distinction between EQS and MQS laws. That is, if $\partial \mathbf{B}/\partial t$ is negligible in an MQS system, Faraday's law again reduces to (1). Thus, the first half of this chapter provides an understanding of steady conduction in some MQS as well as EQS systems. In Chap. 8, we determine the magnetic field intensity from a given distribution of current density. Provided that rates of change are slow enough so that effects of magnetic induction can be ignored, the solution to the steady conduction problem as addressed in Secs. 7.2–7.6 provides the distribution of the magnetic field source, the current density, needed to begin Chap. 8.

Just how fast can the fields vary without producing effects of magnetic induction? For EQS systems, the answer to this question comes in Secs. 7.7–7.9. The EQS effects of finite conductivity and finite rates of change are in sharp contrast to their MQS counterparts, studied in the last half of Chap. 10.

7.1 CONDUCTION CONSTITUTIVE LAWS

In the presence of materials, fields vary in space over at least two length scales. The *microscopic scale* is typically the distance between atoms or molecules while the much larger *macroscopic scale* is typically the dimension of an object made from the material. As developed in the previous chapter, fields in polarized media are averages over the microscopic scale of the dipoles. In effect, the experimental determination of the polarization constitutive law relating the macroscopic $\mathbf{P}$ and $\mathbf{E}$ (Sec. 6.4) does not deal with the microscopic field.

With the understanding that experimentally measured values will again be used to evaluate macroscopic parameters, we assume that the average force acting on an unpaired or free charge, q, within matter is of the same form as the Lorentz force, (1.1.1).

$$\mathbf{f} = q(\mathbf{E} + \mathbf{v} \times \mu_o \mathbf{H}) \tag{1}$$

By contrast with a polarization charge, a free charge is not bound to the atoms and molecules, of which matter is constituted, but under the influence of the electric and magnetic fields can travel over distances that are large compared to interatomic or intermolecular distances. In general, the charged particles collide with the atomic

or molecular constituents, and so the force given by (1) does not lead to uniform acceleration, as it would for a charged particle in free space. In fact, in the conventional conduction process, a particle experiences so many collisions on time scales of interest that the average velocity it acquires is quite low. This phenomenon gives rise to two consequences. First, inertial effects can be disregarded in the time average balance of forces on the particle. Second, the velocity is so low that the forces due to magnetic fields are usually negligible. (The magnetic force term leads to the Hall effect, which is small and very difficult to observe in metallic conductors, but because of the relatively larger translational velocities reached by the charge carriers in semiconductors, more easily observed in these.)

With the driving force ascribed solely to the electric field and counterbalanced by a "viscous" force, proportional to the average translational velocity $\mathbf{v}$ of the charged particle, the force equation becomes

$$\mathbf{f} = \pm|q_\pm|\mathbf{E} = \nu_\pm \mathbf{v} \tag{2}$$

where the upper and lower signs correspond to particles of positive and negative charge, respectively. The coefficients $\nu_\pm$ are positive constants representing the time average "drag" resulting from collisions of the carriers with the fixed atoms or molecules through which they move.

Written in terms of the *mobilities*, $\mu_\pm$, the velocities of the positive and negative particles follow from (2) as

$$\mathbf{v}_\pm = \pm\mu_\pm \mathbf{E} \tag{3}$$

where $\mu_\pm = |q_\pm|/\nu_\pm$. The mobility is defined as positive. The positive and negative particles move with and against the electric field intensity, respectively.

Now suppose that there are two types of charged particles, one positive and the other negative. These might be the positive sodium and negative chlorine ions resulting when salt is dissolved in water. In a metal, the positive charges represent the (zero mobility) atomic sites, while the negative particles are electrons. Then, with N_+ and N_-, respectively, defined as the number of these charged particles per unit volume, the current density is

$$\mathbf{J}_u = N_+|q_+|\mathbf{v}_+ - N_-|q_-|\mathbf{v}_- \tag{4}$$

A flux of negative particles comprises an electrical current that is in a direction opposite to that of the particle motion. Thus, the second term in (4) appears with a negative sign. The velocities in this expression are related to $\mathbf{E}$ by (3), so it follows that the current density is

$$\mathbf{J}_u = (N_+|q_+|\mu_+ + N_-|q_-|\mu_-)\mathbf{E} \tag{5}$$

In terms of the same variables, the unpaired charge density is

$$\rho_u = N_+|q_+| - N_-|q_-| \tag{6}$$

Ohmic Conduction. In general, the distributions of particle densities N_+ and N_- are determined by the electric field. However, in many materials, the quantity in brackets in (5) is a property of the material, called the *electrical conductivity* σ.

$$\boxed{\mathbf{J}_u = \sigma\mathbf{E}; \qquad \sigma \equiv (N_+|q_+|\mu_+ + N_-|q_-|\mu_-)} \tag{7}$$

The MKS units of σ are (ohm - m)$^{-1}$ $\equiv$ Siemens/m = S/m.

In these materials, the charge densities N_+q_+ and N_-q_- keep each other in (approximate) balance so that there is little effect of the applied field on their sum. Thus, the conductivity $\sigma(\mathbf{r})$ is specified as a function of position in nonuniform media by the distribution $N_\pm$ in the material and by the local mobilities, which can also be functions of $\mathbf{r}$.

The conduction constitutive law given by (7) is *Ohm's law* generalized in a field-theoretical sense. Values of the conductivity for some common materials are given in Table 7.1.1. It is important to keep in mind that any constitutive law is of restricted use, and Ohm's law is no exception. For metals and semiconductors, it is usually a good model on a sufficiently large scale. It is also widely used in dealing with electrolytes. However, as materials become semi-insulators, it can be of questionable validity.

Unipolar Conduction. To form an appreciation for the implications of Ohm's law, it will be helpful to contrast it with the law for *unipolar conduction*. In that case, charged particles of only one sign move in a neutral background, so that the expressions for the current density and charge density that replace (5) and (6) are

$$\boxed{\mathbf{J}_u = |\rho|\mu\mathbf{E}} \tag{8}$$

$$\rho_u = \rho \tag{9}$$

where the charge density ρ now carries its own sign. Typical of situations described by these relations is the passage of ions through air.

Note that a current density exists in unipolar conduction only if there is a *net* charge density. By contrast, for Ohmic conduction, where the current density and the charge density are given by (7) and (6), respectively, there can be a current density at a location where there is no *net* charge density. For example, in a metal, negative electrons move through a background of fixed positively charged atoms. Thus, in (7), $\mu_+ = 0$ and the conductivity is due solely to the electrons. But it follows from (6) that the positive charges do have an important effect, in that they can nullify the charge density of the electrons. We will often find that in an Ohmic conductor there is a current density where there is no net unpaired charge density.

7.2 STEADY OHMIC CONDUCTION

To set the stage for the next two sections, consider the fields in a material that has a linear polarizability and is described by Ohm's law, (7.1.7).

$$\boxed{\mathbf{J} = \sigma(\mathbf{r})\mathbf{E}; \qquad \mathbf{D} = \epsilon(\mathbf{r})\mathbf{E}} \tag{1}$$

TABLE 7.1.1
CONDUCTIVITY OF VARIOUS MATERIALS

Metals and Alloys in Solid State	
	$\sigma-$ mhos/m at 20°C
Aluminum, commercial hard drawn	3.54×10^7
Copper, annealed	5.80×10^7
Copper, hard drawn	5.65×10^7
Gold, pure drawn	4.10×10^7
Iron, 99.98%	1.0×10^7
Steel	$0.5–1.0 \times 10^7$
Lead	0.48×10^7
Magnesium	2.17×10^7
Nichrome	0.10×10^7
Nickel	1.28×10^7
Silver, 99.98%	6.14×10^7
Tungsten	1.81×10^7
Semi-insulating and Dielectric Solids	
Bakelite (average range)*	$10^{-8} - 10^{10}$
Celluloid*	10^{-8}
Glass, ordinary*	10^{-12}
Hard rubber*	$10^{-14} - 10^{-16}$
Mica*	$10^{-11} - 10^{-15}$
Paraffin*	$10^{-14} - 10^{-16}$
Quartz, fused*	less than 10^{-17}
Sulfur*	less than 10^{-16}
Teflon*	less than 10^{-16}
Liquids	
Mercury	0.10×10^7
Alcohol, ethyl, 15° C	3.3×10^{-4}
Water, Distilled, 18° C	2×10^{-4}
Corn Oil	5×10^{-11}

*For highly insulating materials. Ohm's law is of dubious validity and conductivity values are only useful for making estimates.

In general, these properties are functions of position, $\mathbf{r}$. Typically, electrodes are used to constrain the potential over some of the surface enclosing this material, as suggested by Fig. 7.2.1.

In this section, we suppose that the excitations are essentially constant in

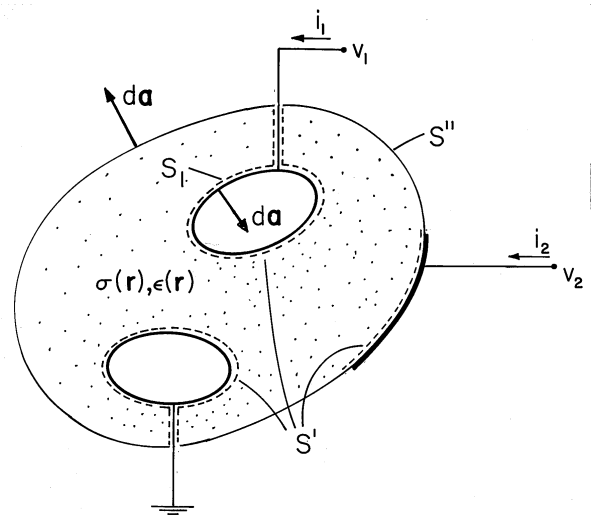


Fig. 7.2.1 Configuration having volume enclosed by surfaces S', upon which the potential is constrained, and S'', upon which its normal derivative is constrained.

time, in the sense that the rate of accumulation of charge at any given location has a negligible influence on the distribution of the current density. Thus, the time derivative of the unpaired charge density in the charge conservation law, (7.0.3), is negligible. This implies that the current density is solenoidal.

$$\boxed{\nabla \cdot \sigma \mathbf{E} = 0} \tag{2}$$

Of course, in the EQS approximation, the electric field is also irrotational.

$$\nabla \times \mathbf{E} = 0 \Leftrightarrow \mathbf{E} = -\nabla \Phi \tag{3}$$

Combining (2) and (3) gives a second-order differential equation for the potential distribution.

$$\nabla \cdot \sigma \nabla \Phi = 0 \tag{4}$$

In regions of uniform conductivity (σ = constant), it assumes a familiar form.

$$\nabla^2 \Phi = 0 \tag{5}$$

In a uniform conductor, the potential distribution satisfies Laplace's equation.

It is important to realize that the physical reasons for obtaining Laplace's equation for the potential distribution in a uniform conductor are quite different from those that led to Laplace's equation in the electroquasistatic cases of Chaps. 4 and 5. With steady conduction, the governing requirement is that the divergence of the current density vanish. The unpaired charge density does not influence the current distribution, but is rather determined by it. In a uniform conductor, the continuity constraint on **J** happens to imply that there is no unpaired charge density.

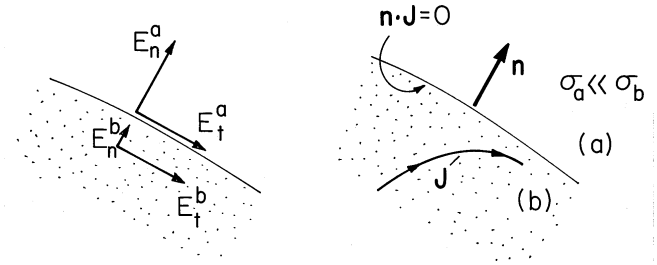


Fig. 7.2.2 Boundary between region (a) that is insulating relative to region (b).

In a nonuniform conductor, (4) shows that there is an accumulation of unpaired charge. Indeed, with σ a function of position, (2) becomes

$$\sigma \nabla \cdot \mathbf{E} + \mathbf{E} \cdot \nabla \sigma = 0 \tag{6}$$

Once the potential distribution has been found, Gauss' law can be used to determine the distribution of unpaired charge density.

$$\rho_u = \epsilon \nabla \cdot \mathbf{E} + \mathbf{E} \cdot \nabla \epsilon \tag{7}$$

Equation (6) can be solved for $div\,\mathbf{E}$ and that quantity substituted into (7) to obtain

$$\boxed{\rho_u = -\frac{\epsilon}{\sigma}\mathbf{E} \cdot \nabla \sigma + \mathbf{E} \cdot \nabla \epsilon} \tag{8}$$

Even though the distribution of ϵ plays no part in determining $\mathbf{E}$, through Gauss' law, it does influence the distribution of unpaired charge density.

Continuity Conditions. Where the conductivity changes abruptly, the continuity conditions follow from (2) and (3). The condition

$$\boxed{\mathbf{n} \cdot (\sigma_a \mathbf{E}^a - \sigma_b \mathbf{E}^b) = 0} \tag{9}$$

is derived from (2), just as (1.3.17) followed from Gauss' law. The continuity conditions implied by (3) are familiar from Sec. 5.3.

$$\boxed{\mathbf{n} \times (\mathbf{E}^a - \mathbf{E}^b) = 0 \Leftrightarrow \Phi^a - \Phi^b = 0} \tag{10}$$

Illustration. Boundary Condition at an Insulating Surface

Insulated wires and ordinary resistors are examples where a conducting medium is bounded by one that is essentially insulating. What boundary condition should be used to determine the current distribution inside the conducting material?

In Fig. 7.2.2, region (a) is relatively insulating compared to region (b), $\sigma_a \ll \sigma_b$. It follows from (9) that the normal electric field in region (a) is much greater than in region (b), $E_n^a \gg E_n^b$. According to (10), the tangential components of $\mathbf{E}$ are equal, $E_t^a = E_t^b$. With the assumption that the normal and tangential components of $\mathbf{E}$ are of the same order of magnitude in the insulating region, these two statements establish the relative magnitudes of the normal and tangential components of $\mathbf{E}$, respectively, sketched in Fig. 7.2.2. We conclude that in the relatively conducting region (b), the normal component of $\mathbf{E}$ is essentially zero compared to the tangential component. Thus, to determine the fields in the relatively conducting region, the boundary condition used *at an insulating surface* is

$$\boxed{\mathbf{n} \cdot \mathbf{J} = 0 \Rightarrow \mathbf{n} \cdot \nabla \Phi = 0} \tag{11}$$

At an insulating boundary, inside the conductor, the normal derivative of the potential is zero, while the boundary potential adjusts itself to make this true. Current lines are diverted so that they remain tangential to the insulating boundary, as sketched in Fig. 7.2.2.

Just as Gauss' law embodied in (8) is used to find the unpaired volume charge density *ex post facto*, Gauss' continuity condition (6.5.3) serves to evaluate the unpaired surface charge density. Combined with the current continuity condition, (9), it becomes

$$\boxed{\sigma_{su} = \mathbf{n} \cdot \epsilon_a \mathbf{E}^a \left(1 - \frac{\epsilon_b}{\epsilon_a} \frac{\sigma_a}{\sigma_b}\right)} \tag{12}$$

Conductance. If there are only two electrodes contacting the conductor of Fig. 7.2.1 and hence one voltage $v_1 = v$ and current $i_1 = i$, the voltage-current relation for the terminal pair is of the form

$$i = Gv \tag{13}$$

where G is the conductance. To relate G to field quantities, (2) is integrated over a volume V enclosed by a surface S, and Gauss' theorem is used to convert the volume integral to one of the current $\sigma \mathbf{E} \cdot d\mathbf{a}$ over the surface S. This integral law is then applied to the surface shown in Fig. 7.2.1 enclosing the electrode that is connected to the positive terminal. Where it intersects the wire, the contribution is $-i$, so that the integral over the closed surface becomes

$$-i + \int_{S_1} \sigma \mathbf{E} \cdot d\mathbf{a} = 0 \tag{14}$$

where S_1 is the surface where the perfectly conducting electrode having potential v_1 interfaces with the Ohmic conductor.

Division of (14) by the terminal voltage v gives an expression for the conductance defined by (13).

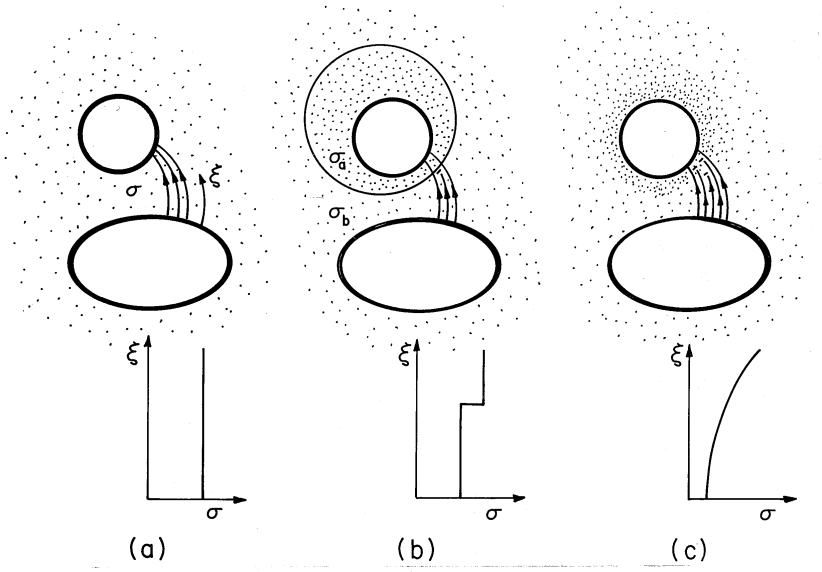


Fig. 7.2.3 Typical configurations involving a conducting material and perfectly conducting electrodes. (a) Region of interest is filled by material having uniform conductivity. (b) Region composed of different materials, each having uniform conductivity. Conductivity is discontinuous at interfaces. (c) Conductivity is smoothly varying.

$$\boxed{G = \frac{i}{v} = \frac{\int_{S_1} \sigma \mathbf{E} \cdot d\mathbf{a}}{v}} \tag{15}$$

Note that the linearity of the equation governing the potential distribution, (4), assures that i is proportional to v. Hence, (15) is independent of v and, indeed, a parameter characterizing the system independent of the excitation.

A comparison of (15) for the conductance with (6.5.6) for the capacitance suggests an analogy that will be developed in Sec. 7.5.

Qualitative View of Fields in Conductors. Three classes of steady conduction configurations are typified in Fig. 7.2.3. In the first, the region of interest is one of uniform conductivity bounded either by surfaces with constrained potentials or by perfect insulators. In the second, the conductivity varies abruptly but by a finite amount at interfaces, while in the third, it varies smoothly. Because Gauss' law plays no role in determining the potential distribution, the permittivity distributions in these three classes of configurations are arbitrary. Of course, they do have a strong influence on the resulting distributions of unpaired charge density.

A qualitative picture of the electric field distribution within conductors emerges from arguments similar to those used in Sec. 6.5 for linear dielectrics. Because $\mathbf{J}$ is solenoidal and has the same direction as $\mathbf{E}$, it passes from the high-potential to the low-potential electrodes through tubes within which lines of $\mathbf{J}$ neither terminate nor originate. The $\mathbf{E}$ lines form the same tubes but either terminate or originate on

the sum of unpaired and polarization charges. The sum of these charge densities is $div\,\epsilon_o\mathbf{E}$, which can be determined from (6).

$$\rho_u + \rho_p = \nabla \cdot \epsilon_o\mathbf{E} = -\epsilon_o\mathbf{E} \cdot \frac{\nabla\sigma}{\sigma} = -\epsilon_o\mathbf{J} \cdot \frac{\nabla\sigma}{\sigma^2} \tag{16}$$

At an abrupt discontinuity, the sum of the surface charges determines the discontinuity of normal $\mathbf{E}$. In view of (9),

$$\sigma_{su} + \sigma_{sp} = \mathbf{n} \cdot (\epsilon_o\mathbf{E}^a - \epsilon_o\mathbf{E}^b) = \mathbf{n} \cdot \epsilon_o\mathbf{E}^a\big(1 - \frac{\sigma_a}{\sigma_b}\big) \tag{17}$$

Note that the distribution of ϵ plays no part in shaping the $\mathbf{E}$ lines.

In following a typical current tube from high potential to low in the uniform conductor of Fig. 7.2.3a, no conductivity gradients are encountered, so (16) tells us there is no source of $\mathbf{E}$. Thus, it is no surprise that Φ satisfies Laplace's equation throughout the uniform conductor.

In following the current tube through the discontinuity of Fig. 7.2.3b, from low to high conductivity, (17) shows that there is a negative surface source of $\mathbf{E}$. Thus, $\mathbf{E}$ tends to be excluded from the more conducting region and intensified in the less conducting region.

With the conductivity increasing smoothly in the direction of $\mathbf{E}$, as illustrated in Fig. 7.2.3c, $\mathbf{E} \cdot \nabla\sigma$ is positive. Thus, the source of $\mathbf{E}$ is negative and the $\mathbf{E}$ lines attenuate along the flux tube.

Uniform and piece-wise uniform conductors are commonly encountered, and examples in this category are taken up in Secs. 7.4 and 7.5. Examples where the conductivity is smoothly distributed are analogous to the smoothly varying permittivity configurations exemplified in Sec. 6.7. In a simple one-dimensional configuration, the following example illustrates all three categories.

Example 7.2.1. One-Dimensional Resistors

The resistor shown in Fig. 7.2.4 has a uniform cross-section of area A in any $x - z$ plane. Over its length d it has a conductivity $\sigma(y)$. Perfectly conducting electrodes constrain the potential to be v at $y = 0$ and to be zero at $y = d$. The cylindrical conductor is surrounded by a perfect insulator.

The potential is assumed to depend only on y. Thus, the electric field and current density are y directed, and the condition that there be no component of $\mathbf{E}$ normal to the insulating boundaries is automatically satisfied. For the one-dimensional field, (4) reduces to

$$\frac{d}{dy}\big(\sigma\frac{d\Phi}{dy}\big) = 0 \tag{18}$$

The quantity in parentheses, the negative of the current density, is conserved over the length of the resistor. Thus, with J_o defined as constant,

$$\sigma\frac{d\Phi}{dy} = -J_o \tag{19}$$

This expression is now integrated from the lower electrode to an arbitrary location y.

$$\int_v^\Phi d\Phi = -\int_0^y \frac{J_o}{\sigma}dy \Rightarrow \Phi = v - \int_0^y \frac{J_o}{\sigma}dy \tag{20}$$

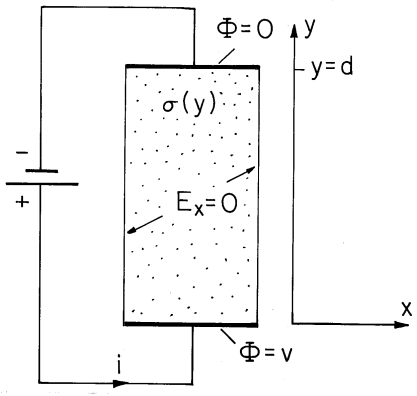


Fig. 7.2.4 Cylindrical resistor having conductivity that is a function of position y between the electrodes. The material surrounding the conductor is insulating.

Evaluation of this expression where $y = d$ and $\Phi = 0$ relates the current density to the terminal voltage.

$$v = \int_0^d \frac{J_o}{\sigma} dy \Rightarrow J_o = v / \int_0^d \frac{dy}{\sigma} \tag{21}$$

Introduction of this expression into (20) then gives the potential distribution.

$$\Phi = v\left[1 - \int_0^y \frac{dy}{\sigma} / \int_0^d \frac{dy}{\sigma}\right] \tag{22}$$

The conductance, defined by (15), follows from (21).

$$G = \frac{AJ_o}{v} = A / \int_0^d \frac{dy}{\sigma} \tag{23}$$

These relations hold for any one-dimensional distribution of σ. Of course, there is no dependence on ϵ, which could have any distribution. The permittivity could even depend on x and z. In terms of the circuit analogy suggested in the introduction, the resistors determine the distribution of voltages regardless of the interconnected capacitors.

Three special cases conform to the three categories of configurations illustrated in Fig. 7.2.3.

Uniform Conductivity. If σ is uniform, evaluation of (22) and (23) gives

$$\Phi = v\left(1 - \frac{y}{d}\right) \tag{24}$$

$$G = \frac{A\sigma}{d} \tag{25}$$

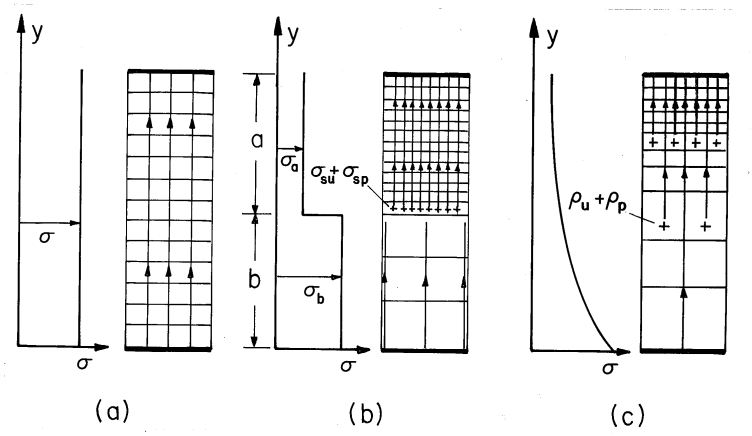


Fig. 7.2.5 Conductivity, potential, charge density, and field distributions in special cases for the configuration of Fig. 7.2.4. (a) Uniform conductivity. (b) Layers of uniform but different conductivities. (c) Exponentially varying conductivity.

The potential and electric field are the same as they would be between plane parallel electrodes in free space in a uniform perfect dielectric. However, because of the insulating walls, the conduction field remains uniform regardless of the length of the resistor compared to its transverse dimensions.

It is clear from (16) that there is no volume charge density, and this is consistent with the uniform field that has been found. These distributions of σ, Φ, and $\mathbf{E}$ are shown in Fig. 7.2.5a.

Piece-Wise Uniform Conductivity. With the resistor composed of uniformly conducting layers in series, as shown in Fig. 7.2.5b, the potential and conductance follow from (22) and (23) as

$$\Phi = \begin{cases} v\left\{1 - \frac{G}{A}\frac{y}{\sigma_b}\right\} & 0 < y < b \\ v\left\{1 - \frac{G}{A}[(b/\sigma_b) + (y-b)/\sigma_a]\right\} & b < y < a+b \end{cases} \tag{26}$$

$$G = \frac{A}{[(b/\sigma_b) + (a/\sigma_a)]} \tag{27}$$

Again, there are no sources to distort the electric field in the uniformly conducting regions. However, at the discontinuity in conductivity, (17) shows that there is surface charge. For $\sigma_b > \sigma_a$, this surface charge is positive, tending to account for the more intense field shown in Fig. 7.2.5b in the upper region.

Smoothly Varying Conductivity. With the exponential variation $\sigma = \sigma_o \exp(-y/d)$, (22) and (23) become

$$\Phi = v\left[1 - \frac{(e^{y/d} - 1)}{(e-1)}\right] \tag{28}$$

$$G = \frac{A\sigma_o}{d(e-1)} \tag{29}$$

Here the charge density that accounts for the distribution of $\mathbf{E}$ follows from (16).

$$\rho_u + \rho_p = \frac{\epsilon_o J_o}{\sigma_o d} e^{y/d} \tag{30}$$

Thus, the field is shielded from the lower region by an exponentially increasing volume charge density.

7.3 DISTRIBUTED CURRENT SOURCES AND ASSOCIATED FIELDS

Under steady conditions, conservation of charge requires that the current density be solenoidal. Thus, $\mathbf{J}$ lines do not originate or terminate. We have so far thought of current tubes as originating outside the region of interest, on the boundaries. It is sometimes convenient to introduce a volume distribution of current sources, $s(\mathbf{r}, t)$ A/m^3, defined so that the steady charge conservation equation becomes

$$\boxed{\oint_S \mathbf{J} \cdot d\mathbf{a} = \int_V s dv \Leftrightarrow \nabla \cdot \mathbf{J} = s} \tag{1}$$

The motivation for introducing a distributed source of current becomes clear as we now define singular sources and think about how these can be realized physically.

Distributed Current Source Singularities. The analogy between (1) and Gauss' law begs for the definition of point, line, and surface current sources, as depicted in Fig. 7.3.1. In returning to Sec. 1.3 where the analogous singular charge distributions were defined, it should be kept in mind that we are now considering a source of current density, not of electric flux.

A point source of current gives rise to a net current i_p out of a volume V that shrinks to zero while always enveloping the source.

$$\oint_S \mathbf{J} \cdot d\mathbf{a} = i_p \qquad i_p \equiv \lim_{\substack{s \to \infty \\ V \to 0}} \int_V s dv \tag{2}$$

Such a source might be used to represent the current distribution around a small electrode introduced into a conducting material. As shown in Fig. 7.3.1d, the electrode is connected to a source of current i_p through an insulated wire. At least under steady conditions, the wire and its insulation can be made fine enough so that the current distribution in the surrounding conductor is not disturbed.

Note that if the wire and its insulation are considered, the current density remains solenoidal. A surface surrounding the spherical electrode is pierced by the

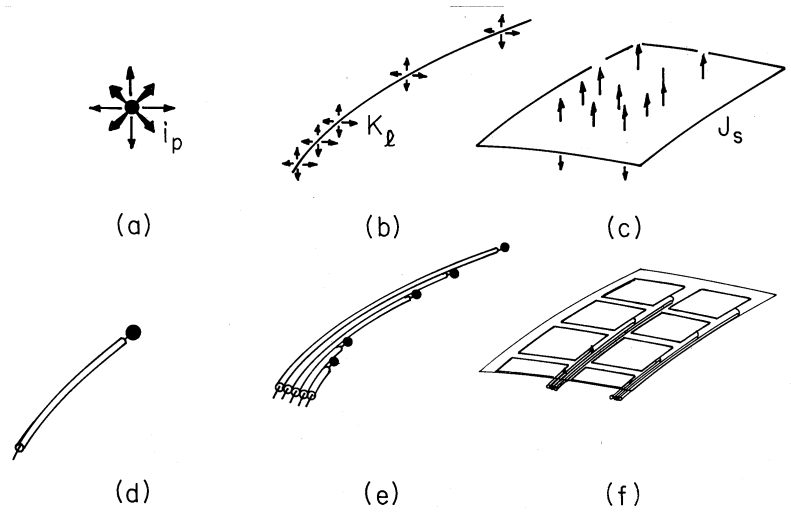


Fig. 7.3.1 Singular current source distributions represented conceptually by the top row, suggesting how these might be realized physically by the bottom row by electrodes fed through insulated wires.

wire. The contribution to the integral of $\mathbf{J}\cdot d\mathbf{a}$ from this part of the surface integral is equal and opposite to that of the remainder of the surface surrounding the electrode. The point source is, in this case, an artifice for ignoring the effect of the insulated wire on the current distribution.

The tubular volume having a cross-sectional area A used to define a line charge density in Sec. 1.3 (Fig. 1.3.4) is equally applicable here to defining a line current density.

$$K_l \equiv \lim_{\substack{s\to\infty \\ A\to 0}} \int_A s\,da \tag{3}$$

In general, K_l is a function of position along the line, as shown in Fig. 7.3.1b. If this is the case, a physical realization would require a bundle of insulated wires, each terminated in an electrode segment delivering its current to the surrounding medium, as shown in Fig. 7.3.1e. Most often, the line source is used with two-dimensional flows and describes a uniform wire electrode driven at one end by a current source.

The surface current source of Figs. 7.3.1c and 7.3.1f is defined using the same incremental control volume enclosing the surface source as shown in Fig. 1.3.5.

$$\boxed{J_s \equiv \lim_{\substack{s\to\infty \\ h\to 0}} \int_{\xi-\frac{h}{2}}^{\xi+\frac{h}{2}} s\,d\xi} \tag{4}$$

Note that J_s is the *net* current density entering the surrounding material at a given location.

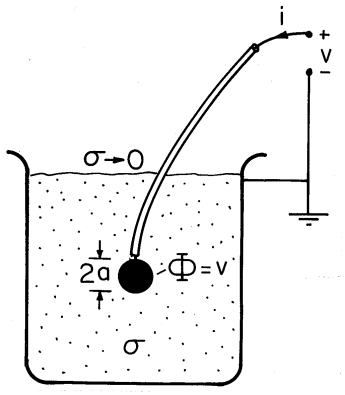


Fig. 7.3.2 For a small spherical electrode, the conductance relative to a large conductor at "infinity" is given by (7).

Fields Associated with Current Source Singularities. In the immediate vicinity of a point current source immersed in a uniform conductor, the current distribution is spherically symmetric. Thus, with $\mathbf{J} = \sigma\mathbf{E}$, the integral current continuity law, (1), requires that

$$4\pi r^2 \sigma E_r = i_p \tag{5}$$

From this, the electric field intensity and potential of a point source follow as

$$E_r = \frac{i_p}{4\pi\sigma r^2} \Rightarrow \Phi = \frac{i_p}{4\pi\sigma r} \tag{6}$$

Example 7.3.1. Conductance of an Isolated Spherical Electrode

A simple way to measure the conductivity of a liquid is based on using a small spherical electrode of radius a, as shown in Fig. 7.3.2. The electrode, connected to an insulated wire, is immersed in the liquid of uniform conductivity σ. The liquid is in a container with a second electrode having a large area compared to that of the sphere, and located many radii a from the sphere. Thus, the potential drop associated with a current i that passes from the spherical electrode to the large electrode is largely in the vicinity of the sphere.

By definition the potential at the surface of the sphere is v, so evaluation of the potential for a point source, (6), at $r = a$ gives

$$v = \frac{i}{4\pi\sigma a} \Rightarrow G \equiv \frac{i}{v} = 4\pi\sigma a \tag{7}$$

This conductance is analogous to the capacitance of an isolated spherical electrode, as given by (4.6.8). Here, a fine insulated wire connected to the sphere would have little effect on the current distribution.

The conductance associated with a contact on a conducting material is often approximated by picturing the contact as a hemispherical electrode, as shown in Fig. 7.3.3. The region above the surface is an insulator. Thus, there is no current density and hence no electric field intensity normal to this surface. Note that this condition

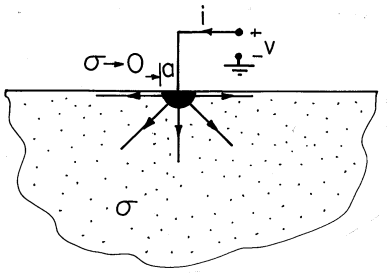


Fig. 7.3.3 Hemispherical electrode provides contact with infinite half-space of material with conductance given by (8).

is satisfied by the field associated with a point source positioned on the conductor-insulator interface. An additional requirement is that the potential on the surface of the electrode be v. Because current is carried by only half of the spherical surface, it follows from reevaluation of (6a) that the conductance of the hemispherical surface contact is

$$G = 2\pi\sigma a \tag{8}$$

The fields associated with uniform line and surface sources are analogous to those discussed for line and surface charges in Sec. 1.3.

The superposition principle, as discussed for Poisson's equation in Sec. 4.3, is equally applicable here. Thus, the fields associated with higher-order source singularities can again be found by superimposing those of the basic singular sources already defined. Because it can be used to model a battery imbedded in a conductor, the dipole source is of particular importance.

Example 7.3.2. Dipole Current Source in Spherical Coordinates

A positive point current source of magnitude i_p is located at $z = d$, just above a negative source (a sink) of equal magnitude at the origin. The source-sink pair, shown in Fig. 7.3.4, gives rise to fields analogous to those of Fig. 4.4.2. In the limit where the spacing d goes to zero while the product of the source strength and this spacing remains finite, this pair of sources forms a dipole. Starting with the potential as given for a source at the origin by (6), the limiting process is the same as leading to (4.4.8). The charge dipole moment qd is replaced by the current dipole moment $i_p d$ and $\epsilon_o \to \sigma$, $qd \to i_p d$. Thus, the potential of the dipole current source is

$$\Phi = \frac{i_p d}{4\pi\sigma}\frac{\cos\theta}{r^2} \tag{9}$$

The potential of a polar dipole current source is found in Prob. 7.3.3.

Method of Images. With the new boundary conditions describing steady current distributions come additional opportunities to exploit symmetry, as discussed in Sec. 4.7. Figure 7.3.5 shows a pair of equal magnitude point current sources located at equal distances to the right and left of a planar surface. By contrast with the point charges of Fig. 4.7.1, these sources are of the same sign. Thus,

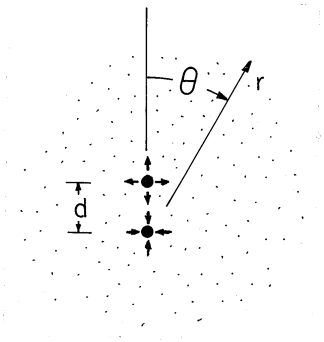


Fig. 7.3.4 Three-dimensional dipole current source has potential given by (9).

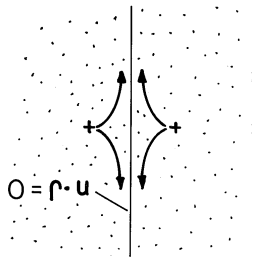


Fig. 7.3.5 Point current source and its image representing an insulating boundary.

the electric field normal to the surface is zero rather than the tangential field. The field and current distribution in the right half is the same as if that region were filled by a uniform conductor and bounded by an insulator on its left.

7.4 SUPERPOSITION AND UNIQUENESS OF STEADY CONDUCTION SOLUTIONS

The physical laws and boundary conditions are different, but the approach in this section is similar to that of Secs. 5.1 and 5.2 treating Poisson's equation.

In a material having the conductivity distribution $\sigma(\mathbf{r})$ and source distribution $s(\mathbf{r})$, a steady potential distribution Φ must satisfy (7.2.4) with a source density $-s$ on the right. Typically, the configurations of interest are as in Fig. 7.2.1, except that we now include the possibility of a distribution of current source density in the volume V. Electrodes are used to constrain this potential over some of the surface enclosing the volume V occupied by this material. This part of the surface, where the material contacts the electrodes, will be called S'. We will assume here that on the remainder of the enclosing surface, denoted by S'', the normal current density is specified. Depicted in Fig. 7.2.1 is the special case where the boundary S'' is insulating and hence where the normal current density is zero. Thus, according to

(7.2.1), (7.2.3), and (7.3.1), the desired $\mathbf{E}$ and $\mathbf{J}$ are found from a solution Φ to

$$\nabla \cdot \sigma \nabla \Phi = -s \tag{1}$$

where

$$\Phi = \Phi_i \quad \text{on} \quad S_i'$$

$$-\mathbf{n} \cdot \sigma \nabla \Phi = J_i \quad \text{on} \quad S_i''$$

Except for the possibility that part of the boundary is a surface S'' where the normal current density rather than the potential is specified, the situation here is analogous to that in Sec. 5.1. The solution can be divided into a particular part [that satisfies the differential equation of (1) at each point in the volume, but not the boundary conditions] and a homogeneous part. The latter is then adjusted to make the sum of the two satisfy the boundary conditions.

Superposition to Satisfy Boundary Conditions. Suppose that a system is composed of a source-free conductor ($s = 0$) contacted by one reference electrode at ground potential and n electrodes, respectively, at the potentials v_j, $j = 1, \ldots n$. The contacting surfaces of these electrodes comprise the surface S'. As shown in Fig. 7.2.1, there may be other parts of the surface enclosing the material that are insulating ($J_i = 0$) and denoted by S''. The solution can be represented as the sum of the potential distributions associated with each of the electrodes of specified potential while the others are grounded.

$$\Phi = \sum_{j=1}^{n} \Phi_j \tag{2}$$

where

$$\nabla \cdot \sigma \nabla \Phi_j = 0$$

$$\Phi_j = \begin{cases} v_j & \text{on } S_i', \quad j = i \\ 0 & \text{on } S_i', \quad j \neq i \end{cases}$$

Each Φ_j satisfies (1) with $s = 0$ and the boundary condition on S_i'' with $J_i = 0$. This decomposition of the solution is familiar from Sec. 5.1. However, the boundary condition on the insulating surface S'' requires a somewhat broadened view of what is meant by the respective terms in (2). As the following example illustrates, modes that have zero derivatives rather than zero amplitude at boundaries are now useful for satisfying the insulating boundary condition.

Example 7.4.1. Modal Solution with an Insulating Boundary

In the two-dimensional configuration of Fig. 7.4.1, a uniformly conducting material is grounded along its left edge, bounded by insulating material along its right edge,

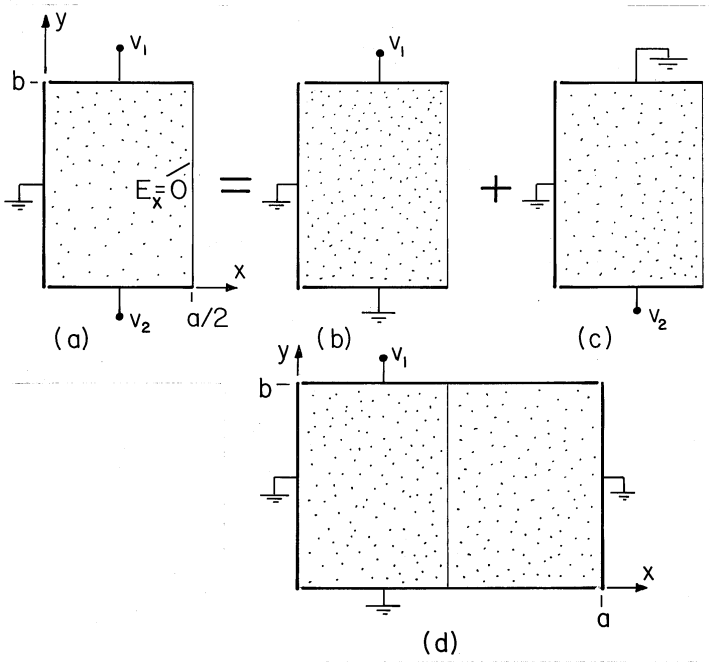


Fig. 7.4.1 (a) Two terminal pairs attached to conducting material having one wall at zero potential and another that is insulating. (b) Field solution is broken into part due to potential v_1 and (c) potential v_2. (d) The boundary condition at the insulating wall is satisfied by using the symmetry of an equivalent problem with all of the walls constrained in potential.

and driven by electrodes having the potentials v_1 and v_2 at the top and bottom, respectively.

Decomposition of the potential, as called for by (2), amounts to the superposition of the potentials for the two problems of (b) and (c) in the figure. Note that for each of these, the normal derivative of the potential must be zero at the right boundary.

Pictured in part (d) of Fig. 7.4.1 is a configuration familiar from Sec. 5.5. The potential distribution for the configuration of Fig. 5.5.2, (5.5.9), is equally applicable to that of Fig. 7.4.1. This is so because the symmetry requires that there be no x-directed electric field along the surface $x = a/2$. In turn, the potential distribution for part (c) is readily determined from this one by replacing $v_1 \rightarrow v_2$ and $y \rightarrow b - y$. Thus, the total potential is

$$\Phi = \sum_{\substack{n=1 \\ \text{odd}}}^{\infty} \frac{4}{\pi} \left\{ \frac{v_1}{n} \frac{\sinh\left(\frac{n\pi}{a}y\right)}{\sinh\left(\frac{n\pi}{a}b\right)} \sin\frac{n\pi}{a}x + \frac{v_2}{n} \frac{\sinh\left[\frac{n\pi}{a}(b-y)\right]}{\sinh\left(\frac{n\pi b}{a}\right)} \sin\frac{n\pi}{a}x \right\} \tag{3}$$

If we were to solve this problem without reference to Sec. 5.5, the modes used to expand the electrode potential would be zero at $x = 0$ and have zero derivative at the insulating boundary (at $x = a/2$).

The Conductance Matrix. With S_i' defined as the surface over which the i-th electrode contacts the conducting material, the current emerging from that electrode is

$$i_i = \int_{S_i} \sigma \nabla \Phi \cdot d\mathbf{a} \tag{4}$$

[See Fig. 7.2.1 for definition of direction of $d\mathbf{a}$.] In terms of the potential decomposition represented by (2), this expression becomes

$$i_i = \sum_{j=1}^{n} \int_{S_i'} \sigma \nabla \Phi_j \cdot d\mathbf{a} = \sum_{j=1}^{n} G_{ij} v_j \tag{5}$$

where the conductances are

$$\boxed{G_{ij} = \frac{\int_{S_i'} \sigma \nabla \Phi_j \cdot d\mathbf{a}}{v_j}} \tag{6}$$

Because Φ_j is by definition proportional to v_j, these parameters are independent of the excitations. They depend only on the physical properties and geometry of the configuration.

Example 7.4.2. Two Terminal Pair Conductance Matrix

For the system of Fig. 7.4.1, (5) becomes

$$\begin{bmatrix} i_1 \\ i_2 \end{bmatrix} = \begin{bmatrix} G_{11} & G_{12} \\ G_{21} & G_{22} \end{bmatrix} \begin{bmatrix} v_1 \\ v_2 \end{bmatrix} \tag{7}$$

With the potential given by (3), the *self-conductances* G_{11} and G_{22} and the *mutual conductances* G_{12} and G_{21} follow by evaluation of (5). This potential is singular in the left-hand corners, so the self-conductances determined in this way are represented by a series that does not converge. However, the mutual conductances are determined by integrating the current density over an electrode that is at the same potential as the grounded wall, so they are well represented. For example, with c defined as the length of the conducting block in the z direction,

$$G_{12} = \frac{\sigma c}{v_2} \int_0^{a/2} \frac{\partial \Phi_2}{\partial y}\Big|_{y=b} dx = \frac{4}{\pi} \sigma c \sum_{\substack{n=1 \\ \text{odd}}}^{\infty} \frac{1}{n \sinh\left(\frac{n\pi b}{a}\right)} \tag{8}$$

Uniqueness. With Φ_i, J_i, $\sigma(\mathbf{r})$, and $s(\mathbf{r})$ given, a steady current distribution is uniquely specified by the differential equation and boundary conditions of (1). As in Sec. 5.2, a proof that a second solution must be the same as the first hinges on defining a difference potential $\Phi_d = \Phi_a - \Phi_b$ and showing that, because $\Phi_d = 0$ on S_i' and $\mathbf{n} \cdot \sigma \nabla \Phi_d = 0$ on S_i'' in Fig. 7.2.1, Φ_d must be zero.

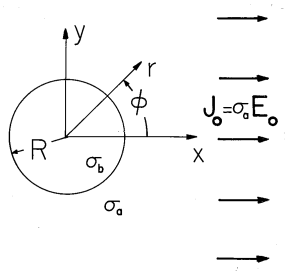


Fig. 7.5.1 Conducting circular rod is immersed in a conducting material supporting a current density that would be uniform in the absence of the rod.

7.5 STEADY CURRENTS IN PIECE-WISE UNIFORM CONDUCTORS

Conductor configurations are often made up from materials that are uniformly conducting. The conductivity is then uniform in the subregions occupied by the different materials but undergoes step discontinuities at interfaces between regions. In the uniformly conducting regions, the potential obeys Laplace's equation, (7.2.5),

$$\nabla^2\Phi = 0 \tag{1}$$

while at the interfaces between regions, the continuity conditions require that the normal current density and tangential electric field intensity be continuous, (7.2.9) and (7.2.10).

$$\mathbf{n}\cdot(\sigma_a\mathbf{E}^a - \sigma_b\mathbf{E}^b) = 0 \tag{2}$$

$$\Phi^a - \Phi^b = 0 \tag{3}$$

Analogy to Fields in Linear Dielectrics. If the conductivity is replaced by the permittivity, these laws are identical to those underlying the examples of Sec. 6.6. The role played by $\mathbf{D}$ is now taken by $\mathbf{J}$. Thus, the analysis for the following example has already been carried out in Sec. 6.6.

Example 7.5.1. Conducting Circular Rod in Uniform Transverse Field

A rod of radius R and conductivity σ_b is immersed in a material of conductivity σ_a, as shown in Fig. 7.5.1. Perhaps imposed by means of plane parallel electrodes far to the right and left, there is a uniform current density far from the cylinder.

The potential distribution is deduced using the same steps as in Example 6.6.2, with $\epsilon_a \to \sigma_a$ and $\epsilon_b \to \sigma_b$. Thus, it follows from (6.6.21) and (6.6.22) as

$$\Phi_a = -RE_o\cos\phi\left[\left(\frac{r}{R}\right) - \left(\frac{R}{r}\right)\frac{(\sigma_b-\sigma_a)}{(\sigma_b+\sigma_a)}\right] \tag{4}$$

$$\Phi_b = \frac{-2\sigma_a}{\sigma_a+\sigma_b}E_o r\cos\phi \tag{5}$$

and the lines of *electric field intensity* are as shown in Fig. 6.6.6. Note that although the lines of $\mathbf{E}$ and $\mathbf{J}$ are in the same direction and have the same pattern in each of the

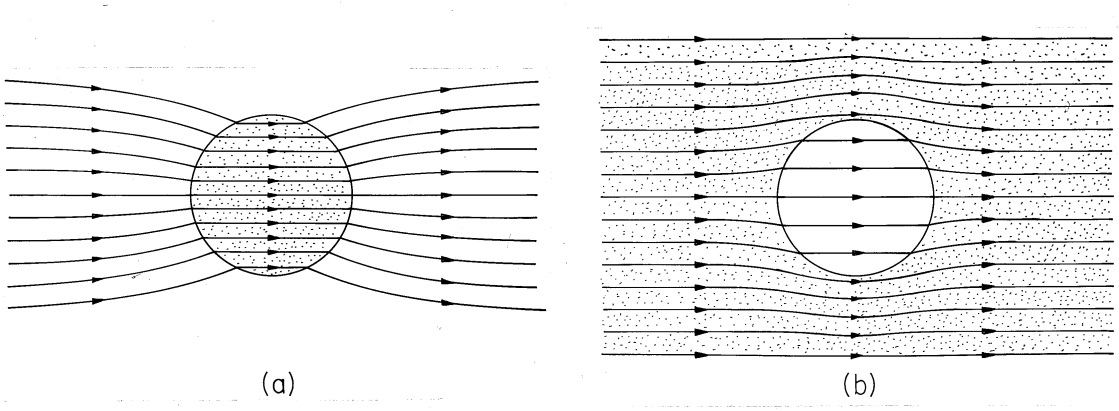


Fig. 7.5.2 Distribution of current density in and around the rod of Fig. 7.5.1. (a) $\sigma_b \geq \sigma_a$. (b) $\sigma_a \geq \sigma_b$.

regions, they have very different behaviors where the conductivity is discontinuous. In fact, the normal component of the current density is continuous at the interface, and the spacing between lines of **J** must be preserved across the interface. Thus, in the distribution of *current density* shown in Fig. 7.5.2, the lines are continuous. Note that the current tends to concentrate on the rod if it is more conducting, but is diverted around the rod if it is more insulating.

A surface charge density resides at the interface between the conducting media of different conductivities. This surface charge density acts as the source of **E** on the cylindrical surface and is identified by (7.2.17).

Inside-Outside Approximations. In exploiting the formal analogy between fields in linear dielectrics and in Ohmic conductors, it is important to keep in mind the very different physical phenomena being described. For example, there is no conduction analog to the free space permittivity ϵ_o. There is no minimum value of the conductivity, and although ϵ can vary between a minimum of ϵ_o in free space and $1000\epsilon_o$ or more in special solids, the electrical conductivity is even more widely varying. The ratio of the conductivity of a copper wire to that of its insulation exceeds 10^{21}.

Because some materials are very good conductors while others are very good insulators, steady conduction problems can exemplify the determination of fields for large ratios of physical parameters. In Sec. 6.6, we examined field distributions in cases where the ratios of permittivities were very large or very small. The "inside-outside" viewpoint is applicable not only to approximating fields in dielectrics but to finding the fields in the transient EQS systems in the latter part of this chapter and in MQS systems with magnetization and conduction.

Before attempting a more general approach, consider the following example, where the fields in and around a resistor are described.

Example 7.5.2. Fields in and around a Conductor

The circular cylindrical conductor of Fig. 7.5.3, having radius b and length L, is surrounded by a perfectly conducting circular cylindrical "can" having inside

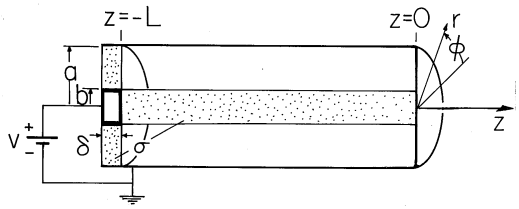


Fig. 7.5.3 Circular cylindrical conductor surrounded by coaxial perfectly conducting "can" that is connected to the right end by a perfectly conducting "short" in the plane $z = 0$. The left end is at potential v relative to right end and surrounding wall and is connected to that wall at $z = -L$ by a washer-shaped resistive material.

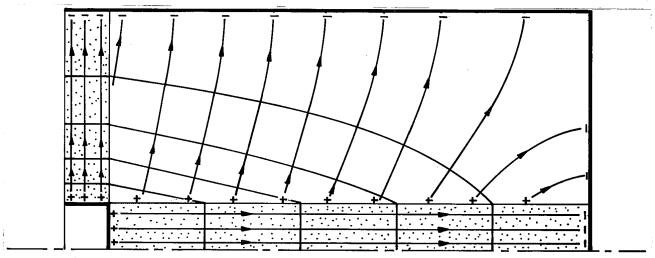


Fig. 7.5.4 Distribution of potential and electric field intensity for the configuration of Fig. 7.5.3.

radius a. With respect to the surrounding perfectly conducting shield, a dc voltage source applies a voltage v to the perfectly conducting disk. A washer-shaped material of thickness δ and also having conductivity σ is connected between the perfectly conducting disk and the outer can. What are the distributions of Φ and $\mathbf{E}$ in the conductors and in the annular free space region?

Note that the fields within each of the conductors are fully specified without regard for the shape of the can. The surfaces of the circular cylindrical conductor are either constrained in potential or bounded by free space. On the latter, the normal component of $\mathbf{J}$, and hence of $\mathbf{E}$, is zero. Thus, in the language of Sec. 7.4, the potential is constrained on S' while the normal derivative of Φ is constrained on the insulating surfaces S''. For the center conductor, S' is at $z = 0$ and $z = -L$ while S'' is at $r = b$. For the washer-shaped conductor, S' is at $r = b$ and $r = a$ and S'' is at $z = -L$ and $z = -(L + \delta)$. The theorem of Sec. 7.4 shows that the potential inside each of the conductors is uniquely specified. Note that this is true regardless of the arrangement outside the conductors.

In the cylindrical conductor, the solution for the potential that satisfies Laplace's equation and all these boundary conditions is simply a linear function of z.

$$\Phi^b = -\frac{v}{L}z \tag{6}$$

Thus, the electric field intensity is uniform and z directed.

$$\mathbf{E}^b = \frac{v}{L}\mathbf{i_z} \tag{7}$$

These equipotentials and $\mathbf{E}$ lines are sketched in Fig. 7.5.4. By way of reinforcing what is new about the insulating surface boundary condition, note that (6) and (7) apply to the cylindrical conductor regardless of its cross-section geometry and its length. However, the longer it is, the more stringent is the requirement that the annular region be insulating compared to the central region.

In the washer-shaped conductor, the axial symmetry requires that the potential not depend on z. If it depends only on the radius, the boundary conditions on the insulating surfaces are automatically satsfied. Two solutions to Laplace's equation are required to meet the potential constraints at $r = a$ and $r = b$. Thus, the solution is assumed to be of the form

$$\Phi^c = Alnr + B \tag{8}$$

The coefficients A and B are determined from the radial boundary conditions, and it follows that the potential within the washer-shaped conductor is

$$\Phi^c = v\frac{ln\left(\frac{r}{a}\right)}{ln\left(\frac{b}{a}\right)} \tag{9}$$

The "inside" fields can now be used to determine those in the insulating annular "outside" region. The potential is determined on all of the surface surrounding this region. In addition to being zero on the surfaces $r = a$ and $z = 0$, the potential is given by (6) at $r = b$ and by (9) at $z = -L$. So, in turn, the potential in this annular region is uniquely determined.

This is one of the few problems in this book where solutions to Laplace's equation that have both an r and a z dependence are considered. Because there is no ϕ dependence, Laplace's equation requires that

$$\left(\frac{\partial^2}{\partial z^2} + \frac{1}{r}\frac{\partial}{\partial r}r\frac{\partial}{\partial r}\right)\Phi = 0 \tag{10}$$

The linear dependence on z of the potential at $r = b$ suggests that solutions to Laplace's equation take the product form $R(r)z$. Substitution into (10) then shows that the r dependence is the same as given by (9). With the coefficients adjusted to make the potential $\Phi_a(a, -L) = 0$ and $\Phi_a(b, -L) = v$, it follows that in the outside insulating region

$$\Phi^a = \frac{v}{ln\left(\frac{a}{b}\right)}ln\left(\frac{r}{a}\right)\frac{z}{L} \tag{11}$$

To sketch this potential and the associated **E** lines in Fig. 7.5.4, observe that the equipotentials join points of the given potential on the central conductor with those of the same potential on the washer-shaped conductor. Of course, the zero potential surface is at $r = a$ and at $z = 0$. The lines of electric field intensity that originate on the surfaces of the conductors are perpendicular to these equipotentials and have tangential components that match those of the inside fields. Thus, at the surfaces of the finite conductors, the electric field in region (a) is neither perpendicular nor tangential to the boundary.

For a positive potential v, it is clear that there must be positive surface charge on the surfaces of the conductors bounding the annular insulating region. Remember that the normal component of **E** on the conductor sides of these surfaces is zero. Thus, there is a surface charge that is proportional to the normal component of **E** on the insulating side of the surfaces.

$$\sigma_s(r = b) = \epsilon_o E_r^a(r = b) = -\frac{\epsilon_o v}{b\,ln(a/b)}\frac{z}{L} \tag{12}$$

The order in which we have determined the fields makes it clear that this surface charge is the one required to accommodate the field configuration outside

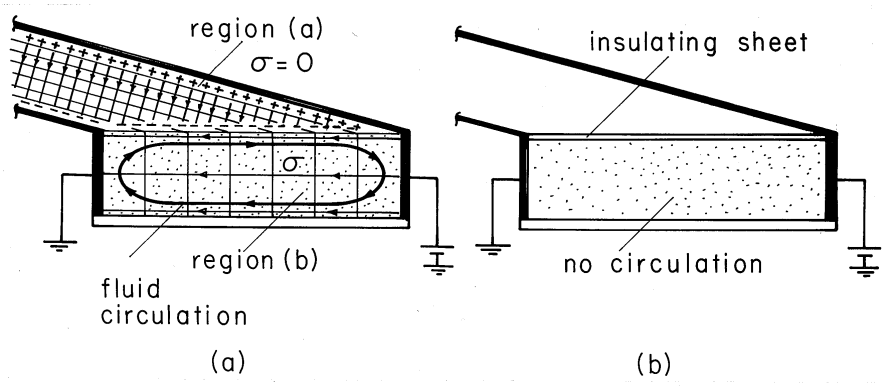


Fig. 7.5.5 Demonstration of the absence of volume charge density and existence of a surface charge density for a uniform conductor. (a) A slightly conducting oil is contained by a box constructed from a pair of electrodes to the left and right and with insulating walls on the other two sides and the bottom. The top surface of the conducting oil is free to move. The resulting surface force density sets up a circulating motion of the liquid, as shown. (b) With an insulating sheet resting on the interface, the circulating motion is absent.

the conducting regions. A change in the shield geometry changes Φ^a but does not alter the current distribution within the conductors. In terms of the circuit analogy used in Sec. 7.0, the potential distributions have been completely determined by the rod-shaped and washer-shaped resistors. The charge distribution is then determined *ex post facto* by the "distributed capacitors" surrounding the resistors.

The following demonstration shows that the unpaired charge density is zero in the volume of a uniformly conducting material and that charges do indeed tend to accumulate at discontinuities of conductivity.

Demonstration 7.5.1. Distribution of Unpaired Charge

A box is constructed so that two of its sides and its bottom are plexiglas, the top is open, and the sides shown to left and right in Fig. 7.5.5 are highly conducting. It is filled with corn oil so that the region between the vertical electrodes in Fig. 7.5.5 is semi-insulating. The region above the free surface is air and insulating compared to the corn oil. Thus, the corn oil plays a role analogous to that of the cylindrical rod in Example 7.5.2. Consistent with its insulating transverse boundaries and the potential constraints to left and right is an "inside" electric field that is uniform.

The electric field in the outside region (a) determines the distribution of charge on the interface. Since we have determined that the inside field is uniform, the potential of the interface varies linearly from v at the right electrode to zero at the left electrode. Thus, the equipotentials are evenly spaced along the interface. The equipotentials in the outside region (a) are planes joining the inside equipotentials and extending to infinity, parallel to the canted electrodes. Note that this field satisfies the boundary conditions on the slanted electrodes and matches the potential on the liquid interface. The electric field intensity is uniform, originating on the upper electrode and terminating either on the interface or on the lower slanted electrode. Because both the spacing and the potential difference vary linearly with horizontal distance, the negative surface charge induced on the interface is uniform.

Wherever there is an unpaired charge density, the corn oil is subject to an electrical force. There is unpaired charge in the immediate vicinity of the interface in the form of a surface charge, but not in the volume of the conductor. Consistent with this prediction is the observation that with the application of about 20 kV to electrodes having 20 cm spacing, the liquid is set into a circulating motion. The liquid moves rapidly to the right at the interface and recirculates in the region below. Note that the force at the interface is indeed to the right because it is proportional to the product of a negative charge and a negative electric field intensity. The fluid moves as though each part of the interface is being pulled to the right. But how can we be sure that the circulation is not due to forces on unpaired charges in the fluid volume?

An alteration to the same experiment answers this question. With a plexiglas sheet placed on the interface, it is mechanically pinned down. That is, the electrical force acting on the unpaired charges in the immediate vicinity of the interface is countered by viscous forces tending to prevent the fluid from moving tangential to the solid boundary. Yet because the sheet is insulating, the field distribution within the conductor is presumably unaltered from what it was before.

With the plexiglas sheet in place, the circulations of the first experiment are no longer observed. This is consistent with a model that represents the corn-oil as a uniform Ohmic conductor[1]. (For a mathematical analysis, see Prob. 7.5.3.)

In general, there is a two-way coupling between the fields in adjacent uniformly conducting regions. If the ratio of conductivities is either very large or very small, it is possible to calculate the fields in an "inside" region ignoring the effect of "outside" regions, and then to find the fields in the "outside" region. The region in which the field is first found, the "inside" region, is usually the one to which the excitation is applied, as illustrated in Example 7.5.2. This will be further illustrated in the following example, which pursues an approximate treatment of Example 7.5.1. The exact solutions found there can then be compared to the approximate ones.

Example 7.5.3. Approximate Current Distribution around Relatively Insulating and Conducting Rods

Consider first the field distribution around and then in a circular rod that has a small conductivity relative to its surroundings. Thus, in Fig. 7.5.1, $\sigma_a \gg \sigma_b$. Electrodes far to the left and right are used to apply a uniform field and current density to region (a). It is therefore in this inside region outside the cylinder that the fields are first approximated.

With the rod relatively insulating, it imposes on region (a) the approximate boundary condition that the normal current density, and hence the radial derivative of the potential, be zero at the rod surface, where $r = R$.

$$\mathbf{n} \cdot \mathbf{J}^a \approx 0 \Rightarrow \frac{\partial \Phi^a}{\partial r} \approx 0 \quad \text{at} \quad r = R \tag{13}$$

Given that the field at infinity must be uniform, the potential distribution in region (a) is now uniquely specified. A solution to Laplace's equation that satisfies this condition at infinity and includes an arbitrary coefficient for hopefully satisfying the

[1] See film *Electric Fields and Moving Media*, produced by the National Committee for Electrical Engineering Films and distributed by Education Development Center, 39 Chapel St., Newton, Mass. 02160.

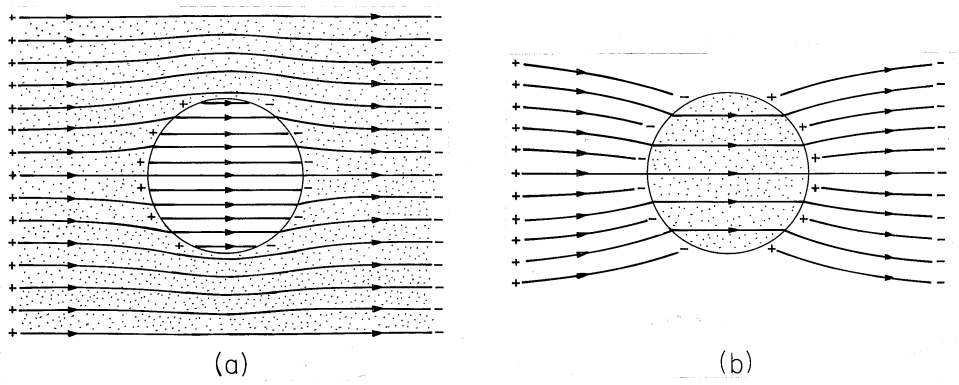


Fig. 7.5.6 Distributions of *electric field* intensity around conducting rod immersed in conducting medium: (a) $\sigma_a \gg \sigma_b$; (b) $\sigma_b \gg \sigma_a$. Compare these to distributions of *current density* shown in Fig. 7.5.2.

first condition is

$$\Phi^a = -E_o r\cos\phi + A\frac{\cos\phi}{r} \tag{14}$$

With A adjusted to satisfy (13), the approximate potential in region (a) is

$$\Phi^a = -E_o\Big(r + \frac{R^2}{r}\Big)\cos\phi \tag{15}$$

This is the potential in the exterior region, implying the field lines shown in Fig. 7.5.6a.

Now that we have obtained the approximate potential at $r = R$, $\Phi_b = -2E_oR\cos(\phi)$, we can in turn approximate the potential in region (b).

$$\Phi^b = Br\cos\phi = -2E_o r\cos\phi \tag{16}$$

The field lines associated with this potential are also shown in Fig. 7.5.6a. Note that if we take the limits of (4) and (5) where $\sigma_a/\sigma_b \gg 1$, we obtain these potentials.

Contrast these steps with those that are appropriate in the opposite extreme, where $\sigma_a/\sigma_b \ll 1$. There the rod tends to behave as an equipotential and the boundary condition at $r = R$ is $\Phi_a = \text{constant} = 0$. This condition is now used to evaluate the coefficient A in (14) to obtain

$$\Phi^a = -E_o\Big(r - \frac{R^2}{r}\Big)\cos\phi \tag{17}$$

This potential implies that there is a current density at the rod surface given by

$$J_r^a(r=R) = -\sigma_a\frac{\partial\Phi^a}{\partial r}(r=R) = 2\sigma_a E_o\cos\phi \tag{18}$$

The normal current density at the inside surface of the rod must be the same, so the coefficient B in (16) can be evaluated.

$$\Phi_b = -\frac{2\sigma_a}{\sigma_b}E_o r\cos\phi \tag{19}$$

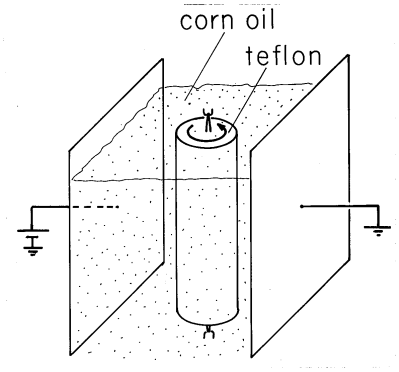


Fig. 7.5.7 Rotor of insulating material is immersed in somewhat conducting corn oil. Plane parallel electrodes are used to impose constant electric field, so from the top, the distribution of electric field should be that of Fig. 7.5.6a, at least until the rotor begins to rotate spontaneously in either direction.

Now the field lines are as shown in Fig. 7.5.6b.

Again, the approximate potential distributions given by (17) and (19), respectively, are consistent with what is obtained from the exact solutions, (4) and (5), in the limit $\sigma_a/\sigma_b \ll 1$.

In the following demonstration, a surprising electromechanical response has its origins in the charge distribution implied by the potential distributions found in Example 7.5.3.

Demonstration 7.5.2. Rotation of an Insulating Rod in a Steady Current

In the apparatus shown in Fig. 7.5.7, a teflon rod is mounted at its ends on bearings so that it is free to rotate. It, and a pair of plane parallel electrodes, are immersed in corn oil. Thus, from the top, the configuration is as shown in Fig. 7.5.1. The applied field $E_o = v/d$, where v is the voltage applied between the electrodes and d is their spacing. In the experiment, $R = 1.27$ cm , $d = 11.8$ cm, and the applied voltage is 10–20 kV.

As the voltage is raised, there is a threshold at which the rod begins to rotate. With the voltage held fixed at a level above the threshold, the ensuing rotation is continuous and in either direction. [See footnote 1.]

To explain this "motor," note that even though the corn oil used in the experiment has a conductivity of $\sigma_a = 5 \times 10^{-11}$ S/m, that is still much greater than the conductivity σ_b of the rod. Thus, the potential around and in the rod is given by (15) and (16) and the $\mathbf{E}$ field distribution is as shown in Fig. 7.5.6a. Also shown in this figure is the distribution of unpaired surface charge, which can be evaluated using (16).

$$\sigma_s(r=R) = \mathbf{n} \cdot (\epsilon_a E_r^a - \epsilon_b E_r^b) = \epsilon_b \frac{\partial \Phi^b}{\partial r}(r=R) = -2\epsilon_b E_o \cos\phi \tag{20}$$

Positive charges on the left electrode induce charges of the *same* sign on the nearer side of the rod, as do the negative charges on the electrode to the right. Thus, when static, the rod is in a posture analogous to that of a compass needle oriented

backwards in a magnetic field. Its static state is unstable and it attempts to reorient itself in the field. The continuous rotation results because once it begins to rotate, additional fields are generated that allow the charge to leak off the cylinder through currents in the surrounding oil.

Note that if the rod were much more conducting than its surroundings, charges on the electrodes would induce charges of opposite sign on the nearer surfaces of the rod. This more familiar situation is the one shown in Fig. 7.5.6b.

The condition requiring that there be no normal current density at an insulating boundary can have a dramatic effect on fringing fields. This has already been illustrated by Example 7.5.2, where the field was uniform in the central conductor no matter what its length relative to its radius. Whenever we take the resistance of a wire having length L, cross-sectional area A, and conductivity σ as being $L/\sigma A$, we exploit this boundary condition.

The conduction analogue of Example 6.6.3 gives a further illustration of how an insulating boundary ducts the electric field intensity. With $\epsilon_a \to \sigma_a$ and $\epsilon_b \to \sigma_b$, the configuration of Fig. 6.6.8 becomes the edge of a plane parallel resistor filled out to the edge of the electrodes by a material having conductivity σ_b. The fringing field then depends on the conductivity σ_a of the surrounding material.

The fringing field that would result if the entire region were filled by a material having a uniform conductivity is shown in Fig. 6.6.9a. By contrast, the field distribution with the conducting material extending only to the edge of the electrode is shown in Fig. 6.6.9b. The field inside is exactly uniform and independent of the geometry of what is outside. Of course, there is always a fringing field outside that does depend on the outside geometry. But because there is little associated current density, the resistance is unaffected by this part of the field.

7.6 CONDUCTION ANALOGS

The potential distribution for steady conduction is determined by solving (7.4.1)

$$\nabla \cdot \sigma \nabla \Phi_c = -s \tag{1}$$

in a volume V having conductivity $\sigma(\mathbf{r})$ and current source distribution $s(\mathbf{r})$, respectively.

On the other hand, if the volume is filled by a perfect dielectric having permittivity $\epsilon(\mathbf{r})$ and unpaired charge density distribution $\rho_u(\mathbf{r})$, respectively, the potential distribution is determined by the combination of (6.5.1) and (6.5.2).

$$\nabla \cdot \epsilon \nabla \Phi_e = -\rho_u \tag{2}$$

It is clear that solutions pertaining to one of these physical situations are solutions for the other, provided that the boundary conditions are also analogous. We have been exploiting this analogy in Sec. 7.5 for piece-wise continuous systems. There, solutions for the fields in dielectrics were applied to conduction problems. Of course, measurements made on dielectrics can also be used to predict steady conduction phemonena.

Conversely, fields found either theoretically or by experimentation in a steady conduction situation can be used to describe those in perfect dielectrics. When measurements are used, the latter procedure is a particularly useful one, because conduction processes are conveniently simulated and comparatively easy to measure. It is more difficult to measure the potential in free space than in a conductor, and to measure a capacitance than a resistance.

Formally, a quantitative analogy is established by introducing the constant ratios for the magnitudes of the properties, sources, and potentials, respectively, in the two systems throughout the volumes and on the boundaries. With k_1 and k_2 defined as scaling constants,

$$\frac{\epsilon}{\sigma} = k_1, \qquad \frac{\Phi_c}{\Phi_e} = k_2, \qquad \frac{k_2}{k_1} = \frac{s}{\rho_u} \tag{3}$$

substitution of the conduction variables into (2) converts it into (1). The boundary conditions on surfaces S' where the potential is constrained are analogous, provided the boundary potentials also have the constant ratio k_2 given by (3).

Most often, interest is in systems where there are no volume source distributions. Thus, suppose that the capacitance of a pair of electrodes is to be determined by measuring the conductance of analogously shaped electrodes immersed in a conducting material. The ratio of the measured capacitance to conductance, the ratio of (6.5.6) to (7.2.15), follows from substituting $\epsilon = k_1\sigma$, (3a),

$$\frac{C}{G} = \frac{\int_{S_1} \epsilon \mathbf{E} \cdot d\mathbf{a}/v}{\int_{S_1} \sigma \mathbf{E} \cdot d\mathbf{a}/v} = \frac{k_1 \int_{S_1} \sigma \mathbf{E} \cdot d\mathbf{a}/v}{\int_{S_1} \sigma \mathbf{E} \cdot d\mathbf{a}/v} = k_1 = \frac{\epsilon}{\sigma} \tag{4}$$

In multiple terminal pair systems, the capacitance matrix defined by (5.1.12) and (5.1.13) is similarly deduced from measurement of a conductance matrix, defined in (7.4.6).

Demonstration 7.6.1. Electrolyte-Tank Measurements

If great accuracy is required, fields in complex geometries are most easily determined numerically. However, especially if the capacitance is sought– and not a detailed field mapping– a conduction analog can prove convenient. A simple experiment to determine the capacitance of a pair of electrodes is shown in Fig. 7.6.1, where they are mounted on insulated rods, contacted through insulated wires, and immersed in tap water. To avoid electrolysis, where the conductors contact the water, low-frequency ac is used. Care should be taken to insure that boundary conditions imposed by the tank wall are either analogous or inconsequential.

Often, to motivate or justify approximations used in analytical modeling of complex systems, it is helpful to probe the potential distribution using such an experiment. The probe consists of a small metal tip, mounted and wired like the electrodes, but connected to a divider. By setting the probe potential to the desired rms value, it is possible to trace out equipotential surfaces by moving the probe in such a way as to keep the probe current nulled. Commercial equipment is automated with a feedback system to perform such measurements with great precision. However, given the alternative of numerical simulation, it is more likely that such approaches are appropriate in establishing rough approximations.

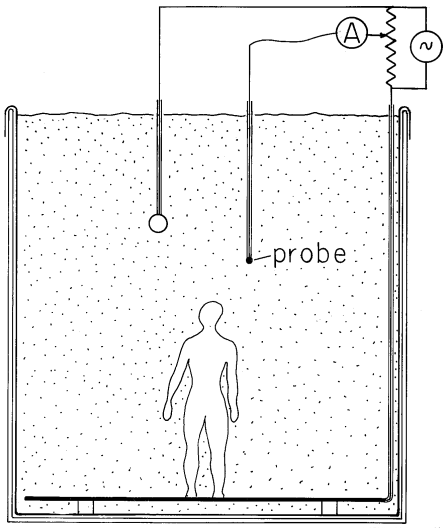


Fig. 7.6.1 Electrolytic conduction analog tank for determining potential distributions in complex configurations.

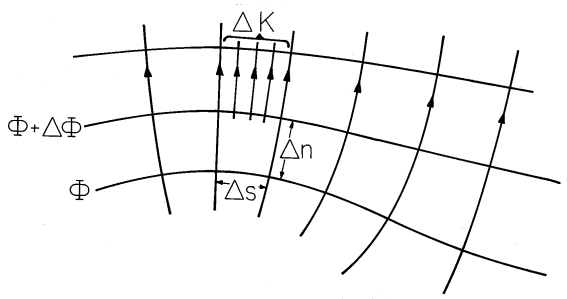


Fig. 7.6.2 In two dimensions, equipotential and field lines predicted by Laplace's equation form a grid of curvilinear squares.

Mapping Fields that Satisfy Laplace's Equation. Laplace's equation determines the potential distribution in a volume filled with a material of uniform conductivity that is source free. Especially for two-dimensional fields, the conduction analog then also gives the opportunity to refine the art of sketching the equipotentials of solutions to Laplace's equation and the associated field lines.

Before considering how a sheet of conducting paper provides the medium for determining two-dimensional fields, it is worthwhile to identify the properties of a field sketch that indeed represents a two-dimensional solution to Laplace's equation.

A review of the many two-dimensional plots of equipotentials and fields given in Chaps. 4 and 5 shows that they form a grid of curvilinear rectangles. In terms of variables defined for the field sketch of Fig. 7.6.2, where the distance between equipotentials is denoted by Δn and the distance between $\mathbf{E}$ lines is Δs, the ratio $\Delta n/\Delta s$ tends to be constant, as we shall now show.

The condition that the field be irrotational gives

$$\mathbf{E} = -\nabla\Phi \Rightarrow |\mathbf{E}| \approx \frac{|\Delta\Phi|}{|\Delta n|} \tag{5}$$

while the steady charge conservation law implies that along a flux tube,

$$\nabla \cdot \sigma\mathbf{E} = 0 \Rightarrow \sigma|\mathbf{E}|\Delta s = \text{constant} \equiv \Delta K \tag{6}$$

Thus, along a flux tube,

$$\sigma\frac{\Delta\Phi}{\Delta n}\Delta s = \Delta K \Rightarrow \frac{\Delta s}{\Delta n} = \frac{\Delta K}{\sigma\Delta\Phi} = \text{constant} \tag{7}$$

If each of the flux tubes carries the same current, and if the equipotential lines are drawn for equal increments of $\Delta\Phi$, then the ratio $\Delta s/\Delta n$ must be constant throughout the mapping. The sides of the curvilinear rectangles are commonly made equal, so that the equipotentials and field lines form a grid of curvilinear squares.

The faithfulness to Laplace's equation of a map of equipotentials at equal increments in potential can be checked by sketching in the perpendicular field lines. With the field lines forming curvilinear squares in the starting region, a correct distribution of the equipotentials is achieved when a grid of squares is maintained throughout the region. With some practice, it is possible to iterate between refinements of the equipotentials and the field lines until a satisfactory map of the solution is sketched.

Demonstration 7.6.2. Two-Dimensional Solution to Laplace's Equation by Means of Teledeltos Paper

For the mapping of *two-dimensional* fields, the conduction analog has the advantage that it is not necessary to make the electrodes and conductor "infinitely" long in the third dimension. Two-dimensional current distributions will result even in a thin-sheet conductor, provided that it has a conductivity that is large compared to its surroundings. Here again we exploit the boundary condition applying to the surfaces of the paper. As far as the fields inside the paper are concerned, a two-dimensional current distribution automatically meets the requirement that there be no current density normal to those parts of the paper bounded by air.

A typical field mapping apparatus is as simple as that shown in Fig. 7.6.3. The paper has the thickness Δ and a conductivity σ. The electrodes take the form of silver paint or copper tape put on the upper surface of the paper, with a shape simulating the electrodes of the actual system. Because the paper is so thin compared to dimensions of interest in the plane of the paper surface, the currents from the electrodes quickly assume an essentially uniform profile over the cross-section of the paper, much as suggested by the inset to Fig. 7.6.3.

In using the paper, it is usual to deal in terms of a surface resistance $1/\Delta\sigma$. The conductance of the plane parallel electrode system shown in Fig. 7.6.4 can be used to establish this parameter.

$$\frac{i}{v} = \frac{w\Delta\sigma}{S} \equiv G_p \Rightarrow \Delta\sigma = G_p\frac{S}{w} \tag{8}$$

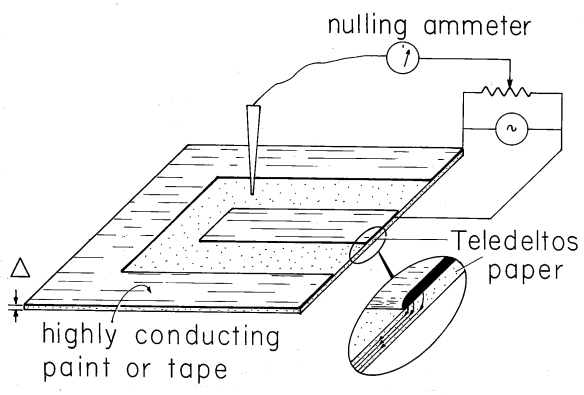


Fig. 7.6.3 Conducting paper with attached electrodes can be used to determine two-dimensional potential distributions.

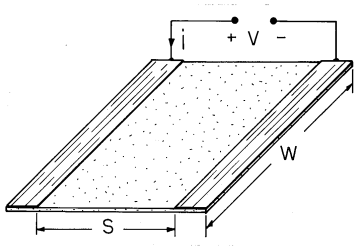


Fig. 7.6.4 Apparatus for determining surface conductivity $\Delta\sigma$ of paper used in experiment shown in Fig. 7.6.3.

The units are simply ohms, and $1/\Delta\sigma$ is the resistance of a square of the material having any sidelength. Thus, the units are commonly denoted as "ohms/square."

To associate a conductance as measured at the terminals of the experiment shown in Fig. 7.6.3 with the capacitance of a pair of electrodes having length l in the third dimension, note that the surface integrations used to define C and G reduce to

$$C = \frac{l}{v}\oint_C \epsilon\mathbf{E}\cdot d\mathbf{s}; \qquad G = \frac{\Delta}{v}\oint_C \sigma\mathbf{E}\cdot d\mathbf{s} \tag{9}$$

where the surface integrals have been reduced to line integrals by carrying out the integration in the third dimension. The ratio of these quantities follows in terms of the surface conductance $\Delta\sigma$ as

$$\frac{C}{G} = \frac{lk_1}{\Delta} = \frac{l\epsilon}{\Delta\sigma} \tag{10}$$

Here G is the conductance as actually measured using the conducting paper, and C is the capacitance of the two-dimensional capacitor it simulates.

In Chap. 9, we will find that magnetic field distributions as well can often be found by using the conduction analog.

TABLE 7.7.1
CHARGE RELAXATION TIMES OF TYPICAL MATERIALS

	$\sigma - \mathrm{S/m}$	ϵ/ϵ_o	$\tau_e - s$
Copper	5.8×10^{7}	1	1.5×10^{-19}
Water, distilled	2×10^{-4}	81	3.6×10^{-6}
Corn oil	5×10^{-11}	3.1	0.55
Mica	$10^{-11} - 10^{-15}$	5.8	$5.1 - 5.1 \times 10^{4}$

7.7 CHARGE RELAXATION IN UNIFORM CONDUCTORS

In a region that has uniform conductivity and permittivity, charge conservation and Gauss' law determine the unpaired charge density throughout the *volume* of the material, without regard for the boundary conditions. To see this, Ohm's law (7.1.7) is substituted for the current density in the charge conservation law, (7.0.3),

$$\nabla \cdot \sigma \mathbf{E} + \frac{\partial \rho_u}{\partial t} = 0 \tag{1}$$

and Gauss' law (6.2.15) is written using the linear polarization constitutive law, (6.4.3).

$$\nabla \cdot \epsilon \mathbf{E} = \rho_u \tag{2}$$

In a region where σ and ϵ are uniform, these parameters can be pulled outside the divergence operators in these equations. Substitution of $div\,\mathbf{E}$ found from (2) into (1) then gives the charge relaxation equation for ρ_u.

$$\boxed{\frac{\partial \rho_u}{\partial t} + \frac{\rho_u}{\tau_e} = 0; \qquad \tau_e \equiv \frac{\epsilon}{\sigma}} \tag{3}$$

Note that it has not been assumed that $\mathbf{E}$ is irrotational, so *the unpaired charge obeys this equation whether the fields are EQS or not.*

The solution to (3) takes on the same appearance as if it were an ordinary differential equation, say predicting the voltage of an RC circuit.

$$\rho_u = \rho_i(x, y, z)e^{-t/\tau_e} \tag{4}$$

However, (3) is a partial differential equation, and so the coefficient of the exponential in (4) is an arbitrary function of the spatial coordinates. The *relaxation time* τ_e has the typical values illustrated in Table 7.7.1.

The function $\rho_i(x, y, z)$ is the unpaired charge density when $t = 0$. Given any initial distribution, the subsequent distribution of ρ_u is given by (4). Once the

unpaired charge density has decayed to zero at a given point, it will remain zero. This is true regardless of the constraints on the surface bounding the region of uniform σ and ϵ. *Except for a transient that can only be initiated from very special initial conditions, the unpaired charge density in a material of uniform conductivity and permittivity is zero. This is true even if the system is not EQS.*

The following example is intended to help emphasize these implications of (3) and (4).

Example 7.7.1. Charge Relaxation in Region of Uniform σ and ϵ

In the region of uniform σ and ϵ shown in Fig. 7.7.1, the initial distribution of unpaired charge density is

$$\rho_i = \begin{cases} \rho_o; & r < a \\ 0; & a < r \end{cases} \tag{5}$$

where ρ_o is a constant.

It follows from (4) that the subsequent distribution is

$$\rho_u = \begin{cases} \rho_o e^{-t/\tau_e}; & r < a \\ 0; & a < r \end{cases}$$

As pictured in Fig. 7.7.1, the charge density in the spherical region $r < a$ remains uniform as it decays to zero with the time constant τ_e. The charge density in the surrounding region is initially zero and remains so throughout the transient.

Charge conservation implies that there must be a current density in the material surrounding the initially charged spherical region. Yet, according to the laws used here, there is never a net unpaired charge density in that region. This is possible because in Ohmic conduction, there are at least two types of charges involved. In the uniformly conducting material, one or both of these migrate in the electric field caused by the net charge [in accordance with (7.1.5)] while exactly neutralizing each other so that $\rho_u = 0$ (7.1.6).

Net Charge on Bodies Immersed in Uniform Materials[2]. The integral charge relaxation law, (1.5.2), applies to the net charge within any volume containing a medium of constant ϵ and σ. If an initially charged particle finds itself suspended in a fluid having uniform σ and ϵ, this charge must decay with the charge relaxation time constant τ_e.

Demonstration 7.7.1. Relaxation of Charge on Particle in Ohmic Conductor

The pair of plane parallel electrodes shown in Fig. 7.7.2 is immersed in a semi-insulating liquid, such as corn oil, having a relaxation time on the order of a second. Initially, a metal particle rests on the lower electrode. Because this particle makes electrical contact with the lower electrode, application of a potential difference results in charge being induced not only on the surfaces of the electrodes but on the surface of the particle as well. At the outset, the particle is an extension of the lower

[2] This subsection is not essential to the material that follows.

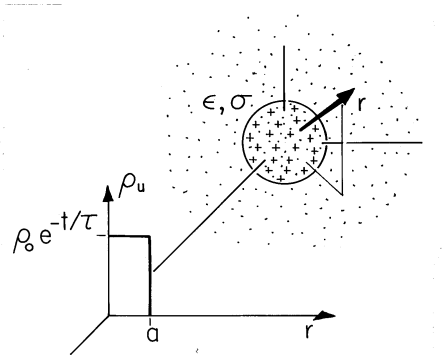


Fig. 7.7.1 Within a material having uniform conductivity and permittivity, initially there is a uniform charge density ρ_u in a spherical region, having radius a. In the surrounding region the charge density is given to be initially zero and found to be always zero. Within the spherical region, the charge density is found to decay exponentially while retaining its uniform distribution.

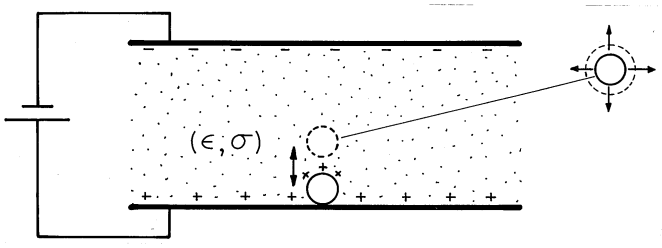


Fig. 7.7.2 The region between plane parallel electrodes is filled by a semi-insulating liquid. With the application of a constant potential difference, a metal particle resting on the lower plate makes upward excursions into the fluid. [See footnote 1.]

electrode. Thus, there is an electrical force on the particle that is upward. Note that changing the polarity of the voltage changes the sign of both the particle charge and the field, so the force is always upward.

As the voltage is raised, the electrical force outweighs the net gravitational force on the particle and it lifts off. As it separates from the lower electrode, it does so with a net charge sufficient to cause the electrical force to start it on its way toward charges of the opposite sign on the upper electrode. However, if the liquid is an Ohmic conductor with a relaxation time shorter than that required for the particle to reach the upper electrode, the net charge on the particle decays, and the upward electrical force falls below that of the downward gravitational force. In this case, the particle falls back to the lower electrode without reaching the upper one. Upon contacting the lower electrode, its charge is renewed and so it again lifts off. Thus, the particle appears to bounce on the lower electrode.

By contrast, if the oil has a relaxation time long enough so that the particle can reach the upper electrode before a significant fraction of its charge is lost, then the particle makes rapid excursions between the electrodes. Contact with the upper electrode results in a charge reversal and hence a reversal in the electrical force as well.

The experiment demonstrates that as long as a particle is electrically isolated

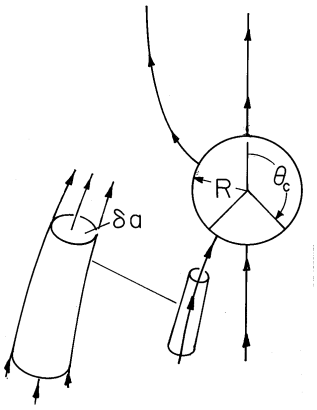


Fig. 7.7.3 Particle immersed in an initially uniform electric field is charged by unipolar current of positive ions following field lines to its surface. As the particle charges, the "window" over which it can collect ions becomes closed.

in an Ohmic conductor, its charge will decay to zero and will do so with a time constant that is the relaxation time ϵ/σ. According to the Ohmic model, once the particle is surrounded by a uniformly conducting material, it cannot be given a net charge by any manipulation of the potentials on electrodes bounding the Ohmic conductor. The charge can only change upon contact with one of the electrodes.

We have found that a particle immersed in an *Ohmic* conductor can only discharge. This is true even if it finds itself in a region where there is an externally imposed conduction current. By contrast, the next example illustrates how a *unipolar* conduction process can be used to charge a particle. The ion-impact charging (or field charging) process is put to work in electrophotography and air pollution control.

Example 7.7.2. Ion-Impact Charging of Macroscopic Particles

The particle shown in Fig. 7.7.3 is itself perfectly conducting. In its absence, the surrounding region is filled by an un-ionized gas such as air permeated by a uniform z-directed electric field. Positive ions introduced at $z \to -\infty$ then give rise to a unipolar current having a density given by the unipolar conduction law, (7.1.8). With the introduction of the particle, some of the lines of electric field intensity can terminate on the particle. These carry ions to the particle. Other lines originate on the particle and it is assumed that there is no mechanism for the particle surface to initiate ions that would then carry charge away from the particle along these lines. Thus, as the particle intercepts some of the ion current, it charges up.

Here the particle-charging process is described as a sequence of steady states. The charge conservation equation (7.0.3) obtained by using the unipolar conduction law (7.1.8) then requires that

$$\nabla \cdot (\mu\rho\mathbf{E}) = 0 \tag{6}$$

Thus, the "field" $\rho\mathbf{E}$ (consisting of the product of the charge density and the electric field intensity) forms flux tubes. These have walls tangential to $\mathbf{E}$ and incremental

cross-sectional areas $\delta\mathbf{a}$, as illustrated in Figs.7.7.3 and 2.7.5, such that $\rho\mathbf{E}\cdot\delta\mathbf{a}$ remains constant.

As a second approximation, it is assumed that the dominant sources for the electric field are on the boundaries, either on the surface of the particle or at infinity. Thus, the ions in the volume of the gas are low enough in concentration so that their volume charge density makes a negligible contribution to the electric field intensity. At each point in the volume of the gas,

$$\nabla\cdot\epsilon_o\mathbf{E}\approx 0 \tag{7}$$

From this statement of Gauss' law, it follows that the $\mathbf{E}$ lines also form flux tubes along which $\mathbf{E}\cdot\delta\mathbf{a}$ is conserved. Because both $\mathbf{E}\cdot\delta\mathbf{a}$ and $\rho\mathbf{E}\cdot\delta\mathbf{a}$ are constant along a given $\mathbf{E}$ line, it is necessary that the charge density ρ be constant along these lines. This fact will now be used to calculate the current of ions to the particle.

At a given instant in the charging process, the particle has a net charge q. Its surface is an equipotential and it finds itself in an electric field that is uniform at infinity. The distribution of electric field for this situation was found in Example 5.9.2. Lines of electric field intensity terminate on the southern end of the sphere over the range $\pi\geq\theta\geq\theta_c$, where θ_c is shown in Figs. 7.7.3 and 5.9.2. In view of the unipolar conduction law, these lines carry with them a current density. Thus, there is a net current into the particle given by

$$i=\int_{\theta_c}^{\pi}-\mu\rho E_r(r=R,\theta)(2\pi R\sin\theta R d\theta) \tag{8}$$

Because ρ is constant along an electric field line and ρ is uniform far from the charge-collecting particles, it is a constant over the surface of integration.

It follows from (5.9.13) that the normal electric field needed to evaluate (8) is

$$E_r=-\frac{\partial\Phi}{\partial r}\Big|_{r=R}=3E_a\cos\theta+\frac{q}{4\pi\epsilon_o R^2} \tag{9}$$

Substitution of (9) into (8) gives

$$i=-\mu\rho 6\pi R^2E_a\int_{\theta_c}^{\pi}\Big(\cos\theta+\frac{q}{q_c}\Big)\sin\theta d\theta \tag{10}$$

where, as in Example 5.9.2, $q_c=12\pi\epsilon_o R^2E_a$ and

$$-\cos\theta_c=\frac{q}{q_c} \tag{11}$$

Remember, θ_c is the angle at which the radial electric field switches from being outward to inward. Thus, it is a function of the amount of charge on the particle. Substitution of (11) into (10) and some manipulation gives the net current to the particle as

$$i=\frac{q_c}{\tau_i}\Big(1-\frac{q}{q_c}\Big)^2 \tag{12}$$

where $\tau_i=4\epsilon_o/\mu\rho$.

From (10) it is clear that the current depends on the particle charge. As charge accumulates on the particle, the angle θ_c increases and so the southern surface over

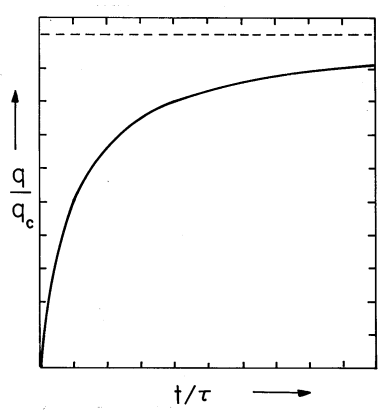


Fig. 7.7.4 Normalized particle charge as a function of normalized time. The saturation charge q_c and charging time τ are given after (10) and (12), respectively.

which electric field lines terminate decreases. By the time $q = q_c$, the collection surface is zero and, as implied by (12), the current goes to zero.

If the charging process is slow enough to be viewed as a sequence of stationary states, the current given by (12) is equal to the rate of increase of the particle charge.

$$\frac{dq}{dt} = i \Rightarrow \frac{d(q/q_c)}{d(t/\tau_i)} = \left(1 - \frac{q}{q_c}\right)^2 \tag{13}$$

Divided by what is on the right and multiplied by the denominator on the left, this expression can be integrated.

$$\int_0^{q/q_c} \frac{d\left(\frac{q'}{q_c}\right)}{\left(1 - \frac{q'}{q_c}\right)^2} = \int_0^{t/\tau_i} d\left(\frac{t}{\tau_i}\right) \tag{14}$$

The result is a charging law that is not exponential but rather

$$\frac{q}{q_c} = \frac{t/\tau_i}{1 + t/\tau_i} \tag{15}$$

This charging transient is shown in Fig. 7.7.4. By contrast with a particle placed in a conduction current that is Ohmic, a particle subjected to a unipolar current will charge up to the saturation charge q_c. Note that the charging time, $\tau_i = 4\epsilon_o/\mu\rho$, again takes the form of ϵ divided by a "conductivity."

Demonstration 7.7.2. Electrostatic Precipitation

Once dust, smoke, or fume particles are charged, they can be subjected to an electric field and pulled out of the gas in which they are interspersed. In large precipitators used to filter combustion gases before they are released from a stack, the charging and precipitation processes are carried out in one region. The apparatus of Fig. 7.7.5 illustrates this process.

A fine wire is stretched along the axis of a grounded conducting cylinder having a radius of 5–10 cm. With the wire at a voltage of 10–30 kv, a hissing sound gives

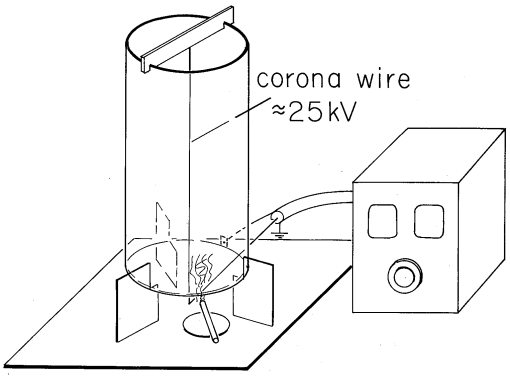


Fig. 7.7.5 Electrostatic precipitator consisting of fine wire at high voltage relative to surrounding conducting transparent coaxial cylinder. Ions created in corona discharge in the immediate vicinity of the wire follow field lines toward outer wall, some terminating on smoke particles. Once charged by the mechanism described in Example 7.7.2, the smoke particles are precipitated on the outer wall.

evidence of ionization of the air in the immediate vicinity of the wire. This corona discharge provides positive and negative ion pairs adjacent to the wire. If the wire is positive, some of the positive ions are drawn out of this region and migrate to the cylindrical outer wall. Thus, outside the corona discharge region there is a unipolar conduction current of the type postulated in Example 7.7.2. The ion mobility is typically $(1 \rightarrow 2) \times 10^{-4}$ (m/s)/(v/m), while the field is on the order of 5×10^5 v/m, so the ion velocity (7.1.3) is in the range of $50 - 100$ m/s.

Smoke particles, mixed with air rising through the cylinder, can be seen to be removed from the gas within a second or so. Large polyethylene particles dropped in from the top can be more readily seen to collect on the walls. In a practical precipitator, the collection electrodes are periodically rapped so that chunks of the collected material drop into a hopper below.

Most of the time required to clear the air of smoke is spent by the particle in migrating to the wall after it has been charged. The charging time constant τ_i is typically only a few milliseconds.

This demonstration further emphasizes the contrast between the behavior of a macroscopic particle when immersed in an Ohmic conductor, as in the previous demonstration, and when subjected to unipolar conduction. A particle immersed in a unipolar "conductor" becomes charged. In a uniform Ohmic conductor, it can only discharge.

7.8 ELECTROQUASISTATIC CONDUCTION LAWS FOR INHOMOGENEOUS MATERIALS

In this section, we extend the discussion of transients to situations in which the electrical permittivity and Ohmic conductivity are arbitrary functions of space.

$$\epsilon = \epsilon(\mathbf{r}), \qquad \sigma = \sigma(\mathbf{r}) \tag{1}$$

Distributions of these parameters, as exemplified in Figs. 6.5.1 and 7.2.3, might be uniform, piece-wise uniform, or smoothly nonuniform. The specific examples falling into these categories answer three questions.

(a) Where does the unpaired charge density, found in Sec. 7.7, tend to accumulate when it disappears from a region having uniform properties.
(b) With the unpaired charge density determined by the self-consistent EQS laws, what is the equation governing the potential distribution throughout the volume of interest?
(c) What boundary and initial conditions make the solutions to this equation unique?

The laws studied in this section and exemplified in the next describe both the perfectly insulating limit of Chap. 6 and the conduction dominated limit of Secs. 7.1–7.6. More important, as suggested in Sec. 7.0, they describe how these limiting situations are related in EQS systems.

Evolution of Unpaired Charge Density. With a nonuniform conductivity distribution, the statement of charge conservation and Ohm's law expressed by (7.7.1) becomes

$$\sigma\nabla\cdot\mathbf{E}+\mathbf{E}\cdot\nabla\sigma+\frac{\partial\rho_u}{\partial t}=0 \tag{2}$$

Similarly, with a nonuniform permittivity, Gauss' law as given by (7.7.2) becomes

$$\epsilon\nabla\cdot\mathbf{E}+\mathbf{E}\cdot\nabla\epsilon=\rho_u \tag{3}$$

Elimination of $\nabla\cdot\mathbf{E}$ between these equations gives an expression that is the generalization of the charge relaxation equation, (7.7.3).

$$\frac{\partial\rho_u}{\partial t}+\frac{\rho_u}{(\epsilon/\sigma)}=-\mathbf{E}\cdot\nabla\sigma+\frac{\sigma}{\epsilon}\mathbf{E}\cdot\nabla\epsilon \tag{4}$$

Wherever the electric field has a component in the direction of a gradient of σ or ϵ, the unpaired charge density can be present and can be temporally increasing or decreasing. If a steady state has been established, in the sense that time rates of change are negligible, the charge distribution is given by (4), because then, $\partial\rho_u/\partial t=0$. Note that this is the distribution of (7.2.8) that prevails for steady conduction. We can therefore expect that the charge density found to disappear from a region of uniform properties in Sec. 7.7 will reappear at surfaces of discontinuity of σ and ϵ or in regions where ϵ and σ vary smoothly.

Electroquasistatic Potential Distribution. To evaluate (4), the self-consistent electric field intensity is required. With the objective of determining that field, Gauss' law, (7.7.2), is used to eliminate ρ_u from the charge conservation statement, (7.7.1).

$$\nabla\cdot\sigma\mathbf{E}+\frac{\partial}{\partial t}(\nabla\cdot\epsilon\mathbf{E})=0 \tag{5}$$

For the first time in the analysis of charge relaxation, we now introduce the electroquasistatic approximation

$$\nabla \times \mathbf{E} \simeq 0 \Rightarrow \mathbf{E} = -\nabla\Phi \tag{6}$$

and (5) becomes the desired expression governing the evolution of the electric potential.

$$\boxed{\nabla \cdot \left(\sigma\nabla\Phi + \frac{\partial}{\partial t}\epsilon\nabla\Phi\right) = 0} \tag{7}$$

Uniqueness. Consider now the initial and boundary conditions that make solutions to (7) unique. Suppose that throughout the volume V, the initial charge distribution is given as

$$\rho_u(\mathbf{r}, t = 0) = \rho_i(\mathbf{r}) \tag{8}$$

and that on the surface S enclosing this volume, the potential is a given function of time

$$\Phi = \Phi_i(\mathbf{r}, t) \text{ on } S \text{ for } t \geq 0. \tag{9}$$

Thus, when $t = 0$, the initial distribution of electric field intensity satisfies Gauss' law. The initial potential distribution satisfies the same law as for regions occupied by perfect dielectrics.

$$\nabla \cdot \epsilon\nabla\Phi_i = -\rho_i \tag{10}$$

Given the boundary condition of (9) when $t = 0$, it follows from Sec. 5.2 that the initial distribution of potential is uniquely determined.

Is the subsequent evolution of the field uniquely determined by (7) and the initial and boundary conditions? To answer this question, we will take a somewhat more formal approach than used in Sec. 5.2 but nevertheless use the same reasoning. Supose that there are two solutions, $\Phi = \Phi_a$ and $\Phi = \Phi_b$, that satisfy (7) and the same initial and boundary conditions.

Equation (7) is written first with $\Phi = \Phi_a$ and then with $\Phi = \Phi_b$. With $\Phi_d \equiv \Phi_a - \Phi_b$, the difference between these two equations becomes

$$\nabla \cdot \left[\sigma\nabla\Phi_d + \frac{\partial}{\partial t}(\epsilon\nabla\Phi_d)\right] = 0 \tag{11}$$

Multiplication of (11) by Φ_d and integration over the volume V gives

$$\int_V \Phi_d \nabla \cdot \left[\sigma\nabla\Phi_d + \frac{\partial}{\partial t}(\epsilon\nabla\Phi_d)\right] dv = 0 \tag{12}$$

The objective in the following manipulation is to turn this integration either into one over positive definite quantities or into an integration over the surface S, where the boundary conditions determine the potential. The latter is achieved if the integrand can be expressed as a divergence. Thus, the vector identity

$$\nabla \cdot \psi\mathbf{A} = \psi\nabla \cdot \mathbf{A} + \mathbf{A} \cdot \nabla\psi \tag{13}$$

is used to write (12) as

$$\int_V \nabla \cdot \left[\Phi_d\left(\sigma\nabla\Phi_d + \frac{\partial}{\partial t}\epsilon\nabla\Phi_d\right)\right]dv - \int_V \left(\sigma\nabla\Phi_d + \frac{\partial}{\partial t}\epsilon\nabla\Phi_d\right)\cdot\nabla\Phi_d dv = 0 \tag{14}$$

and then Gauss' theorem converts the first integral to one over the surface S enclosing V.

$$\oint_S \Phi_d\left(\sigma\nabla\Phi_d + \frac{\partial}{\partial t}\epsilon\nabla\Phi_d\right)\cdot d\mathbf{a} - \int_V \left[\sigma|\nabla\Phi_d|^2 + \frac{\partial}{\partial t}\left(\frac{1}{2}\epsilon|\nabla\Phi_d|^2\right)\right]dv = 0 \tag{15}$$

The conversion of (12) to (15) is an example of a three-dimensional integration by parts. The surface integral is analogous to an evaluation at the endpoints of a one-dimensional integral.

If both Φ_a and Φ_b satisfy the same condition on S, namely (9), then the difference potential is zero on S for all $0 \leq t$. Thus, the surface integral in (15) vanishes. We are left with the requirement that for $0 \leq t$,

$$\frac{d}{dt}\int_V \frac{1}{2}\epsilon|\nabla\Phi_d|^2 dv = -\int_V \sigma|\nabla\Phi_d|^2 dv \tag{16}$$

Because both Φ_a and Φ_b satisfy the same initial conditions, Φ_d must initially be zero. Thus, for $\nabla\Phi_d$ to change to a nonzero value from zero, the derivative on the left must be positive. However, the integral on the right can only be zero or negative. Thus, Φ_d must stay zero for all time. We conclude that the fields found using (7), the initial condition of (8), and boundary conditions of (9) are unique.

7.9 CHARGE RELAXATION IN UNIFORM AND PIECE-WISE UNIFORM SYSTEMS

Configurations composed of subregions where the material has uniform properties are already familiar from Secs. 6.6 and 7.5. The conductivity and permittivity are then step functions of position, and the terms on the right in (7.8.4) are spatial impulses. Thus, the charge density tends to accumulate at interfaces between regions and is represented by a surface charge density.

We consider first the evolution of the potential distribution in a region having uniform properties. With the inhomogeneities represented by the continuity conditions, the discussion is then extended to piece-wise uniform configurations.

Fields in Regions Having Uniform Properties. Where ϵ and σ are uniform, (7.8.7) becomes

$$\nabla^2\left[\frac{\partial\Phi}{\partial t} + \frac{\Phi}{(\epsilon/\sigma)}\right] = 0 \tag{1}$$

This expression is satisfied either if the potential obeys the relaxation equation

$$\frac{\partial \Phi_p}{\partial t} + \frac{\Phi_p}{(\epsilon/\sigma)} = 0 \tag{2}$$

or if it satisfies Laplace's equation

$$\nabla^2 \Phi_h = 0 \tag{3}$$

In general, the potential is a linear combination of these solutions.

$$\Phi = \Phi_p + \Phi_h \tag{4}$$

The potential satisfying (2) is that associated with the relaxation of the charge density initially distributed in the volume of the material. We can think of this as being a particular solution, because the divergence of the associated electric displacement $\mathbf{D} = \epsilon \mathbf{E} = -\epsilon \nabla \Phi_p$ gives the unpaired charge density, (7.7.4), at each point in the volume V for $t > 0$. The solutions Φ_h to Laplace's equation can then be used to make the sum of the two solutions satisfy the boundary conditions.

Given that the initial charge density throughout the volume is $\rho_i(\mathbf{r})$, the subsequent distribution is given by (7.7.4). One particular solution for the potential that then satisfies Poisson's equation throughout the volume follows from evaluating the superposition integral [(4.5.3) with $\epsilon_o \to \epsilon$] over that volume.

$$\Phi_p = \int_{V'} \frac{\rho_i(\mathbf{r}')}{4\pi\epsilon|\mathbf{r} - \mathbf{r}'|} dv' e^{-t/(\epsilon/\sigma)} \tag{5}$$

Note that this potential indeed satisfies (2) and the initial conditions on the charge density in the volume. Of course, the integral could be extended to charges outside the volume V, and the particular solution would be equally valid.

The solutions to Laplace's equation make it possible to make the total potential satisfy boundary conditions. Because an initial distribution of volume charge density cannot be initiated by means of boundary electrodes, the decay of an initial charge density is not usually of interest. The volume potential is most often simply a solution to Laplace's equation. Before delving into these more common examples, consider one that illustrates the more general situation.

Example 7.9.1. Potential Associated with Relaxation of Volume Charge

In Example 7.7.1, the decay of charge having a spherical distribution in space was described. This could be done without regard for boundary constraints. To determine the associated potential, we stipulate the nature of the boundary surrounding the uniform material in which the charge is initially embedded.

The uniform material fills the upper half-space and is bounded in the plane $z = 0$ by a perfect conductor constrained to zero potential. As shown in Fig. 7.9.1, when $t = 0$, there is an initial distribution of charge density that is uniform and of

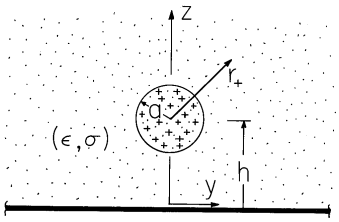


Fig. 7.9.1 Infinite half-space of material having uniform conductivity and permittivity is bounded from below by a perfectly conducting plate. When $t = 0$, there is a uniform charge density in a spherical region.

density ρ_o throughout a spherical region of radius a centered at $z = h$ on the z axis, where $h > a$.

In terms of a spherical coordinate system centered on the z axis at $z = h$, a particular solution for the potential follows from the integral form of Gauss' law, much as in Example 1.3.1. With r_+ denoting the radial distance from the center of the spherical region,

$$\Phi_p = \begin{cases} \frac{3a^2 - r_+^2}{6\epsilon}\rho_o e^{-t/\tau}; & r_+ < a \\ \frac{a^3\rho_o}{3\epsilon r_+}e^{-t/\tau}; & a < r_+ \end{cases} \tag{6}$$

where $r_+ = [x^2 + y^2 + (z-h)^2]^{1/2}$ and $\tau \equiv \epsilon/\sigma$.

Note that this potential satisfies (2) and the initial condition but does not satisfy the zero potential condition at $z = 0$. To satisfy the latter, we add a potential that is a solution to Laplace's equation, (3), everywhere in the upper half-space. This is the potential associated with an image charge density $-\rho_o exp(-t/\tau)$ distributed uniformly over a spherical region of radius a centered at $z = -h$.

$$\Phi_h = \frac{-a^3\rho_o}{3\epsilon r_-}e^{-t/\tau} \tag{7}$$

where $r_- = [x^2 + y^2 + (z+h)^2]^{1/2}, \quad z > 0$.

Thus, the total potential $\Phi = \Phi_p + \Phi_h$ that satisfies both the initial conditions and boundary conditions for $0 < t$ is

$$\Phi = \begin{cases} \frac{3a^2 - r_+^2}{6\epsilon}\rho_o e^{-t/\tau} - \frac{a^3\rho_o}{3\epsilon r_-}e^{-t/\tau}; & r_+ < a \\ \frac{a^3\rho_o}{3\epsilon}\left(\frac{1}{r_+} - \frac{1}{r_-}\right)e^{-t/\tau}; & a < r_+ \end{cases} \tag{8}$$

At each instant in time, the potential distribution is the same as if the charge and its image were static. As the charge relaxes, so does its image. Note that the charge relaxes to the boundary without producing a net charge density anywhere outside the spherical region where the charge was initiated.

Continuity Conditions in Piece-Wise Uniform Systems. Where the material properties undergo step discontinuities, the differential equations are represented by continuity conditions. The one representing the condition that the field be irrotational, (7.8.6), is the same as that in Sec. 5.3.

$$\mathbf{n} \times (\mathbf{E}^a - \mathbf{E}^b) = 0 \Leftrightarrow \Phi^a - \Phi^b = 0 \tag{9}$$

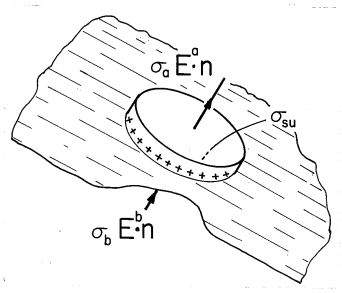


Fig. 7.9.2 Incremental volume for writing charge conservation boundary condition.

The continuity condition representing Gauss' law, (7.7.2), is also familiar (6.2.16).

$$\boxed{\sigma_{su} = \mathbf{n} \cdot (\epsilon_a \mathbf{E}^a - \epsilon_b \mathbf{E}^b)} \tag{10}$$

The continuity condition representing charge conservation, (7.7.1), is (1.5.12). With the current density expressed in terms of Ohm's law, this continuity condition becomes

$$\boxed{\mathbf{n} \cdot (\sigma_a \mathbf{E}^a - \sigma_b \mathbf{E}^b) + \frac{\partial}{\partial t}\sigma_{su} = 0} \tag{11}$$

For the incremental volume of Fig. 7.9.2, this continuity condition requires that if the conduction current entering the volume from region (b) exceeds that leaving to region (a), there must be an increasing surface charge density within the volume.

The fact that we are solving a second-order differential equation, (7.8.7), suggests that there are really only two continuity conditions. Thus, Gauss' continuity condition only serves to relate the field to the unknown surface charge density, and the combination of (10) and (11) comprise one continuity condition.

$$\mathbf{n} \cdot (\sigma_a \mathbf{E}^a - \sigma_b \mathbf{E}^b) + \frac{\partial}{\partial t}\mathbf{n} \cdot (\epsilon_a \mathbf{E}^a - \epsilon_b \mathbf{E}^b) = 0 \tag{12}$$

This continuity condition and the one on the tangential field or potential, (9), are needed to splice together solutions representing fields in piece-wise uniform configurations.

The following example illustrates how the time dependence of the continuity condition allows the fields and charge distribution to evolve from the distributions for perfect dielectrics described in the latter part of Chap. 6 to the steady conduction distributions discussed in the first part of this chapter.

Example 7.9.2. Maxwell's Capacitor

A configuration that brings out the roles of polarization and conduction in the field evolution while avoiding geometric complications is shown in Fig. 7.9.3. The space

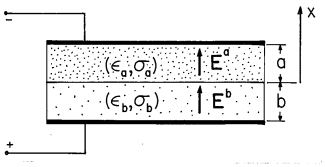


Fig. 7.9.3 Maxwell's capacitor.

between perfectly conducting parallel plates is filled by layers of material. The one above has thickness a, permittivity ϵ_a, and conductivity σ_a, while for the one below, these parameters are b, ϵ_b, and σ_b, respectively. When $t = 0$, a switch is closed and the potential V of a battery is applied across the two electrodes. Initially, there is no unpaired charge between the electrodes either in the volume or on the interface.

The electrodes are assumed long enough so that the fringing can be neglected and the fields in each of the materials taken as uniform.

$$\mathbf{E} = \mathbf{i_x} \begin{cases} E_a(t); & 0 < x < a \\ E_b(t); & -b < x < 0 \end{cases} \tag{13}$$

The linear potential associated with this distribution satisfies Laplace's equation, (3). Because there is no initial charge density in the volumes of the layers, the particular part of the potential, the solution to (2), is zero.

The voltage source imposes the condition that the line integral of the electric field between the plates must be equal to $v(t)$.

$$\int_{-b}^{a} E_x dx = v(t) = aE_a + bE_b \tag{14}$$

Because the layers are conducting, they respond to the application of the voltage with conduction currents. Since the currents differ, they cause a time rate of change of unpaired surface charge density at the interface between the layers, as expressed by (12).

$$(\sigma_a E_a - \sigma_b E_b) + \frac{d}{dt}(\epsilon_a E_a - \epsilon_b E_b) = 0 \tag{15}$$

Note that the boundary conditions on tangential $\mathbf{E}$ at the electrode surfaces and at the interface are automatically satisfied.

Given the driving voltage, these last two expressions comprise two equations in the two unknowns E_a and E_b. Thus, the solution to (14) for E_b and substitution into (15) gives a first-order differential equation for the field response in the upper layer.

$$(b\epsilon_a + a\epsilon_b)\frac{dE_a}{dt} + (b\sigma_a + a\sigma_b)E_a = \sigma_b v + \epsilon_b \frac{dv}{dt} \tag{16}$$

In particular, consider the response to a step in voltage, $v = Vu_{-1}(t)$. The drive on the right in (16) then consists of a step and an impulse. The impulse must be matched by an impulse on the left. That is, the field E_a also undergoes a step change when $t = 0$. To identify the magnitude of this step, integrate (16) from 0^- to 0^+.

$$\begin{aligned}(b\epsilon_a + a\epsilon_b)\int_{0^-}^{0^+} \frac{dE_a}{dt}dt + (b\sigma_a + a\sigma_b)\int_{0^-}^{0^+} E_a dt \\ = \sigma_b \int_{0^-}^{0^+} v dt + \epsilon_b \int_{0^-}^{0^+} \frac{dv}{dt}dt\end{aligned} \tag{17}$$

The result is a relationship between the jumps in voltage and in field.

$$\left(\epsilon_a + \frac{a}{b}\epsilon_b\right)[E_a(0^+) - E_a(0^-)] = \frac{\epsilon_b}{b}[v(0^+) - v(0^-)] \tag{18}$$

Because $v(0^-) = 0$ and $E_a(0^-) = 0$, it follows that

$$E_a(0^+) = \epsilon_b \frac{V}{b\epsilon_a + a\epsilon_b} \tag{19}$$

For $t > 0$, the particular plus homogeneous solution to (16) is

$$E_a = \sigma_b \frac{V}{b\sigma_a + a\sigma_b} + Ae^{-t/\tau} \tag{20}$$

where

$$\tau \equiv \frac{b\epsilon_a + a\epsilon_b}{b\sigma_a + a\sigma_b}.$$

The coefficient A is adjusted to make E_a meet the initial condition given by (19). Thus, the field transient in the upper layer is found to be

$$E_a = \frac{\sigma_b V}{(b\sigma_a + a\sigma_b)}(1 - e^{-t/\tau}) + \frac{\epsilon_b V}{(b\epsilon_a + a\epsilon_b)}e^{-t/\tau} \tag{21}$$

It follows from (14) that the field in the lower layer is then

$$E_b = \frac{V}{b} - \frac{a}{b}E_a \tag{22}$$

The unpaired surface charge density, (10), follows from these fields.

$$\sigma_{su} = \frac{V(\sigma_b\epsilon_a - \sigma_a\epsilon_b)}{(b\sigma_a + a\sigma_b)}(1 - e^{-t/\tau}) \tag{23}$$

The field and unpaired surface charge density transients are shown in Fig. 7.9.4. The curves are drawn to depict a lower layer that has a somewhat greater permittivity and a much greater conductivity than the upper layer. Just after the step in voltage, when $t = 0^+$, the surface charge density remains zero. Thus, the electric fields are at first what they would be if the layers were regarded as perfectly insulating dielectrics. As the surface charge accumulates, these fields approach values consistent with steady conduction. The limiting surface charge density approaches a saturation value that could be found by first evaluating the steady conduction fields and then finding σ_{su}. Note that this surface charge can be positive or negative. With the lower region much more conducting than the upper one ($\sigma_b\epsilon_a \gg \sigma_a\epsilon_b$) the surface charge is positive. In this case, the field ends up tending to be shielded out of the lower layer.

Piece-wise continuous configurations can often be represented by capacitor-resistor networks. An exact circuit representation of Maxwell's capacitor is shown in Fig. 7.9.5. The voltages across the capacitors are simply $v_a = E_a a$ and $v_b = E_b b$. In the circuit, the surface charge density given by (23) is the sum of the net charge per unit area on the lower plate of the top capacitor and that on the upper plate of the lower capacitor.

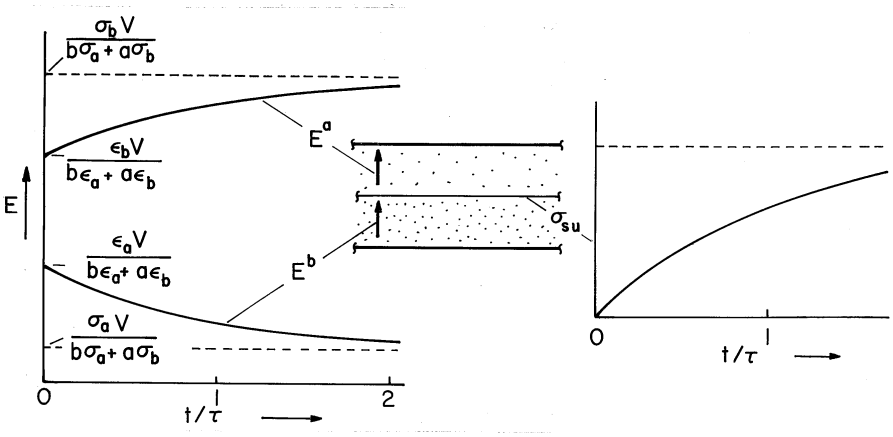


Fig. 7.9.4 With a step in voltage applied to the plane parallel configuration of Fig. 7.9.3, the electric field intensity above and below the interface responds as shown on the left, while the unpaired surface charge density has the time dependence shown on the right.

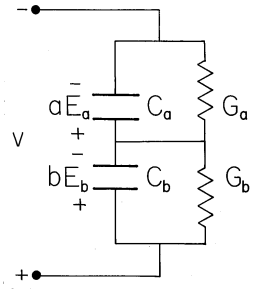


Fig. 7.9.5 Maxwell's capacitor, Fig. 7.9.3, is exactly equivalent to the circuit shown.

Nonuniform Fields in Piece-Wise Uniform Systems. We continue now to consider examples with no initial charge density in the regions having uniform conductivity and dielectric constant. Since it is not possible to establish a charge density in these regions by means of boundary constraints, this is almost always the situation in practice. The field distributions in the uniform subregions have potentials that satisfy Laplace's equation, (3). These are "spliced" together at the interfaces between regions and constrained at boundaries by conditions that vary with time. The continuity conditions vary with time to account for the accumulation of unpaired charge at the interfaces between regions.

Maxwell's capacitor, Example 7.9.2, illustrates most features of the surface charge relaxation process. The response to a step function of voltage across an electrode pair is at first the field distribution of a system of perfect dielectrics, as developed in Chap. 6. After many charge relaxation times, steady conduction prevails, and the fields are as described in Sec. 7.5. In the remainder of this section, configurations will be considered that, by contrast to Maxwell's capacitor, have fields that change their shape as the relaxation process evolves.

The interplay of polarization and conduction processes is also evident in the

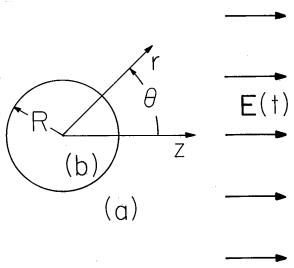


Fig. 7.9.6 A spherical material with conductivity σ_b and permittivity ϵ_b is surrounded by a material with conductivity and permittivity (σ_a, ϵ_a). An electric field $E(t)$ that is uniform far from the sphere is applied.

sinusoidal steady state response of a system. Just as the Maxwell capacitor has short-time and long-time responses dominated by the "capacitors" and "resistors," respectively, the high-frequency and low-frequency responses are dominated by polarization and conduction, respectively. This too will now be illustrated.

Example 7.9.3. Spherical Semi-insulating Material Embedded in a Second Material Stressed by Uniform Electric Field

An electric field intensity $E(t)$ is imposed on a material having permittivity and conductivity (ϵ_a, σ_a), perhaps by means of plane parallel electrodes. At the origin of a spherical coordinate system embedded in this material is a spherical region having permittivity and conductivity (ϵ_b, σ_b) and radius R, as shown in Fig. 7.9.6. Limiting cases include a conducting sphere surrounded by free space ($\epsilon_a = \epsilon_o$, $\sigma_a = 0$) or an insulating spherical cavity surrounded by a conducting material ($\sigma_b = 0$).

In each of the regions, the potential must satisfy Laplace's equation. From our experience with the potentials for perfect dielectric and for steady conduction configurations, we can expect that the boundary conditions can be satisfied using combinations of uniform and dipole fields. With the understanding that the coefficients $A(t)$ and $B(t)$ are functions of time, the solutions to Laplace's equation are therefore postulated to take the form

$$\Phi = \begin{cases} -E(t)r\cos\theta + A(t)\frac{\cos\theta}{r^2}; & r > R \\ B(t)r\cos\theta; & r < R \end{cases} \tag{24}$$

Note that the uniform part of the exterior field has been matched at $r \to \infty$ to the given driving field.

Continuity of the tangential electric field at $r = R$, (9), requires that these potential functions match at $r = R$.

$$\Phi^a(r = R) = \Phi^b(r = R) \tag{25}$$

Conservation of charge, with the surface charge density represented using Gauss' law, (12), makes the further requirement that

$$(\sigma_a E_r^a - \sigma_b E_r^b) + \frac{\partial}{\partial t}(\epsilon_a E_r^a - \epsilon_b E_r^b) = 0 \tag{26}$$

In substituting the potentials of (24) into these two conditions, no derivatives with respect to θ are taken, so each term has the θ dependence $\cos(\theta)$. It is for this

reason that such a simple solution can be used to satisfy the continuity conditions. Substitution into (25) relates the coefficients

$$-ER + \frac{A}{R^2} = BR \Rightarrow B = -E + \frac{A}{R^3} \tag{27}$$

and with this relation used to eliminate B, substitution into (26) results in a differential equation for $A(t)$, with $E(t)$ as a driving function.

$$(2\epsilon_a + \epsilon_b)\frac{dA}{dt} + (2\sigma_a + \sigma_b)A = (\sigma_b - \sigma_a)R^3E(t) + (\epsilon_b - \epsilon_a)R^3\frac{dE}{dt} \tag{28}$$

Step Response. Note that expression (28) has the same form as that for Maxwell's capacitor, (16). The procedure leading to the field response to a step function of applied field, $E = E_o u_{-1}(t)$, is therefore identical to that illustrated in Example 7.9.2. In fact, comparison of these equations makes it clear that the required solution, given that there were no initial fields (when $t = 0^-$), is

$$A = E_o R^3 \left[\frac{\sigma_b - \sigma_a}{2\sigma_a + \sigma_b}(1 - e^{-t/\tau}) + \frac{\epsilon_b - \epsilon_a}{2\epsilon_a + \epsilon_b}e^{-t/\tau} \right] \tag{29}$$

where the relaxation time $\tau = (2\epsilon_a + \epsilon_b)/(2\sigma_a + \sigma_b)$. The coefficient B follows from (27). Thus, the potential of (24) is determined for $t \geq 0$.

$$\Phi = -E_o R\cos\theta \begin{cases} \frac{r}{R} + \left[\frac{\sigma_a - \sigma_b}{2\sigma_a + \sigma_b}(1 - e^{-t/\tau}) + \frac{\epsilon_a - \epsilon_b}{2\epsilon_a + \epsilon_b}e^{-t/\tau} \right](\frac{R}{r})^2; & R < r \\ \frac{r}{R}\left[1 + \frac{\sigma_a - \sigma_b}{2\sigma_a + \sigma_b}(1 - e^{-t/\tau}) + \frac{\epsilon_a - \epsilon_b}{2\epsilon_a + \epsilon_b}e^{-t/\tau} \right]; & r < R \end{cases} \tag{30}$$

The accumulation of unpaired surface charge at $r = R$ accounts for the redistribution of potential with time. It follows from (10) that

$$\sigma_{su} = \epsilon_a E_r^a - \epsilon_b E_r^b = 3E_o \frac{(\epsilon_a\sigma_b - \epsilon_b\sigma_a)}{(2\sigma_a + \sigma_b)}(1 - e^{-t/\tau})\cos\theta \tag{31}$$

Thus, the unpaired surface charge density accumulates at the poles of the sphere, exponentially approaching a saturation value at a rate determined by the relaxation time τ. *Just after the field is turned on, this surface charge density is zero and the field distribution should be that for a uniform field applied to perfect dielectrics.* Indeed, evaluated when $t = 0$, (30) gives the potential for perfect dielectrics. In the opposite extreme, *where many relaxation times have passed so that the exponentials in (30) are negligible, the potential assumes the distribution for steady conduction.*

A graphical portrayal of this field transient is given in Fig. 7.9.7. The case shown was chosen because it involves a drastic redistribution of the field as time progresses. The spherical region is highly conducting compared to its surroundings, but the exterior material is highly polarizable compared to the spherical region. Thus, just after the switch is closed, the field lines tend to be trapped in the outer region. As time progresses and conduction rules, these lines tend to pass through

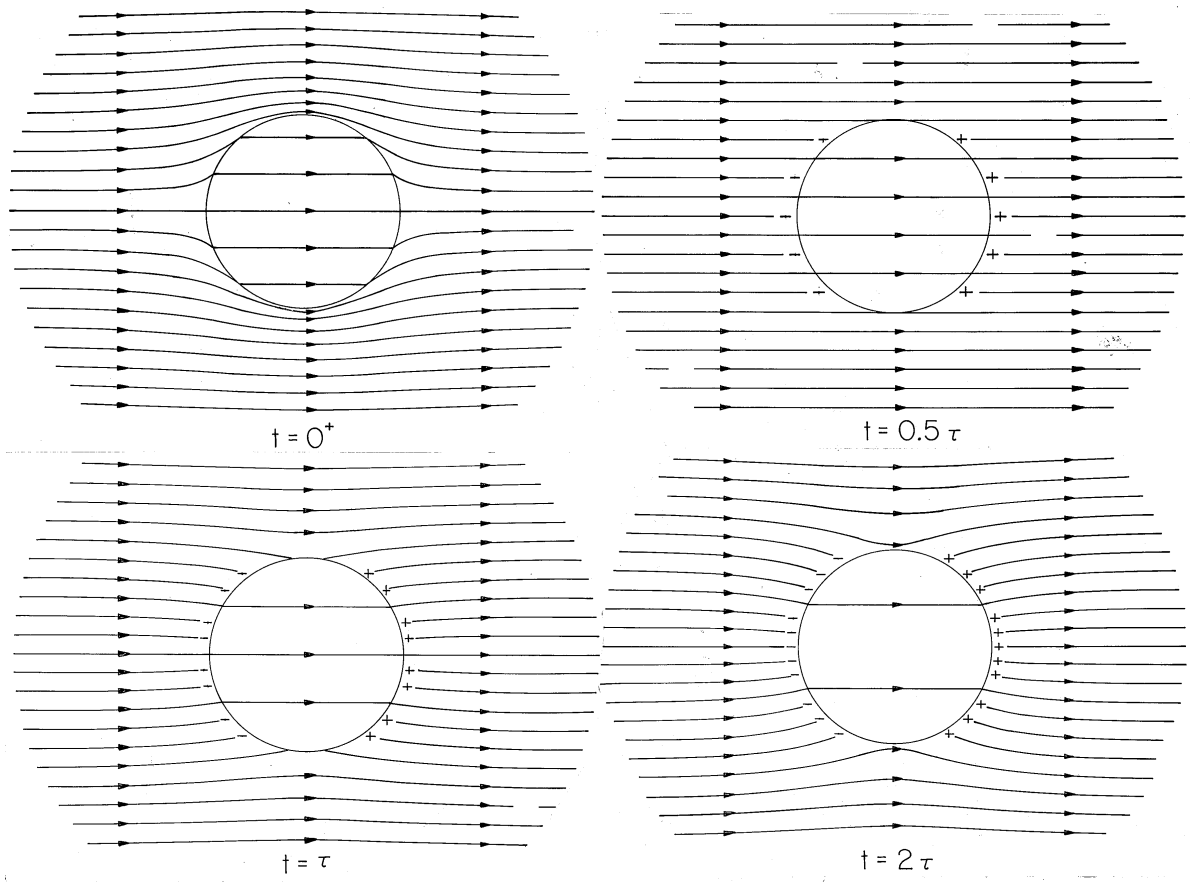


Fig. 7.9.7 Evolution of the *displacement flux density* **D** in and around the sphere of Fig. 7.9.6 and of σ_{su} in response to the application of a step in applied field. The sphere is more conducting than its surroundings ($\sigma_a/\sigma_b = 0.2$), while the outer region has a greater permittivity than the inner one, $\epsilon_a/\epsilon_b = 5$. Thus, when the distribution of **D** is determined by the polarization just after the field is applied, the field lines tend to be trapped in the outer region. By the time $t = 0.5\,\tau$, enough σ_{su} has been induced to cancel the field associated with σ_{sp}, and the *electric field intensity* is essentially uniform. In the final state, conduction alone determines the distribution of **E**. However, it is **D** that is shown in the figure, so, in fact, the permittivities do contribute to the final relative intensities.

the highly conducting sphere. The temporal scale of the transient is determined by the relaxation time τ.

Sinusoidal Steady State Response. Consider now the sinusoidal steady state that results from applying the uniform field

$$E(t) = E_p \cos \omega t = Re E_p e^{j\omega t} \tag{32}$$

As in dealing with ac circuits, where the currents and voltages are also solutions to constant coefficient ordinary differential equations, the response is now assumed to have the same frequency ω as the drive but to have a yet to be determined amplitude and phase represented by the complex coefficients A and B.

$$A(t) = Re\hat{A}e^{j\omega t}; \qquad B(t) = Re\hat{B}e^{j\omega t} \tag{33}$$

Substitution of (32) and (33a) into (28) gives an expression that can be solved for $\hat{A}$ in terms of the drive, E_p.

$$\hat{A} = \frac{[(\sigma_b - \sigma_a) + j\omega(\epsilon_b - \epsilon_a)]}{(2\sigma_a + \sigma_b) + j\omega(2\epsilon_a + \epsilon_b)} R^3 E_p \tag{34}$$

In turn, the complex amplitude B follows from this result and (27).

$$\hat{B} = -E_p + \frac{\hat{A}}{R^3} = -3E_p \frac{(\sigma_a + j\omega\epsilon_a)}{(2\sigma_a + \sigma_b) + j\omega(2\epsilon_a + \epsilon_b)} \tag{35}$$

Now, with the amplitudes in (31) and (32) given by these expressions, the sinusoidal steady state fields postulated with (24) are determined.

$$\Phi = -Re\, E_p R \cos\theta e^{j\omega t} \begin{cases} \frac{r}{R} + \left[\frac{(\sigma_a - \sigma_b) + j\omega(\epsilon_a - \epsilon_b)}{(2\sigma_a + \sigma_b) + j\omega(2\epsilon_a + \epsilon_b)}\right](\frac{R}{r})^2; & r > R \\ 3\frac{r}{R}\frac{(\sigma_a + j\omega\epsilon_a)}{(2\sigma_a + \sigma_b) + j\omega(2\epsilon_a + \epsilon_b)}; & R > r \end{cases} \tag{36}$$

The surface charge density associated with these fields is then

$$\sigma_{su} = Re \frac{3E_p(\sigma_b\epsilon_a - \sigma_a\epsilon_b)}{(2\sigma_a + \sigma_b) + j\omega(2\epsilon_a + \epsilon_b)} \cos\theta e^{j\omega t} \tag{37}$$

With the frequency rather than the time as the parameter, these expressions can be interpreted analogously to the step function response, (30) and (31). In the high-frequency limit, where

$$\frac{\omega(2\epsilon_a + \epsilon_b)}{2\sigma_a + \sigma_b} \equiv \omega\tau \gg 1; \qquad \omega\left[\frac{(\epsilon_a - \epsilon_b)}{(\sigma_a - \sigma_b)}\right] \gg 1 \tag{38}$$

the conductivity terms become negligible in (36), the coefficients $\hat{A}$ and $\hat{B}$ become independent of frequency and real. Thus, the fields are in temporal phase with the applied field and sinusoidally varying versions of what would be found if the materials were assumed to be perfect dielectrics. *If the frequency is high compared to the reciprocal charge relaxation times, the field distributions are the same as they would be just after a step in applied field* [when $t = 0^+$ in (30)].

With the inequalities of (38) reversed, the terms involving the permittivity in (36) are negligible, the coefficients $\hat{A}$ and $\hat{B}$ are again real and hence the fields are just as they would be for stationary conduction except that they vary sinusoidally with time. Thus, *in the low frequency limit, the fields are sinusoidally varying versions of the steady conduction fields* that prevail long after a step in applied field [(30) in the limit $t \to \infty$].

These high- and low-frequency limits are consistent with the frequency dependence of the unpaired surface charge density, given by (37). At low frequencies, this surface charge density varies sinusoidally in or out of phase with the applied field and with an amplitude consistent with steady conduction. As the frequency is made to greatly exceed the reciprocal relaxation time, the magnitude of this charge falls to zero. In this high-frequency limit, there is insufficient time during one cycle for significant charge to relax to the spherical interface. Thus, at high frequencies the fields become the same as if the unpaired charge density were ignored and the dielectrics assumed to be perfectly insulating.

In the two demonstrations that close this section, an obvious objective is the association of the previous example with practical situations. The approximations used to rederive the relevant fields cast further light on the physical processes at work.

Demonstration 7.9.1. Capacitively Induced Fields in a Person in the Vicinity of a High-Voltage Power Line

A person standing under a conventional power line, as in Fig. 7.9.8a, is subject to a 60 Hz alternating electric field intensity that is typically 5×10^4 v/m. In response to this field, body currents are induced. Common experience suggests that these are not large enough to create discomfort, but are the currents appreciable enough to be of long-term medical concern?

In the bare-handed maintenance of power lines, a person is brought to within arms length of the line by an insulated hoist, as shown in Fig. 7.9.8b. Without shielding, the body is in this case subjected to much more intense fields, perhaps 5×10^5 v/m. For the first person proving out this technique, the estimation of fields and currents within the body was of considerable interest.

To the layman, these imposed fields seem to imply that a body one meter in length would be subject to a voltage difference of 50 kV at the ground and 500 kV near the line. However, as we will now illustrate, surrounded by air, the body does an excellent job of shielding out the electric field.

The hemispherical conductor resting on a ground plane, shown in Fig. 7.9.9, is a model for an individual on (and in electrical contact with) the ground. In the experiment, the hemisphere is jello, molded to have the radius R and having a conductivity essentially that of the salt water used in its making. (To obtain the physiological conductivity of 0.2 S/m, unflavored gelatine is made using 0.02 M NaCl, a solution of 1.12 grams/liter.)

Presumably, the potential in and around the hemisphere is given by (30). The $z = 0$ plane is at zero potential for the spherical region described, and so the potential applies equally well to the hemisphere on the ground plane. Parameters are $(\epsilon_a, \sigma_a) = (\epsilon_o, 0)$ in the air and $(\epsilon_b, \sigma_b) = (\epsilon, \sigma)$ in the hemisphere. A conductivity typical of physiological tissue is $\sigma = .2$ S/m. As a result, the charge relaxation time based on the permittivity of the body ($\epsilon_b = 81\epsilon_o$) and the conductivity of the body is extremely short, $\tau = 4 \times 10^{-9}$ s. This makes it possible to approximate the potential distribution using the two simple steps that follow.

First, because the charge can relax to the surface in a time that is far shorter than $1/\omega$, and because the hemisphere is surrounded by material that has far less conductivity, as far as the field in the air is concerned, its surface is an equipotential.

$$\Phi_a(r = R) \simeq 0 \tag{39}$$

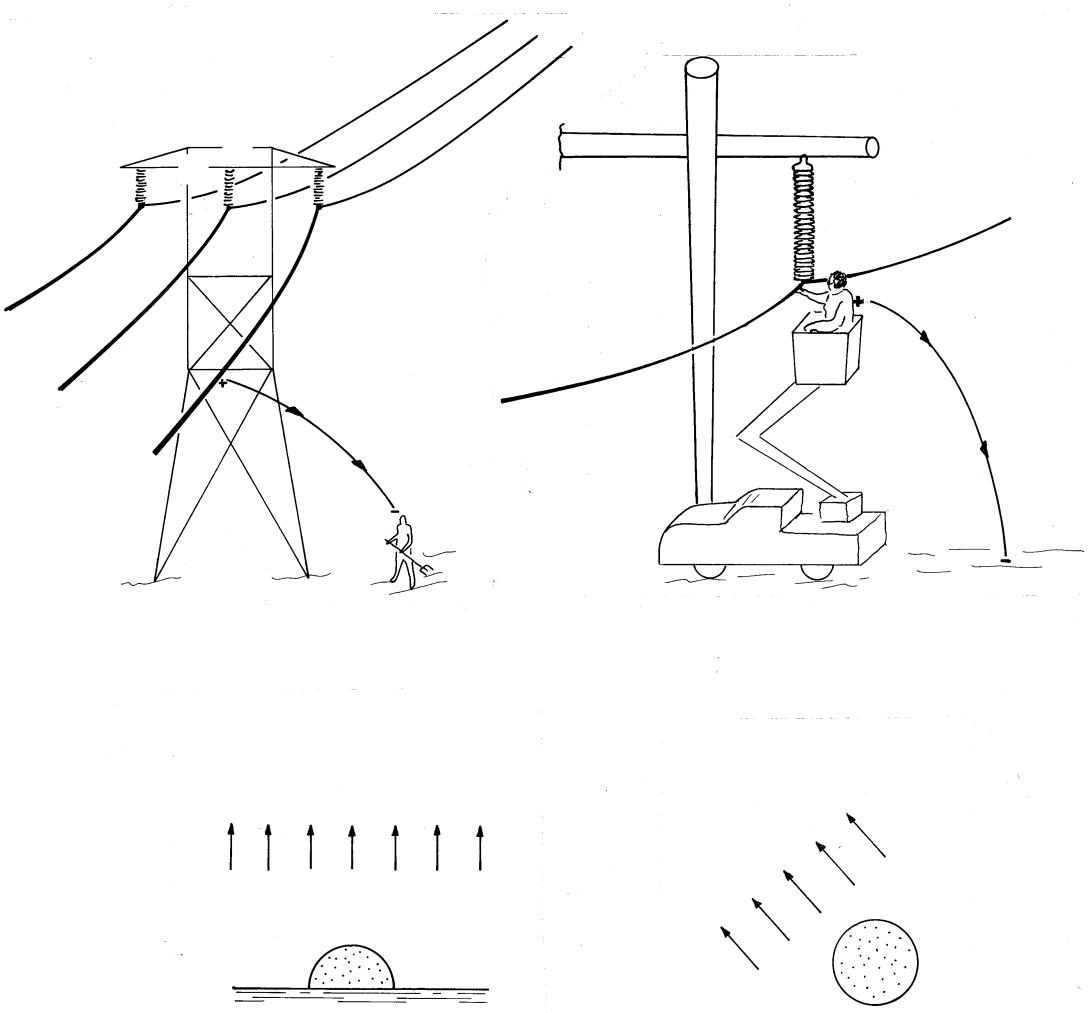


Fig. 7.9.8 (a) Person in vicinity of power line terminates lines of electric field intensity and hence is subject to currents associated with induced charge. The electric field intensity at the ground is as much as 5×10^4 V/m. (b) Worker carrying out "bare-handed maintenance" is subject to field that depends greatly on shielding provided, but can be 5×10^5 V/m or more. (c) Hemispherical model for person on ground in (a). (d) Spherical model for person near line without shielding, (b).

Thus, the potential distribution can be written by inspection [or by recourse to (5.9.7)] as

$$\Phi_a \simeq -E_p R \cos \omega t \left[\left(\frac{r}{R} \right) - \left(\frac{R}{r} \right)^2 \right] \cos \theta \tag{40}$$

Because of the short relaxation time and high conductivity for the sphere relative to the air, the surface charge density is essentially determined by the exterior field.

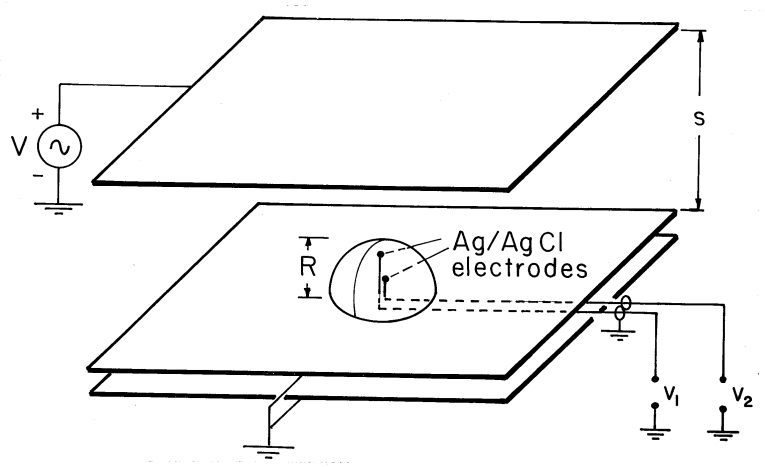


Fig. 7.9.9 Demonstration of currents induced in flesh-simulating hemisphere by field applied in surrounding air.

Thus, the conservation of charge continuity condition, (12), is approximately

$$\sigma E_r^b(r=R) \simeq \frac{\partial}{\partial t}[\epsilon_o E_r^a(r=R)] \tag{41}$$

The rate of change of the surface charge density on the right in this expression has already been determined, so the expression serves to evaluate the normal conduction current density just inside the hemispherical surface.

$$E_r^b(r=R) = -\frac{3\omega\epsilon_o E_p}{\sigma}\sin\omega t\cos\theta \tag{42}$$

In the interior region, the potential is uniform and thus takes the form $Br\cos(\theta)$. Evaluation of the coefficient B by using (42) then gives the approximate potential distribution within the hemisphere.

$$\Phi^b \simeq \frac{3\omega\epsilon_o}{\sigma}E_p r\ \cos\theta\sin\omega t = \frac{3\omega\epsilon_o}{\sigma}E_p z\sin\omega t \tag{43}$$

In retrospect, note that the potentials given by (40) and (43) are obtained by taking the appropriate limit of the potential obtained without making approximations, (36).

Inside the hemisphere, the conditions for essentially steady conduction prevail. Thus, the potential predicted by (43) is probed by means of metal spheres (Ag/AgCl electrodes) embedded in the jello and connected to an oscilloscope through insulated wires. Inside the hemisphere, surface charge stored on the surfaces of the insulated wires has a minor effect on the current distribution.

Typical experimental values for a 250 Hz excitation are $R = 3.8$ cm, $s = 12.7$ cm, $v = 565$ V peak, and $\sigma = 0.2$ S/m. With the probes located at $z = 2.86$ cm and $z = 0.95$ cm, the measured potentials are 25 μV peak and 10 μV peak, respectively. With the given parameters, (43) gives 26.5 μV peak and 8.8 μV peak, respectively.

What are the typical current densities that would be induced in a person in the vicinity of a power line? According to (41), for the person on the ground in a

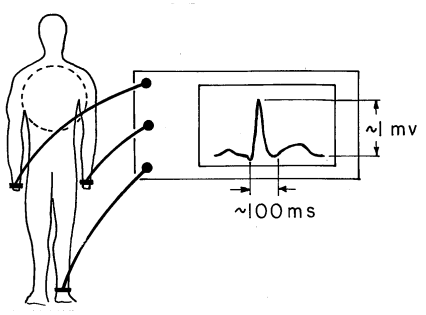


Fig. 7.9.10 Configuration for an electrocardiogram, including voltages typically generated at body periphery by the heart.

field of 5×10^4 V/m (Fig. 7.9.8a), the current density is $J_z = \sigma E_z = 0.05\mu\text{A/cm}^2$. For the person doing bare-handed maintenance where the field is perhaps 5×10^5 V/m (Fig. 7.9.8b), the model is a sphere in a uniform field (Fig. 7.9.8d). The current density is again given by (43), $J_z = \sigma E_z = 0.5\mu\text{A/cm}^2$.

Of course, the geometry of a person is not spherical. Thus, it can be expected that the field will concentrate more in the actual situation than for the hemispherical or spherical models. The approximations introduced in this demonstration would greatly simplify the development of a numerical model.

Have we found estimates of current densities suggesting danger, especially for the maintenance worker? Physiological systems are far too complex for there to be a simple answer to this question. However, matters are placed in some perspective by recognizing that currents of diverse origins exist in the body so long as it lives. In the next demonstration, electrocardiogram potentials are used to estimate current densities that result from the muscular contractions of the heart. The magnitude of the current density found there will lend some perspective to that determined here.

The approximate analysis introduced in support of the previous demonstration is an example of the "inside-outside" viewpoint introduced in Sec. 7.5. The exterior insulating region, where the field was applied, was "inside," while the interior conducting region was "outside." The following demonstration continues this theme with a contrasting example, where the excitation is in the conducting region.

Demonstration 7.9.2. Currents Induced by the Heart

The configuration for taking an electrocardiogram is typically as shown in Fig. 7.9.10. With care taken to balance out 60 Hz signals induced in each of the electrodes by external fields, the electrical signals induced by the muscle contractions in the heart are easily measured using a conventional oscilloscope. In practice, many electrodes are used so that detailed information on the distribution of the muscle contractions can be discerned.

Here we simply represent the heart by a dipole source of current at the center of a conducting sphere, somewhat as depicted in Figs. 7.9.10 and 7.9.11. Relatively little current is induced in the limbs, so that potentials measured at the extremities roughly reflect the potentials on the surface of the equivalent sphere. Given that typical potential differences are on the order of millivolts, what current dipole moment can we attribute to the heart, and what are the typical current densities in its neighborhood?

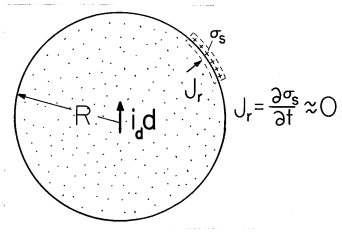


Fig. 7.9.11 Body and heart modeled by spherical conductor and dipole current.

With the heart represented by a current source of dipole moment $i_p d$ at the center of the spherical "torso," the electric potential at the origin approaches that for the dipole current source, (7.3.9).

$$\Phi_b(r \to 0) \to \frac{i_p d}{4\pi\sigma}\frac{\cos\theta}{r^2} \tag{44}$$

At the surface $r = R$, the spherical body is being surrounded by an insulator. Thus, again using Fig. 7.9.11, any normal conduction current must be accounted for by the accumulation of surface charge. Because the relaxation time is so short compared to the $1s$ period typical of the heart, the current density associated with the buildup of surface charge is extremely small. As a result, the current distribution inside the sphere is as though the normal current density at $r = R$ were zero.

$$\frac{\partial\Phi_b}{\partial r}(r = R) \simeq 0 \tag{45}$$

Thus, the potential within the body is fully determined without regard for constraints from the surrounding region. The solution to Laplace's equation that satisfies these last two conditions is

$$\Phi_b \simeq \frac{i_p d}{4\pi\sigma R^2}\left[\left(\frac{R}{r}\right)^2 + 2\left(\frac{r}{R}\right)\right]\cos\theta \tag{46}$$

Because the potential is continuous at $r = R$, the potential on the surface of the "torso" follows from evaluation of this expression at $r = R$.

$$\Phi_a(r = R) = \Phi_b(r = R) = \frac{3(i_p d)}{4\pi\sigma R^2}\cos\theta \tag{47}$$

Thus, given that the potential difference between $\theta = 45$ degrees and $\theta = 135$ degrees is 1 mV, that $R = 25$ cm, and that $\sigma = 0.2$ S/m, it follows from (47) that the peak current dipole moment of the heart is 3.7×10^{-5} A - m.

Typical current densities can now be found using (46) to evaluate the electric field intensity. For example, the current density at the radius $R/2$ just above the dipole source is

$$\begin{aligned} J_z &= \sigma E_z\left(r = \frac{R}{2},\ \theta = 0\right) = \frac{7(i_p d)}{2\pi R^3} \\ &= 2.6 \times 10^{-3}\mathrm{A/m^2} = 0.26\,\mu\mathrm{A/cm^2} \end{aligned} \tag{48}$$

Note that at the particular position selected the current density exceeds with some margin that to which the maintenance worker is subjected in the previous demonstration.

To begin to correlate the state and function of the heart with electrocardiograms, it is necessary to represent the heart by a current dipole that not only has a special temporal signature but rotates with time as well[1,2]. Unfortunately, much of the medical literature on the subject takes the analogy between electric dipoles (Sec.4.4) and current dipoles (Sec. 7.3) literally. The heart is described as an electric dipole[2], which it certainly is not. If it were, its fields would be shielded out by the surrounding conducting flesh.

REFERENCES

[1] R. Plonsey, **Bioelectric Phenomena**, McGraw-Hill Book Co., N.Y. (1969), p. 205.

[2] A. C. Burton, **Physiology and Biophysics of the Circulation**, Year Book Medical Pub., Inc., Chicago, Ill. 2nd ed., pp. 125-138.

7.10 SUMMARY

This chapter can be divided into three parts. In the first, Sec. 7.1, conduction constitutive laws are related to the average motions of microscopic charge carriers. Ohm's law, as it relates the current density $\mathbf{J}_u$ to the electric field intensity $\mathbf{E}$

$$\mathbf{J}_u = \sigma\mathbf{E} \tag{1}$$

is found to describe conduction in certain materials which are constituted of at least one positive and one negative species of charge carrier. As a reminder that the current density can be related to field variables in many ways other than Ohm's law, the unipolar conduction law is also derived in Sec. 7.1, (7.1.8). But in this chapter and those to follow, the conduction law (1) is used almost exclusively.

The second part of this chapter, Secs. 7.2–7.6, is concerned with "steady" conduction. A summary of the differential laws and corresponding continuity conditions is given in Table 7.10.1. Under steady conditions, the unpaired charge density is determined from the last expressions in the table after the first two have been used to determine the electric potential and field intensity.

In the third part of this chapter, Secs. 7.7–7.9, the dynamics of EQS systems is developed and exemplified. The laws used to determine the electric potential and field intensity, given by the first two lines in Table 7.10.2, are valid for frequencies and characteristic times that are arbitrary relative to electrical relaxation times, provided those times are themselves long compared to times required for an electromagnetic wave to propagate through the system. The last expressions identify how the unpaired charge density is relaxing under dynamic conditions.

In EQS systems, the magnetic induction makes a negligible contribution and the electric field intensity is essentially irrotational. Thus, $\mathbf{E}$ is represented by

TABLE 7.10.1
SUMMARY OF LAWS FOR STEADY STATE OHMIC CONDUCTION

	Differential Law	Eq. No.	Continuity Condition	Eq. No.
Faraday's Law	$\nabla \times \mathbf{E} \simeq 0 \Leftrightarrow \mathbf{E} = -\nabla\Phi$	(7.0.1)	$\Phi^a - \Phi^b = 0$	(7.2.10)
Charge conservation	$\nabla \cdot \sigma\mathbf{E} = s$	(7.2.2) (7.3.1)	$\mathbf{n} \cdot (\sigma_a\mathbf{E}^a - \sigma_b\mathbf{E}^b) = J_s$	(7.2.9) (7.3.4)
Unpaired charge distribution	$\rho_u = -\frac{\epsilon}{\sigma}\mathbf{E} \cdot \nabla\sigma + \mathbf{E} \cdot \nabla\epsilon$	(7.2.8)	$\sigma_{su} = \mathbf{n} \cdot \epsilon_a\mathbf{E}^a\left(1 - \frac{\epsilon_b\sigma_a}{\epsilon_a\sigma_b}\right)$	(7.2.12)

TABLE 7.10.2
SUMMARY OF EQS LAWS FOR INHOMOGENEOUS OHMIC MEDIA

	Differential Law	Eq. No.	Continuity Condition	Eq. No.
Faraday's law	$\mathbf{E} = -\nabla\Phi$	(7.0.1)	$\Phi^a - \Phi^b = 0$	(7.2.10)
Charge conservation, Ohm's law, and Gauss' law	$\nabla \cdot \left[\sigma\mathbf{E} + \frac{\partial}{\partial t}(\epsilon\mathbf{E})\right] = s$	(7.8.5) (7.3.2)	$\mathbf{n} \cdot (\sigma_a\mathbf{E}^a - \sigma_b\mathbf{E}^b) + \frac{\partial}{\partial t}\mathbf{n} \cdot (\epsilon_a\mathbf{E}^a - \epsilon_b\mathbf{E}^b) = J_s$	(7.9.12) (7.3.4)
Relaxation of unpaired charge density	$\frac{\partial\rho_u}{\partial t} + \frac{\rho_u}{\epsilon/\sigma} = -\mathbf{E} \cdot \nabla\sigma + \frac{\sigma}{\epsilon}\mathbf{E} \cdot \nabla\epsilon$	(7.8.4)	$\frac{\partial\sigma_{su}}{\partial t} + \mathbf{n} \cdot (\sigma_a\mathbf{E}^a - \sigma_b\mathbf{E}^b) = 0$	(7.9.11)

$-grad\,(\Phi)$ in both Table 7.10.1 and Table 7.10.2. In the EQS approximation, neglecting the magnetic induction is tantamount to ignoring the finite transit time effects of electromagnetic waves. This we saw in Chap. 3 and will see again in Chaps. 14 and 15.

In MQS systems, fields may be varying so slowly that the effect of magnetic induction on the current flow is again ignorable. In that case, the laws of Table 7.10.1 are once again applicable. So it is that the second part of this chapter is a logical base from which to begin the next chapter. At least under steady conditions we already know how to predict the distribution of the current density, the source of the magnetic field intensity.

How rapidly can MQS fields vary without having the magnetic induction come into play? We will answer this question in Chap. 10.

PROBLEMS

7.1 Conduction Constitutive Laws

7.1.1 In a metal such as copper, where each atom contributes approximately one conduction electron, typical current densities are the result of electrons moving at a surprisingly low velocity. To estimate this velocity, assume that each atom contributes one conduction electron and that the material is copper, where the molecular weight $M_o = 63.5$ and the mass density is $\rho = 8.9 \times 10^3 kg/m^3$. Thus, the density of electrons is approximately $(A_o/M_o)\rho$, where $A_o = 6.023 \times 10^{26}$ molecules/kg-mole is Avogadro's number. Given σ from Table 7.1.1, what is the mobility of the electrons in copper? What electric field intensity is required to drive a current density of 1 amp/cm^2? What is the electron velocity?

7.2 Steady Ohmic Conduction

7.2.1* The circular disk of uniformly conducting material shown in Fig. P7.2.1 has a dc voltage v applied to its surfaces at $r = a$ and $r = b$ by means of perfectly conducting electrodes. The other boundaries are interfaces with free space. Show that the resistance $R = ln(a/b)/2\pi\sigma d$.

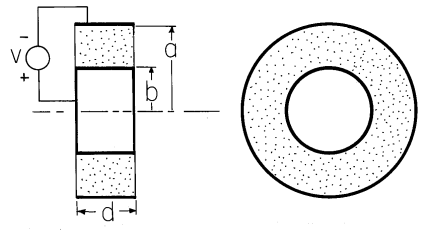


Fig. P7.2.1

7.2.2 In a spherical version of the resistor shown in Fig. P7.2.1, a uniformly conducting material is connected to a voltage source v through spherical perfectly conducting electrodes at $r = a$ and $r = b$. What is the resistance?

7.2.3* By replacing $\epsilon \rightarrow \sigma$, resistors are made to have the same geometry as shown in Fig. P6.5.1. In general, the region between the plane parallel perfectly conducting electrodes is filled by a material of conductivity $\sigma = \sigma(x)$. The boundaries of the conductor that interface with the surrounding free space have normals that are either in the x or the z direction.

(a) Show that even if d is large compared to l and c, $\mathbf{E}$ between the plates is $(v/d)\mathbf{i_y}$.

(b) If the conductor is piece-wise uniform, with sections having conductivities σ_a and σ_b of width a and b, respectively, as shown in Fig. P6.5.1a, show that the conductance $G = c(\sigma_b b + \sigma_a a)/d$.

(c) If $\sigma = \sigma_a(1 + x/l)$, show that $G = 3\sigma_a cl/2d$.

7.2.4 A pair of uniform conductors form a resistor having the shape of a circular cylindrical half-shell, as shown in Fig. P7.2.4. The boundaries at $r = a$ and $r = b$, and in planes parallel to the paper, interface with free space. Show that for steady conduction, all boundary conditions are satisfied by a simple piece-wise continuous potential that is an exact solution to Laplace's equation. Determine the resistance.

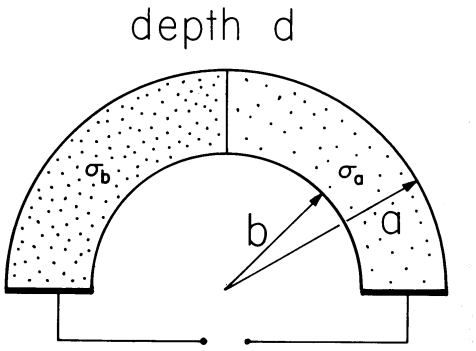


Fig. P7.2.4

7.2.5* The region between the planar electrodes of Fig. 7.2.4 is filled with a material having conductivity $\sigma = \sigma_o/(1 + y/a)$, where σ_o and a are constants. The permittivity ϵ is uniform.

(a) Show that $G = A\sigma_o/d(1 + d/2a)$.

(b) Show that $\rho_u = \epsilon G v/A\sigma_o a$.

7.2.6 The region between the planar electrodes of Fig. 7.2.4 is filled with a uniformly conducting material having permittivity $\epsilon = \epsilon_a/(1 + y/a)$.

(a) What is G?

(b) What is ρ_u in the conductor?

7.2.7* A section of a spherical shell of conducting material with inner radius b and outer radius a is shown in Fig. P7.2.7. Show that if $\sigma = \sigma_o(r/a)^2$, the conductance $G = 6\pi(1 - \cos\alpha/2)ab^3\sigma_o/(a^3 - b^3)$.

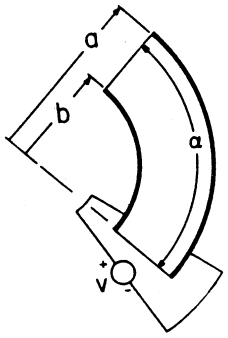


Fig. P7.2.7

7.2.8 In a cylindrical version of the geometry shown in Fig. P7.2.7, the material between circular cylindrical outer and inner electrodes of radii a and b, respectively, has conductivity $\sigma = \sigma_o(a/r)$. The boundaries parallel to the page interface free space and are a distance d apart. Determine the conductance G.

7.3 Distributed Current Sources and Associated Fields

7.3.1* An infinite half-space of uniformly conducting material in the region $y > 0$ has an interface with free space in the plane $y = 0$. There is a point current source of I amps located at $(x, y, z) = (0, h, 0)$ on the y axis. Using an approach analogous to that used in Prob. 6.6.5, show that the potential inside the conductor is

$$\Phi_a = \frac{I}{4\pi\sigma\sqrt{x^2 + (y-h)^2 + z^2}} + \frac{I}{4\pi\sigma\sqrt{x^2 + (y+h)^2 + z^2}}. \qquad (a)$$

Now that the potential of the interface is known, show that the potential in the free space region outside the conductor, where $y < 0$, is

$$\Phi_b = \frac{2I}{4\pi\sigma\sqrt{x^2 + (y-h)^2 + z^2}} \qquad (b)$$

7.3.2 The half-space $y > 0$ is of uniform conductivity while the remaining space is insulating. A uniform line current source of density K_l (A/m) runs parallel to the plane $y = 0$ along the line $x = 0,\ y = h$.

(a) Determine Φ in the conductor.
(b) In turn, what is Φ in the insulating half-space?

7.3.3* A two-dimensional dipole current source consists of uniform line current sources $\pm K_l$ have the spacing d. The cross-sectional view is as shown in

Fig. 7.3.4, with $\theta \to \phi$. Show that the associated potential is

$$\Phi = \frac{K_l d}{2\pi\sigma}\frac{\cos\phi}{r} \qquad (a)$$

in the limit $K_l \to \infty,\ d \to 0,\ K_l d$ finite.

7.4 Superposition and Uniqueness of Steady Conduction Solutions

7.4.1* A material of uniform conductivity has a spherical insulating cavity of radius b at its center. It is surrounded by segmented electrodes that are driven by current sources in such a way that at the spherical outer surface $r = a$, the radial current density is $J_r = -J_o \cos\theta$, where J_o is a given constant.

(a) Show that inside the conducting material, the potential is

$$\Phi = \frac{J_o b}{\sigma}\frac{\left[(r/b) + \frac{1}{2}(b/r)^2\right]}{\left[1 - (b/a)^3\right]}\cos\theta; \qquad b < r < a. \qquad (a)$$

(b) Evaluated at $r = b$, this gives the potential on the surface bounding the insulating cavity. Show that the potential in the cavity is

$$\Phi = \frac{3J_o}{2\sigma}\frac{r\cos\theta}{\left[1 - (b/a)^3\right]}; \qquad r < b \qquad (b)$$

7.4.2 A uniformly conducting material has a spherical interface at $r = a$, with a surrounding insulating material and a spherical boundary at $r = b$ $(b < a)$, where the radial current density is $J_r = J_o \cos\theta$, essentially independent of time.

(a) What is Φ in the conductor?
(b) What is Φ in the insulating region surrounding the conductor?

7.4.3 In a system that stretches to infinity in the $\pm x$ and $\pm z$ directions, there is a layer of uniformly conducting material having boundaries in the planes $y = 0$ and $y = -a$. The region $y > 0$ is free space, while a potential $\Phi = V\cos\beta x$ is imposed on the boundary at $y = -a$.

(a) Determine Φ in the conducting layer.
(b) What is Φ in the region $y > 0$?

7.4.4* The uniformly conducting material shown in cross-section in Fig. P7.4.4 extends to infinity in the $\pm z$ directions and has the shape of a 90-degree section from a circular cylindrical annulus. At $\phi = 0$ and $\phi = \pi/2$, it is in contact with grounded electrodes. The boundary at $r = a$ interfaces free

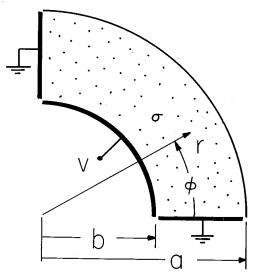


Fig. P7.4.4

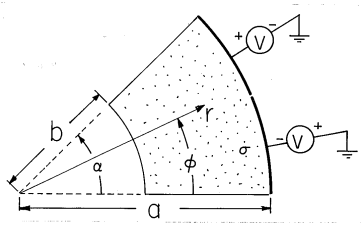


Fig. P7.4.5

space, while at $r = b$, an electrode constrains the potential to be v. Show that the potential in the conductor is

$$\Phi = \sum_{\substack{m=1 \\ \text{odd}}}^{\infty} \frac{4V}{m\pi} \frac{[(r/b)^{2m} + (a/b)^{4m}(b/r)^{2m}]}{[1 + (a/b)^{4m}]} \sin 2m\phi \qquad (a)$$

7.4.5 The cross-section of a uniformly conducting material that extends to infinity in the $\pm z$ directions is shown in Fig. P7.4.5. The boundaries at $r = b$, at $\phi = 0$, and at $\phi = \alpha$ interface insulating material. At $r = a$, voltage sources constrain $\Phi = -v/2$ over the range $0 < \phi < \alpha/2$, and $\Phi = v/2$ over the range $\alpha/2 < \phi < \alpha$.

(a) Find an infinite set of solutions for Φ that satisfy the boundary conditions at the three insulating surfaces.
(b) Determine Φ in the conductor.

7.4.6 The system of Fig. P7.4.4 is altered so that there is an electrode on the boundary at $r = a$. Determine the mutual conductance between this electrode and the one at $r = b$.

7.5 Steady Currents in Piece-Wise Uniform Conductors

7.5.1* A sphere having uniform conductivity σ_b is surrounded by material having the uniform conductivity σ_a. As shown in Fig. P7.5.1, electrodes at "infin-

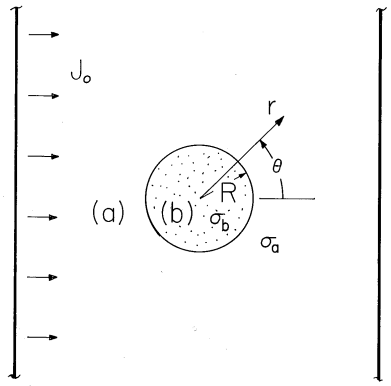


Fig. P7.5.1

ity" to the right and left impose a uniform current density J_o at infinity. Steady conduction prevails. Show that

$$\Phi = -\frac{J_o R}{\sigma_a} \begin{cases} \left[\frac{r}{R} + \left(\frac{\sigma_a - \sigma_b}{2\sigma_a + \sigma_b}\right)\left(\frac{R}{r}\right)^2\right]\cos\theta; & R < r \\ \left(\frac{3\sigma_a}{\sigma_b + 2\sigma_a}\right)\left(\frac{r}{R}\right)\cos\theta; & r < R \end{cases} \qquad (a)$$

7.5.2 Assume at the outset that the sphere of Prob. 7.5.1 is much more highly conducting than its surroundings.

(a) As far as the fields in region (a) are concerned, what is the boundary condition at $r = R$?
(b) Determine the approximate potential in region (a) and compare to the appropriate limiting potential from Prob. 7.5.1.
(c) Based on this potential in region (a), determine the approximate potential in the sphere and compare to the appropriate limit of Φ as found in Prob. 7.5.1.
(d) Now, assume that the sphere is much more insulating than its surroundings. Repeat the steps of parts (a)–(c).

7.5.3* A rectangular box having depth b, length l and width much larger than b has an insulating bottom and metallic ends which serve as electrodes. In Fig. P7.5.3a, the right electrode is extended upward and then back over the box. The box is filled to a depth b with a liquid having uniform conductivity. The region above is air. The voltage source can be regarded as imposing a potential in the plane $z = -l$ between the left and top electrodes that is linear.

(a) Show that the potential in the conductor is $\Phi = -vz/l$.
(b) In turn, show that in the region above the conductor, $\Phi = v(z/l)(x - a)/a$.
(c) What are the distributions of ρ_u and σ_u?

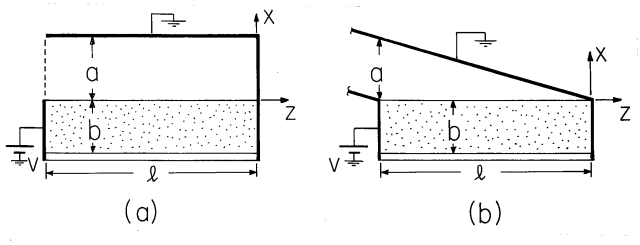


Fig. P7.5.3

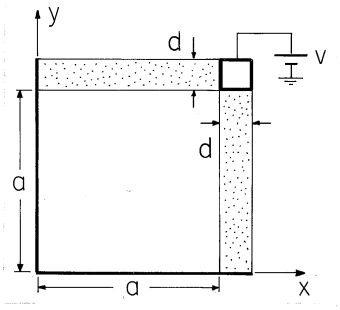


Fig. P7.5.4

(d) Now suppose that the upper electrode is slanted, as shown in Fig. P7.5.3b. Show that Φ in the conductor is unaltered but in the region between the conductor and the slanted plate, $\Phi = v[(z/l) + (x/a)]$.

7.5.4 The structure shown in Fig. P7.5.4 is infinite in the $\pm z$ directions. Each leg has the same uniform conductivity, and conduction is stationary. The walls in the x and in the y planes are perfectly conducting.

(a) Determine Φ, $\mathbf{E}$, and $\mathbf{J}$ in the conductors.
(b) What are Φ and $\mathbf{E}$ in the free space region?
(c) Sketch Φ and $\mathbf{E}$ in this region and in the conductors.

7.5.5 The system shown in cross-section by Fig. P7.5.6a extends to infinity in the $\pm x$ and $\pm z$ directions. The material of uniform conductivity σ_a to the right is bounded at $y = 0$ and $y = a$ by electrodes at zero potential. The material of uniform conductivity σ_b to the left is bounded in these planes by electrodes each at the potential v. The approach to finding the fields is similar to that used in Example 6.6.3.

(a) What is Φ^a as $x \to \infty$ and Φ^b as $x \to -\infty$?
(b) Add to each of these solutions an infinite set such that the boundary conditions are satisfied in the planes $y = 0$ and $y = a$ and as $x \to \pm\infty$.
(c) What two boundary conditions relate Φ^a to Φ^b in the plane $x = 0$?
(d) Use these conditions to determine the coefficients in the infinite series, and hence find Φ throughout the region between the electrodes.

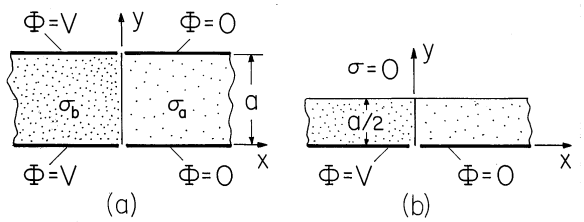


Fig. P7.5.5

(e) In the limits $\sigma_b \gg \sigma_a$ and $\sigma_b = \sigma_a$, sketch Φ and $\mathbf{E}$. (A numerical evaluation of the expressions for Φ is not required.)

(f) Shown in Fig. P7.5.6b is a similar system but with the conductors bounded from above by free space. Repeat the steps (a) through (e) for the fields in the conducting layer.

7.6 Conduction Analogs

7.6.1* In deducing (4) relating the capacitance of electrodes in an insulating material to the conductance of electrodes having the same shape in a conducting material, it is assumed that not only are the ratios of all dimensions in one situation the same as in the other (the systems are geometrically similar), but that the actual size of the two physical situations is the same. Show that if the systems are again geometrically similar but the length scale of the capacitor is l_ϵ while that of the conduction cell is l_σ, $RC = (\epsilon/\sigma)(l_\epsilon/l_\sigma)$.

7.7 Charge Relaxation in Uniform Conductors

7.7.1* In the two-dimensional configuration of Prob. 4.1.4, consider the field transient that results if the region within the cylinder of rectangular cross-section is filled by a material having uniform conductivity σ and permittivity ϵ.

(a) With the initial potential given by (a) of Prob. 4.1.4, with $\epsilon_o \to \epsilon$ and ρ_o a given constant, show that $\rho_u(x, y, t = 0)$ is given by (c) of Prob. 4.1.4.

(b) Show that for $t > 0$, ρ is given by (c) of Prob. 4.1.4 multiplied by $\exp(-t/\tau)$, where $\tau = \epsilon/\sigma$.

(c) Show that for $t > 0$, the potential is given by (a) of Prob. 4.1.4 multiplied by $\exp(-t/\tau)$.

(d) Show that for $t > 0$, the current $i(t)$ from the electrode segment is (f) of Prob. 4.1.4

7.7.2 When $t = 0$, the only net charge in a material having uniform σ and ϵ is the line charge of Prob. 4.5.4. As a function of time for $t > 0$, determine

the

(a) line charge density,
(b) charge density elsewhere in the medium, and
(c) the potential $\Phi(x, y, z, t)$.

7.7.3* When $t = 0$, the charged particle of Example 7.7.2 has a charge $q = q_o < -q_c$.

(a) Show that, as long as q remains less than $-q_c$, the net current to the particle is $i = -\frac{\mu\rho}{\epsilon}q$.
(b) Show that, as long as $q < -q_c$, $q = q_o \exp(-t/\tau_1)$ where $\tau_1 = \epsilon/\mu\rho$.

7.7.4 Relative to the potential at infinity on a plane passing through the equator of the particle in Example 7.7.2, what is the potential of the particle when its charge reaches $q = q_c$?

7.8 Electroquasistatic Conduction Laws for Inhomogeneous Materials

7.8.1* Use an approach similar to that illustrated in this section to show uniqueness of the solution to Poisson's equation for a given initial distribution of ρ and a given potential $\Phi = \Phi_\Sigma$ on the surface S', and a given current density $-(\sigma\nabla\Phi + \partial\epsilon\nabla\Phi/\partial t) \cdot \mathbf{n} = J_\Sigma$ on S'' where $S' + S''$ encloses the volume of interest V.

7.9 Charge Relaxation in Uniform and Piece-Wise Uniform Systems

7.9.1* We return to the coaxial circular cylindrical electrode configurations of Prob. 6.5.5. Now the material in region (2) of each has not only a uniform permittivity ϵ but a uniform conductivity σ as well. Given that $V(t) = Re\hat{V}\exp(j\omega t)$,

(a) show that $\mathbf{E}$ in the first configuration of Fig. P6.5.5 is $\mathbf{i_r}v/rln(a/b)$,
(b) while in the second configuration,

$$\mathbf{E} = \frac{\mathbf{i_r}}{r}Re\frac{\hat{v}}{Det}\begin{cases} j\omega\epsilon_o; & R < r < a \\ \sigma + j\omega\epsilon; & b < r < R \end{cases} \qquad (a)$$

where $Det = [\sigma\, ln(a/R)] + j\omega[\epsilon_o\, ln(R/b) + \epsilon ln(a/R)]$.
(c) Show that in the first configuration a length l (into the paper) is equivalent to a conductance G in parallel with a capacitance C where

$$G = \frac{[\sigma\alpha]l}{ln\,(a/b)}; \qquad C = \frac{[\epsilon_o(2\pi - \alpha) + \epsilon\alpha]l}{ln\,(a/b)} \qquad (b)$$

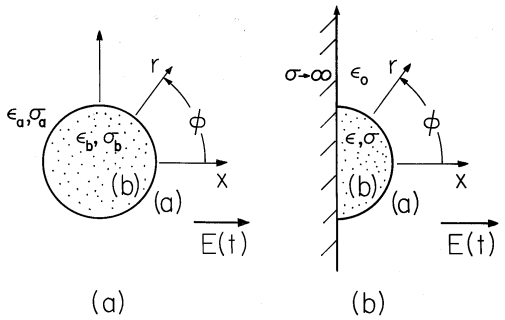


Fig. P7.9.4

while in the second, it is equivalent to the circuit of Fig. 7.9.5 with

$$G_a = 0; \qquad G_b = \frac{2\pi\sigma l}{ln\,(R/b)}$$

$$C_a = \frac{2\pi\epsilon_o l}{ln\,(a/R)}; \qquad C_b = \frac{2\pi\epsilon l}{ln\,(R/b)} \tag{c}$$

7.9.2 Interpret the configurations shown in Fig. P6.5.5 as spherical. An outer spherically shaped electrode has inside radius a, while an inner electrode positioned on the same center has radius b. Region (1) is free space while (2) has uniform ϵ and σ.

(a) For $V = V_o\cos(\omega t)$, determine $\mathbf{E}$ in each region.
(b) What are the elements in the equivalent circuit for each?

7.9.3* Show that the hemispherical electrode of Fig. 7.3.3 is equivalent to a circuit having a conductance $G = 2\pi\sigma a$ in parallel with a capacitance $C = 2\pi\epsilon a$.

7.9.4 The circular cylinder of Fig. P7.9.4a has ϵ_b and σ_b and is surrounded by material having ϵ_a and σ_a. The electric field $E(t)\mathbf{i_x}$ is applied at $x = \pm\infty$.

(a) Find the potential in and around the cylinder and the surface charge density that result from applying a step in field to a system that initially is free of charge.
(b) Find these quantities for the sinusoidal steady state response.
(c) Argue that these fields are equally applicable to the description of the configuration shown in Fig. P7.9.4b with the cylinder replaced by a half-cylinder on a perfectly conducting ground plane. In the limit where the exterior region is free space while the half-cylinder is so conducting that its charge relaxation time is short compared to times characterizing the applied field ($1/\omega$ in the sinusoidal steady state case), what are the approximate fields in the exterior and in the interior regions? (See Prob. 7.9.5 for a direct calculation of these approximate fields.)

7.9.5* The half-cylinder of Fig. P7.9.4b has a relaxation time that is short compared to times characterizing the applied field $E(t)$. The surrounding region is free space ($\sigma_a = 0$).

(a) Show that in the exterior region, the potential is approximately

$$\Phi^a \simeq -aE(t)\left[\frac{r}{a} - \frac{a}{r}\right]\cos\phi \qquad (a)$$

(b) In turn, show that the field inside the half-cylinder is approximately

$$\Phi^b \simeq -\frac{2\epsilon_o}{\sigma}\frac{dE}{dt}r\cos\phi \qquad (b)$$

7.9.6 An electric dipole having a z-directed moment $p(t)$ is situated at the origin and at the center of a spherical cavity of free space having a radius a in a material having uniform ϵ and σ. When $t < 0$, $p = 0$ and there is no charge anywhere. The dipole is a step function of time, instantaneously assuming a moment p_o when $t = 0$.

(a) An instant after the dipole is established, what is the distribution of Φ inside and outside the cavity?
(b) Long after the electric dipole is turned on and the fields have reached a steady state, what is the distribution of Φ?
(c) Determine $\Phi(r, \theta, t)$.

7.9.7* A planar layer of semi-insulating material has thickness d, uniform permittivity ϵ, and uniform conductivity σ, as shown in Fig. P7.9.7. From below it is bounded by contacting electrode segments that impose the potential $\Phi = V\cos\beta x$. The system extends to infinity in the $\pm x$ and $\pm z$ directions.

(a) The potential has been applied for a long time. Show that at $y = 0$, $\sigma_{su} = \epsilon_o V\beta\cos\beta x/\cosh\beta d$.
(b) When $t = 0$, the applied potential is turned off. Show that this unpaired surface charge density decays exponentially from the initial value from part (a) with the time constant $\tau = (\epsilon_o\tanh\beta d + \epsilon)/\sigma$.

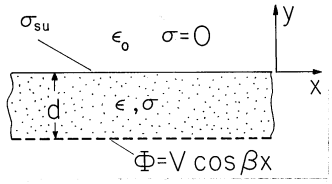


Fig. P7.9.7

7.9.8* Region (b), where $y < 0$, has uniform permittivity ϵ and conductivity σ, while region (a), where $0 < y$, is free space. Before $t = 0$ there are no

charges. When $t = 0$, a point charge Q is suddenly "turned on" at the location $(x, y, z) = (0, h, 0)$.

(a) Show that just after $t = 0$,

$$\Phi^a = \frac{Q}{4\pi\epsilon_o\sqrt{x^2 + (y-h)^2 + z^2}} - \frac{q_b}{4\pi\epsilon_o\sqrt{x^2 + (y+h)^2 + z^2}} \qquad (a)$$

$$\Phi^b = \frac{q_a}{4\pi\epsilon_o\sqrt{x^2 + (y-h)^2 + z^2}} \qquad (b)$$

where $q_b \to Q[(\epsilon/\epsilon_o) - 1]/[(\epsilon/\epsilon_o) + 1]$ and $q_a \to 2Q/[(\epsilon/\epsilon_o) + 1]$.

(b) Show that as $t \to \infty$, $q_b \to Q$ and the field in region (b) goes to zero.
(c) Show that the transient is described by (a) and (b) with

$$q_b = Q\left[1 - \left(\frac{2\epsilon_o}{\epsilon + \epsilon_o}\right)\exp(-t/\tau)\right] \qquad (c)$$

$$q_a = Q\left[\frac{2\epsilon_o}{(\epsilon + \epsilon_o)}\right]\exp(-t/\tau) \qquad (d)$$

where $\tau = (\epsilon_o + \epsilon)/\sigma$.

7.9.9* The cross-section of a two-dimensional system is shown in Fig. P7.9.9. The parallel plate capacitor to the left of the plane $x = 0$ extends to $x = -\infty$, with the lower electrode at potential $v(t)$ and the upper one grounded. This upper electrode extends to the right to the plane $x = b$, where it is bent downward to $y = 0$ and inward to the plane $x = 0$ along the surface $y = 0$. Region (a) is free space while region (b) to the left of the plane $x = 0$ has uniform permittivity ϵ and conductivity σ. The applied voltage $v(t)$ is a step function of magnitude V_o.

(a) The voltage has been on for a long-time. What are the field and potential distributions in region (b)? Having determined Φ^b, what is the potential in region (a)?
(b) Now, Φ is to be found for $t > 0$. Example 6.6.3 illustrates the approach that can be used. Show that in the limit $t \to \infty$, Φ becomes the result of part (a).
(c) In the special case where $\epsilon = \epsilon_o$, sketch the evolution of the field from the time just after the voltage is applied to the long-time limit of part (a).

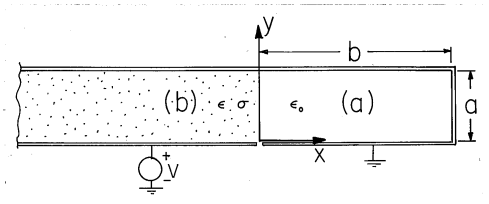


Fig. P7.9.9

8

MAGNETOQUASISTATIC FIELDS: SUPERPOSITION INTEGRAL AND BOUNDARY VALUE POINTS OF VIEW

8.0 INTRODUCTION

MQS Fields: Superposition Integral and Boundary Value Views

We now follow the study of electroquasistatics with that of magnetoquasistatics. In terms of the flow of ideas summarized in Fig. 1.0.1, we have completed the EQS column to the left. Starting from the top of the MQS column on the right, recall from Chap. 3 that the laws of primary interest are Ampère's law (with the displacement current density neglected) and the magnetic flux continuity law (Table 3.6.1).

$$\boxed{\nabla \times \mathbf{H} = \mathbf{J}} \tag{1}$$

$$\boxed{\nabla \cdot \mu_o \mathbf{H} = 0} \tag{2}$$

These laws have associated with them continuity conditions at interfaces. If the interface carries a surface current density $\mathbf{K}$, then the continuity condition associated with (1) is (1.4.16)

$$\mathbf{n} \times (\mathbf{H}^a - \mathbf{H}^b) = \mathbf{K} \tag{3}$$

and the continuity condition associated with (2) is (1.7.6).

$$\mathbf{n} \cdot (\mu_o \mathbf{H}^a - \mu_o \mathbf{H}^b) = 0 \tag{4}$$

In the absence of magnetizable materials, these laws determine the magnetic field intensity $\mathbf{H}$ given its source, the current density $\mathbf{J}$. By contrast with the electroquasistatic field intensity $\mathbf{E}$, $\mathbf{H}$ is not everywhere irrotational. However, it is solenoidal everywhere.

The similarities and contrasts between the primary EQS and MQS laws are the topic of this and the next two chapters. The similarities will streamline the development, while the contrasts will deepen the understanding of both MQS and EQS systems. Ideas already developed in Chaps. 4 and 5 will also be applicable here. Thus, this chapter alone plays the role for MQS systems taken by these two earlier chapters for EQS systems.

Chapter 4 began by expressing the irrotational $\mathbf{E}$ in terms of a scalar potential. Here $\mathbf{H}$ is not generally irrotational, although it may be in certain source-free regions. On the other hand, even with the effects of magnetization that are introduced in Chap. 9, the generalization of the magnetic flux density $\mu_o\mathbf{H}$ has no divergence anywhere. Therefore, Sec. 8.1 focuses on the solenoidal character of $\mu_o\mathbf{H}$ and develops a vector form of Poisson's equation satisfied by the vector potential, from which the H field may be obtained.

In Chap. 4, where the electric potential was used to represent an irrotational electric field, we paused to develop insights into the nature of the scalar potential. Similarly, here we could delve into the way in which the vector potential represents the flux of a solenoidal field. For two reasons, we delay developing this interpretation of the vector potential for Sec. 8.6. First, as we see in Sec. 8.2, the superposition integral approach is often used to directly relate the source, the current density, to the magnetic field intensity without the intetermediary of a potential. Second, many situations of interest involving current-carrying coils can be idealized by representing the coil wires as surface currents. In this idealization, all of space is current free except for some surfaces within which surface currents flow. But, because $\mathbf{H}$ is irrotational everywhere except through these surfaces, this means that the H field may be expressed as the gradient of a *scalar* potential. Further, since the magnetic field is divergence free (at least as treated in this chapter, which does not deal with magnetizable materials), the *scalar* potential obeys Laplace's equation. Thus, most methods developed for EQS systems using solutions to Laplace's equation can be applied to the solution to MQS problems as well. In this way, we find "dual" situations to those solved already in earlier chapters. The method extends to time-varying quasistatic magnetic fields in the presence of perfect conductors in Sec. 8.4. Eventually, in Chap. 9, we shall extend the approach to problems involving piece-wise uniform and linear magnetizable materials.

Vector Field Uniquely Specified. A vector field is uniquely specified by its curl and divergence. This fact, used in the next sections, follows from a slight modification to the uniqueness theorem discussed in Sec. 5.2. Suppose that the vector and scalar functions $\mathbf{C}(\mathbf{r})$ and $D(\mathbf{r})$ are given and represent the curl and divergence, respectively, of a vector function $\mathbf{F}$.

$$\nabla \times \mathbf{F} = \mathbf{C}(\mathbf{r}) \tag{5}$$

$$\nabla \cdot \mathbf{F} = D(\mathbf{r}) \tag{6}$$

The same arguments used in this earlier uniqueness proof then shows that $\mathbf{F}$ is uniquely specified provided the functions $\mathbf{C}(\mathbf{r})$ and $D(\mathbf{r})$ are given everywhere and have distributions consistent with $\mathbf{F}$ going to zero at infinity. Suppose that $\mathbf{F}_a$ and $\mathbf{F}_b$ are two different solutions of (5) and (6). Then the difference solution

$\mathbf{F}_d = \mathbf{F}_a - \mathbf{F}_b$ is both irrotational and solenoidal.

$$\nabla \times \mathbf{F}_d = 0 \tag{7}$$

$$\nabla \cdot \mathbf{F}_d = 0 \tag{8}$$

The difference solution is governed by the same equations as in Sec. 5.2. With $\mathbf{F}_d$ taken to be the gradient of a Laplacian potential, the remaining steps in the uniqueness argument are equally applicable here.

The uniqueness proof shows the importance played by the two differential vector operations, curl and divergence. Among the many possible combinations of the partial derivatives of the vector components of $\mathbf{F}$, these two particular combinations have the remarkable property that their specification gives full information about $\mathbf{F}$.

In Chap. 4, we determined a vector field $\mathbf{F} = \mathbf{E}$ given that the vector source $\mathbf{C} = 0$ and the scalar source $D = \rho/\epsilon_o$. In Secs. 8.1 we find the vector field $\mathbf{F} = \mathbf{H}$, given that the scalar source $D = 0$ and that the vector source is $\mathbf{C} = \mathbf{J}$.

The strategy in this chapter parallels that for Chaps. 4 and 5. We can again think of dividing the fields into two parts, a particular part due to the current density, and a homogeneous part that is needed to satisfy boundary conditions. Thus, with the understanding that the superposition principle makes it possible to take the fields as the sum of particular and homogeneous solutions, (1) and (2) become

$$\nabla \times \mathbf{H}_p = \mathbf{J} \tag{9}$$

$$\nabla \cdot \mu_o \mathbf{H}_p = 0 \tag{10}$$

$$\nabla \times \mathbf{H}_h = 0 \tag{11}$$

$$\nabla \cdot \mu_o \mathbf{H}_h = 0 \tag{12}$$

In sections 8.1–8.3, it is presumed that the current density is given everywhere. The resulting vector and scalar superposition integrals provide solutions to (9) and (10) while (11) and (12) are not relevant. In Sec. 8.4, where the fields are found in free-space regions bounded by perfect conductors, (11) and (12) are solved and boundary conditions are met without the use of particular solutions. In Sec. 8.5, where currents are imposed but confined to surfaces, a boundary value approach is taken to find a particular solution. Finally, Sec. 8.6 concludes with an example in which the region of interest includes a volume current density (which gives rise to a particular field solution) bounded by a perfect conductor (in which surface currents are induced that introduce a homogeneous solution).

8.1 THE VECTOR POTENTIAL AND THE VECTOR POISSON EQUATION

A general solution to (8.0.2) is

$$\boxed{\mu_o \mathbf{H} = \nabla \times \mathbf{A}} \tag{1}$$

where $\mathbf{A}$ is the *vector potential*. Just as $\mathbf{E} = -grad\Phi$ is the "integral" of the EQS equation $curl\mathbf{E} = 0$, so too is (1) the "integral" of (8.0.2). Remember that we could add an arbitrary constant to Φ without affecting $\mathbf{E}$. In the case of the vector potential, we can add the gradient of an arbitrary scalar function to $\mathbf{A}$ without affecting $\mathbf{H}$. Indeed, because $\nabla \times (\nabla\psi) = 0$, we can replace $\mathbf{A}$ by $\mathbf{A'} = \mathbf{A} + \nabla\psi$. The curl of $\mathbf{A}$ is the same as of $\mathbf{A'}$.

We can interpret (1) as the specification of $\mathbf{A}$ in terms of the assumedly known physical $\mathbf{H}$ field. But as pointed out in the introduction, to uniquely specify a vector field, both its curl and divergence must be given. In order to specify $\mathbf{A}$ uniquely, we must also give its divergence. Just what we specify here is a matter of convenience and will vary in accordance with the application. In MQS systems, we shall find it convenient to make the vector potential solenoidal

$$\nabla \cdot \mathbf{A} = 0 \tag{2}$$

Specification of the potential in this way is sometimes called setting the gauge, and with (2) we have established the *Coulomb gauge*.

We turn now to the evaluation of $\mathbf{A}$, and hence $\mathbf{H}$, from the MQS Ampère's law and magnetic flux continuity law, (8.0.1) and (8.0.2). The latter is automatically satisfied by letting the magnetic flux density be represented in terms of the vector potential, (1). Substituting (1) into Ampère's law (8.0.1) then gives

$$\nabla \times (\nabla \times \mathbf{A}) = \mu_o \mathbf{J} \tag{3}$$

The following identity holds.

$$\nabla \times (\nabla \times \mathbf{A}) = \nabla(\nabla \cdot \mathbf{A}) - \nabla^2 \mathbf{A} \tag{4}$$

The reason for defining $\mathbf{A}$ as solenoidal was to eliminate the $\nabla \cdot \mathbf{A}$ term in this expression and to reduce (3) to the *vector Poisson's equation*.

$$\boxed{\nabla^2 \mathbf{A} = -\mu_o \mathbf{J}} \tag{5}$$

The vector Laplacian on the left in this expression is defined *in Cartesian coordinates* as having components that are the scalar Laplacian operating on the respective components of $\mathbf{A}$. Thus, (5) is equivalent to three scalar Poisson's equations, one for each Cartesian component of the vector equation. For example, the z component is

$$\nabla^2 A_z = -\mu_o J_z \tag{6}$$

With the identification of $A_z \rightarrow \Phi$ and $\mu_o J_z \rightarrow \rho/\epsilon_o$, this expression becomes the scalar Poisson's equation of Chap. 4, (4.2.2). The integral of this latter equation is the superposition integral, (4.5.3). Thus, identification of variables gives as the integral of (6)

$$A_z = \frac{\mu_o}{4\pi} \int_{V'} \frac{J_z(\mathbf{r'})}{|\mathbf{r} - \mathbf{r'}|} dv' \tag{7}$$

and two similar equations for the other two components of $\mathbf{A}$. Reconstructing the vector $\mathbf{A}$ by multiplying (7) by $\mathbf{i_z}$ and adding the corresponding x and y components, we obtain the *superposition integral for the vector potential*.

$$\boxed{\mathbf{A}(\mathbf{r}) = \frac{\mu_o}{4\pi}\int_{V'}\frac{\mathbf{J}(\mathbf{r}')}{|\mathbf{r}-\mathbf{r}'|}dv'} \tag{8}$$

Remember, $\mathbf{r}'$ is the coordinate of the current density source, while $\mathbf{r}$ is the coordinate of the point at which $\mathbf{A}$ is evaluated, the observer coordinate. Given the current density everywhere, this integration provides the vector potential. Hence, in principle, the flux density $\mu_o\mathbf{H}$ is determined by carrying out the integration and then taking the curl in accordance with (1).

The theorem at the end of Sec. 8.0 makes it clear that the solution provided by (8) is indeed unique when the current density is given everywhere.

In order that $\nabla\times\mathbf{A}$ be a physical flux density, $\mathbf{J}(\mathbf{r})$ cannot be an arbitrary vector field. Because $div(curl)$ of any vector is identically equal to zero, the divergence of the quasistatic Ampère's law, (8.0.1), gives $\nabla\cdot(\nabla\times\mathbf{H}) = 0 = \nabla\cdot\mathbf{J}$ and thus

$$\nabla\cdot\mathbf{J} = 0 \tag{9}$$

The current distributions of magnetoquasistatics must be solenoidal.

Of course, we know from the discussion of uniqueness given in Sec. 8.0 that (9) does not uniquely specify the current distribution. In an Ohmic conductor, stationary current distributions satisfying (9) were determined in Secs. 7.1–7.5. Thus, any of these distributions can be used in (8). Even under dynamic conditions, (9) remains valid for MQS systems. However, in Secs. 8.4–8.6 and as will be discussed in detail in Chap. 10, if time rates of change become too rapid, Faraday's law demands a rotational electric field which plays a role in determining the distribution of current density. For now, we assume that the current distribution is that for steady Ohmic conduction.

Two-Dimensional Current and Vector Potential Distributions.

Suppose a current distribution $\mathbf{J} = \mathbf{i_z}J_z(x,y)$ exists through all of space. Then the vector potential is z directed, according to (8), and its z component obeys the scalar Poisson equation

$$A_z = \frac{\mu_o}{4\pi}\int\frac{J_z(x',y')dv'}{|\mathbf{r}-\mathbf{r}'|} \tag{10}$$

But this is formally the same expression, (4.5.3), as that of the scalar potential produced by a charge distribution $\rho(x',y')$.

$$\Phi = \frac{1}{4\pi\epsilon_o}\int\frac{\rho(x',y')dv'}{|\mathbf{r}-\mathbf{r}'|} \tag{11}$$

It was inconvenient to integrate the above equation directly. Instead, we determined the field of a line charge from symmetry and Gauss' law and integrated the resulting expression to obtain the potential (4.5.18)

$$\Phi = -\frac{\lambda_l}{2\pi\epsilon_o}ln\Big(\frac{r}{r_o}\Big) \tag{12}$$

where r is the distance from the line charge $r = \sqrt{(x-x')^2+(y-y')^2}$ and r_o is the reference radius. The scalar potential can thus be evaluated from the two-dimensional integral

$$\Phi = -\frac{1}{2\pi\epsilon_o}\int\int \rho(x',y')ln\left(\sqrt{(x-x')^2+(y-y')^2}/r_o\right)dx'dy' \tag{13}$$

The vector potential of a two-dimensional z-directed current distribution obeys the same equation and thus has a solution by analogy, after a proper interchange of parameters.

$$A_z = -\frac{\mu_o}{2\pi}\int J_z(x',y')ln\left(\sqrt{(x-x')^2+(y-y')^2}/r_o\right)dx'dy' \tag{14}$$

Two important consequences emerge from this derivation.

(a) Every two-dimensional EQS potential $\Phi(x,y)$ produced by a given charge distribution $\rho(x,y)$, has an MQS analog vector potential $A_z(x,y)$ caused by a current density $J_z(x,y)$ with the same spatial distribution as $\rho(x,y)$. The magnetic field follows from (1) and thus

$$\begin{aligned}\mu_o\mathbf{H} = \nabla\times\mathbf{A} &= \left(\mathbf{i_x}\frac{\partial}{\partial x}+\mathbf{i_y}\frac{\partial}{\partial y}\right)\times\mathbf{i_z}A_z\\ &= -\mathbf{i_z}\times\left(\mathbf{i_x}\frac{\partial A_z}{\partial x}+\mathbf{i_y}\frac{\partial A_z}{\partial y}\right)\\ &= -\mathbf{i_z}\times\nabla A_z\end{aligned} \tag{15}$$

Therefore the lines of magnetic flux density are perpendicular to the gradient of A_z. A plot of field lines and equipotential lines of the EQS problem is transformed into a plot of an MQS field problem by interpreting the equipotential lines as the lines of magnetic flux density. *Lines of constant A_z are lines of magnetic flux.*

(b) The vector potential of a line current of magnitude i along the z direction is given by analogy with (12),

$$A_z = -\frac{\mu_o}{2\pi}i\ ln\ (r/r_o) \tag{16}$$

which is consistent with the magnetic field $\mathbf{H} = \mathbf{i}_\phi(i/2\pi r)$ given by (1.4.10), if one makes use of the curl expression in polar coordinates,

$$\mu_o\mathbf{H} = \frac{1}{r}\frac{\partial A_z}{\partial\phi}\mathbf{i_r} - \frac{\partial A_z}{\partial r}\mathbf{i}_\phi \tag{17}$$

The following illustrates the integration called for in (8). The fields associated with singular current distributions will be used in later sections and chapters.

Example 8.1.1. Field Associated with a Current Sheet

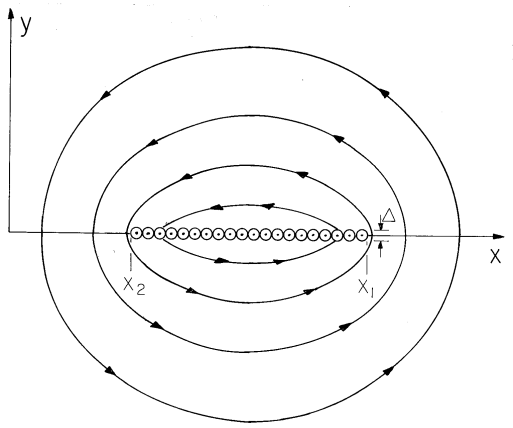


Fig. 8.1.1 Cross-section of surfaces of constant A_z and lines of magnetic flux density for the uniform sheet of current shown.

A z-directed current density is uniformly distributed over a strip located between x_2 and x_1 as shown in Fig. 8.1.1. The thickness of the sheet, Δ, is very small compared to other dimensions of interest. So, the integration of (14) in the y direction amounts to a multiplication of the current density by Δ. The vector potential is therefore determined by completing the integration on x'

$$A_z = -\frac{\mu_o K_o}{2\pi}\int_{x_2}^{x_1} ln\left(\sqrt{(x-x')^2+y^2}/r_o\right)dx' \tag{18}$$

where $K_o \equiv J_z\Delta$.

This integral is carried out in Example 4.5.3, where the two dimensional electric potential of a charged strip was determined. Thus, with $\sigma_o/\epsilon_o \rightarrow \mu_o K_o$, (4.5.24) becomes the desired vector potential.

The profiles of surfaces of constant A_z are shown in Fig. 8.1.1. Remember, these are also the lines of magnetic flux density, $\mu_o\mathbf{H}$.

Example 8.1.2. Two-Dimensional Magnetic Dipole Field

A pair of closely spaced conductors carrying oppositely directed currents of magnitude i is shown in Fig. 8.1.2. The currents extend to + and − infinity in the z direction, so the resulting fields are two-dimensional and can be represented by A_z. In polar coordinates, the distance from the right conductor, which is at a distance d from the z axis, to the observer location is essentially $r - d\cos\phi$. The A_z for each wire takes the form of (16), with r the distance from the wire to the point of observation. Thus, superposition of the vector potentials due to the two wires gives

$$A_z = -\frac{\mu_o i}{2\pi}[ln(r-d\cos\phi) - lnr] = -\frac{\mu_o i}{2\pi} ln\big(1-\frac{d}{r}\cos\phi\big) \tag{19}$$

In the limit $d \ll r$, this expression becomes

$$A_z = \mu_o \frac{id}{2\pi}\frac{\cos\phi}{r} \tag{20}$$

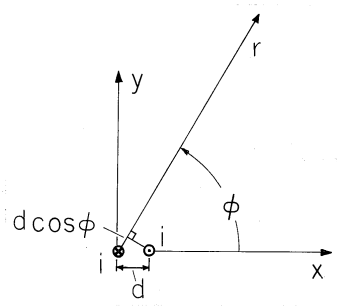


Fig. 8.1.2 A pair of wires having the spacing d carry the current i in opposite directions parallel to the z axis. The two-dimensional dipole field is shown in Fig. 8.1.3.

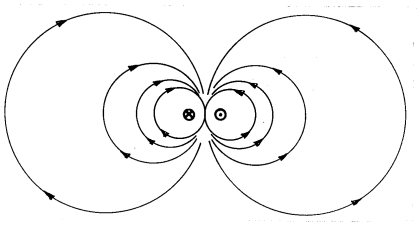


Fig. 8.1.3 Cross-sections of surfaces of constant A_z and hence lines of magnetic flux density for configuration of Fig. 8.1.2.

Thus, the surfaces of constant A_z have intersections with planes of constant z that are circular, as shown in Fig. 8.1.3. These are also the lines of magnetic flux density, which follow from (17).

$$\mu_o \mathbf{H} = \frac{\mu_o i d}{2\pi}\left(-\frac{\sin\phi}{r^2}\mathbf{i_r} + \frac{\cos\phi}{r^2}\mathbf{i}_\phi \right) \tag{21}$$

If the line currents are replaced by line charges, the resulting equipotential lines (intersections of the equipotential surfaces with the $x-y$ plane) coincide with the magnetic field lines shown in Fig. 8.1.3. Thus, the lines of electric field intensity for the electric dual of the magnetic configuration shown in Fig. 8.1.3 originate on the positive line charge on the right and terminate on the negative line charge at the left, following lines that are perpendicular to those shown.

8.2 THE BIOT-SAVART SUPERPOSITION INTEGRAL

Once the vector potential has been determined from the superposition integral of Sec. 8.1, the magnetic flux density follows from an evaluation of *curl* $\mathbf{A}$. However, in certain field evaluations, it is best to have a superposition integral for the field itself. For example, in numerical calculations, numerical derivatives should be avoided.

The field superposition integral follows by operating on the vector potential as given by (8.1.8) before the integration has been carried out.

$$\mathbf{H} = \frac{1}{\mu_o}\nabla \times \mathbf{A} = \frac{1}{4\pi}\nabla \times \int_{V'} \left[\frac{\mathbf{J}(\mathbf{r}')}{|\mathbf{r}-\mathbf{r}'|}\right] dv' \tag{1}$$

The integration is with respect to the source coordinates denoted by $\mathbf{r}'$, while the *curl* operation involves taking derivatives with respect to the observer coordinates $\mathbf{r}$. Thus, the curl operation can be carried out before the integral is completed, and (1) becomes

$$\mathbf{H} = \frac{1}{4\pi}\int_{V'} \nabla \times \left[\frac{\mathbf{J}(\mathbf{r}')}{|\mathbf{r}-\mathbf{r}'|}\right] dv' \tag{2}$$

The *curl* operation required to evaluate the integrand in this expression can be carried out without regard for the particular dependence of the current density because the derivatives are with respect to $\mathbf{r}$, not $\mathbf{r}'$. To make this evaluation, observe that the *curl* operates on the product of the vector $\mathbf{J}$ and the scalar $\psi = |\mathbf{r}-\mathbf{r}'|^{-1}$, and that operation obeys the vector identity

$$\nabla \times (\psi \mathbf{J}) = \psi \nabla \times \mathbf{J} + \nabla\psi \times \mathbf{J} \tag{3}$$

Because $\mathbf{J}$ is independent of $\mathbf{r}$, the first term on the right is zero. Thus, (2) becomes

$$\mathbf{H} = \frac{1}{4\pi}\int_{V'} \nabla\left(\frac{1}{|\mathbf{r}-\mathbf{r}'|}\right) \times \mathbf{J} dv' \tag{4}$$

To evaluate the gradient in this expression, consider the special case when $\mathbf{r}'$ is at the origin in a spherical coordinate system, as shown in Fig. 8.2.1. Then

$$\nabla(1/r) = -\frac{1}{r^2}\mathbf{i}_\mathbf{r} \tag{5}$$

where $\mathbf{i}_\mathbf{r}$ is the unit vector directed from the source coordinate at the origin to the observer coordinate at (r, θ, ϕ).

We now move the source coordinate from the origin to the arbitrary location $\mathbf{r}'$. Then the distance r in (5) is replaced by the distance $|\mathbf{r}-\mathbf{r}'|$. To replace the unit vector $\mathbf{i}_\mathbf{r}$, the *source-observer unit vector* $\mathbf{i}_{\mathbf{r}'\mathbf{r}}$ is defined as being *directed from an arbitrary source coordinate to the observer coordinate P*. In terms of this source-observer unit vector, illustrated in Fig. 8.2.2, (5) becomes

$$\nabla\left(\frac{1}{\mathbf{r}-\mathbf{r}'}\right) = -\frac{\mathbf{i}_{\mathbf{r}'\mathbf{r}}}{|\mathbf{r}-\mathbf{r}'|^\mathbf{2}} \tag{6}$$

Substitution of this expression into (4) gives the *Biot-Savart Law* for the magnetic field intensity.

$$\boxed{\mathbf{H} = \frac{1}{4\pi}\int_{V'} \frac{\mathbf{J}(\mathbf{r}') \times \mathbf{i}_{\mathbf{r}'\mathbf{r}}}{|\mathbf{r}-\mathbf{r}'|^\mathbf{2}} dv'} \tag{7}$$

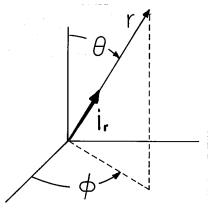


Fig. 8.2.1 Spherical coordinate system with $\mathbf{r}'$ located at origin.

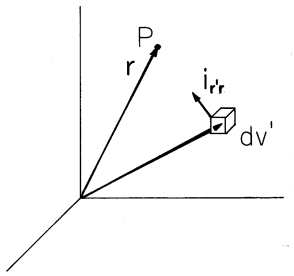


Fig. 8.2.2 Source coordinate $\mathbf{r}'$ and observer coordinate $\mathbf{r}$ showing unit vector $\mathbf{i}_{\mathbf{r}'\mathbf{r}}$ directed from $\mathbf{r}'$ to $\mathbf{r}$.

In evaluating the integrand, the cross-product is evaluated at the source coordinate $\mathbf{r}'$. The integrand represents the contribution of the current density at $\mathbf{r}'$ *to the field at* $\mathbf{r}$. The following examples illustrate the Biot-Savart law.

Example 8.2.1. On Axis Field of Circular Cylindrical Solenoid

The cross-section of an N-turn solenoid of axial length d and radius a is shown in Fig. 8.2.3. There are many turns, so the current i passing through each is essentially ϕ directed. To keep the integration simple, we confine ourselves to finding $\mathbf{H}$ on the z axis, which is the axis of symmetry.

In cylindrical coordinates, the source coordinate incremental volume element is $dv' = r'd\phi' dr' dz'$. For many windings uniformly distributed over a thickness Δ, the current density is essentially the total number of turns multiplied by the current per turn and divided by the area through which the current flows.

$$\mathbf{J} \cong \mathbf{i}_\phi \frac{Ni}{\Delta d} \tag{8}$$

The superposition integral, (7), is carried out first on r'. This extends from $r' = a$ to $r' = a + \Delta$ over the radial thickness of the winding. Because $\Delta \ll a$, the source-observer distance and direction remain essentially constant over this interval, and so the integration amounts to a multiplication by Δ. The axial symmetry requires that $\mathbf{H}$ on the z axis be z directed. The integration over z' and ϕ' is

$$H_z = \frac{1}{4\pi} \int_{d/2}^{-d/2} \int_0^{2\pi} \left(\frac{Ni}{d}\right) \frac{(\mathbf{i}_\phi \times \mathbf{i}_{r'r})_z}{|\mathbf{r} - \mathbf{r}'|^2} a d\phi' dz' \tag{9}$$

In terms of the angle α shown in Fig. 8.2.3 and its inset, the source-observer unit vector is

$$\mathbf{i}_{r'r} = -\mathbf{i}_\mathbf{r} \sin\alpha - \mathbf{i}_\mathbf{z} \cos\alpha \tag{10}$$

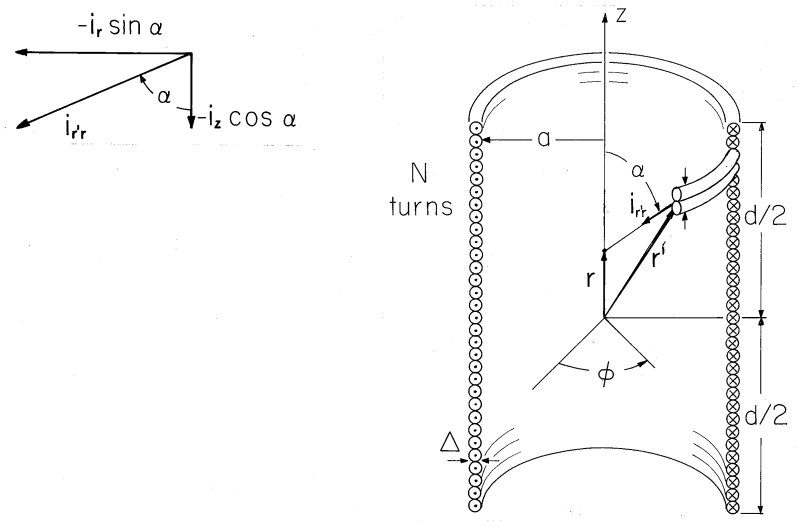


Fig. 8.2.3 A solenoid consists of N turns uniformly wound over a length d, each turn carrying a current i. The field is calculated along the z axis, so the observer coordinate is at $\mathbf{r}$ on the z axis.

so that

$$(\mathbf{i}_\phi \times \mathbf{i}_{r'r})_z = \sin\alpha = \frac{a}{\sqrt{a^2+(z'-z)^2}}; \quad |\mathbf{r}-\mathbf{r}'|^2 = a^2+(z'-z)^2 \tag{11}$$

The integrand in (9) is ϕ' independent, and the integration over ϕ' amounts to multiplication by 2π.

$$H_z = \frac{Ni}{2d}\int_{-d/2}^{d/2} \frac{a^2 dz'}{[a^2+(z'-z)^2]^{3/2}} \tag{12}$$

With the substitution $z'' = z' - z$, it follows that

$$\begin{aligned} H_z &= \frac{Ni}{2d}\frac{z''}{\sqrt{a^2+z''^2}}\Big]_{-\frac{d}{2}-z}^{\frac{d}{2}-z} \\ &= \frac{Ni}{2d}\left[\frac{\frac{d}{2a}-\frac{z}{a}}{\sqrt{1+\left(\frac{d}{2a}-\frac{z}{a}\right)^2}} + \frac{\frac{d}{2a}+\frac{z}{a}}{\sqrt{1+\left(\frac{d}{2a}+\frac{z}{a}\right)^2}}\right] \end{aligned} \tag{13}$$

In the limit where $d/2a \ll 1$, the solenoid becomes a circular coil with N turns concentrated at $r = a$ in the plane $z = 0$. The field intensity at the center of this coil follows from (13) as the amp-turns divided by the loop diameter.

$$H_z \to \frac{Ni}{2a} \tag{14}$$

Thus, a 100-turn circular loop having a radius $a = 5$ cm (that is large compared to its axial length d) and carrying a current of $i = 1$ A would have a field intensity of

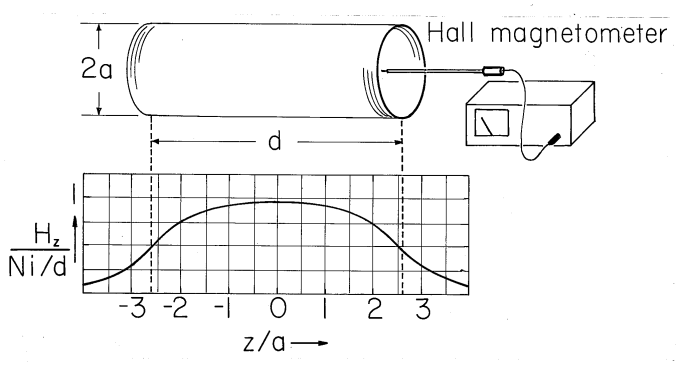


Fig. 8.2.4 Experiment for documenting the axial **H** predicted in Example 8.2.1. Profile of normalized H_z is for $d/2a = 2.58$.

1000 A/m at its center. The flux density measured by a magnetometer would then be $B_z = \mu_o H_z = 4\pi \times 10^{-7}(1000)$ tesla $= 4\pi$ gauss.

Further implications of this finding are discussed in the following demonstration.

Demonstration 8.2.1. Fields of a Circular Cylindrical Solenoid

The solenoid shown in Fig. 8.2.4 has $N = 141$ turns, an axial length $d = 70.5$ cm, and a radius $a = 13.6$ cm. A Hall-type magnetometer measures the magnitude and direction of **H** in and around the coil. The on-axis distribution of H_z predicted by (13) for the experimental length-to-diameter ratio $d/2a = 2.58$ is shown in Fig. 8.2.4. With $i = 1$ amp, the flux density at the center approaches 2.5 gauss. The accuracy with which theory and experiment agree is likely to be limited only by such matters as the care with which the probe can be mounted and the calibration of the magnetometer. Care must also be taken that there are no magnetizable materials, such as iron, in the vicinity of the coil. To avoid contributions from the earth's magnetic field (which is on the order of a gauss), ac fields should be used. If ac is used, there should be no large conducting objects near by in which eddy currents might be induced. (Magnetization and eddy currents, respectively, are taken up in the next two chapters.)

The infinitely long solenoid can be regarded as the analog for MQS systems of the "plane parallel plate capacitor." Just as the capacitor can be constructed to create a uniform electric field between the plates with zero field outside the region bounded by the plates, so too the long solenoid gives rise to a uniform magnetic field throughout the interior region and an exterior field that is zero. This can be seen by probing the field not only as a function of axial position but of radius as well. For the finite length solenoid, the on-axis interior field designated by H_∞ in Fig. 8.2.4 is given by (13) for locations on the z axis where $d/2 \gg z$.

$$H_z \to H_\infty \equiv \left[\frac{d/2a}{\sqrt{1+\left(\frac{d}{2a}\right)^2}}\right]\frac{Ni}{d} \tag{15}$$

In the limit where the solenoid is also very long compared to its radius, where $d/2a \gg 1$, this expression becomes

$$H_\infty \to \frac{Ni}{d} \tag{16}$$

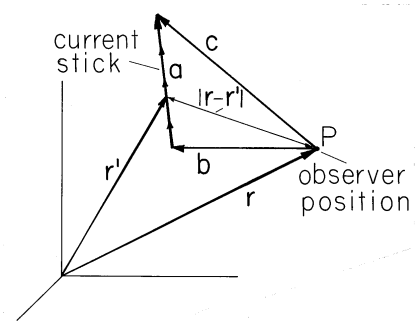


Fig. 8.2.5 A line current i is uniformly distributed over the length of the vector $\mathbf{a}$ originating at $\mathbf{r}+\mathbf{b}$ and terminating at $\mathbf{r}+\mathbf{c}$. The resulting magnetic field intensity is determined at the observer position $\mathbf{r}$.

Probing of the field shows the field maintains the value and direction of (16) over the interior cross-section as well. It also shows that the magnetic field intensity just outside the windings at an axial location that is several radii a from the coil ends is relatively small.

Continuity of magnetic flux requires that the total flux passing through the solenoid in the z direction must be returned in the $-z$ direction outside the solenoid. How, then, can the exterior field of a long solenoid be negligible compared to that inside? The outside flux returns in the $-z$ direction through a much larger exterior area than the area πa^2 through which the interior flux passes. In fact, as the coil becomes infinitely long, this return flux spreads out over an exterior area that stretches to infinity in the x and y directions. The field intensity just outside the winding tends to zero as the coil is made very long.

Stick Model for Computing Fields of Electromagnet. The Biot-Savart superposition integral can be completed analytically for relatively few configurations. Nevertheless, its evaluation amounts to no more than a summation of the field contributions from each of the current elements. Thus, on the computer, its evaluation is a straightforward matter.

Many practical current distributions are, or can be approximated by, connected straight-line current segments, or current "sticks." We will now use the Biot-Savart law to find the field at an arbitrary observer position $\mathbf{r}$ associated with a current stick having an arbitrary location. The result is a practical resource, because a numerical summation over differential volume current elements can then be replaced by one over the sticks.

The current stick, shown in Fig. 8.2.5, is represented by a vector $\mathbf{a}$. Thus, the current is uniformly distributed between the base of this vector at $\mathbf{r}+\mathbf{b}$ and the tip of the vector at $\mathbf{r}+\mathbf{c}$. The source coordinate $\mathbf{r}'$ is located along the current stick. The objective in the following paragraphs is to carry out an integration over the length of the current stick and obtain an expression for $\mathbf{H}(\mathbf{r})$. Because the current stick does not represent a solenoidal current density at its ends, the field derived is of physical significance only if used in conjunction with other current sticks that together represent a continuous current distribution.

The detailed view of the current stick, Fig. 8.2.6, shows the source coordinate ξ denoting the position along the stick. The origin of this coordinate is at the point

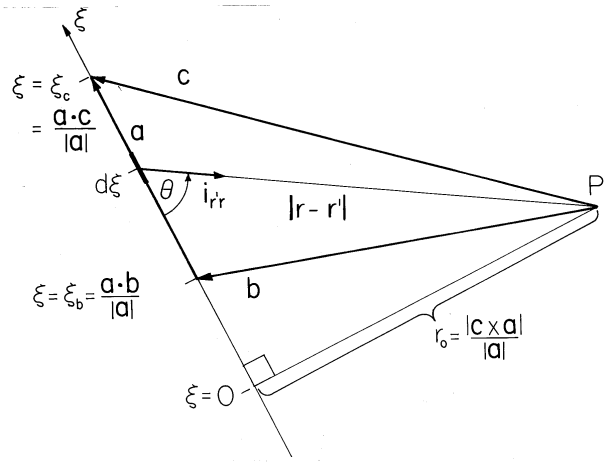


Fig. 8.2.6 View of current element from Fig. 8.2.5 in plane containing **b** and **c**, and hence **a**.

on a line through the stick that is closest to the observer coordinate.

The projection of **b** onto a vector **a** is $\xi_b = \mathbf{a} \cdot \mathbf{b}/|\mathbf{a}|$. Thus, the current stick begins at this distance from $\xi = 0$, as shown in Fig. 8.2.6, and terminates at ξ_c, the projection of **c** onto the axis of **a**, as also shown.

The cross-product $\mathbf{c} \times \mathbf{a}/|\mathbf{a}|$ is perpendicular to the plane of Fig. 8.2.6 and equal in magnitude to the projection of **c** onto a vector that is perpendicular to **a** and in the plane of Fig. 8.2.6. Thus, the shortest distance between the observer position and the axis of the current stick is $r_o = |\mathbf{c} \times \mathbf{a}|/|\mathbf{a}|$. It follows from this fact and the definition of the cross-product that

$$d\mathbf{s} \times \mathbf{i}_{r'r} = d\xi \frac{\left[\frac{\mathbf{c}\times\mathbf{a}}{|a|}\right]}{|\mathbf{r} - \mathbf{r}'|} \tag{17}$$

where $d\mathbf{s}$ is the differential along the line current and

$$|\mathbf{r} - \mathbf{r}'| = (\xi^2 + r_o^2)^{1/2}$$

Integration of the Biot-Savart law, (7), is first performed over the cross-section of the stick. The cross-sectional dimensions are small, so during this integration, the integrand remains essentially constant. Thus, the current density is replaced by the total current and the integral reduced to one on the axial coordinate ξ of the stick.

$$\mathbf{H} = \frac{i}{4\pi} \int_{\xi_b}^{\xi_c} \frac{d\mathbf{s} \times \mathbf{i}_{r'r}}{|\mathbf{r} - \mathbf{r}'|^2} \tag{18}$$

In view of (17), this integral is expressed in terms of the source coordinate integration variable ξ as

$$\mathbf{H} = \frac{i}{4\pi} \int_{\xi_b}^{\xi_c} \frac{\mathbf{c} \times \mathbf{a} d\xi}{|a|(\xi^2 + r_o^2)^{3/2}} \tag{19}$$

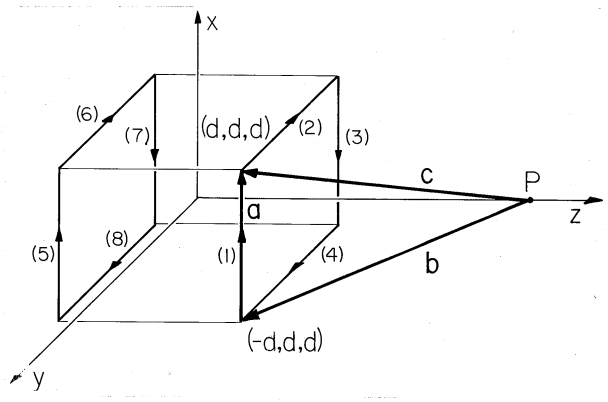


Fig. 8.2.7 A pair of square N-turn coils produce a field at P on the z axis that is the superposition of the fields H_z due to the eight linear elements comprising the coils. The coils are centered on the z axis.

This integral is carried out to obtain

$$\mathbf{H} = \frac{i}{4\pi}\frac{\mathbf{c}\times\mathbf{a}}{|a|}\left[\frac{\xi}{r_o^2[\xi^2+r_o^2]^{1/2}}\right]_{\xi_b}^{\xi_c} \tag{20}$$

In evaluating this expression at the integration endpoints, note that by definition,

$$(\xi_c^2+r_o^2)^{1/2} = |c|; \qquad (\xi_b^2+r_o^2)^{1/2} = |b| \tag{21}$$

so that (20) becomes an expression for the field intensity at the observer location expressed in terms of vectors **a**, **b**, and **c** that serve to define the relative location of the current stick.[1]

$$\boxed{\mathbf{H} = \frac{i}{4\pi}\frac{\mathbf{c}\times\mathbf{a}}{|\mathbf{c}\times\mathbf{a}|^2}\left(\frac{\mathbf{a}\cdot\mathbf{c}}{|c|}-\frac{\mathbf{a}\cdot\mathbf{b}}{|b|}\right)} \tag{22}$$

The following illustrates how this expression can be used repetitively to determine the field induced by currents represented in a piece-wise fashion by current sticks. Expressed in Cartesian coordinates, the vectors are a convenient way to specify the sticks making up a complex winding. On the computer, the evaluation of (22) is then conveniently carried out by a subroutine that is used many times.

Example 8.2.2. Axial Field of a Pair of Square Coils

Shown in Fig. 8.2.7 is a pair of coils, each having N turns carrying a current i in such a direction that the fields induced by each coil reinforce along the z axis. The four linear sections of the two coils comprise the sides of a cube, centered at the origin and with dimensions $2d$.

[1] Private communication, Mr. John G. Aspinall.

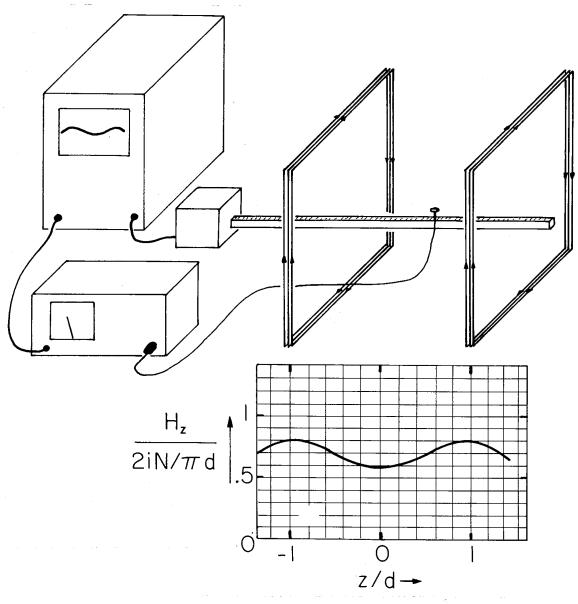


Fig. 8.2.8 Demonstration of axial field generated by pair of square coils having spacing equal to the side lengths.

We confine ourselves to finding **H** along the z axis where, by symmetry, it has only a z component. Thus, for an observer at $(0, 0, z)$, the vectors specifying element (1) of the right-hand coil in Fig. 8.2.7 are

$$\begin{aligned} \mathbf{a} &= 2d\mathbf{i_x} \\ \mathbf{b} &= -d\mathbf{i_x} + d\mathbf{i_y} + (d-z)\mathbf{i_z} \\ \mathbf{c} &= d\mathbf{i_x} + d\mathbf{i_y} + (d-z)\mathbf{i_z} \end{aligned} \tag{23}$$

Evaluation of the z component of (22) then gives the part of H_z due to element (1). Because of the axial symmetry, the field induced by elements (2), (3), and (4) in the same coil are the same as already found for element (1). The field induced by element (5) in the second coil is similarly found starting from vectors that are the same as in (23), except that $d \to -d$ in the z components of **b** and **c**. Here too, the other three elements each contribute the same field as already found. Thus, the axial field intensity, the sum of the contributions from the individual coils, is

$$\begin{aligned} H_z = -\frac{2iN}{\pi d}\Bigg\{ &\frac{1}{\left[\left(1-\frac{z}{d}\right)^2+1\right]\left[2+\left(1-\frac{z}{d}\right)^2\right]^{1/2}} \\ &+ \frac{1}{\left[\left(1+\frac{z}{d}\right)^2+1\right]\left[2+\left(1+\frac{z}{d}\right)^2\right]^{1/2}}\Bigg\} \end{aligned} \tag{24}$$

This distribution is plotted on the inset to Fig. 8.2.8. Because the fields induced by the separate coils reinforce, the pair can be used to produce a relatively uniform field in the midregion.

Demonstration 8.2.2. Field of Square Pair of Coils

In the experiment of Fig. 8.2.8, the axial field is probed by means of a Hall magnetometer. The output is connected to the vertical trace of a high persistence scope. The probe is mounted on a carriage that is attached to a potentiometer in such a way that there is an output voltage proportional to the horizontal position of the probe. This is used to control the horizontal scope deflection. The result is a trace that follows the predicted contour. The plot is shown in terms of normalized coordinates that can be used to compare theory to experiment using any size of coils and any level of current.

8.3 THE SCALAR MAGNETIC POTENTIAL

The vector potential $\mathbf{A}$ describes magnetic fields that possess curl wherever there is a current density $\mathbf{J}(\mathbf{r})$. In the space free of current,

$$\boxed{\nabla \times \mathbf{H} = 0} \tag{1}$$

and thus $\mathbf{H}$ ought to be derivable there from the gradient of a potential.

$$\boxed{\mathbf{H} = -\nabla \Psi} \tag{2}$$

Because

$$\nabla \cdot \mu_o \mathbf{H} = 0 \tag{3}$$

we further have

$$\boxed{\nabla^2 \Psi = 0} \tag{4}$$

The potential obeys Laplace's equation.

Example 8.3.1. The Scalar Potential of a Line Current

A line current is a source singularity (at the origin of a polar coordinate system if it is placed along its z axis). From Ampère's integral law applied to the contour C of Fig. 1.4.4, we have

$$\oint_C \mathbf{H} \cdot d\mathbf{s} = 2\pi r H_\phi = \int_S \mathbf{J} \cdot d\mathbf{a} = i \tag{5}$$

and thus

$$H_\phi = \frac{i}{2\pi r} \tag{6}$$

It follows that the potential Ψ that has H_ϕ of (6) as the negative of its gradient is

$$\Psi = -\frac{i}{2\pi}\phi \tag{7}$$

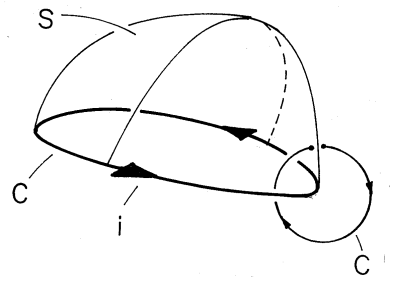


Fig. 8.3.1 Surface spanning loop, contour following loop, and contour for $\oint \mathbf{H} \cdot d\mathbf{s}$.

Note that the potential is multiple valued as the origin is encircled more than once. This property reflects the fact that strictly, **H** is not curl free in all of space. As the origin is encircled, Ampère's integral law identifies **J** as the source of the curl of **H**.

Because Ψ is a solution to Laplace's equation, it must possess an EQS analog. The electroquasistatic potential

$$\Phi = -\frac{V}{2\pi}\phi; \qquad 0 < \phi < 2\pi \tag{8}$$

describes the fringing field of a capacitor of semi-infinite extent, extending from $x = 0$ to $x = +\infty$, with a voltage V across the plates, in the limit as the spacing between the plates is negligible (Fig. 5.7.2 with V reversed in sign). It can also be interpreted as the field of a semi-infinite dipole layer with the dipole density $\pi_s = \sigma_s d = \epsilon_o V$ defined by (4.5.27), where d is the spacing between the surface charge densities, $\pm\sigma_s$, on the outside surfaces of the semi-infinite plates (Fig. 5.7.2 with the signs of the charges reversed). We now have further opportunity to relate H fields of current-carrying wires to EQS analogs involving dipole layers.

The Scalar Potential of a Current Loop. A current loop carrying a current i has a magnetic field that is curl free everywhere except at the location of the wire. We shall now determine the scalar potential produced by the current loop. The line integral $\oint \mathbf{H} \cdot d\mathbf{s}$ enclosing the current does not give zero, and hence paths that enclose the current in the loop are not allowed, if the potential is to be single valued. Suppose that we mount over the loop a surface S spanning the loop which is not crossed by any path of integration. The actual shape of the surface is arbitrary, but the contour C_l is defined by the wire which is its edge. The potential is then made single valued. The discontinuity of potential across the surface follows from Ampère's law

$$\int_C \mathbf{H} \cdot d\mathbf{s} = i \tag{9}$$

where the broken circle on the integral sign is to indicate a path as shown in Fig. 8.3.1 that goes from one side of the surface to a point on the opposite side. Thus, the potential Ψ of a current loop has the discontinuity

$$\int \mathbf{H} \cdot d\mathbf{s} = \int (-\nabla\Psi) \cdot d\mathbf{s} = \Delta\Psi = i \tag{10}$$

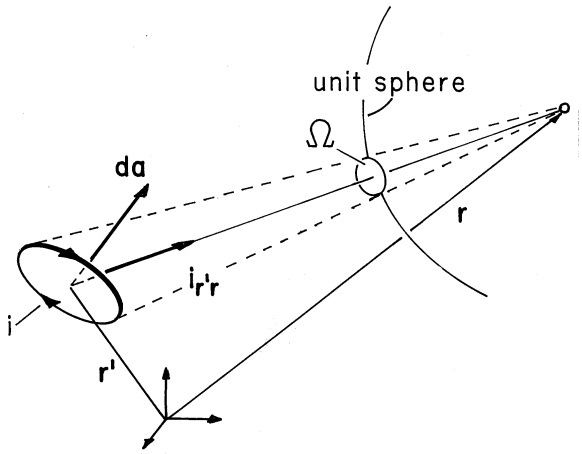


Fig. 8.3.2 Solid angle for observer at $\mathbf{r}$ due to current loop at $\mathbf{r}'$.

We have found in electroquasistatics that a uniform dipole layer of magnitude π_s on a surface S produces a potential that experiences a constant potential jump π_s/ϵ_o across the surface, (4.5.31). Its potential was (4.5.30)

$$\Phi(\mathbf{r}) = \frac{\pi_s}{4\pi\epsilon_o}\Omega \tag{11}$$

where Ω is the solid angle subtended by the rim of the surface as seen by an observer at the point $\mathbf{r}$. Thus, we conclude that the scalar potential Ψ, a solution to Laplace's equation with a constant jump i across the surface S spanning the wire loop, must have a potential jump $\pi_s/\epsilon_o \to i$, and hence the solution

$$\boxed{\Psi(\mathbf{r}) = \frac{i}{4\pi}\Omega} \tag{12}$$

where again the solid angle is that subtended by the contour along the wire as seen by an observer at the point $\mathbf{r}$ as shown by Fig. 8.3.2. In the example of a dipole layer, the surface S specified the physical distribution of the dipole layer. In the present case, S is arbitrary as long as it spans the contour C of the wire. This is consistent with the fact that the solid angle Ω is invariant with respect to changes of the surface S and depends only on the geometry of the rim.

Example 8.3.2. The H Field of Small Loop

Consider a small loop of area a at the origin of a spherical coordinate system with the normal to the surface parallel to the z axis. According to (12), the scalar potential of the loop is then

$$\Psi = \frac{i}{4\pi}\frac{\mathbf{i}_r \cdot \mathbf{i}_z a}{r^2} = \frac{ia}{4\pi}\frac{\cos\theta}{r^2} \tag{13}$$

This is the potential of a dipole. The H field follows from using (2)

$$\mathbf{H} = -\nabla\Psi = \frac{ia}{4\pi r^3}[2\cos\theta\mathbf{i}_r + \sin\theta\mathbf{i}_\theta] \tag{14}$$

As far as its field around and far from the loop is concerned, the current loop can be viewed as if it were a "magnetic" dipole, consisting of two equal and opposite magnetic charges $\pm q_m$ spaced a distance d apart (Fig. 4.4.1 with $q \to q_m$). The magnetic charges (monopoles) are sources of divergence of the magnetic flux $\mu_o\mathbf{H}$ analogous to electric charges as sources of divergence of the displacement flux density $\epsilon_o\mathbf{E}$. Thus, if Maxwell's equations are modified to include the action of a magnetic charge density

$$\rho_m = \lim_{\Delta V\to 0}\frac{q_m}{\Delta V}$$

in units of voltsec/m^4, then the new magnetic Gauss' law must be

$$\nabla\cdot\mu_o\mathbf{H} = \rho_m \tag{15}$$

in analogy with

$$\nabla\cdot\epsilon_o\mathbf{E} = \rho \tag{16}$$

Now, magnetic monopoles have been postulated by Dirac, and recent searches for the existence of such monopoles have been apparently successful[2]. Because the search is so difficult, it is apparent that, if they exist at all, they are very rare in nature. Here the introduction of magnetic charge is a matter of convenience so that the field produced by a small current loop can be pictured as the field of a *magnetic dipole*. This can serve as a mnemonic for the reconstruction of the field. Thus, if it is remembered that the potential of the electric dipole is

$$\Phi = \frac{\mathbf{p}\cdot\mathbf{i}_{\mathbf{r}'\mathbf{r}}}{4\pi\epsilon_o|\mathbf{r}-\mathbf{r}'|^2} \tag{17}$$

the potential of a magnetic dipole can be easily recalled as

$$\Psi = \frac{\mathbf{p}_m\cdot\mathbf{i}_{\mathbf{r}'\mathbf{r}}}{4\pi\mu_o|\mathbf{r}-\mathbf{r}'|^2} \tag{18}$$

where

$$p_m \equiv q_m d = \mu_o ia = \mu_o m \tag{19}$$

The magnetic dipole moment is defined as the product of the magnetic charge, q_m, and the separation, d, or by μ_o times the current times the area of the current loop. Another symbol is used commonly for the "dipole moment" of a current loop, $m \equiv ia$, the product of the current times the area of the loop without the factor μ_o. The reader must gather from the context whether the words dipole moment refer to p_m or $m = p_m/\mu_o$. The magnetic field intensity $\mathbf{H}$ of a magnetic dipole at the origin, (14), is

$$\mathbf{H} = -\nabla\Psi = \frac{m}{4\pi r^3}(2\cos\theta\mathbf{i}_\mathbf{r} + \sin\theta\mathbf{i}_\theta) \tag{20}$$

Of course, the details of the field produced by the current loop and the magnetic charge-dipole differ in the near field. One has $\nabla\cdot\mu_o\mathbf{H} \neq 0$, and the other has a solenoidal $\mathbf{H}$ field.

[2] *Science* Vol. 216, (June 4, 1982).

8.4 MAGNETOQUASISTATIC FIELDS IN THE PRESENCE OF PERFECT CONDUCTORS

There are physical situations in which the current distribution is not prespecified but is given by some equivalent information. Thus, for example, a *perfectly conducting* body in a time-varying magnetic field supports surface currents that shield the **H** field from the interior of the body. The effect of the conductor on the magnetic field is reminiscent of the EQS situations of Sec. 4.6, where charges distributed themselves on the surface of a conductor in such a way as to shield the electric field out of the material.

We found in Chap. 7 that the EQS model of a perfect conductor described the low-frequency response of systems in the sinusoidal steady state, or the long-time response to a step function drive. We will find in Chap. 10 that the MQS model of a perfect conductor represents the high-frequency sinusoidal steady state response or the short-time response to a step drive.

Usually, we use the model of perfect conductivity to describe bodies of high but finite conductivity. The value of conductivity which justifies use of the perfect conductor model depends on the frequency (or time scale in the case of a transient) as well as the geometry and size, as will be seen in Chap. 10. When the material is cooled to the point where it becomes superconducting, a type I superconductor (for example lead) expels any mangetic field that might have originally been within its interior, while showing zero resistance to currrent flow. Thus, even for dc, the material acts on the magnetic field like a perfect conductor. However, type I materials also act to exclude the flux from the material, so they should be regarded as perfect conductors in which flux cannot be trapped. The newer "high temperature ceramic superconductors," such as $Y_1Ba_2Cu_3O_7$, show a type II regime. In this class of superconductors, there can be trapped flux if the material is cooled in a dc field. "High temperature superconductors" are those that show a zero resistance at temperatures above that of liquid nitrogen, 77 degrees Kelvin.

As for EQS systems, Faraday's continuity condition, (1.6.12), requires that the tangential **E** be continuous at a boundary between free space and a conductor. By definition, a stationary perfect conductor cannot have an electric field in its interior. Thus, in MQS as well as EQS systems, there can be no tangential **E** at the surface of a perfect conductor. But the primary laws determining **H** in the free space region, Ampère's law with $\mathbf{J} = 0$ and the flux continuity condition, do not involve the electric field. Rather, they involve the magnetic field, or perhaps the vector or scalar potential. Thus, it is desirable to also state the boundary condition in terms of **H** or Ψ.

Boundary Conditions and Evaluation of Induced Surface Current Density. To identify the boundary condition on the magnetic field at the surface of a perfect conductor, observe first that the magnetic flux continuity condition requires that if there is a time-varying flux density $\mathbf{n} \cdot \mu_o \mathbf{H}$ normal to the surface on the free space side, then there must be the same flux density on the conductor side. But this means that there is then a time-varying flux density in the volume of the perfect conductor. Faraday's law, in turn, requires that there be a *curl* of **E** in the conductor. For this to be true, **E** must be finite there, a contradiction of our defini-

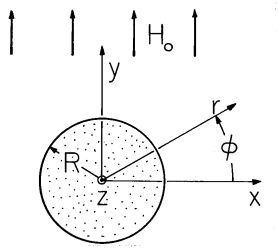


Fig. 8.4.1 Perfectly conducting circular cylinder of radius R in a magnetic field that is y directed and of magnitude H_o far from the cylinder.

tion of the perfect conductor. We conclude that *there can be no normal component of a time-varying magnetic flux density at a perfectly conducting surface.*

$$\boxed{\mathbf{n} \cdot \mu_o \mathbf{H} = 0} \tag{1}$$

Correspondingly, if the **H** field is the gradient of the scalar potential Ψ, we find that

$$\frac{\partial \Psi}{\partial n} = 0 \tag{2}$$

on the surface of a perfect conductor. This should be contrasted with the boundary condition for an EQS potential Φ which must be constant on the surface of a perfect conductor. This boundary condition can be used to determine the magnetic field distribution in the neighborhood of a perfect conductor. Once this has been done, Ampère's continuity condition, (1.4.16), can be used to find the surface current density that has been induced by the time-varying magnetic field. With **n** directed from the perfect conductor into the region of free space,

$$\boxed{\mathbf{K} = \mathbf{n} \times \mathbf{H}} \tag{3}$$

Because there is no time-varying magnetic field in the conductor, only the tangential field intensity on the free space side of the surface is required in this evaluation of the surface current density.

Example 8.4.1. Perfectly Conducting Cylinder in a Uniform Magnetic Field

A perfectly conducting cylinder having radius R and extending to $z = \pm\infty$ is immersed in a uniform time-varying magnetic field. This field is y directed and has intensity H_o at infinity, as shown in Fig. 8.4.1. What is the distribution of **H** in the neighborhood of the cylinder?

In the free space region around the cylinder, there is no current density. Thus, the field can be written as the gradient of a scalar potential (in two dimensions)

$$\mathbf{H} = -\nabla \Psi \tag{4}$$

The far field has the potential

$$\Psi = -H_o y = -H_o r \sin\phi; \qquad r \to \infty \tag{5}$$

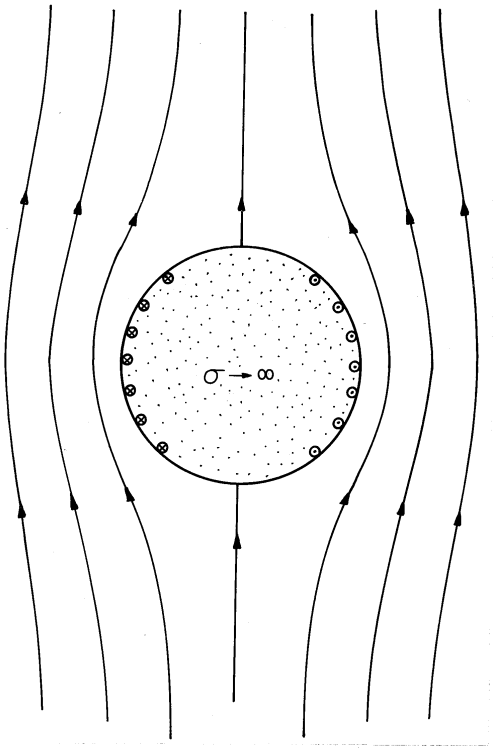


Fig. 8.4.2 Lines of magnetic field intensity for perfectly conducting cylinder in transverse magnetic field.

The condition $\partial\Psi/\partial n = 0$ on the surface of the cylinder suggests that the boundary condition at $r = R$ can be satisfied by adding to (5) a dipole solution proportional to $\sin\phi/r$. By inspection,

$$\Psi = -H_o \sin\phi R\Big(\frac{r}{R} + \frac{R}{r}\Big) \tag{6}$$

has the property $\partial\Psi/\partial r = 0$ at $r = R$. The magnetic field follows from (6) by taking its negative gradient

$$\mathbf{H} = -\nabla\Psi = H_o \sin\phi\mathbf{i}_\mathbf{r}\Big(1 - \frac{R^2}{r^2}\Big) + H_o\cos\phi\mathbf{i}_\phi\Big(1 + \frac{R^2}{r^2}\Big) \tag{7}$$

The current density induced on the surface of the cylinder, and responsible for generating the magnetic field that excludes the field from the interior of the cylinder, is found by evaluating (3) at $r = R$.

$$\mathbf{K} = \mathbf{n}\times\mathbf{H} = \mathbf{i}_\mathbf{z}H_\phi(r = R) = \mathbf{i}_\mathbf{z}2H_o\cos\phi \tag{8}$$

The field intensity of (7) and this surface current density are shown in Fig. 8.4.2. Note that the polarity of $\mathbf{K}$ is such that it gives rise to a magnetic dipole field that tends to buck out the imposed field. Comparison of (7) and the field of a two-dimensional dipole, (8.1.21), shows that the induced moment is $id = 2\pi H_o R^2$.

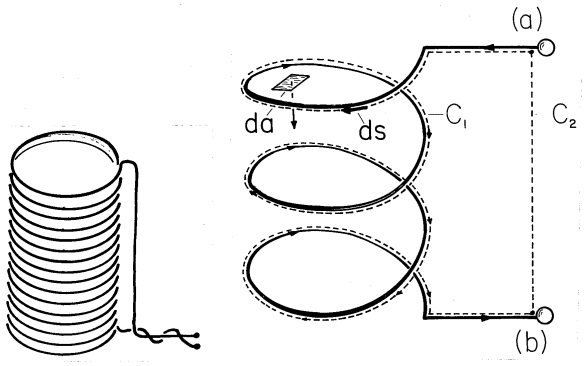


Fig. 8.4.3 A coil having terminals at (a) and (b) links flux through surface enclosed by a contour composed of C_1 adjacent to the perfectly conducting material and C_2 completing the circuit between the terminals. The direction of positive flux is that of $d\mathbf{a}$, defined with respect to $d\mathbf{s}$ by the right-hand rule (Fig. 1.4.1). For the effect of magnetic induction to be negligible in the neighborhood of the terminals, the coil should have many turns, as shown by the inset.

There is an analogy to steady conduction ($\mathbf{H} \leftrightarrow \mathbf{J}$) in the neighborhood of an insulating rod immersed in a conductor carrying a uniform current density. In Demonstration 7.5.2, an electric dipole field also bucked out an imposed uniform field ($\mathbf{J}$) in such a way that there was no normal field on the surface of a cylinder.

Voltage at the Terminals of a Perfectly Conducting Coil. Faraday's law was the underlying reason for the vanishing of the flux density normal to a perfect conductor. By stating this boundary condition in terms of the magnetic field alone, we have been able to formulate the magnetic field of perfect conductors without explicitly solving for the distribution of electric field intensity. It would seem that for the determination of the voltage induced by a time-varying magnetic field at the terminals of the coil, knowledge of the E field would be necessary. In fact, as we now take care to define the circumstances required to make the terminal voltage of a coil a well-defined variable, we shall see that we can put off the detailed determination of $\mathbf{E}$ for Chap. 10.

The EMF at point (a) relative to that at point (b) was defined in Sec. 1.6 as the line integral of $\mathbf{E} \cdot d\mathbf{s}$ from (a) to (b). In Sec. 4.1, where the electric field was irrotational, this integral was then defined as the *voltage* at point (a) relative to (b). We shall continue to use this terminology, which is consistent with that used in circuit theory.

If the voltage is to be a well-defined quantity, independent of the layout of the connecting wires, the terminals of the coil shown in Fig. 8.4.3 must be in a region where the magnetic induction is negligible compared to that in other regions and where, as a result, the electric field is irrotational. To determine the voltage, the integral form of Faraday's law, (1.6.1), is applied to the closed line integral C shown in Fig. 8.4.3.

$$\oint_C \mathbf{E} \cdot d\mathbf{s} = -\frac{d}{dt} \int_S \mu_o \mathbf{H} \cdot d\mathbf{a} \tag{9}$$

The contour goes from the terminal at (a) to that at (b) along the coil wire and closes through a path outside the coil. However, we know that $\mathbf{E}$ is zero along the perfectly conducting wire. Hence, the entire contribution to the line integral comes from the short path between the terminals. Thus, the left side of (9) reduces to

$$\begin{aligned}\int_{C_1+C_2} \mathbf{E}\cdot d\mathbf{s} &= \int_{b\ C_2}^{a} \mathbf{E}\cdot d\mathbf{s} = -\int_{b\ C_2}^{a} \nabla\Phi\cdot d\mathbf{s} \\ &= -(\Phi_a-\Phi_b) = -v\end{aligned} \tag{10}$$

It follows from Faraday's law, (9), that the terminal voltage is

$$\boxed{v = \frac{d\lambda}{dt}} \tag{11}$$

where λ is the *flux linkage*[3]

$$\boxed{\lambda \equiv \int_S \mu_o \mathbf{H}\cdot d\mathbf{a}} \tag{12}$$

By definition, the surface S spans the closed contour C. Thus, as shown in Fig. 8.4.3, it has as its edge the perfectly conducting coil, C_1, and the contour used to close the circuit in the region where the terminals are located, C_2. If the magnetic induction is negligible in the latter region, the electric field is irrotational. In that case, the specific contour, C_2, is arbitrary, and the EMF between the terminals becomes the voltage of circuit theory.

Our discussion has emphasized the importance of having the terminals in a region where the magnetic induction, $\partial\mu_o\mathbf{H}/\partial t$, is negligible. If a time-varying magnetic field is significant in this region, then different arrangements of the leads connecting the terminals to the voltmeter will result in different voltmeter readings. (We will emphasize this point in Sec. 10.1, where we develop an appreciation for the electric field implied by Faraday's law throughout the free space region surrounding the perfect conductors.) However, there remains the task of identifying configurations in which the flux linkage is not appreciably affected by the layout of leads connected to the terminals. In the absence of magnetizable materials, this is generally realized by making coils with many turns that are connected to the outside world through leads arranged to link a minimum of flux. The inset to Fig. 8.4.3 shows an example. The large number of turns assures a magnetic field within the coil that is much larger than that associated with the wires that connect the coil to the terminals. By intertwining these wires, or at least having them close together, the terminal voltage becomes independent of the detailed wire layout.

Demonstration 8.4.1. Surface used to Define the Flux Linkage

[3] We drop the subscript f on the symbol λ for flux linkage where there is no chance to mistake it for line charge density.

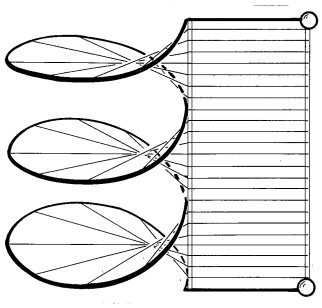


Fig. 8.4.4 To visualize the surface enclosed by the contour $C_1 + C_2$ of Fig. 8.4.3, imagine filling it in with yarn strung on a frame representing the contour.

The surface S used to define λ in (12) is often geometrically complex. It is helpful to picture the surface in terms of a model. Shown in Fig. 8.4.4 is a three-turn coil. The surface is filled in by stringing yarn between a vertical rod joining the terminals in the external region and points on the wire. The surface is filled in by connecting points of decreasing altitude on the rod to points of increasing distance along the wire. Note from Fig. 8.4.3 that $d\mathbf{a}$ and $d\mathbf{s}$ are related by the right-hand rule, where the latter is directed along the contour from the positive terminal to the negative one.

Another way of demonstrating the relationship of the surface to the coil geometry takes advantage of the phenomenon familiar from blowing bubbles. A small coil, closed along the external segment between the terminals, can be dipped into materials like soap solution to form a continuous film having the wire as one continuous edge. In fact, if the film is formed from a material that hardens into a plastic sheet, a permanent model for the surface is obtained.

Inductance. When the flux linked by the perfectly conducting coil of Fig. 8.4.3 is due entirely to a current i in the coil itself, λ is proportional to i, $\lambda = Li$. Thus, the *inductance* L, defined as

$$\boxed{L \equiv \frac{\lambda}{i} = \frac{\int_S \mu_o \mathbf{H} \cdot d\mathbf{a}}{i}} \tag{13}$$

becomes a parameter that is only a function of geometric variables and μ_o. In this case, the terminal voltage given by (11) assumes a form familiar from circuit theory.

$$\boxed{v = L\frac{di}{dt}} \tag{14}$$

The following example illustrates this rule.

Example 8.4.2. Inductance of a Long Solenoid

In Demonstration 8.2.1, we examined the field of a long N-turn solenoid and found that in the limit where the length d becomes very large, the field intensity along the axis is

$$H_z = \frac{Ni}{d} \tag{15}$$

where i is the current in each turn.

For an infinitely long solenoid this is not only the field on the axis of symmetry but everywhere inside the solenoid. To see this, observe that a uniform magnetic field intensity satisfies both Ampère's law and the flux continuity condition throughout the free space interior region. (A uniform field is irrotational and solenoidal.) Further, with the field given by (15) inside the coil and taken as zero outside, Ampère's continuity condition (1.4.16) is satisfied at the surface of the coil where $K_\phi = Ni/d$. The normal flux continuity condition is automatically satisfied, since there is no flux density normal to the coil surface.

Because the field is uniform over the circular cylindrical cross-section, the magnetic flux Φ_λ[4] passing through one turn of the solenoid is simply the cross-sectional area A of the solenoid multiplied by the flux density $\mu_o H$.

$$\Phi_\lambda = \mu_o H_z A = \frac{\mu_o AN}{d} i \tag{16}$$

The flux linkage, defined by (12), is obtained by summing the contributions of all the turns.

$$\lambda = \sum_{\text{turns}} \Phi_\lambda = \frac{\mu_o N^2 A}{d} i \tag{17}$$

Thus, from (13),

$$L = \frac{\lambda}{i} = \frac{\mu_o N^2 A}{d} \tag{18}$$

For the circular cylindrical solenoid of radius a, $A = \pi a^2$. The same arguments used to see that the interior field of a solenoid of circular cross-section is given by (15) show that the solenoid can have an arbitrary cross-sectional geometry and the field will still be given by (15) everywhere inside and be zero outside. Thus, (18) is applicable to a solenoid of arbitrary cross-section.

Example 8.4.3. Dipole Moment Induced in Perfectly Conducting Sphere by Imposed Uniform Magnetic Field

If a highly conducting material is immersed in a magnetic field, it will modify the field in its vicinity via a surface current that cancels the field in its interior. If the material is spherical, we can superimpose the field of a dipole and the uniform field to exactly satisfy the boundary condition on the conducting surface. For a sphere having radius R in an imposed field $H_o\mathbf{i_z}$, as shown in Fig. 8.4.5, what is the equivalent dipole moment m?

The imposed field is conveniently analyzed into radial and azimuthal components. Then the irrotational and solenoidal field proposed to satisfy the boundary conditions is the sum of that uniform field and the field of a dipole at the origin, as given by (8.3.14) together with the definition (8.3.19).

$$\mathbf{H} = H_o\big(\cos\theta\mathbf{i_r} - \sin\theta\mathbf{i}_\theta\big) + \frac{m}{4\pi}\Big(\frac{2\cos\theta}{r^3}\mathbf{i_r} + \frac{\sin\theta}{r^3}\mathbf{i}_\theta\Big) \tag{19}$$

[4] We use the symbol Φ_λ for the flux through one turn of a coil or a loop.

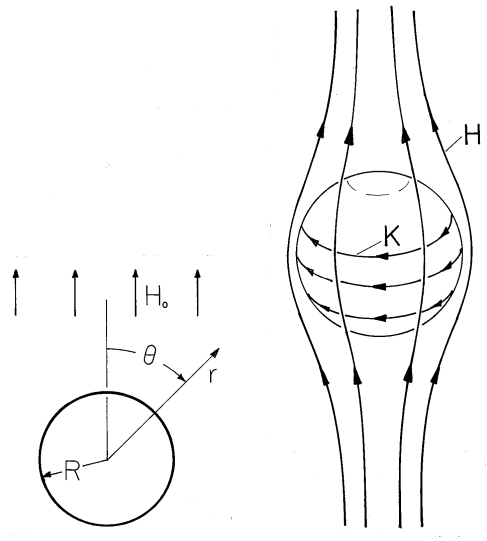


Fig. 8.4.5 Immersed in a uniform magnetic field, a perfectly conducting sphere has the same effect as an oppositely directed magnetic dipole.

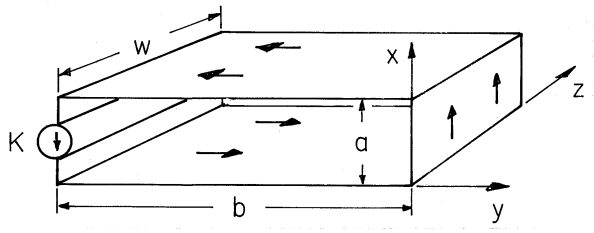


Fig. 8.4.6 One-turn solenoid.

By design, this field already approaches the uniform field at infinity. To satisfy the condition that $\mathbf{n} \cdot \mu_o \mathbf{H} = 0$ at $r = R$,

$$\mu_o H_r(r = R) = 0 \Rightarrow \frac{2m}{4\pi R^3} \cos\theta + H_o \cos\theta = 0 \tag{20}$$

It follows that the equivalent dipole moment is

$$m = -2\pi H_o R^3 \tag{21}$$

The surface currents induced in the sphere which buck out the imposed magnetic flux are responsible for the dipole moment, as illustrated in Fig. 8.4.5.

Example 8.4.4. One-Turn "Solenoid"

The structure of perfectly conducting sheets shown in Fig. 8.4.6 has width w much greater than a and is excited by a uniform (in the z direction) current per unit length K at $y = -b$.

The H-field solution that satisfies the boundary condition $\mathbf{n} \cdot \mathbf{H} = 0$ and $\mathbf{n} \times \mathbf{H} = \mathbf{K}$ on the perfect conductor is

$$H_z = -K \tag{22}$$

What is the voltage that appears across the current generator? From (11) and (12) we conclude

$$v = \frac{d\lambda}{dt} \tag{23}$$

with

$$\lambda = \int \mu_o \mathbf{H} \cdot d\mathbf{a} = \mu_o K a b = \mu_o \frac{ab}{w} i$$

where i is the total current supplied by the generator. The voltage is thus

$$v = L\frac{di}{dt} \tag{24}$$

where

$$L = \mu_o \frac{ab}{w}$$

8.5 PIECE-WISE MAGNETIC FIELDS

In a typical physical situation to which the scalar potential is applicable, layers of wire are used to make a winding that is thin compared to other dimensions of interest. Currents are then confined to surfaces that separate the regions where $\mathbf{H}$ is irrotational. Thus, the sources of the magnetic field intensity can be represented as surface currents. The field produced by these currents is then found by choosing source-free solutions in the space surrounding the current-carrying surfaces and "connecting" these solutions across the surfaces by the proper boundary conditions. This procedure is analogous to finding EQS potentials produced by charge sheets in Chap. 5. Solutions to Laplace's equation were set up on the two sides of a charge sheet and the jump in normal $\epsilon_o \mathbf{E}$ adjusted to equal the surface charge density.

In the MQS situation, the H field obeys Ampère's continuity condition, (1.4.16).

$$\mathbf{n} \times (\mathbf{H}^a - \mathbf{H}^b) = \mathbf{K} \tag{1}$$

At this same surface, the magnetic flux continuity condition, (1.7.6), also applies.

$$\mathbf{n} \cdot (\mu_o \mathbf{H}^a - \mu_o \mathbf{H}^b) = 0 \tag{2}$$

Remember that in Chap. 5, continuity of tangential $\mathbf{E}$ was implied by making the electric potential continuous. By contrast, according to (1), where there is a surface current density, the tangential $\mathbf{H}$ is discontinuous and this implies that *the magnetic scalar potential Ψ is not generally continuous.* To see this, consider the application of Ampère's integral law to an incremental surface that is pierced by the surface current density, as shown in Fig. 8.5.1. If $\mathbf{H}$ is finite, then in the limit where the width w goes to zero, the contributions to the line integral from the segments $B \to B'$ and $A' \to A$ vanish, and so

$$\oint_C \mathbf{H} \cdot d\mathbf{s} = \int_S \mathbf{J} \cdot d\mathbf{a} \Rightarrow -(\nabla \Psi^a - \nabla \Psi^b) \cdot \mathbf{i}_s = \mathbf{K} \cdot \mathbf{i}_n \tag{3}$$

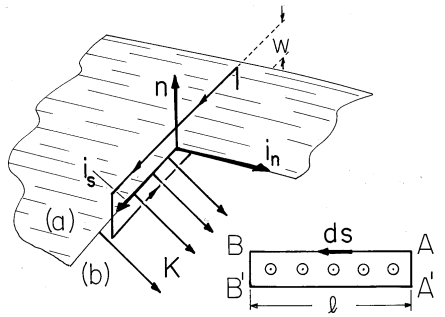


Fig. 8.5.1 Contour enclosing surface current density **K** on surface having normal **n**. Integration of Ampère's law on surface enclosed by the contour shows that the magnetic scalar potential is, in general, discontinuous across the surface.

where the unit vectors $\mathbf{i}_s$ and $\mathbf{i}_n$ are defined in Fig. 8.5.1.

Multiplication of (3) by the incremental line element ds and integration over the length of the incremental surface gives

$$-\int_A^B (\nabla\Psi^a - \nabla\Psi^b)\cdot\mathbf{i}_s ds = \int_A^B \mathbf{K}\cdot\mathbf{i}_n ds \tag{4}$$

In view of the gradient integral theorem, (4.1.16), the integrals on the left can be carried out to obtain

$$(\Psi_B - \Psi_A) - (\Psi_{B'} - \Psi_{A'}) = -\int_A^B \mathbf{K}\cdot\mathbf{i}_n ds \tag{5}$$

Now think of $A-A'$ as a fixed reference position on the surface, where Ψ_A is defined as being equal to $\Psi_{A'}$. It then follows that the discontinuity in Ψ at the location $B-B'$ is a measure of the net current passing normal to the strip joining $A-A'$ to $B-B'$.

A further contrast with the electric field comes from the normal field continuity condition, (2). *At a surface carrying a surface current density in free space, the normal derivative of* Ψ *is continuous.*

The following example shows how to find Ψ, and hence **H**, when a surface current distribution is given.

Example 8.5.1. The Spherical Coil

The magnetic field intensity produced inside a properly wound spherical coil has the important property that it is uniform. This should be contrasted with the field of a long solenoid that is uniform only to the extent that the fringing field can be neglected.

The coil is wound of thin wire so that the turns density is sinusoidally distributed between the north and south poles of a sphere. To the extent that we can disregard the slight pitch in the coil needed to connect the loops with each other, loops of appropriately varying diameter, spaced evenly as projected onto the z axis,

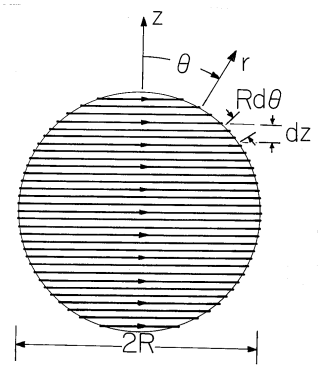


Fig. 8.5.2 Cross-section of "flux ball" consisting of sphere with winding on its surface that is of uniform turns density with respect to the z axis.

automatically simulate such a distribution. The coil, with a radius R and a wire carrying the current i, is shown in Fig. 8.5.2.

To deduce the surface current density representing this winding, note that the density of turns on the surface is the total number, N, divided by the total length, $2R$, and so the number of turns in the incremental length dz is $(N/2R)dz$. Because $z = r\cos\theta$, a differential length dz corresponds to an angular increment $d\theta$: $dz = -\sin\theta R d\theta$. Therefore, the number of turns in the differential length $Rd\theta$ as measured along the periphery of the sphere is $(N/2R)\sin\theta$. With each turn carrying the current i, the surface current density is

$$\mathbf{K} = \mathbf{i}_\phi \frac{N}{2R} i \sin\theta \tag{6}$$

In the spaces interior and exterior to the surface of the sphere, $\mathbf{H}$ is both irrotational and solenoidal. Hence, it is represented by scalar magnetic potentials.

The ϕ component of (1) is the link between the surface current density and the induced field.

$$H_\theta^a - H_\theta^b = \frac{N}{2R} i \sin\theta \tag{7}$$

To obtain H_θ, the derivative of Ψ with respect to θ must be taken, and this suggests that the θ dependence of Ψ be taken as $\cos\theta$. The field is finite at the origin and zero at infinity, so, from the three solutions to Laplace's equation given in Sec. 5.9, we select

$$\Psi = C(r/R)\cos\theta; \qquad r < R \tag{8}$$

$$\Psi = A(R/r)^2 \cos\theta; \qquad r > R \tag{9}$$

The continuity conditions, used now to determine the coefficients A and C, are in terms of the field intensity. Thus, (8) and (9) are used to write $\mathbf{H}$ in the two regions as

$$\mathbf{H} = -\frac{C}{R}(\mathbf{i}_\mathbf{r}\cos\theta - \mathbf{i}_\theta \sin\theta); \qquad r < R \tag{10}$$

$$\mathbf{H} = \frac{A}{R}(R/r)^3(\mathbf{i}_\mathbf{r} 2\cos\theta + \mathbf{i}_\theta \sin\theta); \qquad r > R \tag{11}$$

Substitution of the appropriate components into the continuity conditions, (2) and (7), gives

$$-\frac{C}{R} = \frac{2A}{R} \tag{12}$$

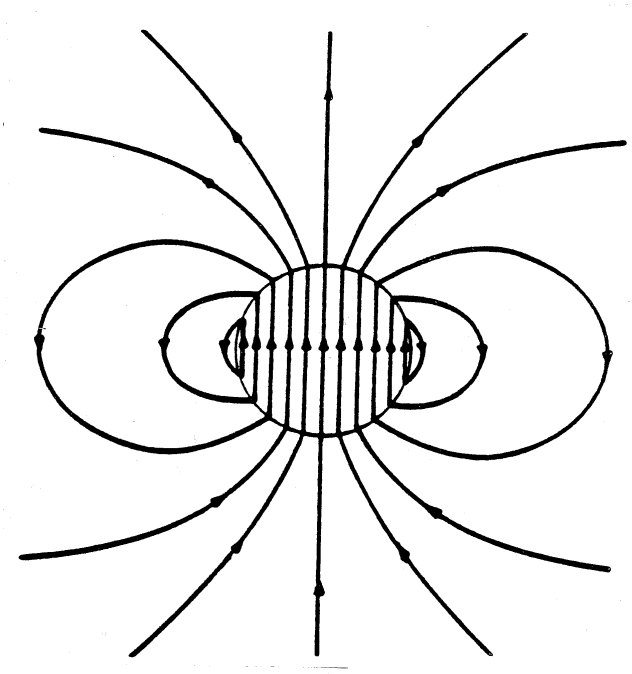


Fig. 8.5.3 Magnetic field intensity of "flux-ball" shown in Fig. 8.5.2.

$$\frac{A}{R} - \frac{C}{R} = \frac{Ni}{2R} \tag{13}$$

Thus, the magnetic field intensity of (10) and (11) is evaluated by setting $C = -2A = -Ni/3$.

$$\mathbf{H} = \frac{Ni}{3R}(\mathbf{i}_\mathbf{r}\cos\theta - \mathbf{i}_\theta \sin\theta); \qquad r < R \tag{14}$$

$$\mathbf{H} = \frac{Ni}{6R}(R/r)^3(\mathbf{i}_\mathbf{r}2\cos\theta + \mathbf{i}_\theta \sin\theta); \qquad r > R \tag{15}$$

The exterior lines of magnetic field intensity are those of a dipole, while the interior field is uniform. Thus, the total picture, shown in Fig. 8.5.3, is one of field lines circulating from south to north inside the sphere and back from north to south on the outside around currents that follow lines of equilatitude around the sphere.

The magnetic potential follows by substituting $C = -2A = -Ni/3$ for C and A in (8) and (9).

$$\Psi = -\frac{Ni}{3}\frac{r}{R}\cos\theta; \qquad r < R \tag{16}$$

$$\Psi = \frac{Ni}{6}(R/r)^2\cos\theta; \qquad r > R \tag{17}$$

Note that these potentials are equal at the equator of the sphere and become increasingly disparate as the poles are approached. With the vertical dimension used to denote Ψ, a sketch of Ψ evaluated in a plane of fixed ϕ would appear as shown in Fig. 8.5.4. Inside, Ψ slopes linearly from its highest value at the south pole to its lowest at the north. Outside, Ψ has its highest value at the north pole and lowest at

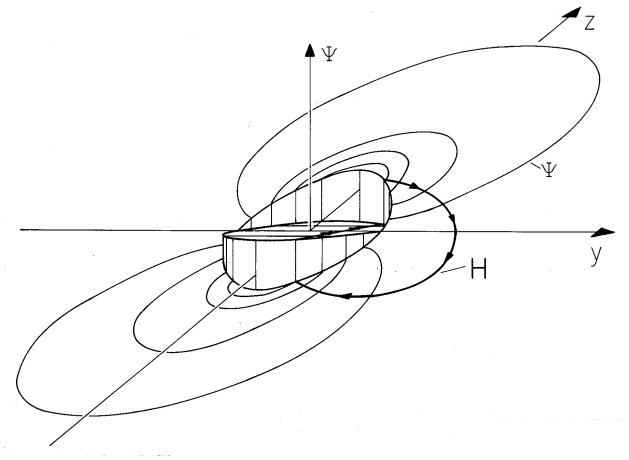


Fig. 8.5.4 Magnetic scalar potential for "flux ball" of Fig. 8.5.2. The vertical axis is Ψ. A line of $\mathbf{H}$ closes on itself as it circulates around surface current, going down the potential "hills" inside and outside the sphere and recovering its altitude at the surfaces of discontinuity at $r = R$, containing the surface current density.

the south. This is consistent with the picture afforded by Fig. 8.5.1 and (5). Even though it closes on itself, the line of $\mathbf{H}$ shown goes continuously "down hill." The potential Ψ regains its altitude in the region of discontinuity.

Finally, we illustrate the computation of the inductance of a coil modeled by a surface current and represented in terms of the magnetic scalar potential. To compute the total flux linked by the winding, first consider the flux linked by one turn at the location $r = R$ and $\theta = \theta'$. Using the flat surface at $z' = R\cos\theta'$ that is enclosed by this circular turn, the flux is

$$\Phi_\lambda = \int_0^{R\sin\theta'} \mu_o H_z 2\pi r dr = \pi(R\sin\theta')^2 \mu_o H_z \tag{18}$$

In this particular problem, H_z is uniform inside the sphere, so this integration amounts to multiplying the area enclosed by the turn by the normal flux density.

The turns density multiplied by $Rd\theta$ gives the number of turns linking this flux in an increment of peripheral length. Thus, the total flux is obtained by carrying out a second integration over all of the turns.

$$\lambda = \int_0^\pi \Phi_\lambda \frac{N}{2R}\sin\theta' R d\theta' = \int_0^\pi i\frac{\pi N^2 R\mu_o}{6}\sin^3\theta' d\theta' = Li \tag{19}$$

$$L \equiv \frac{2}{9}\pi N^2 \mu_o R \tag{20}$$

Demonstration 8.5.1. Field and Inductance of a Spherical Coil

In the experiment shown in Fig. 8.5.5, the "flux ball" has 64 turns and a radius of $R = 5$ cm. The turns are wound on a plastic sphere that essentially has the magnetic properties of free space.

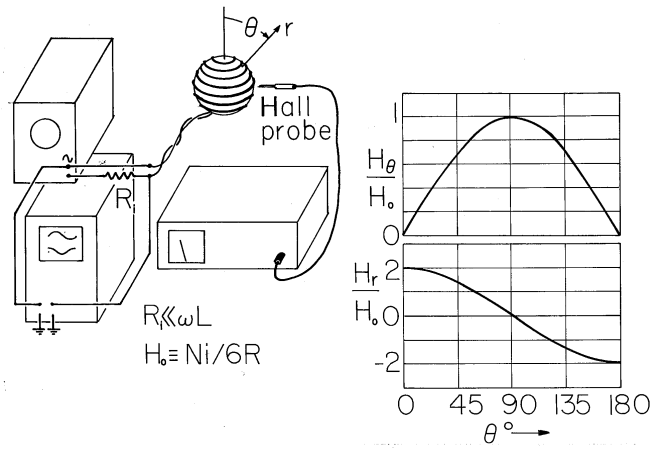


Fig. 8.5.5 Demonstration of fields surrounding the magnetic "flux ball."

The Hall magnetometer makes it possible to probe the magnitude and direction of the field outside the coil. For example, at the north pole, where the magnetic flux density is perpendicular to the sphere surface, the flux density is vertical and for $i = 1$ A predicted by either (14) or (15) to be $\mu_o Ni/3R = 5.36 \times 10^{-4} T = 5.36$ gauss. The inductance is determined by measuring the voltage and current, varying the frequency to determine that it is high enough to assure that the resistance of the coil plays a negligible role in the terminal impedance (the impedance should be of magnitude ωL, and hence vary linearly with frequency). The inductance predicted by (20) is 180 μH, and the value measured using the oscilloscope is typically within 10 percent.

8.6 VECTOR POTENTIAL AND THE BOUNDARY VALUE POINT OF VIEW

We have found that many interesting MQS cases can be treated by the use of the scalar potential obeying Laplace's equation. The vector potential, defined by (8.1.1), is necessary when analyzing fields with nonzero curl. There are other cases as well in which its use may be advantageous. The vector potential is the natural variable for evaluating the flux passing through a surface. In view of (8.1.1), integration of the flux density over the open surface S of Fig. 8.6.1 gives

$$\lambda = \int_S \mu_o \mathbf{H} \cdot d\mathbf{a} = \int_S \nabla \times \mathbf{A} \cdot d\mathbf{a} \tag{1}$$

and it follows from Stokes' theorem that this flux is equal to the line integral of $\mathbf{A} \cdot d\mathbf{s}$ around the contour enclosing the surface.

$$\boxed{\lambda = \oint_C \mathbf{A} \cdot d\mathbf{s}} \tag{2}$$

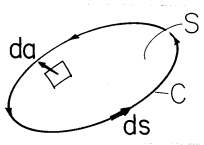


Fig. 8.6.1 Open surface S having area element $d\mathbf{a}$ enclosed by contour C having directed differential length $d\mathbf{s}$.

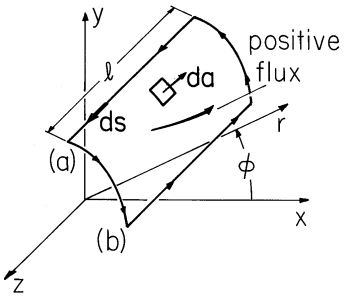


Fig. 8.6.2 Surface S with sides of length l parallel to the z axis at locations (a) and (b). The contour direction is consistent with the flux being positive, as shown.

In certain important cases, $\mathbf{A}$ has only one component and a vector field is again represented in terms of one scalar function. Two such cases are identified in the following subsections.

Vector Potential for Two-Dimensional Fields. Suppose that the flux density is parallel to the $x-y$ plane and is independent of z. It can then be represented by a vector potential having only a z component.

$$\mathbf{A} = A_z(x,y)\mathbf{i_z} \tag{3}$$

Note that the divergence of this $\mathbf{A}$ is automatically zero and that in Cartesian coordinates, the components of the flux density are given in terms of A_z by

$$\mu_o\mathbf{H} = \nabla \times \mathbf{A} = \frac{\partial A_z}{\partial y}\mathbf{i_x} - \frac{\partial A_z}{\partial x}\mathbf{i_y} \tag{4}$$

Consider now the evaluation of the net flux of magnetic flux density through a surface S that has length l in the z direction, as shown in Fig. 8.6.2. The points (a) and (b) denote the coordinates of the corners of the contour enclosing S. The contour consists of a pair of parallel straight segments of length l parallel to the z axis, one at the location (a) in the $x-y$ plane and the other at (b), and contours joining (a) and (b) in $x-y$ planes. Contributions to the contour integral, (2), from these latter segments of C are zero, because $\mathbf{A}$ is perpendicular to $d\mathbf{s}$. Integration along the z-directed segments amounts to multiplication of A_z evaluated at (a) or (b) by the length of the segment. Thus, (1) becomes

$$\boxed{\lambda = l(A_z^a - A_z^b)} \tag{5}$$

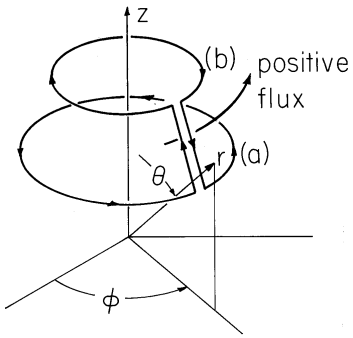


Fig. 8.6.3 Difference between axisymmetric stream function Λ_s evaluated at (a) and (b) is net flux through surface enclosed by the contour shown.

The vector potential at (a) relative to (b) is the net magnetic flux per unit length passing through a surface of unit length in the z direction subtended between the two points and a corresponding pair at unity distance along the z axis. Note that the flux has a sign, relative to the direction of the contour integration, governed by the right-hand rule (Fig. 1.4.1).

Vector Potential for Axisymmetric Fields in Spherical Coordinates.
If the magnetic flux density is invariant with respect to rotation around the z axis, having components in the r and θ directions only, the vector potential again has a single component.

$$\mathbf{A} = A_\phi(r,\theta)\mathbf{i}_\phi \tag{6}$$

The net flux through the annular surface "spanned" over the contour shown in Fig. 8.6.3, having constant outer and inner radii denoted by (a) and (b), respectively, is given by the contributions to (2) of the azimuthal segments, A_ϕ multiplied by the circumferences. The contour is closed by adjacent oppositely directed segments joining points (a) and (b) in a plane of constant ϕ. Thus, the contributions to the line integral of (2) from these segments cancel, even if $\mathbf{A}$ had components in the direction of $d\mathbf{s}$ on these segments. Thus, the net flux through the annulus is simply the *axisymmetric stream function* Λ at (a) relative to that at (b).[5]

$$\boxed{\lambda = \Lambda_s^a - \Lambda_s^b} \tag{7}$$

where

$$\Lambda_s \equiv 2\pi r \sin\theta A_\phi \tag{8}$$

Lines of flux density are tangential to the axisymmetric surfaces of constant Λ_s. Just as A_z provides a ready visualization of the flux lines in two dimensions, Λ_s portrays the axisymmetric flux lines.

[5] With $\mathbf{A}$ used to represent the velocity distribution of an incompressible fluid, Λ_s (or $\Lambda_s/2\pi$) is called Stokes' stream function.

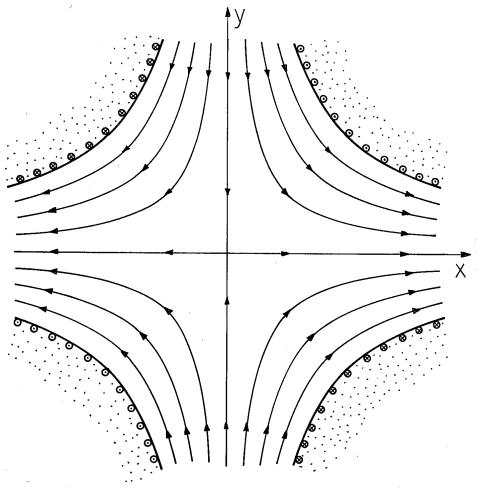


Fig. 8.6.4 Surfaces of constant A_z and hence lines of magnetic field intensity for field trapped between perfectly conducting electrodes.

Boundary Value Solution by "Inspection". In two-dimensional configurations, any surface of constant A_z can be replaced by the surface of a perfect conductor. Moreover, in the free space region between conductors, A_z satisfies Laplace's equation. Thus, any two-dimensional configuration from Chaps. 4 and 5 can be replaced by one where the potential lines are field lines. The equipotential (constant Φ) surfaces of the EQS perfect conductors become the perfectly conducting (constant A_z) surfaces of an MQS system.

Illustration. Field Trapped between Hyperbolic Perfect Conductors

The two-dimensional potential distribution of Example 4.1.1 suggests the vector potential $A_z = \Lambda_o xy/a^2$. The lines of magnetic field intensity, which are the surfaces of constant A_z, are shown in Fig. 8.6.4. Here, the surfaces $A_z = \pm\Lambda_o$ are taken as being the surfaces of perfect conductors. Thus, the current density on the surfaces of these conductors are, given by using (4) to determine $\mathbf{H}$ and, in turn, (8.4.3) to find K_z. These currents shield the fields from the volume of the perfect conductors. The net flux per unit length passing downward between the upper pair of conductors is [in view of (7)] simply $2\Lambda_o$.

This solution is the superposition of the fields of four line currents. Two directed in the $+z$ direction are at infinity in the first and third quadrants, while two in the $-z$ direction are in the second and fourth quadrants.

Example 8.6.1. Field and Inductance of Oppositely Directed Currents in Parallel Perfectly Conducting Cylinders

The cross-section of a pair of parallel perfectly conducting cylinders that extend to $\pm\infty$ in the z direction is shown in Fig. 8.6.5. The conductors have the same geometry as in the EQS case considered in Example 4.6.3. However, they should be regarded as shorted at one end and driven by a current source i at the other. Thus, current in the $+z$ direction in the right conductor is returned in the left conductor.

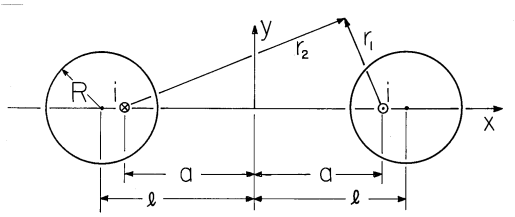


Fig. 8.6.5 Cross-section of perfectly conducting parallel conductors having radius R and spacing $2l$. Fields of oppositely directed line currents having spacing $2a$ are shown to satisfy normal flux boundary condition on circular cylindrical surfaces of conductors.

Although the net current in each conductor is given, its distribution on the surface of the conductors is to be determined.

Example 4.6.3 suggests our strategy. Instead of superimposing the potentials Φ of a pair of line charges of opposite sign, we superimpose the A_z of oppositely directed line currents. With r_1 and r_2 the distances from the observer coordinate to the source coordinates, defined in Fig. 8.6.5, it follows from the vector potential for a line current given by (8.1.16) that

$$A_z = -\frac{\mu_o i}{2\pi}(ln\, r_1 - ln\, r_2) \tag{9}$$

With the identification of variables

$$A_z \rightarrow \Phi; \qquad \frac{\mu_o i}{2\pi} \rightarrow \frac{\lambda_l}{2\pi\epsilon_o} \tag{10}$$

this expression is identical to that for the antidual EQS configuration, (4.6.18). We can conclude that the line currents should be located at $a = (l^2 - R^2)^{1/2}$, and that the constant k used in that deduction (4.6.20) is identified using (10).

$$k \equiv \exp\left(\frac{2\pi\Lambda}{\mu_o i}\right) = \frac{l+a}{R} \tag{11}$$

Here, the potential U in (4.6.20) is replaced by the flux per unit length Λ. Thus, the surfaces of constant A_z are circular cylinders and represent the field lines shown in Fig. 8.6.6.

The inductance per unit length L is now deduced from (11).

$$L \equiv \frac{2\Lambda}{i} = \frac{\mu_o}{\pi} ln\Big(\frac{l+a}{R}\Big) = \frac{\mu_o}{\pi} ln\left|\frac{l}{R} + \sqrt{\Big(\frac{l}{R}\Big)^2 - 1}\right| \tag{12}$$

In the limit where the conductors represent wires that are thin compared to their spacing, the inductance per unit length of (12) is approximated using (4.6.28).

$$L \approx \frac{\mu_o}{\pi} ln\Big(\frac{2l}{R}\Big) \tag{13}$$

Once the vector potential has been determined, it is possible to evaluate the distribution of current density on the conductors. Note that the currents tend to concentrate on the inside surfaces of the conductors, where the magnetic field intensity is more intense.

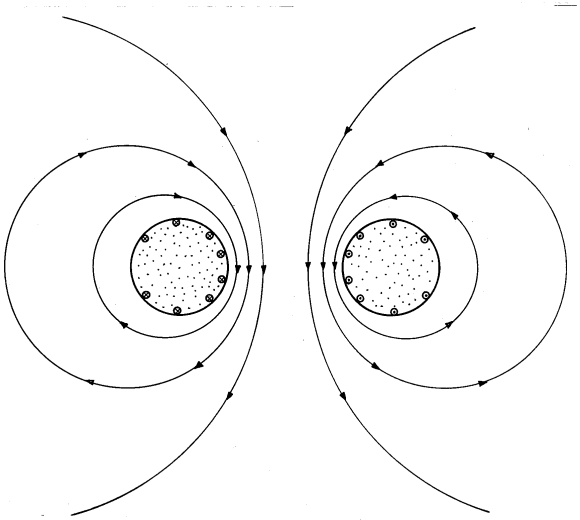


Fig. 8.6.6 Surfaces of constant A_z and hence lines of magnetic field intensity for the parallel conductor configuration shown in the same cross-sectional view by Fig. 8.6.5.

We are one step short of a general relationship between the capacitance per unit length and inductance per unit length of a pair of parallel perfect conductors, regardless of the cross-sectional geometry. With Φ and A_z defined as zero on one of the conductors, evaluated on the other conductor they represent the voltage and the flux linkage per unit length, respectively. Thus, with the understanding that Φ and A_z are evaluated on the second conductor, $L = A_z/i$, and $C = \lambda_l/\Phi$, (4.6.5). Here, i and λ_l, respectively, are the line current and line charge density that give rise to the same fields as do those sources actually on the surfaces of the conductors. These quantitities are related by (10), so we can conclude that regardless of the cross-sectional geometry, the product of the inductance per unit length and the capacitance per unit length is

$$LC = \frac{A_z\lambda_l}{i\Phi} = \mu_o\epsilon_o = \frac{1}{c^2} \tag{14}$$

where c is the velocity of light (3.1.16).

Note that inductance per unit length of parallel circular conductors given by (12) and the capacitance per unit length for the same conductors under "open circuit" conditions (4.6.27) satisfy the general relation (14).

Method of Images. In the presence of a planar perfect conductor, the zero normal flux condition can be satisfied by symmetrically mounting source distributions on both sides of the plane. This approach is familiar from Sec. 4.7, where the boundary condition required a plane of symmetry on which the tangential electric field was zero. Here we require that the field intensity be tangential to the boundary. For two-dimensional configurations, the analogy between the electric potential and A_z makes the image method of Sec. 4.7 directly applicable here. In both cases, the symmetry plane is one of constant potential (Φ or A_z).

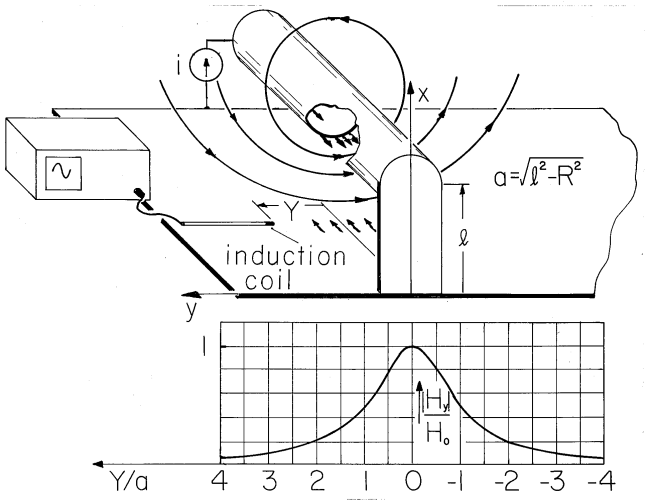


Fig. 8.6.7 With the frequency high enough so that the currents distribute themselves with a negligible normal flux density on the conductors, the field intensity tangential to the conducting plane is that predicted by (16) and shown by the graph. At low frequencies, the current tends to be uniformly distributed in the planar conductor.

The most obvious example is an infinitely long line current at a distance $d/2$ from a perfectly conducting plane. If Fig. 4.7.1 were a picture of line charges rather than point charges, this would be the dual situation. The appropriate image is then an oppositely directed line current located at a distance $d/2$ to the other side of the perfectly conducting plane. By making a pair of symmetrically located line currents the image for this pair of currents, the boundary condition on yet another plane can be satisfied, the analog to the configuration of Fig. 4.7.3.

The following demonstration is intended to emphasize that the perfectly conducting symmetry plane carries a surface current that terminates the field in the region of interest.

Demonstration 8.6.1. Surface Currents Induced in Ground Plane by Overhead Conductor

The metal cylinder mounted over a metal ground plane shown in Fig. 8.6.7 is familiar from Demonstration 4.7.1. Rather than being insulated from the ground plane and driven by a voltage source, this cylinder is shorted to the ground plane at one end and driven by a current source at the other. The height l is small compared to the length, so that the two-dimensional model describes the field distribution in the midregion.

A probe is used to measure the magnetic flux density tangential to the metal ground plane. The distribution of this field, and hence of the surface current density in the adjacent metal, can be determined by recognizing that the ground plane boundary condition of no normal flux density is met by symmetrically mounting a distribution of oppositely directed currents below the metal sheet. This is just what was done in determining the fields for the pair of cylindrical conductors, Fig. 8.6.5.

Thus, (9) is the image solution for the region $x \geq 0$. In terms of x and y,

$$A_z = -\frac{\mu_o i}{2\pi} ln \frac{\sqrt{(a-x)^2+y^2}}{\sqrt{(a+x)^2+y^2}} \tag{15}$$

The flux density tangential to the ground plane at the location $y = Y$ is

$$\mu_o H_y(x=0) = -\frac{\partial A_z}{\partial x}(x=0) = -\mu_o \frac{i}{\pi a}\left[\frac{1}{1+\left(\frac{Y}{a}\right)^2}\right] \tag{16}$$

Normalized to $H_o = i/\pi a$, this distribution is shown as a function of the probe position, Y, in the inset to Fig. 8.6.7.

The role of the surface current density implied by this tangential field is demonstrated by the same probe measurement of the magnetic flux density normal to the conducting sheet. Provided that the frequency is high enough so that the sheet does indeed behave as a perfect conductor, this flux density is small compared to that tangential to the sheet. This is also true at the surface of the cylindrical conductor.

To appreciate the physical origins of this distribution, a dc current source is used in place of the ac source. The distribution of current in the sheet is then dictated by the rules of steady conduction, as enunciated in the first half of Chap. 7. If the sheet is long enough compared to its width, the current is uniformly distributed over the sheet and over the cross-section of the cylinder. By contrast with the high-frequency ac case, where the field is terminated by surface currents in the sheet, the magnetic field now extends below the sheet.

The method of images is not restricted to the two-dimensional situations where there is a convenient analogy between Φ and A_z. In the following example, involving a three-dimensional field, the symmetry conditions are viewed without the aid of the vector potential.

Example 8.6.2. Current Loop above a Perfectly Conducting Plane

A current loop with time-varying current i is mounted a distance h above a perfectly conducting plane, as shown in Fig. 8.6.8. Its axis is inclined at an angle θ with respect to the normal to the plane. What is the net field produced by the current loop and the currents it induces in the plane?

To satisfy the boundary condition in the plane of the perfectly conducting sheet, an image loop is mounted as shown in Fig. 8.6.9. For each current segment in the actual loop, there is a segment in the image loop giving rise to an oppositely directed vertical component of **H**. Thus, the net normal flux density in the plane of the perfect conductor is zero.

Two-Dimensional Boundary Value Problems. The vector potential of a two-dimensional field parallel to the $x-y$ plane is z directed and thus only one scalar function describes fully the associated field, as already pointed out earlier. In problems in which currents are confined to the boundaries, the scalar potential can be used as effectively as the vector potential. The lines of steepest descent of the scalar potential are the lines of constant height of the vector potential. When the

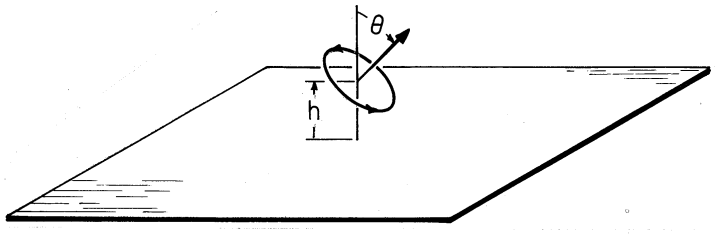


Fig. 8.6.8 Current loop at distance h above a perfectly conducting plane.

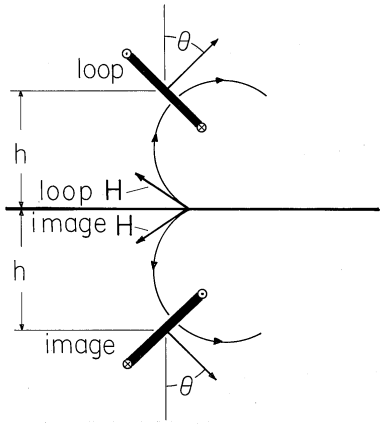


Fig. 8.6.9 Cross-section of configuration of Fig. 8.6.8, showing image dipole giving rise to field that cancels the flux density normal to the planar perfect conductor.

region of interest contains current distributions, then use of the vector potential is required. We shall consider both situations in the examples to follow.

Example 8.6.3. Inductive Attenuator

The cross-section of two conducting electrodes that extend to infinity in the $\pm z$ directions is shown in Fig. 8.6.10. The time-varying current in the $+z$ direction in the electrode at $y = b$ is returned in the $-z$ direction through the $\sqcup$-shaped electrode. This current is so rapidly varying that the electrodes behave as though they were perfectly conducting. The gaps of width Δ insulating the electrodes from each other are small compared to the other dimensions of interest. The magnetic flux (per unit length in the z direction) passing through these gaps in the directions shown is defined as $\Lambda(t)$.

The magnetic fields are two dimensional and there are no sources in the region of interest. Thus, $\mu_o\mathbf{H}$ can be represented in terms of A_z, which satisfies

$$\nabla^2 A_z = 0 \tag{17}$$

The walls are perfectly conducting in the sense that they are modeled as having no normal $\mu_o\mathbf{H}$. This means that A_z is constant on these walls. We define A_z to be zero on the vertical and bottom walls. Thus, A_z must be equal to Λ on the upper

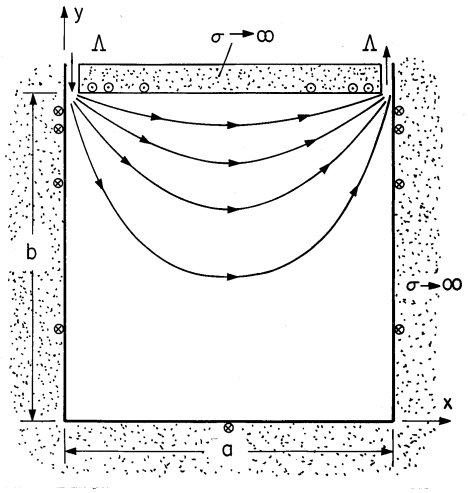


Fig. 8.6.10 Cross-section of inductive attenuator.

electrode, so that the flux per unit length in the z direction through the gaps is Λ.

$$A_z(0,y)=0, \quad A_z(a,y)=0, \quad A_z(x,0)=0, \quad A_z(x,b)=\Lambda \tag{18}$$

The boundary value problem is now formally identical to the EQS capacitive attenuator that was the theme of Sec. 5.5, with the identification of variables

$$\Phi \rightarrow A_z, \qquad V \rightarrow \Lambda \tag{19}$$

Thus, it follows from (5.5.9) that

$$A_z=\sum_{\substack{n=1\\ \text{odd}}}^{\infty}\frac{4\Lambda(t)}{n\pi}\frac{\sinh\left(\frac{n\pi}{a}y\right)}{\sinh\left(\frac{n\pi b}{a}\right)}\sin\left(\frac{n\pi}{a}x\right) \tag{20}$$

The lines of magnetic flux density are the lines of constant A_z. They are the *equipotential* "lines" of Fig. 5.5.3, shown in Fig. 8.6.10 with arrows added to indicate the field direction. Remember, there is a z-directed surface current density that is proportional to the tangential field intensity. For the flux lines shown, K_z is out of the page in the upper electrode and returned into the page on the side walls and (to an extent determined by b relative to a) on the bottom wall as well.

From the cross-sectional view given by Fig. 8.6.10, the provision for the current through the driven plate at the top to recirculate through the side and bottom plates is not shown. The following demonstration emphasizes the implied current paths at the ends of the configuration.

Demonstration 8.6.2. Inductive Attenuator

One configuration described by Example 8.6.3 is shown in Fig. 8.6.11. Here the upper plate is shorted to the adjacent walls at the near end and driven at the far end through a step-down transformer by a 20 kHz oscillator. The driving voltage $v(t)$ at the far end of the upper plate is measured by means of an oscilloscope. The lower

plate is shorted to the side walls at the far end and also connected to these walls at the near end, but in such a way that the induced current $i(t)$ can be measured by means of a current probe.

The walls and upper and lower plates are made from brass or copper. To insure that the resistances of the plate terminations are negligible, they are made from heavy copper wire with the connections soldered. (To make it possible to adjust the spacing b, braided wire is used for the shorts on the lower electrode.)

If the length w of the plates in the z direction is large compared to a and b, $\mathbf{H}$ within the volume follows from (20). The surface current density K_z in the lower plate then follows from evaluation of the tangential $\mathbf{H}$ on its surface. In turn, the total current follows from integration of K_z over the width, a, of the plate.

$$i = -\frac{1}{\mu_o}\sum_{\substack{n=1\\ \text{odd}}}^{\infty}\frac{16\Lambda}{2n\pi}\frac{1}{\sinh\left(\frac{n\pi b}{a}\right)} \tag{21}$$

With the objective of relating this current to the driving voltage, note that (8.4.11) gives

$$v = w\frac{d\Lambda}{dt} \tag{22}$$

so that with the driving voltage a sinusoid of magnitude V,

$$v = V\cos(\omega t) \Rightarrow \Lambda = \frac{V}{w\omega}\sin(\omega t) \tag{23}$$

Thus, in terms of the driving voltage, the output current is $i_o\sin(\omega t)$, where it follows from (21) and (23) that

$$i_o = -I\sum_{\substack{n=1\\ \text{odd}}}^{\infty}\frac{1}{2n\sinh\left(\frac{n\pi b}{a}\right)}; \qquad I \equiv \frac{16V}{\pi w\omega\mu_o} \tag{24}$$

We have found that the output current, normalized to I, has the dependence on spacing between upper and lower plates shown by the inset to Fig. 8.6.11. With the spacing b small compared to a, almost all of the current through the upper plate is returned in the lower one, and the field between is essentially uniform. As the spacing b becomes comparable to the distance a between the side walls, most of the current through the upper electrode is returned in these side walls. Thus, for large b/a, the normalized output current of Fig. 8.6.11 reflects the exponential decay in the $-y$ direction of the field.

Value is added to this demonstration if it is compared to its EQS antidual, Demonstration 5.5.1. For the EQS configuration, the lower plate was properly constrained to essentially the same potential as the walls by connecting it to these side walls through a resistance (which was then used to measure the induced current). Up to frequencies above 100 Hz in the EQS case, this resistance could be as high as that of the oscilloscope (say 1 MΩ) and still constrain the lower plate to essentially the same zero potential as the walls. In the MQS case, we did not use a resistance to connect the lower plate to the side walls (and hence provide a means of measuring the output current), because that resistance would have had to be extremely low, even at 20 kHz, to prevent flux from leaking through the gaps between the lower plate and the side walls. We used the current probe instead. The effects of finite conductivity in MQS systems are the subject of Chap. 10.

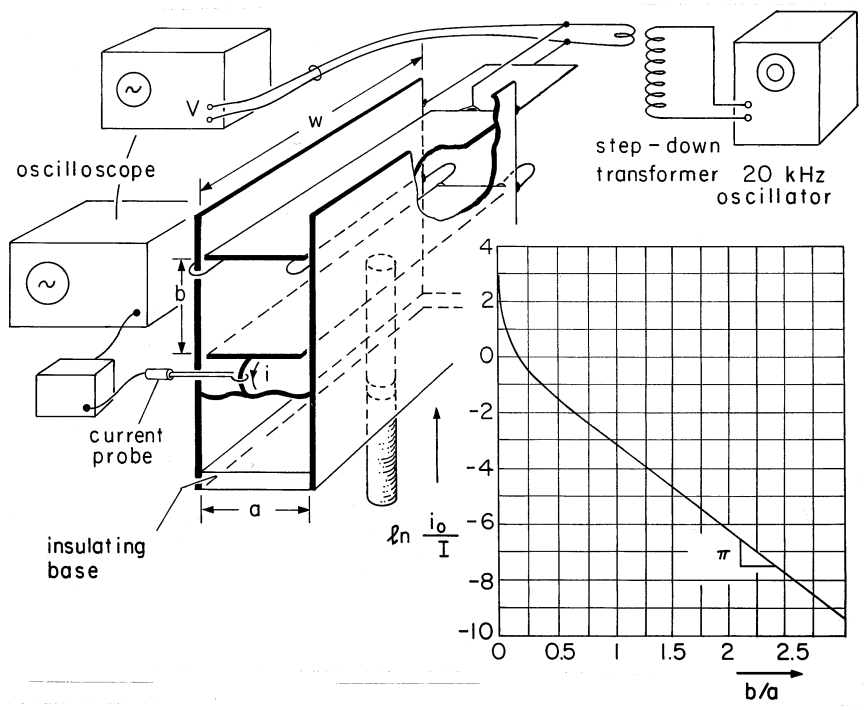


Fig. 8.6.11 Inductive attenuator demonstration.

In a final example, we exemplify how the particular and homogeneous solutions are combined to satisfy boundary conditions while also illustrating how the inductance of a distributed winding is determined.

Example 8.6.4. Field and Inductance of Distributed Winding Bounded by Perfect Conductor

The cross-section of a distributed winding of radius a is shown in Fig. 8.6.12. It consists of turns carrying current i in the $+z$ direction at a location (r, ϕ) and returning the current at $(r, -\phi)$ in the $-z$ direction. The density of turns, each carrying the current i in the $+z$ direction for $0 \leq \phi \leq \pi$ and in the $-z$ direction for $\pi < \phi < 2\pi$, is

$$n = n_o |\sin \phi| \tag{25}$$

The total number of wires N in the left-hand half of the coil is

$$N = \int_0^a \int_0^\pi n_o \sin \phi r dr d\phi = n_o a^2 \tag{26}$$

so that the current density is

$$\mathbf{J} = \mathbf{i_z} i n_o \sin \phi = \mathbf{i_z} i \frac{N}{a^2} \sin \phi \tag{27}$$

The windings are very long in the z direction so that effects of the end turns are ignored and the fields taken as independent of z.

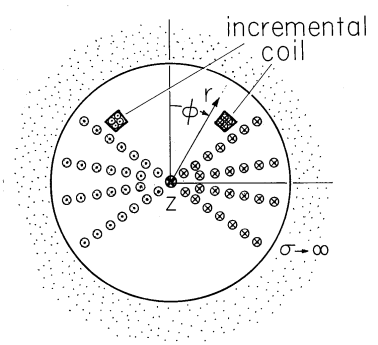


Fig. 8.6.12 Cross-section of two-dimensional distributed winding surrounded by perfectly conducting material. A typical coil consists of wires carrying current in the $+z$ direction at (r, ϕ) somewhere to the right $(0 < \phi < \pi)$, and returning it in the $-z$ direction at $(r, -\phi)$ to the left.

The coil is bounded at $r = a$ by a perfect conductor. With the following steps we determine the field distribution throughout the winding and finally, its inductance.

The vector potential is z independent and must satisfy Poisson's equation (8.1.6). In polar coordinates,

$$\frac{1}{r}\frac{\partial}{\partial r}\left(r\frac{\partial A_z}{\partial r}\right) + \frac{1}{r^2}\frac{\partial^2 A_z}{\partial \phi^2} = -\mu_o J_z \tag{28}$$

First we look for a particular solution. If it is to take a product form, inspection shows that $\sin\phi$ is the appropriate ϕ dependence. Substitution of an r dependence r^n shows that the equation can be satisfied if $n = 2$. Thus, we have "guessed" a particular solution.

$$A_{zp} = -\frac{\mu_o N i}{3}\frac{r^2}{a^2}\sin\phi \tag{29}$$

The magnetic flux density normal to the perfectly conducting surface at $r = a$ must be zero, so the total vector potential must be constant there. It follows that one must add a vector potential with no associated current density in the region $r < a$, a homogeneous solution A_{zh}. At $r = a$, the homogeneous solution, A_{zh}, must be the negative of the particular solution, A_{zp}.

$$[A_{zp} + A_{zh}]_{r=a} = 0 \Rightarrow A_{zh}(r = a) = \frac{\mu_o N i}{3}\sin\phi \tag{30}$$

A linear combination of the two solutions to Laplace's equation that have the same ϕ dependence as this condition is

$$A_{zh} = Cr\sin\phi + \frac{D}{r}\sin\phi \tag{31}$$

The coefficient D must be zero so that the solution is finite at the origin. The coefficient C is then adjusted to make (31) satisfy the condition of (30). Hence, the sum of the particular and homogeneous solutions is

$$A_z = -\frac{\mu_o N i}{3}\left[\left(\frac{r}{a}\right)^2 - \frac{r}{a}\right]\sin\phi \tag{32}$$

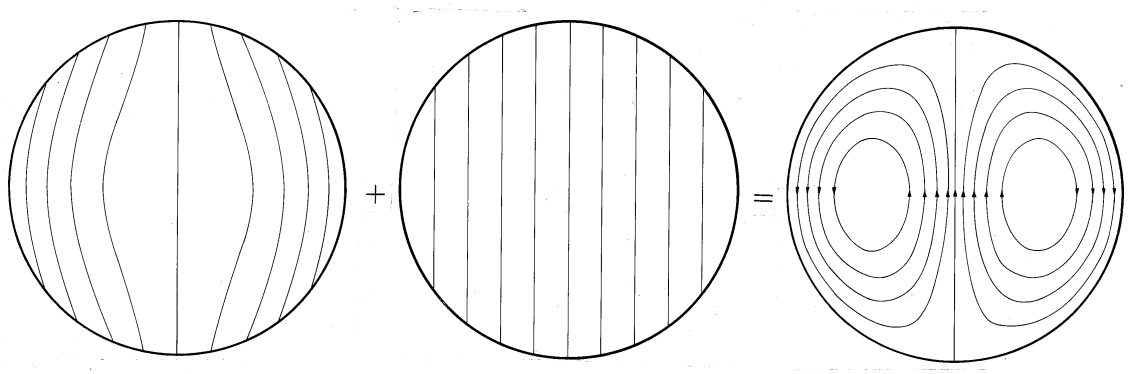


Fig. 8.6.13 Graphical representation of the surfaces of constant A_z for the system of Fig. 8.6.12 as the sum of particular and homogeneous solutions.

A graphical representation of what has been accomplished is given in Fig. 8.6.13, where the surfaces of constant A_z (and hence the lines of field intensity) are shown for the particular, homogeneous, and total solutions.

Each turn of the coil links a different magnetic flux. Thus, to determine the total flux linked by the distribution of turns, it is necessary to carry out an integration. To do this, first observe that the flux linked by the turns with their right legs within the area $rd\phi dr$ in the neighborhood of (r, ϕ) and their left legs within a similar area in the neighborhood of $(r, -\phi)$ is

$$\Phi_\lambda = l[A_z(r,\phi) - A_z(r,-\phi)]n_o \sin\phi r d\phi dr \tag{33}$$

Here, l is the length of the system in the z direction.

The total flux linked by all of the turns is obtained by integrating over all of the turns.

$$\lambda = ln_o \int_0^a \int_0^\pi [A_z(r,\phi) - A_z(r,-\phi)]r \sin\phi d\phi dr \tag{34}$$

Substitution for A_z from (32) and use of (26) then gives

$$\lambda = Li \qquad \text{with} \qquad L \equiv \frac{\pi}{36} l\mu_o N^2 \tag{35}$$

where L will be recognized as the inductance.

8.7 SUMMARY

Just as Chap. 4 was initiated with the representation of an irrotational vector field **E**, this chapter began by focusing on the solenoidal character of the magnetic flux density. Thus, $\mu_o\mathbf{H}$ was portrayed as the curl of another vector, the vector potential **A**.

The determination of the magnetic field intensity, given the current density everywhere, was pursued first using the vector potential. The integration of the

vector Poisson's equation for **A** was the first of many exploitations of analogies between EQS and MQS descriptions. In Cartesian coordinates, the superposition integral for **A**, (8.1.8) in Table 8.7.1, has components that are analogous to the scalar potential superposition integral, (4.5.3), from Table 4.9.1. Similarly, the two-dimensional superposition integral, (8.1.14), has as its analog (4.5.20) from Table 4.9.l.

Especially if a computer is to be used, it is often most practical to work directly with the magnetic field intensity. The Biot-Savart law, (8.2.7) in Table 8.7.1, gives **H** directly as an integration over the given distribution of current density.

In many applications, the current distribution can be approximated by piecewise continuous straight-line segments. In this case, the total field is conveniently represented by the superposition of contributions given by (8.2.22) in Table 8.7.1 due to the individual "sticks."

In regions free of current density, **H** is not only solenoidal, but also irrotational. Thus, like the electric field intensity of Chap. 4, it can be represented by a scalar potential Ψ, $\mathbf{H} = -\nabla\Psi$. The magnetic scalar potential is, in general, discontinuous across a surface carrying a surface current density. It is its normal derivative that is continuous. The scalar potential provides an elegant representation of the fields in free space regions surrounding current loops. The superposition integral, (8.3.12) in Table 8.7.1, is written in terms of the solid angle Ω.

Through the combined effects of Faraday's law, flux continuity, and Ohm's law, currents are induced in a conductor by a time-varying magnetic field. In a perfect conductor, these currents are on the surface, distributed in such a way as to shield the magnetic field out of the conductor. As a result, the normal component of the magnetic flux density must be zero on the surface of a perfect conductor.

Although useful for representing any solenoidal field, the vector potential is especially useful in the situations summarized by Table 8.7.2. It is especially convenient for describing systems with perfectly conducting boundaries. In two dimensions, the boundary condition on a perfect conductor is satisfied by making the vector potential constant on the boundary. The approaches of Chaps. 4 and 5 apply equally well to solving MQS boundary value problems involving perfect conductors. In fact, the two-dimensional EQS and MQS configurations of perfect conductors in free space, exemplified by the configurations of Figs. 4.7.2 and 8.6.7, were found to be duals. Formally, the solution for **H** follows from that for **E** by identifying $\Phi \rightarrow A_z$, $\rho/\epsilon_o \rightarrow \mu_o J_z$. However, while the electric field intensity **E** is perpendicular to the surfaces of constant Φ, **H** is tangential to the surfaces of constant A_z.

The boundary conditions obeyed by the vector potential at surfaces of discontinuity (containing surface currents) reflect the discontinuity in tangential H field and the continuity of the normal flux density. The vector potential itself must be continuous (a discontinuity of **A** would imply an infinite **H** in the surface)

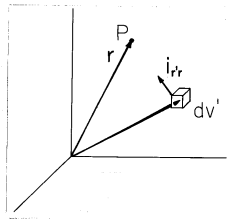
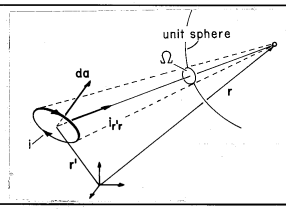
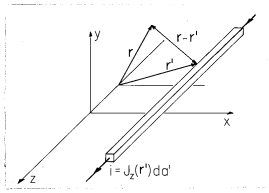
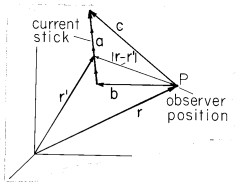
$$(\mathbf{A}^a - \mathbf{A}^b) = 0 \tag{1}$$

where Ampère's continuity condition

$$\mathbf{n} \times [(\nabla \times \mathbf{A})^a - (\nabla \times \mathbf{A})^b] = \mu_o \mathbf{K} \tag{2}$$

requires that *curl* **A** have discontinuous tangential components. The condition that **A** be continuous, (1), guarantees the continuity of the normal flux density. [According to (1), the integral of $\mathbf{A} \cdot d\mathbf{s}$ around an incremental closed contour lying on one

TABLE 8.7.1

Three-dimensional vector potential $\mathbf{A}(\mathbf{r}) = \frac{\mu_o}{4\pi}\int_{V'}\frac{\mathbf{J}(\mathbf{r}')dv'}{\lvert\mathbf{r}-\mathbf{r}'\rvert}$ Three-dimensional magnetic field intensity (Biot-Savart law) $\mathbf{H} = \frac{1}{4\pi}\int_{V'}\frac{\mathbf{J}(\mathbf{r}')\times\mathbf{i}_{r'r}}{\lvert\mathbf{r}-\mathbf{r}'\rvert^2}dv'$	(8.1.8) (8.2.7)	
$\Psi(\mathbf{r}) = \frac{i}{4\pi}\Omega$ $\Omega \equiv \int_S \frac{\mathbf{i}_{r'r}\cdot d\mathbf{a}'}{\lvert\mathbf{r}-\mathbf{r}'\rvert^2}$	(8.3.12) (4.5.29)	
Two-dimensional vector potential $A_z = -\frac{\mu_o}{2\pi}\int_{S'} ln\left(\frac{\lvert\mathbf{r}-\mathbf{r}'\rvert}{r_o}\right)\cdot J_z(\mathbf{r}')da'$	(8.1.14)	
Current "Stick" field $\mathbf{H} = \frac{i}{4\pi}\frac{\mathbf{c}\times\mathbf{a}}{\lvert\mathbf{c}\times\mathbf{a}\rvert^2}\left(\frac{\mathbf{a}\cdot\mathbf{c}}{\lvert c\rvert} - \frac{\mathbf{a}\cdot\mathbf{b}}{\lvert b\rvert}\right)$	(8.2.22)	

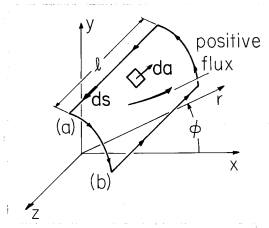
side of the surface is equal to that on the other. Thus, the normal flux which each of these integrals represents, is the same as well.]

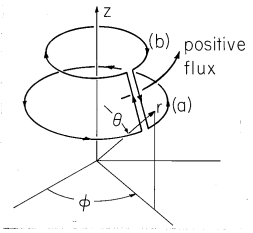
In fluid mechanics, the scalar A_z would be called a "stream-function", because in two dimensions, lines of constant vector potential constitute the flux lines. In axisymmetric configurations, the flux lines are lines of constant Λ_s, as defined in Table 8.7.2. Of course, a similar representation can be used for any solenoidal vector. For example, an expression for the two-dimensional lines of electric field intensity in a region free of charge density could be obtained by finding a vector potential representation of **E**. Thus, in these special cases, the vector potential is convenient for plotting any solenoidal field.

The electric potential Φ of EQS systems, evaluated on the surface of a perfectly

TABLE 8.7.2

Two-Dimensional cartesian coordinates	Eq. No.	
$\mathbf{A} = A_z(x,y)\mathbf{i_z}$	(8.6.3)	
$\mu_o\mathbf{H} = \frac{\partial A_z}{\partial y}\mathbf{i_x} - \frac{\partial A_z}{\partial x}\mathbf{i_y}$	(8.6.4)	
$\lambda = l(A_z^a - A_z^b)$	(8.6.5)	
Two-dimensional polarcoordinates		
$\mathbf{A} = A_z(r,\phi)\mathbf{i_z}$		
$\mu_o\mathbf{H} = \frac{1}{r}\frac{\partial A_z}{\partial \phi}\mathbf{i_r} - \frac{\partial A_z}{\partial r}\mathbf{i}_\phi$	(8.6.7)	
$\lambda = l(A_z^a - A_z^b)$	(8.6.5)	
Axisymmetric spherical coordinates		
$\mathbf{A} = A_\phi(r,\theta)\mathbf{i}_\phi$	(8.6.6)	
$\mu_o\mathbf{H} = \frac{1}{2\pi r^2 \sin\theta}\left(\frac{\partial \Lambda_s}{\partial \theta}\mathbf{i_r} - r\frac{\partial \Lambda_s}{\partial r}\mathbf{i}_\phi\right)$		
$\Lambda_s \equiv 2\pi r \sin\theta A_\phi$	(8.6.8)	
$\lambda = \Lambda_s^a - \Lambda_s^b$	(8.6.7)	





conducting capacitor electrode, can be used to evaluate the terminal voltage. The vector potential is similarly related to the terminal characteristics of a lumped parameter element, this time an inductor. Indeed, we found in Sec. 8.6 that the flux per unit length linked by a pair of conductors in two dimensions was simply the difference of vector potentials evaluated on the two conductors. In Sec. 8.4, we found that the terminal voltage is the time rate of change of this flux linkage.

The division of the field into particular and homogeneous parts makes possible a number of different approaches to obtaining the total field. The particular part can be obtained using the vector potential, using the Biot-Savart law, or by superimposing the fields of thin coils represented in terms the scalar magnetic potential. The homogeneous solution is both irrotational and solenoidal, so it is possible to use either the vector or the scalar potential to represent this part of the field everywhere. The vector potential helps determine the net flux, as required for calculating the inductance, but is of limited usefulness for three-dimensional configurations. The scalar potential does not directly portray the net flux, but does generally apply to three-dimensional configurations.

P R O B L E M S

8.1 The Vector Potential and the Vector Poisson Equation

8.1.1 A solenoid has radius a, length d, and turns N, as shown in Fig. 8.2.3. The length d is much greater than a, so it can be regarded as being infinite. It is driven by a current i.

(a) Show that Ampère's differential law and the magnetic flux continuity law [(8.0.1) and (8.0.2)], as well as the associated continuity conditions [(8.0.3) and (8.0.4)], are satisfied by an interior magnetic field intensity that is uniform and an exterior one that is zero.
(b) What is the interior field?
(c) $\mathbf{A}$ is continuous at $r = a$ because otherwise the $\mathbf{H}$ field would have a singularity. Determine $\mathbf{A}$.

8.1.2* A two-dimensional magnetic quadrupole is composed of four line currents of magnitudes i, two in the positive z direction at $x = 0$, $y = \pm d/2$ and two in the negative z direction at $x = \pm d/2, y = 0$. (With the line charges representing line currents, the cross-section is the same as shown in Fig. P4.4.3.) Show that in the limit where $r \gg d$, $A_z = -(\mu_o i d^2/4\pi)(r^{-2}) \cos 2\phi$. (Note that distances must be approximated accurately to order d^2.)

8.1.3 A two-dimensional coil, shown in cross-section in Fig. P8.1.3, is composed of N turns of length l in the z direction that is much greater than the width w or spacing d. The thickness of the windings in the y direction is much less than w and d. Each turn carries the current i. Determine $\mathbf{A}$.

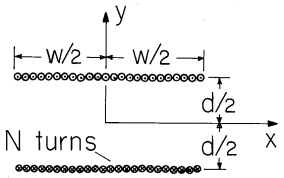


Fig. P8.1.3

8.2 The Biot-Savart Superposition Integral

8.2.1* The washer-shaped coil shown in Fig. P8.2.1 has a thickness Δ that is much less than the inner radius b and outer radius a. It supports a current density $\mathbf{J} = J_o \mathbf{i}_\phi$. Show that along the z axis,

$$\mathbf{H} = \frac{\Delta J_o \mathbf{i_z}}{2}\left[\frac{b}{\sqrt{b^2+z^2}} - \frac{a}{\sqrt{a^2+z^2}} + ln\frac{(a+\sqrt{a^2+z^2})}{(b+\sqrt{b^2+z^2})}\right] \qquad (a)$$

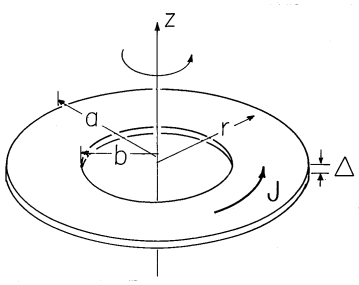


Fig. P8.2.1

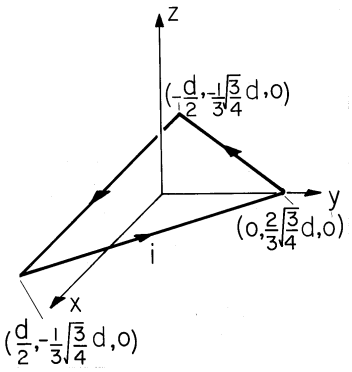


Fig. P8.2.5

8.2.2* A coil is wound so that the wire forms a spherical shell of radius R with the wire essentially running in the ϕ direction. With the wire driven by a current source, the resulting current distribution is a surface current at $r = R$ having the density $\mathbf{K} = K_o \sin\theta \mathbf{i}_\phi$, where K_o is a given constant. There are no other currents. Show that at the center of the coil, $\mathbf{H} = (2K_o/3)\mathbf{i_z}$.

8.2.3 In the configuration of Prob. 8.2.2, the surface current density is uniformly distributed, so that $\mathbf{K} = K_o \mathbf{i}_\phi$, where K_o is again a constant. Find $\mathbf{H}$ at the center of the coil.

8.2.4 Within a spherical region of radius R, the current density is $\mathbf{J} = J_o \mathbf{i}_\phi$, where J_o is a given constant. Outside this region is free space and no other sources of $\mathbf{H}$. Determine $\mathbf{H}$ at the origin.

8.2.5* A current i circulates around a loop having the shape of an equilateral triangle having sides of length d, as shown in Fig. P8.2.5. The loop is in the $z = 0$ plane. Show that along the z axis,

$$\mathbf{H} = i\sqrt{3/4}\frac{d^2\mathbf{i_z}}{4\pi}\left(z^2 + \frac{d^2}{12}\right)^{-1}\left(\frac{d^2}{3} + z^2\right)^{-1/2} \qquad (a)$$

8.2.6 For the two-dimensional coil of Prob. 8.1.3, use the Biot-Savart superposition integral to find $\mathbf{H}$ along the x axis.

8.2.7* Show that $\mathbf{A}$ induced at point P by the current stick of Figs. 8.2.5 and 8.2.6 is

$$\mathbf{A} = \frac{\mu_o i}{4\pi}\frac{\mathbf{a}}{|\mathbf{a}|} ln\left[\frac{\frac{\mathbf{c}\cdot\mathbf{a}}{|\mathbf{a}|}+|\mathbf{c}|}{\frac{\mathbf{b}\cdot\mathbf{a}}{|\mathbf{a}|}+|\mathbf{b}|}\right] \qquad (a)$$

8.3 The Scalar Magnetic Potential

8.3.1 Evaluate the H field on the axis of a circular loop of radius R carrying a current i. Show that your result is consistent with the result of Example 8.3.2 at distances from the loop much greater than R.

8.3.2 Determine Ψ for two infinitely long parallel thin wires carrying currents i in opposite directions parallel to the z axis of a Cartesian coordinate system and located along $x = \pm a$. Show that the lines $\Psi = \text{const}$ in the $x-y$ plane are circles.

8.3.3 Find the scalar potential on the axis of a stack of circular loops (a coil) of N turns and length l using 8.3.12 for an individual turn, integrating over all the turns. Find $\mathbf{H}$ on the axis.

8.4 Magnetoquasistatic Fields in the Presence of Perfect Conductors

8.4.1* A current loop of radius R is at the center of a conducting spherical shell having radius b. Assume that $R \ll b$ and that $i(t)$ is so rapidly varying that the shell can be taken as perfectly conducting. Show that in spherical coordinates, where $R \ll r < b$

$$\mathbf{H} = \frac{i\pi R^2}{4\pi}\left[2\cos\theta\left(\frac{1}{r^3}-\frac{1}{b^3}\right)\mathbf{i}_\mathbf{r} + \sin\theta\left(\frac{1}{r^3}+\frac{2}{b^3}\right)\mathbf{i}_\theta\right] \qquad (a)$$

8.4.2 The two-dimensional magnetic dipole of Example 8.1.2 is at the center of a conducting shell having radius $a \gg d$. The current $i(t)$ is so rapidly varying that the shell can be regarded as perfectly conducting. What are Ψ and $\mathbf{H}$ in the region $d \ll r < a$?

8.4.3* The cross-section of a two-dimensional system is shown in Fig. P8.4.3. A magnetic flux per unit length $s\mu_o H_o$ is trapped between perfectly conducting plane parallel plates that extend to infinity to the left and right. At the origin on the lower plate is a perfectly conducting half-cylinder of radius R.

(a) Show that if $s \gg R$, then

$$\Psi = H_o R\left(\frac{r}{R}+\frac{R}{r}\right)\cos\phi \qquad (a)$$

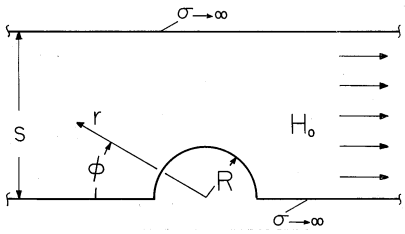


Fig. P8.4.3

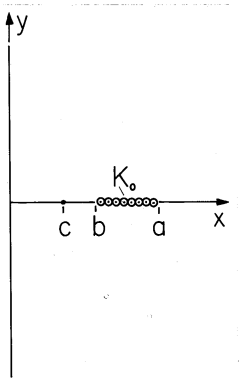


Fig. P8.4.6

(b) Show that a plot of **H** would appear as in the left half of Fig. 8.4.2 turned on its side.

8.4.4 In a three-dimensional version of that shown in Fig. P8.4.3, a perfectly conducting hemispherical bump of radius $s \gg R$ is attached to the lower of two perfectly conducting plane parallel plates. The hemisphere is centered at the origin of a spherical coordinate system such as in Fig. P8.4.3, with $\phi \rightarrow \theta$. The magnetic field intensity is uniform far from the hemisphere. Determine Ψ and **H**.

8.4.5* Running from $z = -\infty$ to $z = +\infty$ at $(x, y) = (0, -h)$ is a wire. The wire is parallel to a perfectly conducting plane at $y = 0$. When $t = 0$, a current step $i = Iu_{-1}(t)$ is applied in the $+z$ direction to the wire.

(a) Show that in the region $y < 0$,

$$\mathbf{H} = \frac{i}{2\pi}\left\{\frac{-(y+h)\mathbf{i_x} + x\mathbf{i_y}}{[x^2+(y+h)^2]} + \frac{(y-h)\mathbf{i_x} - x\mathbf{i_y}}{[x^2+(y-h)^2]}\right\} \qquad \text{for} \quad t > 0 \qquad (a)$$

(b) Show that the surface current density at $y = 0$ is $K_z = -ih/\pi(x^2 + h^2)$.

8.4.6 The cross-section of a system that extends to infinity in the $\pm z$ directions is shown in Fig. P8.4.6. Surrounded by free space, a sheet of current has

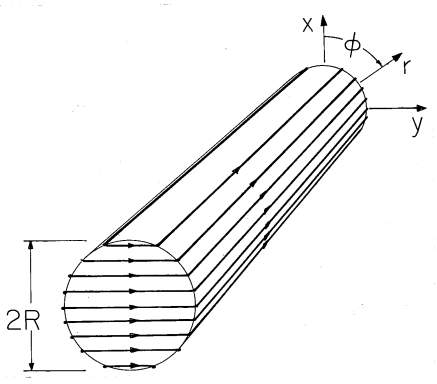


Fig. P8.5.1

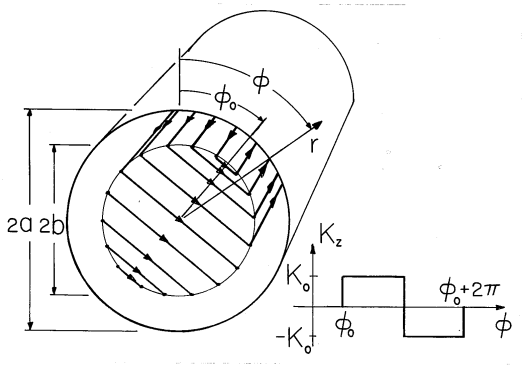


Fig. P8.5.2

the surface current density $K_o\mathbf{i_z}$ uniformly distributed between $x = b$ and $x = a$. The plane $x = 0$ is perfectly conducting.

(a) Determine Ψ in the region $0 < x$.
(b) Find $\mathbf{K}$ in the plane $x = 0$.

8.5 Piece-Wise Magnetic Fields

8.5.1* The cross-section of a cylindrical winding is shown in Fig. P8.5.1. As projected onto the $y = 0$ plane, the number of turns per unit length is constant and equal to $N/2R$. The cylinder can be modeled as infinitely long in the axial direction.

(a) Given that the winding carries a current i, show that

$$\Psi = \frac{Ni}{4}\begin{cases}(R/r)\cos\phi; & R < r\\ -(r/R)\cos\phi; & r < R\end{cases} \qquad (a)$$

and that therefore

$$\mathbf{H} = \frac{Ni}{4R}\begin{cases}(R/r)^2[\cos\phi\mathbf{i_r} + \sin\phi\mathbf{i}_\phi]; & R < r\\ [\cos\phi\mathbf{i_r} - \sin\phi\mathbf{i}_\phi]; & r < R\end{cases} \qquad (b)$$

(b) Show that the inductance per unit length of the winding is $L = \pi\mu_o N^2/8$.

8.5.2 The cross-section of a rotor, coaxial with a perfectly conducting "magnetic shield," is shown in Fig. P8.5.2. Windings consisting of N turns per unit peripheral length are distributed uniformly at $r = b$ so that at a given instant in time, the surface current distribution is as shown. At $r = a$, there is the inner surface of a perfect conductor. The system is very long in the z direction.

(a) What are the continuity conditions on Ψ at $r = b$ and the boundary condition at $r = a$?
(b) Find Ψ, and hence $\mathbf{H}$, in regions (a) and (b) outside and inside the winding, respectively.
(c) With the understanding that the rotor is wound using one wire, so that each turn is in series with the next and a wire carrying the current in the $+z$ direction at ϕ returns the current in the $-z$ direction at $-\phi$, what is the inductance of the rotor coil? Why is it independent of the rotor position ϕ_o?

8.6 Vector Potential

8.6.1* In Example 1.4.1, the magnetic field intensity is determined to be that given by (1.4.7). Define A_z to be zero at the origin.

(a) Show that if H_ϕ is to be finite in the neighborhood of $r = R$, A_z must be continuous there.
(b) Show that $\mathbf{A}$ is given by

$$\mathbf{A} = -\mathbf{i_z}\frac{\mu_o J_o R^2}{3}\begin{cases}\frac{1}{3}(r/R)^3; & r < R\\ ln(r/R) + \frac{1}{3}; & r > R\end{cases} \qquad (a)$$

(c) The loop designated by C' in Fig. 1.4.2 has a length l in the z direction, an inner leg at $r = 0$, and an outer leg at $r = a > R$. Use $\mathbf{A}$ to show that the flux linked is

$$\lambda = -lA_z(a) = \frac{\mu_o J_o R^2 l}{3}\left[ln(a/R) + \frac{1}{3}\right] \qquad (b)$$

8.6.2 For the configuration of Prob. 1.4.2, define A_z as being zero at the origin.

(a) Determine A_z in the regions $r < b$ and $b < r < a$.

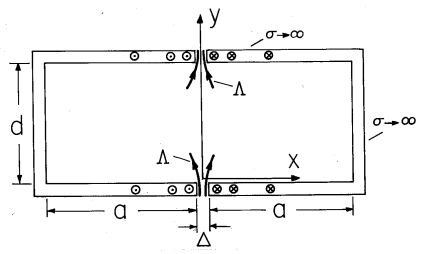


Fig. P8.6.5

(b) Use **A** to determine the flux linked by a closed rectangular loop having length l in the z direction and each of its four sides in a plane of constant ϕ. Two of the sides are parallel to the z axis, one at radius $r = c$ and the other at $r = 0$. The other two, respectively, join the ends of these segments, running radially from $r = 0$ to $r = c$.

8.6.3* In cylindrical coordinates, $\mu_o\mathbf{H} = \mu_o[H_r(r,z)\mathbf{i_r} + H_z(r,z)\mathbf{i_z}]$. That is, the magnetic flux density is axially symmetric and does not have a ϕ component.

(a) Show that

$$\mathbf{A} = [\Lambda_c(r,z)/r]\mathbf{i}_\phi \tag{a}$$

(b) Show that the flux passing between contours at $r = a$ and $r = b$ is

$$\lambda = 2\pi[\Lambda_c(a) - \Lambda_c(b)] \tag{b}$$

8.6.4* For the inductive attenuator considered in Example 8.6.3 and Demonstration 8.6.2:

(a) derive the vector potential, (20), without identifying this MQS problem with its EQS counterpart.
(b) Show that the current is as given by (21).
(c) In the limit where $b/a \gg 1$, show that the response has the dependence on b/a shown in the plot of Fig. 8.6.11.
(d) Show that in the opposite limit, where $b/a \ll 1$, the total current in the lower plate (21) is consistent with a magnetic field intensity between the upper and lower plates that is uniform (with respect to y) and hence equal to $(\Lambda/b\mu_o)\mathbf{i_x}$. Note that

$$\sum_{\substack{n=1\\ \text{odd}}}^{\infty} \frac{1}{n^2} = \frac{\pi^2}{8} \tag{a}$$

8.6.5 Perfectly conducting electrodes are composed of sheets bent into the shape of ⊔'s, as shown in Fig. P8.6.5. The length of the system in the z direction is very large compared to the length $2a$ or height d, so the fields can be

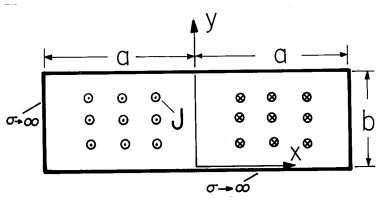


Fig. P8.6.6

regarded as two dimensional. The insulating gaps have a width Δ that is small compared to all dimensions. Passing through these gaps is a magnetic flux (per unit length in the z direction) $\Lambda(t)$. One method of solution is suggested by Example 6.6.3.

(a) Find **A** in regions (a) and (b) to the right and left, respectively, of the plane $x = 0$.
(b) Sketch **H**.

8.6.6* The wires comprising the winding shown in cross-section by Fig. P8.6.6 carry current in the $-z$ direction over the range $0 < x < a$ and return this current over the range $-a < x < 0$. These windings extend uniformly over the range $0 < y < b$. Thus, the current density in the region of interest is $\mathbf{J} = -in_o \sin(\pi x/a)\mathbf{i_z}$, where i is the current carried by each wire and $|n_o \sin(\pi x/a)|$ is the number of turns per unit area. This region is surrounded by perfectly conducting walls at $y = 0$ and $y = b$ and at $x = -a$ and $x = a$. The length l in the z direction is much greater than either a or b.

(a) Show that

$$\mathbf{A} = \mathbf{i_z}\mu_o i n_o (a/\pi)^2 \sin\left(\frac{\pi x}{a}\right)\left[\frac{\cosh\frac{\pi}{a}\left(y-\frac{b}{2}\right)}{\cosh\left(\frac{\pi b}{2a}\right)} - 1\right] \qquad (a)$$

(b) Show that the inductance of the winding is

$$L = 2\mu_o n_o^2 l \frac{a^4}{\pi^3}\left[\left(\frac{\pi b}{2a}\right) - \tanh\left(\frac{\pi b}{2a}\right)\right] \qquad (b)$$

(c) Sketch **H**.

8.6.7 In the configuration of Prob. 8.6.6, the rectangular region is uniformly filled with wires that all carry their current in the z direction. There are n_o of these wires per unit area. The current carried by each wire is returned in the perfectly conducting walls.

(a) Determine **A**.
(b) Assume that all the wires are connected to the wall by a terminating plate at $z = l$ and that each is driven by a current source $i(t)$ in the plane $z = 0$. Note that it has been assumed that each of these current

sources is the same function of time. What is the voltage $v(x, y, t)$ of these sources?

8.6.8 In the configuration of Prob. 8.6.6, the turns are uniformly distributed. Thus, n_o is a constant representing the number of wires per unit area carrying current in the $-z$ direction in the region $0 < x$. Assume that the wire carrying current in the $-z$ direction at the location (x, y) returns the current at $(-x, y)$.

(a) Determine $\mathbf{A}$.
(b) Find the inductance L.

9

MAGNETIZATION

9.0 INTRODUCTION

The sources of the magnetic fields considered in Chap. 8 were conduction currents associated with the motion of unpaired charge carriers through materials. Typically, the current was in a metal and the carriers were conduction electrons. In this chapter, we recognize that materials provide still other magnetic field sources. These account for the fields of permanent magnets and for the increase in inductance produced in a coil by insertion of a magnetizable material.

Magnetization effects are due to the propensity of the atomic constituents of matter to behave as magnetic dipoles. It is natural to think of electrons circulating around a nucleus as comprising a circulating current, and hence giving rise to a magnetic moment similar to that for a current loop, as discussed in Example 8.3.2.

More surprising is the magnetic dipole moment found for individual electrons. This moment, associated with the electronic property of *spin*, is defined as the *Bohr magneton*

$$m_e = \pm \frac{e}{m} \frac{1}{2} \hbar \tag{1}$$

where e/m is the electronic charge-to-mass ratio, 1.76×10^{11} coulomb/kg, and $2\pi\hbar$ is Planck's constant, $\hbar = 1.05 \times 10^{-34}$ joule-sec so that m_e has the units $A - m^2$. The quantum mechanics of atoms and molecules dictates that, whether due to the orbits or to the spins, the electronic contributions to their net dipole moments *tend* to cancel. Those that do make a contribution are typically in unfilled shells.

An estimate of the moment that would result if each atom or molecule of a material contributed only one Bohr magneton shows that the orbital and spin contributions from all the electrons comprising a typical solid had better tend to cancel or the resulting field effects would be prodigious indeed. Even if each atom or molecule is made to contribute only one Bohr magneton of magnetic moment, a

magnetic field results comparable to that produced by extremely large conduction currents. To make this apparent, compare the magnetic field induced by a current loop having a radius R and carrying a current i (Fig. 9.0.la) to that from a spherical collection of dipoles (Fig. 9.0.1b), each having the magnetic moment of only one electron.

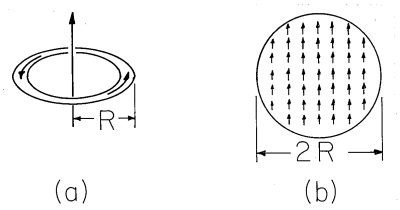


Fig. 9.0.1 (a) Current i in loop of radius R gives dipole moment $\mathbf{m}$. (b) Spherical material of radius R has dipole moment approximated as the sum of atomic dipole moments.

In the case of the spherical material, we consider the net dipole moment to be simply the moment m_e of a single molecule multiplied by the number of molecules. The number of molecules per unit mass is Avogadro's number ($A_0 = 6.023 \times 10^{26}$ molecules/kg-mole) divided by the molecular weight, M_o. The mass is the volume multiplied by the mass density ρ (kg/m^3). Thus, for a sphere having radius R, the sum of the dipole moments is

$$m = m_e\left(\frac{4}{3}\pi R^3\rho\right)\left(\frac{A_o}{M_o}\right) \tag{2}$$

Suppose that the current loop shown in Fig. 9.0.1a has the same radius R as the sphere. What current i would give rise to a magnetic moment equal to that from the sphere of hypothetical material? If the moment of the loop, given by (8.3.19) as being $m = i\pi R^2$, is set equal to that of the sphere, (2), it follows that i must be

$$i = m_e\frac{4}{3}R\rho\frac{A_o}{M_o} \tag{3}$$

Hence, for iron (where $\rho = 7.86 \times 10^3$ and $M_o = 56$) and a radius of 10 cm, the current required to produce the same magnetic moment is $10^5 A$.

Material magnetization can either be permanent or be induced by the application of a field, much as for the polarizable materials considered in Chap. 6. In most materials, the average moment per molecule that can be brought into play is much less than one Bohr magneton. However, highly magnetizable materials can produce net magnetic moments comparable to that estimated in (2).

The development of magnetization in this chapter parallels that for polarization in Chap. 6. Just as the polarization density was used in Sec. 6.1 to represent the effect of electric dipoles on the electric field intensity, the magnetization density introduced in Sec. 9.1 will account for the contributions of magnetic dipoles to the magnetic field intensity. The MQS laws and continuity conditions then collected in Sec. 9.2 are the basis for the remaining sections, and for Chap. 10 as well.

Because permanent magnets are so common, the permanent magnetization fields considered in Sec. 9.3 are more familiar than the permanent polarization electric fields of Sec. 6.3. Similarly, the force experienced as a piece of iron is brought

into a magnetic field is common evidence of the induced magnetization described by the constitutive laws of Sec. 9.4.

The extensive analogy between polarization and magnetization makes most of the examples from Chap. 6 analogous to magnetization examples. This is especially true in Secs. 9.5 and 9.6, where materials are considered that have a magnetization that is linearly related to the magnetic field intensity. Thus, these sections not only build on the insights gained in the earlier sections on polarization, but give the opportunity to expand on both topics as well. The magnetic circuits considered in Sec. 9.7 are of great practical interest and exemplify an approximate way for the evaluation of fields in the presence of strongly magnetized materials. The saturation of magnetizable materials is of primary practical concern. The problems for Secs. 9.6 and 9.7 are an introduction to fields in materials that are magnetically nonlinear.

We generalize Faraday's law in Sec. 9.2 so that it can be used in this chapter to predict the voltage at the terminals of coils in systems that include magnetization. This generalization is used to determine terminal relations that include magnetization in Sec. 9.5. The examples in the subsequent sections study the implications of Faraday's law with magnetization included. As in Chap. 8, we confine ourselves in this chapter to examples that can be modeled using the terminal variables of perfectly conducting circuits. The MQS laws, generalized in Sec. 9.2 to include magnetization, form the basis for the discussion of electric fields in MQS systems that is the theme of Chap. 10.

9.1 MAGNETIZATION DENSITY

The sources of magnetic field in matter are the (more or less) aligned magnetic dipoles of individual electrons or currents caused by circulating electrons.[1] We now describe the effect on the magnetic field of a distribution of magnetic dipoles representing the material.

In Sec. 8.3, we defined the magnitude of the magnetic moment m of a circulating current loop of current i and area a as $m = ia$. The moment vector, $\mathbf{m}$, was defined as normal to the surface spanning the contour of the loop and pointing in the direction determined by the right-hand rule. In Sec. 8.3, where the moment was in the z direction in spherical coordinates, the loop was found to produce the magnetic field intensity

$$\mathbf{H} = \frac{\mu_o m}{4\pi\mu_o r^3}[2\cos\theta\mathbf{i}_\mathbf{r} + \sin\theta\mathbf{i}_\theta] \tag{1}$$

This field is analogous to the electric field associated with a dipole having the moment $\mathbf{p}$. With $\mathbf{p}$ directed along the z axis, the electric dipole field is given by taking the gradient of (4.4.10).

$$\mathbf{E} = \frac{p}{4\pi\epsilon_o r^3}[2\cos\theta\mathbf{i}_\mathbf{r} + \sin\theta\mathbf{i}_\theta] \tag{2}$$

[1] Magnetic monopoles, which would play a role with respect to magnetic fields analogous to that of the charge with respect to electric fields, may in fact exist, but are certainly not of engineering significance. See *Science*, Research News, "In search of magnetic monopoles," Vol. 216, p. 1086 (June 4, 1982).

Thus, the dipole fields are obtained from each other by making the identifications

$$\boxed{\mathbf{p} \leftrightarrow \mu_o \mathbf{m}} \tag{3}$$

In Sec. 6.1, a spatial distribution of electric dipoles is represented by the polarization density $\mathbf{P} = N\mathbf{p}$, where N is the number density of dipoles. Similarly, here we define a *magnetization density* as

$$\boxed{\mathbf{M} = N\mathbf{m}} \tag{4}$$

where again N is the number of dipoles per unit volume. Note that just as the analog of the dipole moment $\mathbf{p}$ is $\mu_o\mathbf{m}$, the analog of the polarization density $\mathbf{P}$ is $\mu_o\mathbf{M}$.

9.2 LAWS AND CONTINUITY CONDITIONS WITH MAGNETIZATION

Recall that the effect of a spatial distribution of electric dipoles upon the electric field is described by a generalization of Gauss' law for electric fields, (6.2.1) and (6.2.2),

$$\nabla \cdot \epsilon_o \mathbf{E} = -\nabla \cdot \mathbf{P} + \rho_u \tag{1}$$

The effect of the spatial distribution of magnetic dipoles upon the magnetic field intensity is now similarly taken into account by generalizing the magnetic flux continuity law.

$$\boxed{\nabla \cdot \mu_o \mathbf{H} = -\nabla \cdot \mu_o \mathbf{M}} \tag{2}$$

In this law, there is no analog to an unpaired electric charge density.

The continuity condition found by integrating (2) over an incremental volume enclosing a section of an interface having a normal $\mathbf{n}$ is

$$\boxed{\mathbf{n} \cdot \mu_o(\mathbf{H}^a - \mathbf{H}^b) = -\mathbf{n} \cdot \mu_o(\mathbf{M}^a - \mathbf{M}^b)} \tag{3}$$

Suggested by the analogy to the description of polarization is the definition of the quantities on the right in (2) and (3), respectively, as the *magnetic charge density* ρ_m and the *magnetic surface charge density* σ_{sm}.

$$\boxed{\rho_m \equiv -\nabla \cdot \mu_o \mathbf{M}} \tag{4}$$

$$\boxed{\sigma_{sm} \equiv -\mathbf{n} \cdot \mu_o(\mathbf{M}^a - \mathbf{M}^b)} \tag{5}$$

Faraday's Law Including Magnetization. The modification of the magnetic flux continuity law implies that another of Maxwell's equations must be generalized. In introducing the flux continuity law in Sec. 1.7, we observed that it was almost inherent in Faraday's law. Because the divergence of the curl is zero, the divergence of the *free space* form of Faraday's law reduces to

$$\nabla \cdot (\nabla \times \mathbf{E}) = 0 = -\frac{\partial}{\partial t} \nabla \cdot \mu_o \mathbf{H} \tag{6}$$

Thus, in free space, $\mu_o \mathbf{H}$ must have a divergence that is at least constant in time. The magnetic flux continuity law adds the information that this constant is zero. In the presence of magnetizable material, (2) shows that the quantity $\mu_o(\mathbf{H} + \mathbf{M})$ is solenoidal. To make Faraday's law consistent with this requirement, the law is now written as

$$\boxed{\nabla \times \mathbf{E} = -\frac{\partial}{\partial t} \mu_o (\mathbf{H} + \mathbf{M})} \tag{7}$$

Magnetic Flux Density. The grouping of $\mathbf{H}$ and $\mathbf{M}$ in Faraday's law and the flux continuity law makes it natural to *define* a new variable, the *magnetic flux density* $\mathbf{B}$.

$$\boxed{\mathbf{B} \equiv \mu_o (\mathbf{H} + \mathbf{M})} \tag{8}$$

This quantity plays a role that is analogous to that of the electric displacement flux density $\mathbf{D}$ defined by (6.2.14). Because there are no macroscopic quantities of monopoles of magnetic charge, its divergence is zero. That is, the flux continuity law, (2), becomes simply

$$\boxed{\nabla \cdot \mathbf{B} = 0} \tag{9}$$

and the corresponding continuity condition, (3), becomes simply

$$\boxed{\mathbf{n} \cdot (\mathbf{B}^a - \mathbf{B}^b) = 0} \tag{10}$$

A similar simplification is obtained by writing Faraday's law in terms of the magnetic flux density. Equation (7) becomes

$$\boxed{\nabla \times \mathbf{E} = -\frac{\partial \mathbf{B}}{\partial t}} \tag{11}$$

If the magnetization is specified independent of $\mathbf{H}$, it is usually best to have it entered explicitly in the formulation by not introducing $\mathbf{B}$. However, if $\mathbf{M}$ is given

as a function of **H**, especially if it is linear in **H**, it is most convenient to remove **M** from the formulation by using **B** as a variable.

Terminal Voltage with Magnetization. In Sec. 8.4, where we discussed the terminal voltage of a perfectly conducting coil, there was no magnetization. The generalization of Faraday's law to include magnetization requires a generalization of the terminal relation.

The starting point in deriving the terminal relation was Faraday's integral law, (8.4.9). This law is generalized to included magnetization effects by replacing $\mu_o\mathbf{H}$ with **B**. Otherwise, the derivation of the terminal relation, (8.4.11), is the same as before. Thus, the terminal voltage is again

$$\boxed{v = \frac{d\lambda}{dt}} \tag{12}$$

but now the flux linkage is

$$\boxed{\lambda \equiv \int_S \mathbf{B} \cdot d\mathbf{a}} \tag{13}$$

In Sec. 9.4 we will see that Faraday's law of induction, as reflected in these last two relations, is the basis for measuring **B**.

9.3 PERMANENT MAGNETIZATION

As the modern-day versions of the lodestone, which made the existence of magnetic fields apparent in ancient times, permanent magnets are now so cheaply manufactured that they are used at home to pin notes on the refrigerator and so reliable that they are at the heart of motors, transducers, and information storage systems. To a first approximation, a permanent magnet can be modeled by a material having a specified distribution of magnetization density **M**. Thus, in this section we consider the magnetic field intensity generated by prescribed distributions of **M**.

In a region where there is no current density **J**, Ampère's law requires that **H** be irrotational. It is then often convenient to represent the magnetic field intensity in terms of the scalar magnetic potential Ψ introduced in Sec. 8.3.

$$\mathbf{H} = -\nabla\Psi \tag{1}$$

From the flux continuity law, (9.2.2), it then follows that Ψ satisfies Poisson's equation.

$$\nabla^2\Psi = -\frac{\rho_m}{\mu_o}; \quad \rho_m \equiv -\nabla \cdot \mu_o\mathbf{M} \tag{2}$$

A specified magnetization density leads to a prescribed magnetic charge density ρ_m. The situation is analogous to that considered in Sec. 6.3, where the polarization density was prescribed and, as a result, where ρ_p was known.

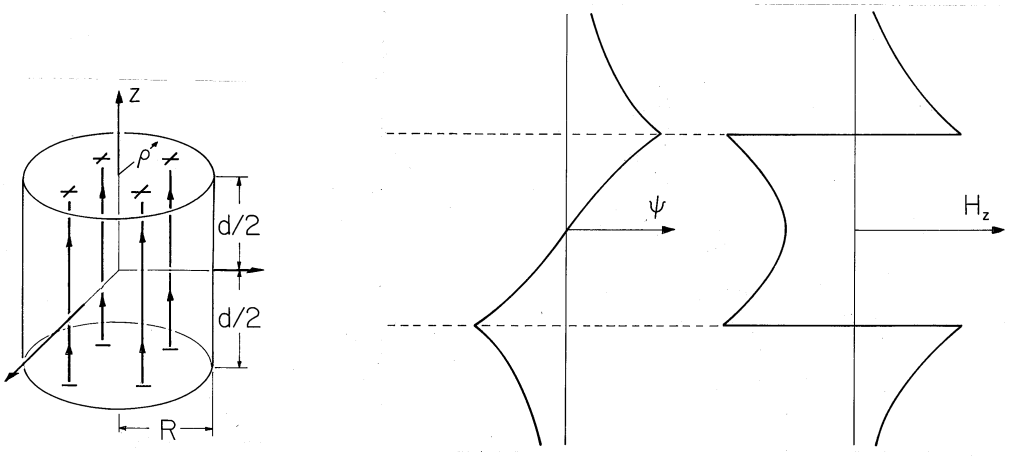


Fig. 9.3.1 (a) Cylinder of circular cross-section uniformly magnetized in the direction of its axis. (b) Axial distribution of scalar magnetic potential and (c) axial magnetic field intensity. For these distributions, the cylinder length is assumed to be equal to its diameter.

Of course, the net magnetic charge of a magnetizable body is always zero, because

$$\int_V \rho_m dv = \oint_S \mu_o \mathbf{H} \cdot d\mathbf{a} = 0 \tag{3}$$

if the integral is taken over the entire volume containing the body. Techniques for solving Poisson's equation for a prescribed charge distribution developed in Chaps. 4 and 5 are directly applicable here. For example, if the magnetization is given throughout all space and there are no other sources, the magnetic scalar potential is given by a superposition integral. Just as the integral of (4.2.2) is (4.5.3), so the integral of (2) is

$$\boxed{\Psi = \int_{V'} \frac{\rho_m(\mathbf{r}')dv}{4\pi\mu_o|\mathbf{r}-\mathbf{r}'|}} \tag{4}$$

If the region of interest is bounded by material on which boundary conditions are specified, (4) provides the particular solution.

Example 9.3.1. Magnetic Field Intensity of a Uniformly Magnetized Cylinder

The cylinder shown in Fig. 9.3.1 is uniformly magnetized in the z direction, $\mathbf{M} = M_o\mathbf{i_z}$. The first step toward finding the resulting $\mathbf{H}$ within the cylinder and in the surrounding free space is an evaluation of the distribution of magnetic charge density. The uniform $\mathbf{M}$ has no divergence, so $\rho_m = 0$ throughout the volume. Thus, the source of $\mathbf{H}$ is on the surfaces where $\mathbf{M}$ originates and terminates. In view of (9.2.3), it takes the form of the surface charge density

$$\sigma_{sm} = -\mathbf{n} \cdot \mu_o(\mathbf{M}^a - \mathbf{M}_b) = \pm\mu_o M_o \tag{5}$$

The upper and lower signs refer to the upper and lower surfaces.

In principle, we could use the superposition integral to find the potential everywhere. To keep the integration simple, we confine ourselves here to finding it on the z axis. The integration of (4) then reduces to integrations over the endfaces of the cylinder.

$$\Psi = \int_0^R \frac{\mu_o M_o 2\pi\rho' d\rho'}{4\pi\mu_o\sqrt{\rho'^2 + \left(z - \frac{d}{2}\right)^2}} - \int_0^R \frac{\mu_o M_o 2\pi\rho' d\rho'}{4\pi\mu_o\sqrt{\rho'^2 + \left(z + \frac{d}{2}\right)^2}} \tag{6}$$

With absolute magnitudes used to make the expressions valid regardless of position along the z axis, these integrals become

$$\begin{aligned}\Psi = &\frac{dM_o}{2}\left[\sqrt{\left(\frac{R}{d}\right)^2 + \left(\frac{z}{d} - \frac{1}{2}\right)^2} - \left|\frac{z}{d} - \frac{1}{2}\right|\right. \\ &\left. - \sqrt{\left(\frac{R}{d}\right)^2 + \left(\frac{z}{d} + \frac{1}{2}\right)^2} + \left|\frac{z}{d} + \frac{1}{2}\right|\right]\end{aligned} \tag{7}$$

The field intensity follows from (1)

$$H_z = -\frac{dM_o}{2}\left[\frac{\left(\frac{z}{d} - \frac{1}{2}\right)}{\sqrt{\left(\frac{R}{d}\right)^2 + \left(\frac{z}{d} - \frac{1}{2}\right)^2}} - \frac{\left(\frac{z}{d} + \frac{1}{2}\right)}{\sqrt{\left(\frac{R}{d}\right)^2 + \left(\frac{z}{d} + \frac{1}{2}\right)^2}} + u\right] \tag{8}$$

where $u \equiv 0$ for $|z| > d/2$ and $u \equiv 2$ for $-d/2 < z < d/2$. Here, from top to bottom, respectively, the signs correspond to evaluating the field above the upper surface, within the magnet, and below the bottom surface.

The axial distributions of Ψ and H_z shown in Fig. 9.3.1 are consistent with a three-dimensional picture of a field that originates on the top face of the magnet and terminates on the bottom face. As for the spherical magnet (the analogue of the permanently polarized sphere shown in Fig. 6.3.1), the magnetic field intensity inside the magnet has a direction opposite to that of $\mathbf{M}$.

In practice, $\mathbf{M}$ would most likely be determined by making measurements of the external field and then deducing $\mathbf{M}$ from this field.

If the magnetic field intensity is generated by a combination of prescribed currents and permanent magnetization, it can be evaluated by superimposing the field due to the current and the magnetization. For example, suppose that the uniformly magnetized circular cylinder of Fig. 9.3.1 were surrounded by the N-turn solenoid of Fig. 8.2.3. Then the axial field intensity would be the sum of that for the current [predicted by the Biot-Savart law, (8.2.7)], and for the magnetization [predicted by the negative gradient of (4)].

Example 9.3.2. Retrieval of Signals Stored on Magnetizable Tape

Permanent magnetization is used for a permanent record in the tape recorder. Currents in an electromagnet are used to induce the permanent magnetization, exploiting the hysteresis in the magnetization of certain materials, as will be discussed

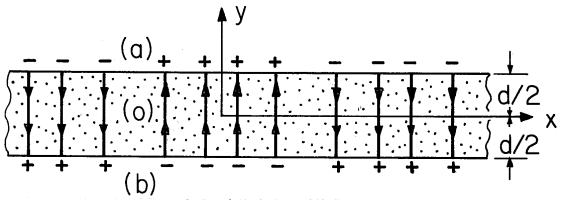


Fig. 9.3.2 Permanently magnetized tape has distribution of **M** representing a Fourier component of a recorded signal. From a frame of reference attached to the tape, the magnetization is static.

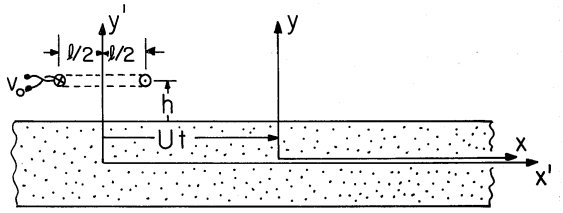


Fig. 9.3.3 From the frame of reference of a sensing coil, the tape is seen to move in the x' direction with the velocity U.

in Sec. 9.4. Here we look at a model of perpendicular magnetization, an actively pursued research field. The conventional recording is done by producing magnetization **M** parallel to the tape.

In a thin tape at rest, the magnetization density shown in Fig. 9.3.2 is assumed to be uniform over the thickness and to be of the simple form

$$\mathbf{M} = M_o \cos \beta x \mathbf{i_y} \tag{9}$$

The magnetic field is first determined in a frame of reference attached to the tape, denoted by (x, y, z) as defined in Fig. 9.3.2. The tape moves with a velocity U with respect to a fixed sensing "head," and so our second step will be to represent this field in terms of fixed coordinates. With Fig. 9.3.3 in view, it is clear that these coordinates, denoted by (x', y', z'), are related to the moving coordinates by

$$x' = x + Ut \rightarrow x = x' - Ut; \qquad y = y' \tag{10}$$

Thus, from the fixed reference frame, the magnetization takes the form of a traveling wave.

$$\mathbf{M} = M_o \cos \beta (x' - Ut) \mathbf{i_y} \tag{11}$$

If **M** is observed at a fixed location x', it has a sinusoidal temporal variation with the frequency $\omega = \beta U$. This relationship between the fixed frame frequency and the spatial periodicity suggests how the distribution of magnetization is established by "recording" a signal having the frequency ω.

The magnetization density has no divergence in the volume of the tape, so the field source is a surface charge density. With upper and lower signs denoting the upper and lower tape surfaces, it follows that

$$\sigma_m = \pm \mu_o M_o \cos \beta x \tag{12}$$

The continuity conditions to be satisfied at the upper and lower surfaces represent the continuity of magnetic flux (9.2.3)

$$\begin{aligned} \mu_o H_y^a - \mu_o H_y^o &= \mu_o M_o \cos \beta x \quad \text{at} \quad y = \frac{d}{2} \\ \mu_o H_y^o - \mu_o H_y^b &= -\mu_o M_o \cos \beta x \quad \text{at} \quad y = -\frac{d}{2} \end{aligned} \tag{13}$$

and the continuity of tangential **H**

$$\begin{aligned} \Psi_a &= \Psi_o \quad \text{at} \quad y = \frac{d}{2} \\ \Psi_o &= \Psi_b \quad \text{at} \quad y = -\frac{d}{2} \end{aligned} \tag{14}$$

In addition, the field should go to zero as $y \to \pm\infty$.

Because the field sources are confined to surfaces, the magnetic scalar potential must satisfy Laplace's equation, (2) with $\rho_m = 0$, in the bulk regions delimited by the interfaces. Motivated by the "odd" symmetry of the source with respect to the $y = 0$ plane and its periodicity in x, we pick solutions to Laplace's equation for the magnetic potential above (a), inside (o), and below (b) the tape that also satisfy the odd symmetry condition of having $\Psi(y) = -\Psi(-y)$.

$$\begin{aligned} \psi_a &= A\, e^{-\beta y} \cos \beta x \\ \psi_o &= C\, \sinh \beta y \cos \beta x \\ \psi_b &= -A\, e^{\beta y} \cos \beta x \end{aligned} \tag{15}$$

Subject to the requirement that $\beta > 0$, the exterior potentials go to zero at $y = \pm\infty$. The interior function is made an odd function of y by excluding the $\cosh(\beta y)\cos(\beta x)$ solution to Laplace's equation, while the exterior functions are made odd by making the coefficients equal in magnitude and opposite in sign. Thus, only two coefficients remain to be determined. These follow from substituting the assumed solution into either of (13) and either of (14), and then solving the two equations to obtain

$$\begin{aligned} A &= \frac{M_o}{\beta} e^{\beta d/2} \left(1 + \coth \frac{\beta d}{2}\right)^{-1} \\ C &= \frac{M_o}{\beta} \left[\left(1 + \coth \frac{\beta d}{2}\right) \sinh \frac{\beta d}{2}\right]^{-1} \end{aligned} \tag{16}$$

The conditions at one interface are automatically satisfied if those at the other are met. This is a proof that the assumed solutions have indeed been correct. Our foresight in defining the origin of the y axis to be at the symmetry plane and exploiting the resulting odd dependence of Ψ on y has reduced the number of undetermined coefficients from four to two.

This field is now expressed in the fixed frame coordinates. With A defined by (16a) and x and y given in terms of the fixed frame coordinates by (10), the magnetic potential above the tape has been determined to be

$$\Psi_a = \frac{M_o}{\beta} \frac{e^{-\beta(y' - \frac{d}{2})}}{\left(1 + \coth \frac{\beta d}{2}\right)} \cos \beta(x' - Ut) \tag{17}$$

Next, we determine the output voltage of a fixed coil, positioned at a height h above the tape, as shown in Fig. 9.3.3. This detecting "head" has N turns, a length l in the x' direction, and width w in the z direction. With the objective of finding the flux linkage, we use (17) to determine the y-directed flux density in the neighborhood of the coil.

$$B_y = -\mu_o \frac{\partial \Psi_a}{\partial y'} = \frac{\mu_o M_o e^{-\beta(y' - \frac{d}{2})}}{\left(1 + \coth \frac{\beta d}{2}\right)} \cos \beta(x' - Ut) \tag{18}$$

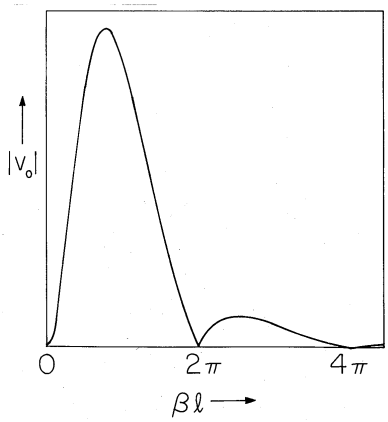


Fig. 9.3.4 Magnitude of sensing coil output voltage as a function of $\beta l = 2\pi l/\Lambda$, where Λ is the wavelength of the magnetization. If the magnetization is produced by a fixed coil driven at the angular frequency ω, the horizontal axis, which is then $\omega l/U$, is proportional to the recording frequency.

The flux linkage follows by multiplying the number of turns N times B_y integrated over the surface in the plane $y = h + \frac{1}{2}d$ spanned by the coil.

$$\begin{aligned}\lambda &= wN\int_{-l/2}^{l/2} B_y\big(y' = h + \frac{d}{2}\big)dx' \\ &= \frac{\mu_o M_o wNe^{-\beta h}}{\beta\big(1+\coth\frac{\beta d}{2}\big)}\big[\sin\beta\big(\frac{l}{2}-Ut\big)+\sin\beta\big(\frac{l}{2}+Ut\big)\big]\end{aligned} \tag{19}$$

The dependence on l is clarified by using a trigonometric identity to simplify the last term in this expression.

$$\lambda = \frac{2\mu_o M_o wNe^{-\beta h}}{\beta\big(1+\coth\frac{\beta d}{2}\big)}\sin\frac{\beta l}{2}\cos\beta Ut \tag{20}$$

Finally, the output voltage follows from (9.2.12).

$$v_o = \frac{d\lambda}{dt} = -\frac{2\mu_o M_o wUN}{\big(1+\coth\frac{\beta d}{2}\big)}e^{-\beta h}\sin\frac{\beta l}{2}\sin\beta Ut \tag{21}$$

The strong dependence of this expression on the wavelength of the magnetization, $2\pi/\beta$, reflects the nature of fields predicted using Laplace's equation. It follows from (21) that the output voltage has the angular frequency $\omega = \beta U$. Thus, (21) can also be regarded as giving the frequency response of the sensor. The magnitude of v_o has the dependence on either the normalized β or ω shown in Fig. 9.3.4.

Two phenomena underlie the voltage response. The periodic dependence reflects the relationship between the length l of the coil and the wavelength $2\pi/\beta$ of the magnetization. When the coil length is equal to the wavelength, there is as much positive as negative flux linking the coil at a given instant, and the signal falls to zero. This is also the condition when l is any multiple of a wavelength and accounts for the $\sin(\frac{1}{2}\beta l)$ term in (21).

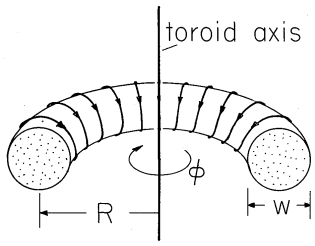


Fig. 9.4.1 Toroidal coil with donut-shaped magnetizable core.

The strong decay of the envelope of the output signal as the frequency is increased, and hence the wavelength decreased, reflects a property of Laplace's equation that frequently comes into play in engineering electromagnetic fields. The shorter the wavelength, the more rapid the decay of the field in the direction perpendicular to the tape. With the sensing coil at a fixed height above the tape, this means that once the wavelength is on the order of $2\pi h$, there is an essentially exponential decrease in signal with increasing frequency. Thus, there is a strong incentive to place the coil as close to the tape as possible.

We should expect that if the tape is very thin compared to the wavelength, the field induced by magnetic surface charges on the top surface would tend to be canceled by those of opposite sign on the surface just below. This effect is accounted for by the term $[1 + \coth(\frac{1}{2}\beta d)]$ in the denominator of (21).

In a practical recording device, the sensing head of the previous example would incorporate magnetizable materials. To predict how these affect the fields, we need a law relating the field to the magnetization it induces. This is the subject of the next section.

9.4 MAGNETIZATION CONSTITUTIVE LAWS

The permanent magnetization model of Sec. 9.3 is a somewhat artificial example of the magnetization density $\mathbf{M}$ specified, independent of the magnetic field intensity. Even in the best of permanent magnets, there is actually some dependence of $\mathbf{M}$ on $\mathbf{H}$.

Constitutive laws relate the magnetization density $\mathbf{M}$ or the magnetic flux density $\mathbf{B}$ to the macroscopic $\mathbf{H}$ within a material. Before discussing some of the more common relations and their underlying physics, it is well to have in view an experiment giving direct evidence of the constitutive law of magnetization. The objective is to observe the establishment of $\mathbf{H}$ by a current in accordance with Ampère's law, and deduce $\mathbf{B}$ from the voltage it induces in accordance with Faraday's law.

Example 9.4.1. Toroidal Coil

A coil of toroidal geometry is shown in Fig. 9.4.1. It consists of a donut-shaped core filled with magnetizable material with N_1 turns tightly wound on its periphery. By means of a source driving its terminals, this coil carries a current i. The resulting

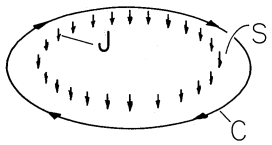


Fig. 9.4.2 Surface S enclosed by contour C used with Ampère's integral law to determine $\mathbf{H}$ in the coil shown in Fig. 9.4.1.

current distribution can be assumed to be so smooth that the fine structure of the field, caused by the finite size of the wires, can be disregarded. We will ignore the slight pitch of the coil and the associated small current component circulating around the axis of the toroid.

Because of the toroidal geometry, the H field in the magnetizable material is determined by Ampère's law and symmetry considerations. Symmetry about the toroidal axis suggests that $\mathbf{H}$ is ϕ directed. The integral MQS form of Ampère's law is written for a contour C circulating about the toroidal axis within the core and at a radius r. Because the major radius R of the torus is large compared to the minor radius $\frac{1}{2}w$, we will ignore the variation of r over the cross-section of the torus and approximate r by an average radius R. The surface S spanned by this contour and shown in Fig. 9.4.2 is pierced N_1 times by the current i, giving a total current of $N_1 i$. Thus, the azimuthal field inside the core is essentially

$$2\pi r H_\phi = N_1 i \rightarrow H_\phi \equiv H = \frac{N_1 i}{2\pi r} \simeq \frac{N_1 i}{2\pi R} \tag{1}$$

Note that the same argument shows that the magnetic field intensity outside the core is zero.

In general, if we are given the current distribution and wish to determine $\mathbf{H}$, recourse must be made not only to Ampère's law but to the flux continuity condition as well. In the idealized toroidal geometry, where the flux lines automatically close on themselves without leaving the magnetized material, the flux continuity condition is automatically satisfied. Thus, in the toroidal configuration, the $\mathbf{H}$ imposed on the core is determined by a measurement of the current i and the geometry.

How can we measure the magnetic flux density in the core? Because $\mathbf{B}$ appears in Faraday's law of induction, the measurement of the terminal voltage of an additional coil, having N_2 turns also wound on the donut-shaped core, gives information on $\mathbf{B}$. The terminals of this coil are terminated in a high enough impedance so that there is a negligible current in this second winding. Thus, the $\mathbf{H}$ field established by the current i remains unaltered.

The flux linked by each turn of the sensing coil is essentially the flux density multiplied by the cross-sectional area $\pi w^2/4$ of the core. Thus, the flux linked by the terminals of the sensing coil is

$$\lambda_2 = \frac{\pi w^2}{4} N_2 B \tag{2}$$

and flux density in the core material is directly reflected in the terminal flux-linkage.

The following demonstration shows how (1) and (2) can be used to infer the magnetization characteristic of the core material from measurement of the terminal current and voltage of the first and second coils.

Demonstration 9.4.1. Measurement of $B - H$ Characteristic

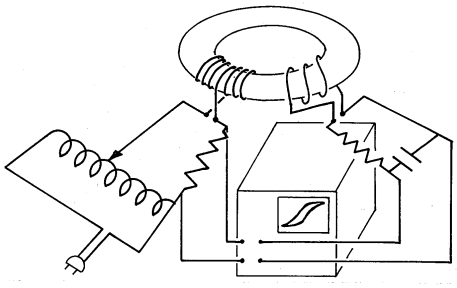


Fig. 9.4.3 Demonstration in which the $B - H$ curve is traced out in the sinusoidal steady state.

The experiment shown in Fig. 9.4.3 displays the magnetization characteristic on the oscilloscope. The magnetizable material is in the donut-shaped toroidal configuration of Example 9.4.1 with the N_1-turn coil driven by a current i from a Variac. The voltage across a series resistance then gives a horizontal deflection of the oscilloscope proportional to H, in accordance with (1).

The terminals of the N_2 turn-coil are connected through an integrating network to the vertical deflection terminals of the oscilloscope. Thus, the vertical deflection is proportional to the integral of the terminal voltage, to λ, and hence through (2), to $\mathbf{B}$.

In the discussions of magnetization characteristics which follow, it is helpful to think of the material as comprising the core of the torus in this experiment. Then the magnetic field intensity $\mathbf{H}$ is proportional to the current i, while the magnetic flux density $\mathbf{B}$ is reflected in the voltage induced in a coil linking this flux.

Many materials are *magnetically linear* in the sense that

$$\boxed{\mathbf{M} = \chi_m \mathbf{H}} \tag{3}$$

Here χ_m is the *magnetic susceptibility*. More commonly, the constitutive law for a magnetically linear material is written in terms of the magnetic flux density, defined by (9.2.8).

$$\boxed{\mathbf{B} = \mu \mathbf{H}; \qquad \mu \equiv \mu_o(1 + \chi_m)} \tag{4}$$

According to this law, the magnetization is taken into account by replacing the permeability of free space μ_o by the *permeability* μ of the material. For purposes of comparing the magnetizability of materials, the *relative permeability* μ/μ_o is often used.

Typical susceptibilities for certain elements, compounds, and common materials are given in Table 9.4.1. Most common materials are only slightly magnetizable. Some substances that are readily polarized, such as water, are not easily magnetized. Note that the magnetic susceptibility can be either positive or negative and that there are some materials, notably iron and its compounds, in which it can be enormous. In establishing an appreciation for the degree of magnetizability that can be expected of a material, it is helpful to have a qualitative picture of its mi-

TABLE 9.4.1
RELATIVE SUSCEPTIBILITIES OF COMMON MATERIALS

	Material	χ_m
PARAMAGNETIC	Mg	1.2×10^{-5}
	Al	2.2×10^{-5}
	Pt	3.6×10^{-4}
	air	3.6×10^{-7}
	O_2	2.1×10^{-6}
DIAMAGNETIC	Na	-0.24×10^{-5}
	Cu	-1.0×10^{-5}
	diamond	-2.2×10^{-5}
	Hg	-3.2×10^{-5}
	H_2O	-0.9×10^{-5}
FERROMAGNETIC	Fe (dynamo sheets)	5.5×10^{3}
	Fe (lab specimens)	8.8×10^{4}
	Fe (crystals)	1.4×10^{6}
	Si-Fe transformer sheets	7×10^{4}
	Si-Fe crystals	3.8×10^{6}
	μ-metal	10^{5}
FERRIMAGNETIC	Fe_3O_4	100
	ferrites	5000

croscopic origins, beginning at the atomic level but including the collective effects of groups of atoms or molecules that result when they become as densely packed as they are in solids. These latter effects are prominent in the most easily magnetized materials.

The magnetic moment of an atom (or molecule) is the sum of the orbital and spin contributions. Especially in a gas, where the atoms are dilute, the magnetic susceptibility results from the (partial) alignment of the individual magnetic moments by a magnetic field. Although the spin contributions to the moment tend to cancel, many atoms have net moments of one or more Bohr magnetons. At room temperature, the orientations of the moments are mostly randomized by thermal agitation, even under the most intense fields. As a result, an applied field can give rise to a significant magnetization only at very low temperatures. A *paramagnetic material* displays an appreciable susceptibility only at low temperatures.

If, in the absence of an applied field, the spin contributions to the moment of an atom very nearly cancel, the material can be *diamagnetic*, in the sense that it displays a slightly negative susceptibility. With the application of a field, the

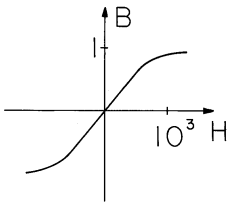


Fig. 9.4.4 Typical magnetization curve without hysteresis. For typical ferromagnetic solids, the saturation flux density is in the range of 1–2 Tesla. For ferromagnetic domains suspended in a liquid, it is .02–.04 Tesla.

orbiting electrons are slightly altered in their circulations, giving rise to changes in moment in a direction opposite to that of the applied field. Again, thermal energy tends to disorient these moments. At room temperature, this effect is even smaller than that for paramagnetic materials.

At very low temperatures, it is possible to raise the applied field to such a level that essentially all the moments are aligned. This is reflected in the saturation of the flux density $\mathbf{B}$, as shown in Fig. 9.4.4. At low field intensity, the slope of the magnetization curve is μ, while at high field strengths, there are no more moments to be aligned and the slope is μ_o. As long as the field is raised and lowered at a rate slow enough so that there is time for the thermal energy to reach an equilibrium with the magnetic field, the B-H curve is single valued in the sense that the same curve is followed whether the magnetic field is increasing or decreasing, and regardless of its rate of change.

Until now, we have been considering the magnetization of materials that are sufficiently dilute so that the atomic moments do not interact with each other. In solids, atoms can be so closely spaced that the magnetic field due to the moment of one atom can have a significant effect on the orientation of another. In *ferromagnetic* materials, this mutual interaction is all important.

To appreciate what makes certain materials ferromagnetic rather than simply paramagnetic, we need to remember that the electrons which surround the nuclei of atoms are assigned by quantum mechanical principles to layers or "shells." Each shell has a particular maximum number of electrons. The electron behaves as if it possessed a net angular momentum, or spin, and hence a magnetic moment. A filled shell always contains an even number of electrons which are distributed spatially in such a manner that the total spin, and likewise the magnetic moment, is zero.

For the majority of atoms, the outermost shell is unfilled, and so it is the outermost electrons that play the major role in determining the net magnetic moment of the atom. This picture of the atom is consistent with paramagnetic and diamagnetic behavior. However, the transition elements form a special class. They have unfilled *inner* shells, so that the electrons responsible for the net moment of the atom are surrounded by the electrons that interact most intimately with the electrons of a neighboring atom. When such atoms are as closely packed as they are in solids, the combination of the interaction between magnetic moments and of electrostatic coupling results in the *spontaneous* alignment of dipoles, or *ferromagnetism*. The underlying interaction between atoms is both magnetic and electrostatic, and can be understood only by invoking quantum mechanical arguments.

In a ferromagnetic material, atoms naturally establish an array of moments that reinforce. Nevertheless, on a macroscopic scale, ferromagnetic materials are

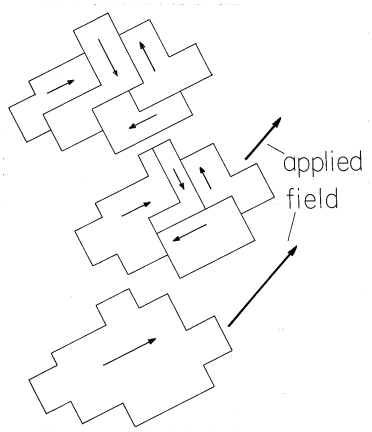


Fig. 9.4.5 Polycrystalline ferromagnetic material viewed at the domain level. In the absence of an applied magnetic field, the domain moments tend to cancel. (This presumes that the material has not been left in a magnetized state by a previously applied field.) As a field is applied, the domain walls shift, giving rise to a net magnetization. In ideal materials, saturation results as all of the domains combine into one. In materials used for bulk fabrication of transformers, imperfections prevent the realization of this state.

not necessarily permanently magnetized. The spontaneous alignment of dipoles is commonly confined to microscopic regions, called domains. The moments of the individual domains are randomly oriented and cancel on a macroscopic scale.

Macroscopic magnetization occurs when a field is applied to a solid, because those domains that have a magnetic dipole moment nearly aligned with the applied field grow at the expense of domains whose magnetic dipole moments are less aligned with the applied field. The shift in domain structure caused by raising the applied field from one level to another is illustrated in Fig. 9.4.5. The domain walls encounter a resistance to propagation that balances the effect of the field.

A typical trajectory traced out in the $B-H$ plane as the field is applied to a typical ferromagnetic material is shown in Fig. 9.4.6. If the magnetization is zero at the outset, the initial trajectory followed as the field is turned up starts at the origin. If the field is then turned down, the domains require a certain degree of coercion to reduce their average magnetization. In fact, with the applied field turned off, there generally remains a flux density, and the field must be reversed to reduce the flux density to zero. The trajectory traced out if the applied field is slowly cycled between positive and negative values many times is the one shown in the figure, with the *remanence flux density* $\mathbf{B}_r$ when $H = 0$ and a *coercive field intensity* $\mathbf{H}_c$ required to make the flux density zero. Some values of these parameters, for materials used to make permanent magnets, are given in Table 9.4.2.

In the toroidal geometry of Example 9.4.1, H is proportional to the terminal current i. Thus, imposition of a sinusoidally varying current results in a sinusoidally varying H, as illustrated in Fig. 9.4.6b. As the i and hence H increases, the trajectory in the $B-H$ plane is the one of increasing H. With decreasing H, a different trajectory is followed. In general, it is not possible to specify B simply by giving H (or even the time derivatives of H). When the magnetization state reflects the previous states of magnetization, the material is said to be *hysteretic*. The $B-H$

TABLE 9.4.2

MAGNETIZATION PARAMETERS FOR PERMANENT MAGNET

From *American Institute of Physics Handbook,* McGraw-Hill, p. 5–188.

Material	H_c (A/m)	B_r (Tesla)
Carbon steel	4000	1.00
Alnico 2	43,000	0.72
Alnico 7	83,500	0.70
Ferroxdur 2	143,000	.34

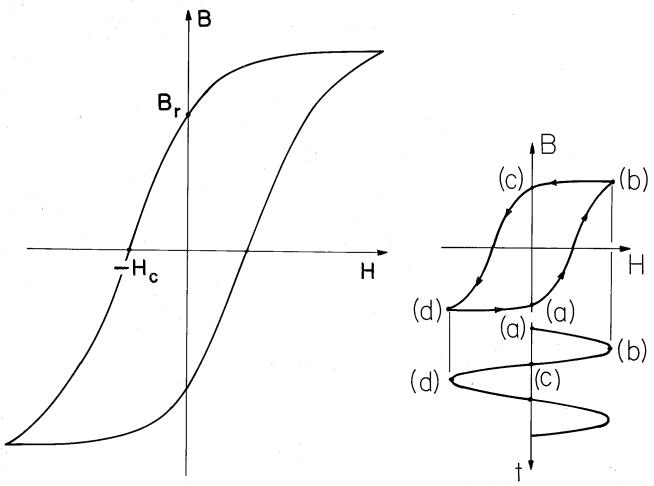


Fig. 9.4.6 Magnetization characteristic for material showing hysteresis with typical values of B_r and H_c given in Table 9.4.2. The curve is obtained after many cycles of sinusoidal excitation in apparatus such as that of Fig. 9.4.3. The trajectory is traced out in response to a sinusoidal current, as shown by the inset.

trajectory representing the response to a sinusoidal H is then called the hysteresis loop.

Hysteresis can be both harmful and useful. Permanent magnetization is one result of hysteresis, and as we illustrated in Example 9.3.2, this can be the basis for the storage of information on tapes. When we develop a picture of energy dissipation in Chap. 11, it will be clear that hysteresis also implies the generation of heat, and this can impose limits on the use of magnetizable materials.

Liquids having significant magnetizabilities have been synthesized by permanently suspending macroscopic particles composed of single ferromagnetic domains.

Here also the relatively high magnetizability comes from the ferromagnetic character of the individual domains. However, the very different way in which the domains interact with each other helps in gaining an appreciation for the magnetization of ferromagnetic polycrystalline solids.

In the absence of a field imposed on the synthesized liquid, the thermal molecular energy randomizes the dipole moments and there is no residual magnetization. With the application of a low frequency H field, the suspended particles assume an average alignment with the field and a single-valued $B - H$ curve is traced out, typically as shown in Fig. 9.4.4. However, as the frequency is raised, the reorientation of the domains lags behind the applied field, and the $B - H$ curve shows hysteresis, much as for solids.

Although both the solid and the liquid can show hysteresis, the two differ in an important way. In the solid, the magnetization shows hysteresis even in the limit of zero frequency. In the liquid, hysteresis results only if there is a finite rate of change of the applied field.

Ferromagnetic materials such as iron are metallic solids and hence tend to be relatively good electrical conductors. As we will see in Chap. 10, this means that unless care is taken to interrupt conduction paths in the material, currents will be induced by a time-varying magnetic flux density. Often, these *eddy currents* are undesired. With the objective of obtaining a highly magnetizable insulating material, iron atoms can be combined into an oxide crystal. Although the spontaneous interaction between molecules that characterizes ferromagnetism is indeed observed, the alignment of neighbors is antiparallel rather than parallel. As a result, such pure oxides do not show strong magnetic properties. However, a mixed-oxide material like Fe_3O_4 (magnetite) is composed of sublattice oxides of differing moments. The spontaneous antiparallel alignment results in a net moment. The class of relatively magnetizable but electrically insulating materials are called *ferrimagnetic*.

Our discussion of the origins of magnetization began at the atomic level, where electronic orbits and spins are fundamental. However, it ends with a discussion of constitutive laws that can only be explained by bringing in additional effects that occur on scales much greater than atomic or molecular. Thus, the macroscopic $\mathbf{B}$ and $\mathbf{H}$ used to describe magnetizable materials can represent averages with respect to scales of domains or of macroscopic particles. In Sec. 9.5 we will make an artificial diamagnetic material from a matrix of "perfectly" conducting particles. In a time-varying magnetic field, a magnetic moment is induced in each particle that tends to cancel that being imposed, as was shown in Example 8.4.3. In fact, the currents induced in the particles and responsible for this induced moment are analogous to the induced changes in electronic orbits responsible on the atomic scale for diamagnetism[1].

9.5 FIELDS IN THE PRESENCE OF MAGNETICALLY LINEAR INSULATING MATERIALS

In this and the next two sections, we study materials with the linear magnetization characteristic of (9.4.4). With the understanding that μ is a prescribed function of position, $\mathbf{B} = \mu\mathbf{H}$, the MQS forms of Ampère's law and the flux continuity law are

$$\boxed{\nabla \times \mathbf{H} = \mathbf{J}} \tag{1}$$

$$\boxed{\nabla \cdot \mu \mathbf{H} = 0} \tag{2}$$

In this chapter, we assume that the current density $\mathbf{J}$ is confined to perfect conductors. We will find in Chap. 10 that a time-varying magnetic flux implies an electric field. Thus, wherever a conducting material finds itself in a time-varying field, there is the possibility that *eddy currents* will be induced. It is for this reason that the magnetizable materials considered in this and the next sections are presumed to be insulating. If the fields of interest vary slowly enough, these induced currents can be negligible.

Ferromagnetic materials are often metallic, and hence also conductors. However, materials can be made both readily magnetizable and insulating by breaking up the conduction paths. By engineering at the molecular or domain scale, or even introducing laminations of magnetizable materials, the material is rendered essentially free of a current density $\mathbf{J}$. The considerations that determine the thickness of laminations used in transformers to prevent eddy currents will be taken up in Chap. 10.

In the regions outside the perfect conductors carrying the current $\mathbf{J}$ of (1), $\mathbf{H}$ is irrotational and $\mathbf{B}$ is solenoidal. Thus, we have a choice of representations. Either, as in Sec. 8.3, we can use the scalar magnetic potential and let $\mathbf{H} = -\nabla\Psi$, or we can follow the lead from Sec. 8.6 and use the vector potential to represent the flux density by letting $\mathbf{B} = \nabla \times \mathbf{A}$.

Where there are discontinuities in the permeability and/or thin coils modeled by surface currents, the continuity conditions associated with Ampère's law and the flux continuity law are used. With $\mathbf{B}$ expressed using the linear magnetization constitutive law, (1.4.16) and (9.2.10) become

$$\boxed{\mathbf{n} \times (\mathbf{H}^a - \mathbf{H}^b) = \mathbf{K}} \tag{3}$$

$$\boxed{\mathbf{n} \cdot (\mu_a \mathbf{H}^a - \mu_b \mathbf{H}^b) = 0} \tag{4}$$

The classification of physical configurations given in Sec. 6.5 for linearly polarizable materials is equally useful here. In the first of these, the region of interest is of uniform permeability. The laws summarized by (1) and (2) are the same as for free space except that μ_o is replaced by μ, so the results of Chap. 6 apply directly. Configurations made up of materials having essentially uniform permeabilities are of the greatest practical interest by far. Thus, piece-wise uniform systems are the theme of Secs. 9.6 and 9.7. The smoothly inhomogeneous systems that are the last category in Fig. 9.5.1 are of limited practical interest. However, it is sometimes useful, perhaps in numerical simulations, to regard the uniform and piece-wise uniform systems as special cases of the smoothly nonuniform systems.

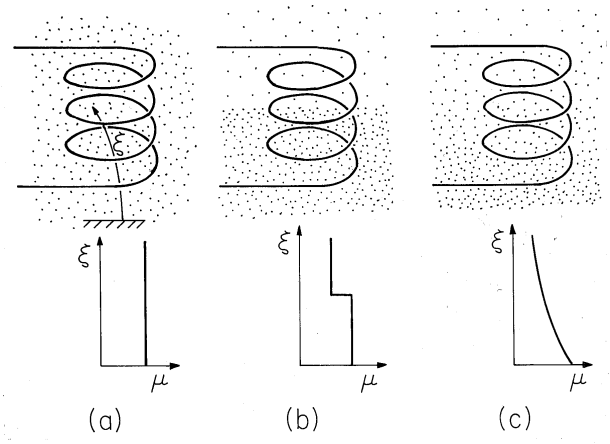


Fig. 9.5.1 (a) Uniform permeability, (b) piece-wise uniform permeability, and (c) smoothly inhomogeneous configurations involving linearly magnetizable material.

Inductance in the Presence of Linearly Magnetizable Materials. In the presence of linearly magnetizable materials, the magnetic flux density is again proportional to the excitation currents. If fields are produced by a single perfectly conducting coil, its inductance is the generalization of that introduced with (8.4.13).

$$L \equiv \frac{\lambda}{i} = \frac{\int_S \mu \mathbf{H} \cdot d\mathbf{a}}{i} \tag{5}$$

The surface S spanning a contour defined by the perfectly conducting wire is the same as that shown in Figs. 8.4.3 and 8.4.4. The effect of having magnetizable material is, of course, represented in (5) by the effect of this material on the intensity, direction, and distribution of $\mathbf{B} = \mu\mathbf{H}$.

For systems in the first category of Fig. 9.5.1, where the entire region occupied by the field is filled by a material of uniform permeability μ, the effect of the magnetization on the inductance is clear. The solutions to (1) and (2) for $\mathbf{H}$ are not altered in the presence of the permeable material. It then follows from (5) that the inductance is simply proportional to μ.

Because it imposes a magnetic field intensity that never leaves the core material, the toroid of Example 9.4.1 is a special case of a piece-wise uniform magnetic material that acts as if all of space were filled with the magnetizable material. As shown by the following example, the inductance of the toroid is therefore also proportional to μ.

Example 9.5.1. Inductance of a Toroid

If the toroidal core of the winding shown in Fig. 9.4.1 and used in the experiment of Fig. 9.4.3 were made a linearly magnetizable material, what would be the voltage needed to supply the driving current i? If we define the flux linkage of the driving coil as λ_1,

$$v = \frac{d\lambda_1}{dt} \tag{6}$$

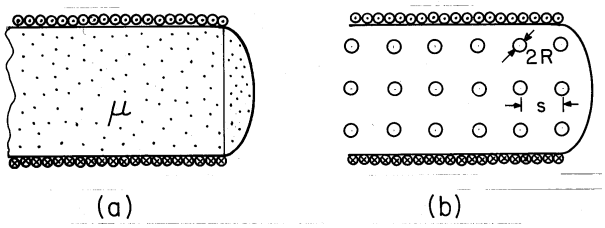


Fig. 9.5.2 (a) Solenoid of length d and radius a filled with material of uniform permeability μ. (b) Solenoid of (a) filled with artificial diamagnetic material composed of an array of metal spheres having radius R and spacing s.

We now find the inductance L, where $\lambda_1 = Li$, and hence determine the required input voltage.

The flux linked by one turn of the driving coil is essentially the cross-sectional area of the toroid multiplied by the flux density. The total flux linked is this quantity multiplied by the total turns N_1.

$$\lambda_1 = N_1\big(\frac{1}{4}\pi w^2\big)B \tag{7}$$

According to the linear constitutive law, the flux density follows from the field intensity as $\mathbf{B} = \mu\mathbf{H}$. For the toroid, H is related to the driving current i by (9.4.1), so

$$B = \mu H = \mu\big(\frac{N_1}{2\pi R}\big)i \tag{8}$$

The desired relation is the combination of these last two expressions.

$$\lambda_1 = Li; \qquad L \equiv \frac{1}{8}\mu\frac{w^2}{R}N_1^2 \tag{9}$$

As predicted, the inductance is proportional to μ. Although inductances are generally increased by bringing paramagnetic and especially ferromagnetic materials into their fields, the effect of introducing ferromagnetic materials into coils can be less dramatic than in the toroidal geometry for reasons discussed in Sec. 9.6. The dependence of the inductance on the square of the turns results because not only is the field induced by the current i proportional to the number of turns, but so too is the amount of the resulting flux that is linked by the coil.

Example 9.5.2. An Artificial Diamagnetic Material

The cross-section of a long (ideally "infinite") solenoid filled with material of uniform permeability is shown in Fig. 9.5.2a. The azimuthal surface current K_ϕ results in an axial magnetic field intensity $H_z = K_\phi$. We presume that the axial length d is very large compared to the radius a of the coil. Thus, the field inside the coil is uniform while that outside is zero. To see that this simple field solution is indeed correct, note that it is both irrotational and solenoidal everywhere except at the surface $r = a$, and that there the boundary conditions, (3) and (4), are satisfied.

For an n-turn coil carrying a current i, the surface current density $K_\phi = ni/d$. Thus, the magnetic field intensity is related to the terminal current by

$$H_z = \frac{ni}{d} \tag{10}$$

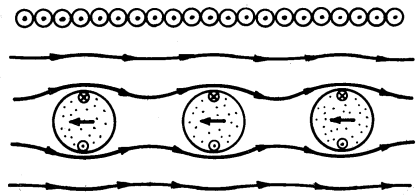


Fig. 9.5.3 Inductance of the coil in Fig. 9.5.2b is decreased because perfectly conducting spheres tend to reduce its effective cross-sectional area.

In the linearly magnetized core region, the flux density is $B_z = \mu H_z$, and so it is also uniform. As a result, the flux linked by each turn is simply $\pi a^2 B_z$ and the total flux linked by the coil is

$$\lambda = n\pi a^2 \mu H_z \tag{11}$$

Substitution from (1) then gives

$$\lambda = Li, \qquad L \equiv \frac{\pi \mu a^2 n^2}{d} \tag{12}$$

where L is the inductance of the coil. Because the coil is assumed to be very long, its inductance is increased by a factor μ/μ_o over that of a coil in free space, much as for the toroid of Example 9.5.1.

Now suppose that the permeable material is actually a cubic array of metal spheres, each having a radius R, as shown in Fig. 9.5.2b. The frequency of the current i is presumably high enough so that each sphere can be regarded as perfectly conducting in the MQS sense discussed in Sec. 8.4. The spacing s of the spheres is large compared to their radius, so that the field of one sphere does not produce an appreciable field at the positions of its neighbors. Each sphere finds itself in an essentially uniform magnetic field.

The dipole moment of the currents induced in a sphere by a magnetic field that is uniform at infinity was calculated in Example 8.4.3, (8.4.21).

$$m = -2\pi H_o R^3 \tag{13}$$

Because the induced currents must produce a field that bucks out the imposed field, a negative moment is induced by a positive field.

By definition, the magnetization density is the number of magnetic moments per unit volume. For a cubic array with spacing s between the sphere centers, the number per unit volume is s^{-3}. Thus, the magnetization density is simply

$$M = Nm = -2\pi H_o \Big(\frac{R}{s}\Big)^3 \tag{14}$$

Comparison of this expression to (9.4.3), which defines the susceptibility χ_m, shows that

$$\chi_m = -2\pi \Big(\frac{R}{s}\Big)^3 \tag{15}$$

As we might have expected from the antiparallel moment induced in a sphere by an imposed field, the susceptibility is negative. The permeability, related to χ_m by (9.4.4), is therefore less than 1.

$$\mu = \mu_o(1 + \chi_m) = \mu_o\Big[1 - 2\pi\Big(\frac{R}{s}\Big)^3\Big] \tag{16}$$

The perfectly conducting spheres effectively reduce the cross-sectional area of the flux, as suggested by Fig. 9.5.3, and hence reduce the inductance. With the introduction of the array of metal spheres, the inductance goes from a value given by (12) with $\mu = \mu_o$ to one with μ given by (16).

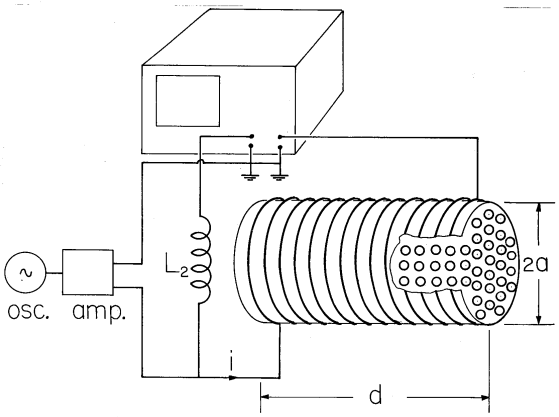


Fig. 9.5.4 Experiment to measure the decrease of inductance that results when the artificial diamagnetic array of Fig. 9.5.2b is inserted into a solenoid.

Faraday's law of induction is also responsible for diamagnetism due to atomic moments. Instead of inducing circulating conduction currents in a metal sphere, as in this example, the time-varying field induces changes in the orbits of electrons about the nucleus that, on the average, contribute an antiparallel magnetic moment to the atom.

The following demonstration is the MQS analog of the EQS Demonstration 6.6.1. In the latter, a measurement was made of the change in capacitance caused by inserting an artificial dielectric between capacitor plates. Here the change in inductance is observed as an artificial diamagnetic material is inserted into a solenoid. Although the spheres are modeled as perfectly conducting in both demonstrations, we will find in Chap. 10 that the requirements to justify this assumption in this MQS example are very different from those for its EQS counterpart.

Demonstration 9.5.1. Artificial Diamagnetic Material

The experiment shown in Fig. 9.5.4 measures the change in solenoid inductance when an array of conducting spheres is inserted. The coil is driven at the angular frequency ω by an oscillator-amplifier. Over the length d shown in the figure, the field tends to be uniform. The circuit shown schematically in Fig. 9.5.5 takes the form of a bridge with the inductive reactance of L_2 used to balance the reactance of the central part of the empty solenoid.

The input resistances of the oscilloscope's balanced amplifiers, represented by R_s, are large compared to the inductor reactances. These branches dominate over the inductive reactances in determining the current through the inductors and, as a result, the inductor currents remain essentially constant as the inductances are varied. With the reactance of the inductor L_2 balancing that of the empty solenoid, these currents are equal and the balanced amplifier voltage $v_o = 0$. When the array of spheres is inserted into the solenoid, the currents through both legs remain essentially constant. Thus, the resulting voltage v_o is the change in voltage across the solenoid

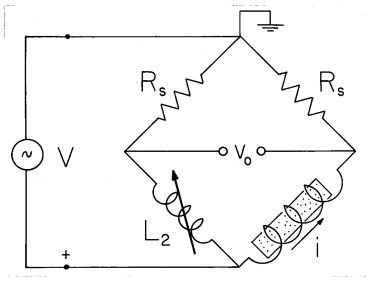


Fig. 9.5.5 Bridge used to measure the change in inductance in the experiment of Fig. 9.5.4.

caused by its change in inductance ΔL.

$$v_o = (\Delta L)\frac{di}{dt} \rightarrow |\hat{v}_o| = \omega(\Delta L)|\hat{i}| \tag{17}$$

In the latter expression, the current and voltage indicated by a circumflex are either peak or rms sinusoidal steady state amplitudes. In view of (12), this expression becomes

$$|\hat{v}_o| = \omega(\mu - \mu_o)\frac{\pi a^2 n^2}{d}|\hat{i}| \tag{18}$$

In terms of the sphere radius and spacing, the change in permeability is given by (16), so the voltage measured by the balanced amplifiers is

$$|\hat{v}_o| = \frac{2\pi^2 \omega a^2 n^2}{d}\left(\frac{R}{s}\right)^3|\hat{i}| \tag{19}$$

To evaluate this expression, we need only the frequency and amplitude of the coil current, the number of turns in the length d, and other dimensions of the system.

Induced Magnetic Charge: Demagnetization. The complete analogy between linearly polarized and linearly magnetized materials is profitably carried yet another step. Magnetic charge is induced where μ is spatially varying, and hence the magnetizable material can introduce sources that revise the free space field distribution. In the linearly magnetizable material, the distribution of these sources is not known until after the fields have been determined. However, it is often helpful in qualitatively predicting the field effects of magnetizable materials to picture the distribution of induced magnetic charges.

Using a vector identity, (2) can be written

$$\mu\nabla \cdot \mathbf{H} + \mathbf{H} \cdot \nabla\mu = 0 \tag{20}$$

Rearrangement of this expression shows that the source of $\mu_o\mathbf{H}$, the magnetic charge density, is

$$\nabla \cdot \mu_o\mathbf{H} = -\frac{\mu_o}{\mu}\mathbf{H} \cdot \nabla\mu \equiv \rho_m \tag{21}$$

Most often we deal with piece-wise uniform systems where variations in μ are confined to interfaces. In that case, it is appropriate to write the continuity of flux density condition in the form

$$\mathbf{n} \cdot \mu_o(\mathbf{H}^a - \mathbf{H}^b) = \mathbf{n} \cdot \mu_o \mathbf{H}^a \big(1 - \frac{\mu_a}{\mu_b}\big) \equiv \sigma_{sm} \tag{22}$$

where σ_{sm} is the magnetic surface charge density. The following illustrates the use of this relation.

Illustration. The Demagnetization Field

A sphere of material having uniform permeability μ is placed in an initially uniform upward-directed field. It is clear from (21) that there are no distortions of the uniform field from magnetic charge induced in the volume of the material. Rather, the sources of induced field are located on the surface where the imposed field has a component normal to the permeability discontinuity. It follows from (22) that positive and negative magnetic surface charges are induced on the top and bottom parts of the surface, respectively.

The **H** field caused by the induced magnetic surface charges originates at the positive charge at the top and terminates on the negative charge at the bottom. This is illustrated by the magnetization analog of the permanently polarized sphere, considered in Example 6.3.1. Our point here is that the field resulting from these induced magnetic surface charges tends to cancel the one imposed. Thus, the field intensity available to magnetize the material is reduced.

The remarks following (6.5.11) apply equally well here. The roles of **E**, **D**, and ϵ are taken by **H**, **B**, and μ. In regions of uniform permeability, (1) and (2) are the same laws considered in Chap. 8, and where the current density is zero, Laplace's equation governs. As we now consider piece-wise nonuniform systems, the effect of the material is accounted for by the continuity conditions.

9.6 FIELDS IN PIECE-WISE UNIFORM MAGNETICALLY LINEAR MATERIALS

Whether we choose to represent the magnetic field in terms of the magnetic scalar potential Ψ or the vector potential **A**, in a current-free region having uniform permeability it assumes a distribution governed by Laplace's equation. That is, where μ is constant and $\mathbf{J} = 0$, (9.5.1) and (9.5.2) require that **H** is both solenoidal and irrotational. If we let $\mathbf{H} = -\nabla\Psi$, the field is automatically irrotational and

$$\boxed{\nabla^2\Psi = 0} \tag{1}$$

is the condition that it be solenoidal. If we let $\mu\mathbf{H} = \nabla\times\mathbf{A}$, the field is automatically solenoidal. The condition that it also be irrotational (together with the requirement that **A** be solenoidal) is then[2]

[2] $\nabla \times \nabla \times \mathbf{A} = \nabla(\nabla \cdot \mathbf{A}) - \nabla^2\mathbf{A}$

$$\boxed{\nabla^2 \mathbf{A} = 0} \tag{2}$$

Thus, in Cartesian coordinates, each component of $\mathbf{A}$ satisfies the same equation as does Ψ.

The methods illustrated for representing piece-wise uniform dielectrics in Sec. 6.6 are applicable here as well. The major difference is that here, currents are used to excite the field whereas there, unpaired charges were responsible for inducing the polarization. The sources are now the current density and surface current density rather than unpaired volume and surface charges. Thus, the external excitations drive the curl of the field, in accordance with (9.5.1) and (9.5.3), rather than its divergence.

The boundary conditions needed at interfaces between magnetically linear materials are

$$\boxed{\mathbf{n} \cdot (\mu_a \mathbf{H}^a - \mu_b \mathbf{H}^b) = 0} \tag{3}$$

for the normal component of the magnetic field intensity, and

$$\boxed{\mathbf{n} \times (\mathbf{H}^a - \mathbf{H}^b) = \mathbf{K}} \tag{4}$$

for the tangential component, in the presence of a surface current. As before, we shall find it convenient to represent windings by equivalent surface currents.

Example 9.6.1. The Spherical Coil with a Permeable Core

The spherical coil developed in Example 8.5.1 is now filled with a uniform core having the permeability μ. With the field intensity again represented in terms of the magnetic scalar potential, $\mathbf{H} = -\nabla\Psi$, the analysis differs only slightly from that already carried out. Laplace's equation, (1), again prevails inside and outside the coil. At the coil surface, the tangential $\mathbf{H}$ again suffers a discontinuity equal to the surface current density in accordance with Ampère's continuity condition, (4). The effect of the permeable material is only felt through the flux continuity condition, (3), which requires that

$$\mu_o H_r^a - \mu H_r^b = 0 \tag{5}$$

Thus, the normal flux continuity condition of (8.5.12) is generalized to include the effect of the permeable material by

$$-\frac{\mu C}{R} = \frac{2\mu_o A}{R} \tag{6}$$

and it follows that the coefficients needed to evaluate Ψ, and hence $\mathbf{H}$, are now

$$A = \frac{Ni}{2\left(1 + \frac{2\mu_o}{\mu}\right)}; \qquad C = -\frac{\mu_o}{\mu}\frac{Ni}{\left(1 + \frac{2\mu_o}{\mu}\right)} \tag{7}$$

Substitution of these coefficients into (8.5.10) and (8.5.11) gives the field inside and outside the spherical coil.

$$\mathbf{H} = \begin{cases} \frac{\mu_o}{\mu}\frac{Ni}{\left(1+\frac{2\mu_o}{\mu}\right)R}(\mathbf{i_r}\cos\theta - \mathbf{i}_\theta\sin\theta) = \frac{\mu_o}{\mu+2\mu_o}\frac{Ni}{R}\mathbf{i_z}; & r<R \\ \frac{Ni}{2\left(1+\frac{2\mu_o}{\mu}\right)R}\left(\frac{R}{r}\right)^3(\mathbf{i_r}2\cos\theta + \mathbf{i}_\theta\sin\theta); & r>R \end{cases} \tag{8}$$

If the coil is highly permeable, these expressions show that the field intensity inside is much less than that outside. In the limit of "infinite permeability," where $\mu_o/\mu \to 0$, the field inside is zero while that outside becomes

$$H_\theta(r=R) = \frac{Ni}{2R}\sin\theta \tag{9}$$

This is the surface current density, (8.5.6). *A surface current density backed by a highly permeable material terminates the tangential magnetic field.* Thus, Ampère's continuity condition relating the fields to each side of the surface is replaced by a boundary condition on the field on the low permeability side of the interface. Using this boundary condition, that H_θ^a be equal to the given K_θ, (8.5.6), the solution for the exterior Ψ and $\mathbf{H}$ can be written by inspection in the limit when $\mu \to \infty$.

$$\Psi_a = \frac{Ni}{2}\left(\frac{R}{r}\right)^2\cos\theta; \qquad \mathbf{H} = \frac{Ni}{2R}\left(\frac{R}{r}\right)^3(\mathbf{i_r}2\cos\theta + \mathbf{i}_\theta\sin\theta) \tag{10}$$

The interior magnetic flux density can in turn be *approximated* by using this exterior field to compute the flux density normal to the surface. Because this flux density must be the same inside, finding the interior field reduces to solving Laplace's equation for Ψ subject to the boundary condition that

$$-\mu\frac{\partial\Psi_b}{\partial r}(r=R) = \mu_o\frac{Ni}{R}\cos\theta \tag{11}$$

Again, the solution represents a uniform field and can be written by inspection.

$$\Psi_b = -\frac{\mu_o}{\mu}Ni\frac{r}{R}\cos\theta \tag{12}$$

The $\mathbf{H}$ field, the gradient of the above expression, is indeed that given by (8a) in the limit where μ_o/μ is small. Note that the interior $\mathbf{H}$ goes to zero as the permeability goes to infinity, but the interior flux density $\mathbf{B}$ remains finite. This fact makes it clear that the inductance of the coil must remain finite, even in the limit where $\mu \to \infty$.

To determine an expression for the inductance that is valid regardless of the core permeability, (8a) can be used to evaluate (8.5.18). Note that the internal flux density $\mathbf{B}$ that replaces $\mu_o H_z$ is $3\mu/[\mu+2\mu_o]$ times larger than the flux density in the absence of the magnetic material. This enhancement factor increases monotonically with the ratio μ/μ_o but reaches a maximum of only 3 in the limit where this ratio goes to infinity. Once again, we have evidence of the core demagnetization caused by the surface magnetic charge induced on the surface of the sphere.

With the uniformity of the field inside the sphere known in advance, a much simpler derivation of (8a) gives further insight into the role of the magnetization.

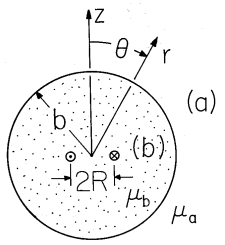


Fig. 9.6.1 Sphere of material having uniform permeability with N-turn coil of radius R at its center. Because $R \ll b$, the coil can be modeled as a dipole. The surrounding region has permeability μ_a.

Thus, in the core, the H-field is the superposition of two fields. The first is caused by the surface current, and given by (8a) with $\mu = \mu_o$.

$$H_i = \frac{Ni}{3R}\mathbf{i_z} \tag{13}$$

The second is due to the uniform magnetization $\mathbf{M} = M\mathbf{i_z}$, which is given by the magnetization analog to (6.3.15) ($\mathbf{E} \to \mathbf{H}$, $\mathbf{P} \to \mu_o\mathbf{M}$, $\epsilon_o \to \mu_o$).

$$\mathbf{H}_M = -\frac{M_o}{3}\mathbf{i_z} \tag{14}$$

The net internal magnetic field intensity is the sum of these.

$$\mathbf{H} = \left(\frac{Ni}{3R} - \frac{M_o}{3}\right)\mathbf{i_z} \tag{15}$$

Only now do we introduce the constitutive law relating M_o to H_z, $M_o = \chi_m H_z$. [In Sec. 9.8 we will exploit the fact that the relation could be nonlinear.] If this law is introduced into (15), and that expression solved for H_z, a result is obtained that is familiar from from (8a).

$$H_z = \frac{Ni/3R}{1 + \frac{1}{3}\chi_m} = \frac{\mu_o}{\mu}\frac{Ni/R}{\left(1 + \frac{2\mu_o}{\mu}\right)} \tag{16}$$

This last calculation again demonstrates how the field $Ni/3R$ is reduced by the magnetization through the "feedback factor" $1/[1 + (\chi_m/3)]$.

Magnetic circuit models, introduced in the next section, exploit the capacity of highly permeable materials to guide the magnetic flux. The example considered next uses familiar solutions to Laplace's equation to illustrate how this guiding takes place. We will make reference to this case study when the subject of magnetic circuits is initiated.

Example 9.6.2. Field Model for a Magnetic Circuit

A small coil with N turns and excited by a current i is used to make a magnetic field in a spherically shaped material of permeability μ_b. As shown in Fig. 9.6.1, the coil has radius R, while the μ sphere has radius b and is surrounded by a magnetic medium of permeability μ_a.

Because the coil radius is small compared to that of the sphere, it will be modeled as a dipole having its moment $m = \pi R^2 i$ in the z direction. It follows from (8.3.13) that the magnetic scalar potential for this dipole is

$$\Psi_{\text{dipole}} = \frac{R^2 N i}{4}\frac{\cos\theta}{r^2} \tag{17}$$

No surface current density exists at the surface of the sphere. Thus, Ampère's continuity law requires that

$$H_\theta^a - H_\theta^b = 0 \rightarrow \Psi_a = \Psi_b \quad \text{at} \quad r = b \tag{18}$$

Also, at the interface, the flux continuity condition is

$$\mu_a H_r^a - \mu_b H_r^b = 0 \quad \text{at} \quad r = b \tag{19}$$

Finally, the only excitation of the field is the coil at the origin, so we require that the field decay to zero far from the sphere.

$$\Psi_a \rightarrow 0 \quad \text{as} \quad r \rightarrow \infty \tag{20}$$

Given that the scalar potential has the θ dependence $\cos(\theta)$, we look for solutions having this same θ dependence. In the exterior region, the solution representing a uniform field is ruled out because there is no field at infinity. In the neighborhood of the origin, we know that Ψ must approach the dipole field. These two conditions are implicit in the assumed solutions

$$\Psi_a = A\frac{\cos\theta}{r^2}; \qquad \Psi_b = \frac{R^2 N i}{4}\frac{\cos\theta}{r^2} + Cr\cos\theta \tag{21}$$

while the coefficients A and C are available to satisfy the two remaining continuity conditions, (18) and (19). Substitution gives two expressions which are linear in A and C and which can be solved to give

$$A = \frac{3}{4}\frac{\mu_b N i R^2}{(\mu_b + 2\mu_a)}; \qquad C = \frac{Ni}{b^3}\frac{R^2(\mu_b - \mu_a)}{2(\mu_b + 2\mu_a)} \tag{22}$$

We thus conclude that the scalar magnetic potential outside the sphere is that of a dipole

$$\Psi_a = \frac{3}{4}\frac{\mu_b N i}{(\mu_b + 2\mu_a)}\left(\frac{R}{r}\right)^2\cos\theta \tag{23}$$

while inside it is that of a dipole plus that of a uniform field.

$$\Psi_b = \frac{Ni}{4}\left[\left(\frac{R}{r}\right)^2\cos\theta + \frac{2(\mu_b - \mu_a)}{(\mu_b + 2\mu_a)}\left(\frac{R}{b}\right)^2\frac{r}{b}\cos\theta\right] \tag{24}$$

For increasing values of the relative permeability, the equipotentials and field lines are shown in Fig. 9.6.2. With $\mu_b/\mu_a = 1$, the field is simply that of the dipole at the origin. In the opposite extreme, where the ratio of permeabilities is 100, it has

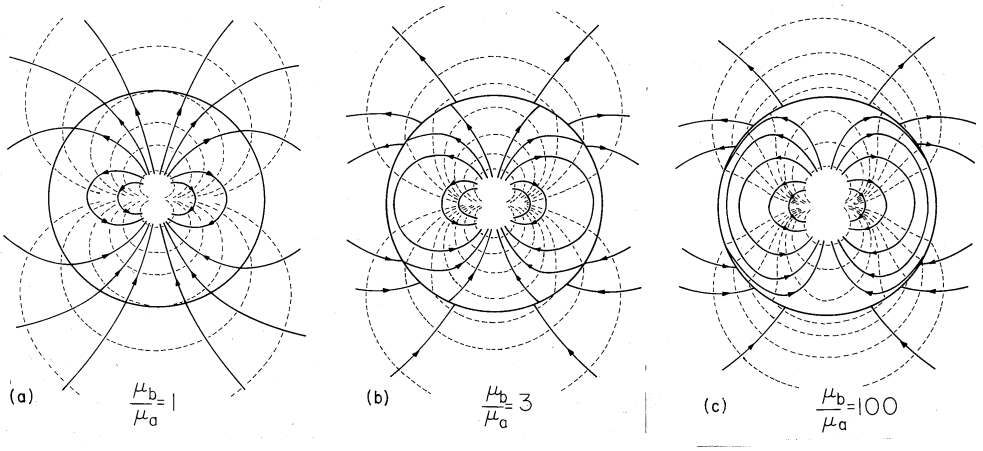


Fig. 9.6.2 Magnetic potential and lines of field intensity in and around the magnetizable sphere of Fig. 9.6.1. (a) With the ratio of permeabilities equal to 1, the dipole field extends into the surrounding free space region without modification. (b) With $\mu_b/\mu_a = 3$, field lines tend to be more confined to the sphere. (c) With $\mu_b/\mu_a = 100$, the field lines (and hence the flux lines) tend to remain inside the sphere.

become clear that the interior field lines tend to become tangential to the spherical surface.

The results of Fig. 9.6.2 can be elaborated by taking the limit of μ_b/μ_a going to infinity. In this limit, the scalar potentials are

$$\Psi_a = \frac{3}{4}Ni\left(\frac{R}{r}\right)^2\cos\theta \tag{25}$$

$$\Psi_b = \frac{Ni}{r}\left(\frac{R}{b}\right)^2\left[\left(\frac{b}{r}\right)^2 + 2\left(\frac{r}{b}\right)\right]\cos\theta \tag{26}$$

In the limit of a large permeability of the medium in which the coil is imbedded relative to that of the surrounding medium, guidance of the magnetic flux occurs by the highly permeable medium. Indeed, in this limit, the flux produced by the coil goes to infinity, whereas the flux of the field $\int \mathbf{H}\cdot d\mathbf{a}$ escaping from the sphere (the so-called "fringing") stays finite, because the exterior potential stays finite. The magnetic flux $\int \mathbf{B}\cdot d\mathbf{a}$ is guided within the sphere, and practically no magnetic flux escapes. The flux lines on the inside surface of the highly permeable sphere can be practically tangential as indeed predicted by (26).

Another limit of interest is when the outside medium is highly permeable and the coil is situated in a medium of low permeability (like free space). In this limit, one obtains

$$\Psi_a = 0 \tag{27}$$

$$\Psi_b = \frac{Ni}{4}\left(\frac{R}{b}\right)^2\left[\left(\frac{b}{r}\right)^2 - \frac{r}{b}\right]\cos\theta \tag{28}$$

The surface at $r = b$ becomes an equipotential of Ψ. The magnetic field is perpendicular to the surface. The highly permeable medium behaves in a way analogous to a perfect conductor in the electroquasistatic case.

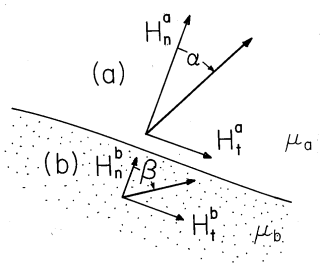


Fig. 9.6.3 Graphical representation of the relations between components of **H** at an interface between a medium of permeability μ_a and a material having permeability μ_b.

In order to gain physical insight, two types of approximate boundary conditions have been illustrated in the previous example. These apply when one region is of much greater permeability than another. In the limit of infinite permeability of one of the regions, the two continuity conditions at the interface between these regions reduce to one boundary condition on the fields in one of the regions. We conclude this section with a summary of these boundary conditions.

At a boundary between regions (a) and (b), having permeabilities μ_a and μ_b, respectively, the normal flux density μH_n is continuous. If there is no surface current density, the tangential components H_t are also continuous. Thus, the magnetic field intensity to either side of the interface is as shown in Fig. 9.6.3. With the angles between **H** and the normal on each side of the interface denoted by α and β, respectively,

$$\tan\alpha = \frac{H_t^a}{H_n^a}; \qquad \tan\beta = \frac{H_t^b}{H_n^b} \tag{29}$$

The continuity conditions can be used to express $\tan(\alpha)$ in terms of the fields on the (b) side of the interface, so it follows that

$$\frac{\tan\alpha}{\tan\beta} = \frac{\mu_a}{\mu_b} \tag{30}$$

In the limit where $\mu_a/\mu_b \to 0$, there are therefore two possibilities. Either $\tan(\alpha) \to 0$, so that $\alpha \to 0$ and **H** in region (a) becomes perpendicular to the boundary, or $\tan(\beta) \to \infty$ so that $\beta \to 90$ degrees and **H** in region (b) becomes tangential to the boundary. Which of these two possibilities pertains depends on the excitation configuration.

Excitation in Region of High Permeability. In these configurations, a closed contour can be found within the highly permeable material that encircles current-carrying wires. For the coil at the center of the highly permeable sphere considered in Example 9.6.2, such a contour is as shown in Fig. 9.6.4. As $\mu_b \to \infty$, the flux density **B** also goes to infinity. In this limit, the flux escaping from the body can be ignored compared to that guided by the body. The boundary is therefore one at which the interior flux density is essentially tangential.

$$\mathbf{n} \cdot \mathbf{B} = 0 \tag{31}$$

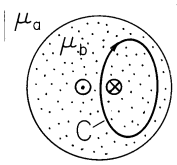


Fig. 9.6.4 Typical contour in configuration of Fig. 9.6.1 encircling current without leaving highly permeable material.

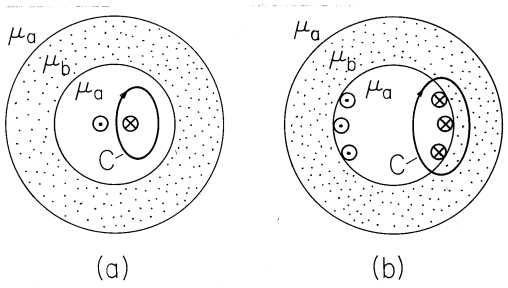


Fig. 9.6.5 (a) With coil in the low permeability region, the contour encircling the current must pass through low permeability material. (b) With coil on the surface between regions, contours encircling current must still leave highly permeable region.

Once the field has been determined in the infinitely permeable material, continuity of tangential **H** is used to provide a boundary condition on the free space side of the interface.

Excitation in Region of Low Permeability. In this second class of configurations, there is no closed contour within the highly permeable material that encircles a current-carrying wire. If the current-carrying wires are within the free space region, as in Fig. 9.6.5a, a contour must leave the highly permeable material to encircle the wire. In the limit where $\mu_b \to \infty$, the magnetic field intensity in the highly permeable material approaches zero, and thus **H** on the interior side of the interface becomes perpendicular to the boundary.

$$\mathbf{n} \times \mathbf{H} = 0 \tag{32}$$

With wires on the interface between regions comprising a surface current density, as illustrated in Fig. 9.6.5b, it is still not possible to encircle the current without following a contour that leaves the highly permeable material. Thus, the case of a surface current is also in this second category. The tangential **H** is terminated by the surface current density. Thus, the boundary condition on **H** on the interior side of the interface carrying the surface current **K** is

$$\mathbf{n} \times \mathbf{H} = \mathbf{K} \tag{33}$$

This boundary condition was illustrated in Example 9.6.1.

Once the fields in the interior region have been found, continuity of normal flux density provides a boundary condition for determining the flux distribution in the highly permeable region.

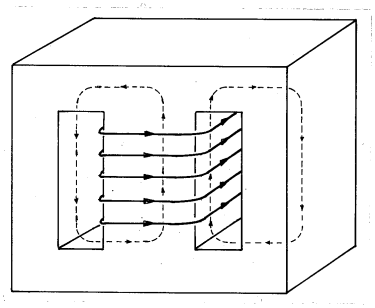


Fig. 9.7.1 Highly magnetizable core in which flux induced by winding can circulate in two paths.

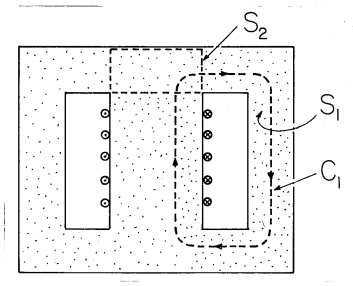


Fig. 9.7.2 Cross-section of highly permeable core showing contour C_1 spanned by surface S_1, used with Ampére's integral law, and closed surface S_2, used with the integral flux continuity law.

9.7 MAGNETIC CIRCUITS

The availability of relatively inexpensive magnetic materials, with magnetic susceptibilities of the order of 1000 or more, allows the production of high magnetic flux densities with relatively small currents. Devices designed to exploit these materials include compact inductors, transformers, and rotating machines. Many of these are modeled as the magnetic circuits that are the theme of this section.

A magnetic circuit typical of transformer cores is shown in Fig. 9.7.1. A core of high permeability material has a pair of rectangular windows cut through its center. Wires passing through these windows are wrapped around the central column. The flux generated by this coil tends to be guided by the magnetizable material. It passes upward through the center leg of the material, and splits into parts that circulate through the legs to left and right.

Example 9.6.2, with its highly permeable sphere excited by a small coil, offered the opportunity to study the trapping of magnetic flux. Here, as in that case with $\mu_b/\mu_a \gg 1$, the flux density inside the core tends to be tangential to the surface. Thus, the magnetic flux density is guided by the material and the field distribution within the core tends to be independent of the exterior configuration.

In situations of this type, where the ducting of the magnetic flux makes it possible to approximate the distribution of magnetic field, the MQS integral laws serve much the same purpose as do Kirchhoff's laws for electrical circuits.

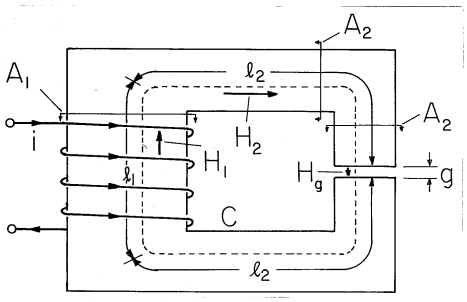


Fig. 9.7.3 Cross-section of magnetic circuit used to produce a magnetic field intensity H_g in an air gap.

The MQS form of Ampère's integral law applies to a contour, such as C_1 in Fig. 9.7.2, following a path of circulating magnetic flux.

$$\oint_{C_1} \mathbf{H} \cdot d\mathbf{s} = \int_{S_1} \mathbf{J} \cdot d\mathbf{a} \tag{1}$$

The surface enclosed by this contour in Fig. 9.7.2 is pierced N times by the current carried by the wire, so the surface integral of the current density on the right in (1) is, in this case, Ni. The same equation could be written for a contour circulating through the left leg, or for one circulating around through the outer legs. Note that the latter would enclose a surface S through which the net current would be zero.

If Ampère's integral law plays a role analogous to Kirchhoff's voltage law, then the integral law expressing continuity of magnetic flux is analogous to Kirchhoff's current law. It requires that through a closed surface, such as S_2 in Fig. 9.7.2, the net magnetic flux is zero.

$$\oint_{S_2} \mathbf{B} \cdot d\mathbf{a} = 0 \tag{2}$$

As a result, the flux entering the closed surface S_2 in Fig. 9.7.2 through the central leg must be equal to that leaving to left and right through the upper legs of the magnetic circuit. We will return to this particular magnetic circuit when we discuss transformers.

Example 9.7.1. The Air Gap Field of an Electromagnet

The magnetic circuit of Fig. 9.7.3 might be used to produce a high magnetic field intensity in the narrow air gap. An N-turn coil is wrapped around the left leg of the highly permeable core. Provided that the length g of the air gap is not too large, the flux resulting from the current i in this winding is largely guided along the magnetizable material.

By approximating the fields in sections of the circuit as being essentially uniform, it is possible to use the integral laws to determine the field intensity in the gap. In the left leg, the field is approximated by the constant H_1 over the length l_1 and cross-sectional area A_1. Similarly, over the lengths l_2, which have the cross-sectional areas A_2, the field intensity is approximated by H_2. Finally, under the assumption that the gap width g is small compared to the cross-sectional dimensions of the gap, the field in the gap is represented by the constant H_g. The line

integral of **H** in Ampère's integral law, (1), is then applied to the contour C that follows the magnetic field intensity around the circuit to obtain the left-hand side of the expression

$$H_1 l_l + 2H_2 l_2 + gH_g = Ni \tag{3}$$

The right-hand side of this equation represents the surface integral of $\mathbf{J} \cdot \mathbf{da}$ for a surface S having this contour as its edge. The total current through the surface is simply the current through one wire multiplied by the number of times it pierces the surface S.

We presume that the magnetizable material is operated under conditions of magnetic linearity. The constitutive law then relates the flux density and field intensity in each of the regions.

$$B_1 = \mu H_1; \quad B_2 = \mu H_2; \quad B_g = \mu_o H_g \tag{4}$$

Continuity of magnetic flux, (2), requires that the total flux through each section of the circuit be the same. With the flux densities expressed using (4), this requires that

$$A_1 \mu H_1 = A_2 \mu H_2 = A_2 \mu_o H_g \tag{5}$$

Our objective is to determine H_g. To that end, (5) is used to write

$$H_2 = \frac{\mu_o}{\mu} H_g; \qquad H_1 = \frac{\mu_o}{\mu} \frac{A_2}{A_1} H_g \tag{6}$$

and these relations used to eliminate H_1 and H_2 in favor of H_g in (3). From the resulting expression, it follows that

$$H_g = \frac{Ni}{\left(\frac{\mu_o}{\mu}\frac{A_2}{A_1} l_1 + \frac{2\mu_o}{\mu} l_2 + g\right)} \tag{7}$$

Note that in the limit of infinite core permeability, the gap field intensity is simply Ni/g.

If the magnetic circuit can be broken into sections in which the field intensity is essentially uniform, then the fields may be determined from the integral laws. The previous example is a case in point. A more general approach is required if the core is of complex geometry or if a more accurate model is required.

We presume throughout this chapter that the magnetizable material is sufficiently insulating so that even if the fields are time varying, there is no current density in the core. As a result, the magnetic field intensity in the core can be represented in terms of the scalar magnetic potential introduced in Sec. 8.3.

$$\mathbf{H} = -\nabla \Psi \tag{8}$$

According to Ampère's integral law, (1), integration of $\mathbf{H} \cdot d\mathbf{s}$ around a closed contour must be equal to the "Ampère turns" Ni passing through the surface spanning the contour. With **H** expressed in terms of Ψ, integration from (a) to (b) around a contour such as C in Fig. 9.7.4, which encircles a net current equal to the product of the turns N and the current per turn i, gives $\Psi_a - \Psi_b \equiv \Delta\Psi = Ni$. With (a) and (b) adjacent to each other, it is clear that Ψ is multiple-valued. To specify the principal value of this multiple-valued function we must introduce a

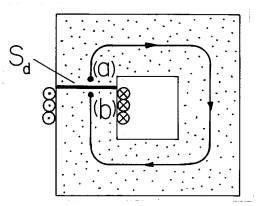


Fig. 9.7.4 Typical magnetic circuit configuration in which the magnetic scalar potential is first determined inside the highly magnetizable material. The principal value of the multivalued scalar potential inside the core is taken by not crossing the surface S_d.

discontinuity in Ψ somewhere along the contour. In the circuit of Fig. 9.7.4, this discontinuity is defined to occur across the surface S_d.

To make the line integral of $\mathbf{H} \cdot d\mathbf{s}$ from any point just above the surface S_d around the circuit to a point just below the surface equal to Ni, the potential is required to suffer a discontinuity $\Delta\Psi = Ni$ across S_d. Everywhere inside the magnetic material, Ψ satisfies Laplace's equation. If, in addition, the normal flux density on the walls of the magnetizable material is required to vanish, the distribution of Ψ within the core is uniquely determined. Note that only the discontinuity in Ψ is specified on the surface S_d. The magnitude of Ψ on one side or the other is not specified. Also, the normal derivative of Ψ, which is proportional to the normal component of $\mathbf{H}$, must be continuous across S_d.

The following simple example shows how the scalar magnetic potential can be used to determine the field inside a magnetic circuit.

Example 9.7.2. The Magnetic Potential inside a Magnetizable Core

The core of the magnetic circuit shown in Fig. 9.7.5 has outer and inner radii a and b, respectively, and a length d in the z direction that is large compared to a. A current i is carried in the z direction through the center hole and returned on the outer periphery by N turns. Thus, the integral of $\mathbf{H} \cdot d\mathbf{s}$ over a contour circulating around the magnetic circuit must be Ni, and a surface of discontinuity S_d is arbitrarily introduced as shown in Fig. 9.7.5. With the boundary condition of no flux leakage, $\partial\Psi/\partial r = 0$ at $r = a$ and at $r = b$, the solution to Laplace's equation within the core is uniquely specified.

In principle, the boundary value problem can be solved even if the geometry is complicated. For the configuration shown in Fig. 9.7.5, the requirement of no radial derivative suggests that Ψ is independent of r. Thus, with A an arbitrary coefficient, a reasonable guess is

$$\Psi = A\phi = -Ni\left(\frac{\phi}{2\pi}\right) \tag{9}$$

The coefficient A has been selected so that there is indeed a discontinuity Ni in Ψ between $\phi = 2\pi$ and $\phi = 0$.

The magnetic field intensity given by substituting (9) into (8) is

$$\mathbf{H} = \frac{A}{r}\mathbf{i}_\phi = \frac{Ni}{2\pi r}\mathbf{i}_\phi \tag{10}$$

Note that $\mathbf{H}$ is continuous, as it should be.

Now that the inside field has been determined, it is possible, in turn, to find the fields in the surrounding free space regions. The solution for the inside field, together

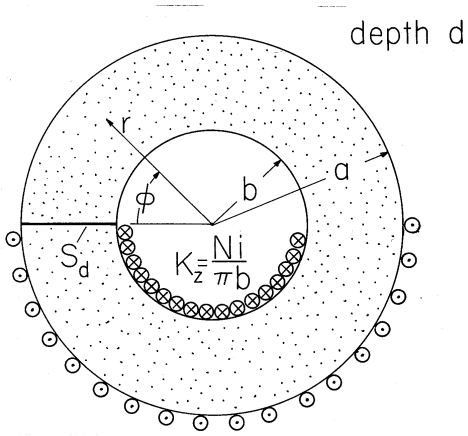


Fig. 9.7.5 Magnetic circuit consisting of a core having the shape of a circular cylindrical annulus with an N-turn winding wrapped around half of its circumferential length. The length of the system into the paper is very long compared to the outer radius a.

with the given surface current distribution at the boundary between regions, provides the tangential field at the boundaries of the outside regions. Within an arbitrary constant, a boundary condition on Ψ is therefore specified. In the outside regions, there is no closed contour that both stays within the region and encircles current. In these regions, Ψ is continuous. Thus, the problem of finding the "leakage" fields is reduced to finding the boundary value solution to Laplace's equation.

This inside-outside approach gives an approximate field distribution that is justified only if the relative permeability of the core is very large. Once the outside field is approximated in this way, it can be used to predict how much flux has left the magnetic circuit and hence how much error there is in the calculation. Generally, the error will be found to depend not only on the relative permeability but also on the geometry. If the magnetic circuit is composed of legs that are long and thin, then we would expect the leakage of flux to be large and the approximation of the inside-outside approach to become invalid.

Electrical Terminal Relations and Characteristics. Practical inductors (chokes) often take the form of magnetic circuits. With more than one winding on the same magnetic circuit, the magnetic circuit serves as the core of a transformer. Figure 9.7.6 gives the schematic representation of a transformer. Each winding is modeled as perfectly conducting, so its terminal voltage is given by (9.2.12).

$$v_1 = \frac{d\lambda_1}{dt}; \qquad v_2 = \frac{d\lambda_2}{dt} \tag{11}$$

However, the flux linked by one winding is due to two currents. If the core is magnetically linear, we have a flux linked by the first coil that is the sum of a flux linkage $L_{11}i_1$ due to its own current and a flux linkage L_{12} due to the current in the second winding. The situation for the second coil is similar. Thus, the flux linkages are related to the terminal currents by an *inductance matrix*.

$$\begin{bmatrix} \lambda_1 \\ \lambda_2 \end{bmatrix} = \begin{bmatrix} L_{11} & L_{12} \\ L_{21} & L_{22} \end{bmatrix} \begin{bmatrix} i_1 \\ i_2 \end{bmatrix} \tag{12}$$

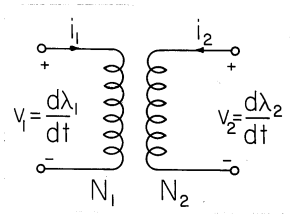


Fig. 9.7.6 Circuit representation of a transformer as defined by the terminal relations of (12) or of an ideal transformer as defined by (13).

The coefficients L_{ij} are functions of the core and coil geometries and properties of the material, with L_{11} and L_{22} the familiar *self-inductances* and L_{12} and L_{21} the *mutual inductances*.

The word "transformer" is commonly used in two ways, each often represented schematically, as in Fig. 9.7.6. In the first, the implication is only that the terminal relations are as summarized by (12). In the second usage, where the device is said to be an *ideal transformer*, the terminal relations are given as voltage and current ratios. For an ideal transformer,

$$\frac{i_2}{i_1} = -\frac{N_1}{N_2}; \qquad \frac{v_2}{v_1} = \frac{N_2}{N_1} \tag{13}$$

Presumably, such a device can serve to step up the voltage while stepping down the current. The relationships between terminal voltages and between terminal currents is linear, so that such a device is "ideal" for processing signals.

The magnetic circuit developed in the next example is that of a typical transformer. We have two objectives. First, we determine the inductances needed to complete (12). Second, we define the conditions under which such a transformer operates as an ideal transformer.

Example 9.7.3. A Transformer

The core shown in Fig. 9.7.7 is familiar from the introduction to this section, Fig. 9.7.1. The "windows" have been filled up by a pair of windings, having the turns N_1 and N_2, respectively. They share the center leg of the magnetic circuit as a common core and generate a flux that circulates through the branches to either side.

The relation between the terminal voltages for an ideal transformer depends only on unity coupling between the two windings. That is, if we call Φ_λ the magnetic flux through the center leg, the flux linking the respective coils is

$$\lambda_1 = N_1\Phi_\lambda; \qquad \lambda_2 = N_2\Phi_\lambda \tag{14}$$

These statements presume that there is no leakage flux which would link one coil but bypass the other.

In terms of the magnetic flux through the center leg, the terminal voltages follow from (14) as

$$v_1 = N_1\frac{d\Phi_\lambda}{dt}; \qquad v_2 = N_2\frac{d\Phi_\lambda}{dt} \tag{15}$$

From these expressions, without further restrictions on the mode of operation, follows the relation between the terminal voltages of (13).

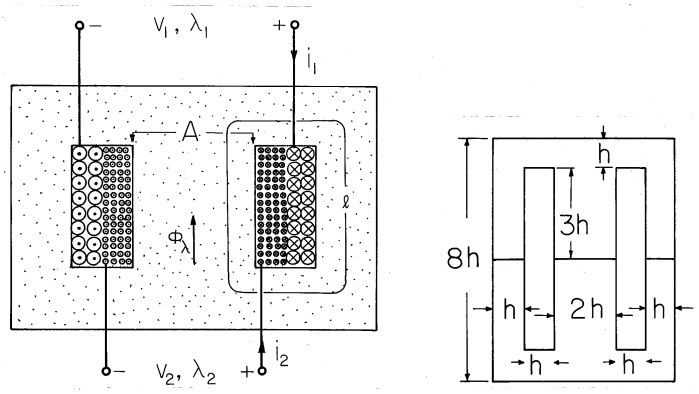


Fig. 9.7.7 In a typical transformer, coupling is optimized by wrapping the primary and secondary on the same core. The inset shows how full use is made of the magnetizable material in the core manufacture.

We now use the integral laws to determine the flux linkages in terms of the currents. Because it is desirable to minimize the peak magnetic flux density at each point throughout the core, and because the flux through the center leg divides evenly between the two circuits, the cross-sectional areas of the return legs are made half as large as that of the center leg.[3] As a result, the magnitude of $\mathbf{B}$, and hence $\mathbf{H}$, can be approximated as constant throughout the core. [Note that we have now used the flux continuity condition of (2).]

With the average length of a circulating magnetic field line taken as l, Ampère's integral law, (1), gives

$$Hl = N_1 i_1 + N_2 i_2 \tag{16}$$

In view of the presumed magnetic linearity of the core, the flux through the cross-sectional area A of the center leg is

$$\Phi_\lambda = AB = A\mu H \tag{17}$$

and it follows from these last two expressions that

$$\Phi_\lambda = \frac{A\mu N_1}{l} i_1 + \frac{A\mu N_2}{l} i_2. \tag{18}$$

Multiplication by the turns N_1 and then N_2, respectively, gives the flux linkages λ_1 and λ_2.

$$\lambda_1 = \left(\frac{A\mu N_1^2}{l}\right) i_1 + \left(\frac{A\mu N_1 N_2}{l}\right) i_2$$

$$\lambda_2 = \left(\frac{A\mu N_1 N_2}{l}\right) i_1 + \left(\frac{A\mu N_2^2}{l}\right) i_2 \tag{19}$$

[3] To optimize the usage of core material, the relative dimensions are often taken as in the inset to Fig. 9.7.7. Two cores are cut from rectangular sections measuring $6h \times 8h$. Once the windows have been removed, the rectangle is cut in two, forming two "E" cores which can then be combined with the "I's" to form two complete cores. To reduce eddy currents, the core is often made from varnished laminations. This will be discussed in Chap. 10.

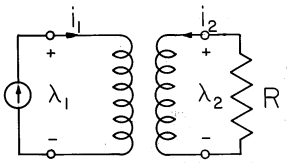


Fig. 9.7.8 Transformer with a load resistance R that includes the internal resistance of the secondary winding.

Comparison of this expression with (12) identifies the self- and mutual inductances as

$$L_{11} = \frac{A\mu N_1^2}{l}; \quad L_{22} = \frac{A\mu N_2^2}{l}; \quad L_{12} = L_{21} = \frac{A\mu N_1 N_2}{l} \tag{20}$$

Note that the mutual inductances are equal. In Sec. 11.7, we shall see that this is a consequence of energy conservation. Also, the self-inductances are related to either mutual inductance by

$$\sqrt{L_{11}L_{22}} = L_{12} \tag{21}$$

Under what conditions do the terminal currents obey the relations for an "ideal transformer"?

Suppose that the (1) terminals are selected as the "primary" terminals of the transformer and driven by a current source $I(t)$, and that the terminals of the (2) winding, the "secondary," are connected to a resistive load R. To recognize that the winding in fact has an internal resistance, this load includes the winding resistance as well. The electrical circuit is as shown in Fig. 9.7.8.

The secondary circuit equation is

$$-i_2 R = \frac{d\lambda_2}{dt} \tag{22}$$

and using (12) with $i_1 = I$, it follows that the secondary current i_2 is governed by

$$L_{22}\frac{di_2}{dt} + i_2 R = -L_{21}\frac{dI}{dt} \tag{23}$$

For purposes of illustration, consider the response to a drive that is in the sinusoidal steady state. With the drive angular frequency equal to ω, the response has the same time dependence in the steady state.

$$I = Re\ \hat{I}e^{j\omega t} \Rightarrow i_2 = Re\ \hat{i}_2 e^{j\omega t} \tag{24}$$

Substitution into (23) then shows that the complex amplitude of the response is

$$\hat{i}_2 = -\frac{j\omega L_{21}\hat{I}}{j\omega L_{22} + R} = -\frac{N_1}{N_2}\hat{i}_1 \frac{1}{1 + \frac{R}{j\omega L_{22}}} \tag{25}$$

The ideal transformer-current relation is obtained if

$$\frac{\omega L_{22}}{R} \gg 1 \tag{26}$$

In that case, (25) reduces to

$$\hat{i}_2 = -\frac{N_1}{N_2}\hat{i}_1 \tag{27}$$

When the ideal transformer condition, (26), holds, the first term on the left in (23) overwhelms the second. What remains if the resistance term is neglected is the statement

$$\frac{d}{dt}(L_{21}i_1 + L_{22}i_2) = \frac{d\lambda_2}{dt} = 0 \tag{28}$$

We conclude that *for ideal transformer operation, the flux linkages are negligible.* This is crucial to having a transformer behave as a linear device. Whether represented by the inductance matrix of (12) or by the ideal relations of (13), linear operation hinges on having a linear relation between $\mathbf{B}$ and $\mathbf{H}$ in the core, (17). By operating in the regime of (26) so that $\mathbf{B}$ is small enough to avoid saturation, (17) tends to remain valid.

9.8 SUMMARY

The magnetization density $\mathbf{M}$ represents the density of magnetic dipoles. The moment $\mathbf{m}$ of a single microscopic magnetic dipole was defined in Sec. 8.2. With $\mu_o\mathbf{m} \leftrightarrow \mathbf{p}$ where $\mathbf{p}$ is the moment of an electric dipole, the magnetic and electric dipoles play analogous roles, and so do the H and E fields. In Sec. 9.1, it was therefore natural to define the magnetization density so that it played a role analogous to the polarization density, $\mu_o\mathbf{M} \leftrightarrow \mathbf{P}$. As a result, the magnetic charge density ρ_m was considered to be a source of $\nabla \cdot \mu_o\mathbf{H}$. The relations of these sources to the magnetization density are the first expressions summarized in Table 9.8.1. The second set of relations are different forms of the flux continuity law, including the effect of magnetization. If the magnetization density is given, (9.2.2) and (9.2.3) are most useful. However, if $\mathbf{M}$ is induced by $\mathbf{H}$, then it is convenient to introduce the magnetic flux density $\mathbf{B}$ as a variable. The correspondence between the fields due to magnetization and those due to polarization is $\mathbf{B} \leftrightarrow \mathbf{D}$.

The third set of relations pertains to linearly magnetizable materials. There is no magnetic analog to the unpaired electric charge density.

In this chapter, the MQS form of Ampère's law was also required to determine $\mathbf{H}$.

$$\nabla \times \mathbf{H} = \mathbf{J} \tag{1}$$

In regions where $\mathbf{J}$=0, $\mathbf{H}$ is indeed analogous to $\mathbf{E}$ in the polarized EQS systems of Chap. 6. In any case, if $\mathbf{J}$ is given, or if it is on perfectly conducting surfaces, its contribution to the magnetic field intensity is determined as in Chap. 8.

In Chap. 10, we introduce the additional laws required to determine $\mathbf{J}$ self-consistently in materials of finite conductivity. To do this, it is necessary to give careful attention to the electric field associated with MQS fields. In this chapter, we have generalized Faraday's law, (9.2.11),

$$\nabla \times \mathbf{E} = -\frac{\partial \mathbf{B}}{\partial t} \tag{2}$$

so that it can be used to determine $\mathbf{E}$ in the presence of magnetizable materials. Chapter 10 brings this law to the fore as it plays a key role in determining the self-consistent $\mathbf{J}$.

TABLE 9.8.1
SUMMARY OF MAGNETIZATION RELATIONS AND LAWS

Magnetization Charge Density and Magnetization Density			
$\rho_m \equiv -\nabla \cdot \mu_o \mathbf{M}$	(9.2.4)	$\sigma_{sm} = -\mathbf{n} \cdot \mu_o(\mathbf{M}^a - \mathbf{M}^b)$	(9.2.5)
Magnetic Flux Continuity with Magnetization			
$\nabla \cdot \mu_o \mathbf{H} = \rho_m$	(9.2.2)	$\mathbf{n} \cdot \mu_o(\mathbf{H}^a - \mathbf{H}^b) = \sigma_{sm}$	(9.2.3)
$\nabla \cdot \mathbf{B} = 0$	(9.2.9)	$\mathbf{n} \cdot (\mathbf{B}^a - \mathbf{B}^b) = 0$	(9.2.10)
where			
$\mathbf{B} \equiv \mu_o(\mathbf{H} + \mathbf{M})$	(9.2.8)		
Magnetically Linear Magnetization			
Constitutive law			
$\mathbf{M} = \chi_m \mathbf{H}; \chi_m \equiv \dfrac{\mu}{\mu_o} - 1$	(9.4.3)		
$\mathbf{B} = \mu \mathbf{H}$	(9.4.4)		
Magnetization source distribution			
$\rho_m = -\dfrac{\mu_o}{\mu} \mathbf{H} \cdot \nabla \mu$	(9.5.21)	$\sigma_{sm} = \mathbf{n} \cdot \mu_o \mathbf{H}^a \left(1 - \dfrac{\mu_a}{\mu_b}\right)$	(9.5.22)

REFERENCES

[1] Purcell, E. M., **Electricity and Magnetism**, McGraw-Hill Book Co., N. Y., 2nd Ed., (1985), p. 413.

PROBLEMS

9.2 Laws and Continuity Conditions with Magnetization

9.2.1 Return to Prob. 6.1.1 and replace $\mathbf{P} \rightarrow \mathbf{M}$. Find ρ_m and σ_{sm}.

9.2.2* A circular cylindrical rod of material is uniformly magnetized in the y' direction transverse to its axis, as shown in Fig. P9.2.2. Thus, for $r < R$, $\mathbf{M} = M_o[\mathbf{i_x} \sin\gamma + \mathbf{i_y} \cos\gamma]$. In the surrounding region, the material forces $\mathbf{H}$ to be zero. (In Sec. 9.6, it will be seen that such a material is one of infinite permeability.)

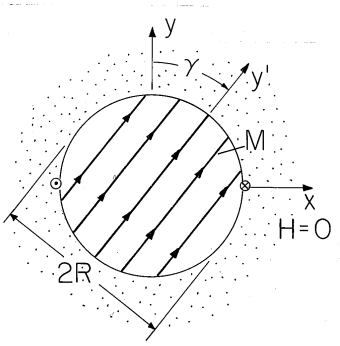


Fig. P9.2.2

(a) Show that if $\mathbf{H} = \mathbf{0}$ everywhere, both Ampère's law and (9.2.2) are satisfied.

(b) Suppose that the cylinder rotates with the angular velocity Ω so that $\gamma = \Omega t$. Then, $\mathbf{B}$ is time varying even though there is no $\mathbf{H}$. A one-turn rectangular coil having depth d in the z direction has legs running parallel to the z axis in the $+z$ direction at $x = -R$, $y = 0$ and in the $-z$ direction at $x = R$, $y = 0$. The other legs of the coil are perpendicular to the z axis. Show that the voltage induced at the terminals of this coil by the time-varying magnetization density is $v = -\mu_o 2RdM_o\Omega \sin\Omega t$.

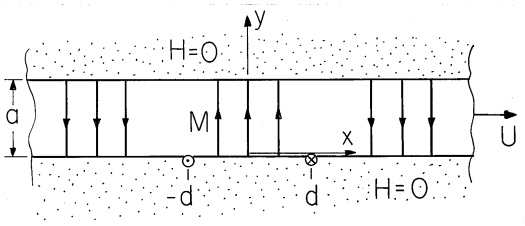


Fig. P9.2.3

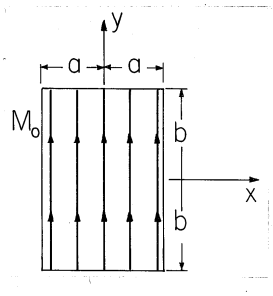


Fig. P9.3.1

9.2.3 In a region between the planes $y = a$ and $y = 0$, a material that moves in the x direction with velocity U has the magnetization density $\mathbf{M} = M_o\mathbf{i_y}\cos\beta(x - Ut)$, as shown in Fig. P9.2.2. The regions above and below are constrained so that $\mathbf{H} = \mathbf{0}$ there and so that the integral of $\mathbf{H}\cdot d\mathbf{s}$ between $y = 0$ and $y = a$ is zero. (In Sec. 9.7, it will be clear that these materials could be the pole faces of a highly permeable magnetic circuit.)

(a) Show that Ampère's law and (9.2.2) are satisfied if $\mathbf{H} = \mathbf{0}$ throughout the magnetizable layer of material.

(b) A one-turn rectangular coil is located in the $y = 0$ plane, one leg running in the $+z$ direction at $x = -d$ (from $z = 0$ to $z = l$) and another running in the $-z$ direction at $x = d$ (from $z = l$ to $z = 0$). What is the voltage induced at the terminals of this coil by the motion of the layer?

9.3 Permanent Magnetization

9.3.1* The magnet shown in Fig. P9.3.1 is much longer in the $\pm z$ directions than either of its cross-sectional dimensions $2a$ and $2b$. Show that the scalar magnetic potential is

$$\begin{aligned}\Psi = \frac{M_o}{2\pi}\Bigg\{ & (x-a)ln\frac{\sqrt{(x-a)^2+(y-b)^2}}{\sqrt{(x-a)^2+(y+b)^2}} \\ & -(x+a)ln\frac{\sqrt{(x+a)^2+(y-b)^2}}{\sqrt{(x+a)^2+(y+b)^2}} \\ & +(y-b)\left[\tan^{-1}\left(\frac{x-a}{y-b}\right)-\tan^{-1}\left(\frac{x+a}{y-b}\right)\right] \\ & -(y+b)\left[\tan^{-1}\left(\frac{x-a}{y+b}\right)-\tan^{-1}\left(\frac{x+a}{y+b}\right)\right]\Bigg\}\end{aligned} \qquad (a)$$

(Note Example 4.5.3.)

9.3.2* In the half-space $y > 0$, $\mathbf{M} = M_o \cos(\beta x) \exp(-\alpha y)\mathbf{i_y}$, where α and β are given positive constants. The half-space $y < 0$ is free space. Show that

$$\Psi = \frac{M_o}{2} \begin{cases} \left[\frac{-2\alpha}{\alpha^2 - \beta^2} e^{-\alpha y} + \frac{e^{-\beta y}}{\alpha - \beta} \right] \cos \beta x; & y > 0 \\ -\frac{e^{\beta y}}{\alpha + \beta} \cos \beta x; & y < 0 \end{cases} \qquad (a)$$

9.3.3 In the half-space $y < 0$, $\mathbf{M} = M_o \sin(\beta x) \exp(\alpha y)\mathbf{i_x}$, where α and β are positive constants. The half-space $y > 0$ is free space. Find the scalar magnetic potential.

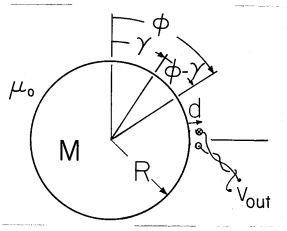


Fig. P9.3.4

9.3.4 For storage of information, the cylinder shown in Fig. P9.3.4 has the magnetization density

$$\mathbf{M} = M_o (r/R)^{p-1} [\mathbf{i_r} \cos p(\phi - \gamma) - \mathbf{i}_\phi \sin p(\phi - \gamma)] \qquad (a)$$

where p is a given integer. The surrounding region is free space.

(a) Determine the magnetic potential Ψ.
(b) A magnetic pickup is comprised of an N-turn coil located at $\phi = \pi/2$. This coil has a dimension a in the ϕ direction that is small compared to the periodicity length $2\pi R/p$ in that direction. Every turn is essentially at the radius $d + R$. Determine the output voltage v_{out} when the cylinder rotates, $\gamma = \Omega t$.
(c) Show that if the density of information on the cylinder is to be high (p is to be high), then the spacing between the coil and the cylinder, d, must be small.

9.4 Magnetization Constitutive Laws

9.4.1* The toroidal core of Example 9.4.1 and Demonstration 9.4.1 is filled by a material having the single-valued magnetization characteristic $\mathbf{M} = M_o \tanh(\alpha H)$, where $\mathbf{M}$ and $\mathbf{H}$ are collinear.

(a) Show that the $B - H$ characteristic is of the type illustrated in Fig. 9.4.4.

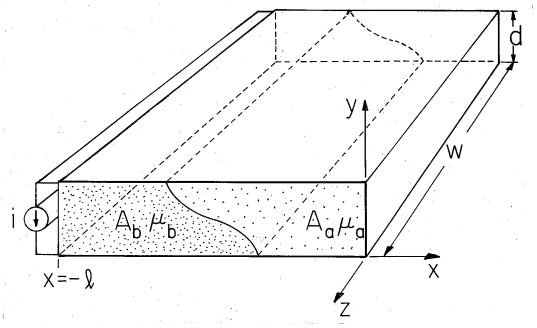


Fig. P9.5.1

(b) Show that if $i = i_o \cos \omega t$, the output voltage is

$$v = \frac{\mu_o \pi w^2 N_2}{4} \frac{d}{dt}\left[\frac{N_1 i_o}{2\pi R}\cos \omega t + M_o \tanh\left(\frac{\alpha N_1 i_o}{2\pi R}\cos \omega t\right)\right] \qquad (a)$$

(c) Show that the characteristic is essentially linear, provided that $\alpha N_1 i_o / 2\pi R \ll 1$.

9.4.2 The toroidal core of Demonstration 9.4.1 is driven by a sinusoidal current $i(t)$ and responds with the hysteresis characteristic of Fig. 9.4.6. Make qualitative sketches of the time dependence of

(a) $B(t)$
(b) the output voltage $v(t)$.

9.5 Fields in the Presence of Magnetically Linear Insulating Materials

9.5.1* A perfectly conducting sheet is bent into a $\supset$ shape to make a one-turn inductor, as shown in Fig. P9.5.1. The width w is much larger than the dimensions in the $x - y$ plane. The region inside the inductor is filled with two linearly magnetizable materials having permeabilities μ_a and μ_b, respectively. The cross-section of the system in any $x-y$ plane is the same. The cross-sectional areas of the magnetizable materials are A_a and A_b, respectively. Given that the current $i(t)$ is uniformly distributed over the width w of the inductor, show that $\mathbf{H} = (i/w)\mathbf{i_z}$ in both of the magnetizable materials. Show that the inductance $L = (\mu_a A_a + \mu_b A_b)/w$.

9.5.2 Perfectly conducting coaxial cylinders, shorted at one end, form the one-turn inductor shown in Fig. P9.5.2. The total current i flowing on the surface at $r = b$ of the inner cylinder is returned through the short and the outer conductor at $r = a$. The annulus is filled by materials of uniform permeability with an interface at $r = R$, as shown.

(a) Determine $\mathbf{H}$ in the annulus. (A simple solution can be shown to satisfy all the laws and continuity conditions.)

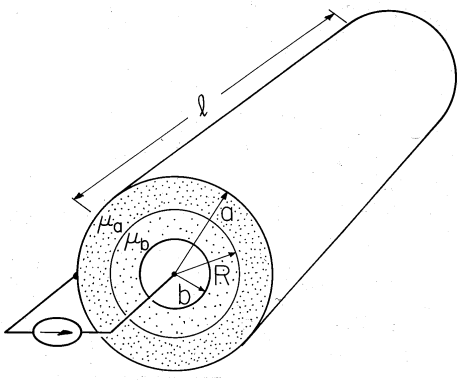


Fig. P9.5.2

(b) Find the inductance.

9.5.3* The piece-wise uniform material in the one-turn inductor of Fig. P9.5.1 is replaced by a smoothly inhomogeneous material having the permeability $\mu = -\mu_m x/l$, where μ_m is a given constant. Show that the inductance is $L = d\mu_m l/2w$.

9.5.4 The piece-wise uniform material in the one-turn inductor of Fig. P9.5.2 is replaced by one having the permeability $\mu = \mu_m(r/b)$, where μ_m is a given constant. Determine the inductance.

9.5.5* Perfectly conducting coaxial cylinders, shorted at one end, form a one-turn inductor as shown in Fig. P9.5.5. Current flowing on the surface at $r = b$ of the inner cylinder is returned on the inner surface of the outer cylinder at $r = a$. The annulus is filled by sectors of linearly magnetizable material, as shown.

(a) Assume that in the regions (a) and (b), respectively, $\mathbf{H} = \mathbf{i}_\phi A/r$ and $\mathbf{H} = \mathbf{i}_\phi C/r$, and show that with A and C functions of time, these fields satisfy Ampère's law and the flux continuity law in the respective regions.
(b) Use the flux continuity condition at the interfaces between regions to show that $C = (\mu_a/\mu_b)A$.
(c) Use Ampère's integral law to relate C and A to the total current i in the inner conductor.
(d) Show that the inductance is $L = l\mu_a\, ln(a/b)/[\alpha + (2\pi - \alpha)\mu_a/\mu_b]$.
(e) Show that the surface current densities at $r = b$ adjacent to regions (a) and (b), respectively, are $K_z = A/b$ and $K_z = C/b$.

9.5.6 In the one-turn inductor of Fig. P9.5.1, the material of piece-wise uniform permeability is replaced by another such material. Now the region between the plates in the range $0 < z < a$ is filled by material having uniform permeability μ_a, while $\mu = \mu_b$ in the range $a < z < w$. Determine the inductance.

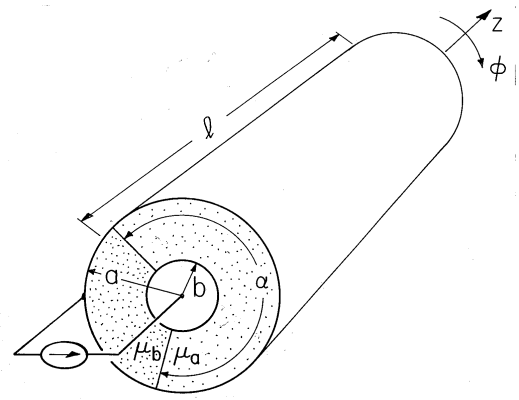


Fig. P9.5.5

9.6 Fields in Piece-Wise Uniform Magnetically Linear Materials

9.6.1* A winding in the $y = 0$ plane is used to produce the surface current density $\mathbf{K} = K_o \cos\beta z \mathbf{i}_\mathbf{x}$. Region (a), where $y > 0$, is free space, while region (b), where $y < 0$, has permeability μ.

(a) Show that

$$\Psi = \frac{K_o \sin\beta z}{\beta(1+\mu/\mu_o)} \begin{cases} -\frac{\mu}{\mu_o} e^{-\beta y}; & y > 0 \\ e^{\beta y}; & y < 0 \end{cases} \qquad (a)$$

(b) Now consider the same problem, but assume at the outset that the material in region (b) has infinite permeability. Show that it agrees with the limit $\mu \to \infty$ of the first expression of part (a).

(c) In turn, use the result of part (b) as a starting point in finding an approximation to Ψ in the highly permeable material. Show that this result agrees with the limit of the second result of part (a) where $\mu \gg \mu_o$.

9.6.2 The planar region $-d < y < d$ is bounded from above and below by infinitely permeable materials, as shown in Fig. P9.6.2. Region (a) to the right and region (b) to the left are separated by a current sheet in the plane $x = 0$ with the distribution $\mathbf{K} = \mathbf{i}_\mathbf{z} K_o \sin(\pi y/2d)$. The system extends to infinity in the $\pm x$ directions and is two dimensional.

(a) In terms of Ψ, what are the boundary conditions at $y = \pm d$.

(b) What continuity conditions relate Ψ in regions (a) and (b) where they meet at $x = 0$?

(c) Determine Ψ.

9.6.3* The cross-section of a two-dimensional cylindrical system is shown in Fig. P9.6.3. A region of free space having radius R is surrounded by material

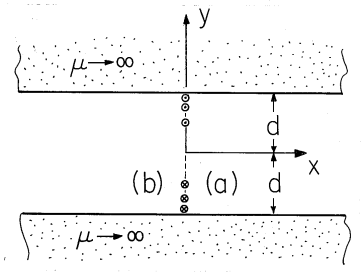


Fig. P9.6.2

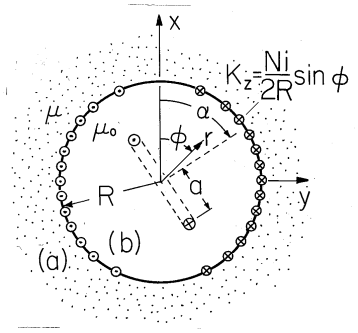


Fig. P9.6.3

having permeability μ which can be considered as extending to infinity. A winding at $r = R$ is driven by the current i and has turns density $(N/2R)\sin\phi$ (turns per unit length in the ϕ direction). Thus, at $r = R$, there is a current density $\mathbf{K} = (N/2R)i\sin\phi\mathbf{i_z}$.

(a) Show that

$$\Psi = \frac{(N/2)i\cos\phi}{(1+\mu/\mu_o)} \begin{cases} \frac{R}{r}; & r > R \\ -(\mu/\mu_o)(r/R); & r < R \end{cases} \qquad (a)$$

(b) An n-turn coil having a spacing between conductors of $2a$ is now placed at the center. The magnetic axis of this coil is inclined at the angle α relative to the x axis. This coil has length l in the z direction. Show that the mutual inductance between this coil and the one at $r = R$ is $L_m = \mu_o a\, lnN\cos\alpha/R[1 + (\mu_o/\mu)]$.

9.6.4 The cross-section of a motor or generator is shown in Fig. 11.7.7. The two coils comprising the stator and rotor windings and giving rise to the surface current densities of (11.7.24) and (11.7.25) have flux linkages having the forms given by (11.7.26).

(a) Assume that the permeabilities of the rotor and stator are infinite, and determine the vector potential in the air gap.
(b) Determine the self-inductances L_s and L_r and magnitude of the peak mutual inductance, M, in (11.7.26). Assume that the current in the $+z$ direction at ϕ is returned at $\phi + \pi$.

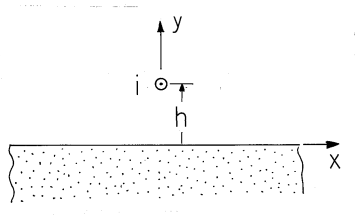


Fig. P9.6.5

9.6.5 A wire carrying a current i in the z direction is suspended a height h above the surface of a magnetizable material, as shown in Fig. P9.6.5. The wire extends to "infinity" in the $\pm z$ directions. Region (a), where $y > 0$, is free space. In region (b), where $y < 0$, the material has uniform permeability μ.

(a) Use the method of images to determine the fields in the two regions.
(b) Now assume that $\mu \gg \mu_o$ and find $\mathbf{H}$ in the upper region, assuming at the outset that $\mu \to \infty$.
(c) In turn, use this approximate result to find the field in the permeable material.
(d) Show that the results of (b) and (c) are consistent with those from the exact analysis in the limit where $\mu \gg \mu_o$.

9.6.6* A conductor carries the current $i(t)$ at a height h above the upper surface of a material, as shown in Fig. P9.6.5. The force per unit length on the conductor is $\mathbf{f} = \mathbf{i} \times \mu_o \mathbf{H}$, where $\mathbf{i}$ is a vector having the direction and magnitude of the current $i(t)$, and $\mathbf{H}$ does not include the self-field of the line current.

(a) Show that if the material is a perfect conductor, $\mathbf{f} = \mu_o \mathbf{i_y} i^2/4\pi h$.
(b) Show that if the material is infinitely permeable, $\mathbf{f} = -\mu_o \mathbf{i_y} i^2/4\pi h$.

9.6.7* Material having uniform permeability μ is bounded from above and below by regions of infinite permeability, as shown in Fig. P9.6.7. With its center at the origin and on the surface of the lower infinitely permeable material is a hemispherical cavity of free space having radius a that is much less than d. A field that has the uniform intensity H_o far from the hemispherical surface is imposed in the z direction.

(a) Assume $\mu \gg \mu_o$ and show that the approximate magnetic potential in the magnetizable material is $\Psi = -H_o a[(r/a) + (a/r)^2/2]\cos\theta$.
(b) In turn, show that the approximate magnetic potential inside the hemisphere is $\Psi = -3H_o z/2$.

9.6.8 In the magnetic tape configuration of Example 9.3.2, the system is as shown in Fig. 9.3.2 except that just below the tape, in the plane $y = -d/2$, there is an infinitely permeable material, and in the plane $y = a > d/2$ above the tape, there is a second infinitely permeable material. Find the voltage v_o.

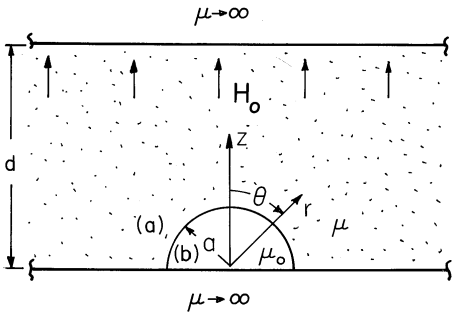


Fig. P9.6.7

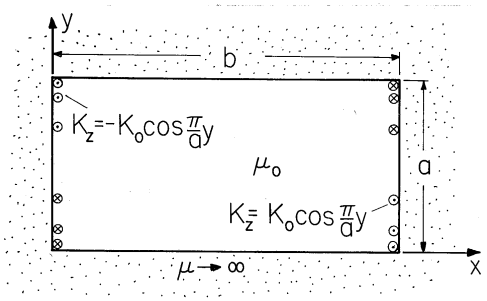


Fig. P9.6.9

9.6.9* A cylindrical region of free space of rectangular cross-section is surrounded by infinitely permeable material, as shown in Fig. P9.6.9. Surface currents are imposed by means of windings in the planes $x = 0$ and $x = b$. Show that

$$\Psi = \frac{K_o a}{\pi} \sin \frac{\pi y}{a} \frac{\cosh \frac{\pi}{a}\left(x - \frac{b}{2}\right)}{\cosh\left(\frac{\pi b}{2a}\right)} \qquad (a)$$

9.6.10* A circular cylindrical hole having radius R is cut through a material having permeability μ_a. A conductor passing through this hole has permeability μ_b and carries the uniform current density $\mathbf{J} = J_o \mathbf{i_z}$, as shown in Fig. P9.6.10. A field that is uniform far from the hole, where it is given by $\mathbf{H} = H_o \mathbf{i_x}$, is applied by external means. Show that for $r < R$, and $R < r$, respectively,

$$A_z = \begin{cases} \frac{-\mu_b J_o r^2}{4} - \frac{2\mu_b H_o R}{(1+\mu_b/\mu_a)} \frac{r}{R} \sin\phi \\ \frac{-\mu_a J_o R^2}{2}\left[ln(r/R) + \frac{1}{2}\frac{\mu_b}{\mu_a}\right] - \mu_a H_o R\left[\frac{r}{R} - \frac{(\mu_a - \mu_b)}{(\mu_a + \mu_b)}\frac{R}{r}\right]\sin\phi \end{cases} \qquad (a)$$

9.6.11* Although the introduction of a magnetizable sphere into a uniform magnetic field results in a distortion of that field, nevertheless, the field within the sphere is uniform. This fact makes it possible to determine the field distribution in and around a spherical particle even when its magnetization characteristic is nonlinear. For example, consider the fields in and around the sphere of material shown together with its $B - H$ curve in Fig. P9.6.11.

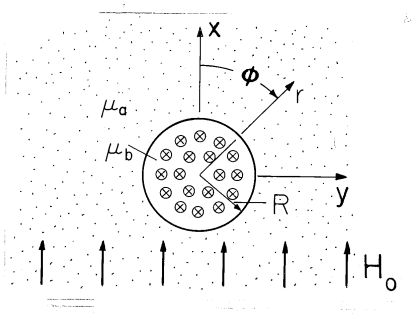


Fig. P9.6.10

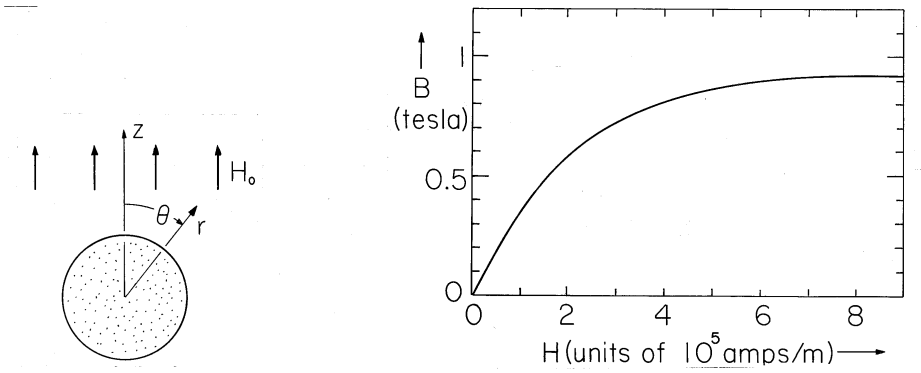


Fig. P9.6.11

(a) Assume that the magnetization density is $\mathbf{M} = M\mathbf{i_z}$, where M is a constant to be determined, and show that the magnetic field intensity inside the sphere is uniform, z directed, and of magnitude $H = H_o - M/3$, and hence that the magnetic flux density, B, in the sphere is related to the magnitude of the magnetic field intensity H by

$$B = 3\mu_o H_o - 2\mu_o H \qquad (a)$$

(b) Draw this *load line* in the $B-H$ plane, showing that it is a straight line with intercepts $3H_o/2$ and $3\mu_o H_o$ with the H and B axes, respectively.

(c) Show how (B, H) in the sphere are determined, given the applied field intensity H_o, by graphically finding the point of intersection between the $B - H$ curve of Fig. P9.6.11 and (a).

(d) Show that if $H_o = 4 \times 10^5$ A/m, $B = 0.75$ tesla and $H = 3.1 \times 10^5$ A/m.

9.6.12 The circular cylinder of magnetizable material shown in Fig. P9.6.12 has the $B - H$ curve shown in Fig. P9.6.11. Determine $\mathbf{B}$ and $\mathbf{H}$ inside the cylinder resulting from the application of a field intensity $\mathbf{H} = H_o\mathbf{i_x}$ where $H_o = 4 \times 10^5$ A/m.

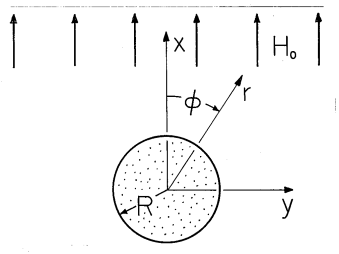


Fig. P9.6.12

9.6.13 The spherical coil of Example 9.6.1 is wound around a sphere of material having the $B - H$ curve shown in Fig. P9.6.11. Assume that $i = 800$ A, $N = 100$ turns, and $R = 10$ cm, and determine B and H in the material.

9.7 Magnetic Circuits

9.7.1* The magnetizable core shown in Fig. P9.7.1 extends a distance d into the paper that is large compared to the radius a. The driving coil, having N turns, has an extent Δ in the ϕ direction that is small compared to dimensions of interest. Assume that the core has a permeability μ that is very large compared to μ_o.

(a) Show that the approximate $\mathbf{H}$ and Ψ inside the core (with Ψ defined to be zero at $\phi = \pi$) are

$$\mathbf{H} = \frac{Ni}{2\pi r}\mathbf{i}_\phi; \qquad \Psi = \frac{Ni}{2}\left(1 - \frac{\phi}{\pi}\right) \tag{a}$$

(b) Show that the approximate magnetic potential in the central region is

$$\Psi = \sum_{m=1}^{\infty} \frac{Ni}{m\pi}(r/b)^m \sin m\phi \tag{b}$$

9.7.2 For the configuration of Prob. 9.7.1, determine Ψ in the region outside the core, $r > a$.

9.7.3* In the magnetic circuit shown in Fig. P9.7.3, an N-turn coil is wrapped around the center leg of an infinitely permeable core. The sections to right and left have uniform permeabilities μ_a and μ_b, respectively, and the gap lengths a and b are small compared to the other dimensions of these sections. Show that the inductance $L = N^2 w[(\mu_b d/b) + (\mu_a c/a)]$.

9.7.4 The magnetic circuit shown in Fig. P9.7.4 is constructed from infinitely permeable material, as is the hemispherical bump of radius R located on the surface of the lower pole face. A coil, having N turns, is wound around

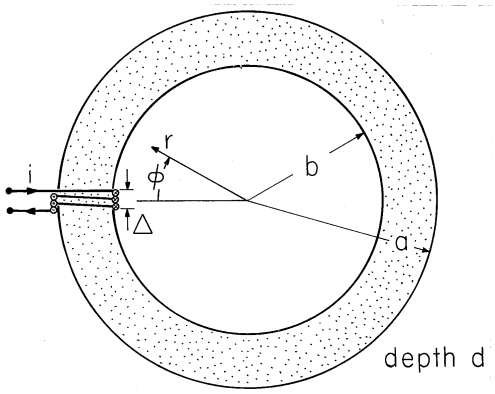


Fig. P9.7.1

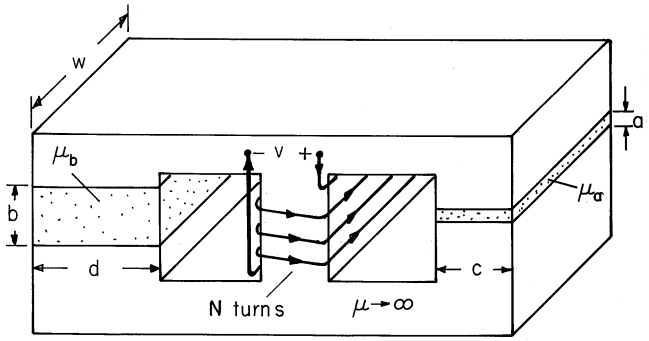


Fig. P9.7.3

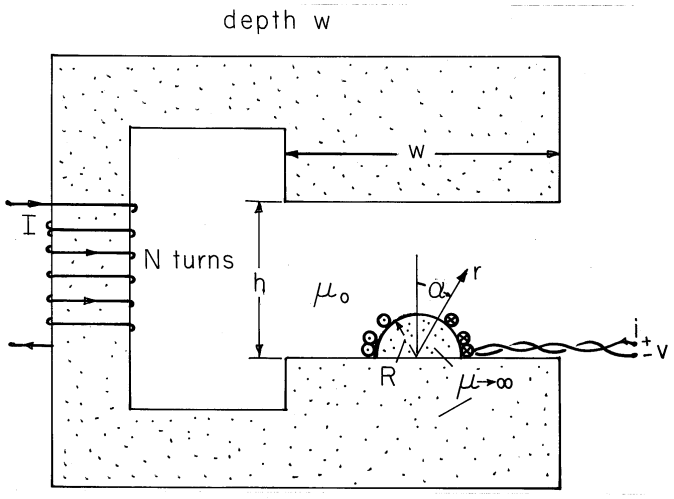


Fig. P9.7.4

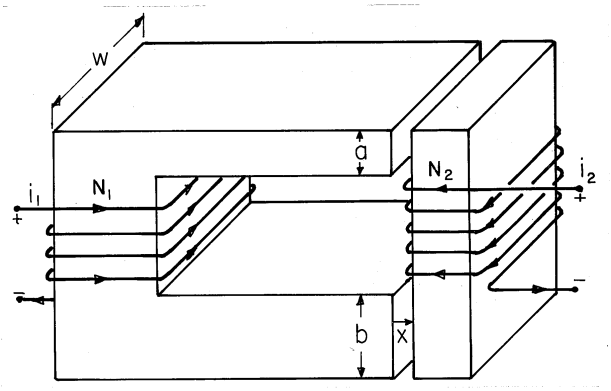


Fig. P9.7.5

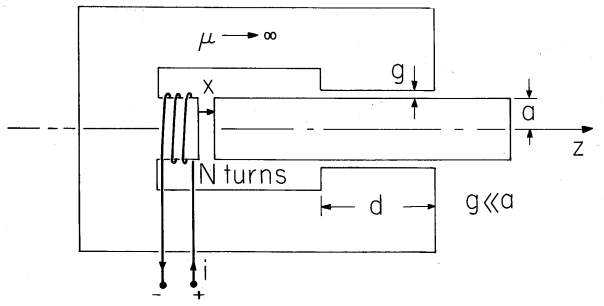


Fig. P9.7.6

the left leg of the magnetic circuit. A second coil is wound around the hemisphere in a distributed fashion. The turns per unit length, measured along the periphery of the hemisphere, is $(n/R)\sin\alpha$, where n is the total number of turns. Given that $R \ll h \ll w$, find the mutual inductance of the two coils.

9.7.5* The materials comprising the magnetic circuit of Fig. P9.7.5 can be regarded as having infinite permeability. The air gaps have a length x that is much less than a or b, and these dimensions, in turn, are much less than w. The coils to left and right, respectively, have total turns N_1 and N_2. Show that the self- and mutual inductances of the coils are

$$L_{11} = N_1^2 L_o, \quad L_{12} = L_{21} = N_1 N_2 L_o,$$

$$L_{22} = N_2^2 L_o, \quad L_o \equiv \frac{aw\mu_o}{x(1 + a/b)} \qquad (a)$$

9.7.6 The magnetic circuit shown in Fig. P9.7.6 has rotational symmetry about the z axis. Both the circular cylindrical plunger and the remainder of the magnetic circuit can be regarded as infinitely permeable. The air gaps have

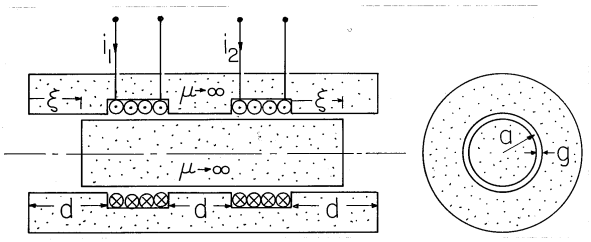


Fig. P9.7.7

widths x and g that are small compared to a and d. Determine the inductance of the coil.

9.7.7 Two cross-sectional views of an axisymmetric magnetic circuit that could be used as an electromechanical transducer are shown in Fig. P9.7.7. Surrounding an infinitely permeable circular cylindrical rod having a radius slightly less than a is an infinitely permeable stator having a hole down its center with a radius slightly greater than a. A pair of coils, having turns N_1 and N_2 and driven by currents i_1 and i_2, respectively are wound around the center rod and positioned in slots in the surrounding stator. The longitudinal position of the rod, denoted by ξ, is limited in range so that the ends of the rod are always well inside the ends of the stator. Thus, $\mathbf{H}$ in each of the air gaps is essentially uniform. Determine the inductance matrix, (9.7.12).

9.7.8 Fields in and around the magnetic circuit shown in Fig. P9.7.8 are to be considered as independent of z. The outside walls are infinitely permeable, while the horizontal central leg has uniform permeability μ that is much less than that of the sides but nevertheless much greater than μ_o. Coils having total turns N_1 and N_2, respectively, are wound around the center leg. These have evenly distributed turns in the planes $x = l/2$ and $x = -l/2$, respectively. The regions above and below the center leg are free space.

(a) Define $\Psi = 0$ at the origin of the given coordinates. As far as Ψ is concerned inside the center leg, what boundary conditions must Ψ satisfy if the central leg is treated as the "inside" of an "inside-outside" problem?
(b) What is Ψ in the center leg?
(c) What boundary conditions must Ψ satisfy in region (a)?
(d) What is Ψ, and hence $\mathbf{H}$, in region (a)? (A simple exact solution is suggested by Prob. 7.5.3.) For the case where $N_1 i_1 = N_2 i_2$, sketch ψ and $\mathbf{H}$ in regions (a) and (b).

9.7.9 The magnetic circuit shown in Fig. P9.7.9 is excited by an N-turn coil and consists of infinitely permeable legs in series with ones of permeability μ, one to the right of length l_2 and the other to the left of length l_1. This second leg has wrapped on its periphery a metal strap having thickness $\Delta \ll w$, conductivity σ, and height l_1. With a terminal current $i = i_o \cos \omega t$, determine $\mathbf{H}$ within the left leg.

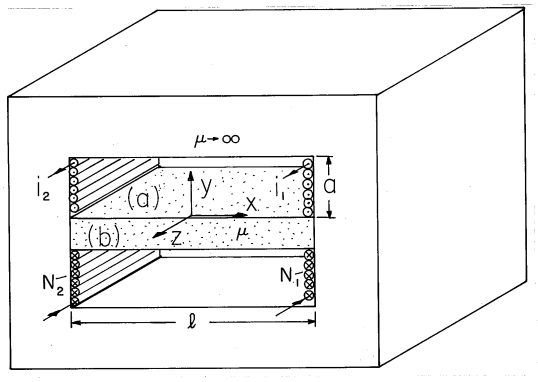


Fig. P9.7.8

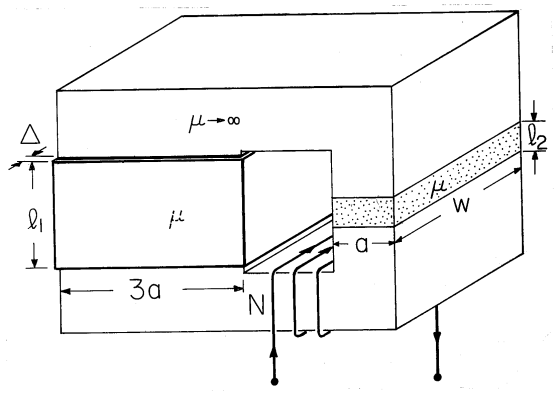


Fig. P9.7.9

9.7.10* The graphical approach to determining fields in magnetic circuits to be used in this and the next example is similar to that illustrated by Probs. 9.6.11–9.6.13. The magnetic circuit of a high-field magnet is shown in Fig. P9.7.10. The two coils each have N turns and carry a current i.

(a) Show that the *load line* for the circuit is

$$B = -\frac{\mu_o}{d}(l_2 + l_1)H + \frac{2Ni\mu_o}{d} \qquad (a)$$

(b) For $N = 500$, $d = 1$ cm, $l_1 = 0.8m$, $l_2 = 0.2$ m, and $i = 10$ amps, find the flux density B in its air gap.

9.7.11 In the magnetic circuit of Fig. P9.7.11, the infinitely permeable core has a gap with cross-sectional area A and height $a + b$, where the latter is much less than the dimensions of the former. In this gap is a material having height b and the $M - H$ relation also shown in the figure. Within the material and in the air gap, $\mathbf{H}$ is approximated as being uniform.

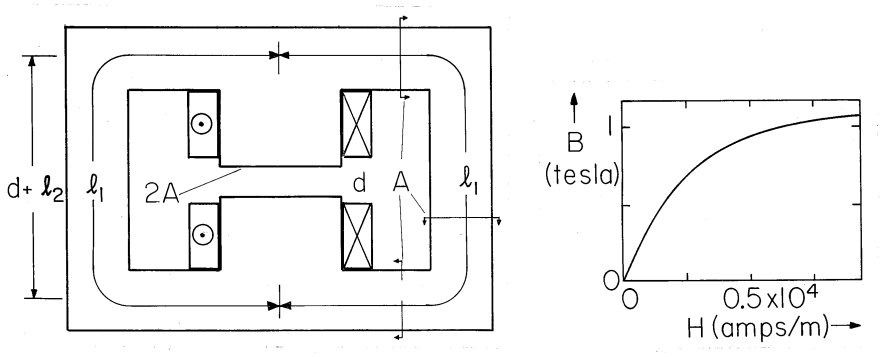


Fig. P9.7.10

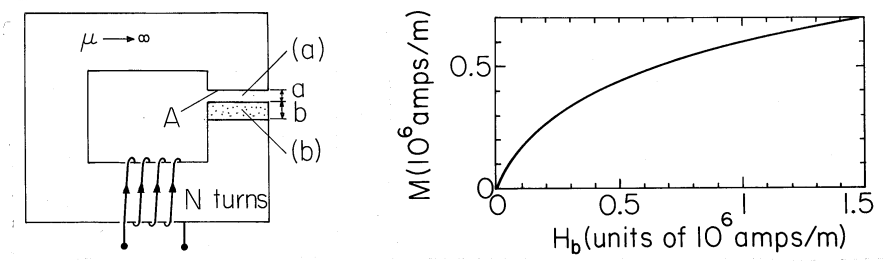


Fig. P9.7.11

(a) Determine the load line relation between H_b, the field intensity in the material, M, and the driving current i.
(b) If $Ni/a = 0.5 \times 10^6$ amps/m and $b/a = 1$, what is M, and hence B?

10

MAGNETOQUASISTATIC RELAXATION AND DIFFUSION

10.0 INTRODUCTION

In the MQS approximation, Ampère's law relates the magnetic field intensity $\mathbf{H}$ to the current density $\mathbf{J}$.

$$\boxed{\nabla \times \mathbf{H} = \mathbf{J}} \tag{1}$$

Augmented by the requirement that $\mathbf{H}$ have no divergence, this law was the theme of Chap. 8. Two types of physical situations were considered. Either the current density was imposed, or it existed in perfect conductors. In both cases, we were able to determine $\mathbf{H}$ without being concerned about the details of the electric field distribution.

In Chap. 9, the effects of magnetizable materials were represented by the magnetization density $\mathbf{M}$, and the magnetic flux density, defined as $\mathbf{B} \equiv \mu_o(\mathbf{H}+\mathbf{M})$, was found to have no divergence.

$$\boxed{\nabla \cdot \mathbf{B} = 0} \tag{2}$$

Provided that $\mathbf{M}$ is either given or instantaneously determined by $\mathbf{H}$ (as was the case throughout most of Chap. 9), and that $\mathbf{J}$ is either given or subsumed by the boundary conditions on perfect conductors, these two magnetoquasistatic laws determine $\mathbf{H}$ throughout the volume.

In this chapter, our first objective will be to determine the distribution of $\mathbf{E}$ around perfect conductors. Then we shall broaden our physical domain to include finite conductors, especially in situations where currents are caused by an $\mathbf{E}$ that

is induced by the time rate of change of **B**. In both cases, we make explicit use of Faraday's law.

$$\boxed{\nabla \times \mathbf{E} = -\frac{\partial \mathbf{B}}{\partial t}} \tag{3}$$

In the EQS systems considered in Chaps. 4–7, the curl of **H** generated by the time rate of change of the displacement flux density was not of interest. Ampère's law was adequately incorporated by the continuity law. However, in MQS systems, the curl of **E** generated by the magnetic induction on the right in (1) is often of primary importance. We had fields that depended on time rates of change in Chap. 7.

We have already seen the consequences of Faraday's law in Sec. 8.4, where MQS systems of perfect conductors were considered. The electric field intensity **E** inside a perfect conductor must be zero, and hence **B** has to vanish inside the perfect conductor if **B** varies with time. This leads to $\mathbf{n} \cdot \mathbf{B} = 0$ on the surface of a perfect conductor. Currents induced in the surface of perfect conductors assure the proper discontinuity of $\mathbf{n} \times \mathbf{H}$ from a finite value outside to zero inside.

Faraday's law was in evidence in Sec. 8.4 and accounted for the voltage at terminals connected to each other by perfect conductors. Faraday's law makes it possible to have a voltage at terminals connected to each other by a perfect "short." A simple experiment brings out some of the subtlety of the voltage definition in MQS systems. Its description is followed by an overview of the chapter.

Demonstration 10.0.1. Nonuniqueness of Voltage in an MQS System

A magnetic flux is created in the toroidal magnetizable core shown in Fig. 10.0.1 by driving the winding with a sinsuoidal current. Because it is highly permeable (a ferrite), the core guides a magnetic flux density **B** that is much greater than that in the surrounding air.

Looped in series around the core are two resistors of unequal value, $R_1 \neq R_2$. Thus, the terminals of these resistors are connected together to form a pair of "nodes." One of these nodes is grounded. The other is connected to high-impedance voltmeters through two leads that follow the different paths shown in Fig. 10.0.1. A dual-trace oscilloscope is convenient for displaying the voltages.

The voltages observed with the leads connected to the same node not only differ in magnitude but are 180 degrees out of phase.

Faraday's integral law explains what is observed. A cross-section of the core, showing the pair of resistors and voltmeter leads, is shown in Fig. 10.0.2. The scope resistances are very large compared to R_1 and R_2, so the current carried by the voltmeter leads is negligible. This means that if there is a current i through one of the series resistors, it must be the same as that through the other.

The contour C_c follows the closed circuit formed by the series resistors. Faraday's integral law is now applied to this contour. The flux passing through the surface S_c spanning C_c is defined as Φ_λ. Thus,

$$\oint_{C_1} \mathbf{E} \cdot d\mathbf{s} = -\frac{d\Phi_\lambda}{dt} = i(R_1 + R_2) \tag{4}$$

where

$$\Phi_\lambda \equiv \int_{S_c} \mathbf{B} \cdot d\mathbf{a} \tag{5}$$

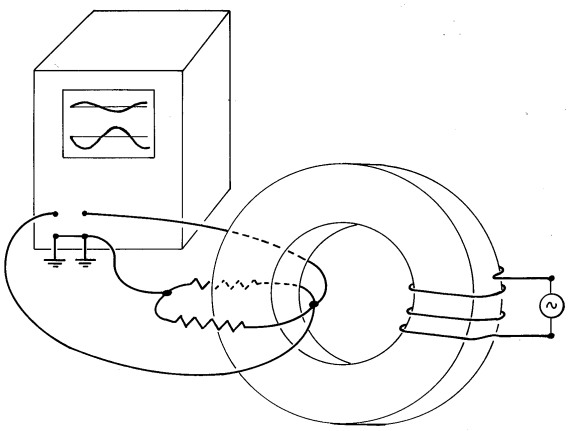


Fig. 10.0.1 A pair of unequal resistors are connected in series around a magnetic circuit. Voltages measured between the terminals of the resistors by connecting the nodes to the dual-trace oscilloscope, as shown, differ in magnitude and are 180 degrees out of phase.

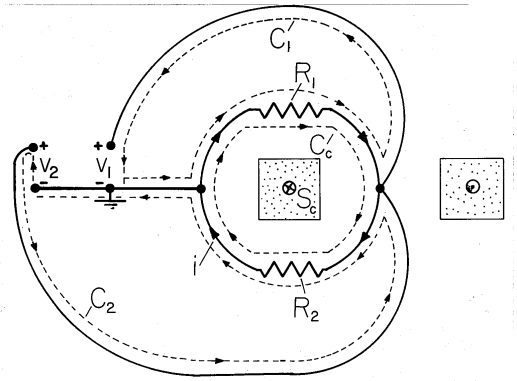


Fig. 10.0.2 Schematic of circuit for experiment of Fig. 10.0.1, showing contours used with Faraday's law to predict the differing voltages v_1 and v_2.

Given the magnetic flux, (4) can be solved for the current i that must circulate around the loop formed by the resistors.

To determine the measured voltages, the same integral law is applied to contours C_1 and C_2 of Fig. 10.0.2. The surfaces spanning the contours link a negligible flux density, so the circulation of $\mathbf{E}$ around these contours must vanish.

$$\oint_{C_1} \mathbf{E} \cdot d\mathbf{s} = v_1 + iR_1 = 0 \tag{6}$$

$$\oint_{C_2} \mathbf{E} \cdot d\mathbf{s} = -v_2 + iR_2 = 0 \tag{7}$$

The observed voltages are found by solving (4) for i, which is then substituted into (6) and (7).

$$v_1 = \frac{R_1}{R_1 + R_2} \frac{d\Phi_\lambda}{dt} \tag{8}$$

$$v_2 = -\frac{R_2}{R_1 + R_2} \frac{d\Phi_\lambda}{dt} \tag{9}$$

From this result it follows that

$$\frac{v_1}{v_2} = -\frac{R_1}{R_2} \tag{10}$$

Indeed, the voltages not only differ in magnitude but are of opposite signs.

Suppose that one of the voltmeter leads is disconnected from the right node, looped through the core, and connected directly to the grounded terminal of the same voltmeter. The situation is even more remarkable because we now have a voltage at the terminals of a "short." However, it is also more familiar. We recognize from Sec. 8.4 that the measured voltage is simply $d\lambda/dt$, where the flux linkage is in this case Φ_λ.

In Sec. 10.1, we begin by investigating the electric field in the free space regions of systems of perfect conductors. Here the viewpoint taken in Sec. 8.4 has made it possible to determine the distribution of **B** without having to determine **E** in the process. The magnetic induction appearing on the right in Faraday's law, (1), is therefore known, and hence the law prescribes the curl of **E**. From the introduction to Chap. 8, we know that this is not enough to uniquely prescribe the electric field. Information about the divergence of **E** must also be given, and this brings into play the electrical properties of the materials filling the regions between the perfect conductors.

The analyses of Chaps. 8 and 9 determined **H** in two special situations. In one case, the current distribution was prescribed; in the other case, the currents were flowing in the surfaces of perfect conductors. To see the more general situation in perspective, we may think of MQS systems as analogous to networks composed of inductors and resistors, such as shown in Fig. 10.0.3. In the extreme case where the source is a rapidly varying function of time, the inductors alone determine the currents. Finding the current distribution in this "high frequency" limit is analogous to finding the **H**-field, and hence the distribution of surface currents, in the systems of perfect conductors considered in Sec. 8.4. Finding the electric field in perfectly conducting systems, the objective in Sec. 10.1 of this chapter, is analogous to determining the distribution of voltage in the circuit in the limit where the inductors dominate.

In the opposite extreme, if the driving voltage is slowly varying, the inductors behave as shorts and the current distribution is determined by the resistive network alone. In terms of fields, the response to slowly varying sources of current is essentially the steady current distribution described in the first half of Chap. 7. Once this distribution of **J** has been determined, the associated magnetic field can be found using the superposition integrals of Chap. 8.

In Secs. 10.2–10.4, we combine the MQS laws of Chap. 8 with those of Faraday and Ohm to describe the evolution of **J** and **H** when neither of these limiting cases prevails. We shall see that the field response to a step of excitation goes from a

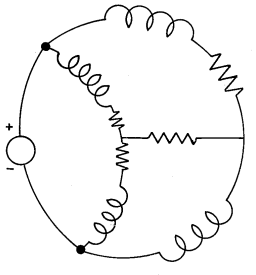


Fig. 10.0.3 Magnetoquasistatic systems with Ohmic conductors are generalizations of inductor-resistor networks. The steady current distribution is determined by the resistors, while the high-frequency response is governed by the inductors.

distribution governed by the perfect conductivity model just after the step is applied (the circuit dominated by the inductors), to one governed by the steady conduction laws for $\mathbf{J}$, and Biot-Savart for $\mathbf{H}$ after a long time (the circuit dominated by the resistors with the flux linkages then found from $\lambda = Li$). Under what circumstances is the perfectly conducting model appropriate? The characteristic times for this magnetic field diffusion process will provide the answer.

10.1 MAGNETOQUASISTATIC ELECTRIC FIELDS IN SYSTEMS OF PERFECT CONDUCTORS

The distribution of $\mathbf{E}$ around the conductors in MQS systems is of engineering interest. For example, the amount of insulation required between conductors in a transformer is dependent on the electric field.

In systems composed of perfect conductors and free space, the distribution of magnetic field intensity is determined by requiring that $\mathbf{n} \cdot \mathbf{B} = 0$ on the perfectly conducting boundaries. Although this condition is required to make the electric field tangential to the perfect conductor vanish, as we saw in Sec. 8.4, it is not necessary to explicitly refer to $\mathbf{E}$ in finding $\mathbf{H}$. Thus, in Faraday's law of induction, (10.0.3), the right-hand side is known. The source of *curl* $\mathbf{E}$ is thus known. To determine the source of *div* $\mathbf{E}$, further information is required.

The regions outside the perfect conductors, where $\mathbf{E}$ is to be found, are presumably filled with relatively insulating materials. To identify the additional information necessary for the specification of $\mathbf{E}$, we must be clear about the nature of these materials. There are three possibilities:

- Although the material is much less conducting than the adjacent "perfect" conductors, the charge relaxation time is far shorter than the times of interest. Thus, $\partial\rho/\partial t$ is negligible in the charge conservation equation and, as a result, the current density is solenoidal. Note that this is the situation in the MQS approximation. In the following discussion, we will then presume that if this situation prevails, the region is filled with a material of *uniform* conductivity, in which case $\mathbf{E}$ is solenoidal within the material volume. (Of course, there

may be surface charges on the boundaries.)

$$\nabla \cdot \mathbf{E} = 0 \tag{1}$$

- The second situation is typical when the "perfect" conductors are surrounded by materials commonly used to insulate wires. The charge relaxation time is generally much longer than the times of interest. Thus, no unpaired charges can flow into these "insulators" and they remain charge free. Provided they are of uniform permittivity, the E field is again solenoidal within these materials.
- If the charge relaxation time is on the same order as times characterizing the currents carried by the conductors, then the distribution of unpaired charge is governed by the combination of Ohm's law, charge conservation, and Gauss' law, as discussed in Sec. 7.7. If the material is not only of uniform conductivity but of uniform permittivity as well, this charge density is zero in the volume of the material. It follows from Gauss' law that $\mathbf{E}$ is once again solenoidal in the material volume. Of course, surface charges may exist at material interfaces.

The electric field intensity is broken into particular and homogeneous parts

$$\mathbf{E} = \mathbf{E}_p + \mathbf{E}_h \tag{2}$$

where, in accordance with Faraday's law, (10.0.3), and (1),

$$\nabla \times \mathbf{E}_p = -\frac{\partial \mathbf{B}}{\partial t} \tag{3}$$

$$\nabla \cdot \mathbf{E}_p = 0 \tag{4}$$

and

$$\nabla \times \mathbf{E}_h = 0 \tag{5}$$

$$\nabla \cdot \mathbf{E}_h = 0. \tag{6}$$

Our approach is reminiscent of that taken in Chap. 8, where the roles of $\mathbf{E}$ and $\partial\mathbf{B}/\partial t$ are respectively taken by $\mathbf{H}$ and $-\mathbf{J}$. Indeed, if all else fails, the particular solution can be generated by using an adaptation of the Biot-Savart law, (8.2.7).

$$\mathbf{E}_p = -\frac{1}{4\pi}\int_{V'} \frac{\frac{\partial \mathbf{B}}{\partial t}(\mathbf{r}') \times \mathbf{i}_{\mathbf{r}'\mathbf{r}}}{|\mathbf{r}-\mathbf{r}'|^{\mathbf{2}}} dv' \tag{7}$$

Given a particular solution to (3) and (4), the boundary condition that there be no tangential $\mathbf{E}$ on the surfaces of the perfect conductors is satisfied by finding a solution to (5) and (6) such that

$$\mathbf{n} \times \mathbf{E} = 0 \Rightarrow \mathbf{n} \times \mathbf{E}_h = -\mathbf{n} \times \mathbf{E}_p \tag{8}$$

on those surfaces.

Given the particular solution, the boundary value problem has been reduced to one familiar from Chap. 5. To satisfy (5), we let $\mathbf{E}_h = -\nabla\Phi$. It then follows from (6) that Φ satisfies Laplace's equation.

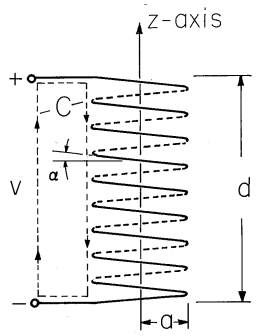


Fig. 10.1.1 Side view of long inductor having radius a and length d.

Example 10.1.1. Electric Field around a Long Coil

What is the electric field distribution in and around a typical inductor? An approximate analysis for a coil of many turns brings out the reason why transformer and generator designers often speak of the "volts per turn" that must be withstood by insulation. The analysis illustrates the concept of breaking the solution into a particular rotational field and a homogeneous conservative field.

Consider the idealized coil of Fig. 10.1.1. It is composed of a thin, perfectly conducting wire, wound in a helix of length d and radius a. The magnetic field can be found by approximating the current by a surface current $\mathbf{K}$ that is ϕ directed about the z axis of a cylindrical coodinate system having the z axis coincident with the axis of the coil. For an N-turn coil, this surface current density is $K_\phi = Ni/d$. If the coil is very long, $d \gg a$, the magnetic field produced within is approximately uniform

$$H_z = \frac{Ni}{d} \tag{9}$$

while that outside is essentially zero (Example 8.2.1). Note that the surface current density is just that required to terminate $\mathbf{H}$ in accordance with Ampère's continuity condition.

With such a simple magnetic field, a particular solution is easily obtained. We recognize that the perfectly conducting coil is on a natural coordinate surface in the cylindrical coordinate system. Thus, we write the z component of (3) in cylindrical coordinates and look for a solution to $\mathbf{E}$ that is independent of ϕ. The solution resulting from an integration over r is

$$\mathbf{E}_p = \mathbf{i}_\phi \begin{cases} -\frac{\mu_o r}{2}\frac{dH_z}{dt} & r < a \\ -\frac{\mu_o a^2}{2r}\frac{dH_z}{dt} & r > a \end{cases} \tag{10}$$

Because there is no magnetic field outside the coil, the outside solution for $\mathbf{E_p}$ is irrotational.

If we adhere to the idealization of the wire as an inclined current sheet, the electric field along the wire in the sheet must be zero. The particular solution does not satisfy this condition, and so we now must find an irrotational and solenoidal $\mathbf{E_h}$ that cancels the component of $\mathbf{E_p}$ tangential to the wire.

A section of the wire is shown in Fig. 10.1.2. What axial field E_z must be added to that given by (10) to make the net $\mathbf{E}$ perpendicular to the wire? If E_z and E_ϕ are to be components of a vector normal to the wire, then their ratio must be

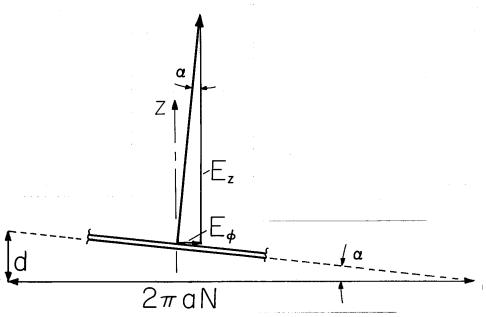


Fig. 10.1.2 With the wire from the inductor of Fig. 10.1.1 stretched into a straight line, it is evident that the slope of the wire in the inductor is essentially the total length of the coil, d, divided by the total length of the wire, $2\pi aN$.

the same as the ratio of the total length of the wire to the length of the coil.

$$\frac{E_z}{E_\phi} = \frac{2\pi aN}{d}; \qquad r = a \tag{11}$$

Using (9) and (10) at $r = a$, we have

$$E_z = -\frac{\mu_o \pi a^2 N^2}{d^2}\frac{di}{dt} \tag{12}$$

The homogeneous solution possesses this field E_z on the surface of the cylinder of radius a and length d. This field determines the potential Φ_h over the surface (within an arbitrary constant). Since $\nabla^2\Phi_h = 0$ everywhere in space and the tangential E_h field prescribes Φ_h on the cylinder, Φ_h is uniquely determined everywhere within an additive constant. Hence, the conservative part of the field is determined everywhere.

The voltage between the terminals is determined from the line integral of $\mathbf{E} \cdot d\mathbf{s}$ between the terminals. The field of the particular solution is ϕ-directed and gives no contribution. The entire contribution to the line integral comes from the homogeneous solution (12) and is

$$v = -E_z d = \frac{\mu_o N^2 \pi a^2}{d}\frac{di}{dt} \tag{13}$$

Note that this expression takes the form Ldi/dt, where the inductance L is in agreement with that found using a contour coincident with the wire, (8.4.18).

We could think of the terminal voltage as the sum of N "voltages per turn" $E_z d/N$. If we admit to the finite size of the wires, the electric stress between the wires is essentially this "voltage per turn" divided by the distance between wires.

The next example identifies the particular and homogeneous solutions in a somewhat more formal fashion.

Example 10.1.2. Electric Field of a One-Turn Solenoid

The cross-section of a one-turn solenoid is shown in Fig. 10.1.3. It consists of a circular cylindrical conductor having an inside radius a much less than its length in

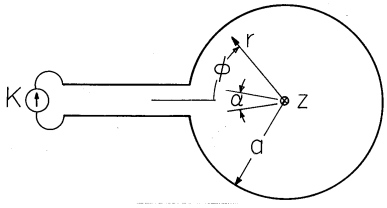


Fig. 10.1.3 A one-turn solenoid of infinite length is driven by the distributed source of current density, $K(t)$.

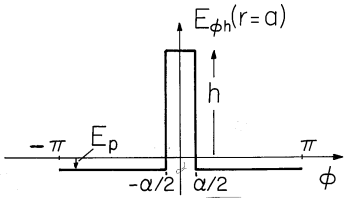


Fig. 10.1.4 Tangential component of homogeneous electric field at $r = a$ in the configuration of Fig. 10.1.3.

the z direction. It is driven by a distributed current source $K(t)$ through the plane parallel plates to the left. This current enters through the upper sheet conductor, circulates in the ϕ direction around the one turn, and leaves through the lower plate. The spacing between these plates is small compared to a.

As in the previous example, the field inside the solenoid is uniform, axial, and equal to the surface current

$$\mathbf{H} = \mathbf{i_z} K(t) \tag{14}$$

and a particular solution can be found by applying Faraday's integral law to a contour having the arbitrary radius $r < a$, (10).

$$\mathbf{E}_p = E_{\phi p}\mathbf{i}_\phi; \qquad E_{\phi p} \equiv -\frac{\mu_o r}{2}\frac{dK}{dt} \tag{15}$$

This field clearly does not satisfy the boundary condition at $r = a$, where it has a tangential value over almost all of the surface. The homogeneous solution must have a tangential component that cancels this one. However, this field must also be conservative, so its integral around the circumference at $r = a$ must be zero. Thus, the plot of the ϕ component of the homogeneous solution at $r = a$, shown in Fig. 10.1.4, has no average value. The amplitude of the tall rectangle is adjusted so that the net area under the two functions is zero.

$$E_{\phi p}(2\pi - \alpha) = h\alpha \Rightarrow h = E_{\phi p}\Big(\frac{2\pi}{\alpha} - 1\Big) \tag{16}$$

The field between the edges of the input electrodes is approximated as being uniform right out to the contacts with the solenoid.

We now find a solution to Laplace's equation that matches this boundary condition on the tangential component of $\mathbf{E}$. Because E_ϕ is an even function of ϕ, Φ is taken as an odd function. The origin is included in the region of interest, so the polar coordinate solutions (Table 5.7.1) take the form

$$\Phi = \sum_{n=1}^{\infty} A_n r^n \sin n\phi \tag{17}$$

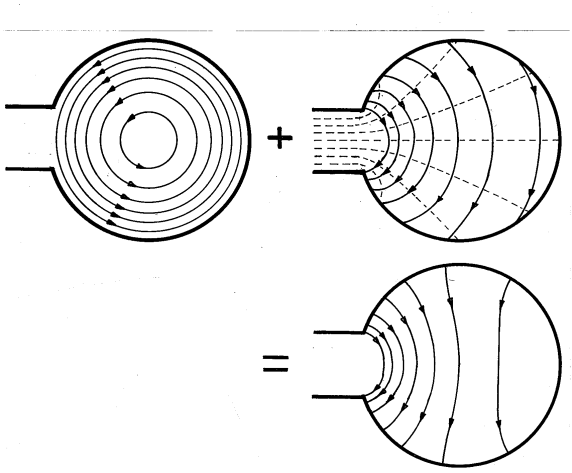


Fig. 10.1.5 Graphical representation of solution for the electric field in the configuration of Fig. 10.1.3.

It follows that

$$E_{\phi h} = -\frac{1}{r}\frac{\partial \Phi}{\partial \phi} = -\sum_{n=1}^{\infty} nA_n r^{n-1}\cos n\phi. \tag{18}$$

The coefficients A_n are evaluated, as in Sec. 5.5, by multiplying both sides of this expression by $\cos(m\phi)$ and integrating from $\phi = -\pi$ to $\phi = \pi$.

$$\begin{aligned}\int_{-\pi}^{-\alpha/2} - E_{\phi p}\cos m\phi d\phi + \int_{-\alpha/2}^{\alpha/2} E_{\phi p}\left(\frac{2\pi}{\alpha} - 1\right)\cos m\phi d\phi \\ + \int_{\alpha/2}^{\pi} -E_{\phi p}\cos m\phi d\phi = -mA_m a^{m-1}\pi\end{aligned} \tag{19}$$

Thus, the coefficients needed to evaluate the potential of (17) are

$$A_m = -\frac{4E_{\phi p}(r=a)}{m^2 a^{m-1}\alpha}\sin\frac{m\alpha}{2} \tag{20}$$

Finally, the desired field intensity is the sum of the particular solution, (15), and the homogeneous solution, the gradient of (17).

$$\begin{aligned}\mathbf{E} = -\frac{\mu_o a}{2}\frac{dK}{dt}\left[\frac{r}{a}\mathbf{i}_\phi + 4\sum_{n=1}^{\infty}\frac{\sin\frac{n\alpha}{2}}{\alpha n}\left(\frac{r}{a}\right)^{n-1}\cos n\phi\mathbf{i}_\phi\right. \\ \left. + 4\sum_{n=1}^{\infty}\frac{\sin\frac{n\alpha}{2}}{n\alpha}\left(\frac{r}{a}\right)^{n-1}\sin n\phi\mathbf{i}_\mathbf{r}\right]\end{aligned} \tag{21}$$

The superposition of fields represented in this solution is shown graphically in Fig. 10.1.5. A conservative field is added to the rotational field. The former has

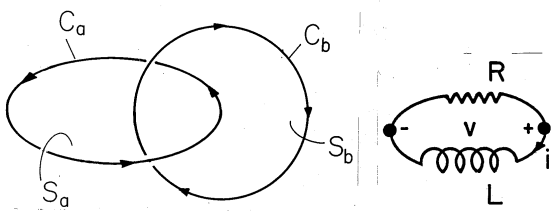


Fig. 10.2.1 Current induced in accordance with Faraday's law circulates on contour C_a. Through Ampère's law, it results in magnetic field that follows contour C_b.

a potential at $r = a$ that is a linearly increasing function of ϕ between the input electrodes, increasing from a negative value at the lower electrode at $\phi = -\alpha/2$, passing through zero at the midplane, and reaching an equal positive value at the upper electrode at $\phi = \alpha/2$. The potential decreases in a linear fashion from this high as ϕ is increased, again passing through zero at $\phi = 180$ degrees, and reaching the negative value upon returning to the lower input electrode. Equipotential lines therefore join points on the solenoid periphery with points at the same potential between the input electrodes. Note that the electric field associated with this potential indeed has the tangential component required to cancel that from the rotational part of the field, the proof of this being in the last of the plots.

Often the vector potential provides conveniently a particular solution. With **B** replaced by $\nabla \times \mathbf{A}$,

$$\nabla \times \left(\mathbf{E} + \frac{\partial \mathbf{A}}{\partial t} \right) = 0 \tag{22}$$

Suppose **A** has been determined. Then the quantity in parantheses must be equal to the gradient of a potential Φ so that

$$\mathbf{E} = -\frac{\partial \mathbf{A}}{\partial t} - \nabla \Phi \tag{23}$$

In the examples treated, the first term in this expression is the particular solution, while the second is the homogeneous solution.

10.2 NATURE OF FIELDS INDUCED IN FINITE CONDUCTORS

If a conductor is situated in a time-varying magnetic field, the induced electric field gives rise to currents. From Sec. 8.4, we have shown that these currents prevent the penetration of the magnetic field into a perfect conductor. How high must σ be to treat a conductor as perfect? In the next two sections, we use specific analytical models to answer this question. Here we preface these developments with a discussion of the interplay between the laws of Faraday, Ampère and Ohm that determines the distribution, duration, and magnitude of currents in conductors of finite conductivity.

The integral form of Faraday's law, applied to the surface S_a and contour C_a of Fig. 10.2.1, is

$$\oint_{C_a} \mathbf{E} \cdot d\mathbf{s} = -\frac{d}{dt} \int_{S_a} \mathbf{B} \cdot d\mathbf{a} \tag{1}$$

Ohm's law, $\mathbf{J} = \sigma\mathbf{E}$, introduced into (1), relates the current density circulating around a tube following C_a to the enclosed magnetic flux.

$$\oint_{C_a} \frac{\mathbf{J}}{\sigma} \cdot d\mathbf{s} = -\frac{d}{dt}\int_{S_a} \mathbf{B} \cdot d\mathbf{a} \tag{2}$$

This statement applies to every circulating current "hose" in a conductor. Let us concentrate on one such hose. The current flows parallel to the hose, and therefore $\mathbf{J} \cdot d\mathbf{s} = Jds$. Suppose that the cross-sectional area of the hose is $A(s)$. Then $JA(s) = i$, the current in the hose, and

$$\oint \frac{A(s)}{\sigma} ds = R \tag{3}$$

is the resistance of the hose. Therefore,

$$iR = -\frac{d\lambda}{dt} \tag{4}$$

Equation (2) describes how the time-varying magnetic flux gives rise to a circulating current. Ampère's law states how that current, in turn, produces a magnetic field.

$$\oint_{C_b} \mathbf{H} \cdot d\mathbf{s} = \int_{S_b} \mathbf{J} \cdot d\mathbf{a} \tag{5}$$

Typically, that field circulates around a contour such as C_b in Fig. 10.2.1, which is pierced by $\mathbf{J}$. With Gauss' law for $\mathbf{B}$, Ampère's law provides the relation for $\mathbf{H}$ produced by $\mathbf{J}$. This information is summarized by the "lumped circuit" relation

$$\lambda = Li \tag{6}$$

The combination of (4) and (6) provides a differential equation for the circuit current $i(t)$. The equivalent circuit for the differential equation is the series interconnection of a resistor R with an inductor L, as shown in Fig. 10.2.1. The solution is an exponentially decaying function of time with the time constant L/R.

The combination of (2) and (5)– of the laws of Faraday, Ampère, and Ohm– determine $\mathbf{J}$ and $\mathbf{H}$. The field problem corresponds to a continuum of "circuits." We shall find that the time dependence of the fields is governed by time constants having the nature of L/R. This time constant will be of the form

$$\tau_m = \mu\sigma l_1 l_2 \tag{7}$$

In contrast with the charge relaxation time ϵ/σ of EQS, this *magnetic diffusion time* depends on the product of two characteristic lengths, denoted here by l_1 and l_2. For given time rates of change and electrical conductivity, the larger the system, the more likely it is to behave as a perfect conductor.

Although we will not use the integral laws to determine the fields in the finite conductivity systems of the next sections, they are often used to make engineering

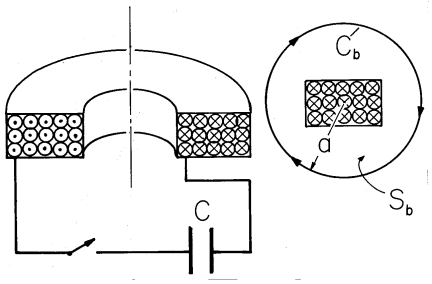


Fig. 10.2.2 When the spark gap switch is closed, the capacitor discharges into the coil. The contour C_b is used to estimate the average magnetic field intensity that results.

approximations. The following demonstration is quantified using rough approximations in a style that typifies how field theory is often applied to practical problems.

Demonstration 10.2.1. Edgerton's Boomer

The capacitor in Fig. 10.2.2, $C = 25\mu F$, is initially charged to $v = 4kV$. The spark gap switch is then closed so that the capacitor can discharge into the 50-turn coil. This demonstration has been seen by many visitors to Prof. Harold Edgerton's Strobe Laboratory at M.I.T.

Given that the average radius of a coil winding $a = 7$ cm, and that the height of the coil is also on the order of a, roughly what magnetic field is generated? Ampère's integral law, (5), can be applied to the contour C_b of the figure to obtain an approximate relation between the average $\mathbf{H}$, which we will call H_1, and the coil current i_1.

$$H_1 \approx \frac{N_1 i_1}{2\pi a} \tag{8}$$

To determine i_1, we need the inductance L_{11} of the coil. To this end, the flux linkage of the coil is approximated by N_1 times the product of the average coil area and the average flux density.

$$\lambda \approx N_1(\pi a^2)\mu_o H_1 \tag{9}$$

From these last two equations, one obtains $\lambda = L_{11} i_1$, where the inductance is

$$L_{11} \approx \frac{\mu_o a N_1^2}{2} \tag{10}$$

Evaluation gives $L_{11} = 0.1$ mH.

With the assumption that the combined resistance of the coil, switch, and connecting leads is small enough so that the voltage across the capacitor and the current in the inductor oscillate at the frequency

$$\omega = \frac{1}{\sqrt{CL_{11}}} \tag{11}$$

we can determine the peak current by recognizing that the energy $\frac{1}{2}Cv^2$ initially stored in the capacitor is one quarter of a cycle later stored in the inductor.

$$\frac{1}{2}L_{11}i_p^2 \approx \frac{1}{2}Cv_p^2 \Rightarrow i_p = v_p\sqrt{C/L_{11}} \tag{12}$$

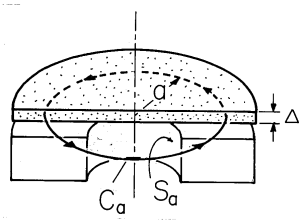


Fig. 10.2.3 Metal disk placed on top of coil shown in Fig. 10.2.2.

Thus, the peak current in the coil is $i_1 = 2,000A$. We know both the capacitance and the inductance, so we can also determine the frequency with which the current oscillates. Evaluation gives $\omega = 20 \times 10^3 s^{-1}$ ($f = 3$kHz).

The H field oscillates with this frequency and has an amplitude given by evaluating (8). We find that the peak field intensity is $H_1 = 2.3 \times 10^5$ A/m so that the peak flux density is 0.3 T (3000 gauss).

Now suppose that a conducting disk is placed just above the driver coil as shown in Fig. 10.2.3. What is the current induced in the disk? Choose a contour that encloses a surface S_a which links the upward-directed magnetic flux generated at the center of the driver coil. With E defined as an average azimuthally directed electric field in the disk, Faraday's law applied to the contour bounding the surface S_a gives

$$2\pi a E_\phi = -\frac{d}{dt}\int_{S_a} \mathbf{B}\cdot d\mathbf{a} \approx -\frac{d}{dt}(\mu_o H_1 \pi a^2) \tag{13}$$

The average current density circulating in the disk is given by Ohm's law.

$$J_\phi = \sigma E_\phi = -\frac{\sigma \mu_o a}{2}\frac{dH_1}{dt} \tag{14}$$

If one were to replace the disk with his hand, what current density would he feel? To determine the peak current, the derivative is replaced by ωH_1. For the hand, $\sigma \approx 1$ S/m and (14) gives 20 mA/cm^2. This is more than enough to provide a "shock."

The conductivity of an aluminum disk is much larger, namely 3.5×10^7 S/m. According to (14), the current density should be 35 million times larger than that in a human hand. However, we need to remind ourselves that in using Ampère's law to determine the driving field, we have ignored contributions due to the induced current in the disk.

Ampère's integral law can also be used to approximate the field induced by the current in the disk. Applied to a contour that loops around the current circulating in the disk rather than in the driving coil, (2) requires that

$$H_{ind} \approx \frac{i_2}{2\pi a} \approx \frac{\Delta a J_\phi}{2\pi a} \tag{15}$$

Here, the cross-sectional area of the disk through which the current circulates is approximated by the product of the disk thickness Δ and the average radius a.

It follows from (14) and (15) that the induced field gets to be on the order of the imposed field when

$$\frac{H_{ind}}{H_1} \approx \frac{\Delta \sigma \mu_o a}{4\pi}\frac{1}{|H_1|}\left|\frac{dH_1}{dt}\right| \approx \frac{\tau_m}{4\pi}\omega \tag{16}$$

where

$$\tau_m \equiv \mu_o \sigma \Delta a \tag{17}$$

Note that τ_m takes the form of (7), where $l_1 = \Delta$ and $l_2 = a$.

For an aluminum disk of thickness $\Delta = 2$ mm, $a = 7$ cm, $\tau_m = 6$ ms, so $\omega\tau_m/4\pi \approx 10$, and the field associated with the induced current is comparable to that imposed by the driving coil.[1] The surface of the disk is therefore one where $\mathbf{n} \cdot \mathbf{B} \approx 0$. The lines of magnetic flux density passing upward through the center of the driving coil are trapped between the driver coil and the disk as they turn radially outward. These lines are sketched in Fig. 10.2.4.

In the terminology introduced with Example 9.7.4, the disk is the secondary of a transformer. In fact, τ_m is the time constant L_{22}/R of the secondary, where L_{22} and R are the inductance and resistance of a circuit representing the disk. Indeed, the condition for ideal transformer operation, (9.7.26), is equivalent to having $\omega\tau_m/4\pi \gg 1$. The windings in power transformers are subject to the forces we now demonstrate.

If an aluminum disk is placed on the coil and the switch closed, a number of applications emerge. First, there is a bang, correctly suggesting that the disk can be used as an acoustic transducer. Typical applications are to deep-sea acoustic sounding. The force density $\mathbf{F}(N/m^3)$ responsible for this sound follows from the Lorentz law (Sec. 11.9)

$$\mathbf{F} = \mathbf{J} \times \mu_o \mathbf{H} \tag{18}$$

Note that regardless of the polarity of the driving current, and hence of the average $\mathbf{H}$, this force density acts upward. It is a force of repulsion. With the current distribution in the disk represented by a surface current density K, and $\mathbf{B}$ taken as one half its average value (the factor of 1/2 will be explained in Example 11.9.3), the total upward force on the disk is

$$\mathbf{f} = \int_V \mathbf{J} \times \mathbf{B} dV \approx \frac{1}{2} KB(\pi a^2)\mathbf{i_z} \tag{19}$$

By Ampère's law, the surface current K in the disk is equal to the field in the region between the disk and the driver, and hence essentially equal to the average H. Thus, with an additional factor of $\frac{1}{2}$ to account for time averaging the sinusoidally varying drive, (19) becomes

$$f \approx f_o \equiv \frac{1}{4}\mu_o H^2(\pi a^2) \tag{20}$$

In evaluating this expression, the value of $\mathbf{H}$ adjacent to the disk with the disk resting on the coil is required. As suggested by Fig. 10.2.4, this field intensity is larger than that given by (8). Suppose that the field is intensified in the gap between coil and plate by a factor of about 2 so that $H \simeq 5 \times 10^5 A$. Then, evaluation of (20) gives $10^3 N$ or more than 1000 times the force of gravity on an $80g$ aluminum disk. How high would the disk fly? To get a rough idea, it is helpful to know that the driver current decays in several cycles. Thus, the average driving force is essentially an impulse, perhaps as pictured in Fig. 10.2.5 having the amplitude of (20) and a duration $T = 1$ ms. With the aerodynamic drag ignored, Newton's law requires that

$$M\frac{dV}{dt} = f_o T u_o(t) \tag{21}$$

[1] As we shall see in the next sections, because the calculation is not self-consistent, the inequality $\omega\tau_m \gg 1$ indicates that the induced field is comparable to and not in excess of the one imposed.

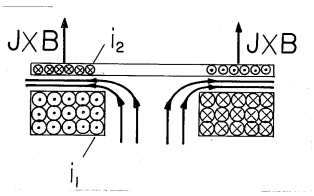


Fig. 10.2.4 Currents induced in the metal disk tend to induce a field that bucks out that imposed by the driving coil. These currents result in a force on the disk that tends to propel it upward.

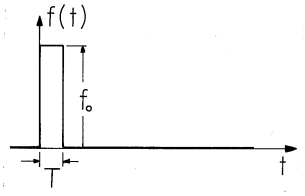


Fig. 10.2.5 Because the magnetic force on the disk is always positive and lasts for a time T shorter than the time it takes the disk to leave the vicinity of the coil, it is represented by an impulse of magnitude f_oT.

where $M = 0.08kg$ is the disk mass, V is its velocity, and $u_o(t)$ is the unit impulse. Integration of this expression from $t = 0^-$ (when the velocity $V = 0$) to $t = 0^+$ gives

$$MV(O^+) = f_oT \tag{22}$$

For the numbers we have developed, this initial velocity is about 10 m/s or about 20 miles/hr. Perhaps of more interest is the height h to which the disk would be expected to travel. If we require that the initial kinetic energy $\frac{1}{2}MV^2$ be equal to the final potential energy Mgh ($g = 9.8$ m/s^2), this height is $\frac{1}{2}V^2/g \simeq 5$ m.

The voltage and capacitance used here for illustration are modest. Even so, if the disk is thin and malleable, it is easily deformed by the field. Metal forming and transport are natural applications of this phenomenon.

10.3 DIFFUSION OF AXIAL MAGNETIC FIELDS THROUGH THIN CONDUCTORS

This and the next section are concerned with the influence of thin-sheet conductors of finite conductivity on distributions of magnetic field. The demonstration of the previous section is typical of physical situations of interest. By virtue of Faraday's law, an applied field induces currents in the conducting sheet. Through Ampère's law, these in turn result in an induced field tending to buck out the imposed field. The resulting field has a time dependence reflecting not only that of the applied field but the conductivity and dimensions of the conductor as well. This is the subject of the next two sections.

A class of configurations with remarkably simple fields involves one or more sheet conductors in the shape of cylinders of infinite length. As illustrated in Fig.

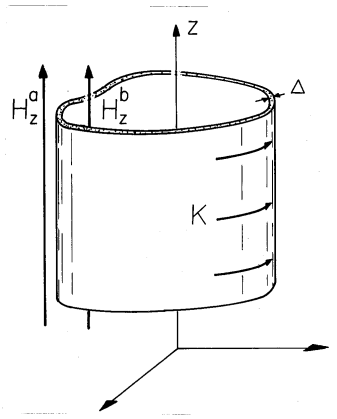


Fig. 10.3.1 A thin shell having conductivity σ and thickness Δ has the shape of a cylinder of arbitrary cross-section. The surface current density $K(t)$ circulates in the shell in a direction perpendicular to the magnetic field, which is parallel to the cylinder axis.

10.3.1, these are uniform in the z direction but have an arbitrary cross-sectional geometry. In this section, the fields are z directed and the currents circulate around the z axis through the thin sheet. Fields and currents are pictured as independent of z.

The current density **J** is divergence free. If we picture the current density as flowing in planes perpendicular to the z axis, and as essentially uniform over the thickness Δ of the sheet, then the surface current density must be independent of the azimuthal position in the sheet.

$$K = K(t) \tag{1}$$

Ampère's continuity condition, (9.5.3), requires that the adjacent axial fields are related to this surface current density by

$$\boxed{-H_z^a + H_z^b = K} \tag{2}$$

In a system with a single cylinder, with a given circulating surface current density K and insulating materials of uniform properties both outside (a) and inside (b), a uniform axial field inside and no field outside is the exact solution to Ampère's law and the flux continuity condition. (We saw this in Demonstration 8.2.1 and in Example 8.4.2. for a solenoid of circular cross-section.) In a system consisting of nested cylinders, each having an arbitrary cross-sectional geometry and each carrying its own surface current density, the magnetic fields between cylinders would be uniform. Then (2) would relate the uniform fields to either side of any given sheet.

In general, K is not known. To relate it to the axial field, we must introduce the laws of Ohm and Faraday. The fact that K is uniform makes it possible to exploit the integral form of the latter law, applied to a contour C that circulates through the cylinder.

$$\oint_C \mathbf{E} \cdot d\mathbf{s} = -\frac{d}{dt}\int_S \mathbf{B} \cdot d\mathbf{a} \tag{3}$$

To replace $\mathbf{E}$ in this expression, we multiply $\mathbf{J} = \sigma\mathbf{E}$ by the thickness Δ to relate the surface current density to E, the magnitude of $\mathbf{E}$ inside the sheet.

$$K \equiv \Delta J = \Delta\sigma E \Rightarrow E = \frac{K}{\Delta\sigma} \tag{4}$$

If Δ and σ are uniform, then E (like K), is the same everywhere along the sheet. However, either the thickness or the conductivity could be functions of azimuthal position. If σ and Δ are given, the integral on the left in (3) can be taken, since K is constant. With s denoting the distance along the contour C, (3) and (4) become

$$\boxed{K \oint_C \frac{ds}{\Delta(s)\sigma(s)} = -\frac{d}{dt}\int_S \mathbf{B}\cdot d\mathbf{a}} \tag{5}$$

Of most interest is the case where the thickness and conductivity are uniform and (5) becomes

$$\frac{KP}{\Delta\sigma} = -\frac{d}{dt}\int_S \mathbf{B}\cdot d\mathbf{a} \tag{6}$$

with P denoting the peripheral length of the cylinder.

The following are examples based on this model.

Example 10.3.1. Diffusion of Axial Field into a Circular Tube

The conducting sheet shown in Fig. 10.3.2 has the shape of a long pipe with a wall of uniform thickness and conductivity. There is a uniform magnetic field $\mathbf{H} = \mathbf{i_z}H_o(t)$ in the space outside the tube, perhaps imposed by means of a coaxial solenoid. What current density circulates in the conductor and what is the axial field intensity H_i inside?

Representing Ohm's law and Faraday's law of induction, (6) becomes

$$\frac{K}{\Delta\sigma}2\pi a = -\frac{d}{dt}(\mu_o\pi a^2 H_i) \tag{7}$$

Ampère's law, represented by the continuity condition, (2), requires that

$$K = -H_o + H_i \tag{8}$$

In these two expressions, H_o is a given driving field, so they can be combined into a single differential equation for either K or H_i. Choosing the latter, we obtain

$$\frac{dH_i}{dt} + \frac{H_i}{\tau_m} = \frac{H_o}{\tau_m} \tag{9}$$

where

$$\tau_m = \frac{1}{2}\mu_o\sigma\Delta a \tag{10}$$

This expression pertains regardless of the driving field. In particular, suppose that before $t = 0$, the fields and surface current are zero, and that when $t = 0$, the outside H_o is suddenly turned on. The appropriate solution to (9) is the combination

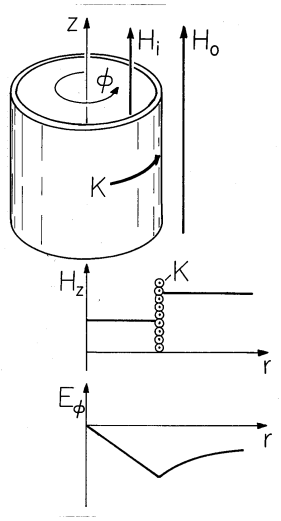


Fig. 10.3.2 Circular cylindrical conducting shell with external axial field intensity $H_o(t)$ imposed. The response to a step in applied field is a current density that initially shields the field from the inner region. As this current decays, the field penetrates into the interior and is finally uniform throughout.

of the particular solution $H_i = H_o$ and the homogeneous solution $\exp(-t/\tau_m)$ that satisfies the initial condition.

$$H_i = H_o(1 - e^{-t/\tau_m}) \tag{11}$$

It follows from (8) that the associated surface current density is

$$K = -H_o e^{-t/\tau_m} \tag{12}$$

At a given instant, the axial field has the radial distribution shown in Fig. 10.3.2b. Outside, the field is imposed to be equal to H_o, while inside it is at first zero but then fills in with an exponential dependence on time. After a time that is long compared to τ_m, the field is uniform throughout. Implied by the discontinuity in field intensity at $r = a$ is a surface current density that initially terminates the outside field. When $t = 0$, $K = -H_o$, and this results in a field that bucks out the field imposed on the inside region. The decay of this current, expressed by (12), accounts for the penetration of the field into the interior region.

This example illustrates what one means by "perfect conductor approximation." A perfect conductor would shield out the magnetic field forever. A physical conductor shields it out for times $t \ll \tau_m$. Thus, in the MQS approximation, a conductor can be treated as perfect for times that are short compared with the characteristic time τ_m. The electric field $E_\phi \equiv E$ is given by applying (3) to a contour having an arbitrary radius r.

$$2\pi r E = -\frac{d}{dt}(\mu_o H_i \pi r^2) \Rightarrow E = -\frac{\mu_o r}{2}\frac{dH_i}{dt} \qquad r < a \tag{13}$$

$$\begin{aligned} 2\pi r E &= -\frac{d}{dt}(\mu_o H_i \pi a^2) - \frac{d}{dt}[\mu_o H_o \pi (r^2 - a^2)] \Rightarrow \\ E &= -\frac{\mu_o a}{2}\left[\frac{a}{r}\frac{dH_i}{dt} + \left(\frac{r}{a} - \frac{a}{r}\right)\frac{dH_o}{dt}\right] \qquad r > a \end{aligned} \tag{14}$$

At $r = a$, this particular solution matches that already found using the same integral law in the conductor. In this simple case, it is not necessary to match boundary conditions by superimposing a homogeneous solution taking the form of a conservative field.

We consider next an example where the electric field is not simply the particular solution.

Example 10.3.2. Diffusion into Tube of Nonuniform Conductivity

Once again, consider the circular cylindrical shell of Fig. 10.3.2 subject to an imposed axial field $H_o(t)$. However, now the conductivity is a function of azimuthal position.

$$\sigma = \frac{\sigma_o}{1 + \alpha \cos \phi} \tag{15}$$

The integral in (5), resulting from Faraday's law, becomes

$$K \oint_C \frac{ds}{\Delta(s)\sigma(s)} = \frac{K}{\Delta\sigma_o} \int_0^{2\pi} (1 + \alpha \cos \phi) a d\phi = \frac{2\pi a}{\Delta\sigma_o} K \tag{16}$$

and hence

$$\frac{2\pi a}{\Delta\sigma_o} K = -\frac{d}{dt}(\pi a^2 \mu_o H_i) \tag{17}$$

Ampère's continuity condition, (2), once again becomes

$$K = -H_o + H_i \tag{18}$$

Thus, H_i is determined by the same expressions as in the previous example, except that σ is replaced by σ_o. The surface current response to a step in imposed field is again the exponential of (12).

It is the electric field distribution that is changed. Using (15), (4) gives

$$E = \frac{K}{\Delta\sigma_o}(1 + \alpha \cos \phi) \tag{19}$$

for the electric field inside the conductor. The E field in the adjacent free space regions is found using the familiar approach of Sec. 10.1. The particular solution is the same as for the uniformly conducting shell, (13) and (14). To this we add a homogeneous solution $\mathbf{E}_h = -\nabla\Phi$ such that the sum matches the tangential field given by (19) at $r = a$. The ϕ-independent part of (19) is already matched by the particular solution, and so the boundary condition on the homogeneous part requires that

$$-\frac{1}{a}\frac{\partial \Phi}{\partial \phi}(r = a) = \frac{K\alpha}{\Delta\sigma_o} \cos \phi \Rightarrow \Phi(r = a) = -\frac{K\alpha a}{\Delta\sigma_o} \sin \phi \tag{20}$$

Solutions to Laplace's equation that vary as $\sin(\phi)$ match this condition. Outside, the appropriate r dependence is $1/r$ while inside it is r. With the coefficients of these potentials adjusted to match the boundary condition given by (20), it follows that the electric field outside and inside the shell is

$$\mathbf{E} = \begin{cases} -\frac{\mu_o r}{2}\frac{dH_i}{dt}\mathbf{i}_\phi - \nabla\Phi_i & r < a \\ -\frac{\mu_o a}{2}\left[\frac{a}{r}\frac{dH_i}{dt} + \left(\frac{r}{a} - \frac{a}{r}\right)\frac{dH_o}{dt}\right]\mathbf{i}_\phi - \nabla\Phi_o & a < r \end{cases} \tag{21}$$

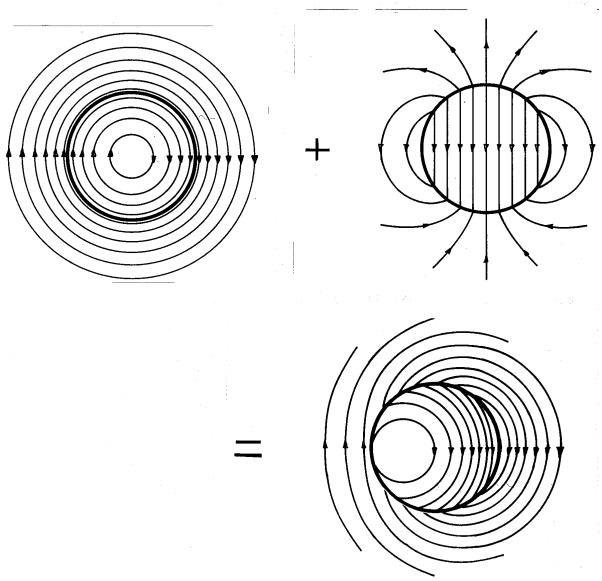


Fig. 10.3.3 Electric field induced in regions inside and outside shell (having conductivity that varies with azimuthal position) portrayed as the sum of a particular rotational and homogeneous conservative solution. Conductivity is low on the right and high on the left, $\alpha = 0.5$.

where

$$\Phi_i = -\frac{K\alpha}{\Delta\sigma_o} r \sin\phi \tag{22}$$

$$\Phi_o = -\frac{K\alpha a^2}{\Delta\sigma_o} \frac{\sin\phi}{r} \tag{23}$$

These expressions can be evaluated using (11) and (12) for H_i and K for the electric field associated with a step in applied field. It follows that **E**, like the surface current and the induced **H**, decays exponentially with the time constant of (10). At a given instant, the distribution of **E** is as illustrated in Fig. 10.3.3. The total solution is the sum of the particular rotational and homogeneous conservative parts. The degree to which the latter influences the total field depends on α, which reflects the inhomogeneity in conductivity.

For positive α, the conductivity is low on the right (when $\phi = 0$) and high on the left in Fig. 10.3.3. In accordance with (7.2.8), positive unpaired charge is induced in the transition region where the current flows from high to low conductivity, and negative charge is induced in the transition region from low to high conductivity. The field of the homogeneous solution shown in the figure originates and terminates on the induced charges.

We shall return to models based on conducting cylindrical shells in axial fields. Systems of conducting shells can be used to represent the nonuniform flow of current in thick conductors. The model will also be found useful in determining the rate of induction heating for cylindrical objects.

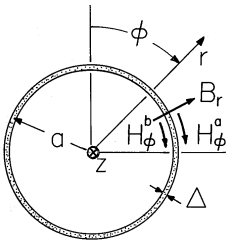


Fig. 10.4.1 Cross-section of circular cylindrical conducting shell having its axis perpendicular to the magnetic field.

10.4 DIFFUSION OF TRANSVERSE MAGNETIC FIELDS THROUGH THIN CONDUCTORS

In this section we study magnetic induction of currents in thin conducting shells by fields transverse to the shells. In Sec. 10.3, the magnetic fields were automatically tangential to the conductor surfaces, so we did not have the opportunity to explore the limitations of the boundary condition $\mathbf{n} \cdot \mathbf{B} = 0$ used to describe a "perfect conductor." In this section the imposed fields generally have components normal to the conducting surface.

The steps we now follow can be applied to many different geometries. We specifically consider the circular cylindrical shell shown in cross-section in Fig. 10.4.1. It has a length in the z direction that is very large compared to its radius a. Its conductivity is σ, and it has a thickness Δ that is much less than its radius a. The regions outside and inside are specified by (a) and (b), respectively.

The fields to be described are directed in planes perpendicular to the z axis and do not depend on z. The shell currents are z directed. A current that is directed in the $+z$ direction at one location on the shell is returned in the $-z$ direction at another. The closure for this current circulation can be imagined to be provided by perfectly conducting endplates, or by a distortion of the current paths from the z direction near the cylinder ends (end effect).

The shell is assumed to have essentially the same permeability as free space. It therefore has no tendency to guide the magnetic flux density. Integration of the *magnetic flux continuity* condition over an incremental volume enclosing a section of the shell shows that the normal component of $\mathbf{B}$ is continuous through the shell.

$$\mathbf{n} \cdot (\mathbf{B}^a - \mathbf{B}^b) = 0 \Rightarrow B_r^a = B_r^b \tag{1}$$

Ohm's law relates the axial current density to the axial electric field, $J_z = \sigma E_z$. This density is presumed to be essentially uniformly distributed over the radial cross-section of the shell. Multiplication of both sides of this expression by the thickness Δ of the shell gives an expression for the surface current density in the shell.

$$K_z \equiv \Delta J_z = \Delta \sigma E_z \tag{2}$$

Faraday's law is a vector equation. Of the three components, the radial one is dominant in describing how the time-varying magnetic field induces electric fields, and hence currents, tangential to the shell. In writing this component, we assume that the fields are independent of z.

$$\frac{1}{a}\frac{\partial E_z}{\partial \phi} = -\frac{\partial B_r}{\partial t} \tag{3}$$

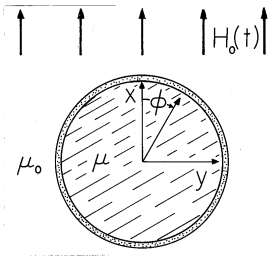


Fig. 10.4.2 Circular cylindrical conducting shell filled by insulating material of permeability μ and surrounded by free space. A magnetic field $H_o(t)$ that is uniform at infinity is imposed transverse to the cylinder axis.

Ampère's continuity condition makes it possible to express the surface current density in terms of the tangential fields to either side of the shell.

$$K_z = H_\phi^a - H_\phi^b \tag{4}$$

These last three expressions are now combined to obtain the desired continuity condition.

$$\boxed{\frac{1}{\Delta\sigma a}\frac{\partial}{\partial\phi}(H_\phi^a - H_\phi^b) = -\frac{\partial B_r}{\partial t}} \tag{5}$$

Thus, the description of the shell is encapsulated in the two continuity conditions, (1) and (5).

The thin-shell model will now be used to place in perspective the idealized boundary condition of perfect conductivity. In the following example, the conductor is subjected to a field that is suddenly turned on. The field evolution with time places in review the perfect conductivity mode of MQS systems in Chap. 8 and the magnetization phenomena of Chap. 9. Just after the field is turned on, the shell acts like the perfect conductors of Chap. 8. As time goes on, the shell currents decay to zero and only the magnetization of Chap. 9 persists.

Example 10.4.1. Diffusion of Transverse Field into Circular Cylindrical Conducting Shell with a Permeable Core

A permeable circular cylindrical core having radius a is shown in Fig. 10.4.2. It is surrounded by a thin conducting shell, having thickness Δ and conductivity σ. A uniform time-varying magnetic field intensity $H_o(t)$ is imposed transverse to the axis of the shell and core. The configuration is long enough in the axial direction to justify representing the fields as independent of the axial coordinate z.

Reflecting the fact that the region outside (o) is free space while that inside (i) is the material of linear permeability are the constitutive laws

$$\mathbf{B}^o = \mu_o\mathbf{H}^o; \qquad \mathbf{B}^i = \mu\mathbf{H}^i \tag{6}$$

For the two-dimensional fields in the $r-\phi$ plane, where the sheet current is in the z direction, the scalar potential provides a convenient description of the field.

$$\mathbf{H} = -\nabla\Psi \tag{7}$$

We begin by recognizing the form taken by Ψ far from the cylinder.

$$\Psi = -H_o r \cos\phi \tag{8}$$

Note that substitution of this relation into (7) indeed gives the uniform imposed field.

Given the ϕ dependence of (8), we assume solutions of the form

$$\Psi^o = -H_o r \cos\phi + A\frac{\cos\phi}{r} \tag{9}$$

$$\Psi^i = Cr\cos\phi$$

where A and C are coefficients to be determined by the continuity conditions. In preparation for the evaluation of these conditions, the assumed solutions are substituted into (7) to give the flux densities

$$\mathbf{B}^o = \mu_o\big(H_o + \frac{A}{r^2}\big)\cos\phi\mathbf{i}_\mathbf{r} - \mu_o\big(H_o - \frac{A}{r^2}\big)\sin\phi\mathbf{i}_\phi \tag{10}$$

$$\mathbf{B}^i = -\mu C(\cos\mathbf{i}_\mathbf{r} - \sin\phi\mathbf{i}_\phi)$$

Should we expect that these functions can be used to satisfy the continuity conditions at $r = a$ given by (1) and (5) at every azimuthal position ϕ? The inside and outside radial fields have the same ϕ dependence, so we are assured of being able to adjust the two coefficients to satisfy the flux continuity condition. Moreover, in evaluating (5), the ϕ derivative of H_ϕ has the same ϕ dependence as B_r. Thus, satisfying the continuity conditions is assured.

The first of two relations between the coefficients and H_o follows from substituting (10) into (1).

$$\mu_o\big(H_o + \frac{A}{a^2}\big) = -\mu C \tag{11}$$

The second results from a similar substitution into (5).

$$-\frac{1}{\Delta\sigma a}\big(H_o - \frac{A}{a^2}\big) - \frac{C}{\Delta\sigma a} = -\mu_o\left(\frac{dH_o}{dt} + \frac{1}{a^2}\frac{dA}{dt}\right) \tag{12}$$

With C eliminated from this latter equation by means of (11), we obtain an ordinary differential equation for $A(t)$.

$$\frac{dA}{dt} + \frac{A}{\tau_m} = -a^2\frac{dH_o}{dt} + \frac{H_o a}{\mu_o\Delta\sigma}\big(1 - \frac{\mu_o}{\mu}\big) \tag{13}$$

The time constant τ_m takes the form of (10.2.7).

$$\tau_m = \mu_o\sigma\Delta a\big(\frac{\mu}{\mu + \mu_o}\big) \tag{14}$$

In (13), the time dependence of the imposed field is arbitrary. The form of this expression is the same as that of (7.9.28), so techniques for dealing with initial conditions and for determining the sinusoidal steady state response introduced there are directly applicable here.

Response to a Step in Applied Field. Suppose there is no field inside or outside the conducting shell before $t = 0$ and that H_o is a step function of magnitude H_m turned on when $t = 0$. With D a coefficient determined by the initial condition, the solution to (13) is the sum of a particular and a homogeneous solution.

$$A = H_m a^2 \frac{(\mu - \mu_o)}{(\mu + \mu_o)} + De^{-t/\tau_m} \tag{15}$$

Integration of (13) from $t = 0^-$ to $t = 0^+$ shows that $A(0) = -H_m a^2$, so that D is evaluated and (15) becomes

$$A = H_m a^2 \left[\frac{(\mu - \mu_o)}{(\mu + \mu_o)} (1 - e^{-t/\tau_m}) - e^{-t/\tau_m} \right] \tag{16}$$

This expression makes it possible to evaluate C using (11). Finally, these coefficients are substituted into (9) to give the potential outside and inside the shell.

$$\Psi^o = -H_m a \left\{ \frac{r}{a} - \frac{a}{r} \left[\frac{(\mu - \mu_o)}{(\mu + \mu_o)} (1 - e^{-t/\tau_m}) - e^{-t/\tau_m} \right] \right\} \cos\phi \tag{17}$$

$$\Psi^i = -H_m a \frac{r}{a} \frac{2\mu_o}{(\mu + \mu_o)} (1 - e^{-t/\tau_m}) \cos\phi \tag{18}$$

The field evolution represented by these expressions is shown in Fig. 10.4.3, where lines of $\mathbf{B}$ are portrayed. When the transverse field is suddenly turned on, currents circulate in the shell in such a direction as to induce a field that bucks out the one imposed. For an applied field that is positive, this requires that the surface current be in the $-z$ direction on the right and returned in the $+z$ direction on the left. This surface current density can be analytically expressed first by using (10) to evaluate Ampère's continuity condition

$$K_z = H_\phi^o - H_\phi^i = \left[-H_o \left(1 - \frac{\mu_o}{\mu} \right) + \frac{A}{a^2} \left(1 + \frac{\mu_o}{\mu} \right) \right] \sin\phi \tag{19}$$

and then by using (15).

$$K_z = -2H_m e^{-t/\tau_m} \sin\phi \tag{20}$$

With the decay of K_z, the external field goes from that for a perfect conductor (where $\mathbf{n} \cdot \mathbf{B} = 0$) to the field that would have been found if there were no conducting shell. The magnetizable core tends to draw this field into the cylinder.

The coefficient A represents the amplitude of a two-dimensional dipole that has a field equivalent to that of the shell current. Just after the field is applied, A is negative and hence the equivalent dipole moment is directed opposite to the imposed field. This results in a field that is diverted around the shell. With the passage of time, this dipole moment can switch sign. This sign reversal occurs only if $\mu > \mu_o$, making it clear that it is due to the magnetization of the core. In the absence of the core, the final field is uniform.

Under what conditions can the shell be regarded as perfectly conducting? The answer involves not only σ but also the time scale and the size, and to some extent,

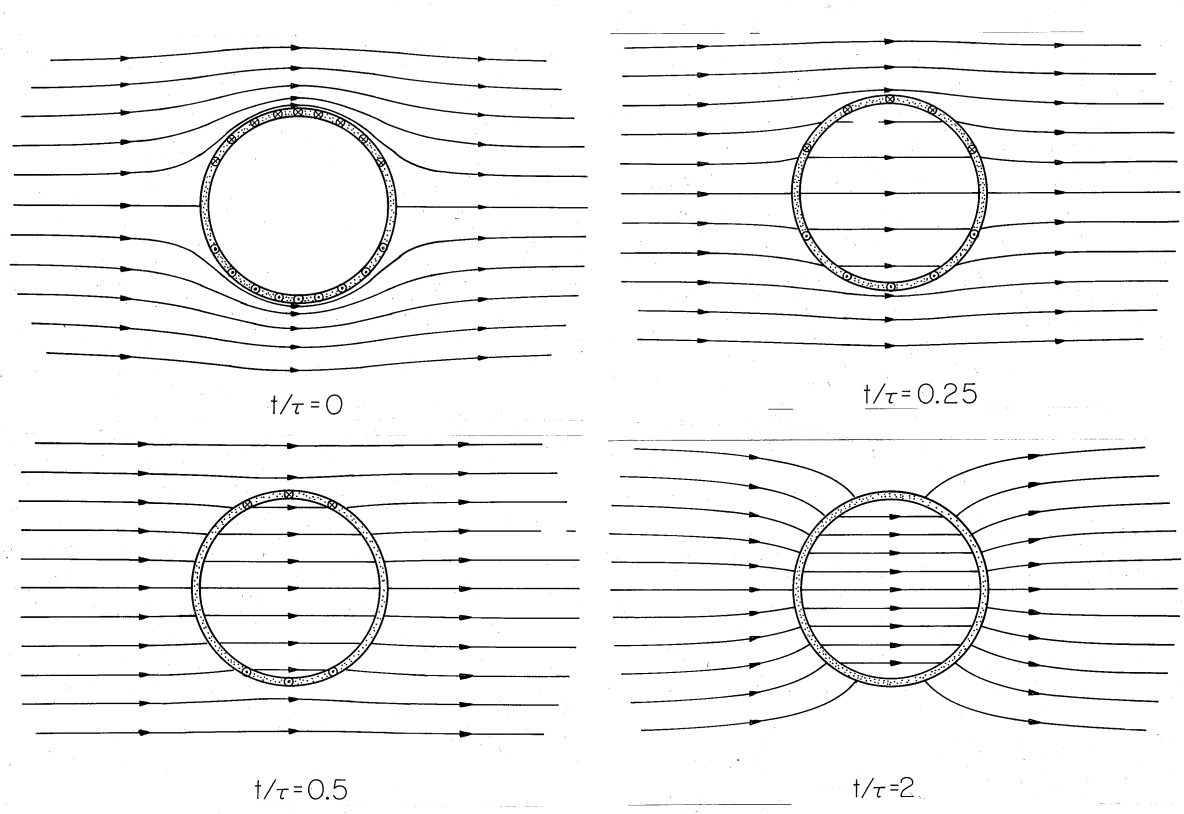


Fig. 10.4.3 When $t = 0$, a magnetic field that is uniform at infinity is suddenly imposed on the circular cylindrical conducting shell. The cylinder is filled by an insulating material of permeability $\mu = 200\mu_o$. When $t/\tau = 0$, an instant after the field is applied, the surface currents completely shield the field from the central region. As time goes on, these currents decay, until finally the field is no longer influenced by the conducting shell. The final field is essentially perpendicular to the highly permeable core. In the absence of this core, the final field would be uniform.

the permeability. For our step response, the shell shields out the field for times that are short compared to τ_m, as given by (14).

Demonstration 10.4.1. Currents Induced in a Conducting Shell

The apparatus of Demonstration 10.2.1 can be used to make evident the shell currents predicted in the previous example. A cylinder of aluminum foil is placed on the driver coil, as shown in Fig. 10.4.4. With the discharge of the capacitor through the coil, the shell is subjected to an abruptly applied field. By contrast with the step function assumed in the example, this field oscillates and decays in a few cycles. However, the reversal of the field results in a reversal in the induced shell current, so regardless of the time dependence of the driving field, the force density $\mathbf{J} \times \mathbf{B}$ is in the same direction.

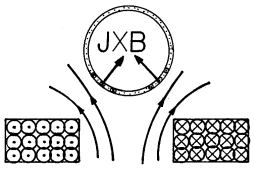


Fig. 10.4.4 In an experiment giving evidence of the currents induced when a field is suddenly applied transverse to a conducting cylinder, an aluminum foil cylinder, subjected to the field produced by the experiment of Fig. 10.2.2, is crushed.

The force associated with the induced current is inward. If the applied field were truly uniform, the shell would then be "squashed" inward from the right and left by the field. Because the field is not really uniform, the cylinder of foil is observed to be compressed inward more at the bottom than at the top, as suggested by the force vectors drawn in Fig. 10.4.4. Remember that the postulated currents require paths at the ends of the cylinder through which they can circulate. In a roll of aluminum foil, these return paths are through the shell walls in those end regions that extend beyond the region of the applied field.

The derivation of the continuity conditions for a circular cylindrical shell follows a format that is applicable to other geometries. Examples are a planar sheet and a spherical shell.

10.5 MAGNETIC DIFFUSION LAWS

The self-consistent evolution of the magnetic field intensity $\mathbf{H}$ with its source $\mathbf{J}$ induced in Ohmic materials of finite conductivity is familiar from the previous two sections. In the models so far considered, the induced currents were in thin conducting shells. Thus, in the processes of magnetic relaxation described in these sections, the currents were confined to thin regions that could be represented by dynamic continuity conditions.

In this and the next two sections, the conductor extends throughout at least part of a volume of interest. Like $\mathbf{H}$, the current density in Ampère's law

$$\nabla \times \mathbf{H} = \mathbf{J} \tag{1}$$

is an unknown function. For an Ohmic material, it is proportional to the local electric field intensity.

$$\mathbf{J} = \sigma \mathbf{E} \tag{2}$$

In turn, $\mathbf{E}$ is induced in accordance with Faraday's law

$$\nabla \times \mathbf{E} = -\frac{\partial \mu \mathbf{H}}{\partial t} \tag{3}$$

The conductor is presumed to have uniform conductivity σ and permeability μ. For linear magnetization, the magnetic flux continuity law is

$$\nabla \cdot \mu \mathbf{H} = 0 \tag{4}$$

In the MQS approximation the current density **J** is also solenoidal, as can be seen by taking the divergence of Ampère's law.

$$\nabla \cdot \mathbf{J} = 0 \tag{5}$$

In the previous two sections, we combined the continuity conditions implied by (1) and (4) with the other laws to obtain dynamic continuity conditions representing thin conducting sheets. The regions between sheets were insulating, and so the field distributions in these regions were determined by solving Laplace's equation. Here we combine the differential laws to obtain a new differential equation that takes on the role of Laplace's equation in determining the distribution of magnetic field intensity.

If we solve Ohm's law, (2), for **E** and substitute for **E** in Faraday's law, we have in one statement the link between magnetic induction and induced current density.

$$\nabla \times \left(\frac{\mathbf{J}}{\sigma} \right) = -\frac{\partial \mu \mathbf{H}}{\partial t} \tag{6}$$

The current density is eliminated from this expression by using Ampère's law, (1). The result is an expression of **H** alone.

$$\nabla \times \left(\frac{\nabla \times \mathbf{H}}{\sigma} \right) = -\frac{\partial \mu \mathbf{H}}{\partial t} \tag{7}$$

This expression assumes a somewhat more familiar appearance when σ and μ are constants, so that they can be taken outside the operations. Further, it follows from (4) that **H** is solenoidal so the use of a vector identity[2] turns (7) into

$$\boxed{\frac{1}{\mu\sigma} \nabla^2 \mathbf{H} = \frac{\partial \mathbf{H}}{\partial t}} \tag{8}$$

At each point in a material having uniform conductivity and permeability, the magnetic field intensity satisfies this vector form of the *diffusion equation*. The distribution of current density implied by the **H** found by solving this equation with appropriate boundary conditions follows from Ampère's law, (1).

Physical Interpretation. With the understanding that **H** and **J** are solenoidal, the derivation of (8) identifies the feedback between source and field that underlies the magnetic diffusion process. The effect of the (time-varying) field on the source embodied in the combined laws of Faraday and Ohm, (6), is perhaps best appreciated by integrating (6) over any fixed open surface S enclosed by a contour C. By Stokes' theorem, the integration of the curl over the surface transforms into an integration around the enclosing contour. Thus, (6) implies that

$$-\oint_C \frac{\mathbf{J}}{\sigma} \cdot d\mathbf{s} = \frac{d}{dt} \int_S \mu \mathbf{H} \cdot d\mathbf{a} \tag{9}$$

[2] $\nabla \times \nabla \times \mathbf{H} = \nabla(\nabla \cdot \mathbf{H}) - \nabla^2 \mathbf{H}$

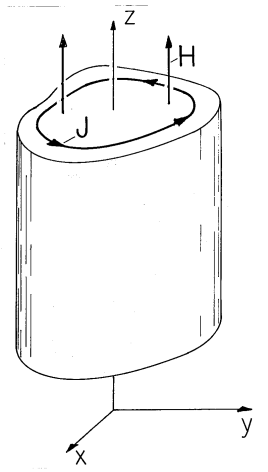


Fig. 10.5.1 Configurations in which cylindrically shaped conductors having axes parallel to the magnetic field have currents transverse to the field in $x-y$ planes.

and requires that the electromotive force around *any* closed path must be equal to the time rate of change of the enclosed magnetic flux. Numerical approaches to solving magnetic diffusion problems may in fact approximate a system by a finite number of circuits, each representing a current tube with its own resistance and flux linkage. To represent the return effect of the current on **H**, the diffusion equation also incorporates Ampère's law, (1).

The relaxation of axial fields through thin shells, developed in Sec. 10.3, is an example where the geometry of the conductor and the symmetry make the current tubes described by (9) readily discernible. The diffusion of an axial magnetic field H_z into the volume of cylindrically shaped conductors, as shown in Fig. 10.5.1, is a generalization of the class of axial problems described in Sec. 10.3. As the only component of **H**, $H_z(x,y)$ must satisfy (8).

$$\frac{1}{\mu\sigma}\nabla^2 H_z = \frac{\partial H_z}{\partial t} \tag{10}$$

The current density is then directed transverse to this field and given in terms of H_z by Ampère's law.

$$\mathbf{J} = \mathbf{i_x}\frac{\partial H_z}{\partial y} - \mathbf{i_y}\frac{\partial H_z}{\partial x} \tag{11}$$

Thus, the current density circulates in $x-y$ planes.

Methods for solving the diffusion equation are natural extensions of those used in previous chapters for dealing with Laplace's equation. Although we confine ourselves in the next two sections to diffusion in one spatial dimension, the thin-shell models give an intuitive impression as to what can be expected as magnetic fields diffuse into solid conductors having a wide range of geometries.

Consider the coaxial thin shells shown in Fig. 10.5.2 as a model for a solid cylindrical conductor. Following the approach outlined in Sec. 10.3, suppose that the exterior field H_o is an imposed function of time. Then the fields between sheets (H_1

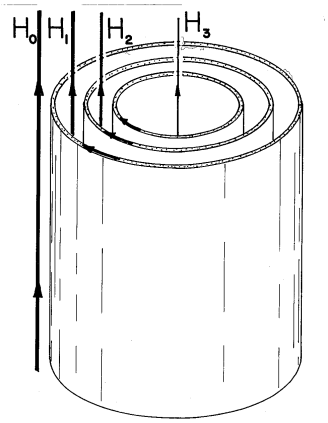


Fig. 10.5.2 Example of an axial field configuration composed of coaxial conducting shells of infinite axial length. When an exterior field H_o is applied, currents circulating in the shells tend to shield out the imposed field.

and H_2) and in the central region (H_3) are determined by a system of three ordinary differential equations having $H_o(t)$ as a drive. Associated with the evolution of these fields are surface currents in the shells that tend to shield the field from the region within. In the limit where the number of shells is infinite, the field distribution in a solid conductor could be represented by such coupled thin shells. However, the more practical approach used in the next sections is to solve the diffusion equation exactly. The situations considered are in cartesian rather than polar coordinates.

10.6 MAGNETIC DIFFUSION TRANSIENT RESPONSE

The self-consistent distribution of current density and magnetic field intensity in the volume of a uniformly conducting material is determined from the laws given in Sec. 10.5 and summarized by the magnetic diffusion equation (10.5.8). In this section, we illustrate magnetic diffusion phenomena by considering the transient that results when a current is abruptly turned on or off.

In contrast to Laplace's equation, the diffusion equation involves a time rate of change, and so it is necessary to deal with the time dependence in much the same way as the space dependence. The diffusion process considered in this section is in one spatial dimension, with time as the second "dimension." Our approach builds on product solutions and the solution of boundary value problems by superposition, as introduced in Chap. 5.

The class of configurations of interest is illustrated in Fig. 10.6.1. Perfectly conducting electrodes are driven along their edges at $x = -b$ by a distributed current source. The uniformly conducting material is sandwiched between these electrodes. The current originating in the source then circulates in the x direction through the electrode in the $y = 0$ plane to a point where it passes in the y direction through the conducting material. It is then returned to the source through the other perfectly conducting plate. Note that this configuration is a special case of

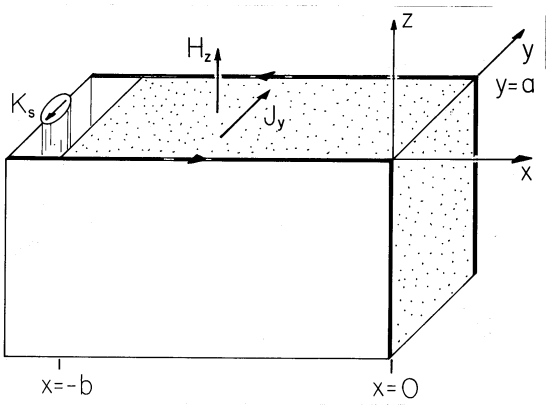


Fig. 10.6.1 A block of uniformly conducting material having length b and thickness a is sandwiched between perfectly conducting electrodes that are driven along their edges at $x = -b$ by a distributed current source. Current density and field intensity in the block are, respectively, y and z directed, each depending on (x, t).

that shown in Fig. 10.5.1, where the current density is transverse to a magnetic field intensity that has only one component, H_z.

If this field and the associated current density are indeed independent of y, then it follows from (10.5.10) and (10.5.11) that H_z satisfies the one-dimensional diffusion equation

$$\frac{1}{\mu\sigma}\frac{\partial^2 H_z}{\partial x^2} = \frac{\partial H_z}{\partial t} \tag{1}$$

and the only component of the current density is related to H_z by Ampère's law

$$\mathbf{J} = -\mathbf{i_y}\frac{\partial H_z}{\partial x} \tag{2}$$

Note that this one-dimensional model correctly requires that the current density, and hence the electric field intensity, be normal to the perfectly conducting electrodes at $y = 0$ and $y = a$.

The distributed current source, perfectly conducting sheets and conducting block form a closed path for currents that circulate in $x-y$ planes. These extend to infinity in the $+$ and $-z$ directions in the manner of an infinite one-turn solenoid. The field outside the outermost of these current paths is therefore taken as being zero. Ampère's continuity condition then requires that at the surface $x = -b$, where the distributed current source is located, the enclosed magnetic field intensity be equal to the imposed surface current density K_s. In the plane $x = 0$, the situation is similar except that there is no surface current density, and so the magnetic field intensity must be zero. Thus, consistent with solving a differential equation that is second order in x, are the two boundary conditions

$$H_z(-b, t) = K_s(t), \qquad H_z(0, t) = 0 \tag{3}$$

The equation is first order in its time dependence, suggesting that to complete the specification of the transient solution, the initial value of H_z must also be given.

$$H_z(x, 0) = H_i(x) \tag{4}$$

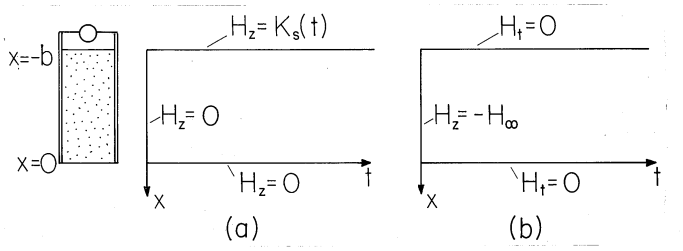


Fig. 10.6.2 Boundary and initial conditions for one-dimensional magnetic diffusion pictured in the $x - t$ plane. (a) The total fields at the ends of the block are constrained to be equal to the driving surface current density and to zero, respectively, while there is one initial condition when $t = 0$. (b) The transient part of the solution is zero at the boundaries and satisfies the initial condition that makes the total solution assume the current value when $t = 0$.

It is helpful to picture the boundary and initial conditions needed to uniquely specify solutions to (2) in the $x - t$ plane, as shown in Fig. 10.6.2a. Here the conducting block can be pictured as extending from $x = 0$ to $x = -b$, with the field between a function of x that evolves in the t "direction." Presumably, the distribution of H_z in the $x-t$ space is predicted by (1) with the boundary conditions of (3) at $x = 0$ and $x = -b$ and the initial condition of (4) when $t = 0$.

Is the solution for $H_z(t)$ uniquely specified by (1), the boundary conditions of (3), and the initial condition of (4)? A proof that it is can be made following a line of reasoning suggested by the EQS uniqueness arguments of Sec. 7.8.

Suppose that the drive is a step function of time, so that the final state is one of uniform steady conduction. Then, the linearity of (1) makes it possible to think of the total field as being the superposition of this steady field and a transient part.

$$H_z = H_\infty(x) + H_t(x,t) \tag{5}$$

The steady solution, which presumably prevails as $t \to \infty$, satisfies (1) with the time derivative set equal to zero,

$$\frac{\partial^2 H_\infty}{\partial x^2} = 0 \tag{6}$$

while the transient part satisfies the complete equation.

$$\frac{1}{\mu\sigma}\frac{\partial^2 H_t}{\partial x^2} = \frac{\partial H_t}{\partial t} \tag{7}$$

Because the steady solution satisfies the boundary conditions for all time $t > 0$, the boundary conditions satisfied by the transient part are homogeneous.

$$H_t(-b,t) = 0; \qquad H_t(0,t) = 0 \tag{8}$$

However, the steady solution does not satisfy the initial condition. The transient solution is therefore adjusted so that the total solution does.

$$H_t(x,0) = H_i(x) - H_\infty(x) \tag{9}$$

The conditions satisfied by the transient part of the solution on the boundaries in the $x-t$ space are pictured in Fig. 10.6.2b.

Product Solutions to the One-Dimensional Diffusion Equation. The approach now used to find the H_t that satisfies (7) and the conditions of (8) and (9) is familiar from finding Cartesian coordinate product solutions to Laplace's equation in two dimensions in Sec. 5.4. Here the second "dimension" is t and we consider solutions that take the form $H_t = X(x)T(t)$. Substitution into (7) and division by XT gives

$$\frac{1}{X}\frac{d^2X}{dx^2} - \frac{\mu\sigma}{T}\frac{dT}{dt} = 0 \tag{10}$$

With the first term taken as $-k^2$ and the second as k^2, it follows that

$$\frac{1}{X}\frac{d^2X}{dx^2} = -k^2 \Rightarrow \frac{d^2X}{dx^2} + k^2X = 0 \tag{11}$$

and

$$-\frac{\mu\sigma}{T}\frac{dT}{dt} = k^2 \Rightarrow \frac{dT}{dt} + \frac{k^2}{\mu\sigma}T = 0 \tag{12}$$

Given the boundary conditions of (8), the appropriate solution to (11) is

$$X = \sin kx; \qquad k = \frac{n\pi}{b} \tag{13}$$

where n can be any integer. Associated with each of these modes is a time dependence given by (12) as a decaying exponential with the time constant

$$\tau_n = \frac{\mu\sigma b^2}{(n\pi)^2} \tag{14}$$

Thus, we are led to a transient part of the solution that is itself a superposition of modes, each satisfying the boundary conditions.

$$H_t = \sum_{n=1}^{\infty} C_n \sin\left(\frac{n\pi}{b}x\right)e^{-t/\tau_n} \tag{15}$$

When $t = 0$, the modes take the form of a Fourier series. Thus, the coefficients C_n can be used to satisfy the initial condition, (9).

In the following example, the coefficients are evaluated for specific initial conditions. However, because the "short time" and "long time" field and current distributions are known at the outset, much of the dynamics can be anticipated at the outset. For times that are very short compared to the magnetic diffusion time $\mu\sigma b^2$, the conducting block must act as a perfect conductor. In this short time limit, we know from Chap. 8 that the current from the distributed source is confined to the surface at $x = -b$. Thus, for early times, the distribution represented by the series of (15) tends to be an impulse function of x. After many magnetic diffusion

times, the current reaches a steady state and achieves a distribution that would be predicted in the first half of Chap. 7. The following example fills in the evolution from the field of a perfectly conducting system to that for steady conduction.

Example 10.6.1. Response to a Step in Current

When $t = 0$, suppose that there are no currents or associated fields. Then the current source suddenly becomes the constant K_p. The solution to (6) that is zero at $x = 0$ and is K_p at $x = -b$ is

$$H_\infty = -K_p \frac{x}{b} \tag{16}$$

This is the field associated with a constant current density K_p/b that is uniformly distributed over the cross-section of the block.

Because there is no initial magnetic field, it follows from (9) that the initial transient part of the field must cancel the steady part.

$$H_t(x,0) = K_p \frac{x}{b} \tag{17}$$

This must be the distribution of H_t given by (15) when $t = 0$.

$$K_p \frac{x}{b} = \sum_{n=1}^{\infty} C_n \sin\left(\frac{n\pi}{b}x\right) \tag{18}$$

Following the procedure familiar from Sec. 5.5, the coefficients C_n are now evaluated by multiplying both sides of this expression by $\sin(m\pi/b)$, multiplying by dx, and integrating from $x = -b$ to $x = 0$.

$$\int_{-b}^{0} K_p \frac{x}{b} \sin\left(\frac{m\pi}{b}x\right)dx = \sum_{n=1}^{\infty} C_n \int_{-b}^{0} \sin\left(\frac{n\pi}{b}x\right)\sin\left(\frac{m\pi}{b}x\right)dx \tag{19}$$

From the series on the right, only the term $m = n$ is not zero. Carrying out the integration on the left[3] then gives an expression that can be solved for C_m. Replacing $m \to n$ then gives

$$C_n = -2K_p \frac{(-1)^n}{n\pi} \tag{20}$$

Finally, (16) and (15) [the latter evaluated using (20)] are superimposed as required by (5) to give the desired description of how the field evolves as a function of space and time.

$$H_z = -K_p \frac{x}{b} - \sum_{n=1}^{\infty} 2K_p \frac{(-1)^n}{n\pi} \sin\left(\frac{n\pi x}{b}\right) e^{-t/\tau_n} \tag{21}$$

The distribution of current density follows from this expression substituted into Ampère's law, (2).

$$J_y = \frac{K_p}{b} + \sum_{n=1}^{\infty} 2K_p \frac{(-1)^n}{b} \cos\left(\frac{n\pi x}{b}\right) e^{-t/\tau_n} \tag{22}$$

[3] $\int \sin(u)u\,du = \sin(u) - u\cos(u)$

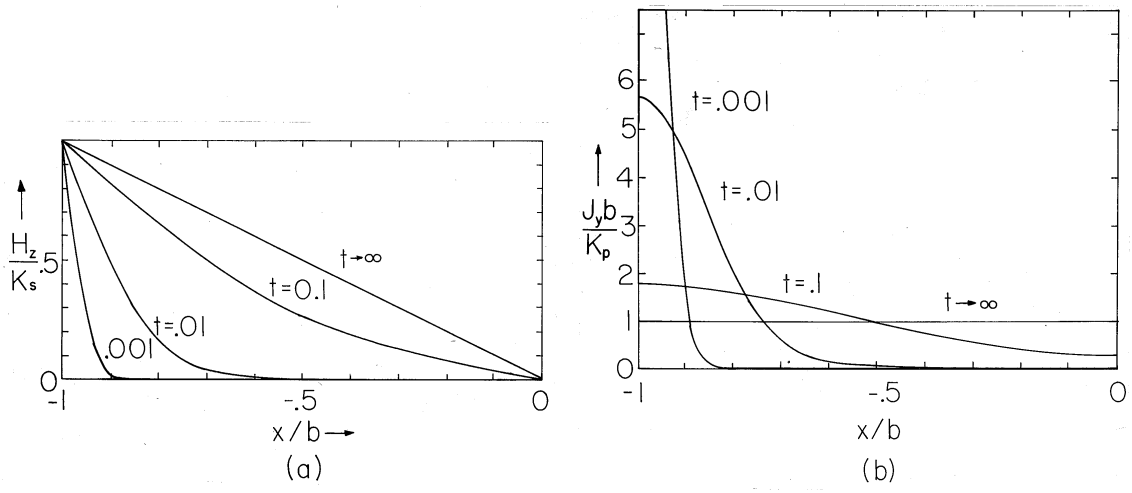


Fig. 10.6.3 (a) Distribution of H_z in the conducting block of Fig. 10.6.1 in response to applying a step in current with no initial field. In terms of time normalized to the magnetic diffusion time based on the length b, the field diffuses into the block, finally assuming the linear distribution expected for steady conduction. (b) Distribution of J_y with normalized time as a parameter. The initial distribution is an impulse (a surface current density) at $x = -b$, while the final distribution is uniform.

These expressions are pictured in Fig. 10.6.3. Note that the higher the order of a term, the more rapid its exponential decay with time. As a result, the most terms in the series are needed when $t = 0^+$. These are needed to make the initial magnetic field intensity zero and the initial current density an impulse at $x = -b$. Because the lowest mode in the transient part of either H_z or J_y has the longest time constant, the long-time response is dominated by the steady response and the first term in the series. Of course, with the decay of the transient part, the field approaches a linear x dependence while the current density assumes the uniform distribution expected for a steady current.

10.7 SKIN EFFECT

If the surface current source driving the conducting block of Fig. 10.6.1 is a sinusoidal function of time

$$K_s(t) = Re\hat{K}_s e^{j\omega t} \tag{1}$$

the current density tends to circulate through the block in the neighborhood of the surface adjacent to the source. This tendency for the sinusoidal steady state current to return to the source through the thin zone or skin region nearest to the source gives another view of magnetic diffusion.

To illustrate skin effect in specific terms we return to the one-dimensional diffusion configuration of Sec. 10.6, Fig. 10.6.1. Once again, the distributions of H_z

and J_y are governed by the one-dimensional diffusion equation and Ampère's law, (10.6.1) and (10.6.2).

The diffusion equation is linear and has coefficients that are independent of time. We can expect a sinusoidal steady state response having the same frequency as the drive, (1). The solution to the diffusion equation is therefore taken as having a product form, but with the time dependence stipulated at the outset.

$$H_z = Re\hat{H}_z(x)e^{j\omega t} \tag{2}$$

At a given location x, the coefficient of the exponential is a complex number specifying the magnitude and phase of the field.

Substitution of (2) into the diffusion equation, (10.6.1), shows that the complex amplitude has an x dependence governed by

$$\frac{d^2\hat{H}_z}{dx^2} - \gamma^2\hat{H}_z = 0 \tag{3}$$

where $\gamma^2 \equiv j\omega\mu\sigma$.

Solutions to (3) are simply $\exp(\mp\gamma x)$. However, γ is complex. If we note that $\sqrt{j} = (1+j)/\sqrt{2}$, then it follows that

$$\gamma = \sqrt{j\omega\mu\sigma} = (1+j)\sqrt{\frac{\omega\mu\sigma}{2}} \tag{4}$$

In terms of the *skin depth* δ, defined by

$$\delta \equiv \sqrt{\frac{2}{\omega\mu\sigma}} \tag{5}$$

One can also write (4) as

$$\gamma = \frac{(1+j)}{\delta} \tag{6}$$

With C_+ and C_- arbitrary coefficients, solutions to (3) are therefore

$$\hat{H}_z = C_+e^{-(1+j)\frac{x}{\delta}} + C_-e^{(1+j)\frac{x}{\delta}} \tag{7}$$

Before considering a detailed example where these coefficients are evaluated using the boundary conditions, consider the $x-t$ dependence of the field represented by the first solution in (7). Substitution into (2) gives

$$H_z = Re\left[C_1e^{-\frac{x}{\delta}}e^{j(\omega t-\frac{x}{\delta})}\right] \tag{8}$$

making it clear that the field magnitude is an exponentially decaying function of x. Within the envelope with the decay length δ shown in Fig. 10.7.1, the field propagates in the x direction. That is, points of constant phase on the field distribution have $\omega t - x/\delta =$ constant and hence move in the x direction with the velocity $\omega\delta$.

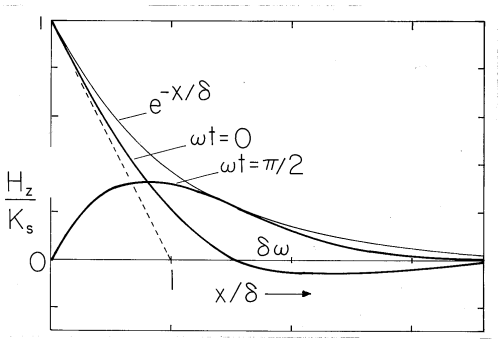


Fig. 10.7.1 Magnetic diffusion wave in the sinusoidal steady state, showing envelope with decay length δ and instantaneous field at two different times. The point of zero phase propagates with the velocity $\omega\delta$.

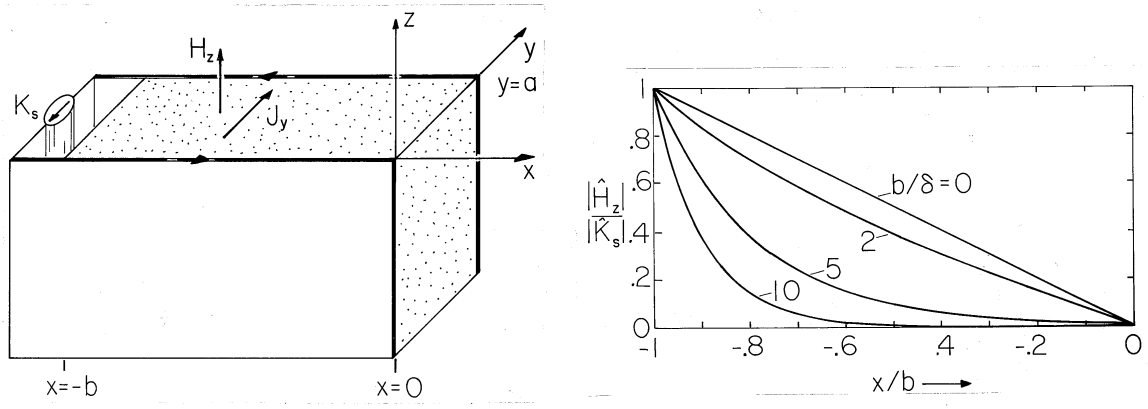


Fig. 10.7.2 (a) One-dimensional magnetic diffusion in the sinusoidal steady state in the same configuration as considered in Sec. 10.6. (b) Distribution of the magnitude of H_z in the conducting block of (a) as a function of the skin depth. Decreasing the skin depth is equivalent to raising the frequency.

Although the phase propagation signifies that at a given instant, the field (and current density) are positive in one region while negative in another, the propagation is difficult to discern because the decay is very rapid.

The second solution in (7) represents a similar diffusion wave, but decaying and propagating in the $-x$ rather than the $+x$ direction. The following illustrates how the two diffusion waves combine to satisfy boundary conditions.

Example 10.7.1. Diffusion into a Conductor of Finite Thickness

We consider once again the field distribution in a conducting material sandwiched between perfectly conducting plates, as shown in either Fig. 10.7.2 or Fig. 10.6.1. The surface current density of the drive is given by (1) and it is assumed that any transient reflecting the initial conditions has died out. How does the frequency dependence of the field distribution in the conducting block reflect the magnetic diffusion process?

Boundary conditions on H_z are the same as in Sec. 10.6, $H_z(-b,t) = K_s(t)$ and $H_z(0,t) = 0$. These are satisfied by adjusting the complex amplitude so that

$$\hat{H}_z(-b) = \hat{K}_s; \qquad \hat{H}_z(0) = 0 \tag{9}$$

It follows from (7) that the second of these is satisfied if $C_+ = -C_-$. The first condition then serves to evaluate C_+ and hence C_-, so that

$$\hat{H}_z = \hat{K}_s \frac{\left(e^{-(1+j)\frac{x}{\delta}} - e^{(1+j)\frac{x}{\delta}}\right)}{\left(e^{(1+j)\frac{b}{\delta}} - e^{-(1+j)\frac{b}{\delta}}\right)} \tag{10}$$

This expression represents the superposition of fields propagating and decaying in the $\pm x$ directions, respectively. Evaluated at a given location x, it is a complex number. In accordance with (2), H_z is the real part of this number multiplied by $\exp(j\omega t)$. The magnitude of H_z is the magnitude of (10), and is shown with the skin depth as a parameter by Fig. 10.7.2.

Consider the field distribution in two limits. First, suppose that the skin depth is very large compared to the thickness b of the conducting block. This might be the limit in which the frequency is made very low compared to the reciprocal magnetic diffusion time based on the conductor thickness.

$$\delta \gg b \Rightarrow \frac{2}{\omega\mu\sigma} \gg b^2 \Rightarrow \frac{2}{\mu\sigma b^2} \gg \omega \tag{11}$$

In this limit, the arguments of the exponentials in (10) are small. Using the approximation $\exp(u) \approx 1 + u$, (10) becomes

$$\hat{H}_z \to \hat{K}_s \frac{\left[1 - (1+j)\frac{x}{\delta}\right] - \left[1 + (1+j)\frac{x}{\delta}\right]}{\left[1 + (1+j)\frac{b}{\delta}\right] - \left[1 - (1+j)\frac{b}{\delta}\right]} = -\hat{K}_s \frac{x}{b} \tag{12}$$

Substitution of this complex amplitude into (2) gives the space-time dependence.

$$H_z \to \frac{-x}{b} Re\hat{K}_s e^{j\omega t} \tag{13}$$

The field has the linear distribution expected if the current density is uniformly distributed over the length of the conductor. In this large skin depth limit, the field and current density spatial distributions are essentially the same as if the current source were time independent.

In the opposite extreme, the skin depth is short compared to the conductor length. Perhaps this is accomplished by making the frequency very high compared to the reciprocal magnetic diffusion time based on the conductor length.

$$\delta \ll b \Rightarrow \frac{2}{\mu\sigma b^2} \ll \omega \tag{14}$$

Then, the first term in the denominator of (10) is large compared with the second. Division of the numerator by this first term gives

$$\hat{H}_z \to \hat{K}_s \left[e^{-(1+j)\frac{x+b}{\delta}} - e^{(1+j)\frac{x-b}{\delta}}\right] \approx \hat{K}_s e^{-(1+j)\left(\frac{x+b}{\delta}\right)} \tag{15}$$

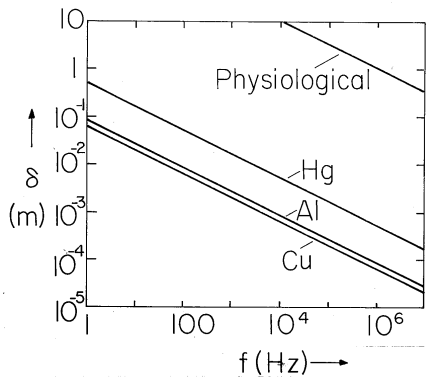


Fig. 10.7.3 Skin depth as a function of frequency.

In justifying the second of these expressions, remember that x is negative throughout the region of interest. Substitution of (15) into (2) shows that in this short skin depth limit

$$H_z = Re\left\{\hat{K}_s e^{-\left(\frac{(x+b)}{\delta}\right)} e^{j\left[\omega t - \frac{(x+b)}{\delta}\right]}\right\} \tag{16}$$

With the origin shifted from $x = 0$ to $x = -b$, this field has the $x - t$ dependence of the diffusion wave represented by (8). So it is that in the short skin depth limit, the distribution of the field magnitude shown in Fig. 10.7.2 has the exponential decay typical of skin effect.

The skin depth, (5), is inversely proportional to the square root of $\omega\mu\sigma$. Thus, an order of magnitude variation in frequency or in conductivity only changes δ by about a factor of about 3. Even so, skin depths found under practical conditions are widely varying because these parameters have enormous ranges. In good conductors, such as copper or aluminum, Fig. 10.7.3 illustrates how δ varies from about 1 cm at 60 Hz to less than 0.1 mm at l MHz. Of interest in determining magnetically induced currents in flesh is the curve for skin depth in materials having the "physiological" conductivity of about 0.2 S/m (Demonstration 7.9.1).

If the frequency is high enough so that the skin depth is small compared with the dimensions of interest, then the fields external to the conductor are essentially determined using the perfect conductivity model introduced in Sec. 8.4. In Demonstration 8.6.1, the fields around a conductor above a ground plane line were derived and the associated surface current densities deduced. If these currents are in the sinusoidal steady state, we can now picture them as actually extending into the conductors a distance that is on the order of δ.

Although skin effect determines the paths of current flow at radio frequencies, as the following demonstrates, it can be important even at 60 Hz.

Demonstration 10.7.1. Skin Effect

The core of magnetizable material shown in Fig. 10.7.4 passes through a slit cut from an aluminum block and through a winding that is driven at a frequency in the range of 60–240 Hz. The winding and the block of aluminum, respectively, comprise

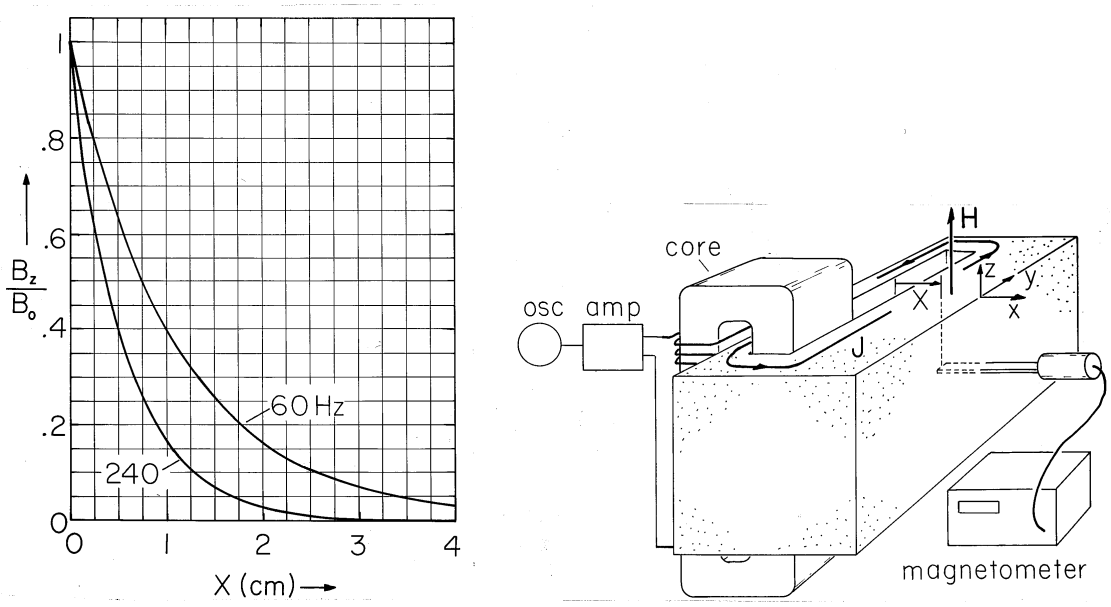


Fig. 10.7.4 Demonstration of skin effect. Currents induced in the conducting block tend to follow paths of minimum reactance nearest to the slot. Thus, because the aluminum block is thick compared to the skin depth, the field intensity observed decreases exponentially with distance X. In the experiment, the block is $10 \times 10 \times 26$ cm with thickness of 6 cm between the right face of the slot and the right side of the block. In aluminum at 60 Hz, $\delta = 1.1$ cm, while at 240 Hz δ is half of that. To avoid distortion of the field, the yoke is placed at one end of the slot.

the primary and secondary of a transformer. In effect, the secondary is composed of one turn that is shorted on itself.

The thickness b of the aluminum block is somewhat larger than a skin depth at 60 Hz. Therefore, currents circulating through the block around the leg of the magnetic circuit tend to follow the paths of least reactance closest to the slit. By making the length of the block and slit in the y direction large compared to b, we expect to see distributions of current density and associated magnetic field intensity at locations in the block well removed from the ends that have the x dependence found in Example 10.7.1.

In the limit where δ is small compared to b, the magnitude of the expected magnetic flux density B_z (normalized to its value where $X = 0$) has the exponential decay with distance x of the inset to Fig. 10.7.4. The curves shown are for aluminum at frequencies of 60 Hz and 240 Hz. According to (5), increasing the frequency by a factor of 4 should decrease the skin depth by a factor of 2. Provision is made for measuring this field by having a small slit milled in the block with a large enough width to permit the insertion of a magnetometer probe oriented to measure the magnetic flux density in the z direction.

As we have seen in this and previous sections, currents induced in a conductor tend to exclude the magnetic field from some region. Conductors are commonly used as shields that isolate a region from its surroundings. Typically, the conductor is made thick compared to the skin depth based on the fields to be shielded out.

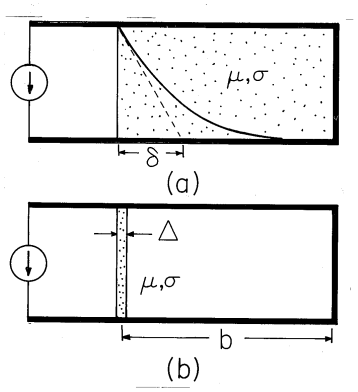


Fig. 10.7.5 Perfectly conducting ⊃-shaped conductors are driven by a distributed current source at the left. The magnetic field is shielded out of the region to the right enclosed by the perfect conductors by: (a) a block of conductor that fills the region and has a thickness b that is large compared to a skin depth; and (b) a sheet conductor having a thickness Δ that is less than the skin depth.

However, our studies of currents induced in thin conducting shells in Secs. 10.3 and 10.4 make it clear that this can be too strict a requirement for good shielding. The thin-sheet model can now be seen to be valid if the skin depth δ is *large* compared to the thickness Δ of the sheet. Yet, we found that for a cylindrical shell of radius R, provided that $\omega\mu\sigma\Delta R \gg 1$, a sinusoidally varying applied field would be shielded from the interior of the shell. Apparently, under certain circumstances, even a conductor that is thin compared to a skin depth can be a good shield.

To understand this seeming contradiction, consider the one-dimensional configurations shown in Fig. 10.7.5. In the first of the two, plane parallel perfectly conducting electrodes again sandwich a block of conductor in a system that is very long in a direction perpendicular to the paper. However, now the plates are shorted by a perfect conductor at the right. Thus, at very low frequencies, all of the current from the source circulates through the perfectly conducting plates, bypassing the block. As a result, the field throughout the conductor is uniform. As the frequency is raised, the electric field generated by the time-varying magnetic flux drives a current through the block much as in Example 10.7.1, with the current in the block tending to circulate through paths of least reactance near the left edge of the block. For simplicity, suppose that the skin depth δ is shorter than the length of the block b, so that the decay of current density and field into the block is essentially the exponential sketched in Fig. 10.7.5a. With the frequency high enough to make the skin depth short compared to b, the field tends to be shielded from points within the block.

In the configuration of Fig. 10.7.5b, the block is replaced by a sheet having the same σ and μ but a thickness Δ that is less than a skin depth δ. Is it possible that this thin sheet could suppress the field in the region to the right as well as the thick conductor?

The answer to this question depends on the location of the observer and the extent b of the region with which he or she is associated. In the conducting block, shielding is poor in the neighborhood of the left edge but rapidly improves at

distances into the interior that are of the order of δ or more. By contrast, the sheet conductor can be represented as a current divider. The surface current, K_s, of the source is tapped off by the sheet of conductivity per unit width $G = \sigma\Delta/h$ (where h is the height of the structure) connected to the inductance (assigned to unit width) $L = \mu bh$ of the single-turn inductor. The current through the single-turn inductor is

$$K_s \frac{1/j\omega L}{\left(G + \frac{1}{j\omega L}\right)} = \frac{K_s}{1 + j\omega LG} \tag{17}$$

This current, and the associated field, is shielded out effectively when $|\omega LG| = \omega\mu\sigma b\Delta \gg 1$. With the sheet, the shielding strategy is to make equal use of all of the volume to the right for generating an electric field in the sheet conductor. The efficiency of the shielding is improved by making $\omega\mu\sigma\Delta b$ large: The interior field is made small by making the shielded volume large.

10.8 SUMMARY

Before tackling the concepts in this chapter, we had studied MQS fields in two limiting situations:

- In the first, currents in Ohmic conductors were essentially stationary, with distributions governed by the steady conduction laws investigated in Secs. 7.2–7.6. The associated magnetic fields were then found by using these current distributions as sources. In the absence of magnetizable material, the Biot-Savart law of Sec. 8.2 could be used for this purpose. With or without magnetizable material, the boundary value approaches of Secs. 8.5 and 9.6 were applicable.

- In the second extreme, where fields were so rapidly varying that conductors were "perfect," the effect on the magnetic field of currents induced in accordance with the laws of Faraday, Ampère, and Ohm was to nullify the magnetic flux density normal to conducting surfaces. The boundary value approach used to find self-consistent fields and surface currents in this limit was the subject of Secs. 8.4 and 8.6.

In this chapter, the interplay of the laws of Faraday, Ohm, and Ampère has again been used to find self-consistent MQS fields and currents. However, in this chapter, the conductivity has been finite. This has made it possible to explore the dynamics of fields with source currents that were neither distributed throughout the volumes of conductors in accordance with the laws of steady conduction nor confined to the surfaces of perfect conductors.

In dealing with perfect conductors in Chaps. 8 and 9, the all-important role of $\mathbf{E}$ could be placed in the background. Left for a study of this chapter was the electric field induced by a time-varying magnetic induction. So, we began in Sec. 10.1 by picturing the electric field in systems of perfect conductors. The approach was familiar from solving EQS (Chap. 5) and MQS (Chap. 8) boundary value problems involving Poisson's equation. The electric field intensity was represented by the superposition of a particular part having a curl that balanced $-\partial\mathbf{B}/\partial t$ at

each point in the volume, and an irrotational part that served to make the total field tangential to the surfaces of the perfect conductors.

Having developed some insight into the rotational electric fields induced by magnetic induction, we then undertook case studies aimed at forming an appreciation for spatial and temporal distributions of currents and fields in finite conductors. By considering the effects of finite conductivity, we could answer questions left over from the previous two chapters.

- Under what conditions are distributions of current and field quasistationary in the sense of being essentially snapshots of a sequence of static fields?
- Under what conditions do they consist of surface currents and fields having negligible normal components at the surfaces of conductors?

We now know that the answer comes in terms of characteristic magnetic diffusion (or relaxation) times τ that depend on the electrical conductivity, the permeability, and the product of lengths.

$$\tau = \mu\sigma\Delta b \tag{1}$$

The lengths in this expression make it clear that the size and topology of the conductors plays an important role. This has been illustrated by the thin-sheet models of Secs. 10.3 and 10.4 and one-dimensional magnetic diffusion into the bulk of conductors in Secs. 10.6 and 10.7. In each of these classes of configurations, the role played by τ has been illustrated by the step response and by the sinusoidal steady state response. For the former, the answer to the question, "When is a conductor perfect?" was literal. The conductor tended to be perfect for times that were short compared to a properly defined τ. For the latter, the answer came in the form of a condition on the frequency. If $\omega\tau \gg 1$, the conductor tended to be perfect.

In the sinusoidal state, a magnetic field impressed at the surface of a conductor penetrates a distance δ into the conductor that is the skin depth and is given by setting $\omega\tau = \omega\mu\sigma\delta^2 = 2$ and solving for δ.

$$\delta = \sqrt{\frac{2}{\omega\mu\sigma}} \tag{2}$$

It is true that conductors will act as perfect conductors if this skin depth is much shorter than all other dimensions of interest. However, the thin sheet model of Sec. 10.4 teaches the important lesson that the skin depth may be larger than the conductor thickness and yet the conductor can still act to shield out the normal flux density. Indeed, in Sec. 10.4 it was assumed that the current was uniform over the conductor cross-section and hence that the skin depth was large, not small, compared to the conductor thickness. Demonstration 8.6.1, where current passes through a cylindrical conductor at a distance l above a conducting ground plane, is an example. It would be found in that demonstration that if l is large compared to the conductor thickness, the surface current in the ground plane would distribute itself in accordance with the perfectly conducting model even if the frequency is so low that the skin depth is somewhat larger than the thickness of the ground plane. If Δ is the ground plane thickness, we would expect the normal flux density to be small so long as $\omega\tau_m = \omega\mu\sigma\Delta l \gg 1$. Typical of such situations is that the electrical dissipation due to conduction is confined to thin conductors and the magnetic

energy storage occupies relatively larger regions that are free of dissipation. Energy storage and power dissipation are subjects taken up in the next chapter.

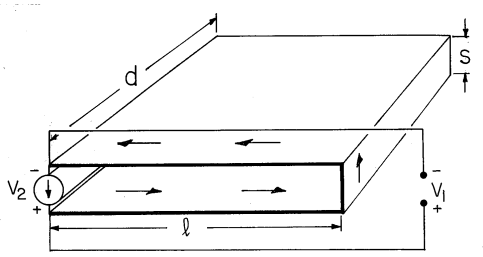


Fig. P10.0.2

PROBLEMS

10.1 Introduction

10.1.1* In Demonstration 10.0.1, the circuit formed by the pair of resistors is replaced by the one shown in Fig. 10.0.1, composed of four resistors of equal resistance R. The voltmeter might be the oscilloscope shown in Fig. 10.0.1. The "grounded" node at (4) is connected to the negative terminal of the voltmeter.

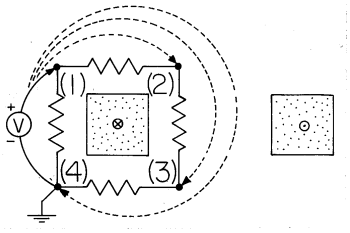


Fig. P10.0.1

(a) Show that the voltage measured with the positive lead connected at (1), so that the voltmeter is across one of the resistors, is $v = (d\Phi_\lambda/dt)/4$.

(b) Show that if the positive voltmeter lead is connected to (2), then to (3), and finally to (4) (so that the lead is wrapped around the core once and connected to the same grounded node as the negative voltmeter lead), the voltages are, respectively, twice, three times, and four times this value. Show that this last result is as would be expected for a transformer with a one-turn secondary.

10.1.2 Plane parallel perfectly conducting plates are shorted to form the one-turn inductor shown in Fig. 10.0.2. The current source is distributed so that it supplies i amps over the width d.

(a) Given that d and l are much greater than the spacing s, determine the voltage measured across the terminals of the current source by the voltmeter v_2.

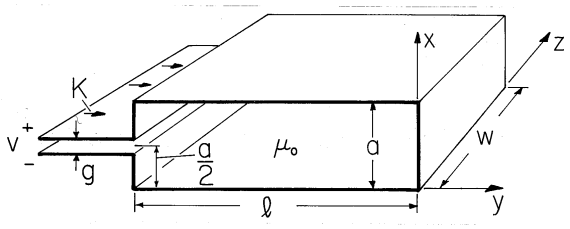


Fig. P10.1.2

(b) What is the voltage measured by the voltmeter v_1 connected as shown in the figure across these same terminals?

10.2 Magnetoquasistatic Electric Fields in Systems of Perfect Conductors

10.2.1* In Prob. 8.4.1, the magnetic field of a dipole surrounded by a perfectly conducting spherical shell is found. Show that

$$\mathbf{E} = \mathbf{i}_\phi \frac{\mu_o a^2}{4R^2} \frac{dI}{dt} \left[\frac{r}{R} - (R/r)^2 \right] \sin\theta \qquad (a)$$

in the region between the dipole and the shell.

10.2.2 The one-turn inductor of Fig. P10.1.2 is driven at the left by a current source that evenly distributes the surface current density $K(t)$ over the width w. The dimensions are such that $g \ll a \ll w$.

(a) In terms of $K(t)$, what is $\mathbf{H}$ between the plates?
(b) Determine a particular solution having the form $\mathbf{E}_p = \mathbf{i}_\mathbf{x} E_{xp}(y,t)$, and find $\mathbf{E}$.

10.2.3 The one-turn solenoid shown in cross-section in Fig. P10.1.3 consists of perfectly conducting sheets in the planes $\phi = 0$, $\phi = \alpha$, and $r = a$. The latter is broken at the middle and driven by a current source of $K(t)$ amps/unit length in the z direction. The current circulates around the perfectly conducting path provided by the sheets, as shown in the figure. Assume that the angle $\alpha \gg \delta$ and that the system is long enough in the z direction to justify taking the fields as two dimensional.

(a) In terms of $K(t)$, what is $\mathbf{H}$ in the pie-shaped region?
(b) What is $\mathbf{E}$ in this region?

10.2.4* By constrast with previous examples and problems in this section, consider here the induction of currents in materials that have relatively *low* conductivity. An example would be the induction heating of silicon in the manufacture of semiconductor devices. The material in which the currents are to be induced takes the form of a long circular cylinder of radius b.

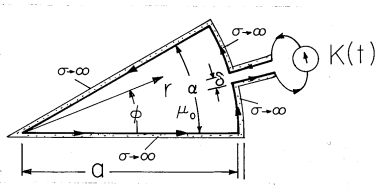


Fig. P10.1.3

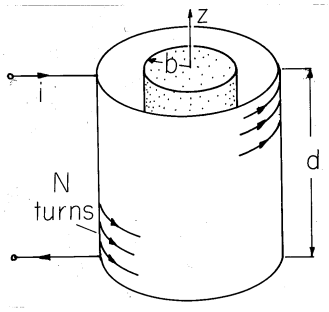


Fig. P10.1.4

A long solenoid surrounding this material has N turns, a length d that is much greater than its radius, and a driving current $i(t)$, as shown in Fig. P10.1.4.

Because the material to be heated has a small conductivity, the induced currents are small and contribute a magnetic field that is small compared to that imposed. Thus, the approach to determining the distribution of current induced in the semiconductor is 1) to first find $\mathbf{H}$, ignoring the effect of the induced current. This amounts to solving Ampère's law and the flux continuity law with the current density that of the excitation coil. Then, 2) with $\mathbf{B}$ known, the electric field in the semiconductor is determined using Faraday's law and the MQS form of the conservation of charge law, $\nabla \cdot (\sigma \mathbf{E}) = 0$. The approach to finding the fields can then be similar to that illustrated in this section.

(a) Show that in the semiconductor and in the annulus, $\mathbf{B} \approx (\mu_o N i/d)\mathbf{i_z}$.
(b) Use the symmetry about the z axis to show that in the semiconductor, where there is no radial component of $\mathbf{J}$ and hence of $\mathbf{E}$ at $r = b$, $\mathbf{E} = -(\mu_o N r/2d)(di/dt)\mathbf{i}_\phi$.
(c) To investigate the conditions under which this approximation is useful, suppose that the excitation is sinusoidal, with angular frequency ω. Approximate the magnetic field intensity $H_{induced}$ associated with the induced current. Show that for the approximation to be good, $H_{induced}/H_{imposed} = \omega \mu_o \sigma b^2/4 \ll 1$.

10.2.5 The configuration for this problem is the same as for Prob. 10.1.4 except that the slightly conducting material is now a cylinder having a rectangular cross-section, as shown in Fig. P10.1.5. The imposed field is therefore the same as before.

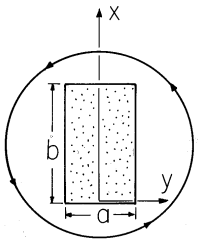


Fig. P10.1.5

(a) In terms of the coordinates shown, find a particular solution for $\mathbf{E}$ that takes the form $\mathbf{E} = \mathbf{i_y} E_{yp}(x,t)$ and satisfies the boundary conditions at $x = 0$ and $x = b$.
(b) Determine $\mathbf{E}$ inside the material of rectangular cross-section.
(c) Sketch the particular, homogeneous, and total electric fields, making clear how the first two add up to satisfy the boundary conditions. (Do not take the time to evaluate your analytical formula but rather use your knowledge of the nature of the solutions and the boundary conditions that they must satisfy.)

10.3 Nature of Fields Induced in Finite Conductors

10.3.1* The "Boomer" might be modeled as a transformer, with the disk as the one-turn secondary terminated in its own resistance. We have found here that if $\omega\tau_m \gg 1$, then the flux linked by the secondary is small. In Example 9.7.4, it was shown that operation of a transformer in its "ideal" mode also implies that the flux linked by the secondary be small. There it was found that to achieve this condition, the time constant L_{22}/R of the secondary must be long compared to times of interest. Approximate the inductance and resistance of the disk in Fig. 10.2.3 and show that L_{22}/R is indeed roughly the same as the time given by (10.2.17).

10.3.2 It is proposed that the healing of bone fractures can be promoted by the passage of current through the bone normal to the fracture. Using magnetic induction, a transient current can be induced without physical contact with the patient. Suppose a nonunion of the radius (a nonhealing fracture in the long bone of the forearm, as shown in Fig. P10.2.2) is to be treated. How would you arrange a driving coil so as to induce a longitudinal current along the bone axis through the fracture?

10.3.3* Suppose that a driving coil like that shown in Fig. 10.2.2 is used to produce a magnetic flux through a conductor having the shape of the circular cylindrical shell shown in Fig. 10.3.2. The shell has a thickness Δ and radius a. Following steps parallel to those represented by (10.2.13)–(10.2.16), show that H_{ind}/H_1 is *roughly* $\omega\tau_m$, where τ_m is given by (10.3.10). (Assume that the applied field is essentially uniform over the dimensions of the shell.)

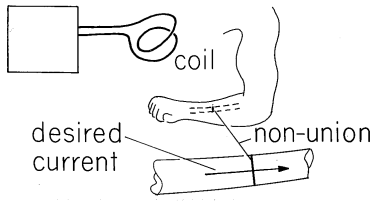


Fig. P10.2.2

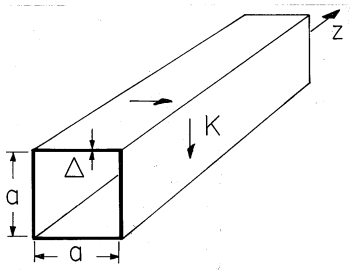


Fig. P10.3.1

10.4 Diffusion of Axial Magnetic Fields through Thin Conductors

10.4.1* A metal conductor having thickness Δ and conductivity σ is formed into a cylinder having a square cross-section, as shown in Fig. P10.3.1. It is very long compared to its cross-sectional dimensions a. When $t = 0$, there is a surface current density K_o circulating uniformly around the shell. Show that the subsequent surface current density is $K(t) = K_o \exp(-t/\tau_m)$ where $\tau_m = \mu_o \sigma \Delta a/4$.

10.4.2 The conducting sheet of thickness Δ shown in cross-section by Fig. P10.3.2 forms a one-turn solenoid having length l that is large compared to the length d of two of the sides of its right-triangular cross-section. When $t = 0$, there is a circulating current density J_o uniformly distributed in the conductor.

(a) Determine the surface current density $K(t) = \Delta J(t)$ for $t > 0$.

(b) A high-impedance voltmeter is connected as shown between the lower right and upper left corners. What $v(t)$ is measured?

(c) Now lead (1) is connected following path (2). What voltage is measured?

10.4.3* A system of two concentric shells, as shown in Fig. 10.5.2 without the center shell, is driven by the external field $H_o(t)$. The outer and inner shells have thicknesses Δ and radii a and b, respectively.

(a) Show that the fields H_1 and H_2, between the shells and inside the in-

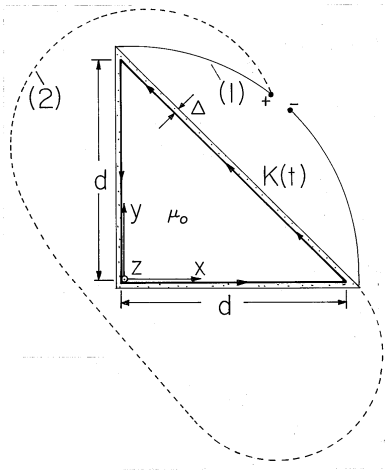


Fig. P10.3.2

ner shell, respectively, are governed by the equations ($\tau_m = \mu_o\sigma\Delta b/2$)

$$\tau_m \frac{dH_2}{dt} + H_2 - H_1 = 0 \qquad (a)$$

$$\tau_m(b/a)\frac{dH_2}{dt} + \tau_m\left(\frac{a}{b} - \frac{b}{a}\right)\frac{dH_1}{dt} + H_1 = H_o(t) \qquad (b)$$

(b) Given that $H_o = H_m \cos\omega t$, show that the sinusoidal steady state fields are $H_1 = Re\{[H_m(1+j\omega\tau_m)/D]\exp j\omega t\}$ and $H_2 = Re\{[H_m/D]\exp j\omega t\}$ where $D = [1 + j\omega\tau_m(a/b - b/a)](1 + j\omega\tau_m) + j\omega\tau_m(b/a)$.

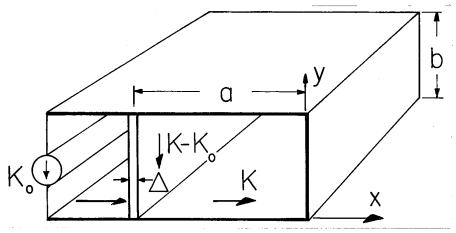


Fig. P10.3.4

10.4.4 The $\supset$-shaped perfect conductor shown in Fig. P10.3.4 is driven along its left edge by a current source having the uniformly distributed density $K_o(t)$. At $x = -a$ there is a thin sheet having the nonuniform conductivity $\sigma = \sigma_o/[1 + \alpha\cos(\pi y/b)]$. The length in the z direction is much greater than the other dimensions.

(a) Given $K_o(t)$, find a differential equation for $K(t)$.
(b) In terms of the solution $K(t)$ to this equation, determine $\mathbf{E}$ in the region $-a < x < 0,\ 0 < y < b$.

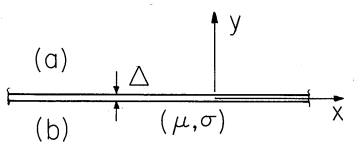


Fig. P10.4.1

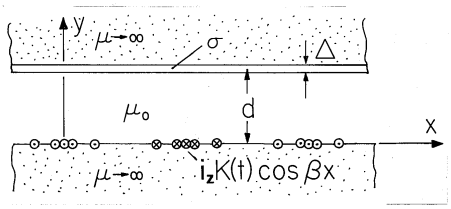


Fig. P10.4.2

10.5 Diffusion of Transverse Magnetic Fields through Thin Conductors

10.5.1* A thin planar sheet having conductivity σ and thickness Δ extends to infinity in the x and z directions, as shown in Fig. P10.4.1. Currents in the sheet are z directed and independent of z.

(a) Show that the sheet can be represented by the boundary conditions

$$B_y^a - B_y^b = 0 \qquad (a)$$

$$\frac{\partial}{\partial x}(H_x^a - H_x^b) = -\Delta\sigma\frac{\partial B_y}{\partial t} \qquad (b)$$

(b) Now consider the special case where the regions above and below are free space and extend to infinity in the $+y$ and $-y$ directions, respectively. When $t = 0$, there is a surface current density in the sheet $\mathbf{K} = \mathbf{i_z} K_o \sin\beta x$, where K_o and β are given constants. Show that for $t > 0$, $K_z = K_o \exp(-t/\tau)$ where $\tau = \mu_o\sigma\Delta/2\beta$.

10.5.2 In the two-dimensional system shown in cross-section by Fig. P10.4.2, a planar air gap of width d is bounded from above in the surface $y = d$ by a thin conducting sheet having conductivity σ and thickness Δ. This sheet is, in turn, backed by a material of infinite permeability. The region below is also infinitely permeable and at the interface $y = 0$ there is a winding used to impose the surface current density $\mathbf{K} = K(t)\cos\beta x\mathbf{i_z}$. The system extends to infinity in the $\pm x$ and $\pm z$ directions.

(a) The surface current density $K(t)$ varies so rapidly that the conducting sheet acts as a perfect conductor. What is Ψ in the air gap?

(b) The current is slowly varying so that the sheet supports little induced current. What is Ψ in the air gap?

(c) Determine $\Psi(x, y, t)$ if there is initially no magnetic field and a step, $K = K_o u_{-1}(t)$, is applied. Show that the early and long-time response matches that expected from parts (a) and (b).

10.5.3* The cross-section of a *spherical* shell having conductivity σ, radius R and thickness Δ is as shown in Fig. 8.4.5. A magnetic field that is uniform and z directed at infinity is imposed.

(a) Show that boundary conditions representing the shell are

$$B_r^a - B_r^b = 0 \qquad (a)$$

$$\frac{1}{R\sin\theta}\frac{\partial}{\partial\theta}\left[\sin\theta(H_\theta^a - H_\theta^b)\right] = -\mu_o\Delta\sigma\frac{\partial H_r}{\partial t} \qquad (b)$$

(b) Given that the driving field is $H_o(t) = Re\{\hat{H}_o\exp(j\omega t)\}$, show that the magnetic moment of a dipole at the origin that would have an effect on the external field equivalent to that of the shell is

$$\mathbf{m} = Re\{\frac{-j\omega\tau(2\pi R^3\hat{H}_o)}{1+j\omega\tau}\exp(j\omega t)\}$$

where $\tau \equiv \mu_o\sigma\Delta R/3$.

(c) Show that in the limit where $\omega\tau \to \infty$, the result is the same as found in Example 8.4.3.

10.5.4 A magnetic dipole, having moment $i(t)a$ (as defined in Example 8.3.2) oriented in the z direction is at the center of a spherical shell having radius R, thickness Δ, and conductivity σ, as shown in Fig. P10.4.4. With $i = Re\{\hat{i}\exp(j\omega t)\}$, the system is in the sinusoidal steady state.

(a) In terms of $i(t)a$, what is Ψ in the neighborhood of the origin?
(b) Given that the shell is perfectly conducting, find Ψ. Make a sketch of $\mathbf{H}$ for this limit.
(c) Now, with σ finite, determine Ψ.
(d) Take the appropriate limit of the fields found in (c) to recover the result of (b). In terms of the parameters that have been specified, under what conditions does the shell behave as though it had infinite conductivity?

10.5.5* In the system shown in cross-section in Fig. P10.4.5, a thin sheet of conductor, having thickness Δ and conductivity σ, is wrapped around a circular cylinder having infinite permeability and radius b. On the other side of an air gap at the radius $r = a$ is a winding, used to impose the surface current density $\mathbf{K} = K(t)\sin 2\phi\mathbf{i_z}$, backed by an infinitely permeable material in the region $a < r$.

(a) The current density varies so rapidly that the sheet behaves as an infinite conductor. In this limit, show that Ψ in the air gap is

$$\Psi = -\frac{aK}{2}\frac{\left[\left(\frac{r}{b}\right)^2 + \left(\frac{b}{r}\right)^2\right]}{\left[\left(\frac{a}{b}\right)^2 + \left(\frac{b}{a}\right)^2\right]}\cos 2\phi \qquad (a)$$

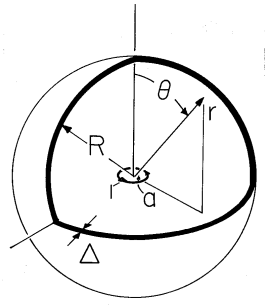


Fig. P10.4.4

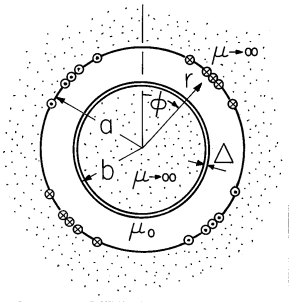


Fig. P10.4.5

(b) Now suppose that the driving current is so slowly varying that the current induced in the conducting sheet is negligible. Show that

$$\Psi = -\frac{aK}{2}\frac{\left[\left(\frac{r}{b}\right)^2 - \left(\frac{b}{r}\right)^2\right]}{\left[\left(\frac{a}{b}\right)^2 - \left(\frac{b}{a}\right)^2\right]}\cos 2\phi \qquad (b)$$

(c) Show that if the fields are zero when $t < 0$ and there is a step in current, $K(t) = K_o u_{-1}(t)$

$$\Psi = \frac{aK_o \cos 2\phi}{\left(\frac{a}{b}\right)^2 - \left(\frac{b}{a}\right)^2}\left\{\frac{\left[\left(\frac{r}{a}\right)^2 - \left(\frac{a}{r}\right)^2\right]}{\left(\frac{a}{b}\right)^2 + \left(\frac{b}{a}\right)^2}e^{-t/\tau} - \frac{\left[\left(\frac{r}{b}\right)^2 - \left(\frac{b}{r}\right)^2\right]}{2}\right\} \qquad (c)$$

where

$$\tau = \frac{\mu_o \sigma \Delta b}{2}\frac{\left[\left(\frac{b}{a}\right)^2 + \left(\frac{a}{b}\right)^2\right]}{\left[\left(\frac{a}{b}\right)^2 - \left(\frac{b}{a}\right)^2\right]} \qquad (d)$$

Show that the early and long-time responses do indeed match the results found in parts (a) and (b).

10.5.6 The configuration is as described in Prob. 10.4.5 except that the conducting shell is on the outside of the air gap at $r = a$, while the windings are on the inside surface of the air gap at $r = b$. Also, the windings are now arranged

so that the imposed surface current density is $\mathbf{K} = K_o(t)\sin\phi$. For this configuration, carry out parts (a), (b), and (c) of Prob. 10.4.5.

10.6 Magnetic Diffusion Laws

10.6.1* Consider a class of problems that are analogous to those described by (10.5.10) and (10.5.11), but with $\mathbf{J}$ rather than $\mathbf{H}$ written as a solution to the diffusion equation.

(a) Use (10.5.1)–(10.5.5) to show that

$$\nabla^2(\mathbf{J}/\sigma) = \mu\frac{\partial \mathbf{J}}{\partial t} \tag{a}$$

(b) Now consider $\mathbf{J}$ (rather than $\mathbf{H}$) to be z directed but independent of z, $\mathbf{J} = J_z(x,y,t)\mathbf{i_z}$, and $\mathbf{H}$ (rather than $\mathbf{J}$) to be transverse, $\mathbf{H} = H_x(x,y,t)\mathbf{i_x} + H_y(x,y,t)\mathbf{i_y}$. Show that

$$\nabla^2\left(\frac{J_z}{\sigma}\right) = \mu\frac{\partial J_z}{\partial t} \tag{b}$$

where $\mathbf{H}$ can be found from $\mathbf{J}$ using

$$\frac{\partial \mathbf{H}}{\partial t} = -\frac{\partial}{\partial y}\left(\frac{J_z}{\sigma\mu}\right)\mathbf{i_x} + \frac{\partial}{\partial x}\left(\frac{J_z}{\sigma\mu}\right)\mathbf{i_y} \tag{c}$$

Note that these expressions are of the same form as (10.5.8), (10.5.10), and (10.5.11), respectively, but with the roles of $\mathbf{J}$ and $\mathbf{H}$ reversed.

10.7 Magnetic Diffusion Step Response

10.7.1* In the configuration of Fig. 10.6.1, a steady state has been established with $K_s = K_p =$ constant. When $t = 0$, this driving current is suddenly turned off. Show that $\mathbf{H}$ and $\mathbf{J}$ are given by (10.6.21) and (10.6.22) with the first term in each omitted and the sign of the summation in each reversed.

10.7.2 Consider the configuration of Fig. 10.6.1 but with a perfectly conducting electrode in the plane $x = 0$ "shorting" the electrode at $y = 0$ to the one at $y = a$.

(a) A steady driving current has been established with $K_s = K_p =$ constant. What are the steady $\mathbf{H}$ and $\mathbf{J}$ in the conducting block?

(b) When $t = 0$, the driving current is suddenly turned off. Determine $\mathbf{H}$ and $\mathbf{J}$ for $t > 0$.

10.8 Skin Effect

10.8.1* For Example 10.7.1, the conducting block has length d in the z direction.

(a) Show that the impedance seen by the current source is

$$Z = \frac{a(1+j)}{d\sigma\delta}\frac{\left[e^{(1+j)b/\delta} + e^{-(1+j)b/\delta}\right]}{\left[e^{(1+j)b/\delta} - e^{-(1+j)b/\delta}\right]} \qquad (a)$$

(b) Show that in the limit where $b \ll \delta$, Z becomes the dc resistance $a/db\sigma$.

(c) Show that in the opposite extreme where $b \gg \delta$, so that the current is concentrated near the surface, the block impedance has resistive and inductive-reactive parts of equal magnitude and that the resistance is equivalent to that for a slab having thickness δ in the x direction carrying a current that is uniformly distributed with respect to x.

10.8.2 In the configuration of Example 10.7.1, the perfectly conducting electrodes are terminated by a perfectly conducting electrode in the plane $x = 0$.

(a) Determine the sinusoidal steady state response $\mathbf{H}$.

(b) Show that even though the current source is now "shorted" by perfectly conducting electrodes, the high-frequency field distribution is still given by (10.7.16), so that in this limit, the current still concentrates at the surface.

(c) Determine the impedance of a length d (in the z direction) of the block.

11

ENERGY, POWER FLOW, AND FORCES

11.0 INTRODUCTION

One way to decide whether a system is electroquasistatic or magnetoquasistatic is to consider the relative magnitudes of the electric and magnetic energy storages. The subject of this chapter therefore makes a natural transition from the quasistatic laws to the complete set of electrodynamic laws. In the order introduced in Chaps. 1 and 2, but now including polarization and magnetization,[1] these are Gauss' law [(6.2.1) and (6.2.3)]

$$\nabla \cdot (\epsilon_o \mathbf{E} + \mathbf{P}) = \rho_u \tag{1}$$

Ampère's law (6.2.11),

$$\nabla \times \mathbf{H} = \mathbf{J}_u + \frac{\partial}{\partial t}(\epsilon_o \mathbf{E} + \mathbf{P}) \tag{2}$$

Faraday's law (9.2.7),

$$\nabla \times \mathbf{E} = -\frac{\partial}{\partial t}\mu_o(\mathbf{H} + \mathbf{M}) \tag{3}$$

and the magnetic flux continuity law (9.2.2).

$$\nabla \cdot \mu_o(\mathbf{H} + \mathbf{M}) = 0 \tag{4}$$

Circuit theory describes the excitation of a two-terminal element in terms of the voltage v applied between the terminals and the current i into and out of the respective terminals. The power supplied through the terminal pair is vi. One objective in this chapter is to extend the concept of power flow in such a way that power is thought to flow throughout space, and is not associated only with

[1] For polarized and magnetized media at rest.

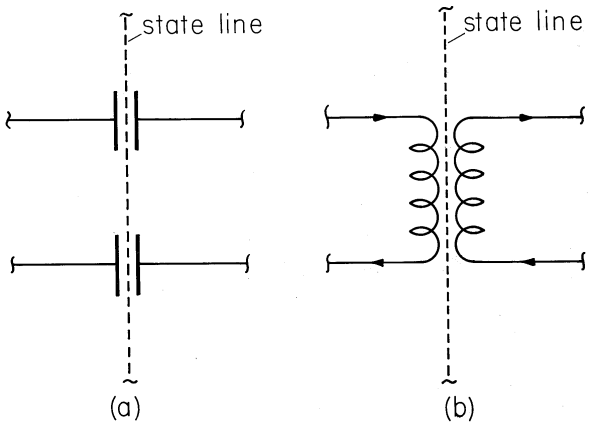


Fig. 11.0.1 If the border between two states passes between the plates of a capacitor or between the windings of a transformer, is there power flow that should be overseen by the federal government?

current flow into and out of terminals. The basis for this extension is the laws of electrodynamics, (1)–(4).

Even if a system can be represented by a circuit, the need for the generalization of the circuit-theoretical power flow concept is apparent if we try to understand how electrical energy is transferred within, rather than between, circuit elements. The limitations of the circuit viewpoint would be crucial to testimony of an expert witness in litigation concerning the authority of the Federal Power Commission[2] to regulate power flowing between states. If the view is taken that passage of current across a border is a prerequisite for power flow, either of the devices shown in Fig. 11.0.1 might be installed at the border to "launder" the power. In the first, the state line passes through the air gap between capacitor plates, while in the second, it separates the primary from the secondary in a transformer.[3] In each case, the current never leaves the state where it is generated. Yet in the examples shown, power generated in one state can surely be consumed in another, and a meaningful discussion of how this takes place must be based on a broadened view of power flow.

From the circuit-theoretical viewpoint, energy storage and rate of energy dissipation are assigned to circuit elements as a whole. Power flowing through a terminal pair is expressed as the product of a potential difference v between the terminals and the current i in one terminal and out of the other. Thus, the terminal voltage v and current i do provide a meaningful description of power flow into a surface S that encloses the circuit shown in Fig. 11.0.2. The surface S does not pass "inside" one of the elements.

Power Flow in a Circuit. For the circuit of Fig. 11.0.2, Kirchhoff's laws

[2] Now the Federal Energy Regulatory Commission.

[3] To be practical, the capacitor would be constructed with an enormous number of interspersed plates, so that in order to keep the state line in the air gap, a gerrymandered border would be required. Contemplation of the construction of a practical transformer, as described in Sec. 9.7, reveals that the state line would be even more difficult to explain in the MQS case.

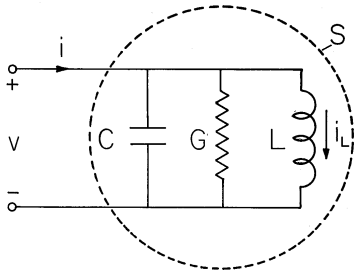


Fig. 11.0.2 Circuit used to review the derivation of energy conservation statement for circuits.

combine with the terminal relations for the capacitor, inductor, and resistor to give

$$i = C\frac{dv}{dt} + i_L + Gv \tag{5}$$

$$v = L\frac{di_L}{dt} \tag{6}$$

Motivated by the objective to obtain a statement involving vi, we multiply the first of these laws by the terminal voltage v. To eliminate the term vi_L on the right, we also multiply the second equation by i_L. Thus, with the addition of the two relations, we obtain

$$vi = vC\frac{dv}{dt} + i_L L\frac{di_L}{dt} + Gv^2 \tag{7}$$

Because L and C are assumed to be constant, we can use the relation $udu = d(\frac{1}{2}u^2)$ to rewrite this expression as

$$vi = \frac{dw}{dt} + Gv^2 \tag{8}$$

where

$$w = \frac{1}{2}Cv^2 + \frac{1}{2}Li_L^2$$

With its origins solely in the circuit laws, (8) can be regarded as giving no more information than inherent in the original laws. However, it gives insights into the circuit dynamics that are harbingers of what can be expected from the more general statement to be derived in Sec. 11.1. These come from considering some extremes.

- If the terminals are open ($i = 0$), and if the resistor is absent ($G = 0$), w is constant. Thus, the *energy* w is conserved in this limiting case. The solution to the circuit laws must lead to the conclusion that the sum of the electric energy $\frac{1}{2}Cv^2$ and the magnetic energy $\frac{1}{2}Li_L^2$ is constant.
- Again, with $G = 0$, but now with a current supplied to the terminals, (8) becomes

$$vi = \frac{dw}{dt} \tag{9}$$

Because the right-hand side is a perfect time derivative, the expression can be integrated to give

$$\int_0^t vidt = w(t) - w(0) \tag{10}$$

Regardless of the details of how the currents and voltage vary with time, the time integral of the *power* vi is solely a function of the initial and final total energies w. Thus, if w were zero to begin with and vi were positive, at some later time t, the total energy would be the positive value given by (10). To remove the total energy from the inductor and capacitor, vi must be reversed in sign until the integration has reduced w to zero. Because the process is reversible, we say that the energy w is *stored* in the capacitor and inductor.

- If the terminals are again open ($i = 0$) but the resistor is present, (8) shows that the stored energy w must decrease with time. Because Gv^2 is positive, this process is not reversible and we therefore say that the energy is *dissipated* in the resistor.

In circuit theory terms, (8) is an example of an energy conservation theorem. According to this theorem, *electrical energy* is *not* conserved. Rather, of the electrical energy supplied to the circuit at the rate vi, part is stored in the capacitor and inductor and indeed conserved, and part is dissipated in the resistor. The energy supplied to the resistor is *not conserved in electrical form.* This energy is dissipated in heat and becomes a new kind of energy, thermal energy.

Just as the circuit laws can be combined to describe the flow of power between the circuit elements, so Maxwell's equations are the basis for a field-theoretical view of power flow. The reasoning that casts the circuit laws into a power flow statement parallels that used in the next section to obtain the more general field-theoretical law, so it is worthwhile to review how the circuit laws are combined to obtain a statement describing power flow.

Overview. The energy conservation theorem derived in the next two sections will also not be a conservation theorem in the sense that electrical energy is conserved. Rather, in addition to accounting for the storage of energy, it will include conversion of energy into other forms as well. Indeed, one of the main reasons for our interest in power flow is the insight it gives into other subsystems of the physical world [e.g. the thermodynamic, chemical, or mechanical subsystems]. This will be evident from the topics of subsequent sections.

The conservation of energy statement assumes as many special forms as there are different constitutive laws. This is one reason for pausing with Sec. 11.1 to summarize the integral and differential forms of the conservation law, regardless of the particular application. We shall reference these expressions throughout the chapter. The derivation of Poynting's theorem, in the first part of Sec. 11.2, is motivated by the form of the general conservation theorem. As subsequent sections evolve, we shall also make continued reference to this law in its general form.

By specializing the materials to Ohmic conductors with linear polarization and magnetization constitutive laws, it is possible to make a clear identification of the origins of electrical energy storage and dissipation in media. Such systems are considered in Sec. 11.3, where the flow of power from source to "sinks" of thermal

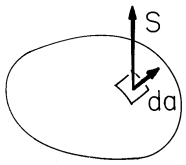


Fig. 11.1.1 Integral form of energy conservation theorem applies to system within arbitrary volume V enclosed by surface S.

dissipation is illustrated. Processes of energy storage and dissipation are developed in greater depth in Secs. 11.4 and 11.5.

Through Sec. 11.5, the assumption is that materials are at rest. In Secs. 11.6 and 11.7, the power input is studied in the presence of motion of materials. These sections illustrate how the energy conservation law is used to determine electric and magnetic forces on macroscopic media. The discussion in these sections is confined to a determination of total forces. Consistent with the field theory point of view is the concept of a distributed force per unit volume, a force density. Rigorous derivations of macroscopic force densities are based on energy arguments paralleling those of Secs. 11.6 and 11.7.

In Sec. 11.8, we shall look at microscopic models of force density distributions that provide a picture of the origin of these distributions. Finally, Sec. 11.9 is an introduction to the macroscopic force densities needed to put electromechanical coupling on a continuum basis.

11.1 INTEGRAL AND DIFFERENTIAL CONSERVATION STATEMENTS

The circuit with theoretical conservation theorem (11.0.8) equates the power flowing into the circuit to the rate of change of the energy stored and the rate of energy dissipation. In a field, theoretical generalization, the energy must be imagined distributed through space with an energy density W (joules/m^3), and the power is dissipated at a local rate of dissipation per unit volume P_d (watts/m^3). The power flows with a density $\mathbf{S}$ (watts/m^2), a vector, so that the power crossing a surface S_a is given by $\int_{S_a} \mathbf{S} \cdot d\mathbf{a}$. With these field-theoretical generalizations, the power flowing into a volume V, enclosed by the surface S must be given by

$$\boxed{-\oint_S \mathbf{S} \cdot d\mathbf{a} = \frac{d}{dt}\int_V W dv + \int_V P_d dv} \tag{1}$$

where the minus sign takes care of the fact that the term on the left is the power flowing *into* the volume.

According to the right-hand side of this equation, this input power is equal to the rate of increase of the total energy stored plus the power dissipation. The total energy is expressed as an integral over the volume of an *energy density*, W. Similarly, the total power dissipation is the integral over the volume of a *power dissipation density* P_d.

The volume is taken as being fixed, so the time derivative can be taken inside the volume integration on the right in (1). With the use of Gauss' theorem, the surface integral on the left is then converted to one over the volume and the term transferred to the right-hand side.

$$\int_V \left(\nabla \cdot \mathbf{S} + \frac{\partial W}{\partial t} + P_d\right) dv = 0 \tag{2}$$

Because V is arbitrary, the integrand must be zero and a *differential statement of energy conservation* follows.

$$\boxed{\nabla \cdot \mathbf{S} + \frac{\partial W}{\partial t} + P_d = 0} \tag{3}$$

With an appropriate definition of $\mathbf{S}$, W and P_d, (1) and (3) could describe the flow, storage, and dissipation not only of electromagnetic energy, but of thermal, elastic, or fluid mechanical energy as well. In the next section we will use Maxwell's equations to determine these variables for an electromagnetic system.

11.2 POYNTING'S THEOREM

The objective in this section is to derive a statement of energy conservation from Maxwell's equations in the form identified in Sec. 11.1. The conservation theorem includes the effects of both displacement current and of magnetic induction. The EQS and MQS limits, respectively, can be taken by neglecting those terms having their origins in the magnetic induction $\partial\mu_o(\mathbf{H} + \mathbf{M})/\partial t$ on the one hand, and in the displacement current density $\partial(\epsilon_o\mathbf{E} + \mathbf{P})/\partial t$ on the other.

Ampère's law, including the effects of polarization, is (11.0.2).

$$\nabla \times \mathbf{H} = \mathbf{J}_u + \frac{\partial \epsilon_o \mathbf{E}}{\partial t} + \frac{\partial \mathbf{P}}{\partial t} \tag{1}$$

Faraday's law, including the effects of magnetization, is (11.0.3).

$$\nabla \times \mathbf{E} = -\frac{\partial \mu_o \mathbf{H}}{\partial t} - \frac{\partial \mu_o \mathbf{M}}{\partial t} \tag{2}$$

These field-theoretical laws play a role analogous to that of the circuit equations in the introductory section. What we do next is also analogous. For the circuit case, we form expressions that are quadratic in the dependent variables. Several considerations guide the following manipulations. One aim is to derive an expression involving power dissipation or conversion densities and time rates of change of energy storages. The power per unit volume imparted to the current density of unpaired charge follows directly from the Lorentz force law (at least in free space). The force on a particle of charge q is

$$\mathbf{f} = q(\mathbf{E} + \mathbf{v} \times \mu_o \mathbf{H}) \tag{3}$$

The rate of work on the particle is

$$\mathbf{f} \cdot \mathbf{v} = q\mathbf{v} \cdot \mathbf{E} \tag{4}$$

If the particle density is N and only one species of charged particles exists, then the rate of work per unit volume is

$$N\mathbf{f} \cdot \mathbf{v} = qN\mathbf{v} \cdot \mathbf{E} = \mathbf{J}_u \cdot \mathbf{E} \tag{5}$$

Thus, one must anticipate that an energy conservation law that applies to free space must contain the term $\mathbf{J}_u \cdot \mathbf{E}$. In order to obtain this term, one should dot multiply (1) by $\mathbf{E}$.

A second consideration that motivates the form of the energy conservation law is the aim to obtain a perfect divergence of density of power flow. Dot multiplication of (1) by $\mathbf{E}$ generates $(\nabla \times \mathbf{H}) \cdot \mathbf{E}$. This term is made into a perfect divergence if one adds to it $-(\nabla \times \mathbf{E}) \cdot \mathbf{H}$, i.e., if one subtracts (2) dot multiplied by $\mathbf{H}$.

Indeed,

$$(\nabla \times \mathbf{E}) \cdot \mathbf{H} - (\nabla \times \mathbf{H}) \cdot \mathbf{E} = \nabla \cdot (\mathbf{E} \times \mathbf{H}) \tag{6}$$

Thus, subtracting (2) dot multiplied by $\mathbf{H}$ from (1) dot multiplied by $\mathbf{E}$ one obtains

$$\boxed{\begin{aligned} -\nabla \cdot (\mathbf{E} \times \mathbf{H}) = & \frac{\partial}{\partial t}\left(\frac{1}{2}\epsilon_o \mathbf{E} \cdot \mathbf{E}\right) + \mathbf{E} \cdot \frac{\partial \mathbf{P}}{\partial t} \\ & + \frac{\partial}{\partial t}\left(\frac{1}{2}\mu_o \mathbf{H} \cdot \mathbf{H}\right) \\ & + \mathbf{H} \cdot \frac{\partial \mu_o \mathbf{M}}{\partial t} + \mathbf{E} \cdot \mathbf{J}_u \end{aligned}} \tag{7}$$

In writing the first and third terms on the right, we have exploited the relation $u \cdot du = d(\frac{1}{2}u^2)$. These two terms now take the form of the energy storage term in the power theorem, (11.1.3). The desire to obtain expressions taking this form is a third consideration contributing to the choice of ways in which (1) and (2) were combined. We could have seen at the outset that dotting $\mathbf{E}$ with (1) and subtracting (2) after it had been dotted with $\mathbf{H}$ would result in terms on the right taking the desired form of "perfect" time derivatives.

In the electroquasistatic limit, the magnetic induction terms on the right in Faraday's law, (2), are neglected. It follows from the steps leading to (7) that in the EQS approximation, the third and fourth terms on the right of (7) are negligible. Similarly, in the magnetoquasistatic limit, the displacement current, the last two terms on the right in Ampère's law, (1), is neglected. This implies that for MQS systems, the first two terms on the right in (7) are negligible.

Systems Composed of Perfect Conductors and Free Space. Quasistatic examples in this category are the EQS systems of Chaps. 4 and 5 and the MQS systems of Chap. 8, where perfect conductors are surrounded by free space. Whether quasistatic or electrodynamic, in these configurations, $\mathbf{P} = 0$, $\mathbf{M} = 0$; and where there is a current density $\mathbf{J}_u$, the perfect conductivity insures that $\mathbf{E} = 0$. Thus,

the second and last two terms on the right in (7) are zero. For perfect conductors surrounded by free space, the differential form of the power theorem becomes

$$\boxed{-\nabla \cdot \mathbf{S} = \frac{\partial W}{\partial t}} \tag{8}$$

with

$$\boxed{\mathbf{S} = \mathbf{E} \times \mathbf{H}} \tag{9}$$

and

$$\boxed{W = \frac{1}{2}\epsilon_o \mathbf{E} \cdot \mathbf{E} + \frac{1}{2}\mu_o \mathbf{H} \cdot \mathbf{H}} \tag{10}$$

where $\mathbf{S}$ is the *Poynting vector* and W is the sum of the *electric and magnetic energy densities*. The electric and magnetic fields are confined to the free space regions. Thus, power flow and energy storage pictured in terms of these variables occur entirely in the free space regions.

Limiting cases governed by the EQS and MQS laws, respectively, are distinguished by having predominantly electric and magnetic energy densities. The following simple examples illustrate the application of the power theorem to two simple quasistatic situations. Applications of the theorem to electrodynamic systems will be taken up in Chap. 12.

Example 11.2.1. Plane Parallel Capacitor

The plane parallel capacitor of Fig. 11.2.1 is familiar from Example 3.3.1. The circular electrodes are perfectly conducting, while the region between the electrodes is free space. The system is driven by a voltage source distributed around the edges of the electrodes. Between the electrodes, the electric field is simply the voltage divided by the plate spacing (3.3.6),

$$\mathbf{E} = \frac{v}{d}\mathbf{i_z} \tag{11}$$

while the magnetic field that follows from the integral form of Ampère's law is (3.3.10).

$$\mathbf{H} = \frac{r}{2}\epsilon_o \frac{d}{dt}\left(\frac{v}{d}\right)\mathbf{i}_\phi \tag{12}$$

Consider the application of the integral version of (8) to the surface S enclosing the region between the electrodes in Fig. 11.2.1. First we determine the power flowing into the volume through this surface by evaluating the left-hand side of (8). The density of power flow follows from (11) and (12).

$$\mathbf{S} = \mathbf{E} \times \mathbf{H} = -\frac{r}{2}\frac{\epsilon_o}{d^2} v \frac{dv}{dt}\mathbf{i_r} \tag{13}$$

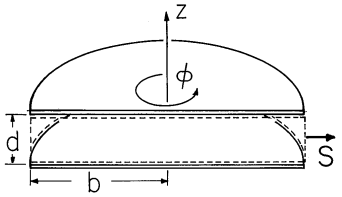


Fig. 11.2.1 Plane parallel circular electrodes are driven by a distributed voltage source. Poynting flux through surface denoted by dashed lines accounts for rate of change of electric energy stored in the enclosed volume.

The top and bottom surfaces have normals perpendicular to this vector, so the only contribution comes from the surface at $r = b$. Because $\mathbf{S}$ is constant on that surface, the integration amounts to a multiplication.

$$-\oint_S \mathbf{E}\times\mathbf{H}\cdot d\mathbf{a} = (2\pi bd)\Big(\frac{b}{2}\frac{\epsilon_o}{d^2}v\frac{dv}{dt}\Big) = \frac{d}{dt}\Big(\frac{1}{2}Cv^2\Big) \tag{14}$$

where

$$C \equiv \frac{\pi b^2\epsilon_o}{d}$$

Here the expression has been written as the rate of change of the energy stored in the capacitor. With $\mathbf{E}$ again given by (11), we double-check the expression for the time rate of change of energy storage.

$$\frac{d}{dt}\int_V \frac{1}{2}\epsilon_o\mathbf{E}\cdot\mathbf{E}dv = \frac{d}{dt}\left[\frac{1}{2}\epsilon_o(d\pi b^2)\Big(\frac{v}{d}\Big)^2\right] = \frac{d}{dt}\Big(\frac{1}{2}Cv^2\Big) \tag{15}$$

From the field viewpoint, power flows into the volume through the surface at $r = b$ and is stored in the form of electrical energy in the volume between the plates. In the quasistatic approximation used to evaluate the electric field, the magnetic energy storage is neglected at the outset because it is small compared to the electric energy storage. As a check on the implications of this approximation, consider the total magnetic energy storage. From (12),

$$\begin{aligned}\int_V \frac{1}{2}\mu_o\mathbf{H}\cdot\mathbf{H}dv &= \frac{1}{2}\mu_o\left[\frac{1}{2}\frac{\epsilon_o}{d}\Big(\frac{dv}{dt}\Big)\right]^2 d\int_0^b r^2 2\pi r dr \\ &= \frac{\mu_o\epsilon_o b^2}{16}C\Big(\frac{dv}{dt}\Big)^2\end{aligned} \tag{16}$$

Comparison of this expression with the electric energy storage found in (15) shows that the EQS approximation is valid provided that

$$\frac{\mu_o\epsilon_o b^2}{8}\Big|\frac{dv}{dt}\Big|^2 \ll v^2 \tag{17}$$

For a sinusoidal excitation of frequency ω, this gives

$$\Big(\frac{b\omega}{\sqrt{8}\,c}\Big)^2 \ll 1 \tag{18}$$

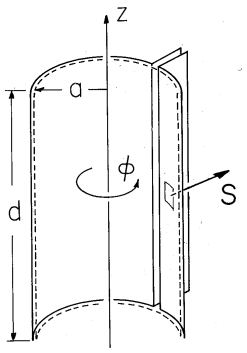


Fig. 11.2.2 One-turn solenoid surrounding volume enclosed by surface S denoted by dashed lines. Poynting flux through this surface accounts for the rate of change of magnetic energy stored in the enclosed volume.

where c is the free space velocity of light (3.1.16). The result is familiar from Example 3.3.1. *The requirement that the propagation time b/c of an electromagnetic wave be short compared to a period $1/\omega$ is equivalent to the requirement that the magnetic energy storage be negligible compared to the electric energy storage.*

A second example offers the opportunity to apply the integral version of (8) to a simple MQS system.

Example 11.2.2. Long Solenoidal Inductor

The perfectly conducting one-turn solenoid of Fig. 11.2.2 is familiar from Example 10.1.2. In terms of the terminal current $i = Kd$, the magnetic field intensity inside is (10.1.14),

$$\mathbf{H} = \frac{i}{d}\mathbf{i_z} \tag{19}$$

while the electric field is the sum of the particular and conservative homogeneous parts [(10.1.15) for the particular part and $\mathbf{E}_h$ for the conservative part].

$$\mathbf{E} = -\frac{\mu_o}{2}\frac{dH_z}{dt}r\mathbf{i}_\phi + \mathbf{E}_h \tag{20}$$

Consider how the power flow through the surface S of the volume enclosed by the coil is accounted for by the time rate of change of the energy stored. The Poynting flux implied by (19) and (20) is

$$\mathbf{S} = \mathbf{E} \times \mathbf{H} = \left[-\frac{\mu_o a}{2d^2}\frac{d}{dt}\left(\frac{1}{2}i^2\right) + \frac{i}{d}E_{\phi h}\right]\mathbf{i_r} \tag{21}$$

This Poynting vector has no component normal to the top and bottom surfaces of the volume. On the surface at $r = a$, the first term in brackets is constant, so the integration on S amounts to a multiplication by the area. Because $\mathbf{E_h}$ is irrotational, the integral of $\mathbf{E}_h \cdot d\mathbf{s} = E_{\phi h} r d\phi$ around a contour at $r = a$ must be zero. For this reason, there is no net contribution of $\mathbf{E}_h$ to the surface integral.

$$-\oint_S \mathbf{E} \times \mathbf{H} \cdot d\mathbf{a} = 2\pi a d\left(\frac{\mu_o a}{2d^2}\right)\frac{d}{dt}\left(\frac{1}{2}i^2\right) = \frac{d}{dt}\left(\frac{1}{2}Li^2\right); \tag{22}$$

where

$$L \equiv \frac{\mu_o \pi a^2}{d}$$

Here the result shows that the power flow is accounted for by the rate of change of the stored magnetic energy. Evaluation of the right hand side of (8), ignoring the electric energy storage, indeed gives the same result.

$$\frac{d}{dt}\int_V \frac{1}{2}\mu_o \mathbf{H}\cdot\mathbf{H}dv = \frac{d}{dt}\left[\pi a^2 d\frac{1}{2}\mu_o\left(\frac{i}{d}\right)^2\right] = \frac{d}{dt}\left(\frac{1}{2}Li^2\right) \tag{23}$$

The validity of the quasistatic approximation is examined by comparing the magnetic energy storage to the neglected electric energy storage. Because we are only interested in an order of magnitude comparison and we know that the homogeneous solution is proportional to the particular solution (10.1.21), the latter can be approximated by the first term in (20).

$$\begin{aligned}\int_V \frac{1}{2}\epsilon_o \mathbf{E}\cdot\mathbf{E}dv &\simeq \frac{1}{2}\epsilon_o \frac{\mu_o^2}{4d^2}\left(\frac{di}{dt}\right)^2\left[d\int_0^a r^2 2\pi r dr\right] \\ &= \frac{\mu_o\epsilon_o a^2}{16}L\left(\frac{di}{dt}\right)^2\end{aligned} \tag{24}$$

We conclude that *the MQS approximation is valid provided that the angular frequency ω is small compared to the time required for an electromagnetic wave to propagate the radius a of the solenoid and that this is equivalent to having an electric energy storage that is negligible compared to the magnetic energy storage.*

$$\frac{\mu_o\epsilon_o a^2}{8}\left(\frac{di}{dt}\right)^2 \ll i^2 \rightarrow \left(\frac{\omega a}{\sqrt{8}c}\right)^2 \ll 1 \tag{25}$$

A note of caution is in order. If the gap between the "sheet" terminals is made very small, the electric energy storage of the homogeneous part of the E field can become large. If it becomes comparable to the magnetic energy storage, the structure approaches the condition of resonance of the circuit consisting of the gap capacitance and solenoid inductance. In this limit, the MQS approximation breaks down. In practice, the electric energy stored in the gap would be dominated by that in the connecting plates, and the resonance could be described as the coupling of MQS and EQS systems as in Example 3.4.1.

In the following sections, we use (7) to study the storage and dissipation of energy in macroscopic media.

11.3 OHMIC CONDUCTORS WITH LINEAR POLARIZATION AND MAGNETIZATION

Consider a stationary material described by the constitutive laws

$$\begin{aligned}\mathbf{P} &= \epsilon_o \chi_e \mathbf{E} \\ \mu_o \mathbf{M} &= \mu_o \chi_m \mathbf{H}\end{aligned} \tag{1}$$

$$\mathbf{J}_u = \sigma\mathbf{E}$$

where the susceptibilities χ_e and χ_m, and hence the permittivity and permeability ϵ and μ, as well as the conductivity σ, are all independent of time. Expressed in terms of these constitutive laws for $\mathbf{P}$ and $\mathbf{M}$, the polarization and magnetization terms in (11.2.7) become

$$\mathbf{E}\cdot\frac{\partial\mathbf{P}}{\partial t} = \frac{\partial}{\partial t}\big(\frac{1}{2}\epsilon_o\chi_e\mathbf{E}\cdot\mathbf{E}\big)$$

$$\mathbf{H}\cdot\frac{\partial\mu_o\mathbf{M}}{\partial t} = \frac{\partial}{\partial t}\big(\frac{1}{2}\mu_o\chi_m\mathbf{H}\cdot\mathbf{H}\big) \tag{2}$$

Because these terms now appear in (11.2.7) as perfect time derivatives, it is clear that in a material having "linear" constitutive laws, energy is *stored* in the polarization and magnetization processes.

With the substitution of these terms into (11.2.7) and Ohm's law for $\mathbf{J}_u$, a conservation law is obtained in the form discussed in Sec. 11.1. For an electrically and magnetically linear material that obeys Ohm's law, the integral and differential conservation laws are (11.1.1) and (11.1.3), respectively, with

$$\boxed{\mathbf{S} = \mathbf{E}\times\mathbf{H}} \tag{3a}$$

$$\boxed{W = \frac{1}{2}\epsilon\mathbf{E}\cdot\mathbf{E} + \frac{1}{2}\mu\mathbf{H}\cdot\mathbf{H}} \tag{3b}$$

$$\boxed{P_d = \sigma\mathbf{E}\cdot\mathbf{E}} \tag{3c}$$

The power flux density $\mathbf{S}$ and the energy density W appear as in the free space conservation theorem of Sec. 11.2. The energy storage in the polarization and magnetization is included by simply replacing the free space permittivity and permeability by ϵ and μ, respectively.

The term P_d is always positive and seems to represent a rate of power loss from the electromagnetic system. That P_d indeed represents power converted to thermal form is motivated by considering the origins of the Ohmic conduction law. In terms of the bipolar conduction model introduced in Sec. 7.1, positive and negative carriers, respectively, experience the forces $\mathbf{f}_+$ and $\mathbf{f}_-$. These forces are balanced by collisions with the surrounding particles, and hence the work done by the field in forcing the migration of the particles is converted into thermal energy. If the velocity of the families of particles are, respectively, $\mathbf{v}_+$ and $\mathbf{v}_-$, and the number densities N_+ and N_-, respectively, then the rate of work performed on the carriers (per unit volume) is

$$P_d = N_+\mathbf{f}_+\cdot\mathbf{v}_+ + N_-\mathbf{f}_-\cdot\mathbf{v}_- \tag{4}$$

In recognition of the balance between collision forces and electrical forces, the forces of (4) are replaced by $|q_+|\mathbf{E}$ and $-|q_-|\mathbf{E}$, respectively.

$$P_d = N_+|q_+|\mathbf{E}\cdot\mathbf{v}_+ - N_-|q_-|\mathbf{E}\cdot\mathbf{v}_- \tag{5}$$

If, in turn, the velocities are written as the products of the respective mobilities and the macroscopic electric field, (7.1.3), it follows that

$$P_d = (N_+|q_+|\mu_+ + N_-|q_-|\mu_-)\mathbf{E}\cdot\mathbf{E} = \sigma\mathbf{E}\cdot\mathbf{E} \tag{6}$$

where the definition of the conductivity σ (7.1.7) has been used.

The power dissipation density $P_d = \sigma\mathbf{E}\cdot\mathbf{E}$ (watts/m^3) represents a rate of energy loss from the electromagnetic system to the thermal system.

Example 11.3.1. The Poynting Vector of a Stationary Current Distribution

In Example 7.5.2, we studied the electric fields in and around a circular cylindrical conductor fed by a battery in parallel with a disk-shaped conductor. Here we determine the Poynting vector field and explore its spatial relationship to the dissipation density.

First, within the circular cylindrical conductor [region (b) in Fig. 11.3.1], the electric field was found to be uniform, (7.5.7),

$$\mathbf{E}^b = \frac{v}{L}\mathbf{i_z} \tag{7}$$

while in the surrounding free space region, it was [from (7.5.11)]

$$\mathbf{E}^a = -\frac{v}{L\,ln(a/b)}\left[\frac{z}{r}\mathbf{i_r} + ln(r/a)\mathbf{i_z}\right] \tag{8}$$

and in the disk-shaped conductor [from (7.5.9)]

$$\mathbf{E}^c = \frac{v}{ln(a/b)}\frac{1}{r}\mathbf{i_r} \tag{9}$$

By symmetry, the magnetic field intensity is ϕ directed. The ϕ component of $\mathbf{H}$ is most easily evaluated from the integral form of Ampère's law. The current density in the circular conductor follows from (7) as $J_o = \sigma v/L$. Then,

$$2\pi r H_\phi = J_o\pi r^2 \rightarrow H^b_\phi = \frac{J_o r}{2}; \qquad r < b \tag{10}$$

$$2\pi r H_\phi = J_o\pi b^2 \rightarrow H^a_\phi = \frac{J_o b^2}{2r}; \qquad b < r < a \tag{11}$$

The magnetic field distribution in the disk conductor is also deduced from Ampère's law. In this region, it is easiest to evaluate the r component of Ampère's differential law with the current density $\mathbf{J}^c = \sigma\mathbf{E}^c$, with $\mathbf{E}^c$ given by (9). Integration of this partial differential equation on z then gives a linear function of z plus

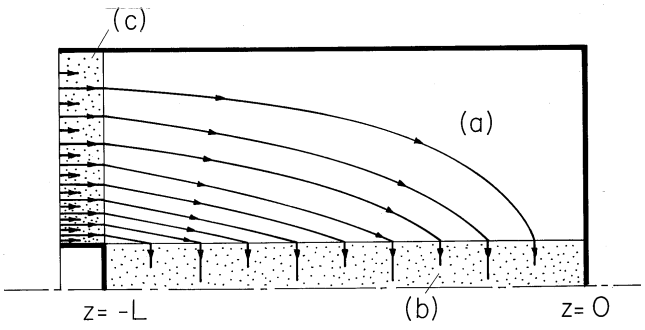


Fig. 11.3.1 Distribution of Poynting flux in coaxial resistors and associated free space. The configuration is the same as for Example 7.5.2. A source to the left supplies current to disk-shaped and circular cylindrical resistive materials. The outer and right-end conductors are perfectly conducting. Note that there is a Poynting flux in the free space interior region even when the currents are stationary.

an "integration constant" that is a function of r. The latter is determined by the requirement that H_ϕ be continuous at $z = -L$.

$$H_\phi^c = -\frac{\sigma}{ln(a/b)}\frac{v}{r}(L+z) + J_o\frac{b^2}{2r}; \qquad b < r < a \tag{12}$$

It follows from these last four equations that the Poynting vector inside the circular cylindrical conductor, in the surrounding space, and in the disk-shaped electrode is

$$\mathbf{S}^b = -\frac{v}{L}\frac{J_o}{2}r\mathbf{i_r} \tag{13}$$

$$\mathbf{S}^a = -\frac{vb^2J_o}{ln(a/b)2rL}\Big(\frac{z}{r}\mathbf{i_z} - ln\frac{r}{a}\mathbf{i_r}\Big) \tag{14}$$

$$\mathbf{S}^c = \left[\frac{-\sigma}{ln^2(a/b)}\frac{v^2}{r^2}(L+z) + \frac{J_o v}{ln(a/b)}\frac{b^2}{2r^2}\right]\mathbf{i_z} \tag{15}$$

This distribution of $\mathbf{S}$ is sketched in Fig. 11.3.1. Wherever there is a dissipation density, there must be a negative divergence of $\mathbf{S}$. Thus, in the conductors, the $\mathbf{S}$ lines terminate in the volume. In the free space region (a), $\mathbf{S}$ is solenoidal. Even with the fields perfectly stationary in time, the power is seen to flow through the *open space* to be absorbed in the volume where the dissipation takes place. The integral of the Poynting vector over the surface surrounding the inner conductor gives what we would expect either from the circuit point of view

$$-\oint \mathbf{E}\times\mathbf{H}\cdot d\mathbf{a} = (2\pi bL)\Big(\frac{v}{L}\Big)\Big(\frac{J_o b}{2}\Big) = v(\pi b^2 J_o) = vi \tag{16}$$

where i is the total current through the cylinder, or from an evaluation of the right-hand side of the integral conservation law.

$$\int_V \sigma\mathbf{E}\cdot\mathbf{E}dv = (\pi b^2 L)\sigma\Big(\frac{v}{L}\Big)^2 = v\Big(\pi b^2\sigma\frac{v}{L}\Big) = vi \tag{17}$$

An Alternative Conservation Theorem for Electroquasistatic Systems. In describing electroquasistatic systems, it is inconvenient to require that the magnetic field intensity be evaluated. We consider now an alternative conservation theorem that is specialized to EQS systems. We will find an alternative expression for $\mathbf{S}$ that does not involve $\mathbf{H}$. In the process of finding an alternative distribution of $\mathbf{S}$, we *illustrate the danger of ascribing meaning to* $\mathbf{S}$ *evaluated at a point, rather than integrated over a closed surface.*

In the EQS approximation, $\mathbf{E}$ is irrotational. Thus,

$$\mathbf{E} = -\nabla\Phi \tag{18}$$

and the power input term on the left in the integral conservation law, (11.1.1), can be expressed as

$$-\oint_S \mathbf{E}\times\mathbf{H}\cdot d\mathbf{a} = \oint_S \nabla\Phi\times\mathbf{H}\cdot d\mathbf{a} \tag{19}$$

Next, the vector identity

$$\nabla\times(\Phi\mathbf{H}) = \nabla\Phi\times\mathbf{H} + \Phi\nabla\times\mathbf{H} \tag{20}$$

is used to write the right-hand side of (19) as

$$-\oint_S \mathbf{E}\times\mathbf{H}\cdot d\mathbf{a} = \oint_S \nabla\times(\Phi\mathbf{H})\cdot d\mathbf{a} - \oint_S \Phi\nabla\times\mathbf{H}\cdot d\mathbf{a} \tag{21}$$

The first integral on the right is zero because the curl of a vector is divergence free and a field with no divergence has zero flux through a closed surface. Ampère's law can be used to eliminate *curl* $\mathbf{H}$ from the second.

$$-\oint_S \mathbf{E}\times\mathbf{H}\cdot d\mathbf{a} = -\oint_S \Phi\big(\mathbf{J}+\frac{\partial\mathbf{D}}{\partial t}\big)\cdot d\mathbf{a} \tag{22}$$

In this way, we have determined an alternative expression for $\mathbf{S}$, *valid only in the electroquasistatic approximation.*

$$\boxed{\mathbf{S} = \Phi\big(\mathbf{J}+\frac{\partial\mathbf{D}}{\partial t}\big)} \tag{23}$$

The density of power flow, expressed by (23) as the product of a potential and *total current density* consisting of the sum of the conduction and displacement current densities, has a form similar to that used in circuit theory.

The power flux density of (23) is convenient in describing EQS systems, where the effects of magnetic induction are not significant. To be consistent with the EQS approximation, the conservation law must be used with the magnetic energy density neglected.

Example 11.3.2. Alternative EQS Power Flux Density for Stationary Current Distribution

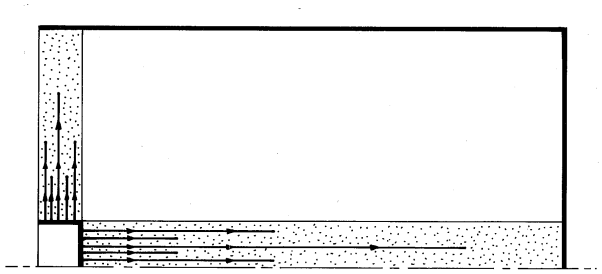


Fig. 11.3.2 Distribution of electroquasistatic flux density for the same system as shown in Fig. 11.3.1.

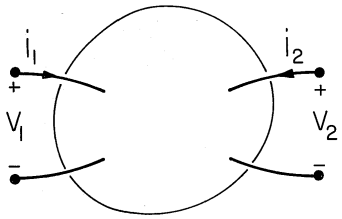


Fig. 11.3.3 Arbitrary EQS system accessed through terminal pairs.

To contrast the alternative EQS power flow density with the Poynting flux density, consider again the coaxial resistor configuration of Example 11.3.1. Because the fields are stationary, the EQS power flux density is

$$\mathbf{S} = \Phi\mathbf{J} \tag{24}$$

By contrast with the Poynting flux density, this vector field is zero in the free space region. In the circular cylindrical conductor, the potential and current density are [(7.5.6) and (7.5.7)]

$$\Phi^b = -\frac{v}{L}z; \qquad \mathbf{J}^b = \sigma\mathbf{E}^b = \frac{\sigma v}{L}\mathbf{i_z} \tag{25}$$

and it follows that the power flux density is simply

$$\mathbf{S} = -\frac{\sigma v^2}{L^2}z\mathbf{i_z} \tag{26}$$

There is a similar, radially directed flux density in the disk-shaped resistor.

The alternative distribution of $\mathbf{S}$, shown in Fig. 11.3.2, is clearly very different from that shown in Fig. 11.3.1 for the Poynting flux density.

Poynting Power Density Related to Circuit Power Input. Suppose that the surface S described by the conservation theorem encloses a system that is accessed through terminal pairs, as shown in Fig. 11.3.3. Under what circumstances is the integral of $\mathbf{S} \cdot d\mathbf{a}$ over S equivalent to summing the voltage-current product of the terminals of the wires connected to the system?

Two attributes of the fields on the surface S enclosing the system are required. *First, the contribution of the magnetic induction to* $\mathbf{E}$ *must be negligible on* S. If this is so, then regardless of what is inside S (for example, both EQS and MQS systems), *on the surface* S, the electric field can be taken as irrotational. It follows that in taking the integral over a closed surface of the Poynting power density, we can just as well use (23).

$$-\oint_S \mathbf{E}\times\mathbf{H}\cdot d\mathbf{a} = -\oint_S \Phi\big(\mathbf{J}+\frac{\partial \mathbf{D}}{\partial t}\big)\cdot d\mathbf{a} \tag{27}$$

By contrast with the EQS systems treated in deriving this expression, it now holds only on the surface S, not necessarily on surfaces inside the volume enclosed by S.

Second, on the surface S*, the contribution of the displacement current must be negligible.* This is equivalent to requiring that S is chosen parallel to the displacement flux density. In this case, the total power into the system reduces to

$$-\oint_S \mathbf{E}\times\mathbf{H}\cdot d\mathbf{a} = -\oint_S \Phi\mathbf{J}\cdot d\mathbf{a} \tag{28}$$

The integrand has value only where the surface S intersects a wire. If taken as perfectly conducting (but nevertheless in a region where $\partial\mathbf{B}/\partial t$ is zero and hence $\mathbf{E}$ is irrotational), the wires have potentials that are uniform over their cross-sections. Thus, in (28), Φ is equal to the voltage of the terminal. In integrating the current density over the cross-section of the wire, note that $d\mathbf{a}$ is directed out of the surface, while a positive terminal current is directed into the surface. Thus,

$$-\oint_S \mathbf{E}\times\mathbf{H}\cdot d\mathbf{a} = \sum_{i=1}^{n} v_i i_i \tag{29}$$

and the input power expressed by (28) is equivalent to what would be expected from circuit theory.

Poynting Flux and Electromagnetic Radiation. Power cannot be supplied to or lost by a quasistatic system of finite extent through a surface at infinity. Such a power supply or loss requires radiation, and electromagnetic waves are neglected when either the magnetic induction or the displacement current density are neglected. To prove this statement, consider an EQS system of finite net charge. Its electric field intensity decays like $1/r^2$ at infinity, where r is the distance to a far-off point from some origin chosen within the system. At a great distance, the currents appear equivalent to current loop sources. Hence, the magnetic field intensity has the $1/r^3$ decay typical of a magnetic dipole. It follows that the Poynting vector decays at least as fast as $1/r^5$, so that the flux of $\mathbf{E}\times\mathbf{H}$ integrated over the "sphere" at infinity of area $4\pi r^2$ gives zero contribution. Because it is only that part of $\mathbf{E}\times\mathbf{H}$ resulting from electromagnetic radiation that contributes at infinity, Poynting's theorem is shown in Sec. 12.5 to be a powerful tool for dealing with antennae.

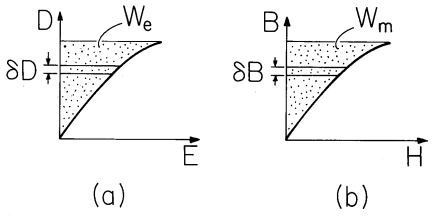


Fig. 11.4.1 Single-valued constitutive laws showing energy density associated with variables at the endpoints of the curves: (a) electric energy density; and (b) magnetic energy density.

11.4 ENERGY STORAGE

In the conservation theorem, (11.2.7), we have identified the terms $\mathbf{E}\cdot\partial\mathbf{P}/\partial t$ and $\mathbf{H}\cdot\partial\mu_o\mathbf{M}/\partial t$ as the rate of energy supplied per unit volume to the polarization and magnetization of the material. For a linear isotropic material, we found that these terms can be written as derivatives of energy density functions. In this section, we seek a more general description of energy storage. First, nonlinear materials are considered from the field viewpoint. Then, for those systems that can be described in terms of electrical terminal pairs, energy storage is formulated in terms of terminal variables. We will find the results of this section directly applicable to finding electric and magnetic forces in Secs. 11.6 and 11.7.

Energy Densities. Consider a material in which $\mathbf{E}$ and $\mathbf{D}\equiv(\epsilon_o\mathbf{E}+\mathbf{P})$ are collinear. With E and D representing the magnitudes of these vectors, this material is presumed to be described by a constitutive law in which E is a single-valued function of D, such as that sketched in Fig. 11.4.1a. In the case of a linear constitutive law, the curve is a straight line with a slope equal to the permittivity ϵ.

Consider a material in which $\mathbf{E}$ and $\mathbf{P}$ are collinear (isotropic material). Then, of course, $\mathbf{E}$ and $\mathbf{D}\equiv\epsilon_o\mathbf{E}+\mathbf{P}$ are collinear as well. One may graph the magnitude of D versus E and obtain a complete characterization of the material. Now the power per unit volume imparted to the polarization is $\mathbf{E}\cdot\partial\mathbf{P}/\partial t$. If one adds to it the rate of energy supply to the field per unit volume (the free space part) $\mathbf{E}\cdot\partial\epsilon_o\mathbf{E}/\partial t$, one obtains for the power per unit volume

$$\boxed{\mathbf{E}\cdot\frac{\partial}{\partial t}(\epsilon_o\mathbf{E}+\mathbf{P})=\mathbf{E}\cdot\frac{\partial\mathbf{D}}{\partial t}=E\frac{\partial D}{\partial t}} \tag{1}$$

The power supplied to the unit volume can now be written as the time derivative of a function of D, $W_e(D)$. Indeed, if we define the area above the graph in Fig. 11.4.1 as W_e, then

$$\boxed{\frac{\partial W_e}{\partial t}=\frac{\partial W_e}{\partial D}\frac{\partial D}{\partial t}=E\frac{\partial D}{\partial t}} \tag{2}$$

Thus, $E(\partial D/\partial t)$ is the derivative of the function $W_e(D)$. This function is the energy stored per unit volume, because the energy supplied per unit volume expressed by the integral

$$\int_{-\infty}^{t} dt E \frac{\partial D}{\partial t} = \int_0^D E\delta D = W_e(D) \tag{3}$$

is a function of the final value D of the displacement flux, and we assumed that the fields E and D were zero at $t = -\infty$. Here, δD represents the differential of D, usually denoted by dD. We will use δ rather than d to avoid confusion between differentials used in carrying out volume, surface and line integrals and the differential used here, which implies an integration in a "state space" having the "dimension" D.

Similar arguments show that if $\mathbf{B} \equiv \mu_o(\mathbf{H} + \mathbf{M})$ and $\mathbf{H}$ are collinear, and if H is a single-valued function of B, then

$$\boxed{\mathbf{H} \cdot \frac{\partial \mathbf{B}}{\partial t} = \frac{\partial W_m}{\partial t}} \tag{4}$$

where

$$\boxed{W_m = W_m(B) = \int_0^B H\delta B} \tag{5}$$

With (1) and (4) replacing the first four terms on the right in the energy theorem of (11.2.7), it is clear that the energy density $W = W_e + W_m$. The electric and magnetic energy densities have the geometric interpretations as areas on the graphs representing the constitutive laws in Fig. 11.4.1.

Energy Storage in Terms of Terminal Variables. It was shown in Sec. 11.3 that the power input to a system could be represented by the sum of the vi products for each of the terminal pairs, (11.3.29), provided certain conditions were met in the neighborhoods of the terminals. The description of energy storage in a loss-free system in terms of terminal variables will be found useful in determining electric and magnetic forces. With the assumption that all of the power input to a system is accounted for by a time rate of change of the energy stored, the energy conservation statement for a system becomes

$$\sum_{i=1}^{n} v_i i_i = \frac{dw}{dt} \tag{6}$$

where

$$w = \int_V W dv$$

and the integral is carried over the volume of the system. If the system is *electroquasistatic*, conservation of charge requires that the terminal current be the time rate of change of the charge on the electrode to which the positive terminal is attached.

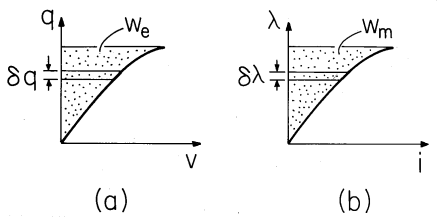


Fig. 11.4.2 Single-valued terminal relations showing total energy stored when variables are at the endpoints of the curves: (a) electric energy storage; and (b) magnetic energy storage.

$$\boxed{i_i = \frac{dq_i}{dt}} \tag{7}$$

Further, $w = w_e$, the stored electric energy. Thus, one concludes from (6) that

$$\sum_{i=1}^{n} v_i \frac{dq_i}{dt} = \frac{dw_e}{dt} \Rightarrow dw_e = \sum_{i=1}^{n} v_i dq_i \tag{8}$$

The second expression states that with the addition of an incremental amount of charge dq_i to an electrode having the voltage v_i goes an incremental change in the stored energy w_e. Integration on the charges then gives the total energy

$$\boxed{w_e = \sum_{i=1}^{n} \int v_i dq_i} \tag{9}$$

To complete this integral, each of the terminal voltages must be a known function of the associated charges.

$$\boxed{v_i = v_i(q_1, \ldots\ q_n)} \tag{10}$$

Integration is then carried out along any path in the state space $(q_1 \ldots q_n)$ that begins at the origin and ends with the desired charges on the electrodes (and hence the desired terminal voltages). For a single terminal pair, the energy can be pictured as the area shown in Fig. 11.4.2a.

If the system is magnetoquasistatic, the conservation law for a lossless system that can be described by terminal relations again takes the form of (6). However, rather than expressing the currents as derivatives of electrode charges, the voltages are derivatives of the fluxes linked by the respective terminal pairs.

$$\boxed{v_i = \frac{d\lambda_i}{dt}} \tag{11}$$

Then, (6) leads to

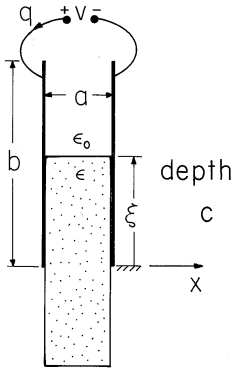


Fig. 11.4.3 Capacitor partially filled by free space and by dielectric having permittivity ϵ.

$$\boxed{w_m = \sum_{i=1}^{n} \int i_i d\lambda_i} \tag{12}$$

To complete this integral, we require the terminal currents as functions of the terminal flux linkages.

$$\boxed{i_i = i_i(\lambda_i \ldots \lambda_n)} \tag{13}$$

For a single terminal pair system, w_m is portrayed in Fig. 11.4.2b.

The most general way to compute the total energy stored in a system is to integrate the energy densities given by (3) and (5) over the volumes of the respective systems. If systems can be described in terms of terminal relations and are loss free, (9) and (12) must lead to the same answers. Note that (D, E) and (q, v) are the field and circuit variables in the EQS systems, while (B, H) and (λ, i) have corresponding roles in MQS systems.

Example 11.4.1. An Electrically Linear System

A dielectric slab of permittivity ϵ partially fills the region between plane parallel perfectly conducting electrodes, as shown in Fig. 11.4.3. With the fringing field ignored, we find the total energy stored by two methods. First, the energy density is integrated over the volume. Then, the terminal relation is used to evaluate the total energy.

An exact solution for the electric field well between the electrodes is simply $\mathbf{E} = \mathbf{i}_\mathbf{x}(v/a)$. Note that this field satisfies the boundary conditions at the interface between the dielectric slab and the free space region above and at the electrodes. We assume that $a \ll b$ and therefore neglect the fringing fields.

The energy density in the linear dielectric, where $\mathbf{D} = \epsilon\mathbf{E}$, follows from evaluation of (3).

$$W_e = \int_0^D E\delta D = \frac{1}{2}\frac{D^2}{\epsilon} = \frac{1}{2}\epsilon E^2; \tag{14}$$

$$E = \frac{v}{a}$$

In the free space region, the same result applies with $\epsilon \to \epsilon_o$.

Integration of these energy densities over the regions in which they apply amounts to a multiplication by the respective volumes. Thus, the total energy is

$$w_e = \int_V W_e dV = \frac{1}{2}\epsilon\left(\frac{v}{a}\right)^2(\xi ca) + \frac{1}{2}\epsilon_o\left(\frac{v}{a}\right)^2[(b-\xi)ca] \tag{15}$$

Note that this expression takes the form

$$w_e = \frac{1}{2}Cv^2 \tag{16}$$

where

$$C \equiv \frac{c}{a}[\epsilon_o b + \xi(\epsilon - \epsilon_o)]$$

In terms of the terminal variables, where $q = Cv$, the total energy follows from an evaluation of (9).

$$w_e = \int v dq = \int \frac{q}{C} dq = \frac{1}{2}\frac{q^2}{C} = \frac{1}{2}Cv^2 \tag{17}$$

Once the integration has been carried out, the last expression is written by again using the relation $q = Cv$. Note that the volume integration of the energy density and the integration in terms of the terminal variables give the same result.

The next example considers an MQS system with two terminal pairs and thus illustrates the integration called for in evaluating the energy from the terminal relations. Also, the energy stored in coupled inductors is often of practical interest.

Example 11.4.2. Coupled Coils; Transformers

An example of a two terminal pair lossless MQS system is a pair of coupled coils having the terminal relations

$$\begin{bmatrix}\lambda_1\\ \lambda_2\end{bmatrix} = \begin{bmatrix}L_{11} & L_{12}\\ L_{21} & L_{22}\end{bmatrix}\begin{bmatrix}i_1\\ i_2\end{bmatrix} \tag{18}$$

In this case, (12) becomes

$$dw_m = i_1 d\lambda_1 + i_2 d\lambda_2 \tag{19}$$

To evaluate this expression, we need to substitute for the currents written in terms of the flux linkages. This requires the inversion of (18). For linear systems, this is easily done, but not for nonlinear systems. To avoid inversion, we rewrite the right-hand side of (19), which becomes

$$dw_m = d(i_1\lambda_1 + i_2\lambda_2) - \lambda_1 di_1 - \lambda_2 di_2 \tag{20}$$

and regroup terms

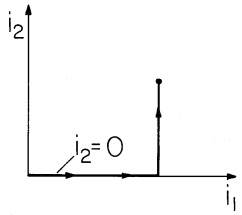


Fig. 11.4.4 Integration path in state space consisting of terminal currents.

$$\boxed{dw'_m = \lambda_1 di_1 + \lambda_2 di_2} \tag{21}$$

where the *coenergy* is defined as

$$\boxed{w'_m = (i_1\lambda_1 + i_2\lambda_2) - w_m} \tag{22}$$

Equation (21) can be integrated when the flux linkages are expressed in terms of the currents, and that is the form in which the terminal relations are given by (18). Once the coenergy w'_m has been found, w_m follows from (22).

The integration of (19) is a line integral in a state space (i_1, i_2). If energy is conserved, we must be able to carry out this integration along any path that begins with the currents turned off and ends with the currents at the desired values. In the path represented by Fig. 11.4.4, the current i_1 is turned up first while holding the current i_2 to zero. Then, with i_1 held fixed at its final value, the current i_2 is raised from zero to its final value. For this path, the integration of (22) becomes

$$w'_m = \int_0^{i_1} \lambda_1(i'_1, 0)di'_1 + \int_0^{i_2} \lambda_2(i_1, i'_2)di'_2 \tag{23}$$

Substitution for the flux linkages from (18) and evaluation of the integrals then gives

$$w'_m = \frac{1}{2}L_{11}i_1^2 + L_{12}i_1i_2 + \frac{1}{2}L_{22}i_2^2 \tag{24}$$

If the integration is carried out along a path where the roles of i_1 and i_2 are reversed, the expression obtained is (24) with $L_{12} \to L_{21}$. To make the energy stored independent of path, the mutual inductances must be equal.

$$L_{12} = L_{21} \tag{25}$$

This relation, which we found to hold for the transformer of Example 9.7.4, is required if energy is to be conserved. The energy is now evaluated by substituting this expression and the flux linkages expressed using (18) into (22) solved for w_m. It follows that

$$w'_m = w_m \tag{26}$$

Evaluation of the energy stored in a unity-coupled transformer, where the inductances take the form of (9.7.20), gives

$$w_m = \frac{A\mu}{l}\left(\frac{1}{2}N_1^2i_1^2 + N_1N_2i_1i_2 + \frac{1}{2}N_2^2i_2^2\right) \tag{27}$$

Operating under "ideal" conditions [in the sense that $i_2/i_1 = -N_1/N_2$, (9.7.13)], the transformer does not store energy, $w_m = 0$. Thus, according to the power theorem in the form of (6), under ideal operating conditions, the power input at one terminal pair instantaneously appears as a power output at the second terminal pair.

Examples have so far involved linear polarization and magnetization constitutive laws. In the following, the EQS energy storage in a material having a nonlinear polarization constitutive law is determined.

Example 11.4.3. Energy Storage in Electrically Nonlinear Material

To represent the tendency of the polarization to saturate as the electric field is raised, a constitutive law might take the form

$$D = \left(\frac{\alpha_1}{\sqrt{1 + \alpha_2 E^2}} + \epsilon_o \right) E \tag{28}$$

Here, α_1 and α_2 are parameters descriptive of the specific material, and $\mathbf{D}$ is collinear with $\mathbf{E}$. This constitutive law is portrayed graphically in Fig. 11.4.5.

Because D is given as a function of E that is not easily solved for E as a function of D, the computation of the electric energy density using (3) is inconvenient. However, we can observe that

$$\delta W_e = E\delta D = \delta(ED) - D\delta E \tag{29}$$

and then regroup terms so that the expression becomes

$$\boxed{\delta W_e' = D\delta E} \tag{30}$$

where

$$\boxed{W_e' = ED - W_e} \tag{31}$$

Integration now leads to the *coenergy density* W_e', but the energy density W_e can then be found using (31) and the constitutive law.

Specifically, evaluation of (30) using (28) gives the coenergy density

$$W_e' = \int D\delta E = \frac{\alpha_1}{\alpha_2}\left(\sqrt{1 + \alpha_2 E^2} - 1\right) + \frac{1}{2}\epsilon_o E^2 \tag{32}$$

It follows from (31) that the energy density is

$$W_e = ED - W_e' = \frac{\alpha_1}{\alpha_2}\left(\frac{\sqrt{1 + \alpha_2 E^2} - 1}{\sqrt{1 + \alpha_2 E^2}} \right) + \frac{1}{2}\epsilon_o E^2 \tag{33}$$

A graphical representation of the energy and coenergy functions is given in Fig. 11.4.5. The area "under the curve" with D as the integration variable is W_e, (3), and the area under the curve with E as the integration variable is W_e', (31).

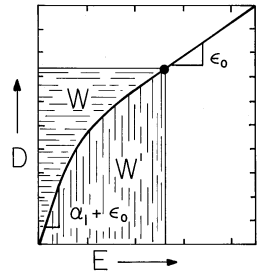


Fig. 11.4.5 Single-valued nonlinear constitutive law. Areas representing energy density W and coenergy density W' are not equal in this case.

11.5 ELECTROMAGNETIC DISSIPATION

The heat generated by electromagnetic fields is often the controlling feature of an engineering design. Semiconductors inevitably produce heat, and the distribution and magnitude of the heat source is an important consideration whether the application is to computers or power conversion. Often, the generation of heat poses a fundamental limitation on the performance of equipment. Examples where the generation of heat is desirable include the heating coil of an electric stove and the microwave irradiation of food in a microwave oven.

Ohmic conduction is the primary cause of heat generation in metals, but it also operates in semiconductors, electrolytes, and (at low frequencies) in semi-insulating liquids and solids. The mechanism responsible for this type of heating was discussed in Sec. 11.3. The dissipation density associated with Ohmic conduction is $\sigma \mathbf{E} \cdot \mathbf{E}$.

An Ohmic current can be imposed by making electrical contact with the material, as for the heating element in a stove. If the material is a good conductor, such currents can also be induced by magnetic induction (without electrical contact). The currents induced by time-varying magnetic fields in Chap. 10 are an example. *Induction heating* is an MQS process and often used in processing metals. Currents induced in transformer cores by the time-varying magnetic flux are an example of undesirable heating. In this context, the associated losses (which are minimized by laminating the core) are said to be due to *eddy currents*.

Ohmic heating can also be induced by "capacitive" coupling. In the EQS examples of Sec. 7.9, *dielectric heating* is caused by the currents associated with the accumulation of unpaired charges.

Whether due to magnetic induction or capacitive coupling, the generation of heat is described by the dissipation density $P_d = \sigma \mathbf{E} \cdot \mathbf{E}$ identified in Sec. 11.3. However, the polarization and magnetization terms in the conservation theorem, (11.2.7), can also be responsible for energy dissipation. This occurs when the (electric or magnetic) dipoles do not align instantaneously with the fields. The polarization and magnetization constitutive laws differ from the laws postulated in Sec. 11.3.

As an example suggesting how the polarization term in (11.2.7) can represent dissipation, picture the artificial dielectric of Demonstration 6.6.1 (the ping-pong ball dielectric) but with spheres that are highly resistive rather than perfectly conducting. The accumulation of charge on the poles of the spheres in response to the application of an electric field is described by a *rate*, rather than a *magnitude*, that

is proportional to the field. Thus, we would expect $\partial \mathbf{P}/\partial t$ rather than $\mathbf{P}$ to be proportional to $\mathbf{E}$. With γ a coefficient representing the properties and geometry of the spheres, the polarization constitutive law would then take the form

$$\frac{\partial \mathbf{P}}{\partial t} = \gamma \mathbf{E} \tag{1}$$

If this law is used to express the polarization term in the conservation law, the second term on the right in (11.2.7), a positive definite quantity results.

$$\mathbf{E} \cdot \frac{\partial \mathbf{P}}{\partial t} = \gamma \mathbf{E} \cdot \mathbf{E} \tag{2}$$

As might be expected from the physical origins of the constitutive law, the polarization term now represents dissipation rather than energy storage.

When materials are placed in electric fields having frequencies so high that conduction effects are negligible, losses due to the polarization of dipoles become the dominant heating mechanism. The artificial diamagnetic material considered in Demonstration 9.5.1 suggests how analogous losses are associated with the dynamic magnetization of a material. If the spherical particles comprising the artificial diamagnetic material have a finite conductivity, the induced dipole moments are not in phase with an applied sinusoidal field. What amounts to Ohmic dissipation on the particle scale is accounted for on the macroscopic scale by a modified constitutive law of magnetization.

The most common losses due to magnetization are encountered in ferromagnetic materials. *Hysteresis losses* occur because of the coercion required to obtain alignment of ferromagnetic domains. We will end this section with the relationship between the hysteresis curve of Fig. 9.4.6 and the dissipation density.

Energy Conservation for Temporally Periodic Systems. Many practical situations involve fields that vary with time in a periodic fashion. The sinusoidal steady state is the most common example. If the energy conservation law (11.0.8) is integrated over one period T, the energy storage term makes no contribution.

$$\int_0^T \frac{dw}{dt} dt = w(T) - w(0) = 0 \tag{3}$$

As a result, the time average of the conservation law states that the time average of the input power goes into the time average of the dissipation. The time average of the integral form of the conservation law, (11.1.1), becomes

$$-\langle \oint_S \mathbf{S} d\mathbf{a} \rangle = \langle \int_V P_d dv \rangle \tag{4}$$

This expression, which assumes that the dynamics are periodic but not necessarily sinusoidal, gives us two ways to compute the total energy dissipation. Either we can use the right-hand side and integrate the power dissipation density over the

volume, or we can use the left-hand side and integrate the time average of $\mathbf{S} \cdot d\mathbf{a}$ over the surface enclosing the volume.

Consider the sinusoidal steady state as a particular case. If $\mathbf{P}$ and $\mathbf{M}$ are related to $\mathbf{E}$ and $\mathbf{H}$ by linear differential equations, an approach can be taken that is familiar from circuit theory. The phase and amplitude of each field at a given location are represented by a complex amplitude. For example, the electric and magnetic field intensities are written as

$$\mathbf{E} = Re\hat{\mathbf{E}}(\mathbf{r})e^{j\omega t}; \qquad \mathbf{H} = Re\hat{\mathbf{H}}(\mathbf{r})e^{j\omega t} \tag{5}$$

A complex vector $\hat{\mathbf{E}}(\mathbf{r})$ has three complex scalar components $\hat{E}_x(\mathbf{r})$, $\hat{E}_y(\mathbf{r})$, and $\hat{E}_z(\mathbf{r})$. The meaning of each is the same as the meaning of a complex voltage in circuit theory: e.g., the magnitude of $\hat{E}_x(\mathbf{r})$, $|\hat{E}_x(\mathbf{r})|$, gives the peak amplitude of the x component of the electric field varying cosinusoidally with time, and the phase of $\hat{E}_x(\mathbf{r})$ gives the phase advance of the cosine time function.

In determining the time averages of products of quantities that are in the sinusoidal steady state, it is helpful to make use of the *time average theorem*. With $*$ designating the complex conjugate,

$$\boxed{\langle Re\hat{A}e^{j\omega t} Re\hat{B}e^{j\omega t}\rangle = \frac{1}{2}Re\hat{A}\hat{B}^*} \tag{6}$$

This can be shown by using the identity

$$Re\hat{C}e^{j\omega t} = \frac{1}{2}(\hat{C}e^{j\omega t} + \hat{C}^* e^{-j\omega t}) \tag{7}$$

Induction Heating. In this case, the heating is represented by Ohmic conduction and P_d given by (11.3.3c). The examples from Chaps. 7 and 10 involving conductors of finite conductivity offer the opportunity to apply this relation to the evaluation of the right-hand side of (4). If the same total time average power is calculated using the left-hand side of this expression, it may seem that Ohm's law is not required. However, remember that this law is also reflected in the field quantities used to calculate $\mathbf{S}$.

Example 11.5.1. Induction Heating of the Thin Shell

The thin conducting shell of Fig. 11.5.1, in a field $H_o(t)$ applied collinear with its axis, was described in Example 10.3.1. Here the applied field is in the sinusoidal steady state

$$H_o = Re\hat{H}_o e^{j\omega t} \tag{8}$$

According to (10.3.9), the complex amplitude of the response, the magnetic field inside the shell, is

$$\hat{H}_i = \frac{\hat{H}_o}{1 + j\omega\tau_m} \tag{9}$$

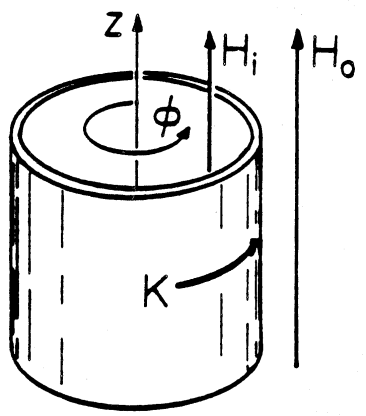


Fig. 11.5.1 Circular cylindrical conducting shell in imposed axial magnetic field intensity $H_o(t)$.

where $\tau_m = \frac{1}{2}\mu_o\sigma\Delta a$.

The complex amplitude of the surface current density circulating in the shell follows from (10.3.8).

$$\hat{K} = -\hat{H}_o + \frac{\hat{H}_o}{1 + j\omega\tau_m} = -\frac{j\omega\tau_m\hat{H}_o}{1 + j\omega\tau_m} \tag{10}$$

Because the current density is uniform over the radial cross-section of the shell, the dissipation density can be written in terms of the surface current density $K = \Delta\sigma E$.

$$P_d = \sigma\mathbf{E}\cdot\mathbf{E} = \frac{K^2}{\Delta^2\sigma} \tag{11}$$

It follows from the application of the time average theorem, (6), that the total time average dissipation is

$$\langle \int_V P_d dv\rangle = \langle \int_V \frac{1}{2} Re\frac{\hat{K}\hat{K}^*}{\Delta^2\sigma} dv\rangle = \frac{2\pi a\Delta l}{2\Delta^2\sigma} Re\hat{K}\hat{K}^* \tag{12}$$

where l is the shell length. To complete the derivation based on an integration of the density over the volume of the conductor, this expression can be evaluated using (10).

$$\langle p_d\rangle \equiv \langle \int_V P_d dv\rangle = p_o\frac{(\omega\tau_m)^2}{1 + (\omega\tau_m)^2}; \qquad p_o \equiv \frac{\pi a l}{\sigma\Delta}|\hat{H}_o|^2 \tag{13}$$

The same result is found by evaluating the time average of the Poynting flux density integrated over a surface that is just outside the shell at $r = a$. To see this, we again use the time average theorem, (6), and recognize that the surface integral amounts to a multiplication by the surface area of the shell.

$$-\langle \oint_S (\mathbf{E}\times\mathbf{H})\cdot d\mathbf{a}\rangle = \oint_S \frac{1}{2} Re\hat{E}_\phi\hat{H}_o^* da = \frac{2\pi a l}{2} Re\hat{E}_\phi\hat{H}_o^* \tag{14}$$

To evaluate this expression, (10) is used to determine E_ϕ

$$\hat{E}_\phi = \frac{\hat{K}}{\Delta\sigma} = -\frac{j\omega\tau_m\hat{H}_o}{\Delta\sigma(1 + j\omega\tau_m)} = -\frac{j\omega\tau_m(1 - j\omega\tau_m)\hat{H}_o}{\Delta\sigma[1 + (\omega\tau_m)^2]} \tag{15}$$

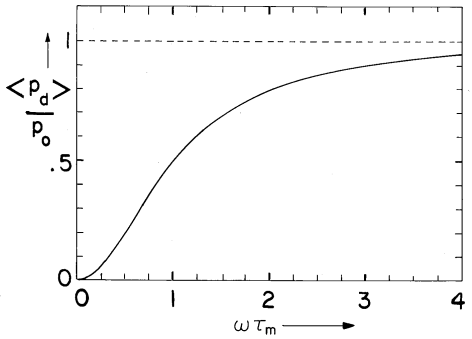


Fig. 11.5.2 Time average power dissipation density normalized to p_o as defined with (13) as a function of the frequency normalized to the magnetic diffusion time defined with (9).

Evaluation of (14) then gives

$$-\langle \oint \mathbf{E} \times \mathbf{H} \cdot d\mathbf{a} \rangle = p_o \frac{(\omega\tau_m)^2}{1+(\omega\tau_m)}; \qquad p_o \equiv \frac{\pi a l}{\sigma\Delta}|\hat{H}_o|^2 \tag{16}$$

which is the same result as found by integrating the dissipation density over the volume, (13).

The dependence of the time average power dissipation on the normalized frequency is shown in Fig. 11.5.2. At very low frequencies, the induced current is not large enough to have an appreciable effect on the imposed field. Thus, the electric field is proportional to the time rate of change of the *applied field*, and because the dissipation is proportional to the square of $\mathbf{E}$, the power dissipation increases as the square of ω. At high frequencies, the induced current can be no more than that required to shield the imposed field from the region inside the shell. As a result, the dissipation reaches an asymptotic limit.

Which of the two approaches is best for finding the total power dissipation? The answer depends on what field information is available. Certainly, the notion that the total heat generated can be found by integrating over a surface that is completely outside the heated material is a fundamental consequence of Poynting's theorem.

Dielectric Heating. In the sinusoidal steady state, we can identify the power dissipation density associated with polarization by finding the time average

$$\langle P_d \rangle = \langle \mathbf{E} \cdot \frac{\partial \mathbf{D}}{\partial t} \rangle \tag{17}$$

In view of the time average theorem, (6), this becomes

$$\langle P_d \rangle = \frac{1}{2} Re j\omega \hat{\mathbf{D}} \cdot \hat{\mathbf{E}}^* \tag{18}$$

If the polarization $\mathbf{P}$ does not follow the electric field $\mathbf{E}$ instantaneously, yet the material is still linear and isotropic, the complex vector $\hat{\mathbf{P}}$ can be related to $\hat{\mathbf{E}}$ by

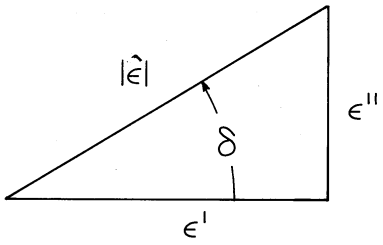


Fig. 11.5.3 Definition of angle δ defining the loss tangent $\tan(\delta)$ in terms of the real and the negative of the imaginary parts of the complex permittivity.

a complex susceptibility. Or, instead, the complex displacement flux density vector $\hat{\mathbf{D}}$ is related to $\hat{\mathbf{E}}$ by a complex dielectric constant.

$$\hat{\mathbf{D}} = \hat{\epsilon}\hat{\mathbf{E}} = (\epsilon' - j\epsilon'')\hat{\mathbf{E}} \tag{19}$$

Here $\hat{\epsilon}$ is the *complex permittivity* with real and imaginary parts ϵ' and $-\epsilon''$, respectively.

Evaluation of (18) using this constitutive law gives

$$\langle P_d \rangle = \frac{\omega}{2}|\hat{\mathbf{E}}|^2 Re j\hat{\epsilon} = \frac{\omega}{2}|\hat{\mathbf{E}}|^2\epsilon'' \tag{20}$$

Thus, ϵ'' represents the electrical dissipation associated with the polarization process.

In the literature, the *loss tangent* $\tan\delta$ is often used to represent dissipation. It is the tangent of the phase angle δ of the complex dielectric constant defined in terms ϵ' and ϵ'' in Fig. 11.5.3. Thus,

$$\tan\delta = \frac{\epsilon''}{\epsilon'}; \qquad \cos\delta = \frac{\epsilon'}{|\hat{\epsilon}|}; \qquad \sin\delta = \frac{\epsilon''}{|\hat{\epsilon}|} \tag{21}$$

From this definition, it follows from Eulers formula that

$$\epsilon' - j\epsilon'' = |\hat{\epsilon}|(\cos\delta - j\sin\delta) = |\hat{\epsilon}|e^{-j\delta} \tag{22}$$

Given the complex amplitude of the electric field, $\mathbf{D}$ is

$$\mathbf{D} = Re\{|\hat{\epsilon}|\hat{\mathbf{E}}e^{j(\omega t-\delta)}\} \tag{23}$$

If the electric field is $\mathbf{E}_o\cos(\omega t)$, then $\mathbf{D}$ is $|\hat{\epsilon}|\mathbf{E}_o\cos(\omega t - \delta)$. The electric displacement lags the electric field by the phase angle δ.

In terms of the loss tangent defined by (21), the time average electrical dissipation density of (20) becomes

$$\langle P_d \rangle = \frac{\omega\epsilon'}{2}|\hat{E}|^2\tan\delta \tag{24}$$

Usually the loss tangent and ϵ' are measured. In the following example, we compute the complex permittivity from a model of the polarizable medium and

find the electrical dissipation on a macroscopic basis. In this special case we have the option of finding the time average loss by considering each of the dipoles on a microscopic basis. This is not generally possible, because the interactions among dipoles that are neglected in this example are usually too complicated for an analytic treatment.

Example 11.5.2. An Artificial Lossy Dielectric

By putting together examples considered in Chaps. 6 and 7, we can illustrate the origins of the complex permittivity. The artificial dielectric of Example 6.6.1 and Demonstration 6.6.1 had "molecules" consisting of perfectly conducting spheres. As a result, the polarization was pictured as instantaneously in step with the applied field. We consider now the result of having spheres that have finite conductivity.

The response of a single sphere having a finite conductivity σ and permittivity ϵ surrounded by free space is a special case of Example 7.9.3. The response to a sinusoidal drive is summarized by (7.9.36), where we set $\sigma_a = 0$, $\epsilon_a = \epsilon_o$, $\sigma_b = \sigma$, and $\epsilon_b = \epsilon$. All that is required from this solution for the potential is the moment of a dipole that would give rise to the same exterior field as does the sphere. Comparison of the potential of a dipole, (4.4.10), to that given by (7.9.36a) shows that the complex amplitude of the moment is

$$\hat{p} = 4\pi\epsilon_o R^3 \frac{\left[1 + j\omega\tau_e \frac{(\epsilon-\epsilon_o)}{2\epsilon_o+\epsilon}\right]}{1 + j\omega\tau_e}\hat{E} \tag{25}$$

where $\tau_e \equiv (2\epsilon_o + \epsilon)/\sigma$. If mutual interactions between dipoles are ignored, the polarization density $\mathbf{P}$ is this moment of a single dipole multiplied by the number of dipoles per unit volume, N. For a cubic array with a distance s between the dipoles (the centers of the spheres), $N = 1/s^3$. Thus, the complex amplitude of the electric displacement is

$$\hat{D} = \epsilon_o\hat{E} + \hat{P} = \epsilon_o\hat{E} + \frac{\hat{p}}{s^3} \tag{26}$$

Combining this result with the moment given by (25) yields the desired constitutive law in the form $\hat{\mathbf{D}} = \hat{\epsilon}\hat{\mathbf{E}}$, where the complex permittivity is

$$\hat{\epsilon} = \epsilon_o\left\{1 + 4\pi\left(\frac{R}{s}\right)^3 \frac{\left[1 + j\omega\tau_e \frac{(\epsilon-\epsilon_o)}{2\epsilon_o+\epsilon}\right]}{1 + j\omega\tau_e}\right\} \tag{27}$$

The time average power dissipation density follows from this expression and (20).

$$\langle P_d\rangle = \frac{2\pi\epsilon_o}{\tau_e}\left(\frac{R}{s}\right)^3\left[\frac{3\epsilon_o}{2\epsilon_o+\epsilon}\right]\frac{(\omega\tau_e)^2}{1+(\omega\tau_e)^2}|\hat{E}|^2 \tag{28}$$

The dependence of the power dissipation on frequency has the same form as for the induction heating example, Fig. 11.5.2. At low frequencies, the surface charges induced at the north and south poles of each sphere are completely determined by the external field. Thus, the current density within the sphere that makes possible the accumulation of these surface charges is proportional to the time rate of change of the applied field. At low frequencies, the dissipation is proportional to the square

of the volume current and hence to the square of the time rate of change of the applied field. As a result, at low frequencies, the dissipation density increases with the square of the frequency.

As the frequency is raised, less surface charge is induced on the spheres. Although the amount of charge induced is inversely proportional to the frequency, there is a compensating effect because the volume currents are responsible for the dissipation, and these are proportional to the time rate of change of the charge. Thus, the dissipation density reaches a saturation value as the frequency becomes very high.

One tool used to form a picture of atomic, molecular, and domain physics is dielectric spectroscopy. Using this approach, the frequency dependence of the complex permittivity is used to gain insight into the microscopic structure.

Magnetization, like polarization, can also be the source of dissipation. The time average dissipation density due to magnetization follows by taking the time averge of the third and fourth terms on the right in the basic power theorem, (11.2.7). Combined, these terms give

$$\langle P_d \rangle = \langle \mathbf{H} \cdot \frac{\partial \mathbf{B}}{\partial t} \rangle \tag{29}$$

For small-signal applications, this source of dissipation is dealt with by introducing a complex permeability $\hat{\mu}$ such that $\hat{\mathbf{B}} = \hat{\mu}\hat{\mathbf{H}}$. The role of the complex permeability is similar to that of the complex permittivity. The artificial diamagnetic material of Example 9.5.2 and Demonstration 9.5.1 can be used to exemplify the concept. Instead of perfectly conducting spheres that give rise to a magnetic moment instantaneously induced antiparallel to the applied field, spherical shells of finite conductivity would be used. The dipole moment induced in the individual spherical shells would be deduced following the same approach as in Sec. 10.4. The resulting dipole moment would not be in phase with an applied sinusoidally varying magnetic field. The derivation of an equivalent complex permeability would follow from the same line of reasoning as used in the previous example.

Hysteresis Losses. Under periodic conditions in magnetizable solids, B and H are related by the hysteresis curve described in Sec. 9.4 and illustrated again in Fig. 11.5.4. What time average power dissipation is implied by the hysteresis?

As before, B and H are collinear. However, neither is now a single-valued function of the other. Evaluation of (29) is accomplished by breaking the cycle into two parts, each involving a single-valued relationship between B and H. The first is the upswing "trajectory" from $A \rightarrow C$ in Fig. 11.5.4. Over this half-cycle, which takes B from B_A to B_C, the trajectory is $H_+(B)$. With B taken as B_A when $t = 0$, it follows from (11.4.4) and (11.4.5) that

$$\int_0^{T/2} \mathbf{H} \cdot \frac{\partial \mathbf{B}}{\partial t} dt = \int_{B_A}^{B_C} \frac{dW_m}{dt} dt = \int_{B_A}^{B_C} H_+ \delta B \tag{30}$$

This is the area under the curve of H versus B between A and C in Fig. 11.5.4, traversed on the "upswing." A similar evaluation for the "downswing," where the

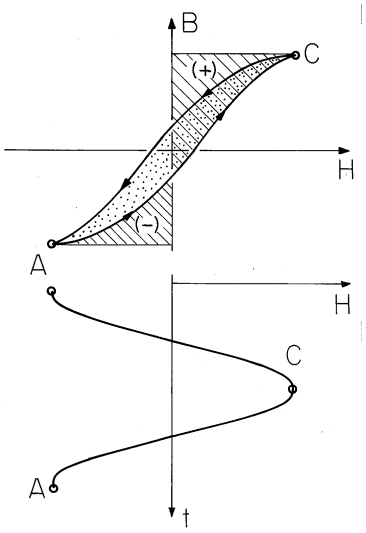


Fig. 11.5.4 With the application of a sinusoidal magnetic field intensity, a steady state is reached in which the hysteresis loop shown in the $B-H$ plane is traced out in the direction shown. The dashed area represents the energy density associated with upward traversal from A to C. The dotted area inside the loop represents the energy density dissipated per traversal of the loop.

trajectory is $H_-(B)$, gives

$$\int_{T/2}^{T} \mathbf{H}\cdot\frac{\partial \mathbf{B}}{\partial t}dt = \int_{B_C}^{B_A} H_-\delta B = -\int_{B_A}^{B_C} H_-\delta B \tag{31}$$

The time average power dissipation, (29), then is the sum of these two contributions divided by T.

$$\langle P_d\rangle = \frac{1}{T}\Big[\int_{B_A}^{B_C} H_+\delta B - \int_{B_A}^{B_C} H_-\delta B\Big] \tag{32}$$

Thus, the area within the hysteresis loop is the energy dissipated in one cycle.

11.6 ELECTRICAL FORCES ON MACROSCOPIC MEDIA

Electrical forces on macroscopic materials have their origins in the forces exerted on the microscopic particles of which the materials are composed. Macroscopic fields have been used to describe conduction, polarization, and magnetization. In Chaps. 6, 7 and 9, polarization, current, and magnetization densities, respectively, were related to the macroscopic field variables through constitutive laws. Typically, the parameters in these laws are determined from measurements. Thus, the experimentally determined relations make it unnecessary to take detailed account of how the microscopic fields are averaged.

Because the definition of the average is already implicit in our macroscopic formulation of Maxwell's equations, we must now take care that our use of macroscopic field quantities for representing electromagnetic forces is self-consistent. The

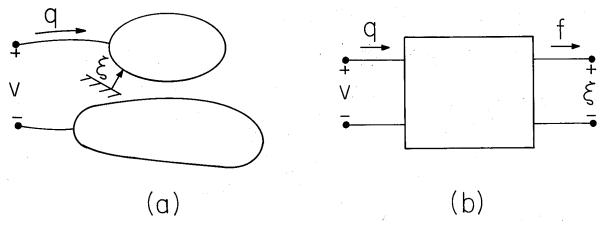


Fig. 11.6.1 (a) Electroquasistatic system having one electrical terminal pair and one mechanical degree of freedom. (b) Schematic representation of EQS subsystem with coupling to external mechanical system represented by a mechanical terminal pair.

force on a macroscopic volume element ΔV of a material is the sum of the forces on the charged particles and magnetic dipoles constituting the material. Consider the simple case in which no magnetic dipoles are present. Then

$$\mathbf{f} = \sum_i q_i \{\mathbf{E}(\mathbf{r}_i) + \mathbf{v}_i \times \mu_o \mathbf{H}(\mathbf{r}_i)\} \tag{1}$$

where the summation is over all the charges within ΔV at their respective positions. Now, the fields $\mathbf{E}(\mathbf{r}_i)$ and $\mathbf{H}(\mathbf{r}_i)$ are the *microscopic* fields that vary greatly from point $\mathbf{r}_i$ to point $\mathbf{r}_j$ in the material. The macroscopic fields $\mathbf{E}(\mathbf{r})$ and $\mathbf{H}(\mathbf{r})$ are averaged (smoothed) versions of these fields, whose sources are the averaged charge densities

$$\rho \equiv \sum_i \frac{q_i}{\Delta V} \tag{2}$$

and

$$\mathbf{J} \equiv \sum_i \frac{q_i \mathbf{v}_i}{\Delta V} \tag{3}$$

where the velocity $\mathbf{v}_i$ of the microscopic particles should be distinguished from that of the macroscopic material in which they are embedded or through which they move. The average of a product is not equal to the product of the averages. Thus, one could not find the force density $\mathbf{F} = \mathbf{f}/\Delta V$ from the expression $\rho\mathbf{E}+\mathbf{J}\times\mu_o\mathbf{H}$, as the product of the averaged charge density and averaged electric field plus averaged current density times averaged magnetic flux density. Other methods have to be used to determine the force. One of the most useful is the energy method. Given the constitutive law for the material, which represents the interrelationship between macroscopic field variables, conservation of energy provides a way of deducing the self-consistent force acting on the material.

In this and the next section, we illustrate how total forces can be determined using conservation of energy as a *premise*. In this section, the EQS systems considered have only one mechanical degree of freedom and only one electrical terminal pair. In the next section, MQS systems are considered and the approach is broadened to a somewhat more general class of systems. A parallel approach determines the force density rather than the total force. After expanding on microscopic forces in Sec. 11.8, we shall review macroscopic force densities in Sec. 11.9.

Typical of the electroquasistatic problems considered in this section is the pair of metallic electrodes shown in Fig. 11.6.1. With the application of a voltage,

unpaired charges of opposite polarity are induced on the electrode surfaces. The electrical state of the system is specified by giving the geometry and the potential difference v between the electrodes. Here we picture one electrode as movable, with its position denoted by ξ. The two terminal pair system of Fig. 11.6.1b is useful to include mechanical effects via an additional terminal pair. If we think of the net unpaired charge q on the electrode as an electrical terminal variable complementing v, then the force of electrical origin f complements the mechanical displacement ξ.

Given the electrical terminal relation $v = v(q, \xi)$, we now use an energy conservation principle to determine the force $f = f(q, \xi)$ that acts to increase the displacement ξ. The electrical terminal relation can either be regarded as a measured function or be predicted using the macroscopic field laws and constitutive laws for the materials within the "box."

It is now *assumed* that there is no conversion of electrical energy to thermal form within the box of Fig. 11.6.1b. Mechanisms for conversion of energy to heat are modeled by elements outside the box. For example, the finite conductivity of any dielectric is taken into account by a resistance external to the system. Thus, the electrical power input to what is defined as the "box," the electroquasistatic subsystem, must either result in a change in the electrical energy stored or mechanical power expended as the force f acts on the mechanical system. The integral form of the power conservation theorem, (11.1.1), is generalized to include the rate of work by the force f

$$-\oint_S \mathbf{S} \cdot d\mathbf{a} = \frac{d}{dt}\int_V W_e dv + f\frac{d\xi}{dt} \tag{4}$$

In Sec. 11.4, we represented the quasistatic net electrical power input on the left in this expression in circuit theory terms. With the total energy w_e defined as the integral of the energy density over the entire volume of the system, (4) becomes

$$v\frac{dq}{dt} = \frac{dw_e}{dt} + f\frac{d\xi}{dt} \tag{5}$$

where the electrical power input is the product $vi = vdq/dt$. Multiplication of (4) by dt converts a statement of power flow to one of energy conservation.

$$\boxed{vdq = dw_e + fd\xi} \tag{6}$$

If an increment of charge dq is placed on an electrode at potential v, an increment of energy vdq is added to the system that produces a change in the total stored energy dw_e, an increment of work $fd\xi$ done on an external mechanical system, or some combination of both. Here, $f(q, \xi)$ is the as yet unknown force. Solved for dw_e, this energy conservation statement is

$$dw_e = vdq - fd\xi \tag{7}$$

This expression describes what might be termed a quasistatic electrical and mechanical *subsystem*. The *state* of this subsystem is specified by prescribing the geometry (ξ) and the charge on the electrode, for then the voltage of the electrode follows

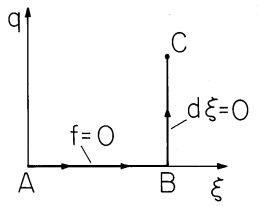


Fig. 11.6.2 Path of line integration in state space (q, ξ) used to find energy at location C.

from the terminal relation $v(q, \xi)$. The state of the subsystem is fully determined by the variables (q, ξ), which are therefore regarded as *independent variables*. In terms of the two terminal pairs shown in Fig. 11.6.1b, one of each pair of terminal variables has been chosen as an independent variable.

The incremental change in $w_e(q, \xi)$ associated with incremental changes of dq and $d\xi$ in the independent variables is

$$dw_e = \frac{\partial w_e}{\partial q} dq + \frac{\partial w_e}{\partial \xi} d\xi \tag{8}$$

Because q and ξ can be independently specified, (7) and (8) must hold for any combination of dq and dξ. For example, they must hold if the position of the electrode is held fixed so that $d\xi = 0$ and the charge is changed by the incremental amount dq. They must also describe the change in energy resulting from making an incremental displacement $d\xi$ of the electrode under open circuit conditions, where $dq = 0$. Indeed, (7) and (8) hold if q and ξ are changed by *arbitrary* incremental amounts, and so it follows that the coefficients of dq in (7) and (8) must be equal to each other, as must the coefficients of dξ.

$$\boxed{v = \frac{\partial}{\partial q} w_e(q, \xi); \qquad f = -\frac{\partial}{\partial \xi} w_e(q, \xi)} \tag{9}$$

Given the total energy, written in terms of the independent variables (q, ξ), the second of these relations provides the desired force. Integration of the energy density over the volume of the system is one way to determine w_e. Another is to integrate (7) along a line in the state space (q, ξ) designed so that the integral can be carried out without having to know f.

$$w_e(q, \xi) = \int (v dq - f d\xi) \tag{10}$$

Such a path[4] is shown in Fig. 11.6.2, where it is assumed that the force of electrical origin f is zero if the charge q is zero. Thus, in integrating along the contour $q = 0$ from $A \rightarrow B$, $dq = 0$ and $f = 0$, so there is no contribution. The remainder of the integral, from $B \rightarrow C$, is carried out with ξ fixed, so $d\xi = 0$, and (10) reduces to

[4] Note the analogy with the line integral $\int (E_x dx + E_y dy)$ of a two-dimensional conservation field that results in the potential $\phi(x, y)$.

$$\boxed{w_e = -\int_0^{\xi} f(0,\xi')d\xi' + \int_0^{q} v(q',\xi)dq' = \int_0^{q} v(q',\xi)dq'} \tag{11}$$

We have accounted for the energy required to place the subsystem in the state (q,ξ). In physical terms, the mathematical steps represent first assembling the subsystem mechanically with no electrical excitation. Because there is no force acting on the electrode as it is put in place, no work is involved. Then, with its location fixed, the electrode is charged by means of an electrical source.

Suppose that the subsystem is electrically linear, so that either as a result of mathematical modeling or of measurements on the actual system, the electrical terminal relation takes the form

$$v = \frac{q}{C(\xi)} \tag{12}$$

Then, with this relation used to evaluate (11), it follows that the energy is

$$w_e = \int_0^{q} \frac{q'}{C} dq' = \frac{1}{2}\frac{q^2}{C} \tag{13}$$

Finally, the desired force of electrical origin follows from substituting this expression into (9b).

$$f = -\frac{1}{2}q^2\frac{dC^{-1}}{d\xi} = \frac{1}{2}\left(\frac{q}{C}\right)^2\frac{dC}{d\xi} \tag{14}$$

Note that with a similar substitution into (9a), the terminal relation of (12) is obtained.

Once the partial derivative with respect to ξ has been taken while holding the proper independent variable (q) fixed, the force can be written in terms of variables other than the independent ones. Thus, with the use of the terminal relation, (12), the force is written in terms of the terminal voltage v as

$$\boxed{f = \frac{1}{2}v^2\frac{dC}{d\xi}} \tag{15}$$

The following example gives the opportunity to apply this result to a specific configuration.

Example 11.6.1. Force on a Capacitor Plate

The region between the plane parallel electrodes shown in Fig. 11.6.3 is filled by a layer of dielectric having permittivity ϵ and thickness b and an air gap ξ. The total distance between electrodes, $b+\xi$, is small compared to the linear dimensions of the plates, so fringing fields will be ignored. Thus, the electric fields E_a and E_b in the air gap and in the dielectric, respectively, are uniform. What force on the upper electrode results from applying the voltage v between the electrodes?

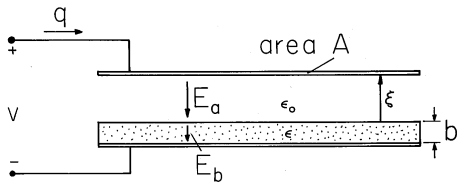


Fig. 11.6.3 Specific example of EQS systems having one electrical and one mechanical terminal pair.

First we determine the charge q on the upper electrode. To this end, the integral of $\mathbf{E}$ from the upper electrode to the lower one must be equal to the applied voltage, so

$$v = \xi E_a + bE_b \tag{16}$$

Further, there is presumably no unpaired surface charge at the interface between the dielectric layer and the air gap. Thus, Gauss' continuity condition requires that

$$\epsilon_o E_a = \epsilon E_b \tag{17}$$

Elimination of E_b between these equations gives

$$E_a = \frac{v}{\xi + b\frac{\epsilon_o}{\epsilon}} \tag{18}$$

In terms of this electric field at the surface of the upper electrode, Gauss' continuity condition shows that the total charge on the upper electrode is

$$q = D_a A = \epsilon_o E_a A \tag{19}$$

and so it follows from (18) that the electrical terminal relation can be written in terms of a capacitance C.

$$q = Cv; \qquad C \equiv \frac{\epsilon_o A}{\xi + b\frac{\epsilon_o}{\epsilon}} \tag{20}$$

Because the dielectric is described by a linear constitutive law, we have obtained an electrical terminal relation where v is a linear function of q.

The force acting on the upper electrode follows from a substitution of (20) into (15).

$$f = -\frac{1}{2}v^2 \frac{\epsilon_o A}{\left(\xi + b\frac{\epsilon_o}{\epsilon}\right)^2} \tag{21}$$

By definition, if f is positive, it acts in the direction of ξ. Here we find that regardless of the polarity of the applied voltage, f is negative. This is to be expected, because charges of one polarity on the upper electrode are attracted toward those of opposite polarity on the lower electrode.

In describing energy conversion, a minus sign can be extremely important. For example, vdq is the incremental energy *into* the electroquasistatic subsystem, while $fd\xi$ is the energy *leaving* that subsystem as the force of electrical origin acts *on* the external mechanical system. Thus, if f is positive, it acts on the mechanical system in such a direction as to increase the associated displacement.

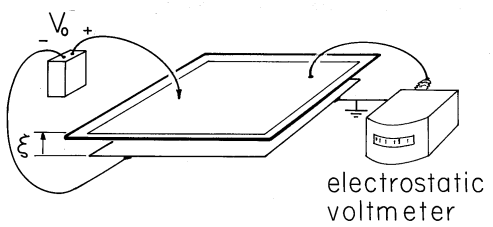


Fig. 11.6.4 Apparatus used to demonstrate amplification of voltage as the upper electrode is raised. (The electrodes are initially charged and then the voltage source is removed so q = constant.) The electrodes, consisting of foil mounted on insulating sheets, are about 1 m × 1 m, with the upper one insulated from the frame, which is used to control its position. The voltage is measured by the electrostatic voltmeter, which "loads" the system with a capacitance that is small compared to that of the electrodes and (at least on a dry day) a negligible resistance.

Rotating motors and generators are examples where the conversion of energy between electrical and mechanical form is a cyclic process. In these cases, the subsystem returns to its original state once each cycle. The energy converted per cycle is determined by integrating the energy conservation law, (6), around the closed path in the state space representing this process.

$$\oint v dq = \oint dw_e + \oint f d\xi \tag{22}$$

Because the energy stored in the system must return to its original value, there is no net contribution of the energy storage term in (22). For a cyclic process, the net electrical energy input per cycle must be equal to the net mechanical power output per cycle.

$$\oint v dq = \oint f d\xi \tag{23}$$

The following demonstration is primarily intended to give further insight into the implications of the conservation of energy principle for a cyclic process.

Demonstration 11.6.1. An Energy Conversion Cycle

The experiment shown in Fig. 11.6.4 is based on the plane parallel capacitor configuration analyzed in Example 11.6.1. The lower electrode, aluminum foil mounted on a table top, is covered by a thin sheet of plastic. The upper one is also foil, but taped to an insulating sheet which is attached to a frame. This electrode can then be manually raised and lowered to effectively control the displacement ξ.

With the letters A through D used to designate states of the system, we consider the following energy conversion cycle.

- $A \rightarrow B$. With $v = 0$, the upper electrode rests on the plastic sheet. A voltage V_o is applied.
- $B \rightarrow C$. With the voltage source removed so that the upper electrode is electrically isolated, it is raised to the position $\xi = L$.
- $C \rightarrow D$. The upper electrode is shorted, so that its voltage returns to zero.
- $D \rightarrow A$. The upper electrode is returned to its original position at $\xi = 0$.

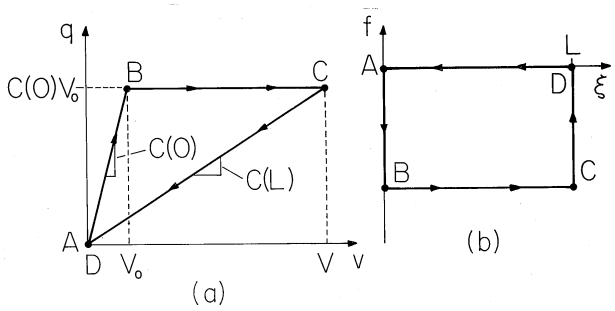


Fig. 11.6.5 Closed paths followed in cyclic conversion of energy from mechanical to electrical form: (a) in (q, v) plane; and (b) in (f, ξ) plane.

Is electrical energy converted to mechanical form, or vice versa?

The process in carrying out the closed integrals on the left-hand and right-hand sides of (23) as the cycle is carried out can be pictured in the (q, v) and (f, ξ) planes, respectively, as shown in Fig. 11.6.5. From $A \to B$, $q = C(0)v$, where $C(\xi)$ is given by (20). Thus, the trajectory in the (q, v) plane is a straight line ending at the voltage $v = V_o$ of the source. Because the upper electrode has remained at its original position, the trajectory in the (f, ξ) plane is along the $\xi = 0$ axis. The force on the electrode caused by raising its voltage to V_o follows from (21).

$$f = -\frac{1}{2}\frac{v^2 C^2}{\epsilon_o A} \Rightarrow f_B = -\frac{1}{2}\frac{[V_o C(0)]^2}{\epsilon_o A} \tag{24}$$

Now, from $B \to C$, the voltage source is removed so that as the upper electrode is raised to $\xi = L$, its charge is conserved. This means that the trajectory in the (q, v) plane is one where $q = \text{constant} = V_o C(0)$. The voltage reached by the upper electrode can be found by requiring that q be conserved.

$$V_o C(0) = V C(L) \Rightarrow V = V_o \frac{C(0)}{C(L)} \tag{25}$$

In the experiment, the thickness b of the dielectric sheet is a fraction of a millimeter, while the final elevation $\xi = L$ might be 20 cm. (If the displacement is larger than this, the fringing field comes into play and the expression for the capacitance is no longer valid.) Thus, as the sheet is raised, an original voltage of 500 V is easily amplified to 10 - 20 kV. This is readily observed by means of an electrostatic voltmeter attached to the upper electrode, as shown in Fig. 11.6.4.

To determine the trajectory $B \to C$ in the (f, ξ) plane, observe from (14) or (24) that as a function of q, the force is independent of ξ.

$$f = -\frac{1}{2}\frac{q^2}{\epsilon_o A} \tag{26}$$

The trajectory $B \to C$ in the (f, ξ) plane is therefore one of constant f_B given by (24). In general, $f(q, \xi)$ is not independent of ξ, but in plane parallel geometry, it is.

The system is now returned to its original state in two steps. First, from $C \to D$, the upper electrode remains at $\xi = L$ and is shorted to ground. In the (q, v) plane, the state returns to the origin along the straight line given by $q = C(L)v$, (20). In the (f, ξ) plane, the force drops to zero with $\xi = L$. Second, from $D \to A$,

the upper electrode is returned to its original position. The values of (q, v) remain zero, while the trajectory in the (f, ξ) plane is $f = 0$.

The experiment is simple enough so that we can use physical reasoning to decide the direction of energy conversion. Although the force of gravity is likely to exceed the electrical force of attraction between the electrodes, as far as the electrical subsystem is concerned, the upper electrode is raised against a downward electrical force. Because the charge is removed before it is lowered, there is no electrical force on the electrode as it is lowered. Thus, net work is done on the EQS subsystem. The right-hand side of (23), the net work done by the subsystem on the external mechanical system, is thus negative.

Evaluation of one or the other of the two sides of the energy conversion law, (23), provides two other ways to determine the direction of energy conversion. Consider first the electrical input energy. The integral has contributions from $A \rightarrow B$ (where the source is used to charge the upper electrode) and from $C \rightarrow D$ (where the electrode is discharged). The areas under the respective triangles representing the integral of vdq are

$$\oint vdq = \int_A^B vdq + \int_C^D vdq = \frac{1}{2}C(0)V_o^2 - \frac{1}{2}C(L)V^2 \tag{27}$$

In view of the expression for $C(\xi)$, (20), this expression can be written as

$$\oint vdq = \frac{1}{2}C(0)V_o^2\left[1 - \frac{C(0)}{C(L)}\right] = -\frac{1}{2}C(0)V_o^2\frac{L}{b}\frac{\epsilon}{\epsilon_o} \tag{28}$$

This expression is clearly negative, indicating that the net electrical energy flow is out of the electrical terminal pair. This is consistent with having a net mechanical energy input to the system.

The net mechanical output energy per cycle expressed by the right-hand side of (23) should be equal to (28). To see that this is so, we recognize that the integral consists of two possible contributions, from $B \rightarrow C$ and $D \rightarrow A$. During the latter, $f = 0$, so the magnitude of the integral is simply the area of the rectangle in Fig. 11.6.5b.

$$\oint fd\xi = -\frac{1}{2}V_o^2\frac{C^2(0)}{\epsilon_o A}L = -\frac{1}{2}C(0)V_o^2\frac{L}{b}\frac{\epsilon}{\epsilon_o} \tag{29}$$

As required by the conservation law, this mechanical energy output is negative and is equal to the net electrical input energy given by (28).

With the sequence of electrical and mechanical terminal constraints described above, there is a net conversion of energy from mechanical to electrical form. The system acts as an electrical generator with energy provided by whoever raises and lowers the upper electrode. With the voltage applied when the electrode is at its largest displacement, and the electrode grounded before it is raised, the energy flow is from the electrical voltage source to the mechanical system. In this case, the system acts as a motor. We will have the opportunity to exemplify a practical motor in the next section. Most motors are MQS rather than EQS. However, a practical EQS device that is designed to convert energy from mechanical to electrical form is the capacitor microphone, a version of which was described in Example 6.3.3.

Electrical forces have their origins in forces on unpaired charges and on dipoles. The force on the upper capacitor plate of Example 11.6.1 is due to the unpaired charges. The equal and opposite force on the combination of electrode and dielectric

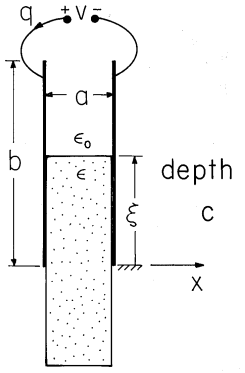


Fig. 11.6.6 Slab of dielectric partially extending between capacitor plates. The spacing, a, is much less than either b or the depth c of the system into the paper. Further, the upper surface at ξ is many spacings a away from the upper and lower edges of the capacitor plates, as is the lower surface as well.

is in part due to unpaired charges and in part to dipoles induced in the dielectric. The following exemplifies a total force that is entirely due to polarization.

Example 11.6.2. Force on a Dielectric Material

We return to the configuration of Example 11.4.1, where a dielectric slab extends a distance ξ into the region between plane parallel electrodes, as shown in Fig. 11.6.6. The capacitance was found in Example 11.4.1 to be (11.4.16).

$$C = \frac{c}{a}[\epsilon_o b + \xi(\epsilon - \epsilon_o)] \tag{30}$$

It follows from (15) that there is a force tending to draw the dielectric into the region between the electrodes.

$$f = \frac{1}{2}v^2\frac{c}{a}(\epsilon - \epsilon_o) \tag{31}$$

This force results because dipoles induced by the fringing field experience forces in the ξ direction that are passed on to the material in which they are embedded. Even though the force is due to the fringing fields, the net force does not depend on the details of that field. This is evident from our energy arguments because, at least as long as the upper edge of the slab is well within the region between the plates and the lower edge never reaches the vicinity of the electrodes, the energy storage in *the fringing fields does not change when the slab is moved.*

Further discussion of the force density responsible for the force on the dielectric will be given in Sec. 11.9. Its physical reality is demonstrated next.

Demonstration 11.6.2. Force on a Liquid Dielectric

In the experiment shown in Fig. 11.6.7, capacitor plates are dipped into a dish full of dielectric liquid. Thus, with the application of the voltage, it rises against gravity. To demonstrate the relationship between the voltage and the force, the spacing between the electrodes is a slowly varying function of radial position. With r denoting the radial distance from an axis where an extension of the electrodes would join, and α

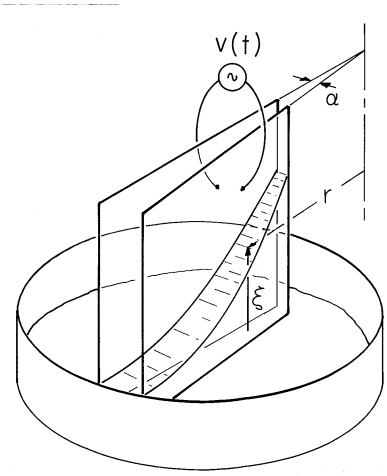


Fig. 11.6.7 In a demonstration of the polarization force, a pair of conducting transparent electrodes are dipped into a liquid (corn oil dyed with food coloring). They are closer together at the upper right than at the lower left, so when a voltage is applied, the electric field intensity decreases with increasing distance, r, from the apex. As a result, the liquid is seen to rise to a height that varies as $1/r^2$. The electrodes are about 10 cm × 10 cm, with an electric field exceeding the nominal breakdown strength of air at atmospheric pressure, 3×10^6 V/m. The experiment is therefore carried out under pressurized nitrogen.

the angle between the electrodes, the spacing at a distance r is αr. Thus, in (31), the spacing between electrodes $a \to \alpha r$ and the force per unit radial distance tending to push the liquid upward is a function of the radial position.

$$\frac{f}{c} = \frac{1}{2}\frac{v^2}{\alpha r}(\epsilon - \epsilon_o) \tag{32}$$

This force must raise a column of liquid having a height ξ and width αr. With the mass density of the liquid defined as ρ, the total mass per radial distance raised by this force is therefore $\alpha r \xi \rho$. Force equilibrium is therefore represented by setting the force per unit radial length equal to this mass multiplied by the gravitational acceleration g.

$$\frac{1}{2}\frac{v^2}{\alpha r}(\epsilon - \epsilon_o) = \alpha r \xi \rho g \tag{33}$$

This expression can be solved for $\xi(r)$.

$$\xi = \frac{1}{2}\frac{v^2(\epsilon - \epsilon_o)}{\alpha^2 \rho g}\frac{1}{r^2} \tag{34}$$

In the experiment,[5] the electrodes are constructed from tin-oxide coated glass. They are then both conducting and transparent. As a result, the height to which the liquid rises can be seen to obey (34), both as to its magnitude and its radial dependence on r.

[5] See film *Electric Fields and Moving Media* from series by National Committee for Electrical Engineering Films, Education Development Center, 39 Chapel St., Newton, Mass. 02160.

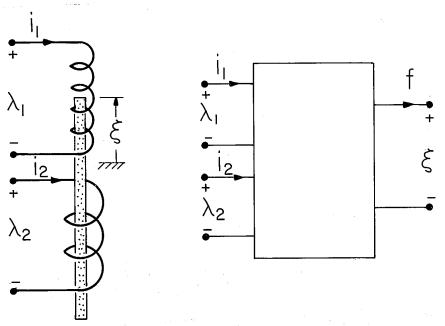


Fig. 11.7.1 (a) Magnetoquasistatic system with two electrical terminal pairs and one mechanical degree of freedom. (b) MQS subsystem representing (a).

To obtain an appreciable rise of the liquid without exceeding the field strength for electrical breakdown between the electrodes, the atmosphere over the liquid must be pressurized. Also, to avoid effects of unpaired charges injected at high field strengths by the electrodes, the applied voltage is alternating and, because the force is proportional to the square of the applied field, the height of rise is proportional to the rms value of the voltage.

11.7 MACROSCOPIC MAGNETIC FORCES

In this section, an energy principle is applied to the determination of net forces in MQS systems. With Sec. 11.6 as background, it is appropriate to include the case of multiple terminal pairs. As in Sec. 11.4, the coenergy is again found to be a convenient alternative to the energy.

The MQS system is shown schematically in Fig. 11.7.1. It has two electrical terminal pairs and one mechanical degree of freedom. The magnetoquasistatic subsystem now described by an energy principle excludes electrical dissipation and all aspects of the mechanical system, mechanical energy storage and dissipation. The energy principle then states that the input of electrical power through the electrical terminal pairs either goes into a rate of change of the stored magnetic energy or into a rate of change of the work done on the external mechanical world.

$$v_1 i_1 + v_2 i_2 = \frac{dw_m}{dt} + f\frac{d\xi}{dt} \tag{1}$$

As in Sec. 11.6, our starting point in finding the force is a postulated principle of energy conservation. Because the system is presumably MQS, in accordance with (11.3.29), the left-hand side represents the net flux of power into the system. With the addition of the last term and the inherent assumption that there is no electrical dissipation in the subsystem being described, (1) is more than the recasting of Poynting's theorem.

In an MQS system, the voltages are the time rates of change of the flux linkages. With these derivatives substituted into (1) and the expression multiplied by dt, it becomes

$$\boxed{i_1 d\lambda_1 + i_2 d\lambda_2 = dw_m + f d\xi} \tag{2}$$

This energy principle states that the increments of electrical energy put into the MQS subsystem (as increments of flux $d\lambda_1$ and $d\lambda_2$ through the terminals multiplied by their currents i_1 and i_2, respectively) either go into the total energy, which is increased by the amount dw_m, or into work on the external mechanical system, subject to the force f and experiencing a displacement $d\xi$.

With the energy principle written as in (2), the flux linkages are the independent variables. We saw in Example 11.4.2 that it is inconvenient to specify the flux linkages as functions of the currents. With the objective of casting the currents as the independent variables, we now recognize that

$$i_1 d\lambda_1 = d(i_1\lambda_1) - \lambda_1 di_1; \qquad i_2 d\lambda_2 = d(i_2\lambda_2) - \lambda_2 di_2 \tag{3}$$

and substitute into (2) to obtain

$$dw'_m = \lambda_1 di_1 + \lambda_2 di_2 + f d\xi \tag{4}$$

where the coenergy function, seen before in Sec. 11.4, is defined as

$$w'_m = i_1\lambda_1 + i_2\lambda_2 - w_m \tag{5}$$

We picture the MQS subsystem as having flux linkages λ_1 and λ_2, a force f and a total energy w_m that are specified once the currents i_1 and i_2 and the displacement ξ are stipulated. According to (4), the coenergy is a function of the independent variables i_1, i_2, and ξ, $w'_m = w'_m(i_1, i_2, \xi)$, and the change in w'_m can also be written as

$$dw'_m = \frac{\partial w'_m}{\partial i_1} di_1 + \frac{\partial w'_m}{\partial i_2} di_2 + \frac{\partial w'_m}{\partial \xi} d\xi \tag{6}$$

Because the currents and displacement are independent variables, (4) and (6) can hold only if the coefficients of like terms on the right are equal. Thus,

$$\boxed{\lambda_1 = \frac{\partial w'_m}{\partial i_1}; \qquad \lambda_2 = \frac{\partial w'_m}{\partial i_2}; \qquad f = \frac{\partial w'_m}{\partial \xi}} \tag{7}$$

The last of these three expressions is the key to finding the force f.

Reciprocity Condition. Before we find the coenergy and hence f, consider the implication of the first two expressions in (7) for the electrical terminal relations. Taking the derivative of λ_1 with respect to i_2, and of λ_2 with respect to i_1, shows that

$$\boxed{\frac{\partial \lambda_1}{\partial i_2} = \frac{\partial^2 w'_m}{\partial i_1 \partial i_2} = \frac{\partial^2 w'_m}{\partial i_2 \partial i_1} = \frac{\partial \lambda_2}{\partial i_1}} \tag{8}$$

Although this *reciprocity condition* must reflect conservation of energy for any lossless system, magnetically linear or not, consider its implications for a system described by the linear terminal relations.

$$\begin{bmatrix} \lambda_1 \\ \lambda_2 \end{bmatrix} = \begin{bmatrix} L_{11} & L_{12} \\ L_{21} & L_{22} \end{bmatrix} \begin{bmatrix} i_1 \\ i_2 \end{bmatrix} \tag{9}$$

Application of (8) shows that energy conservation requires the equality of the mutual inductances.

$$L_{12} = L_{21} \tag{10}$$

This relation has been derived in Example 11.4.2 from a related but different point of view.

Finding the Coenergy. To find w'_m, we integrate (4) along a path in the state space (i_1, i_2, ξ) arranged so that the integral can be carried out without having to know f.

$$\boxed{w'_m = \int (\lambda_1 di_1 + \lambda_2 di_2 + f d\xi)} \tag{11}$$

Thus, the first leg of the line integral is carried out on ξ with the currents equal to zero. Provided that $f = 0$ in the absence of these currents, this means that the integral of $f d\xi$ makes no contribution.

The payoff from our formulation in terms of the coenergy rather than the energy comes in being able to carry out the remaining integration using terminal relations in which the flux linkages are expressed in terms of the currents. For the linear terminal relations of (9), this line integration was illustrated in Example 11.4.2, where it was found that

$$w'_m = \frac{1}{2} L_{11} i_1^2 + L_{12} i_1 i_2 + \frac{1}{2} L_{22} i_2^2 \tag{12}$$

Evaluation of the Force. In general, the inductances in this expression are functions of ξ. Thus, the force f follows from substituting this expression into (7c).

$$\boxed{f = \frac{1}{2} i_1^2 \frac{dL_{11}}{d\xi} + i_1 i_2 \frac{dL_{12}}{d\xi} + \frac{1}{2} i_2^2 \frac{dL_{22}}{d\xi}} \tag{13}$$

Of course, this expression applies to systems having a single electrical terminal pair as a special case where $i_2 = 0$.

This generalization of the energy method to multiple electrical terminal pair systems suggests how systems with two or more mechanical degrees of freedom are treated.

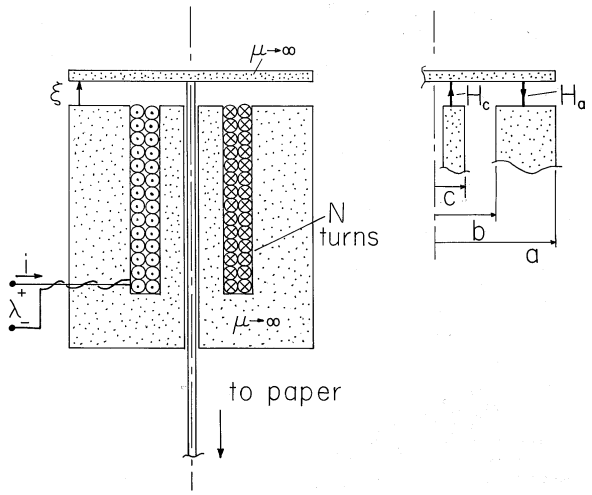


Fig. 11.7.2 Cross-section of axially symmetric transducer similar to the ones used to drive dot matrix printers.

Example 11.7.1. Driver for a Matrix Printer

A transducer that is similar to those used to drive an impact printer is shown in Fig. 11.7.2. The device, which is symmetric about the axis, might be one of seven used to drive wires in a high-speed matrix printer. The objective is to transduce a current i that drives the N-turn coil into a longitudinal displacement ξ of the permeable disk at the top. This disk is attached to one end of a wire, the other end of which is used to impact the ribbon against paper, imprinting a dot.

The objective here is to determine the force f acting on the plunger at the top. For simplicity, we make a highly idealized model in which the magnetizable material surrounding the coil and filling its core, as well as that of the movable disk, is regarded as perfectly permeable. Moreover, the air gap spacing ξ is small compared to the radial dimension a, so the magnetic field intensity is approximated as uniform in the air gap. The wire is so fine that the magnetizable material removed to provide clearance for the wire can be disregarded.

With H_a and H_c defined as shown by the inset to Fig. 11.7.2, Ampère's integral law is applied to a contour passing upward through the center of the core, across the air gap at the center, radially outward in the disk, and then downward across the air gap and through the outer part of the stator to encircle the winding in the infinitely permeable material.

$$H_a\xi + H_c\xi = Ni \tag{14}$$

A second relation between H_a and H_c follows from requiring that the net flux out of the disk must be zero.

$$\mu_o H_a \pi(a^2 - b^2) = \mu_o H_c \pi c^2 \tag{15}$$

Using this last expression to replace H_c in (14) results in

$$H_c = \frac{Ni}{\xi\left(1 + \frac{c^2}{a^2 - b^2}\right)} \tag{16}$$

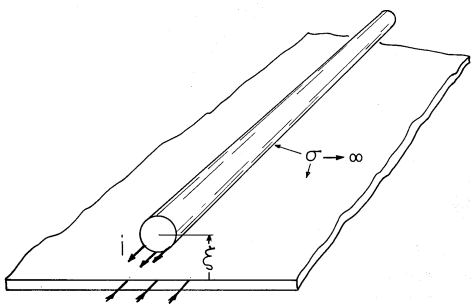


Fig. 11.7.3 Cross-section of perfectly conducting current-carrying wire over a perfectly conducting ground plane.

The magnetic flux linking every turn in the coil is $\mu_o H_c \pi c^2$. Thus, the total flux linked by the coil is

$$\lambda = Li; \qquad L = \frac{\mu_o N^2 \pi c^2}{\xi\left(1 + \frac{c^2}{a^2 - b^2}\right)} \tag{17}$$

Finally, the force follows from an evaluation of (13) (specialized to the single terminal pair system of this example).

$$f = \frac{1}{2} i^2 \frac{dL}{d\xi} = -\frac{1}{2} i^2 \frac{\mu_o N^2 \pi c^2}{\xi^2\left(1 + \frac{c^2}{a^2 - b^2}\right)} \tag{18}$$

As might have been expected by one who has observed magnetizable materials pulled into a magnetic field, the force is negative. Given the definition of ξ in Fig. 11.7.2, the application of a current will tend to close the air gap. To write a dot, the current is applied. To provide for a return of the plunger to its original position when the current is removed, a spring is inserted in the air gap.

In the magnetic transducer of the previous example, the force on the driver disk is due to magnetization. The next example illustrates the force associated with the current density.

Example 11.7.2. Force on a Wire over a Perfectly Conducting Plane

The cross-section of a perfectly conducting wire with its center a distance ξ above a perfectly conducting ground plane is shown in Fig. 11.7.3. The configuration is familiar from Demonstration 8.6.1. The current carried by the wire is returned in the ground plane. The distribution of this current on the surfaces of the wire and ground plane is consistent with the requirement that there be no flux density normal to the perfectly conducting surfaces. What is the force per unit length f acting on the wire?

The inductance per unit length is half of that for a pair of conductors having the center-to-center spacing 2ξ. Thus, it is half of that given by (8.6.12).

$$L = \frac{\mu_o}{2\pi} ln\left[\frac{\xi}{R} + \sqrt{\left(\frac{\xi}{R}\right)^2 - 1}\right] \tag{19}$$

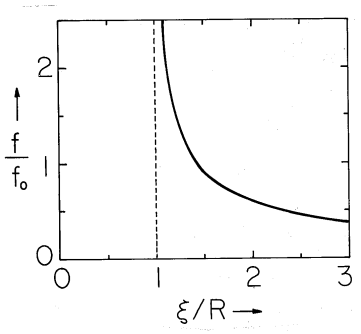


Fig. 11.7.4 The force tending to levitate the wire of Fig. 11.7.3 as a function of the distance to the ground plane normalized to the radius R of wire.

The force per unit length in the ξ direction then follows from an evaluation of (13) (again adapted to the single terminal pair situation).

$$f = \frac{1}{2} i^2 \frac{dL}{d\xi} = f_o \frac{1}{\sqrt{(\xi/R)^2 - 1}}; \qquad f_o = \frac{\mu_o i^2}{4\pi R} \tag{20}$$

The dependence of this force on the elevation above the ground plane is shown in Fig. 11.7.4. In the limit where the elevation is large compared to the radius of the conductor, (20) becomes

$$f \to \frac{1}{4} \frac{\mu_o i^2}{\pi \xi} \tag{21}$$

In Sec. 11.8, we will identify the force density acting on materials carrying a current density $\mathbf{J}$ as being $\mathbf{J} \times \mu_o \mathbf{H}$. Note that the upward force predicted by (20) is indeed consistent with the direction of this force density.

The force on a thin wire, (21), can be derived from this force density by recognizing that the contribution of the self-field of the wire to the total force per unit length is zero. Thus, the force per unit length can be computed using for $\mathbf{B}$ the flux density caused by the image current a distance 2ξ away. The flux density due to this image current has a magnitude that follows from Ampère's integral law as $\mu_o i/2\pi(2\xi)$. This field is essentially uniform over the cross-section of the wire, so the integral of the force density $\mathbf{J} \times \mathbf{B}$ over the cross-section of the wire amounts to an integration of the current density $\mathbf{J}$ over the cross-section. The latter is the total current i, and so we are led to a force per unit length of magnitude $\mu_o i^2/2\pi(2\xi)$, which is in agreement with (21).

The following is a demonstration of the force on current-carrying conductors exemplified previously. It also provides a dramatic demonstration of the existence of induced currents.

Demonstration 11.7.1. Steady State Magnetic Levitation

In the experiment shown in Fig. 11.7.5, the current-carrying wire of the previous example has been wound into a pancake shaped coil that is driven by about 20 amps of 60 Hz current. The conductor beneath is an aluminum sheet of 1.3 cm thickness. Even at 60 Hz, this conductor tends to act as a perfect conductor. This follows from

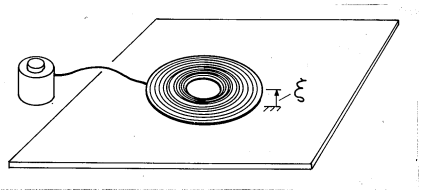


Fig. 11.7.5 When the pancake coil is driven by an ac current, it floats above the aluminum plate. In this experiment, the coil consists of 250 turns of No. 10 copper wire with an outer radius of 16 cm and an inner one of 2.5 cm. The aluminum sheet has a thickness of 1.3 cm. With a 60 Hz current i of about 20 amp rms, the height above the plate is 2 cm.

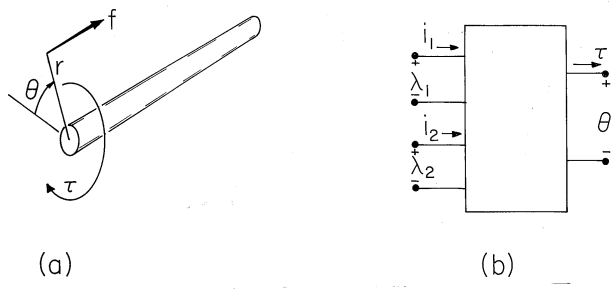


Fig. 11.7.6 (a) The force f, acting through a lever-arm of length r, produces a torque $\tau = rf$. (b) Mechanical terminal pair representing a rotational degree of freedom.

an evaluation of the product of the angular frequency ω and the time constant τ_m estimated in Sec. 10.2. From (10.2.17), $\omega\tau_m = \omega\mu_o\sigma\Delta a \approx 20$, where the average radius is $a = 9$ cm, Δ is the sheet thickness and the sheet conductivity is given by Table 7.1.1.

The time average force, of the type described in Example 11.7.2, is sufficiently large to levitate the coil. As the current is increased, its height above the aluminum sheet increases, as would be expected from the dependence of the force on the height for a single wire, Fig. 11.7.4.

The Torque of Electrical Origin. In some of the most important transducers, the mechanical response takes the form of a rotation rather than a translation. The shaft shown in Fig. 11.7.6a might be attached to the rotor of a motor or generator. A force f acting through a lever arm of length r that rotates the shaft through an incremental angle $d\theta$ causes a displacement $d\xi = rd\theta$. Thus, the incremental work done on the mechanical system $fd\xi$ becomes

$$fd\xi \rightarrow \tau d\theta \tag{22}$$

where τ is defined as the *torque*.

If the two terminal pair MQS system of Fig. 11.7.1 had a rotational rather than a displacement degree of freedom, the representation would be the same as has been outlined, except that $f \rightarrow \tau$ and $\xi \rightarrow \theta$. The mechanical terminal pair is now represented as in Fig. 11.7.6b.

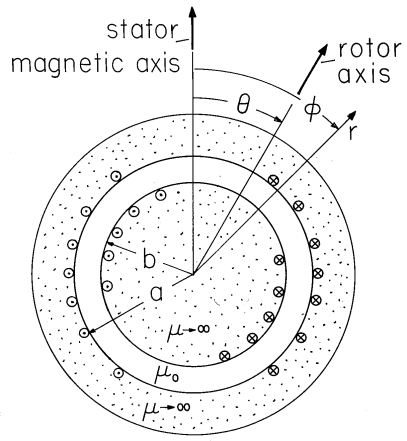


Fig. 11.7.7 Cross-section of rotating machine.

The torque follows from (13) as

$$\tau = \frac{1}{2} i_1^2 \frac{dL_{11}}{d\theta} + i_1 i_2 \frac{dL_{12}}{d\theta} + \frac{1}{2} i_2^2 \frac{dL_{22}}{d\theta} \tag{23}$$

Among the types of magnetic rotating motors and generators that could be used to exemplify the torque of (23), we now choose a synchronous machine. Although other types of motors are more common, it is a near certainty that if these words are being read with the aid of electrical illumination, the electricity used is being generated by means of a synchronous generator.

Example 11.7.3. A Synchronous Machine

The cross-section of a stator and rotor modeling a rotating machine is shown in Fig. 11.7.7. The rotor consists of a highly permeable circular cylindrical material mounted on a shaft so that it can undergo a rotation measured by the angle θ. Surrounding this rotor is a stator, composed of a highly permeable material. In slots, on the inner surface of the stator and on the outer surface of the rotor, respectively, are windings with sinusoidally varying turn densities. These windings, driven by the currents i_1 and i_2, respectively, give rise to current distributions that might be modeled by surface current densities

$$K_z = i_1 N_s \sin\phi \quad \text{at} \quad r = a \tag{24}$$

$$K_z = i_2 N_r \sin(\phi - \theta) \quad \text{at} \quad r = b \tag{25}$$

where N_s and N_r are constants descriptive of the windings. Thus, the current distribution shown on the stator in Fig. 11.7.7 is fixed and gives rise to a magnetic field having the fixed vertical axis shown in the figure. The rotor coil gives rise to a similar field except that its axis is at the angle θ of the rotor. The rotor magnetic axis, also shown in Fig. 11.7.7, therefore rotates with the rotor.

Electrical Terminal Relations. With the rotor and stator materials taken as infinitely permeable, the air gap fields are determined by using (24) and (25) to

write boundary conditions on the tangential **H** and then solving Laplace's equation for the air gap magnetic fields (Secs. 9.6 and 9.7). The flux linked by the respective coils is then of the form

$$\begin{aligned}\begin{bmatrix}\lambda_1\\ \lambda_2\end{bmatrix} &= \begin{bmatrix}L_{11} & L_{12}(\theta)\\ L_{12}(\theta) & L_{22}\end{bmatrix}\begin{bmatrix}i_1\\ i_2\end{bmatrix}\\ &= \begin{bmatrix}L_s & M\cos\theta\\ M\cos\theta & L_r\end{bmatrix}\begin{bmatrix}i_1\\ i_2\end{bmatrix}\end{aligned} \tag{26}$$

where the *self-inductances* L_s and L_r and peak *mutual inductance* M are constants.

The dependence of the inductance matrix on the angle of the rotor, θ, can be reasoned physically. The rotor is modeled as a smooth circular cylinder, so in the absence of a rotor current i_2, there can be no effect of the rotor angle θ on the flux linked by the stator winding. Hence, the stator self-inductance is independent of θ. Similar reasoning shows that the rotor self-inductance must be independent of rotor angle θ. The θ dependence of the mutual inductance is plausible because the flux λ_1 linked by the stator, due to the current in the rotor, must peak when the magnetic axes of the coils are aligned ($\theta = 0$) and must be zero when they are perpendicular ($\theta = 90$ degrees).

Torque Evaluation. The magnetic torque on the rotor follows directly from using (26) to evaluate (23).

$$\tau = i_1 i_2 \frac{d}{d\theta} M\cos\theta = -i_1 i_2 M\sin\theta \tag{27}$$

This torque depends on the currents and θ in such a way that the magnetic axis of the rotor tends to align with that of the stator. With $\theta = 0$, the axes are aligned and there is no torque. If θ is slightly positive and the currents are both positive, the torque is negative. This is as would be expected with the magnetic axis of the stator vertical and that of the rotor in the first quadrant (as in Fig. 11.7.7).

Synchronous Operation. In the synchronous mode of operation, the stator current is constrained to be sinusoidal while that on the rotor is a constant. To avoid having to describe the mechanical system, we will assume that the shaft is attached to a mechanical load that makes the angular velocity Ω constant. Thus, the electrical and mechanical terminals are constrained so that

$$\begin{aligned} i_1 &= I_1\cos\omega t\\ i_2 &= I_2\\ \theta &= \Omega t - \gamma\end{aligned} \tag{28}$$

Under what circumstances can we derive a time average torque on the shaft, and hence a net conversion of energy with each rotation?

With the constraints of (28), the torque follows from (27) as

$$\tau = -I_1 I_2 M\cos\omega t\sin(\Omega t - \gamma) \tag{29}$$

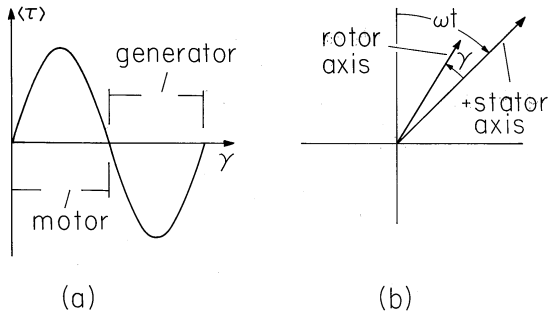


Fig. 11.7.8 (a) Time average torque as a function of angle γ. (b) The rotor magnetic axis lags the clockwise rotating component of the stator magnetic field axis by the angle γ.

A trigonometric identity[6] makes the implications of this result more apparent.

$$\tau = -\frac{I_1 I_2 M}{2}\Big\{\sin[(\omega+\Omega)t-\gamma]+\sin[-(\omega-\Omega)t-\gamma]\Big\} \tag{30}$$

There is no time average value of either of these sinusoidal functions of time unless one or the other of the frequencies, $(\omega+\Omega)$ and $(\omega-\Omega)$, is zero. For example, with the rotation frequency equal to that of the excitation,

$$\omega = \Omega \tag{31}$$

the time average torque is

$$\langle\tau\rangle = \frac{I_1 I_2 M}{2}\sin\gamma \tag{32}$$

The dependence of the time average torque on the phase angle γ is shown in Fig. 11.7.8a. With γ between 0 and 180 degrees, there is a positive time average torque acting on the external mechanical system in the direction of rotation Ω. In this range, the machine acts as a *motor* to convert energy from electrical to mechanical form. In the range of γ from 180 degrees to 360 degrees, energy is converted from mechanical to electrical form and operation is as a generator.

Stator Field Analyzed into Traveling Waves. From (30), it is clear that a time-average torque results from either a forward ($\Omega = \omega$) or a backward ($\Omega = -\omega$) rotation. This suggests that the field produced by the stator winding is the superposition of fields having magnetic axes rotating in the clockwise and counterclockwise directions. Formally, this can be seen by rewriting the stator surface current density, (24), using the electrical and mechanical constraints of (28). With the use once again of the double-angle trigonometric identity, the distribution of surface current density is separated into two parts.

$$K_z = N_s I_1 \cos\omega t \sin\phi = \frac{N_s I_1}{2}[\sin(\phi+\omega t)+\sin(\phi-\omega t)] \tag{33}$$

[6] $\sin(x)\cos(y) = \frac{1}{2}(\sin(x+y)+\sin(x-y))$

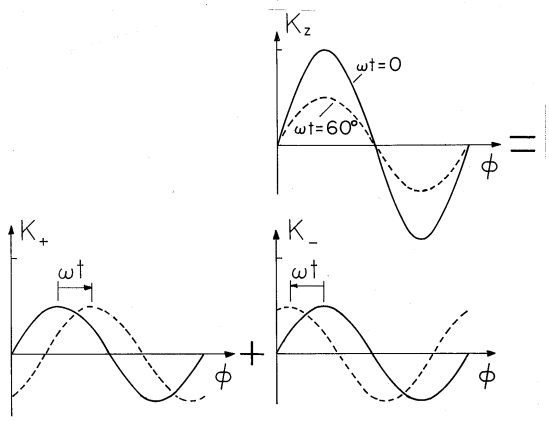


Fig. 11.7.9 With the sinusoidally distributed stator current excited by a current that varies sinusoidally with time, the surface current is a standing wave which can be analyzed into the sum of oppositely propagating traveling waves.

The sinusoidal excitation produces a standing-wave surface current with nodes at $\theta = 0$ and 180 degrees. This is the first distribution in Fig. 11.7.9. Analyzed as it is on the right in (33), and pictured in Fig. 11.7.9, it is the sum of two countertraveling waves. The magnetic axis of the wave traveling to the right is at $\phi = \omega t$.

We now have the following picture of the synchronous operation found to give rise to the time average torque. The field of the stator is composed of rotating parts, one with a magnetic axis that rotates in a clockwise direction at angular velocity ω, and the other rotating in the opposite direction. The frequency condition of (31) therefore represents a synchronous condition in which the "forward" component of the stator field and the magnetic axis of the rotor rotate at the same angular velocity.

In view of the definition of γ given in (28), if γ is positive, the rotor magnetic axis lags the stator axis by the angle γ, as shown in Fig. 11.7.8. When the machine operates as a motor, the forward component of the stator magnetic field "pulls" the rotor along. When the device operates as a generator, γ is negative and the rotor magnetic axis leads that of the forward component of the stator field. For generator operation, the rotor magnetic axis "pulls" the forward component of the stator field.

11.8 FORCES ON MICROSCOPIC ELECTRIC AND MAGNETIC DIPOLES

The energy principle was used in the preceding sections to derive the macroscopic forces on polarizable and magnetizable materials. The same principle can also be applied to derive the force distributions, the force densities. For this purpose, one needs more than a purely electromagnetic description of the system. In order to develop the simple model for the force density distribution, we need the expression for the force on an electric dipole for polarizable media, and on a magnetic dipole for magnetizable media. The force on an electric dipole will be derived simply from the Lorentz force law. We have not stated a corresponding force law for magnetic charges. Even though these are not found in nature as isolated charges but only

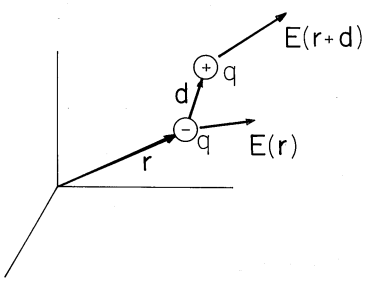


Fig. 11.8.1 An electric dipole experiences a net electric force if the positive charge q is subject to an electric field $\mathbf{E}(\mathbf{r}+\mathbf{d})$ that differs from $\mathbf{E}(\mathbf{r})$ acting on the negative charge q.

as dipoles, it is nevertheless convenient to state such a law. This will be done by showing how the electric force law follows from the energy principle. By analogy a corresponding law on magnetic charges will be derived from which the force on a magnetic dipole will follow.

Force on an Electric Dipole. The force on a stationary electric charge is given by the Lorentz law with $\mathbf{v} = 0$.

$$\mathbf{f} = q\mathbf{E} \tag{1}$$

A dipole is the limit of two charges of equal magnitude and opposite sign spaced a distance $\mathbf{d}$ apart, in the limit

$$\lim_{\substack{q\to\infty \\ |d|\to 0}} (q\mathbf{d}) = \mathbf{p}$$

with $\mathbf{p}$ being finite. Charges q of opposite polarity, separated by the vector distance $\mathbf{d}$, are shown in Fig. 11.8.1. The total force on the dipole is the sum of the forces on the individual charges.

$$\mathbf{f} = q[\mathbf{E}(\mathbf{r}+\mathbf{d}) - \mathbf{E}(\mathbf{r})] \tag{2}$$

Unless the electric field at the location $\mathbf{r}+\mathbf{d}$ of the positive charge differs from that at the location $\mathbf{r}$ of the negative charge, the separate contributions cancel.

In order to develop an expression for the force on the dipole in the limit where the spacing $\mathbf{d}$ of the charges is small compared to distances over which the field varies appreciably, (2) is written in Cartesian coordinates and the field at the positive charge expanded about the position of the negative charge. Thus, the x component is

$$\begin{aligned} f_x &= q[E_x(x+d_x,\ y+d_y,\ z+d_z) - E_x(x,y,z)] \\ &= q\left[E_x(x,y,z) + d_x\frac{\partial E_x}{\partial x} + d_y\frac{\partial E_x}{\partial y} + d_z\frac{\partial E_x}{\partial z}\right. \\ &\quad \left. + \ldots - E_x(x,y,z)\right] \end{aligned} \tag{3}$$

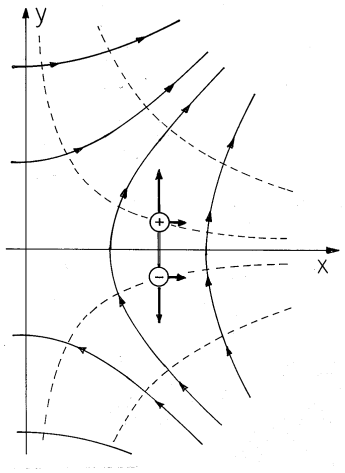


Fig. 11.8.2 Dipole having y direction and positioned on the x axis in field of (6) experiences force in the x direction.

The first and last terms cancel. In more compact notation, this expression is therefore

$$f_x = \mathbf{p} \cdot \nabla E_x \tag{4}$$

where we have identified the dipole moment $\mathbf{p} \equiv q\mathbf{d}$. The other force components follow in a similar fashion, with y and z playing the role of x. The three components are then summarized in the vector expression

$$\boxed{\mathbf{f} = \mathbf{p} \cdot \nabla \mathbf{E}} \tag{5}$$

The derivation provides an explanation of how $\mathbf{p}\cdot\nabla\mathbf{E}$ is evaluated in Cartesian coordinates. The i-th component of (5) is obtained by dotting $\mathbf{p}$ with the gradient of the i-th component of $\mathbf{E}$.

Illustration. Force on a Dipole

Suppose that a dipole finds itself in the field

$$\Phi = -V_o \frac{xy}{a^2}; \qquad \mathbf{E} = -\nabla\Phi = \frac{V_o}{a^2}(y\mathbf{i_x} + x\mathbf{i_y}) \tag{6}$$

which is familiar from Example 4.1.1. It follows from (5) that the force is

$$\mathbf{f} = \frac{V_o}{a^2}(p_y\mathbf{i_x} + p_x\mathbf{i_y}) \tag{7}$$

According to this expression, the y-directed dipole on the x axis in Fig. 11.8.2 experiences a force in the x direction. The y-directed force is zero because E_y is the same at the respective locations of the charges. The x-directed force exists because E_x goes from being positive just above the x axis to negative just below. Thus, the x-directed contributions to the force of each of the charges is in the same direction.

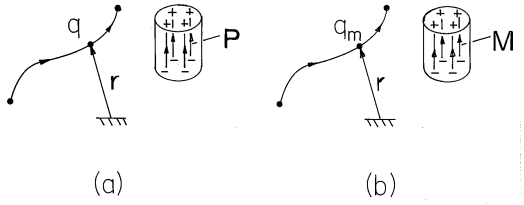


Fig. 11.8.3 (a) Electric charge brought into field created by permanent polarization. (b) Analogous magnetic charge brought into field of permanent magnet.

Force on Electric Charge Derived from Energy Principle. The force on an electric charge is stated in the Lorentz law. This law is also an ingredient in Poynting's theorem, and in the identification of energy and power flow. Indeed, $\mathbf{E} \cdot \mathbf{J}_u$ was recognized from the Lorentz law as the power density imparted to the current density of unpaired charge. The energy principle can be used to derive the force law on a microscopic charge "in reverse". This seems to be the hard way to obtain the Lorentz law of force on a stationary charge. Yet we go through the derivation for three reasons.

(a) The derivation of force from the EQS energy principle is shown to be consistent with the Lorentz force on a stationary charge.
(b) The derivation shows that the field can be produced by permanently polarized material objects, and yet the energy principle can be employed in a straightforward manner.
(c) The same principle can be applied to derive the microscopic MQS force on a magnetic charge.

Let us consider an EQS field produced by charge distributions and permanent polarizations $\mathbf{P}_p$ in free space as sketched in Fig. 11.8.3a. By analogy, we will then have found the force on a magnetic charge in the field of a permanent magnet, Fig. 11.8.3b. The Poynting theorem identifies the rate of energy imparted to the polarization per unit volume as

$$\frac{\text{rate of change of energy}}{\text{volume}} = \mathbf{E} \cdot \frac{\partial}{\partial t}\epsilon_o \mathbf{E} + \mathbf{E} \cdot \frac{\partial \mathbf{P}_p}{\partial t} \tag{8}$$

Because $\mathbf{P}_p$ is a permanent polarization, $\partial \mathbf{P}_p / \partial t = 0$, and the permanent polarization does not contribute to the change in energy associated with introducing a point charge. Hence, as charge is brought into the vicinity of the permanent polarization, the change of energy density is

$$\delta W_e = \mathbf{E} \cdot \delta(\epsilon_o \mathbf{E}) \tag{9}$$

where δ stands for the differential change of $\epsilon_o \mathbf{E}$. The change of energy is

$$\delta w_e = \int_V dv \mathbf{E} \cdot \delta(\epsilon_o \mathbf{E}) \tag{10}$$

where V includes all of space. The electroquasistatic E field is the negative gradient of the potential

$$\mathbf{E} = -\nabla \Phi \tag{11}$$

Introducing this into (10), one has

$$\delta w_e = -\int_V dv \nabla\Phi \cdot \delta(\epsilon_o \mathbf{E}) = -\int_V dv \nabla \cdot [\Phi \delta(\epsilon_o \mathbf{E})] + \int_V dv \Phi \nabla \cdot (\delta \epsilon_o \mathbf{E}) \tag{12}$$

where we have "integrated by parts," using an identity.[7] The first integral can be written as an integral over the surface enclosing the volume V. Since V is all of space, the surface is at infinity. Because $\mathbf{E}\Phi$ vanishes at infinity at least as fast as $1/r^3$ ($1/r^2$ for E, $1/r$ for Φ, where r is the distance from the origin of a coordinate system mounted within the electroquasistatic structure), the surface integral vanishes. Now

$$\nabla \cdot \delta(\epsilon_o \mathbf{E}) = \delta\rho_u \tag{13}$$

from Gauss' law, where $\delta\rho_u$ is the change of unpaired charge. Thus, from (12),

$$\delta w_e = \int_V \Phi \delta\rho_u dv \tag{14}$$

so the change of energy is equal to the charge increment $\delta\rho_u dv$ introduced at $\mathbf{r}$ times the potential Φ at $\mathbf{r}$, summed over all the charges.

Suppose that one introduces only a small test charge q, so that $\rho_u dv = q$ at point $\mathbf{r}$. Then

$$\delta w_e(\mathbf{r}) = q\Phi(\mathbf{r}) \tag{15}$$

The change of energy is the potential Φ at the point at which the charge is introduced times the charge. This form of the energy interprets the potential of an EQS field as the work to be done in bringing a charge from infinity to the point of interest.

If the charge is introduced at $\mathbf{r}+\Delta\mathbf{r}$, then the change in total energy associated with introducing that charge is

$$\delta w_e(\mathbf{r} + \Delta\mathbf{r}) = q[\Phi(\mathbf{r}) + \Delta\mathbf{r} \cdot \nabla\Phi(\mathbf{r})] \tag{16}$$

Introduction of a charge q at $\mathbf{r}$, subsequent removal of the charge, and introduction of the charge at $\mathbf{r} + \Delta\mathbf{r}$ is equivalent to the displacement of the charge from $\mathbf{r}$ to $\mathbf{r} + \Delta\mathbf{r}$. If there is a net energy decrease, then work must have been done by the force $\mathbf{f}$ exerted by the field on the charge. The work done by the field on the charge is

$$-[\delta w_e(\mathbf{r} + \Delta\mathbf{r}) - \delta w_e(\mathbf{r})] = -q\Delta\mathbf{r} \cdot \nabla\Phi(\mathbf{r}) = \Delta\mathbf{r} \cdot \mathbf{f} \tag{17}$$

and therefore

$$\mathbf{f} = -q\nabla\Phi = q\mathbf{E} \tag{18}$$

Thus, the Lorentz law for a stationary charge is implied by the EQS laws.

Before we attack the problem of force on a magnetic charge, we explore some features of the electroquasistatic case. In (17), q is a small test charge. Electric test

[7] $(\nabla\psi) \cdot \mathbf{A} = \nabla \cdot (\mathbf{A}\psi) - (\nabla \cdot \mathbf{A})\psi$

charges are available as electrons. But suppose that in analogy with the magnetic case, no free electric charge was available. Then one could still produce a test charge by the following artifice. One could polarize a very long-thin rod of cross-section a, with a uniform polarization density $\mathbf{P}$ along the axis of the rod (Sec. 6.1). At one end of the rod, there would be a polarization charge $q = Pa$, at the other end there would be a charge of equal magnitude and opposite sign. If the rod were of very long length, while the end with positive charge could be used as the "test charge," the end of opposite charge would be outside the field and experience no force. Here the charge representing the polarization of the rod has been treated as unpaired.

We are now ready to derive the force on a magnetic charge.

Force on a Magnetic Charge and Magnetic Dipole. The attraction of a magnetizable particle to a magnet is the result of the force exerted by a magnetic field on a magnetic dipole. Even in this case, because the particle is macroscopic, the force is actually the sum of forces acting on the microscopic atomic constituents of the material. As pointed out in Secs. 9.0 and 9.4, the magnetization characteristics of macroscopic media such as the iron particle relate back to the magnetic moment of molecules, atoms, and even individual electrons. Given that a particle has a magnetic moment $\mathbf{m}$ as defined in Sec. 8.2, what is the force on the particle in a magnetic field intensity $\mathbf{H}$? The particle can be comprised of a macroscopic material such as a piece of iron. However, to distinguish between forces on macroscopic media and microscopic particles, we should consider here that the force is on an elementary particle, such as an atom or electron.

We have shown how one derives the force on an electric charge in an electric field from the energy principle. The electric field could have been produced by permanently polarized dielectric bodies. In analogy, one could produce a magnetic field by permanently magnetized magnetic bodies. In the EQS case, the test charge could have been produced by a long, uniformly and permanently polarized cylindrical rod. In the magnetic case, an "isolated" magnetic charge could be produced by a long, uniformly and permanently magnetized rod of cross-sectional area a. If the magnetization density is $\mathbf{M}$, then the analogy is

$$\nabla \cdot \mathbf{P} \leftrightarrow \nabla \cdot \mu_o \mathbf{M}, \qquad \Phi \leftrightarrow \Psi, \qquad q\mathbf{E} \leftrightarrow q_m \mathbf{H} \tag{19}$$

where, for the uniformly magnetized rod, and the magnetic charge

$$q_m = \mu_o M a \tag{20}$$

is located at one end of the rod, the charge $-q_m$ at the other end of the rod (Example 9.3.1). The force on a magnetic charge is thus, in analogy with (18),

$$\boxed{\mathbf{f} = q_m \mathbf{H}} \tag{21}$$

which is the extension of the Lorentz force law for a stationary electric charge to the magnetic case. Of course, the force on a dipole is, in analogy to (5) (see Fig. 11.8.4),

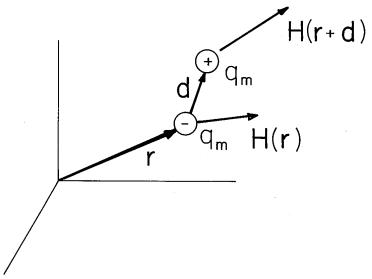


Fig. 11.8.4 Magnetic dipole consisting of positive and negative magnetic charges q_m.

$$\boxed{\mathbf{f} = q_m \mathbf{d} \cdot \mathbf{H} = \mu_o \mathbf{m} \cdot \nabla \mathbf{H}} \tag{22}$$

where $\mathbf{m}$ is the magnetic dipole moment.

We have seen in Example 8.3.2 that a magnetic dipole of moment $\mathbf{m}$ can be made up of a circulating current loop with magnitude $m = ia$, where i is the current and a the area of the loop. Thus, the force on a current loop could also be evaluated from the Lorentz law for electric currents as

$$\mathbf{f} = i \int d\mathbf{s} \times \mu_o \mathbf{H} \tag{23}$$

with i the total current in the loop. Use of vector identities indeed yields (22) in the MQS case. Thus, this could be an alternate way of deriving the force on a magnetic dipole. We prefer to derive the law independently via a Lorentz force law for stationary magnetic charges, because an important dispute on the validity of the magnetic dipole model rested on the correct interpretation of the force law[1–3]. While the details of the dispute are beyond the scope of this textbook, some of the issues raised are fundamental and may be of interest to the reader who wants to explore how macroscopic formulations of the electrodynamics of moving media based on magnetization represented by magnetic charge (Chap. 9) or by circulating currents are reconciled.

The analogy between the polarization and magnetization was emphasized by Prof. L. J. Chu[2], who taught the introductory electrical engineering course in electromagnetism at MIT in the fifties. He derived the force law for moving magnetic charges, of which (21) is the special case for a stationary charge. His approach was soon criticized by Tellegen[3], who pointed out that the accepted model of magnetization is that of current loops being the cause of magnetization. While this in itself would not render the magnetic charge model invalid, Tellegen pointed out that the force computed from (23) in a dynamic field does not lead to (22), but to

$$\mathbf{f} = \mu_o \mathbf{m} \cdot \nabla \mathbf{H} - \mu_o \epsilon_o \mathbf{m} \times \frac{\partial \mathbf{E}}{\partial t} \tag{24}$$

Because the force is different depending upon whether one uses the magnetic charge model or the circulating current model for the magnetic dipole, so his reasoning went, and because the circulating current model is the physically correct one, the

magnetic charge model is incorrect. The issue was finally settled[4] when it was shown that the force (24) as computed by Tellegen was incorrect. Equation (23) assumes that i could be described as constant around the current loop and pulled out from under the integral. However, in a time-varying electric field, the charges induced in the loop cause a current whose contribution precisely cancels the second term in (24). Thus, both models lead to the same force on a magnetic dipole and it is legitimate to use either model. The magnetic model has the advantage that a stationary dipole contains no "moving parts," while the current model does contain moving charges. Hence the circulating current formalism is by necessity more complicated and more likely to lead to error.

Comparison of Coulomb's Force on an Electron to the Force on its Magnetic Dipole. Why is it possible to accurately describe the motions of an electron in vacuum by the Lorentz force law without including the magnetic force associated with its dipole moment? The answer is that the magnetic dipole effect on the electron is relatively small. To obtain an estimate of the magnitude of the magnetic dipole effect, we compare the forces produced by a typical (but large) electric field achievable without electrical breakdown in air on the charge e of the electron, and by a typical (but large) magnetic field gradient acting on the magnetic dipole moment of the electron. Taking for $\mathbf{E}$ the value 10^6 V/m, with $e \approx 1.6 \times 10^{-19}$ coulomb,

$$f_e = eE \approx 1.6 \times 10^{-13} N \tag{25}$$

A $\mathbf{B}$ of 1 tesla (10,000 gauss) is a typical large flux density produced by an iron core electromagnet. Let us assume that a flux density variation of this order can be produced over a distance of 1 cm, which is, in practice, a rather high gradient. Yet taking this value and a moment of one Bohr magneton (9.0.1), we obtain from (22) for the force on the electron

$$f_m = 1.8 \times 10^{-25} N \tag{26}$$

Note that the electric force associated with the net charge is much greater than the magnetic one due to the magnetic dipole moment. Because of the large ratio f_e/f_m for fields of realistic magnitudes, experiments designed to detect magnetic dipole effects on fundamental particles did not utilize particles having a net charge, but rather used neutral atoms (most notably, the Stern-Gerlach experiment[8]). Indeed, a stray electric field on the order of 10^{-6} V/m would deflect an electron as strongly as a magnetic field gradient of the very large magnitude assumed in calculating (26).

The small magnetic dipole moment of the electron can become very important in solid matter because macroscopic solids are largely neutral. Hence, the forces exerted upon the positive and negative charges within matter by an applied electric field more or less cancel. In such a case, the forces on the electronic magnetic dipoles in an applied magnetic field can dominate and give rise to the significant macroscopic force observed when an iron filing is picked up by a magnet.

[8] W. Gerlach and O. Stern, "Uber die Richtungsquantelung im Magnetfeld," *Ann. d. Physik*, 4th series, Vol. 74, (1924), pp. 673-699.

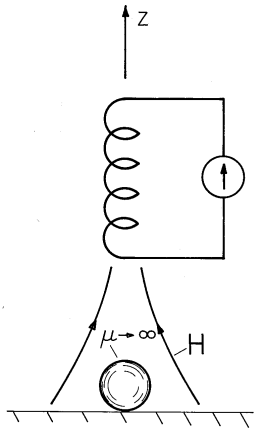


Fig. 11.8.5 By dint of its field gradient, a magnet can be used to pick up a spherical magnetizable particle.

Example 11.8.1. Magnetization Force on a Macroscopic Particle

Suppose that we wanted to know the force exerted on an iron particle by a magnet. Could the microscopic force, (22), be used? The energy method derivation shows that, provided the particle is surrounded by free space, the answer is yes. The particle is taken as being spherical, with radius R, as shown in Fig. 11.8.5. It is assumed to have such a large magnetizability that its permeability can be taken as infinite. Further, the radius R is much smaller than other dimensions of interest, especially those characterizing variations in the applied field in the neighborhood of the particle.

Because the particle is small compared to dimensions over which the field varies significantly, we can compute its *moment* by approximating the local field as uniform. Thus, the magnetic potential is determined by solving Laplace's equation in the region around the particle subject to the conditions that $\mathbf{H}$ be the uniform field H_o at "infinity" and Ψ be constant on the surface of the particle. The calculation is fully analogous to that for the electric potential surrounding a perfectly conducting sphere in a uniform electric field. In the electric analog, the dipole moment was found to be (6.6.5), $\mathbf{p} = 4\pi\epsilon_o R^3\mathbf{E}$. Therefore, it follows from the analogy provided by (19) that the magnetic dipole moment at the particle location is

$$\mu_o m = 4\pi\mu_o R^3 H \Rightarrow \mathbf{m} = 4\pi R^3\mathbf{H} \tag{27}$$

Directly below the magnet, $\mathbf{H}$ has only a z component. Thus, the dipole moment follows from (27) as

$$\mathbf{m} = 4\pi R^3 H_z\mathbf{i_z} \tag{28}$$

Evaluation of (22) therefore gives

$$f_z = 4\pi R^3 H_z\frac{\partial H_z}{\partial z} \tag{29}$$

where H_z and its derivative are evaluated at the location of the particle.

A typical axial distribution of H_z is shown in Fig. 11.8.6 together with two pictures aimed at gaining insight into the origins of the magnetic dipole force. In

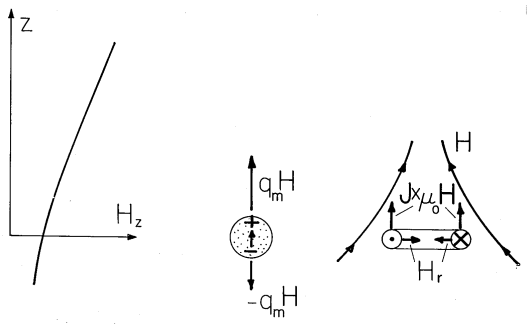


Fig. 11.8.6 In an increasing axial field, the force on a dipole is upward whether the dipole is modeled as a pair of magnetic charges or as a circulating current.

the first, the dipole is again depicted as a pair of magnetic monopoles, induced to form a moment collinear with the **H**. Because the field is more intense at the north pole of the particle than at the south pole, there is then a net force.

Alternatively, suppose that the dipole is actually a circulating current, so that the force is given by (23). Even though the energy argument makes it clear that the force is again given by (22), the physical picture is different. Because **H** is solenoidal, an intensity that increases with z implies that the field just off axis has a component that is directed radially inward. It is this radial component of the flux density crossed with the current density that results in an upward force on each segment of the loop.

REFERENCES

[1] P. Penfield, Jr., and H. A. Haus, **Electrodynamics of Moving Media**, MIT Press, Cambridge, Mass. (1967).

[2] R. M. Fano, L. J. Chu, and R. B. Adler, **Electromagnetic Fields, Energy, and Forces**, John Wiley and Sons, New York (1960).

[3] D. B. H. Tellegen, "Magnetic-dipole models," *Am. J. Phys.* Vol. 30 (Sept. 1962), pp. 650-652.

[4] H. A. Haus and P. Penfield, Jr., "Force on a current loop," *Phys. Lett.*, Vol. 26A (March 1968), pp. 412-413.

11.9 MACROSCOPIC FORCE DENSITIES

A macroscopic force density $\mathbf{F}(\mathbf{r})$ is the force per unit volume acting on a medium in the neighborhood of $\mathbf{r}$. Fundamentally, the electromagnetic force density is the result of forces acting on those microscopic particles embedded in the material that are charged, or that have electric or magnetic dipole moments. The forces acting on these individual particles are passed along through interparticle forces to the

macroscopic material as a whole. In the limit where that volume becomes small, the force density can then be regarded as the sum of the microscopic forces over a volume element ΔV.

$$\mathbf{F} = \lim_{\Delta V \to 0} \sum_{\Delta V} \mathbf{f} \tag{1}$$

Of course, the linear dimensions of ΔV are large compared to the microscopic scale.

Strictly, the forces in this sum should be evaluated using the microscopic fields. However, we can gain insight concerning the form taken by the force density by using the macroscopic fields in this evaluation. This is the basis for the following discussions of the force densities associated with unpaired charges and with conduction currents (the Lorentz force density) and with the polarization and magnetization of media (the Kelvin force density).

To be certain that the usage of macroscopic fields in describing the force densities is consistent with that implicit in the constitutive laws already introduced to describe conduction, polarization, and magnetization, the electromagnetic force densities should be derived using energy arguments. These derivations are extensions of those of Secs. 11.6 and 11.7 for forces. We end this section with a discussion of the results of such derivations and of circumstances under which they will predict the same total forces or even material deformations as those derived here.

The Lorentz Force Density. Without restricting the generality of the resulting force density, suppose that the electrical force on a material is due to two species of charged particles. One has N_+ particles per unit volume, each with a charge q_+, while the other has density N_- and a charge equal to $-q_-$. With $\mathbf{v}$ denoting the velocity of the macroscopic material and $\mathbf{v}_\pm$ representing the respective velocities of the carriers relative to that material, the Lorentz force law gives the force on the individual particles.

$$\mathbf{f}_+ = q_+[\mathbf{E} + (\mathbf{v}_+ + \mathbf{v}) \times \mu_o \mathbf{H}] \tag{2}$$

$$\mathbf{f}_- = -q_-[\mathbf{E} + (\mathbf{v}_- + \mathbf{v}) \times \mu_o \mathbf{H}] \tag{3}$$

Note that q_- is a positive number.

In typical solids and fluids, the charged particles are either bonded to the material or migrate relative to the material, suffering many collisions with the neutral material during times of interest. In either case, the inertia of the particles is inconsequential, so that on the average, the forces on the individual particles are passed along to the macroscopic material. In either situation, the force density on the material is the sum of (2) and (3), respectively, multiplied by the charged particle densities.

$$\mathbf{F} = N_+ \mathbf{f}_+ + N_- \mathbf{f}_- \tag{4}$$

Substitution of (2) and (3) into this expression gives the *Lorentz force density*

$$\boxed{\mathbf{F} = \rho_u \mathbf{E} + \mathbf{J} \times \mu_o \mathbf{H}} \tag{5}$$

where ρ_u is the unpaired charge density (7.1.6) and $\mathbf{J}$ is the current density.

$$\rho_u = N_+ q_+ - N_- q_-; \qquad \mathbf{J} = N_+ q_+ (\mathbf{v} + \mathbf{v}_+) - N_- q_- (\mathbf{v} + \mathbf{v}_-) \tag{6}$$

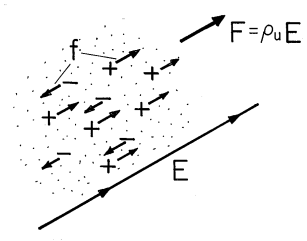


Fig. 11.9.1 The electric Lorentz force density ρ_u is proportional to the *net* charge density because the charges individually pass their force to the material in which they are embedded.

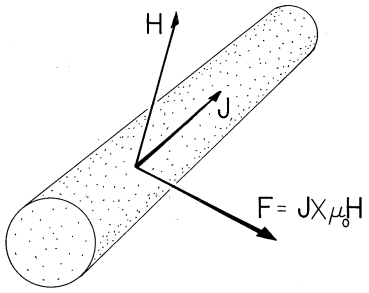


Fig. 11.9.2 The magnetic Lorentz force density $\mathbf{J} \times \mu_o \mathbf{H}$.

Because the material is in motion, with velocity $\mathbf{v}$, the current density $\mathbf{J}$ has not only the contribution familiar from Sec. 7.1 (7.1.4) due to the migration of the carriers relative to the material, but one due to the net charge carried by the moving material as well.

In EQS systems, the first term in (5) usually outweighs the second, while in MQS systems (where the unpaired charge density is negligible), the second term tends to dominate.

The derivation and Fig. 11.9.1 suggest why the electric term is proportional to the *net* charge density. In a given region, the force density resulting from the positively charged particles tends to be canceled by that due to the negatively charged particles, and the net force density is therefore proportional to the difference in absolute magnitudes of the charge densities. We exploited this fact in Chap. 7 to let electrically induced material motions evidence the distribution of the unpaired charge density. For example, in Demonstration 7.5.1, the unpaired charge density was restricted to an interface, and as a result, the motion of the fluid was suppressed by constraining the interface. A more recent example is the force on the upper electrode in the capacitor transducer of Example 11.6.1. Here again the force density is confined to a thin region on the surface of the conducting electrode.

The magnetic term in (6), pictured in Fig. 11.9.2 as acting on a current-carrying wire, is also familiar. This force density was responsible for throwing the metal disk into the air in the experiment described in Sec. 10.2. The force responsible for the levitation of the pancake coil in Demonstration 11.7.1 was also the net effect of the Lorentz force density, acting either over the volume of the coil conductors or over that of the conducting sheet below. In MQS systems, where the contribution of the "convection" current $\rho_u \mathbf{v}$ is negligible, the current density is typically due

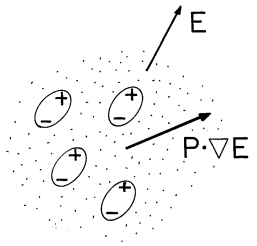


Fig. 11.9.3 The electric Kelvin force density results because the force on the individual dipoles is passed on to the neutral medium.

to conduction. Note that this means that the velocity of the charge carriers is determined by the electric field they experience in the conductor, and not simply by the motion of the conductor. The current density $\mathbf{J}$ in a moving conductor is generally not in the direction of motion.[9]

The Kelvin Polarization Force Density. If microscopic particles carrying a net charge were the only contributors to a macroscopic force density, it would not be possible to explain the forces on polarized materials that are free of unpaired charge. Example 11.6.2 and Demonstration 11.6.2 highlighted the polarization force. The experiment was carried out in such a way that the dielectric material did not support unpaired charge, so the force is not explained by the Lorentz force density.

In EQS cases where $\rho_u = 0$, the macroscopic force density is the result of forces on the microscopic particles with dipole moments. The resulting force density is fundamentally different from that due to unpaired charges; the forces $\mathbf{p} \cdot \nabla \mathbf{E}$ on the individual microscopic particles are passed along by interparticle forces to the medium as a whole. A comparison of Fig. 11.9.3 with Fig. 11.9.1 emphasizes this point. For a single species of particle, the force density is the force on a single dipole multiplied by the number of dipoles per unit volume N_p. By definition, the polarization density $\mathbf{P} = N_p \mathbf{p}$, so it follows that the force density due to polarization is

$$\boxed{\mathbf{F} = \mathbf{P} \cdot \nabla \mathbf{E}} \tag{7}$$

This is often called the *Kelvin polarization force density.*

Example 11.9.1. Force on a Dielectric Material

In Fig. 11.9.4, the cross-section of a pair of electrodes that are dipped into a liquid dielectric is shown. The picture might be of a cross-section from the experiment

[9] Indeed, it is fortunate that the carriers do not have the same velocity as the material, for if they did, it would not be possible to use the magnetic Lorentz force density for electromechanical energy conversion. If we recognize that the rate at which a force $\mathbf{f}$ does work on a particle that moves at the velocity $\mathbf{v}$ is $\mathbf{v} \cdot \mathbf{f}$, then it follows from the Lorentz force law, (1.1.1), that the rate of doing work on individual particles through the agent of the magnetic field is $\mathbf{v} \cdot (\mathbf{v} \times \mu_o \mathbf{H})$. The cross-product is perpendicular to $\mathbf{v}$, so this rate of doing work must be zero.

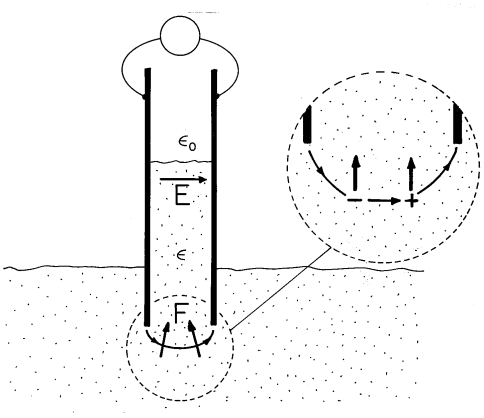


Fig. 11.9.4 In terms of the Kelvin force density, the dielectric liquid is pushed into the field region between capacitor plates because of the forces on individual dipoles in the fringing field.

of Demonstration 11.6.2. With the application of a potential difference to the electrodes, the dielectric rises between the electrodes. According to (7), what is the distribution of force density causing this rise?

For the liquid dielectric, the polarization constitutive law is taken as linear [(6.4.2) and (6.4.4)]

$$\mathbf{P} = (\epsilon - \epsilon_o)\mathbf{E} \tag{8}$$

so that with the understanding that ϵ is a function of position (uniform in the liquid, ϵ_o in the gas, and taking a step at the interface), the force density of (7) becomes

$$\mathbf{F} = (\epsilon - \epsilon_o)\mathbf{E} \cdot \nabla\mathbf{E} \tag{9}$$

By using a vector identity[10] and invoking the EQS approximation where $\nabla \times \mathbf{E} = 0$, this expression is written as

$$\mathbf{F} = \frac{1}{2}(\epsilon - \epsilon_o)\nabla(\mathbf{E} \cdot \mathbf{E}) \tag{10}$$

A second identity[11] converts this expression into one that will now prove useful in picturing the distribution of force density.

$$\mathbf{F} = \frac{1}{2}\nabla[(\epsilon - \epsilon_o)\mathbf{E} \cdot \mathbf{E}] - \frac{1}{2}\mathbf{E} \cdot \mathbf{E}\nabla(\epsilon - \epsilon_o) \tag{11}$$

Provided that the interface is well removed from the fringing fields at the top and bottom edges of the electrodes, the electric field is uniform not only in the dielectric and gas above and below the interface between the electrodes, but through the interface as well. Thus, throughout the region between the electrodes, there is no gradient of $\mathbf{E}$, and hence, according to (7), no Kelvin force density. The Kelvin force density is therefore confined to the fringing field region where the fluid surrounds the lower edges of the electrodes. In this region, ϵ is uniform, so the force density reduces to the first term in (11). Expressed by this term, the direction and

[10] $\mathbf{A} \cdot \nabla\mathbf{A} = (\nabla \times \mathbf{A}) \times \mathbf{A} + \frac{1}{2}\nabla(\mathbf{A} \cdot \mathbf{A})$

[11] $\nabla(\psi\phi) = \psi\nabla\phi + \phi\nabla\psi$

magnitude of the force density is determined by the gradient of the scalar $\mathbf{E} \cdot \mathbf{E}$. Thus, where $\mathbf{E}$ is varying in the fringing field, it is directed generally upward and into the region of greater field intensity, as suggested by Fig. 11.9.4. The force on the dipole shown by the inset lends further credence to the dipolar origins of the force density.

Although there is no physical basis for doing so, it might seem reasonable to take the force density caused by polarization as being $\rho_p\mathbf{E}$. After all, it is the polarization charge density ρ_p that was used in Chap. 6 to represent the effect of the media on the macroscopic electric field intensity $\mathbf{E}$. The experiment of Demonstration 11.6.2, pictured in Fig. 11.6.7, makes it clear that this force density is not correct. With the interface well removed from the fringing fields, there is no polarization charge density anywhere in the liquid, either at the interface or in the fringing field. If $\rho_p\mathbf{E}$ were the correct force density, it would be zero throughout the fluid volume except at the interfaces with the conducting electrodes. There, the forces are perpendicular to the surface of the electrodes. Such a force distribution could not cause the fluid to rise.

The Kelvin Magnetization Force Density. Forces caused by magnetization are probably the most commonly experienced electromagnetic forces. They account for the attraction between a magnet and a piece of iron. In Example 11.7.1, this force density acts on the disk of magnetizable material.

Given that the magnetizable material is made up of microscopic dipoles, each experiencing a force of the nature of (11.8.22), and that the magnetization density $\mathbf{M}$ is the number of these per unit volume multiplied by $\mathbf{m}$, it follows from the arguments of the preceding section that the force density due to magnetization is

$$\boxed{\mathbf{F} = \mu_o \mathbf{M} \cdot \nabla \mathbf{H}} \tag{12}$$

This is sometimes called the *Kelvin magnetization force density.*

Example 11.9.2. Force Density in a Magnetized Fluid

With the dielectric liquid replaced by a ferrofluid having a uniform permeability μ, and the electrodes replaced by the pole faces of an electromagnet, the physical configuration shown in Fig. 11.9.4 becomes the one of Fig. 11.9.5, illustrating the magnetization force density. In such fluids[1], the magnetization results from an essentially permanent suspension of magnetized particles. Each particle comprises a magnetic dipole and passes its force on to the liquid medium in which it is suspended. Provided that the magnetization obeys a linear law, the discussion of the distribution of force density given in Example 11.9.1 applies equally well here.

Alternative Force Densities. We now return to comments made at the beginning of this section. The fields used to express the Lorentz and Kelvin force densities are macroscopic. To assure consistency between the averages implied by these force densities and those already inherent in the constitutive laws, an energy principle can be used. The approach is a continuum version of that exemplified

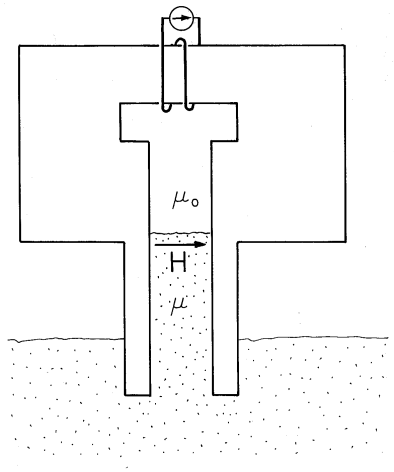


Fig. 11.9.5 In an experiment that is the magnetic analog of that shown in Fig. 11.9.4, a magnetizable liquid is pushed upward into the field region between the pole faces by the forces on magnetic dipoles in the fringing region at the bottom.

for lumped parameter systems in Secs. 11.7 and 11.8. In the lumped parameter systems, electrical terminal relations were used to determine a total energy, and energy conservation was used to determine the force. In the continuum system[2], the electrical constitutive law is used to find an energy density, and energy conservation used, in turn, to find a force density. This energy method, like the one exemplified in Secs. 11.7 and 11.8 for lumped parameter systems, describes systems that are loss free. In making practical use of the result, it is assumed that it will be applicable even if there are losses. A more general method, which invokes a *principle of virtual power*[3], allows for dissipation but requires more empirical information than the polarization or magnetization constitutive law as a starting point.

Force densities derived from more rigorous arguments than given here can have very different distributions from the superposition of the Lorentz and Kelvin force densities. We would expect that the arguments break down when the microscopic particles become so densely packed that the field experienced by one is significantly altered by its nearest neighbor. But surely the difference between the magnetic force density of Lorentz and Kelvin (LK)

$$\mathbf{F}_{\mathrm{LK}} = \mathbf{J} \times \mu_o \mathbf{H} + \mu_o \mathbf{M} \cdot \nabla \mathbf{H} \tag{13}$$

we have derived here and the *Korteweg-Helmholtz force density* (KH) for incompressible media

$$\mathbf{F}_{\mathrm{KH}} = \mathbf{J} \times \mathbf{B} - \frac{1}{2}\mathbf{H} \cdot \mathbf{H} \nabla \mu \tag{14}$$

cited in the literature[2] is not due to interactions between microscopic particles. This latter force density is often obtained for an *incompressible* material from energy arguments. [Note that with $-\nabla\mu$ and $\mathbf{H} \cdot \mathbf{H}$, respectively, playing the roles of $dL/d\xi$ and i^2, the magnetization term in (14) takes a form found for the force on a magnetizable material in Sec. 11.7.]

In Example 11.9.2 (where $\mathbf{J} = \mathbf{0}$), we found the force density of (13) to be confined to the fringing field. By contrast, (14) gives no force density in the fringing region (where μ is uniform), but rather puts it all at the interface. According to this latter equation, through the agent of a surface force density (a force density that is a spatial impulse at the interface), the field pulls upward on the interface.

The question may then be asked whether, and how, the two force density expressions can be reconciled. The answer is that if $\mu_o\mathbf{M} = (\mu - \mu_o)\mathbf{H}$, they predict the same motion for any volume-conserving material deformations such as those of an incompressible fluid. We shall demonstrate this for the case of a liquid, such as shown in Fig. 11.9.5, but allowing for the action of a current $\mathbf{J}$ as well. As the first step in the derivation, we shall show that (13) and (14) differ by the gradient of a scalar, $\pi(\mathbf{r})$.

To see this, use a vector identity[12] to write (13) as

$$\mathbf{F}_{\mathrm{LK}} = \mathbf{J} \times \mu_o\mathbf{H} + (\mu - \mu_o)[(\nabla \times \mathbf{H}) \times \mathbf{H} + \frac{1}{2}\nabla(\mathbf{H} \cdot \mathbf{H})] \tag{15}$$

The MQS form of Ampère's law makes it possible to substitute $\nabla \times \mathbf{H}$ for $\mathbf{J}$ in this expression, which then becomes

$$\mathbf{F}_{\mathrm{LK}} = \mathbf{J} \times \mathbf{B} + \frac{1}{2}(\mu - \mu_o)\nabla(\mathbf{H} \cdot \mathbf{H}) \tag{16}$$

The second term in this expression is then expanded using a second vector identity[13]

$$\mathbf{F}_{\mathrm{LK}} = \mathbf{J} \times \mathbf{B} - \frac{1}{2}\mathbf{H} \cdot \mathbf{H}\nabla\mu + \nabla\big[\frac{1}{2}(\mu - \mu_o)\mathbf{H} \cdot \mathbf{H}\big] \tag{17}$$

This expression differs from (14) by the last term, which indeed takes the form $\nabla\pi$ where

$$\pi = \frac{1}{2}(\mu - \mu_o)\mathbf{H} \cdot \mathbf{H} \tag{18}$$

Now consider Newton's force law for an elemental volume of material. Using the Korteweg-Helmholtz force density, (14), it takes the form

$$\mathbf{F}_{\mathrm{inertial}} = \mathbf{F}_m - \nabla p + \mathbf{F}_{\mathrm{KH}} \tag{19}$$

where p is the internal fluid pressure and $\mathbf{F}_m$ is the sum of all other mechanical contributions to the force density. Alternatively, using (13) written as (17) as the force density, this same law is represented by

$$\mathbf{F}_{\mathrm{inertial}} = \mathbf{F}_m - \nabla p + \mathbf{F}_{\mathrm{KH}} + \nabla\pi = \mathbf{F}_m - \nabla p' + \mathbf{F}_{\mathrm{KH}} \tag{20}$$

For an incompressible material, none of the other laws needed to describe the continuum (such as mass conservation) involve the pressure.[14] Thus, if (19) is used, p

[12] $\mathbf{A} \cdot \nabla\mathbf{A} = (\nabla \times \mathbf{A}) \times \mathbf{A} + \frac{1}{2}\nabla(\mathbf{A} \cdot \mathbf{A})$

[13] $\nabla(\psi\phi) = \psi\nabla\phi + \phi\nabla\psi$

[14] For example, for a compressible fluid, the pressure depends on mass density and temperature, so the pressure does appear in the physical laws. Indeed, in the constitutive law relating these values, the pressure has a well-defined value. However, in an incompressible fluid, the constitutive law relating the pressure to mass density and temperature is not relevant to the prediction of material motion.

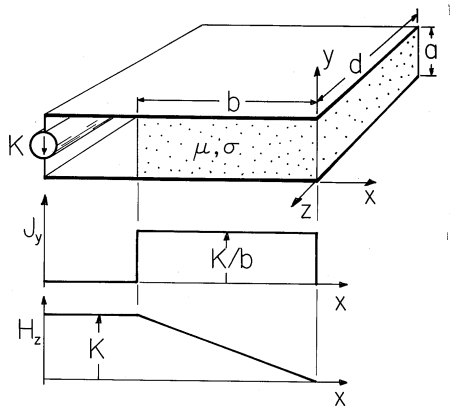


Fig. 11.9.6 The block having uniform permeability and conductivity carries a uniform current density in the y direction which produces a z-directed magnetic field intensity. Although the force densities of (13) and (14) have very different distributions in the block, they predict the same net force.

appears only in that equation and if (20) is used, $p' \equiv p - \pi$ appears only in that expression. This means that p and p' play identical roles in predicting the deformation. In an incompressible material, it is the role of the pressure to adjust itself so that only volume conserving deformations are allowed.[15] The two formulations would differ in what one would call the pressure, but would result in the same material deformation and velocity. An example is the height of rise of the fluid between the parallel plates in Fig. 11.9.5.

Included in the class of incompressible deformations are rigid body motions. If used self-consistently, force densities that differ by the gradient of a "π" will predict the same motions of rigid bodies. Thus, the net force on a body surrounded by free space will be the same whether found using the Lorentz-Kelvin or the Korteweg-Helmholtz force density. The following example illustrates this concept.

Example 11.9.3. Magnetic Force on a Magnetizable Current-Carrying Material

A block of conducting material having permeability μ is shown in Fig. 11.9.6 sandwiched between perfectly conducting plates. A current source, distributed over the left edges of these electrodes, drives a constant surface current density K in the $+x$ direction along the left edge of the lower electrode. This current passes through the block in the y direction as a current density

$$\mathbf{J} = \frac{K}{b}\mathbf{i_y} \tag{21}$$

and is returned to the source in the $-x$ direction at the left edge of the upper electrode. The thickness a of the block is small compared to its other two dimensions, so the magnetic field between the electrodes is z directed and dependent only on x.

[15] Like the "perfectly permeable material" of magnetic circuits, in which $\mathbf{B}$ remains finite as $\mathbf{H}$ goes to zero, the "perfectly incompressible" material is one in which the pressure remains finite even as the material becomes infinitely "stiff" to all but those deformations that conserve volume.

From Ampère's law it follows that

$$\frac{\partial H_z}{\partial x} = -J_y \Rightarrow \mathbf{H} = -\mathbf{i_z}\frac{K}{b}x \tag{22}$$

in the conducting block.

The alternative force densities, (13) and (14), have very different distributions in the block. Yet we must find that the net force on the block, found by integrating each over its volume, is the same. To see that this is so, consider first the sum of the Lorentz and Kelvin force densities, (13).

There is no x component of the magnetic field intensity, so for this particular configuration, the magnetization term makes no contribution to (13). Evaluation of the first term using (19) and (20) then gives

$$(F_x)_{\mathrm{LK}} = -\frac{K^2}{b^2}\mu_o x \tag{23}$$

Integration of this force density over the volume amounts to a multiplication by the cross-sectional area ad, and integration on x. Thus, the net force predicted by using the force density of Lorentz and Kelvin is

$$(f_x)_{\mathrm{LK}} = ad\int_{-b}^{0} -\frac{K^2\mu_o x}{b^2}dx = \frac{1}{2}adK^2\mu_o \tag{24}$$

Now, the Korteweg-Helmholtz force density given by (14) is evaluated. The permeability μ is uniform throughout the interior of the block, so the magnetization term is again zero there. However, μ is a step function at the ends of the block, where $x = -b$ and $x = 0$. Thus, $\nabla\mu$ is an impulse there and we must take care to include the contributions from the surface regions in our integration. Evaluation of the x component of (14) using (21) and (22) gives

$$(F_x)_{\mathrm{KH}} = -\frac{\mu K^2}{b^2}x - \frac{1}{2}H_z^2\frac{\partial\mu}{\partial x} \tag{25}$$

Integration of (25) over the volume of the block therefore gives

$$(f_x)_{\mathrm{KH}} = ad\left[\int_{-b}^{0}\frac{-K^2\mu}{b^2}xdx - \int_{-b^-}^{-b^+}\frac{1}{2}H_z^2\frac{\partial\mu}{\partial x}dx\right] \tag{26}$$

Note that H_z is constant through the interface at $x = -b$. Thus, the integration of the last term can be carried out. Simplification of this expression gives the same total force as found before, (24).

The distributions of the force densities given by (13) and (14) are generally different, even very different. It is therefore natural to ask which of the two is the "right" one. In general, until the "other" force densities acting on the medium in question are specified, this question cannot be answered. Here, where a discussion of continuum mechanics is beyond our purview, we have identified a class of mechanical deformations (namely, those that are volume conserving or "incompressible"), where these force densities are equally valid. In fact, any other force density differing from these by a term having the form $\nabla\pi$ would also be valid. The combined

Lorentz and Kelvin force densities have the advantage of a satisfying physical interpretation. However, the derivation has the weakness of making an *ad hoc* use of the macroscopic fields. Force densities resulting from an energy argument have the advantage of dealing rigorously with the macroscopic fields.

REFERENCES

[1] R. E. Rosensweig, "Magnetic Fluids," *Scientific American*, (Oct. 1982), pp. 136-145.

[2] J. R. Melcher, **Continuum Electromechanics**, MIT Press, Cambridge, Mass. (1981), chap. 3.

[3] P. Penfield and H. A. Haus, **Electrodynamics of Moving Media**, MIT Press, Cambridge, Mass. (1967).

11.10 SUMMARY

Far reaching as they are, the laws summarized by Maxwell's equations are directly applicable to the description of only one of many physical subsystems of scientific and engineering interest. Like those before it, this chapter has been concerned with the electromagnetic subsystem. However, by casting the electromagnetic laws into statements of power flow, we have come to recognize how the electromagnetic subsystem couples to the thermodynamic subsystem through the power dissipation density and to the mechanical subsystem through forces and force densities of electromagnetic origin.

The basis for a self-consistent macroscopic description of any continuum subsystem is a power flow statement having the forms identified in Sec. 11.1. Describing the energy and power flow in and into a volume V enclosed by a surface S, the integral conservation of energy statement takes the form (11.1.1).

$$-\oint_S \mathbf{S}\cdot d\mathbf{a} = \frac{d}{dt}\int_V W dv + \int_V P_d dv \tag{1}$$

The differential form of the conservation of energy statement is implied by the above.

$$-\nabla\cdot\mathbf{S} = \frac{\partial W}{\partial t} + P_d \tag{2}$$

Poynting's theorem, the subject of Sec. 11.2, is obtained starting from the laws of Faraday and Ampère to obtain an expression of the form of (2). For materials that are Ohmic ($\mathbf{J}=\sigma\mathbf{E}$) and that are linearly polarizable and magnetizable ($\mathbf{D}=\epsilon\mathbf{E}$ and $\mathbf{B}=\mu\mathbf{H}$), the *power flux density* $\mathbf{S}$ (or *Poynting's vector*), *energy density* W, and *power dissipation density* P_d were shown in Sec. 11.3 to be

$$\mathbf{S} = \mathbf{E}\times\mathbf{H} \tag{3}$$

$$W = \frac{1}{2}\epsilon \mathbf{E}\cdot\mathbf{E} + \frac{1}{2}\mu \mathbf{H}\cdot\mathbf{H} \tag{4}$$

$$P_d = \sigma \mathbf{E}\cdot\mathbf{E} \tag{5}$$

Of course, taking the free space limit where ϵ and μ assume their free space values and $\sigma = 0$ gives the free space conservation statement discussed in Sec. 11.2.

In Sec. 11.3, we found that in EQS systems, an alternative to Poynting's vector is (11.3.24).

$$\mathbf{S} = \Phi\left(\mathbf{J} + \frac{\partial \mathbf{D}}{\partial t}\right) \tag{6}$$

This expression is of practical importance, because it can be evaluated without determining $\mathbf{H}$, which is generally not of interest in EQS systems.

An important application of the integral form of the energy conservation statement is to lumped parameter systems. In these cases, the surface S of (1) encloses a system that is connected to the outside world through terminals. It is then convenient to describe the power flow in terms of the terminal variables. It was shown in Sec. 11.3 (11.3.29), that the net power into the system represented by the left-hand side of (1) becomes

$$-\oint_S \mathbf{E}\times\mathbf{H}\cdot d\mathbf{a} = \sum_{i=1}^{n} v_i i_i \tag{7}$$

provided that the magnetic induction and the electric displacement current through the surface S are negligible.

This set the stage for the application of the integral form of the energy conservation theorem to lumped parameter systems.

In Sec. 11.4, attention focused on the energy storage term, the first terms on the right in (1) and (2). The energy density concept was broadened to include materials having constitutive laws relating the flux densities to the field intensities that were single valued and collinear. With E, D, H, and B representing the field magnitudes, the energy density was found to be the sum of electric and magnetic energy densities.

$$W = W_e + W_m; \qquad W_e = \int_0^D E(D')\delta D'; \qquad W_m = \int_0^B H(B')\delta B' \tag{8}$$

Integrated over the volume V of a system, this function leads to the total energy w.

For quasistatic lumped parameter systems, the total electric or magnetic energy is often conveniently found following a different route. First the terminal relations are determined and then the total energy is found by adding up the increments of energy put into the system as it is energized. In the case of an n terminal pair EQS system, where the relation between terminal voltage v_i and associated charge q_i is $v_i(q_1,\ q_2,\ \ldots q_n)$, the increment of energy is $v_i dq_i$, and the total electric energy is (11.4.9).

$$w_e = \sum_{i=1}^{n} \int v_i dq_i \tag{9}$$

The line integration in an n-dimensional space representing the n independent q_i's was illustrated by Example 11.4.2.

Similarly, for an n terminal pair MQS system where the current i_i is related to the flux linkage λ_i by $i_i = i_i(\lambda_1,\ \lambda_2,\ \ldots \lambda_n)$, the total energy is (11.4.12).

$$w_m = \sum_{i=1}^{n} \int i_i d\lambda_i \tag{10}$$

Note the analogy between these expressions for the total energy of EQS and MQS lumped parameter systems and the electric and magnetic energy densities, respectively, of (8). The transition from the field picture afforded by the energy densities to the lumped parameter characterization is made by $E \to v,\ D \to q$ and by $H \to i,\ B \to \lambda$.

Especially in using the energy to evaluate forces of electrical origin, we found it convenient to define coenergy density functions.

$$W'_e = DE - W_e; \qquad W'_m = BH - W_m \tag{11}$$

It followed that these functions were natural when it was desirable to use E and H as the independent variables rather than D and B.

$$W'_e = \int_0^E D(E')\delta E'; \qquad W'_m = \int_0^H B(H')\delta H' \tag{12}$$

The total coenergy functions for lumped parameter EQS and MQS systems could be found either by integrating these densities over the volume or by again viewing the system in terms of its terminal variables. With the total coenergy functions defined by

$$w'_e = \sum_{i=1}^{n} q_i v_i - w_e; \qquad w'_m = \sum_{i=1}^{n} \lambda_i i_i - w_m \tag{13}$$

it followed that the coenergy functions could be determined from the terminal relations by again carrying out line integrations, but this time with the voltages and currents as the independent variables. For EQS systems,

$$w'_e = \sum_{i=1}^{n} \int q_i dv_i \tag{14}$$

while for MQS systems,

$$w'_m = \sum_{i=1}^{n} \int \lambda_i di_i \tag{15}$$

Again, note the analogy to the respective terms in (12).

The remaining sections of the chapter developed some of the possible implications of the "dissipation" term in the energy conservation statement, the last terms in (1) and (2). In Sec. 11.5, coupling to a thermal subsystem was discussed. In

this section, the disparity between the power input and the rate of increase of the energy stored was accounted for by heating. In addition to Ohmic heating, caused by collisions between the migrating carriers and the neutral media, we considered losses associated with the dynamic polarization and magnetization of materials.

In Secs. 11.6–11.9, we considered coupling to a mechanical subsystem as a second mechanism by which energy could be extracted from (or put into) the electromagnetic subsystem. With the displacement of an object denoted by ξ, we used an energy conservation postulate to infer the total electric or magnetic force acting on the object from the energy functions [(11.6.9), and its magnetic analog]

$$f_e = -\frac{\partial w_e(q_1 \ \ldots \ q_n, \ \xi)}{\partial \xi}; \qquad f_m = -\frac{\partial w_m(\lambda_1 \ \ldots \ \lambda_n, \ \xi)}{\partial \xi} \tag{16}$$

or from the coenergy functions [(11.7.7) and the analogous expression for electric systems].

$$f_e = \frac{\partial w'_e(v_1 \ \ldots \ v_n, \ \xi)}{\partial \xi}; \qquad f_m = \frac{\partial w'_m(i_1 \ \ldots \ i_n, \ \xi)}{\partial \xi} \tag{17}$$

In Sec. 11.8, where the Lorentz force on a particle was generalized to account for electric and magnetic dipole moments, one objective was a microscopic picture that would lend physical insight into the forces on polarized and magnetized materials. The Lorentz force was generalized to include the force on stationary electric and magnetic dipoles, respectively.

$$\mathbf{f} = \mathbf{p} \cdot \nabla \mathbf{E}; \qquad \mathbf{f} = \mu_o \mathbf{m} \cdot \nabla \mathbf{H} \tag{18}$$

The total macroscopic forces resulting from microscopic forces had already been encountered in the previous two sections. The force density describes the interaction between a volume element of the electromagnetic subsystem and a mechanical continuum. The force density inferred by averaging over the forces identified in Sec. 11.8 as acting on microscopic particles was

$$\mathbf{F} = \rho_u \mathbf{E} + \mathbf{J} \times \mu_o \mathbf{H} + \mathbf{P} \cdot \nabla \mathbf{E} + \mu_o \mathbf{M} \cdot \nabla \mathbf{H} \tag{19}$$

A more rigorous approach to finding the force density could be based on a generalization of the energy method introduced in Secs. 11.6 and 11.7. As background for further pursuit of this subject, we have illustrated the importance of including the mechanical continuum with which the force density acts. Before there can be a meaningful answer to the question, "Which force density is correct?" the other force densities acting on the material must be specified. As an illustration, we found that very different electric or magnetic force densities would result in the same deformations of an incompressible material and in the same net force on an object surrounded by free space[1,2].

REFERENCES

[1] P. Penfield, Jr., and H. A. Haus, **Electrodynamics of Moving Media**, MIT Press, Cambridge, Mass. (1967).

[2] J. R. Melcher, **Continuum Electromechanics**, MIT Press, Cambridge, Mass. (1981), chap. 3.

PROBLEMS

11.1 Introduction

11.1.1* A capacitor C, an inductor L, and a resistor R are in series, driven by the voltage $v(t)$ and carrying the current $i(t)$. With v_c defined as the voltage across the capacitor, show that $vi = dw/dt + i^2R$ where $w = \frac{1}{2}Cv_c^2 + \frac{1}{2}Li^2$. Argue that w is the energy stored in the inductor and capacitor, while i^2R is the power dissipated in the resistor.

11.2 Integral and Differential Conservation Statements

11.2.1* Consider a system in which the fields are y and/or z directed and independent of y and z. Then $S = S_x(x,t)\mathbf{i_x}$, $W = W(x,t)$, and $P_d = P_d(x,t)$.

(a) Show that for a volume having area A in any $y-z$ plane and located between $x = x_1$ and $x = x_2$, (1) becomes

$$-[AS_x(x_1) - AS_x(x_2)] = \frac{d}{dt}A\int_{x_2}^{x_1} W dx + A\int_{x_2}^{x_1} P_d dx \qquad (a)$$

(b) Take the limit where $x_1 - x_2 = \Delta x \to 0$ and show that the one-dimensional form of (3) results.

(c) Based on (a), argue that S_x is the power flux density in the x direction.

11.3 Poynting's Theorem

11.3.1* The perfectly conducting plane parallel electrodes of Fig. 13.1.1 are driven at the left by a voltage source $V_d(t)$ and are "open circuit" at the right, as shown in Fig. 13.1.4. The system is EQS.

(a) Show that the power flux density is $\mathbf{S} = \mathbf{i_y}(-\epsilon_o y/a^2)V_d dV_d/dt$.

(b) Using $\mathbf{S}$, show that the power input is $d(\frac{1}{2}CV_d^2)/dt$, where $C = \epsilon_o bw/a$.

(c) Evaluate the right-hand side of (11.1.1) to show that if the magnetic energy storage is neglected, the same result is obtained.

(d) Show that the magnetic energy storage is indeed negligible if b/c is much shorter than times of interest.

11.3.2 The perfectly conducting plane parallel electrodes of Fig. 13.1.1 are driven at the left by a current source $I_d(t)$, as shown in Fig. 13.1.3. The system is MQS.

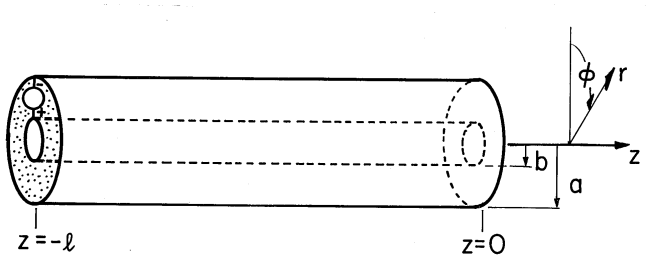


Fig. P11.3.2

(a) Determine **S**.
(b) From **S**, find the input power.
(c) Evaluate the right-hand side of (11.1.1) for a volume enclosing the region between the electrodes, and show that if the electric energy storage is neglected, it is indeed equal to the left-hand side.
(d) Under what conditions is the electric energy storage negligible?

11.4 Ohmic Conductors with Linear Polarization and Magnetization

11.4.1* In Example 7.3.2, a three-dimensional dipole current source drives circulating currents through a uniformly conducting material. This source is so slowly varying with time that time rates of change have a negligible effect. Consider first the power flow as pictured in terms of the Poynting flux density, (3).

(a) Show that

$$\mathbf{E} \times \mathbf{H} = \left(\frac{i_p d}{4\pi}\right)^2 \frac{1}{\sigma} \left| \left(\frac{-2\cos\theta \sin\theta}{r^5}\right) \mathbf{i}_\theta + \frac{\sin^2\theta}{r^5} \mathbf{i}_\mathbf{r} \right| \qquad (a)$$

(b) Show that

$$P_d = \left(\frac{i_p d}{4\pi}\right)^2 \frac{1}{\sigma} \frac{(1 + 3\cos^2\theta)}{r^6} \qquad (b)$$

(c) Using these results, show that (11.1.3) is indeed satisfied.
(d) Now, using the alternative EQS power theorem, evaluate **S** as given by (23) and again show that (11.1.3) is satisfied.
(e) Observe that the latter evaluation is much simpler to carry out and that the latter power flux density is easier to picture.

11.4.2 Coaxial perfectly conducting circular cylindrical electrodes make contact with a uniformly conducting material of conductivity σ in the annulus $b < r < a$, as shown in Fig. P11.3.2. The length l is large compared to a. A voltage source v drives the system at the left, while the electrodes are "open" at the right. Assume that $v(t)$ is so slowly varying that the voltage can be regarded as independent of z.

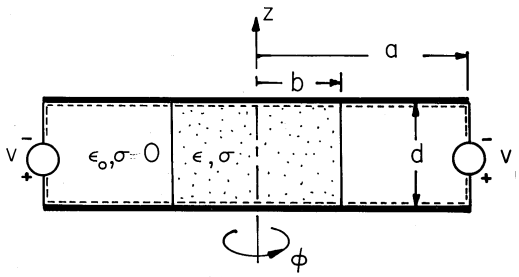


Fig. P11.3.3

(a) Determine **E**, Φ, and **H** in the annulus.
(b) Evaluate the Poynting power flux density **S** [as given by (3)] in the annulus.
(c) Use **S** to evaluate the total power dissipation by integration over the surface enclosing the annulus.
(d) Show that the same result is obtained by integrating P_d over the volume.
(e) Evaluate **S** as given by (23), and use that distribution of the power flux density to determine the total power dissipation.
(f) Make sketches of the alternative distributions of **S**.
(g) Show that the input power is vi, where i is the total current from the voltage source.

11.4.3* A pair of perfectly conducting circular plates having a spacing d form parallel electrodes in a system having cylindrical symmetry about the z axis and the cross-section shown by Fig. P11.3.3. The central region between the plates is filled out to the radius b by a uniformly conducting material having conductivity σ and uniform permittivity ϵ, while the surrounding region, where $b < r < a$, is free space. A distributed voltage source $v(t)$ constrains the potential difference between the outer edges of the electrodes. Assume that the system is EQS.

(a) Show that the Poynting power flux density is

$$\mathbf{S} = -\mathbf{i_r}\begin{cases} \frac{r}{2}\left(\frac{\sigma v}{d} + \frac{\epsilon}{d}\frac{dv}{dt}\right)\frac{v}{d}; & r < b \\ \frac{1}{2r}\left[\frac{1}{d}(\epsilon b^2 + \epsilon_o(r^2 - b^2))\frac{dv}{dt} + \frac{\sigma b^2}{d}v\right]\frac{v}{d}; & b < r < a \end{cases} \qquad (a)$$

(b) Integrate this flux density over a surface enclosing the region between the plates, and show that it is equal to the sum of the rate of change of electric energy storage and the power dissipation.
(c) Now show that the alternative power flux density given by (23) is

$$\mathbf{S} = -\frac{v}{d}(z-d)\mathbf{i_z}\begin{cases} \frac{\sigma v}{d} + \frac{\epsilon_o}{d}\frac{dv}{dt}; & r < b \\ \frac{\epsilon_o}{d}\frac{dv}{dt}; & b < r < a \end{cases} \qquad (b)$$

(d) Carry out part (b) using this distribution of **S**, and show that the result is the same.
(e) Show that the power input is equal to vi, where i is the total current from the voltage source.

11.4.4 In Example 7.5.1, the steady current distribution in and around a conducting circular cylindrical rod immersed in a conducting material was determined. Assume that E_o is so slowly varying that it can be regarded as static.

(a) Determine the distribution of Poynting power flux density $\mathbf{S}$, as given by (3).
(b) Determine the alternative $\mathbf{S}$ given by (23).
(c) Find the power dissipation density P_d in and around the rod.
(d) Show that the differential energy conservation law [(11.1.3) with $\partial W/\partial t = 0$] is satisfied at each point in and around the rod using either of these distributions of $\mathbf{S}$.

11.5 Energy Storage

11.5.1* In Example 8.5.1, the inductance L of a spherically shaped coil was found by "adding up" the flux linkages of the individual windings. Taking an alternative approach to finding L, use the fields found in that example to determine the total energy storage, w_m. Then use the fact that $w_m = \frac{1}{2}Li^2$ to show that L is as given by (8.5.20).

11.5.2 In Prob. 9.6.3, a coil has turns at the interface between a magnetizable material and a circular cylindrical core of free space, as shown in Fig. P9.6.3. Assume that the system has a length l in the z direction and determine the total energy, w_m. (Assume that the rotatable coil carries no current.) Use the fact that $w_m = \frac{1}{2}Li^2$ to find L.

11.5.3* In Example 8.6.4, the fields of a coil distributed throughout a volume were found. Using these fields to evaluate the total energy storage, show that the inductance is as given by (8.6.35).

11.5.4 The magnetic circuit described in Prob. 9.7.5 and shown in Fig. P9.7.5 has two electrical excitations. Determine the total magnetic coenergy, $w'_m(i_1, i_2, x)$.

11.5.5 The cross-section of a motor or generator is shown in Fig. 11.7.7.

(a) Determine the magnetic coenergy density W'_m, and hence the total coenergy w'_m.
(b) By writing w'_m in the form of (11.4.24), determine L_{11}, L_{12}, and L_{22}.

11.5.6* The material in the system of Fig. 11.4.3 has the constitutive law of (28). Show that the total coenergy is

$$w'_e = \left[\frac{\alpha_1}{\alpha_2}\left(\sqrt{1+\frac{\alpha^2 v^2}{a^2}}-1\right)+\frac{1}{2}\epsilon_o\frac{v^2}{a^2}\right]\xi ca+\frac{1}{2}\frac{\epsilon_o v^2}{a}(b-\xi)c \qquad (a)$$

11.5.7 Consider the system shown in Fig. P9.5.1 but with $\mu_a = \mu_o$ and the region where $\mathbf{B} = \mu_b\mathbf{H}$ now filled with a material having the constitutive law

$$\mathbf{B} = \left(\mu_o + \alpha_1/\sqrt{1+\alpha_2 H^2}\right)\mathbf{H} \qquad (a)$$

(a) Determine $\mathbf{B}$ and $\mathbf{H}$ in each region.
(b) Find the coenergy density in each region and hence the total coenergy w'_m as a function of the driving current i.

11.6 Electromagnetic Dissipation

11.6.1* In Example 7.9.2, the Maxwell capacitor has an area A (perpendicular to x), and the terminals are driven by a source $v = Re[\hat{v}\exp(j\omega t)]$. The sinusoidal steady state has been established. Show that the time average power dissipation in the lossy dielectrics is

$$\langle P_d \rangle = \frac{A}{2}\frac{[a\sigma_a(\sigma_b^2+\omega^2\epsilon_b^2)+b\sigma_b(\sigma_a^2+\omega^2\epsilon_a^2)]}{(b\sigma_a+a\sigma_b)^2+\omega^2(b\epsilon_a+a\epsilon_b)^2}|\hat{v}|^2 \qquad (a)$$

11.6.2 In Example 7.9.3, the potential is found in the EQS approximation in and around a lossy dielectric sphere embedded in a lossy dielectric and stressed by a uniform field having a sinusoidal dependence on time (7.9.36).

(a) Find the time average power dissipation density in each region.
(b) What is the total time average power dissipated in the sphere?

11.6.3* Plane parallel perfectly conducting plates having the spacing d are shorted by a perfectly conducting sheet in the plane $x = 0$, as shown in Fig. P11.5.3. A sheet having thickness Δ and conductivity σ is in the plane $x = -b$ and makes contact with the perfectly conducting plates above and below. At their left edges, in the plane $x = -(a+b)$, a source of surface current density, $K(t)$, is connected to the plates. The regions to left and right of the resistive sheet are free space, and w is large compared to a, b, and d.

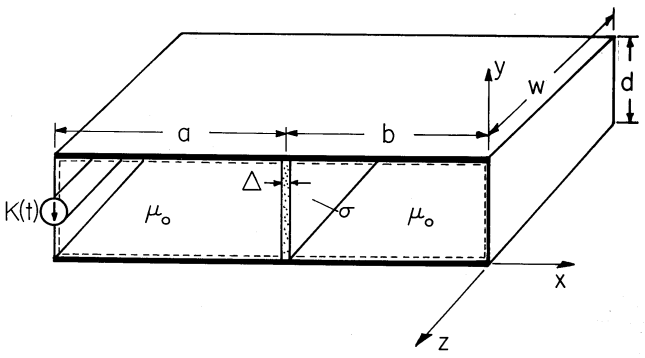


Fig. P11.5.3

(a) Show that the total power dissipation and magnetic energy stored as defined on the right in (11.1.1), are

$$\int_V P_d dv = \Delta\sigma w d\mu_o^2 b^2 \left(\frac{dH^b}{dt}\right)^2; \quad \int_V W dv = \frac{1}{2}\mu_o dw(bH_b^2 + aK^2) \qquad (a)$$

(b) Show that the integral on the left in (11.1.1) over the surface indicated by the dashed line in the figure gives the same result as found in part (a).

11.6.4 In Example 10.4.1, the applied field is $H_o(t) = H_m \cos(\omega t)$ and sinsuoidal steady state conditions prevail. Determine the time average power dissipation in the conducting sheet.

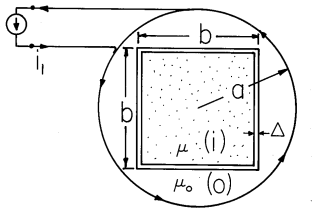


Fig. P11.5.5

11.6.5* The cross-section of an N-turn circular solenoid having radius a is shown in Fig. P11.5.5. It surrounds a thin cylindrical shell of square cross-section, with length b on a side. This shell has thickness Δ and conductivity σ, and is filled by a material having permeability μ. Both the shell and the solenoid have a length d perpendicular to the paper that is large compared to a.

(a) Given that the terminals of the solenoid are driven by the current $i_1 = i_o \cos\omega t$ and the sinusoidal steady state has been established, integrate the time average power dissipation density over the volume of the shell to show that the total time-average power dissipation is

$$p_d = \frac{2b}{\sigma\Delta d} N^2 i_o^2 \left[\frac{(\omega\tau_m)^2}{1 + (\omega\tau_m)^2}\right] \qquad (a)$$

(b) In the sinusoidal steady state, the time average Poynting flux through a surface enclosing the shell goes into the time average dissipation. Use this fact to obtain (a).

11.6.6 In describing the response of macroscopic media to fields in the sinusoidal steady state, it is convenient to use complex constitutive laws. The complex permittivity is introduced by (19). Here we introduce and illustrate the complex *permeability*. Suppose that field quantities take the form

$$\mathbf{E} = Re\hat{\mathbf{E}}(x,y,z)e^{j\omega t}; \qquad \hat{\mathbf{H}} = Re\hat{\mathbf{H}}(x,y,z)e^{j\omega t} \qquad (a)$$

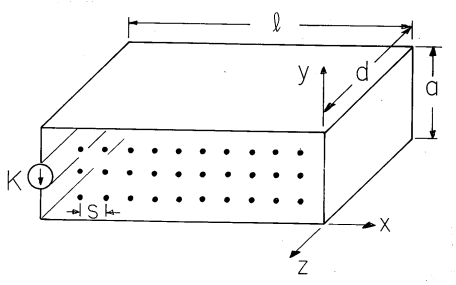


Fig. P11.5.6

(a) Show that in a region where there is no *macroscopic* current density, the MQS laws require that

$$\nabla \times \hat{\mathbf{E}} = -j\omega\hat{\mathbf{B}} \tag{b}$$

$$\nabla \times \hat{\mathbf{H}} = 0 \tag{c}$$

$$\nabla \cdot \hat{\mathbf{B}} = 0 \tag{d}$$

(c) Given that the spherical shell of Prob. 10.4.3 comprises each element in the cubic array of Fig. P11.5.6, each sphere with spacing s such that $s \gg R$, what is the complex permeability μ defined such that $\hat{\mathbf{B}} = \hat{\mu}\hat{\mathbf{H}}$?

(d) A macroscopic material composed of this array of spheres is placed in the one-turn solenoid of rectangular cross-section shown in Fig. P11.5.6. This configuration is long enough in the z direction so that fringing fields can be ignored. At their left edges, the perfectly conducting plates composing the top and bottom of the solenoid are driven by a distributed current source, $K(t)$. With the fringing fields in the neighborhood of the left end ignored, the resulting fields take the form $\mathbf{H} = H_z(x,t)\mathbf{i_z}$ and $\mathbf{E} = E_y(x,t)\mathbf{i_y}$. Use an evaluation of the Poynting flux to determine the total time average power dissipated in the length l, width d, and height a of the material.

11.6.7* In the limit where the skin depth δ is small compared to the length b, the magnetic field distribution in the conductor of Fig. 10.7.2 is given by (10.7.15). Show that (per unit $y-z$ area) the time average power dissipation associated with the current flowing in the "skin" region is $|K_s|^2/2\sigma\delta$ watts/m^2.

11.6.8 The conducting block shown in Fig. 10.7.2 has a length d in the z direction.

(a) Determine the total time average power dissipation.

(b) Show that in the case $\delta \ll b$ this expression reduces to that obtained in Prob. 11.5.7, while in the limit $\delta \gg b$, the result is i^2R where R is the dc resistance of the slab and i is the total current.

11.6.9* The toroid of Fig. 9.4.1 is filled with an insulating material having the magnetization constitutive law of Prob. 9.4.3. Show that from the terminals

of the N_1-turn coil, the circuit is equivalent to one having an inductance $L = \mu_o N_1^2 w^2/8R$ in series with a resistance $R_m = \mu_o \gamma N_1^2 w^2/8R$.

11.6.10 The toroid of Fig. 9.4.1 is filled by a material having the magnetization characteristic shown in Fig. P11.5.10. A sinusoidal current is supplied with a particular amplitude, $i = (2H_c 2\pi R/N_1)\cos(\omega t)$.

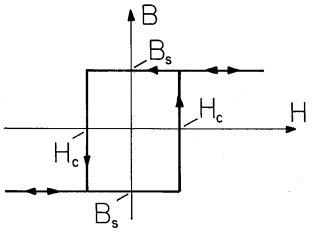


Fig. P11.5.10

(a) Draw a dimensioned plot of $B(t)$.
(b) Find the terminal voltage $v(t)$ and also make a dimensioned plot.
(c) Compute the time average power input, defined as

$$\langle vi \rangle = \frac{1}{T}\int_t^{t+T} vi dt \qquad (a)$$

where $T = 2\pi/\omega$.
(d) Show that the result of part (c) can also be found by recognizing that, during one cycle, there is an energy/unit volume dissipated which is equal to the area enclosed by the $B - H$ characteristic.

11.7 Electrical Forces on Macroscopic Media

11.7.1* A pair of perfectly conducting plates, the upper one fixed and the lower one free to move with the horizontal displacement ξ, have a fixed spacing a as shown in Fig. P11.6.1. Show that the force of electrical origin acting on the lower electrode in the ξ direction is $f = -\epsilon_o v^2 d/2a$.

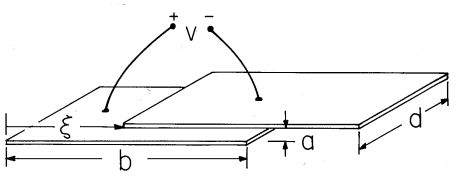


Fig. P11.6.1

11.7.2 In Example 4.6.3, the capacitance per unit length of the pair of parallel circular cylindrical conductors shown in Fig. 4.6.6 was found. Determine the force per unit length acting on the right cylinder in the x direction.

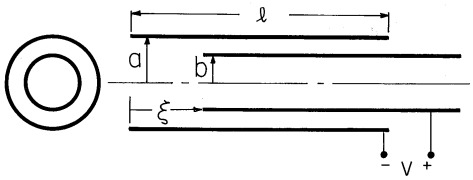


Fig. P11.6.4

11.7.3* The electric transducer shown in cross-section by Fig. P11.6.3 has cylindrical symmetry about the center line. A coaxial pair of perfectly conducting electrodes having length l are excited at the left end by a voltage source $v(t)$. A perfectly insulating dielectric material having permittivity ϵ is free to slide in and out of the annular region between electrodes.

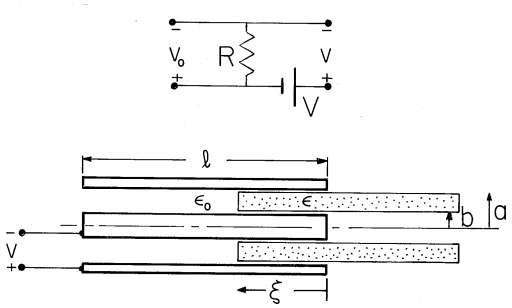


Fig. P11.6.3

(a) Show that the force of electric origin acting on the dielectric material in the axial direction is $f = v^2\pi(\epsilon - \epsilon_o)/ln(a/b)$.
(b) Show that if the electrical terminals are constrained by the circuit shown, R is very small and the plunger suffers the displacement $\xi(t)$ the output voltage is $v_o = -2\pi RV(\epsilon - \epsilon_o)(d\xi/dt)/ln(a/b)$.

11.7.4 The electrometer movement shown in Fig. P11.6.4 consists of concentric, perfectly conducting tubes, the inner one free to move in the axial direction.

(a) Ignore the fringing field and determine the force of electrical origin acting in the direction of ξ.
(b) For the energy conversion cycle of Demonstration 11.6.1, but for this transducer, make dimensioned plots of the cycle in the (q, v) and (f, ξ) planes (analogous to those of Fig. 11.6.5).
(c) By calculating both, show that the electrical energy input in one cycle is equal to the work done on the external mechanical system.

11.7.5* Show that the vertical force on the nonlinear dielectric material of Prob. 11.4.6 is

$$f = \left[\frac{\alpha_1}{\alpha_2}\left(\sqrt{1 + \frac{\alpha_2 v^2}{a^2}} - 1\right) + \frac{1}{2}\epsilon_o\frac{v^2}{a^2}\right]ca - \frac{\epsilon_o v^2 c}{2a} \qquad (a)$$

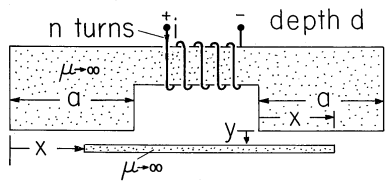


Fig. P11.7.3

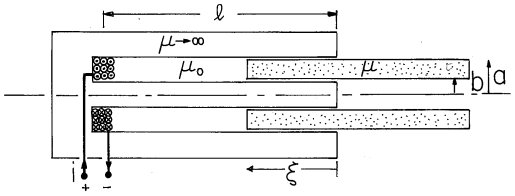


Fig. P11.7.4

11.8 Macroscopic Magnetic Fields

11.8.1* Show that the force acting in the x direction on the movable element of Prob. 9.7.5 (Note Prob. 11.4.4.) is

$$f = -\frac{\mu_o a w}{2x^2(1+a/b)}(N_1^2 i_1^2 + 2N_1 N_2 i_1 i_2 + N_2^2 i_2^2) \qquad (a)$$

11.8.2 Determine the force $f(i,\xi)$ acting in the x direction on the plunger of the magnetic circuit shown in Fig. P9.7.6.

11.8.3* The magnetic transducer shown in Fig. P11.7.3 consists of a magnetic circuit in which the lower element is free to move in the x and y directions. From the energy principle, ignoring fringing fields, show that the force on this element is

$$\mathbf{f} = \frac{\mu_o n^2 d i^2}{2a}\left[\frac{a-2x}{y}\mathbf{i_x} - \frac{x(a-x)}{y^2}\mathbf{i_y}\right] \qquad (a)$$

11.8.4 The magnetic circuit shown in cross-section by Fig. P11.7.4 has cylindrical symmetry. A plunger of permeability μ having outer and inner radii a and b can suffer a displacement ξ into the annular gap of a magnetic circuit otherwise made of infinitely permeable material. The coil has N turns. Assume that the left end of the plunger is well within the magnetic circuit, so that fringing fields can be ignored, and determine the force $f(i,\xi)$ acting to displace the plunger in the ξ direction.

11.8.5* The "variable reluctance" motor shown in cross-section in Fig. P11.7.5 consists of an infinitely permeable yoke and an infinitely permeable rotor

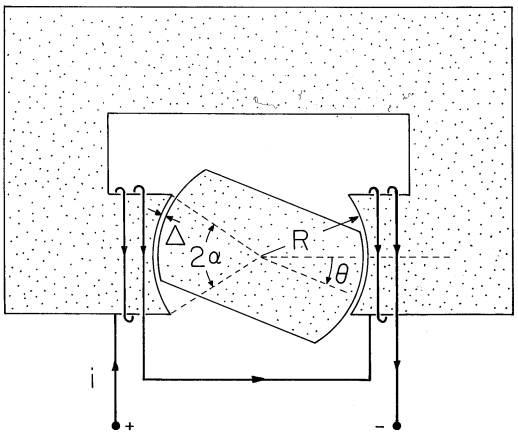


Fig. P11.7.5

element forming a magnetic circuit with two air gaps of length $\Delta \ll R$. The system has depth $d \gg \Delta$ into the paper. Assume that $0 < \theta < \alpha$, as shown, and show that the torque caused by passing a current i through the two N-turn coils is $\tau = -\mu_o R d N^2 i^2/\Delta$.

11.8.6 A "two-phase" synchronous machine is constructed having a cross-section like that shown in Fig. 11.7.7, except that there is an additional winding on the stator. This is identical to the one shown except that it is rotated 90 degrees in the clockwise direction. The current in the stator winding shown in Fig. 11.7.7 is denoted by i_a, while that in the additional winding is i_b. Thus, the magnetic axes of i_a and i_b, respectively, are upward and to the right. With L_s, L_r, and M given constants, the inductance matrix is

$$\begin{bmatrix} \lambda_a \\ \lambda_b \\ \lambda_r \end{bmatrix} = \begin{bmatrix} L_s & 0 & M\cos\theta \\ 0 & L_s & M\sin\theta \\ M\cos\theta & M\sin\theta & L_r \end{bmatrix} \begin{bmatrix} i_a \\ i_b \\ i_r \end{bmatrix} \qquad (a)$$

(a) Determine the coenergy $w'_m(i_a, i_b, \theta)$.
(b) Find the torque on the rotor, $\tau(i_a, i_b, \theta)$.
(c) With $i_a = I\cos(\omega t)$ and $i_b = I\sin(\omega t)$, where I and ω are given constants, argue that the magnetic axis produced by the stator rotates with the angular velocity ω.
(d) Using these current constraints together with $i_r = I_r$ and $\theta = \Omega t - \gamma$, where I_r, γ and Ω are constants, show that under synchronous conditions (where $\omega = \Omega$), the torque is $\tau = MII_r\sin(\gamma)$.

11.9 Forces on Microscopic Electric and Magnetic Dipoles

11.9.1* In a uniform electric field $\mathbf{E}$, a perfectly conducting particle having radius R has a dipole moment $\mathbf{p} = 4\pi\epsilon_o R^3\mathbf{E}$. Provided that R is short compared to

distances over which the field varies, this gives a good approximation to $\mathbf{p}$, even where the field is not uniform. Such a particle is shown at the location $x = X,\ y = Y$ in Fig. P11.8.1, where it is subject to the field produced by a periodic potential $\Phi = V_o \cos(\beta x)$ imposed in the plane $y = 0$.

(a) Show that the potential imposed in the region $0 < y$ is $V_o \cos(\beta x)$ exp $(-\beta y)$.

(b) Show that, provided that the particle has no net charge, the force on the particle is

$$\mathbf{f} = -4\pi\epsilon_o R^3 (V_o\beta)^2 \beta \mathbf{i_y} e^{-2\beta y} \qquad (a)$$

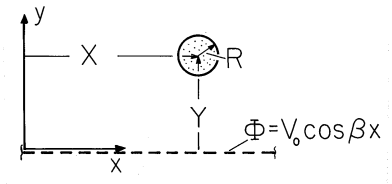


Fig. P11.8.1

11.9.2 The perfectly conducting particle described in Prob. 11.8.1, carrying no net charge but polarized by the imposed electric field, is subjected to the field of a charge Q located at the origin of a spherical coordinate system. In terms of its location R relative to the charged particle at the origin, determine the force on the particle.

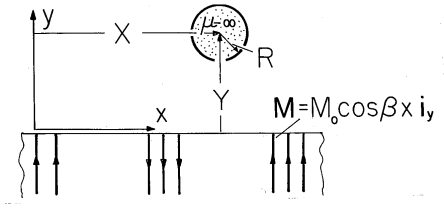


Fig. P11.8.3

11.9.3* In Fig. P11.8.3, permanent magnets in the lower half-space are represented by the magnetization density $\mathbf{M} = M_o \cos(\beta x)\mathbf{i_y}$, where M_o and β are given positive constants.

(a) Show that the resulting magnetic potential in the upper half-space is

$$\Psi = (M_o/2\beta)\cos(\beta x)\exp(-\beta y)$$

(b) A small infinitely permeable particle having the radius R is located at $x = X,\ y = Y$. Show that the magnetization force on the particle is as given by (a) of Prob. 11.8.1, with $V_o \to (M_o/2\beta)$ and $\epsilon_o \to \mu_o$.

11.9.4 A small "infinitely permeable" particle of radius R is a distance Z above an infinitely permeable plane, as shown in Fig. P11.8.4. A uniform field

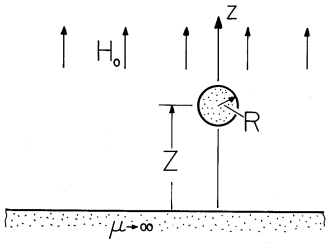


Fig. P11.8.4

$\mathbf{H} = H_o\mathbf{i_z}$ is imposed. Assume that $R \ll Z$, and use (27) to approximate the dipole moment induced in the particle. The effect of the infinitely permeable plane on the field induced by this dipole is equivalent to that of a second image dipole located at $z = -Z$. Thus, there is a force of attraction between the magnetized particle and the infinite plane that is equivalent to that attracting the dipole to its image. Determine the force in the z direction on the particle.

11.10 Macroscopic Force Densities

11.10.1 In Prob. 11.7.2, the total force on a magnetizable plunger is found (Fig. P9.7.6). Find this same force by integrating the force density, (14), over the volume of the plunger.

11.10.2 In Example 10.3.1, the transient current induced by applying a magnetic field intensity H_o to a conducting shell is determined.

(a) Show that there is a radial magnetic force per unit area acting on the shell $T_r = \mu_o K(H_o + H_i)/2$. (Note that the thin-shell model implies that $\mathbf{H}$ varies in an essentially linear fashion with R inside the shell.)
(b) Specifically, show that

$$T_r = -\frac{\mu_o H_o^2}{2}\left(2 - e^{-t/\tau_m}\right)e^{-t/\tau_m} \qquad (a)$$

11.10.3 In Example 10.4.1, the transient current induced in a conducting shell by the application of a transverse magnetic field is found. Suppose that the magnetizable core is absent.

(a) Show that the radial force per unit area acting on the shell is $T_r = \mu_o K(H_\phi^o + H_\phi^i)/2$. (Note that according to the thin-shell model, $\mathbf{H}$ has an essentially linear dependence on r within the shell.)
(b) Determine $T_r(\phi, t)$ and relate the result to Demonstration 10.4.1.

12

ELECTRODYNAMIC FIELDS: THE SUPERPOSITION INTEGRAL POINT OF VIEW

12.0 INTRODUCTION

This chapter and the remaining chapters are concerned with the combined effects of the magnetic induction $\partial\mathbf{B}/\partial t$ in Faraday's law and the electric displacement current $\partial\mathbf{D}/\partial t$ in Ampère's law. Thus, the full Maxwell's equations without the quasistatic approximations form our point of departure. In the order introduced in Chaps. 1 and 2, but now including polarization and magnetization, these are, as generalized in Chaps. 6 and 9,

$$\nabla \cdot (\epsilon_o \mathbf{E}) = \rho_u - \nabla \cdot \mathbf{P} \tag{1}$$

$$\nabla \times \mathbf{H} = \mathbf{J}_u + \frac{\partial}{\partial t}(\epsilon_o \mathbf{E} + \mathbf{P}) \tag{2}$$

$$\nabla \times \mathbf{E} = -\frac{\partial}{\partial t}\mu_o(\mathbf{H} + \mathbf{M}) \tag{3}$$

$$\nabla \cdot (\mu_o \mathbf{H}) = -\nabla \cdot (\mu_o \mathbf{M}) \tag{4}$$

One may question whether a generalization carried out within the formalism of electroquasistatics and magnetoquasistatics is adequate to be included in the full dynamic Maxwell's equations, and some remarks are in order. Gauss' law for the electric field was modified to include charge that accumulates in the polarization process. The accounting for the charge leaving a designated volume was done under no restrictions of quasistatics, and thus (1) can be adopted in the fully dynamic case. Subsequently, Ampère's law was modified to preserve the divergence-free character of the right-hand side. But there was more involved in that step. The term $\partial\mathbf{P}/\partial t$ can be identified unequivocally as the current density associated with a time dependent polarization process, provided that the medium as a whole is at rest. Thus, (2) is the correct generalization of Ampère's law for polarizable media

at rest. If the medium moves with the velocity $\mathbf{v}$, a term $\nabla \times (\mathbf{P} \times \mathbf{v})$ has to be added to the right-hand side[1,2]. The generalization of Gauss' law and Faraday's law for magnetic fields is by analogy. If the material is moving and magnetized, a term $-\mu_o \nabla \times (\mathbf{M} \times \mathbf{v})$ must be added to the right-hand side of (3). We shall not consider such moving polarized or magnetized media in the sequel.

Throughout this chapter, we are generally interested in electromagnetic fields in free space. If the region of interest is filled by a material having an appreciable polarization and or magnetization, the constitutive laws are presumed to represent a linear and isotropic material

$$\mathbf{D} \equiv \epsilon_o \mathbf{E} + \mathbf{P} = \epsilon \mathbf{E} \tag{5}$$

$$\mathbf{B} \equiv \mu_o (\mathbf{H} + \mathbf{M}) = \mu \mathbf{H} \tag{6}$$

and ϵ and μ are assumed uniform throughout the region of interest.[1] Maxwell's equations in linear and isotropic media may be rewritten more simply

$$\nabla \cdot \epsilon \mathbf{E} = \rho_u \tag{7}$$

$$\nabla \times \mathbf{H} = \mathbf{J}_u + \frac{\partial}{\partial t} \epsilon \mathbf{E} \tag{8}$$

$$\nabla \times \mathbf{E} = -\frac{\partial}{\partial t} \mu \mathbf{H} \tag{9}$$

$$\nabla \cdot \mu \mathbf{H} = 0 \tag{10}$$

Our approach in this chapter is a continuation of the one used before. By expressing the fields in terms of superposition integrals, we emphasize the relationship between electrodynamic fields and their sources. Next we take into account the effect of conducting bodies upon the electromagnetic field, introducing the boundary value approach.

We began Chaps. 4 and 8 by expressing an irrotational $\mathbf{E}$ in terms of a scalar potential Φ and a solenoidal $\mathbf{B}$ in terms of a vector potential $\mathbf{A}$. We start this chapter in Sec. 12.1 with the generalization of these potentials to represent the electric and magnetic fields under electrodynamic conditions. Poisson's equation related Φ to its source in Chap. 4 and $\mathbf{A}$ to the current density $\mathbf{J}$ in Chap. 8. What equation relates these potentials to their sources when quasistatic approximations do not apply? In Sec. 12.1, we develop the inhomogeneous wave equation, which assumes the role played by Poisson's equation in the quasistatic cases. It follows from this equation that for linearly polarizable and magnetizable materials, the superposition principle applies to electrodynamics.

The fields associated with source singularities are the next topic, in analogy either with Chaps. 4 or 8. In Sec. 12.2, we start with the field of an elemental charge and build up the field of a dynamic electric dipole. Here we exemplify the launching of an electromagnetic wave and see how the quasistatic electric dipole fields relate to the more general electrodynamic fields. The section concludes by deriving the electrodynamic fields associated with a magnetic dipole from the fields

[1] To make any relation in this chapter apply to free space, let $\epsilon = \epsilon_o$ and $\mu = \mu_o$.

for an electric dipole by exploiting the symmetry of Maxwell's equations in source-free regions.

The superposition integrals developed in Sec. 12.3 provide particular solutions to the inhomogeneous wave equations, just as those of Chaps. 4 and 8, respectively, gave solutions to the scalar and vector Poisson's equations. In describing the operation of antennae, the fields that radiate away from the source are of primary interest. The superposition integrals for these radiation fields are used to find antenna radiation patterns in Sec. 12.4. The discussion of antennae is continued in Sec. 12.5, which has as a theme the complex form of Poynting's theorem. This theorem makes it possible to model the impedance of antennae as "seen" by their driving sources.

In Sec. 12.6, the field sources take the form of surface currents and surface charges. It is generally not convenient to find the associated fields by making direct use of the superposition integrals. Nevertheless, the sources are a "given," and any method that results in the associated fields amounts to solving the superposition integrals. This section provides a first view of the solutions to the wave equation in Cartesian coordinates that will be derived from the boundary value point of view in Chap. 13. In preparation for the boundary value approach of the next chapter, boundary conditions are satisfied by appropriate choices of sources. Thus, the parallel plate waveguide considered from the boundary value point of view in Chap. 13 is seen here from the point of view of waves initiated by given sources. The method of images, taken up in Sec. 12.7, provides further examples of this approach to satisfying boundary conditions.

When boundaries are introduced in this chapter, they are presumed to be perfectly conducting. In Chap. 13, the boundaries can also be interfaces between perfectly insulating dielectrics. In both of these chapters, the theme is dynamical phenomena related to the propagation and reflection of electromagnetic waves. The dynamics are characterized by one or more electromagnetic transit times, τ_{em}. Dynamical phenomena associated with charge relaxation or magnetic diffusion, characterized by τ_e and τ_m, are excluded. We will look at these again in Chaps. 14 and 15.

12.1 ELECTRODYNAMIC FIELDS AND POTENTIALS

In this section, we extend the use of the scalar and vector potentials to the description of electrodynamic fields. In regions of interest, the current density $\mathbf{J}$ of unpaired charge and the charge density ρ_u are prescribed functions of space and time. If there is any material present, it is of uniform permittivity ϵ and permeability μ, $\mathbf{D} = \epsilon\mathbf{E}$ and $\mathbf{B} = \mu\mathbf{H}$. For quasistatic fields in such regions, the potentials Φ and $\mathbf{A}$ are governed by Poisson's equation. In this section, we see the role of Poisson's equation for quasistatic fields taken over by the inhomogeneous wave equation for electrodynamic fields.

In both Chaps. 4 and 8, potentials were introduced so as to satisfy automatically the one of the two laws that was source free. In Chap. 4, we made $\mathbf{E} = -\nabla\Phi$ so that $\mathbf{E}$ was automatically irrotational, $\nabla \times \mathbf{E} = 0$. In Chap. 8 we let $\mathbf{B} = \nabla \times \mathbf{A}$ so that $\mathbf{B}$ was automatically solenoidal, $\nabla \cdot \mathbf{B} = 0$. Of the four laws comprising Maxwell's equations, (12.0.7)–(12.0.10), those of Gauss and Ampère involve

sources, while the last two, Faraday's law and the magnetic flux continuity law, do not. Following the approach used before, potentials should be introduced that automatically satisfy Faraday's law and the magnetic flux continuity law, (12.0.9) and (12.0.10). This is the objective of the following steps.

Given that the magnetic flux density remains solenoidal, the vector potential **A** can be defined just as it was in Chap. 8.

$$\boxed{\mathbf{B} = \mu\mathbf{H} = \nabla \times \mathbf{A}} \tag{1}$$

With $\mu\mathbf{H}$ represented in this way, (12.0.10) is again automatically satisfied and Faraday's law, (12.0.9), becomes

$$\nabla \times \big(\mathbf{E} + \frac{\partial \mathbf{A}}{\partial t}\big) = 0 \tag{2}$$

This expression is also automatically satisfied if we make the quantity in brackets equal to $-\nabla\Phi$.

$$\boxed{\mathbf{E} = -\nabla\Phi - \frac{\partial \mathbf{A}}{\partial t}} \tag{3}$$

With **H** and **E** defined in terms of Φ and **A** as given by (1) and (3), the last two of the four Maxwell's equations, (12.0.9–12.0.10), are automatically satisfied. Note, however, that the potentials that represent given fields **H** and **E** are not fully specified by (1) and (3). We can add to **A** the gradient of any scalar function, thus changing both **A** and Φ without affecting **H** or **E**. A further specification of the potentials will therefore be given shortly.

We now turn to finding the equations that **A** and Φ must obey if the laws of Gauss and Ampère, the first two of (12.0.9-12.0.10), are to be satisfied. Substitution of (1) and (3) into Ampère's law, (12.0.8), gives

$$\nabla \times (\nabla \times \mathbf{A}) = \mu\epsilon \frac{\partial}{\partial t}\big(-\nabla\Phi - \frac{\partial \mathbf{A}}{\partial t}\big) + \mu\mathbf{J}_u \tag{4}$$

A vector identity makes it possible to rewrite the left-hand side so that this equation is

$$\nabla(\nabla \cdot \mathbf{A}) - \nabla^2\mathbf{A} = \mu\epsilon \frac{\partial}{\partial t}\big(-\nabla\Phi - \frac{\partial \mathbf{A}}{\partial t}\big) + \mu\mathbf{J}_u \tag{5}$$

With the gradient and time derivative operators interchanged, this expression is

$$\nabla\big(\nabla \cdot \mathbf{A} + \mu\epsilon\frac{\partial \Phi}{\partial t}\big) - \nabla^2\mathbf{A} = -\mu\epsilon\frac{\partial^2 \mathbf{A}}{\partial t^2} + \mu\mathbf{J}_u \tag{6}$$

To uniquely specify **A**, we must not only stipulate its curl, but give its divergence as well. This point was made in Sec. 8.0. In Sec. 8.1, where we were concerned with MQS fields, we found it convenient to make **A** solenoidal. Here,

where we have kept the displacement current, we set the divergence of $\mathbf{A}$ so that the term in brackets on the left is zero.

$$\boxed{\nabla \cdot \mathbf{A} = -\mu\epsilon \frac{\partial \Phi}{\partial t}} \tag{7}$$

This choice of $\nabla \cdot \mathbf{A}$ is called the choice of the *Lorentz gauge*. In this gauge, the expression representing Ampère's law, (6), reduces to one involving $\mathbf{A}$ alone, to the exclusion of Φ.

$$\boxed{\nabla^2 \mathbf{A} - \mu\epsilon \frac{\partial^2 \mathbf{A}}{\partial t^2} = -\mu \mathbf{J}_u} \tag{8}$$

The last of Maxwell's equations, Gauss' law, is satisfied by making Φ obey the differential equation that results from the substitution of (3) into (12.0.7).

$$\nabla \cdot \epsilon\Big(-\nabla\Phi - \frac{\partial \mathbf{A}}{\partial t}\Big) = \rho_u \Rightarrow \nabla^2 \Phi + \frac{\partial}{\partial t}(\nabla \cdot \mathbf{A}) = -\frac{\rho_u}{\epsilon} \tag{9}$$

We can substitute for $\nabla \cdot \mathbf{A}$ using (7), thus eliminating $\mathbf{A}$ from this expression.

$$\boxed{\nabla^2 \Phi - \mu\epsilon \frac{\partial^2 \Phi}{\partial t^2} = -\frac{\rho_u}{\epsilon}} \tag{10}$$

In summary, with $\mathbf{H}$ and $\mathbf{E}$ defined in terms of the vector potential $\mathbf{A}$ and scalar potential Φ by (1) and (3), the distributions of these potentials are governed by the *vector and scalar inhomogeneous wave equations* (8) and (10), respectively. The *unpaired* charge density and the *unpaired* current density are the "sources" in these equations. In representing the fields in terms of the potentials, it is understood that the "gauge" of $\mathbf{A}$ has been set so that $\mathbf{A}$ and Φ are related by (7).

The time derivatives in (8) and (10) are the result of retaining both the displacement current and the magnetic induction. Thus, in the quasistatic limits, these terms are neglected and we return to vector and scalar potentials governed by Poisson's equation.

Superposition Principle. The inhomogeneous wave equations satisfied by $\mathbf{A}$ and Φ [(8) and (10)] as well as the gauge condition, (7), are linear when the sources on the right are prescribed. That is, if solutions $\mathbf{A_a}$ and Φ_a are associated with sources $\mathbf{J}_a$ and ρ_a,

$$(\mathbf{J}_a,\ \rho_a) \Rightarrow (\mathbf{A}_a,\ \Phi_a) \tag{11}$$

and similarly, $\mathbf{J}_b$ and ρ_b produce the potentials $\mathbf{A}_b$, Φ_b,

$$(\mathbf{J}_b,\ \rho_b) \Rightarrow (\mathbf{A}_b,\ \Phi_b) \tag{12}$$

then the potentials resulting from the sum of the sources is the sum of the potentials.

$$[(\mathbf{J}_a + \mathbf{J}_b),\ (\rho_a + \rho_b)] \Rightarrow [(\mathbf{A}_a + \mathbf{A}_b),\ (\Phi_a + \Phi_b)] \tag{13}$$

The formal proof of this superposition principle follows from the same reasoning used for Poisson's equation in Sec. 4.3.

In prescribing the charge and current density on the right in (8) and (10), it should be remembered that these sources are related by the law of charge conservation. Thus, although Φ and $\mathbf{A}$ appear in (8) and (10) to be independent, they are actually coupled. This interdependence of the sources is reflected in the link between the scalar and vector potentials established by the gauge condition of (7). Once $\mathbf{A}$ has been found, it is often convenient to use this relation to determine Φ.

Continuity Conditions. Each of Maxwell's equations, (12.0.7)–(12.0.10), as well as the charge conservation law obtained by combining the divergence of Ampère's laws with Gauss' law, implies a continuity condition. In the absence of polarization and magnetization, these conditions were derived from the integral laws in Chap. 1. Generalized to include polarization and magnetization in Chaps. 6 and 9, the continuity conditions for (12.0.7)–(12.0.10) are, respectively,

$$\mathbf{n} \cdot (\epsilon_a \mathbf{E}^a - \epsilon_b \mathbf{E}^b) = \sigma_{su} \tag{14}$$

$$\mathbf{n} \times (\mathbf{H}^a - \mathbf{H}^b) = \mathbf{K}_u \tag{15}$$

$$\mathbf{n} \times (\mathbf{E}^a - \mathbf{E}^b) = 0 \tag{16}$$

$$\mathbf{n} \cdot (\mu_a \mathbf{H}^a - \mu_b \mathbf{H}^b) = 0 \tag{17}$$

The derivation of these conditions is the same as given at the end of the sections introducing the respective integral laws in Chap. 1, except that $\mu_o \mathbf{H}$ is replaced by $\mu \mathbf{H}$ in Faraday's law and $\epsilon_o \mathbf{E}$ by $\epsilon \mathbf{E}$ in Ampère's law.

In Secs. 12.6 and 12.7, and in the following chapters, these conditions are used to relate electrodynamic fields to surface currents and surface charges. At the outset, we recognize that two of these continuity conditions are, like Faraday's law and the law of magnetic flux continuity, not independent of each other. Further, just as the laws of Ampère and Gauss imply the charge conservation relation between $\mathbf{J}_u$ and ρ_u, the continuity conditions associated with these laws imply the charge conservation continuity condition obeyed by the surface currents and surface charge densities.

To see the first interdependence, Faraday's law is integrated over a surface S enclosed by a contour C *lying in the plane of the interface*, as shown in Fig. 12.1.1a. Stokes' theorem is then used to write

$$\oint_C \mathbf{E} \cdot d\mathbf{s} = -\frac{d}{dt} \int_S \mu \mathbf{H} \cdot d\mathbf{a} \tag{18}$$

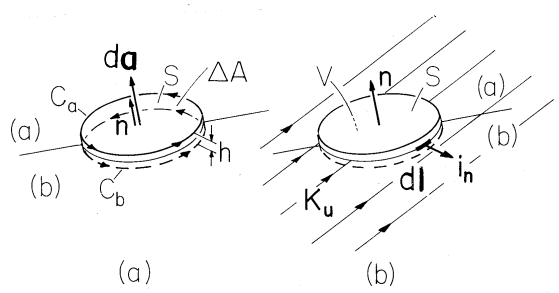


Fig. 12.1.1 (a) Surface S just above or just below the interface. (b) Volume V of incremental thickness h enclosing a section of the interface.

Whether taken on side (a) or side (b) of the interface, the line integral on the left is the same. This follows from Faraday's continuity law (16). Thus, if we take the difference between (18) evaluated on side (a) and on side (b), we obtain

$$\frac{d}{dt}(\mu_a \mathbf{H}^a - \mu_b \mathbf{H}^b) \cdot \mathbf{n} = 0 \tag{19}$$

By making the tangential electric field continuous, we have assured the continuity of the time derivative of the normal magnetic flux density. *For a sinusoidally time-dependent process, matching the tangential electric field automatically assures the matching of the normal magnetic flux densities.*

In particular, consider a surface of a conductor that is "perfect" in the MQS sense. The electric field inside such a conductor is zero. From (16), the tangential component of **E** just outside the conductor must also be zero. In view of (19), we conclude that the normal flux density at a perfectly conducting surface must be time independent. This boundary condition is familiar from the last half of Chap. 8.[2]

Given that the divergence of Ampère's law combines with Gauss' law to give conservation of charge,

$$\nabla \cdot \mathbf{J}_u + \frac{\partial \rho_u}{\partial t} = 0 \tag{20}$$

we should expect that there is a second relationship among the conditions of (14)–(17), this time between the surface charge density and surface current density that appear in the first two. Integration of (20) over the volume of the "pillbox" shown in Fig. 12.1.1b gives

$$\lim_{\substack{h \to 0 \\ \Delta A \to 0}} \left[\oint_S \mathbf{J}_u \cdot d\mathbf{a} + \frac{d}{dt} \int_V \rho_u dV \right] = 0 \tag{21}$$

In the limit where first the thickness h and then the area ΔA go to zero, these integrals reduce to ΔA times

$$\mathbf{n} \cdot (\mathbf{J}_u^a - \mathbf{J}_u^b) + \nabla_\Sigma \cdot \mathbf{K}_u + \frac{\partial \sigma_u}{\partial t} = 0 \tag{22}$$

[2] Note that the absence of a time-varying normal flux density does not imply that there is no tangential **E**. The surface of a material that is an infinite conductor in one direction but an insulator in the other might have no normal $\mu\mathbf{H}$ and yet support a tangential **E** in the direction of zero conductivity.

The first term is the contribution to the first integral in (21) from the surfaces on the (a) and (b) sides of the interface, respectively, having normals $+\mathbf{n}$ and $-\mathbf{n}$. The second term, which is written in terms of the "surface divergence" defined in terms of a vector $\mathbf{F}$ by

$$\nabla_\Sigma \cdot \mathbf{F} \equiv \lim_{\Delta A \to 0} \oint_C \mathbf{F} \cdot \mathbf{i}_n dl \tag{23}$$

results because the surface current density makes a finite contribution to the first integral in (21) even though the thickness h of the volume goes to zero. [In (23), $\mathbf{i}_n$ is the unit normal to the volume V, as shown in the figure.] Such a surface current density can be used to represent currents imposed over a region having a thickness that is small compared to other dimensions of interest. It can also represent the current on the surface of a perfect conductor. (In using the conservation of charge continuity condition in Secs. 7.6 and 7.7, this term was not present because the surfaces described by this continuity condition were not carrying surface currents.) In terms of coordinates local to the point of interest, the surface divergence can be thought of as a two-dimensional divergence. The last term in (22) results from the integration of the charge density over the volume. Because there is a surface charge density, there is net charge inside the volume even in the limit where $h \to 0$.

When we specify $\mathbf{K}_u$ and σ_u in (14) and (15), it is with the understanding that they obey the charge conservation continuity condition, (22). But, we also conclude that the charge conservation law is implied by the laws of Ampère and Gauss, and so we know that if (14) and (15) are satisfied, then so too is (22).

When perfectly conducting boundaries are described in Chaps. 13 and 14, the surface current and charge found on a perfectly conducting boundary using the continuity conditions from the laws of Ampère and Gauss will automatically satisfy the charge conservation condition. Further, a zero tangential electric field on a perfect conductor automatically implies that the normal magnetic flux density vanishes.

With the inhomogeneous wave equation playing the role of Poisson's equation, the stage is now set for a scenario paralleling that for electroquasistatics in Chap. 4 and for magnetoquasistatics in Chap. 8. The next section identifies the fields associated with source singularities. Section 12.3 develops superposition integrals for the response to given distributions of the sources. Henceforth, in this and the next chapter, we shall drop the subscript u from the source quantities.

12.2 ELECTRODYNAMIC FIELDS OF SOURCE SINGULARITIES

Given the response to an elemental source, the fields associated with an arbitrary distribution of sources can be found by superposition. This approach will be formalized in the next section and can be utilized for determining the radiation patterns of many antenna arrays. The fields resulting from this superposition principle form a particular solution that can be combined with solutions to the homogeneous wave equation to satisfy the boundary conditions imposed by perfectly conducting boundaries.

We begin by identifying the potential Φ associated with a time varying point charge $q(t)$. In a closed system, where the net charge is invariant, an increase in

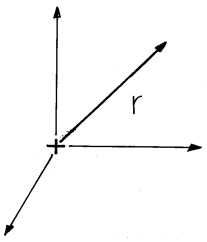


Fig. 12.2.1 A point charge located at the origin of a spherical coordinate system.

charge at one point must be compensated by a decrease in charge elsewhere. Thus, as we shall see in identifying the fields of an electric dipole, physically meaningful fields are the superposition of those produced by at least two point charges of opposite sign. Conservation of charge further requires that this shift in the distribution of net charge from one region to another be accounted for by a current. This current is the source term in the inhomogeneous wave equation for the vector potential.

Potential of a Point Charge. Consider the potential Φ predicted by the inhomogeneous wave equation, (12.1.10), for a time varying point charge $q(t)$ located at the origin of the spherical coordinate system shown in Fig. 12.2.1.

By definition, ρ is zero everywhere except at the origin, where it is singular.[3] In the immediate neighborhood of the origin, we should expect that the potential varies so rapidly with r that the Laplacian would dominate the second time derivative in the inhomogeneous wave equation, (12.1.10). Then, in the vicinity of the origin, we should expect the potential for a point charge to be the same as for Poisson's equation, namely $q(t)/(4\pi\epsilon r)$ (4.4.1). From Sec. 3.1, we have a hint as to how the combined effects of the magnetic induction and electric displacement current represented by the second time derivative in the inhomogeneous wave-equation, (12.1.10), should affect this potential. We can expect that the response at a radial position r will be delayed by the time required for an electromagnetic wave to reach that position from the origin. For a wave propagating at the velocity c, this time is r/c. Thus, we make the educated guess that the solution to (12.1.10) for a point charge at the origin is

$$\Phi = \frac{q\left(t - \frac{r}{c}\right)}{4\pi\epsilon r} \tag{1}$$

where $c = 1/\sqrt{\mu\epsilon}$. According to (1), given that the time dependence of the point charge is $q(t)$, the potential at radius r is given by the familiar potential for a point charge, provided that $t \to (t - r/c)$.

Verification that Φ of (1) is a solution to the inhomogeneous wave equation (12.1.10) takes two steps. First, the expression is substituted into the *homogeneous* wave equation [(12.1.10) with no source] to see that it is satisfied everywhere except at the origin. In carrying out this step, note that Φ is a function of the spherical

[3] Of course, charge conservation requires that there be a current supplying this time-varying charge and that through action of this current, if charge accumulates at the origin, there must be a reduction of charge somewhere else. The simplest example of a source obeying charge conservation is the dipole.

radial coordinate r alone. Thus, $\nabla^2\Phi$ is simply $r^{-2}\partial(r^2\partial\Phi/\partial r)/\partial r$. This operation gives the same result as the operation $r^{-1}\partial^2(r\Phi)/\partial r^2$. Thus, evaluated using the potential of (1), the terms on the left in the inhomogeneous wave equation, (12.1.10), become

$$\nabla^2\Phi - \frac{1}{c^2}\frac{\partial^2\Phi}{\partial t^2} = \frac{1}{4\pi\epsilon}\left[\frac{1}{r}\frac{\partial^2}{\partial r^2}q\big(t-\frac{r}{c}\big) - \frac{1}{r}\frac{1}{c^2}\frac{\partial^2}{\partial t^2}q\big(t-\frac{r}{c}\big)\right] = 0 \tag{2}$$

for $r \neq 0$. In carrying out this evaluation, note that $\partial q/\partial r = -q'/c$ and $\partial q/\partial t = q'$ where the prime indicates a derivative with respect to the argument. Thus, the homogeneous wave equation is satisfied everywhere except at the origin.

In the second step, we confirm that (1) is the dynamic potential of a point charge. We integrate the inhomogeneous wave equation in the neighborhood of $r = 0$, (12.1.10), over a small spherical volume of radius r centered on the origin.

$$\int_V \Big(-\nabla\cdot\nabla\Phi + \mu\epsilon\frac{\partial^2\Phi}{\partial t^2}\Big)dv = \int_V \frac{\rho}{\epsilon}dv \tag{3}$$

The Laplacian has been written in terms of its definition in anticipation of using Gauss' theorem to convert the first integral to one over the surface at r. In the limit where r is small, the integration of the second time derivative term gives no contribution.

$$\begin{aligned}\int_V \mu\epsilon\frac{\partial^2\Phi}{\partial t^2}dv &= \mu\epsilon\frac{\partial^2}{\partial t^2}\lim_{r\to 0}\int_V \Phi dv \\ &= \mu\epsilon\frac{\partial^2}{\partial t^2}\lim_{r\to 0}\int_0^r \frac{q4\pi r^2}{4\pi\epsilon r}dr = 0\end{aligned} \tag{4}$$

Integration of the first term on the left in (3) is familiar from Chap. 4, because Gauss' theorem converts the volume integration to one over the enclosing surface and we therefore have

$$\begin{aligned}-\int \nabla\cdot\nabla\Phi dv &= -\oint_S \nabla\Phi\cdot d\mathbf{a} = -4\pi r^2\frac{\partial\Phi}{\partial r} \\ &= -4\pi r^2\big(-\frac{q}{4\pi\epsilon r^2}\big) = \frac{q}{\epsilon}\end{aligned} \tag{5}$$

In the limit where $r \to 0$, the integral on the right in (3) gives q/ϵ. Thus, it reduces to the same expression obtained using (1) to evaluate the left-hand side of (3). We conclude that (1) is indeed the solution to the inhomogeneous wave equation for a point charge at the origin.

Electric Dipole Field. An electric dipole consists of a pair of charges $\pm q(t)$ separated by the distance d, as shown in Fig. 12.2.2. As one charge increases in magnitude at the expense of the other, there is an elemental current $i(t)$ directed between the two along the z axis. Charge conservation requires that

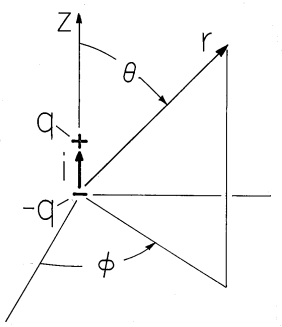


Fig. 12.2.2 A dynamic dipole in which the time-variation of the charge is accounted for by the elemental current $i(t)$.

$$\boxed{i = \frac{dq}{dt}} \tag{6}$$

This current can be pictured as a singularity in the distribution of the current density J_z. In fact, the role played by ρ/ϵ as the source of Φ on the right in (12.1.10) is played by μJ_z in determining A_z in (12.1.8). Just as q can be regarded as the integral of the charge density ρ over the elemental volume occupied by that charge density, μid is μJ_z first integrated over the cross-sectional area in the $x-y$ plane of the current tube joining the charges (to give μi) and then integrated over the length d of the tube. Thus, we exploit the analogy between the z component of the vector inhomogeneous wave equation for A_z and that for Φ, (12.1.8) and (12.1.10), to write the vector potential associated with an incremental current element at the origin. The solution to (12.1.8) is the same as that to (12.1.10) with $q/\epsilon \to \mu id$.

$$\boxed{A_z = \frac{\mu d i\left(t - \frac{r}{c}\right)}{4\pi r}} \tag{7}$$

Remember that r is a spherical coordinate, so it is best to convert this expression into spherical coordinates. Figure 12.2.3 shows that

$$A_r = A_z \cos\theta; \qquad A_\theta = -A_z \sin\theta \tag{8}$$

Thus, in spherical coordinates, (7) becomes the vector potential for an electric dipole.

$$\mathbf{A} = \frac{\mu d}{4\pi}\left[\frac{i\left(t - \frac{r}{c}\right)}{r}\cos\theta \mathbf{i}_\mathbf{r} - \frac{i\left(t - \frac{r}{c}\right)}{r}\sin\theta \mathbf{i}_\theta\right] \tag{9}$$

The dipole scalar potential is the superposition of the potentials due to the individual charges, (5). The positive charge is located on the z axis at $z = d$, while the negative one is at the origin, so superposition gives

$$\Phi = \frac{1}{4\pi\epsilon}\left\{\frac{q\left[t - \left(\frac{r}{c} - \frac{d}{c}\cos\theta\right)\right]}{r - d\cos\theta} - \frac{q\left[t - \frac{r}{c}\right]}{r}\right\} \tag{10}$$

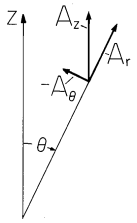


Fig. 12.2.3 The z-directed potential is analyzed into its components in spherical coordinates.

where, in a way familiar from Sec. 4.4, the distance from the point of observation to the charge at $z = d$ is approximated by $r - d\cos\theta$. With q' indicating a derivative with respect to the argument, expansion in a Taylor's series based on $d\cos\theta \ll r$ gives

$$\Phi \simeq \frac{1}{4\pi\epsilon}\left\{\left(\frac{1}{r}+\frac{d\cos\theta}{r^2}\right)q\big(t-\frac{r}{c}\big)+\frac{d}{c}\frac{\cos\theta}{r}q'\big(t-\frac{r}{c}\big)-\frac{q\big(t-\frac{r}{c}\big)}{r}\right\} \tag{11}$$

and keeping terms that are linear in d results in the desired scalar potential for the electric dipole.

$$\Phi = \frac{d}{4\pi\epsilon}\left[\frac{q\big(t-\frac{r}{c}\big)}{r^2}+\frac{q'\big(t-\frac{r}{c}\big)}{cr}\right]\cos\theta \tag{12}$$

The vector potential (9) and scalar potential (12) obey (12.1.7), as can be confirmed by differentiation and use of the conservation law (6). We can now evaluate the magnetic and electric fields associated with these scalar and vector potentials. The magnetic field intensity follows by evaluating (12.1.1) using (9). [Remember that conservation of charge requires that $q' = i$, in accordance with (6).]

$$\boxed{\mathbf{H} = \frac{d}{4\pi}\left[\frac{i'\big(t-\frac{r}{c}\big)}{cr}+\frac{i\big(t-\frac{r}{c}\big)}{r^2}\right]\sin\theta\mathbf{i}_\phi} \tag{13}$$

To find $\mathbf{E}$, (12.1.3) is evaluated using (9) and (12).

$$\boxed{\begin{aligned}\mathbf{E} = \frac{d}{4\pi\epsilon}\Bigg\{&2\left[\frac{q\big(t-\frac{r}{c}\big)}{r^3}+\frac{q'\big(t-\frac{r}{c}\big)}{cr^2}\right]\cos\theta\mathbf{i}_\mathbf{r}\\&+\left[\frac{q\big(t-\frac{r}{c}\big)}{r^3}+\frac{q'\big(t-\frac{r}{c}\big)}{cr^2}+\frac{q''\big(t-\frac{r}{c}\big)}{c^2r}\right]\sin\theta\mathbf{i}_\theta\Bigg\}\end{aligned}} \tag{14}$$

As can be seen by comparing (14) to (4.4.10), in the limit where $c \to \infty$, this electric field becomes the electric field found from the electroquasistatic dipole potential. Note that the quasistatic field is proportional to q (rather than its first or second temporal derivative) and decays as $1/r^3$. The first and second time derivatives of q are of order q/τ and q/τ^2 respectively, where τ is the typical time interval

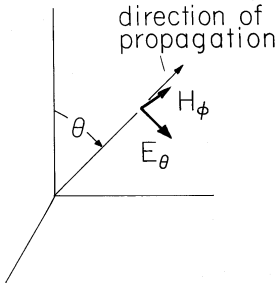


Fig. 12.2.4 Far fields constituting a plane wave propagating in the radial direction.

within which q experiences an appreciable change. Thus, these time derivative terms are small compared to the quasistatic terms if $r/c \ll \tau$. What we have found gives substance to the arguments given for the EQS approximation in Sec. 3.3. That is, we have found that the quasistatic approximation is justified if the condition of (3.3.5) prevails.

The combination of electric displacement current and magnetic induction leading to the inhomogeneous wave equation has three dramatic effects on the dipole fields. First, the response at a location r is delayed[4] by the transit time r/c. Second, the electric field is not only proportional to $q(t-r/c)$, but also to $q'(t-r/c)$ and $q''(t-r/c)$. Third, the part of the electric field that is proportional to q'' decreases with radius in proportion to $1/r$. Associated with this "far field" is a magnetic field, the first term in (13), that similarly decreases as $1/r$. Together, these fields comprise an electromagnetic wave propagating radially outward from the dipole antenna.

$$\begin{aligned} \lim_{r\to\infty} \mathbf{H} &\to \frac{d}{4\pi}\frac{i'\left(t-\frac{r}{c}\right)\sin\theta \mathbf{i}_\phi}{cr} \\ \lim_{r\to\infty} \mathbf{E} &\to \frac{d}{4\pi\epsilon}\frac{q''\left(t-\frac{r}{c}\right)}{c^2 r}\sin\theta \mathbf{i}_\theta \end{aligned} \tag{15}$$

Note that these field components are orthogonal to each other and transverse to the radial direction of propagation, as shown in Fig. 12.2.4.

To appreciate the significance of the $1/r$ dependence of the fields in (15), consider the Poynting flux, (11.2.9), associated with these fields.

$$\lim_{r\to\infty}[\mathbf{E}\times\mathbf{H}] = \left(\frac{d}{4\pi}\right)^2\sqrt{\mu/\epsilon}\frac{\left[q''\left(t-\frac{r}{c}\right)\right]^2}{c^2 r^2}\sin^2\theta \tag{16}$$

The power flow out through a spherical surface at the radius r follows from this expression as

$$\begin{aligned} P = \oint \mathbf{E}\times\mathbf{H}\cdot d\mathbf{a} &= \int_0^\pi \left(\frac{d}{4\pi}\right)^2\sqrt{\mu/\epsilon}\frac{(q'')^2}{c^2 r^2}\sin^2\theta 2\pi r^2\sin\theta d\theta \\ &= \frac{d^2}{6\pi}\sqrt{\mu/\epsilon}\frac{\left[q''\left(t-\frac{r}{c}\right)\right]^2}{c^2} \end{aligned} \tag{17}$$

[4] In addition to the retarded response highlighted here, an "advanced" response, where $t-r/c \to t+r/c$, is also a solution to the inhomogeneous wave equation. Because it does not fit with our idea of causality, it is not used here.

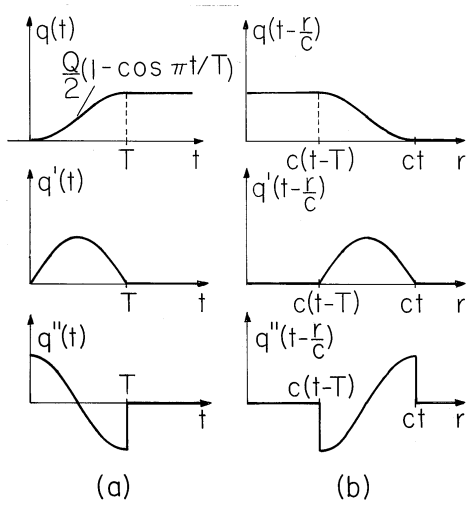


Fig. 12.2.5 (a) Time dependence of the dipole charge $q(t)$ as well as its first and second derivatives. (b) The radial dependence of the functions needed to evaluate the dipole fields resulting from the turn-on transient of (a) when $t > T$.

Because the far fields of the dipole vary as $1/r$, and hence the power flux density is proportional to $1/r^2$, and because the area of the surface at r increases as r^2, we conclude that there is a net power flowing outward from the dipole at infinity. These far field components are called the *radiation field.*

Example 12.2.1. Turn-on Fields of an Electric Dipole

To help establish the physical significance of the electric dipole expressions for **E** and **H**, (13) and (14), consider the fields associated with charging an electric dipole through the transient shown in Fig. 12.2.5a. Over a period T, the charge increases from zero to Q with a continuous first derivative but a second derivative that suffers a finite discontinuity, as shown in the figure. Multiplied by appropriate factors of $1/r$, $1/r^2$, and $1/r^3$, the field distributions are made up of these three functions, with t replaced by $t - r/c$. Thus, at a given instant in time, the factors $q(t - r/c)$, $q'(t - r/c)$, and $q''(t - r/c)$ have the radial distributions shown in Fig. 12.2.5b.

The electric and magnetic fields are shown at three successive instants in time in Fig. 12.2.6. The transient part of the field is confined to an annular region with its outside radius at $r = ct$ (the wave front) and inner radius at $r = c(t - T)$. Inside this latter radius, the fields are static and composed only of those terms varying as $1/r^3$. Thus, when $t = T$ (Fig. 12.2.6a), all of the field is transient, because the source has just reached a constant state. At the subsequent times $t = 2T$ and $t = 3T$, the fields left behind by the outward propagating rear of the wave transient, the **E** field of a static electric dipole and $\mathbf{H} = \mathbf{0}$, are as shown in Figs. 12.2.6b and 6c.

The flow of charges to the poles of the dipole produces an electromagnetic wave which reveals its identity once the annular region of the transient fields propagates out of the range of the near field. Note that the electric and magnetic fields shown in the outward propagating wave of Fig. 12.2.6c are mutually sustaining. In accordance with Faradays' law, the curl of **E**, which is ϕ directed and tends to be largest midway

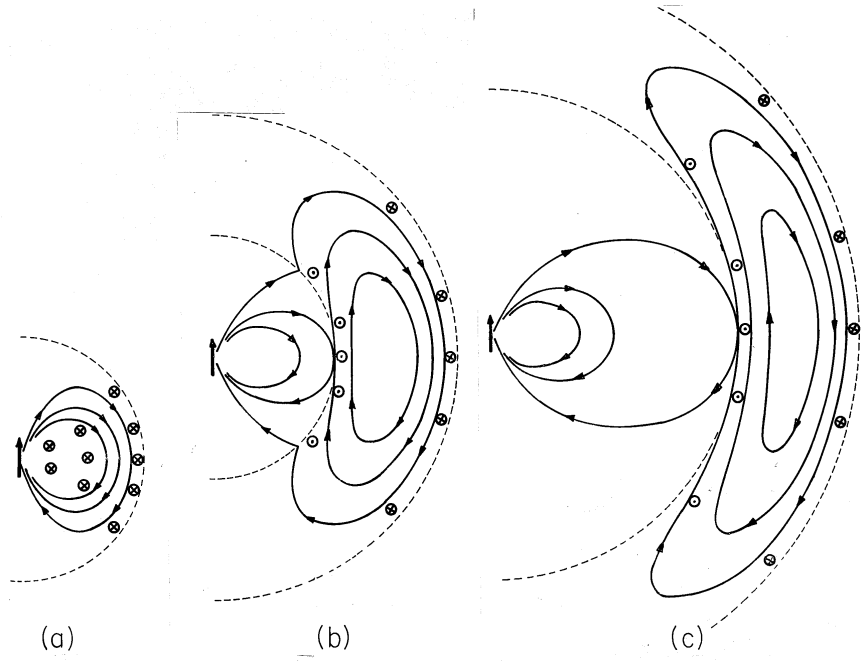


Fig. 12.2.6 Electric fields (solid lines) and magnetic fields resulting from turning on an electric dipole in accordance with the temporal dependence indicated in Fig. 12.2.5. The fields are zero outside the wave front indicated by the outermost broken line. (a) For $t < T$, the entire field is in a transient state. (b) By the time $t > T$, the fields due to the transient are seen to be propagating outward between the expanding spherical surfaces at $r = ct$ and $r = c(t - T)$. Inside the latter surface, which is also indicated by a broken line, the fields are static. (c) At still later times, the propagating wave divorces itself from the dipole as the electric field generated by the magnetic induction, and the magnetic field generated by the displacement current, become self-sustaining.

between the front and back of the wave, is balanced by a time rate of change of $\mathbf{B}$ which also has its largest value in the same region.[5] Similarly, to satisfy Ampère's law, the θ-directed curl of $\mathbf{H}$, which also peaks midway between the front and back of the wave, is balanced by a time rate of change of $\mathbf{D}$ that peaks in the same region.

It is instructive to review the discussion given in Sec. 3.3 of EQS and MQS approximations and their relation to electromagnetic waves. The electric dipole considered here in detail is the prototype system sketched in Fig. 3.3.1a. We have indeed found that if the condition of (3.3.5) is met, the EQS fields dominate. We should expect that if the current carried by the elemental loop of the prototype MQS system of Fig. 3.3.1b is a rapidly varying function of time, then the magnetic dipole (considered in the MQS limit in Sec. 8.3) also gives rise to a radiation field

[5] In discerning a time rate of change implied by the figure, remember that the fields in the region of the spherical shell indicated by the two broken-line circles in Figs. 12.2.6b and 12.2.6c are propagating outward.

much like that discussed here. These fields are considered at the conclusion of this section.

Electric Dipole in the Sinusoidal Steady State. In the sections that follow, the fields of the electric dipole will be superimposed to obtain field patterns from antennae used at radio and microwave frequencies. In most of these practical situations, the field sources, q and i, are essentially in the sinusoidal steady state. In particular,

$$i = \text{Re } \hat{i}e^{j\omega t} \tag{18}$$

where $\hat{i}$ is a complex number representing both the phase and amplitude of the current. Then, the general expression for the vector potential of the electric dipole, (7), becomes

$$A_z = \text{Re } \frac{\mu d\hat{i}}{4\pi r} e^{j\omega(t-\frac{r}{c})} \tag{19}$$

Separation of the time dependence from the space dependence in solving the inhomogeneous wave equation is accomplished by the use of complex vector functions of space multiplied by $\exp j\omega t$. With the understanding that the time dependence is recovered by multiplying by $\exp(j\omega t)$ and taking the real part, we will now deal with the complex amplitudes of the fields and drop the factor $\exp j\omega t$. Thus, (19) becomes

$$A_z = \text{Re } \hat{A}_z e^{j\omega t}; \qquad \hat{A}_z = \frac{\mu d\hat{i}}{4\pi} \frac{e^{-jkr}}{r} \tag{20}$$

where the *wave number* $k \equiv \omega/c$.

In terms of complex amplitudes, the magnetic and electric field intensities of the electric dipole follow from (13) and (14) as [by substituting $q \rightarrow \text{Re } (\hat{i}/j\omega) \exp(-jkr) \exp(j\omega t)$]

$$\hat{\mathbf{H}} = j\frac{kd\hat{i}}{4\pi}\left(\frac{1}{jkr} + 1\right) \sin\theta \frac{e^{-jkr}}{r} \mathbf{i}_\phi \tag{21}$$

$$\begin{aligned} \hat{\mathbf{E}} = & j\frac{kd\hat{i}}{4\pi}\sqrt{\mu/\epsilon}\left\{2\left[\frac{1}{(jkr)^2} + \frac{1}{jkr}\right]\cos\theta \mathbf{i}_\mathbf{r}\right. \\ & \left. + \left[\frac{1}{(jkr)^2} + \frac{1}{jkr} + 1\right]\sin\theta \mathbf{i}_\theta\right\}\frac{e^{-jkr}}{r} \end{aligned} \tag{22}$$

The far fields are given by terms with the $1/r$ dependence.

$$\boxed{\hat{H}_\phi = j\frac{kd\hat{i}}{4\pi}\sin\theta\frac{e^{-jkr}}{r}} \tag{23}$$

$$\boxed{\hat{E}_\theta = \sqrt{\mu/\epsilon}\hat{H}_\phi} \tag{24}$$

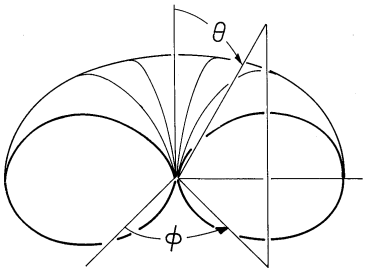


Fig. 12.2.7 Radiation pattern of short electric dipole, shown in the range $\pi/2 < \phi < 3\pi/2$.

These fields, which are a special case of those pictured in Fig. 12.2.4, propagate radially outward. The far field pattern is a radial progression of the fields shown between the broken lines in Fig. 12.2.6c. (The response shown is the result of one half of a cycle.)

It follows from (23) and (24) that for a short dipole in the sinusoidal steady state, the power radiated per unit solid angle is[6]

$$\frac{4\pi r^2\langle S_r\rangle}{4\pi} = r^2\frac{1}{2}\mathrm{Re}\,\hat{\mathbf{E}}\times\hat{\mathbf{H}}^*\cdot\mathbf{i_r} = \frac{1}{2}\sqrt{\mu/\epsilon}\frac{(kd)^2}{(4\pi)^2}|\hat{i}|^2\sin^2\theta \tag{25}$$

Equation (25) expresses the dependence of the radiated power on the direction (θ,ϕ), and can be called the radiation pattern. Often, only the functional dependence, $\Psi(\theta,\phi)$ is identified with the "radiation pattern." In the case of the short electric dipole,

$$\Psi(\theta,\phi) = \sin^2\theta \tag{26}$$

and the radiation pattern is as shown in Fig. 12.2.7.

The Far-Field and Uniformly Polarized Plane Waves. For an observer far from the dipole, the variation of the field with respect to radius is more noticeable than that with respect to the angle θ. Further, if kr is large, the radial variation represented by $\exp(-jkr)$ dominates over the much weaker dependence due to the factor $1/r$. This term makes the fields tend to repeat themselves every wavelength $\lambda = 2\pi/k$. At frequencies of the order used for VHF television, the wavelength is on the order of a meter, while the station antenna is typically kilometers away. Thus, over the dimensions of a receiving antenna, the variations due to the factor $1/r$ and the θ variation in (23) and (24) are insignificant. By contrast, the receiving antenna has dimensions on the order of λ, and so the radial variation represented by $\exp(-jkr)$ is all-important. Far from the dipole, where spatial variations transverse to the radial direction of propagation are unimportant, and where the slow decay due to the $1/r$ term is negligible, the fields take the form of *uniform plane waves*. With the local spherical coordinates replaced by Cartesian coordinates, as shown in Fig. 12.2.8, the fields then take the form

$$\mathbf{E} = E_z(y,t)\mathbf{i_z}; \qquad \mathbf{H} = H_x(y,t)\mathbf{i_x} \tag{27}$$

[6] Here we use the time average theorem of (11.5.6).

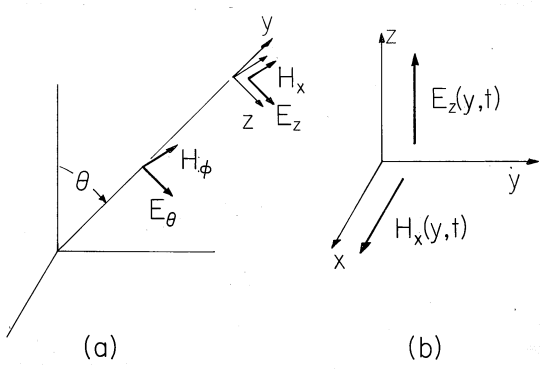


Fig. 12.2.8 (a) Radiation field of electric dipole. (b) Cartesian representation in neighborhood of remote point.

That is, the fields depend only on y, which plays the role of r, and are directed transverse to y. Instead of the far fields given by (15), we have traveling-wave fields that, by virtue of their independence of the transverse coordinates, are called *plane waves*. To emphasize that the dipole has indeed launched a plane wave, in (15) we replace

$$\frac{d}{4\pi\epsilon}\frac{q''(t-\frac{r}{c})}{c^2 r}\sin\theta \rightarrow E_+(t-\frac{y}{c}) \tag{28}$$

and recognize that $i' = q''$, (6), so that

$$\mathbf{E} = E_+(t-\frac{y}{c})\mathbf{i_z}; \qquad \mathbf{H} = \sqrt{\epsilon/\mu}E_+(t-\frac{y}{c})\mathbf{i_x} \tag{29}$$

The dynamics of such plane waves are described in Chap. 14. Note that the ratio of the magnitudes of $\mathbf{E}$ and $\mathbf{H}$ is the *intrinsic impedance* $\zeta \equiv \sqrt{\mu/\epsilon}$. In free space, $\zeta = \zeta_o \equiv \sqrt{\mu_o/\epsilon_o} \approx 377\Omega$.

Magnetic Dipole Field. Given the magnetic and electric fields of an electric dipole, (13) and (14), what are the electrodynamic fields of a magnetic dipole? We answer this question by exploiting a far-reaching property of Maxwell's equations, (12.0.7)–(12.0.10), as they apply where $\mathbf{J}_u = 0$ and $\rho_u = 0$. In such regions, Maxwell's equations are replicated by replacing $\mathbf{H}$ by $-\mathbf{E}$, $\mathbf{E}$ by $\mathbf{H}$, ϵ by μ, and μ by ϵ. It follows that because (13) and (14) are solutions to Maxwell's equations, then so are the fields.

$$\mathbf{E} = -\frac{d}{4\pi}(\frac{q''_m}{cr} + \frac{q'_m}{r^2})\sin\theta\mathbf{i}_\phi \tag{30}$$

$$\mathbf{H} = \frac{d}{4\pi\mu}\left[2(\frac{q_m}{r^3} + \frac{q'_m}{cr^2})\cos\theta\mathbf{i_r} + (\frac{q_m}{r^3} + \frac{q'_m}{cr^2} + \frac{q''_m}{c^2 r})\sin\theta\mathbf{i}_\theta\right] \tag{31}$$

Of course, q_m must now be interpreted as a source of divergence of $\mathbf{H}$, i.e., a magnetic charge. Substitution shows that these fields do indeed satisfy Maxwell's equations with $\mathbf{J} = 0$ and $\rho = 0$, except at the origin. To discover the source singularity at the origin giving rise to these fields, they are examined in the limit

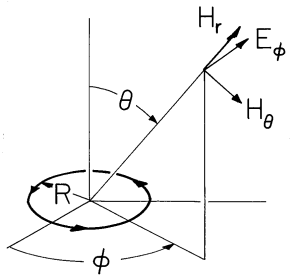


Fig. 12.2.9 Magnetic dipole giving rise to the fields of (33) and (34).

where $r \to 0$. Observe that in the neighborhood of the origin, terms proportional to $1/r^3$ dominate $\mathbf{H}$ as given by (31). Close to the source, $\mathbf{H}$ takes the form of a magnetic dipole. This can be seen by a comparison of this near field to that given by (8.3.20) for a magnetic dipole.

$$dq_m\big(t-\frac{r}{c}\big)=\mu m\big(t-\frac{r}{c}\big) \tag{32}$$

With this identification of the source, (30) and (31) become

$$\boxed{\mathbf{E}=-\frac{\mu}{4\pi}\left[\frac{m''\big(t-\frac{r}{c}\big)}{cr}+\frac{m'\big(t-\frac{r}{c}\big)}{r^2}\right]\sin\theta\mathbf{i}_\phi} \tag{33}$$

$$\boxed{\begin{aligned}\mathbf{H}=\frac{1}{4\pi}\Bigg\{&2\left[\frac{m\big(t-\frac{r}{c}\big)}{r^3}+\frac{m'\big(t-\frac{r}{c}\big)}{cr^2}\right]\cos\theta\mathbf{i}_\mathbf{r}\\&+\left[\frac{m\big(t-\frac{r}{c}\big)}{r^3}+\frac{m'\big(t-\frac{r}{c}\big)}{cr^2}+\frac{m''\big(t-\frac{r}{c}\big)}{c^2r}\right]\sin\theta\mathbf{i}_\theta\Bigg\}\end{aligned}} \tag{34}$$

The small current loop of Fig. 12.2.9, which has a magnetic moment $m=\pi R^2 i$, could be the source of the fields given by (33) and (34). If the current driving this loop were turned on in a manner analogous to that considered in Example 12.2.1, the field left behind the outward propagating pulse would be the magnetic dipole field derived in Example 8.3.2.

The complex amplitudes of the far fields for the magnetic dipole are the counterpart of the fields given by (23) and (24) for an electric dipole. They follow from the first term of (33) and the last term of (34) as

$$\boxed{\hat{H}_\theta=-\frac{k^2}{4\pi}\hat{m}\sin\theta\frac{e^{-jkr}}{r}} \tag{35}$$

$$\boxed{\hat{E}_\phi=-\sqrt{\mu/\epsilon}\hat{H}_\theta} \tag{36}$$

In Sec. 12.4, it will be seen that the radiation fields of the electric dipole can be superimposed to describe the radiation patterns of current distributions and of antenna arrays. A similar application of (35) and (36) to describing the radiation patterns of antennae composed of arrays of magnetic dipoles is illustrated by the problems.

12.3 SUPERPOSITION INTEGRAL FOR ELECTRODYNAMIC FIELDS

With the identification in Sec. 12.2 of the fields associated with point charge and current sources, we are ready to construct fields produced by an arbitrary distribution of sources. Just as the superposition integral of Sec. 4.5 was based on the linearity of Poisson's equation, the superposition principle for the dynamic fields hinges on the linear nature of the inhomogeneous wave equations of Sec. 12.1.

Transient Response. The scalar potential for a point charge q at the origin, given by (12.2.1), can be generalized to describe a point charge at an arbitrary source position $\mathbf{r}'$ by replacing the distance r by $|\mathbf{r}-\mathbf{r}'|$ (see Fig. 4.5.1). Then, the point charge is replaced by the charge density ρ evaluated at the source position multiplied by the incremental volume element dv'. With these substitutions in the scalar potential of a point charge, (12.2.1), the potential at an observer location $\mathbf{r}$ is the integrand of the expression

$$\boxed{\Phi(\mathbf{r},t)=\int_{V'}\frac{\rho\left(\mathbf{r}',\ t-\frac{|\mathbf{r}-\mathbf{r}'|}{c}\right)}{4\pi\epsilon|\mathbf{r}-\mathbf{r}'|}dv'} \tag{1}$$

The integration over the source coordinates $\mathbf{r}'$ then superimposes the fields at $\mathbf{r}$ due to all of the sources. Given the charge density everywhere, this integral comprises the solution to the inhomogeneous wave equation for the scalar potential, (12.1.10).

In Cartesian coordinates, any one of the components of the vector inhomogeneous wave-equation, (12.1.8), obeys a scalar equation. Thus, with $\rho/\epsilon \rightarrow \mu J_i$, (1) becomes the solution for A_i, whether i be x, y or z.

$$\boxed{\mathbf{A}(\mathbf{r},t)=\mu\int_{V'}\frac{\mathbf{J}\left(\mathbf{r}',\ t-\frac{|\mathbf{r}-\mathbf{r}'|}{c}\right)}{4\pi|\mathbf{r}-\mathbf{r}'|}dv'} \tag{2}$$

We should keep in mind that conservation of charge implies a relationship between the current and charge densities of (1) and (2). Given the current density, the charge density is determined to within a time-independent distribution. An alternative, and often less involved, approach to finding $\mathbf{E}$ avoids the computation of the charge density. Given $\mathbf{J}$, $\mathbf{A}$ is found from (2). Then, the gauge condition, (12.1.7), is used to find Φ. Finally, $\mathbf{E}$ is found from (12.1.3).

Sinusoidal Steady State Response. In many practical situations involving radio, microwave, and optical frequency systems, the sources are essentially in the sinusoidal steady state.

$$\rho = \text{Re}\ \hat{\rho}(\mathbf{r})e^{j\omega t} \Rightarrow \Phi = \text{Re}\hat{\Phi}(\mathbf{r})e^{j\omega t} \tag{3}$$

Equation (1) is evaluated by using the charge density given by (3), with $\mathbf{r} \rightarrow \mathbf{r}'$ and $t \rightarrow t - |\mathbf{r} - \mathbf{r}'|/c$

$$\begin{aligned} \Phi &= \text{Re} \int_{V'} \frac{\hat{\rho}(\mathbf{r}')e^{j\omega\left(t - \frac{|\mathbf{r}-\mathbf{r}'|}{c}\right)}}{4\pi\epsilon|\mathbf{r} - \mathbf{r}'|} dv' \\ &= \text{Re}\left[\int_{V'} \frac{\hat{\rho}(\mathbf{r}')e^{-jk|\mathbf{r}-\mathbf{r}'|}}{4\pi\epsilon|\mathbf{r} - \mathbf{r}'|} dv'\right] e^{j\omega t} \end{aligned} \tag{4}$$

where $k \equiv \omega/c$. Thus, the quantity in brackets in the second expression is the complex amplitude of Φ at the location $\mathbf{r}$. With the understanding that the time dependence will be recovered by multiplying this complex amplitude by $\exp(j\omega t)$ and taking the real part, the superposition integral for the complex amplitude of the potential is

$$\boxed{\hat{\Phi} = \int_{V'} \frac{\hat{\rho}(\mathbf{r}')e^{-jk|\mathbf{r}-\mathbf{r}'|}}{4\pi\epsilon|\mathbf{r} - \mathbf{r}'|} dv'} \tag{5}$$

From (2), the same reasoning gives the superposition integral for the complex amplitude of the vector potential.

$$\boxed{\hat{\mathbf{A}} = \frac{\mu}{4\pi} \int_{V'} \frac{\hat{\mathbf{J}}(\mathbf{r}')e^{-jk|\mathbf{r}-\mathbf{r}'|}}{|\mathbf{r} - \mathbf{r}'|} dv'} \tag{6}$$

The superposition integrals are often used to find the radiation patterns of driven antenna arrays. In these cases, the distribution of current, and hence charge, is independently prescribed everywhere. Section 12.4 illustrates this application of the superposition integral.

If fields are to be found in confined regions of space, with part of the source distribution on boundaries, the fields given by the superposition integrals represent particular solutions to the inhomogeneous wave equations. Following the same approach as used in Sec. 5.1 for solving boundary value problems involving Poisson's equation, the boundary conditions can then be satisfied by superimposing on the solution to the *inhomogeneous* wave equation solutions satisfying the *homogeneous* wave equation.

12.4 ANTENNA RADIATION FIELDS IN THE SINUSOIDAL STEADY STATE

Antennae are designed to transmit and receive electromagnetic waves. As we know from Sec. 12.2, the superposition integrals for the scalar and vector potentials result

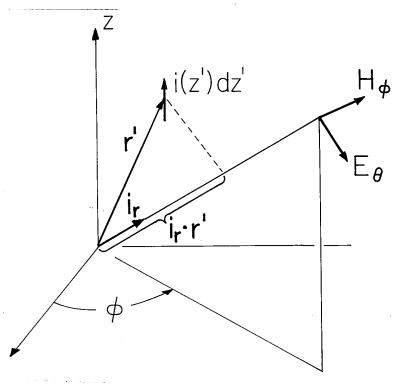


Fig. 12.4.1 Incremental current element at $\mathbf{r}'$ is source for radiation field at (r, θ, ϕ).

in both the radiation and near fields. If we confine our interest to the fields far from the antenna, extensive simplifications are achieved.

Many types of antennae are composed of driven conducting elements that are extremely thin. This often makes it possible to use simple arguments to approximate the distribution of current over the length of the conductor. With the current distribution specified at the outset, the superposition integrals of Sec. 12.3 can then be used to determine the associated fields.

An element idz' of the current distribution of an antenna is pictured in Fig. 12.4.1 at the source location $\mathbf{r}'$. If this element were at the origin of the spherical coordinate system shown, the associated radiation fields would be as given by (12.2.23) and (12.2.24). With the distance to the current element r' much less than r, how do we adapt these expressions so that they represent the fields when the incremental source is located at $\mathbf{r}'$ rather than at the origin?

The current elements comprising the antenna are typically within a few wavelengths of the origin. By contrast, the distance r (say, from a TV transmitting antenna, where the wavelength is on the order of 1 meter, to a receiver 10 kilometers away) is far larger. For an observer in the neighborhood of a point (r, θ, ϕ), there is little change in $\sin\theta/r$, and hence in the *magnitude* of the field, caused by a displacement of the current element from the origin to $\mathbf{r}'$. However, the *phase* of the electromagnetic wave launched by the current element is strongly influenced by changes in the distance from the element to the observer that are of the order of a wavelength. This is seen by writing the argument of the exponential term in terms of the wavelength λ, $jkr = j2\pi r/\lambda$.

With the help of Fig. 12.4.1, we see that the distance from the source to the observer is $r - \mathbf{r}' \cdot \mathbf{i}_\mathbf{r}$. Thus, for the current element located at $\mathbf{r}'$ in the neighborhood of the origin, the radiation fields given by (12.2.23) and (12.2.24) are

$$\boxed{\hat{H}_\phi \simeq \frac{jk}{4\pi} \sin\theta \frac{e^{-jk(r-\mathbf{r}'\cdot\mathbf{i}_\mathbf{r})}}{r} i(\mathbf{r}')dz'} \tag{1}$$

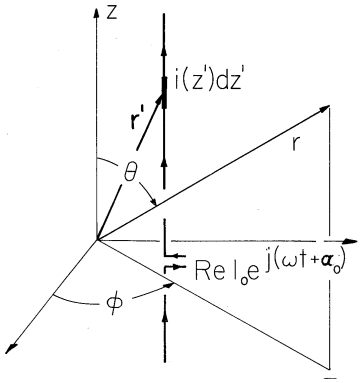


Fig. 12.4.2 Line current distribution as source of radiation field.

$$\boxed{\hat{E}_\theta \simeq \sqrt{\frac{\mu}{\epsilon}}\hat{H}_\phi} \tag{2}$$

Because **E** and **H** are vector fields, yet another approximation is implicit in writing these expressions. In shifting the current element, there is a slight shift in the coordinate directions at the observer location. Again, because r is much larger than $|\mathbf{r}'|$, this slight change in the direction of the field can be ignored. Thus, radiation fields due to a superposition of current elements can be found by simply superimposing the fields as though they were parallel vectors.

Distributed Current Distribution. A wire antenna, driven by a given current distribution Re $[\hat{i}(z)\exp(j\omega t)]$, is shown in Fig. 12.4.2. At the terminals, the complex amplitude of this current is $\hat{i} = I_o \exp(j\omega t + \alpha_o)$. It follows from (1) and the superposition principle that the magnetic radiation field for this antenna is

$$\hat{H}_\phi \simeq \frac{jk}{4\pi}\sin\theta\frac{e^{-jkr}}{r}\int \hat{i}(z')e^{jk\mathbf{r}'\cdot\mathbf{i}_\mathbf{r}}dz' \tag{3}$$

Note that the role played by id for the incremental dipole is now played by $i(z')dz'$. For convenience, we define a field pattern function $\psi_o(\theta)$ that gives the θ dependence of the E and H fields

$$\boxed{\psi_o(\theta) \equiv \frac{\sin\theta}{l}\int \frac{\hat{i}(z')}{I_o}e^{j(k\mathbf{r}'\cdot\mathbf{i}_\mathbf{r}-\alpha_o)}dz'} \tag{4}$$

where l is the length of the antenna and $\psi_o(\theta)$ is dimensionless. With the aid of $\psi_o(\theta)$, one may write (3) in the form

$$\boxed{\hat{H}_\phi \simeq \frac{jkl}{4\pi}\frac{e^{-jkr}}{r}I_o e^{j\alpha_o}\psi_o(\theta)} \tag{5}$$

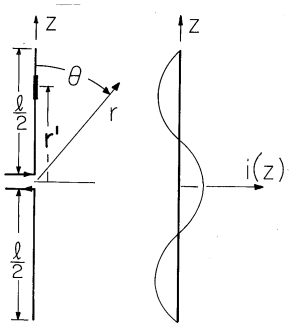


Fig. 12.4.3 Center-fed wire antenna with standing-wave distribution of current.

By definition, $\hat{i}(\hat{z}') = I_o \exp(j\alpha_o)$ if z' is evaluated at the terminals of the antenna. Thus, ψ_o is neither a function of I_o nor of α_o. In order to evaluate (5), one needs to know the current dependence on z', $\hat{i}(z')$. One can show that the current distribution on a (open-ended) thin wire is made up of a "standing wave" with the dependence $\sin(2\pi s/\lambda)$ upon the coordinate s measured along the wire, from the end of the wire. The proof of this statement will be presented in Chapter 14, when we shall discuss the current distribution in a coaxial cable.

Example 12.4.1. Radiation Pattern of Center-Fed Wire Antenna

A wire antenna, fed at its midpoint and on the z axis, is shown in Fig. 12.4.3. The current distribution is "given" according to the above remarks.

$$\hat{i} = -I_o \frac{\sin k(|z| - l/2)}{\sin(kl/2)} e^{j\alpha_o} \tag{6}$$

In setting up the radiation field superposition integral, (5), observe that $\mathbf{r}' \cdot \mathbf{i}_\mathbf{r} = z' \cos\theta$.

$$\psi_o = \frac{\sin\theta}{l} \int_{-l/2}^{l/2} \frac{-\sin k(|z'| - l/2)}{\sin(kl/2)} e^{jkz' \cos\theta} dz' \tag{7}$$

Evaluation of the integral[7] then gives

$$\psi_o = \frac{2}{kl \sin(kl/2)} \left[\frac{\cos(kl/2) - \cos\left(\frac{kl}{2}\cos\theta\right)}{\sin\theta} \right] \tag{8}$$

The radiation pattern of the wire antenna is proportional to the absolute value squared of the θ-dependent factor of ψ_o

$$\Psi(\theta) = \left[\frac{\cos(kl/2) - \cos\left(\frac{kl}{2}\cos\theta\right)}{\sin\theta} \right]^2 \tag{9}$$

[7] To carry out the integration, first express the integration over the positive and negative segments of z' as separate integrals. With the sine functions represented by the sum of complex exponentials, the integration is reduced to a sum of integrations of complex exponentials.

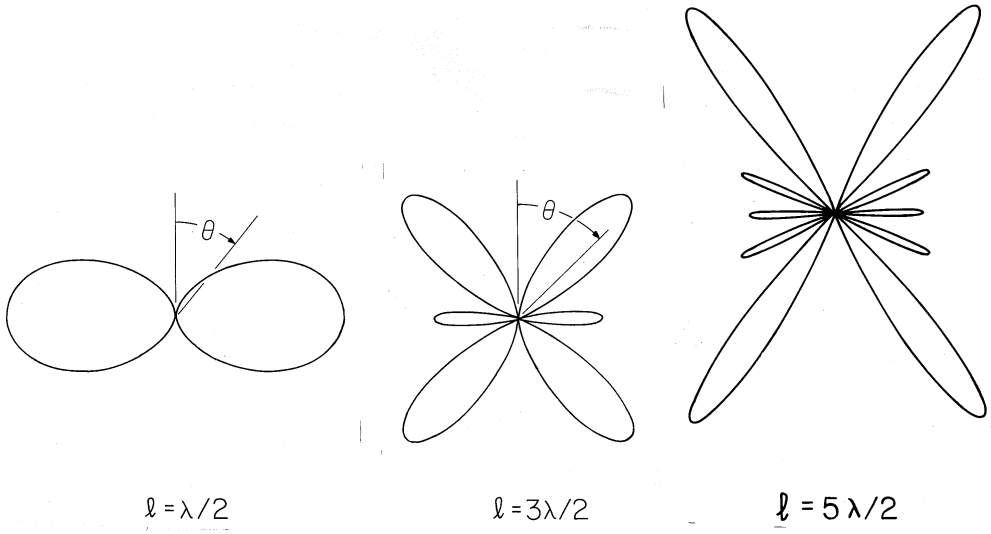


Fig. 12.4.4 Radiation patterns for center-fed wire antennas.

In viewing the plots of this radiation pattern shown in Fig. 12.4.4, remember that it is the same in any plane of constant ϕ. Thus, a three-dimensional picture of the function $\Psi(\theta, \phi)$ is generated by rotating one of these patterns about the z axis.

The radiation pattern for a half-wave antenna differs little from that for the short dipole, shown in Fig. 12.2.7. Because of the interference between waves generated by segments having different phases and amplitudes, the pattern for longer wires is more complex. As the length of the antenna is increased to many wavelengths, the number of lobes increases.

Arrays. Desired radiation patterns are often obtained by combining driven elements into arrays. To illustrate, consider an array of $1 + n$ elements, the first at the origin and designated by "0". The others are designated by $i = 1 \dots n$ and respectively located at $\mathbf{a}_i$. We can find the radiation pattern for the array by summing over the contributions of the separate elements. Each of these takes the form of (5), with $r \to r - \mathbf{a}_i \cdot \mathbf{i}_\mathbf{r}$, $I_o \to I_i$, $\alpha_o \to \alpha_i$, and $\psi_o(\theta) \to \psi(\theta)$.

$$\hat{H}_\phi \simeq \frac{jkl}{4\pi r} \sum_{i=0}^{n} e^{-jk(r-\mathbf{a}_i \cdot \mathbf{i}_\mathbf{r})} I_i e^{j\alpha_i} \psi_i(\theta) \tag{10}$$

In the special case where the magnitude (but not the phase) of each element is the same and the elements are identical, so that $I_i = I_o$ and $\psi_i = \psi_o$, this expression can be written as

$$\hat{H}_\theta \simeq \frac{jkl}{4\pi} I_o e^{j\alpha_o} \frac{e^{-jkr}}{r} \psi_o(\theta) \psi_a(\theta, \phi) \tag{11}$$

where the *array factor* is

$$\psi_a(\theta, \phi) \equiv \sum_{i=0}^{n} e^{jk\mathbf{a}_i \cdot \mathbf{i}_\mathbf{r}} e^{j(\alpha_i - \alpha_o)} \tag{12}$$

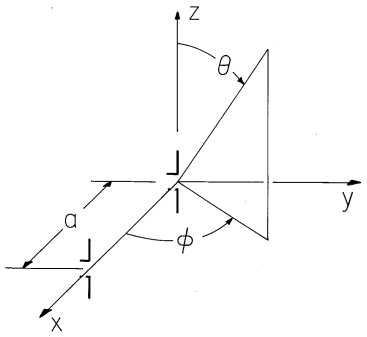


Fig. 12.4.5 Array consisting of two elements with spacing, a.

Note that the radiation pattern of the array is represented by the square of the product of ψ_o, representing the pattern for a single element, and the array factor ψ_a. If the $n+1$ element array is considered one element in a second array, these same arguments could be repeated to show that the radiation pattern of the array of arrays is represented by the square of the product of ψ_o, ψ_a and the square of the array factor of the second array.

Example 12.4.2. Two-Element Arrays

The elements of an array have a spacing a, as shown in Fig. 12.4.5. The array factor follows from evaluation of (12), where $\mathbf{a}_o = 0$ and $\mathbf{a}_1 = a\mathbf{i}_\mathbf{x}$. The projection of $\mathbf{i}_\mathbf{r}$ into $\mathbf{i}_\mathbf{x}$ gives (see Fig. 12.4.5)

$$\mathbf{a}_1 \cdot \mathbf{i}_\mathbf{r} = a \sin\theta \cos\phi \tag{13}$$

It follows that

$$\psi_a = 1 + e^{j(ka \sin\theta \cos\phi + \alpha_1 - \alpha_o)} \tag{14}$$

It is convenient to write this expression as a product of a part that determines the phase and a part that determines the amplitude.

$$\psi_a = 2e^{j(ka \sin\theta \cos\phi + \alpha_1 - \alpha_o)/2} \cos\left[\frac{ka}{2} \sin\theta \cos\phi + \frac{1}{2}(\alpha_1 - \alpha_o)\right] \tag{15}$$

Dipoles in Broadside Array. With the elements short compared to a wavelength, the individual patterns are those of a dipole. It follows from (4) that

$$\psi_o = \sin\theta \tag{16}$$

With the dipoles having a half-wavelength spacing and driven in phase,

$$a = \frac{\lambda}{2} \Rightarrow ka = \pi, \qquad \alpha_1 - \alpha_o = 0 \tag{17}$$

The magnitude of the array factor follows from (15).

$$|\psi_a| = 2\left|\cos\left(\frac{\pi}{2} \sin\theta \cos\phi\right)\right| \tag{18}$$

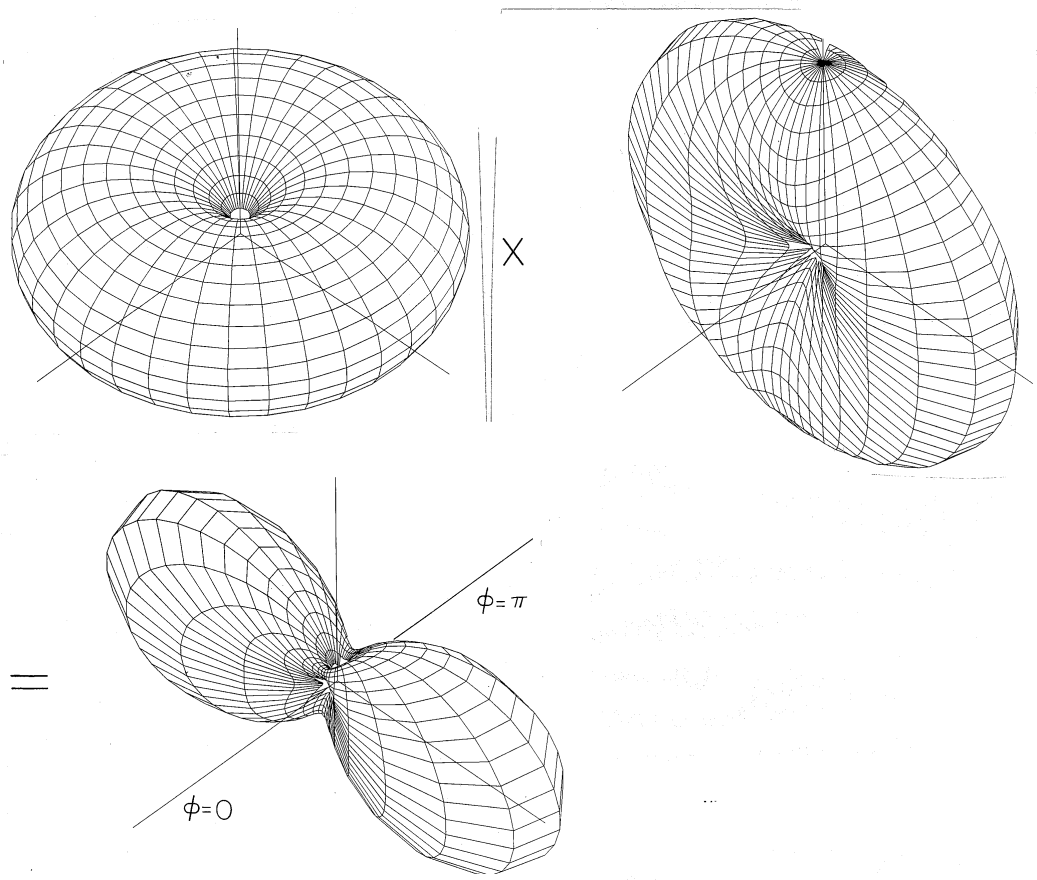


Fig. 12.4.6 Radiation pattern of dipoles in phase, half-wave spaced, is product of pattern for individual elements multiplied by the array factor.

The radiation pattern for the array follows from (16) and (18).

$$\Psi = |\psi_o|^2 |\psi_a|^2 = 4 \sin^2 \theta \cos^2 \left(\frac{\pi}{2} \sin \theta \cos \phi \right) \tag{19}$$

Figure 12.4.6 geometrically portrays how the single-element pattern and array pattern multiply to provide the radiation pattern. With the elements a half-wavelength apart and driven in phase, electromagnetic waves arrive in phase at points along the y axis and reinforce. There is no radiation in the $\pm x$ directions, because a wave initiated by one element arrives out of phase with the wave being initiated by that second element. As a result, the waves reinforce along the y axis, the "broadside" direction, while they cancel along the x axis.

Dipoles in End-Fire Array. With quarter-wave spacing and driven 90 degrees out of phase,

$$a = \frac{\lambda}{4}, \qquad \alpha_1 - \alpha_o = \frac{\pi}{2} \tag{20}$$

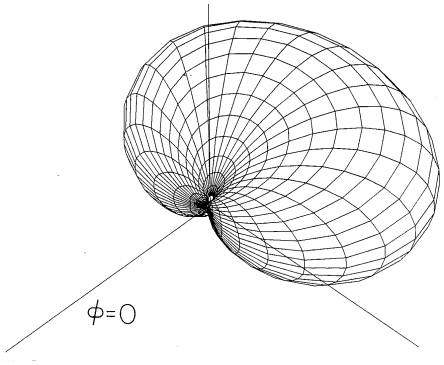


Fig. 12.4.7 Radiation pattern for dipoles quarter-wave spaced, 90 degrees out of phase.

the magnitude of the array factor follows from (15) as

$$|\psi_a| = 2\Big|\cos\Big[\frac{\pi}{4}\sin\theta\cos\phi + \frac{\pi}{4}\Big]\Big| \tag{21}$$

The radiation pattern follows from (16) and (21).

$$\Psi = |\psi_o|^2|\psi_a|^2 = 4\sin^2\theta\cos^2\Big[\frac{\pi}{4}\sin\theta\cos\phi + \frac{\pi}{4}\Big] \tag{22}$$

Shown graphically in Fig. 12.4.7, the pattern is now in the $-x$ direction. Waves initiated in the $-x$ direction by the element at $x = a$ arrive in phase with those originating from the second element. Thus, the wave being initiated by that second element in the $-x$ direction is reinforced. By contrast, the wave initiated in the $+x$ direction by the element at $x = 0$ arrives 180 degrees out of phase with the wave being initiated in the $+x$ direction by the other element. Thus, radiation in the $+x$ direction cancels, and the array is unidirectional.

Finite Dipoles in End-Fire Array. Finally, consider a pair of finite length elements, each having a length l, as in Fig. 12.4.3. The pattern for the individual elements is given by (8). With the elements spaced as in Fig. 12.4.5, with $a = \lambda/4$ and driven 90 degrees out of phase, the magnitude of the array factor is given by (21). Thus, the amplitude of the radiation pattern is

$$\Psi = 4\left[\frac{\cos\left(\frac{kl}{2}\right) - \cos\left(\frac{kl}{2}\cos\theta\right)}{\sin\theta}\right]^2\left(\cos^2\Big[\frac{\pi}{4}\sin\theta\cos\phi + \frac{\pi}{4}\Big]\right)^2 \tag{23}$$

For elements of length $l = 3\lambda/2$ ($kl = 3\pi$), this pattern is pictured in Fig. 12.4.8.

Gain. The time average power flux density, $\langle S_r(\theta,\ \phi)\rangle$, normalized to the power flux density averaged over the surface of a sphere, is called the *gain* of an antenna.

$$G = \frac{\langle S_r(\theta,\ \phi)\rangle}{\frac{1}{4\pi r^2}\int_0^{\pi}\int_0^{2\pi}\langle S_r\rangle r\sin\theta d\phi r d\theta} \tag{24}$$

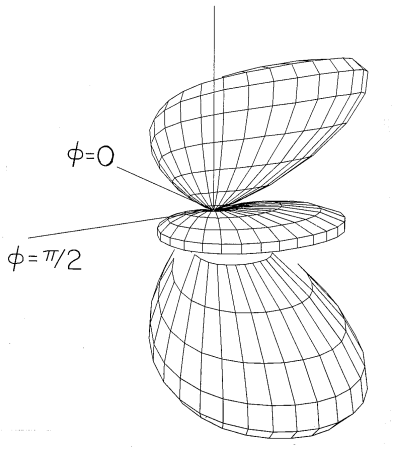


Fig. 12.4.8 Radiation pattern for two center-fed wire antennas, quarter-wave spaced, 90 degrees out-of-phase, each having length $3\lambda/2$.

If the direction is not specified, it is implied that G is the gain in the direction of maximum gain.

The radial power flux density is the Poynting flux, defined by (11.2.9). Using the time average theorem, (11.5.6), and the fact that the ratio of $\mathbf{E}$ to $\mathbf{H}$ for the radiation field is $\sqrt{\mu/\epsilon}$, (2), gives

$$\langle S_r \rangle = \frac{1}{2} Re\hat{\mathbf{E}} \times \hat{\mathbf{H}}^* = \frac{1}{2} Re\hat{E}_\theta \hat{H}_\phi^* = \frac{1}{2}\sqrt{\epsilon/\mu}|\hat{E}_\theta|^2 \tag{25}$$

Because the radiation pattern expresses the $(\theta,\ \phi)$ dependence of $|E_\theta|^2$ with a multiplicative factor that is in common to the numerator and denominator of (24), G can be evaluated using the radiation pattern Ψ for $\langle S_r \rangle$.

Example 12.4.3. Gain of an Electric Dipole

For the electric dipole, it follows from (1) and (2) that the radiation pattern is proportional to $\sin^2(\theta)$. The gain in the θ direction is then

$$G = \frac{\sin^2\theta}{\frac{1}{2}\int_0^\pi \sin^3\theta d\theta} = \frac{3}{2}\sin^2\theta \tag{26}$$

and the "gain" is 3/2.

12.5 COMPLEX POYNTING'S THEOREM AND RADIATION RESISTANCE

To the generator supplying its terminal current, a radiating antenna appears as a load with an impedance having a resistive part. This is true even if the antenna is made from perfectly conducting material and therefore incapable of converting

electrical power to heat. The power radiated away from the antenna must be supplied through its terminals, much as if it were dissipated in a resistor. Indeed, if there is no electrical dissipation in the antenna, the power supplied at the terminals is that radiated away. This statement of power conservation makes it possible to determine the equivalent resistance of the antenna simply by using the far fields that were the theme of Sec. 12.4.

Complex Poynting's Theorem. For systems in the sinusoidal steady state, a useful alternative to the form of Poynting's theorem introduced in Secs. 11.1 and 11.2 results from writing Maxwell's equations in terms of complex amplitudes *before* they are combined to provide the desired theorem. That is, we assume at the outset that fields and sources take the form

$$\mathbf{E} = Re\hat{\mathbf{E}}(x,y,z)e^{j\omega t} \tag{1}$$

Suppose that the region of interest is composed either of free space or of perfect conductors. Then, substitution of complex amplitudes into the laws of Ampère and Faraday, (12.0.8) and (12.0.9), gives

$$\nabla \times \hat{\mathbf{H}} = \hat{\mathbf{J}} + j\omega\epsilon\hat{\mathbf{E}} \tag{2}$$

$$\nabla \times \hat{\mathbf{E}} = -j\omega\mu\hat{\mathbf{H}} \tag{3}$$

The manipulations that are now used to obtain the desired "complex Poynting's theorem" parallel those used to derive the real, time-dependent form of Poynting's theorem in Sec. 11.2. We *dot* $\mathbf{E}$ with the complex conjugate of (2) and subtract the dot product of the complex conjugate of $\mathbf{H}$ with (3). It follows that[8]

$$-\nabla \cdot (\hat{\mathbf{E}} \times \hat{\mathbf{H}}^*) = \hat{\mathbf{E}} \cdot \hat{\mathbf{J}}^* + j\omega(\mu\hat{\mathbf{H}} \cdot \hat{\mathbf{H}}^* - \epsilon\hat{\mathbf{E}} \cdot \hat{\mathbf{E}}^*) \tag{4}$$

The object of this manipulation was to obtain the "perfect" divergence on the left, because this expression can then be integrated over a volume V and Gauss' theorem used to convert the volume integral on the left to an integral over the enclosing surface S.

$$\begin{aligned} -\oint_S \frac{1}{2}(\hat{\mathbf{E}} \times \hat{\mathbf{H}}^*) \cdot d\mathbf{a} = & j\omega 2 \int_V \frac{1}{4}(\mu\hat{\mathbf{H}} \cdot \hat{\mathbf{H}}^* - \epsilon\hat{\mathbf{E}} \cdot \hat{\mathbf{E}}^*)dv \\ & + \int_V \frac{1}{2}\hat{\mathbf{E}} \cdot \hat{\mathbf{J}}_u^* dv \end{aligned} \tag{5}$$

This expression has been multiplied by $\frac{1}{2}$, so that its real part represents the time average flow of power, familiar from Sec. 11.5. Note that the real part of the first term on the right is zero. The real part of (5) equates the time average of the Poynting vector flux into the volume with the time average of the power imparted to the current density of unpaired charge, $\mathbf{J}_u$, by the electric field. This information

[8] $\nabla \cdot (\mathbf{A} \times \mathbf{B}) = \mathbf{B} \cdot \nabla \times \mathbf{A} - \mathbf{A} \cdot \nabla \times \mathbf{B}$

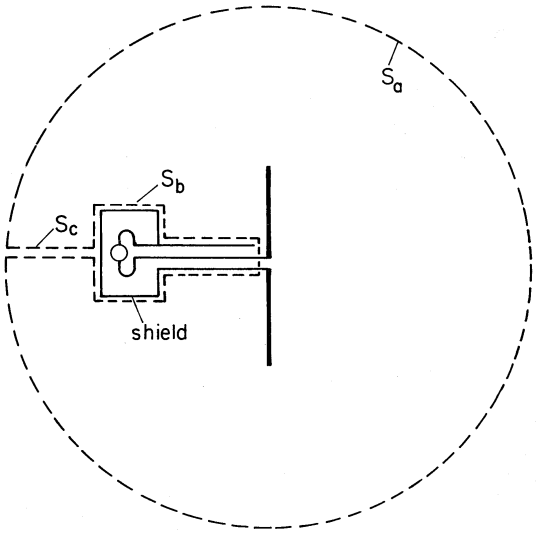


Fig. 12.5.1 Surface S encloses the antenna but excludes the source. Spherical part of S is at "infinity."

is equivalent to the time average of the (real form of) Poynting's theorem. The imaginary part of (5) relates the difference between the time average magnetic and electric energies in the volume V to the imaginary part of the complex Poynting flux into the volume. The imaginary part of the complex Poynting theorem conveys additional information.

Radiation Resistance. Consider the perfectly conducting antenna system surrounded by the spherical surface, S, shown in Fig. 12.5.1. To exclude sources from the enclosed volume, this surface is composed of an outer surface, S_a, that is far enough from the antenna so that only the radiation field makes a contribution, a surface S_b that surrounds the source(s), and a surface S_c that can be envisioned as the wall of a system of thin tubes connecting S_a to S_b in such a way that $S_a + S_b + S_c$ is indeed the surface enclosing V. By making the connecting tubes very thin, contributions to the integral on the left in (5) from the surface S_c are negligible. We now write, and then explain, the terms in (5) as they describe this radiation system.

$$-\int_{S_a} \frac{1}{2}\sqrt{\epsilon/\mu}|\hat{E}_\theta|^2 da + \sum_{i=1}^{n} \frac{1}{2}\hat{v}_i\hat{i}_i^* = j2\omega \int_V \frac{1}{2}\left(\frac{1}{2}\mu|\hat{\mathbf{H}}|^2 - \frac{1}{2}\epsilon|\hat{\mathbf{E}}|^2\right)dv \qquad (6)$$

The first term is the contribution from integrating the radiation Poynting flux over S_a, where (12.4.2) serves to eliminate $\mathbf{H}$. The second term comes from the surface integral in (5) of the Poynting flux over the surface, S_b, enclosing the sources (generators). Think of the generators as enclosed by perfectly conducting boxes powered by terminal pairs (coaxial cables) to which the antennae are attached. We have shown in Sec. 11.3 (11.3.29) that the integral of the Poynting flux over S_b is

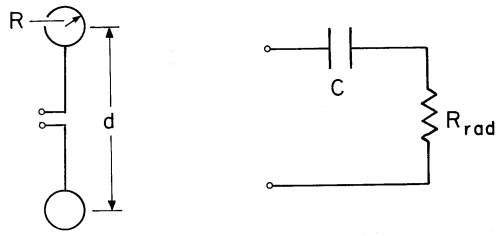


Fig. 12.5.2 End-loaded dipole and equivalent circuit.

equivalent to the sum of voltage-current products expressing power flow from the circuit point of view. The first term on the right is the same as the first on the right in (5). Finally, the last term in (5) makes no contribution, because the only regions where $\mathbf{J}$ exists within V are those modeled here as perfectly conducting and hence where $\mathbf{E} = 0$.

Consider a single antenna with one input terminal pair. The antenna is a linear system, so the complex voltage must be proportional to the complex terminal current.

$$\hat{v} = Z_{\text{ant}}\hat{i} \tag{7}$$

Here, Z_{ant} is the impedance of the antenna. In terms of this impedance, the time average power can be written as

$$\frac{1}{2}Re(\hat{v}\hat{i}^*) = \frac{1}{2}Re(Z_{\text{ant}})|\hat{i}|^2 = \frac{1}{2}Re(Z_{\text{ant}})|\hat{I}_o|^2 \tag{8}$$

It follows from the real part of (6) that the *radiation resistance*, R_{rad}, is

$$Re(Z_{\text{ant}}) \equiv R_{\text{rad}} = \sqrt{\epsilon/\mu}\int_{S_a}|E_\theta|^2\frac{da}{|\hat{I}_o|^2} \tag{9}$$

The imaginary part of Z_{out} describes the reactive power supplied to the antenna.

$$Im(Z_{\text{ant}}) = \frac{\omega\int(\mu|\hat{\mathbf{H}}|^2 - \epsilon|\hat{\mathbf{E}}|^2)dv}{|I_o|^2} \tag{10}$$

The radiation field contributions to this integral cancel out. If the antenna elements are short compared to a wavelength, contributions to (10) are dominated by the quasistatic fields. Thus, the electric dipole contributions are dominated by the electric field (and the reactance is capacitive), while those for the magnetic dipole are inductive. By making the antenna on the order of a wavelength, the magnetic and electric contributions to (10) are often made to essentially cancel. An example is a half-wavelength version of the wire antenna in Example 12.4.1. The equivalent circuit for such resonant antennae is then solely the radiation resistance.

Example 12.5.1. Equivalent Circuit of an Electric Dipole

An "end-loaded" electric dipole is composed of a pair of perfectly conducting metal spheres, each of radius R, as shown in Fig. 12.5.2. These spheres have a spacing, d, that is short compared to a wavelength but large compared to the radius, R, of the spheres.

The equivalent circuit is also shown in Fig. 12.5.2. The statement that the sum of the voltage drops around the circuit is zero requires that

$$\hat{v} = \frac{\hat{i}}{j\omega C} + R_{\rm rad}\hat{i} \tag{11}$$

A statement of power flow is obtained by multiplying this expression by the complex conjugate of the complex amplitude of the current.

$$\frac{1}{2}\hat{v}\hat{i}^* = -\frac{j\omega}{2C}\hat{q}\hat{q}^* + \frac{1}{2}R_{\rm rad}\hat{i}\hat{i}^*; \qquad \hat{i} \equiv j\omega\hat{q} \tag{12}$$

Here the dipole charge, q, is defined such that $i = dq/dt$. The real part of this expression takes the same form as the statement of complex power flow for the antenna, (6). Thus, with $\hat{E}_\theta$ provided by (12.2.23) and (12.2.24), we can solve for the radiation resistance:

$$R_{\rm rad} = \sqrt{\mu/\epsilon}\frac{(kd)^2}{(4\pi)^2}\int_0^\pi \frac{\sin^2\theta(2\pi r\sin\theta)rd\theta}{r^2} = \frac{(kd)^2}{6\pi}\sqrt{\mu/\epsilon} \tag{13}$$

Note that because $k \equiv \omega/c$, this radiation resistance is proportional to the square of the frequency.

The imaginary part of the impedance is given by the right-hand side of (10). The radiation field contributions to this integral cancel out. In integrating over the near field, the electric energy storage dominates and becomes essentially that associated with the quasistatic capacitance of the pair of spheres. We assume that the spheres are connected by wires that are extremely thin, so that their effect can be ignored. Then, the capacitance is the series capacitance of two isolated spheres, each having a capacitance of $4\pi\epsilon R$.

$$C = 2\pi\epsilon R \tag{14}$$

Radiation fields are solutions to the full Maxwell equations. In contrast, EQS fields were analyzed ignoring the magnetic flux linkage in Faraday's law. The approximation is justified if the size of the system is small compared with a wavelength. The following example treats the scattering of particles that are small compared with the wavelength. The fields around the particles are EQS, and the currents induced in the particles are deduced from the EQS approximation. These currents drive radiation fields, resulting in Rayleigh scattering. The theory of Rayleigh scattering explains why the sky is blue in color, as the following example shows.

Example 12.5.2. Rayleigh Scattering

Consider a spatial distribution of particles in the field of an infinite parallel plane wave. The particles are assumed to be small as compared to the wavelength of the plane wave. They get polarized in the presence of an electric field $\mathbf{E}_a$, acquiring a dipole moment

$$\mathbf{p} = \epsilon_o\alpha\mathbf{E}_a \tag{15}$$

where α is the polarizability. These particles could be atoms or molecules, such as the molecules of nitrogen and oxygen of air exposed to visible light. They could also

be conducting spheres of radius R. In the latter case, the dipole moment produced by an applied electric field E_a is given by (6.6.5) and the polarizability is

$$\alpha = 4\pi R^3 \tag{16}$$

If the frequency of the polarizing wave is ω and its propagation constant $k = \omega/c$, the far field radiated by the particle, expressed in a spherical coordinate system with its $\theta = 0$ axis aligned with the electric field of the wave, is, from (12.2.22),

$$E_\theta = -\sqrt{\frac{\mu_o}{\epsilon_o}}\frac{k\omega\hat{p}}{4\pi}\sin\theta\frac{e^{-jkr}}{r} \tag{17}$$

where $\hat{i}d = j\omega\hat{p}$ is used in the above expression. The power radiated by each dipole, i.e., the power scattered by a dipole, is

$$\begin{aligned} P_{\text{Scatt}} &= \int_{S_a}\frac{1}{2}\sqrt{\frac{\epsilon_o}{\mu_o}}|\hat{E}_\theta|^2 = \frac{1}{2}\sqrt{\frac{\mu_o}{\epsilon_o}}\left|\frac{\omega k\hat{p}}{4\pi}\right|^2\frac{1}{r^2}\int_0^\pi\int_0^{2\pi} d\phi r^2\sin^3\theta d\theta \\ &= \frac{1}{2}\sqrt{\frac{\mu_o}{\epsilon_o}}\left|\frac{\omega k\hat{p}}{4\pi}\right|^2\frac{8\pi}{3} = \frac{1}{12\pi}\sqrt{\frac{\mu_o}{\epsilon_o}}\frac{\omega^4}{c^2}\epsilon_o^2\alpha^2\hat{\mathbf{E}}^2 \end{aligned} \tag{18}$$

The scattered power increases with the fourth power of frequency when α is not a function of frequency. The polarizability of N_2 and O_2 is roughly frequency independent. Of the visible radiation, the blue (high) frequencies scatter much more than the red (low) frequencies. This is the reason for the blue color of the sky. The same phenomenon accounts for the polarization of the scattered radiation. Along a line L at a large angle from the line from the observer O to the sun S, only the electric field perpendicular to the plane LOS produces radiation visible at the observer position (note the $\sin^2\theta$ dependence of the radiation). Thus, the scattered radiation observed at O has an electric field perpendicular to LOS.

The present analysis has made two approximations. First, of course, we assumed that the particle is small compared with a wavelength. Second, we computed the induced polarization from the unperturbed field E_θ of the incident plane wave. This assumes that the particle perturbs the wave negligibly, that the scattered power is very small compared to the power in the wave. Of course, the incident wave decreases in intensity as it proceeds through the distribution of scatterers, but this macroscopic change can be treated as a simple attenuation proportional to the density of scatterers.

12.6 PERIODIC SHEET-SOURCE FIELDS: UNIFORM AND NONUNIFORM PLANE WAVES

This section introduces the electrodynamic fields associated with surface sources. The physical systems analyzed are generalizations, on the one hand, of such EQS situations as Example 5.6.2, where sinusoidal surface charge densities produced a Laplacian field decaying away from the surface charge source. On the other hand, the MQS sinusoidal surface current sources producing magnetic fields that decay

away from their source (for example, Prob. 8.6.9) are generalized to the fully dynamic case. In both cases, one expects that the quasistatic approximation will be contained in the limit where the spatial period of the source is much smaller than the wavelength $\lambda = 2\pi/\omega\sqrt{\mu\epsilon}$. When the spatial period of the source approaches, or exceeds, the wavelength, new phenomena ought to be revealed. Specifically, distributions of surface current density $\mathbf{K}$ and surface charge density σ_s are given in the $x-z$ plane.

$$\mathbf{K} = K_x(x,t)\mathbf{i_x} + K_z(x,t)\mathbf{i_z} \tag{1}$$

$$\sigma_s = \sigma_s(x,t) \tag{2}$$

These are independent of z and are typically periodic in space and time, extending to infinity in the x and z directions.

Charge conservation links $\mathbf{K}$ and σ_s. A two-dimensional version of the charge conservation law, (12.1.22), requires that there must be a time rate of decrease of surface charge density σ_s wherever there is a two-dimensional divergence of $\mathbf{K}$.

$$\frac{\partial K_x}{\partial x} + \frac{\partial K_z}{\partial z} + \frac{\partial \sigma_s}{\partial t} = 0 \Rightarrow \frac{\partial K_x}{\partial x} + \frac{\partial \sigma_s}{\partial t} = 0 \tag{3}$$

The second expression results because K_z is independent of z.

Under the assumption that the only sources are those in the $x-z$ plane, it follows that the fields can be pictured as the superposition of those due to (K_x, σ_s) given to satisfy (3) and due to K_z. It is therefore convenient to break the fields produced by these two kinds of sources into two categories.

Transverse Magnetic (TM) Fields. The source distribution (K_x, σ_s) does not produce a z component of the vector potential $\mathbf{A}$, $A_z = 0$. This follows because there is no z component of the current in the superposition integral for $\mathbf{A}$, (12.3.2). However, there are both current and charge sources, so that the superposition integral for Φ requires that in addition to an $\mathbf{A}$ that lies in $x-y$ planes, there is an electric potential as well.

$$\mathbf{A} = A_x(x,y,t)\mathbf{i_x} + A_y(x,y,t)\mathbf{i_y}; \qquad \Phi = \Phi(x,y,t) \tag{4}$$

Because the source distribution is independent of z, we have taken these potentials to be also two dimensional. It follows that $\mathbf{H}$ *is transverse to the* $x-y$ *coordinates upon which the fields depend*, while $\mathbf{E}$ lies in the $x-y$ plane.

$$\mathbf{H} = \frac{1}{\mu}\nabla \times \mathbf{A} = H_z(x,y,t)\mathbf{i_z}$$

$$\mathbf{E} = -\nabla\Phi - \frac{\partial \mathbf{A}}{\partial t} = E_x(x,y,t)\mathbf{i_x} + E_y(x,y,t)\mathbf{i_y} \tag{5}$$

Sources and fields for these transverse magnetic (TM) fields have the relative orientations shown in Fig. 12.6.1.

We will be concerned here with sources that are in the sinusoidal steady state. Although $\mathbf{A}$ and Φ could be used to derive the fields, in what follows it is more

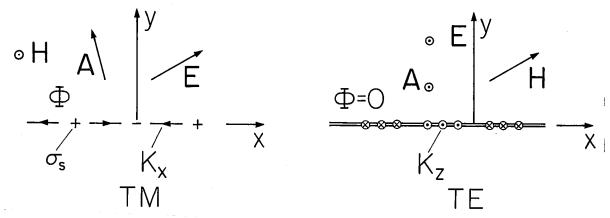


Fig. 12.6.1 Transverse magnetic and electric sources and fields.

convenient to deal directly with the fields themselves. The complex amplitude of H_z, the only component of $\mathbf{H}$, is conveniently used to represent $\mathbf{E}$ in the free space regions to either side of the sheet. This can be seen by using the x and y components of Ampère's law to write

$$\boxed{E_x = \frac{1}{j\omega\epsilon}\frac{\partial \hat{H}_z}{\partial y}} \tag{6}$$

$$\boxed{\hat{E}_y = -\frac{1}{j\omega\epsilon}\frac{\partial \hat{H}_z}{\partial x}} \tag{7}$$

for the only two components of $\mathbf{E}$.

The relationship between $\mathbf{H}$ and its source is obtained by taking the curl of the vector wave equation for $\mathbf{A}$, (12.1.8). The curl operator commutes with the Laplacian and time derivative, so that the result is the inhomogeneous wave equation for $\mathbf{H}$.

$$\boxed{\nabla^2\mathbf{H} - \mu\epsilon\frac{\partial^2\mathbf{H}}{\partial t^2} = -\nabla\times\mathbf{J}} \tag{8}$$

For the sheet source, the driving term on the right is zero everywhere except in the $x-z$ plane. Thus, in the free space regions, the z component of this equation gives a differential equation for the complex amplitude of H_z.

$$\boxed{(\frac{\partial^2}{\partial x^2} + \frac{\partial^2}{\partial y^2})\hat{H}_z + \omega^2\mu\epsilon\hat{H}_z = 0} \tag{9}$$

This expression is a two-dimensional example of the *Helmholtz equation.* Given sinusoidal steady state source distributions of (K_x, σ_s) consistent with charge conservation, (3), the continuity conditions can be used to relate these sources to the fields described by (6), (7), and (9).

Product Solutions to the Helmholtz Equation. One theme of this section is the solution to the Helmholtz equation, (9). Note that this equation resulted from the time-dependent wave equation by separation of variables, by assuming solutions of the form $H_z(x,y)T(t)$, where $T(t) = \exp(j\omega t)$. We now look for solutions expressing the $x-y$ dependence that take the product form $X(x)Y(y)$. The process is familiar from Sec. 5.4, but the resulting family of solutions is of wider variety, and it is worthwhile to focus on their nature before applying them to particular examples.

With the substitution of the product solution $H_z = X(x)Y(y)$, (9) becomes

$$\frac{1}{X}\frac{d^2X}{dx^2} + \frac{1}{Y}\frac{d^2Y}{dy^2} + \omega^2\mu\epsilon = 0 \tag{10}$$

This expression is satisfied if the first and second terms are constants

$$-k_x^2 - k_y^2 + \omega^2\mu\epsilon = 0 \tag{11}$$

and it follows that parts of the total solution are governed by the ordinary differential equations

$$\frac{d^2X}{dx^2} + k_x^2 X = 0; \qquad \frac{d^2Y}{dy^2} + k_y^2 Y = 0. \tag{12}$$

Although k_x and k_y are constants, as long as they satisfy (11) they can be real or imaginary. In this chapter, we are interested in solutions that are periodic in the x direction, so we can think of k_x as being real and $k_x^2 > 0$. Furthermore, the value of k_x is fixed by the assumed functional form of the surface currents and charges. Equation (11) then determines k_y from given values of k_x and ω. In solving (11) for k_y, we must take the square root of a quantity that can be positive or negative. By way of distinguishing the two roots of (11) solved for k_y, we define

$$\boxed{\beta \equiv \begin{cases} |\sqrt{\omega^2\mu\epsilon - k_x^2}|; & \omega^2\mu\epsilon > k_x^2 \\ -j|\sqrt{k_x^2 - \omega^2\mu\epsilon}|; & \omega^2\mu\epsilon < k_x^2 \end{cases}} \tag{13}$$

and write the two solutions to (11) as

$$k_y \equiv \mp\beta \tag{14}$$

Thus, β is defined as either positive real or negative imaginary, and what we have found for the product solution $X(x)Y(y)$ are combinations of products

$$\hat{H}_z\alpha \left\{ \begin{matrix} \cos k_x x \\ \sin k_x x \end{matrix} \right\} \left\{ \begin{matrix} e^{-j\beta y} \\ e^{j\beta y} \end{matrix} \right\} \tag{15}$$

Note that if $\omega^2\mu\epsilon < k_x^2$, k_y is defined by (13) and (14) such that the field, which is periodic in the x direction, decays in the $+y$ direction for the upper solution but decays in the $-y$ direction for the lower solution. These fields resemble solutions to

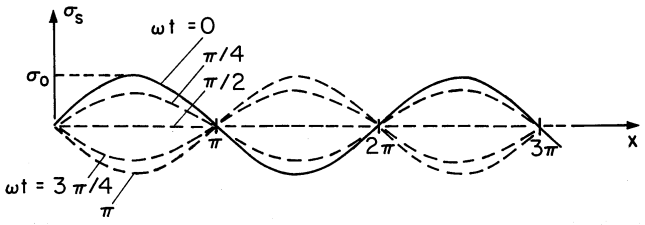


Fig. 12.6.2 Standing wave of surface charge density.

Laplace's equation. Indeed, in the limit where $\omega^2\mu\epsilon \ll k_x^2$, the Helmholtz equation becomes Laplace's equation.

As the frequency is raised, the rate of decay in the $\pm y$ directions decreases until k_y becomes real, at which point the solutions take a form that is in sharp contrast to those for Laplace's equation. With $\omega^2\mu\epsilon > k_x^2$, the solutions that we assumed to be periodic in the x direction are *also periodic in the y direction.*

The wave propagation in the y direction that renders the solutions periodic in y is more evident if the product solutions of (15) are written with the time dependence included.

$$H_z \,\alpha \left\{ \begin{matrix} \cos k_x x \\ \sin k_x x \end{matrix} \right\} e^{j(\omega t \mp \beta y)} \tag{16}$$

For $\omega^2\mu\epsilon > k_x^2$, the upper and lower signs in (16) [and hence in (14)] correspond to waves propagating in the positive and negative y directions, respectively.

By taking a linear combination of the trigonometric functions in (16), we can also form the complex exponential $\exp(jk_x x)$. Thus, another expression of the solutions given by (16) is as

$$H_z \,\alpha\, e^{j(\omega t \mp \beta y \mp k_x x)} \tag{17}$$

Instead of having standing waves in the x direction, as represented by (16), we now have solutions that are traveling in the $\pm x$ directions. Examples 12.6.1 and 12.6.2, respectively, illustrate how standing-wave and traveling-wave fields are excited.

Example 12.6.1. Standing-Wave TM Fields

Consider the field response to a surface charge density that is in the sinusoidal steady state and represented by

$$\sigma_s = Re\left[\hat{\sigma}_o \sin k_x x e^{j\omega t}\right] \tag{18}$$

The complex coefficient $\hat{\sigma}_o$, which determines the temporal phase and magnitude of the charge density at any given location x, is given. Figure 12.6.2 shows this function represented in space and time. The charge density is always zero at the locations $k_x x = n\pi$, where n is any integer, and oscillates between positive and negative peak amplitudes at locations in between. When it is positive in one half-period between nulls, it is negative in the adjacent half-periods. It has the x dependence of a standing wave.

The current density that is consistent with the surface charge density of (18) follows from (3).

$$K_x = Re\left[\frac{j\omega\hat{\sigma}_o}{k_x}\cos k_x x e^{j\omega t}\right] \tag{19}$$

With the surface current density in the z direction zero, the fields excited by these surface sources above and below the sheet are TM. The continuity conditions, (12.1.14)–(12.1.17), relate the fields to the given surface source distributions.

We start with Ampère's continuity condition, the x component of (12.1.15)

$$H_z^a - H_z^b = K_x \quad \text{at} \quad y = 0 \tag{20}$$

because it determines the x dependence of H_z as $\cos k_x x$. Of the possible combinations of solutions given by (15), we let

$$\hat{H}_z = \begin{cases} \hat{A}\cos k_x x e^{-j\beta y} \\ \hat{B}\cos k_x x e^{j\beta y} \end{cases} \tag{21}$$

The upper solution pertains to the upper region. Note that we select a y dependence that represents either a wave propagating in the $+y$ direction (for $\omega^2\mu\epsilon > 0$) or a field that decays in that direction (for $\omega^2\mu\epsilon < 0$). The lower solution, which applies in the lower region, either propagates in the $-y$ direction or decays in that direction. One of two conditions on the coefficients in (21) it follows from substitution of these equations into Ampère's continuity condition, (20).

$$\hat{A} - \hat{B} = \frac{j\omega\hat{\sigma}_o}{k_x} \tag{22}$$

A second condition follows from Faraday's continuity condition, (12.1.16), which requires that the tangential electric field be continuous.

$$\hat{E}_x^a - \hat{E}_x^b = 0 \quad \text{at} \quad y = 0 \tag{23}$$

Substitution of the solutions, (21), into (6) gives $\hat{E}_x^a$ and $\hat{E}_x^b$, from which follows

$$\hat{A} = -\hat{B} \tag{24}$$

Combining (2) and (3) we find

$$\hat{A} = -\hat{B} = \frac{j\omega\hat{\sigma}_o}{2k_x} \tag{25}$$

The remaining continuity conditions are now automatically satisfied. There is no normal flux density, so the flux continuity condition of (12.1.17) is automatically satisfied. But even if there were a y component of $\mathbf{H}$, continuity of tangential $\mathbf{E}$ as expressed by (23) would guarantee that this condition is satisfied.

In summary, the coefficients given by (25) can be used in (21), and those expressions introduced into (6) and (7), to determine the fields as

$$H_z = Re \pm \frac{j\omega\hat{\sigma}_o}{2k_x}\cos k_x x e^{j(\omega t \mp \beta y)} \tag{26}$$

$$E_x = Re - \frac{j\hat{\sigma}_o\beta}{2\epsilon k_x}\cos k_x x e^{j(\omega t \mp \beta y)} \tag{27}$$

$$E_y = Re \pm \frac{\hat{\sigma}_o}{2\epsilon}\sin k_x x e^{j(\omega t \mp \beta y)} \tag{28}$$

These fields are pictured in Fig. 12.6.3 for the case where σ_o is real. In the first field distribution, the frequency is low enough so that $\omega^2\mu\epsilon < k_x^2$. Thus, β as given by (13) has a negative imaginary value. The electric field pattern is shown when $t = 0$. At this instant, $\mathbf{H} = 0$. When $\omega t = \pi/2$, $\mathbf{H}$ is as shown while $\mathbf{E} = 0$. The $\mathbf{E}$ and $\mathbf{H}$ are 90 degrees out of temporal phase. The fields decay in the y direction, much as they would for a spatially periodic surface charge distribution in the EQS limit. Because they decay in the $\pm y$ directions for reasons that do not involve dissipation, these fields are sometimes called *evanescent waves*. The decay has its origins in the nature of quasistatic fields, shaped as they are by Laplace's equation. Indeed, with $\omega^2\mu\epsilon \ll k_x^2$, $\mathbf{E} = -\nabla\Phi$, and we are dealing with scalar solutions Φ to Laplace's equation. The field pattern corresponds to that of Example 5.6.2. As the frequency is raised, the rate of decay in the y direction decreases. The rate of decay, $|\beta|$, reaches zero as the frequency reaches $\omega = k_x/\sqrt{\mu\epsilon} = k_x c$. The physical significance of this condition is seen by recognizing that $k_x = 2\pi/\lambda_x$, where λ_x is the wavelength in the x direction of the imposed surface charge density, and that $\omega = 2\pi/T$ where T is the temporal period of the excitation. Thus, as the frequency is raised to the point where the fields no longer decay in the $\pm y$ directions, the period T has become $T = \lambda_x/c$, and so has become as short as the time required for an electromagnetic wave to propagate the wavelength λ_x.

The second distribution of Fig. 12.6.3 illustrates what happens to the fields as the frequency is raised beyond the cutoff frequency, when $\omega^2\mu\epsilon > k_x^2$. In this case, both $\mathbf{E}$ and $\mathbf{H}$ are shown in Fig. 12.6.3 when $t = 0$. Fields above and below the sheet propagate in the $\pm y$ directions, respectively. As time progresses, the evolution of the fields in the respective regions can be pictured as a translation of these distributions in the $\pm y$ directions with the phase velocities ω/k_y.

Transverse Electric (TE) Fields. Consider the case of a z-directed surface current density $\mathbf{K} = k_z\mathbf{i_z}$. Then, the surface charge density σ_s is zero. It follows from the superposition integral for Φ, (12.3.1), that $\Phi = 0$ and from the superposition integral for $\mathbf{A}$, (12.3.2), that $\mathbf{A} = A_z\mathbf{i_z}$. Equation (12.1.3) then shows that $\mathbf{E}$ is in the z direction, $\mathbf{E} = E_z\mathbf{i_z}$. *The electric field is transverse to the x and y axes*, while the magnetic field lines are in $x - y$ planes. These are the field directions summarized in the second part of Fig. 12.6.1.

In the sinusoidal steady state, it is convenient to use E_z as the function from which all other quantities can be derived, for it follows from Faraday's law that the two components of $\mathbf{H}$ can be written in terms of E_z.

$$\boxed{\hat{H}_x = -\frac{1}{j\omega\mu}\frac{\partial\hat{E}_z}{\partial y}} \tag{29}$$

$$\boxed{\hat{H}_y = \frac{1}{j\omega\mu}\frac{\partial\hat{E}_z}{\partial x}} \tag{30}$$

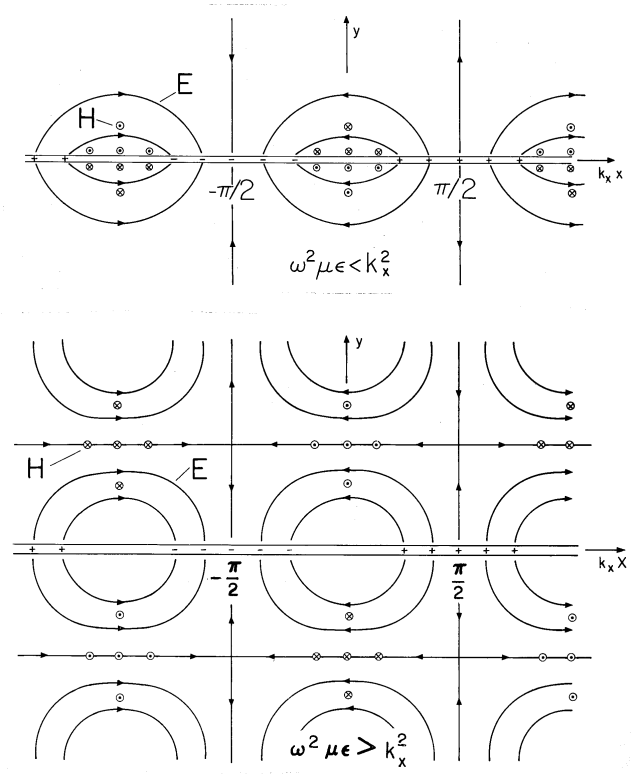


Fig. 12.6.3 TM waves due to standing wave of sources in $y = 0$ plane.

In the free space regions to either side of the sheet, each of the Cartesian components of $\mathbf{E}$ and $\mathbf{H}$ satisfies the wave equation. We have already seen this for $\mathbf{H}$. To obtain an expression playing a similar role for $\mathbf{E}$, we could again return to the wave equations for $\mathbf{A}$ and Φ. A more direct derivation begins by taking the curl of Faraday's law.

$$\nabla \times \nabla \times \mathbf{E} = -\nabla \times \frac{\partial \mu \mathbf{H}}{\partial t} \Rightarrow \nabla(\nabla \cdot \mathbf{E}) - \nabla^2 \mathbf{E} = -\mu \frac{\partial}{\partial t}(\nabla \times \mathbf{H}) \tag{31}$$

On the left, a vector identity has been used, while on the right the order of taking the time derivative and the curl has been reversed. Now, if we substitute for the divergence on the left using Gauss' law, and for the curl on the right using Ampère's law, it follows that

$$\boxed{\nabla^2 \mathbf{E} - \mu\epsilon \frac{\partial^2 \mathbf{E}}{\partial t^2} = \nabla\left(\frac{\rho}{\epsilon}\right) + \mu \frac{\partial \mathbf{J}}{\partial t}} \tag{32}$$

In the free space regions, the driving terms on the right are absent. In the case of transverse electric fields, $\hat{E}_z$ is the only field component. From (32), an assumed

time dependence of the form $\mathbf{E} = Re[\hat{E}_z \mathbf{i_z} \exp(j\omega t)]$ leads to the Helmholtz equation for $\hat{E}_z$

$$\boxed{\left(\frac{\partial^2}{\partial x^2} + \frac{\partial^2}{\partial y^2}\right)\hat{E}_z + \omega^2 \mu\epsilon \hat{E}_z = 0} \tag{33}$$

In retrospect, we see that the TE field relations are obtained from those for the TM fields by replacing $\mathbf{H} \rightarrow -\mathbf{E}$, $\mathbf{E} \rightarrow \mathbf{H}$, $\epsilon \rightarrow \mu$ and $\mu \rightarrow \epsilon$. This could have been expected, because in the free space regions to either side of the source sheet, Maxwell's equations are replicated by such an exchange of variables. The discussion of product solutions to the Helmholtz equation, given following (9), is equally applicable here.

Example 12.6.2. Traveling-Wave TE Fields

This example has two objectives. One is to illustrate the TE fields, while the other is to provide further insights into the nature of electrodynamic fields that are periodic in time and in one space dimension. In Example 12.6.1, these fields were induced by a *standing wave* of surface sources. Here the source takes the form of *a wave traveling in the x direction.*

$$K_z = Re\hat{K}_o e^{j(\omega t - k_x x)} \tag{34}$$

Again, the frequency of the source current, ω, and its spatial dependence, $\exp(-jk_x x)$, are prescribed. The traveling-wave x, t dependence of the source suggests that solutions take the form of (17).

$$\hat{E}_z = \begin{cases} \hat{A}e^{-j\beta y}e^{-jk_x x}; & y > 0 \\ \hat{B}e^{j\beta y}e^{-jk_x x}; & y < 0 \end{cases} \tag{35}$$

Faraday's continuity condition, (12.1.16), requires that

$$\hat{E}_z^a = \hat{E}_z^b \qquad \text{at} \qquad y = 0 \tag{36}$$

and this provides the first of two conditions on the coefficients in (35).

$$\hat{A} = \hat{B} \tag{37}$$

Ampère's continuity condition, (12.1.15), further requires that

$$-(\hat{H}_x^a - \hat{H}_x^b) = \hat{K}_z \qquad \text{at} \qquad y = 0 \tag{38}$$

With H_x found by substituting (35) into (29), this condition shows that

$$\hat{A} = \hat{B} = -\frac{\omega\mu\hat{K}_o}{2\beta} \tag{39}$$

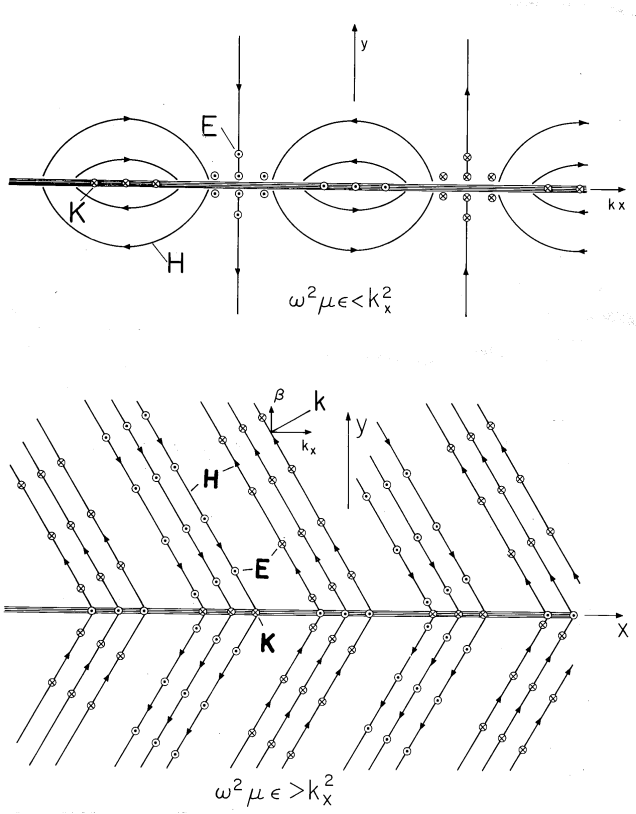


Fig. 12.6.4 TE fields induced by traveling-wave source in the $y = 0$ plane.

With the substitution of these coefficients into (35), we have

$$E_z = Re - \frac{\omega\mu}{2\beta}\hat{K}_o e^{j(\omega t - k_x x)} \begin{cases} e^{-j\beta y}; & y > 0 \\ e^{j\beta y}; & y < 0 \end{cases} \tag{40}$$

Provided that β is as defined by (13), these relations are valid regardless of the frequency. However, to emphasize the effect on the field when the frequency is such that $\omega^2\mu\epsilon < k_x^2$, these expressions are written for that case as

$$E_z = Re - \frac{j\omega\mu}{2|\beta|}\hat{K}_o e^{j(\omega t - k_x x)} \begin{cases} e^{-|\beta| y}; & y > 0 \\ e^{|\beta| y}; & y < 0 \end{cases} \tag{41}$$

The space time dependence of E_z, and $\mathbf{H}$ as found by using (40) to evaluate (29) and (30), is illustrated in Fig. 12.6.4. For $\omega^2\mu\epsilon > k_x^2$, the response to the traveling wave of surface current is waves with lines of constant amplitude given by

$$k_x x \pm k_y y = \text{constant} + \omega t \tag{42}$$

Thus, points of constant phase are lines of slope $\mp k_x/k_y$. The velocity of these lines in the x direction, ω/k_x, is called the phase velocity of the wave in the x

direction. The respective waves also have phase velocities in the $\pm y$ directions, in this case $\pm\omega/k_y$. The response to the traveling-current sheet in this high-frequency regime is a pair of uniform plane waves. Their direction of propagation is along the gradient of (42), and it is sometimes convenient to describe such plane waves by a vector wave number $\mathbf{k}$ having the direction of propagation of the planes of constant phase. The waves in the half-plane $Y > 0$ possess the k vector

$$\mathbf{k} = k_x\mathbf{i_x} + k_y\mathbf{i_y} \tag{43}$$

At frequencies low enough so that $\omega^2\mu\epsilon < k_x^2$, points of constant phase lie on lines perpendicular to the x axis. At a given location along the x axis, the fields vary in synchronism but decay in the $\pm y$ directions. In the limit when $\omega^2\mu\epsilon \ll k_x^2$ (or $f \ll c/\lambda_x$, where $\omega \equiv 2\pi f$), the $\mathbf{H}$ fields given by (29) and (30) become the MQS fields of a spatially periodic current sheet that happens to be traveling in the x direction. These "waves" are similar to those predicted by Laplace's equation except that for a given wavelength $2\pi/k_x$ in the x direction, they reach out further in the y direction. (A standing-wave version of this MQS field is exemplified by Prob. 8.6.9.) In recognition of the decay in the y direction, they are sometimes called *nonuniform plane waves* or *evanescent waves*. Note that the frequency demarcating propagation in the $\pm y$ directions from evanescence or decay in the $\pm y$ directions is $f = c/\lambda_x$ or the frequency at which the spatial period of the imposed current sheet is equal to one wavelength for a plane wave propagating in free space.

12.7 ELECTRODYNAMIC FIELDS IN THE PRESENCE OF PERFECT CONDUCTORS

The superposition integral approach is directly applicable to the determination of electrodynamic fields from sources specified throughout all space. In the presence of materials, sources are induced as well as imposed. These sources cannot be specified in advance. For example, if a perfect conductor is introduced, surface currents and charges are induced on its surface in just such a way as to insure that there is neither a tangential electric field at its surface nor a magnetic flux density normal to its surface.

We have already seen how the superposition integral approach can be used to find the fields in the vicinity of perfect conductors, for EQS systems in Chap. 4 and for MQS systems in Chap. 8. Fictitious sources are located in regions outside that of interest so that they add to those from the actual sources in such a way as to satisfy the boundary conditions. The approach is usually used to provide simple analytical descriptions of fields, in which case its application is a bit of an art– but it can also be the basis for practical numerical analyses involving complex systems.

We begin with a reminder of the boundary conditions that represent the influence of the sources induced on the surface of a perfect conductor. Such a conductor is defined as one in which $\mathbf{E} \to 0$ because $\sigma \to \infty$. Because the tangential electric field must be continuous across the boundary, it follows from Faraday's continuity condition that just outside the surface of the perfect conductor (having the unit normal $\mathbf{n}$)

$$\mathbf{n} \times \mathbf{E} = 0 \tag{1}$$

In Sec. 8.4, and again in Sec. 12.1, it was argued that (1) implies that the normal magnetic flux density just outside a perfectly conducting surface must be constant.

$$\frac{\partial}{\partial t}(\mathbf{n} \cdot \mu\mathbf{H}) = 0 \tag{2}$$

The physical origins and limitations of this boundary condition were one of the subjects of Chap. 10.

Method of Images. The symmetry considerations used to satisfy boundary conditions in Secs. 4.7 and 8.6 on certain planes of symmetry are equally applicable here, even though the fields now suffer time delays under transient conditions and phase delays in the sinusoidal steady state. We shall illustrate the method of images for an incremental dipole. It follows by superposition that the same method can be used with arbitrary source distributions.

Suppose that we wished to determine the fields associated with an electric dipole over a perfectly conducting ground plane. This dipole is the upper one of the two shown in Fig. 12.7.1. The associated electric and magnetic fields were determined in Sec. 12.2, and will be called $\mathbf{E}_p$ and $\mathbf{H}_p$, respectively. To satisfy the condition that there be no tangential electric field on the perfectly conducting plane, that plane is made one of symmetry in an equivalent configuration in which a second "image" dipole is mounted, having a direction and intensity such that at any instant, its charges are the negatives of those of the first dipole. That is, the + charge of the upper dipole is imaged by a negative charge of equal magnitude with the plane of symmetry perpendicular to and bisecting a line joining the two. The second dipole has been arranged so that at each instant in time, it produces a tangential $\mathbf{E} = \mathbf{E}_h$ that just cancels that of the first at each location on the symmetry plane. With

$$\mathbf{E} = \mathbf{E}_h + \mathbf{E}_p \tag{3}$$

we have made $\mathbf{E}$ satisfy (1) and hence (2) on the ground plane.

There are two ways of conceptualizing the "method of images." The one given here is consistent with the superposition integral point of view that is the theme of this chapter. The second takes the boundary value point of view of the next chapter. These alternative points of view are familiar from Chaps. 4 and 5 for EQS systems and from the first and second halves of Chap. 8 for MQS systems. From the boundary value point of view, in the upper half-space, $\mathbf{E}_p$ and $\mathbf{H}_p$ are particular solutions, satisfying the inhomogeneous wave equation everywhere in the volume of interest. In this region, the fields $\mathbf{E}_h$ and $\mathbf{H}_h$ due to the image dipole are then solutions to the homogeneous wave equation. Physically, they represent fields induced by sources on the perfectly conducting boundary.

To emphasize that the symmetry arguments apply regardless of the temporal details of the excitations, the fields shown in Fig. 12.7.1 are those of the electric dipole during the turn-on transient discussed in Example 12.2.1. At an arbitrary point on the ground plane, the "real" dipole produces fields that are not necessarily in the plane of the paper or perpendicular to it. Yet symmetry requires that the tangential $\mathbf{E}$ due to the sum of the fields is zero on the ground plane, and Faraday's law requires that the normal $\mathbf{H}$ is zero as well.

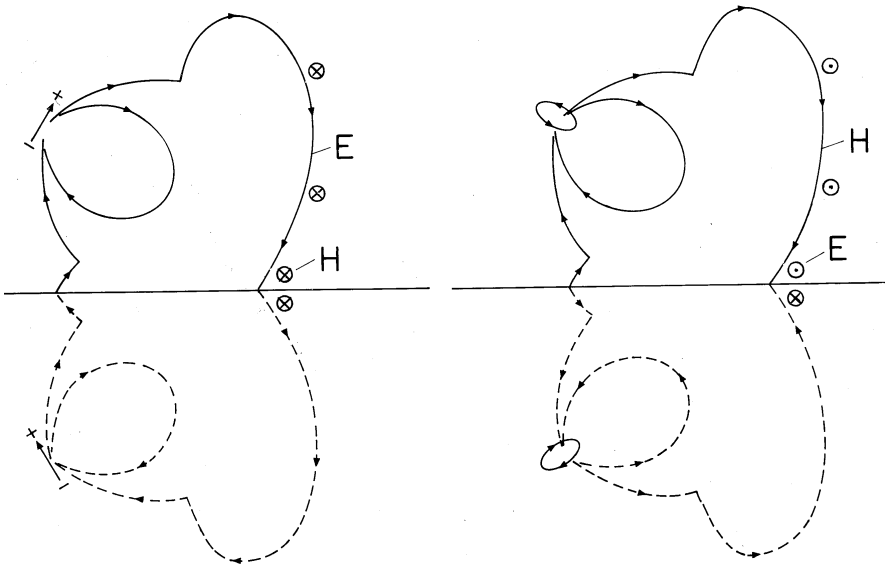


Fig. 12.7.1 Dipoles over a ground plane together with their images: (a) electric dipole; and (b) magnetic dipole.

In the case of the magnetic dipole over a ground plane shown in Fig. 12.7.1b, finding the image dipole is easiest by nulling the magnetic flux density normal to the ground plane, rather than the electric field tangential to the ground plane. The fields shown are the dual [(12.2.33)–(12.2.34)] of those for the electric dipole turn-on transient of Example 12.2.1. If we visualize the dipole as due to magnetic charge, the image charge is now of the same sign, rather than opposite sign, as the source.

Image methods are commonly used in extending the superposition integral techniques to antenna field patterns in order to treat the effects of a ground plane and of reflectors.

Example 12.7.1. Ground Planes and Reflectors

Quarter-Wave Antenna above a Ground Plane. The center-fed wire antenna of Example 12.4.1, shown in Fig. 12.7.2a, has a plane of symmetry, $\theta = \pi/2$, on which there is no tangential electric field. Thus, provided the terminal current remains the same, the field in the upper half-space remains unaltered if a perfectly conducting ground plane is placed in this plane. The radiation electric field is therefore given by (12.4.2), (12.4.5), and (12.4.8). Note that the lower half of the wire antenna serves as an image for the top half. Whether used for AM broadcasting or as a microwave mobile antenna (on the roof of an automobile), the height is usually a quarter-wavelength. In this case, $kl = \pi$, and these relations give

$$|\hat{E}_\theta| = \frac{1}{4}\sqrt{\mu/\epsilon}\frac{I_o}{r}|\psi_o(\theta)| \tag{4}$$

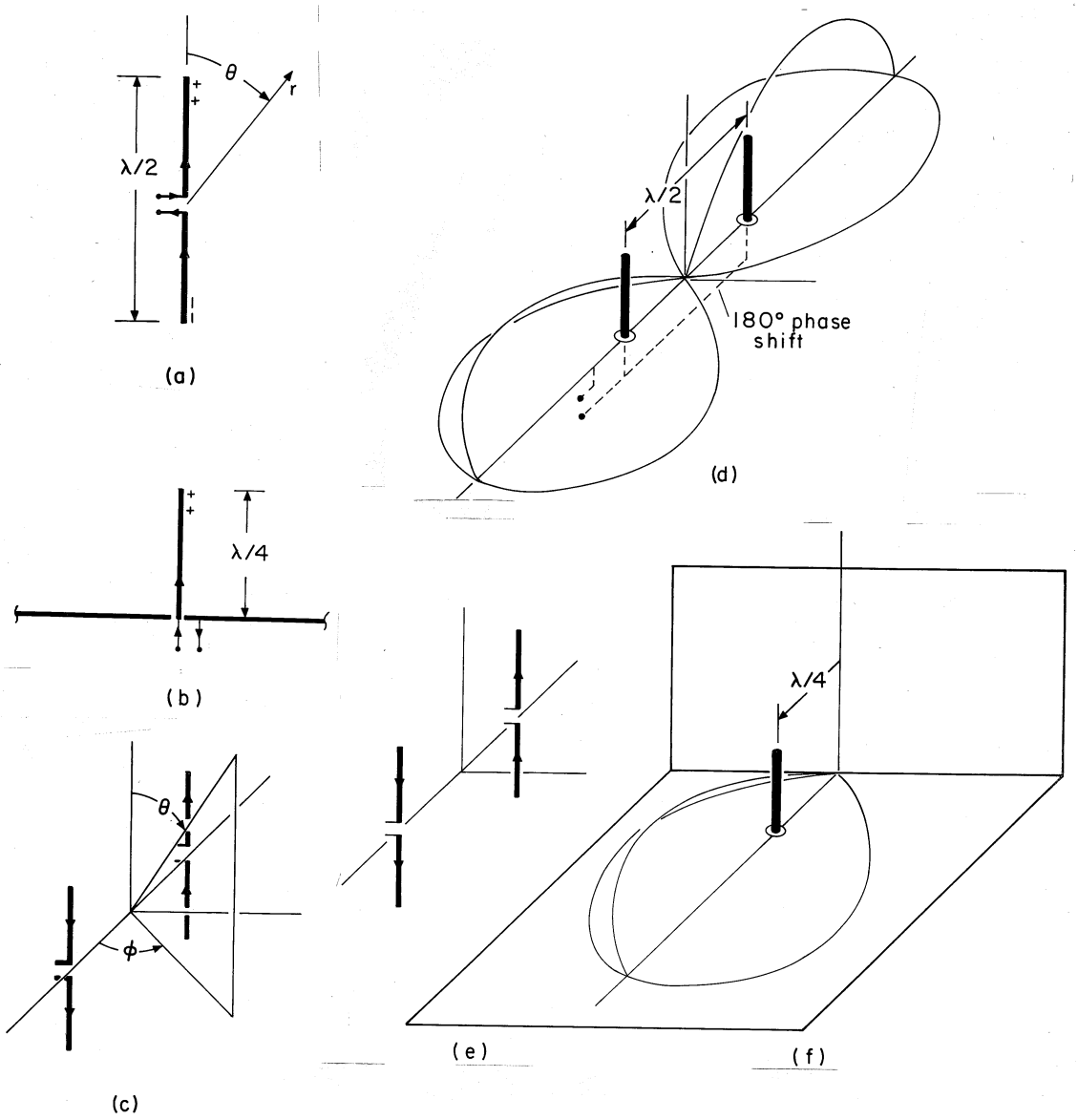


Fig. 12.7.2 Equivalent image systems for three physical systems.

where the radiation intensity pattern is

$$\psi_o = \frac{2}{\pi} \frac{\cos\left(\frac{\pi}{2}\cos\theta\right)}{\sin\theta} \tag{5}$$

Although the radiation pattern for the quarter-wave ground plane is the same as that for the half-wave center-fed wire antenna, the radiation resistance is half as

much. This follows from the fact that the surface of integration in (12.5.9) is now a hemisphere rather than a sphere.

$$R_{\text{rad}} = \frac{1}{2\pi}\sqrt{\mu/\epsilon}\int_0^{\pi/2}\frac{\cos^2\left(\frac{\pi}{2}\cos\theta\right)}{\sin\theta}d\theta = \sqrt{\mu/\epsilon}\frac{0.61}{2\pi} \tag{6}$$

The integral can be converted to a sine integral, which is tabulated. [9] In free space, this radiation resistance is 37Ω.

Two-Element Array over Ground Plane. The radiation pattern from an array of elements vertical to a ground plane can be deduced using the same image arguments. The pair of center-fed half-wave elements shown in Fig. 12.7.2c have lower elements that serve as images for the quarter-wave vertical elements over a ground plane shown in Fig. 12.7.2d.

If we consider elements with a half-wave spacing that are driven 180 degrees out of phase, the array factor is given by (12.4.15) with $ka = \pi$ and $\alpha_1 - \alpha_o = \pi$. Thus, with ψ_o from (5), the electric radiation field is

$$|\hat{E}_\theta| = \frac{1}{4}\sqrt{\mu/\epsilon}\frac{I_o}{r}|\psi_o(\theta)\psi_a(\theta,\phi)| \tag{7}$$

where

$$\psi_o\psi_a = \frac{4}{\pi}\cos\left[\frac{\pi}{2}(\sin\theta\cos\phi + 1)\right]\frac{\cos\left(\frac{\pi}{2}\cos\theta\right)}{\sin\theta} \tag{8}$$

The radiation pattern is proportional to the square of this function and is sketched in Fig. 12.7.2d. The field initiated by one element arrives in the far field at $\phi = 0$ and $\phi = \pi$ with a phase that reinforces that from the second element. The fields produced from the elements arrive out of phase in the "broadside" directions, and so the pattern nulls in those directions ($\phi = \pm\pi/2$).

Phased arrays of two or more verticals are often used by AM stations to provide directed broadcasting, with the ground plane preferably wet land, often with buried "radial" conductors to make the ground plane more nearly like a perfect conductor.

Ground-Plane with Reflector. The radiation pattern for the pair of vertical elements has no electric field tangential to a vertical plane located midway between the elements. Thus, the effect of one of the elements is equivalent to that of a reflector having a distance of a quarter-wavelength from the vertical element. This is the configuration shown in Fig. 12.7.2f.

The radiation resistance of the vertical quarter wave element with a reflector follows from (12.5.9), evaluated using (7). Now the integration is over the quarter-sphere which, together with the ground plane and the reflector plane, encloses the element at a radius of many wavelengths.

$$R_{\text{rad}} = \frac{\sqrt{\mu/\epsilon}}{\pi^2}\int_0^{\pi/2}\int_{-\pi/2}^{\pi/2}\frac{\cos^2\left[\frac{\pi}{2}(\sin\theta\cos\phi+1)\right]\cos^2\left(\frac{\pi}{2}\cos\theta\right)}{\sin\theta}d\phi d\theta \tag{9}$$

[9] It is perhaps easiest to carry out the integral numerically, as can be done with a programmable calculator. Note that the integrand is zero at $\theta = 0$.

Demonstration 12.7.1. Ground-Planes, Phased Arrays, and Reflectors

The experiment shown in Fig. 12.7.3 demonstrates the effect of the phase shift on the radiation pattern of the array considered in Example 12.7.1. The spacing and length of the vertical elements are 7.9 cm and 3.9 cm, respectively, which corresponds to $\lambda/2$ and $\lambda/4$ respectively at a frequency of 1.9 GHz. The ground plane consists of an aluminum sheet, with the array mounted on a section of the sheet that can be rotated. Thus, the radiation pattern in the plane $\theta = \pi/2$ can be measured by rotating the array, keeping the receiving antenna, which is many wavelengths away, fixed.

An audible tone can be used to indicate the amplitude of the received signal. To this end, the 1.9 GHz source is modulated at the desired audio frequency and detected at the receiver, amplified, and made audible through a loud speaker.

The 180 degree phase shift between the drives for the two driven elements is obtained by inserting a "line stretcher" in series with the coaxial line feeding one of the elements. By effectively lengthening the transmission line, the delay in the transmission line wave results in the desired phase delay. (Chapter 14 is devoted to the dynamics of signals propagating on such transmission lines.) The desired 180 degree phase shift is produced by rotating the array to a broadside position (the elements equidistant from the receiving antenna) and tuning the line stretcher so that the signals are nulled. With a further 90 degree rotation so that the elements are in the end-fire array position (in line with the receiving antenna), the detected signal should peak.

One vertical element can be regarded as the image for the other in a physical situation in which one element is backed at a quarter-wavelength by a reflector. This quarter-wave ground plane with a reflector is demonstrated by introducing a sheet of aluminum halfway between the original elements, as shown in Fig. 12.7.3. With the introduction of the sheet, the "image" element is shielded from the receiving antenna. Nevertheless, the detected signal should be essentially unaltered.

The experiment suggests many other interesting and practical configurations. For example, if the line stretcher is used to null the signal with the elements in end-fire array position, the elements are presumably driven in phase. Then, the signal should peak if the array is rotated 90 degrees so that it is broadside to the receiver.

Boundaries at the Nodes of Standing Waves. The TM fields found in Example 12.6.1 were those produced by a surface charge density taking the form of a standing wave in the $y = 0$ plane. Examination of the analytical expressions for $\mathbf{E}$, (12.6.27)–(12.6.28), and of their graphical portrayal, Fig. 12.6.3, shows that at every instant in time, $\mathbf{E}$ was normal to the planes where $k_x x = n\pi$ (n any integer), whether the waves were evanescent or propagating in the $\pm y$ directions. That is, the fields have nodal planes (of no tangential $\mathbf{E}$) parallel to the $y-z$ plane. These fields would therefore remain unaltered by the introduction of thin, perfectly conducting sheets in these planes.

Example 12.7.2. TM Fields between Parallel Perfect Conductors

To be specific, suppose that the fields found in Example 12.6.1 are to "fit" within a region bounded by perfectly conducting surfaces in the planes $x = 0$ and $x = a$. The configuration is shown in Fig. 12.7.4. We adjust k_x so that

$$k_x a = n\pi \Rightarrow k_x = \frac{n\pi}{a} \tag{10}$$

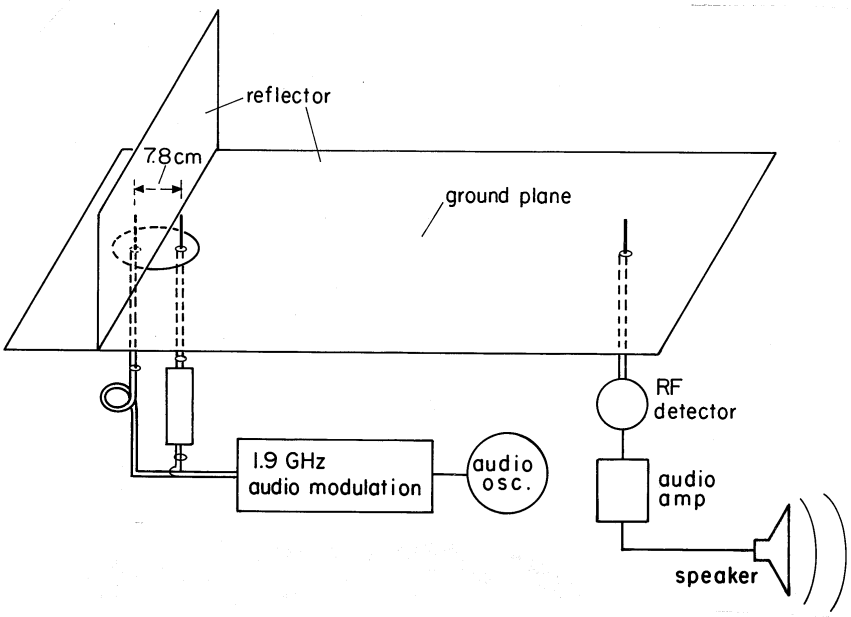


Fig. 12.7.3 Demonstration of phase shift on radiation pattern.

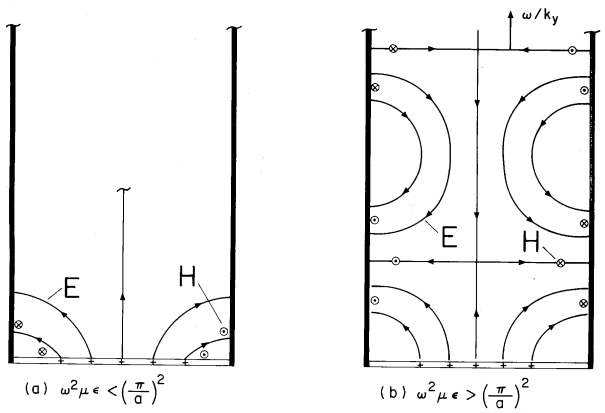


Fig. 12.7.4 The $n = 1$ TM fields between parallel plates (a) evanescent in y direction and (b) propagating in y direction.

where n indicates the number of half-wavelengths in the x direction of the fields shown in Fig. 12.6.3 that have been made to fit between the perfect conductors. To make the fields satisfy the wave equation, k_y must be given by (12.6.14) and (12.6.13). Thus, from this expression and (10), we see that for the *n-th mode* of the TM fields between the plates, the wave number in the y direction is related to the frequency by

$$k_y = \beta = \begin{cases} \sqrt{\omega^2\mu\epsilon - (n\pi/a)^2}; & \omega^2\mu\epsilon > (n\pi/a)^2 \\ -j\sqrt{(n\pi/a)^2 - \omega^2\mu\epsilon}; & \omega^2\mu\epsilon < (n\pi/a)^2 \end{cases} \tag{11}$$

We shall encounter these modes and this *dispersion equation* again in Chap. 13, where waves propagating between parallel plates will be considered from the boundary value point of view. There we shall superimpose these modes and, if need be, comparable TM field modes, to satisfy arbitrary source conditions in the plane $y = 0$. The sources in the plane $y = 0$ will then represent an antenna driving a parallel plate waveguide.

The standing-wave fields of Example 12.6.1 are the superposition of two traveling waves that exactly cancel at the nodal planes to form the standing wave in the x direction. To see this, observe that a standing wave, such as that for the surface charge distribution given by (12.6.18), can be written as the sum of two traveling waves.[10]

$$\sigma_s = \text{Re}\left[\hat{\sigma}_o \sin k_x x e^{j\omega t}\right] = \text{Re}\left[\frac{j\hat{\sigma}_o}{2} e^{j(\omega t - k_x x)} - \frac{j\hat{\sigma}_o}{2} e^{j(\omega t + k_x x)}\right] \tag{12}$$

By superposition, the field responses therefore must take this same form. For example, E_y as given by (12.6.28) can be written as

$$E_y = \text{Re}\ \mp \frac{\hat{\sigma}_o}{4\epsilon j}\left[e^{j(\omega t \mp \beta y - k_x x)} - e^{j(\omega t \mp \beta y + k_x x)}\right] \tag{13}$$

where the upper and lower signs again refer to the regions above and below the sheet of charge density. The first term represents the response to the component of the surface current density that travels to the right while the second is the response from the component traveling to the left. The planes of constant phase for the component waves traveling to the right, as well as their respective directions of propagation, are as for the TE fields of Fig. 12.6.4. Because the traveling wave components of the standing wave have phases that advance in the y direction with the same velocity, have the same wavelength in the x direction and the same frequency, their electric fields in the y-direction exactly cancel in the planes $x = 0$ and $x = a$ at each instant in time. With this recognition, we may construct TE *modes* of the parallel plate conductor structure of Fig. 12.7.4 by superposition of two countertraveling waves, one of which was studied in Example 12.6.2.

12.8 SUMMARY

This chapter has been concerned with the determination of the electrodynamic fields associated with given distributions of current density $\mathbf{J}(\mathbf{r}, t)$ and charge density $\rho(\mathbf{r}, t)$. We began by extending the vector potential $\mathbf{A}$ and scalar potential Φ to situations where both the displacement current density and the magnetic induction are important. The resulting field-potential relations, the first two equations in Table 12.8.1, are familiar from quasistatics, except that $-\partial\mathbf{A}/\partial t$ is added to $-\nabla\Phi$. As defined here, with $\mathbf{A}$ and Φ related by the gauge condition of (12.1.7) in the table, the current density $\mathbf{J}$ is the source of $\mathbf{A}$, while the charge density ρ is the source of

[10] $\sin u = (\exp(ju) - \exp(-ju))/2j$

TABLE 12.8.1

ELECTRODYNAMIC SOURCE-POTENTIAL RELATIONS

$\mathbf{B} = \mu\mathbf{H} = \nabla \times \mathbf{A}$	(12.1.1)	$\mathbf{E} = -\nabla\Phi - \dfrac{\partial \mathbf{A}}{\partial t}$	(12.1.3)
$\nabla^2\mathbf{A} - \mu\epsilon\dfrac{\partial^2\mathbf{A}}{\partial t^2} = -\mu\mathbf{J}$	(12.1.8)	$\mathbf{A} = \mu\displaystyle\int_{V'} \frac{\mathbf{J}\left(\mathbf{r}', t - \frac{\lvert\mathbf{r}-\mathbf{r}'\rvert}{c}\right)}{4\pi\lvert\mathbf{r}-\mathbf{r}'\rvert} dv'$	(12.3.2)
$\nabla^2\Phi - \mu\epsilon\dfrac{\partial^2\Phi}{\partial t^2} = -\dfrac{\rho}{\epsilon}$	(12.1.10)	$\Phi = \displaystyle\int_{V'} \frac{\rho\left(\mathbf{r}', t - \frac{\lvert\mathbf{r}-\mathbf{r}'\rvert}{c}\right)}{4\pi\epsilon\lvert\mathbf{r}-\mathbf{r}'\rvert} dv'$	(12.3.1)
$\nabla\cdot\mathbf{A} + \mu\epsilon\dfrac{\partial\Phi}{\partial t} = 0$	(12.1.7)	$\nabla\cdot\mathbf{J} + \dfrac{\partial\rho}{\partial t} = 0$	(12.1.20)

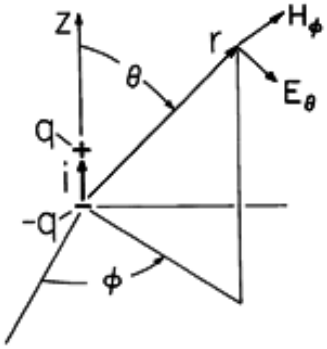
Φ. This is evident from the finding that, written in terms of $\mathbf{A}$ and Φ, Maxwell's equations imply the inhomogeneous wave equations summarized by (12.1.8) and (12.1.10) in Table 12.8.1.

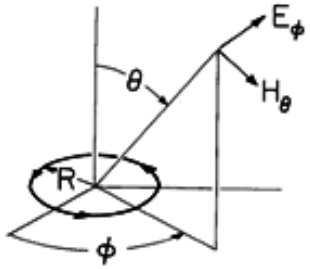
Given the sources everywhere, solutions to the inhomogeneous wave equations are given by the respective superposition integrals of Table 12.8.1. As a reminder that the sources in these integrals are related, the charge conservation law, (12.1.20), is included. The relation between $\mathbf{J}$ and ρ in the superposition integrals implied by charge conservation underlies the gauge relation between $\mathbf{A}$ and ρ, (12.1.7).

The derivation of the superposition integrals began in Sec. 12.2 with the identification of the potentials, and hence fields, associated with dipoles. Here, in remarkably simple terms, it was seen that the effect on the field at $\mathbf{r}$ of the source at $\mathbf{r}'$ is delayed by the time required for a wave to propagate through the intervening distance at the velocity of light, c. In the quasistatic limit, where times of interest are long compared to this delay time, the electric and magnetic dipoles considered in Sec. 12.2 are those familiar from electroquasistatics (Sec. 4.4) and magnetoquasistatics (Sec. 8.3), respectively. With the complete description of electromagnetic radiation from these dipoles, we could place the introduction to quasistatics of Sec. 3.3 on firmer ground.

For the purpose of determining the radiation pattern and radiation resistance of antennae, the radiation fields are of primary interest. For the sinusoidal steady state, Section 12.4 illustrated how the radiation fields could be superimposed to describe the radiation from given distributions of current elements representing an antenna, and how the fields from these elements could be combined to represent the radiation from an array. The elementary solutions from which these fields were constructed are those of an electric dipole, as summarized in Table 12.8.2. A similar

TABLE 12.8.2
DIPOLE RADIATION FIELDS





$\hat{H}_\phi = j\frac{kd}{4\pi}\hat{i}\sin\theta\frac{e^{-jkr}}{r}$	(12.2.23)	$\hat{E}_\phi = -\sqrt{\mu/\epsilon}\hat{H}_\theta$	(12.2.36)
$k \equiv \omega/c$			
$\hat{E}_\theta = \sqrt{\mu/\epsilon}\hat{H}_\phi$	(12.2.24)	$\hat{H}_\theta = -\frac{k^2}{4\pi}\hat{m}\sin\theta\frac{e^{-jkr}}{r}$	(12.2.35)
		$k \equiv \omega/c$	

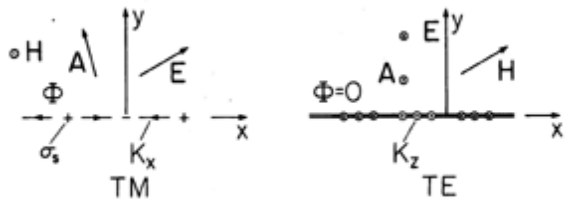
use can be made of the magnetic dipole radiation fields, which are also summarized for reference in the table.

The fields associated with planar sheet sources, the subject of Sec. 12.6, will be encountered again in the next chapter. In Sec. 12.6, the surface sources were taken as given. We found that sources having distributions that were dependent on (x, t) (independent of z) could be classified in accordance with the fields they produced, as summarized by the figures in Table 12.8.3. The TM and TE sources and fields, respectively, are described in terms of H_z and E_z by the relations given in the table. In the limit $\omega^2\mu\epsilon \ll k_x^2$, these source and field cases are EQS and MQS, respectively. This condition on the frequency means that the period $2\pi/\omega$ is much longer than the time λ_x/c for an electromagnetic wave to propagate a distance equal to a wavelength $\lambda_x = 2\pi/k_x$ in the x direction.

In the form of uniform and nonuniform plane waves, the Cartesian coordinate solutions to the homogeneous wave equation for these two-dimensional fields are summarized by the last equations in Table 12.8.3. In this chapter, we have thought of k_x as being imposed by the given source distribution. As the frequency is raised,

TABLE 12.8.3

TWO-DIMENSIONAL ELECTRODYNAMIC FIELDS



$\left(\frac{\partial^2}{\partial x^2}+\frac{\partial^2}{\partial y^2}\right)\hat{H}_z+\omega^2\mu\epsilon\hat{H}_z=0$	(12.6.9)	$\left(\frac{\partial^2}{\partial x^2}+\frac{\partial^2}{\partial y^2}\right)\hat{E}_z+\omega^2\mu\epsilon\hat{E}_z=0$	(12.6.33)
$\hat{E}_x=\frac{1}{j\omega\epsilon}\frac{\partial\hat{H}_z}{\partial y}$	(12.6.6)	$\hat{H}_x=-\frac{1}{j\omega\mu}\frac{\partial\hat{E}_z}{\partial y}$	(12.6.29)
$\hat{E}_y=\frac{-1}{j\omega\epsilon}\frac{\partial\hat{H}_z}{\partial x}$	(12.6.7)	$\hat{H}_y=\frac{1}{j\omega\mu}\frac{\partial\hat{E}_z}{\partial x}$	(12.6.30)

$$\begin{bmatrix}\hat{H}_z\\ \hat{E}_z\end{bmatrix}\propto \mathrm{Re}\,e^{j(\omega t\mp\beta y-k_x x)};\qquad \beta\equiv\begin{cases}|\sqrt{\omega^2\mu\epsilon-k_x^2}|, & \omega^2\mu\epsilon>k_x^2\\ -j|\sqrt{k_x^2-\omega^2\mu\epsilon}|, & \omega^2\mu\epsilon<k_x^2\end{cases}\qquad(12.6.13)$$

with the wavelength along the x direction $\lambda_x = 2\pi/k_x$ fixed, the fields at first decay in the $\pm y$ directions (are evanescent in those directions) and are in temporal synchronism with the sources. These are the EQS and MQS limits. As the frequency is raised, the fields extend further and further in the $\pm y$ directions. At the frequency $f = c/\lambda_x$, the field decay in the $\pm y$ directions gives way to propagation.

In the next chapter, these field solutions will be found fundamental to the description of fields in the presence of perfect conductors and dielectrics.

REFERENCES

[1] H. A. Haus and P. Penfield, Jr., **Electrodynamics of Moving Media**, MIT Press, Cambridge, Mass. (1967).

[2] J. R. Melcher, **Continuum Electromechanics**, Secs. 2.8 and 2.9, MIT Press, Cambridge, Mass. (1982).

P R O B L E M S

12.1 Electrodynamic Fields and Potentials

12.1.1* In Sec. 10.1, the electric field in an MQS system was divided into a particular part $\mathbf{E}_p$ satisfying Faraday's law, and an irrotational part $\mathbf{E}_h$. The latter was adjusted to make the sum satisfy appropriate boundary conditions. Show that in terms of Φ and $\mathbf{A}$, as defined in this section, $\mathbf{E}_p = -\partial\mathbf{A}/\partial t$ and $\mathbf{E}_h = -\nabla\Phi$, where these potentials satisfy (12.1.8) and (12.1.10) with the time derivatives neglected.

12.1.2 In Sec. 3.3, dimensional arguments were used to show that the quasistatic limits were valid in a system having a typical length L and time τ if $L/c \ll \tau$. Use similar arguments to show that the second term on the right in either (12.1.8) or (12.1.10) is negligible when this condition prevails. Note that the resulting equations are those for MQS (8.1.5) and EQS (4.2.2) systems.

12.2 Electrodynamic Fields of Source Singularities

12.2.1 An electric dipole has $q(t) = 0$ for $t < 0$ and $t > T$. When $0 < t < T$, $q(t) = Q[1-\cos(2\pi t/T)]/2$. Use sketches similar to those of Figs. 12.2.5 and 12.2.6 to show the field distributions when $t < T$ and $T < t$.

12.2.2* Use the "interchange of variables" property of Maxwell's equations to show that the sinusoidal steady state far fields of a magnetic dipole, (12.2.35) and (12.2.36), follow directly from (12.2.23), (12.2.24), and (12.2.32).

12.2.3* A magnetic dipole has a moment $m(t)$ having the time dependence shown in Fig. 12.2.5a where $dq(t) \rightarrow \mu m(t)$. Show that the fields are then much as shown in Fig. 12.2.6 with $\mathbf{E} \rightarrow \mathbf{H}$, $\mathbf{H} \rightarrow -\mathbf{E}$, and $\epsilon \leftrightarrow \mu$.

12.4 Antenna Radiation Fields in the Sinusoidal Steady State

12.4.1 An "end-fed" antenna consists of a wire stretching between $z = 0$, where it is driven by the current $I_o\cos(\omega t - \alpha_o)$, and $z = l$. At $z = l$, it is terminated in such a resistance that the current distribution over its length is a wave traveling with the velocity of light in the z direction; $i(z,t) = \mathrm{Re}\,[I_o \exp[j(\omega t - kz + \alpha_o)]]$ where $k \equiv \omega/c$.

(a) Determine the radiation pattern, $\Psi(\theta)$.

(b) For a one-wavelength antenna ($kl = 2\pi$), use a plot of $|\Psi(\theta)|$ to show that the lobes of the radiation pattern tend to be in the direction of the traveling wave.

12.4.2* An antenna is modeled by a distribution of incremental magnetic dipoles, as shown in Fig. P12.4.2. Define $\mathcal{M}(z)$ as a dipole moment per unit length so that for an incremental dipole located at z', $\hat{m} \rightarrow \mathcal{M}(z')dz'$. Given $\mathcal{M}$, show that

$$\hat{E}_\phi = \frac{k^2 l}{4\pi}\sqrt{\mu/\epsilon}\frac{e^{-jkr}}{r}\mathcal{M}_o e^{j\alpha_o}\psi_o(\theta) \qquad (a)$$

where

$$\psi_o(\theta) \equiv \frac{\sin\theta}{l}\int \frac{\mathcal{M}(z')}{\mathcal{M}_o}e^{j(k\mathbf{r}'\cdot\mathbf{i}_\mathbf{r}-\alpha_o)}dz' \qquad (b)$$

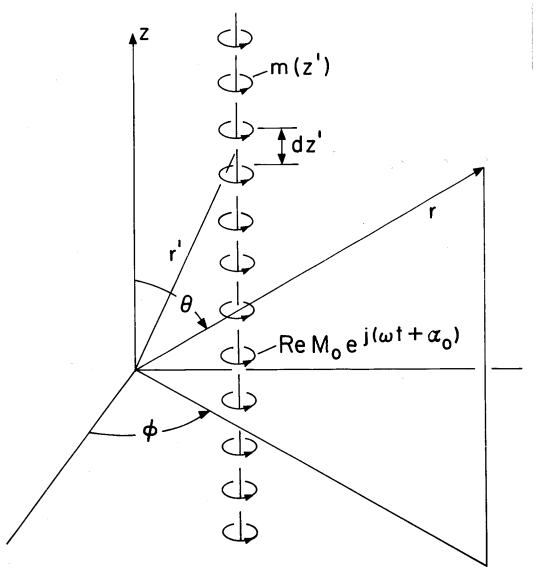


Fig. P12.4.2

12.4.3 A linear distribution of magnetic dipoles, described in general in Prob. 12.4.2, is excited so that $\mathcal{M}(z') = -\mathcal{M}_o \exp(j\alpha_o)\sin\beta(z-l)/\sin\beta l$, $0 \leq z \leq l$ where β is a given parameter (not necessarily ω/c). Determine $\psi_o(\theta)$.

12.4.4* For the three-element array shown in Fig. P12.4.4, the spacing is $\lambda/4$.

(a) Show that the array factor is

$$\psi_a(\theta,\phi) = \left[1 + e^{j\left(\frac{\pi}{2}\cos\phi\sin\theta+\alpha_1-\alpha_o\right)} + e^{j(\pi\cos\phi\sin\theta+\alpha_2-\alpha_o)}\right] \qquad (a)$$

(b) Show that for an array of in-phase short dipoles, the "broadside" radiation intensity pattern is

$$|\psi_o|^2|\psi_a|^2 = \left[1 + 2\cos\left(\frac{\pi}{2}\cos\phi\sin\theta\right)\right]^2\sin^2\theta \qquad (b)$$

(c) Show that for an array of short dipoles differing progressively by 90 degrees so that $\alpha_1 - \alpha_o = \pi/2$ and $\alpha_2 - \alpha_o = \pi$, the end-fire radiation pattern is

$$|\psi_o|^2|\psi_a|^2 = \left\{1 + 2\cos\left[\frac{\pi}{2}(\cos\phi\sin\theta + 1)\right]\right\}^2 \sin^2\theta \qquad (c)$$

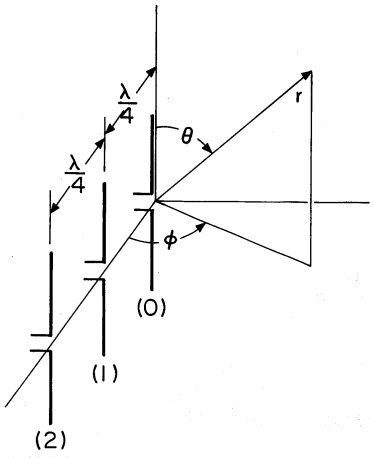


Fig. P12.4.4

12.4.5 Collinear elements have the half-wave spacing and configuration shown in Fig. P12.4.5.

(a) Determine the array factor $\psi_a(\theta)$.
(b) What is the radiation pattern if the elements are "short" dipoles driven in phase?
(c) What is the gain $G(\theta)$ for the array of part (b)?

12.5 Complex Poynting's Theorem and Radiation Resistance

12.5.1* A center-fed wire antenna has a length of $3\lambda/2$. Show that its radiation resistance in free space is 104Ω. (The definite integral can be evaluated numerically.)

12.5.2 The spherical coil of Example 8.5.1 is used as a magnetic dipole antenna. Its diameter is much less than a wavelength, and its equivalent circuit is an inductance L in parallel with a radiation resistance R_{rad}. In terms of the radius R, number of turns N, and frequency ω, what are L and R_{rad}?

12.6 Periodic Sheet Source Fields: Uniform and Nonuniform Plane Waves

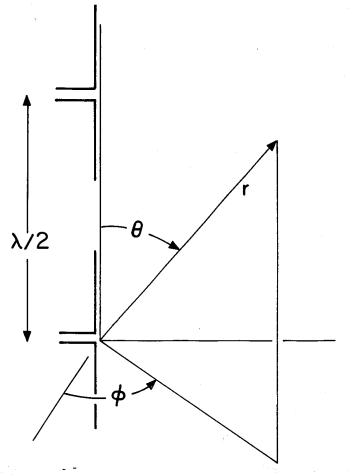


Fig. P12.4.5

12.6.1* In the plane $y = 0$, $K_z = 0$ and the surface charge density is given as the traveling wave $\sigma_s = \text{Re}\ \sigma_o \exp[j(\omega t - k_x x)] = \text{Re}\ [\sigma_o \exp(-jk_x x) \exp(j\omega t)]$, where σ_o, ω, and k_x are given real numbers.

(a) Show that the current density is

$$K_x = \text{Re}\ \frac{\omega\sigma_o}{k_x} e^{j(\omega t - k_x x)} = \text{Re}\left(\frac{\omega\sigma_o e^{-jk_x x}}{k_x}\right) e^{j\omega t} \qquad (a)$$

(b) Show that the fields are

$$\mathbf{H} = \mathbf{i_z} Re\big[\pm \frac{\omega\sigma_o}{2k_x} e^{\mp j\beta y} e^{j(\omega t - k_x x)}\big] \qquad (b)$$

$$\mathbf{E} = \text{Re}\left[\mathbf{i_x}\left(\frac{-\beta\sigma_o}{2\epsilon k_x} e^{\mp j\beta y}\right) + \mathbf{i_y}\big(\pm \frac{\sigma_o}{2\epsilon}\big) e^{\mp j\beta y}\right] e^{j(\omega t - k_x x)} \qquad (c)$$

where upper and lower signs, respectively, refer to the regions where $0 < y$ and $0 > y$.

(c) Sketch the field distributions at a given instant in time for β imaginary and β real.

12.6.2 In the plane $y = 0$, the surface current density is a standing wave, $\mathbf{K} = \text{Re}[\mathbf{i_z} K_o$
$\sin(k_x x) \exp(j\omega t)]$, and there is no surface charge density.

(a) Determine $\mathbf{E}$ and $\mathbf{H}$.
(b) Sketch these fields at a given instant in time for β real and β imaginary.
(c) Show that these fields can be decomposed into waves traveling in the $\pm x$ directions with the phase velocities $\pm\omega/k_x$.

12.6.3* In the planes $y = \pm d/2$, shown in Fig. P12.6.3, there are surface current densities $K_z = \mathrm{Re}\,\hat{K}\exp[j(\omega t - k_x x)]$, where $\hat{K} = \hat{K}^a$ at $y = d/2$ and $\hat{K} = \hat{K}^b$ at $y = -d/2$. The surface charge density is zero in each plane.

(a) Show that

$$E_z = \mathrm{Re}\,\frac{-\omega\mu}{2\beta}\left\{\hat{K}^a\begin{bmatrix}\exp\left[-j\beta\left(y-\frac{d}{2}\right)\right]\\ \exp\left[j\beta\left(y-\frac{d}{2}\right)\right]\\ \exp\left[j\beta\left(y-\frac{d}{2}\right)\right]\end{bmatrix}+\hat{K}^b\begin{bmatrix}\exp\left[-j\beta\left(y+\frac{d}{2}\right)\right]\\ \exp\left[-j\beta\left(y+\frac{d}{2}\right)\right]\\ \exp\left[j\beta\left(y+\frac{d}{2}\right)\right]\end{bmatrix}\right\}e^{j(\omega t-k_x x)}\quad\begin{matrix};\quad \frac{d}{2}<y\\ ;\quad -\frac{d}{2}<y<\frac{d}{2}\\ ;\quad y<-\frac{d}{2}\end{matrix}\qquad (a)$$

(b) Show that if $\hat{K}^b = -\hat{K}^a\exp(-j\beta d)$, the fields cancel in region (b) where $(y < -d/2)$, so that the combined radiation is unidirectional.

(c) Show that under this condition, the field in the region $y > d/2$ is

$$E_z = \mathrm{Re}\,\frac{-\omega\mu j}{\beta}\hat{K}^a e^{-j\beta d}(\sin\beta d)e^{j\left[\omega t-\beta\left(y-\frac{d}{2}\right)-k_x x\right]};\qquad \frac{d}{2}<y \qquad (b)$$

(d) With the structure used to impose the surface currents such that k_x is fixed, show that to maximize the wave radiated in region (a), the frequency should be

$$\omega = \frac{1}{\sqrt{\mu\epsilon}}\sqrt{k_x^2+\left[\frac{(2n+1)\pi}{2d}\right]^2} \qquad (c)$$

and that under this condition, the direction of the radiated wave is $\mathbf{k} = k_x\mathbf{i_x} + [(2n+1)\pi/2d]\mathbf{i_y}$ where $n = 0, 1, 2, \ldots$.

12.6.4 Surface charges in the planes $y = \pm d/2$ shown in Fig. P12.6.3 have the densities $\sigma_s = \mathrm{Re}\,\hat{\sigma}\exp[j(\omega t - k_x x)]$ where $\hat{\sigma} = \hat{\sigma}^a$ at $y = d/2$ and $\hat{\sigma} = \hat{\sigma}^b$ at $y = -d/2$.

(a) How should $\hat{\sigma}^a$ and $\hat{\sigma}^b$ be related to produce field cancellation in region (b)?

(b) Under this condition, what is H_z in region (a)?

(c) What frequencies give a maximum H_z in region (a), and what is the direction of propagation under this condition?

12.7 Electrodynamic Fields in the Presence of Perfect Conductors

12.7.1* An antenna consists of a ground plane with a $3\lambda/4$ vertical element in which a "quarter-wave stub" is used to make the current in the top half-wavelength in phase with that in the bottom quarter-wavelength. In each

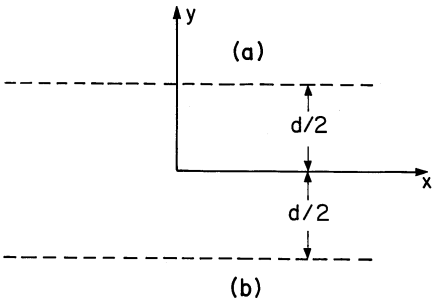


Fig. P12.6.3

section, the current has the sinusoidal distribution shown in Fig. P12.7.1. Show that the radiation intensity factor is

$$|\psi_o|^2|\psi_a|^2 = (2/\pi)^2|\cos[(\pi/2)\cos\theta]|^2|1 + 2\cos(\pi\cos\theta)|^2/|\sin\theta|^2$$

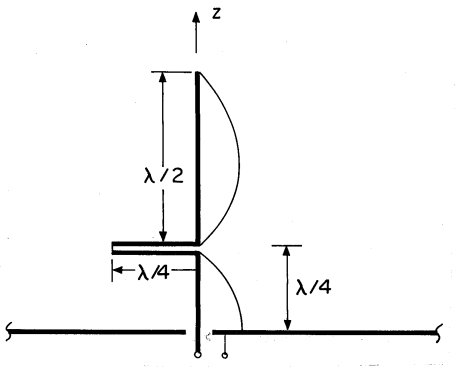


Fig. P12.7.1

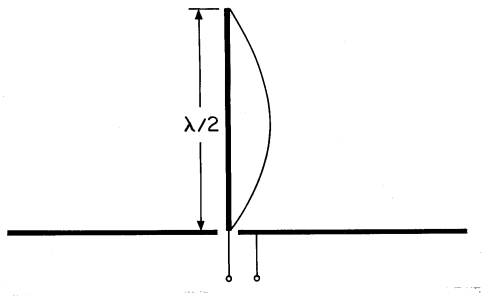


Fig. P12.7.2

12.7.2 A vertical half-wave antenna with a horizontal perfectly conducting ground plane is shown in Fig. P12.7.2. What is its radiation resistance?

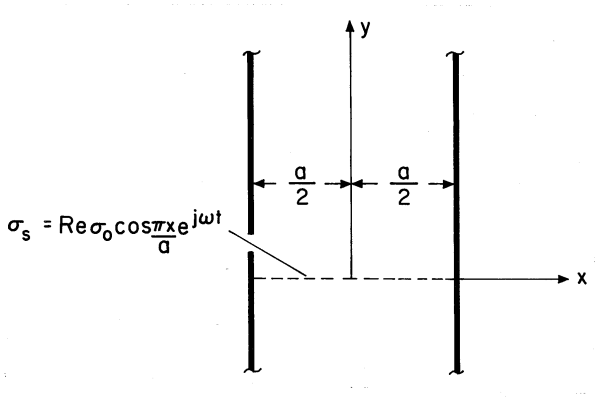


Fig. P12.7.3

12.7.3 Plane parallel perfectly conducting plates in the planes $x = \pm a/2$ form the walls of a waveguide, as shown in Fig. 12.7.3. Waves in the free-space region between are excited by a sheet of surface charge density $\sigma_s = \mathrm{Re}\,\sigma_o \cos(\pi x/a)\exp(j\omega t)$ and $K_z = 0$.

(a) Find the fields in regions $0 < y$ and $0 > y$. (Guess solutions that meet both the continuity conditions at the sheet and the boundary conditions on the perfectly conducting plates.) Are they TE or TM?
(b) What are the distributions of σ_s and $\mathbf{K}$ on the perfectly conducting plates?
(c) What is the "dispersion equation" relating ω to β?
(d) Sketch $\mathbf{E}$ and $\mathbf{H}$ for β imaginary and real.

12.7.4 Consider the configuration of Prob. 12.7.3, but with $\sigma_s = 0$ and $K_z = \mathrm{Re}\,\hat{K}_o \cos(\pi x/a)\exp(j\omega t)$ in the plane $y = 0$. Complete parts (a)-(d) of Prob. 12.7.3.

13

ELECTRODYNAMIC FIELDS: THE BOUNDARY VALUE POINT OF VIEW

13.0 INTRODUCTION

In the treatment of EQS and MQS systems, we started in Chaps. 4 and 8, respectively, by analyzing the fields produced by specified (known) sources. Then we recognized that in the presence of materials, at least some of these sources were induced by the fields themselves. Induced surface charge and surface current densities were determined by making the fields satisfy boundary conditions. In the volume of a given region, fields were composed of particular solutions to the governing quasistatic equations (the scalar and vector Poisson equations for EQS and MQS systems, respectively) and those solutions to the homogeneous equations (the scalar and vector Laplace equation, respectively) that made the total fields satisfy appropriate boundary conditions.

We now embark on a similar approach in the analysis of electrodynamic fields. Chapter 12 presented a study of the fields produced by specified sources (dipoles, line sources, and surface sources) and obeying the inhomogeneous wave equation. Just as in the case of EQS and MQS systems in Chap. 5 and the last half of Chap. 8, we shall now concentrate on solutions to the homogeneous source-free equations. These solutions then serve to obtain the fields produced by sources lying outside (maybe on the boundary) of the region within which the fields are to be found. In the region of interest, the fields generally satisfy the inhomogeneous wave equation. However in this chapter, where there are no sources in the volume of interest, they satisfy the homogeneous wave equation. It should come as no surprise that, following this systematic approach, we shall reencounter some of the previously obtained solutions.

In this chapter, fields will be determined in some limited region such as the volume V of Fig. 13.0.1. The boundaries might be in part perfectly conducting in the sense that on their surfaces, $\mathbf{E}$ is perpendicular and the time-varying $\mathbf{H}$ is tangential. The surface current and charge densities implied by these conditions

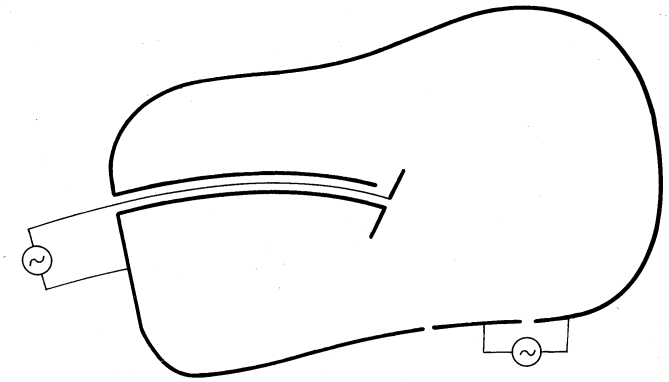


Fig. 13.0.1 Fields in a limited region are in part due to sources induced on boundaries by the fields themselves.

are not known until after the fields have been found. If there is material within the region of interest, it is perfectly insulating and of piece-wise uniform permittivity ϵ and permeability μ.[1] Sources $\mathbf{J}$ and ρ are specified throughout the volume and appear as driving terms in the inhomogeneous wave equations, (12.6.8) and (12.6.32). Thus, the $\mathbf{H}$ and $\mathbf{E}$ fields obey the inhomogeneous wave-equations.

$$\nabla^2\mathbf{H} - \mu\epsilon\frac{\partial^2\mathbf{H}}{\partial t^2} = -\nabla\times\mathbf{J} \tag{1}$$

$$\nabla^2\mathbf{E} - \mu\epsilon\frac{\partial^2\mathbf{E}}{\partial t^2} = \nabla\left(\frac{\rho}{\epsilon}\right) + \mu\frac{\partial\mathbf{J}}{\partial t} \tag{2}$$

As in earlier chapters, we might think of the solution to these equations as the sum of a part satisfying the inhomogeneous equations throughout V (particular solution), and a part satisfying the homogeneous wave equation throughout that region. In principle, the particular solution could be obtained using the superposition integral approach taken in Chap. 12. For example, if an electric dipole were introduced into a region containing a uniform medium, the particular solution would be that given in Sec. 12.2 for an electric dipole. The boundary conditions are generally not met by these fields. They are then satisfied by adding an appropriate solution of the homogeneous wave equation.[2]

In this chapter, the source terms on the right in (1) and (2) will be set equal to zero, and so we shall be concentrating on solutions to the homogeneous wave equation. By combining the solutions of the homogeneous wave equation that satisfy boundary conditions with the source-driven fields of the preceding chapter, one can describe situations with given sources and given boundaries.

In this chapter, we shall consider the propagation of waves in some axial direction along a structure that is uniform in that direction. Such waves are used to transport energy along pairs of conductors (transmission lines), and through

[1] If the region is one of free space, $\epsilon\to\epsilon_o$ and $\mu\to\mu_o$.

[2] As pointed out in Sec. 12.7, this is essentially what is being done in satisfying boundary conditions by the method of images.

waveguides (metal tubes at microwave frequencies and dielectric fibers at optical frequencies). We confine ourselves to the sinusoidal steady state.

Sections 13.1-13.3 study two-dimensional modes between plane parallel conductors. This example introduces the mode expansion of electrodynamic fields that is analogous to the expansion of the EQS field of the capacitive attenuator (in Sec. 5.5) in terms of the solutions to Laplace's equation. The principal and higher order modes form a complete set for the representation of arbitrary boundary conditions. The example is a model for a strip transmission line and hence serves as an introduction to the subject of Chap. 14. The higher-order modes manifest properties much like those found in Sec. 13.4 for hollow pipe guides.

The dielectric waveguides considered in Sec. 13.5 explain the guiding properties of optical fibers that are of great practical interest. Waves are guided by a dielectric core having permittivity larger than that of the surrounding medium but possess fields extending outside this core. Such electromagnetic waves are guided because the dielectric core slows the effective velocity of the wave in the guide to the point where it can match the velocity of a wave in the surrounding region that propagates along the guide but decays in a direction perpendicular to the guide.

The fields considered in Secs. 13.1–13.3 offer the opportunity to reinforce the notions of quasistatics. Connections between the EQS and MQS fields studied in Chaps. 5 and 8, respectively, and their corresponding electrodynamic fields are made throughout Secs. 13.1–13.4.

13.1 INTRODUCTION TO TEM WAVES

The **E** and **H** fields of transverse electromagnetic waves are directed transverse to the direction of propagation. It will be shown in Sec. 14.2 that such TEM waves propagate along structures composed of pairs of perfect conductors of arbitrary cross-section. The parallel plates shown in Fig. 13.1.1 are a special case of such a pair of conductors. The direction of propagation is along the y axis. With a source driving the conductors at the left, the conductors can be used to deliver electrical energy to a load connected between the right edges of the plates. They then function as a *parallel plate transmission line*.

We assume that the plates are wide in the z direction compared to the spacing, a, and that conditions imposed in the planes $y = 0$ and $y = -b$ are independent of z, so that the fields are also z independent. In this section, discussion is limited to either "open" electrodes at $y = 0$ or "shorted" electrodes. Techniques for dealing with arbitrarily terminated transmission lines will be introduced in Chap. 14. The "open" or "shorted" terminals result in standing waves that serve to illustrate the relationship between simple electrodynamic fields and the EQS and MQS limits. These fields will be generalized in the next two sections, where we find that the TEM wave is but one of an infinite number of modes of propagation along the y axis between the plates.

If the plates are open circuited at the right, as shown in Fig. 13.1.1, a voltage is applied at the left at $y = -b$, and the fields are EQS, the **E** that results is x directed. (The plates form a parallel plate capacitor.) If they are "shorted" at the right and the fields are MQS, the **H** that results from applying a current source at the left is z directed. (The plates form a one-turn inductor.) We are now looking

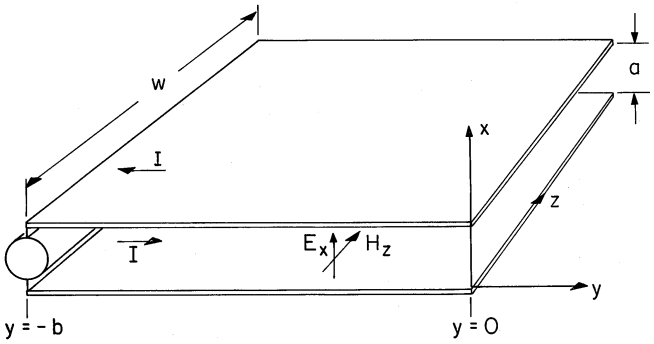


Fig. 13.1.1 Plane parallel plate transmission line.

for solutions to Maxwell's equations (12.0.7)–(12.0.10) that are similarly transverse to the y axis.

$$\mathbf{E} = E_x \mathbf{i_x}; \qquad \mathbf{H} = H_z \mathbf{i_z} \tag{1}$$

Fields of this form automatically satisfy the boundary conditions of zero tangential **E** and normal **H** (normal **B**) on the surfaces of the perfect conductors. These fields have no divergence, so the divergence laws for **E** and **H** [(12.0.7) and (12.0.10)] are automatically satisfied. Thus, the remaining laws, Ampère's law (12.0.8) and Faraday's law (12.0.9) fully describe these TEM fields. We pick out the only components of these laws that are not automatically satisfied by observing that $\partial E_x/\partial t$ drives the x component of Ampère's law and $\partial H_z/\partial t$ is the source term of the z component of Faraday's law.

$$\boxed{\frac{\partial H_z}{\partial y} = \epsilon \frac{\partial E_x}{\partial t}} \tag{2}$$

$$\boxed{\frac{\partial E_x}{\partial y} = \mu \frac{\partial H_z}{\partial t}} \tag{3}$$

The other components of these laws are automatically satisfied if it is assumed that the fields are independent of the transverse coordinates and thus depend only on y.

The effect of the plates is to terminate the field lines so that there are no fields in the regions outside. With Gauss' continuity condition applied to the respective plates, E_x terminates on surface charge densities of opposite sign on the respective electrodes.

$$\sigma_s(x = 0) = \epsilon E_x; \qquad \sigma_s(x = a) = -\epsilon E_x \tag{4}$$

These relationships are illustrated in Fig. 13.1.2a.

The magnetic field is terminated on the plates by surface current densities. With Ampère's continuity condition applied to each of the plates,

$$K_y(x = 0) = -H_z; \qquad K_y(x = a) = H_z \tag{5}$$

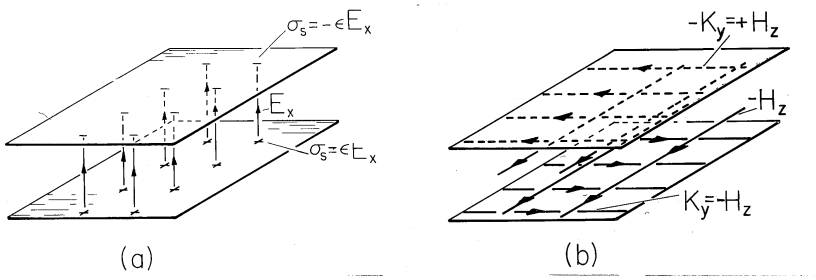


Fig. 13.1.2 (a) Surface charge densities terminating **E** of TEM field between electrodes of Fig. 13.1.1. (b) Surface current densities terminating **H**.

these relationships are represented in Fig. 13.1.2b.

We shall be interested primarily in the sinusoidal steady state. Between the plates, the fields are governed by differential equations having constant coefficients. We therefore assume that the field response takes the form

$$H_z = \mathrm{Re}\,\hat{H}_z(y)e^{j\omega t}; \qquad E_x = \mathrm{Re}\,\hat{E}_x(y)e^{j\omega t} \tag{6}$$

where ω can be regarded as determined by the source that drives the system at one of the boundaries. Substitution of these solutions into (2) and (3) results in a pair of ordinary constant coefficient differential equations describing the y dependence of E_x and H_z. Without bothering to write these equations out, we know that they too will be satisfied by exponential functions of y. Thus, we proceed to look for solutions where the functions of y in (6) take the form $\exp(-jk_y y)$.

$$H_z = \mathrm{Re}\,\hat{h}_z e^{j(\omega t - k_y y)}; \qquad E_x = \mathrm{Re}\,\hat{e}_x e^{j(\omega t - k_y y)} \tag{7}$$

Once again, we have assumed a solution taking a product form. Substitution into (2) then shows that

$$\hat{e}_x = -\frac{k_y}{\omega\epsilon}\hat{h}_z \tag{8}$$

and substitution of this expression into (3) gives the *dispersion equation*

$$k_y = \pm\beta; \qquad \beta \equiv \omega\sqrt{\mu\epsilon} = \frac{\omega}{c} \tag{9}$$

For a given frequency, there are two values of k_y. A linear combination of the solutions in the form of (7) is therefore

$$H_z = \mathrm{Re}\,[A^+ e^{-j\beta y} + A^- e^{j\beta y}]e^{j\omega t} \tag{10}$$

The associated electric field follows from (8) evaluated for the $\pm$ waves, respectively, using $k_y = \pm\beta$.

$$E_x = -\mathrm{Re}\,\sqrt{\mu/\epsilon}[A^+ e^{-j\beta y} - A^- e^{j\beta y}]e^{j\omega t} \tag{11}$$

The amplitudes of the waves, A^+ and A^-, are determined by the boundary conditions imposed in planes perpendicular to the y axis. The following example

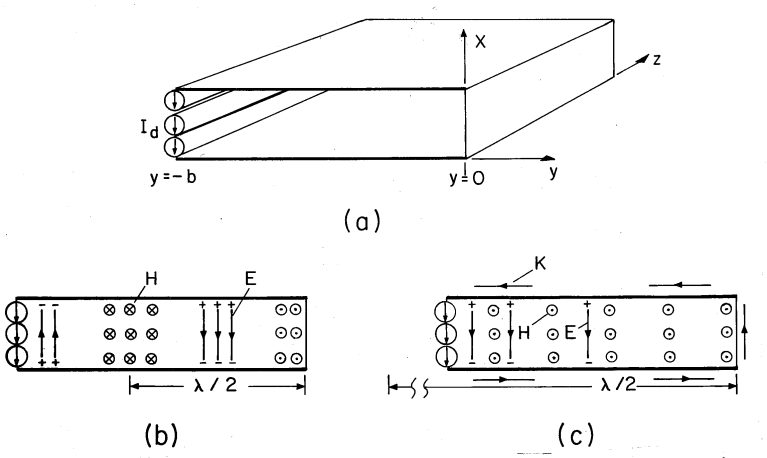


Fig. 13.1.3 (a) Shorted transmission line driven by a distributed current source. (b) Standing wave fields with **E** and **H** shown at times differing by 90 degrees. (c) MQS fields in limit where wavelength is long compared to length of system.

illustrates how the imposition of these *longitudinal boundary conditions* determines the fields. It also is the first of several opportunities we now use to place the EQS and MQS approximations in perspective.

Example 13.1.1. Standing Waves on a Shorted Parallel Plate Transmission Line

In Fig. 13.1.3a, the parallel plates are terminated at $y = 0$ by a perfectly conducting plate. They are driven at $y = -b$ by a current source I_d distributed over the width w. Thus, there is a surface current density $K_y = I_d/w \equiv K_o$ imposed on the lower plate at $y = -b$. Further, in this example we will assume that a distribution of sources is used in the plane $y = -b$ to make this driving surface current density uniform over that plane. In summary, the longitudinal boundary conditions are

$$E_x(0,t) = 0 \tag{12}$$

$$H_z(-b,t) = -\mathrm{Re}\,\hat{K}_o e^{j\omega t} \tag{13}$$

To make E_x as given by (11) satisfy the first of these boundary conditions, we must have the amplitudes of the two traveling waves equal.

$$A^+ = A^- \tag{14}$$

With this relation used to eliminate A^+ in (10), it follows from (13) that

$$A^+ = -\frac{\hat{K}_o}{2\cos\beta b} \tag{15}$$

We have found that the fields between the plates take the form of standing waves.

$$H_z = -\mathrm{Re}\,\hat{K}_o \frac{\cos\beta y}{\cos\beta b} e^{j\omega t} \tag{16}$$

$$E_x = -\mathrm{Re}\, j\hat{K}_o \sqrt{\mu/\epsilon} \frac{\sin \beta y}{\cos \beta b} e^{j\omega t} \tag{17}$$

Note that **E** and **H** are 90° out of temporal phase.[3] When one is at its peak, the other is zero. The distributions of **E** and **H** shown in Fig. 13.1.3b are therefore at different instants in time.

Every half-wavelength π/β from the short, **E** is again zero, as sketched in Fig. 13.1.3b. Beginning at a distance of a quarter-wavelength from the short, the magnetic field also exhibits nulls at half-wavelength intervals. Adjacent peaks in a given field are 180 degrees out of temporal phase.

The MQS Limit. If the driving frequency is so low that a wavelength is much longer than the length b, we have

$$\frac{2\pi b}{\lambda} = \beta b \ll 1 \tag{18}$$

In this limit, the fields are those of a one-turn inductor. That is, with $\sin(\beta y) \approx \beta y$ and $\cos(\beta y) \approx 1$, (16) and (17) become

$$H_z \rightarrow -\mathrm{Re}\, \hat{K}_o e^{j\omega t} \tag{19}$$

$$E_x \rightarrow -\mathrm{Re}\, \hat{K}_o j\omega\mu y e^{j\omega t} \tag{20}$$

The magnetic field intensity is uniform throughout and the surface current density circulates uniformly around the one-turn loop. The electric field increases in a linear fashion from zero at the short to a maximum at the source, where the source voltage is

$$v(t) = \int_0^a E_x(-b,t)dx = \mathrm{Re}\, \hat{K}_o j\omega\mu b a e^{j\omega t} = \frac{d\lambda}{dt} \tag{21}$$

To make it clear that these are the fields of a one-turn solenoid (Example 8.4.4), the flux linkage λ has been identified as

$$\lambda = L\frac{di}{dt}; \qquad i = \mathrm{Re}\, \hat{K}_o w e^{j\omega t}; \qquad L = \frac{ab\mu}{w} \tag{22}$$

where L is the inductance.

The MQS Approximation. In Chap. 8, we would have been led to these same limiting fields by assuming at the outset that the displacement current, the term on the right in (2), is negligible. Then, this one-dimensional form of Ampère's law and (1) requires that

$$\nabla \times \mathbf{H} \approx 0 \Rightarrow \frac{\partial H_z}{\partial y} \approx 0 \Rightarrow H_z = H_z(t) = -\mathrm{Re}\, \hat{K}_o e^{j\omega t} \tag{23}$$

If we now use this finding in Faraday's law, (3), integration on y and use of the boundary condition of (12) gives the same result for **E** as found taking the low-frequency limit, (20).

[3] In making this and the following deductions, it is helpful to take $\hat{K}_o$ as being real.

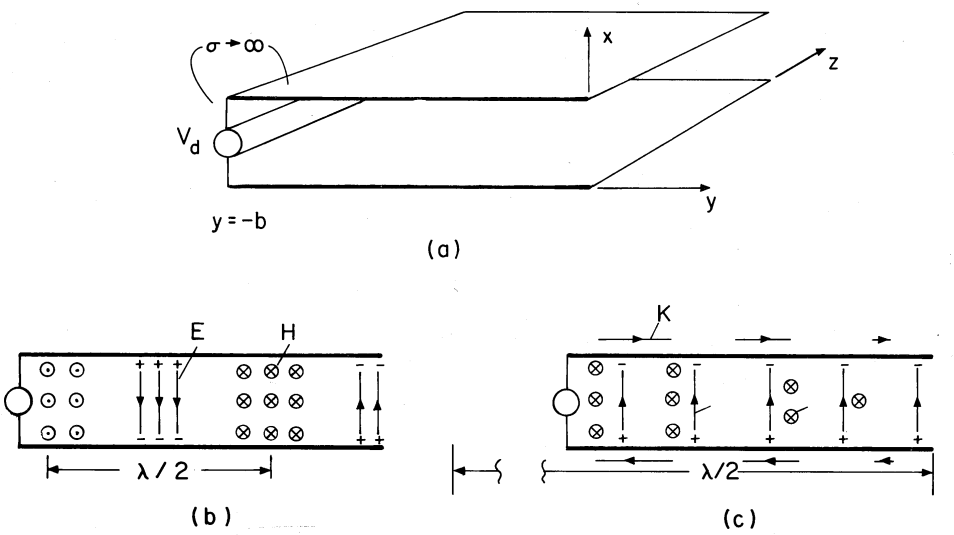


Fig. 13.1.4 (a) Open circuit transmission line driven by voltage source. (b) **E** and **H** at times that differ by 90 degrees. (c) EQS fields in limit where wavelength is long compared to b.

In the previous example, the longitudinal boundary conditions (conditions imposed at planes of constant y) could be satisfied exactly using the TEM mode alone. The short at the right and the distributed current source at the left each imposed a condition that was, like the TEM fields, independent of the transverse coordinates. In almost all practical situations, longitudinal boundary conditions which are independent of the transverse coordinates (used to describe transmission lines) are approximate. The open circuit termination at $y = 0$, shown in Fig. 13.1.4, is a case in point, as is the source which in this case is not distributed in the x direction.

If a longitudinal boundary condition is independent of z, the fields are, in principle, still two dimensional. Between the plates, we can therefore think of satisfying the longitudinal boundary conditions using a superposition of the modes to be developed in the next section. These consist of not only the TEM mode considered here, but of modes having an x dependence. A detailed evaluation of the coefficients specifying the amplitudes of the higher-order modes brought in by the transverse dependence of a longitudinal boundary condition is illustrated in Sec. 13.3. There we shall find that at low frequencies, where these higher-order modes are governed by Laplace's equation, they contribute to the fields only in the vicinity of the longitudinal boundaries. As the frequency is raised beyond their respective cutoff frequencies, the higher-order modes begin to propagate along the y axis and so have an influence far from the longitudinal boundaries.

Here, where we wish to restrict ourselves to situations that are well described by the TEM modes, we restrict the frequency range of interest to well below the lowest cutoff frequency of the lowest of the higher-order modes.

Given this condition, "end effects" are restricted to the neighborhood of a longitudinal boundary. Approximate boundary conditions then determine the distribution of the TEM fields, which dominate over most of the length. In the open

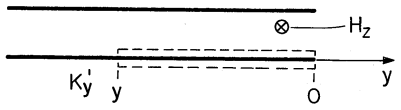


Fig. 13.1.5 The surface current density, and hence, H_z go to zero in the vicinity of the open end.

circuit example of Fig. 13.1.4a, application of the integral charge conservation law to a volume enclosing the end of one of the plates, as illustrated in Fig. 13.1.5, shows that K_y must be essentially zero at $y = 0$. For the TEM fields, this implies the boundary condition[4]

$$H_z(0,t) = 0 \tag{24}$$

At the left end, the vertical segments of perfect conductor joining the voltage source to the parallel plates require that E_x be zero over these segments. We shall show later that the higher-order modes do not contribute to the line integral of $\mathbf{E}$ between the plates. Thus, in so far as the TEM fields are concerned, the requirement is that

$$V_d(t) = \int_0^a E_x(-b,t)dx \Rightarrow E_x(-b,t) = \frac{V_d}{a} \tag{25}$$

Example 13.1.2. Standing Waves on an Open-Circuit Parallel Plate Transmission Line

Consider the parallel plates "open" at $y = 0$ and driven by a voltage source at $y = -b$. Boundary conditions are then

$$H_z(0,t) = 0; \qquad E_x(-b,t) = \mathrm{Re}\,\hat{V}_d e^{j\omega t}/a \tag{26}$$

Evaluation of the coefficients in (10) and (11) so that the boundary conditions in (26) are satisfied gives

$$A^+ = -A^- = -\frac{\hat{V}_d}{2a\cos\beta b}\sqrt{\epsilon/\mu} \tag{27}$$

It follows that the TEM fields between the plates, (10) and (11), are

$$H_z = \mathrm{Re}\, j\frac{\hat{V}_d}{a}\sqrt{\epsilon/\mu}\frac{\sin\beta y}{\cos\beta b}e^{j\omega t} \tag{28}$$

$$E_x = \mathrm{Re}\,\frac{\hat{V}_d}{a}\frac{\cos\beta y}{\cos\beta b}e^{j\omega t} \tag{29}$$

These distributions of $\mathbf{H}$ and $\mathbf{E}$ are shown in Fig. 13.1.4 at times that differ by 90 degrees. The standing wave is similar to that described in the previous example, except that it is now $\mathbf{E}$ rather than $\mathbf{H}$ that peaks at the open end.

[4] In the region outside, the fields are not confined by the plates. As a result, there is actually some radiation from the open end of the line, and this too is not represented by (24). This effect is small if the plate spacing is small compared to a wavelength.

The EQS Limit. In the low frequency limit, where the wavelength is much longer than the length of the plates so that $\beta b \ll 1$, the fields given by (28) and (29) become

$$H_z \rightarrow \mathrm{Re}\, j\frac{\hat{V}_d}{a}\omega\epsilon y e^{j\omega t} \tag{30}$$

$$E_x \rightarrow \mathrm{Re}\,\frac{\hat{V}_d}{a}e^{j\omega t} \tag{31}$$

At low frequencies, the fields are those of a capacitor. The electric field is uniform and simply equal to the applied voltage divided by the spacing. The magnetic field varies in a linear fashion from zero at the open end to its peak value at the voltage source. Evaluation of $-H_z$ at $z = -b$ gives the surface current density, and hence the current i, provided by the voltage source.

$$i = \mathrm{Re}\, j\omega\frac{\epsilon bw}{a}\hat{V}_d e^{j\omega t} \tag{32}$$

Note that this expression implies that

$$i = \frac{dq}{dt}; \qquad q = CV_d; \qquad C = \frac{\epsilon bw}{a} \tag{33}$$

so that the limiting behavior is indeed that of a plane parallel capacitor.

EQS Approximation. How would the quasistatic fields be predicted in terms of the TEM fields? If quasistatic, we expect the system to be EQS. Thus, the magnetic induction is negligible, so that the right-hand side of (3) is approximated as being equal to zero.

$$\nabla \times \mathbf{E} \approx 0 \Rightarrow \frac{\partial E_x}{\partial y} \approx 0 \tag{34}$$

It follows from integration of this expression and using the boundary condition of (26b) that the quasistatic $\mathbf{E}$ is

$$E_x = \frac{V_d}{a} \tag{35}$$

In turn, this result provides the displacement current density in Ampère's law, the right-hand side of (2).

$$\frac{\partial H_z}{\partial y} \simeq \epsilon\frac{d}{dt}\left(\frac{V_d}{a}\right) \tag{36}$$

The right-hand side of this expression is independent of y. Thus, integration with respect to y, with the "constant" of integration evaluated using the boundary condition of (26a), gives

$$H_z \simeq \epsilon\frac{d}{dt}V_d\frac{y}{a} \tag{37}$$

For the sinusoidal voltage drive assumed at the outset in the description of the TEM waves, this expression is consistent with that found in taking the quasistatic limit, (30).

Demonstration 13.1.1. Visualization of Standing Waves

A demonstration of the fields described by the two previous examples is shown in Fig. 13.1.6. A pair of sheet metal electrodes are driven at the left by an oscillator. A fluorescent lamp placed between the electrodes is used to show the distribution of the rms electric field intensity.

The gas in the tube is ionized by the oscillating electric field. Through the field-induced acceleration of electrons in this gas, a sufficient velocity is reached so that collisions result in ionization and an associated optical radiation. What is seen is a time average response to an electric field that is oscillating far more rapidly than can be followed by the eye.

Because the light is proportional to the magnitude of the electric field, the observed 0.75 m distance between nulls is a half-wavelength. It can be inferred that the generator frequency is $f = c/\lambda = 3 \times 10^8/1.5 = 200$ MHz. Thus, the frequency is typical of the lower VHF television channels.

With the right end of the line shorted, the section of the lamp near that end gives evidence that the electric field there is indeed as would be expected from Fig. 13.1.3b, where it is zero at the short. Similarly, with the right end open, there is a peak in the light indicating that the electric field near that end is maximum. This is consistent with the picture given in Fig. 13.1.4b. In going from an open to a shorted condition, the positions of peak light intensity, and hence of peak electric field intensity, are shifted by $\lambda/4$.

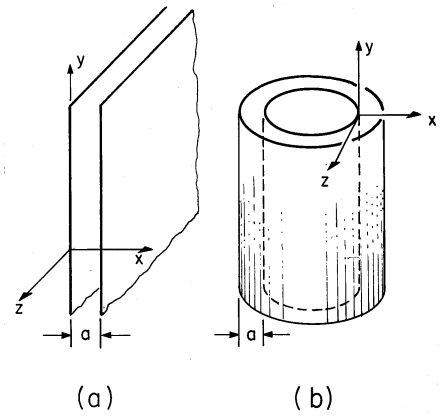


Fig. 13.2.1 (a) Plane parallel perfectly conducting plates. (b) Coaxial geometry in which z-independent fields of (a) might be approximately obtained without edge effects.

13.2 TWO-DIMENSIONAL MODES BETWEEN PARALLEL PLATES

This section treats the boundary value approach to finding the fields between the perfectly conducting parallel plates shown in Fig. 13.2.1a. Most of the mathematical ideas and physical insights that come from a study of modes on perfectly conducting structures that are uniform in one direction (for example, parallel wire and coaxial transmission lines and waveguides in the form of hollow perfectly conducting tubes) are illustrated by this example. In the previous section, we have already seen that the plates can be used as a transmission line supporting TEM waves. In this and the next section, we shall see that they are capable of supporting other electromagnetic waves.

Because the structure is uniform in the z direction, it can be excited in such a way that fields are independent of z. One way to make the structure approximately uniform in the z direction is illustrated in Fig. 13.2.1b, where the region between the plates becomes the annulus of coaxial conductors having very nearly the same radii. Thus, the difference of these radii becomes essentially the spacing a and the z coordinate maps into the ϕ coordinate. Another way is to make the plates very wide (in the z direction) compared to their spacing, a. Then, the fringing fields from the edges of the plates are negligible. In either case, the understanding is that the field excitation is uniformly distributed in the z direction. The fields are now assumed to be independent of z.

Because the fields are two dimensional, the classifications and relations given in Sec. 12.6 and summarized in Table 12.8.3 serve as our starting point. Cartesian coordinates are appropriate because the plates lie in coordinate planes. Fields either have $\mathbf{H}$ transverse to the $x-y$ plane and $\mathbf{E}$ in the $x-y$ plane (TM) or have $\mathbf{E}$ transverse and $\mathbf{H}$ in the $x-y$ plane (TE). In these cases, H_z and E_z are taken as the functions from which all other field components can be derived. We consider sinusoidal steady state solutions, so these fields take the form

$$H_z = \text{Re}\ \hat{H}_z(x,y)e^{j\omega t} \tag{1}$$

$$E_z = \text{Re}\ \hat{E}_z(x,y)e^{j\omega t} \tag{2}$$

These field components, respectively, satisfy the Helmholtz equation, (12.6.9) and (12.6.33) in Table 12.8.3, and the associated fields are given in terms of these components by the remaining relations in that table.

Once again, we find product solutions to the Helmholtz equation, where H_z and E_z are assumed to take the form $X(x)Y(y)$. This formalism for reducing a partial differential equation to ordinary differential equations was illustrated for Helmholtz's equation in Sec. 12.6. This time, we take a more mature approach, based on the observation that the coefficients of the governing equation are independent of y (are constants). As a result, $Y(y)$ will turn out to be governed by a constant coefficient differential equation. This equation will have exponential solutions. Thus, with the understanding that k_y is a yet to be determined constant (that will turn out to have two values), we assume that the solutions take the specific product forms

$$\hat{H}_z = \hat{h}_z(x)e^{-jk_y y} \tag{3}$$

$$\hat{E}_z = \hat{e}_z(x)e^{-jk_y y} \tag{4}$$

Then, the field relations of Table 12.8.3 become

TM Fields:

$$\frac{d^2\hat{h}_z}{dx^2} + p^2\hat{h}_z = 0 \tag{5}$$

where $p^2 \equiv \omega^2\mu\epsilon - k_y^2$

$$\hat{e}_x = -\frac{k_y}{\omega\epsilon}\hat{h}_z \tag{6}$$

$$\hat{e}_y = -\frac{1}{j\omega\epsilon}\frac{d\hat{h}_z}{dx} \tag{7}$$

TE Fields:

$$\frac{d^2\hat{e}_z}{dx^2} + q^2\hat{e}_z = 0 \tag{8}$$

where $q^2 \equiv \omega^2\mu\epsilon - k_y^2$

$$\hat{h}_x = \frac{k_y}{\omega\mu}\hat{e}_z \tag{9}$$

$$\hat{h}_y = \frac{1}{j\omega\mu}\frac{d\hat{e}_z}{dx} \tag{10}$$

The boundary value problem now takes a classic form familiar from Sec. 5.5. What values of p and q will make the electric field tangential to the plates zero? For the TM fields, $\hat{e}_y = 0$ on the plates, and it follows from (7) that it is the derivative of H_z that must be zero on the plates. For the TE fields, E_z must itself be zero at the plates. Thus, the boundary conditions are

TM Fields:

$$\frac{d\hat{h}_z}{dx}(0) = 0; \qquad \frac{d\hat{h}_z}{dx}(a) = 0 \tag{11}$$

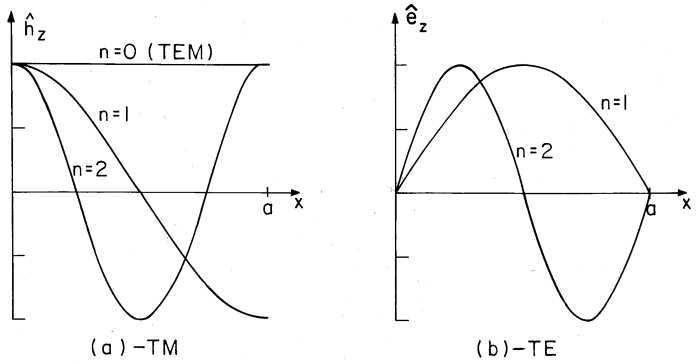


Fig. 13.2.2 Dependence of fundamental fields on x.

TE Fields:

$$\hat{e}_z(0) = 0; \qquad \hat{e}_z(a) = 0 \tag{12}$$

To check that all of the conditions are indeed met at the boundaries, note that if (11) is satisfied, there is neither a tangential **E** nor a normal **H** at the boundaries for the TM fields. (There is no normal **H** whether the boundary condition is satisfied or not.) For the TE field, E_z is the only electric field, and making E_z=0 on the boundaries indeed guarantees that $H_x = 0$ there, as can be seen from (9).

Representing the TM modes, the solution to (5) is a linear combination of $\sin(px)$ and $\cos(px)$. To satisfy the boundary condition, (11), at $x = 0$, we must select $\cos(px)$. Then, to satisfy the condition at $x = a$, it follows that $p = p_n = n\pi/a,\ n = 0, 1, 2, \ldots$

$$\hat{h}_z \propto \cos p_n x \tag{13}$$

$$p_n = \frac{n\pi}{a}, \quad n = 0, 1, 2, \ldots \tag{14}$$

These functions and the associated values of p are called *eigenfunctions* and *eigenvalues*, respectively. The solutions that have been found have the x dependence shown in Fig. 13.2.2a.

From the definition of p given in (5), it follows that for a given frequency ω (presumably imposed by an excitation), the wave number k_y associated with the n-th mode is

$$k_y \equiv \pm\beta_n; \qquad \beta_n \equiv \begin{cases} \sqrt{\omega^2\mu\epsilon - (n\pi/a)^2}; & \omega^2\mu\epsilon > (n\pi/a)^2 \\ -j\sqrt{(n\pi/a)^2 - \omega^2\mu\epsilon}; & \omega^2\mu\epsilon < (n\pi/a)^2 \end{cases} \tag{15}$$

Similar reasoning identifies the modes for the TE fields. Of the two solutions to (8), the one that satisfies the boundary condition at $x = 0$ is $\sin(qx)$. The second boundary condition then requires that q take on certain eigenvalues, q_n.

$$\hat{e}_z \propto \sin q_n x \tag{16}$$

$$q_n = \frac{n\pi}{a} \tag{17}$$

The x dependence of E_z is then as shown in Fig. 13.2.2b. Note that the case $n = 0$ is excluded because it implies a solution of zero amplitude.

For the TE fields, it follows from (17) and the definition of q given with (8) that[5]

$$k_y \equiv \pm\beta_n; \qquad \beta_n \equiv \begin{cases} \sqrt{\omega^2\mu\epsilon - (n\pi/a)^2}; & \omega^2\mu\epsilon > (n\pi/a)^2 \\ -j\sqrt{(n\pi/a)^2 - \omega^2\mu\epsilon}; & \omega^2\mu\epsilon < (n\pi/a)^2 \end{cases} \tag{18}$$

In general, the fields between the plates are a linear combination of all of the modes. In superimposing these modes, we recognize that $k_y = \pm\beta_n$. Thus, with coefficients that will be determined by boundary conditions in planes of constant y, we have the solutions

TM Modes:

$$\begin{aligned} H_z = &\text{Re}\left[A_o^+ e^{-j\beta_o y} + A_o^- e^{j\beta_o y}\right. \\ &\left. + \sum_{n=1}^{\infty}\left(A_n^+ e^{-j\beta_n y} + A_n^- e^{j\beta_n y}\right)\cos\frac{n\pi}{a}x\right]e^{j\omega t} \end{aligned} \tag{19}$$

TE Modes:

$$E_z = \text{Re}\sum_{n=1}^{\infty}\left(C_n^+ e^{-j\beta_n y} + C_n^- e^{j\beta_n y}\right)\sin\frac{n\pi}{a}x\, e^{j\omega t} \tag{20}$$

We shall refer to the n-th mode represented by these fields as the TM_n or TE_n mode, respectively.

We now make an observation about the TM_0 mode that is of far-reaching significance. Its distribution of H_z has no dependence on x [(13) with $p_n = 0$]. As a result, $E_y = 0$ according to (7). Thus, for the TM_0 mode, *both* **E** and **H** are transverse to the axial direction y. This special mode, represented by the $n = 0$ terms in (19), is therefore the *transverse electromagnetic* (TEM) mode featured in the previous section. One of its most significant features is that the relation between frequency ω and wave number in the y direction, k_y, [(15) with $n = 0$] is $k_y = \pm\omega\sqrt{\mu\epsilon} = \pm\omega/c$, the same as for a uniform electromagnetic plane wave. Indeed, as we saw in Sec. 13.1, it *is* a uniform plane wave.

The frequency dependence of k_y for the TEM mode and for the higher-order TM_n modes given by (15) are represented graphically by the $\omega - k_y$ plot of Fig. 13.2.3. For a given frequency, ω, there are two values of k_y which we have called $\pm\beta_n$. The dashed curves represent imaginary values of k_y. Imaginary values correspond to exponentially decaying and "growing" solutions. An exponentially "growing" solution is in fact a solution that decays in the $-y$ direction. Note that the switch from exponentially decaying to propagating fields for the higher-order modes occurs at the *cutoff frequency*

$$\omega_{cn} = \frac{1}{\sqrt{\mu\epsilon}}\left(\frac{n\pi}{a}\right) \tag{21}$$

[5] For the particular geometry considered here, it has turned out that the eigenvalues p_n and q_n are the same (with the exception of $n = 0$). This coincidence does not occur with boundaries having other geometries.

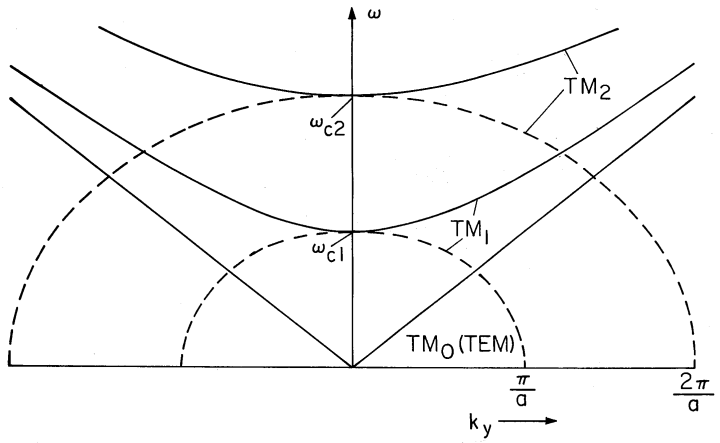


Fig. 13.2.3 Dispersion relation for TM modes.

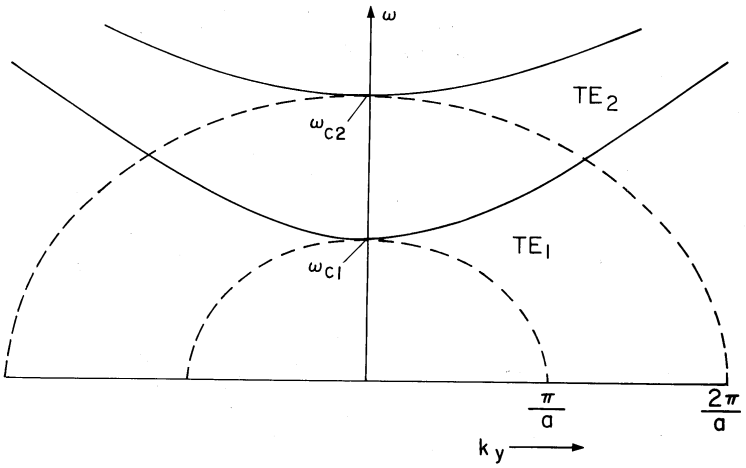


Fig. 13.2.4 Dispersion relation for TE modes.

The velocity of propagation of points of constant phase (for example, a point at which a field component is zero) is ω/k_y. Figure 13.2.3 emphasizes that for all but the TEM mode, the phase velocity is a function of frequency. The equation relating ω to k_y represented by this figure, (15), is often called the *dispersion equation.*

The dispersion equation for the TE modes is shown in Fig. 13.2.4. Although the field distributions implied by each branch are very different, in the case of the plane parallel electrodes considered here, the curves are the same as those for the $\text{TM}_{n\neq 0}$ modes.

The next section will provide greater insight into the higher-order TM and TE modes.

13.3 TE AND TM STANDING WAVES BETWEEN PARALLEL PLATES

In this section, we delve into the relationship between the two-dimensional higher-order modes derived in Sec. 13.2 and their sources. The examples are chosen to relate directly to case studies treated in quasistatic terms in Chaps. 5 and 8.

The matching of a longitudinal boundary condition by a superposition of modes may at first seem to be a purely mathematical process. However, even qualitatively it is helpful to *think* of the influence of an excitation in terms of the resulting modes. For quasistatic systems, this has already been our experience. For the purpose of estimating the dependence of the output signal on the spacing b between excitation and detection electrodes, the EQS response of the capacitive attenuator of Sec. 5.5 could be pictured in terms of the lowest-order mode. In the electrodynamic situations of interest here, it is even more common that one mode dominates. Above its cutoff frequency, a given mode can propagate through a waveguide to regions far removed from the excitation.

Modes obey orthogonality relations that are mathematically useful for the evaluation of the mode amplitudes. Formally, the mode orthogonality is implied by the differential equations governing the transverse dependence of the fundamental field components and the associated boundary conditions. For the TM modes, these are (13.2.5) and (13.2.11).

TM Modes:

$$\frac{d^2\hat{h}_{zn}}{dx^2} + p_n^2\hat{h}_{zn} = 0 \tag{1}$$

where

$$\frac{d\hat{h}_{zn}}{dx}(a) = 0; \qquad \frac{d\hat{h}_{zn}}{dx}(0) = 0$$

and for the TE modes, these are (13.2.8) and (13.2.12).

TE Modes:

$$\frac{d^2\hat{e}_{zn}}{dx^2} + q_n^2\hat{e}_{zn} = 0 \tag{2}$$

where

$$\hat{e}_{zn}(a) = 0; \qquad \hat{e}_{zn}(0) = 0$$

The word "orthogonal" is used here to mean that

$$\int_0^a \hat{h}_{zn}\hat{h}_{zm}dx = 0; \qquad n \neq m \tag{3}$$

$$\int_0^a \hat{e}_{zn}\hat{e}_{zm}dx = 0; \qquad n \neq m \tag{4}$$

These properties of the modes can be seen simply by carrying out the integrals, using the modes as given by (13.2.13) and (13.2.16). More fundamentally, they can be deduced from the differential equations and boundary conditions themselves, (1) and (2). This was illustrated in Sec. 5.5 using arguments that are directly applicable here [(5.5.20)–(5.5.26)].

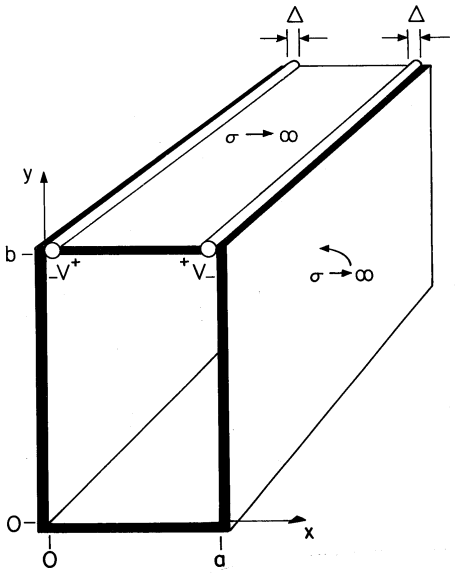


Fig. 13.3.1 Configuration for excitation of TM waves.

The following two examples illustrate how TE and TM modes can be excited in waveguides. In the quasistatic limit, the configurations respectively become identical to EQS and MQS situations treated in Chaps. 5 and 8.

Example 13.3.1. Excitation of TM Modes and the EQS Limit

In the configuration shown in Fig. 13.3.1, the parallel plates lying in the planes $x = 0$ and $x = a$ are shorted at $y = 0$ by a perfectly conducting plate. The excitation is provided by distributed voltage sources driving a perfectly conducting plate in the plane $y = b$. These sources constrain the integral of $\mathbf{E}$ across narrow insulating gaps of length Δ between the respective edges of the upper plate and the adjacent plates. All the conductors are modeled as perfect. The distributed voltage sources maintain the two-dimensional character of the fields even as the width in the z direction becomes long compared to a wavelength. Note that the configuration is identical to that treated in Sec. 5.5. Therefore, we already know the field behavior in the quasistatic (low frequency) limit.

In general, the two-dimensional fields are the sum of the TM and TE fields. However, here the boundary conditions can be met by the TM fields alone. Thus, we begin with H_z, (13.2.19), expressed as a single sum.

$$H_z = \mathrm{Re}\left[\sum_{n=0}^{\infty}(A_n^+ e^{-j\beta_n y} + A_n^- e^{j\beta_n y})\cos\frac{n\pi}{a}x\right]e^{j\omega t} \tag{5}$$

This field and the associated $\mathbf{E}$ satisfy the boundary conditions on the parallel plates at $x = 0$ and $x = a$. Boundary conditions are imposed on the tangential $\mathbf{E}$ at the longitudinal boundaries, where $y = 0$

$$E_x(x, 0, t) = 0 \tag{6}$$

and at the driving electrode, where $y = b$. We assume here that the gap lengths Δ are small compared to other dimensions of interest. Then, the electric field within each gap is conservative and the line integral of E_x across the gaps is equal to the gap voltages $\pm v$. Over the region between $x = \Delta$ and $x = a - \Delta$, the perfectly conducting electrode makes $E_x = 0$.

$$\int_{a-\Delta}^{a} E_x(x, b, t)dx = v; \qquad \int_{0}^{\Delta} E_x(x, b, t)dx = -v \tag{7}$$

Because the longitudinal boundary conditions are on E_x, we substitute H_z as given by (5) into the x component of Faraday's law [(12.6.6) of Table 12.8.3] to obtain

$$E_x = \mathrm{Re}\Big[\sum_{n=0}^{\infty} \frac{-\beta_n}{\omega\epsilon}\big(A_n^+ e^{-j\beta_n y} - A_n^- e^{j\beta_n y}\big)\cos\frac{n\pi}{a}x\Big]e^{j\omega t} \tag{8}$$

To satisfy the condition at the short, (6), $A_n^+ = A_n^-$ and (8) becomes

$$E_x = \mathrm{Re}\Big[\sum_{n=0}^{\infty} \frac{2j\beta_n}{\omega\epsilon}A_n^+ \sin\beta_n y \cos\frac{n\pi}{a}x\Big]e^{j\omega t} \tag{9}$$

This set of solutions satisfies the boundary conditions on three of the four boundaries. What we now do to satisfy the "last" boundary condition differs little from what was done in Sec. 5.5. The A_n^+'s are adjusted so that the summation of product solutions in (9) matches the boundary condition at $y = b$ summarized by (7). Thus, we write (9) with $y = b$ on the right and with the function representing (7) on the left. This expression is multiplied by the m'th eigenfunction, $\cos(m\pi x/a)$, and integrated from $x = 0$ to $x = a$.

$$\int_0^a \hat{E}_x(x, b)\cos\frac{m\pi x}{a}dx = \int_0^a \sum_{n=0}^{\infty} \frac{2j\beta_n A_n^+}{\omega\epsilon}\sin\beta_n b \cdot \cos\frac{n\pi}{a}x\ \cos\frac{m\pi}{a}xdx \tag{10}$$

Because the intervals where $\hat{E}_x(x, b)$ is finite are so small, the cosine function can be approximated by a constant, namely ± 1 as appropriate. On the right-hand side of (10), we exploit the orthogonality condition so as to pick out only one term in the infinite series.

$$\hat{v}[-1 + \cos m\pi] = \frac{2j\beta_m}{\omega\epsilon}\sin\beta_m b\Big(\frac{a}{2}\Big)A_m^+ \tag{11}$$

Of the infinite number of terms in the integral on the right in (10), only the term where $n = m$ has contributed. The coefficients follow from solving (11) and replacing $m \to n$.

$$A_n^+ = \begin{cases} 0; & n \text{ even} \\ \dfrac{-2\omega\epsilon\hat{v}}{j\beta_n a \sin\beta_n b}; & n \text{ odd} \end{cases} \tag{12}$$

With the coefficients $A_n^+ = A_n^-$ now determined, we can evaluate all of the fields. Substitution into (5), and (8) and into the result using (12.6.7) from Table 12.8.3 gives

$$H_z = \mathrm{Re}\left[\sum_{\substack{n=1\\ \mathrm{odd}}}^{\infty} \frac{4j\omega\epsilon\hat{v}}{\beta_n a}\frac{\cos\beta_n y}{\sin\beta_n b}\cos\frac{n\pi}{a}x\right]e^{j\omega t} \tag{13}$$

$$E_x = \mathrm{Re}\left[\sum_{\substack{n=1\\ \mathrm{odd}}}^{\infty} \frac{-4\hat{v}}{a}\frac{\sin\beta_n y}{\sin\beta_n b}\cos\frac{n\pi}{a}x\right]e^{j\omega t} \tag{14}$$

$$E_y = \mathrm{Re}\left[\sum_{\substack{n=1\\ \mathrm{odd}}}^{\infty} \frac{4n\pi}{a}\frac{\hat{v}}{(\beta_n a)}\frac{\cos\beta_n y}{\sin\beta_n b}\sin\frac{n\pi}{a}x\right]e^{j\omega t} \tag{15}$$

Note the following aspects of these fields (which we can expect to see in Demonstration 13.3.1). First, the magnetic field is directed perpendicular to the $x-y$ plane. Second, by making the excitation symmetric, we have eliminated the TEM mode. As a result, the only modes are of order $n = 1$ and higher. Third, at frequencies below the cutoff for the TM_1 mode, β_y is imaginary and the fields decay in the y direction.[6] Indeed, in the quasistatic limit where $\omega^2\mu\epsilon \ll (\pi/a)^2$, the electric field is the same as that given by taking the gradient of (5.5.9). In this same quasistatic limit, the magnetic field would be obtained by using this quasistatic $\mathbf{E}$ to evaluate the displacement current and then solving for the resulting magnetic field subject to the boundary condition that there be no normal flux density on the surfaces of the perfect conductors. Fourth, above the cutoff frequency for the $n = 1$ mode but below the cutoff for the $n = 2$ mode, we should find standing waves having a wavelength $2\pi/\beta_1$.

Finally, note that each of the expressions for the field components has $\sin(\beta_n b)$ in its denominator. With the frequency adjusted such that $\beta_n = n\pi/b$, this function goes to zero and the fields become infinite. This resonance condition results in an infinite response, because we have pictured all of the conductors as perfect. It occurs when the frequency is adjusted so that a wave reflected from one boundary arrives at the other with just the right phase to reinforce, upon a second reflection, the wave currently being initiated by the drive.

The following experiment gives the opportunity to probe the fields that have been found in the previous example. In practical terms, the structure considered might be a parallel plate waveguide.

Demonstration 13.3.1. Evanescent and Standing TM Waves

The experiment shown in Fig. 13.3.2 is designed so that the field distributions can be probed as the excitation is varied from below to above the cutoff frequency of the TM_1 mode. The excitation structures are designed to give fields approximating those found in Example 13.3.1. For convenience, $a = 4.8$ cm so that the excitation frequency ranges above and below a cut-off frequency of 3.1 GHz. The generator is modulated at an audible frequency so that the amplitude of the detected signal is converted to "loudness" of the tone from the loudspeaker.

In this TM case, the driving electrode is broken into segments, each insulated from the parallel plates forming the waveguide and each attached at its center to a

[6] $\sin(ju) = j\sinh(u)$ and $\cos(ju) = \cosh(u)$

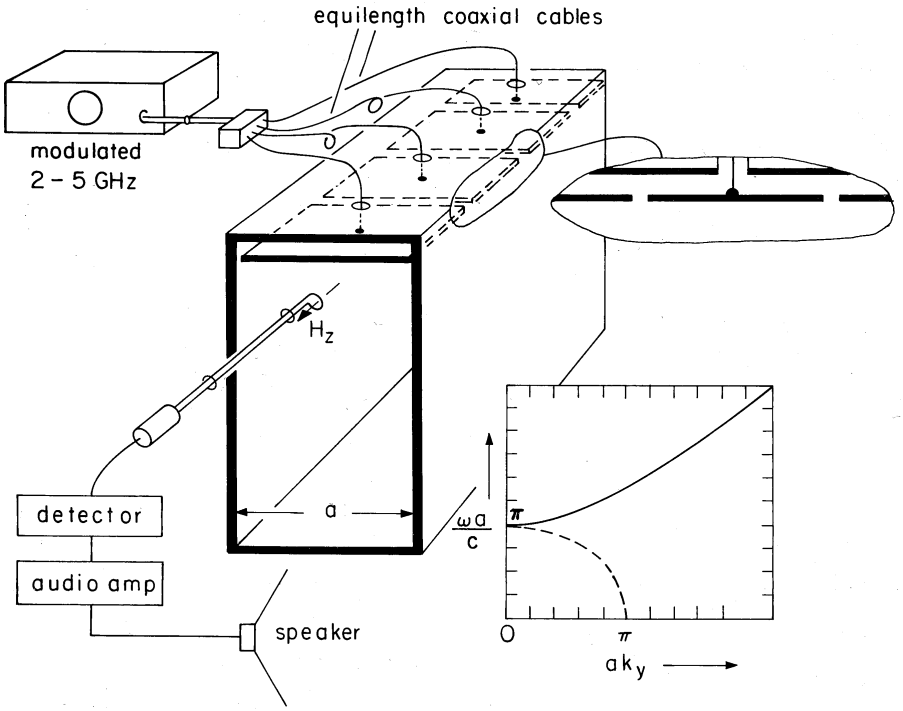


Fig. 13.3.2 Demonstration of TM evanescent and standing waves.

coaxial line from the generator. The segments insure that the fields applied to each part of the electrode are essentially in phase. (The cables feeding each segment are of the same length so that signals arrive at each segment in phase.) The width of the structure in the z direction is of the order of a wavelength or more to make the fields two dimensional. (Remember, in the vicinity of the lowest cutoff frequency, a is about one-half wavelength.) Thus, if the feeder were attached to a contiguous electrode at one point, there would be a tendency for standing waves to appear on the excitation electrode, much as they did on the wire antennae in Sec. 12.4. In the experiment, the segments are about a quarter-wavelength in the z direction but, of course, about a half-wavelength in the x direction.

In the experiment, $\mathbf{H}$ is detected by means of a one-turn coil. The voltage induced at the terminals of this loop is proportional to the magnetic flux perpendicular to the loop. Thus, for the TM fields, the loop detects its greatest signal when it is placed in an $x-y$ plane. To avoid interference with $\mathbf{E}$, the coaxial line connected to the probe as well as the loop itself are kept adjacent to the conducting walls (where H_z peaks anyway).

The spatial features of the field, implied by the normalized ω versus k_y plot of Fig. 13.3.2, can be seen by moving the probe about. With the frequency below cutoff, the field decays in the $-y$ direction. This exponential decay or evanescence decreases to a linear dependence at cutoff and is replaced above cutoff by standing waves. The value of k_y at a given frequency can be deduced from the experiment by measuring the quarter-wave distance from the short to the first null in the magnetic field. Note that if there are asymmetries in the excitation that result in excitation of the TEM mode, the standing waves produced by this mode will tend to obscure

the TM_1 mode when it is evanescent. The TEM waves do not have a cutoff!

As we have seen once again, the TM fields are the electrodynamic generalization of two-dimensional EQS fields. That is, in the quasistatic limit, the previous example becomes the capacitive attenuator of Sec. 5.5.[7]

We have more than one reason to expect that the two-dimensional TE fields are the generalization of MQS systems. First, this was seen to be the case in Sec. 12.6, where the TE fields associated with a given surface current density were found to approach the MQS limit as $\omega^2\mu\epsilon \ll k_y^2$. Second, from Sec. 8.6 we know that for every two-dimensional EQS configuration involving perfectly conducting boundaries, there is an MQS one as well.[8] In particular, the MQS analog of the capacitor attenuator is the configuration shown in Fig. 13.3.3. The MQS **H** field was found in Example 8.6.3.

In treating MQS fields in the presence of perfect conductors, we recognized that the condition of zero tangential **E** implied that there be no time-varying normal **B**. This made it possible to determine **H** without regard for **E**. We could then delay taking detailed account of **E** until Sec. 10.1. Thus, in the MQS limit, a system involving essentially a two-dimensional distribution of **H** can (and usually does) have an **E** that depends on the third dimension. For example, in the configuration of Fig. 13.3.3, a voltage source might be used to drive the current in the z direction through the upper electrode. This current is returned in the perfectly conducting ⊔-shaped walls. The electric fields in the vicinities of the gaps must therefore increase in the z direction from zero at the shorts to values consistent with the voltage sources at the near end. Over most of the length of the system, **E** is across the gap and therefore in planes *perpendicular* to the z axis. This MQS configuration does not excite pure TE fields. In order to produce (approximately) two-dimensional TE fields, provision must be made to make **E** as well as **H** two dimensional. The following example and demonstration give the opportunity to further develop an appreciation for TE fields.

Example 13.3.2. Excitation of TE Modes and the MQS Limit

An idealized configuration for exciting standing TE modes is shown in Fig. 13.3.4. As in Example 13.3.1, the perfectly conducting plates are shorted in the plane $y = 0$. In the plane $y = b$ is a perfectly conducting plate that is segmented in the z direction. Each segment is driven by a voltage source that is itself distributed in the x direction. In the limit where there are many of these voltage sources and perfectly conducting segments, the driving electrode becomes one that both imposes a z-directed **E** and has no z component of **B**. That is, just below the surface of this electrode, wE_z is equal to the sum of the source voltages. One way of approximately realizing this idealization is used in the next demonstration.

Let Λ be defined as the flux per unit length (length taken along the z direction) into and out of the enclosed region through the gaps of width Δ between the driving electrode and the adjacent edges of the plane parallel electrodes. The magnetic field

[7] The example which was the theme of Sec. 5.5 might equally well have been called the "microwave attenuator," for a section of waveguide operated below cutoff is used in microwave circuits to attenuate signals.

[8] The **H** satisfying the condition that $\mathbf{n} \cdot \mathbf{B} = 0$ on the perfectly conducting boundaries was obtained by replacing $\Phi \rightarrow A_z$ in the solution to the analogous EQS problem.

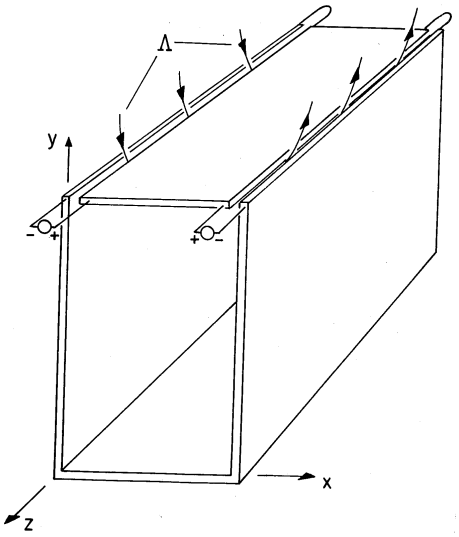


Fig. 13.3.3 Two-dimensional MQS configuration that does not have TE fields.

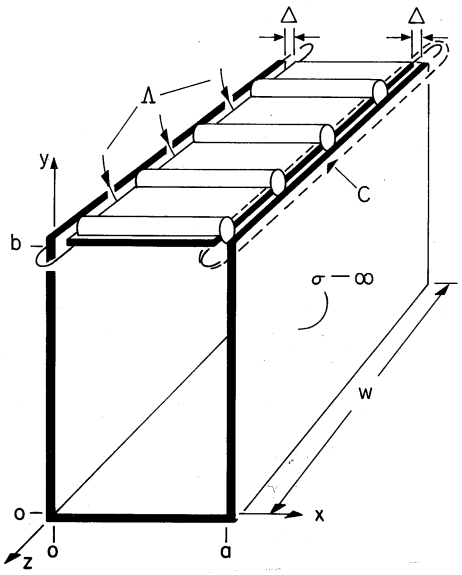


Fig. 13.3.4 Idealized configuration for excitation of TE standing waves.

normal to the driving electrode between the gaps is zero. Thus, at the upper surface, H_y has the distribution shown in Fig. 13.3.5a.

Faraday's integral law applied to the contour C of Fig. 13.3.4 and to a similar contour around the other gap shows that

$$E_z(x,b,t) = -\frac{d\Lambda}{dt} \Rightarrow \hat{E}_z = -j\omega\hat{\Lambda} \tag{16}$$

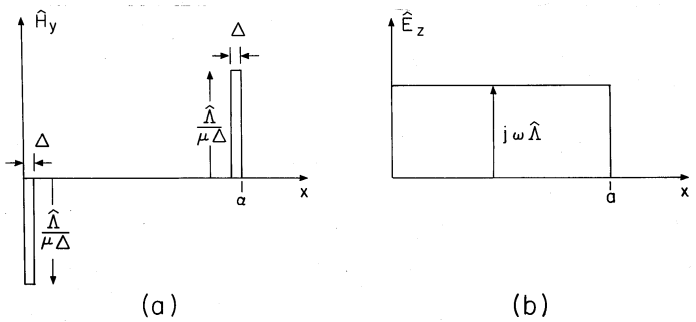


Fig. 13.3.5 Equivalent boundary conditions on normal **H** and tangential **E** at $y = b$.

Thus, either the normal **B** or the tangential **E** on the surface at $y = b$ is specified. The two must be consistent with each other, i.e., they must obey Faraday's law. It is perhaps easiest in this case to deal directly with E_z in finding the coefficients appearing in (13.2.20). Once they have been determined (much as in Example 13.3.1), **H** follows from Faraday's law, (12.6.29) and (12.6.30) of Table 12.8.3.

$$E_z = \mathrm{Re} \sum_{\substack{m=1 \\ \text{odd}}}^{\infty} -\frac{4j\hat{\Lambda}\omega}{m\pi} \frac{\sin \beta_m y}{\sin \beta_m b} \sin \frac{m\pi x}{a} e^{j\omega t} \tag{17}$$

$$H_x = \mathrm{Re} \sum_{\substack{m=1 \\ \text{odd}}}^{\infty} \frac{4\beta_m \hat{\Lambda}}{\mu m\pi} \frac{\cos \beta_m y}{\sin \beta_m b} \sin \frac{m\pi x}{a} e^{j\omega t} \tag{18}$$

$$H_y = \mathrm{Re} \sum_{\substack{m=1 \\ \text{odd}}}^{\infty} \frac{-4\hat{\Lambda}}{\mu a} \frac{\sin \beta_m y}{\sin \beta_m b} \cos \frac{m\pi x}{a} e^{j\omega t} \tag{19}$$

In the quasistatic limit, $\omega^2\mu\epsilon \ll (m\pi/a)^2$, this magnetic field reduces to that found in Example 8.6.3.

A few observations may help one to gain some insights from these expressions. First, if the magnetic field is sensed, then the detection loop must have its axis in the $x - y$ plane. For these TE modes, there should be no signal sensed with the axis of the detection loop in the z direction. This probe can also be used to verify that **H** normal to the perfectly conducting surfaces is indeed zero, while its tangential value peaks at the short. Second, the same decay of the fields below cutoff and appearance of standing waves above cutoff is predicted here, as in the TM case. Third, because **E** is perpendicular to planes of constant z, the boundary conditions on **E**, and hence **H**, are met, even if perfectly conducting plates are placed over the open ends of the guide, say in the planes $z = 0$ and $z = w$. In this case, the guide becomes a closed pipe of rectangular cross-section. What we have found are then a subset of the three-dimensional modes of propagation in a rectangular waveguide.

Demonstration 13.3.2. Evanescent and Standing TE Waves

The apparatus of Demonstration 13.3.1 is altered to give TE rather than TM waves by using an array of "one-turn inductors" rather than the array of "capacitor plates." These are shown in Fig. 13.3.6.

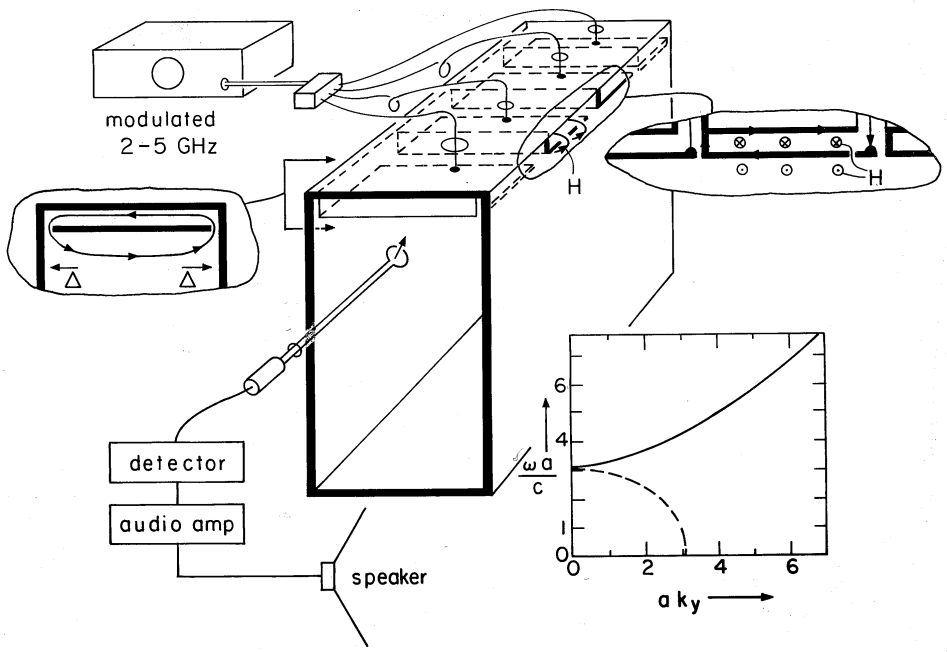


Fig. 13.3.6 Demonstration of evanescent and standing TE waves.

Each member of the array consists of an electrode of width $a - 2\Delta$, driven at one edge by a common source and shorted to the perfectly conducting backing at its other edge. Thus, the magnetic flux through the closed loop passes into and out of the guide through the gaps of width Δ between the ends of the one-turn coil and the parallel plate (vertical) walls of the guide. Effectively, the integral of E_z created by the voltage sources in the idealized model of Fig. 13.3.4 is produced by the integral of E_z between the left edge of one current loop and the right edge of the next.

The current loop can be held in the $x - z$ plane to sense H_y or in the $y - z$ plane to sense H_x to verify the field distributions derived in the previous example. It can also be observed that placing conducting sheets against the open ends of the parallel plate guide, making it a rectangular pipe guide, leaves the characteristics of these two-dimensional TE modes unchanged.

13.4 RECTANGULAR WAVEGUIDE MODES

Metal pipe waveguides are often used to guide electromagnetic waves. The most common waveguides have rectangular cross-sections and so are well suited for the exploration of electrodynamic fields that depend on three dimensions. Although we confine ourselves to a rectangular cross-section and hence Cartesian coordinates, the classification of waveguide modes and the general approach used here are equally applicable to other geometries, for example to waveguides of circular cross-section.

The parallel plate system considered in the previous three sections illustrates

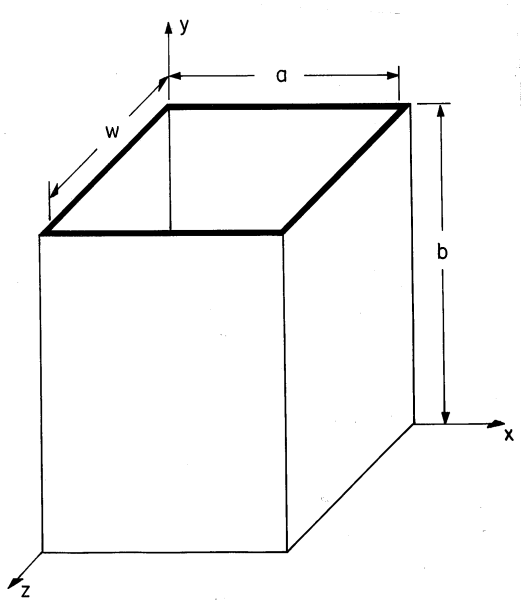


Fig. 13.4.1 Rectangular waveguide.

much of what can be expected in pipe waveguides. However, unlike the parallel plates, which can support TEM modes as well as higher-order TE modes and TM modes, the pipe cannot transmit a TEM mode. From the parallel plate system, we expect that a waveguide will support *propagating* modes only if the frequency is high enough to make the greater interior cross-sectional dimension of the pipe greater than a free space half-wavelength. Thus, we will find that a guide having a larger dimension greater than 5 cm would typically be used to guide energy having a frequency of 3 GHz.

We found it convenient to classify two-dimensional fields as transverse magnetic (TM) or transverse electric (TE) according to whether **E** or **H** was transverse to the direction of propagation (or decay). Here, where we deal with three-dimensional fields, it will be convenient to classify fields according to whether they have **E** or **H** *transverse to the axial direction of the guide.* This classification is used regardless of the cross-sectional geometry of the pipe. We choose again the y coordinate as the axis of the guide, as shown in Fig. 13.4.1. If we focus on solutions to Maxwell's equations taking the form

$$H_y = \text{Re}\ \hat{h}_y(x,z)e^{j(\omega t - k_y y)} \tag{1}$$

$$E_y = \text{Re}\ \hat{e}_y(x,z)e^{j(\omega t - k_y y)} \tag{2}$$

then all of the other complex amplitude field components can be written in terms of the complex amplitudes of these axial fields, H_y and E_y. This can be seen from substituting fields having the form of (1) and (2) into the transverse components of Ampère's law, (12.0.8),

$$-jk_y\hat{h}_z - \frac{\partial \hat{h}_y}{\partial z} = j\omega\epsilon\hat{e}_x \tag{3}$$

$$\frac{\partial \hat{h}_y}{\partial x} + jk_y\hat{h}_x = j\omega\epsilon\hat{e}_z \tag{4}$$

and into the transverse components of Faraday's law, (12.0.9),

$$-jk_y\hat{e}_z - \frac{\partial \hat{e}_y}{\partial z} = -j\omega\mu\hat{h}_x \tag{5}$$

$$\frac{\partial \hat{e}_y}{\partial x} + jk_y\hat{e}_x = -j\omega\mu\hat{h}_z \tag{6}$$

If we take $\hat{h}_y$ and $\hat{e}_y$ as specified, (3) and (6) constitute two algebraic equations in the unknowns $\hat{e}_x$ and $\hat{h}_z$. Thus, they can be solved for these components. Similarly, $\hat{h}_x$ and $\hat{e}_z$ follow from (4) and (5).

$$\hat{h}_x = \left(-jk_y\frac{\partial \hat{h}_y}{\partial x} - j\omega\epsilon\frac{\partial \hat{e}_y}{\partial z}\right)/(\omega^2\mu\epsilon - k_y^2) \tag{7}$$

$$\hat{h}_z = \left(-jk_y\frac{\partial \hat{h}_y}{\partial z} + j\omega\epsilon\frac{\partial \hat{e}_y}{\partial x}\right)/(\omega^2\mu\epsilon - k_y^2) \tag{8}$$

$$\hat{e}_x = \left(j\omega\mu\frac{\partial \hat{h}_y}{\partial z} - jk_y\frac{\partial \hat{e}_y}{\partial x}\right)/(\omega^2\mu\epsilon - k_y^2) \tag{9}$$

$$\hat{e}_z = \left(-j\omega\mu\frac{\partial \hat{h}_y}{\partial x} - jk_y\frac{\partial \hat{e}_y}{\partial z}\right)/(\omega^2\mu\epsilon - k_y^2) \tag{10}$$

We have found that the three-dimensional fields are a superposition of those associated with E_y (so that the magnetic field is transverse to the guide axis), the TM fields, and those due to H_y, the TE modes. The axial field components now play the role of "potentials" from which the other field components can be derived.

We can use the y components of the laws of Ampère and Faraday together with Gauss' law and the divergence law for $\mathbf{H}$ to show that the axial complex amplitudes $\hat{e}_y$ and $\hat{h}_y$ satisfy the two-dimensional Helmholtz equations.

TM Modes $(H_y = 0)$:

$$\frac{\partial^2 \hat{e}_y}{\partial x^2} + \frac{\partial^2 \hat{e}_y}{\partial z^2} + p^2\hat{e}_y = 0 \tag{11}$$

where

$$p^2 = \omega^2\mu\epsilon - k_y^2$$

and

TE Modes $(E_y = 0)$:

$$\frac{\partial^2 \hat{h}_y}{\partial x^2} + \frac{\partial^2 \hat{h}_y}{\partial z^2} + q^2\hat{h}_y = 0 \tag{12}$$

where

$$q^2 = \omega^2 \mu\epsilon - k_y^2$$

These relations also follow from substitution of (1) and (2) into the y components of (13.0.2) and (13.0.1).

The solutions to (11) and (12) must satisfy boundary conditions on the perfectly conducting walls. Because E_y is parallel to the perfectly conducting walls, it must be zero there.

TM Modes:

$$\hat{e}_y(0,z) = 0; \quad \hat{e}_y(a,z) = 0; \quad \hat{e}_y(x,0) = 0; \quad \hat{e}_y(x,w) = 0 \tag{13}$$

The boundary condition on H_y follows from (9) and (10), which express $\hat{e}_x$ and $\hat{e}_z$ in terms of $\hat{h}_y$. On the walls at $x = 0$ and $x = a$, $\hat{e}_z = 0$. On the walls at $z = 0,\ z = w,\ \hat{e}_x = 0$. Therefore, from (9) and (10) we obtain

TE Modes:

$$\frac{\partial h_y}{\partial x}(0,z) = 0; \quad \frac{\partial h_y}{\partial x}(a,z) = 0; \quad \frac{\partial h_y}{\partial z}(x,0) = 0; \quad \frac{\partial h_y}{\partial z}(x,w) = 0 \tag{14}$$

The derivative of $\hat{h}_y$ with respect to a coordinate perpendicular to the boundary must be zero.

The solution to the Helmholtz equation, (11) or (12), follows a pattern that is familiar from that used for Laplace's equation in Sec. 5.4. Either of the complex amplitudes representing the axial fields is represented by a product solution.

$$\begin{bmatrix} \hat{e}_y \\ \hat{h}_y \end{bmatrix} \propto X(x)Z(z) \tag{15}$$

Substitution into (11) or (12) and separation of variables then gives

$$\frac{d^2X}{dx^2} + \gamma^2 X = 0 \tag{16}$$

$$\frac{d^2Z}{dz^2} + \delta^2 Z = 0$$

where

$$-\gamma^2 - \delta^2 + \begin{pmatrix} p^2 \\ q^2 \end{pmatrix} = 0 \tag{17}$$

Solutions that satisfy the TM boundary conditions, (13), are then

TM Modes:

$$X \propto \sin \gamma_m x; \qquad \gamma_m = \frac{m\pi}{a}, \quad m = 1, 2, \ldots \tag{18}$$

$$Z \propto \sin \delta_n z; \qquad \delta_n = \frac{n\pi}{w}, \quad n = 1, 2, \ldots$$

so that

$$p_{mn}^2 = \left(\frac{m\pi}{a}\right)^2 + \left(\frac{n\pi}{w}\right)^2; \qquad m = 1, 2, \ldots, \quad n = 1, 2, \ldots \tag{19}$$

When either m or n is zero, the field is zero, and thus m and n must be equal to an integer equal to or greater than one. For a given frequency ω and mode number (m, n), the wave number k_y is found by using (19) in the definition of p associated with (11)

$$k_y = \pm\beta_{mn}$$

with

$$\beta_{mn} \equiv \begin{cases} \sqrt{\omega^2\mu\epsilon - \left(\frac{m\pi}{a}\right)^2 - \left(\frac{n\pi}{w}\right)^2}; & \omega^2\mu\epsilon > \left(\frac{m\pi}{a}\right)^2 + \left(\frac{n\pi}{w}\right)^2 \\ -j\sqrt{\left(\frac{m\pi}{a}\right)^2 + \left(\frac{n\pi}{w}\right)^2 - \omega^2\mu\epsilon}; & \omega^2\mu\epsilon < \left(\frac{m\pi}{a}\right)^2 + \left(\frac{n\pi}{w}\right)^2 \end{cases} \tag{20}$$

Thus, the TM solutions are

$$E_y = \mathrm{Re} \sum_{m=1}^{\infty} \sum_{n=1}^{\infty} (A_{mn}^{+} e^{-j\beta_{mn} y} + A_{mn}^{-} e^{j\beta_{mn} y}) \sin \frac{m\pi}{a} x \ \sin \frac{n\pi}{w} z \ e^{j\omega t} \tag{21}$$

For the TE modes, (14) provides the boundary conditions, and we are led to the solutions

TE Modes:

$$X \propto \cos \gamma_m x; \qquad \gamma_m = \frac{m\pi}{a}; \quad m = 0, 1, 2, \ldots \tag{22}$$

$$Z \propto \cos \delta_n z; \qquad \delta_n = \frac{n\pi}{a}; \quad n = 0, 1, 2, \ldots$$

Substitution of γ_m and δ_n into (17) therefore gives

$$q_{mn}^2 = \left(\frac{m\pi}{a}\right)^2 + \left(\frac{n\pi}{w}\right)^2; \qquad m = 0, 1, 2, \ldots, \quad n = 0, 1, 2, \ldots, \tag{23}$$

$$(m, n) \neq (0, 0)$$

The wave number k_y is obtained using this eigenvalue in the definition of q associated with (12). With the understanding that either m or n can now be zero, the expression is the same as that for the TM modes, (20). However, both m and n cannot be zero. If they were, it follows from (22) that the axial $\mathbf{H}$ would be uniform over any given cross-section of the guide. The integral of Faraday's law over the cross-section of the guide, with the enclosing contour C adjacent to the perfectly conducting boundaries as shown in Fig. 13.4.2, requires that

$$\oint \mathbf{E} \cdot d\mathbf{s} = -\mu A \frac{dH_y}{dt} \tag{24}$$

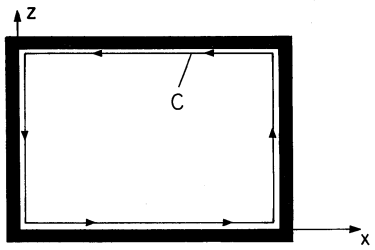


Fig. 13.4.2 Cross-section of guide with contour adjacent to perfectly conducting walls.

where A is the cross-sectional area of the guide. Because the contour on the left is adjacent to the perfectly conducting boundaries, the line integral of $\mathbf{E}$ must be zero. It follows that for the $m = 0,\ n = 0$ mode, $H_y = 0$. If there were such a mode, it would have both $\mathbf{E}$ and $\mathbf{H}$ transverse to the guide axis. We will show in Sec. 14.2, where TEM modes are considered in general, that TEM modes cannot exist within a perfectly conducting pipe.

Even though the dispersion equations for the TM and TE modes only differ in the allowed lowest values of (m, n), the field distributions of these modes are very different.[9] The superposition of TE modes gives

$$H_y = \mathrm{Re} \sum_{m=0}^{\infty} \sum_{n=0}^{\infty} (C_{mn}^{+} e^{-j\beta_{mn} y} + C_{mn}^{-} e^{j\beta_{mn} y}) \cdot \cos \frac{m\pi}{a} x \, \cos \frac{n\pi}{w} z \, e^{j\omega t} \tag{25}$$

where $m \cdot n \neq 0$. The frequency at which a given mode switches from evanescence to propagation is an important parameter. This *cutoff frequency* follows from (20) as

$$\omega_c = \frac{1}{\sqrt{\mu\epsilon}} \sqrt{\left(\frac{m\pi}{a}\right)^2 + \left(\frac{n\pi}{w}\right)^2} \tag{26}$$

TM Modes:

$$m \neq 0, \quad n \neq 0$$

TE Modes:

$$m \quad \text{and} \quad n \quad \text{not both zero}$$

Rearranging this expression gives the normalized cutoff frequency as functions of the aspect ratio a/w of the guide.

$$\underline{\omega}_c \equiv \frac{\omega_c w}{c\pi} = \sqrt{(w/a)^2 m^2 + n^2} \tag{27}$$

These normalized cutoff frequencies are shown as functions of w/a in Fig. 13.4.3.

The numbering of the modes is standardized. The dimension w is chosen as $w \leq a$, and the first index m gives the variation of the field along a. The TE_{10}

[9] In other geometries, such as a circular waveguide, this coincidence of p_{mn} and q_{mn} is not found.

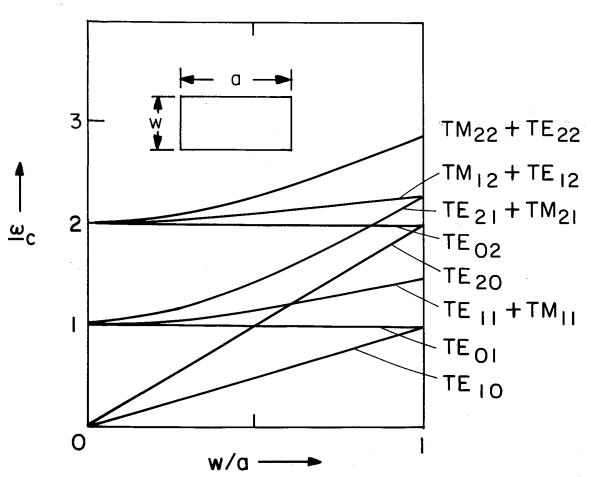


Fig. 13.4.3 Normalized cutoff frequencies for lowest rectangular waveguide modes as a function of aspect ratio.

mode then has the lowest cutoff frequency and is called the *dominant* mode. All other modes have higher cutoff frequencies (except, of course, in the case of the square cross-section for which TE_{01} has the same cutoff frequency). Guides are usually designed so that at the frequency of operation only the dominant mode is propagating, while all higher-order modes are "cutoff."

In general, an excitation of the guide at a cross-section $y =$ constant excites all waveguide modes. The modes with cutoff frequencies higher than the frequency of excitation decay away from the source. Only the dominant mode has a sinusoidal dependence upon y and thus possesses fields that are periodic in y and "dominate" the field pattern far away from the source, at distances larger than the transverse dimensions of the waveguide.

Example 13.4.1. TE_{10} Standing Wave Fields

The section of rectangular guide shown in Fig. 13.4.4 is excited somewhere to the right of $y = 0$ and shorted by a conducting plate in the plane $y = 0$. We presume that the frequency is above the cutoff frequency for the TE_{10} mode and that $a > w$ as shown. The frequency of excitation is chosen to be below the cutoff frequency for all higher order modes and the source is far away from $y = 0$ (i.e., at $y \gg a$). The field in the guide is then that of the TE_{10} mode. Thus, H_y is given by (25) with $m = 1$ and $n = 0$. What is the space-time dependence of the standing waves that result from having shorted the guide?

Because of the short, $E_z(x, y = 0, z) = 0$. In order to relate the coefficients C_{10}^+ and C_{10}^-, we must determine $\hat{e}_z$ from $\hat{h}_y$ as given by (25) using (10)

$$E_z = \text{Re } j\omega\mu\frac{a}{\pi}(C_{10}^+ e^{-j\beta_{10}y} + C_{10}^- e^{j\beta_{10}y}) \sin\frac{\pi x}{a} e^{j\omega t} \tag{28}$$

and because $\hat{e}_z = 0$ at the short, it follows that

$$C_{10}^+ = -C_{10}^- \tag{29}$$

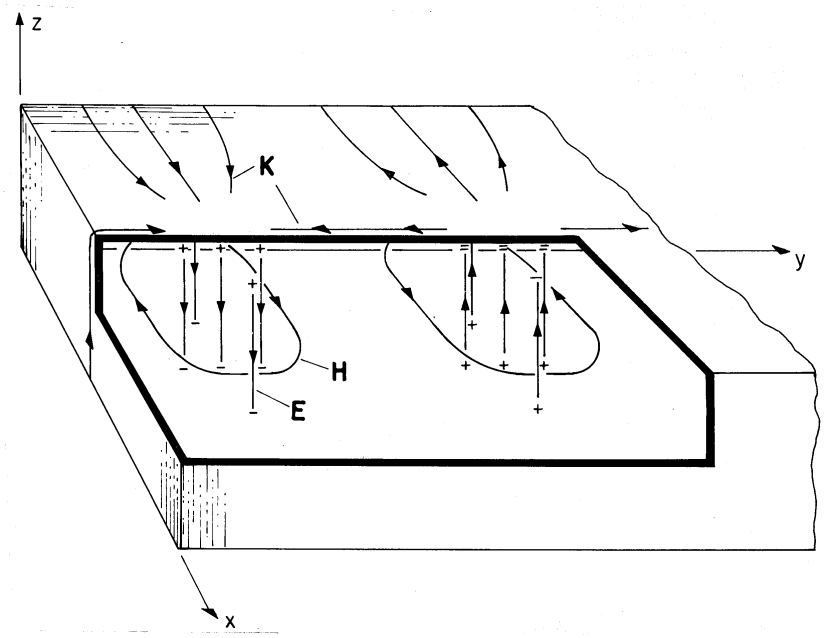


Fig. 13.4.4 Fields and surface sources for TE_{10} mode.

so that

$$E_z = \text{Re}\left[2\omega\mu\frac{a}{\pi}C_{10}^{+}\sin\beta_{10}y\sin\frac{\pi}{a}xe^{j\omega t}\right] \tag{30}$$

and this is the only component of the electric field in this mode. We can now use (29) to evaluate (25).

$$H_y = -\text{Re}\left[2jC_{10}^{+}\sin\beta_{10}y\cos\frac{\pi}{a}xe^{j\omega t}\right] \tag{31}$$

In using (7) to evaluate the other component of $\mathbf{H}$, remember that in the C_{mn}^{+} term of (25), $k_y = \beta_{mn}$, while in the C_{mn}^{-} term, $k_y = -\beta_{mn}$.

$$H_x = \text{Re}\left[2j\beta_{10}\frac{a}{\pi}C_{10}^{+}\cos\beta_{10}y\sin\frac{\pi}{a}xe^{j\omega t}\right] \tag{32}$$

To sketch these fields in the neighborhood of the short and deduce the associated surface charge and current densities, consider C_{10}^{+} to be real. The j in (31) and (32) shows that H_x and H_y are 90 degrees out of phase with the electric field. Thus, in the field sketches of Fig. 13.4.4, $\mathbf{E}$ and $\mathbf{H}$ are shown at different instants of time, say $\mathbf{E}$ when $\omega t = \pi$ and $\mathbf{H}$ when $\omega t = \pi/2$. The surface charge density is where E_z terminates and originates on the upper and lower walls. The surface current density can be inferred from Ampère's continuity condition. The temporal oscillations of these fields should be pictured with $\mathbf{H}$ equal to zero when $\mathbf{E}$ peaks, and with $\mathbf{E}$ equal to zero when $\mathbf{H}$ peaks. At planes spaced by multiples of a half-wavelength along the y axis, $\mathbf{E}$ is always zero.

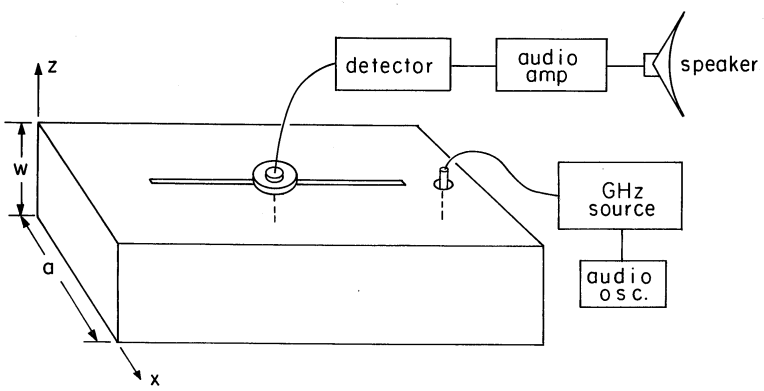


Fig. 13.4.5 Slotted line for measuring axial distribution of TE_{10} fields.

The following demonstration illustrates how a movable probe designed to couple to the electric field is introduced into a waveguide with minimal disturbance of the wall currents.

Demonstration 13.4.1. Probing the TE_{10} Mode.

A waveguide slotted line is shown in Fig. 13.4.5. Here the line is shorted at $y = 0$ and excited at the right. The probe used to excite the guide is of the capacitive type, positioned so that charges induced on its tip couple to the lines of electric field shown in Fig. 13.4.4. This electrical coupling is an alternative to the magnetic coupling used for the TE mode in Demonstration 13.3.2.

The y dependence of the field pattern is detected in the apparatus shown in Fig. 13.4.5 by means of a second capacitive electrode introduced through a slot so that it can be moved in the y direction and not perturb the field, i.e., the wall is cut *along* the lines of the surface current $\mathbf{K}$. From the sketch of $\mathbf{K}$ given in Fig. 13.4.4, it can be seen that $\mathbf{K}$ is in the y direction along the center line of the guide.

The probe can be used to measure the wavelength $2\pi/k_y$ of the standing waves by measuring the distance between nulls in the output signal (between nulls in E_z). With the frequency somewhat below the cutoff of the TE_{10} mode, the spatial decay away from the source of the evanescent wave also can be detected.

13.5 DIELECTRIC WAVEGUIDES: OPTICAL FIBERS

Waves can be guided by dielectric rods or slabs and the fields of these waves occupy the space within and around these dielectric structures. Especially at optical wavelengths, dielectric fibers are commonly used to guide waves. In this section, we develop the properties of waves guided by a planar sheet of dielectric material. The waves that we find are typical of those found in integrated optical systems and in the more commonly used optical fibers of circular cross-section.

A planar version of a dielectric waveguide is pictured in Fig. 13.5.1. A dielectric of thickness $2d$ and permittivity ϵ_i is surrounded by a dielectric of permittivity $\epsilon < \epsilon_i$. The latter might be free space with $\epsilon = \epsilon_o$. We are interested in how this

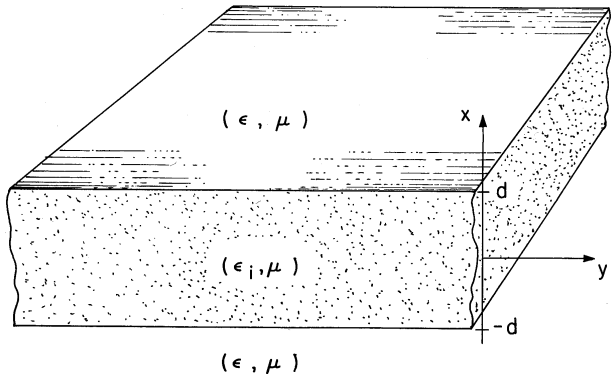


Fig. 13.5.1 Dielectric slab waveguide.

structure might be used to guide waves in the y direction and will confine ourselves to fields that are independent of z.

With a source somewhere to the left (for example an antenna imbedded in the dielectric), there is reason to expect that there are fields outside as well as inside the dielectric. We shall look for field solutions that propagate in the y direction and possess fields solely inside and near the layer. The fields external to the layer decay to zero in the $\pm x$ directions. Like the waves propagating along waveguides, those guided by this structure have transverse components that take the form

$$E_z = \text{Re}\ \hat{e}_z(x)e^{j(\omega t - k_y y)} \tag{1}$$

both inside and outside the dielectric. That is, the fields inside and outside the dielectric have the same frequency ω, the same phase velocity ω/k_y, and hence the same wavelength $2\pi/k_y$ in the y direction. Of course, whether such fields can actually exist will be determined by the following analysis.

The classification of two-dimensional fields introduced in Sec. 12.6 is applicable here. The TM and TE fields can be made to independently satisfy the boundary conditions so that the resulting modes can be classified as TM or TE.[10] Here we will confine ourselves to the transverse electric modes. In the exterior and interior regions, where the permittivities are uniform but different, it follows from substitution of (1) into (12.6.33) (Table 12.8.3) that

$$\frac{d^2\hat{e}_z}{dx^2} - \alpha_x^2\hat{e}_z = 0; \qquad \alpha_x = \sqrt{k_y^2 - \omega^2\mu\epsilon}; \quad d < x \text{ and } x < -d \tag{2}$$

$$\frac{d^2\hat{e}_z}{dx^2} + k_x^2\hat{e}_z = 0; \qquad k_x = \sqrt{\omega^2\mu\epsilon_i - k_y^2}; \quad -d < x < d \tag{3}$$

A guided wave is one that is composed of a nonuniform plane wave in the exterior regions, decaying in the $\pm x$ directions and propagating with the phase velocity ω/k_y in the y direction. In anticipation of this, we have written (2) in

[10] Circular dielectric rods do not support simple TE or TM waves; in that case, this classification of modes is not possible.

terms of the parameter α_x, which must then be real and positive. Through the continuity conditions, the exterior wave must match up to the interior wave at the dielectric surfaces. The solutions to (3) are sines and cosines if k_x is real. In order to match the interior fields onto the nonuniform plane waves on both sides of the guide, it is necessary that k_x be real.

We now set out to find the wave numbers k_y that not only satisfy the wave equations in each of the regions, represented by (2) and (3), but the continuity conditions at the interfaces as well. The configuration is symmetric about the $x = 0$ plane so we can further divide the modes into those that have even and odd functions $E_z(x)$. Thus, with A an arbitrary factor, appropriate even solutions to (2) and (3) are

$$\hat{e}_z = \begin{cases} Ae^{-\alpha_x(x-d)}; & d < x \\ A\dfrac{\cos k_x x}{\cos k_x d}; & -d < x < d \\ Ae^{\alpha_x(x+d)}; & x < -d \end{cases} \tag{4}$$

To simplify the algebra, we have displaced the origin in the exterior solutions so that just the coefficient, A, is obtained when $\hat{e}_z$ is evaluated at the respective interfaces. With a similar objective, the interior solution has been divided by the constant $\cos(k_x d)$ so that at the boundaries, $\hat{e}_z$ also becomes A. In this way, we have adjusted the interior coefficient so that $\hat{e}_z$ is continuous at the boundaries.

Because this transverse field is the only component of **E**, all of the continuity conditions on **E** are now satisfied. The permeabilities of all regions are presumed to be the same, so both tangential and normal components of **H** must be continuous at the boundaries. From (12.6.29), the continuity of normal $\mu\mathbf{H}$ is guaranteed by the continuity of E_z in any case. The tangential field is obtained using (12.6.30).

$$\hat{h}_y = \frac{1}{j\omega\mu}\frac{d\hat{e}_z}{dx} \tag{5}$$

Substitution of (4) into (5) gives

$$\hat{h}_y = \frac{1}{j\omega\mu}\begin{cases} -\alpha_x Ae^{-\alpha_x(x-d)}; & d < x \\ -k_x A\frac{\sin k_x x}{\cos k_x d}; & -d < x < d \\ \alpha_x Ae^{\alpha_x(x+d)}; & x < -d \end{cases} \tag{6}$$

The assumption that E_z is even in x has as a consequence the fact that the continuity condition on tangential **H** is satisfied by the same relation at both boundaries.

$$-\alpha_x A = -k_x A\tan k_x d \Rightarrow \frac{\alpha_x}{k_x} = \tan k_x d \tag{7}$$

Our goal is to determine the propagation constant k_y for a given ω. If we were to substitute the definitions of α_x and k_x into this expression, we would have this dispersion equation, $\mathrm{D}(\omega,k_y)$, implicitly relating k_y to ω. It is more convenient to solve for α_x and k_x first, and then for k_y.

Elimination of k_y between the expressions for α_x and k_x given with (2) and (3) gives a second expression for α_x/k_x.

$$\frac{\alpha_x}{k_x} = \sqrt{\frac{\omega^2\mu\epsilon_i d^2}{(k_x d)^2}\left(1 - \frac{\epsilon}{\epsilon_i}\right) - 1} \tag{8}$$

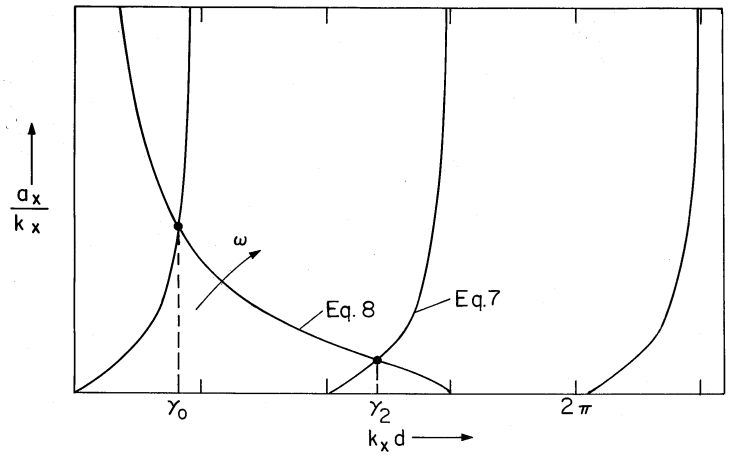


Fig. 13.5.2 Graphical solution to (7) and (8).

The solutions for the values of the normalized transverse wave numbers ($k_x d$) can be pictured as shown in Fig. 13.5.2. Plotted as functions of $k_x d$ are the right-hand sides of (7) and (8). The points of intersection, $k_x d = \gamma_m$, are the desired solutions. For the frequency used to make Fig. 13.5.2, there are two solutions. These are designated by even integers because the odd modes (Prob. 13.5.1) have roots that interleave these even modes.

As the frequency is raised, an additional even TE-guided mode is found each time the curve representing (8) reaches a new branch of (7). This happens at frequencies ω_c such that $\alpha_x/k_x = 0$ and $k_x d = m\pi/2$, where $m = 0, 2, 4, \ldots$ From (8),

$$\omega_c = \frac{m\pi}{2d} \frac{1}{\sqrt{\mu(\epsilon_i - \epsilon)}} \tag{9}$$

The $m = 0$ mode has no cutoff frequency.

To finally determine k_y from these eigenvalues, the definition of k_x given with (3) is used to write

$$k_y d = \sqrt{\omega^2 \mu \epsilon_i d^2 - (k_x d)^2} \tag{10}$$

and the dispersion equation takes the graphical form of Fig. 13.5.3. To make Fig. 13.5.2, we had to specify the ratio of permittivities, so that ratio is also implicit in Fig. 13.5.3.

Features of the dispersion diagram, Fig. 13.5.3, can be gathered rather simply. Where a mode is just cutoff because $\omega = \omega_c$, $\alpha_x = 0$, as can be seen from Fig. 13.5.2. From (2), we gather that $k_y = \omega_c \sqrt{\mu\epsilon}$. Thus, at cutoff, a mode must have a propagation constant k_y that lies on the straight broken line to the left, shown in Fig. 13.5.3. At cutoff, each mode has a phase velocity equal to that of a plane wave in the medium exterior to the layer.

In the high-frequency limit, where ω goes to infinity, we see from Fig. 13.5.2 that k_xd approaches the constant $k_x \to (m+1)\pi/2d$. That is, in (3), k_x becomes a constant even as ω goes to infinity and it follows that in this high frequency limit $k_y \to \omega\sqrt{\mu\epsilon_i}$.

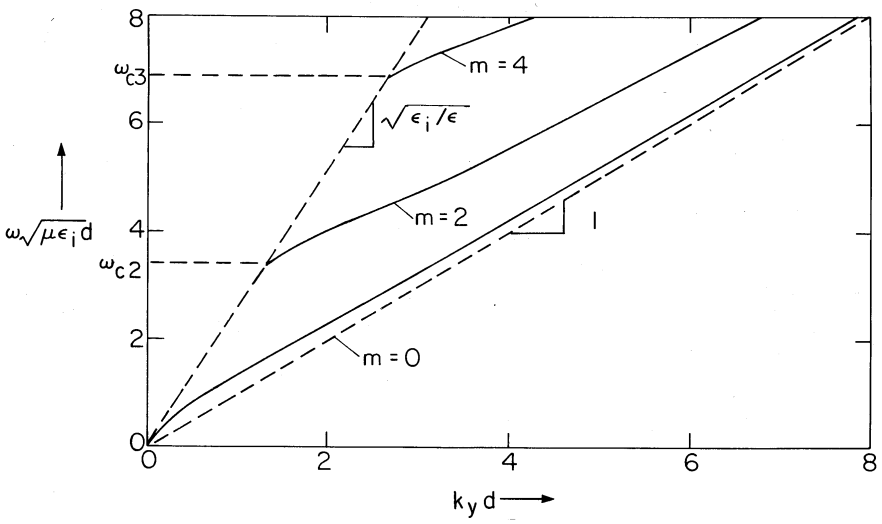


Fig. 13.5.3 Dispersion equation for even TE modes with $\epsilon_i/\epsilon = 6.6$.

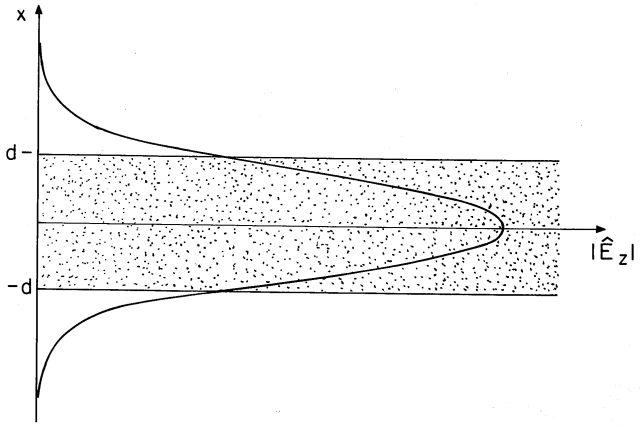


Fig. 13.5.4 Distribution of transverse **E** for TE_0 mode on dielectric waveguide of Fig. 13.5.1.

The physical reasons for this behavior follow from the nature of the mode pattern as a function of frequency. When $\alpha_x \to 0$, as the frequency approaches cutoff, it follows from (4) that the fields extend far into the regions outside of the layer. The wave approaches an infinite parallel plane wave having a propagation constant that is hardly affected by the layer. In the opposite extreme, where ω goes to infinity, the decay of the external field is rapid, and a given mode is well confined inside the layer. Again, the wave assumes the character of an infinite parallel plane wave, but in this limit, one that propagates with the phase velocity of a plane wave in a medium with the dielectric constant of the layer.

The distribution of E_z of the $m = 0$ mode at one frequency is shown in Fig. 13.5.4. As the frequency is raised, each mode becomes more confined to the layer.

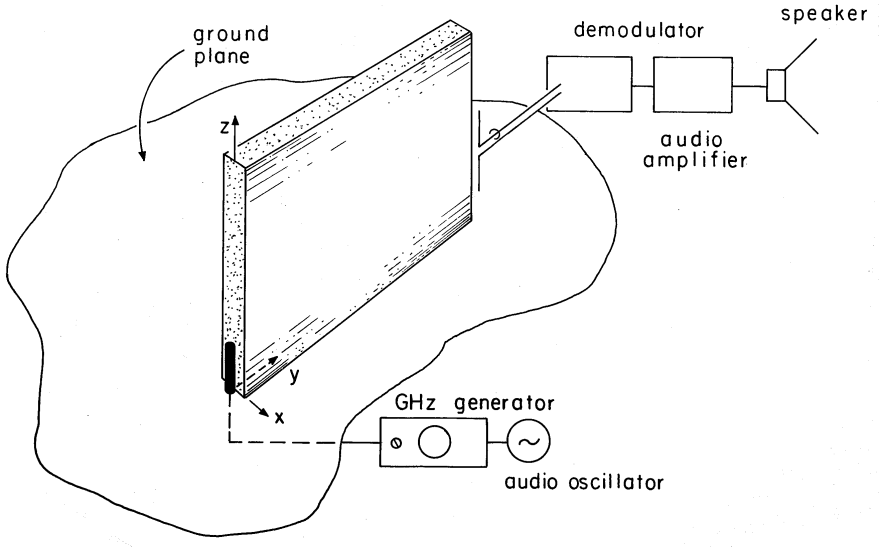


Fig. 13.5.5 Dielectric waveguide demonstration.

Demonstration 13.5.1. Microwave Dielectric Guided Waves

In the experiment shown in Fig. 13.5.5, a dielectric slab is demonstrated to guide microwaves. To assure the excitation of only an $m = 0$ TE-guided wave, but one as well confined to the dielectric as possible, the frequency is made just under the cutoff frequency ω_{c2}. (For a 2 cm thick slab having $\epsilon_i/\epsilon_o = 6.6$, this is a frequency just under 6 GHz.) The $m = 0$ wave is excited in the dielectric slab by means of a vertical element at its left edge. This assures excitation of E_z while having the symmetry necessary to avoid excitation of the odd modes.

The antenna is mounted at the center of a metal ground plane. Thus, without the slab, the signal at the receiving antenna (which is oriented to be sensitive to E_z) is essentially the same in all directions perpendicular to the z axis. With the slab, a sharply increased signal in the vicinity of the right edge of the slab gives qualitative evidence of the wave guidance. The receiving antenna can also be used to probe the field decay in the x direction and to see that this decay increases with frequency.[11]

13.6 SUMMARY

There are two perspectives from which this chapter can be reviewed. First, it can be viewed as a sequence of specific examples that are useful for dealing with radio frequency, microwave, and optical systems. Secs. 13.1–13.3 are concerned with the propagation of energy along parallel plates, first acting as a transmission line and then as a waveguide. Practical systems to which the derived properties of the TEM and higher-order modes are directly applicable are strip lines used at frequencies

[11] To make the excitation independent of z, a collinear array of in-phase dipoles could be used for the excitation. This is not necessary to demonstrate the qualitative features of the guide.

that extend from dc to the microwave range. The rectangular waveguide of Sec. 13.4 might well be a section of "plumbing" from a microwave communication system, and the dielectric waveguide of Sec. 13.5 has many of the properties of an optical fiber. Second, the mathematical analysis of waves exemplified in this chapter is generally applicable to other more complex systems that are uniform in one direction.

When the structures described in this chapter are used to transport energy from one location to another, they are generally not terminated in "shorts" and "opens" and hence, generally, do not simply support standing waves. The object is usually to carry energy from an antenna to a receiver or from a generator to a load whether that be an antenna or a light bulb. Such energy transport is accomplished by the traveling waves featured in the next chapter.

PROBLEMS

13.1 Introduction to TEM Waves

13.1.1* With a short at $y = 0$, it is possible to find the fields for Example 13.1.1 by recognizing at the outset that standing wave solutions meeting the homogeneous boundary condition of (12) are of the form $E_x = \mathrm{Re}\, A \sin(\beta y) \exp(j\omega t)$.

(a) Use (13.1.2) and (13.1.3) to determine the associated H_z and the dispersion equation (relation between β and ω).
(b) Now use the boundary condition at $y = -b$ to show that the fields are as given by (13.1.16) and (13.1.17).

13.1.2* Take the approach outlined in Prob. 13.1.1 for finding the fields [(13.1.28) and (13.1.29)] in Example 13.1.2.

13.1.3 Assume that $\hat{K}_o$ is real and express the standing wave of (13.1.17) so as to make it evident that it is the sum of equal-amplitude waves traveling in the $\pm y$ directions, each with a magnitude of phase velocity $\omega/\beta = c$ and wavelength $2\pi/\beta$.

13.1.4* Coaxial perfectly conducting circular cylinders having outer and inner radii a and b, respectively, form the transmission line shown in Fig. P13.1.4.

(a) If the conductors were "open circuit" at $z = 0$ and driven by a voltage source V at $z = -l$, show that the EQS electric field is radial and given by $V/[r\, ln(a/b)]$.
(b) If the conductors were "shorted" at $z = 0$ and driven by a current source I at $z = -l$, show that the MQS magnetic field intensity is ϕ directed and given by $I/2\pi r$.
(c) With the motivation provided by these limiting solutions, show that solutions to all of Maxwell's equations (in the region between the conductors) that satisfy the boundary conditions on the surfaces of the coaxial conductors are

$$\mathbf{E} = \mathbf{i}_\mathbf{r} \frac{V(z,t)}{ln\left(\frac{a}{b}\right) r}; \qquad \mathbf{H} = \mathbf{i}_\phi \frac{I(z,t)}{2\pi r} \tag{a}$$

provided that V and I are now functions not only of t but of z as well that satisfy equations taking the same form as (13.1.2) and (13.1.3).

$$\frac{\partial I}{\partial z} = -C \frac{\partial V}{\partial t}; \qquad C \equiv \frac{2\pi\epsilon}{ln\left(\frac{a}{b}\right)} \tag{b}$$

$$\frac{\partial V}{\partial z} = -L \frac{\partial I}{\partial t}; \qquad L \equiv \frac{ln\left(\frac{a}{b}\right)\mu}{2\pi} \tag{c}$$

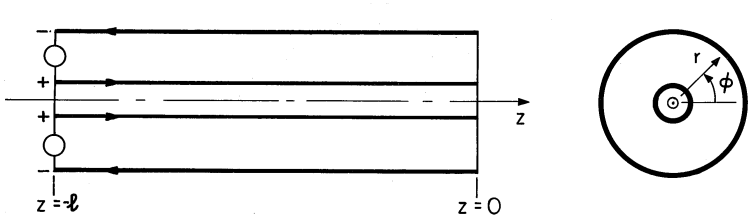


Fig. P13.1.4

13.1.5 For the coaxial configuration of Prob. 13.1.4, there is a perfectly conducting "short" at $z = 0$, and the conductors are driven by a current source $I = \mathrm{Re}[I_o e^{j\omega t}]$ at $z = -l$.

(a) Find $I(z,t)$ and $V(z,t)$ and hence $\mathbf{E}$ and $\mathbf{H}$.
(b) Take the low frequency limit where $\omega\sqrt{\mu\epsilon}l \ll 1$ and show that $\mathbf{E}$ and $\mathbf{H}$ are the same as for a coaxial inductor.
(c) Find $\mathbf{E}$ and $\mathbf{H}$ directly from the MQS laws and show that they agree with the results of part (b).

13.1.6 For the coaxial configuration of Prob. 13.1.4, the conductors are "open circuited" at $z = 0$ and driven by a voltage source $V = \mathrm{Re}\,[V_o \exp(j\omega t]$ at $x = -l$.

(a) Find $I(z,t)$ and $V(z,t)$ and hence $\mathbf{E}$ and $\mathbf{H}$.
(b) Take the low-frequency limit where $\omega\sqrt{\mu\epsilon}l \ll 1$ and show that $\mathbf{E}$ and $\mathbf{H}$ are the same as for a coaxial capacitor.
(c) Find $\mathbf{E}$ and $\mathbf{H}$ directly from the EQS laws and show that they agree with the results of (b).

13.2 Two-Dimensional Modes Between Parallel Plates

13.2.1* Show that each of the higher-order modes propagating in the $+y$ direction, represented by A_n^+ and C_n^+ in (13.2.19) and (13.2.20), respectively, can be regarded as the sum of plane waves propagating in the directions represented by the vector wave number

$$\mathbf{k} = \pm\frac{n\pi}{a}\mathbf{i_x} + \beta_n\mathbf{i_y} \qquad (a)$$

and interfering in the planes $x = 0$ and $x = a$ so as to satisfy the boundary conditions.

13.2.2 The TM and TE modes can themselves be classified into odd or even modes that, respectively, have $\hat{h}_z$ or $\hat{e}_z$ odd or even functions of x. With this in mind, the origin of the coordinate system is moved so that it is midway between the perfectly conducting plates, as shown in Fig. P13.2.2.

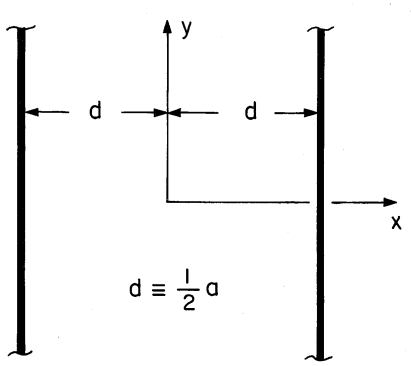


Fig. P13.2.2

(a) Find the odd TM and TE solutions. Note that when the boundary condition is met at $x = d \equiv a/2$ for these functions, it is automatically met at $x = -d$.

(b) Find the even TM and TE solutions, again noting that if the conditions are met at $x = d$, then they are at $x = -d$ as well.

13.3 TE and TM Standing Waves between Parallel Plates

13.3.1* Starting with (13.3.1) (for TM modes) and (13.3.2) (for TE modes) use steps similar to those illustrated by (5.5.20)–(5.5.26) to obtain the orthogonality conditions of (13.3.3) and (13.3.4), respectively.

13.3.2 In the system of Example 13.3.1, the wall at $y = 0$ is replaced by that shown in Fig. P13.3.2. A strip electrode is embedded in, but insulated from, the wall at $y = 0$. The resistance R is low enough so that $\mathbf{E}$ tangential to the boundary at $y = 0$, even at the insulating gaps between the strip electrode and the surrounding wall, is negligible.

(a) Determine the output voltage v_o in terms of v.

(b) For $b/a = 2$, describe the dependence of $|v_o|$ on frequency over the range $\omega\sqrt{\mu\epsilon}\,a = 0 \rightarrow \pi\sqrt{5/4}$, specifying the low-frequency range where the response has a linear dependence on frequency and the resonance frequencies.

(c) What is the distribution of $H_z(x, y)$ at the resonance frequencies?

13.3.3* In the two-dimensional system of Fig. P13.3.3, each driven electrode has the same nature as the one in Fig. 13.3.1. The origin of the y axis has been chosen to be in the plane of symmetry.

(a) Use the symmetry to argue that $H_z(y = 0) = 0$.

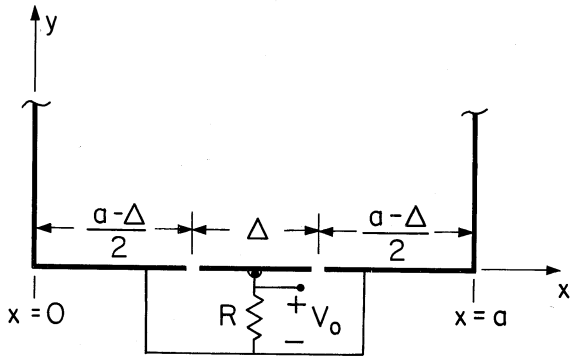


Fig. P13.3.2

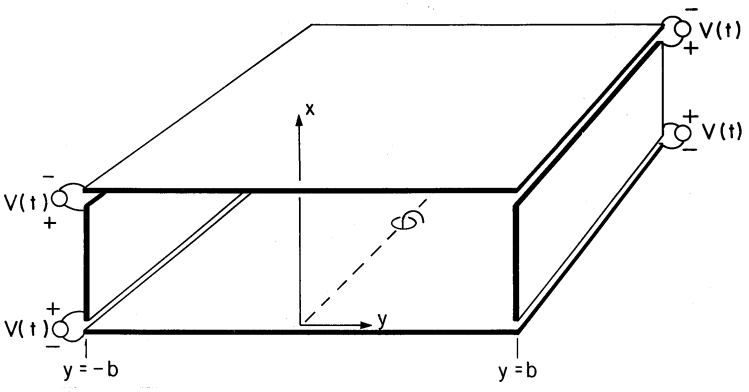


Fig. P13.3.3

(b) Show that in the interior region,

$$H_z = \mathrm{Re} \sum_{\substack{n=1 \\ \text{odd}}}^{\infty} \frac{-4j\omega\epsilon\hat{v}}{\beta_n a} \frac{\sin \beta_n y}{\cos \beta_n b} \cos \frac{n\pi x}{a} e^{j\omega t} \qquad (a)$$

13.3.4 The one-turn loop of Fig. P13.3.4 has dimensions that are small compared to a, b, or wavelengths of interest and has area A in the $x - y$ plane.

(a) It is used to detect the TM H field at the middle of the bottom electrode in Fig. 13.3.1. Assume that the resistance is large enough so that the current induced in this loop gives rise to a magnetic field that is negligible compared to that already found. In terms of H_z, what is v_o?

(b) At what locations $x = X$ of the loop is $|v_o|$ a maximum?

(c) If the same loop were in the plate at $y = 0$ in the configuration of Fig. 13.1.3 and used to detect H_z at $y = 0$ for the TEM fields of Example

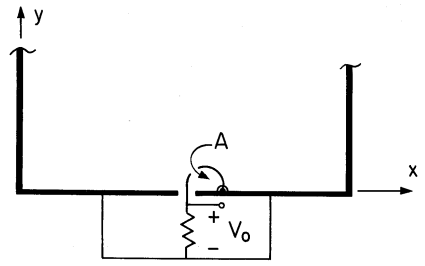


Fig. P13.3.4

13.1.1, what would be the dependence of $|v_o|$ on the location $x = X$ of the loop?

(d) If the loop were located in the plate at $y = 0$ in the TE configuration of Fig. 13.3.4, how should the loop be oriented to detect $\mathbf{H}$?

13.3.5 In the system shown in Fig. P13.3.5, $\Delta \ll d$ and the driving sources $v = \mathrm{Re}[\hat{v}\exp(j\omega t)]$ are uniformly distributed in the z direction so that the fields are two dimensional. Thus, the driving electrode is like that of Fig. 13.3.1 except that it spans the width d rather than the full width a. Find $\mathbf{H}$ and $\mathbf{E}$ in terms of v.

13.3.6 In the system shown in Fig. P13.3.6, the excitation electrode is like that for Fig. 13.3.4 except that it has a width d rather than a. Find $\mathbf{H}$ and $\mathbf{E}$ in terms of $\hat{\Lambda}$.

13.4 Rectangular Waveguide Modes

13.4.1* Show that an alternative method of exciting and detecting the TE_{10} mode in Demonstration 13.4.1 is to introduce one-turn loops as shown in Fig. P13.4.1. The excitation loop is inserted through a hole in the conducting wall while the detection loop passes through a slot, so that it can be moved in the y direction. The loops are each in the $y - z$ plane. To minimize disturbance of the field, the detection loop is terminated in a high enough impedance so that the field from the current in the loop is negligible. Compare the y dependence of the detected signal to that measured using the electric probe.

13.4.2 A rectangular waveguide has $w/a = 0.75$. Presuming that all TE and TM modes are excited in the guide, in what order do the lowest six modes begin to propagate in the y direction as the frequency is raised?

13.4.3* The rectangular waveguide shown in Fig. P13.4.3 is terminated in a perfectly conducting plate at $y = 0$ that makes contact with the guide walls. An electrode at $y = b$ has a gap of width $\Delta \ll a$ and $\Delta \ll w$ around its

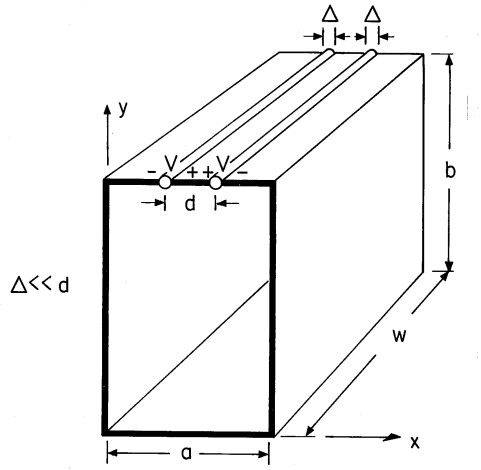


Fig. P13.3.5

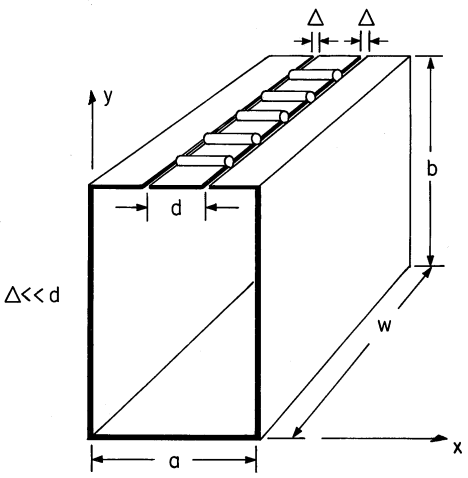


Fig. P13.3.6

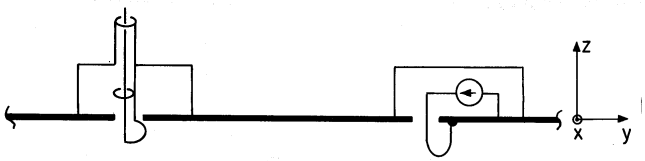


Fig. P13.4.1

edges. Distributed around this gap are sources that constrain the field from the edges of the plate to the guide walls to $v(t)/\Delta = \mathrm{Re}(\hat{v}/\Delta)\exp(j\omega t)$.

(a) Argue that the fields should be TM and use the boundary condition

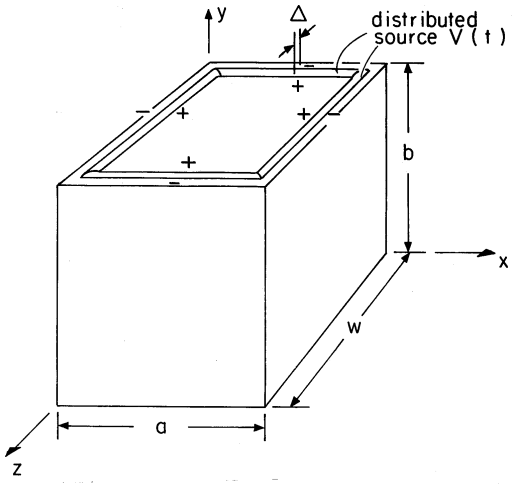


Fig. P13.4.3

at $y = 0$ to show that

$$\hat{E}_y = \sum_{m=1}^{\infty}\sum_{n=1}^{\infty} 2A^{+}_{mn}\cos\beta_{mn}y \sin\frac{m\pi}{a}x \sin\frac{n\pi}{w}z \qquad (a)$$

[Hint: If (13.4.9) and (13.4.10) are used, remember that $k_y = +\beta_{mn}$ for the A^{+}_{mn} mode but $k_y = -\beta_{mn}$ for the A^{-}_{mn} mode.]

(b) Show that, for m and n both odd, $A^{+}_{mn} = 8\hat{v}(\omega^2\mu\epsilon - \beta^2_{mn})/nm\pi^2\beta_{mn}\sin(k_{mn}b)$, while for either m or n even, $A^{+}_{mn} = 0$.

(c) Show that for these modes the resonance frequencies (normalized to $1/\sqrt{\mu\epsilon}a$) are

$$\omega\sqrt{\mu\epsilon}a = \pi\sqrt{m^2 + \left(\frac{a}{w}n\right)^2 + \left(\frac{a}{b}p\right)^2} \qquad (b)$$

where m, n, and p are integers, m and n odd.

(d) Show that under quasistatic conditions, the field which has been found is consistent with that implied by the EQS potential given by (5.10.10) and (5.10.15).

13.4.4 The rectangular waveguide shown in Fig. P13.4.3 is terminated in a perfectly conducting plate at $y = 0$ that makes contact with the guide walls. However, instead of the excitation electrode shown, at $y = b$ there is the perfectly conducting plate with a square hole cut in its center, shown in Fig. P13.4.4. In this hole, the pole faces of a magnetic circuit are flush with the plate and are used to excite fields within the guide. Approximate the normal fields over the surface of the pole faces as

$$H_y = \begin{cases} \hat{H}_o & \text{for } \frac{a}{2} < x < \frac{a+\Delta}{2} \text{ and } \frac{w-\Delta}{2} < z < \frac{w+\Delta}{2} \\ -\hat{H}_o & \text{for } \frac{a-\Delta}{2} < x < \frac{a}{2} \text{ and } \frac{w-\Delta}{2} < z < \frac{w+\Delta}{2} \end{cases} \qquad (a)$$

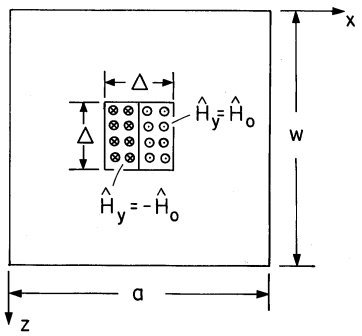


Fig. P13.4.4

where $\hat{H}_o$ is a complex constant. (Note that, if the magnetic circuit is driven by a one turn coil, the terminal voltage $v = j\omega(\Delta^2/2)\mu\hat{H}_o$.) Determine H_y, and hence **E** and **H**, inside the guide.

13.5 Dielectric Waveguides: Optical Fibers

13.5.1* For the dielectric slab waveguide of Fig. 13.5.1, consider the TE modes that have E_z an odd function of z.

(a) Show that the dispersion relation between ω and k_y is again found from (13.5.10), but with $(k_x d)$ found by simultaneously solving (13.5.8) and

$$\frac{\alpha_x}{k_x} = -\cot k_x d \qquad (a)$$

(b) Sketch the graphical solution for $k_x d \equiv \gamma_m$ (m odd) and show that the cutoff frequency is again given by (13.5.9), but with m odd rather than even.

(c) Show that these odd modes also have the asymptote of unity slope shown in Fig. 13.5.3.

(d) Sketch the odd mode dispersion relation on that for the even modes (Fig. 13.5.3).

13.5.2 For the dielectric slab waveguide shown in Fig. 13.5.1, $\epsilon_i/\epsilon = 2.5$, $\mu = \mu_o$, and $d = 1$ cm. In Hz, what is the highest frequency that can be used to guide only one TE mode. (Note the result of Prob. 13.5.1.)

13.5.3* The dielectric slab waveguide of Fig. 13.5.1 is the same as that considered in this problem except that it now has a permeability μ_i that differs from that outside, where it is μ.

(a) Show that (13.5.7) and (13.5.8), respectively, are replaced by

$$\frac{\alpha_x}{k_x} = \frac{\mu}{\mu_i}\begin{bmatrix} \tan k_x d \\ -\cot k_x d \end{bmatrix} \begin{matrix} ;\text{even} \\ ;\text{odd} \end{matrix} \qquad (a)$$

$$\frac{\alpha_x}{k_x} = \sqrt{\frac{\omega^2 \mu_i \epsilon_i d^2}{(k_x d)^2}\left(1 - \frac{\mu\epsilon}{\mu_i \epsilon_i}\right) - 1} \qquad (b)$$

(b) Show that making $\mu_i > \mu$ lowers the cutoff frequency.
(c) For a given frequency, does making $\mu_i/\mu > 1$ increase or decrease the wavelength $\lambda \equiv 2\pi/k_y$?

13.5.4 The dielectric slab of Fig. 13.5.1 has permittivity ϵ_i and permeability μ_i, while in the surrounding regions these are ϵ and μ, respectively. Consider the TM modes.

(a) Determine expressions analogous to (13.5.7), (13.5.8), and (13.5.10) that can be used to determine the dispersion relation $\omega = \omega(k_y)$ for modes that have H_z even and odd functions of x.
(b) What are the cutoff frequencies?
(c) For $\mu_i = \mu$ and $\epsilon_i = \epsilon = 2.5$, draw the dispersion plot for the lowest three modes that is analogous to that of Fig. 13.5.3.

14

ONE-DIMENSIONAL WAVE DYNAMICS

14.0 INTRODUCTION

Examples of conductor pairs range from parallel conductor transmission lines carrying gigawatts of power to coaxial lines carrying microwatt signals between computers. When these lines become very long, times of interest become very short, or frequencies become very high, electromagnetic wave dynamics play an essential role. The transmission line model developed in this chapter is therefore widely used.

Equally well described by the transmission line model are plane waves, which are often used as representations of radiation fields at radio, microwave, and optical frequencies. For both qualitative and quantitative purposes, there is again a need to develop convenient ways of analyzing the dynamics of such systems. Thus, there are practical reasons for extending the analysis of TEM waves and one-dimensional plane waves given in Chap. 13.

The wave equation is ubiquitous. Although this equation represents most accurately electromagnetic waves, it is also applicable to acoustic waves, whether they be in gases, liquids or solids. The dynamic interaction between excitation amplitudes (E and H fields in the electromagnetic case, pressure and velocity fields in the acoustic case) is displayed very clearly by the solutions to the wave equation. The developments of this chapter are therefore an investment in understanding other more complex dynamic phenomena.

We begin in Sec. 14.1 with the distributed parameter ideal transmission line. This provides an exact representation of plane (one-dimensional) waves. In Sec. 14.2, it is shown that for a wide class of two-conductor systems, uniform in an axial direction, the transmission line equations provide an exact description of the TEM fields. Although such fields are in general three dimensional, their propagation in the axial direction is exactly represented by the one-dimensional wave equation to the extent that the conductors and insulators are perfect. The distributed parameter

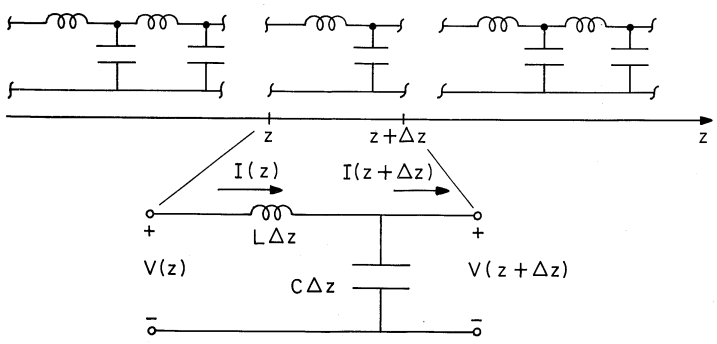


Fig. 14.1.1 Incremental length of distributed parameter transmission line.

model is also commonly used in an approximate way to describe systems that do not support fields that are exactly TEM.

Sections 14.3–14.6 deal with the space-time evolution of transmission line voltage and current. Sections 14.3–14.4, which concentrate on the transient response, are especially applicable to the propagation of digital signals. Sections 14.5-14.6 concentrate on the sinusoidal steady state that prevails in power transmission and communication systems.

The effects of electrical losses on electromagnetic waves, propagating through lossy media or on lossy structures, are considered in Secs. 14.7–14.9. The distributed parameter model is generalized to include the electrical losses in Sec. 14.7. A limiting form of this model provides an "exact" representation of TEM waves in lossy media, either propagating in free space or along pairs of perfect conductors embedded in uniform lossy media. This limit is developed in Sec. 14.8. Once the conductors are taken as being "perfect," the model is exact and the model is equivalent to the physical system. However, a second limit of the lossy transmission line model, which is exemplified in Sec. 14.9, is not "exact." In this case, conductor losses give rise to an electric field in the direction of propagation. Thus, the fields are not TEM and this section gives a more realistic view of how quasi-one-dimensional models are often used.

14.1 DISTRIBUTED PARAMETER EQUIVALENTS AND MODELS

The theme of this section is the *distributed parameter transmission line* shown in Fig. 14.1.1. Over any finite axial length of interest, there is an infinite set of the basic units shown in the inset, an infinite number of capacitors and inductors. The parameters L and C are defined per unit length. Thus, for the segment shown between $z + \Delta z$ and z, $L\Delta z$ is the series inductance (in Henrys) of a section of the distributed line having length Δz, while $C\Delta z$ is the shunt capacitance (in Farads).

In the limit where the incremental length $\Delta z \to 0$, this distributed parameter transmission line serves as a model for the propagation of three types of electromagnetic fields.[1]

[1] To facilitate comparison with quasistatic fields, the direction of wave propagation for TEM waves in Chap. 13 was taken as y. It is more customary to make it z.

- First, it gives an exact representation of uniformly polarized electromagnetic plane waves. Whether these are waves in free space, perhaps as launched by the dipole considered in Sec. 12.2, or TEM waves between plane parallel perfectly conducting electrodes, Sec. 13.1, these fields depend only on one spatial coordinate and time.
- Second, we will see in the next section that the distributed parameter transmission line represents exactly the (z,t) dependence of TEM waves propagating on pairs of axially uniform perfect conductors forming transmission lines of arbitrary cross-section. Such systems are a generalization of the parallel plate transmission line. By contrast with that special case, however, the fields generally depend on the transverse coordinates. These fields are therefore, in general, three dimensional.
- Third, it represents in an approximate way, the (z,t) dependence for systems of large aspect ratio, having lengths over which the fields evolve in the z direction (e.g., wavelengths) that are long compared to the transverse dimensions. To reflect the approximate nature of the model and the two- or three-dimensional nature of the system it represents, it is sometimes said to be *quasi-one-dimensional*.

We can obtain a pair of partial differential equations governing the transmission line current $I(z,t)$ and voltage $V(z,t)$ by first requiring that the currents into the node of the elemental section sum to zero

$$I(z) - I(z+\Delta z) = C\Delta z \frac{\partial V}{\partial t} \tag{1}$$

and then requiring that the series voltage drops around the circuit also sum to zero.

$$V(z) - V(z+\Delta z) = L\Delta z \frac{\partial I}{\partial t} \tag{2}$$

Then, division by Δz and recognition that

$$\lim_{\Delta z \to 0} \frac{f(z+\Delta z) - f(z)}{\Delta z} = \frac{\partial f}{\partial z} \tag{3}$$

results in the *transmission line equations*.

$$\boxed{\frac{\partial I}{\partial z} = -C\frac{\partial V}{\partial t}} \tag{4}$$

$$\boxed{\frac{\partial V}{\partial z} = -L\frac{\partial I}{\partial t}} \tag{5}$$

The remainder of this section is an introduction to some of the physical situations represented by these laws.

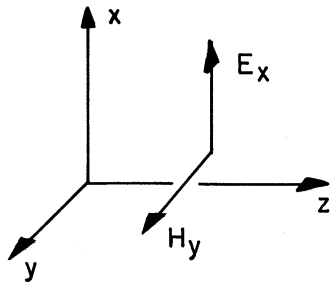


Fig. 14.1.2 Possible polarization and direction of propagation of plane wave described by the transmission line equations.

Plane-Waves. In the following sections, we will develop techniques for describing the space-time evolution of fields on transmission lines. These are equally applicable to the description of electromagnetic plane waves. For example, suppose the fields take the form shown in Fig. 14.1.2.

$$\mathbf{E} = E_x(z,t)\mathbf{i_x}; \qquad \mathbf{H} = H_y(z,t)\mathbf{i_y} \tag{6}$$

Then, the x and y components of the laws of Ampère and Faraday reduce to[2]

$$-\frac{\partial H_y}{\partial z} = \epsilon\frac{\partial E_x}{\partial t} \tag{7}$$

$$\frac{\partial E_x}{\partial z} = -\mu\frac{\partial H_y}{\partial t} \tag{8}$$

These laws are identical to the transmission line equations, (4) and (5), with

$$H_y \leftrightarrow I, \quad E_x \leftrightarrow V, \quad \epsilon \leftrightarrow C, \quad \mu \leftrightarrow L \tag{9}$$

With this identification of variables and parameters, the discussion is equally applicable to plane waves, whether we are considering wave transients or the sinusoidal steady state in the following sections.

Ideal Transmission Line. The TEM fields that can exist between the parallel plates of Fig. 14.1.3 can either be regarded as plane waves that happen to meet the boundary conditions imposed by the electrodes or as a special case of transmission line fields. The following example illustrates the transition to the second viewpoint.

Example 14.1.1. Plane Parallel Plate Transmission Line

In this case, the fields E_x and H_y pictured in Fig. 14.1.2 and described by (7) and (8) can exist unaltered between the plates of Fig. 14.1.3. If the voltage and current are defined as

$$V = E_x a; \qquad I = H_y w \tag{10}$$

[2] Compare with (13.1.2) and (13.1.3) for fields in $x - z$ plane and propagating in the y direction.

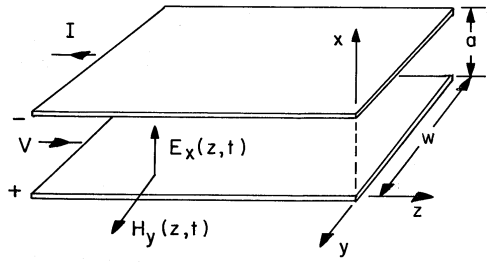


Fig. 14.1.3 Example of transmission line where conductors are parallel plates.

Equations (7) and (8) become identical to the transmission line equations, (4) and (5), with the capacitance and inductance per unit length defined as

$$C = \frac{w\epsilon}{a}; \qquad L = \frac{a\mu}{w} \tag{11}$$

Note that these are indeed the C and L that would be found in Chaps. 5 and 8 for the pair of perfectly conducting plates shown in Fig. 14.1.3 if they had unit length in the z direction and were, respectively, "open circuited" and "short circuited" at the right end.

As an alternative to a field description, the distributed $L-C$ transmission line model gives circuit theory interpretation to the physical processes at work in the actual system. As expressed by (1) and hence (4), the current I can be a function of z because some of it can be diverted into charging the "capacitance" of the line. This is an alternative way of representing the effect of the displacement current density on the right in Ampère's law, (7). The voltage V is a function of z because the inductance of the line causes a voltage drop, even though the conductors are pictured as having no resistance. This follows from (2) and (5) and embodies the same information as did Faraday's differential law (8). The integral of $\mathbf{E}$ from one conductor to the other at some location z can differ from that at another location because of the flux linked by a contour consisting of these integration paths and closing by contours along the perfect conductors.

In the next section, we will generalize our picture of TEM waves and see that (4) and (5) *exactly* describe transverse waves on pairs of perfect conductors of arbitrary cross-section. Of course, L and C are the inductance per unit length and capacitance per unit length of the particular conductor pair under consideration. The fields depend not only on the independent variables (z,t) appearing explicitly in the transmission line equations, but upon the transverse coordinates as well. Thus, the parallel plate transmission line and the generalization of that line considered in the next section are examples for which the distributed parameter model is exact.

In these cases, TEM waves are exact solutions to the boundary value problem at all frequencies, including frequencies so high that the wavelength of the TEM wave is comparable to, or smaller than, the transverse dimensions of the line. As one would expect from the analysis of Secs. 13.1–13.3, higher-order modes propagating in the z direction are also valid solutions. These are not described by the transmission line equations (4) and (5).

Quasi-One-Dimensional Models. The distributed parameter model is also often used to represent fields that are *not quite* TEM. As an example where an approximate model consists of the distributed $L-C$ network, suppose that the region between the plane parallel plate conductors is filled to the level $x=d<a$ by a dielectric of one permittivity with the remainder filled by a material having a different permittivity. The region between the conductors is then one of nonuniform permittivity. We would find that it is not possible to exactly satisfy the boundary conditions on both the tangential and normal electric fields at the interface between dielectrics with an electric field that only had components transverse to z.[3] Even so, if the wavelength is very long compared to the transverse dimensions, the distributed parameter model provides a useful approximate description. The capacitance per unit length used in this model reflects the effect of the nonuniform dielectric in an approximate way.

14.2 TRANSVERSE ELECTROMAGNETIC WAVES

The parallel plates of Sec. 13.1 are a special case of the general configuration shown in Fig. 14.2.1. The conductors have the same cross-section in any plane $z=$ constant, but their cross-sectional geometry is arbitrary.[4] The region between the pair of perfect conductors is filled by a material having uniform permittivity ϵ and permeability μ. In this section, we show that such a structure can support fields that are transverse to the axial coordinate z, and that the $z-t$ dependence of these fields is described by the ideal transmission line model.

Two common transmission line configurations are illustrated in Fig. 14.2.2.

The TEM fields are conveniently pictured in terms of the vector and scalar potentials, $\mathbf{A}$ and Φ, generalized to describe electrodynamic fields in Sec. 12.1. This is because such fields have only an axial component of $\mathbf{A}$.

$$\mathbf{A}=A_z(x,y,z,t)\mathbf{i_z} \tag{1}$$

Indeed, evaluation in Cartesian coordinates, shows that even though A_z is in general not only a function of the transverse coordinates but of the axial coordinate z as well, there is no longitudinal component of $\mathbf{H}$.

To insure that the electric field is also transverse to the z axis, the z component of the expression relating $\mathbf{E}$ to $\mathbf{A}$ and Φ (12.1.3) must be zero.

$$E_z=-\frac{\partial\Phi}{\partial z}-\frac{\partial A_z}{\partial t}=0 \tag{2}$$

A second relation between Φ and A_z is the gauge condition, (12.1.7), which in view of (1) becomes

$$\frac{\partial A_z}{\partial z}=-\mu\epsilon\frac{\partial\Phi}{\partial t} \tag{3}$$

[3] We can see that a uniform plane wave cannot describe such a situation because the propagational velocities of plane waves in dielectrics of different permittivities differ.

[4] The direction of propagation is now z rather than y.

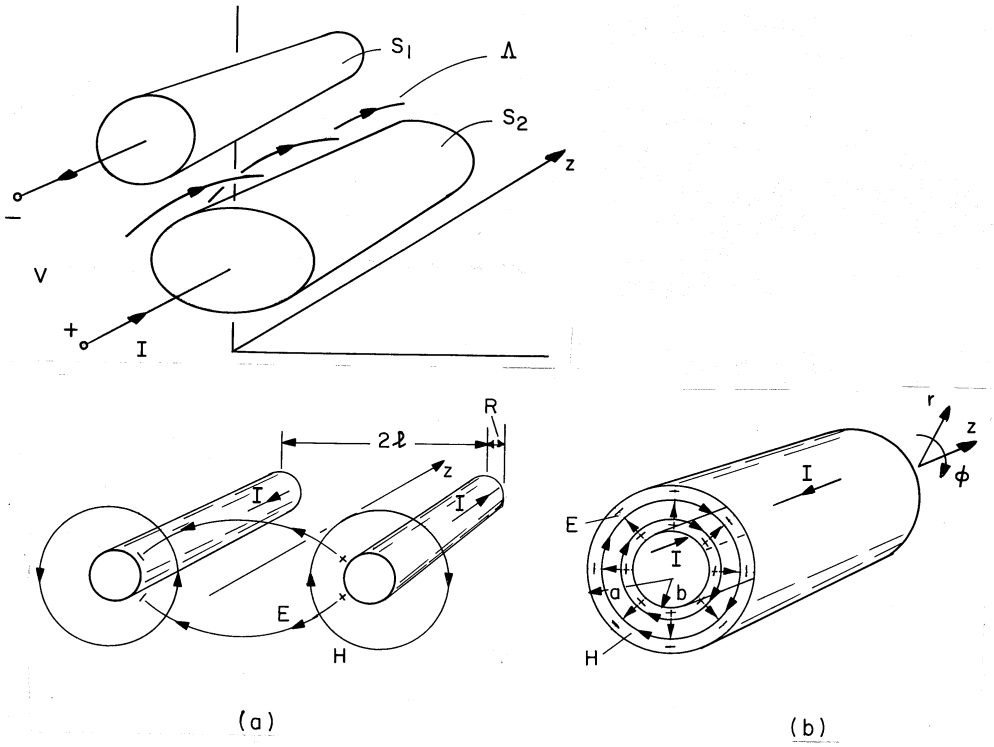


Fig. 14.2.1 Configuration of two parallel perfect conductors supporting TEM fields.

Fig. 14.2.2 Two examples of transmission lines that support TEM waves: (a) parallel wire conductors; and (b) coaxial conductors.

These last two equations combine to show that both Φ and A_z must satisfy

the one-dimensional wave equation. For example, elimination of $\partial^2 A_z/\partial z\partial t$ between the z derivative of (2) and the time derivative of (3) gives

$$\frac{\partial^2 \Phi}{\partial z^2} = \mu\epsilon \frac{\partial^2 \Phi}{\partial t^2} \tag{4}$$

A similar manipulation, with the roles of z and t reversed, shows that A_z also satisfies the one-dimensional wave equation.

$$\frac{\partial^2 A_z}{\partial z^2} = \mu\epsilon \frac{\partial^2 A_z}{\partial t^2} \tag{5}$$

Even though the potentials satisfy the one-dimensional wave equations, in general they depend on the transverse coordinates. In fact, the differential equation governing the dependence on the transverse coordinates is the two-dimensional Laplace's equation. To see this, observe that the three-dimensional Laplacian consists of a part involving derivatives with respect to the transverse coordinates and a second derivative with respect to z.

$$\nabla^2 = \nabla_T^2 + \frac{\partial^2}{\partial z^2} \tag{6}$$

In general, Φ and $\mathbf{A}$ satisfy the three-dimensional wave equation, the homogeneous forms of (12.1.8) and (12.1.10). But, in view of (4) and (5), these expressions reduce to

$$\nabla_T^2 \Phi = 0 \tag{7}$$

$$\nabla_T^2 A_z = 0 \tag{8}$$

where the Laplacian ∇_T^2 is the two-dimensional Laplacian, written in terms of the transverse coordinates.

Even though the fields actually depend on z, *the transverse dependence is as though the fields were quasistatic and two dimensional.*

The boundary conditions on the surfaces of the conductors require that there be no tangential $\mathbf{E}$ and no normal $\mathbf{B}$. The latter condition prevails if A_z is constant on the surfaces of the conductors. This condition is familiar from Sec. 8.6. With A_z defined as zero on the surface S_1 of one of the conductors, as shown in Fig. 14.2.1, it is equal to the flux per unit length passing between the conductors when evaluated anywhere on the second conductor. Thus, the boundary conditions imposed on A_z are

$$A_z = 0 \text{ on } S_1; \qquad A_z = \Lambda(z,t) \text{ on } S_2 \tag{9}$$

As described in Sec. 8.6, where two-dimensional magnetic fields were represented in terms of A_z, Λ is the flux per unit length passing between the conductors. Because $\mathbf{E}$ is transverse to z and $\mathbf{A}$ has only a z component, $\mathbf{E}$ is found from Φ by taking the transverse gradient just as if the fields were two dimensional. The boundary condition on $\mathbf{E}$, met by making Φ constant on the surfaces of the conductors, is therefore familiar from Chaps. 4 and 5.

$$\Phi = 0 \text{ on } S_1; \qquad \Phi = V(z,t) \text{ on } S_2 \tag{10}$$

By definition, Λ is equal to the inductance per unit length L times the total current I carried by the conductor having the surface S_2.

$$\Lambda = LI \tag{11}$$

The first of the transmission line equations is now obtained simply by evaluating (2) on the boundary S_2 of the second conductor and using the definition of Λ from (11).

$$\boxed{\frac{\partial V}{\partial z} + L\frac{\partial I}{\partial t} = 0} \tag{12}$$

The second equation follows from a similar evaluation of (3). This time we introduce the capacitance per unit length by exploiting the relation $LC = \mu\epsilon$, (8.6.14).

$$\boxed{\frac{\partial I}{\partial z} + C\frac{\partial V}{\partial t} = 0} \tag{13}$$

The integral of $\mathbf{E}$ between the conductors within a given plane of constant z is V, and can be interpreted as the voltage between the two conductors. The total current carried in the $+z$ direction through a plane of constant z by one of the conductors and returned in the $-z$ direction by the other is I. *Because effects of magnetic induction are important, V is a function of z. Similarly, because the displacement current is important, the current I is also a function of z.*

Example 14.2.1. Parallel Plate Transmission Line

Between the perfectly conducting parallel plates of Fig. 14.1.3, solutions to (7) and (8) that meet the boundary conditions of (9) and (10) are

$$A_z = \Lambda(z,t)\big(1 - \frac{x}{a}\big) = \frac{a\mu}{w}\big(1 - \frac{x}{a}\big)I(z,t) \tag{14}$$

$$\Phi = \big(1 - \frac{x}{a}\big)V(z,t) \tag{15}$$

In the EQS context of Chap. 5, the latter is the potential associated with a uniform electric field between plane parallel electrodes, while in the MQS context of Example 8.4.4, (14) is the vector potential associated with the uniform magnetic field inside a one-turn solenoid. The inductance per unit length follows from (11) and the evaluation of (14) on the surface S_2, and one way to evaluate the capacitance per unit length is to use the relation $LC = \mu\epsilon$.

$$L = \frac{\mu a}{w}; \qquad C = \frac{\mu\epsilon}{L} = \frac{\epsilon w}{a} \tag{16}$$

Every two-dimensional example from Chap. 4 with perfectly conducting boundaries is a candidate for supporting TEM fields that propagate in a direction perpendicular to the two dimensions. For every solution to (7) meeting the boundary

conditions of (10), there is one to (8) satisfying the conditions of (9). This follows from the antiduality exploited in Chap. 8 to describe the magnetic fields with perfectly conducting boundaries (Example 8.6.3). The next example illustrates how we can draw upon results from these earlier chapters.

Example 14.2.2. Parallel Wire Transmission Line

For the parallel wire configuration of Fig. 14.2.2a, the capacitance per unit length was derived in Example 4.6.3, (4.6.27).

$$C = \frac{\pi\epsilon}{ln\left[\frac{l}{R} + \sqrt{\left(\frac{l}{R}\right)^2 - 1}\right]} \tag{17}$$

The inductance per unit length was derived in Example 8.6.1, (8.6.12).

$$L = \frac{\mu}{\pi} ln\left[\frac{l}{R} + \sqrt{\left(\frac{l}{R}\right)^2 - 1}\right] \tag{18}$$

Of course, the product of these is $\mu\epsilon$.

At any given instant, the electric and magnetic fields have a cross-sectional distribution depicted by Figs. 4.6.5 and 8.6.6, respectively. The evolution of the fields with z and t are predicted by the one-dimensional wave equation, (4) or (5), or a similar equation resulting from combining the transmission line equations.

Propagation is in the z direction. With the understanding that the fields have transverse distributions that are identical to the EQS and MQS patterns, the next sections focus on the evolution of the fields with z and t.

No TEM Fields in Hollow Pipes. From the general description of TEM fields given in this section, we can see that TEM modes will not exist inside a hollow perfectly conducting pipe. This follows from the fact that both A_z and Φ must be constant on the walls of such a pipe, and solutions to (7) and (8) that meet these conditions are that A_z and Φ, respectively, are equal to these constants throughout. From Sec. 5.2, we know that these solutions to Laplace's equation are unique. The $\mathbf{E}$ and $\mathbf{H}$ they represent are zero, so there can be no TEM fields. This is consistent with the finding for rectangular waveguides in Sec. 13.4. The parallel plate configuration considered in Secs. 13.1–13.3 could support TEM modes because it was assumed that in any given cross-section (perpendicular to the axial position), the electrodes were insulated from each other.

Power-flow and Energy Storage. The transmission line model expresses the fields in terms of V and I. For the TEM fields, this is not an approximation but rather an elegant way of dealing with a class of three-dimensional time-dependent fields. To emphasize this point, we now show the equivalence of power flow and energy storage as derived from the transmission line model and from Poynting's theorem.

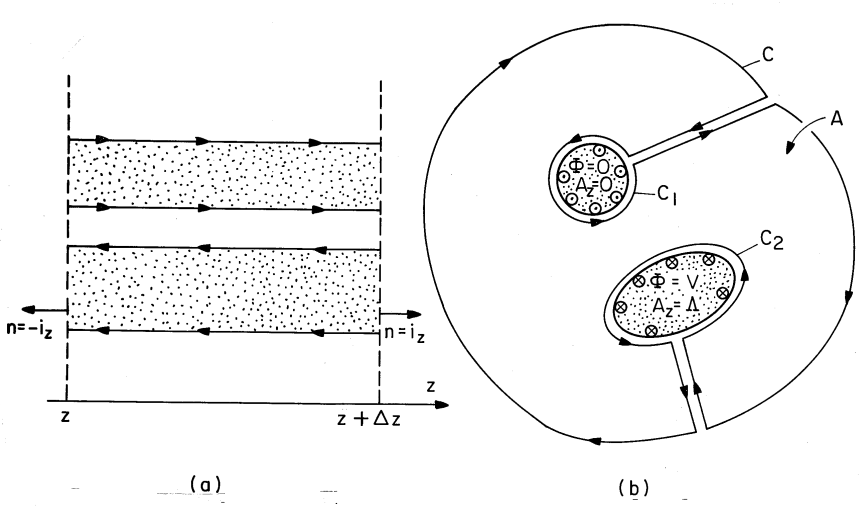


Fig. 14.2.3 Incremental length of transmission line and its cross-section.

An incremental length, Δz, of a two-conductor system and its cross-section are pictured in Fig. 14.2.3. A one-dimensional version of the energy conservation law introduced in Sec. 11.1 can be derived from the transmission line equations using manipulations analogous to those used to derive Poynting's theorem in Sec. 11.2. We multiply (14.1.4) by V and (14.1.5) by I and add. The result is a one-dimensional statement of energy conservation.

$$\boxed{-\frac{\partial}{\partial z}(VI) = \frac{\partial}{\partial t}(\frac{1}{2}CV^2 + \frac{1}{2}LI^2)} \tag{19}$$

This equation has intuitive "appeal." The power flowing in the z direction is VI, and the energy per unit length stored in the electric and magnetic fields is $\frac{1}{2}CV^2$ and $\frac{1}{2}LI^2$, respectively. Multiplied by Δz, (19) states that the amount by which the power flow at z exceeds that at $z + \Delta z$ is equal to the rate at which energy is stored in the length Δz of the line.

We can obtain the same result from the three-dimensional Poynting's integral theorem, (11.1.1), evaluated using (11.3.3), and applied to a volume element of incremental length Δz but one having the cross-sectional area A of the system (if need be, one extending to infinity).

$$\begin{aligned} -\Big[\int_A \mathbf{E}\times\mathbf{H}\cdot\mathbf{i_z}da\Big|_{z+\Delta z} - \int_A \mathbf{E}\times\mathbf{H}\cdot\mathbf{i_z}da\Big|_z\Big] \\ = \frac{\partial}{\partial t}\int_A (\frac{1}{2}\epsilon\mathbf{E}\cdot\mathbf{E} + \frac{1}{2}\mu\mathbf{H}\cdot\mathbf{H})da\Delta z \end{aligned} \tag{20}$$

Here, the integral of Poynting's flux density, $\mathbf{E}\times\mathbf{H}$, over a closed surface S has been converted to one over the cross-sectional areas A in the planes z and $z + \Delta z$. The closed surface is in this case a cylinder having length Δz in the z direction

and a lateral surface described by the contour C in Fig. 14.2.3b. The integrals of Poynting's flux density over the various parts of this lateral surface (having circumference C and length Δz) either are zero or cancel. For example, on the surfaces of the conductors denoted by C_1 and C_2, the contributions are zero because $\mathbf{E}$ is perpendicular. Thus, the contributions to the integral over S come only from integrations over A in the planes $z+\Delta z$ and z. Note that in writing these contributions on the left in (20), the normal to S on these surfaces is $\mathbf{i_z}$ and $-\mathbf{i_z}$, respectively.

To see that the integrals of the Poynting flux over the cross-section of the system are indeed simply VI, $\mathbf{E}$ is written in terms of the potentials (12.1.3).

$$\int_A \mathbf{E}\times\mathbf{H}\cdot\mathbf{i_z}da = \int_A \Big(-\nabla\Phi - \frac{\partial \mathbf{A}}{\partial t}\Big)\times\mathbf{H}\cdot\mathbf{i_z}da \tag{21}$$

The surface of integration has its normal in the z direction. Because $\mathbf{A}$ is also in the z direction, the cross-product of $\partial\mathbf{A}/\partial t$ with $\mathbf{H}$ must be perpendicular to z, and therefore makes no contribution to the integral. A vector identity then converts the integral to

$$\begin{aligned}\int_A \mathbf{E}\times\mathbf{H}\cdot\mathbf{i_z}da &= \int_A -\nabla\Phi\times\mathbf{H}\cdot\mathbf{i_z}da\\ &= -\int_A \nabla\times(\Phi\mathbf{H})\cdot\mathbf{i_z}da\\ &+\int_A \Phi\nabla\times\mathbf{H}\cdot\mathbf{i_z}da\end{aligned} \tag{22}$$

In Fig. 14.2.3, the area A, enclosed by the contour C, is insulating. Thus, because $\mathbf{J}=0$ in this region and the electric field, and hence the displacement current, are perpendicular to the surface of integration, Ampère's law tells us that the integrand in the second integral is zero. The first integral can be converted, by Stokes' theorem, to a line integral.

$$\int_A \mathbf{E}\times\mathbf{H}\cdot\mathbf{i_z}da = -\oint_C \Phi\mathbf{H}\cdot d\mathbf{s} \tag{23}$$

On the contour, $\Phi=0$ on C_1 and at infinity. The contributions along the segments connecting C_1 and C_2 to infinity cancel, and so the only contribution comes from C_2. On that contour, $\Phi=V$, so Φ is a constant. Finally, again because the displacement current is perpendicular to $d\mathbf{s}$, Ampère's integral law requires that the line integral of $\mathbf{H}$ on the contour C_2 enclosing the conductor having potential V be equal to $-I$. Thus, (23) becomes

$$\int_A \mathbf{E}\times\mathbf{H}\cdot\mathbf{i_z}da = -V\oint_{C_2}\mathbf{H}\cdot d\mathbf{s} = VI \tag{24}$$

The axial power flux pictured by Poynting's theorem as passing through the insulating region between the conductors can just as well be represented by the current and voltage of one of the conductors. To formalize the equivalence of these points of view, (24) is used to evaluate the left-hand side of Poynting's theorem, (20), and that expression divided by Δz.

$$\begin{aligned}&-\frac{[V(z+\Delta z)I(z+\Delta z)-V(z)I(z)]}{\Delta z}\\ &\quad=\frac{\partial}{\partial t}\int_A\Big(\frac{1}{2}\epsilon\mathbf{E}\cdot\mathbf{E}+\frac{1}{2}\mu\mathbf{H}\cdot\mathbf{H}\Big)da\end{aligned} \tag{25}$$

In the limit $\Delta z \to 0$, this statement is equivalent to that implied by the transmission line equations, (19), because the electric and magnetic energy storages per unit length are

$$\frac{1}{2}CV^2 = \int_A \frac{1}{2}\epsilon \mathbf{E}\cdot\mathbf{E}da; \qquad \frac{1}{2}LI^2 = \int_A \frac{1}{2}\mu \mathbf{H}\cdot\mathbf{H}da \tag{26}$$

In summary, for TEM fields, we are justified in thinking of a transmission line as storing energies per unit length given by (26) and as carrying a power VI in the z direction.

14.3 TRANSIENTS ON INFINITE TRANSMISSION LINES

The transient response of transmission lines or plane waves is of interest for time-domain reflectometry and for radar. In these applications, it is the delay and shape of the response to pulse-like signals that provides the desired information. Even more common is the use of pulses to represent digitally encoded information carried by various types of cables and optical fibers. Again, pulse delays and reflections are often crucial, and an understanding of how these are endemic to common communications systems is one of the points in this and the next section.

The next four sections develop insights into dynamic phenomena described by the one-dimensional wave equation. This and the next section are concerned with transients and focus on initial as well as boundary conditions to create an awareness of the key role played by causality. Then, with the understanding that effects of the turn-on transient have died away, the sinusoidal steady state response is considered in Secs. 14.5–14.6,

The evolution of the transmission line voltage $V(z,t)$, and hence the associated TEM fields, is governed by the one-dimensional wave equation. This follows by combining the transmission line equations, (14.1.4)-(5), to obtain one expression for V.

$$\frac{\partial^2 V}{\partial z^2} = \frac{1}{c^2}\frac{\partial^2 V}{\partial t^2}; \qquad c \equiv \frac{1}{\sqrt{LC}} = \frac{1}{\sqrt{\mu\epsilon}} \tag{1}$$

This equation has a remarkably general pair of solutions

$$V = V_+(\alpha) + V_-(\beta) \tag{2}$$

where V_+ and V_- are *arbitrary* functions of variables α and β that are defined as particular combinations of the independent variables z and t.

$$\alpha = z - ct \tag{3}$$

$$\beta = z + ct \tag{4}$$

To see that this general solution in fact satisfies the wave equation, it is only necessary to perform the derivatives and substitute them into the equation. To that end, observe that

$$\frac{\partial V_\pm}{\partial z} = V'_\pm; \qquad \frac{\partial V_\pm}{\partial t} = \mp cV'_\pm \tag{5}$$

where primes indicate the derivative with respect to the argument of the function. Carrying out the same process once more gives the second derivatives required to evaluate the wave equation.

$$\frac{\partial^2 V_\pm}{\partial z^2} = V_\pm''; \qquad \frac{\partial^2 V_\pm}{\partial t^2} = c^2 V_\pm'' \tag{6}$$

Substitution of these expression for the derivatives in (1) shows that (1) is satisfied. Functions having the form of (2) are indeed solutions to the wave equation.

According to (2), V is a superposition of fields that propagate, without changing their shape, in the positive and negative z directions. With α maintained constant, the component V_+ is constant. With α a constant, the position z increases with time according to the law

$$z = \alpha + ct \tag{7}$$

The shape of the second component of (2) remains invariant when β is held constant, as it is if the z coordinate decreases at the rate c. The functions $V_+(z - ct)$ and $V_-(z + ct)$ represent forward and backward waves proceeding without change of shape at the speed c in the $+z$ and $-z$ directions respectively. We conclude that the voltage can be represented as a superposition of forward and backward waves, V_+ and V_-, which, if the space surrounding the conductors is free space (where $\epsilon = \epsilon_o$ and $\mu = \mu_o$), propagate with the velocity $c \simeq 3 \times 10^8$ m/s of light.

Because $I(z, t)$ also satisfies the one-dimensional wave equation, it also can be written as the sum of traveling waves.

$$I = I_+(\alpha) + I_-(\beta) \tag{8}$$

The relationships between these components of I and those of V are found by substitution of (2) and (8) into either of the transmission line equations, (14.1.4)–(14.1.5), which give the same result if it is remembered that $c = 1/\sqrt{LC}$. In summary, as fundamental solutions to the equations representing the ideal transmission line, we have

$$\boxed{V = V_+(\alpha) + V_-(\beta)} \tag{9}$$

$$\boxed{I = \frac{1}{Z_o}[V_+(\alpha) - V_-(\beta)]} \tag{10}$$

where

$$\alpha = z - ct; \qquad \beta = z + ct \tag{11}$$

Here, Z_o is defined as the *characteristic impedance* of the line.

$$\boxed{Z_o \equiv \sqrt{L/C}} \tag{12}$$

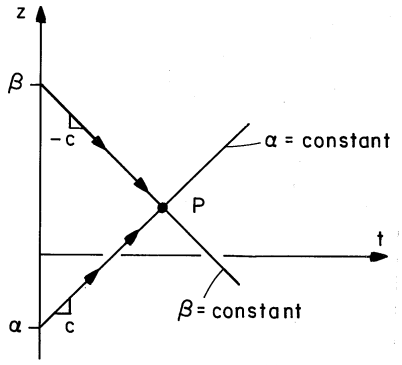


Fig. 14.3.1 Waves initiated at $z = \alpha$ and $z = \beta$ propagate along the lines of constant α and β to combine at P.

Typically, Z_o is the intrinsic impedance $\sqrt{\mu/\epsilon}$ multiplied by a function of the ratio of dimensions describing the cross-sectional geometry of the line.

Illustration. Characteristic Impedance of Parallel Wires

For example, the parallel wire transmission line of Example 14.2.2 has the characteristic impedance

$$\sqrt{L/C} = \frac{1}{\pi} ln \left[\frac{l}{R} + \sqrt{\left(\frac{l}{R}\right)^2 - 1} \right] \sqrt{\mu/\epsilon} \tag{13}$$

where for free space, $\sqrt{\mu/\epsilon} \approx 377\Omega$.

Response to Initial Conditions. The specification of the distribution of V and I at an initial time, $t = 0$, leads to two traveling waves. It is helpful to picture the field evolution in the $z - t$ plane shown in Fig. 14.3.1. In this plane, the $\alpha =$ constant and $\beta =$ constant *characteristic lines* are straight and have slopes $\pm c$, respectively.

When $t = 0$, we are given that along the z axis,

$$V(z, 0) = V_i(z) \tag{14}$$

$$I(z, 0) = I_i(z) \tag{15}$$

What are these fields at some later time, such as at P in Fig. 14.3.1?

We answer this question in two steps. First, we use the initial conditions to establish the separate components V_+ and V_- at each position when $t = 0$. To this end, the initial conditions of (14) and (15) are substituted for the quantities on the left in (9) and (10) to obtain two equations for these unknowns.

$$V_+ + V_- = V_i \tag{16}$$

$$\frac{1}{Z_o}(V_+ - V_-) = I_i \tag{17}$$

These expressions can then be solved for the components in terms of the initial conditions.

$$\boxed{V_+ = \frac{1}{2}\Big(I_i Z_o + V_i\Big)} \tag{18}$$

$$\boxed{V_- = \frac{1}{2}\Big(-I_i Z_o + V_i\Big)} \tag{19}$$

The second step combines these components to determine the field at P in Fig. 14.3.1. Here we use the invariance of V_+ along the line $\alpha =$ constant and the invariance of V_- along the line $\beta =$ constant. The way in which these components combine at P to give V and I is summarized by (9) and (10). The total voltage at P is the sum of the components, while the current is the characteristic admittance Z_o^{-1} multiplied by the difference of the components.

The following examples illustrate how the initial conditions determine the invariants (the waves $V_\pm$ propagating in the $\pm z$ directions) and how these invariants in turn determine the fields at a subsequent time and different position. They show how the response at P in Fig. 14.3.1 is determined by the initial conditions at just two locations, indicated in the figure by the points $z = \alpha$ and $z = \beta$. Implicit in our understanding of the dynamics is causality. The response at the location P at some *later* time is the result of conditions at $(z = \alpha, t = 0)$ that propagate with the velocity c in the $+z$ direction and conditions at $(z = \beta, t = 0)$ that propagate in the $-z$ direction with velocity c.

Example 14.3.1. Initiation of a Pure Traveling Wave

In Example 3.1.1, we were introduced to a uniform plane wave composed of a single component traveling in the $+z$ direction. The particular initial conditions for E_x and H_y [(3.1.9) and (3.1.10)] were selected so that the response would be composed of just the wave propagating in the $+z$ direction. Given that the initial distribution of E_x is

$$E_x(z,0) = E_i(z) = E_o e^{-z^2/2a^2} \tag{20}$$

can we now show how to select a distribution of H_y such that there is no part of the response propagating in the $-z$ direction?

In applying the transmission line to plane waves, we make the identification (14.1.9)

$$V \leftrightarrow E_x, \quad I \leftrightarrow H_y, \quad C \leftrightarrow \epsilon_o, \quad L \leftrightarrow \mu_o \Rightarrow Z_o \leftrightarrow \sqrt{\frac{\mu_o}{\epsilon_o}} \tag{21}$$

We are assured that $E_- = 0$ by making the right-hand side of (19) vanish. Thus, we make

$$H_i = \sqrt{\frac{\epsilon_o}{\mu_o}} E_i = \sqrt{\frac{\epsilon_o}{\mu_o}} E_o e^{-z^2/2a^2} \tag{22}$$

It follows from (18) and (19) that along the characteristic lines passing through $(z, 0)$,

$$E_+ = E_i; \qquad E_- = 0 \tag{23}$$

and from (9) and (10) that the subsequent fields are

$$E_x = E_+ = E_o e^{-(z-ct)^2/2a^2} \tag{24}$$

$$H_y = \sqrt{\frac{\epsilon_o}{\mu_o}} E_+ = \sqrt{\frac{\epsilon_o}{\mu_o}} E_o e^{-(z-ct)^2/2a^2} \tag{25}$$

These are the traveling electromagnetic waves found "the hard way" in Example 3.1.1.

The following example gives further substance to the two-step process used to deduce the fields at P in Fig. 14.3.1 from those at $(z = \alpha, t = 0)$ and $(z = \beta, t = 0)$. First, the components V_+ and V_-, respectively, are deduced at $(z = \alpha, t = 0)$ and $(z = \beta, t = 0)$ from the initial conditions. Because V_+ is invariant along the line $\alpha =$ constant while V_- is invariant along the line $\beta =$ constant, we can then combine these components to determine the fields at P.

Example 14.3.2. Initiation of a Wave Transient

Suppose that when $t = 0$ there is a uniform voltage V_p between the positions $z = -d$ and $z = d$, but that outside this range, $V = 0$. Further, suppose that initially, $I = 0$ over the entire length of the line.

$$V_i = \begin{cases} V_p; & -d < z < d \\ 0; & z < -d \text{ and } d < z \end{cases} \tag{26}$$

What are the subsequent distributions of V and I? Once we have found these responses, we will see how such initial conditions might be realized physically.

The initial conditions are given a pictorial representation in Fig. 14.3.2, where $V(z, 0) = V_i$ and $I(z, 0) = I_i$ are shown as the solid and broken distributions when $t = 0$.

It follows from (18) and (19) that

$$V_+ = \begin{cases} 0; & \alpha < -d, \ d < \alpha \\ \frac{1}{2}V_p; & -d < \alpha < d \end{cases}, \qquad V_- = \begin{cases} 0; & \beta < -d, \ d < \beta \\ \frac{1}{2}V_p; & -d < \beta < d \end{cases} \tag{27}$$

Now that the initial conditions have been used to identify the wave components $V_\pm$, we can use (9) and (10) to establish the subsequent V and I. These are also shown in Fig. 14.3.2 using the axis perpendicular to the $z - t$ plane to represent either $V(z, t)$ (the solid lines) or $I(z, t)$ (the dashed lines). Shown in this figure are the initial and two subsequent field distributions. At point P_1, both V_+ and V_- are zero, so that both V and I are also zero. At points like P_2, where the wave propagating from $z = d$ has arrived but that from $z = -d$ has not, V_+ is $V_p/2$ while V_- remains zero. At points like P_3, neither the wave propagating in the $-z$ direction from $z = d$ or that propagating in the $+z$ direction from $z = -d$ has yet arrived, V_+ and V_- are given by (27), and the fields remain the same as they were initially.

By the time $t = d/c$, the wave transient has resolved itself into two pulses propagating in the $+z$ and $-z$ directions with the velocity c. These pulses consist

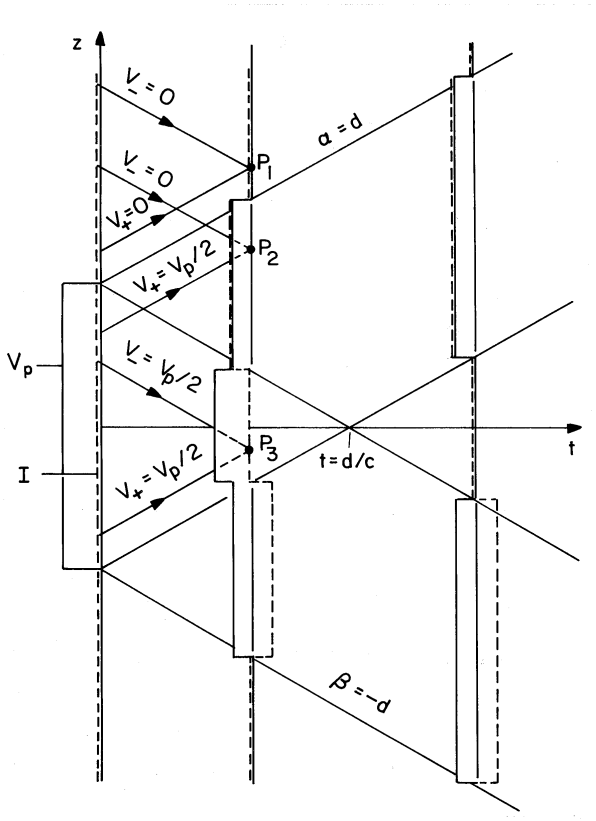


Fig. 14.3.2 Wave transient pictured in the $z-t$ plane. When $t = 0$, $I = 0$ and V assumes a uniform value over the range $-d < z < d$ and is zero outside this range.

of a voltage and a current that are in a constant ratio equal to the characteristic impedance, Z_o.

With the help of the step function $u_{-1}(z)$, defined by

$$u_{-1}(z) \equiv \begin{cases} 0; & z < 0 \\ 1; & 0 < z \end{cases} \tag{28}$$

we can carry out these same steps in analytical terms. The initial conditions are

$$I(z,0) = 0$$

$$V(z,0) = V_p[u_{-1}(z+d) - u_{-1}(z-d)] \tag{29}$$

The wave components follow from (18) and (19) and are expressed in terms of the variables α and β because they are invariant along lines where these parameters, respectively, are constant.

$$\begin{aligned} V_+ &= \frac{1}{2}V_p[u_{-1}(\alpha+d) - u_{-1}(\alpha-d)] \\ V_- &= \frac{1}{2}V_p[u_{-1}(\beta+d) - u_{-1}(\beta-d)] \end{aligned} \tag{30}$$

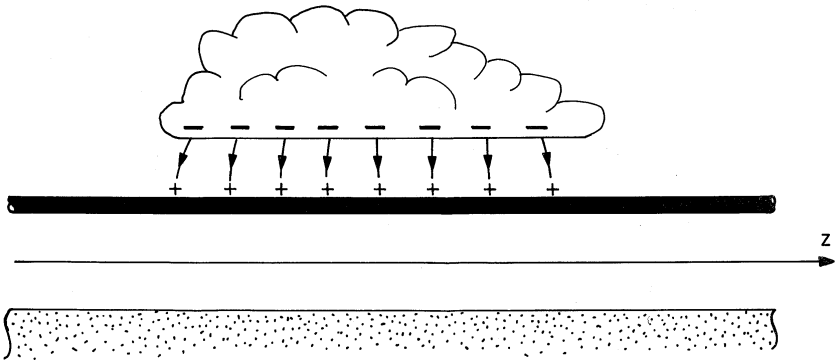


Fig. 14.3.3 Thunderstorm over power line modeled by initial conditions of Fig. 14.3.2.

The voltage and current at the point P in Fig. 14.3.1 follow from substitution of these expresions into (9) and (10). With α and β expressed in terms of (z,t) using (11), it follows that

$$\begin{aligned} V =& \frac{1}{2}V_p[u_{-1}(z-ct+d)-u_{-1}(z-ct-d)] \\ &+\frac{1}{2}V_p[u_{-1}(z+ct+d)-u_{-1}(z+ct-d)] \end{aligned}$$

$$\begin{aligned} I =& \frac{1}{2}\frac{V_p}{Z_o}[u_{-1}(z-ct+d)-u_{-1}(z-ct-d)] \\ &-\frac{1}{2}\frac{V_p}{Z_o}[u_{-1}(z+ct+d)-u_{-1}(z+ct-d)] \end{aligned} \tag{31}$$

These are analytical expressions for the the functions depicted by Fig. 14.3.2.

When our lights blink during a thunderstorm, it is possibly due to circuit interruption resulting from a power line transient initiated by a lightning stroke. Even if the discharge does not strike the power line, there can be transients resulting from an accumulation of charge on the line imaging the charge in the cloud above, as shown in Fig. 14.3.3. When the cloud is discharged to ground by the lightning stroke, initial conditions are established that might be modeled by those considered in this example. Just after the lightning discharge, the images for the charge accumulated on the line are on the ground below.

14.4 TRANSIENTS ON BOUNDED TRANSMISSION LINES

Transmission lines are generally connected to a source and to a load, as shown in Fig. 14.4.1a. More complex systems composed of interconnected transmission lines can usually be decomposed into subsystems having this basic configuration. A generator at $z = 0$ is connected to a load at $z = l$ by a transmission line having the length l. In this section, we build upon the traveling wave picture introduced in Sec. 14.3 to describe transients at a boundary initiated by a source.

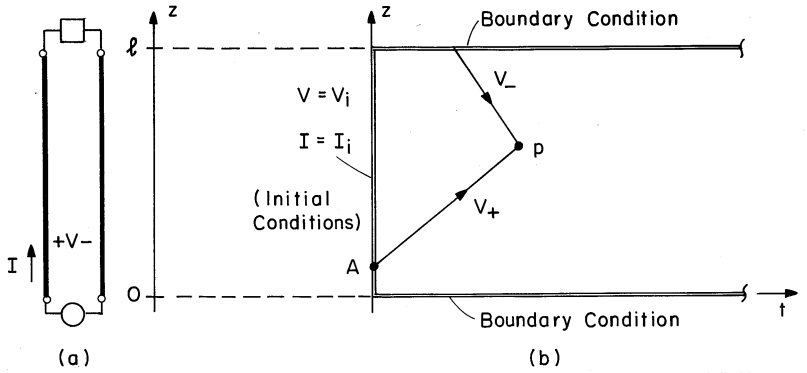


Fig. 14.4.1 (a)Transmission line with terminations. (b) Initial and boundary conditions in $z-t$ plane.

In picturing the evolution with time of the voltage $V(z,t)$ and current $I(z,t)$ on a terminated line, it is again helpful to use the $z-t$ plane shown in Fig. 14.4.1b. The load and generator impose boundary conditions at $z=l$ and $z=0$. In addition to satisfying these conditions, the distributions of V and I must also satisfy the respective initial values $V=V_i(z)$ and $I=I_i(z)$ when $t=0$, introduced in Sec. 14.3. Thus, our goal is to find V and I in the $\subset$-shaped region of $z-t$ space shown in Fig. 14.4.1b.

In Sec. 14.3, we found that the transmission line equations, (14.1.4) and (14.1.5), have solutions

$$V=V_+(\alpha)+V_-(\beta) \tag{1}$$

$$I=\frac{1}{Z_o}[V_+(\alpha)-V_-(\beta)] \tag{2}$$

where

$$\alpha=z-ct; \qquad \beta=z+ct \tag{3}$$

and $c=1/\sqrt{LC}$ and $Z_o=\sqrt{L/C}$.

A mathematical way of saying that V_+ and V_-, respectively, represent waves traveling in the $+z$ and $-z$ directions is to say that these quantities are invariants on the characteristic lines $\alpha=$ constant and $\beta=$ constant in the $z-t$ plane.

There are two steps in finding V and I.

- First, the initial conditions, and now the boundary conditions as well, are used to determine V_+ and V_- along the two families of characteristic lines in the region of the $z-t$ plane of interest. This is done with the understanding that causality prevails in the sense that the dynamics evolve in the "direction" of increasing time. Thus it is where a characteristic line enters the $\subset$-shaped region of Fig. 14.4.1b and goes to the right that the invariant for that line is set.

- Second, the solution at a given point of intersection for the lines $\alpha=$ constant and $\beta=$ constant are found in accordance with (1) and (2). This second step can be pictured as in Fig. 14.4.1b. In physical terms, the total voltage or

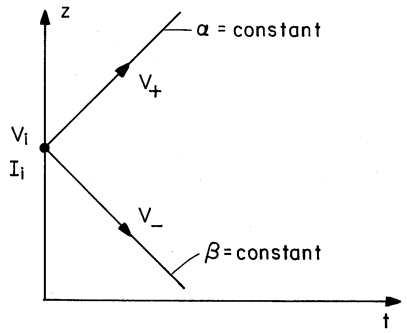


Fig. 14.4.2 Characteristic lines originating on initial conditions.

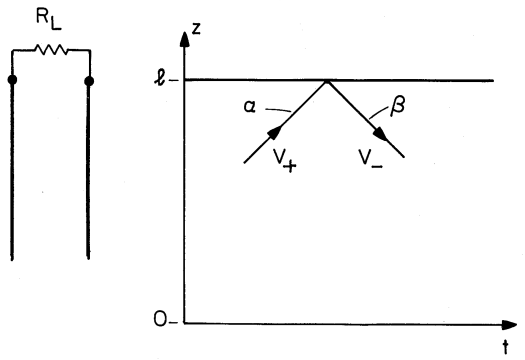


Fig. 14.4.3 Characteristic line originating on load.

current is the superposition of traveling waves propagating along the characteristic lines that intersect at the point of interest.

To complete the first step, note that a characteristic line passing through a given point P has three possible origins. First, it can originate on the $t = 0$ axis, in which case the invariants, $V_{\pm}$, are determined by the initial conditions. This was the only possibility on the infinite transmission line considered in Sec. 14.3. The initial voltage and current where the characteristic line originates when $t = 0$ in Fig. 14.4.2 is used to evaluate (1) and (2), and the simultaneous solution of these expressions then gives the desired invariants.

$$V_+ = \frac{1}{2}(V_i + Z_o I_i) \tag{4}$$

$$V_- = \frac{1}{2}(V_i - Z_o I_i) \tag{5}$$

The second origin of a characteristic line is the boundary at $z = l$, as shown in Fig. 14.4.3. In particular, we consider the load resistance R_L as the termination that imposes the boundary condition

$$V(l, t) = R_L I(l, t) \tag{6}$$

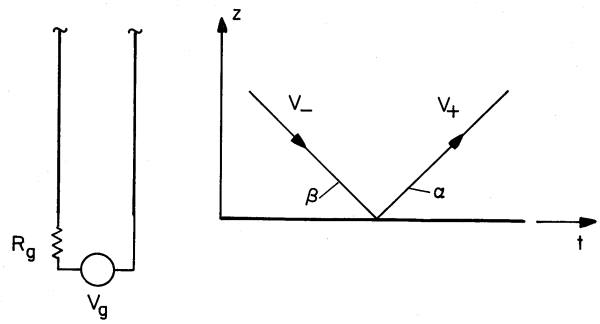


Fig. 14.4.4 Characteristic lines originating on generator end of line.

The problems will illustrate how the same approach illustrated here can also be used to describe terminations composed of arbitrary circuits. Certainly, the case where the load is a pure resistance is the most important type of termination, for reasons that will be clear shortly.

Again, because phenomena proceed in the $+t$ "direction," the incident wave V_+ and the boundary condition at $z = l$ conspire to determine the reflected wave V_- on the characteristic line $\beta =$ constant originating on the boundary at $z = l$ (Fig. 14.4.3). To say this mathematically, we substitute (1) and (2) into (6)

$$V_+ + V_- = \frac{R_L}{Z_o}(V_+ - V_-) \tag{7}$$

and solve for V_-.

$$\boxed{V_- = V_+\Gamma_L; \qquad \Gamma_L \equiv \frac{\left(\frac{R_L}{Z_o} - 1\right)}{\left(\frac{R_L}{Z_o} + 1\right)}} \tag{8}$$

Here, V_+ and V_- are evaluated at $z = l$, and hence with $\alpha = l - ct$ and $\beta = l + ct$. Given the incident wave V_+, we multiply it by the *reflection coefficient* Γ_L and determine V_-.

The third possible origin of a characteristic line passing through the given point P is on the boundary at $z = 0$, as shown in Fig. 14.4.4. Here the line has been terminated in a source modeled as an ideal voltage source, $V_g(t)$, in series with a resistance R_g. In this case, it is the wave traveling in the $-z$ direction (represented by V_- and incident on the boundary from the left in Fig. 14.4.4) that combines with the boundary condition there to determine the reflected wave V_+.

The boundary condition is the constraint of the circuit on the voltage and current at the terminals.

$$V(0,t) = V_g - R_g I(0,t) \tag{9}$$

Substitution of (1) and (2) then gives an expression that can be solved for V_+, given V_- and $V_g(t)$.

$$\boxed{V_+ = \frac{V_g}{\frac{R_g}{Z_o}+1} + V_-\Gamma_g; \qquad \Gamma_g \equiv \frac{\left(\frac{R_g}{Z_o}-1\right)}{\left(\frac{R_g}{Z_o}+1\right)}} \tag{10}$$

The following examples illustrate the two steps necessary to determine the transient response. First, $V_\pm$ are found over the range of time of interest using the initial conditions [(4) and (5) and Fig. 14.4.2] and boundary conditions [(8) and Fig. 14.4.3 and (10) and Fig. 14.4.4]. Then, the wave-components are superimposed to find V and I ((1) and (2) and Fig. 14.4.1.) To appreciate the space-time significance of the equations used in this process, it is helpful to have in mind the associated $z-t$ sketches.

Matching. The reflection of waves from the terminations of a line results in responses that can persist long after a signal has propagated the length of the transmission line. As a practical matter, it is therefore often desirable to eliminate reflections by *matching* the line.

From (8), it follows that wave reflection is eliminated at the load by making the load resistance equal to the characteristic impedance of the line, $R_L = Z_o$. Similarly, from (10), there will be no reflection of the wave V_- at the source if the resistance R_g is made equal to Z_o.

Consider first an example in which the response is made simple because the line is matched to its load.

Example 14.4.1. Matching

In the configuration shown in Fig. 14.4.5a, the load has a resistance R_L while the generator is an ideal voltage source $V_g(t)$ in series with the resistor R_g. The load is matched to the line, $R_L = Z_o$. As a result, according to (8), there are no V_- waves on characteristics originating at the load.

$$R_L = Z_o \Rightarrow V_- = 0 \tag{11}$$

Suppose that the driving voltage consists of a pulse of amplitude V_p and duration T, as shown in Fig. 14.4.5b. Further, suppose that when $t = 0$ the line voltage and current are both zero, $V_i = 0$, and $I_i = 0$. Then, it follows from (4) and (5) that V_+ and V_- are both zero on the respective characteristic lines originating on the $t = 0$ axis, as shown in Fig. 14.4.5b. By design, (8) gives $V_- = 0$ for the $\beta =$ constant characteristics originating at the load. Finally, because $V_- = 0$ for all characteristic lines incident on the source (whether they originate on the initial conditions or on the load), it follows from (10) that on characteristic lines originating at $z = 0$, V_+ is as shown in Fig. 14.4.5b. We now know V_+ and V_- everywhere.

It follows from (1) and (2) that V and I are as shown in Fig. 14.4.5. Because $V_- = 0$, the voltage and current both take the form of a pulse of temporal duration T and spatial length cT, propagating from source to load with the velocity c.

To express analytically what has been found, we know that at $z = 0$, $V_- = 0$ and in turn from (10) that at $z = 0$,

$$V_+ = \frac{V_g(t)}{\left(\frac{R_g}{Z_o}+1\right)} \tag{12}$$

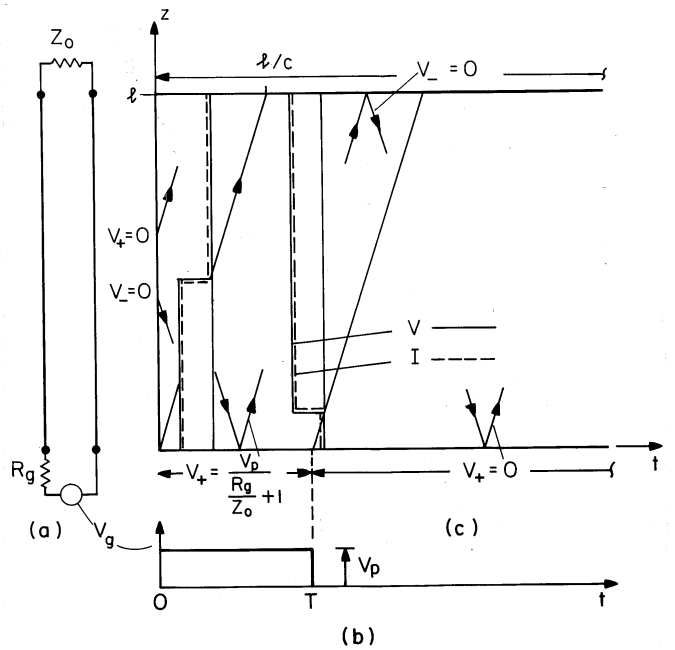


Fig. 14.4.5 (a) Matched line. (b) Wave components in $z-t$ plane. (c) Response in $z-t$ plane.

This is the value of V_+ along any line of constant α originating on the $z=0$ axis. For example, along the line $\alpha=-ct'$ passing through the $z=0$ axis when $t=t'$,

$$V_+ = \frac{V_g(t')}{\left(\frac{R_g}{Z_o}+1\right)} \tag{13}$$

We can express this result in terms of $z-t$ by introducing $\alpha=-ct'$ into (3), solving that expression for t', and introducing that expression for t' in (13). The result is just what we have already pictured in Fig. 14.4.5.

$$V(z,t) = V_+(\alpha) = \frac{V_g\left(t-\frac{z}{c}\right)}{\left(\frac{R_g}{Z_o}+1\right)} \tag{14}$$

Regardless of the shape of the voltage pulse, it appears undistorted at some location z but delayed by z/c.

Note that at any location on the matched line, including the terminals of the generator, $V/I=Z_o$. The matched line appears to the generator as a resistance equal to the characteristic impedance of the line.

We have assumed in this example that the initial voltage and current are zero over the length of the line. If there were finite initial conditions, their response with the generator voltage set equal to zero would add to that obtained here because the wave equation is linear and superposition holds. Initial conditions give rise to waves V_+ and V_- propagating in the $+z$ and $-z$ directions, respectively. However, because there are no reflected waves at the load, the effect of the initial conditions could not last longer at the generator than the time l/c required for V_- to reach $z=0$ from

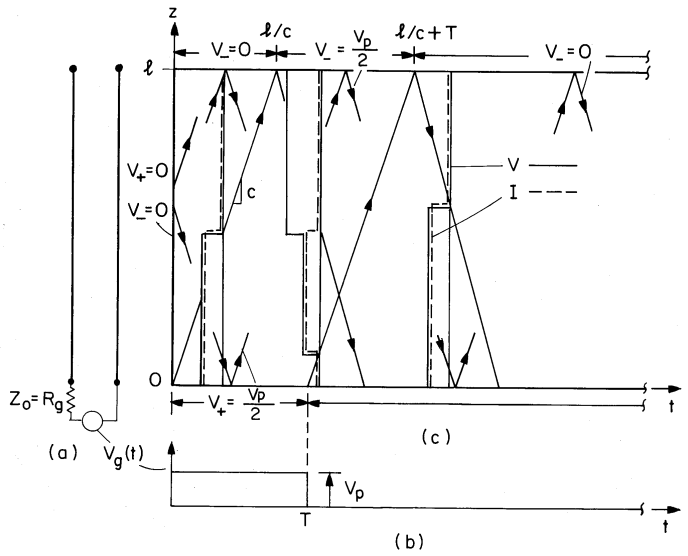


Fig. 14.4.6 (a) Open line. (b) Wave components in $z-t$ plane. (c) Response in $z-t$ plane.

$z = l$. They would not last longer at the load than the time $2l/c$, when any resulting wave reflected from the generator would return to the load.

Open circuit and short circuit terminations result in complete reflection. For the open circuit, $I = 0$ at the termination, and it follows from (2) that $V_+ = V_-$. For a short, $V = 0$, and (1) requires that $V_+ = -V_-$. Note that these limiting relations follow from (8) by making R_L infinite and zero in the respective cases.

In the following example, we see that an open circuit termination can result in a voltage that is momentarily as much as twice that of the generator.

Example 14.4.2. Open Circuit Termination

The transmission line of Fig. 14.4.6 is terminated in an infinite load resistance and driven by a generator modeled as a voltage source in series with a resistance R_g equal to the characteristic impedance Z_o. As in the previous example, the driving voltage is a pulse of time duration T, as shown in Fig. 14.4.6b. When $t = 0$, V and I are zero. In this example, we illustrate the effect of matching the generator resistance to the line and of having complete reflection at the load.

The boundary at $z = l$, (8), requires that

$$V_- = V_+ \tag{15}$$

while that at the generator, (10), is simply

$$V_+ = \frac{V_g}{2} \tag{16}$$

Because the generator is matched, this latter condition establishes V_+ on characteristic lines originating on the $z = 0$ axis without regard for V_-. These are summarized along the t axis in Fig. 14.4.6b.

To establish the values of V_- on characteristic lines originating at the load, we must know values of the incident V_+. Because I and V are both initially zero, the incident V_+ at the load is zero until t=l/c. From (15), V_- is also zero. From $t = l/c$ until $t = l/c + T$, the incident $V_+ = V_p/2$ and V_- on the characteristic lines originating at the open circuit during this time interval follows from (15) as $V_p/2$. Finally, for all greater times, the incident wave is zero at the load and so also is the reflected wave. The values of $V_\pm$ for characteristic lines originating on the associated segments of the boundaries and on the $t = 0$ axis are summarized in Fig. 14.4.6c.

With the values of $V_\pm$ determined, we now use (1) and (2) to make the picture also shown in Fig. 14.4.6c of the distributions of V and I at progressive instants in time. Because of the matched condition at the generator, the transient is over by the time the pulse has made one round trip. To make the current at the open circuit termination zero, the voltage doubles during that period when both incident and reflected waves exist at the termination.

The configuration of Fig. 14.4.6 was regarded in the previous example as an "open circuit transmission line" driven by a voltage source in series with a resistor. If we had been given the same configuration in Chap. 7, we would have taken it to be a "capacitor" in series with the resistor and the voltage source. The next example puts the EQS approximation in perspective by showing how it represents the dynamics when the resistance R_g is large compared to Z_o. A clue as to what happens when this ratio is large comes from writing it in the form

$$\frac{R_g}{Z_o} = R_g\sqrt{C/L} = \frac{R_gCl}{l\sqrt{CL}} = \frac{R_gCl}{(l/c)} \tag{17}$$

Here, R_gCl is the charging time of the capacitor and l/c is the electromagnetic wave transit time. When this ratio is large, the time for the transient to complete itself is many wave transit times. Thus, as will now be seen, the exponential charging of the capacitor is made up of many small steps associated with the electromagnetic wave passing "to and fro" over the length of the line.

Example 14.4.3. Quasistatic Transient as the Limit of an Electrodynamic Transient

The transmission line shown to the left in Fig. 14.4.7 is open at $z = l$ and driven at $z = 0$ by a step in voltage, $V_g = V_p u_{-1}(t)$. We are especially interested in the response with the series resistance, R_g, very large compared to Z_o. For simplicity, we assume that the initial voltage and current are zero.

The boundary condition imposed at the open termination, where $z = l$, is $I = 0$. From (2),

$$V_+ = V_- \tag{18}$$

while at the source, (10) pertains with $V_g = V_p$ a constant[5]

$$V_+ = V_g + V_-\Gamma_g; \qquad V_g \equiv \frac{V_p}{\left(\frac{R_g}{Z_o} + 1\right)} \tag{19}$$

[5] Be careful to distinguish the constant V_g as defined in this example from the source voltage $V_g(t) = V_p U_{-1}(t)$.

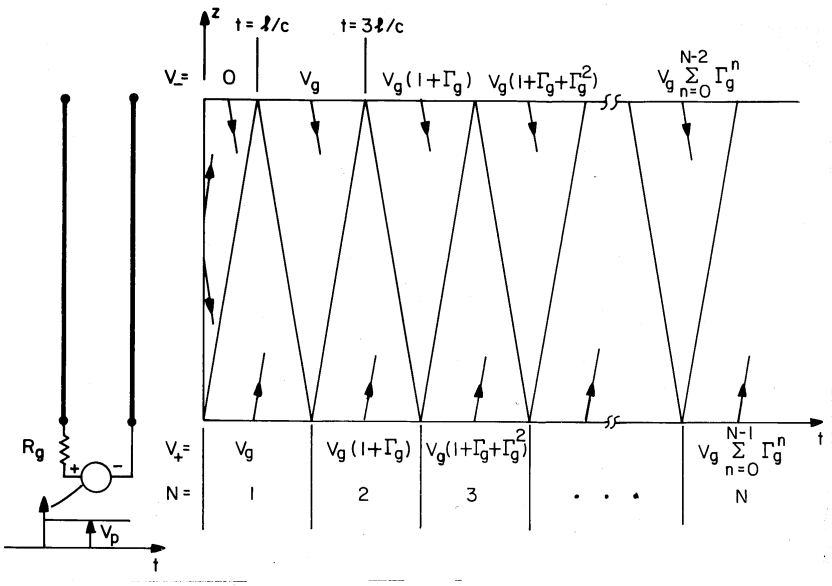


Fig. 14.4.7 Wave components of open line to a step in voltage in series with a high resistance.

with the reflection coefficient of the generator defined as

$$\Gamma_g \equiv \frac{\frac{R_g}{Z_o} - 1}{\frac{R_g}{Z_o} + 1} \tag{20}$$

Starting with characteristic lines originating at $t = 0$, where the initial conditions determine that V_+ and V_- are zero, we can now use these boundary conditions to determine V_- on lines originating at the load and V_+ on lines originating at $z = 0$. These values are shown in Fig. 14.4.7. Thus, $V_\pm$ are now known everywhere in the $\subset$-shaped region.

The voltage and current now follow from (1) and (2). In particular, consider the response at the generator terminals, where $z = 0$. In Fig. 14.4.7, the t axis has been divided into intervals of duration $2l/c$, the first denoted by $N = 1$, the second by $N = 2$, etc. We have found that the wave components incident on and reflected from the $z = 0$ boundary in the N-th interval are

$$V_- = V_g \sum_{n=0}^{N-2} \Gamma_g^n \tag{21}$$

$$V_+ = V_g \sum_{n=0}^{N-1} \Gamma_g^n \tag{22}$$

It follows from (2) that the current at $z = 0$ during this time interval is

$$I(0,t) = \frac{V_p}{R_g} \frac{1}{1 + \frac{Z_o}{R_g}} \Gamma_g^{N-1}; \qquad 2(N-1)\frac{l}{c} < t < 2N\frac{l}{c} \tag{23}$$

In turn, this current can be used to evaluate the terminal voltage.

$$V(0,t) = V_p\left(1 - \frac{\Gamma_g^{N-1}}{1+\frac{Z_o}{R_g}}\right) \tag{24}$$

With R_g/Z_o very large, it follows from (20) that

$$\Gamma_g \to \left(1 - 2\frac{Z_o}{R_g}\right) \tag{25}$$

In this same limit, the term $1+Z_o/R_g$ in (24) is essentially unity. Thus, (24) becomes approximately

$$V(0,t) \to V_p\left[1 - \left(1 - \frac{2Z_o}{R_g}\right)^{N-1}\right]; \qquad 2(N-1)\frac{l}{c} < t < \frac{2Nl}{c} \tag{26}$$

We suspect that in the limit where the round-trip transit time $2l/c$ is short compared to the charging time $\tau = R_gCl$, this voltage becomes the step response of the series capacitor and resistor.

$$V(0,t) \to V_p(1 - e^{-t/\tau}] \tag{27}$$

To see that this is indeed the case, we exploit the fact that

$$\lim_{x\to 0}(1-x)^{1/x} = e^{-1} \tag{28}$$

by writing (26) in the form

$$V(0,t) \to V_p\left\{1 - \left[\left(1 - \frac{2Z_o}{R_g}\right)^{1/(2Z_o/R_g)}\right]^{(N-1)(2Z_o/R_g)}\right\} \tag{29}$$

It follows that in the limit where Z_o/R_g is small,

$$V(0,t) \to V_p\left[1 - e^{-(N-1)(2Z_o/R_g)}\right]; \qquad 2(N-1)\frac{l}{c} < t < 2N\frac{l}{c} \tag{30}$$

Remember that N represents the interval of time during which the expression is valid. If we take the time as being that when the interval begins, then

$$2(N-1)\frac{l}{c} \sim t \Rightarrow 2(N-1) = \frac{t}{(l/c)} \tag{31}$$

Substitution of this expression for $2(N-1)$ into (30) and use of (17) then shows that in this high-resistance limit, the voltage does indeed take the exponential form for a charging capacitor, (27), with a charging time $\tau = R_gCl$. In the example of $V(0,t)$ shown in Fig. 14.4.8, there are 10 round-trip transit times in one charging time, $R_gCl = 20l/c$.

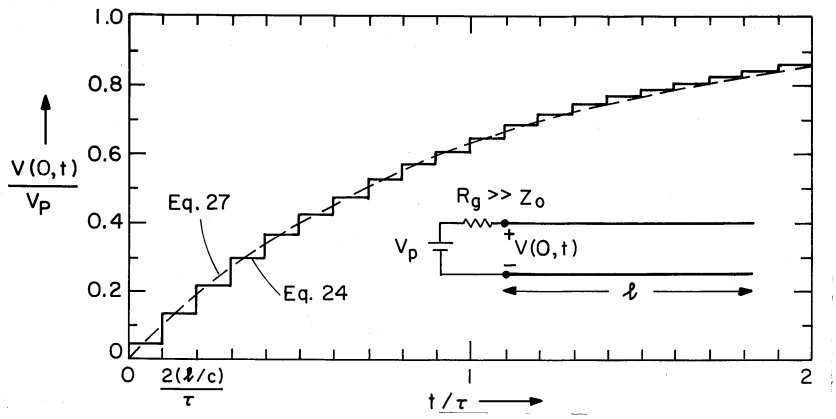


Fig. 14.4.8 Response of open circuit transmission line to step in voltage in series with a high resistance. The smooth curve is predicted by the EQS model.

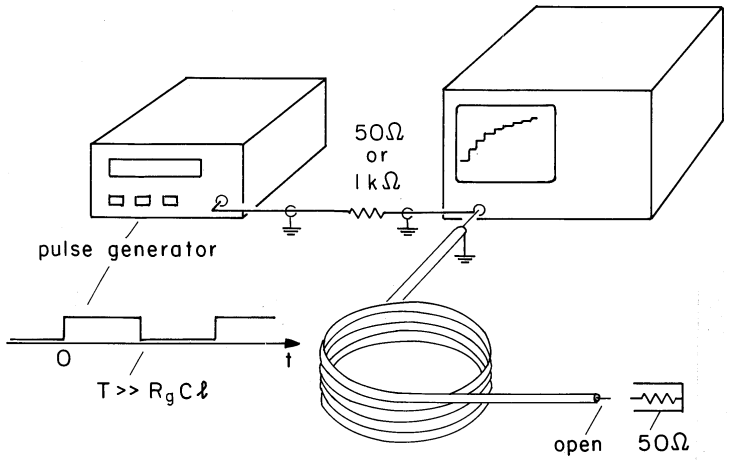


Fig. 14.4.9 Oscilloscope displays voltage at terminals of line under conditions of Examples 14.4.1-3.

The following demonstration is typical of a variety of demonstrations that are easily carried out using a good oscilloscope and a stretch of transmission line.

Demonstration 14.4.1. Transmission Line Matching, Reflection, and Quasistatic Charging

The apparatus shown in Fig. 14.4.9 is all that is required to demonstrate the phenomena described in the examples. In a typical experiment, a 10 m length of cable is used, in which case the wave transit time is about 0.05 μs. Thus, to resolve the transient, the oscilloscope must have a frequency response that extends to 100 MHz.

To achieve matching of the generator, as called for in Example 14.4.2, $R_g = Z_o$. Typically, for a coaxial cable, this is 50 Ω.

To see the charging transient of Example 14.4.3 with 10 round trip transit times in the capacitive charging time, it follows from (17) that we should make $R_g/Z_o = 20$. Thus, for a coaxial cable having $Z_o = 50\Omega$, $R_g = 1k\Omega$.

14.5 TRANSMISSION LINES IN THE SINUSOIDAL STEADY STATE

The method used in Sec. 14.4 is equally applicable to finding the response to a sinusoidal excitation of an ideal transmission line. Rather than exciting the line by a voltage step or a voltage pulse, as in the examples of Sec. 14.4, the source may produce a sinusoidal excitation. In that case, there is a part of the response that is in the sinusoidal steady state and a part that accounts for the initial conditions and the transient associated with turning on the source. Provided that the boundary conditions are (like the transmission line equations) linear, we can express the response as a superposition of these two parts.

$$V(z,t) = V_s(z,t) + V_t(z,t) \tag{1}$$

Here, V_s is the sinusoidal steady state response, determined without regard for the initial conditions but satisfying the boundary conditions. Added to this to make the total solution satisfy the initial conditions is V_t. This transient solution is defined to satisfy the boundary conditions with the drive equal to zero and to make the total solution satisfy the initial conditions. If we were interested in it, this transient solution could be found using the methods of the previous section. In an actual physical situation, this part of the solution is usually dissipated in the resistances of the terminations and the line itself. Then the sinusoidal steady state prevails. In this and the next section, we focus on this part of the solution.

With the understanding that the boundary conditions, like those describing the transmission line, are linear differential equations with constant coefficients, the response will be sinusoidal and at the same frequency, ω, as the drive. Thus, we assume at the outset that

$$V = \mathrm{Re}\,\hat{V}(z)e^{j\omega t}; \qquad I = \mathrm{Re}\,\hat{I}(z)e^{j\omega t} \tag{2}$$

Substitution of these expressions into the transmission line equations, (14.1.4)–(14.1.5), shows that the z dependence is governed by the ordinary differential equations

$$\boxed{\frac{d\hat{I}}{dz} = -j\omega C\hat{V}} \tag{3}$$

$$\boxed{\frac{d\hat{V}}{dz} = -j\omega L\hat{I}} \tag{4}$$

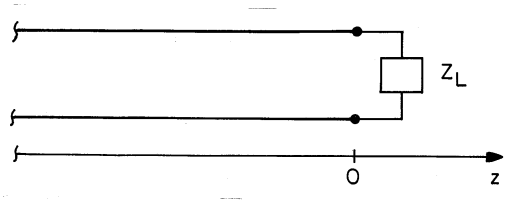


Fig. 14.5.1 Termination at $z = 0$ in load impedance.

Again because of the constant coefficients, these linear equations have two solutions, each having the form $\exp(-jkz)$. Substitution shows that

$$\boxed{\hat{V} = \hat{V}_+ e^{-j\beta z} + \hat{V}_- e^{j\beta z}} \tag{5}$$

where $\beta \equiv \omega\sqrt{LC}$. In terms of the same two arbitrary complex coefficients, it also follows from substitution of this expression into (14.1.5) that

$$\boxed{\hat{I} = \frac{1}{Z_o}\left(\hat{V}_+ e^{-j\beta z} - \hat{V}_- e^{j\beta z}\right)} \tag{6}$$

where $Z_o = \sqrt{L/C}$.

What we have found are solutions having the same traveling wave forms as identified in Sec. 14.3, (14.3.9)–(14.3.10). This can be seen by using (2) to recover the time dependence and writing these two expressions as

$$V = \mathrm{Re}\left[\hat{V}_+ e^{-j\beta\left(z-\frac{\omega}{\beta}t\right)} + \hat{V}_- e^{j\beta\left(z+\frac{\omega}{\beta}t\right)}\right] \tag{7}$$

$$I = \mathrm{Re}\,\frac{1}{Z_o}\left[\hat{V}_+ e^{-j\beta\left(z-\frac{\omega}{\beta}t\right)} - \hat{V}_- e^{j\beta\left(z+\frac{\omega}{\beta}t\right)}\right] \tag{8}$$

The velocity of the waves is $\pm\omega/\beta = 1/\sqrt{LC}$. Because the coefficients $\hat{V}_\pm$ are complex, they represent both the amplitude and phase of these traveling waves. Thus, the solutions could be sinusoids, cosinusoids, or any combination of these having the given arguments. In working with standing waves in Sec. 13.2, we demonstrated how the coefficients could be adjusted to satisfy simple boundary conditions. Here we introduce a point of view that is convenient in dealing with complicated terminations.

Transmission Line Impedance. The transmission line shown in Fig. 14.5.1 is terminated in a load impedance Z_L. By definition, Z_L is the complex number

$$\frac{\hat{V}(0)}{\hat{I}(0)} = Z_L \tag{9}$$

In general, it could represent any linear system composed of resistors, inductors, and capacitors. The complex amplitudes $\hat{V}_{\pm}$ are determined by this and another boundary condition. This second condition represents the termination of the line somewhere to the left in Fig. 14.5.1.

At any location on the line, the impedance is found by taking the ratio of (5) and (6).

$$\boxed{Z(z) \equiv \frac{\hat{V}(z)}{\hat{I}(z)} = Z_o \frac{1 + \Gamma_L e^{2j\beta z}}{1 - \Gamma_L e^{2j\beta z}}} \tag{10}$$

Here, Γ_L is the *reflection coefficient* of the load.

$$\boxed{\Gamma_L \equiv \frac{\hat{V}_-}{\hat{V}_+}} \tag{11}$$

Thus, Γ_L is simply the ratio of the complex amplitudes of the traveling wave components.

At the location $z = 0$, where the line is connected to the load and (9) applies, this expression becomes

$$\boxed{\frac{Z_L}{Z_o} = \frac{1 + \Gamma_L}{1 - \Gamma_L}} \tag{12}$$

The boundary condition, expressed by (12), is sufficient to determine the reflection coefficient. That is, from (12) it follows that

$$\Gamma_L = \frac{(Z_L/Z_o - 1)}{(Z_L/Z_o + 1)} \tag{13}$$

Given the load impedance, Γ_L follows from this expression. The line impedance at a location z to the left then follows from the use of this expression to evaluate (10).

The following examples lead to important implications of (11) while indicating the usefulness of the impedance point of view.

Example 14.5.1. Impedance Matching

Given an incident wave V_+, how can we eliminate the reflected wave represented by V_-? By definition, there is no reflected wave if the reflection coefficient, (11), is zero. It follows from (13) that

$$\Gamma_L = 0 \Rightarrow Z_L = Z_o \tag{14}$$

Note that Z_o is real, which means that the matched load is equivalent to a resistance, $R_L = Z_o$. Thus, our finding is consistent with that of Sec. 14.4, where we found that

such a termination would eliminate the reflected wave, sinusoidal steady state or not.

It follows from (10) that the line has the same impedance, Z_o, at any location z, when terminated in its characteristic impedance. Because V_-=0, it follows from (7) that the voltage takes the form

$$V = \mathrm{Re}\,\hat{V}_+ e^{j(\omega t - \beta z)} \tag{15}$$

The voltage has the distribution in space and time of a sinusoid traveling in the z direction with the velocity $1/\sqrt{LC}$. At any given location, the voltage is sinusoidal in time at the (angular) frequency ω. The amplitude is the same, regardless of z.[6]

The previous example illustrated that at any location, a transmission line terminated in a resistance equal to its characteristic impedance has an impedance which is also resistive and equal to Z_o. The next example illustrates what happens in the opposite extreme, where the termination dissipates no energy and the response is a pure standing wave rather than the pure traveling wave of the matched line.

Example 14.5.2. Short Circuit Impedance and Standing Waves

With a short circuit at $z = 0$, (5) makes it clear that $V_- = -V_+$. Thus, the reflection coefficient defined by (11) is $\Gamma_L = -1$. We come to the same conclusion from the evaluation of (13).

$$Z_L = 0 \Rightarrow \Gamma_L = -1 \tag{16}$$

The impedance at some location z then follows from (10) as

$$\frac{Z(-l)}{Z_o} \equiv j\frac{X}{Z_o} = j\tan\beta l \tag{17}$$

In view of the definition of β,

$$\beta l = \frac{\omega l}{c} = 2\pi\frac{l}{\lambda} \tag{18}$$

and so we can think of βl as being proportional either to the frequency or to the length of the line measured in wavelengths λ. The impedance of the line is a reactance X having the dependence on either of these quantities shown in Fig. 14.5.2.

At low frequencies (or for a length that is short compared to a quarter-wavelength), X is positive and proportional to ω. As should be expected from either Chap. 8 or Example 13.1.1, the reactance is that of an inductor.

$$\beta l \ll 1 \Rightarrow X \to (\beta l)\sqrt{L/C} = \omega L l \tag{19}$$

As the frequency is raised to the point where the line is a quarter-wavelength long, the impedance is infinite. A shorted quarter-wavelength line has the impedance of an open circuit! As the frequency is raised still further, the reactance becomes capacitive, decreasing with increasing frequency until the half-wavelength line exhibits

[6] By contrast with Demonstration 13.1.1, where the light emitted by the fluorescent tube indicated that the electric field peaked at some locations and nulled at others, the distribution of light for a matched line would be "flat."

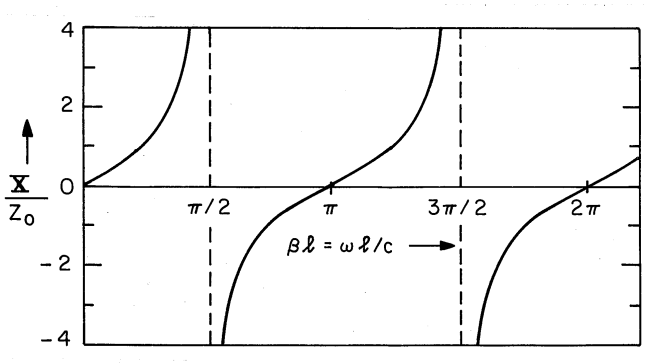


Fig. 14.5.2 Reactance as a function of normalized frequency for a shorted line.

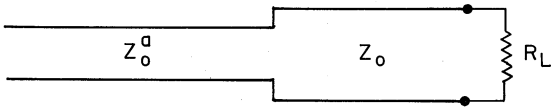


Fig. 14.5.3 A quarter-wave matching section.

the impedance of the termination, a short. That the impedance repeats itself as the line is increased in length by a half-wavelength is evident from Fig. 14.5.2.

We consider next an example that illustrates one of many methods for matching a load resistance R_L to a line having a characteristic impedance not equal to R_L.

Example 14.5.3. Quarter-Wave Matching Section

A quarter-wavelength line, as shown in Fig. 14.5.3, has the useful property of converting a normalized load impedance Z_L/Z_o to a normalized impedance that is the reciprocal of that impedance, Z_o/Z_L. To see this, we evaluate the impedance, (10), a quarter-wavelength from the load, where $\beta z = -\pi/2$, and then use (12).

$$Z\left(\beta z = -\frac{\pi}{2}\right) = \frac{Z_o^2}{Z_L} \tag{20}$$

Thus, if we wanted to match a line having the characteristic impedance Z_o^a to a load resistance $Z_L = R_L$, we could interpose a quarter-wavelength section of line having as its characteristic impedance a Z_o that is the geometric mean of the load resistance and the characteristic impedance of the line to be matched.

$$Z_o = \sqrt{Z_o^a R_L} \tag{21}$$

The idea of using quarter-wavelength sections to achieve matching will be continued in the next example.

The transmission line model is equally well applicable to electromagnetic plane waves. The equivalence was pointed out in Sec. 14.1. When these waves are optical, the permeability of common materials remains μ_o, and the polarizability is

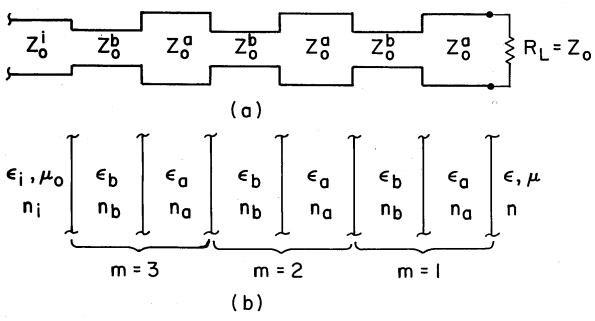


Fig. 14.5.4 (a) Cascaded quarter-wave transmission line sections. (b) Optical coating represented by (a).

described by the *index of refraction*, n, defined such that

$$\mathbf{D} = n^2 \epsilon_o \mathbf{E} \tag{22}$$

Thus, $n^2\epsilon_o$ takes the place of the dielectric constant, ϵ. The appropriate value of $n^2\epsilon_o$ is likely to be very different from the value of ϵ used for the same material at low frequencies.[7]

The following example illustrates the application of the transmission line viewpoint to an optical problem.

Example 14.5.4. Quarter-Wave Cascades for Reduction of Reflection

When *one* quarter-wavelength line is used to transform from one specified impedance to another, it is necessary to specify the characteristic impedance of the quarter-wave section. In optics, where it is desirable to minimize reflections that result from the passage of light from one transparent medium to another, it is necessary to specify the index of refraction of the quarter wave section. Given other constraints on the materials, this often is not possible. In this example, we see how the use of multiple layers gives some flexibility in the choice of materials.

The matching section of Fig. 14.5.4a consists of m pairs of quarter-wave sections of transmission line, respectively, having characteristic impedances Z_o^a and Z_o^b. This represents equally well the cascaded pairs of quarter wave layers of dielectric shown in Fig. 14.5.4b, interposed between materials of dielectric constants ϵ and ϵ_i. Alternatively, these layers are represented by their indices of refraction, n_a and n_b, interposed between materials having indices n_i and n.

First, we picture the matching problem in terms of the transmission line. The load resistance R_L represents the material to the right of the cascade. This region is pictured as an infinite transmission line having characteristic impedance Z_o. Thus, it presents a load to the cascade of resistance $R_L = Z_o$. To determine the impedance at the other side of the cascade, we make repeated use of the impedance transformation for a quarter-wave section, (20). To begin with, the impedance at the terminals of the first quarter-wave section is

$$Z = \frac{(Z_o^a)^2}{Z_o} \tag{23}$$

[7] With fields described in the frequency domain, ϵ, and hence n^2, are in general complex functions of frequency, as in Sec. 11.5.

With this taken as the load resistance in (20), the impedance at the terminals of the second section is

$$Z = \left(\frac{Z_o^b}{Z_o^a}\right)^2 Z_o \tag{24}$$

This can now be regarded as the impedance transformation for the pair of quarter-wave sections. If we now make repeated use of (24) to represent the impedance transformation for the quarter-wave sections taken in pairs, we find that the impedance at the terminals of m pairs is

$$Z = \left(\frac{Z_o^b}{Z_o^a}\right)^{2m} Z_o \tag{25}$$

Now, to apply this result to the optics configuration, we identify (14.1.9)

$$\begin{aligned} R_L \to \sqrt{\mu_o/\epsilon} \equiv \zeta_L &= \frac{\zeta_o}{n}; \\ Z_o^a = \sqrt{\mu_o/\epsilon_a} \equiv \zeta_a &= \frac{\zeta_o}{n_a}; \\ Z_o^b = \sqrt{\mu_o/\epsilon_b} \equiv \zeta_b &= \frac{\zeta_o}{n_b} \end{aligned} \tag{26}$$

and have from (25) for the intrinsic impedance of the cascade

$$\zeta = \zeta_L \left(\frac{\zeta_b}{\zeta_a}\right)^{2m} \tag{27}$$

In terms of the indices of refraction,

$$\frac{n}{n_i} = \left(\frac{n_a}{n_b}\right)^{2m} \tag{28}$$

If this condition on the optical properties and number of the layer pairs is fulfilled, the wave can propagate through the interface between regions of indices n_i and n without reflection. Given materials having n_a/n_b less than n/n_i, it is possible to pick the number of layer pairs, m, to satisfy the condition (at least approximately).

Coatings are commonly used on lenses to prevent reflection. In such applications, the waves processed by the lens generally have a spectrum of frequencies. Thus, optimization of the matching coatings is more complex than pictured here, where it has been assumed that the light is at a single frequency (is monochromatic).

It has been assumed here that the electromagnetic wave has normal incidence at the dielectric interface. Waves arriving at the interface at an angle can also be pictured in terms of the transmission line. In practical applications, the design of lens coatings to prevent reflection over a range of angles of incidence is a further complication.[8]

[8] H. A. Haus, *Waves and Fields in Optoelectronics*, Prentice-Hall, Inc., Englewood Cliffs, N.J. (1984), pp. 43-46.

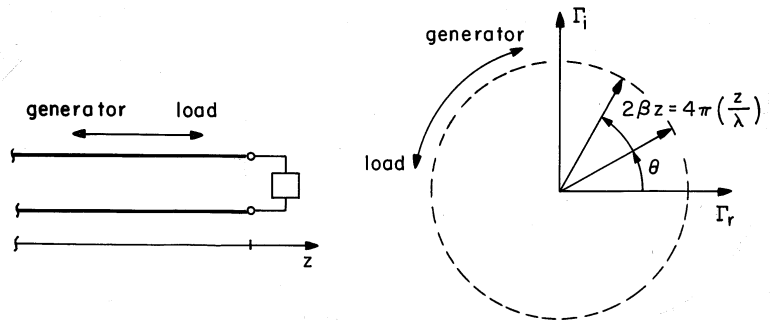


Fig. 14.6.1 (a)Transmission line conventions. (b) Reflection coefficient dependence on z in the complex Γ plane.

14.6 REFLECTION COEFFICIENT REPRESENTATION OF TRANSMISSION LINES

In Sec. 14.5, we found that a quarter-wavelength of transmission line turned a short circuit into an open circuit. Indeed, with an appropriate length (or driven at an appropriate frequency), the shorted line could have an inductive or a capacitive reactance. In general, the impedance observed at the terminals of a transmission line has a more complicated dependence on the termination.

Typical microwave measurements are made with a length of transmission line between the observation point and the terminals of the device under study, whether that be an antenna or a transistor. In this section, the objective is a way of visualizing the relation between the impedance at the "generator" terminals and the impedance of the "load." We will find that a representation of the variables in the reflection coefficient plane is valuable both conceptually and practically.

At a location z, the impedance of the transmission line shown in Fig. 14.6.1a is (14.5.10)

$$\boxed{\frac{Z(z)}{Z_o} = \frac{1+\Gamma(z)}{1-\Gamma(z)}} \tag{1}$$

where the reflection coefficient at the location z is defined as the complex function

$$\boxed{\Gamma(z) = \frac{\hat{V}_-}{\hat{V}_+} e^{j2\beta z}} \tag{2}$$

At the load position, where $z = 0$, the reflection coefficient is equal to Γ_L as defined by (14.5.11).

Like the impedance, the reflection coefficient is a function of z. Unlike the impedance, Γ has an easily pictured z dependence. Regardless of z, the magnitude of Γ is the same. Thus, as pictured in the complex Γ plane of Fig. 14.6.1b, it is a complex vector of magnitude $|\hat{V}_-/\hat{V}_+|$ and angle $\theta + 2\beta z$, where θ is the angle at

the position $z = 0$. With z defined as increasing from the generator to the load, the dependence of the reflection coefficient on z is as summarized in the figure. As we move from the generator toward the load, z increases and hence Γ rotates in the counterclockwise direction.

In summary, once the complex number Γ is established at one location z, its variation as we move toward the load or toward the generator can be pictured as a rotation at constant magnitude in the counterclockwise or clockwise directions, respectively. Typically, Γ is established at the location of the load, where the impedance, Z_L, is known. Then Γ at any location z follows from (1) solved for Γ.

$$\boxed{\Gamma = \frac{\left(\frac{Z}{Z_o} - 1\right)}{\left(\frac{Z}{Z_o} + 1\right)}} \tag{3}$$

With the magnitude and phase of Γ established at the load, the reflection coefficient can be found at another location by a simple rotation through an angle $4\pi(z/\lambda)$, as shown in Fig. 14.6.1b. The impedance at this second location would then follow from evaluation of (1).

Smith Chart. We save ourselves the trouble of evaluating (1) or (3), either to establish Γ at the load or to infer the impedance implied by Γ at some other location, by mapping Z/Z_o in the Γ plane of Fig. 14.6.1b. To this end, we define the normalized impedance as having a resistive part r and a reactive part x

$$\frac{Z}{Z_o} = r + jx \tag{4}$$

and plot the contours of constant r and of constant x in the Γ plane. This makes it possible to see directly what Z is implied by each value of Γ. Effectively, such a mapping provides a graphical solution of (1). The next few steps summarize how this mapping of the contours of constant r and x in the $\Gamma_r - \Gamma_i$ plane can be made with ruler and compass.

First, (1) is written using (4) on the left and $\Gamma = \Gamma_r + j\Gamma_i$ on the right. The real and imaginary parts of this equation must be equal, so it follows that

$$r = \frac{(1 - \Gamma_r^2 - \Gamma_i^2)}{(1 - \Gamma_r)^2 + \Gamma_i^2} \tag{5}$$

$$x = \frac{2\Gamma_i}{(1 - \Gamma_r)^2 + \Gamma_i^2} \tag{6}$$

These expressions are quadratic in Γ_r and Γ_i. By completing the squares, they can be written as

$$\left(\Gamma_r - \frac{r}{r+1}\right)^2 + \Gamma_i^2 = \left(\frac{1}{1+r}\right)^2 \tag{7}$$

$$(\Gamma_r - 1)^2 + \left(\Gamma_i - \frac{1}{x}\right)^2 = \left(\frac{1}{x}\right)^2 \tag{8}$$

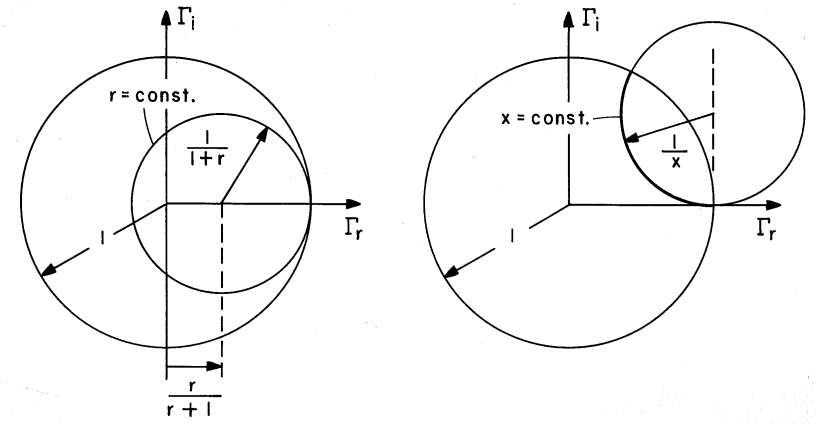


Fig. 14.6.2 (a) Circle of constant normalized resistance, r, in Γ plane. (b) Circle of constant normalized reactance, x, in Γ plane.

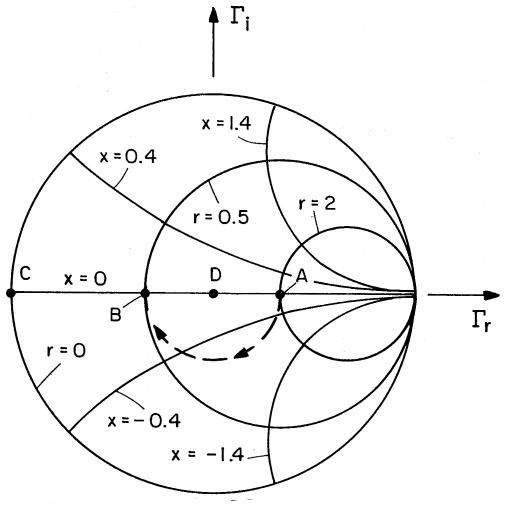


Fig. 14.6.3 Smith chart.

Thus, the contours of constant normalized resistance, r, and of constant normalized reactance, x, are the circles shown in Figs. 14.6.2a–14.6.2b.

Putting these contours together gives the lines of constant r and x in the complex Γ plane shown in Fig. 14.6.3. This is called a *Smith chart.*

Illustration. Impedance with Simple Terminations

How do we interpret the examples of Sec. 14.5 in terms of the Smith chart?

- **Quarter-wave Section.** In Example 14.5.3 we found that a normalized resistive load r_L was transformed into its reciprocal by a quarter-wave line. Suppose that $r_L = 2$ (the load resistance is $2Z_o$) and $x = 0$. Then, the load is

at A in Fig. 14.6.3. A quarter-wavelength toward the generator is a rotation of 180 degrees in a clockwise direction, with Γ following the trajectory from $A \rightarrow B$ in Fig. 14.6.3. Note that the impedance at B is indeed the reciprocal of that at A, $r = 0.5, x = 0$.

- **Impedance of Short Circuit Line.** Consider next the shorted line of Example 14.5.2. The load resistance r_L is 0, and reactance x_L is 0 as well, so we begin at the point C in Fig. 14.6.3. Now, we can trace out the impedance as we move away from the short toward the generator by rotating along the trajectory of unit radius in the clockwise direction. Note that all along this trajectory, $r = 0$. The normalized reactance then traces out the values given in Fig. 14.5.2, first taking on positive (inductive) values until it becomes infinite at $\lambda/4$ (rotation of 180 degrees), and then negative (capacitive) values until it returns to C, when the line has a length of $\lambda/2$.

- **Matched Line.** For the matched load of Example 14.5.1, we start out with $r_L = 1$ and $x_L = 0$. This is point D at the origin in Fig. 14.6.3. Thus, the trajectory of Γ is a circle of zero radius, and the impedance remains $r_L = 1$ over the length of the line.

While taking measurements on a transmission line terminated in a particular device, the Smith chart is often used to have an immediate picture of the impedance at the terminals. Even though the chart could be replaced by a programmable calculator, the overview provided by the Smith chart is important. Not only does it provide insight concerning the impedance, it can be used to picture the spatial evolution of the voltage and current, as we now see.

Standing Wave Ratio. Once the reflection coefficient has been established, the voltage and current distributions are determined (to within a factor determined by the source). That is, in terms of Γ, (14.5.5) becomes

$$\hat{V} = \hat{V}_+ e^{-j\beta z}[1 + \Gamma(z)] \tag{9}$$

The exponential factor has an amplitude that is independent of z. Thus, $[1 + \Gamma(z)]$ represents the z dependence of the voltage amplitude. This complex quantity can be pictured in the Γ plane as shown in Fig. 14.6.4a. Remember, as we move from load to generator, Γ rotates in the clockwise direction. As it does so, $1+\Gamma$ varies between a maximum value of $1 + |\Gamma|$ and a minimum value of $1 - |\Gamma|$. According to (9), we can now picture the spatial distribution of the voltage amplitude. Convenient for describing this distribution is the *voltage standing wave ratio* (VSWR), defined as the ratio of the maximum voltage amplitude to the minimum voltage amplitude. From Fig. 14.6.4a, we can see that this ratio is

$$\boxed{\text{VSWR} = \frac{(1+\Gamma)_{\max}}{(1+\Gamma)_{\min}} = \frac{1+|\Gamma|}{1-|\Gamma|}} \tag{10}$$

The distribution of voltage amplitude is shown for several VSWR's in Fig. 14.6.4b. We have already seen such distributions in two extremes. With the short

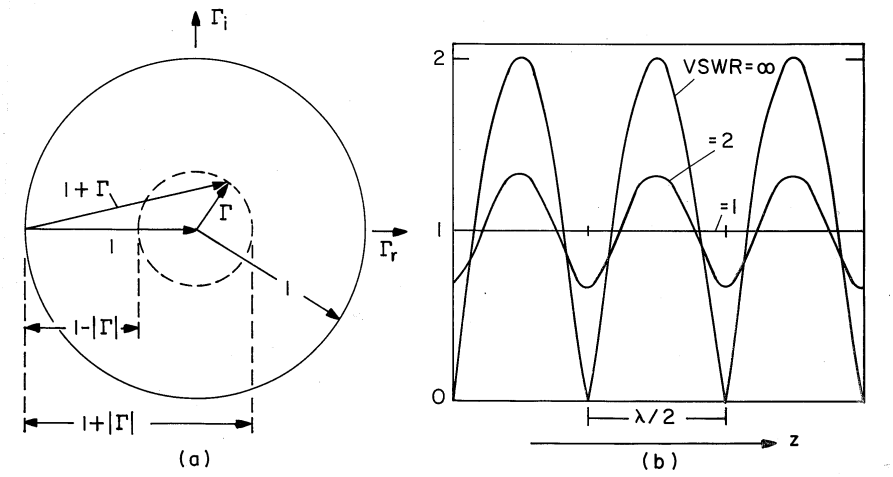


Fig. 14.6.4 (a) Normalized line voltage $1 + \Gamma$. (b) Distribution of voltage amplitude for three VSWR's.

circuit or open circuit terminations considered in Sec. 13.1, the reflection coefficient was on the unit circle and the VSWR was infinite. Indeed, the infinite VSWR envelope of Fig. 14.6.4b is that of a standing wave, with nulls every half-wavelength. The opposite extreme is also familiar. Here, the line is matched and the reflection coefficient is on a circle of zero radius. Thus, the VSWR is unity and the distribution of voltage amplitude is uniform.

Measurement of the VSWR and the location of a voltage null provides the information needed to determine a line termination. This follows by first using (10) to evaluate the magnitude of the reflection coefficient from the measured VSWR.

$$|\Gamma| = \frac{\text{VSWR} - 1}{\text{VSWR} + 1} \tag{11}$$

Thus, the radius of the circle representing the voltage distribution on the line has been determined. Second, a determination of the position of a null is tantamount to locating (to within a half-wavelength) the position on the line where Γ passes through the negative real axis. The distance from this point to the load, in wavelengths, then determines where the load is located on this circle. The corresponding impedance is that of the load.

Demonstration 14.6.1. VSWR and Load Impedance

In the slotted line shown in Fig. 14.6.5, a movable probe with its attached detector provides a measure of the line voltage as a function of z. The distance between the load and the voltage probe can be measured directly. By using a frequency of 3 GHz and an air-insulated cable (having a permittivity that is essentially that of free space, so that the wave velocity is 3×10^8 m/s), the wavelength is conveniently 10 cm.

The characteristic impedance of the coaxial cable is 50 Ω, so with terminations of 50 Ω, 100 Ω, and a short, the observed distribution of voltage is as shown in Fig. 14.6.4b for VSWR's of 1, 2, and ∞. (To plot data points on these curves, the

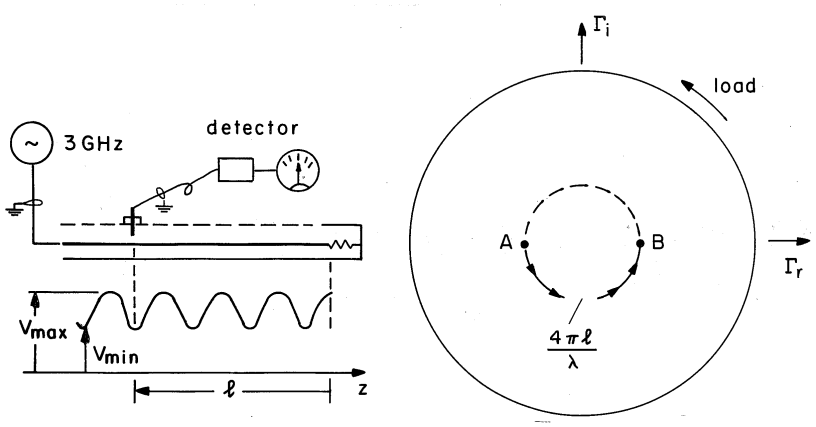


Fig. 14.6.5 Demonstration of distribution of voltage magnitude as function of VSWR.

measured values should be normalized to match the peak voltage of the appropriate distribution.)

Figure 14.6.5 illustrates how a measurement of the VSWR and position of a null can be used to infer the termination. Addition of a half-wavelength to l means an additional revolution in the Γ plane, so which null is used to define the distance l makes no difference. The trajectory drawn in the illustration is for the 100 Ω termination.

Admittance in the Reflection Coefficient Plane. Commonly, transmission lines are interconnected in parallel. It is then convenient to work with the admittance rather than the impedance. The Smith chart describes equally well the evolution of the admittance with z.

With $Y_o = 1/Z_o$ defined as the characteristic admittance, it follows from (1) that

$$\frac{Y}{Y_o} = \frac{1-\Gamma}{1+\Gamma} \tag{12}$$

If $\Gamma \to -\Gamma$, this expression becomes identical to that relating the normalized impedance to Γ, (1). Thus, the contours of constant normalized conductance, g, and normalized susceptance, y,

$$\frac{Y}{Y_o} \equiv g + jy \tag{13}$$

are those of the normalized impedance, r and x, rotated by 180 degrees. Rotate by 180 degrees the impedance form of the Smith chart and the admittance form is obtained! The contours of r and x, respectively, become those of g and y.[9]

[9] Usually, Γ is not explicitly evaluated. Rather, the admittance is given at one point on the Γ circle (and hence on the chart) and determined (by a rotation through the appropriate angle on the chart) at another point. Thus, for most applications, the chart need not even be rotated. However, if Γ is to be evaluated directly from the admittance, it should be remembered that the coordinates are actually $-\Gamma_r$ and $-\Gamma_i$.

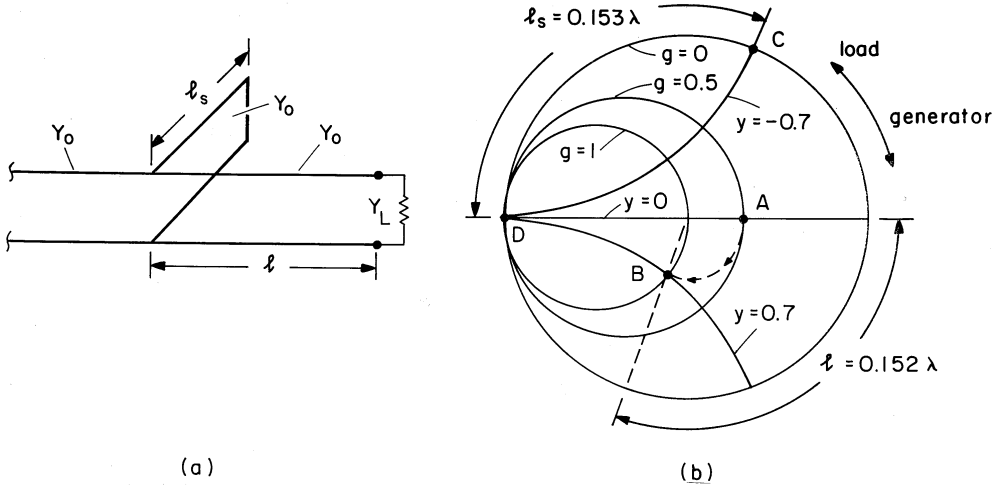


Fig. 14.6.6 (a) Single stub matching. (b) Admittance Smith chart.

The admittance form of the Smith chart is used in the following example.

Example 14.6.1. Single Stub Matching

In Fig. 14.6.6a, the load admittance Y_L is to be matched to a transmission line having characteristic admittance Y_o by means of a "stub" consisting of a shorted section of line having the same characteristic admittance Y_o. Variables that can be used to accomplish the matching are the distance l from the load to the stub and the length l_s of the stub.

Matching is accomplished in two steps. First, the length l is adjusted so that the real part of the admittance at the position where the stub is attached is equal to Y_o. Then the length of the shorted stub is adjusted so that it's susceptance cancels that of the line. Here, we see the reason for using the admittance form of the Smith chart, shown in Fig. 14.6.6b. The stub and the line are connected in parallel so that their admittances add.

The two steps are pictured in Fig. 14.6.6b for the case where the normalized load admittance is $g + jy = 0.5$, at A on the chart. The real part of the admittance becomes equal to the characteristic admittance on the circle $g = 1$; we adjust the length l so that the stub is connected at B, where the $|\Gamma|$ constant curve intersects the $g = 1$ circle. In the particular example shown, this length is $l = 0.152\lambda$. From the chart, one reads off a positive susceptibility at this point of about $y = 0.7$. We can determine the stub length l_s that gives the negative of this susceptance by again using the chart. The desired admittance of the stub is at C, where $g = 0$ and $y = -0.7$. In the case of the stub, the "load" is the short, where the admittance is infinite, at D on the chart. Following the $|\Gamma| = 1$ circle in the clockwise direction (from the "load" toward the "generator") from the short at D to the desired admittance at C then gives the length of the stub. For the example, $l_s = 0.153\lambda$.

To the left of the point where the stub is attached, the line should have a unity VSWR. The following demonstrates this concept.

Demonstration 14.6.2. Single Stub Matching

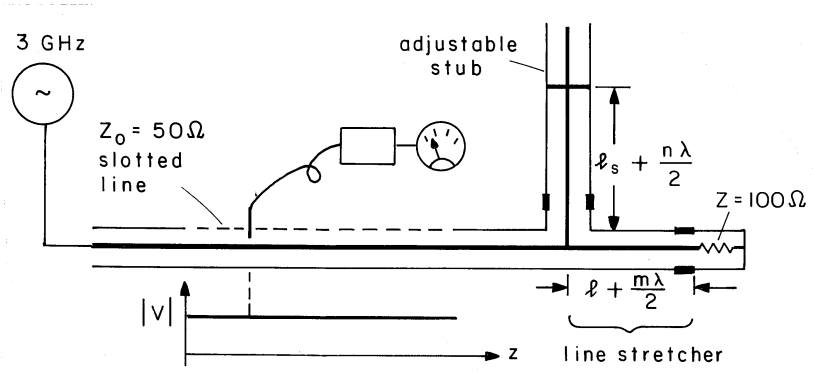


Fig. 14.6.7 Single stub matching demonstration.

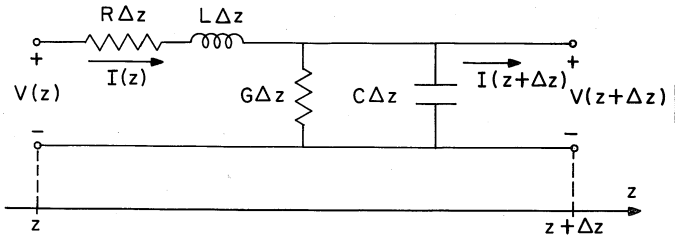


Fig. 14.7.1 Incremental section of lossy distributed line.

In Fig. 14.6.7, the previous demonstration has been terminated with an adjustable length of line (a line stretcher) and a stub. The slotted line makes it possible to see the effect on the VSWR of matching the line. With a load of $Z = 100\Omega$ and the stub and line stretcher adjusted to the values found in the previous example, the voltage amplitude is found to be independent of the position of the probe in the slotted line. Of course, we can add a half-wavelength to either l or l_s and obtain the same condition.

14.7 DISTRIBUTED PARAMETER EQUIVALENTS AND MODELS WITH DISSIPATION

The distributed parameter transmission line of Sec. 14.1 is now generalized to include certain types of dissipation by using the incremental circuit shown in Fig. 14.7.1 . The capacitance per unit length C is shunted by a conductance per unit length G and in series with the inductance per unit length L is the resistance per unit length R.

If the line really were made up of so many lumped parameter elements that it could be described by continuum equations, G would be the conductance per unit length of the lossy capacitors (Sec. 7.9) and R would be the resistance per unit length of the inductors. More often, G and R (like L and C) are either equivalent to or a model of a physical system. Examples are discussed in the next two sections.

The steps leading to the generalized transmission line equations are suggested by Eqs. 14.1.1 through 14.1.5. In requiring that the currents at the terminal on the right sum to zero, there is now an additional current through the shunt conductance. In the limit where $\Delta z \to 0$,

$$\boxed{\frac{\partial I}{\partial z} = -C\frac{\partial V}{\partial t} - GV} \tag{1}$$

Similarly, in summing the voltages around the loop, there is now a voltage drop across the series resistance. Again, in the limit $\Delta z \to 0$,

$$\boxed{\frac{\partial V}{\partial z} = -L\frac{\partial I}{\partial t} - RI} \tag{2}$$

As should be expected, with the introduction of dissipation represented by G and R, $V(z,t)$ and $I(z,t)$ no longer take the form of waves propagating without distortion. That is, substitution shows that solutions no longer take the form of (14.4.1)–(14.4.3). As a result, we would have to work considerably harder than in Secs. 14.3–14.4 to describe transients on lossy transmission lines. However, although somewhat more involved then before, the sinusoidal steady state response follows from the approach illustrated in Secs. 14.5–14.6.

With the objective of describing the sinusoidal steady state, complex amplitude representations of V and I (14.5.2) are substituted into (1) and (2) to give

$$\frac{d\hat{I}}{dz} = -(j\omega C + G)\hat{V} \tag{3}$$

$$\frac{d\hat{V}}{dz} = -(j\omega L + R)\hat{I} \tag{4}$$

To obtain an expression for the voltage alone, (3) is substituted into the derivative of (4).

$$\frac{d^2\hat{V}}{dz^2} - (j\omega L + R)(j\omega C + G)\hat{V} = 0 \tag{5}$$

With the voltage found from this equation, the current follows from (4).

$$\hat{I} = \frac{-1}{R + j\omega L}\frac{d\hat{V}}{dz} \tag{6}$$

Albeit complex, the coefficient in (5) is constant, so it is again appropriate to look for exponential solutions. Using the convention established in Sec. 14.5, we look for solutions $\exp(-jkz)$. Substitution into (5) then shows that

$$k^2 = -(j\omega L + R)(j\omega C + G) \tag{7}$$

So as to be clear in distinguishing the two roots of this dispersion equation, we *define* β as having a positive real part and write the roots as

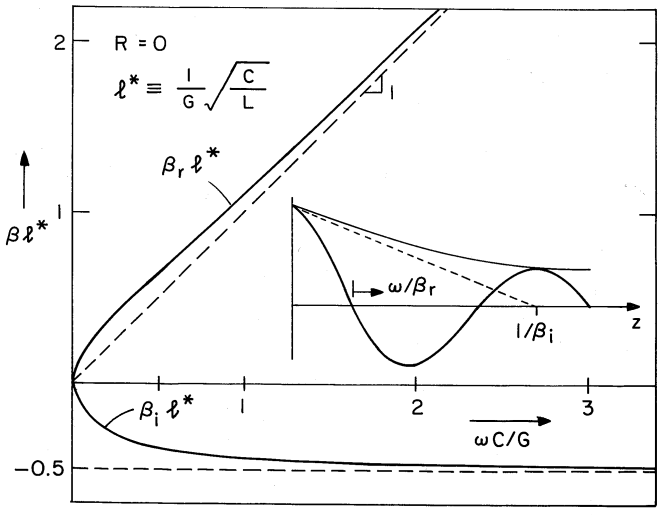


Fig. 14.7.2 Roots of (7) as functions of normalized ω. The real and imaginary parts, respectively, of the complex wave number β relate to the phase velocity and rate of decay of the wave, as shown.

$$\boxed{k = \pm\beta; \qquad \beta \equiv \sqrt{(\omega^2 LC - RG) - j\omega(RC + LG)}; \qquad \text{Re}\,\beta > 0} \tag{8}$$

These roots, $k = k_r + jk_i$, are pictured as a function of frequency in Fig. 14.7.2. From (7), k^2 is in the lower half-plane. It follows that the value of k having a positive real part (defined as β) has a negative imaginary part.

These definitions take on physical significance when the solutions to (5) are written as

$$\hat{V} = \hat{V}_+ e^{-j\beta z} + \hat{V}_- e^{j\beta z} \tag{9}$$

because it is then clear that we have defined β so that V_+ represents a wave with points of constant phase propagating in the $+z$ direction. Note that because β_i is negative, this wave decays in the $+z$ direction, as shown in Fig. 14.7.2. Similarly, $\hat{V}_-$ is the complex amplitude at $z = 0$ of a wave that decays in the $-z$ direction and has phases propagating in the $-z$ direction.[10]

In terms of the two coefficients $\hat{V}_\pm$, the current expression follows from substituting (9) into (6)

$$\hat{I} = \frac{1}{Z_o}(\hat{V}_+ e^{-j\beta z} - \hat{V}_- e^{j\beta z}) \tag{10}$$

where the complex characteristic impedance is now defined as

[10] It is important not to generalize from this finding. The direction of propagation of points of constant phase (the phase propagation direction, PPG, is not, in general, indicative of the directions of propagation of the wave; i.e., a source positioned on an infinite line at $z = 0$ does not necessarily cause waves with positive PPG to go away from the source in the $+z$ direction and with negative PPG to go away in the $-z$ direction. The direction of propagation is usually determined by the direction of the group velocity (GV). In the presence of loss, waves with positive GV decay in the $+z$-direction, with negative GV in the $-z$-direction.

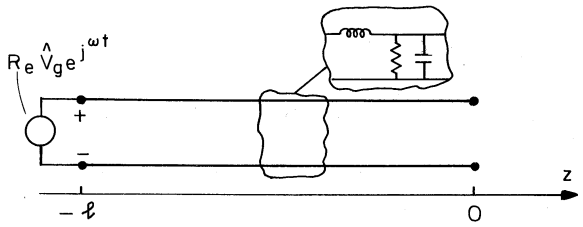


Fig. 14.7.3 Open circuit lossy line.

$$\boxed{Z_o \equiv \frac{(R + j\omega L)}{j\beta}} \tag{11}$$

Comparison of (9) and (10) with (14.5.5) and (14.5.6) shows that the impedance and reflection coefficient descriptions are applicable, provided we generalize β and Z_o to be the complex numbers given by (8) and (11). That these quantities are now complex is an inconvenience[11] and a warning that some ideas established for the ideal line need to be reexamined. For example, reasoning as in Sec. 14.5 shows that a pure resistance can no longer be used to match the line. Further, it is not possible to match the line at all frequencies with any finite number of lumped elements.

Example 14.7.1. Signal Attenuation on an Open Circuit Line

The lossy transmission line shown in Fig. 14.7.3 is open at the right and driven by a voltage source of complex amplitude V_g at the left. What is the voltage measured at the open circuit?

The open circuit at $z = 0$ requires that $I(0) = 0$, and hence [from (10)] that $V_+ = V_-$. Thus, the voltage, as given by (9), is

$$\hat{V} = \hat{V}_+(e^{-j\beta z} + e^{j\beta z}) = \hat{V}_g \frac{(e^{-j\beta z} + e^{j\beta z})}{(e^{j\beta l} + e^{-j\beta l})} \tag{12}$$

Here we have adjusted the coefficient $\hat{V}_+$ so that the voltage is $\hat{V}_g$ at the left end, where the voltage source is connected. As a function of time, the voltage distribution is therefore

$$V(z,t) = \mathrm{Re}\hat{V}_g \frac{(e^{-j\beta z} + e^{j\beta z})}{(e^{j\beta l} + e^{-j\beta l})} e^{j\omega t} \tag{13}$$

Much of the complicated phenomenon represented by this simple expression is encapsulated in the complex wave number. To illustrate, consider the voltage measured at $z = 0$, which from (13) has the complex amplitude

$$\hat{V}(0) = \frac{\hat{V}_g}{\cos \beta l} \tag{14}$$

If a calculator or computer is not available for evaluating the cosine of a complex number, then we can use the double-angle identity to write

$$\cos \beta l = \cos(\beta_r l + j\beta_i l) = \cos \beta_r l \cosh \beta_i l - j \sin \beta_r l \sinh \beta_i l \tag{15}$$

[11] Circumvented by having a calculator programmed to carry out operations on complex variables.

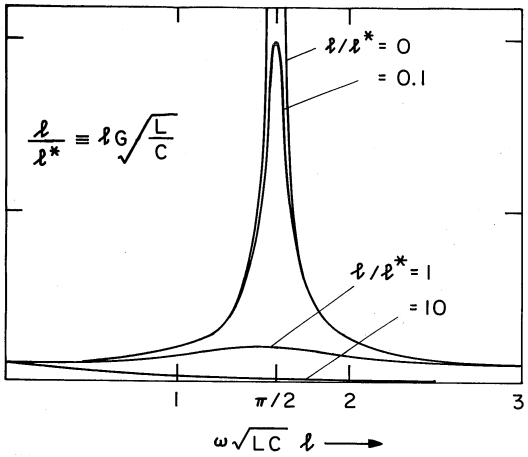


Fig. 14.7.4 Frequency response for open circuit lossy line.

For the case where all of the loss is due to the shunt conductance ($R = 0$), the frequency response is illustrated in Fig. 14.7.4. The four responses shown are for increasing amounts of loss, perhaps introduced by increasing G.

At very low frequencies, the output voltage simply follows the driving voltage. This is because we have considered the case where $R = 0$ and with the frequency so low that the inductor has no effect, the output terminals are connected to the source through a negligible impedance.

As the frequency is raised, consider first the response with no loss ($l/l^* = 0$). As the frequency approaches that required to make the line a quarter-wavelength long, the impedance of the line at the generator approaches zero and the current approaches infinity. This resonance condition results in the infinite response at $z = 0$. (As the frequency is raised further, these resonance conditions occur each time the frequency is such that the line has a length equal to a quarter-wavelength plus a multiple of a half-wavelength.) With the addition of a slight amount of loss ($l/l^* = 0.1$), the response is finite even under the resonance conditions. Further increasing the loss ($l/l^* = 1$) results in a response with a dull peak at the resonance point. Still larger losses ($l/l^* = 10$) bring in skin effect and monotonic attenuation of the voltage over the length of the line. Phenomena underlying this response are discussed in the next section.

14.8 UNIFORM AND TEM WAVES IN OHMIC CONDUCTORS ($R = 0$)

Transverse electromagnetic (TEM) waves that propagate in the z direction and are polarized in the x direction have electric and magnetic fields

$$\mathbf{E} = E_x(z,t)\mathbf{i_x}; \qquad \mathbf{H} = H_y(z,t)\mathbf{i_y} \tag{1}$$

We consider here how waves having this form propagate through a material with not only uniform permittivity ϵ and permeability μ (as in Secs. 14.1–14.6) but now

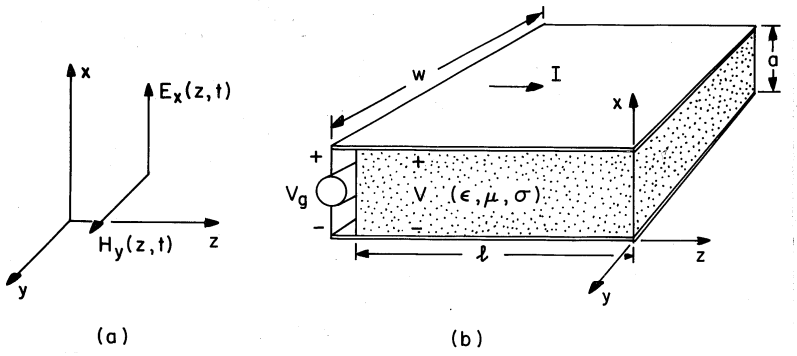


Fig. 14.8.1 (a) TEM fields in uniform lossy material. (b) Perfectly conducting electrodes with material having uniform σ as well as ϵ and μ between. With fringing field ignored, fields in the material have the transverse character of (a).

a uniform conductivity σ as well. As suggested by Fig. 14.8.1a, these fields might constitute plane waves in "infinite" media. They might also be the fields between the perfectly conducting planar electrodes of Fig. 14.8.1b. Our first objective in this section is to see that both the TEM fields in "infinite media" and on the "strip line" are described *exactly* by the distributed parameter model of Sec. 14.7 with $R = 0$. The ohmic loss introduces a conductance per unit length G.

With the introduction of fields having the form of (1) into the laws of Faraday and Ampère, only two of the six equations are not automatically satisfied. These are the x component of Ampère's law with Ohm's law used to express the conduction current

$$-\frac{\partial H_y}{\partial z} = \sigma E_x + \frac{\partial \epsilon E_x}{\partial t} \tag{2}$$

and the y component of Faraday's law

$$\frac{\partial E_x}{\partial z} = -\frac{\partial \mu H_y}{\partial t} \tag{3}$$

Except for the conduction current, the first term on the right in (2), these are the same equations as featured in Secs. 14.1-14.6. They become the plane parallel transmission-line equations if (2) is multiplied by the plate width w and (3) is multiplied by $-a$, where a is the plate spacing

$$\frac{\partial I}{\partial z} = -GV - C\frac{\partial V}{\partial t} \tag{4}$$

$$\frac{\partial V}{\partial z} = -L\frac{\partial I}{\partial t} \tag{5}$$

where the current I and voltage V are

$$I \equiv K_z w = -H_y w; \qquad V \equiv -E_x a \tag{6}$$

and

$$G = \frac{\sigma w}{a}; \qquad C = \frac{\epsilon w}{a}; \qquad L = \frac{\mu a}{w} \tag{7}$$

These are the same equations found for the distributed parameter line of Sec. 14.7 with $R = 0$. Thus, whether representing a plane wave in a uniform lossy material or the transmission-line filled with such a uniform medium, the distributed parameter model is "exact."

From the point of view taken in Sec. 14.2, the geometry of the parallel conductors in the "strip line" is a special case. In the problems, the derivation of the transmission line equations given in Sec. 14.2 is generalized to include the effects of a uniformly conducting material in the space between the perfect conductors. Regardless of their cross-sectional geometry, so long as the pair of conductors are perfectly conducting and the material between them is uniform, the fields are exactly TEM and exactly represented by the distributed parameter model. Not only is $\sqrt{LC} = \sqrt{\mu\epsilon}$ (8.6.14), but so also is $C/G = \epsilon/\sigma$ (7.6.4), regardless of the cross-sectional geometry.

We now suppose that sinusoidal steady state conditions have been established. Then the voltage and current are represented by (14.7.9) and (14.7.10) with the wave number and characteristic impedance given by (14.7.8) and (14.7.11) with $R = 0$ and L, C, and G given by (7).

$$\beta = \sqrt{\omega^2\mu\epsilon - j\omega\mu\sigma} \tag{8}$$

$$Z_o = \frac{\omega\mu a}{w\beta} \tag{9}$$

Example 14.8.1. TEM Fields in a Lossy Material between Plane Parallel Plates Terminated in an Open Circuit

With an "open circuit" at $z = 0$ and driven by a voltage source at $z = -l$, the parallel plate configuration of Fig. 14.7.1b is equivalent to the open circuit transmission line of Example 14.7.1. With the understanding that β is now given by (8), it follows from (14.7.13) that

$$V = \mathrm{Re}\,\hat{V}_g \frac{[e^{-j\beta l(z/l)} + e^{j\beta l(z/l)}]}{e^{j\beta l} + e^{-j\beta l}} e^{j\omega t} \tag{10}$$

Using the values of $\hat{V}_+ = \hat{V}_-$ implied by (14.7.12) in (14.7.10) results in the current distribution

$$I = \mathrm{Re}\,\frac{\hat{V}_g}{Z_o} \frac{[e^{-j\beta l(z/l)} - e^{j\beta l(z/l)}]}{e^{j\beta l} + e^{-j\beta l}} e^{j\omega t} \tag{11}$$

where Z_o is evaluated using (9).

The voltage and current have been specified as a superposition of forward and backward waves, which, respectively, decay in the directions in which their phases propagate. The distribution of the square of the magnitude of V (of E_x) predicted by (10) (and hence of the time average dissipation density or time average electric energy density) is illustrated by Fig. 14.8.2. In this case, the electrical dissipation is small enough so that a standing wave pattern is evident. The wave propagating and decaying to the right interferes with the wave propagating and decaying to the left in such a way that the boundary condition at $z = 0$ is satisfied. In the neighborhood of $z = 0$, where the wave traveling to the left has not yet decayed appreciably, the two waves interfere to form the familiar standing wave pattern. However, at the left, the wave traveling to the left has largely decayed and so interferes with the wave

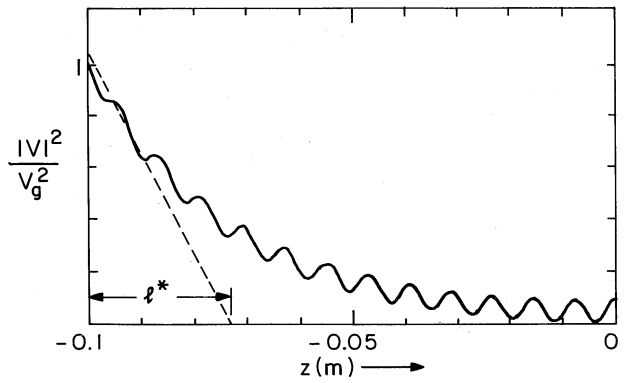


Fig. 14.8.2 Square of the magnitude of $\hat{V}$ as a function of position z for a slightly damped electromagnetic wave. $\omega = 12 \times 10^{10}$ rad/s, $l = 0.1$ m, $\epsilon = \epsilon_o$, $\mu = \mu_o$, and $\sigma = 0.1$ S/m, so $\omega\epsilon/\sigma = \omega\tau_e = 10.6$ and $l^* = 0.0265$ m.

traveling to the right to produce no more than a ripple in the total field magnitude. Further insights concerning these field distributions will come from considering some limits of the dispersion equation discussed next.

The first and second terms under the radical in the dispersion equation, (8), represent the displacement and conduction current densities, respectively. The relative importance of these current densities is determined by the relationship between the frequency and the reciprocal charge relaxation time. This is evident if (8) is written as

$$\beta = \omega\sqrt{\mu\epsilon}\sqrt{1 - \frac{j}{\omega\tau_e}} \tag{12}$$

where $\tau_e \equiv \epsilon/\sigma$ is the charge relaxation time.

Displacement Current Much Greater Than Conduction Current:.
$\omega\tau_e \gg 1$. In this limit, the waves are essentially electromagnetic, with some damping due to the finite conductivity. The second term under the radical in (12) is small compared to the first. Thus, the expression can be given a convenient approximation by using the first two terms in a binomial expansion.[12]

$$\beta \approx \omega\sqrt{\mu\epsilon} - \frac{j}{2l^*} \tag{13}$$

The natural distance over which the electromagnetic wave decays by $1/e$ is $2l^*$, where the *characteristic length* l^* is defined in (13) as

$$\boxed{l^* \equiv \frac{1}{\sigma}\sqrt{\epsilon/\mu}} \tag{14}$$

[12] With $x \equiv -j/\omega\tau_e$, $(1+x)^{1/2} \approx (1 + \frac{1}{2}x)$

Note that this length is the reciprocal of the intrinsic impedance conductivity product. With $\tau_e = C/G$, the dependence of β on ω given by (13) approximates the high-frequency range of Fig. 14.7.2.

In the case of Fig. 14.8.2, $\omega\epsilon/\sigma = 10.6$, so that the conditions for this low loss limit are met. Because the attenuation length for the electric field is $2l^*$, the attenuation length for the square of the magnitude of E_x is l^*, as shown in the figure, and the length of the system l is several times larger than the characteristic length l^*.

Conduction Current Much Greater Than Displacement Current: $\omega\tau_e \ll 1$. In this limit, the effects of displacement current are ignored altogether so that the first term under the radical is neglected compared to the second, and the dispersion equation is approximated by

$$\beta \approx \sqrt{-j\omega\mu\sigma} = \frac{(1-j)}{\delta} \tag{15}$$

Here, $\delta \equiv \sqrt{2/\omega\mu\sigma}$ is the skin depth, familiar from Sec. 10.7.[13] Thus, in this regime, the decay length is δ while the wavelength is $2\pi\delta$. The dependence of β on ω given by (15) approximates β in the low-frequency range of Fig. 14.7.2.

Example 14.8.2. Overview of TEM Fields in Open Circuit Transmission Line Filled with Lossy Material

Given the properties and dimensions of a simple system and a characteristic time for the dynamics, what are its dominant electromagnetic features? In this example, with the voltage source driving the system of Fig. 14.8.1b (so that the characteristic time is $1/\omega$), the system could be essentially a:

(1) resistor, in which case E_x would be uniform (Sec. 7.2)

(2) lossy capacitor, also with an essentially uniform E_x (Sec. 7.9)

(3) distribution of inductors and resistors with the distribution of E_x governed by magnetic diffusion (Sec. 10.7)

(4) lossy transmission line supporting slightly damped electromagnetic waves

With the objective of having a summary way of picturing these possibilities, we recognize that the field distributions [(10) and (11)] are exponential functions of $\beta l(z/l)$. Thus, βl encapsulates the field distribution. In terms of dimensionless parameters, $\omega\tau_e$ (representing the frequency) and l/l^* (representing the length), we write (12) as

$$\beta l = \sqrt{\omega\tau_e(\omega\tau_e - j)}\,\frac{l}{l^*} \tag{16}$$

and conclude that the field distributions are governed by two parameters, the length of the system relative to the characteristic length (l/l^*) and the frequency relative to

[13] As defined by (10.7.2), the product of ω and the magnetic diffusion time based on this length, $\mu\sigma\delta^2$, is equal to 2.

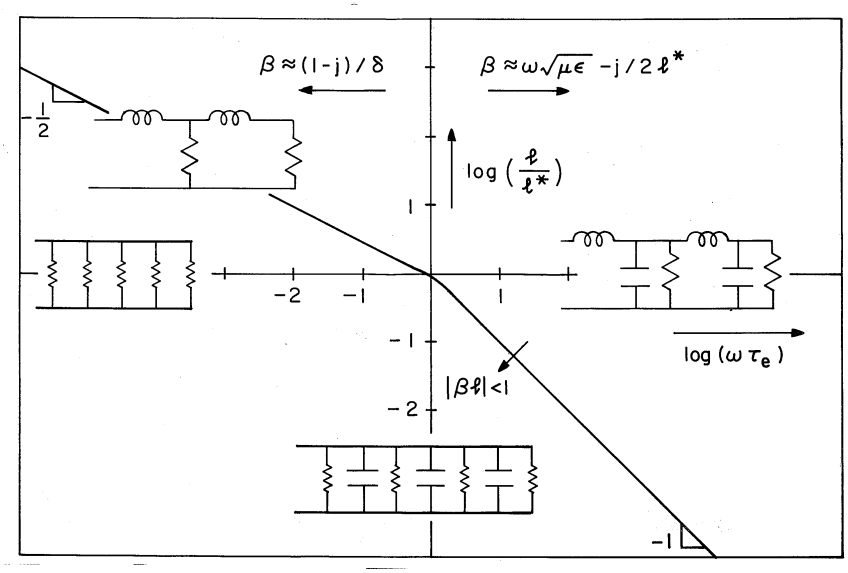


Fig. 14.8.3 In the length-frequency plane, regimes for TEM fields in material of uniform ϵ, μ, and σ between perfect conductors having length l (Fig. 14.8.1a). The length is normalized to $l^* = (\sigma\sqrt{\mu/\epsilon})^{-1}$ and the angular frequency to $\tau_e = \epsilon/\sigma$.

the reciprocal charge relaxation time ($\omega\tau_e$). The logs of these variables are the coordinates in Fig. 14.8.3. The origin of the plot is at the length equal to the characteristic length, l^*, and the angular frequency equal to the reciprocal charge relaxation time, $(\epsilon/\sigma)^{-1}$. These coordinates provide for a systematic overview of the electromagnetic regimes.

The approximate expressions for the wave number given by (13) and (15), respectively, apply to the right and left of the vertical axis, as indicated at the top of Fig. 14.8.3. It is tempting to jump to the conclusion that there are simply two regimes, the one to the right where the fields are composed of slightly damped electromagnetic waves, and the one to the left involving "skin-effect." However, this is not the whole story, because it does not take into account the length of the system. It is really βl, and not β alone, that determines the field distribution between the plates.

Whether representing a slightly damped electromagnetic wave or magnetic diffusion (skin effect), a small value of βl means that there is little variation of the voltage over the length of the system. In the cases where $|\beta l| \ll 1$, the exponentials expressing the z dependence can be approximated by the first terms in a Taylor's series. Thus, in this regime, the voltage (E_x) follows from (10) as being essentially uniform

$$V \approx \mathrm{Re}\,\hat{V}_g e^{j\omega t} \tag{17}$$

and the current (H_y) given by (11) takes on an esssentially linear distribution.

$$I \approx \frac{\hat{V}_g}{Z_o}(-j\beta l)\frac{z}{l}e^{j\omega t} = \mathrm{Re}\ -\hat{V}_g\frac{w\sigma}{a}(1+j\omega\tau_e)ze^{j\omega t} \tag{18}$$

The regime in Fig. 14.8.3 where this limit pertains, follows from the dispersion equation, (16).

$$|\beta l| = \frac{l}{l^*}(\omega\tau_e)^{1/2}[(\omega\tau_e)^2 + 1]^{1/4} \ll 1 \tag{19}$$

The line along which $\beta l = 1$ can be conveniently pictured by making this expression an equality, solving for l/l^* and taking the log.

$$\log\left(\frac{l}{l^*}\right) = -\frac{1}{2}\log(\omega\tau_e) - \frac{1}{4}\log[(\omega\tau_e)^2 + 1] \tag{20}$$

This makes it clear that for large values of $\omega\tau_e$, the line of demarcation has a slope of -1, while for small values, its slope is $-1/2$. This line is shown in Fig. 14.8.3. In the region well to the southwest of this line, the electric field distribution is essentially uniform. The circuits drawn on the respective regions in Fig. 14.8.3 picture the four limiting cases.

In terms of this figure, picture what happens as the frequency is raised for systems that are larger than the matching length, $l \gg l^*$. In this case, raising the frequency follows a trajectory in the upper half-plane from the left to the right. With the frequency very low, the voltage and current distributions are approximated by (17) and (18). Because $\omega\tau_e \ll 1$, it follows from the latter equation that the system is essentially a resistor. As the line $\beta l = 1$ is approached, $\omega\tau_e$ is still small, so that effects of the displacement current are negligible. That the variation of the fields that comes into play is due to magnetic diffusion is clear from the appropriate limiting expression for β, (15). Indeed, the line $\beta l = 1$ in this quadrant approaches the line along which the angular frequency is equal to the reciprocal magnetic diffusion time based on the length l,

$$\omega\tau_m = \omega\mu\sigma l^2 = 1 \tag{21}$$

as can be seen by rewriting this expression as

$$\log\left(\frac{l}{l^*}\right) = -\frac{1}{2}\log(\omega\tau_e) \tag{22}$$

In the neighborhood of this line, in the second quadrant where the magnetic diffusion line is shown (the distributed transmission line of Sec. 14.7 with $R = 0$ and $C = 0$), the system is magnetoquasistatic (MQS).

As the frequency is raised still further, the displacement current begins to come into effect. The wave number makes a transition from representing the heavily damped waves of magnetic diffusion to the slightly damped electromagnetic waves of the first quadrant.

Consider the contrasting nature of the system with its length much less than the characteristic length, $l \ll l^*$, as the frequency is raised.

As before, to the far left of the figure, the electric field is uniform and the current is that characteristic of a resistor. This regime, like that just above in the second quadrant, is one of quasi-steady conduction. In this regime, the fields are described by the steady conduction approximation which was the subject of the first half of Chap. 7.

By contrast with the situation in the upper half-plane, the fields now remain uniform until the angular frequency passes well beyond the reciprocal charge relaxation time, the vertical axis. Note that in this range, the voltage and current are those for a distribution of conductances shunting perfectly conducting plates, as shown in Fig. 14.8.3. Thus, all of the conductances and capacitances can be lumped together. Up to this frequency range, the system is electroquasistatic (EQS).

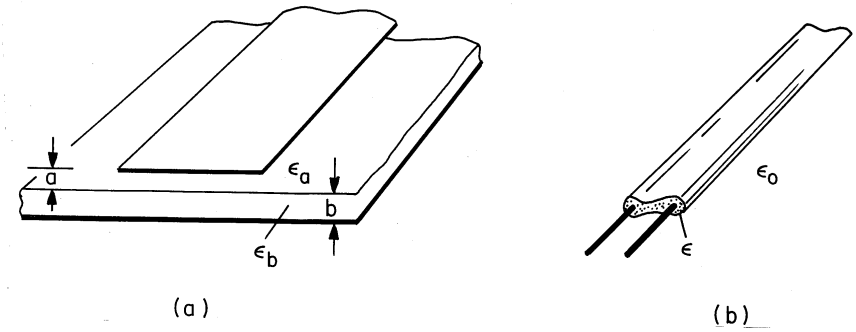


Fig. 14.8.4 (a) Strip line, used for microwave transmission on circuit boards and chips. (b) "Twin lead" commonly used for TV antennae.

As the frequency is raised still further, effects of magnetic induction come into play and conspire with the displacement current to create field distributions typical of electromagnetic waves. This happens in the range where $|\beta l| = 1$, because in this quadrant, the angular frequency is equal to the electromagnetic delay time based on the length of the system,

$$\omega\tau_{em} \equiv \omega\sqrt{\mu\epsilon}l = 1 \tag{23}$$

as can be seen by writing this expression as

$$\log\left(\frac{l}{l^*}\right) = -\log(\omega\tau_e) \tag{24}$$

In this frequency range and further to the right, the field distributions are those for slightly damped electromagnetic waves.

In summary, far to the left in Fig. 14.8.3, quasi-steady conduction prevails. The dynamic process that first comes into play as the frequency is raised is determined by the length of the system relative to the characteristic length. Systems large enough to be in the upper half-plane are in the MQS regime. Those small enough to be in the lower half-plane are in the EQS regime.

The distributed parameter transmission line is often used to represent the evolution of fields on pairs of conductors surrounded by inhomogeneous dielectrics. Practical examples are shown in Fig. 14.8.4, where the dielectric is piece-wise uniform. In these cases, even if the conductors can be represented as perfectly conducting, so that $R = 0$, the fields between the conductors are *not* exactly TEM. Completely transverse waves would propagate with different velocities in the two dielectric regions, and it would not be possible to match boundary conditions at the interfaces. Nevertheless, with C and G, respectively, taken as being the EQS capacitance and conductance per unit length of the open circuit conductors, and L the MQS inductance per unit length of the short circuit conductors, the distributed parameter line of Sec. 14.7 can provide an excellent model.

In cases where the material between the conductors is inhomogeneous, the distributed parameter model provides a good approximation of the principal mode of propagation, provided that the frequency is low enough to insure that the wavelength in the z direction is long compared to the cross-sectional dimensions. For

example, it is shown in the problems that there is a z-directed $\mathbf{E}$ in the strip line of Fig. 14.8.4a, so the fields are not TEM. However, if one neglects fringing fields one can show that E_z is small compared to the transverse fields if

$$\frac{b(\beta a)}{a+b}\left|1-\frac{\epsilon_a}{\epsilon_b}\right| \ll 1 \tag{25}$$

Thus, the distributed parameter model is exact if the dielectric is uniform ($\epsilon_a = \epsilon_b$), and approximately correct if $\beta a = 2\pi a/\lambda$ is small enough to fulfill the inequality.

14.9 QUASI-ONE-DIMENSIONAL MODELS ($G = 0$)

The transmission line model of Sec. 14.7 can also represent the losses in the parallel conductors. With the conductors of finite conductivity, currents in the z direction cause a component of $\mathbf{E}$ in that direction. Because the tangential $\mathbf{E}$ is continuous at the surfaces of the conductors, this axial electric field extends into the insulating region between the conductors as well. We conclude that the fields are no longer exactly TEM when the conductor losses are finite.

Under what circumstances can the series distributed resistance R be used to represent the conductor losses? We will find that the conductivity must be sufficiently low so that the skin depth is large compared to the conductor thickness. One might expect that this model applies only to the case of large R. Interestingly, we find that this "constant resistance" model can remain valid even under circumstances where line losses are small, in the sense that the decay of a wave within a distance of the order of a wavelength is small. This occurs when $|\omega L| \gg R$, i.e., the effect of the distributed inductance is much larger than that of the series resistance. In the opposite extreme, where the effect of the series resistance is large compared to that of the inductance, the model represents EQS charge diffusion. A demonstration is used to exemplify physical situations modeled by this distributed R-C line. These include solid state electronic devices and physiological systems.

We conclude this section with a model that is appropriate if the skin depth is much less than the conductor thickness. By restricting the model to the sinusoidal steady state, the series distributed resistance R can be replaced by a "frequency dependent" resistance. This approximate model is typical of those used for representing losses in metallic conductors at radio frequencies and above.

We assume conductors in which the conduction current dominates the displacement current. In the sinusoidal steady state, this is true if

$$\frac{\omega\epsilon}{\sigma} \equiv \omega\tau_e \ll 1 \tag{1}$$

Thus, as the frequency is raised, the distribution of current density in the conductors is at first determined by quasi-stationary conduction (first half of Chap. 7) and then by the magnetic diffusion processes discussed in Secs. 10.3-10.7. That is, with the frequency low enough so that magnetic diffusion is essentially instantaneous, the current density is uniformly distributed over the conductor cross-sections. Intuitively, we should expect that the constant resistance R only represents conductor

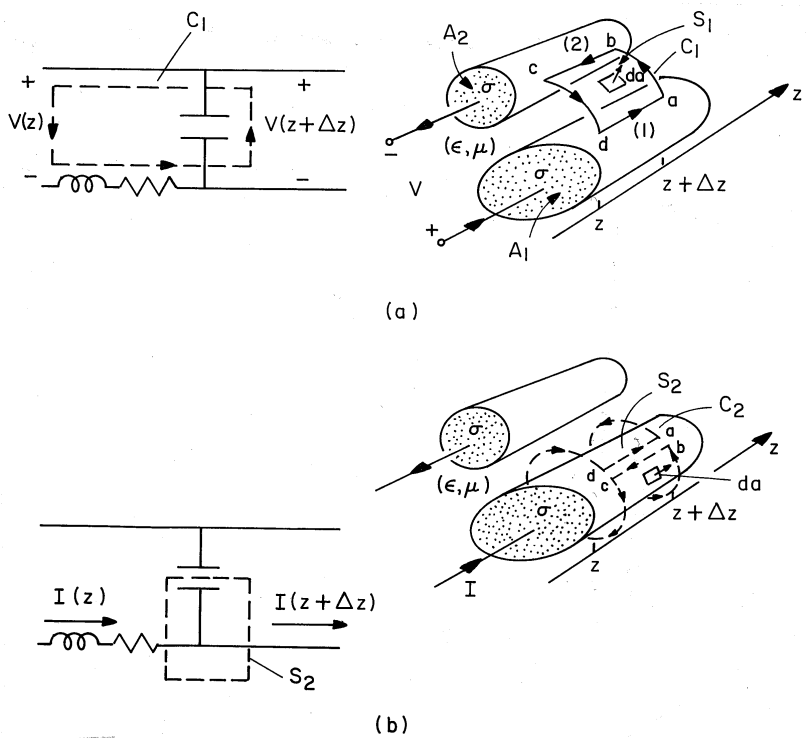


Fig. 14.9.1 (a) Faraday's integral law and, (b) Ampère's integral law applied to an incremental length Δz of line.

losses at frequencies sufficiently low so that the distribution of current density in the conductors does not depend on rates of change.

The equations used to describe the incremental circuit in Sec. 14.7 express the integral laws of Faraday and Ampère for incremental lengths of the transmission line. The "current loop equation" for loop C_1 in the circuit of Fig. 14.9.1a can be derived by applying Faraday's law to the surface S_1 enclosed by the contour C_1, also shown in that figure.

$$\int_a^b \mathbf{E}\cdot d\mathbf{s} + \int_c^d \mathbf{E}\cdot d\mathbf{s} + E_z\big|_{(1)}\Delta z - E_z\big|_{(2)}\Delta z = -\frac{\partial}{\partial t}\int_{S_1}\mu\mathbf{H}\cdot d\mathbf{a} \tag{2}$$

With the line integrals between conductors defined as the voltages and the flux through the surface as $\Delta z L I$, this expression becomes

$$V(z+\Delta z) - V(z) + E_z\big|_{(1)}\Delta z - E_z\big|_{(2)}\Delta z = -\frac{\partial}{\partial t}\int_{S_1}\mu\mathbf{H}\cdot d\mathbf{a} \tag{3}$$

and in the limit where $\Delta z \to 0$, we obtain

$$\frac{\partial V}{\partial z} = -L\frac{\partial I}{\partial t} - E_z\big|_{(1)} + E_z\big|_{(2)} \tag{4}$$

The field equivalent of charge conservation for the circuit node enclosed by the surface S_2 in Fig. 14.9.1b is Ampère's integral law applied to the surface S_2 enclosed by the contour C_2, also shown in that figure. Note that C_2 almost encircles one of the conductors with oppositely directed adjacent segments completing the z-directed parts of the contour. For a surface S_2 of incremental length Δz, Ampère's integral law requires that

$$\int_a^b \mathbf{H} \cdot d\mathbf{s} + \int_c^d \mathbf{H} \cdot d\mathbf{s} = \frac{\partial}{\partial t} \int_{S_2} \epsilon \mathbf{E} \cdot d\mathbf{a} \tag{5}$$

where the contributions from the oppositely directed legs in the z direction cancel. Ampère's integral law requires that the integral of $\mathbf{H} \cdot d\mathbf{s}$ on the contours essentially surrounding the conductor be the enclosed current I. Gauss' integral law requires that the surface integral of $\epsilon \mathbf{E} \cdot d\mathbf{a}$ be equal to $\Delta z C V$. Thus, (5) becomes

$$-I(z + \Delta z) + I(z) = C \Delta z \frac{\partial V}{\partial t} \tag{6}$$

and in the limit, the second transmission line equation.

$$\frac{\partial I}{\partial z} = -C \frac{\partial V}{\partial t} \tag{7}$$

If the current density is uniformly distributed over the cross-sectional areas A_1 and A_2 of the respective conductors, it follows that the current densities are related to the total current by

$$I = A_1 J_{z1} = -A_2 J_{z2} \tag{8}$$

In each conductor, $J_z = \sigma E_z$, so the axial electric fields required to complete (4) are related to I by

$$E_{z1} = \frac{J_{z1}}{\sigma_1} = \frac{I}{\sigma_1 A_1}; \qquad E_{z2} = \frac{J_{z2}}{\sigma_1} = -\frac{I}{\sigma_2 A_2} \tag{9}$$

and indeed, the voltage equation is the same as for the distributed line,

$$\frac{\partial V}{\partial z} = -L \frac{\partial I}{\partial t} - RI \tag{10}$$

where the resistance per unit length has been found to be

$$R \equiv \frac{1}{\sigma_1 A_1} + \frac{1}{\sigma_2 A_2} \tag{11}$$

Example 14.9.1. Low-Frequency Losses on Parallel Plate Line

In the parallel plate transmission line shown in Fig. 14.9.2, the conductor thickness is b and the cross-sectional areas are $A_1 = A_2 = bw$. It follows from (11) that the resistance is

$$R = \frac{2}{bw\sigma} \tag{12}$$

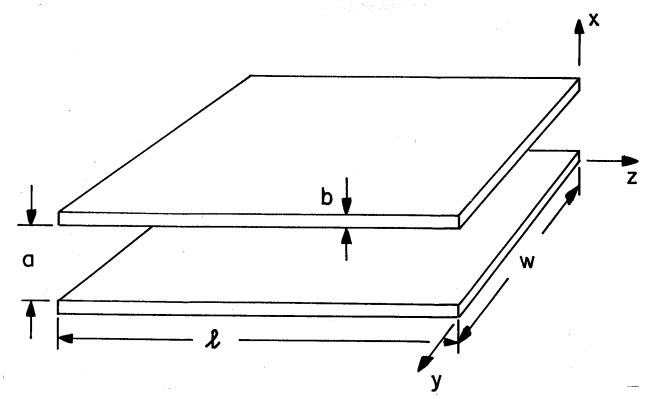


Fig. 14.9.2 Parallel plate transmission line with conductor thickness b that is small compared to skin depth.

Under the assumption that the conductor thickness, b, is much less than the plate spacing,[14] a, the inductance per unit length is the same as found in Example 14.1.1, as is also the capacitance per unit length.

$$L = \frac{a\mu}{w}; \qquad C = \frac{w\epsilon}{a} \tag{13}$$

As the frequency is raised, the current distribution over the cross-sections of the conductors becomes nonuniform when the skin depth δ (10.7.5) gets to be on the order of the plate thickness. Thus, for the model to be valid using the resistance given by (12),

$$\delta \equiv \sqrt{\frac{2}{\omega\mu\sigma}} \gg b \Rightarrow \omega\mu\sigma b \ll \frac{2}{b} \tag{14}$$

With this inequality we require that the effects of magnetic induction in determining the distribution of current in the conductors be negligible. Under what conditions are we justified in ignoring this effect of magnetic induction but nevertheless keeping that represented by the distributed inductance? Put another way, we ask if the inductive reactance $j\omega L$ can be large compared to the resistance R and still satisfy the condition of (14).

$$\omega L \gg R \Rightarrow \frac{2}{a} \ll \omega\mu\sigma b \tag{15}$$

Combined, these last two conditions require that

$$\frac{b}{a} \ll 1 \tag{16}$$

We conclude that as long as the conductor thicknesses are small compared to their spacing, R represents the loss over the full frequency range from dc to the frequency at which the current in the conductors ceases to be uniformly distributed. This is true because the time constant $\tau_m \equiv L/R = \mu\sigma ab$ that determines the frequency at which the resistance is equal to the inductive reactance[15] is much larger than the magnetic diffusion time $\mu\sigma b^2$ based on the thickness of the conductors.

[14] So that the magnetic energy stored in the plates themselves is negligible compared to that between the plates.

[15] Familiar from Sec. 10.3.

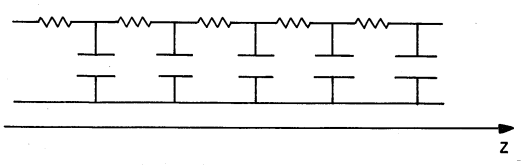


Fig. 14.9.3 Charge diffusion or R-C transmission line.

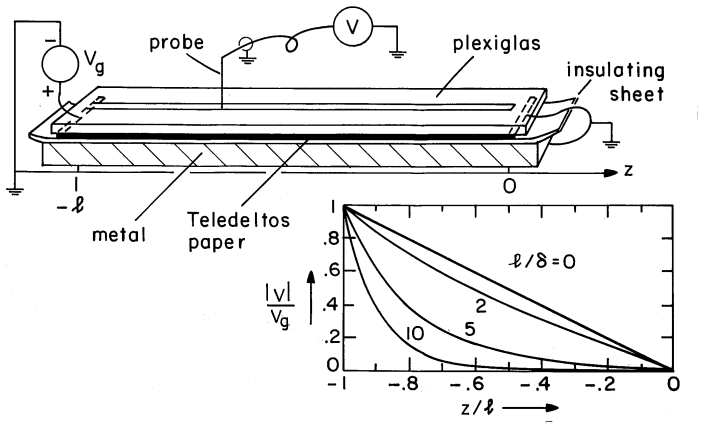


Fig. 14.9.4 Charge diffusion line.

Charge Diffusion Transmission Line. If the resistance is large enough so that the inductance has little effect, the lossy transmission line becomes an EQS model. The line is simply composed of the series resistance shunted by the distributed capacitance of Fig. 14.9.3. To see that the voltage (and hence charge) and current on this line are governed by the diffusion equation, (10) is solved for I, with L set equal to zero,

$$I = -\frac{1}{R}\frac{\partial V}{\partial z} \tag{17}$$

and that expression substituted into the z derivative of (7).

$$\frac{\partial^2 V}{\partial z^2} = RC\frac{\partial V}{\partial t} \tag{18}$$

By contrast with the charge relaxation process undergone by charge in a uniform conductor, the charge in this heterogeneous system diffuses. The distributed R-C line is used to model EQS processes that range from those found in neural conduction to relaxation in semiconductors. We can either view the solution of (17) and (18) as a special case from Sec. 14.7 or exploit the complete analogy to the magnetic diffusion processes described in Secs. 10.6 and 10.7.

Demonstration 14.9.1. Charge Diffusion Line

A simple demonstration of the charge diffusion line is shown in Fig. 14.9.4. A thin insulating sheet is sandwiched between a resistive sheet on top (the same Teledeltos paper used in Demonstration 7.6.2) and a metal plate on the bottom.

With sinusoidal steady state conditions established by means of a voltage source at $z = -l$ and a short circuit at the right, the voltage distribution is the analog of that described for magnetic diffusion in Example 10.7.1. The "skin depth" for the charge diffusion process is given by (10.7.5) with $\mu\sigma \rightarrow RC$.

$$\delta = \sqrt{\frac{2}{\omega RC}} \tag{19}$$

With this the new definition of δ, the magnitude of the voltage measured by means of the high-impedance voltmeter can be compared to the theory, plotted in Fig. 10.7.2. Typical values are $\epsilon = 3.5\epsilon_o$, $b\sigma = 4.5 \times 10^{-4}$ S (where $b\sigma$ is the surface conductivity of the conducting sheet), and $a = 25\,\mu$m, in which case $RC = \epsilon/(b\sigma)a = 2.7 \times 10^{-3}$ sec/m^2 and $\delta \simeq 0.5$ m at a frequency of 500 Hz.

In the previous example, we found that the transmission line model is applicable provided that the conductor thicknesses were small compared to their spacing and to the skin-depth. That the model could be self-consistent from dc up to frequencies at which the inductive impedance dominates resistance is in part attributable to the plane parallel geometry.

To see this, consider a transmission line composed of a circular cylindrical conductor and a thin sheet, as shown in Fig. 8.6.7. In Demonstration 8.6.1, it was found that the condition $\mathbf{n} \cdot \mathbf{B} = 0$ on the conductor surfaces is met at frequencies for which the skin depth is far *greater* than the thickness of the thin sheet conductor. The examples of Sec. 10.4 show why this is possible. The effective magnetic diffusion time that determines the frequency at which currents in the conducting sheet make a transition from a quasi-stationary distribution to one consistent with $\mathbf{n} \cdot \mathbf{B} = 0$ is $\mu\sigma\Delta l$, where Δ is the thickness of the conductor and l is the distance between conductors. This is also the L/R time constant governing the transition from resistance to inductance domination in the distributed electrodynamic model. We conclude that, even though the current may be essentially uniform over the conductor cross section, as the frequency changes from dc to the inductance dominated range, the current can shift its distribution over the conductor surface. Thus, in non-planar geometries, the constant R model can be inadequate even over a frequency range where the skin depth is large compared to the conductor thickness.

Skin Depth Small Compared to All Dimensions of Interest. In transmission lines used at radio frequencies and higher, it is usual for the skin depth to be much less than the conductor thickness, $\delta \ll b$. In the case of Fig. 14.9.2, $2 \ll \omega\mu\sigma b^2$. Provided that $a > b$, it follows from (15) that the inductive reactance dominates resistance. Although the line is then very nearly ideal, it is often long enough so that losses cannot be neglected. We therefore conclude this section by developing a model, restricted to the sinusoidal steady state, that accounts for losses when the skin depth is small compared to all dimensions of interest.

In this case, the axial conduction currents are confined to within a few skin depths of the conductor surfaces. Within a few skin depths, the tangential magnetic field decays from its value at the conductor surface to zero. Because the magnetic field decays so rapidly along a coordinate perpendicular to a given point on the conductor surface, the effects on the magnetic diffusion of spatial variations along

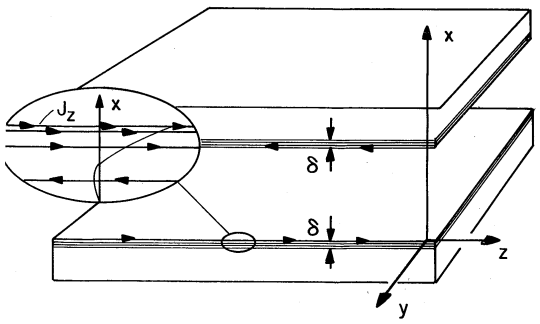


Fig. 14.9.5 Parallel plate transmission line with conductors that are thick compared to the skin depth.

the conductor surface are negligible. For this reason, fields in the conductors can be approximated by the one-dimensional magnetic diffusion process described in Sec. 10.7. The following example illustrates this concept.

Example 14.9.2. High-Frequency Losses on Parallel Plate Line

The parallel plate transmission line is shown again in Fig. 14.9.5, this time with the axial current distribution in the conductors in thin regions on the inner surfaces of the conductors rather than uniform. In the conductors, the displacement current is negligible, so that the magnetic field is governed by the magnetic diffusion equation, (10.5.8). In the sinusoidal steady state, the y component of this equation requires that

$$\frac{1}{\mu\sigma}\left[\frac{\partial^2 \hat{H}_y}{\partial x^2}+\frac{\partial^2 \hat{H}_y}{\partial z^2}\right]=-j\omega\hat{H}_y \tag{20}$$

The first term on the left is of the order of $H_y/(\delta)^2$, while the second is of the order of $H_y k^2 = H_y(2\pi/\lambda)^2$ [where λ is the wavelength in the axial (z) direction]. Thus, the derivative with respect to z can be ignored compared to that with respect to x, provided that

$$\frac{1}{\delta^2} \gg k^2 \Rightarrow \delta \ll \frac{\lambda}{2\pi} \tag{21}$$

In this case, (20) becomes the one-dimensional magnetic diffusion equation studied in Sec. 10.7. In the lower conductor, the magnetic field diffuses in the $-x$ direction, so the appropriate solution to (20) is

$$\hat{H}_y = \hat{H}_o e^{(1+j)x/\delta} \tag{22}$$

where H_o is the magnetic field intensity at the surface of the lower conductor [see (10.7.8)]. Ampère's law gives the current density associated with this field distribution

$$\hat{J}_z = \frac{\partial \hat{H}_y}{\partial x} = \frac{\hat{H}_o(1+j)}{\delta} e^{(1+j)x/\delta} \tag{23}$$

It follows from either integrating this expression over the cross-section of the lower conductor or appealing to Ampère's integral law that the the total current in the lower conductor is

$$\hat{I} = w\int_{-\infty}^{0} \hat{J}_z dx = w\hat{H}_o \tag{24}$$

The axial electric field intensity at the surface of the lower conductor can now be written in terms of this total current by first using Ohm's law and the current density of (23) evaluated at the surface and then using (24) to express this field in terms of the total current.

$$\hat{E}_z(0) = \frac{\hat{J}_z(0)}{\sigma} = \frac{\hat{I}}{w}\frac{(1+j)}{\sigma\delta} \tag{25}$$

A similar derivation gives an axial electric field at the surface of the upper conductor that is the negative of this result. Thus, we can complete the sinusoidal steady state version of the voltage transmission-line equation, (4).

$$\frac{d\hat{V}}{dz} = -\left[j\omega L + \frac{2(1+j)}{w\sigma\delta}\right]\hat{I} \tag{26}$$

Because the magnetic energy stored within the conductor is usually negligible compared to that in the region between conductors,

$$\omega L \gg \frac{2}{w\sigma\delta} \tag{27}$$

and (26) becomes the first of the two sinusoidal steady state transmission line equations.

$$\frac{d\hat{V}}{dz} = -\big(j\omega L + \frac{2}{w\sigma\delta}\big)\hat{I} \tag{28}$$

The second follows directly from (7).

$$\frac{d\hat{I}}{dz} = -j\omega C\hat{V} \tag{29}$$

Comparison of these expressions with those describing the line operating with the conductor thickness much less than the skin depth, (10) and (7), shows that here there is an equivalent distributed resistance.

$$R_{eq} = \frac{2}{w\sigma\delta} = \frac{1}{w}\sqrt{\frac{2\omega\mu}{\sigma}} \tag{30}$$

(Here, μ is the permeability of the conductor, not of the region between conductors.) Note that this is the series dc resistance of conductors having width w and thickness δ. Because δ is inversely proportional to the square root of the frequency, this equivalent resistance increases with the square root of the frequency.

14.10 SUMMARY

The theme in this chapter has been the transmission line. It has been used to represent the evolution of electromagnetic fields through structures generally comprised of a pair of "conductors" embedded in a less conducting, and often highly insulating, medium. We have confined ourselves to systems that are uniform in the direction of evolution, the z direction.

If the conductors can be regarded as perfectly conducting, and the medium in which they are embedded as having uniform permeability, permittivity, and conductivity, the fields are exactly TEM, regardless of the cross-sectional geometry. The relevant laws and distributed parameter model are summarized in Table 14.10.1. Identification of variables as illustrated in the table make the transmission line exactly *equivalent* to a plane wave. Whether L, C, or G represent fields propagating along the conductors or a plane wave, $LC = \mu\epsilon$ and $C/G = \epsilon/\sigma$.

Much of this chapter is devoted to describing the limit where the conductors are not only perfect, but the medium has negligible conductivity ($G = 0$). Transients on this "ideal" transmission line are described by using the relations summarized in Table 14.10.2. The voltage and current at any position and time (z, t) are superpositions of wave components that propagate with the velocity c. These forward and backward wave components are, respectively, invariant on lines in the $z-t$ plane of constant α and β. Along those lines originating on initial conditions, the wave components are as summarized in the second row of the table. The last two rows summarize how the reflected wave component is determined from the incident component at two common terminations.

A summary of the relations used to describe the ideal line in the sinusoidal steady state is given in Table 14.10.3. Because it has a magnitude that is constant and a phase that increases linearly with z, the evolution of voltage and current and of their ratio, the impedance $Z(z)$, is conveniently pictured in terms of the complex reflection coefficient, $\Gamma(z)$. Relations and the complex Γ plane are illustrated in the first row. The mappings of the impedance and of the admittance onto this plane, respectively, are summarized by the second and third rows. Because the magnitude of Γ is constant over a uniform length of line, the trajectory of $Z(z)$ or $Y(z)$ is on a circle of constant radius in the directions of the generator or the load, as indicated. These Smith charts give a convenient overview of how the impedance and admittance vary with position.

In Sec. 14.7, a shunt conductance per unit length, G, (to represent losses in the material between the transmission line conductors) and a series resistance per unit length, R, (for losses in the conductors themselves) was added to the distributed parameter transmission line representation. For the limiting case where the conductors were infinitely conducting, $R = 0$, and the material between of uniform properties, the fields represented by the line were exactly TEM. In the case where the material properties did vary over the cross section, the distributed parameter picture provided a useful model for the line provided that the wavelength was long compared to the cross-sectional dimensions. In specific terms, this model gave the opportunity to consider the dynamical processes considered in Chaps. 7, 10, and 12 (charge relaxation, magnetic diffusion and electromagnetic wave propagation, respectively) in one self consistent situation. What was learned will be generalized in the review of the processes given in Secs. 15.3–15.4.

In Sec. 14.9, where $G = 0$ but R was finite, the specific objective was to understand how the transmission line concept could be used to approximate conductor losses. A broader objective was to again illustrate the use of the distributed parameter line as a model, representing the fields at frequencies sufficiently low so that the wavelength is long compared with the transverse dimensions.

TABLE 14.10.1
TRANSMISSION LINE EQUIVALENTS

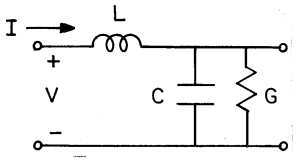
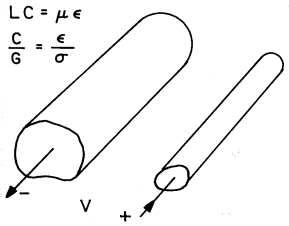
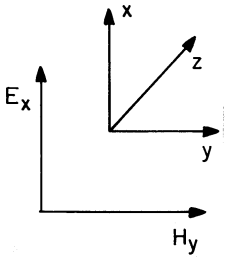
$\frac{\partial I}{\partial z} = -C\frac{\partial V}{\partial t} - GV$	(14.8.4)	
$\frac{\partial V}{\partial z} = -L\frac{\partial I}{\partial t}$	(14.8.5)	
	$I \rightarrow H_y$ $V \rightarrow E_x$ $C \rightarrow \epsilon = n^2\epsilon_o$ $L \rightarrow \mu$ $\frac{C}{G} \rightarrow \epsilon/\sigma$	

TABLE 14.10.2
WAVE TRANSIENTS

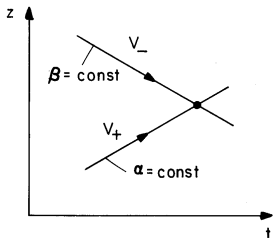
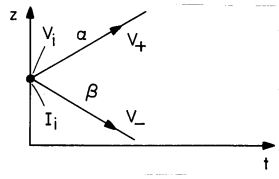
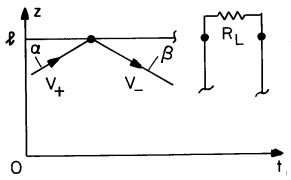
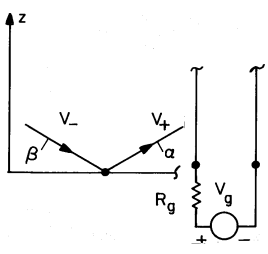
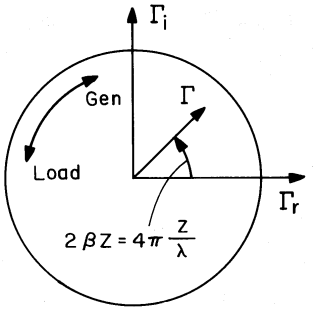
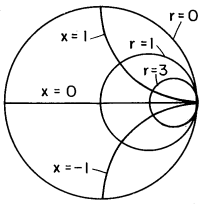
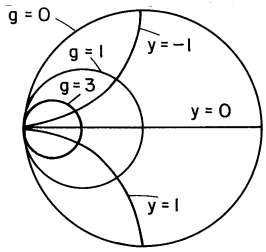
$V = V_+(\alpha) + V_-(\beta)$	(14.3.9)	
$I = \frac{1}{Z_o}(V_+(\alpha) - V_-(\beta))$	(14.3.10)	
$\alpha = z - ct; \quad \beta = z + ct$	(14.3.11)	
$Z_o = \sqrt{L/C}$	(14.3.12)	
$c = 1/\sqrt{LC}$	(14.3.1)	
$V_+ = \frac{1}{2}(V_i + Z_o I_i)$	(14.3.18)	
$V_- = \frac{1}{2}(V_i - Z_o I_i)$	(14.3.19)	
$V_- = V_+ \dfrac{\left(\frac{R_L}{Z_o} - 1\right)}{\left(\frac{R_L}{Z_o} + 1\right)}$	(14.4.8)	
$V_+ = \dfrac{V_g}{\left(\frac{R_g}{Z_o} + 1\right)} + V_- \dfrac{\left(\frac{R_g}{Z_o} - 1\right)}{\left(\frac{R_g}{Z_o} + 1\right)}$	(14.4.10)	

TABLE 14.10.3
SINUSOIDAL-STEADY-STATE $(R = 0,\ G = 0)$

$\hat{V} = \hat{V}_+ e^{-j\beta z}[1 + \Gamma(z)]$	(14.5.5)	
$\hat{I} = \frac{\hat{V}_+ e^{-j\beta z}}{Z_o}[1 - \Gamma(z)]$	(14.5.6)	
$\Gamma \equiv \frac{\hat{V}_-}{\hat{V}_+} e^{j2\beta z}$	(14.6.2)	
$Z_o = \sqrt{L/C}$	(14.3.12)	
$\beta = \omega\sqrt{LC}$	(14.5.5)	
$\frac{Z(z)}{Z_o} = \frac{1 + \Gamma(z)}{1 - \Gamma(z)} \equiv r + jx$	(14.6.1)	
$\Gamma = \frac{\frac{Z}{Z_o} - 1}{\frac{Z}{Z_o} + 1}$	(14.6.3)	
$\frac{Y(z)}{Y_o} = \frac{1 - \Gamma(z)}{1 + \Gamma(z)} = g + jy$	(14.6.12)	
$\Gamma = \frac{1 - \frac{Y}{Y_o}}{1 + \frac{Y}{Y_o}}$		
$Y_o = \sqrt{C/L}$		

PROBLEMS

14.1 Distributed Parameter Equivalents and Models

14.1.1 The "strip line" shown in Fig. P14.1.1 is an example where the fields are *not* exactly TEM. Nevertheless, wavelengths long compared to a and b, the distributed parameter model is applicable. The lower perfectly conducting plate is covered by a planar perfectly insulating layer having properties $(\epsilon_b, \mu_b = \mu_o)$. Between this layer and the upper electrode is a second perfectly insulating material having properties $(\epsilon_a, \mu_a = \mu_o)$. The width w is much greater than $a+b$, so fringing fields can be ignored. Determine L and C and hence the transmission line equations. Show that $LC \neq \mu\epsilon$ unless $\epsilon_a = \epsilon_b$.

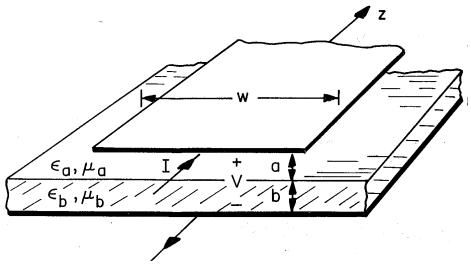


Fig. P14.1.1

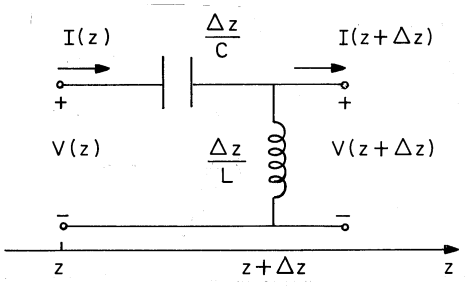


Fig. P14.1.2

14.1.2 An incremental section of a "backward wave" transmission line is as shown in Fig. P14.1.2. The incremental section of length Δz shown has a reciprocal capacitance per unit length $\Delta z C^{-1}$ and reciprocal inductance per unit length $\Delta z L^{-1}$. Show that, by contrast with (4) and (5), in this case the transmission line equations are

$$L\frac{\partial^2 I}{\partial t \partial z} = -V; \qquad C\frac{\partial^2 V}{\partial t \partial z} = -I \tag{a}$$

14.2 Transverse Electromagnetic Waves

14.2.1* For the coaxial configuration of Fig. 14.2.2b,

(a) Show that, defined as zero on the outer conductor, A_z and Φ are

$$A_z = -\mu I ln(r/a)/2\pi; \qquad \Phi = -\lambda_l ln(r/a)/2\pi\epsilon \tag{a}$$

where λ_l is the charge per unit length on the inner conductor.

(b) Using these expressions, show that the L and C needed to complete the transmission line equations are

$$L = \frac{\mu}{2\pi} ln\left(\frac{a}{b}\right); \qquad C = 2\pi\epsilon / ln\left(\frac{a}{b}\right) \tag{b}$$

and hence that $LC = \mu\epsilon$.

14.2.2 A transmission line consists of a conductor having the cross-section shown in Fig. P4.7.5 adjacent to an L-shaped return conductor comprised of "ground planes" in the planes $x = 0$ and $y = 0$, intersecting at the origin. Assuming that the region between these conductors is free space, what are the transmission line parameters L and C?

14.3 Transients on Infinite Transmission Lines

14.3.1 Show that the characteristic impedance of a coaxial cable (Prob. 14.2.1) is

$$Z_o = \sqrt{\mu/\epsilon} ln(a/b)/2\pi \tag{a}$$

For a dielectric having $\epsilon = 2.5\epsilon_o$ and $\mu = \mu_o$, evaluate Z_o for values of $a/b = 2, 10, 100$, and 1000. Would it be reasonable to design such a cable to have $Z_o = 1K\Omega$?

14.3.2 For the parallel conductor line of Fig. 14.2.2 in free space, what value of l/R should be used to make $Z_o = 300$ ohms?

14.3.3 The initial conditions on an infinite line are $V = 0$ and $I = I_p$ for $-d < z < d$ and $I = 0$ for $z < -d$ and $d < z$. Determine $V(z,t)$ and $I(z,t)$ for $0 < t$, presenting the solution graphically, as in Fig. 14.3.2.

14.3.4 On an infinite line, when $t = 0$, $V = V_o \exp(-z^2/2a^2)$, and $I = 0$, determine analytical expressions for $V(z,t)$ and $I(z,t)$.

14.3.5* In the energy conservation theorem for a transmission line, (14.2.19), VI is the power flow. Show that at any location, z, and time, t, it is correct to

think of power flow as the superposition of power carried by the + wave in the $+z$ direction and − wave in the $-z$ direction.

$$VI = \frac{1}{Z_o}[V_+^2 - V_-^2] \qquad (a)$$

14.3.6 Show that the traveling wave solutions of (2) are not solutions of the equations for the "backward wave" transmission line of Prob. 14.1.2.

14.4 Transients on Bounded Transmission Lines

14.4.1 A transmission line, terminated at $z = l$ in an "open circuit," is driven at $z = 0$ by a voltage source V_g in series with a resistor, R_g, that is matched to the characteristic impedance of the line, $R_g = Z_o$. For $t < 0$, $V_g = V_o =$ constant. For $0 < t$, $V_g = 0$. Determine the distribution of voltage and current on the line for $0 < t$.

14.4.2 The transient is to be determined as in Prob. 14.4.1, except the line is now terminated at $z = l$ in a "short circuit."

14.4.3 The transmission line of Fig. 14.4.1 is terminated in a resistance $R_L = Z_o$. Show that, provided that the voltage and current over the length of the line are initially zero, the line has the same effect on the circuit connected at $z = 0$ as would a resistance Z_o.

14.4.4 A transmission line having characteristic impedance Z_a is terminated at $z = l + L$ in a resistance $R_a = Z_a$. At the other end, where $z = l$, it is connected to a second transmission line having the characteristic impedance Z_b. This line is driven at $z = 0$ by a voltage source $V_g(t)$ in series with a resistance $R_b = Z_b$. With $V_g = 0$ for $t < 0$, the driving voltage makes a step change to $V_g = V_o$, a constant voltage. Determine the voltage $V(0, t)$.

14.4.5 A pair of transmission lines is connected as in Prob. 14.4.4. However, rather than being turned on when $t = 0$, the voltage source has been on for a long time and when $t = 0$ is suddenly turned off. Thus, $V_g = V_o$ for $t < 0$ and $V_g = 0$ for $0 < t$. The lines have the same wave velocity c. Determine $V(0, t)$. (Note that, by contrast with the situation in Prob. 14.4.4, the line having characteristic impedance Z_a now has initial values of voltage and current.)

14.4.6 A transmission line is terminated at $z = l$ in a "short" and driven at $z = 0$ by a current source $I_g(t)$ in parallel with a resistance R_g. For $0 < t < T$, $I_g = I_o =$ constant, while for $t < 0$ and $T < t$, $I_g = 0$. For $R_g = Z_o$, determine $V(0, t)$.

14.4.7 With R_g not necessarily equal to Z_o, the line of Prob. 14.4.6 is driven by a step in current; for $t < 0$, $I_g = 0$, while for $0 < t$, $I_g = I_o =$ constant.

(a) Using an approach suggested by Example 14.4.3, determine the current $I(0,t)$.
(b) If the transmission line is MQS, the system can be represented by a parallel inductor and resistor. Find $I(0,t)$ assuming such a model.
(c) Show that in the limit where the round-trip transit time $2l/c$ is short compared to the time $\tau = lL/R_g$, the current $I(0,t)$ found in (a) approaches that predicted by the MQS model.

14.4.8 The transmission line shown in Fig. P14.4.8 is terminated in a series load resistance, R_L, and capacitance C_L.

(a) Show that the algebraic relation between the incident and reflected wave at $z = l$, given by (8) for the load resistance alone, is replaced by the differential equation at $z = l$

$$Z_o C_L \left(\frac{R_L}{Z_o} + 1\right)\frac{dV_-}{dt} + V_- = Z_o C_L \left(\frac{R_L}{Z_o} - 1\right)\frac{dV_+}{dt} + V_+ \qquad (a)$$

which can be solved for the reflected wave $V_-(l,t)$ given the incident wave $V_+(l,t)$.
(b) Show that if the capacitor voltage is V_c when $t = 0$, then

$$V_-(l,0) = \frac{V_c}{\left(\frac{R_L}{Z_o} + 1\right)} + V_+(l,0)\frac{\left(\frac{R_L}{Z_o} - 1\right)}{\left(\frac{R_L}{Z_o} + 1\right)} \qquad (b)$$

(c) Given that $V_g(t) = 0$ for $t < 0$, $V_g(t) = V_o =$ constant for $0 < t$, and that $R_g = Z_o$, determine $V(0,t)$.

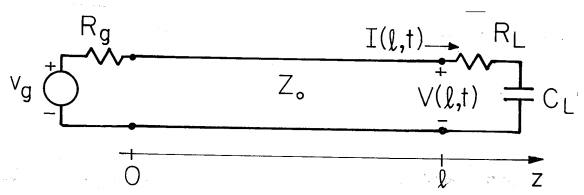


Fig. P14.4.8

14.5 Transmission Lines in the Sinusoidal Steady State

14.5.1 Determine the impedance of a quarter-wave section of line that is terminated, first, in a load capacitance C_L, and second, in a load inductance L_L.

14.5.2 A line having length l is terminated in an open circuit.

(a) Determine the line admittance $Y(-l)$ and sketch it as a function of $\omega l/c$.
(b) Show that the low-frequency admittance is that of a capacitor lC.

14.5.3* A line is matched at $z = 0$ and driven at $z = -l$ by a voltage source $V_g(t) = V_o \sin(\omega t)$ in series with a resistance equal to the characteristic impedance of the line. Thus, the line is as shown in Fig. 14.4.5 with $R_g = Z_o$. Show that in the sinusoidal steady state,

$$V = \mathrm{Re}\frac{1}{2}\hat{V}_g e^{-j\beta(z+l)}e^{j\omega t}; \qquad I = \mathrm{Re}\frac{1}{2Z_o}\hat{V}_g e^{-j\beta(z+l)}e^{j\omega t}$$

where $\hat{V}_g \equiv -jV_o$.

14.5.4 In Prob. 14.5.3, the drive is zero for $t < 0$ and suddenly turned on when $t = 0$. Thus, for $0 < t$, $V_g(t)$ is as in Prob. 14.5.3. With the solution written in the form of (1), where $V_s(z,t)$ is the sinusoidal steady state solution found in Prob. 14.5.3, what are the initial and boundary conditions on the transient part of the solution? Determine $V(z,t)$ and $I(z,t)$.

14.6 Reflection Coefficient Representation of Transmission Lines

14.6.1* The normalized load impedance is $Z_L/Z_o = 2 + j2$. Use the Smith chart to show that the impedance of a quarter-wave line with this termination is $Z/Z_o = (1 - j)/4$. Check this result using (20).

14.6.2 For a normalized load impedance $Z_L/Z_o = 2 + j2$, use (3) to evaluate the reflection coefficient, $|\Gamma|$, and hence the VSWR, (10). Use the Smith chart to check these results.

14.6.3 For the system shown in Fig. 14.6.6a, the load admittance is $Y_L = 2Y_o$. Determine the position, l, and length, l_s, of a shorted stub, also having the characteristic admittance Y_o, that matches the load to the line.

14.6.4 In practice, it may not be possible or convenient to control the position l of the stub, as required for single stub matching of a load admittance Y_L to a line having characteristic admittance Y_o. In that case, a "double stub" matching approach can be used, where two stubs at arbitrary locations but with adjustable lengths are used. At the price of restricting the range of loads that can be matched, suppose that the first stub is attached in parallel with the load and shorted at length l_1, and that the second stub is shorted at length l_2 and connected in parallel with the line at a given distance l from the load. The stubs have the same characteristic admittance as the line. Describe how, given the load admittance and the distance l to the second stub, the lengths l_1 and l_2 would be designed to match the load to the line. (Hint: The first stub can be adjusted in length to locate

the effective load anywhere on the circle on the Smith chart having the normalized conductance g_L of the load.) Demonstrate for the case where $Y_L = 2Y_o$ and $l = 0.042\lambda$.

14.6.5 Use the Smith chart to obtain the VSWR on the line to the left in Fig. 14.5.3 if the load resistance is $R_L/Z_o = 2$ and $Z_o^a = 2Z_0$. (Hint: Remember that the impedance of the Smith chart is normalized to the characteristic impedance at the position in question. In this situation, the lines have different characteristic impedances.)

14.7 Distributed Parameter Equivalents and Models with Dissipation

14.7.1 Following the steps exemplified in Section 14.1, derive (1) and (2).

14.7.2 For Example 14.7.1,

(a) Determine $I(z,t)$.
(b) Find the impedance at $z = -l$.
(c) In the long wave limit, $|\beta l| \ll 1$, what is this impedance and what equivalent circuit does it imply?

14.7.3 The configuration is as in Example 14.7.1 except that the line is shorted at $z = 0$. Determine $V(z,t)$ and $I(z,t)$, and hence the impedance at $z = -l$. In the long wave limit, $|\beta l| \ll 1$, what is this impedance and what equivalent circuit does it imply?

14.7.4* Following steps suggested by the derivation of (14.2.19),

(a) Use (1) and (2) to derive the power theorem

$$-\frac{\partial}{\partial z}(VI) = \frac{\partial}{\partial t}\left(\frac{1}{2}CV^2 + \frac{1}{2}LI^2\right) + I^2R + V^2G \qquad (a)$$

(b) The product of two sinusoidally varying quantities is a constant (time average) part plus a part that varies sinusoidally at twice the frequency. In complex notation,

$$\mathrm{Re}\hat{A}e^{j\omega t}\mathrm{Re}\hat{B}e^{j\omega t} = \frac{1}{2}\mathrm{Re}\hat{A}\hat{B}^* + \frac{1}{2}\mathrm{Re}\hat{A}\hat{B}e^{2j\omega t} \qquad (b)$$

Use (11.5.7) to prove this identity.

(c) Show that, in describing the sinusoidal steady state, the time average of the power theorem becomes

$$-\frac{d}{dz}\left(\frac{1}{2}\mathrm{Re}\hat{V}\hat{I}^*\right) = \frac{1}{2}\mathrm{Re}(\hat{I}\hat{I}^*R + \hat{V}\hat{V}^*G) \qquad (c)$$

Show that for Example 14.7.1, it follows that the time average power input is equal to the integral over the length of the time average power dissipation per unit length.

$$\frac{1}{2}\mathrm{Re}\hat{V}\hat{I}^*\big|_{z=-l} = \int_{-l}^{0}\frac{1}{2}\mathrm{Re}(\hat{I}\hat{I}^*R + \hat{V}\hat{V}^*G)dz \qquad (d)$$

(d) Evaluate the time average input power on the left in this relation and the integral of the time average dissipation per unit length on the right and show that they are indeed equal.

14.8 Uniform and TEM Waves in Ohmic Conductors

14.8.1 In the general TEM configuration of Fig. 14.2.1, the material between the conductors has uniform conductivity, σ, as well as uniform permittivity, ϵ. Following steps like those leading to 14.2.12 and 14.2.13, show that (4) and (5) describe the waves, regardless of cross-sectional geometry. Note the relationship between G and C summarized by (7.6.4).

14.8.2 Although associated with the planar configuration of Fig. 14.8.1 in this section, the transmission line equations, (4) and (5), represent exact field solutions that are, in general, functions of the transverse coordinates as well as z. Thus, the transmission line represents a large family of exact solutions to Maxwell's equations. This follows from Prob. 14.8.1, where it is shown that the transmission line equations apply even if the regions between conductors are coaxial, as shown in Fig. 14.2.2b, with a material of uniform permittivity, permeability, and conductivity between $z = -l$ and $z = 0$. At $z = 0$, the transmission line conductors are "open circuit." At $z = -l$, the applied voltage is Re $\hat{V}_g \exp(j\omega t)$. Determine the electric and magnetic fields in the region between transmission line conductors. Include the dependence of the fields on the transverse coordinates. Note that the axial dependence of these fields is exactly as described in Examples 14.8.1 and 14.8.2.

14.8.3 The terminations and material between the conductors of a transmission line are as described in Prob. 14.8.2. However, rather than being coaxial, the perfectly conducting transmission line conductors are in the parallel wire configuration of Fig. 14.2.2a. In terms of $\Phi(x, y, z, t)$ and $A_z(x, y, z, t)$, determine the electric and magnetic fields over the length of the line, including their dependencies on the transverse coordinates. What are L, C, and G and hence β and Z_o?

14.8.4* The transmission line model for the strip line of Fig. 14.8.4a is derived in Prob. 14.1.1. Because the permittivity is not uniform over the cross-section of the line, the waves represented by the model are not exactly TEM. The approximation is valid as long as the wavelength is long enough so that (25)

is satisfied. In the approximation, E_x is taken as being uniform with x in each of the dielectrics, E^a and E^b, respectively. To estimate the longitudinal field E_z and compare it to E^a,

(a) Use the integral form of the law of induction applied to an incremental surface between $z + \Delta z$ and z and between the perfect conductors to derive Faraday's transmission line equation written in terms of E^a.

$$\left(a + \frac{\epsilon_a}{\epsilon_b} b\right) \frac{\partial E^a}{\partial z} = -\mu_o (a + b) \frac{\partial H_y}{\partial t} \tag{a}$$

(b) Then carry out this same procedure using a surface that again has edges at $z + \Delta z$ and z on the upper perfect conductor, but which has its lower edge at the interface between dielectrics. With the axial electric field at the interface defined as E_z, show that

$$E_z = -a\mu_o \frac{\partial H_y}{\partial t} - a \frac{\partial E^a}{\partial z} = -ab\mu_o \frac{\left(\frac{\epsilon_a}{\epsilon_b} - 1\right)}{\left(a + \frac{\epsilon_a}{\epsilon_b} b\right)} \frac{\partial H_y}{\partial t} \tag{b}$$

(c) Now show that in order for this field to be small compared to E^a, (25) must hold.

14.9 Quasi-One-Dimensional Models ($G = 0$)

14.9.1 The transmission line of Fig. 14.2.2a is comprised of wires having a finite conductivity σ, with the dielectric between of negligible conductivity. With the distribution of V and I described by (7) and (10), what are C, L, and R, and over what frequency range is this model valid? (Note Examples 4.6.3 and 8.6.1.) Give a condition on the dimensions $R \to a$ and l that must be satisfied to have the model be self-consistent over frequencies ranging from where the resistance dominates to where the inductive reactance dominates.

14.9.2 In the coaxial transmission line of Fig. 14.2.2b, the outer conductor has a thickness Δ. Each conductor has the conductivity σ. What are C, L, and R, and over what frequency range are (7) and (10) valid? Give a condition on the transverse dimensions that insures the model being valid into the frequency range where the inductive reactance dominates the resistance.

14.9.3 Find $V(z, t)$ on the charge diffusion line of Fig. 14.9.4 in the case where the applied voltage has been zero for $t < 0$ and suddenly becomes $V_p =$ constant for $0 < t$ and the line is shorted at $z = 0$. (Note Example 10.6.1.)

14.9.4 Find $V(z, t)$ under the conditions of Prob. 14.9.3 but with the line "open circuited" at $z = 0$.

15

OVERVIEW OF ELECTROMAGNETIC FIELDS

15.0 INTRODUCTION

In developing the study of electromagnetic fields, we have followed the course summarized in Fig. 1.0.1. Our quest has been to make the laws of electricity and magnetism, summarized by Maxwell's equations, a basis for understanding and innovation. These laws are both general and simple. But, as a consequence, they are mastered only after experience has been gained through many specific examples. The case studies developed in this text have been aimed at providing this experience. This chapter reviews the examples and intends to foster a synthesis of concepts and applications.

At each stage, simple configurations have been used to illustrate how fields relate to their sources, whether the latter are imposed or induced in materials. Some of these configurations are identified in Section 15.1, where they are used to outline a comparative study of electroquasistatic, magnetoquasistatic, and electrodynamic fields. A review of much of the outline (Fig. 1.0.1) can be made by selecting a particular class of configurations, such as cylinders and spheres, and using it to exemplify the material in a sequence of case studies.

The relationship between fields and their sources is the theme in Section 15.2. Again, following the outline in Fig. 1.0.1, electric field sources are unpaired charges and polarization charges, while magnetic field sources are current and (paired) magnetic charges. Beginning with electroquasistatics, followed by magnetoquasistatics and finally by electrodynamics, our outline first focused on physical situations where the sources were constrained and then were induced by the presence of media. In this text, magnetization has been represented by magnetic charge. An alternative commonly used formulation, in which magnetization is represented by "Ampèrian" currents, is discussed in Sec. 15.2.

As a starting point in the discussions of EQS, MQS, and electrodynamic fields, we have used idealized models for media. The limits in which materials behave as

"perfect conductors" and "perfect insulators" and in which they can be said to have "infinite permittivity or permeability" provide yet another way to form an overview of the material. Such an approach is taken at the end of Sec. 15.2.

Useful as these idealizations are, their physical significance can be appreciated only by considering the relativity of perfection. Although we have introduced the effects of materials by making them ideal, we have then looked more closely and seen that "perfection" is a relative concept. If the fields associated with idealized models are said to be "zero order," the second part of Sec. 15.2 raises the level of maturity reflected in the review by considering the "first order" fields.

What is meant by a "perfect conductor" in EQS and MQS systems is a part of Sec. 15.2 that naturally leads to a review in Sec. 15.3 of how characteristic times can be used to understand electromagnetic field interactions with media. Now that we can see EQS and MQS systems from the perspective of electrodynamics, Sec. 15.3 is aimed at an overview of how the spatial scale, time scale (frequency), and material properties determine the dominant processes. The objective in this section is not only to integrate material, but to add insight into the often iterative process by which a model is made to both encapsulate the essential physics and serve as a basis of engineering innovation.

Energy storage and dissipation, together with the associated forces on macroscopic media, provide yet another overview of electromagnetic systems. This is the theme of Sec. 15.4, which summarizes the reasons why macroscopic forces can usually be classified as being either EQS or MQS.

15.1 SOURCE AND MATERIAL CONFIGURATIONS

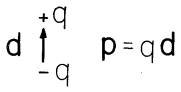
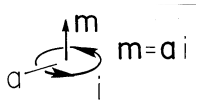
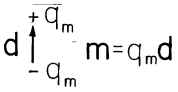
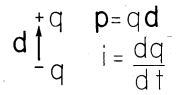
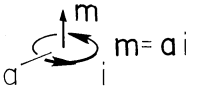
We can use any one of a number of configurations to review physical phenomena outlined in Fig. 1.0.1. The sections, examples, and problems associated with a given physical situation are referenced in the tables used to trace the evolution of a given configuration.

Incremental Dipoles. In homogeneous media, dipole fields are simple solutions to Laplace's equation or the wave equation in two or three dimensions and have been used to represent the range of situations summarized in Table 15.1.1. As introduced in Chap. 4, the dipole represented closely spaced equal and opposite electric charges. Perhaps these charges were produced on a pair of closely spaced conducting objects, as shown in Fig. 3.3.1a. In Chap. 6, the electric dipole was used to represent polarization, and a distinction was made between unpaired and paired (polarization) charges.

In representing conduction phenomena in Chap. 7, the dipole represented a closely spaced pair of current sources. Rather than being a source in Gauss' law, the dipole was a source in the law of charge conservation.

In magnetoquasistatics, there were two types of dipoles. First was the small current loop, where the dipole moment was the product of the area, a, and the circulating current, i. The dipole fields were those from a current loop, far from the loop, such as shown in Fig. 3.3.1b. As we will discuss in Sec. 15.2, we could have used current loop dipoles to represent magnetization. However, in Chap. 9,

TABLE 15.1.1
SUMMARY OF INCREMENTAL DIPOLES

Electroquasistatic charge: Point; Sec. 4.4, Line; Prob. 4.4.1, Sec. 5.7	
Electroquasistatic polarization: Sec. 6.1	
Stationary conduction current: Point; Example 7.3.2 Line; Prob. 7.3.3	
Magnetoquasistatic current: Point; Example 8.3.2 Line; Example 8.1.2	
Magnetoquasistatic magnetization: Sec. 9.1	
Electric Electrodynamic: Point; Sec. 12.2	
Magnetic Electrodynamic: Point; Sec. 12.2	

magnetization was represented by magnetic dipoles, a pair of equal and opposite magnetic charges. Thus, the developments of polarization in Chap. 6 were directly applicable to magnetization.

To create the time-varying positive and negative charges of the electric dipole, a current is required. In Fig. 3.3.1a, this current is supplied by the voltage source. In the EQS limit, the magnetic field associated with this current is negligible, as are the effects of the associated magnetic field. In Chap. 12, where the laws of Faraday and Ampère were made self-consistent, the coupling between these laws was found to result in electromagnetic radiation. Electric dipole radiation existed because the charging currents created some magnetic field and that, in turn, induced a rotational electric field. In the case of the magnetic dipole shown last in Table 15.1.1, electromagnetic waves resulted from a displacement current induced by the time-varying magnetic field that, in turn, produced a more rotational magnetic field.

Planar Periodic Configurations. Solutions to Laplace's equation in Cartesian coordinates are all that is required to study the quasistatic and "steady" situations outlined in Table 15.1.2. The fields used to study these physical situations, which are periodic in a plane that "extends to infinity," are by nature decaying in the direction perpendicular to that plane.

The electrodynamic fields studied in Sec. 12.6 have this same decay in a direction perpendicular to the direction of periodicity as the frequency becomes low. From the point of view of electromagnetic waves, these low frequency, essentially Laplacian, fields are represented by nonuniform plane waves. As the frequency is raised, the nonuniform plane waves become waves that propagate in the direction in which they formerly decayed. Solutions to the wave equation can be spatially periodic in both directions. The TE and TM electrodynamic field configurations that conclude Table 15.1.2 help put into perspective those aspects of the EQS and MQS configurations that do not involve losses.

Cylindrical and Spherical. A few simple solutions to Laplace's equation are sufficient to illustrate the nature of fields in and around cylindrical and spherical material objects. Table 15.1.3 shows how a sequence of case studies begins with EQS and MQS fields, respectively, in systems of "perfect" insulators and "perfect" conductors and culminates in the very different influences of finite conductivity on EQS and MQS fields.

Fields Between Plane Parallel Plates. Uniform and piece-wise uniform quasistatic fields are sufficient to illustrate phenomena ranging from EQS, the "capacitor," to MQS "magnetic diffusion through thin conductors," Table 15.1.4. Closely related TEM fields describe the remaining situations.

Axisymmetric (Coaxial) Fields. The case studies summarized in Table 15.1.4 under this category parallel those for fields between plane parallel conductors.

TABLE 15.1.2
PLANAR PERIODIC CONFIGURATIONS

Field Solutions	
Laplace's equation:	Sec. 5.4
Wave equation:	Sec. 12.6
Electroquasistatic (EQS)	
Constrained Potentials and Surface Charge:	Examp. 5.6.2
Constrained Potentials and Volume Charge:	Examp. 5.6.1
	Probs. 5.6.1-4
Constrained Potentials and Polarization:	Probs. 6.3.1-4
Charge Relaxation:	Probs. 7.9.7-8
Steady Conductor (MQS or EQS)	
Constrained Potential and Insulating Boundary:	Prob. 7.4.3
Magnetoquasistatic (MQS)	
Magnetization:	Examp. 9.3.2
Magnetic diffusion through Thin Conductors:	Probs. 10.4.1-2
Electrodynamic	
Imposed Surface Sources:	Examps. 12.6.1-2
	Probs. 12.6.1-4
Imposed Sources with Perfectly	Examp. 12.7.2
Conducting Boundaries:	Probs. 12.7.3-4
	Probs. 13.2.1
Perfectly Insulating Boundaries:	Sec. 13.5
	Probs. 13.2.3-4
	Probs. 13.5.1-4

TABLE 15.1.3
CYLINDRICAL AND SPHERICAL CONFIGURATIONS

Field Solutions to Laplace's Equation:	Cylindrical; Sec. 5.7	Spherical; Sec. 5.9
Electroquasistatic		
Equipotentials:	Examp. 5.8.1	Examp. 5.9.2
Polarization:		
Permanent:	Prob. 6.3.6	Examp. 6.3.1
		Prob. 6.3.5
Induced:	Examp. 6.6.2	Probs. 6.6.1-2
Charge Relaxation:	Probs. 7.9.4-5	Examp. 7.9.3
		Prob. 7.9.6
Steady Conduction (MQS or EQS)		
Imposed Current:	Examp. 7.5.1	Probs. 7.5.1-2
Magnetoquasistatic		
Imposed Current:	Probs. 8.5.1-2	Examp. 8.5.1
Perfect Conductor:	Probs. 8.4.2-3	Examp. 8.4.3
		Prob. 8.4.1
Magnetization:	Probs. 9.6.3-4,10,12	Probs. 9.6.11,13
Magnetic Diffusion:	Examp. 10.4.1	Probs. 10.4.3-4
	Probs. 10.4.5-6	

TM and TE Fields with Longitudinal Boundary Conditions. The case studies under this heading in Table 15.1.4 offer the opportunity to see the relationship

TABLE 15.1.4. SPECIAL CONFIGURATIONS

Fields Between Plane Parallel Plates	
Capacitor:	Examps. 3.3.1, 6.3.3 Probs. 6.5.1-4, 6.6.8, 11.2.1 11.3.3, 11.6.1
Resistor:	Examps. 7.2.1, 7.5.2
Inductor:	Examp. 8.4.4, Probs. 9.5.1,3,6
Charge Relaxation:	Examp. 7.9.2
Magnetic Diffusion though:	
Thin Conductors:	Prob. 10.3.4
Thick Conductors (TEM):	Examps. 10.6.1, 10.7.1 Probs. 10.3.4, 10.6.1-2, 10.7.1-2
Principle (TEM) Waveguide Modes	Examps. 13.1.1-2
Transmission Line:	Examps. 14.1.1, 14.8.2
Axisymmetric (Coaxial) Fields	
Capacitor:	Probs 6.5.5-6
Resistor:	Examps. 7.5.2 Probs. 7.2.1,4,8
Inductor:	Examp. 3.4.1 Probs. 9.5.2,4-5
Charge Relaxation:	Prob. 7.9.1
TEM Transmission Line	Prob. 13.1.4
TM and TE Fields with Longitudinal Boundary Conditions	
Capacitive Attenuator:	Sec. 5.5
TM Waveguide Fields:	Examp. 13.3.1
Inductive Attenuator:	Examp. 8.6.3
TE Waveguide Fields:	Examp. 13.3.2
Cylindrical Conductor-Pair and Conductor-Plane	
EQS Perfect Conductors:	Examp. 4.6.3
MQS Perfect Conductors:	Examp. 8.6.1
TEM Transmission Line:	Examp. 14.2.2

between fields and their sources, in the quasistatic limits and as electromagnetic waves. The EQS and MQS limits, illustrated by Demonstrations 5.5.1 and 8.6.2, respectively, become the shorted TM and TE waveguide fields of Demonstrations 13.3.1 and 13.3.2.

Cylindrical Conductor Pair and Conductor Plane. The fields used in these configurations are first EQS, then MQS, and finally TEM. The relationship between the EQS and MQS fields and the physical world is illustrated by Demonstrations 4.7.1 and 8.6.1. Regardless of cross-sectional geometry, TEM waves on pairs of perfect conductors are much of the same nature regardless of geometry, as illustrated by Demonstration 13.1.1.

15.2 MACROSCOPIC MEDIA

Source Representation of Macroscopic Media. The primary sources of the EQS electric field intensity were the unpaired and paired charge densities, respectively, describing the influence of macroscopic media on the fields through conduction and polarization (Chap. 6). Although in Chap. 8 the primary source of the MQS magnetic field due to conduction was the unpaired current density, in Chap. 9, magnetization was modeled as the result of orientation of permanent magnetic dipoles made up of a pair of magnetic charges, positive and negative. This is not the conventional way of introducing magnetization. However, the magnetic charge model made possible an analogy between polarization and magnetization that enabled us to introduce magnetization into the field equations by analogy to polarization. More conventional is the approach that treats magnetization as the result of circulating Ampèrian currents. The two approaches lead to the same final result, only the model is different. To illustrate this, let us rewrite Maxwell's equations (12.0.1)–(12.0.4) in terms of $\mathbf{B}$, rather than $\mathbf{H}$

$$\nabla \times \mathbf{E} = -\frac{\partial}{\partial t}\mathbf{B} \tag{1}$$

$$\nabla \times \frac{\mathbf{B}}{\mu_o} = \nabla \times \mathbf{M} + \mathbf{J}_u + \frac{\partial}{\partial t}\epsilon_o \mathbf{E} + \frac{\partial}{\partial t}\mathbf{P} \tag{2}$$

$$\nabla \cdot \epsilon_o \mathbf{E} = -\nabla \cdot \mathbf{P} + \rho_u \tag{3}$$

$$\nabla \cdot \mathbf{B} = 0 \tag{4}$$

Thus, if $\mathbf{B}$ is considered to be the fundamental field variable, rather than $\mathbf{H}$, then the presence of magnetization manifests itself by the appearance of the term $\nabla \times \mathbf{M}$ next to $\mathbf{J}_u$ in Ampère's law. Like $\mathbf{J}_u$, the Ampèrian current density, $\nabla \times \mathbf{M}$, is the source responsible for driving $\mathbf{B}/\mu_o$. Because $\mathbf{B}$ is solenoidal, no sources of divergence appear in Maxwell's equations reformulated in terms of $\mathbf{B}$. The fundamental source representing magnetization is now a current flowing around a small loop (magnetic

dipole). Equations (1)–(4) are, of course, identical in content to (12.0.1)–(12.0.4) because they resulted from the latter by a simple substitution of $\mathbf{B}/\mu_o - \mathbf{M}$ for $\mathbf{H}$. Yet the model of magnetization was changed by this substitution. As mentioned in Sec. 11.8, both models lead to the same result even when relativistic effects are included, but the Ampèrian model calls for greater care and sophistication, because it contains moving parts (currents) in the rest frame. This is the other reason we chose the magnetic charge model extensively developed by L. J. Chu.

Material Idealizations. Much of our analysis of electromagnetic fields has been based on source idealizations. In the case of sources produced by or induced in media, idealizations were made of the media and of the boundary conditions implied by the induced sources. These are summarized by the first and second parts of Table 15.2.1.

The case studies listed in Tables 15.1.2–15.1.4 can be used as themes to exemplify these idealizations.

The Relativity of Perfection. We began modeling EQS and MQS fields in the presence of media by postulating "perfect" conductors. When we studied materials in more detail, we learned that "perfection" is a relative concept. Useful as are the idealizations summarized in Table 15.2.1, they must be used with proper regard for the approximations made. Those idealizations that involve conductivity depend not only on relative material properties for their validity but on size and time-rates of change as well. These are reviewed in the next section.

In each of the three "infinite parameter" idealizations listed in the table, the parameter in one region is large compared to that in another region. The appropriate boundary condition depends on the region of field excitation. The idealization makes it possible to approximate the field in an "inside" region without regard for what is "outside." One of the continuity conditions on the surface of the "inside" region is approximated as being homogeneous. Then the fields in the "outside" region are found by starting with the other continuity condition. Our first introduction to this "inside-outside" approach came in Sec. 7.5. With appropriate regard for replacing a source of curl with a source of divergence, the general discussion given in Sec. 9.6 for magnetizable materials is applicable to the other situations as well.

15.3 CHARACTERISTIC TIMES, PHYSICAL PROCESSES, AND APPROXIMATIONS

Self-Consistency of Approximate Laws. By dealing with EQS and MQS systems, we concentrated on phenomena that result from approximate forms of Maxwell's equations. Terms in the "exact" equations were ignored, and field configurations were derived from these truncated forms of the equations. This way of solving problems is not unique to electromagnetic field theory. Very often it is

TABLE 15.2.1
IDEALIZATIONS

Idealization	Source Constraint	Section
EQS Perfect Insulator	Charges Constrained	4.3-5
Perfectly Polarized	**P** Constrained	6.3
MQS Perfect "Insulator"	Currents Constrained	8.1-3
Perfectly Magnetized	**M** Constrained	9.3
Resonant/Traveling-Wave Electrodynamic Systems	Self-Consistent Charge and Current	12.2-4, 12.6

Idealization	Boundary Condition	Section
EQS Perfect Conductor	Perfectly Conducting Surfaces Equipotentials	4.6-7, 5.1-10
Steady Conduction "Infinite Conductivity"	$\mathbf{n} \times \mathbf{E} \approx 0$ or $\mathbf{n} \cdot \mathbf{J} \approx 0$ on surface	7.2, 9.6
"Infinite" Permittivity	$\mathbf{n} \times \mathbf{E} \approx 0$ or $\mathbf{n} \cdot \mathbf{D} \approx 0$ on surface	9.6
"Infinite" Permeability	$\mathbf{n} \times \mathbf{H} \approx \mathbf{K}$ or $\mathbf{n} \cdot \mathbf{B} \approx 0$ on surface	9.6
MQS Perfect Conductor	$\partial \mathbf{n} \cdot \mathbf{B}/\partial t \approx 0$ on perfectly conducting surfaces	8.4, 8.6 10.1, 12.7 13.1-4

necessary to ignore terms that appear in a "more exact" formulation of a physical problem. When this is done, it is necessary to be fully cognizant of the consequences of such approximations. Thus, the energy conservation relations used in the EQS and MQS approximations are special limiting cases of the Poynting theorem obeyed by the full Maxwell equations. The neglect of the displacement current or magnetic induction is equivalent to the neglect of the electric or magnetic energy storage.

Next, one needs to ascertain whether the problem has been sufficiently specified by the approximate form of the equations and which boundary conditions have to be retained, which discarded. The development of the EQS and MQS approximations, with the proof of the uniqueness theorem, provided examples of the development of a self-consistent formalism within the framework of a set of approximate equations. In systems composed of "perfectly conducting" and "perfectly insulating" media, it is relatively easy to decide whether or not there are subsystems that are EQS or MQS.

A system of perfect conductors surrounded by perfect insulators is likely to be EQS, if it is "open circuit" at zero frequency (a system of capacitors), and MQS, if it is "short circuit" at zero frequency (a system of inductors). However, we are generally not confronted with physical situations in which the materials are labeled as "perfect conductors" or "perfect insulators." Indeed, with the last half of Chap. 7 and Chap. 10 as background, there comes an awareness that in EQS and MQS systems the term "perfect" usually has very different meanings.

Presented with a physical object connected to an electrical source, how do we sort the dominant from the inconsequential electromagnetic phenomena? Generally, this is an iterative process with the first "guess" based on experience and intuition. With the understanding that the combinations of materials and geometries that are of practical interest are far too diverse to make a few simple rules universally applicable, this section is nevertheless aimed at organizing what we have learned so as to promote the insight required to identify dominant physical processes.

From the examination of how finite conductivity influences the distribution of the charge density in the EQS systems of Chap. 7 and the current density in the MQS systems of Chap. 10, and from the discussion of the electrodynamics of lossy materials, we have a good idea of what questions must be asked to determine the electromagnetic nature of simple subsystems. A specific example, familiar from Sec. 14.8, is the conducting block sandwiched between perfectly conducting plane parallel electrodes, shown in Fig. 14.8.1.

- First, what are the electrical properties of the materials? Here this question has been reduced to, What are σ, ϵ, and μ? The most widely ranging of these parameters is the conductivity σ, which can vary from 10^{-14} S/m in common hydrocarbon liquids to almost 10^{8} S/m in copper. Indeed, vacuum and superconducting materials extend this range from absolute zero to infinity.
- Second, what is the size scale l? In common engineering systems, lengths of interest range from the submicrometer scales of semiconductor junctions to lengths for power transmission systems in excess of 1000 kilometers. Of course, even this range is small compared to the subnuclear to supergalactic range provided by nature.
- Third, what time scale τ is of interest? Perhaps the system is driven by a sinusoidally varying source. Then, the time scale would most likely be the reciprocal of the angular frequency $1/\omega$. In common engineering practice, frequencies range from 10^{-2} Hz used to characterize insulation to optical frequencies in the range of 10^{15} Hz. Again, nature provides frequencies that range even more widely, including the reciprocal of millions of years for terrestrial magnetic fields in one extreme and the frequencies of gamma rays in the other.

Similitude and Maxwell's Equations. Consider an arbitrary system, shown in Fig. 15.3.1, having the typical length l and properties

$$\epsilon\underline{\epsilon}(\mathbf{r}), \quad \sigma\underline{\sigma}(\mathbf{r}), \quad \mu\underline{\mu}(\mathbf{r}) \tag{1}$$

where ϵ, σ, and μ are typical magnitudes of dielectric constant, conductivity and permeability, and $\underline{\epsilon}(\mathbf{r}), \underline{\sigma}(\mathbf{r})$, and $\underline{\mu}(\mathbf{r})$ are the spatial distributions, normalized so that their peak values are of the order of unity.

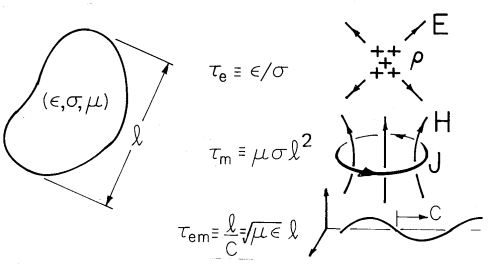


Fig. 15.3.1 Arbitrary system having typical length l, permittivity ϵ, conductivity σ, and permeability μ.

TABLE 15.3.1
SECTIONS EXEMPLIFYING CHARACTERISTIC TIMES

Electroquasistatic charge relaxation time:	Sec. 7.7, 7.9
Magnetoquasistatic magnetic (current) diffusion time:	Sec. 10.2-7
Electromagnetic wave transit time:	Sec. 12.2-7, 14.3-4

From our studies of ohmic conductors in EQS and MQS systems, we know that field distributions are governed by the charge relaxation time τ_e and the magnetic diffusion time τ_m, respectively. Moreover, from our study of electromagnetic waves, we know that the transit time for an electromagnetic wave, τ_{em}, comes into play with electrodynamic effects. Sections in which these three times were exemplified are listed in Table 15.3.1. Thus, we expect to find that in systems having one typical size scale, there are no more than three times that determine the nature of the fields.

$$\tau_e \equiv \frac{\epsilon}{\sigma}; \quad \tau_m \equiv \mu\sigma l^2; \quad \tau_{em} \equiv \frac{l}{c} = l\sqrt{\mu\epsilon} \tag{2}$$

Actually, the electromagnetic transit time is the geometric mean of the other two times, so that only two of these times are independent.

$$\tau_{em} = \sqrt{\tau_e \tau_m} \tag{3}$$

With an excitation having the angular frequency ω, the relative distribution of sources and fields in a system is determined by the product of ω and any pair of these times. This can be seen by writing Maxwell's equations in normalized form. To that end, we use underbars to denote normalized (dimensionless) variables and normalize the spatial coordinates to the typical length l. The time is normalized to the reciprocal of the angular frequency.

$$(x, y, z) = (\underline{x}l, \underline{y}l, \underline{z}l), \quad t = \underline{t}/\omega \tag{4}$$

The fields and charge density are normalized to a typical electric field intensity $\mathcal{E}$.

$$\mathbf{E} = \mathcal{E}\underline{\mathbf{E}}, \quad \mathbf{H} = \mathcal{E}\sqrt{\frac{\epsilon}{\mu}}\underline{\mathbf{H}}, \quad \rho_u = \frac{\epsilon\mathcal{E}}{l}\underline{\rho}_u \tag{5}$$

Then, Maxwell's equations (12.0.7)–(12.0.10), with the constitutive laws of (1), become

$$\underline{\nabla} \cdot \underline{\epsilon}\underline{\mathbf{E}} = \underline{\rho}_u \tag{6}$$

$$\underline{\nabla} \times \underline{\mathbf{H}} = \omega\tau_{em}\Big(\frac{1}{\omega\tau_e}\underline{\mathbf{E}} + \frac{\partial\underline{\epsilon}\underline{\mathbf{E}}}{\partial\underline{t}}\Big) \tag{7a}$$

$$= \frac{1}{\omega\tau_{em}}\omega\tau_m\underline{\mathbf{E}} + \omega\tau_{em}\frac{\partial\underline{\epsilon}\underline{\mathbf{E}}}{\partial\underline{t}} \tag{7b}$$

$$\underline{\nabla} \times \underline{\mathbf{E}} = -\omega\tau_{em}\frac{\partial\underline{\mathbf{H}}}{\partial\underline{t}} \tag{8}$$

$$\underline{\nabla} \cdot \underline{\mu}\underline{\mathbf{H}} = 0 \tag{9}$$

In writing the alternative forms of Ampère's law, (3) has been used.

In a system having the constitutive laws of (1), two parameters specify the fields predicted by Maxwell's equations, (6)–(9). These are any pair of the three ratios of the characteristic times of (2) to the typical time of interest. For the sinusoidal steady state, the time of interest is $1/\omega$. Thus, using the version of Ampère's law given by (7a), the dimensionless parameters $(\omega\tau_{em}, \omega\tau_e)$ specify the fields. Using (7b), the parameters are $(\omega\tau_{em}, \omega\tau_m)$.

Characteristic Times and Lengths. Evidently, the three dimensionless parameters formed by multiplying the characteristic times of (2) by the frequency, ω, (or the reciprocal of some other time typifying the dynamics), are the key to sorting out physical processes.

$$\omega\tau_e = \frac{\omega\epsilon}{\sigma}; \qquad \omega\tau_m = \omega\mu\sigma l^2; \qquad \omega\tau_{em} = \omega l\sqrt{\mu\epsilon} \tag{10}$$

Given two of these parameters and hence the third, we have some clues as to what physical processes are dominant. However, even in a subsystem typified by one permittivity, one conductivity, and one permeability, other parameters may be needed to specify the geometry. Every ratio of dimensions is another dimensionless parameter! To begin with, suppose that we are dealing with a system where all of the dimensions are on the order of the typical length l. The characteristic times make evident why quasistatic systems are either EQS or MQS. They also determine how the effects of finite conductivity come into play either through charge relaxation or magnetic diffusion as the frequency is raised.

Since the electromagnetic transit time is the geometric mean of the charge relaxation and magnetic diffusion times, (3), τ_{em} must lie between the other two times. Thus, the three times are in one of two orders. Either $\tau_m < \tau_e$, in which case

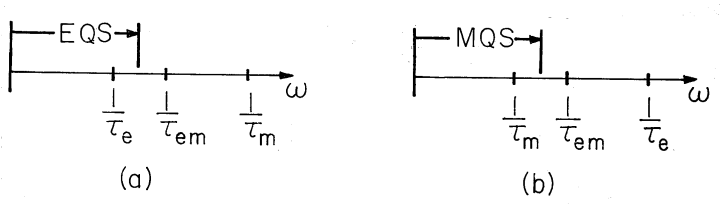


Fig. 15.3.2 Ordering of reciprocal of characteristic times on the frequency axis.

the order of reciprocal times is as shown in Fig. 15.3.2a, or the reverse is true, and the order is as in Fig. 15.3.2b. Moreover, if τ_e is well removed from τ_{em}, then we are assured that τ_m is also very different from τ_{em}.

As the frequency is raised, we first encounter either the charge relaxation phenomena typical of EQS subsystems (Fig. 15.3.2a) or the magnetic diffusion phenomena of MQS subsystems (Fig. 15.3.2b). The respective quasistatic laws for EQS and MQS systems apply for frequencies ranging above the first reciprocal time but below the reciprocal electromagnetic transit time. In both cases, the frequency is well below the reciprocal of the electromagnetic delay time.

The EQS laws follow from (6)–(9) using the first form of (7). A physical situation is characterized by the EQS laws, when the term on the right hand side of Faraday's law, (8), is negligible. From Ampère's law we gather that $\underline{\mathbf{H}}$ is of the order of $\omega\tau_{em}\underline{\mathbf{E}}$ when $\omega\tau_e > 1$, and of order τ_{em}/τ_e when $\omega\tau_e < 1$. In the former case, in which the displacement current density dominates over the conduction current density, one finds for the right hand side in Faraday's law: $(\omega\tau_{em})^2\underline{\mathbf{E}}$. In the latter case, in which the conduction current density is larger than the displacement current density, the right hand side of (8) is $\omega\tau_{em}^2/\tau_e\underline{\mathbf{E}}$. Thus the source of curl in Faraday's law can be neglected when $(\omega\tau_{em})^2 \ll 1$ or $\omega\tau_{em}/\tau_e \ll 1$ whichever is a more stringent limit on ω. The laws of EQS prevail. An analogous, but simpler, argument arrives at the laws of MQS. The argument is simpler, because there is no analog to unpaired electric charge.

In cases where the ordering of characteristic times is as in Fig. 15.3.2b, the MQS laws apply for frequencies beyond the reciprocal magnetic diffusion time but again falling short of the electromagnetic transit time. This can be seen from the normalized Maxwell's equations, this time using (7b). Because $\omega\tau_{em} \ll 1$, the last term in (7b) (the displacement current) is negligible. Thus, we are led to the primary MQS laws, Ampère's law with the displacement current neglected and the continuity law for the magnetic flux density (9). This time, it follows from Ampère's law [(7b) with the last term neglected] that $\mathbf{H} \approx (\omega\tau_m/\omega\tau_{em})\mathbf{E}$, so that the right-hand side of Faraday's law, (8), is of the order of $\omega\tau_m$. Thus, the MQS laws are (10.0.1)–(10.0.3).

As the frequency is raised, so that we move from left to right along the frequency axes of Fig. 15.3.2, we expect dynamical phenomena associated with charge relaxation, electromagnetic waves, and magnetic diffusion to come into play as the frequency comes into the range of the respective reciprocal characteristic times. Actually, because the dynamics can establish their own length scales (for example, the skin depth), matters are sometimes not so simple. However, insight is gained by observing that the length scale l orders these critical frequencies. With the objective of picturing the electromagnetic phenomena in a plane, in which one axis reflects the effect of the frequency while the other axis represents the length scale,

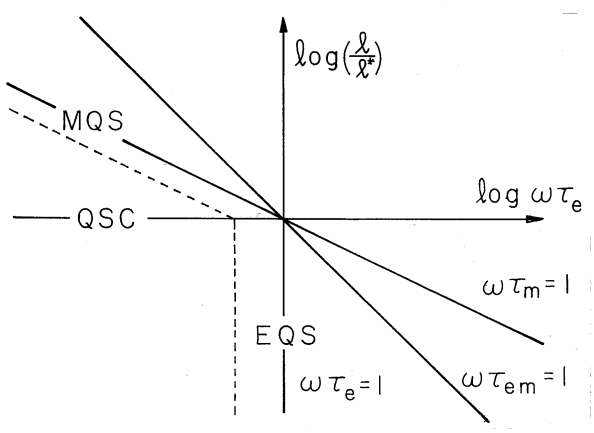


Fig. 15.3.3 In plane where the vertical axis denotes the log of the length scale normalized to the characteristic length defined by (14), and the horizontal axis is the angular frequency multiplied by the charge relaxation time τ_e, the three lines denote possible boundaries between regimes.

we normalize the frequency to the one characteristic time, τ_e, that does not depend on the length. Thus, the frequency conditions for effects of charge relaxation, magnetic diffusion, and electromagnetic waves to be important are, respectively,

$$\omega\tau_e = 1 \tag{11}$$

$$\omega\tau_m = 1 \Rightarrow \omega\tau_e = (l/l^*)^{-2} \tag{12}$$

$$\omega\tau_{em} = 1 \Rightarrow \omega\tau_e = (l/l^*)^{-1} \tag{13}$$

where the *characteristic length* l^* is

$$l^* \equiv \frac{1}{\sigma}\sqrt{\epsilon/\mu} \tag{14}$$

In a plane in which the coordinates are essentially the length scale and the frequency, the lines along which the frequency is equal to the respective reciprocal characteristic times are shown in Fig. 15.3.3. The vertical axis denotes the log of the length scale normalized to the characteristic length, while the horizontal axis is the log of the frequency multiplied by the charge relaxation time. Thus, the origin is where the length is equal to l^* and the frequency is equal to $1/\tau_e$.

Note that for systems having a typical length l less than the reciprocal of the characteristic impedance conductivity product, l^*, the ordering of times is as in Fig. 15.2.1a. If the length is greater than this characteristic length, then the ordering is as in Fig. 15.2.1b. At least for systems having one length scale l and one characteristic time $1/\omega$, *the system can be MQS only if* l *is larger than* l^* *and can be EQS only if* l *is smaller than* l^*. The MQS and EQS regimes of Fig. 15.3.3 both reduce to quasistationary conduction (QSC) at frequencies such that $\omega\tau_m \ll 1$ and $\omega\tau_e \ll 1$, respectively.

Since σ is such a widely varying parameter, the values of l^* also have a wide range. Table 15.3.2 illustrates this fact. In water having physiological conductivity

(in flesh), the characteristic times would coincide if the length scale were about 12 cm at a characteristic frequency ($\omega\tau_e = 1$) f = 45 MHz. For lengths less than about 12 cm, the ordering would be as in Fig. 15.3.2a and for longer lengths, as in Fig. 15.3.2b. However, in copper it would require that the characteristic length be less than an atomic distance to make τ_e exceed τ_m. On such a short length scale, the conductivity model is not valid.[1] In the opposite extreme, a layer of corn oil about 60,000 miles thick would be required to make τ_m exceed τ_e!

Example 15.3.1. Overview of TEM Fields in Open Circuit Transmission Line Filled with Lossy Material (continued)

In Sec. 14.8, we considered the nature of the electromagnetic fields in a conductor sandwiched between "perfectly conducting" plates. Example 14.8.2 was devoted to an overview of electromagnetic regimes pictured in the length-time plane, Fig. 14.8.3, redrawn as Fig. 15.3.3. As the frequency was raised in that example with $l \gg l^*$, the line $\omega\tau_m = 1$ indicated that quasi-stationary conduction had given way to magnetic diffusion (the resistor had become a system of distributed resistors and inductors). In that specific example, this was the line at which the long wave approximation broke down, $\beta l \approx 1$. With $l \ll l^*$, we have seen that as the frequency was raised, the crossing of the line $\omega\tau_e = 1$ denoted that a resistor had changed into a system of distributed resistors in parallel with distributed capacitors.

This example has a misleading simplicity that can be traced to the fact that it actually possesses more than one length scale and conductivity. To impose the TEM fields by means of the source, it was necessary to envision the slab of conductor as making perfect electrical contact with perfectly conducting plates. In reality, the boundary condition used to represent these plates implies conditions on still other parameters, notably the electrical properties and thickness of the plates.

As the frequency is raised for a system in the upper half-plane (l larger than the matching length), why do we not see a transition to electromagnetic waves at $\omega\tau_{em} = 1$ rather than $\omega\tau_e = 1$? The perfectly conducting plates force the displacement current to compete with the conduction current on its "own" length scale (either the skin depth or the electromagnetic wavelength). Thus, in this example, we do not make a transition from magnetic diffusion (with a penetration length determined by the skin depth δ) to a damped electromagnetic wave (with a decay length of twice l^*) until the electromagnetic wavelength $\lambda = 2\pi/\sqrt{\mu\epsilon}\omega$ has become as short as the skin depth. Both are decreasing with increasing frequency. However, the skin depth (which decreases as $1/\sqrt{\omega}$) is equal to the wavelength (which decreases as $1/\omega$) only as the frequency reaches $\omega\tau_e = 2\pi^2$ (for present purposes, "$\omega\tau_e = 1$").

In the lower half-plane, where systems are smaller than the characteristic length, why was the transition at $\omega\tau_e = 1$ evident in the surface current density in the plates but not in the spatial distribution of the fields? The electric field was found to remain uniform until the frequency had been raised to $\omega\tau_{em} = 1$. Here again, the "perfectly conducting" plates obscure the general situation. The conducting block has uniform conductivity. As a result, it can support no volume charge density, regardless of the frequency. In the EQS limit, it is the charge density that shapes the electric field distribution. Here the only charges are at the interfaces between the block and the perfectly conducting plates. Until magnetic induction comes into play at $\omega\tau_{em} = 1$, these surface charges assume whatever distribution they must

[1] Put another way, on a time scale as short as the charge relaxation time in a metal, the inertia of the electrons responsible for the conduction would come into play. (S. Gruber, "On Charge Relaxation in Good Conductors," *Proc. IEEE*, Vol. 61 (1973), pp. 237-238. The inertial force is not included in the conductivity model.

to be consistent with an irrotational electric field. As a result, the plates make the EQS fields essentially uniform, and the appropriate model simplifies to one lumped parameter C in parallel with one lumped parameter R.

15.4 ENERGY, POWER, AND FORCE

Maxwell's equations attribute an excitation ($\mathbf{E}$ and $\mathbf{H}$) to every point in space. Consistent with this view, energy density and power flow density must be associated with every point in space as well. Poynting's theorem, Sec. 11.2, does that. Poynting's theorem identifies energy storage and dissipation associated with the polarization and magnetization processes.

Each self-consistent macroscopic set of equations must possess an energy conservation principle, maybe including terms describing transformation of energy into other forms, like heat, if dissipation is present. An example was given in Sec. 11.3 of a conservation principle for the approximate description of EQS fields with a density of power flow vector that was different from $\mathbf{E} \times \mathbf{H}$. This alternate form of an energy conservation principle was better suited to the EQS description, because it did not contain the $\mathbf{H}$ field which is not usually evaluated in the EQS approximation. Instead, the charge conservation law (derived from Ampère's law) was used to find the currents flowing in the system.

An important application of the concept of energy was the derivation of the force on macroscopic material. The force on a dielectric or magnetic object computed from energy change can include correctly the contributions to the net force from fringing fields even though the field expressions neglect them, if the energy associated with the fringing field does not change in a small displacement of the object.

Energy and Quasistatics. Because magnetic and electric energy storages, respectively, are negligible in EQS and MQS systems, a comparison of energy densities can also be used to establish the validity of a quasistatic approximation. Specifically, we will see that in systems characterized by one length scale, the ratio of magnetic to electric energy storage takes the form

$$\frac{w_m}{w_e} = K\left(\frac{l}{l^*}\right)^2 \tag{1}$$

where l^* is the characteristic length

$$l^* \equiv \frac{1}{\sigma}\sqrt{\epsilon/\mu} \tag{2}$$

familiar from Secs. 14.8[2] and 15.3 and K is of the order of unity.

[2] In Sec. 14.8, twice this length was found to be the decay length for an electromagnetic wave.

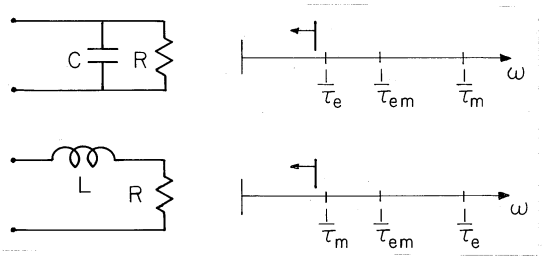


Fig. 15.4.1 Low-frequency equivalent circuits and associated ordering to reciprocal times.

Energy arguments can also be the basis for simple models that modestly extend the frequency range of quasi-stationary conduction. A second object in this section is the illustration of how these models are deduced.

As the frequency is raised, one of two processes leads to a modification in the field sources, and hence of the fields. If l is less than l^*, so that $1/\tau_e$ is the first reciprocal characteristic time encountered as ω is raised, then the current density is progressively altered to supply unpaired charge to regions of nonuniform σ and ϵ. Alternatively, if l is larger than l^*, so that $1/\tau_m$ is the shortest reciprocal characteristic time, magnetic induction alters the current density notonly in its magnitude and time dependence but in its spatial distribution as well.

Fully dynamic fields, in which all three (or more) characteristic times are of the same order of magnitude are difficult to analyze because the distribution of sources is not known until the fields have been solved selfconsistently, often a difficult task. However, if the frequency is lower than the lowest reciprocal time, the field distributions still approximate those for stationary conduction. This makes it possible to approximate the energy storages, and hence to identify both the conditions for the system to be EQS or MQS and to develop models that are appropriate for frequencies approaching the lowest reciprocal characteristic time.

The first step in this process is to determine the quasi-stationary fields. The second is to use these fields to evaluate the total electric and magnetic energy storages as well as the total energy dissipation.

$$w_e = \int_V \frac{1}{2}\epsilon \mathbf{E}\cdot\mathbf{E}dv; \quad w_m = \int_V \frac{1}{2}\mu \mathbf{H}\cdot\mathbf{H}dv; \quad p_d = \int_V \sigma \mathbf{E}\cdot\mathbf{E}dv \tag{3}$$

If it is found that the ratio of magnetic to electric energy storage takes the form of (1), and that if l is either very small or very large compared to the characteristic length, then we can presumably model the system by either the R-C or the L-R circuit of Fig. 15.4.1.

As the third step, parameters in these circuits are determined by comparing w_e, w_m, and p_d, as found from the QSC fields using (3), to these quantities determined in terms of the circuit variables.

$$w_e = \frac{1}{2}Cv^2; \qquad w_m = \frac{1}{2}Li^2; \qquad p_d = Ri^2 \tag{4}$$

In general, the circuit models are valid only up to frequencies approaching, but not equal to, the lowest reciprocal time for the system. In the following example, we

will find that the R-C circuit is an exact model for the EQS system, so that the model is valid even for frequencies beyond $1/\tau_e$. However, because the fields can be strongly altered by rate processes if the frequency is equal to the lowest reciprocal time, it is generally not appropriate to use the equivalent circuits except to take into account energy storage effects coming into play as the frequency *approaches* $1/RC$ or R/L.

Example 15.4.1. Energy Method for Deriving an Equivalent Circuit

The block of uniformly conducting material sandwiched between plane parallel perfectly conducting plates, as shown in Fig. 14.8.1, was the theme of Sec. 14.8. This gives the opportunity to see how the low-frequency model developed here fits into the general picture provided by that section.

In the conducting block, the quasi-stationary conduction (QSC) fields have the distributions

$$\mathbf{E} = \frac{v}{a}\mathbf{i}_\mathbf{x}; \qquad \mathbf{H} = \frac{\sigma v}{a} z \mathbf{i}_\mathbf{y} \tag{5}$$

The total electric and magnetic energies and total dissipation follow from an integration of the respective densities over the volume of the system in accordance with (3)

$$w_e = wal\frac{1}{2}\epsilon\frac{v^2}{a^2}; \quad w_m = \frac{wa\mu}{6}\left(\frac{\sigma v}{a}\right)^2 l^3; \quad p_d = \frac{a}{wl\sigma}i^2 \tag{6}$$

where v and i are the terminal voltage and current.

Comparison of (4) and (6) shows that

$$C = \frac{lw\epsilon}{a}; \qquad L = \frac{a\mu l}{3w}; \qquad R = \frac{a}{lw\sigma} \tag{7}$$

Because the entire volume of the system considered here has uniform properties, there are no sources of the electric field (charge densities) in the volume of the system. As a result, the capacitance C found here is no different than if the volume were filled with a perfectly insulating material. By contrast, if the slab were of nonuniform conductivity, as in Example 7.2.1, the capacitance, and hence equivalent circuit, found by this energy method would not be so "obvious."

The inductance of the equivalent circuit does reflect a distribution of the source of the magnetic field, for the current density is distributed throughout the volume of the slab. By using the energy argument, we have acknowledged that there is a distribution of current paths, each having a different flux linkage. Strictly, when the flux linked by any current path is the same, inductance is only defined for perfectly conducting current paths.

Which equivalent circuit is appropriate? Here we decide by comparing the stored energies.

$$\frac{w_m}{w_e} = \frac{1}{3}\left(\frac{l}{l^*}\right)^2 \tag{8}$$

Thus, as we anticipated with (1), the system can be EQS if $l \ll l^*$ and MQS if $l \gg l^*$. The appropriate equivalent circuit in Fig. 15.4.1 is the $R-C$ circuit if $l \ll l^*$ and is the $L-R$ circuit if $l \gg l^*$.

The simple circuits of Fig. 15.4.1 are not generally valid if the frequency reaches the reciprocal of the longest characteristic time, since the field distributions

have changed by then. In terms of the circuit elements, this means that in order for the circuits to be equivalent to the physical system, the time rates of change must remain slow enough so that $\omega RC < 1$ or $\omega L/R < 1$.

P R O B L E M S

15.1 Source and Material Configurations

15.1.1 A theme from Chap. 5 on has been the use of orthogonal modes to represent field solutions and satisfy boundary conditions. Make a table identifying examples and problems illustrating this theme.

15.2 Macroscopic Media

15.2.1 Field lines in the vicinity of a spherical interface between materials (a) and (b) are shown in Fig. P15.2.1. In each case, describe four idealized physical situations for which the field lines would be appropriate.

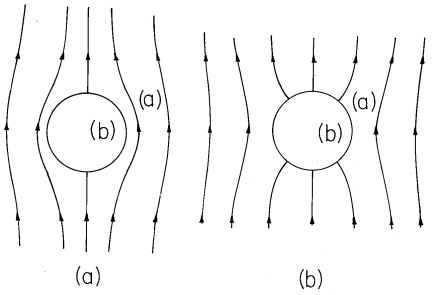


Fig. P15.2.1

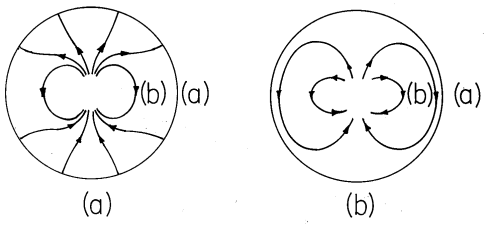


Fig. P15.2.2

15.2.2 Dipoles at the center of a spherical region and associated fields are shown in Fig. P15.2.2. In each case, describe four appropriate idealized physical situations.

15.3 Characteristic Times, Physical Processes, and Approximations

15.3.1 In Fig. 15.3.3, a typical length and time are considered the independent parameters. Suppose that we wish to see the effect of varying the conductivity with the size held fixed. For example, with not only the size but the frequency fixed, the material might be cooling from a very high temperature where it is molten and an ionic conductor to a low temperature where it is a good insulator. Using the conductivity rather than the length for the vertical axis, select a normalization time for the horizontal axis that is independent of conductivity, and construct a diagram analogous to Fig. 15.3.3. Identify a "characteristic" conductivity, σ^*, for normalizing the conductivity.

15.3.2 Figure 7.5.3 shows a circular conductor carrying a current that is returned through a coaxial "perfectly" conducting "can." For sufficiently low frequencies, the electric field and surface charge densities are as shown in Fig. 7.5.4. The magnetic field is described in Example 11.3.1 where the effect of the washer-shaped conductor is neglected.

(a) Sketch $\mathbf{E}$ and $\mathbf{H}$, as well as the distribution of ρ_u and $\mathbf{J}_u$.
(b) Suppose that the length L is on the order of the radius (a), and (b) is not much smaller than (a). As the frequency is raised, argue that either charge relaxation will first dominate in revising the field distribution as in Fig. P15.3.2a, or magnetic diffusion will dominate as in Fig. P15.3.2b. In the latter case, describe the current distribution in the conductor by associating it with an example and a demonstration in this text.
(c) With L allowed to be large compared to (a), under what circumstances will the system behave as the lossy transmission line of Fig. 14.7.1 with $G = 0$? Discuss the EQS and MQS limits where this model applies.

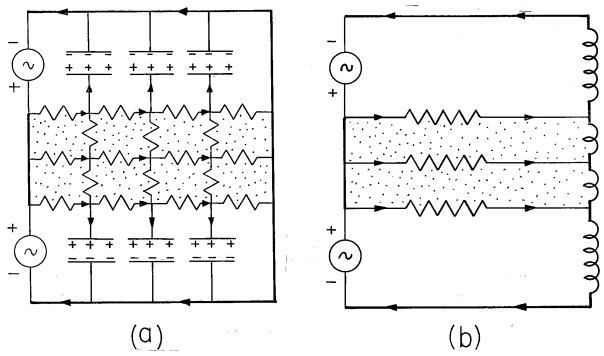


Fig. P15.3.2

15.4 Energy, Power, and Force

15.4.1 For the system considered in Prob. 15.3.2, use the energy approach to

identify the parameters in the low frequency equivalent circuits of Fig. 15.4.1, and write the ratio of energies in the form of (1). Ignore the effect of the washer-shaped conductor.

1

APPENDIX

1.1 VECTOR OPERATIONS

A vector is a quantity which possesses magnitude and direction. In order to describe a vector mathematically, a coordinate system having orthogonal axes is usually chosen. In this text, use is made of the Cartesian, circular cylindrical, and spherical coordinate systems. In these three-dimensional systems, any vector is completely described by three scalar quantities. For example, in Cartesian coordinates, a vector is described with reference to mutually orthogonal coordinate axes. Then the magnitude and orientation of the vector are described by specifying the three projections of the vector onto the three coordinate axes.

In representing a vector[1] $\mathbf{A}$ mathematically, its direction along the three orthogonal coordinate axes must be given. The direction of each axis is represented by a unit vector $\mathbf{i}$, that is, a vector of unit magnitude directed along the axis. In Cartesian coordinates, the three unit vectors are denoted $\mathbf{i_x}$, $\mathbf{i_y}$, $\mathbf{i_z}$. In cylindrical coordinates, they are $\mathbf{i_r}$, $\mathbf{i}_\phi$, $\mathbf{i_z}$, and in spherical coordinates, $\mathbf{i_r}$, $\mathbf{i}_\theta$, $\mathbf{i}_\phi$. $\mathbf{A}$, then, has three vector components, each component corresponding to the projection of $\mathbf{A}$ onto the three axes. Expressed in Cartesian coordinates, a vector is defined in terms of its components by

$$\mathbf{A} = A_x\mathbf{i_x} + A_y\mathbf{i_y} + A_z\mathbf{i_z} \tag{1}$$

These components are shown in Fig. A.1.1.

[1] Vectors are usually indicated either with boldface characters, such as $\mathbf{A}$, or by drawing a line (or an arrow) above a character to indicate its vector nature, as in $\bar{A}$ or $\vec{A}$.

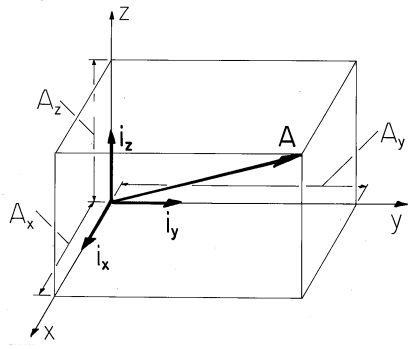


Fig. A.1.1 Vector **A** represented by its components in Cartesian coordinates and unit vectors **i**.

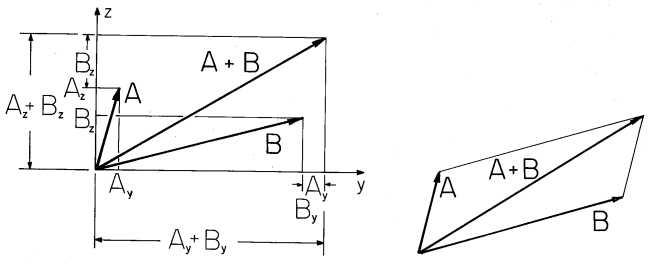


Fig. A.1.2 (a) Graphical representation of vector addition in terms of specific coordinates. (b) Representation of vector addition independent of specific coordinates.

Vector Addition. The sum of two vectors $\mathbf{A} = A_x\mathbf{i_x} + A_y\mathbf{i_y} + A_z\mathbf{i_z}$ and $\mathbf{B} = B_x\mathbf{i_x} + B_y\mathbf{i_y} + B_z\mathbf{i_z}$ is effected by adding the coefficients of each of the components, as shown in two dimensions in Fig. A.1.2a.

$$\mathbf{A} + \mathbf{B} = (A_x + B_x)\mathbf{i_x} + (A_y + B_y)\mathbf{i_y} + (A_z + B_z)\mathbf{i_z} \tag{2}$$

From (2), then, it should be clear that vector addition is both commutative, $\mathbf{A}+\mathbf{B} = \mathbf{B} + \mathbf{A}$, and associative, $(\mathbf{A} + \mathbf{B}) + \mathbf{C} = \mathbf{A} + (\mathbf{B} + \mathbf{C})$.

Graphically, vector summation can be performed without regard to the coordinate system, as shown in Fig. A.1.2b, by noticing that the sum $\mathbf{A} + \mathbf{B}$ is a vector directed along the diagonal of a parallelogram formed by **A** and **B**.

It should be noted that the representation of a vector in terms of its components is dependent on the coordinate system in which it is carried out. That is, changes of coordinate system will require an appropriate vector transformation. Further, the variables used must also be transformed. The transformation of variables and vectors from one coordinate system to another is illustrated by considering a transformation from Cartesian to spherical coordinates.

Example 1.1.1. Transformation of Variables and Vectors

We are given variables in terms of x, y, and z and vectors such as $\mathbf{A} = A_x\mathbf{i_x} + A_y\mathbf{i_y} + A_z\mathbf{i_z}$. We wish to obtain variables in terms of r, θ, and ϕ and vectors expressed as $\mathbf{A} = A_r\mathbf{i_r} + A_\theta\mathbf{i}_\theta + A_\phi\mathbf{i}_\phi$. In Fig. A.1.3a, we see that the point P has two

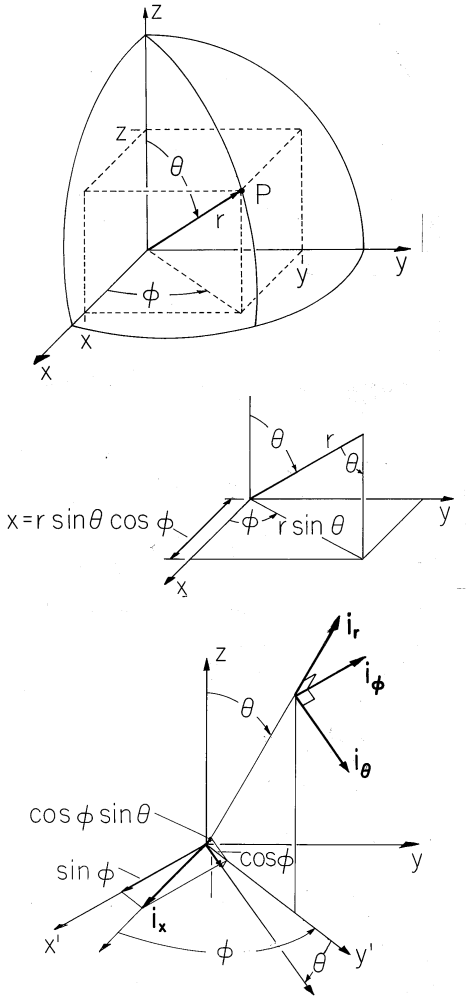


Fig. A.1.3 Specification of a point P in Cartesian and spherical coordinates. (b) Transformation from Cartesian coordinate x to spherical coordinates. (c) Transformation of unit vector in x direction into spherical coordinate coordinates.

representations, one involving the variables x, y and z and the other, r, θ and ϕ. In particular, from Fig. A.1.3b, x is related to the spherical coordinates by

$$x = r \sin\theta \cos\phi \tag{3}$$

In a similar way, the variables y and z evaluated in spherical coordinates can be shown to be

$$y = r \sin\theta \sin\phi \tag{4}$$

$$z = r \cos\theta \tag{5}$$

The vector $\mathbf{A}$ is transformed by resolving each of the unit vectors $\mathbf{i_x}$, $\mathbf{i_y}$, $\mathbf{i_z}$ in terms of the unit vectors in spherical coordinates. For example, $\mathbf{i_x}$ can first be

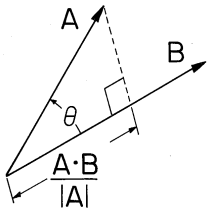


Fig. A.1.4 Illustration for definition of dot product.

resolved into components in the orthogonal coordinates (x', y', z) shown in Fig. A.1.3c. By definition, y' is along the intersection of the $\phi =$ constant and the $x-y$ planes. Also in the $x-y$ plane is x', which is perpendicular to the $y'-z$ plane. Thus, $\sin\phi$, $\cos\phi$, and 0 are the components of $\mathbf{i_x}$ along the x', y', and z axes respectively. These components are in turn resolved into components along the spherical coordinate directions by recognizing that the component $\sin\phi$ along the x' axis is in the $-\mathbf{i}_\phi$ direction while the component of $\cos\phi$ along the y' axis resolves into components $\cos\phi\cos\theta$ in the direction of $\mathbf{i}_\theta$, and $\cos\phi\sin\theta$ in the $\mathbf{i_r}$ direction. Thus,

$$\mathbf{i_x} = \sin\theta\cos\phi\mathbf{i_r} + \cos\theta\cos\phi\mathbf{i}_\theta - \sin\phi\mathbf{i}_\phi \tag{6}$$

Similarly,

$$\mathbf{i_y} = \sin\theta\sin\phi\mathbf{i_r} + \cos\theta\sin\phi\mathbf{i}_\theta + \cos\phi\mathbf{i}_\phi \tag{7}$$

$$\mathbf{i_z} = \cos\theta\mathbf{i_r} - \sin\theta\mathbf{i}_\theta \tag{8}$$

It must be emphasized that the concept of a vector is independent of the coordinate system. (In the same sense, in Chaps. 2 and 4, vector operations are defined independently of the coordinate system in which they are expressed.) A vector can be visualized as having the direction and magnitude of an arrow-tipped line element. This picture makes it possible to deal with vectors in a geometrical language that is independent of the choice of a particular coordinate system, one that will now be used to define the most important vector operations.

For analytical or numerical purposes, the operations are usually carried out in coordinate notation. Then, as illustrated, either in the text that follows or in the problems, each operation will be evaluated in a Cartesian coordinate system.

Definition of Scalar Product. Given vectors $\mathbf{A}$ and $\mathbf{B}$ as illustrated in Fig. A.1.4, the scalar, or dot product, between the two vectors is defined as

$$\mathbf{A}\cdot\mathbf{B} = |\mathbf{A}||\mathbf{B}|\cos\theta \tag{9}$$

where θ is the angle between the two vectors.

It follows directly from its definition that the scalar product is commutative.

$$\mathbf{A}\cdot\mathbf{B} = \mathbf{B}\cdot\mathbf{A} \tag{10}$$

The scalar product is also distributive.

$$(\mathbf{A}+\mathbf{B})\cdot\mathbf{C} = \mathbf{A}\cdot\mathbf{C} + \mathbf{B}\cdot\mathbf{C} \tag{11}$$

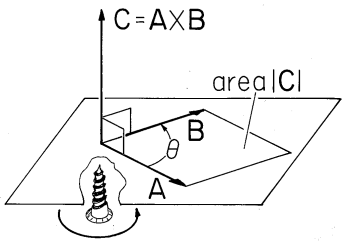


Fig. A.1.5 Illustration for definition of vector-product.

To see this, note that $\mathbf{A} \cdot \mathbf{C}$ is the projection of $\mathbf{A}$ onto $\mathbf{C}$ times the magnitude of $\mathbf{C}$, $|\mathbf{C}|$, and $\mathbf{B} \cdot \mathbf{C}$ is the projection of $\mathbf{B}$ onto $\mathbf{C}$ times $|\mathbf{C}|$. Because projections are additive, (11) follows.

These two properties can be used to define the scalar product in terms of the vector components in Cartesian coordinates. According to the definition of the unit vectors,

$$\mathbf{i_x} \cdot \mathbf{i_x} = \mathbf{i_y} \cdot \mathbf{i_y} = \mathbf{i_z} \cdot \mathbf{i_z} = 1$$

$$\mathbf{i_x} \cdot \mathbf{i_y} = \mathbf{i_x} \cdot \mathbf{i_z} = \mathbf{i_y} \cdot \mathbf{i_z} = 0 \tag{12}$$

With $\mathbf{A}$ and $\mathbf{B}$ expressed in terms of these components, it follows from the distributive and commutative properties that

$$\mathbf{A} \cdot \mathbf{B} = A_x B_x + A_y B_y + A_z B_z \tag{13}$$

Thus, in agreement with (9), the square of the magnitude of a vector is

$$\mathbf{A} \cdot \mathbf{A} = |\mathbf{A}|^2 = A_x^2 + A_y^2 + A_z^2 \tag{14}$$

Definition of Vector Product. The cross-product of vectors $\mathbf{A}$ and $\mathbf{B}$ is a vector $\mathbf{C}$ having a magnitude

$$|\mathbf{C}| = |\mathbf{A}||\mathbf{B}| \sin\theta \tag{15}$$

and having a direction perpendicular to both $\mathbf{A}$ and $\mathbf{B}$. Geometrically, the magnitude of $\mathbf{C}$ is the area of the parallelogram formed by the vectors $\mathbf{A}$ and $\mathbf{B}$. The vector $\mathbf{C}$ has the direction of advance of a right-hand screw, as though driven by rotating $\mathbf{A}$ into $\mathbf{B}$. Put another way, a right-handed coordinate system is formed by $\mathbf{A} - \mathbf{B} - \mathbf{C}$, as is shown in Fig. A.1.5. The commonly accepted notation for the cross-product is

$$\mathbf{C} = \mathbf{A} \times \mathbf{B} \tag{16}$$

It is useful to note that if the vector $\mathbf{A}$ is resolved into two mutually perpendicular vectors, $\mathbf{A} = \mathbf{A}_\perp + \mathbf{A}_\parallel$, where $\mathbf{A}_\perp$ lies in the plane of $\mathbf{A}$ and $\mathbf{B}$ and is perpendicular to $\mathbf{B}$ and $\mathbf{A}_\parallel$ is parallel to $\mathbf{B}$, then

$$\mathbf{A} \times \mathbf{B} = \mathbf{A}_\perp \times \mathbf{B} \tag{17}$$

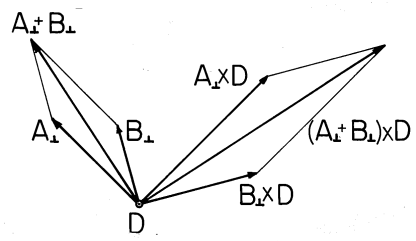


Fig. A.1.6 Graphical representation showing that the vector-product is distributive.

This equality follows from the fact that both cross-products have equal magnitude (since $|\mathbf{A}_\perp \times \mathbf{B}| = |\mathbf{A}_\perp||\mathbf{B}|$ and $|\mathbf{A}|_\perp| = |\mathbf{A}| \sin\theta$) and direction (perpendicular to both $\mathbf{A}$ and $\mathbf{B}$).

The distributive property for the cross-product,

$$(\mathbf{A} + \mathbf{B}) \times \mathbf{D} = \mathbf{A} \times \mathbf{D} + \mathbf{B} \times \mathbf{D} \tag{18}$$

can be shown using (17) and the geometrical construction in Fig. A.1.6 as follows. First, note that $(\mathbf{A} + \mathbf{B})_\perp = (\mathbf{A}_\perp + \mathbf{B}_\perp)$, where $\perp$ denotes a component in the planes of $\mathbf{A}$ and $\mathbf{D}$ or $\mathbf{B}$ and $\mathbf{D}$, respectively, and perpendicular to $\mathbf{D}$. Thus,

$$(\mathbf{A} + \mathbf{B}) \times \mathbf{D} = (\mathbf{A} + \mathbf{B})_\perp \times \mathbf{D} = (\mathbf{A}_\perp + \mathbf{B}_\perp) \times \mathbf{D} \tag{19}$$

Now, we need only show that

$$(\mathbf{A}_\perp + \mathbf{B}_\perp) \times \mathbf{D} = \mathbf{A}_\perp \times \mathbf{D} + \mathbf{B}_\perp \times \mathbf{D} \tag{20}$$

This equation is given graphical expression in Fig. A.1.6 by the vectors $\mathbf{A}_\perp$, $\mathbf{B}_\perp$, and their sum. To within a factor of $|\mathbf{D}|$, the three vectors $\mathbf{A}_\perp \times \mathbf{D}$, $\mathbf{B}_\perp \times \mathbf{D}$, and their sum, are, respectively, the vectors $\mathbf{A}_\perp$, $\mathbf{B}_\perp$, and their sum, rotated by 90 degrees. Thus, the vector addition property already shown for $\mathbf{A}_\perp + \mathbf{B}_\perp$ also applies to $\mathbf{A}_\perp \times \mathbf{D} + \mathbf{B}_\perp \times \mathbf{D}$.

Because interchanging the order of two vectors calls for a reassignment of the direction of the product vector (the direction of $\mathbf{C}$ in Fig. A.1.5), the commutative property does not hold. Rather,

$$\mathbf{A} \times \mathbf{B} = -\mathbf{B} \times \mathbf{A} \tag{21}$$

Using the distributive law, the vector product of two vectors can be constructed in terms of their Cartesian coordinates by using the following properties of the vector products of the unit vectors.

$$\begin{aligned} \mathbf{i_x} \times \mathbf{i_x} &= 0 \qquad \mathbf{i_x} \times \mathbf{i_y} = \mathbf{i_z} \\ \mathbf{i_y} \times \mathbf{i_y} &= 0 \qquad \mathbf{i_y} \times \mathbf{i_z} = -\mathbf{i_z} \times \mathbf{i_y} = \mathbf{i_x} \\ \mathbf{i_z} \times \mathbf{i_z} &= 0 \qquad \mathbf{i_x} \times \mathbf{i_z} = -\mathbf{i_z} \times \mathbf{i_x} = -\mathbf{i_y} \end{aligned} \tag{22}$$

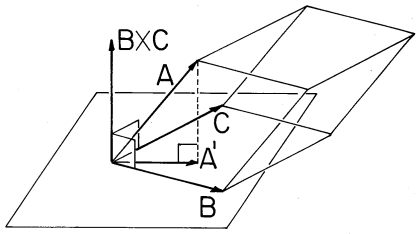


Fig. A.1.7 Graphical representation of scalar triple product.

Thus,

$$\begin{aligned}\mathbf{A}\times\mathbf{B} =& \mathbf{i_x}(A_yB_z - A_zB_y) + \mathbf{i_y}(A_zB_x - A_xB_z)\\ &+ \mathbf{i_z}(A_xB_y - A_yB_x)\end{aligned} \tag{23}$$

A useful mnemonic for finding the cross-product in Cartesian coordinates is realized by noting that the right-hand side of (23) is the determinant of a matrix:

$$\mathbf{A}\times\mathbf{B} = \begin{vmatrix} \mathbf{i_x} & \mathbf{i_y} & \mathbf{i_z} \\ A_x & A_y & A_z \\ B_x & B_y & B_z \end{vmatrix} \tag{24}$$

The Scalar Triple Product. The definition of the scalar triple product of vectors $\mathbf{A}$, $\mathbf{B}$, and $\mathbf{C}$ follows from Fig. A.1.7, and the definition of the scalar and vector products.

$$\mathbf{A}\cdot(\mathbf{B}\times\mathbf{C}) = [|\mathbf{A}|\cos(\mathbf{A},\mathbf{B}\times\mathbf{C})][|\mathbf{B}||\mathbf{C}|\sin(\mathbf{B},\mathbf{C})] \tag{25}$$

The scalar triple product is equal to the volume of the parallelepiped having the three vectors for its three bases. That is, in (25) the second term in square brackets is the area of the base parallelogram in Fig. A.1.7 while the first is the height of the parallelopiped. The scalar triple product is positive if the three vectors form a right-handed coordinate system in the order in which they are written; otherwise it is negative. Hence, a cyclic rearrangement in the order of the vectors leaves the value of the product unchanged.

$$\mathbf{A}\cdot(\mathbf{B}\times\mathbf{C}) = \mathbf{B}\cdot(\mathbf{C}\times\mathbf{A}) = \mathbf{C}\cdot(\mathbf{A}\times\mathbf{B}) \tag{26}$$

It follows that the placing of the cross and the dot in a scalar triple product is arbitrary. The cross and dot can be interchanged without affecting the product.

Using the rules for evaluating the dot product and the cross-product in Cartesian coordinates, we have

$$\mathbf{A}\cdot(\mathbf{B}\times\mathbf{C}) = A_x(B_yC_z - B_zC_y) + A_y(B_zC_x - B_xC_z) + A_z(B_xC_y - B_yC_x) \tag{27}$$

The Double Cross-Product. Consider the vector product $\mathbf{A}\times(\mathbf{B}\times\mathbf{C})$. Is there another, sometimes more useful, way of expressing this double cross-product?

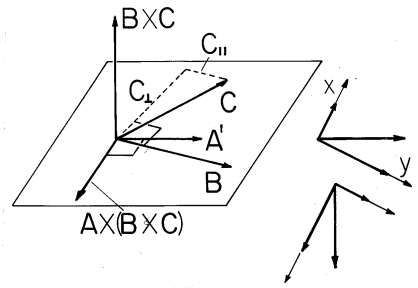


Fig. A.1.8 Graphical representation of double cross-product.

Since the product $\mathbf{B} \times \mathbf{C}$ is perpendicular to the plane defined by $\mathbf{B}$ and $\mathbf{C}$, then the final product $\mathbf{A} \times (\mathbf{B} \times \mathbf{C})$ must lie in the plane of $\mathbf{B}$ and $\mathbf{C}$. Hence, the vector product must be expressible as a linear combination of the vectors $\mathbf{B}$ and $\mathbf{C}$. One way to find the coefficients of this linear combination is to evaluate the product in Cartesian coordinates. Here we prefer to use a geometric derivation.

Because the vector $\mathbf{B} \times \mathbf{C}$ is perpendicular to the plane defined by the vectors $\mathbf{B}$ and $\mathbf{C}$, it follows from Fig. A.1.7 that

$$\mathbf{A} \times (\mathbf{B} \times \mathbf{C}) = \mathbf{A}' \times (\mathbf{B} \times \mathbf{C}) \tag{28}$$

where $\mathbf{A}'$ is the projection of $\mathbf{A}$ onto the plane defined by $\mathbf{B}$ and $\mathbf{C}$. Next, we separate the vector $\mathbf{C}$ into a component parallel to $\mathbf{B}$, $\mathbf{C}_{\|}$, and a component perpendicular to $\mathbf{B}$, $\mathbf{C}_{\perp}$, as shown by Fig. A.1.8, so that

$$\mathbf{A} \times (\mathbf{B} \times \mathbf{C}) = \mathbf{A}' \times (\mathbf{B} \times \mathbf{C}_{\perp}) \tag{29}$$

Then, according to the properties of the cross-product, the magnitude of the vector product is given by

$$|\mathbf{A} \times (\mathbf{B} \times \mathbf{C})| = |\mathbf{A}'||\mathbf{B}||\mathbf{C}_{\perp}| \tag{30}$$

and the direction of the vector product is orthogonal to $\mathbf{A}'$ and lies in the plane defined by the vectors $\mathbf{B}$ and $\mathbf{C}$, as shown in Fig. A.1.8

A rule for constructing a vector perpendicular to a given vector, $\mathbf{A}'$, in an $x - y$ plane is as follows. First, the two components of $\mathbf{A}'$ with respect to any two orthogonal axes (x, y) are determined. Here these are the directions of $\mathbf{C}_{\perp}$ and $\mathbf{B}$ with components $\mathbf{A}' \cdot \mathbf{C}_{\perp}$, and $\mathbf{A}' \cdot \mathbf{B}$, respectively. Then, a new vector is constructed by interchanging the x and y components and changing the sign of one of them. According to this rule, Fig. A.1.8 shows that the vector $\mathbf{A} \times (\mathbf{B} \times \mathbf{C})$ is given by

$$\mathbf{A} \times (\mathbf{B} \times \mathbf{C}) = (\mathbf{A}' \cdot \mathbf{C}_{\perp})\mathbf{B} - (\mathbf{A}' \cdot \mathbf{B})\mathbf{C}_{\perp} \tag{31}$$

Now, because $\mathbf{C}_{\|}$ has the same direction as $\mathbf{B}$,

$$(\mathbf{A}' \cdot \mathbf{B})\mathbf{C}_{\|} = (\mathbf{A}' \cdot \mathbf{C}_{\|})\mathbf{B}, \tag{32}$$

and addition of (31) gives

$$\mathbf{A} \times (\mathbf{B} \times \mathbf{C}) = \mathbf{A}' \cdot (\mathbf{C}_{\perp} + \mathbf{C}_{\|})\mathbf{B} - (\mathbf{A}' \cdot \mathbf{B})(\mathbf{C}_{\perp} + \mathbf{C}_{\|}) \tag{33}$$

Now observe that $\mathbf{A}' \cdot \mathbf{C} = \mathbf{A} \cdot \mathbf{C}$ and $\mathbf{A}' \cdot \mathbf{B} = \mathbf{A} \cdot \mathbf{B}$ (which follow from the definition of $\mathbf{A}'$ as the projection of $\mathbf{A}$ into the $\mathbf{B} - \mathbf{C}$ plane), and the double cross-product becomes

$$\mathbf{A} \times (\mathbf{B} \times \mathbf{C}) = (\mathbf{A} \cdot \mathbf{C})\mathbf{B} - (\mathbf{A} \cdot \mathbf{B})\mathbf{C} \tag{34}$$

This result is particularly convenient because it does not contain any special notation or projections.

The vector identities found in this Appendix are summarized in Table III at the end of the text.

2

APPENDIX

2.1 LINE AND SURFACE INTEGRALS

Consider a path connecting points (a) and (b) as shown in Fig. A.2.1. Assume that a vector field $\mathbf{A}(\mathbf{r})$ exists in the space in which the path is situated. Then the line integral of $\mathbf{A}(\mathbf{r})$ is defined by

$$\int_{(a)}^{(b)} \mathbf{A} \cdot d\mathbf{s} \tag{1}$$

To interpret (1), think of the path between (a) and (b) as subdivided into differential vector segments $d\mathbf{s}$. At every vector segment, the vector $\mathbf{A}(\mathbf{r})$ is evaluated and the dot product is formed. The line integral is then defined as the sum of these dot products in the limit as $d\mathbf{s}$ approaches zero. A line integral over a path that closes on itself is denoted by the symbol $\oint \mathbf{A} \cdot d\mathbf{s}$.

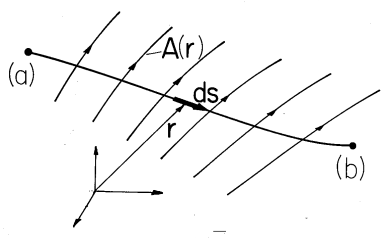


Fig. A.2.1 Configuration for integration of vector field $\mathbf{A}$ along line having differential length $d\mathbf{s}$ between points (a) and (b).

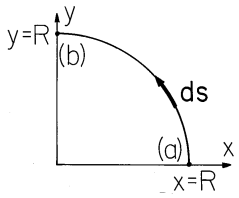


Fig. A.2.2 Integration line having shape of quarter segment of a circle with radius R and differential element $d\mathbf{s}$.

To perform a line integration, the integral must first be reduced to a form that can be evaluated using the rules of integral calculus. This is done with the aid of a coordinate system. The following example illustrates this process.

Example 2.1.1. Line Integral

Given the two-dimensional vector field

$$\mathbf{A} = x\mathbf{i_x} + axy\,\mathbf{i_y} \tag{2}$$

find the line integral along a quarter circle of radius R as shown in Fig. A.2.2.

Using a Cartesian coordinate system, the differential line segment $d\mathbf{s}$ has the components dx and dy.

$$d\mathbf{s} = \mathbf{i_x}dx + \mathbf{i_y}dy \tag{3}$$

Now x and y are not independent but are constrained by the fact that the integration path follows a circle defined by the equation

$$x^2 + y^2 = R^2 \tag{4}$$

Differentiation of (4) gives

$$2xdx + 2ydy = 0 \tag{5}$$

and therefore

$$dy = -\frac{x}{y}dx \tag{6}$$

Thus, the dot product $\mathbf{A} \cdot d\mathbf{s}$ can be written as a function of the variable x alone.

$$\mathbf{A} \cdot d\mathbf{s} = xdx + a\,xydy = (x - ax^2)dx \tag{7}$$

When the path is described in the sense shown in Fig. A.2.4, x decreases from R to zero. Therefore,

$$\int \mathbf{A} \cdot d\mathbf{s} = \int_R^0 (x - ax^2)dx = \Big(\frac{x^2}{2} - \frac{ax^3}{3}\Big)\Big|_R^0 = \frac{aR^3}{3} - \frac{R^2}{2} \tag{8}$$

If the path is not expressible in terms of an analytic function, the evaluation of the line integral becomes difficult. If everything else fails, numerical methods can be employed.

Surface Integrals. Given a vector field $\mathbf{A}(\mathbf{r})$ in a region of space containing a specified (open or closed) surface S, an important form of the surface integral of $\mathbf{A}$ over S is

$$\int_S \mathbf{A} \cdot d\mathbf{a} \tag{9}$$

The vector $d\mathbf{a}$ has a magnitude that represents the differential area of a surface element and a direction that is normal to that area. To interpret (9), think of the surface S as subdivided into these differential area elements $d\mathbf{a}$. At each area element, the differential scalar $\mathbf{A} \cdot d\mathbf{a}$ is evaluated and the surface integral is defined as the sum of these dot products over S in the limit as $d\mathbf{a}$ approaches zero. The surface integral $\int_S \mathbf{A} \cdot d\mathbf{a}$ is also called the "flux" of the vector $\mathbf{A}$ through the surface S.

To evaluate a surface integral, a coordinate system is introduced in which the integration can be performed according to the methods of integral calculus. Then the surface integral is transformed into a double integral in two independent variables. This is best illustrated with the aid of a specific example.

Example 2.1.2. Surface Integral

Given the vector field

$$\mathbf{A} = \mathbf{i}_\mathbf{x} x \tag{10}$$

find the surface integral $\int_S \mathbf{A} \cdot d\mathbf{a}$, where S is one eighth of a spherical surface of radius R in the first octant of a sphere ($0 \le \phi \le \pi/2,\ 0 \le \theta \le \pi/2$).

Because the surface lies on a sphere, it is best to carry out the integration in spherical coordinates. To transform coordinates from Cartesian to spherical, recall from (A.1.3) that the x coordinate is related to r, θ, and ϕ by

$$x = r \sin\theta \cos\phi \tag{11}$$

and from (A.1.6), the unit vector $\mathbf{i}_\mathbf{x}$ is

$$\mathbf{i}_\mathbf{x} = \sin\theta\cos\phi\, \mathbf{i}_\mathbf{r} + \cos\theta\cos\phi\, \mathbf{i}_\theta - \sin\phi\, \mathbf{i}_\phi \tag{12}$$

Therefore, because the area element $d\mathbf{a}$ is

$$d\mathbf{a} = \mathbf{i}_\mathbf{r} R^2 \sin\theta d\theta d\phi \tag{13}$$

the surface integral becomes

$$\begin{aligned} \int_S \mathbf{A} \cdot d\mathbf{a} &= \int_0^{\pi/2} d\theta \int_0^{\pi/2} d\phi R^3 \sin^3\theta \cos^2\phi \\ &= \frac{\pi R^3}{4} \int_0^{\pi/2} d\theta \sin^3\theta = \frac{\pi R^3}{6} \end{aligned} \tag{14}$$

A surface integral of a vector $\mathbf{A}$ over a closed surface is indicated by

$$\oint_S \mathbf{A} \cdot d\mathbf{a} \tag{15}$$

Note also that we use a single integral sign for a surface integral, even though, in fact, two integrations are involved when the integral is actually evaluated in terms of a coordinate system.

2.2 PROOF THAT THE CURL OPERATION RESULTS IN A VECTOR

The definition

$$[curl\,\mathbf{A}]_n = \lim_{a\to 0} \frac{1}{a} \oint \mathbf{A}\cdot d\mathbf{s} \tag{1}$$

assigns a scalar, $[curl\,\mathbf{A}]_n$, to each direction $\mathbf{n}$ at the point P under consideration. The limit must be independent of the shape of the contour C (as long as all its points approach the point P in the limit as the area a of the contour goes to zero). The identification of $curl\,\mathbf{A}$ as a vector also implies a proper dependence of this limit upon the orientation of the normal $\mathbf{n}$ of a. The purpose of this appendix is to show that these two requirements are indeed satisfied by (1). We shall prove the following facts:

1. At a particular point (x, y, z) lying in the plane specified by its normal vector $\mathbf{n}$, the quantity on the right in (1) is independent of the shape of the contour. (The notation $[curl\,\mathbf{A}]_n$, is introduced at this stage only as a convenient abbreviation for the expression on the right.)
2. If $[curl\,\mathbf{A}]_n$ is indeed the component of a vector $[curl\,\mathbf{A}]$ in the $\mathbf{n}$ direction and $\mathbf{n}$ is a unit normal in the $\mathbf{n}$ direction, then

$$[curl\,\mathbf{A}]_n = [\mathrm{curl}\,\mathbf{A}]\cdot\mathbf{n} \tag{2}$$

where $[curl\,\mathbf{A}]$ is a vector defined at the point (x, y, z).

The proof of (1) follows from the fact that any closed contour integral can be built up from a superposition of contour integrals around a large number of rectangular contours C_i, as shown in Fig. A.2.3. All rectangles have sides $\Delta\xi$, $\Delta\eta$. If the entire contour containing the rectangles is small ($a \to 0$), then the contour integral around each rectangle differs from that for the contour C_o at the origin only by a term on the order of the linear dimension of the contour, $a^{1/2}$, times the area $\Delta\xi\Delta\eta$. This is true provided that the distance from the origin to any point on the contour does not exceed $a^{1/2}$ by an order of magnitude and that $\mathbf{A}$ is once differentiable in the neighborhood of the origin. We have

$$\frac{1}{\Delta\xi\Delta\eta}\oint_{C_i}\mathbf{A}\cdot d\mathbf{s} = \frac{1}{\Delta\xi\Delta\eta}\oint_{C_o}\mathbf{A}\cdot d\mathbf{s} + O(a^{1/2}) \tag{3}$$

Therefore,

$$\begin{aligned}\frac{1}{a}\oint_C \mathbf{A}\cdot d\mathbf{s} &= \sum_i \frac{1}{a}\oint_{C_i}\mathbf{A}\cdot d\mathbf{s} = \frac{\Delta\xi\Delta\eta}{a}\sum_i \frac{1}{\Delta\xi\Delta\eta}\oint_{C_i}\mathbf{A}\cdot d\mathbf{s}\\ &= N\frac{\Delta\xi\Delta\eta}{a}\left[\frac{1}{\Delta\xi\Delta\eta}\oint_{C_o}\mathbf{A}\cdot d\mathbf{s} + O(a^{1/2})\right]\end{aligned} \tag{4}$$

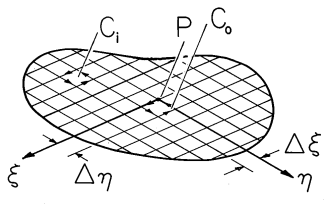


Fig. A.2.3 Separation of closed contour integral into large number of integrals over rectangular contours.

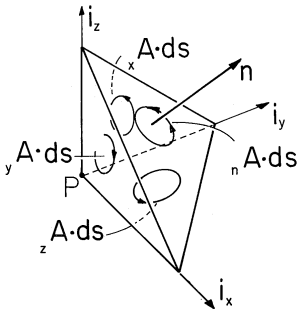


Fig. A.2.4 Arbitrary incremental contour integral having normal **n** analyzed into integration contours enclosing surface, having normals in the directions of the Cartesian coordinates.

where N is the number of rectangles into which the contour C has been subdivided. However, $N = a/(\Delta\xi\Delta\eta)$, and therefore we find

$$\lim_{a\to 0} \sum_i \frac{1}{a} \oint_{C_i} \mathbf{A} \cdot d\mathbf{s} = \lim_{a\to 0} \frac{1}{\Delta\xi\Delta\eta} \oint_{C_o} \mathbf{A} \cdot d\mathbf{s} \tag{5}$$

The expression on the left refers to the original contour, while the expression on the right refers to the rectangular contour at the origin. Since a contour of arbitrary shape can be constructed by a proper arrangement of rectangular contours, we have proven that the expression $\lim_{a\to 0} \int \mathbf{A} \cdot d\mathbf{s}/a$ is independent of the shape of the contour as long as (3) holds.

Turning to the proof that (1) defines the component of a vector, we recognize that the shape of the contour is arbitrary when evaluating $\int \mathbf{A} \cdot d\mathbf{s}/a$. We displace the plane in which the contour lies by a *differential* amount away from the point $P(x, y, z)$, as shown in Fig. A.2.4 which does not affect the value of $[curl\, \mathbf{A}]_n$ as defined in (1). The intersection of the plane with the three coordinate planes through P is a triangle. We pick the triangle for the contour C in (1).

It follows from Fig. A.2.4 that the contour integral around the triangular contour in the plane perpendicular to **n** can also be written as the sum of three integrals around the three triangular contours in the respective coordinate planes. Indeed, each of the added sections of line are traversed in one contour integration in the opposite direction, so that the integrals over the added sections of the line cancel upon summation and we have

$$\oint_n \mathbf{A} \cdot d\mathbf{s} = \oint_x \mathbf{A} \cdot d\mathbf{s} + \oint_y \mathbf{A} \cdot d\mathbf{s} + \oint_z \mathbf{A} \cdot d\mathbf{s} \tag{6}$$

where each contour integral is denoted by the subscript taken from the unit vector normal to the plane of the contour.

We further note that the areas a_x, a_y, a_z of the three triangles in the respective coordinate planes are the projections of the area a onto the corresponding coordinate plane.

$$a_x = a\mathbf{i_x} \cdot \mathbf{n} \tag{7}$$

$$a_y = a\mathbf{i_y} \cdot \mathbf{n} \tag{8}$$

$$a_z = a\mathbf{i_z} \cdot \mathbf{n} \tag{9}$$

Thus, by dividing (6) by a and making use of (7), (8), and (9), we have:

$$\begin{aligned}\frac{1}{a}\oint_n \mathbf{A}\cdot d\mathbf{s} =& \frac{1}{a_x}\oint_x \mathbf{A}\cdot d\mathbf{s}\mathbf{i_x}\cdot\mathbf{n} + \frac{1}{a_y}\oint_y \mathbf{A}\cdot d\mathbf{s}\mathbf{i_y}\cdot\mathbf{n} \\ &+ \frac{1}{a_z}\oint_z \mathbf{A}\cdot d\mathbf{s}\mathbf{i_z}\cdot\mathbf{n}\end{aligned} \tag{10}$$

Now, since the contours are already taken around differential area elements, the limit $a \to 0$ is already implied in (10). Thus, we have the quantities

$$[curl\,\mathbf{A}]_x = \lim_{a_x\to 0}\oint_x \mathbf{A}\cdot d\mathbf{s}/a_x \ldots \tag{11}$$

But (10) is the definition of the component in the $\mathbf{n}$ direction of a vector:

$$curl\,\mathbf{A} = [curl\,\mathbf{A}]_x\mathbf{i_x} + [curl\,\mathbf{A}]_y\mathbf{i_y} + [curl\,\mathbf{A}]_z\mathbf{i_z} \tag{12}$$

It is therefore legitimate to define at every point x, y, z in space a vector quantity, $curl\,\mathbf{A}$, whose x-, y-, and z-components are evaluated as the limiting expressions of (1).